International Journal of
Molecular Sciences

Volume 2

The Tight Junction and Its Proteins

More Than Just a Barrier

Edited by
Michael Fromm and Susanne M. Krug

Printed Edition of the Special Issue Published in
International Journal of Molecular Sciences

www.mdpi.com/journal/ijms

MDPI

The Tight Junction and Its Proteins: More Than Just a Barrier

The Tight Junction and Its Proteins: More Than Just a Barrier

Volume 2

Editors

Michael Fromm
Susanne M. Krug

MDPI • Basel • Beijing • Wuhan • Barcelona • Belgrade • Manchester • Tokyo • Cluj • Tianjin

Editors
Michael Fromm
Charité—Universitätsmedizin Berlin
Germany

Susanne M. Krug
Charité—Universitätsmedizin Berlin
Germany

Editorial Office
MDPI
St. Alban-Anlage 66
4052 Basel, Switzerland

This is a reprint of articles from the Special Issue published online in the open access journal *International Journal of Molecular Sciences* (ISSN 1422-0067) (available at: https://www.mdpi.com/journal/ijms/special_issues/Tight_Junction).

For citation purposes, cite each article independently as indicated on the article page online and as indicated below:

LastName, A.A.; LastName, B.B.; LastName, C.C. Article Title. *Journal Name* **Year**, *Article Number*, Page Range.

Volume 2
ISBN 978-3-03943-300-1 (Pbk)
ISBN 978-3-03943-301-8 (PDF)

Volume 1-2
ISBN 978-3-03943-302-5 (Pbk)
ISBN 978-3-03943-303-2 (PDF)

Cover image courtesy of Susanne M. Krug.

Contents

About the Editors

Michael Fromm is a senior professor and former Head of the Institute of Clinical Physiology at the Charité—Universitätsmedizin Berlin, Germany, where he still works. He has published more than 230 research articles, resulting in an h-index of 61. Through this, he has made seminal contributions to transport mechanisms and barrier functions of intestinal and renal epithelia in health and disease. For some claudins, he has discovered that they form channels selective for ions and/or water. Starting in 2006, he was the coordinator of the Deutsche Forschungsgemeinschaft (DFG) Research Unit "Molecular structure and function of the tight junction", which paved the way to a currently running DFG graduate school focusing on tight junction research. Within this, his lab focuses on protein prerequisites of tricellular tight junction water permeability.

Susanne M. Krug has studied Biochemistry and is now a Group Leader at the Institute of Clinical Physiology at the Charité—Universitätsmedizin Berlin, Germany. She has made remarkable contributions to the understanding of the tricellular tight junction as a regulated passage site for macromolecules, especially in inflamed intestinal epithelium. Presently, she holds three grants of the Deutsche Forschungsgemeinschaft (DFG) and, based on >60 publications, has reached an h-index of 25. Her current research interests still deal with tricellular tight junctions, but also with interaction of immune cells and tight junction proteins in inflammatory bowel diseases.

Preface to "The Tight Junction and Its Proteins: More Than Just a Barrier"

Most accredited FAO statistics predict that in 30 years, the world's population will have reached 9 billion people. In order to satisfy the nutritional needs of humans, the demand for raw materials, especially protein sources, will increase. It has been estimated that by 2050, the production of meat will have increased by 50%, while the demand for fish, milk, and eggs will have grown by 75%. An increase in animal products requires an increase in farmed animals, and this will be accompanied by a significant intensification in livestock farming (higher animal densities and production units, more concentrated feed, pharmaceuticals, and vaccinations, etc.). A large number of animals, farmed in relatively small areas, will result in a larger demand for protein and energy sources on which to feed them and in the deposition of large amounts of excreta, containing nitrogen, phosphorus, organic matter, and fecal microbes, in the water, with a consequent contamination of water systems globally, which will include surface water eutrophication and groundwater nitrate enrichment. Thus, the livestock sector is an important user of natural resources and has a great influence on air, soil, and water quality, the global climate, and biodiversity maintenance. Our research proposes innovative ideas to control the environmental damage through the management of animal nutrition. At the same time, the perception of animals as sentient beings capable of feeling emotions, like joy and pain, will increase in prevalence in the future. Thus, it will be increasingly important to adopt nutritional strategies and breeding techniques capable of increasing animal welfare and at the same time to reduce the use of pharmacological treatments in full respect of the environment, animal health, and food safety.

Michael Fromm, Susanne M. Krug
Editors

International Journal of
Molecular Sciences

MDPI

Review

Role of Tricellular Tight Junction Protein Lipolysis-Stimulated Lipoprotein Receptor (LSR) in Cancer Cells

Takayuki Kohno *, Takumi Konno and Takashi Kojima

Department of Cell Science, Research Institute for Frontier Medicine, Sapporo Medical University, Sapporo 060-8556, Japan
* Correspondence: kohno@sapmed.ac.jp; Tel.: +81-11-611-2111; Fax: +81-11-611-2299

Received: 19 June 2019; Accepted: 19 July 2019; Published: 20 July 2019

Abstract: Maintaining a robust epithelial barrier requires the accumulation of tight junction proteins, LSR/angulin-1 and tricellulin, at the tricellular contacts. Alterations in the localization of these proteins temporarily cause epithelial barrier dysfunction, which is closely associated with not only physiological differentiation but also cancer progression and metastasis. In normal human endometrial tissues, the endometrial cells undergo repeated proliferation and differentiation under physiological conditions. Recent observations have revealed that the localization and expression of LSR/angulin-1 and tricellulin are altered in a menstrual cycle-dependent manner. Moreover, it has been shown that endometrial cancer progression affects these alterations. This review highlights the differences in the localization and expression of tight junction proteins in normal endometrial cells and endometrial cancers and how they cause functional changes in cells.

Keywords: tricellular tight junctions; endometrial cancer; epithelial barrier dysfunction

1. Introduction

The endometrium is a regenerative tissue in which the cells undergo proliferation and differentiation depending on the levels of estrogen, progesterone, or various cytokines. The organization of cell-cell junctions, such as tight junctions, adherence junctions, gap junctions, and desmosomes, has important implications for the homeostatic regulation of many tissues, including the endometrium [1]. Cell-cell junctions are formed not only in bicellular regions but also at tricellular contacts [2]. Several reviews have mentioned that occludin (OCLN) and claudins (CLDNs) have been established as bicellular tight junction proteins involved in the formation and maintenance of epithelial barriers [3–5]. A recent study revealed that their expression and localization are affected by the menstrual cycle [6]. According to the report, CLDN-1, -3, -4, and -7 localized in the subapical region during the proliferative phase of the endometrium, while they were broadly distributed to the lateral region during the secretory phase (Figure 1). Furthermore, it has been shown that robust epithelial barrier formation requires localization of these tight junction proteins at the subapical region by analyzing primary cultured normal human endometrial cells. Recent studies have revealed that the localization of tricellular tight junction proteins, tricellulin and LSR/angulin-1, to tricellular contacts is required for epithelial barrier maturation based on the proper localization of OCLN and CLDNs [7]. A recent study demonstrated that tricellulin localized in the subapical region during the endometrial secretory phase, whereas LSR was broadly distributed to the lateral region [8]. In contrast, during the proliferative phase of endometrium formation, both proteins localized in the subapical region. Furthermore, analysis using primary cultured normal human endometrial cells revealed that localization of LSR to the tricellular contacts is required for the formation of mature epithelial polarity with sufficient barrier function. These findings suggested that LSR and tricellulin are closely related to the functional regulation of

periodic morphological changes in the endometrial tissue. In the normal human endometrium, a part of the mechanism that regulates the localization and expression of tricellular tight junction proteins has been elucidated below.

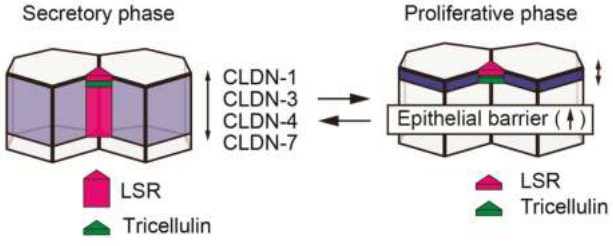

Figure 1. The localization of tight junction proteins is affected by menstrual cycle. In secretory phase of human endometrium, CLDN-1, -3, -4, and -7 are widely distributed to the lateral region. Tricellulin localized in tricellular contacts of the subapical region, whereas LSR is widely distributed to the lateral region. In proliferative phase, CLDNs localized in the subapical tight junction region. Tricellulin and LSR localized in the subapical tricellular contacts.

2. Tricellular Tight Junction Proteins and Cancer

Many oncogenic processes are known to be involved in genetic instability based on failure of DNA mismatch repair pathways [9]. It is an established fact that the abnormal cell growth, dedifferentiation, and EMT are induced by the activation of oncogenes, such as Ras, and/or the inactivation of tumor suppressor genes, such as PTEN and p53 [10]. These adverse events, like a cancer metastasis, are certainly accompanied with reconstitution of cell-cell junctions [11]. While most of the differentiated epithelial cells have established tight junctions, disruption of tight junctions abolishes cell polarity and promotes dedifferentiation [3,12]. Furthermore, a decrease in epithelial barrier function is implicated in cancer cell invasion and metastasis [13]. Epithelial barrier homeostasis is disrupted by decreased expression of tight junction proteins as well as by their overexpression [14]. It still remains largely unknown how expression of tight junction proteins is regulated during the oncogenic process. Interestingly, decreased expression of tricellulin, which regulates epithelial barrier maturation, has been reported to be associated with tumor progression. For instance, in human tonsillar squamous cell carcinoma, decreased expression of tricellulin and CLDN-7 and increased expression of CLDN-1 have been identified [15]. In hepatocellular carcinoma cells, decreased expression of tricellulin has been observed as compared to that in normal hepatocytes [16]. In addition, lower prognosis of intrahepatic cholangiocarcinoma (iCCC) has been shown to correlate with decreased expression of tricellulin [17]. In pancreatic cancer, the decreased expression of tricellulin exhibits a correlation with decreased differentiation [18]. In gastric carcinoma, Snail-induced EMT negatively regulates the expression of tricellulin [19].

Increasing number of studies have reported the relationship between malignant transformation and expression of LSR, which is another tricellular tight junction protein. It has been reported that the expression of LSR is higher in invasive ductal carcinomas compared to that in invasive lobular carcinomas [20]. In addition, LSR is considered as a candidate prognostic biomarker in colon cancer patients [21]. Recent observations have revealed that the expression levels of LSR, tricellulin, and CLDN-1 were higher in head and neck squamous cell carcinoma tissues compared with those in normal palatine tonsils [22]. In addition, by analyzing the immunohistochemical staining using paraffin sections of head and neck squamous cell carcinoma tissue, it has been shown that the expression levels of both LSR and CLDN-1 are increased in cancerous tissues, especially in invasive tissues, compared to those in adjacent dysplasia tissues. Increased expression of CLDN-1 has been observed in advanced head and neck cancer [23]. CLDN-1 has also been shown to be significantly expressed in hypopharyngeal squamous cell carcinoma tissues, suggesting that CLDN-1 is associated with tumor

differentiation and lymph node metastasis [24]. As described above, various cancerous malignancies are associated with changes in the expression and localization of not only bicellular tight junction proteins but also tricellular tight junction proteins. These findings suggested that tricellular tight junction proteins may interact closely with bicellular junctions during malignant transformation in response to reduction of the barrier function.

3. Expression and Localization of the Tricellular Tight Junction Proteins, LSR and Tricellulin, during Endometriosis and Endometrial Carcinoma

During endometriosis, decreased expression levels of CLDN-3, -4, and -7 have been observed [25], and in endometrial cancer, increased expression levels of CLDN-3 and -4 have been reported [26,27]. Since changes in the expression levels of bicellular tight junction proteins were observed during the pathogenesis of the endometrial cancer, it is reasonable to consider that these processes were also accompanied by changes in expression levels of tricellular tight junction proteins. Recently, by analyzing the immunohistochemical staining using paraffin sections of endometriotic and endometrial cancer tissue, it has been found that during endometriosis tricellulin was localized in the subapical region similar to normal human endometrial tissue, while LSR was localized in the subapical region of tricellular contacts in addition to the lateral region [8]. In endometrial carcinoma G1, where the formation of gland-like structure is retained, the expression levels of tricellulin and LSR were distributed unevenly from the subapical to the lateral region of cell-cell junctions. In G2 and G3 endometrial carcinoma, their expression levels were decreased. Taken together, these findings revealed that the grade of malignancy correlated with the decreased expression levels of tricellulin and LSR in addition to changes in the localizations of these proteins (Figure 2). Among cultured cells derived from endometrial cancer, we were able to confirm the expression levels of both tricellulin and LSR in Sawano, HHUA, and JHMUE-1 cells, all of which exhibit an epithelial phenotype, whereas little or no expression was observed in JHMUE-2, which exhibits a fibroblast-like morphology. Since the expression levels of tricellulin and LSR contribute to the maintenance of the morphology of epithelial cells, we hypothesized that depletion of these proteins enhances cell motility. The endometrial cancer cell line, Sawano, endogenously expresses tricellulin and LSR. In Sawano cells with LSR knockdown, the epithelial barrier function was reduced, and thereby, cell motility, cell invasion, and proliferation were enhanced compared to those in the parental control. Thus, the localization of LSR at tricellular contacts is necessary for maintaining the robustness of the epithelial barrier function. The relationship between the exclusion of LSR from tricellular contacts and cancer progression has been discussed below, with a focus on endometrial cancer.

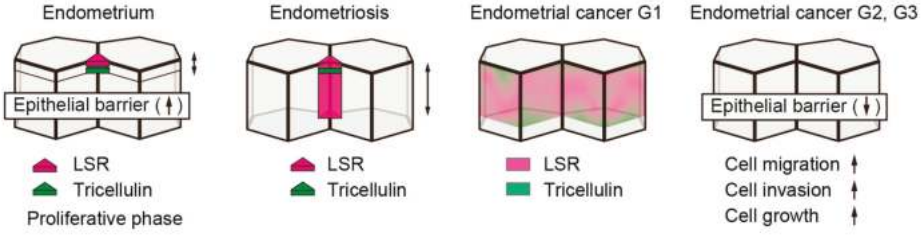

Figure 2. Expression and localization of LSR and tricellulin during endometriosis and in endometrial cancers. LSR and tricellulin localized in tricellular contacts in endometrium. During endometriosis, tricellulin is localized in the subapical region of tricellular contacts and LSR is localized in not only the subapical tricellular contacts but also in the lateral tricellular contacts. In endometrial cancer G1, tricellulin and LSR were distributed unevenly from the subapical to the lateral region of bicellular junctions. In endometrial cancer G2 and G3, the expression levels of tricellulin and LSR were downregulated, resulting in decrease of epithelial barrier and increase of cell migration, cell invasion, and cell growth.

4. Obesity and Endometrial Cancer

Diagnoses of endometrial cancer have increased worldwide in recent years [28]. Obesity is a major risk factor for endometrial cancer [29]. Bioinformatics analysis using cBioProtal and DAVID bioinformatics resources confirmed that expression of genes related to glucose metabolism and lipid metabolism is increased in endometrial cancer [30]. Increase in estrogen, decrease in adiponectin, and increase in inflammatory cytokines are all known as typical cancer-inducing factors [31]. Leptin has also been reported to be involved in endometrial cell proliferation [32]. Previous studies have reported that an increase in circulating adiponectin and leptin-adiponectin ratio may be potential risk factors for breast cancer, colorectal cancer, pancreatic cancer, and endometrial cancer [33,34]. Leptin is produced not only from an adipose tissue, but also from follicles and placenta, and its production is associated with menstrual cycle and pregnancy [35,36]. Leptin is involved in facilitating endometrial cancer progression and metastasis of pancreatic cancer via the activation of JAK2/STAT3 pathway [37,38]. Adiponectin suppresses the progression and development of cancer by antagonizing this pathway [39]. It has been found that in endometrial cancer cells, leptin suppressed the expression of LSR, while adiponectin increased its expression [8]. Moreover, studies using inhibitors suggested that the stimulation with leptin or adiponectin induced an alteration of LSR expression via the PI3K and JAK2/3 pathways.

It has been speculated that there is an interface between the regulatory pathways of the epithelial barrier formation and signaling pathways via the adipocytokine receptor. The knockdown of LSR enhanced cell motility and invasion in Sawano cells. This finding correlated with the cellular response associated with leptin-dependent downregulation of LSR (Figure 3). Interestingly, even in normal human endometrial cells, leptin suppressed LSR expression, while adiponectin increased its expression. It is assumed that obesity is involved in the malignant transformation of endometrial cancer besides attenuating the robust tight junctions of normal endometrium. LSR has been identified as a lipid receptor involved in lipid clearance [40]. In mice, suppression of LSR expression in the liver causes systemic hyperlipidemia, resulting in obesity and weight gain [41]. The differences in the function and role of LSR as a lipoprotein receptor and the involvement of LSR in obesity-dependent epithelial barrier attenuation should be clarified in future studies.

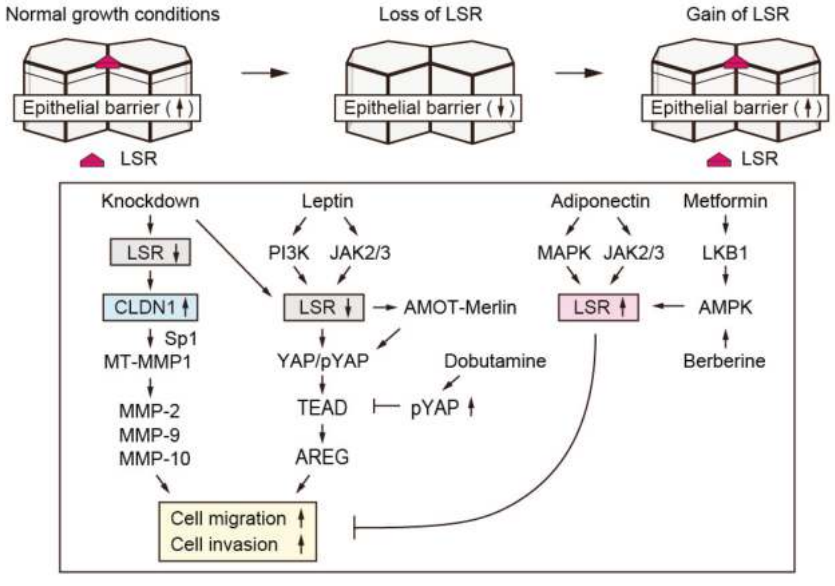

Figure 3. Changes in cellular functions by repression and re-expression of LSR. Under normal growth conditions, LSR localized in tricellular contacts in primary cultured normal human endometrial cells and Sawano cells. The knockdown of LSR enhanced cell motility and cell growth accompanying with decrease in barrier function. Leptin suppressed LSR expression; in contrast, adiponectin induced an increase in its expression. AMPK activator metformin and berberine also induced an increase in LSR expression at the subapical region of tricellular contacts, resulting in the rescue of the LSR-knockdown phenotypes.

5. Glucose Metabolism and Endometrial Cancer

Obesity has been reported to be an independent risk factor for the development of diabetes [42]. Epidemiological studies have shown that metformin, a therapeutic agent for type 2 diabetes, reduces the incidence of endometrial cancer [43]. In addition, berberine, which is a herbal medicine component, has been reported to be not only effective in type 2 diabetes, but also in suppression of growth of cancer [44]. We found that metformin and berberine both increased LSR expression in endometrial cancer cells. The upregulation of LSR expression by these drugs contributed to the suppression of motility and invasion of endometrial cancer cells enhanced by leptin administration. Metformin and berberine also increased LSR expression in primary cultured normal human endometrial cells (Figure 3). Therefore, these drugs may be used to treat diseases based on epithelial barrier disruption. In fact, these drugs, which are categorized as AMPK activators, are currently being considered as potential therapeutic agents for endometrial cancer [43–45].

AMPK is an energy sensor that regulates the levels of intracellular ATP and centrally regulates metabolism [46,47]. Initially, depletion of intracellular ATP was reported to temporarily and reversibly disrupt tight junctions [48]. However, recent studies have indicated that AMPK, rather than affecting the intracellular ATP levels, may directly regulate tight junction proteins [49]. In the report, the authors revealed that AMPK regulates the relocalization of ZO-1 after Ca switch, independently of the intracellular ATP levels. Furthermore, AMPK has been reported to promote stabilization of tight junctions and to enhance barrier function via phosphorylation of the scaffold protein, GIV, which regulates cell polarity [50]. Metformin acts as a therapeutic agent for diabetes via LKB1-mediated phosphorylation of AMPK, which is accompanied by mitochondrial OxPhos suppression [51], suggesting that, in epithelial cells, metformin stabilizes tight junctions via the activation of AMPK.

Interestingly, it has been previously reported that the progression of endometrial cancer correlates with the decrease in AMPK expression [52]. It is necessary to elucidate the signal transduction pathways involved in AMPK-regulated glucose metabolism and the regulation of epithelial barrier function.

6. Mechanisms of Enhancement of Cell Invasion Caused by Decreased LSR Expression

Using immunohistochemical analysis of paraffinized sections of endometrial cancer tissues, we observed a positive expression of LSR and negative expression of CLDN-1 in the gland-like structure region. In contrast, in the invasive front area, LSR expression decreased and CLDN-1 expression increased. Following knockdown of LSR in endometrial cancer Sawano cells, CLDN-1 expression increased, while there was no significant change in the expression levels of CLDN-3, -4, -7, and OCLN. Before LSR knockdown, although CLDN-1 localized in the subapical region, it was widely distributed not only to the subapical region but also to the lateral region after LSR knockdown. These findings suggested that there was a negative relationship between the expression levels of LSR and CLDN-1 (Figure 3). In intestinal epithelial cells, it has been reported that regulation of CLDN-1 expression requires Sp1 binding to the CLDN-1 promoter region [53]. It has been reported that CLDN-1, -4, and -19 harbor Sp1 binding sites in the promoter region [54–56]. We confirmed that Sp1-dependent transcriptional regulation was involved in the enhancement of CLDN-1 expression associated with LSR repression [57].

It has been reported that cell invasion is enhanced via the cleavage of laminin-5 gamma 2 chains by activation of MT-MMP1 and MMP2 in CLDN-1-overexpressing OSC cells [58]. In addition, in SW480 cells, overexpressing CLDN-1, cell invasion is enhanced through the activation of MMP2 and MMP9 [59]. The initial process of cell invasion requires reconstitution of extracellular matrix components, along with the attenuation of cell junctions [60]. Twenty four MMP family members have been identified so far [61]. It has been found that knockdown of LSR increased the expression levels of MT-MMP1, MMP2, MMP9, and MMP10 in Sawano cells [57]. MT-MMP1 has been reported to be a initiating factor that regulates the MMP cascade following the activation of proMMP2 [62]. Interestingly, double knockdown of LSR and CLDN-1 suppressed the increase in cell invasion by LSR knockdown [57]. Little is known about the precise molecular mechanisms underlying the activation of MMPs accompanying the expression of CLDN-1 in endometrial cancer tissues. The suppression of LSR downregulation may regulate the malignant transformation of endometrial cancer.

7. Hippo Pathway and Endometrial Cancer

Relaxation of cell-cell junctions and abnormality of epithelial polarity suppress contact inhibition in epithelial cells, resulting in the induction of abnormal proliferation. The Hippo pathway comprehensively regulates these mechanisms [63]. When the Hippo pathway is turned on, LATS1/2 is phosphorylated via MST1/2. Phosphorylated LATS1/2 phosphorylates YAP, and phosphorylated YAP is degraded via 14-3-3. On the other hand, when the Hippo pathway is blocked, the phosphorylation of YAP is suppressed. The non-phosphorylated form of YAP translocates from the cytoplasm to the nucleus as a transcription cofactor and induces the expression of target genes, such as AREG and DKK1, depending on the expression of the transcription factor TEAD.

We found that YAP is localized in the cytoplasm of the endometrial tissue and in the nucleus in G1, G2, and G3 endometrioid carcinoma, as revealed by immunohistochemical staining using paraffinized sections of endometriotic and endometrial cancer tissues. As mentioned above, cell motility and invasion enhanced by knockdown of LSR were decreased by double knockdown of LSR and YAP. These findings suggested that the decrease in epithelial barrier function caused by the suppression of LSR expression is involved in the regulation of cell motility and invasion via YAP (Figure 3). The β-adrenergic receptor agonist, dobutamine, decreases nuclear YAP levels and increases the amount of cytosolic phosphorylated YAP in human osteoblastoma U2OS cells [64]. Dobutamine has also been reported to suppress the enhancement in the expression of YAP in gastric carcinoma, resulting in the suppression of cell motility and invasion [65]. In addition, in LSR-knocked down Sawano cells,

dobutamine administration suppressed the enhancement in cell motility and invasion via the increase of phosphorylated YAP. The precise molecular mechanisms underlying the phosphorylation of Hippo kinases, such as MST1/2 and LATS1/2, via LSR-mediated epithelial barrier modulation still need to be elucidated.

Under glucose starvation conditions, AMPK is phosphorylated by LKB1 [66]. Phosphorylated AMPK has been reported to suppress nuclear translocation of YAP via the phosphorylation of LATS1/2 and/or direct phosphorylation of YAP [47]. In Sawano cells, under glucose-starving conditions, YAP is localized in the proximity of the cell-cell junctions [67]. In addition, both AMPK and YAP were phosphorylated. Moreover, both cell invasion and cell motility enhanced by LSR knockdown were rescued by glucose starvation. It has been speculated that these mechanisms are probably similar to the effect of treatment of AMPK activator, metformin or berberine, as mentioned above. Glucose starvation also increased LSR expression. Further studies are needed to elucidate the signaling pathways by which glucose starvation regulates epithelial barrier functions in endometrial cancer.

Using DNA microarray and qPCR analysis, it has been found that the expression levels of the transcription factors TEAD and AREG, increased in LSR-knockdown Sawano cells [67]. Moreover, immunohistochemical analysis using paraffinized sections of endometriotic and endometrial cancer tissue showed that AREG was expressed in the cytoplasm and that the expression increased with the progression of cancer stage. In Sawano cells, increasing cell motility and invasion by LSR knockdown was suppressed by knockdown of AREG. These effects were also observed after TEAD knockdown. In parental Sawano cells, knockdown of AREG did not affect cell motility and invasion. Therefore, it is concluded that TEAD-dependent AREG expression via the Hippo pathway is involved in the enhancement of cell motility accompanied by the suppression of LSR expression.

8. Crosstalk between the Hippo Pathway and Tight Junctions

Merlin/NF2 is known as one of the tumor suppressor factors that regulate the Hippo pathway [68]. Merlin localizes to adherens junctions by interacting with E-cadherin, PAR3, and catenin [69]. Merlin also interacts with YAP and AMOT, a scaffold protein of Mst1/2 and LATS1/2 at tight junctions and contributes to the regulation of EMT [70]. It has been suggested that changes in the cell adhesion between adjacent cells, that is, modulation of tight junctions and adherens junctions, regulate the phosphorylation of YAP via the Hippo pathway, leading to the disruption of contact inhibition and normal growth. However, the precise molecular mechanisms have yet to be elucidated.

By immunohistochemical analysis, we found that AMOT localized in the subapical region and the lateral region of endometriosis tissues [67]. In endometrioid adenocarcinoma, positive expression of AMOT was observed in the gland-like structure region. Compared with that in endometrial carcinoma G1, decreased expression of AMOT was observed in G2 and G3. The Motin family consists of AMOT (angiomotin), AMOTL1 (angiomotin-like 1), and AMOTL2 (angiomotin-like 2) [71]. In addition, two isoforms of AMOT, AMOT-p130 and AMOT-p80, have been identified. AMOT-p80 has been identified as an oncogene in hemangioendothelioma, head and neck squamous cell carcinoma, and prostate cancer [72–74]. AMOT-p130 has been reported to exhibit oncogenic functions as well as tumor suppressive functions [71]. AMOTL1 has been shown to act as an oncogene in breast cancer [75] and cervical cancer [76], and AMOTL2 has been reported to act as an oncogene in breast cancer [77] and suppressor glioblastoma carcinogenesis [78]. In endometrial cancer, decreased expression of AMOT was observed during cancer progression [67]. Molecular mechanisms related to AMOT in endometrial cancer would be clarified in the near future.

Using immunostaining analysis, we found that, in Sawano cells, endogenous Merlin localized in the vicinity of the cell-cell junctions identically to the other cells [68,79]. Under these conditions, AMOT is localized in tight junctions. It is known that AMOT interacts with Patj, Pals2, and Mupp1 at the tight junctions and that Merlin binds to the coiled-coil region of AMOT [80]. The Rac GTPase-activating protein, Rich1, binds through this region of AMOT. In mature tight junctions because Merlin binds to AMOT, Rich1 cannot interact with AMOT and localizes to the cytosol, resulting in the inactivation

of Rac. When Merlin is dissociated from AMOT, which is localized at tight junctions, Rich1 binds to the coiled-coil region of AMOT, thereby activating Rac and enhancing cell proliferation and cell motility. In Sawano cells, LSR knockdown decreased the expression levels of both AMOT and Merlin, and AMOT and LSR double knockdown further reduced the expression of Merlin [67]. The report revealed that the increased invasion and motility of Sawano cells by LSR knockdown was suppressed by AMOT knockdown. In the parental Sawano cells, AMOT knockdown increased cell invasion and motility, which were, in turn, suppressed by YAP knockdown. These findings suggested that YAP as well as Rac are involved in the malignant transformation of endometrial cancer cells. Identification of the crosstalk between AMOT/Merlin pathway and Rac/Rich1 pathway is considered to contribute to the elucidation of the malignant transformation mechanisms of endometrial cancer.

9. Changes in LSR Localization Are Associated with Changes in Cell Size Following Changes in Cell Density

An inverse correlation has been reported between cell density and motility of epithelial cells [81,82]. At high cell densities, apparent cell size decreases with increase in cell thickness accompanying decreasing cell motility. Conversely, at low cell densities, cells spread thinly and cell motility increases. In Sawano cells, LSR and tricellulin localized in tricellular contacts under high cell density conditions, while these proteins migrated to the bicellular region under low cell density conditions despite the presence of tricellular contacts [83]. Under these conditions, TER measurements indicated that an epithelial barrier was present even at low cell densities. The localizations of the bicellular tight junction proteins, OCLN and CLDN-4, were not affected by changes in cell density. Furthermore, knockdown of LSR under high cell density conditions induced thin spreading of cells and enhanced cell motility (unpublished observation). These findings suggested that the localization of LSR at tricellular contacts is necessary for the maintenance of static epithelial cell sheets.

An increase in cell density affects the intracellular tension mediated by actomyosin [84]. MRLC2 is localized at bicellular regions in the low density culture of Sawano cells [83]. Phosphorylated form of MRLC2, which represents activated myosin, is also localized in these regions. Under high cell density conditions, MRLC2 accumulated in vesicles or aggregated as particles near the apical cell surface membrane without localization to the apical bicellular region. It has been reported that activated MRLC2 is dephosphorylated by MYPT1, which is a component of the myosin phosphatase complex [85]. MYPT1 is localized in bicellular regions under high cell density conditions; however, under low cell density conditions, this protein was largely delocalized. These findings suggested that there is a high intracellular tension at bicellular regions of low density-grown cells as compared to that of high density-grown cells. When phosphorylated MRLC2 is localized in bicellular regions and MYPT1 is delocalized from there, LSR is localized in bicellular tight junctions. On the other hand, when MYPT1 is localized in bicellular regions, LSR is localized in apical tricellular contacts (Figure 4). Taken together, the localization of LSR altered in a cell density- and/or cellular tension-dependent manner. It is necessary to elucidate how LSR recognizes cell size and intracellular tension.

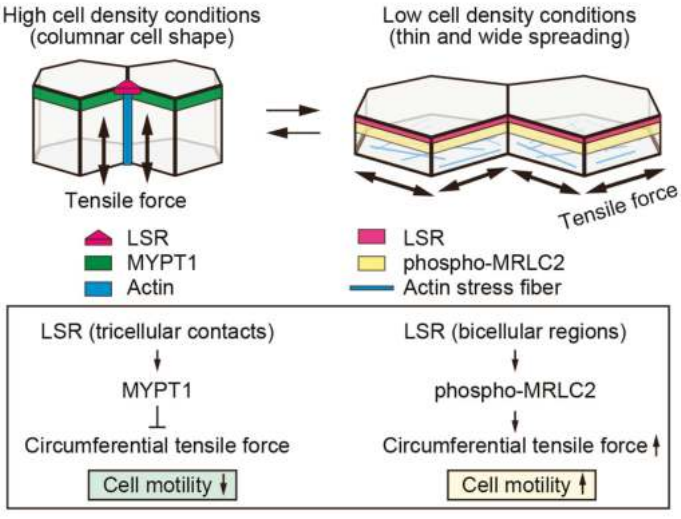

Figure 4. Decreased cellular tension causes LSR to localize at tricellular contacts. At high cell density, where cells were grown with columnar shape, the cellular tension decreased in the circumferential direction because MYPT1 is localized in these regions. Under these conditions, LSR is localized in tricellular contacts. In contrast, higher tension existed in cell-cell junctions at lower cell density because the phosphorylated form of MRLC2 is localized in these regions. In addition, actin stress fibers formed adjacent to the basal membrane. Under these conditions, LSR localized in bicellular junctions. It is noteworthy that thin and wide spreading cells increase cell motility.

10. Decreased Cellular Tension Causes LSR to Localize at Tricellular Contacts

Cellular tension is formed at cell-cell junctions and cell-substrate interface [86]. When the cells occupy a wide spread area, the number of focal contacts, where paxillin and integrins bind to the extracellular matrix, increases at basal membrane, facilitating polymerization of actin cytoskeleton [87]. Myosin, a cross-linked protein of actin fibers, generates cellular tension by contracting actin fibers [88]. Sawano cells cultured at low density conditions were spread thin and wide, and significant stress fiber formation was induced [83]. This suggested that high cellular tension is present under these conditions. Cellular tension is reportedly reduced by ROCK inhibitor, Y27632, muscle and non-muscle myosin II inhibitor, blebbistatin, or MLCK inhibitor, ML-7 [89]. When these reagents were added under low density conditions of Sawano cells where LSR localized in bicellular junctions, LSR localization decreased at bicellular junctions and increased at tricellular contacts. In our preliminary experiments, the focal adhesion kinase FAK localized in bicellular regions under low density of Sawano cells. FAK has been reported to be involved in the control of intestinal barrier functions [90] and blood-testis barrier functions [91]. In Sawano cells, FAK was dislocated from bicellular regions with increasing cell densities; however, the underlying mechanisms are still unclear. It is thought that the relationship between the regulatory mechanism of cellular tension involving FAK and the regulatory mechanism of epithelial barrier functions involving LSR will become clear in future studies.

11. Crosstalk between Intracellular Tension and Cell Junctions

In Sawano cells, LSR is reversibly translocated in a cellular tension- and/or cell size-dependent manner, whereas the localizations of OCLN and CLDN-4 were not affected by these conditions. Interestingly, accumulation of F-actin was observed not only along the lateral region of tricellular contacts but also the circumferential subapical region, leading to increase in cell thickness with the high cell density culture of Sawano cells [83]. Moreover, the actin polymerization inhibitor, Cytochalasin

D, excluded LSR from tricellular contacts, resulting in partial stratification of monolayered Sawano cell sheets. In long-term high-density culture, Sawano cells spontaneously and partially stratified in absence of Cytochalasin D. Under these conditions, the accumulated F-actin disappeared from lateral regions of tricellular contacts near the stratified area. In addition, LSR was translocated from tricellular contacts to the cell surface besides intracellular vesicles. Simultaneously, the epithelial barrier function decreased (unpublished observations). These findings suggested that the accumulation of F-actin at tricellular contacts is implicated in LSR localization to tricellular contacts. It is still not clear how the accumulated actin at tricellular regions regulates cellular tension. It is necessary to analyze the precise mechanism by which LSR localization is regulated by tension formed by actomyosin at tricellular contacts.

There have been almost no reports that LSR interacts directly with the actomyosin cytoskeleton at tricellular contacts. In contrast, it has been revealed that tricellulin promotes localization of both actin and myosin at tricellular contacts via interaction with Cdc42GEF protein Tuba (DNMBP, ARHGEF36) [92]. Cdc42 is one of the key proteins involved in the formation and maturation of epithelial polarity and contributes to the enhancement of cellular tension via MRCK(Cdc42BPA) [93]. MYPT1 is inactivated via phosphorylation by MRCK or ROCK [94,95]. In addition, the accumulation of tricellulin at tricellular contacts is controlled by LSR [7,96]. However, little is known about the downregulation of cellular tension during epithelial cell maturation by these proteins. Reportedly, the non-phosphorylated form of LSR in which mutations have been introduced to serine residues localizes to bicellular junctions [97]. However, the significance of LSR localization at bicellular junctions and its underlying molecular mechanism have not been elucidated yet. It is thought that changes in LSR localization along with changes in cellular tension are associated with acquisition of endometrial cancer motility. Further studies are required in order to understand the precise molecular mechanisms underlying regulation of LSR localization based on the changes in actomyosin activity and cellular tension.

Adherens junctions organize prior to tight junctions during the intercellular closure [98]. Adherens junctions interact with the actin cytoskeleton via the nectin-afadin complex and the cadherin-α/β-catenin complex [4]. Thereby, the actin cytoskeleton forms circumferential actomyosin bundles, contributing to cell polarity and cell thickness [99]. Shroom3 and Lulu1/2 are involved in the regulation of circumferential actomyosin bundles via ROCK [100,101]. Tight junctions are organized by the polarity complex consisting of PAR3, PAR6, and aPKC, which interact with circumferential actomyosin bundles via ZO1/2/3 [102]. For polarized epithelial cells, the cell thickness increases with long-term culture. The process of cell thickening is involved in the rearrangement of the actin cytoskeleton and the microtubule network [103]. Drebrin has been identified as a factor linking the actin cytoskeleton to the microtubule network through the interaction with complex consisting of myosin IIB, spectrin βII, and EB3 [104]. The report has revealed that, in Drebrin knockout cells, the cell thickness was reduced without compromising the cell polarity and the barrier function. Drebrin also localizes to gap junctions by interacting with connexin-43 [105]. Further studies are required to investigate whether Drebrin regulates LSR localization.

12. Hippo Pathway and Cytoskeletal Dynamics

Junctional complexes comprised of tight junctions and adherens junctions are important for the maintenance of apico-basal polarity in planar epithelial cells [4]. Many of these complexes interact with various adaptor proteins via PDZ domains and are linked to actomyosin networks [106]. These interactions allow epithelial cells to maintain apico-basal polarity [107]. Insufficient planar cell polarity is formed when only a few cells exist in a population per unit area [4]. In contrast, planar cell mobility decreases as the number of cells increases in the population until contact inhibition occurs, thereby resulting in apico-basal polarity formation [108]. It is already known that the Hippo pathway participates in these processes. In polarized epithelial cells, the Hippo pathway is involved with the maturation of tight junctions and adherens junctions, as well as the planar cell polarity pathway,

mechanotransduction pathway, and growth factor signaling [82]. YAP (yes-associated protein) is a regulator of cell size [109]. This report revealed that a signal from widely spread cells induced the activation of transcription factors following the nuclear localization of YAP, whereas a signal from narrowly spread cells induced the inhibition of transcription factors following the degradation of YAP outside the nucleus [110]. Moreover, ARHGAP18, a Rho GTPase-activating protein, regulates the cortical actin network through the YAP signaling cascade [111]. A recent study has indicated that in endometrial carcinoma, the nuclear localization of YAP is involved in increased malignancy [112]. MYPT1 is known to activate Merlin [68,79]. The localization of MYPT1 was sensitive to changes in cell density [83]. Therefore, in endometrial cancer cells, the activity of Merlin might be altered by changes in cell density. It is necessary to identify the molecules involved in the crosstalk between the mechanism that regulates the cell size based on YAP expression and the mechanism that regulates the tight junction integrity based on the cellular tension.

13. Conclusions

During endometrial cancer progression, a decreased expression of LSR and increased expression of CLDN-1 have been observed. In primary cultured normal human endometrial cells, leptin reduced the expression of LSR. Obesity is one of the risk factors for endometrial cancer. These findings demonstrated that disruption of epithelial barrier integrity due to translocation of LSR was related to the mechanism of malignant transformation of endometrial cancer. These mechanisms were closely related to the Hippo pathway and also involved the reconstitution of extracellular matrix components. Furthermore, changes in cellular tension were associated with changes in LSR localization. The Hippo pathway has also been reported to be involved in the regulation of cellular tension. The cellular tension influences the translocation of LSR from bicellular junctions to tricellular contacts. On the contrary, the mechanism that causes the disruption of the robust epithelial barrier is poorly understood in endometrial cancer cells. In order to elucidate functional changes in the epithelial barrier during the malignant transformation of normal endometrial cells, it is required to accurately analyze the molecular mechanisms that regulate the localization of tricellular tight junction proteins.

Funding: This research was funded by JSPS KAKENHI Grant Number JP19K05736.

Acknowledgments: This work was supported by the Ministry of Education, Culture, Sports, Science, and Technology of Japan.

Conflicts of Interest: The authors declare no conflicts of interest.

Abbreviations

CLDNs	claudins
EMT	epithelial-mesenchymal transition
HCC	hepatocellular carcinoma
HNSCC	head and neck squamous cell carcinoma
iCCC	intrahepatic cholangiocarcinoma
LSR	lipolysis-stimulated lipoprotein receptor
MLCK	myosin light chain kinase
MYPT1	myosin phosphatase target subunit 1
MRLC2	myosin regulatory light chain 2
OCLN	occludin
OSC	oral squamous cell carcinoma
TER	transepithelial electrical resistance

References

1. Garcia, M.A.; Nelson, W.J.; Chavez, N. Cell-cell junctions organize structural and signaling networks. *Cold Spring Harb. Perspect. Biol.* **2018**, *10*, a029181. [CrossRef] [PubMed]

2. Furuse, M.; Izumi, Y.; Oda, Y.; Higashi, T.; Iwamoto, N. Molecular organization of tricellular tight junctions. *Tissue Barriers* **2014**, *2*, e28960. [CrossRef] [PubMed]
3. Tsukita, S.; Yamazaki, Y.; Katsuno, T.; Tamura, A.; Tsukita, S. Tight junction-based epithelial microenvironment and cell proliferation. *Oncogene* **2008**, *27*, 6930–6938. [CrossRef] [PubMed]
4. Zihni, C.; Mills, C.; Matter, K.; Balda, M.S. Tight junctions: From simple barriers to multifunctional molecular gates. *Nat. Rev. Mol. Cell Biol.* **2016**, *17*, 564–580. [CrossRef] [PubMed]
5. Förster, C. Tight junctions and the modulation of barrier function in disease. *Histochem. Cell Biol.* **2008**, *130*, 55–70. [CrossRef] [PubMed]
6. Someya, M.; Kojima, T.; Ogawa, M.; Ninomiya, T.; Nomura, K.; Takasawa, A.; Murata, M.; Tanaka, S.; Saito, T.; Sawada, N. Regulation of tight junctions by sex hormones in normal human endometrial epithelial cells and uterus cancer cell line Sawano. *Cell Tissue Res.* **2013**, *354*, 481–494. [CrossRef] [PubMed]
7. Furuse, M.; Oda, Y.; Higashi, T.; Iwamoto, N.; Masuda, S. Lipolysis-stimulated lipoprotein receptor: A novel membrane protein of tricellular tight junctions. *Ann. N. Y. Acad. Sci.* **2012**, *1257*, 54–58. [CrossRef]
8. Shimada, H.; Satohisa, S.; Kohno, T.; Takahashi, S.; Hatakeyama, T.; Konno, T.; Tsujiwaki, M.; Saito, T.; Kojima, T. The roles of tricellular tight junction protein lipolysis-stimulated lipoprotein receptor in malignancy of human endometrial cancer cells. *Oncotarget* **2016**, *7*, 27735–27752. [CrossRef]
9. Bilyk, O.; Coatham, M.; Jewer, M.; Postovit, L.M. Epithelial-to-Mesenchymal Transition in the female reproductive tract: From normal functioning to disease pathology. *Front. Oncol.* **2017**, *7*, 1–21. [CrossRef]
10. Sherr, C.J. Principles of tumor suppression. *Cell* **2004**, *116*, 235–246. [CrossRef]
11. Heerboth, S.; Housman, G.; Leary, M.; Longacre, M.; Byler, S.; Lapinska, K.; Willbanks, A.; Sarkar, S. EMT and tumor metastasis. *Clin. Transl. Med.* **2015**, *4*. [CrossRef]
12. Martin, T.A.; Jiang, W.G. Loss of tight junction barrier function and its role in cancer metastasis. *Biochim. Biophys. Acta Biomembr.* **2009**, *1788*, 872–891. [CrossRef]
13. Martin, T.A. The role of tight junctions in cancer metastasis. *Semin. Cell Dev. Biol.* **2014**, *36*, 224–231. [CrossRef]
14. Leech, A.O.; Cruz, R.G.B.; Hill, A.D.K.; Hopkins, A.M. Paradigms lost—An emerging role for over-expression of tight junction adhesion proteins in cancer pathogenesis. *Ann. Transl. Med.* **2015**, *3*, 1–15.
15. Kondoh, A.; Takano, K.I.; Kojima, T.; Ohkuni, T.; Kamekura, R.; Ogasawara, N.; Go, M.; Sawada, N.; Himi, T. Altered expression of claudin-1, claudin-7, and tricellulin regardless of human papilloma virus infection in human tonsillar squamous cell carcinoma. *Acta Otolaryngol.* **2011**, *131*, 861–868. [CrossRef]
16. Patonai, A.; Erdélyi-Belle, B.; Korompay, A.; Somorácz, A.; Straub, B.K.; Schirmacher, P.; Kovalszky, I.; Lotz, G.; Kiss, A.; Schaff, Z. Claudins and tricellulin in fibrolamellar hepatocellular carcinoma. *Virchows Arch.* **2011**, *458*, 679–688. [CrossRef]
17. Somorácz, A.; Korompay, A.; Törzsök, P.; Patonai, A.; Erdélyi-Belle, B.; Lotz, G.; Schaff, Z.; Kiss, A. Tricellulin expression and its prognostic significance in primary liver carcinomas. *Pathol. Oncol. Res.* **2014**, *20*, 755–764. [CrossRef]
18. Korompay, A.; Borka, K.; Lotz, G.; Somorácz, A.; Törzsök, P.; Erdélyi-Belle, B.; Kenessey, I.; Baranyai, Z.; Zsoldos, F.; Kupcsulik, P.; et al. Tricellulin expression in normal and neoplastic human pancreas. *Histopathology* **2012**, *60*, E76–E86. [CrossRef]
19. Masuda, R.; Semba, S.; Mizuuchi, E.; Yanagihara, K.; Yokozaki, H. Negative regulation of the tight junction protein tricellulin by snail-induced epithelial-mesenchymal transition in gastric carcinoma cells. *Pathobiology* **2010**, *77*, 106–113. [CrossRef]
20. Reaves, D.K.; Fagan-Solis, K.D.; Dunphy, K.; Oliver, S.D.; Scott, D.W.; Fleming, J.M. The role of lipolysis stimulated lipoprotein receptor in breast cancer and directing breast cancer cell behavior. *PLoS ONE* **2014**, *9*, e91747. [CrossRef]
21. García, J.M.; Peña, C.; García, V.; Domínguez, G.; Muñoz, C.; Silva, J.; Millán, I.; Diaz, R.; Lorenzo, Y.; Rodriguez, R.; et al. Prognostic value of LISCH7 mRNA in plasma and tumor of colon cancer patients. *Clin. Cancer Res.* **2007**, *13*, 6351–6358. [CrossRef]
22. Takano, K.; Kakuki, T.; Obata, K.; Nomura, K.; Miyata, R.; Kondo, A.; Kurose, M.; Kakiuchi, A.; Kaneko, Y.; Kohno, T.; et al. The behavior and role of lipolysis-stimulated lipoprotein receptor, a component of tricellular tight junctions, in head and neck squamous cell carcinomas. *Anticancer Res.* **2016**, *36*, 5895–5904. [CrossRef]

23. Sappayatosok, K.; Phattarataratip, E. Overexpression of claudin-1 is associated with advanced clinical stage and invasive pathologic characteristics of oral squamous cell carcinoma. *Head Neck Pathol.* **2015**, *9*, 173–180. [CrossRef]
24. Li, W.; Dong, Q.; Li, L.; Zhang, Z.; Cai, X.; Pan, X. Prognostic significance of claudin-1 and cyclin B1 protein expression in patients with hypopharyngeal squamous cell carcinoma. *Oncol. Lett.* **2016**, *11*, 2995–3002. [CrossRef]
25. Grund, S.; Grümmer, R. Direct cell-cell interactions in the endometrium and in endometrial pathophysiology. *Int. J. Mol. Sci.* **2018**, *19*, 2227. [CrossRef]
26. Pan, X.Y.; Wang, B.; Che, Y.C.; Weng, Z.P.; Dai, H.Y.; Peng, W. Expression of claudin-3 and claudin-4 in normal, hyperplastic, and malignant endometrial tissue. *Int. J. Gynecol. Cancer* **2007**, *17*, 233–241. [CrossRef]
27. Konecny, G.E.; Agarwal, R.; Keeney, G.A.; Winterhoff, B.; Jones, M.B.; Mariani, A.; Riehle, D.; Neuper, C.; Dowdy, S.C.; Wang, H.J.; et al. Claudin-3 and claudin-4 expression in serous papillary, clear-cell, and endometrioid endometrial cancer. *Gynecol. Oncol.* **2008**, *109*, 263–269. [CrossRef]
28. Lortet-Tieulent, J.; Ferlay, J.; Bray, F.; Jemal, A. International patterns and trends in endometrial cancer incidence, 1978–2013. *J. Natl. Cancer Inst.* **2018**, *110*, 354–361. [CrossRef]
29. Hopkins, B.D.; Goncalves, M.D.; Cantley, L.C. Obesity and cancer mechanisms: Cancer metabolism. *J. Clin. Oncol.* **2016**, *34*, 4277–4283. [CrossRef]
30. Byrne, F.L.; Poon, I.K.H.; Modesitt, S.C.; Tomsig, J.L.; Chow, J.D.Y.; Healy, M.E.; Baker, W.D.; Atkins, K.A.; Lancaster, J.M.; Marchion, D.C.; et al. Metabolic vulnerabilities in endometrial cancer. *Cancer Res.* **2014**, *74*, 5832–5845. [CrossRef]
31. Gelsomino, L.; Naimo, G.D.; Catalano, S.; Mauro, L.; Andò, S. The emerging role of adiponectin in female malignancies. *Int. J. Mol. Sci.* **2019**, *20*, 2127. [CrossRef]
32. Stern, J.H.; Rutkowski, J.M.; Scherer, P.E. Adiponectin, leptin, and fatty acids in the maintenance of metabolic homeostasis through adipose tissue crosstalk. *Cell Metab.* **2016**, *23*, 770–784. [CrossRef]
33. Ashizawa, N.; Yahata, T.; Quan, J.; Adachi, S.; Yoshihara, K.; Tanaka, K. Serum leptin-adiponectin ratio and endometrial cancer risk in postmenopausal female subjects. *Gynecol. Oncol.* **2010**, *119*, 65–69. [CrossRef]
34. Gong, T.T.; Wu, Q.J.; Wang, Y.L.; Ma, X.X. Circulating adiponectin, leptin and adiponectin-leptin ratio and endometrial cancer risk: Evidence from a meta-analysis of epidemiologic studies. *Int. J. Cancer* **2015**, *137*, 1967–1978. [CrossRef]
35. Dupont, J.Ë.; Reverchon, M.; Cloix, L.; Froment, P.; Ramé, C. Involvement of adipokines, AMPK, PI3K and the PPAR signaling pathways in ovarian follicle development and cancer. *Int. J. Dev. Biol.* **2012**, *56*, 959–967. [CrossRef]
36. Pérez-Pérez, A.; Toro, A.; Vilariño-García, T.; Maymó, J.; Guadix, P.; Dueñas, J.L.; Fernández-Sánchez, M.; Varone, C.; Sánchez-Margalet, V. Leptin action in normal and pathological pregnancies. *J. Cell. Mol. Med.* **2018**, *22*, 716–727. [CrossRef]
37. Fan, Y.; Gan, Y.; Shen, Y.; Cai, X.; Song, Y.; Zhao, F.; Yao, M.; Gu, J.; Tu, H. Leptin signaling enhances cell invasion and promotes the metastasis of human pancreatic cancer via increasing MMP-13 production. *Oncotarget* **2015**, *6*, 16120–16134. [CrossRef]
38. Ahn, J.H.; Choi, Y.S.; Choi, J.H. Leptin promotes human endometriotic cell migration and invasion by up-regulating MMP-2 through the JAK2/STAT3 signaling pathway. *Mol. Hum. Reprod.* **2015**, *21*, 792–802. [CrossRef]
39. Handy, J.A.; Fu, P.P.; Kumar, P.; Mells, J.E.; Sharma, S.; Saxena, N.K.; Anania, F.A. Adiponectin inhibits leptin signalling via multiple mechanisms to exert protective effects against hepatic fibrosis. *Biochem. J.* **2011**, *440*, 385–395. [CrossRef]
40. Stenger, C.; Hanse, M.; Pratte, D.; Mbala, M.L.; Akbar, S.; Koziel, V.; Escanyé, M.C.; Kriem, B.; Malaplate-Armand, C.; Olivier, J.L.; et al. Up-regulation of hepatic lipolysis stimulated lipoprotein receptor by leptin: A potential lever for controlling lipid clearance during the postprandial phase. *FASEB J.* **2010**, *24*, 4218–4228. [CrossRef]
41. Yen, F.T.; Roitel, O.; Bonnard, L.; Notet, V.; Pratte, D.; Stenger, C.; Magueur, E.; Bihain, B.E. Lipolysis stimulated lipoprotein receptor: A novel molecular link between hyperlipidemia, weight gain, and atherosclerosis in mice. *J. Biol. Chem.* **2008**, *283*, 25650–25659. [CrossRef]
42. Parida, S.; Siddharth, S.; Sharma, D. Adiponectin, obesity, and cancer: Clash of the bigwigs in health and disease. *Int. J. Mol. Sci.* **2019**, *20*, 2519. [CrossRef]

43. Lee, T.Y.; Martinez-Outschoorn, U.E.; Schilder, R.J.; Kim, C.H.; Richard, S.D.; Rosenblum, N.G.; Johnson, J.M. Metformin as a therapeutic target in endometrial cancers. *Front. Oncol.* **2018**, *8*, 341. [CrossRef]
44. Wang, H.; Zhu, C.; Ying, Y.; Luo, L.; Huang, D.; Luo, Z. Metformin and berberine, two versatile drugs in treatment of common metabolic diseases. *Oncotarget* **2018**, *9*, 10135–10146. [CrossRef]
45. Umene, K.; Banno, K.; Kisu, I.; Yanokura, M.; Nogami, Y.; Tsuji, K.; Masuda, K.; Ueki, A.; Kobayashi, Y.; Yamagami, W.; et al. New candidate therapeutic agents for endometrial cancer: Potential for clinical practice (Review). *Oncol. Rep.* **2013**, *29*, 855–860. [CrossRef]
46. Mo, J.S.; Meng, Z.; Kim, Y.C.; Park, H.W.; Hansen, C.G.; Kim, S.; Lim, D.S.; Guan, K.L. Cellular energy stress induces AMPK-mediated regulation of YAP and the Hippo pathway. *Nat. Cell Biol.* **2015**, *17*, 500–510. [CrossRef]
47. Wang, W.; Xiao, Z.D.; Li, X.; Aziz, K.E.; Gan, B.; Johnson, R.L.; Chen, J. AMPK modulates Hippo pathway activity to regulate energy homeostasis. *Nat. Cell Biol.* **2015**, *17*, 490–499. [CrossRef]
48. Canfield, P.E.; Geerdes, A.M.; Molitoris, B.A. Effect of reversible ATP depletion on tight-junction integrity in LLC-PK1 cells. *Am. J. Physiol. Physiol.* **2017**, *261*, F1038–F1045. [CrossRef]
49. Zhang, L.; Li, J.; Young, L.H.; Caplan, M.J. AMP-activated protein kinase regulates the assembly of epithelial tight junctions. *Proc. Natl. Acad. Sci. USA* **2006**, *103*, 17272–17277. [CrossRef]
50. Aznar, N.; Patel, A.; Rohena, C.C.; Dunkel, Y.; Joosen, L.P.; Taupin, V.; Kufareva, I.; Farquhar, M.G.; Ghosh, P. AMP-activated protein kinase fortifies epithelial tight junctions during energetic stress via its effector GIV/Girdin. *eLife* **2016**, *5*, 1–33. [CrossRef]
51. Shackelford, D.B.; Shaw, R.J. The LKB1-AMPK pathway: Metabolism and growth control in tumour suppression. *Nat. Rev. Cancer* **2009**, *9*, 563–575. [CrossRef]
52. Zou, J.; Hong, L.; Luo, C.; Li, Z.; Zhu, Y.; Huang, T.; Zhang, Y.; Yuan, H.; Hu, Y.; Wen, T.; et al. Metformin inhibits estrogen-dependent endometrial cancer cell growth by activating the AMPK–FOXO1 signal pathway. *Cancer Sci.* **2016**, *107*, 1806–1817. [CrossRef]
53. Wang, H.B.; Wang, P.Y.; Wang, X.; Wan, Y.L.; Liu, Y.C. Butyrate enhances intestinal epithelial barrier function via up-regulation of tight junction protein claudin-1 transcription. *Dig. Dis. Sci.* **2012**, *57*, 3126–3135. [CrossRef]
54. Dufresne, J.; Cyr, D.G. Activation of an SP binding site is crucial for the expression of claudin 1 in rat epididymal principal cells. *Biol. Reprod.* **2007**, *76*, 825–832. [CrossRef]
55. Honda, H.; Pazin, M.J.; Ji, H.; Wernyj, R.P.; Morin, P.J. Crucial roles of Sp1 and epigenetic modifications in the regulation of the cldn4 promoter in ovarian cancer cells. *J. Biol. Chem.* **2006**, *281*, 21433–21444. [CrossRef]
56. Luk, J.M.; Tong, M.K.; Mok, B.W.; Tam, P.C.; Yeung, W.S.B.; Lee, K.F. Sp1 site is crucial for the mouse claudin-19 gene expression in the kidney cells. *FEBS Lett.* **2004**, *578*, 251–256. [CrossRef]
57. Shimada, H.; Satohisa, S.; Kohno, T.; Konno, T.; Arimoto, C.; Saito, T.; Kojima, T. Downregulation of lipolysis-stimulated lipoprotein receptor promotes cell invasion via claudin-1-mediated matrix metalloproteinases in human endometrial cancer. *Oncol. Lett.* **2017**, *16*, 6776–6782. [CrossRef]
58. Oku, N.; Sasabe, E.; Ueta, E.; Yamamoto, T.; Osaki, T. Tight junction protein claudin-1 enhances the invasive activity of oral squamous cell carcinoma cells by promoting cleavage of laminin-5 γ2 chain via matrix metalloproteinase (MMP)-2 and membrane-type MMP-1. *Cancer Res.* **2006**, *66*, 5251–5257. [CrossRef]
59. Van Itallie, C.M.; Fanning, A.S.; Anderson, J.M.; Boireau, S.; Samuel, M.S.; Pannequin, J.; Ryan, J.L.; Choquet, A.; Chapuis, H.; Rebillard, X.; et al. Claudin-1 regulates cellular transformation and metastatic behavior in colon cancer. *J. Clin. Investig.* **2005**, *115*, 1765–1776.
60. Castro-Castro, A.; Marchesin, V.; Monteiro, P.; Lodillinsky, C.; Rossé, C.; Chavrier, P. Cellular and molecular mechanisms of MT1-MMP-dependent cancer cell invasion. *Annu. Rev. Cell Dev. Biol.* **2016**, *32*, 555–576. [CrossRef]
61. Brown, G.T.; Murray, G.I. Current mechanistic insights into the roles of matrix metalloproteinases in tumour invasion and metastasis. *J. Pathol.* **2015**, *237*, 273–281. [CrossRef]
62. Itoh, Y.; Seiki, M. MT1-MMP: A potent modifier of pericellular microenvironment. *J. Cell. Physiol.* **2006**, *206*, 1–8. [CrossRef]
63. Harvey, K.F.; Zhang, X.; Thomas, D.M. The Hippo pathway and human cancer. *Nat. Rev. Cancer* **2013**, *13*, 246–257. [CrossRef]

64. Bao, Y.; Nakagawa, K.; Yang, Z.; Ikeda, M.; Withanage, K.; Ishigami-Yuasa, M.; Okuno, Y.; Hata, S.; Nishina, H.; Hata, Y. A cell-based assay to screen stimulators of the Hippo pathway reveals the inhibitory effect of dobutamine on the YAP-dependent gene transcription. *J. Biochem.* **2011**, *150*, 199–208. [CrossRef]
65. Zheng, H.X.; Wu, L.N.; Xiao, H.; Du, Q.; Liang, J.F. Inhibitory effects of dobutamine on human gastric adenocarcinoma. *World J. Gastroenterol.* **2014**, *20*, 17092–17099. [CrossRef]
66. Hardie, D.G. AMP-activated protein kinase-an energy sensor that regulates all aspects of cell function. *Genes Dev.* **2011**, *25*, 1895–1908. [CrossRef]
67. Shimada, H.; Abe, S.; Kohno, T.; Satohisa, S.; Konno, T.; Takahashi, S.; Hatakeyama, T.; Arimoto, C.; Kakuki, T.; Kaneko, Y.; et al. Loss of tricellular tight junction protein LSR promotes cell invasion and migration via upregulation of TEAD1/AREG in human endometrial cancer. *Sci. Rep.* **2017**, *7*, 37049. [CrossRef]
68. Cooper, J.; Giancotti, F.G. Molecular insights into NF2/Merlin tumor suppressor function. *FEBS Lett.* **2014**, *588*, 2743–2752. [CrossRef]
69. Gladden, A.B.; Hebert, A.M.; Schneeberger, E.E.; McClatchey, A.I. The NF2 tumor suppressor, Merlin, regulates epidermal development through the establishment of a junctional polarity complex. *Dev. Cell* **2010**, *19*, 727–739. [CrossRef]
70. Zhao, B.; Li, L.; Lu, Q.; Wang, L.H.; Liu, C.Y.; Lei, Q.; Guan, K.L. Angiomotin is a novel Hippo pathway component that inhibits YAP oncoprotein. *Genes Dev.* **2011**, *25*, 51–63. [CrossRef]
71. Huang, T.; Zhou, Y.; Zhang, J.; Cheng, A.S.L.; Yu, J.; To, K.F.; Kang, W. The physiological role of Motin family and its dysregulation in tumorigenesis. *J. Transl. Med.* **2018**, *16*, 98. [CrossRef]
72. Ortiz, A.; Lee, Y.C.; Yu, G.; Liu, H.C.; Lin, S.C.; Bilen, M.A.; Cho, H.; Yu-Lee, L.Y.; Lin, S.H. Angiomotin is a novel component of cadherin-11/β-catenin/p120 complex and is critical for cadherin-11-mediated cell migration. *FASEB J.* **2015**, *29*, 1080–1091. [CrossRef]
73. Hakami, F.; Darda, L.; Stafford, P.; Woll, P.; Lambert, D.W.; Hunter, K.D. The roles of HOXD10 in the development and progression of head and neck squamous cell carcinoma (HNSCC). *Br. J. Cancer* **2014**, *111*, 807–816. [CrossRef]
74. Levchenko, T.; Bratt, A.; Arbiser, J.L.; Holmgren, L. Angiomotin expression promotes hemangioendothelioma invasion. *Oncogene* **2004**, *23*, 1469–1473. [CrossRef]
75. Couderc, C.; Boin, A.; Fuhrmann, L.; Vincent-Salomon, A.; Mandati, V.; Kieffer, Y.; Mechta-Grigoriou, F.; Del Maestro, L.; Chavrier, P.; Vallerand, D.; et al. AMOTL1 promotes breast cancer progression and is antagonized by Merlin. *Neoplasia* **2016**, *18*, 10–24. [CrossRef]
76. Wan, H.Y.; Li, Q.Q.; Zhang, Y.; Tian, W.; Li, Y.N.; Liu, M.; Li, X.; Tang, H. MiR-124 represses vasculogenic mimicry and cell motility by targeting AmotL1 in cervical cancer cells. *Cancer Lett.* **2014**, *355*, 148–158. [CrossRef]
77. Mojallal, M.; Zheng, Y.; Hultin, S.; Audebert, S.; van Harn, T.; Johnsson, P.; Lenander, C.; Fritz, N.; Mieth, C.; Corcoran, M.; et al. AmotL2 disrupts apical–basal cell polarity and promotes tumour invasion. *Nat. Commun.* **2014**, *5*, 4557. [CrossRef]
78. Artinian, N.; Cloninger, C.; Holmes, B.; Benavides-Serrato, A.; Bashir, T.; Gera, J. Phosphorylation of the Hippo pathway component AMOTL2 by the mTORC2 kinase promotes YAP signaling, resulting in enhanced glioblastoma growth and invasiveness. *J. Biol. Chem.* **2015**, *290*, 19387–19401. [CrossRef]
79. Li, W.; Cooper, J.; Karajannis, M.A.; Giancotti, F.G. Merlin: A tumour suppressor with functions at the cell cortex and in the nucleus. *EMBO Rep.* **2012**, *13*, 204–215. [CrossRef]
80. Yi, C.; Troutman, S.; Fera, D.; Stemmer-Rachamimov, A.; Avila, J.L.; Christian, N.; Persson, N.L.; Shimono, A.; Speicher, D.W.; Marmorstein, R.; et al. A tight junction-associated Merlin-Angiomotin complex mediates Merlin's regulation of mitogenic signaling and tumor suppressive functions. *Cancer Cell* **2011**, *19*, 527–540. [CrossRef]
81. Leontieva, O.V.; Demidenko, Z.N.; Blagosklonny, M. V Contact inhibition and high cell density deactivate the mammalian target of rapamycin pathway, thus suppressing the senescence program. *Proc. Natl. Acad. Sci. USA* **2014**, *111*, 8832–8837. [CrossRef]
82. Gumbiner, B.M.; Kim, N.-G. The Hippo-YAP signaling pathway and contact inhibition of growth. *J. Cell Sci.* **2014**, *127*, 709–717. [CrossRef]
83. Kohno, T.; Kikuchi, S.; Ninomiya, T.; Kojima, T. The bicellular tensile force sorts the localization of LSRs in bicellular and tricellular junctions. *Ann. N. Y. Acad. Sci.* **2017**, *1397*, 185–194. [CrossRef]

84. Levayer, R.; Lecuit, T. Biomechanical regulation of contractility: Spatial control and dynamics. *Trends Cell Biol.* **2012**, *22*, 61–81. [CrossRef]
85. Gutzman, J.H.; Sive, H. Epithelial relaxation mediated by the myosin phosphatase regulator Mypt1 is required for brain ventricle lumen expansion and hindbrain morphogenesis. *Development* **2010**, *137*, 795–804. [CrossRef]
86. Mui, K.L.; Chen, C.S.; Assoian, R.K. The mechanical regulation of integrin-cadherin crosstalk organizes cells, signaling and forces. *J. Cell Sci.* **2016**, *129*, 1093–1100. [CrossRef]
87. Parsons, J.T.; Horwitz, A.R.; Schwartz, M.A. Cell adhesion: Integrating cytoskeletal dynamics and cellular tension. *Nat. Rev. Mol. Cell Biol.* **2010**, *11*, 633–643. [CrossRef]
88. Vicente-Manzanares, M.; Ma, X.; Adelstein, R.S.; Horwitz, A.R. Non-muscle myosin II takes centre stage in cell adhesion and migration. *Nat. Rev. Cell Biol.* **2009**, *10*, 778–790. [CrossRef]
89. Amano, M.; Nakayama, M.; Kaibuchi, K. Rho-kinase/ROCK: A key regulator of the cytoskeleton and cell polarity. *Cytoskeleton* **2010**, *67*, 545–554. [CrossRef]
90. Ma, Y.; Semba, S.; Khan, R.I.; Bochimoto, H.; Watanabe, T.; Fujiya, M.; Kohgo, Y.; Liu, Y.; Taniguchi, T. Focal adhesion kinase regulates intestinal epithelial barrier function via redistribution of tight junction. *Biochim. Biophys. Acta* **2013**, *1832*, 151–159. [CrossRef]
91. Siu, E.R.; Wong, E.W.P.; Mruk, D.D.; Porto, C.S.; Cheng, C.Y. Focal adhesion kinase is a blood-testis barrier regulator. *Proc. Natl. Acad. Sci. USA* **2009**, *106*, 9298–9303. [CrossRef]
92. Oda, Y.; Otani, T.; Ikenouchi, J.; Furuse, M. Tricellulin regulates junctional tension of epithelial cells at tricellular contacts via Cdc42. *J. Cell Sci.* **2014**, *127*, 4201–4212. [CrossRef]
93. Riento, K.; Ridley, A.J. ROCKs: Multifunctional kinases in cell behaviour. *Nat. Rev. Mol. Cell Biol.* **2003**, *4*, 446–456. [CrossRef]
94. Kale, V.P.; Hengst, J.A.; Desai, D.H.; Dick, T.E.; Choe, K.N.; Colledge, A.L.; Takahashi, Y.; Sung, S.; Amin, S.G.; Yun, J.K. A novel selective multikinase inhibitor of ROCK and MRCK effectively blocks cancer cell migration and invasion. *Cancer Lett.* **2014**, *354*, 299–310. [CrossRef]
95. Ito, M.; Nakano, T.; Erdodi, F.; Hartshorne, D.J. Myosin phosphatase: Structure, regulation and function. *Mol. Cell. Biochem.* **2004**, *259*, 197–209. [CrossRef]
96. Masuda, S.; Oda, Y.; Sasaki, H.; Ikenouchi, J.; Higashi, T.; Akashi, M.; Nishi, E.; Furuse, M. LSR defines cell corners for tricellular tight junction formation in epithelial cells. *J. Cell Sci.* **2011**, *124*, 548–555. [CrossRef]
97. Nakatsu, D.; Kano, F.; Taguchi, Y.; Sugawara, T.; Nishizono, T.; Nishikawa, K.; Oda, Y.; Furuse, M.; Murata, M. JNK1/2-dependent phosphorylation of angulin-1/LSR is required for the exclusive localization of angulin-1/LSR and tricellulin at tricellular contacts in EpH4 epithelial sheet. *Genes Cells* **2014**, *19*, 565–581. [CrossRef]
98. Takai, Y.; Nakanishi, H. Nectin and afadin: Novel organizers of intercellular junctions. *J. Cell Sci.* **2003**, *116*, 17–27. [CrossRef]
99. Zhang, J.; Betson, M.; Erasmus, J.; Zeikos, K.; Bailly, M.; Cramer, L.P.; Braga, V.M.M. Actin at cell-cell junctions is composed of two dynamic and functional populations. *J. Cell Sci.* **2005**, *118*, 5549–5562. [CrossRef]
100. Chu, C.W.; Gerstenzang, E.; Ossipova, O.; Sokol, S.Y. Lulu regulates shroom-induced apical constriction during neural tube closure. *PLoS ONE* **2013**, *8*, e81854. [CrossRef]
101. Nishimura, T.; Takeichi, M. Shroom3-mediated recruitment of Rho kinases to the apical cell junctions regulates epithelial and neuroepithelial planar remodeling. *Development* **2008**, *135*, 1493–1502. [CrossRef]
102. Rodriguez-Boulan, E.; Macara, I.G. Organization and execution of the epithelial polarity programme. *Nat. Rev. Mol. Cell Biol.* **2014**, *15*, 225–242. [CrossRef]
103. Toya, M.; Kobayashi, S.; Kawasaki, M.; Shioi, G.; Kaneko, M.; Ishiuchi, T.; Misaki, K.; Meng, W.; Takeichi, M. CAMSAP3 orients the apical-to-basal polarity of microtubule arrays in epithelial cells. *Proc. Natl. Acad. Sci. USA* **2015**, *113*, 1–6. [CrossRef]
104. Bazellières, E.; Massey-Harroche, D.; Barthélémy-Requin, M.; Richard, F.; Arsanto, J.P.; Le Bivic, A. Apico-basal elongation requires a drebrin-E-EB3 complex in columnar human epithelial cells. *J. Cell Sci.* **2012**, *125*, 919–931. [CrossRef]
105. Butkevich, E.; Hülsmann, S.; Wenzel, D.; Shirao, T.; Duden, R.; Majoul, I. Drebrin is a novel connexin-43 binding partner that links gap junctions to the submembrane cytoskeleton. *Curr. Biol.* **2004**, *14*, 650–658. [CrossRef]

106. Guillemot, L.; Paschoud, S.; Pulimeno, P.; Foglia, A.; Citi, S. The cytoplasmic plaque of tight junctions: A scaffolding and signalling center. *Biochim. Biophys. Acta Biomembr.* **2008**, *1778*, 601–613. [CrossRef]
107. Miyake, Y.; Inoue, N.; Nishimura, K.; Kinoshita, N.; Hosoya, H.; Yonemura, S. Actomyosin tension is required for correct recruitment of adherens junction components and zonula occludens formation. *Exp. Cell Res.* **2006**, *312*, 1637–1650. [CrossRef]
108. Iden, S.; Collard, J.G. Crosstalk between small GTPases and polarity proteins in cell polarization. *Nat. Rev. Mol. Cell Biol.* **2008**, *9*, 846–859. [CrossRef]
109. Halder, G.; Dupont, S.; Piccolo, S. Transduction of mechanical and cytoskeletal cues by YAP and TAZ. *Nat. Rev. Mol. Cell Biol.* **2012**, *13*, 591–600. [CrossRef]
110. Dupont, S.; Morsut, L.; Aragona, M.; Enzo, E.; Giulitti, S.; Cordenonsi, M.; Zanconato, F.; Le Digabel, J.; Forcato, M.; Bicciato, S.; et al. Role of YAP/TAZ in mechanotransduction. *Nature* **2011**, *474*, 179–183. [CrossRef]
111. Porazinski, S.; Wang, H.; Asaoka, Y.; Behrndt, M.; Miyamoto, T.; Morita, H.; Hata, S.; Sasaki, T.; Krens, S.F.G.; Osada, Y.; et al. YAP is essential for tissue tension to ensure vertebrate 3D body shape. *Nature* **2015**, *521*, 217–221. [CrossRef]
112. Tsujiura, M.; Mazack, V.; Sudol, M.; Kaspar, H.G.; Nash, J.; Carey, D.J.; Gogoi, R. Yes-Associated Protein (YAP) modulates oncogenic features and radiation sensitivity in endometrial cancer. *PLoS ONE* **2014**, *9*, e100974. [CrossRef]

International Journal of
Molecular Sciences

MDPI

Review

Mouse Models of Human Claudin-Associated Disorders: Benefits and Limitations

Murat Seker [1], Cármen Fernández-Rodríguez [2], Luis Alfonso Martínez-Cruz [2] and Dominik Müller [1,*]

[1] Department of Pediatric Gastroenterology, Nephrology and Metabolism, Charité—Universitätsmedizin Berlin, Charité, 13353 Berlin, Germany; murat.seker@charite.de
[2] ClC BioGUNE, Bizkaia Science and Technology Park, 801A, 48160 Derio, Spain; cfernandez@cicbiogune.es (C.F.-R.); amartinez@cicbiogune.es (L.A.M.-C.)
* Correspondence: dominik.mueller@charite.de

Received: 15 October 2019; Accepted: 2 November 2019; Published: 5 November 2019

Abstract: In higher organisms, epithelia separate compartments in order to guarantee their proper function. Such structures are able to seal but also to allow substances to pass. Within the paracellular pathway, a supramolecular structure, the tight junction transport is largely controlled by the temporospatial regulation of its major protein family called claudins. Besides the fact that the expression of claudins has been identified in different forms of human diseases like cancer, clearly defined mutations in the corresponding claudin genes have been shown to cause distinct human disorders. Such disorders comprise the skin and its adjacent structures, liver, kidney, the inner ear, and the eye. From the phenotype analysis, it has also become clear that different claudins can cause a complex phenotype when expressed in different organs. To gain deeper insights into the physiology and pathophysiology of claudin-associated disorders, several mouse models have been generated. In order to model human disorders in detail, they have been designed either as full knockouts, knock-downs or knock-ins by a variety of techniques. Here, we review human disorders caused by CLDN mutations and their corresponding mouse models that have been generated thus far and assess their usefulness as a model for the corresponding human disorder.

Keywords: tight junction; claudin; mutations; kidney; liver; skin; human; mice; disease

1. Introduction

In higher organisms epithelia, endothelia and mesothelia are essential to separate different compartments in order to guarantee their proper function. Such structures can be found ubiquitously, like in skin which separates the body from the surrounding environment, the lung (air/blood) and the intestine (gut lumen/blood). Further, epithelial structures form the blood-brain-barrier [1] and are also essential for liver and kidney function [2]. Epithelia consist of monolayer or multilayer structures [3] but a common prerequisite for their function is polarization, i.e., a clear orientation of apical to basolateral requiring a well-defined maintenance molecular machinery [4]. Moreover, besides providing a tight barrier (e.g., within the bladder), epithelial structures are able to regulate coordinated transport across cellular barriers. Transport across epithelial barriers is provided in general via two systems, the paracellular and the transcellular pathway. Whereas the first provides the organism with a maximum of resorptive capacity by minimal energy expenditure, the latter aims at fine-tuning depending on the actual needs of the organism, regulated also by a subset of various local, regional and global mechanisms [5].

In more detail, the transcellular pathway consists of apical uptake, intracellular buffering, transport and basolateral extrusion mechanisms. This pathway is highly energy dependent and mostly driven by the basolateral Na^+-K^+-ATPase. One of the advantages of such a pathway is its controllability

on several of the steps, e.g., by hormones (e.g., $1,25(OH)_2D_3$ or Parathyroid Hormone (PTH)) and therefore also aims at fine-tuning to provide the organism according to its actual needs and also on middle and long term regulation [6]. Especially for these pathways, it has been shown that mutations in human gene cause distinct monogenetic disorders, like Bartter's [7] and Gitelman's Syndrome [8] with a clear phenotype-genotype correlation. In order to study such genetic effects, mouse models have been generated to study successfully the consequences of human mutations [9–13].

Considering the paracellular pathway, enormous progress has been achieved during the last two decades as it became clear that this pathway, although basically driven by a given electrochemical gradient only, is regulated by several structures and mechanisms. In regions where concentration gradients of solutes across the epithelial layer are high, like the proximal tubule of the kidney, paracellular pathways provide the organism with maximal reabsorption by minimal energy expenditure. More distantly, crosstalk takes place before the transcellular pathway provides the major mechanism. A key component of the paracellular pathway is a supramolecular structure, called tight junction (TJ). The TJ consists of several membrane-bound proteins and their intracellular adapter and scaffolding proteins [14]. The major proteins essential for the TJ are claudins (lat. *claudere*, i.e., to seal). The family of claudins is currently included 27 members in eukaryotes. The claudin proteins are membrane-bound and span four times the plasma membrane with an intracellular C- and N-terminal part. Each of the four provides a functional entity, i.e., either to act as pore-forming or as a sealing component (for a detailed review: [15]). Classification of claudins has been made based on different factors such as sequence similarity and functionality. In this review, we used the latter one which was based on sealing or pore-forming capabilities of claudins reviewed by Krause et al. [16].

In 1999, the group of Lifton showed that the disorder *Familial Hypercalciuria, Hypomagnesemia with Nephroclacinosis (FHHNC*) is caused by mutations in the *CLDN16* gene. This observation provided the first evidence that TJ disorders cause human disorders and diseases [17]. Since then, several other TJ disorders have been shown to cause, when mutated, (*CLDN1, CLDN2 CLDN9 CLDN10, CLDN14, CLDN16, CLDN19*), human disorders [18–23]. Furthermore, expression of claudins are influenced by many factors (e.g., smoking, diet changes, alcohol intake) [24–26] and numerous associations of disordered claudin expression and disease have been described. (for detail reviews see [27,28]).

To model such disorders, genetically modified mice have been generated. Initially, embryonic stem cell technology was used to create such models [29] and later, other approaches have been established successfully [30]. Besides global deletions, regional and local variations of murine gene expression have been established. Although not reported yet, based on current developments, it can be expected that CRISPR/Cas9 technology will take place as a standard procedure [31].

However, even though such models provide insights into physiology and pathophysiology and may open new avenues for the development of therapeutical interventions, they face limitations. Here, we provide an overview of current human claudin-associated disorders and their corresponding mouse models, their impact on physiology and pathophysiology.

2. Claudin Mutations Causing Human Disorders

2.1. Claudin 1

CLDN1 consists of four exons encoding a 211 amino acid protein that conveys barrier properties [16]. It has been shown that claudin-1 interacts with claudin-3 and claudin-5, which are also barrier–forming claudins [32,33]. In the skin, *CLDN1* is expressed in the stratum corneum, stratum basale, stratum granulosum and stratum spinosum [34]. Further, it is expressed in the kidney [35], gall bladder [36], human ovarian epithelium [37] and the inner ear [38]. The expression of *CLDN1* is increased in colorectal cancer [39], lung carcinoma [40], cervical cancer [41] and reduced in larynx cancer [42]. Evans et al. showed that *CLDN1* is involved in Hepatitis C Virus entry into intestinal cells, which is presumably depending on the first extracellular loop (ECL, Figure 1) [43].

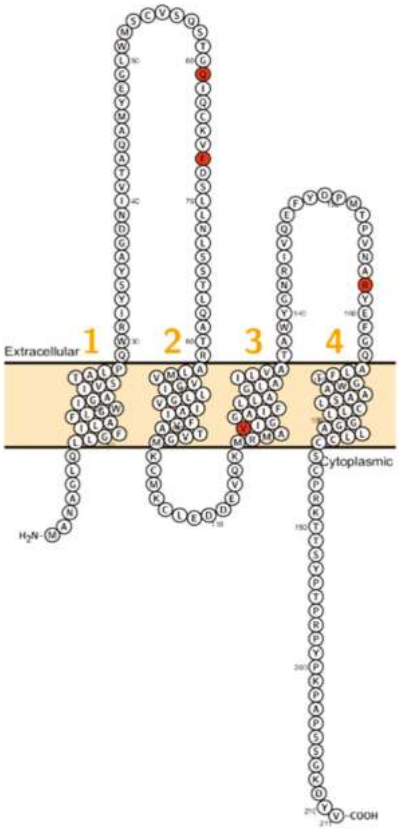

Figure 1. Topology of *CLDN1*. FASTA sequence of *CLDN1* (Uniprot accession no: O95832; plotted by Protter software http://wlab.ethz.ch/protter/). Each amino acid is shown as a single letter code and numbers (orange) indicate transmembrane domains. Mutations shown to be involved in human diseases are shown in red.

In 2002, Baala et al. described a family with autosomal dominant ichthyosis, alopecia, leucocytic vacuoles and sclerosing cholangitis (ILVASC; or neonatal ichthyosis with sclerosing cholangitis (NISCH-Syndrome OMIM 607626) assigned to chromosome 3q27–28 [44]. In 2004 Hadj-Rabia et al. identified in the same kindred a frameshift mutation in *CLDN1* leading to a premature stop codon at position 67 [18] (Figure 1). This finding, that ILVASC/NISCH syndrome is caused by mutations in *CLDN1* has been later confirmed by others [18,44–46]. In 2006, a neonate patient with erythroderma, massive lamellar desquamation and alopecia were reported. The hepatologic aspects were icterus, hyperbilirubinemia and increased biliary acids, liver biopsy showed panlobular cholestasis with acute hepatitis. All reported cases showed that *CLDN1* mutations in humans were not lethal and did not affect fertility.

Furuse and colleagues generated *Cldn1* deficient mice, which exhibited low body weight and died within the first day after birth, possibly attributable to an excessive trans-epithelial water loss (TEWL). *Cldn1* deficient mice displayed also altered lipid composition and defects of the stratum corneum of the skin. On the other hand, *CLDN1* deficient patients also displayed mild wrinkled skin and hyperproliferation of keratinocytes. However, only some patients had liver cell injury [18]. Whether knockout mice were affected by hepatic abnormalities has not been reported, probably due to the perinatal death.

Since the mouse model was limited because of its early lethality, a KD mouse approach was used, that showed reduced expression levels of *Cldn1* and *Cldn1* levels were associated with the severity of the phenotype [47]. *Cldn1* KD mice were born with wrinkled skin similar to KO mice, however, morphological examinations at 8 weeks of age revealed a normal development, which might be explained by the low but still expressed *Cldn1.* The underlying mechanism of TEWL was further investigated by Hirano et al. by using tamoxifen-induced epidermis-specific deletion of *Cldn1* in adult mice. Four days after induction, claudin-1 began depleting from basal layers and was undetectable in granular layers at day eight and tight junction leakage was observed. Neither TEWL nor stratum corneum defects were observed until day 18 suggesting that TJ deterioration is a prerequisite for stratum corneum defects [48].

2.2. Claudin 2

Claudin-2 is one of the two claudins that were initially identified by Furuse et al. in 1998 [49]. In humans, its gene contains two exons encoding a 203 amino acid protein that constitutes cation-selective pores [50]. It is expressed in rat brain [51], proximal tubules of the kidney [52] liver, and epididymis [53].

Its expression is increased in colorectal cancer [54], active ulcerative colitis [55], a severe form of the coeliac disease [56] and inflammatory bowel disease [57] whereas it is downregulated in breast tumors and osteosarcoma [58,59]. It has been shown that miR-16 modulates *CLDN2* expression and causes dysfunctional barrier properties in inflammatory bowel disease [60].

Cldn2 KO mice have been generated by Muto et al. [61]. Mice were morphologically normal at birth. The authors did not observe renal morphological abnormalities under both light and electron microscope. However, further analysis in proximal tubules revealed reduced absorption of Na^+ and higher urinary fractional excretion of Ca^{2+}. The same mice were investigated by a different group, focusing on small intestine showing that *Cldn2* deficient mice have slightly larger intestine and longer intestinal villi. They further demonstrated *Cldn2* dependent Na^+ selective intestinal paracellular permeability. Matsumoto et al. focused on liver and biliary tissues of *Cldn2* deficient mice and similar to the kidney, no obvious morphological abnormalities were observed [62]. The detailed physiological analysis revealed a decreased bile flow in *Cldn2* deficient mice and four weeks under a lithogenic diet, KO mice developed gallstones as a consequence of altered bile composition and flow rate [62]. As *Cldn2* and *Cldn15* play an important role in paracellular ion flow, Wada et al. generated *Cldn2*$^{-/-}$ *Cldn15*$^{-/-}$ double KO (dKO) mice [63]. Deficiency of both genes caused early death by week three, which was attributed to overt hypoglycemia of the dKO animals presumably caused by a disrupted Na^+ flow, which is important for intestinal glucose absorption. Transgenic mice with colon specific overexpression of *Cldn2* displayed an enlarged colon and RNAs of genes involved in cell proliferation were found to be increased. In contrast, for inflammation related RNAs, the opposite was shown, in line with the fact that mice were protected against experimentally induced colitis [64].

Recently a missense mutation of Cldn2 associated with obstructive azoospermia in a four generation spanning family has been identified (Figure 2). Further, it has been shown that different claudins (*CLDN1, CLDN2, CLDN3, CLDN4* and *CLDN7)* are expressed in human epididymal tight junctions [65]. Except for *CLDN2* all these claudins cause, when eliminated, a disruption of the epithelial barrier. Therefore, it has been assumed that malfunction of these claudins might cause infertility in men but has not been proven so far.

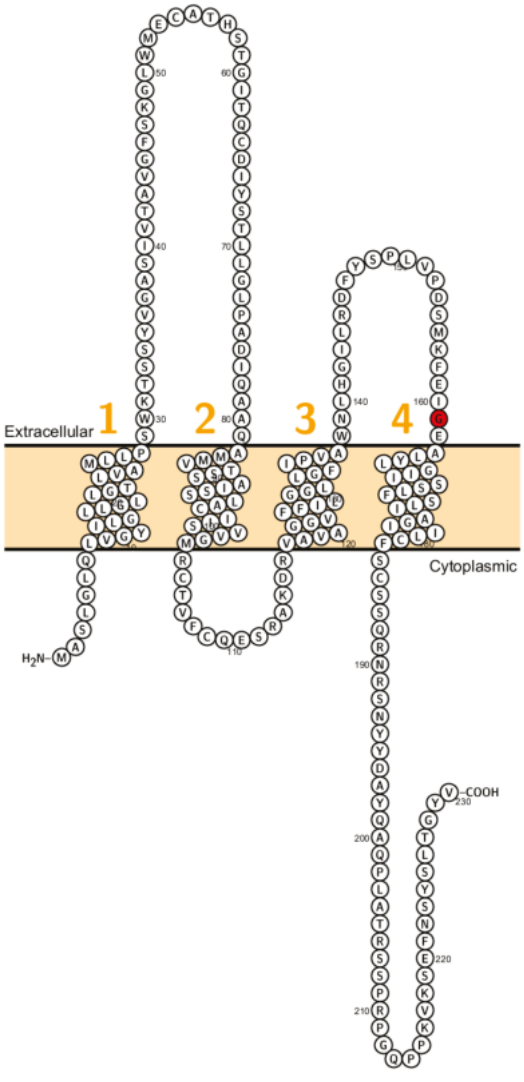

Figure 2. Topology of *CLDN2*. FASTA sequence of *CLDN2* (Uniprot accession no: P57739). Each amino acid is shown as a single letter code and numbers (orange) indicate transmembrane domains. Mutations shown to be involved in human diseases are shown in red.

2.3. Claudin 9

The Claudin-9 gene consists of a single exon encoding a 217 amino acid protein. It constitutes a barrier to K^+ and Na^+. Its expression was found in the inner ear, the liver [66] and the kidney [67].

Zhang et al. showed that claudin-9, together with claudin-6 mediates Hepatitis C Virus (HCV) entry into hepatoma cell lines [66]. Fofana et al. generated monoclonal antibodies against *CLDN9* which inhibit HCVpp (HCV pseudo particles) entry to *CLDN9* expressing cell lines [68].

The expression of *CLDN9* is increased in gastric cancer [69] and promotes cell proliferation and migration of lung metastasis [70]. In cervical carcinoma, RNA expression levels were found to be decreased [71].

Sineni et al. described patients with inherited autosomal recessive hearing loss who had a truncated variant of claudin-9 (p.L29fs). The mutation is located at the beginning of the first ECL (Figure 3). The truncated protein was not detected at the plasma membrane, indicating a dysfunctional TJ and thereby affecting the peri- and endolymphatic ion composition in the inner ear as the cause of hearing impairment [19]. Patients did not display coordination disturbances. This pathophysiological principle has been demonstrated in the past when mutations in BSND have been identified in patients with Bartter syndrome Type 4 [72].

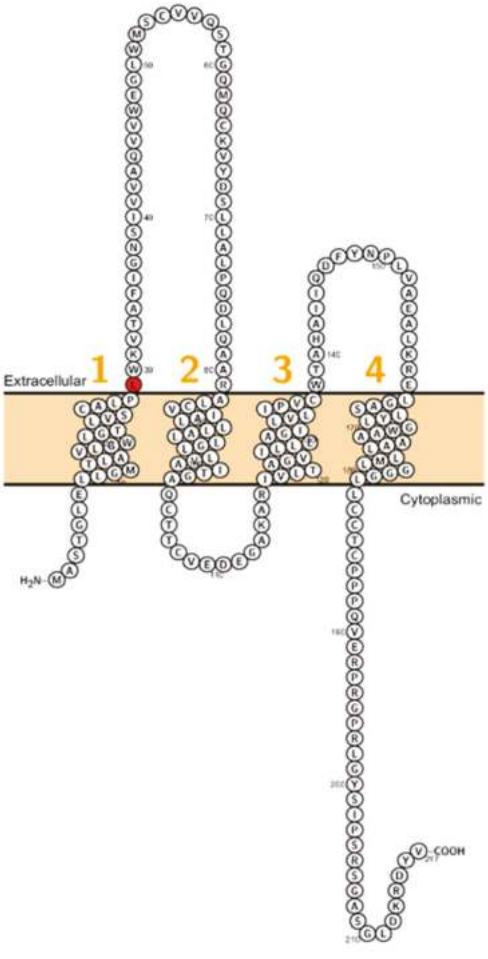

Figure 3. Topology of *CLDN9*. FASTA sequence of *CLDN9* (Uniprot accession no: O95484). Each amino acid is shown as a single letter code and numbers (orange) indicate transmembrane domains. Mutations shown to be involved in human diseases are shown in red.

Mice that carry a missense mutation in *Cldn9* were shown to be deaf. Further analysis showed that Reissner's membrane was morphologically normal when compared to wild type mice and that only the basal but not the apical part of the cochlea was morphologically affected. Inner ear development was normal until postnatal day 14 (P14) then degeneration of the organ of Corti was observed. Since claudin-9 acts as a barrier for Na^+ and K^+, heterologous expression of the mutant in MDCK cells did not affect membrane targeting, indicating that this protein was not functional even when properly

targeted and inserted into the TJ. In both, patients and mice hearing loss are age dependent. In mice at P14, outer hair cells (OHC) appeared normal whereas severe degeneration of OHC was observed at P80. In patients, a younger affected sibling had moderate hearing loss when compared to the older sibling. Neither mutant mice nor human patients had balance problems. Although *Cldn9* is expressed in various tissues, the authors did not report any abnormalities of other organs (e.g., kidney) yet.

2.4. Claudin 10

CLDN10 consists of five exons encoding a 228 amino acid protein. Initially, there were two isoforms described [73], later Günzel et al. described four different splice variants mostly localized at TJs except for the ones that lack exon 4 [74]. Claudin-10a constitutes a pore for anions whereas claudin-10b forms a pore for cations [16,73]. *CLDN10b* is expressed in many tissues including the brain, lung [75], salivary gland [76], mammary gland [77] but *CLDN10a* is exclusively expressed in the kidney [73]. There are no isoform-specific antibodies, but according to RNA hybridization data, *Cldn10b* is highly expressed in medulla and *Cldn10a* in the cortex [73] and based on RNA-Seq data, *Cldn10a* is expressed in the proximal tubule (PT) and *Cldn10b* in thick ascending limb (TAL) [11].

Both isoforms interact with claudin-18 and claudin-19 in a yeast two-hybrid analysis [78], whereas immunofluorescence experiments on kidney sections did not demonstrate colocalization [79]. Additionally, claudin-10 has been implicated in left-right-patterning as well as in tumor progression and invasiveness [80].

Patients with a homozygous mutation in *CLDN10B* (N48K) showed anhidrosis, alacrima, dry mouth, and kidney failure with hypermagnesemia, low urinary Mg^{2+} and Ca^{2+} [81] (Figure 4). Patients did not display overt hypokalemia indicating only a mild renal electrolyte wasting although Meyers et al. described a patient with *CLDN10* mutation who initially presented with hypokalemia and follow-up examinations revealed a developing hypermagnesemia [82]. In fact, *CLDN10* patients exhibit a considerable range of hypohidrosis, hypolacrymia, ichthyosis and xerostomia and a decreased amount of saliva. Functional testing revealed that patients had decreased NaCl absorption in the TAL, too [82].

TAL specific knockout of both isoforms in mice resulted in polyuria, polydipsia and hypermagnesemia. Moreover, acidic urine and calcium deposits in the kidney (nephrocalcinosis) were observed. Quantitative expression analysis of TAL tubules revealed that expression of *Cldn10*, *Cldn16* and *Cldn19* was increased in kidneys of mutant animals [11].

Mice lacking claudin-16 and claudin-10 in the kidney were found to have normal Mg^{2+} in serum and absence of nephrocalcinosis. The authors demonstrated that the deletion of *Cldn10* and the loss of *Cldn16* led to an expansion of the DCT, especially which eventually resulted in increased resorption of Mg^{2+} [83].

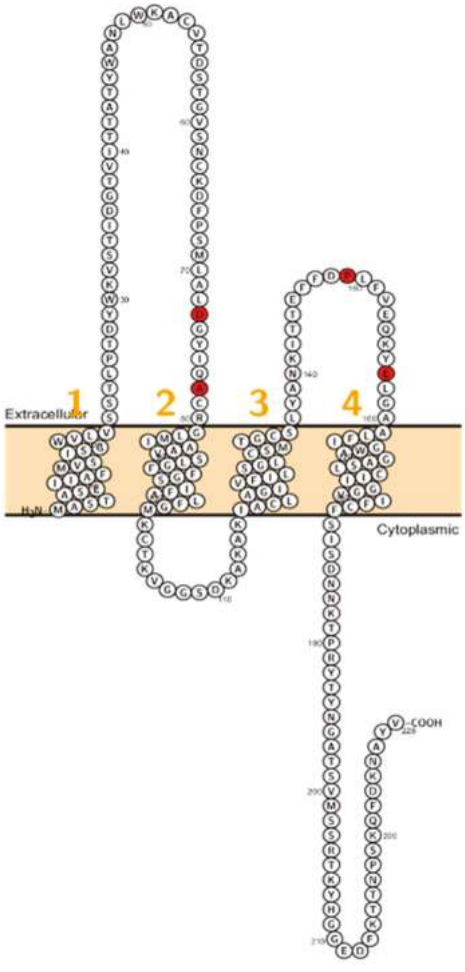

Figure 4. Topology of *CLDN10*. FASTA sequence of *CLDN10* (Uniprot accession no: P78369). Each amino acid is shown as a single letter code and numbers (orange) indicate transmembrane domains. Mutations shown to be involved in human diseases are shown in red.

2.5. Claudin 14

CLDN14 is located on human chromosome 21 and consists of two exons encoding a 239 amino acid protein. It has five protein-coding transcript variants and is classified as a barrier forming claudin [15].

Overexpression of *CLDN14* is associated with gastric and hepatocellular forms of cancer [84].

Cldn14 expression was found in outer and inner ear hair cells and also in the TAL, the DCT [85] and in the liver [12].

Wilcox et al. reported on deaf patients from two large consanguineous families revealing a mutation (V85D) in *CLDN14.* This mutation is predicted to interfere with a phosphorylation site and this residue is conserved between *CLDN3* and *CLDN9* which are expressed in the inner ear too [86]. Immunocytochemistry experiments showed that the mutant failed to localize on the membrane [87]. After this initial study, several other mutations (W56, R81H, G232R) have been reported (Figure 5).

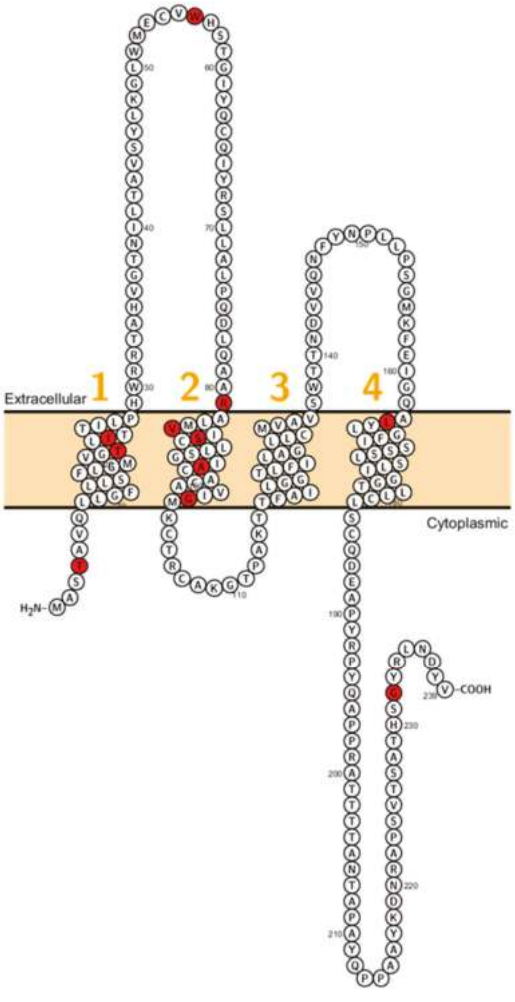

Figure 5. Topology of *CLDN14*. FASTA sequence of *CLDN14* (Uniprot accession no: O95500). Each amino acid is shown as a single letter code and numbers (orange) indicate transmembrane domains. Mutations shown to be involved in human diseases are shown in red.

Examination of *Cldn14* mice that included kidney and liver along with 41 other tissues revealed no morphological differences between knockout and wild type animals. Inner hair cells and outer hair cells (OHC) seemed to develop normally. However, the rapid loss of OHC characterized by disorganization and loss of stereocilia was observed after the first week. Auditory brainstem response (ABR), tests revealed that knockout mice suffer from hearing loss by the third week of age [12].

Although initially no kidney abnormalities were observed neither in mice nor in patients, upon a high calcium diet, *Cldn14* deficient mice developed hypomagnesemia and hypocalciuria. Moreover, it has been shown that two microRNA regulate extracellular Ca^{2+} levels through suppressing *Cldn14* expression under normal diet conditions [85].

Transgenic overexpression of *Cldn14* in TAL of kidney resulted in hypercalciuria and hypermagnesuria [88].

In humans, the hearing loss occurred at the prelingual stage and the severity of hearing loss depends on the mutation. A patient with non-common mutation (A163V) was reported with hearing ability until the age of three, in line with the observation in mice [89].

2.6. Claudin 16

Claudin-16 is a pore forming claudin encoded by *CLDN16* gene [16]. It is expressed in duodenum, jejunum, ileum, colon [90], in tooth germ [91], in salivary glands [92], and also has been found in the endolymphatic duct of the inner ear [93]. The by far highest expression has been found in the thick ascending limb (TAL) of the kidney [94].

Several studies related overexpression of *CLDN16* with different cancer types including ovarian cancer [95] and papillary thyroid carcinoma [96]. Also, claudin-16 might play a role in cell proliferation and differentiation, e.g., breast cancer [97,98].

In the kidney, Claudin-16 is crucial for TJ-specific ion transport in the TAL and handles approximately 25% Ca^{2+} and 70% of Mg^{2+} reabsorption [99]. However, the exact role of claudin-16 remains a matter of debate. Hou and colleagues showed that claudin-16 enhances the permeability of monovalent cations, including Na^{+}, than that of divalent cations, as Mg^{2+} (<50%) [90]. When *Cldn16* was deleted in mice, a cation-to-anion selectivity (P_{Na}/P_{Cl}) but no divalent-to-monovalent cation selectivity (P_{Mg}/P_{Na}) was observed [100]. Other groups have reported a selectivity of Claudin-16 for divalent cations Mg^{2+} and Ca^{2+} [101,102]. Hou et al. have described an interaction with claudin-19 as being necessary for correct TJ integration [78]. Additionally, it has been reported that claudin-14 reduces the cation permeability of claudin-16, but not for the claudin-19 in transfected LLC-PK1 cells. Based on this hypothesis, claudin-14 might act as a negative regulator of divalent cation permeation [85]. Split-ubiquitin yeast 2-hybrid (Y2H) membrane protein interaction assay showed that claudin-14 interacts with the claudin-16 [79]. Other known interactions reported are with syntaxin-8 [102] and with PDZ domain containing RING finger 1 (encoded by *PDZRN*) [103] by electrophysiological experiments [104].

Mutations in human *CLDN16* cause an autosomal recessive disorder called *Familial hypomagnesemia with hypercalcinuria and nephrocalcinosis* (FHHNC) [105] (Figure 6). Other phenotypic features are incomplete distal tubular acidosis, impaired bone homeostasis [94], hypocitraturia and hyperuricemia which can be considered a secondary effect of renal insufficiency. To date, about 66 mutations including missense/nonsense, splicing, small deletion and small indels have been identified. Although still a matter of debate, it is believed that claudin-16 and claudin-19 form a heterodimer/tetramer essential for the divalent cation selectivity of the paracellular channels at the TAL and it has been demonstrated that some mutations disrupt this interaction [106].

Cldn16 deficient mice exhibited hypomagnesia and hypercalciuria and a low urinary pH but did not show nephrocalcinosis which could be explained by the upregulation of several genes (e.g., *Trpm6, Trpv5, Cnnm2*) involved in calcium and magnesium transport or the altered pH. Moreover, mice did not show renal insufficiency [13].

Besides, knockdown mice were generated by RNA interference technology [100] which phenocopied the main features of FHHNC including hypercalcinuria, hypomagnesemia, nephrocalcinosis and urinary Ca^{2+} and Mg^{2+} wasting without showing nephrocalcinosis or renal insufficiency. *Cldn16* KD animals showed increase of 1,25-dihydroxychlecalciferol [100].

For Cldn16 Patients, a genotype-phenotype correlation has been reported [94]. In sharp contrast to humans, although mice recapitulate many features of FHHNC like hypomagnesemia and hypercalciuria, they do not display nephrocalcinosis nor renal insufficiency [100]. Most of the patients with FHHNC nephrocalcinosis develop end stage renal disease with a need of renal transplantation [107]. Recently, amelogenesis imperfecta has been related to the absence of Claudin-16 in the ameloblasts in humans and mice [105] as an additional role of Cldn16 deficiency.

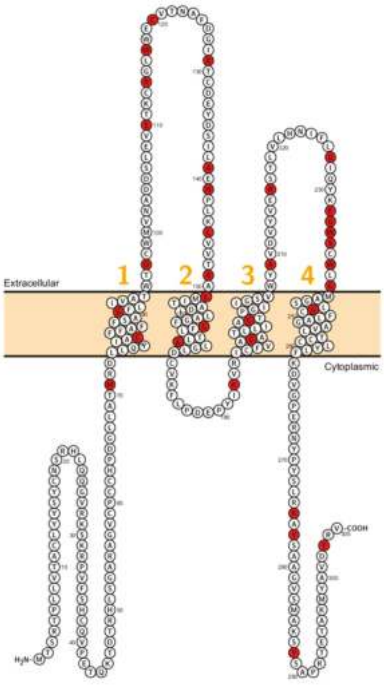

Figure 6. Topology of *CLDN16.* FASTA sequence of *CLDN16* (Uniprot accession no: Q9Y517). Each amino acid is shown as a single letter code and numbers (orange) indicate transmembrane domains. Mutations shown to be involved in human diseases are shown in red.

2.7. Claudin 19

The CLDN-19 gene encodes a 224 amino acid protein. Claudin-19 is a barrier forming claudin and is expressed in the thick ascending limb of the kidney and the retinal pigment epithelium (RPE) and the sheath of myelinated peripheral nerves. Additionally its expression was reported detected in the inner ear [38], stomach [108] and lung [109]. Like claudin-16, claudin-19 plays a major role in the permeability and selectivity of the TJ in TAL.

Claudin-19 interacts with claudin-16, both are involved in the reabsorption of divalent cations in the TAL [79,110]. Gong et al. isolated a stable dimer of claudin-16 with claudin-19 from transfected HEK293 cells and Sf9 cells [85]. The dimerization occurs through the cis-association of the third and the fourth transmembrane domain in both proteins [111]. This hypothesis is complemented by in vivo transgenic animal models, deletion of claudin-16 rendered claudin-19 delocalization from the TJ and vice versa [78]. Selective mutations disrupt the dimerization, triggering a loss of the transport function with FHHNC disease is the consequence [112].

Moreover, claudin-19 and ZO-1 are found by co-immunoprecipitation forming a complex in Madin-Darby canine kidney (MDCK) cells [97]. Meier et al. reported patients presenting by a phenotype of FHHNC disease but with the ocular disease [113,114]. All individuals of these families suffered from severe visual impairment, characterized by macular colobomata, significant myopia, and horizontal nystagmus. The genotype of these patients did not show a mutation in *CLDN16*, but Konrad and colleagues identified three mutations (G20D, Q57E) in *CLDN19*, recapitulating CLDN16 defects but, ocular defects, too. Other reported mutations (L90P and G123R) disrupt the interaction between claudin-16 and claudin-19 [23,112] (Figure 7).

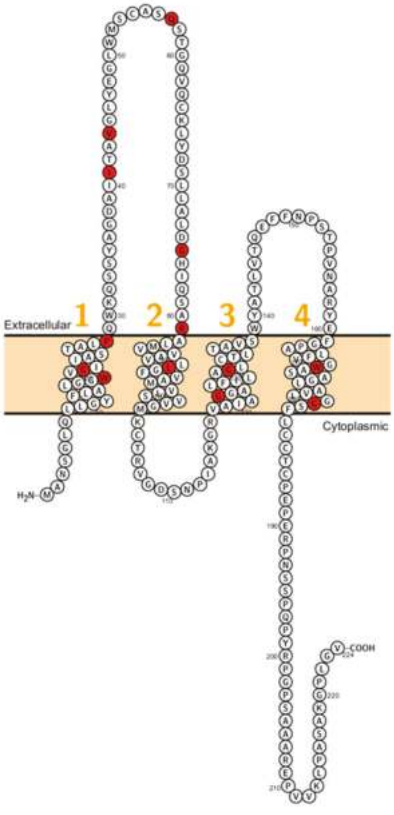

Figure 7. Topology of *CLDN19*. FASTA sequence of *CLDN19* (Uniprot accession no: Q8N6F1). Each amino acid is shown as a single letter code and numbers (orange) indicate transmembrane domains. Mutations shown to be involved in human diseases are shown in red.

Cldn19 KD mice showed a reduction of Mg^{2+} in plasma and excessive losses of Ca^{2+} and Mg^{2+} levels in kidney similar to *Cldn16* KO mice [78]. These mutations are the cause of FHHNC diseases, in which interaction between claudin-16 and-19 is disrupted. The dissociation of these proteins can trigger a loss of the transport function of them and cause FHHNC [112]. On the other hand, knockout mouse of *Cldn19* provokes renal reabsorption deficiency [79].

3. Discussion

Twenty years ago, the seminal work of Lifton's group described mutations in a gene coding for a TJ protein (initially named paracellin-1 and thereafter classified as claudin-16) as being causative for a human disorder (FHHNC) [99]. *CLDN16*, being the first claudin of a continuously expanding group of claudins causing human disorders, has been subject to various investigations on expression, function and also on possibilities of pharmaceutical interventions [115]. To gain further insights, mouse models, either as knockdown or knock out have been established (Table 1). Such models recapitulated some (Hypercalciuria, Hypomagnesemia) but not all (Nephrocalcinosis and renal insufficiency) of the hallmarks of human FHHNC, demonstrating the benefits but also the limitations of such models of TJ disorders. Recently the association of claudin-16 and amelogenesis imperfecta in men and mice has been shown [91].

Table 1. Overview of claudins causing human diseases and corresponding mouse models. The existence (by publication) is indicated by (+) while (−) indicates the absence of a corresponding model.

Human			Mouse			
Claudin	**Human Disorder**	**Hallmarks**	**Knockout**	**Knockdown**	**Conditional Knockout**	**Transgenic Overexpression**
1	NISCH Syndrome	Ichthyosis	Ichthyosis ($Cldn2^{-/-}$)	Ichthyosis	+	+
2	Obstructive azoospermia	Male infertility	Larger intestine ($Cldn2^{-/-}$ $Cldn15^{-/-}$) Hypoglycemia Perinatal lethality	−	−	Larger colon
9	Nonsyndromic sensorioneural deafness	Deafness	Deafness	−	−	−
10	HELIX syndrome	Hypokalemia Hypermagnesemia Nephrocalcinosis	Perinatal lethality	−	Hypokalemi Hypermagnesemia Nephrocalcinosis	−
14	Nonsyndromic sensorioneural deafness	Deafness	Deafness	−	−	Hypercalcuria Hypermagnesemia
16	FHHNC	Hypercalciuria Renal insufficiency Hypomagnesemia Nephrocalcinosis	Hypercalciuria Hypomagnesemia	Hypercalciuria Hypomagnesemia	−	−
19	FHHNC + Eye Involvement	Hypercalciuria Renal insufficiency Hypomagnesemia Nephrocalcinosis Eye involvement	Hypercalciuria Hypomagnesemia	Hypercalciuria Hypomagnesemia Eye abnormalities	−	−

As the example of claudin-16 demonstrates, disorders that are caused by mutations in the corresponding claudin genes are not restricted to a given organ but rather should be considered as 'claudinopathies'. This view would not restrict the consequences to tissue-specific local or regional expression but appreciates the function and loss in all of the organs and tissues where a given claudin is expressed. Moreover, in a given organ, multiple different claudins are expressed and can cause, when mutated a similar phenotype albeit having different underlying pathophysiology. For example, kidney stones are a worldwide problem that affects 12% of the world population regardless of gender [116,117]. Besides *CLDN16* and *CLDN19*, in 2009, a genome-wide association study on an Icelandic and Dutch population revealed that a *CLDN14* variant (rs219780[C]) is associated with kidney stones too.

In this perspective, animal models, especially mice with all their limitations, are indispensable to study the consequences of claudin deficiency.

Funding: This research was funded by the Deutsche Forschungsgemeinschaft (DFG), Research Training Group GRK 2318 (to M.S. and D.M.), and the Open Access Publication Fund of the Charité—Universitätsmedizin Berlin. C.F.R. and L.A.M.C. acknowledge Ministerio Español de Ciencia e Innovación (MICINN) for funding under grants BFU2010-17857 and BFU2016-77408-R], as well as the Spanish Ministry of Economy and Competitiveness (MINECO/FEDER, UE) [REFsBES-2017-080435, BES-2014-068464] and the MICINN CONSOLIDER-INGENIO 2010 Program [grant number CSD2008-00005; BFU2015-70067-REDC]. We also thank MINECO for the Severo Ochoa Excellence Accreditation to CIC bioGUNE (SEV-2016-0644).

Conflicts of Interest: The authors declare no conflict of interest.

References

1. Daneman, R.; Prat, A. The blood-brain barrier. *Cold Spring Harb. Perspect. Biol.* **2015**, *7*, a020412. [CrossRef]
2. Baud, L. Renal Epithelial Cells: Differentiation and Plasticity. *J. Am. Soc. Nephrol.* **2003**, *14*, S1–S2. [CrossRef]
3. Macara, I.G.; Guyer, R.; Richardson, G.; Huo, Y.; Ahmed, S.M. Epithelial homeostasis. *Curr. Biol.* **2014**, *24*, R815–R825. [CrossRef]
4. Roignot, J.; Peng, X.; Mostov, K. Polarity in Mammalian Epithelial Morphogenesis. *Cold Spring Harb. Perspect. Biol.* **2013**, *5*, a013789. [CrossRef] [PubMed]
5. Karasov, W.H. Integrative physiology of transcellular and paracellular intestinal absorption. *J. Exp. Biol.* **2017**, *220*, 2495–2501. [CrossRef]
6. Sterling, T.M.; Nemere, I. Calcium uptake and membrane trafficking in response to PTH or 25(OH)D3 in polarized intestinal epithelial cells. *Steroids* **2007**, *72*, 151–157. [CrossRef] [PubMed]
7. Cunha, T.D.S.; Heilberg, I.P. Bartter syndrome: Causes, diagnosis, and treatment. *Int. J. Nephrol. Renov. Dis.* **2018**, *11*, 291–301. [CrossRef]
8. Knoers, N.V.; Levtchenko, E.N. Gitelman syndrome. *Orphanet J. Rare Dis.* **2008**, *3*, 22. [CrossRef]
9. Furuse, M.; Hata, M.; Furuse, K.; Yoshida, Y.; Haratake, A.; Sugitani, Y.; Noda, T.; Kubo, A.; Tsukita, S. Claudin-based tight junctions are crucial for the mammalian epidermal barrier: A lesson from claudin-1-deficient mice. *J. Cell Biol.* **2002**, *156*, 1099–1111. [CrossRef]
10. Nakano, Y.; Kim, S.H.; Kim, H.M.; Sanneman, J.D.; Zhang, Y.; Smith, R.J.; Marcus, D.C.; Wangemann, P.; Nessler, R.A.; Banfi, B. A claudin-9-based ion permeability barrier is essential for hearing. *PLoS Genet.* **2009**, *5*, e1000610. [CrossRef]
11. Breiderhoff, T.; Himmerkus, N.; Stuiver, M.; Mutig, K.; Will, C.; Meij, I.C.; Bachmann, S.; Bleich, M.; Willnow, T.E.; Müller, D. Deletion of claudin-10 (Cldn10) in the thick ascending limb impairs paracellular sodium permeability and leads to hypermagnesemia and nephrocalcinosis. *Proc. Natl. Acad. Sci. USA* **2012**, *109*, 14241–14246. [CrossRef] [PubMed]
12. Ben-Yosef, T.; Belyantseva, I.A.; Saunders, T.L.; Hughes, E.D.; Kawamoto, K.; Van Itallie, C.M.; Beyer, L.A.; Halsey, K.; Gardner, D.J.; Wilcox, E.R.; et al. Claudin 14 knockout mice, a model for autosomal recessive deafness DFNB29, are deaf due to cochlear hair cell degeneration. *Hum. Mol. Genet.* **2003**, *12*, 2049–2061. [CrossRef]
13. Will, C.; Breiderhoff, T.; Thumfart, J.; Stuiver, M.; Kopplin, K.; Sommer, K.; Gunzel, D.; Querfeld, U.; Meij, I.C.; Shan, Q.; et al. Targeted deletion of murine Cldn16 identifies extra- and intrarenal compensatory mechanisms of Ca^{2+} and Mg^{2+} wasting. *Am. J. Physiol. Ren. Physiol.* **2010**, *298*, F1152–F1161. [CrossRef] [PubMed]

14. Tsukita, S.; Furuse, M. The structure and function of claudins, cell adhesion molecules at tight junctions. *Ann. N. Y. Acad. Sci.* **2000**, *915*, 129–135. [CrossRef]
15. Günzel, D.; Yu, A.S.L. Claudins and the Modulation of Tight Junction Permeability. *Physiol. Rev.* **2013**, *93*, 525–569. [CrossRef] [PubMed]
16. Krause, G.; Winkler, L.; Mueller, S.L.; Haseloff, R.F.; Piontek, J.; Blasig, I.E. Structure and function of claudins. *Biochim. Biophys. Acta* **2008**, *1778*, 631–645. [CrossRef]
17. Sanjad, S.A.; Hariri, A.; Habbal, Z.M.; Lifton, R.P. A novel PCLN-1 gene mutation in familial hypomagnesemia with hypercalciuria and atypical phenotype. *Pediatr. Nephrol.* **2007**, *22*, 503–508. [CrossRef]
18. Hadj-Rabia, S.; Baala, L.; Vabres, P.; Hamel-Teillac, D.; Jacquemin, E.; Fabre, M.; Lyonnet, S.; De Prost, Y.; Munnich, A.; Hadchouel, M.; et al. Claudin-1 gene mutations in neonatal sclerosing cholangitis associated with ichthyosis: A tight junction disease. *Gastroenterology* **2004**, *127*, 1386–1390. [CrossRef]
19. Sineni, C.J.; Yildirim-Baylan, M.; Guo, S.; Camarena, V.; Wang, G.; Tokgoz-Yilmaz, S.; Duman, D.; Bademci, G.; Tekin, M. A truncating CLDN9 variant is associated with autosomal recessive nonsyndromic hearing loss. *Hum. Genet.* **2019**, *138*, 1071–1075. [CrossRef]
20. Hadj-Rabia, S.; Brideau, G.; Al-Sarraj, Y.; Maroun, R.C.; Figueres, M.-L.; Leclerc-Mercier, S.; Olinger, E.; Baron, S.; Chaussain, C.; Nochy, D.; et al. Multiplex epithelium dysfunction due to CLDN10 mutation: The HELIX syndrome. *Genet. Med.* **2017**, *20*, 190–201. [CrossRef]
21. Wilcox, E.R.; Burton, Q.L.; Naz, S.; Riazuddin, S.; Smith, T.N.; Ploplis, B.; Belyantseva, I.; Ben-Yosef, T.; Liburd, N.A.; Morell, R.J.; et al. Mutations in the Gene Encoding Tight Junction Claudin-14 Cause Autosomal Recessive Deafness DFNB29. *Cell* **2001**, *104*, 165–172. [CrossRef]
22. Hampson, G.; A Konrad, M.; Scoble, J. Familial hypomagnesaemia with hypercalciuria and nephrocalcinosis (FHHNC): Compound heterozygous mutation in the claudin 16 (CLDN16) gene. *BMC Nephrol.* **2008**, *9*, 12. [CrossRef] [PubMed]
23. Konrad, M.; Schaller, A.; Seelow, D.; Pandey, A.V.; Waldegger, S.; Lesslauer, A.; Vitzthum, H.; Suzuki, Y.; Luk, J.M.; Becker, C.; et al. Mutations in the tight-junction gene claudin 19 (CLDN19) are associated with renal magnesium wasting, renal failure, and severe ocular involvement. *Am. J. Hum. Genet.* **2006**, *79*, 949–957. [CrossRef] [PubMed]
24. De Santis, S.; Cavalcanti, E.; Mastronardi, M.; Jirillo, E.; Chieppa, M. Nutritional Keys for Intestinal Barrier Modulation. *Front. Immunol.* **2015**, *6*, 612. [CrossRef] [PubMed]
25. Merikallio, H.; Kaarteenaho, R.; Pääkkö, P.; Lehtonen, S.; Hirvikoski, P.; Mäkitaro, R.; Harju, T.; Soini, Y. Impact of smoking on the expression of claudins in lung carcinoma. *Eur. J. Cancer* **2011**, *47*, 620–630. [CrossRef] [PubMed]
26. Ramalingam, A.; Wang, X.; Gabello, M.; Valenzano, M.C.; Soler, A.P.; Ko, A.; Morin, P.J.; Mullin, J.M. Dietary methionine restriction improves colon tight junction barrier function and alters claudin expression pattern. *Am. J. Physiol. Physiol.* **2010**, *299*, C1028–C1035. [CrossRef]
27. Soini, Y. Claudins in lung diseases. *Respir. Res.* **2011**, *12*, 70. [CrossRef]
28. Barmeyer, C.; Schulzke, J.D.; Fromm, M. Claudin-related intestinal diseases. *Semin. Cell Dev. Biol.* **2015**, *42*, 30–38. [CrossRef]
29. Limaye, A.; Hall, B.; Kulkarni, A.B. Manipulation of mouse embryonic stem cells for knockout mouse production. *Curr. Protoc. Cell Biol.* **2009**, *44*, 19.13.1–19.13.24.
30. Kooij, G.; Kopplin, K.; Blasig, R.; Stuiver, M.; Koning, N.; Goverse, G.; van der Pol, S.M.; van Het Hof, B.; Gollasch, M.; Drexhage, J.A.; et al. Disturbed function of the blood-cerebrospinal fluid barrier aggravates neuro-inflammation. *Acta Neuropathol.* **2014**, *128*, 267–277. [CrossRef]
31. Adli, M. The CRISPR tool kit for genome editing and beyond. *Nat. Commun.* **2018**, *9*, 1911. [CrossRef] [PubMed]
32. Daugherty, B.L.; Ward, C.; Smith, T.; Ritzenthaler, J.D.; Koval, M. Regulation of Heterotypic Claudin Compatibility. *J. Biol. Chem.* **2007**, *282*, 30005–30013. [CrossRef] [PubMed]
33. Piontek, J.; Fritzsche, S.; Cording, J.; Richter, S.; Hartwig, J.; Walter, M.; Yu, D.; Turner, J.R.; Gehring, C.; Rahn, H.-P.; et al. Elucidating the principles of the molecular organization of heteropolymeric tight junction strands. *Cell. Mol. Life Sci.* **2011**, *68*, 3903–3918. [CrossRef] [PubMed]
34. Zorko, M.S.; Veraniä, P.; Leskovec, N.K.; Pavloviä, M.D.; Pavlović, M.D.; Veranič, P. Expression of tight-junction proteins in the inflamed and clinically uninvolved skin in patients with venous leg ulcers. *Clin. Exp. Dermatol.* **2009**, *34*, e949–e952. [CrossRef] [PubMed]

35. Reyes, J.L.; Lamas, M.; Martin, D.; Namorado, M.D.C.; Islas, S.; Luna, J.; Tauc, M.; Gonzalez-Mariscal, L.; Gonz, L. The renal segmental distribution of claudins changes with development. *Kidney Int.* **2002**, *62*, 476–487. [CrossRef]
36. Laurila, J.J.; Karttunen, T.; Koivukangas, V.; Laurila, P.A.; Syrjala, H.; Saarnio, J.; Soini, Y.; Ala-Kokko, T.I. Tight junction proteins in gallbladder epithelium: Different expression in acute acalculous and calculous cholecystitis. *J. Histochem. Cytochem.* **2007**, *55*, 567–573. [CrossRef]
37. Zhu, Y.; Brannstrom, M.; Janson, P.O.; Sundfeldt, K. Differences in expression patterns of the tight junction proteins, claudin 1, 3, 4 and 5, in human ovarian surface epithelium as compared to epithelia in inclusion cysts and epithelial ovarian tumours. *Int. J. Cancer* **2006**, *118*, 1884–1891. [CrossRef]
38. Kitajiri, S.-I.; Furuse, M.; Morita, K.; Saishin-Kiuchi, Y.; Kido, H.; Ito, J.; Tsukita, S. Expression patterns of claudins, tight junction adhesion molecules, in the inner ear. *Hear. Res.* **2004**, *187*, 25–34. [CrossRef]
39. Mori, M.; Nakagawa, S.; Miyoshi, N.; Ishii, H.; Mimori, K.; Tanaka, F.; Sekimoto, M.; Doki, Y. Expression of CLDN1 in colorectal cancer: A novel marker for prognosis. *Int. J. Oncol.* **2011**, *39*, 791–796. [CrossRef]
40. Zhang, Z.; Wang, A.; Sun, B.; Zhan, Z.; Chen, K.; Wang, C. Expression of CLDN1 and CLDN10 in lung adenocarcinoma in situ and invasive lepidic predominant adenocarcinoma. *J. Cardiothorac. Surg.* **2013**, *8*, 95. [CrossRef]
41. Zhang, W.-N.; Li, W.; Wang, X.-L.; Hu, Z.; Zhu, D.; Ding, W.-C.; Liu, D.; Li, K.-Z.; Ma, D.; Wang, H. CLDN1 expression in cervical cancer cells is related to tumor invasion and metastasis. *Oncotarget* **2016**, *7*, 87449–87461. [CrossRef] [PubMed]
42. Zhou, S.; Piao, X.; Wang, C.; Wang, R.; Song, Z. Identification of claudin1, 3, 7 and 8 as prognostic markers in human laryngeal carcinoma. *Mol. Med. Rep.* **2019**, *20*, 393–400. [PubMed]
43. Evans, M.J.; Von Hahn, T.; Tscherne, D.M.; Syder, A.J.; Panis, M.; Wölk, B.; Hatziioannou, T.; McKeating, J.A.; Bieniasz, P.D.; Rice, C.M. Claudin-1 is a hepatitis C virus co-receptor required for a late step in entry. *Nature* **2007**, *446*, 801–805. [CrossRef]
44. Baala, L.; Hadj-Rabia, S.; Hamel-Teillac, D.; Hadchouel, M.; Prost, C.; Leal, S.M.; Jacquemin, E.; Sefiani, A.; De Prost, Y.; Courtois, G.; et al. Homozygosity mapping of a locus for a novel syndromic ichthyosis to chromosome 3q27-q28. *J. Investig. Dermatol.* **2002**, *119*, 70–76. [CrossRef] [PubMed]
45. Kirchmeier, P.; Sayar, E.; Hotz, A.; Hausser, I.; Islek, A.; Yilmaz, A.; Artan, R.; Fischer, J. Novel mutation in the CLDN1 gene in a Turkish family with neonatal ichthyosis sclerosing cholangitis (NISCH) syndrome. *Br. J. Dermatol.* **2014**, *170*, 976–978. [CrossRef] [PubMed]
46. Vreeburg, M.; Wagner, A.; Van Geel, M.; Nagtzaam, I.F.; Peeters, V.P.M.; Steijlen, P.M.; Van Steensel, M.A.M. Novel CLDN1 mutation in ichthyosis-hypotrichosis-sclerosing cholangitis syndrome without signs of liver disease. *Br. J. Dermatol.* **2018**, *178*, e202–e203.
47. Tokumasu, R.; Yamaga, K.; Yamazaki, Y.; Murota, H.; Suzuki, K.; Tamura, A.; Bando, K.; Furuta, Y.; Katayama, I.; Tsukita, S. Dose-dependent role of claudin-1 in vivo in orchestrating features of atopic dermatitis. *Proc. Natl. Acad. Sci. USA* **2016**, *113*, E4061–E4068. [CrossRef]
48. Hirano, T.; Yokouchi, M.; Atsugi, T.; Amagai, M.; Kubo, A. Epidermis-specific ablation of claudin-1 in adult mice demonstrates the essential role of a tight junction barrier in skin homeostasis. *J. Dermatol. Sci.* **2016**, *84*, e37. [CrossRef]
49. Furuse, M.; Fujita, K.; Hiiragi, T.; Fujimoto, K.; Tsukita, S. Claudin-1 and -2: Novel integral membrane proteins localizing at tight junctions with no sequence similarity to occludin. *J. Cell Biol.* **1998**, *141*, 1539–1550. [CrossRef]
50. Amasheh, S.; Meiri, N.; Gitter, A.H.; Schöneberg, T.; Mankertz, J.; Schulzke, J.D.; Fromm, M. Claudin-2 expression induces cation-selective channels in tight junctions of epithelial cells. *J. Cell Sci.* **2002**, *115*, 4969–4976. [CrossRef]
51. Lamas, M.; González-Mariscal, L.; Gutiérrez, R. Presence of claudins mRNA in the brain. Selective modulation of expression by kindling epilepsy. *Mol. Brain Res.* **2002**, *104*, 250–254. [CrossRef]
52. Enck, A.H.; Berger, U.V.; Yu, A.S.L. Claudin-2 is selectively expressed in proximal nephron in mouse kidney. *Am. J. Physiol. Physiol.* **2001**, *281*, F966–F974. [CrossRef]
53. Guan, X.; Inai, T.; Shibata, Y. Segment-specific expression of tight junction proteins, claudin-2 and -10, in the rat epididymal epithelium. *Arch. Histol. Cytol.* **2005**, *68*, 213–225. [CrossRef] [PubMed]

54. Kinugasa, T.; Huo, Q.; Higashi, D.; Shibaguchi, H.; Kuroki, M.; Tanaka, T.; Futami, K.; Yamashita, Y.; Hachimine, K.; Maekawa, S.; et al. Selective up-regulation of claudin-1 and claudin-2 in colorectal cancer. *Anticancer Res.* **2007**, *27*, 3729–3734. [CrossRef]
55. Oshima, T.; Miwa, H.; Joh, T. Changes in the expression of claudins in active ulcerative colitis. *J. Gastroenterol. Hepatol.* **2008**, *23*, S146–S150. [CrossRef]
56. Szakál, D.N.; Győrffy, H.; Arató, A.; Cseh, Á.; Molnár, K.; Papp, M.; Dezsofi, A.; Veres, G. Mucosal expression of claudins 2, 3 and 4 in proximal and distal part of duodenum in children with coeliac disease. *Virchows Archiv.* **2010**, *456*, 245–250. [CrossRef]
57. Weber, C.R.; Nalle, S.C.; Tretiakova, M.; Rubin, D.T.; Turner, J.R. Claudin-1 and claudin-2 expression is elevated in inflammatory bowel disease and may contribute to early neoplastic transformation. *Lab. Investig.* **2008**, *88*, 1110–1120. [CrossRef]
58. Kim, T.H.; Huh, J.H.; Lee, S.; Kang, H.; I Kim, G.; An, H.J. Down-regulation of claudin-2 in breast carcinomas is associated with advanced disease. *Histopathology* **2008**, *53*, 48–55. [CrossRef]
59. Zhang, X.; Wang, H.; Li, Q.; Li, T. CLDN2 inhibits the metastasis of osteosarcoma cells via down-regulating the afadin/ERK signaling pathway. *Cancer Cell Int.* **2018**, *18*, 160. [CrossRef]
60. Martínez, C.; Rodiño-Janeiro, B.K.; Lobo, B.; Stanifer, M.L.; Klaus, B.; Granzow, M.; González-Castro, A.M.; Salvo-Romero, E.; Alonso-Cotoner, C.; Pigrau, M.; et al. miR-16 and miR-125b are involved in barrier function dysregulation through the modulation of claudin-2 and cingulin expression in the jejunum in IBS with diarrhoea. *Gut* **2017**, *66*, 1537–1538. [CrossRef]
61. Muto, S.; Hata, M.; Taniguchi, J.; Tsuruoka, S.; Moriwaki, K.; Saitou, M.; Furuse, K.; Sasaki, H.; Fujimura, A.; Imai, M.; et al. Claudin-2–deficient mice are defective in the leaky and cation-selective paracellular permeability properties of renal proximal tubules. *Proc. Natl. Acad. Sci. USA* **2010**, *107*, 8011–8016. [CrossRef] [PubMed]
62. Matsumoto, K.; Imasato, M.; Yamazaki, Y.; Tanaka, H.; Watanabe, M.; Eguchi, H.; Nagano, H.; Hikita, H.; Tatsumi, T.; Takehara, T.; et al. Claudin 2 Deficiency Reduces Bile Flow and Increases Susceptibility to Cholesterol Gallstone Disease in Mice. *Gastroenterology* **2014**, *147*, 1134–1145.e10. [CrossRef] [PubMed]
63. Wada, M.; Tamura, A.; Takahashi, N.; Tsukita, S. Loss of claudins 2 and 15 from mice causes defects in paracellular Na+ flow and nutrient transport in gut and leads to death from malnutrition. *Gastroenterology* **2013**, *144*, 369–380. [CrossRef] [PubMed]
64. Ahmad, R.; Chaturvedi, R.; Olivares-Villagómez, D.; Habib, T.; Asim, M.; Shivesh, P.; Polk, D.B.; Wilson, K.T.; Washington, M.K.; Van Kaer, L.; et al. Targeted colonic claudin-2 expression renders resistance to epithelial injury, induces immune suppression, and protects from colitis. *Mucosal Immunol.* **2014**, *7*, 1340–1353. [CrossRef] [PubMed]
65. Dubé, É.; Dufresne, J.; Chan, P.T.; Hermo, L.; Cyr, D.G. Assessing the Role of Claudins in Maintaining the Integrity of Epididymal Tight Junctions Using Novel Human Epididymal Cell Lines1. *Biol. Reprod.* **2010**, *82*, 1119–1128. [CrossRef]
66. Zheng, A.; Yuan, F.; Li, Y.; Zhu, F.; Hou, P.; Li, J.; Song, X.; Ding, M.; Deng, H. Claudin-6 and Claudin-9 Function as Additional Coreceptors for Hepatitis C Virus. *J. Virol.* **2007**, *81*, 12465–12471. [CrossRef]
67. Abuazza, G.; Becker, A.; Williams, S.S.; Chakravarty, S.; Truong, H.-T.; Lin, F.; Baum, M. Claudins 6, 9, and 13 are developmentally expressed renal tight junction proteins. *Am. J. Physiol. Physiol.* **2006**, *291*, F1132–F1141. [CrossRef]
68. Fofana, I.; Zona, L.; Thumann, C.; Heydmann, L.; Durand, S.C.; Lupberger, J.; Blum, H.E.; Pessaux, P.; Gondeau, C.; Reynolds, G.M.; et al. Functional Analysis of Claudin-6 and Claudin-9 as Entry Factors for Hepatitis C Virus Infection of Human Hepatocytes by Using Monoclonal Antibodies. *J. Virol.* **2013**, *87*, 10405–10410. [CrossRef]
69. Zavala-Zendejas, V.E.; Torres-Martinez, A.C.; Salas-Morales, B.; Fortoul, T.I.; Montano, L.F.; Rendon-Huerta, E.P. Claudin-6, 7, or 9 overexpression in the human gastric adenocarcinoma cell line AGS increases its invasiveness, migration, and proliferation rate. *Cancer Investig.* **2011**, *29*, 1–11. [CrossRef]
70. Sharma, R.K.; Chheda, Z.S.; Das Purkayastha, B.P.; Gomez-Gutierrez, J.G.; Jala, V.R.; Haribabu, B. A spontaneous metastasis model reveals the significance of claudin-9 overexpression in lung cancer metastasis. *Clin. Exp. Metastasis* **2016**, *33*, 263–275. [CrossRef]

71. Zhu, J.; Wang, R.; Cao, H.; Zhang, H.; Xu, S.; Wang, A.; Liu, B.; Wang, Y.; Wang, R. Expression of claudin-5, -7, -8 and -9 in cervical carcinoma tissues and adjacent non-neoplastic tissues. *Int. J. Clin. Exp. Pathol.* **2015**, *8*, 9479–9486. [PubMed]
72. Birkenhäger, R.; Otto, E.; Schürmann, M.J.; Vollmer, M.; Ruf, E.-M.; Maier-Lutz, I.; Beekmann, F.; Fekete, A.; Omran, H.; Feldmann, D.; et al. Mutation of BSND causes Bartter syndrome with sensorineural deafness and kidney failure. *Nat. Genet.* **2001**, *29*, 310–314. [CrossRef] [PubMed]
73. Van Itallie, C.M.; Rogan, S.; Yu, A.; Vidal, L.S.; Holmes, J.; Anderson, J.M. Two splice variants of claudin-10 in the kidney create paracellular pores with different ion selectivities. *Am. J. Physiol. Physiol.* **2006**, *291*, F1288–F1299. [CrossRef] [PubMed]
74. Günzel, D.; Stuiver, M.; Kausalya, P.J.; Haisch, L.; Krug, S.; Rosenthal, R.; Meij, I.C.; Hunziker, W.; Fromm, M.; Muller, D. Claudin-10 exists in six alternatively spliced isoforms that exhibit distinct localization and function. *J. Cell Sci.* **2009**, *122*, 1507–1517. [CrossRef]
75. Zemke, A.C.; Snyder, J.C.; Brockway, B.L.; Drake, J.A.; Reynolds, S.D.; Kaminski, N.; Stripp, B.R. Molecular staging of epithelial maturation using secretory cell-specific genes as markers. *Am. J. Respir. Cell Mol. Biol.* **2009**, *40*, 340–348. [CrossRef]
76. Hashizume, A.; Ueno, T.; Furuse, M.; Tsukita, S.; Nakanishi, Y.; Hieda, Y. Expression patterns of claudin family of tight junction membrane proteins in developing mouse submandibular gland. *Dev. Dyn.* **2004**, *231*, 425–431. [CrossRef]
77. Jakab, C.; Halász, J.; Szasz, A.M.; Batmunkh, E.; Kiss, A.; Schaff, Z.; Rusvai, M.; Galfi, P.; Kulka, J. Expression and localisation of claudin-1,-2,-3,-4,-5,-7 and-10 proteins in the normal canine mammary gland. *Acta Vet. Hung.* **2008**, *56*, 341–352. [CrossRef]
78. Hou, J.; Renigunta, A.; Gomes, A.S.; Hou, M.; Paul, D.L.; Waldegger, S.; Goodenough, D.A. Claudin-16 and claudin-19 interaction is required for their assembly into tight junctions and for renal reabsorption of magnesium. *Proc. Natl. Acad. Sci. USA* **2009**, *106*, 15350–15355. [CrossRef]
79. Milatz, S.; Himmerkus, N.; Wulfmeyer, V.C.; Drewell, H.; Mutig, K.; Hou, J.; Breiderhoff, T.; Muller, D.; Fromm, M.; Bleich, M.; et al. Mosaic expression of claudins in thick ascending limbs of Henle results in spatial separation of paracellular Na^+ and Mg^{2+} transport. *Proc. Natl. Acad. Sci. USA* **2017**, *114*, e219–e227. [CrossRef]
80. Schumann, S.; Buck, V.U.; Classen-Linke, I.; Wennemuth, G.; Grümmer, R. Claudin-3, claudin-7, and claudin-10 show different distribution patterns during decidualization and trophoblast invasion in mouse and human. *Histochem. Cell Biol.* **2015**, *144*, 571–585. [CrossRef]
81. Klar, J.; Piontek, J.; Milatz, S.; Tariq, M.; Jameel, M.; Breiderhoff, T.; Schuster, J.; Fatima, A.; Asif, M.; Sher, M.; et al. Altered paracellular cation permeability due to a rare CLDN10B variant causes anhidrosis and kidney damage. *PLoS Genet.* **2017**, *13*, e1006897. [CrossRef] [PubMed]
82. Meyers, N.; Nelson-Williams, C.; Malaga-Dieguez, L.; Kaufmann, H.; Loring, E.; Knight, J.; Lifton, R.P.; Trachtman, H. Hypokalemia Associated with a Claudin 10 Mutation: A Case Report. *Am. J. Kidney Dis.* **2019**, *73*, 425–428. [CrossRef] [PubMed]
83. Breiderhoff, T.; Himmerkus, N.; Drewell, H.; Plain, A.; Gunzel, D.; Mutig, K.; Willnow, T.E.; Muller, D.; Bleich, M. Deletion of claudin-10 rescues claudin-16-deficient mice from hypomagnesemia and hypercalciuria. *Kidney Int.* **2018**, *93*, 580–588. [CrossRef] [PubMed]
84. Gao, M.; Li, W.; Wang, H.; Wang, G. The distinct expression patterns of claudin-10, -14, -17 and E-cadherin between adjacent non-neoplastic tissues and gastric cancer tissues. *Diagn. Pathol.* **2013**, *8*, 205. [CrossRef] [PubMed]
85. Gong, Y.; Renigunta, V.; Himmerkus, N.; Zhang, J.; Renigunta, A.; Bleich, M.; Hou, J. Claudin-14 regulates renal Ca^{++} transport in response to CaSR signalling via a novel microRNA pathway. *EMBO J.* **2012**, *31*, 1999–2012. [CrossRef] [PubMed]
86. Lee, K.; Ansar, M.; Andrade, P.B.; Khan, B.; Santos-Cortez, R.L.P.; Ahmad, W.; Leal, S.M. Novel CLDN14 mutations in Pakistani families with autosomal recessive non-syndromic hearing loss. *Am. J. Med Genet. Part A* **2012**, *158*, 315–321. [CrossRef]
87. Wattenhofer, M.; Reymond, A.; Falciola, V.; Charollais, A.; Caille, D.; Borel, C.; Lyle, R.; Estivill, X.; Petersen, M.B.; Meda, P.; et al. Different mechanisms preclude mutant CLDN14 proteins from forming tight junctions in vitro. *Hum. Mutat.* **2005**, *25*, 543–549. [CrossRef]

88. Gong, Y.; Hou, J. Claudin-14 underlies Ca(+)(+)-sensing receptor-mediated Ca(+)(+) metabolism via NFAT-microRNA-based mechanisms. *J. Am. Soc. Nephrol.* **2014**, *25*, 745–760. [CrossRef]
89. Pater, J.A.; Benteau, T.; Griffin, A.; Penney, C.; Stanton, S.G.; Predham, S.; Kielley, B.; Squires, J.; Zhou, J.; Li, Q.; et al. A common variant in CLDN14 causes precipitous, prelingual sensorineural hearing loss in multiple families due to founder effect. *Hum. Genet.* **2017**, *136*, 107–118. [CrossRef]
90. Hou, J. Claudins and mineral metabolism. *Curr. Opin. Nephrol. Hypertens.* **2016**, *25*, 308–313. [CrossRef]
91. Bardet, C.; Courson, F.; Wu, Y.; Khaddam, M.; Salmon, B.; Ribes, S.; Thumfart, J.; Yamaguti, P.M.; Rochefort, G.Y.; Figueres, M.L.; et al. Claudin-16 Deficiency Impairs Tight Junction Function in Ameloblasts, Leading to Abnormal Enamel Formation. *J. Bone Miner. Res.* **2016**, *31*, 498–513. [CrossRef] [PubMed]
92. Kriegs, J.O.; Homann, V.; Kinne-Saffran, E.; Kinne, R.K.H. Identification and subcellular localization of paracellin-1 (claudin-16) in human salivary glands. *Histochem. Cell Biol.* **2007**, *128*, 45–53. [CrossRef]
93. Runggaldier, D.; Pradas, L.G.; Neckel, P.H.; Mack, A.F.; Hirt, B.; Gleiser, C. Claudin expression in the rat endolymphatic duct and sac—First insights into regulation of the paracellular barrier by vasopressin. *Sci. Rep.* **2017**, *7*, 45482. [CrossRef] [PubMed]
94. Weber, S.; Schlingmann, K.P.; Peters, M.; Nejsum, L.N.; Nielsen, S.; Engel, H.; Grzeschik, K.H.; Seyberth, H.W.; Gröne, H.J.; Nüsing, R.; et al. Primary gene structure and expression studies of rodent paracellin-1. *J. Am. Soc. Nephrol.* **2001**, *12*, 2664–2672. [PubMed]
95. Rangel, L.B.; Sherman-Baust, C.A.; Wernyj, R.P.; Schwartz, D.R.; Cho, K.R.; Morin, P.J. Characterization of novel human ovarian cancer-specific transcripts (HOSTs) identified by serial analysis of gene expression. *Oncogene* **2003**, *22*, 7225–7232. [CrossRef] [PubMed]
96. Fluge, Ø.; Bruland, O.; Akslen, L.A.; Lillehaug, J.R.; Varhaug, J.E. Gene Expression in Poorly Differentiated Papillary Thyroid Carcinomas. *Thyroid* **2006**, *16*, 161–175.
97. Lee, N.P.; Tong, M.K.; Leung, P.P.; Chan, V.W.; Leung, S.; Tam, P.-C.; Chan, K.-W.; Lee, K.-F.; Yeung, W.S.; Luk, J.M. Kidney claudin-19: Localization in distal tubules and collecting ducts and dysregulation in polycystic renal disease. *FEBS Lett.* **2006**, *580*, 923–931. [CrossRef]
98. Martin, T.A.; Harrison, G.M.; Watkins, G.; Jiang, W.G. Claudin-16 reduces the aggressive behavior of human breast cancer cells. *J. Cell. Biochem.* **2008**, *105*, 41–52. [CrossRef] [PubMed]
99. Simon, D.B.; Lu, Y.; Choate, K.A.; Velazquez, H.; Al-Sabban, E.; Praga, M.; Casari, G.; Bettinelli, A.; Colussi, G.; Rodriguez-Soriano, J.; et al. Paracellin-1, a renal tight junction protein required for paracellular Mg^{2+} resorption. *Science* **1999**, *285*, 103–106. [CrossRef]
100. Hou, J.; Shan, Q.; Wang, T.; Gomes, A.S.; Yan, Q.; Paul, D.L.; Bleich, M.; Goodenough, D.A. Transgenic RNAi Depletion of Claudin-16 and the Renal Handling of Magnesium. *J. Biol. Chem.* **2007**, *282*, 17114–17122. [CrossRef]
101. Kausalya, P.J.; Amasheh, S.; Gunzel, D.; Wurps, H.; Muller, D.; Fromm, M.; Hunziker, W. Disease-associated mutations affect intracellular traffic and paracellular Mg^{2+} transport function of Claudin-16. *J. Clin. Investig.* **2006**, *116*, 878–891. [CrossRef] [PubMed]
102. Ikari, A.; Hirai, N.; Shiroma, M.; Harada, H.; Sakai, H.; Hayashi, H.; Suzuki, Y.; Degawa, M.; Takagi, K. Association of Paracellin-1 with ZO-1 Augments the Reabsorption of Divalent Cations in Renal Epithelial Cells. *J. Biol. Chem.* **2004**, *279*, 54826–54832. [CrossRef] [PubMed]
103. Marunaka, K.; Furukawa, C.; Fujii, N.; Kimura, T.; Furuta, T.; Matsunaga, T.; Endo, S.; Hasegawa, H.; Anzai, N.; Yamazaki, Y.; et al. The RING finger- and PDZ domain-containing protein PDZRN3 controls localization of the Mg(2+) regulator claudin-16 in renal tube epithelial cells. *J. Biol. Chem.* **2017**, *292*, 13034–13044. [CrossRef]
104. Hou, J.; Renigunta, V.; Nie, M.; Sunq, A.; Himmerkus, N.; Quintanova, C.; Bleich, M.; Renigunta, A.; Wolf, M.T.F. Phosphorylated claudin-16 interacts with Trpv5 and regulates transcellular calcium transport in the kidney. *Proc. Natl. Acad. Sci. USA* **2019**, *116*, 19176–19186. [CrossRef] [PubMed]
105. Gimenez-Mascarell, P.; Schirrmacher, C.E.; Martínez-Cruz, L.A.; Muller, D. Novel Aspects of Renal Magnesium Homeostasis. *Front. Pediatr.* **2018**, *6*, 77. [CrossRef]
106. Yamaguti, P.M.; Dos Santos, P.A.C.; Leal, B.S.; Santana, V.B.B.D.M.; Mazzeu, J.F.; Acevedo, A.C.; Neves, F.D.A.R. Identification of the first large deletion in the CLDN16 gene in a patient with FHHNC and late-onset of chronic kidney disease: Case report. *BMC Nephrol.* **2015**, *16*, 92. [CrossRef]

107. Konrad, M.; Hou, J.; Weber, S.; Dötsch, J.; Kari, J.A.; Seeman, T.; Kuwertz-Bröking, E.; Peco-Antic, A.; Tasic, V.; Dittrich, K.; et al. CLDN16 genotype predicts renal decline in familial hypomagnesemia with hypercalciuria and nephrocalcinosis. *J. Am. Soc. Nephrol.* **2008**, *19*, 171–181. [CrossRef]
108. Niimi, T.; Nagashima, K.; Ward, J.M.; Minoo, P.; Zimonjic, D.B.; Popescu, N.C.; Kimura, S. claudin-18, a Novel Downstream Target Gene for the T/EBP/NKX2.1 Homeodomain Transcription Factor, Encodes Lung- and Stomach-Specific Isoforms through Alternative Splicing. *Mol. Cell. Biol.* **2001**, *21*, 7380–7390. [CrossRef]
109. Wolburg, H.; Wolburg-Buchholz, K.; Liebner, S.; Engelhardt, B. Claudin-1, claudin-2 and claudin-11 are present in tight junctions of choroid plexus epithelium of the mouse. *Neurosci. Lett.* **2001**, *307*, 77–80. [CrossRef]
110. Fromm, M.; Piontek, J.; Rosenthal, R.; Gunzel, D.; Krug, S.M. Tight junctions of the proximal tubule and their channel proteins. *Pflüg. Arch.* **2017**, *469*, 877–887. [CrossRef]
111. Gong, Y.; Renigunta, V.; Zhou, Y.; Sunq, A.; Wang, J.; Yang, J.; Renigunta, A.; Baker, L.A.; Hou, J. Biochemical and biophysical analyses of tight junction permeability made of claudin-16 and claudin-19 dimerization. *Mol. Biol. Cell* **2015**, *26*, 4333–4346. [CrossRef] [PubMed]
112. Hou, J.; Renigunta, A.; Konrad, M.; Gomes, A.S.; Schneeberger, E.E.; Paul, D.L.; Waldegger, S.; Goodenough, D.A. Claudin-16 and claudin-19 interact and form a cation-selective tight junction complex. *J. Clin. Investig.* **2008**, *118*, 619–628. [CrossRef] [PubMed]
113. Meier, W.; Blumberg, A.; Imahorn, W.; De Luca, F.; Wildberger, H.; Oetliker, O. Idiopathic hypercalciuria with bilateral macular colobomata: A new variant of oculo-renal syndrome. *Helvetica Paediatr. Acta* **1979**, *34*, 257–269.
114. Rodriguez-Soriano, J.; Vallo, A. Pathophysiology of the renal acidification defect present in the syndrome of familial hypomagnesaemia-hypercalciuria. *Pediatr. Nephrol.* **1994**, *8*, 431–435. [CrossRef] [PubMed]
115. Takahashi, A.; Kondoh, M.; Suzuki, H.; Yagi, K. Claudin as a target for drug development. *Curr. Med. Chem.* **2011**, *18*, 1861–1865. [CrossRef] [PubMed]
116. Pawar, A.S.; Thongprayoon, C.; Cheungpasitporn, W.; Sakhuja, A.; Mao, M.A.; Erickson, S.B. Incidence and characteristics of kidney stones in patients with horseshoe kidney: A systematic review and meta-analysis. *Urol. Ann.* **2018**, *10*, 87–93.
117. Alelign, T.; Petros, B. Kidney Stone Disease: An Update on Current Concepts. *Adv. Urol.* **2018**, *2018*, 3068365. [CrossRef]

International Journal of
Molecular Sciences

MDPI

Article

Intestinal Preservation Injury: A Comparison Between Rat, Porcine and Human Intestines

John Mackay Søfteland [1,2], Anna Casselbrant [3], Ali-Reza Biglarnia [4], Johan Linders [4], Mats Hellström [2], Antonio Pesce [5], Arvind Manikantan Padma [2], Lucian Petru Jiga [6], Bogdan Hoinoiu [7], Mihai Ionac [7] and Mihai Oltean [1,2,*]

1 The Transplant Institute, Sahlgrenska University Hospital, 413 45 Gothenburg, Sweden
2 Laboratory for Transplantation and Regenerative Medicine, Institute of Clinical Sciences, Sahlgrenska Academy at the University of Gothenburg, Sahlgrenska Science Park Medicinaregatan 8, 413 90 Gothenburg, Sweden
3 Department of Gastrosurgical Research and Education, Institute of Clinical Sciences, Sahlgrenska Academy at the University of Gothenburg, Sahlgrenska University Hospital, 41345 Gothenburg, Sweden
4 Department of Transplantation, Skåne University Hospital, 205 02 Malmö, Sweden
5 Department of Medical and Surgical Sciences and Advanced Technologies, University of Catania, Via Santa Sofia 86, 95123 Catania, Italy
6 Department for Plastic, Aesthetic, Reconstructive and Hand Surgery, Evangelisches Krankenhaus Oldenburg, Medical Campus University of Oldenburg, Steinweg 13–17, 26122 Oldenburg, Germany
7 Pius Branzeu Center for Laparoscopic Surgery and Microsurgery, University of Medicine and Pharmacy, P-ta. E. Murgu 2, 300041 Timisoara, Romania
* Correspondence: mihai.oltean@surgery.gu.se; Tel.: +46-704-906-156

Received: 21 June 2019; Accepted: 25 June 2019; Published: 27 June 2019

Abstract: Advanced preservation injury (PI) after intestinal transplantation has deleterious short- and long-term effects and constitutes a major research topic. Logistics and costs favor rodent studies, whereas clinical translation mandates studies in larger animals or using human material. Despite diverging reports, no direct comparison between the development of intestinal PI in rats, pigs, and humans is available. We compared the development of PI in rat, porcine, and human intestines. Intestinal procurement and cold storage (CS) using histidine–tryptophan–ketoglutarate solution was performed in rats, pigs, and humans. Tissue samples were obtained after 8, 14, and 24 h of CS), and PI was assessed morphologically and at the molecular level (cleaved caspase-3, zonula occludens, claudin-3 and 4, tricellulin, occludin, cytokeratin-8) using immunohistochemistry and Western blot. Intestinal PI developed slower in pigs compared to rats and humans. Tissue injury and apoptosis were significantly higher in rats. Tight junction proteins showed quantitative and qualitative changes differing between species. Significant interspecies differences exist between rats, pigs, and humans regarding intestinal PI progression at tissue and molecular levels. These differences should be taken into account both with regards to study design and the interpretation of findings when relating them to the clinical setting.

Keywords: tight junctions; organ preservation; intestine; transplantation; ischemia; intestinal mucosa

1. Introduction

Intestinal transplantation is the established therapeutic alternative in patients with complicated intestinal failure, with results continuously improving over the last two decades [1]. However, the post-transplant course is frequently marred by life-threatening complications due to ischemia–reperfusion injury (IRI), immunosuppression, and acute rejection, and patient management remains challenging [2–4]. Hence, further translational research is warranted to develop novel

strategies to alleviate IRI, identify noninvasive biomarkers of rejection, and test alternative immunosuppressive strategies.

Intestinal grafts withstand the shortest cold storage (CS) period of all abdominal organs. In the clinical setting, CS is kept below ten hours due to concerns of mucosal sloughing and epithelial barrier breakdown, which may favor bacterial translocation and graft edema [5,6]. Numerous experimental approaches targeting the preservation injury have been tested in rats [7], but virtually none have been implemented clinically due to the lack of consistent evidence, including preclinical safety studies.

Rats have the advantage of simpler logistics, lower costs, and a relatively straightforward surgical procedure. Rat models have provided valuable insights into the physiology, immunology, and pathology of the transplanted intestine [8,9]. Nonetheless, anatomical, physiological, and immunological differences prevent the direct translation of many findings into clinical practice, and pigs are frequently used as a preclinical model to confirm the results of small animal studies [10–13]. Pigs share numerous anatomical and physiological similarities with humans, are easily accessible and affordable, and their use as livestock animals relieves some ethical concerns.

In spite of their use in intestinal preservation research, no direct comparison exists between rat and porcine intestines, to link the abundant data from rodents with this important preclinical model. To our knowledge, the extent to which the results obtained using porcine or rat intestines apply to the human intestine also remains unclear. Hence, it is unclear if and how the sequence and speed of development of the cellular and molecular alterations in rodents resemble the ones described in pigs and how this wealth of experimental data ultimately compares to the clinical setting. In this study, we set out to compare the development of the intestinal preservation injury in rats, pigs, and humans under similar conditions of procurement and CS.

2. Results

2.1. Histology

Intestinal CS induced the typical subepithelial lifting and edema in the vast majority of samples irrespective of species but the extent and speed of development of the subepithelial cleft revealed differences between species. Rat intestines developed significant subepithelial edema and even epithelial shedding (median Chiu/Park score 3) already after eight hours of CS, whereas the porcine intestines showed significantly lower injury score and mild edema or even normal histology (median Chiu/Park score 1) ($p < 0.001$). At the same time-point, human intestines exhibited mild or moderate subepithelial edema (median score 3)—a lesser injury than in rats ($p = 0.04$), but higher than in pigs ($p = 0.02$) (Figure 1A).

At both latter time-points, rat intestines showed a significantly more severe mucosal injury compared to porcine intestines; human intestines revealed significantly worse morphology compared to pigs after 24 h ($p < 0.01$). A particular feature in the porcine and human intestines was the significant lifting of the mucosa from the muscular layer (submucosal edema), a feature not present in the rat intestines.

Throughout the study, goblet cell (GC) counts indicated different patterns between the three species. Control rat intestine had significantly more GC than pig ileum (148 ± 28 vs 71 ± 23, $p < 0.05$). In rat and human intestines, CS induced a decrease in mucus-filled GC on the villi, which became significant after 14 h, whereas the amount of GC in porcine intestines did not differ significantly from the baseline throughout the entire experiment (Figure 1B).

Normal pig intestines had significantly higher enterocyte density and significantly fewer polymorphonuclear neutrophils (PMN) in the villi compared to rat and human intestines (Figure 2).

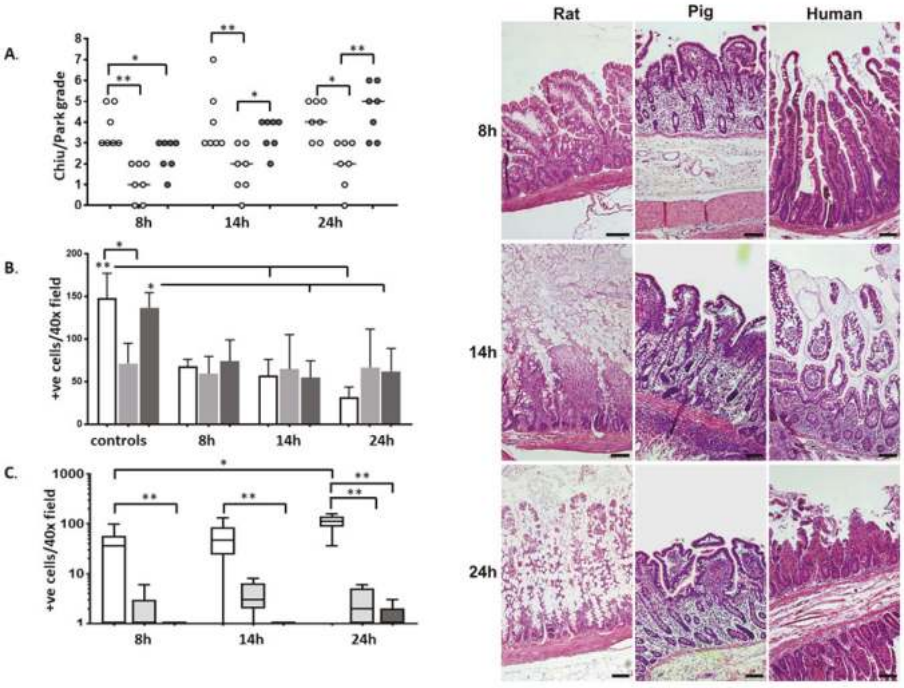

Figure 1. Light microscopy of rat (white), pig (light grey), and human (dark grey) intestines after different periods of cold storage (CS). (**A**) Summary of the tissue injury (Chiu score) induced by CS with each dot representing one individual ($n = 7$) and the bar showing the median value; (**B**) goblet cell count; (**C**) enterocyte apoptosis quantified by caspase-3 positive cells (box plot showing the median, 5–95th percentile, and lowest and highest values at each time point). * $p < 0.05$, ** $p < 0.01$. A large number of apoptotic enterocytes (positive for active caspase-3) were found in rat intestines after 8 h of CS. Rat intestines had more apoptotic enterocytes than human intestines at all time points (Figure 1C). Right: representative microphotographs from each species at each of the three time-points (hematoxillin eosin stain, original magnification ×100, scale bar 100 microns).

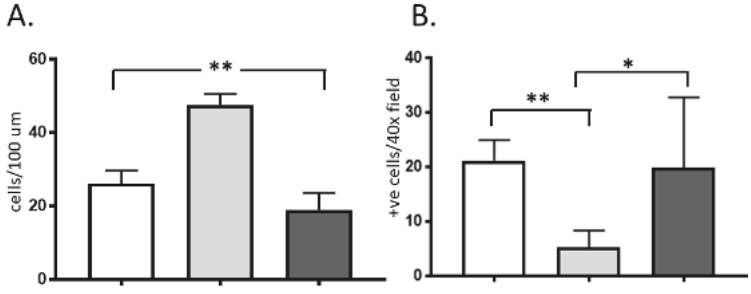

Figure 2. Enterocyte (**A**) and polymorphonuclear (PMN) leukocyte (**B**) counts in rat, (white bar) pig (light grey), and human (dark grey) intestines ($n = 7$). Enterocytes were counted using 4′,6-diamidino-2-phenylindole (DAPI) staining on the sides of longitudinally oriented villi on several 100 μm segments; PMNs were counted in villi on ten random fields at high magnification (×400) (data shown as mean ± SD). * $p < 0.05$, ** $p < 0.01$.

2.2. Immunohistochemistry

In all three species, zonula occludens (ZO)-1 was detected as an intense, thin fluorescent signal at the apical tips of the basolateral membrane, from the crypts to the tip of the villi. Whereas ZO-1 staining in rats and humans frequently appeared like a line or large dots, ZO-1 staining in pigs often had the appearance of a dotted line or small dots (probably due to a narrower apical membrane and higher cellularity). Claudin-3 was visualized as a thin, reticular signal along the entire basolateral membrane. Claudin-3 frequently colocalized with ZO-1 in an area corresponding to the apical edge of the basolateral membrane (data not shown).

After eight hours of CS, ZO-1 staining became absent or discontinuous at the tip of some villi in rat intestines but overall it was maintained along the entire villus (Figure 3). Pig and human intestines revealed a strong immunosignal along the entire contour of the villi. In rats, claudin-3 staining was found between enterocytes but showed a widespread de-colocalization from ZO-1 as well as some cytoplasmic staining. Both pig and human showed strong claudin-3 staining as a sharp, reticular fluorescence signal along the entire basolateral membrane (Figure S1).

In rats, fourteen hours of CS led to a marked decrease in the ZO-1 immunostaining, which was preserved only towards the base of the villi and in the crypts. Porcine and human intestines continued, however, to show unchanged, well-preserved ZO-1 expression along the villus. Claudin-3 staining between enterocytes became more diffuse while cytoplasmic staining was also noted. Overall, the staining pattern remained thin and fibrillar but with a tendency towards less sharp, diffuse membrane staining and cytoplasmic staining. Stronger subjunctional intensity was also noted in some samples.

After 24 h, all rat intestines completely lacked villus staining for ZO-1, while both porcine and human continued to show immunofluorescent staining frequently reaching villus tips. In both pig and human intestines, claudin-3 revealed more diffuse, discontinuous staining along the basolateral membrane with an obvious subjunctional staining gradient.

2.3. Western Blot Analysis

All proteins analyzed by Western blot were detected in rat, pig, and human samples. Generally, all proteins studied were found to have the lowest expression in the rat small intestine. After eight hours of CS, the expression of claudin-3, claudin-4, tricellulin, and ZO-1 was significantly higher in human samples compared to rat samples. This difference persisted after fourteen and 24 h for claudin-4 but subsided for claudin-3, tricellulin, and ZO-1.

In four out of six tight junction (TJ) proteins studied (occludin, tricellulin, claudin-3, ZO-1) no differences between species were found after 14 h and 24 h of CS.

Pig tissue expressed more occludin at eight hours as well as more Ck8 protein at all time points compared to rats (Figure 4).

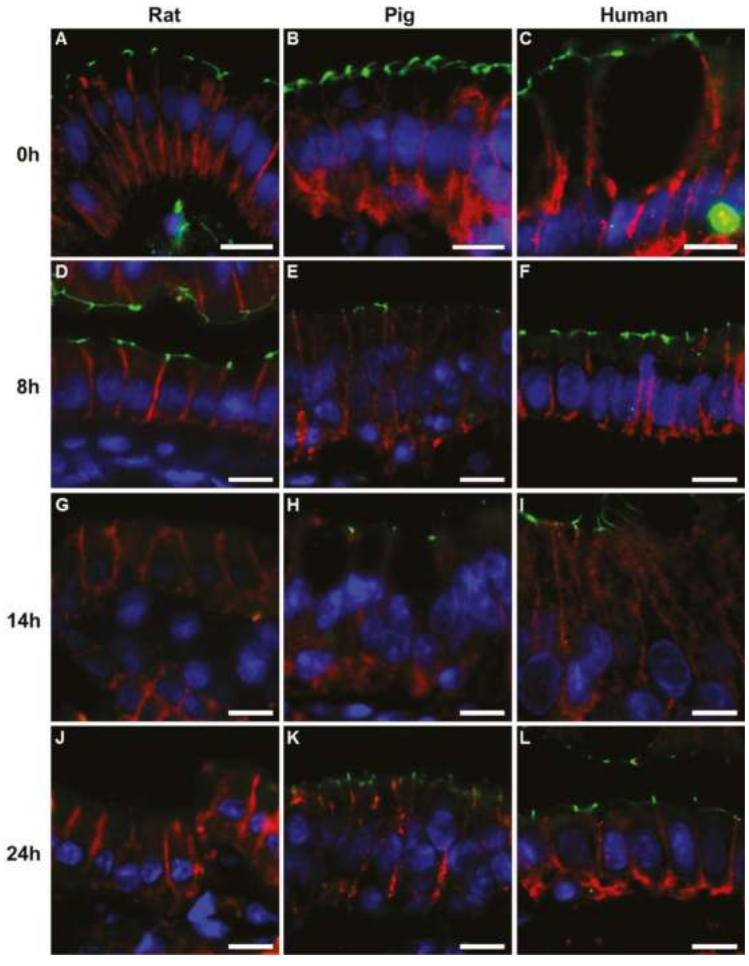

Figure 3. Immunofluorescent staining for zonula occludens (ZO)-1 (green) and claudin-3 (red) after various periods of cold storage (CS); strong immunofluorescent signal for both proteins after 8 h CS in rat (**A**), pig (**B**), and human intestine (**C**); after 14 h, ZO-1 signal was lost in rat (**D**) but not pig (**E**) or human (**F**) intestinal mucosa; after 24 h (**J**–**L**) of CS, ZO-1 staining was absent and claudin-3 revealed diffuse membrane staining and cytoplasmic staining in rat intestines (**G**), while in pig (**H**) and human (**I**) intestines, ZO-1 signal was maintained and claudin-3 stained more diffuse, stronger on the subjunctional basolateral membrane, together with some cytoplasmic staining. Nuclei were stained blue using 4′,6-diamidino-2-phenylindole (DAPI). Images were acquired from areas where enterocytes still remained attached to the lamina propria and as close to the villus tip as possible. Original magnification ×400, scale bar, 10 μm.

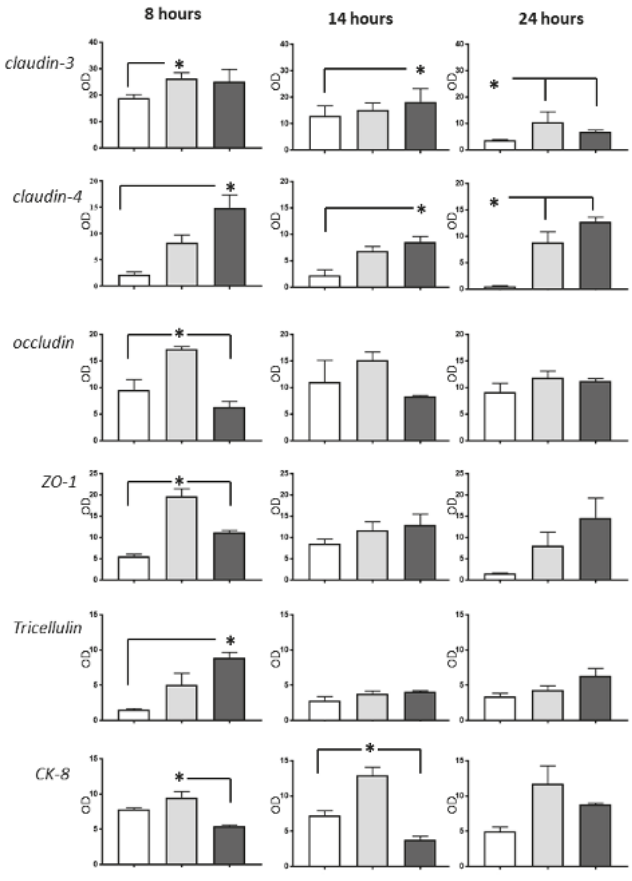

Figure 4. Western blot analysis of several junctional proteins and cytokeratin (CK)-8 in rat (white bars), pig (light grey bars), and human (dark grey bars) intestines after different periods of cold storage. Samples (15 µg) from the three species from the same time-point were run simultaneously (n = 3–4). Results (mean ± standard error) were normalized to glyceraldehyde-3-phosphate dehydrogenase and presented as semiquantitative results (optical density, OD); * $p < 0.05$.

3. Discussion

Ischemia–reperfusion injury remains a major concern after intestinal transplantation as tissue damage may favor bacterial translocation and sepsis, anastomotic leaks, and intestinal graft edema with risk for abdominal compartment syndrome [2]. Moreover, an advanced ischemic injury may promote the later occurrence of graft fibrosis and graft dysmotility [14]. The susceptibility of the intestine to ischemic injury and the life-threatening complications it may lead to, continues to mandate a search for protective and therapeutic interventions.

Although some studies infer a higher resilience of porcine intestines towards intestinal ischemia as compared to rats [15–17], to our knowledge this is the first direct comparison between these species. The sequential evaluation of the intestinal preservation injury in this study found a substantially different pattern of changes in human intestines compared with rats and pigs, both regarding the time course and the type of tissue damage. Rat and human intestines developed significant mucosal changes already after eight hours of CS whereas porcine intestines revealed near-normal epithelium

after the same time span. Conversely, both the human and porcine intestines developed significant submucosal edema, a feature not observed in rodents.

Goblet cells are critical for the integrity and repair of the intestinal epithelium and are considered a good marker of intestinal health [18]. GC mucus depletion occurs rapidly after the onset of intestinal ischemia [19]. In rats and humans, goblet cell count decreased during the CS compared to normal tissue, whereas this phenomenon was absent in the porcine ileum, which revealed a stable GC number throughout the experiment. Interestingly, control porcine tissue had less GC compared to both rats and humans. It is unclear whether this finding is intrinsic to (juvenile) pigs or it is the result of preoperative fasting as a decrease in amount and mucus content of GC count have been reported early and after fasting or weaning and in malnourished piglets [20]. Notably, the initial GC count seemed higher in the human intestines, while it is likely that the human organ donors did not receive any enteral nutrition during the day preceding the organ procurement either.

Pigs developed mucosal alterations at the later time points compared to humans and rats. For example, the epithelial lesion recorded after 24 h (massive epithelial lifting, grade 3) in the pig intestines usually occurred between 8 and 14 h of CS in rat and human intestines. Part of the explanation for these interspecies differences may be the higher mucosal cellularity in pigs, leading to a higher TJ density. The lesser amount of tissue PMNs in pigs may also play a role as the hypoxic, stressed leukocytes could release its lytic enzymes in the surrounding tissue already before reperfusion [21,22]. The practical consequence of this finding is that preservation studies using pig intestines would require longer CS periods than in rats to attain a significant tissue injury. When designing experimental studies that mimic the human situation it may be prudent to adjust the ischemia time required to create a comparable injury to reflect the interspecies differences.

Caspase-3 activation and increased apoptosis has been reported earlier following CS of rat kidneys, livers, and intestines [23–26]. Similarly, we found abundant active caspase-3 in rat intestines; however, caspase-3 positive pig or human enterocytes were significantly fewer. This intriguing finding is difficult to explain considering that humans had very few caspase-3 positive enterocytes but it may also reflect interspecies differences. In another study, under similar conditions (60 min of intestinal ischemia and 120 min of reperfusion) 75% of rat Paneth cells entered apoptosis, whereas only 25% of the human Paneth cells were found apoptotic [27].

Ischemia and ATP depletion disrupt the actin cytoskeleton in various types of cells and tissues [28,29]. The actin cytoskeleton plays essential roles in the functional and structural integrity of the cells, including the structure and function of tight junctions. Thus, one suggested mechanism behind the TJ dysfunction is the strain on the TJs by the neighboring, contracting cells. Internalization of TJ proteins and TJ disassembly have been shown to occur rapidly after various stimuli, followed by TJ dysfunction and increased permeability [30]. Earlier studies revealed quantitative TJ protein changes during intestinal ischemia [31] yet the qualitative changes (i.e., cytoplasmic shift, altered membrane staining pattern) revealed by the immunofluorescence claudin-3 staining may be equally relevant. Herein, the progress of injury seems to have coincided with the occurrence of significant qualitative and quantitative alterations in claudin expression (particularly the TJ-sealing protein, claudin-3), whereas the expression of ZO-1 seems to have limited importance for injury development. In addition, it is tempting to speculate that the rapid TJ-protein alterations in the non-fasted rats, particularly tricellulin and ZO-1, may be also due to the mucosal exposure to the aggressive intestinal chyle containing bile acids, pancreatic enzymes combined with the depletion of the protective CG and mucus layer.

An advantage of the current study is the systematic use of distal small intestine. The different digestive functions of the various intestinal segments are also reflected in the varying content of different junctional proteins [32]. Hence, we minimized the differences between different anatomical areas as responsible for the differences noted between various junctional proteins in different species. An inherent drawback of the study was the use of human intestines from brain dead organ donors. This setting was both necessary and relevant as it mirrored the clinical situation of intestinal procurement and preservation for transplantation. Nonetheless, this may have induced additional changes and

differences compared to the young, healthy animals, as brain death induces both local and systemic inflammatory processes [33,34]. The relatively short period of brain death customarily encountered in Sweden may have limited the effect of donor inflammation on the intestine. Besides brain death, organ donors may also have been subjected to hemodynamic instability, cardiac arrest, trauma, or medical interventions (vasopressors, fluid resuscitation) that may potentially have affected the intestine. Whereas some of these factors were present in our human tissue donors, these factors not always preclude intestinal donation [35]. Discordant age between study subjects (young animals vs middle-aged organ donors) could also be regarded as another limitation. Though the current practice usually restricts the use of intestinal donors older than 50 [36], the impact of age on the development of intestinal preservation injury is yet unknown. Last but not least, the antibodies used in the study may have different affinity to different species. This implies that a higher protein expression detected on the Western blot does not always reflect its real tissue expression but rather shows the antibody–antigen affinity, which may differ between species.

In conclusion, this report provides the first direct comparison of the development of intestinal preservation injury in the rat, pig, and human at histological and molecular levels. The current results suggest that porcine intestines have a slower development of the tissue injury compared to human intestines, while rat intestines appear to have a faster injury development. These differences should be taken into account when designing experimental studies to allow meaningful endpoints and results.

4. Materials and Methods

4.1. Animals, Surgery, and Sampling

Male, Sprague–Dawley rats (n = 7) aged around 3 months were purchased from Charles River (Sulzfeld, Germany), housed in the University animal quarters, and acclimatized for one week. The rats received rat chow and water ad libitum and were not fasted before surgery. The study followed the regulations outlined by the European Union (2010/63/EU) and was reviewed and approved by the Gothenburg committee of the Swedish Animal Welfare Agency (#135/07). Under 2.5% isoflurane anesthesia, the small intestine was perfused with and stored in ice-cold histidine–tryptophan–ketoglutarate solution (HTK, Custodiol®, Fresenius Kohler Chemie GmbH, Alsbach-Hähnlein, Germany) as described earlier [15]. The distal half (ileum) was resected and its ends were tightly ligated using silk 3/0. After 8 h, 14 h, and 24 h of CS 3 cm segments of ileum were sampled and stored in 4% buffered formalin or snap frozen.

Landrace pigs of either sex (n = 7), weighing around 30 kg were purchased from a commercial supplier and housed individually at the Pius Branzeu Center in Timisoara. Animals were acclimatized for one week, fed once daily with standard pig diet and provided with water ad libitum. Food was withdrawn 24 h before surgery but animals' unrestricted access to water was maintained. All experiments were reviewed and approved by the Ethics and Deontology Committee for Research on Animals of the University of Medicine and Pharmacy, Timisoara, Romania (13008/9 May 2013). Following premedication with ketamine (20 mg/kg; Pfizer Pharma GmbH, Germany), xylazine (2 mg/kg), and atropine (0.05 mg/kg), pigs were intubated and ventilated using a mixture of isoflurane and oxygen. Using a previously described approach [16] and following perfusion with 1.5 L HTK solution, the complete small intestine was then excised. In an ice basin on a backtable, the last meter of the ileum was resected, placed in ice-cold HTK solution, and sampled after 8 h, 14 h, and 24 h of CS. Samples were stored in 4% buffered formalin or snap frozen.

4.2. Human Organ Donors

Ileal segments were obtained from seven deceased brain dead (DBD) multiorgan donors with an intensive care unit stay of less than four days. Donor median age was 48 years (range 14–63) (additional donor information is provided in Table S1). The donors (or next of kin) previously consented for tissue

use for medical research. The use of human tissue in the study was reviewed and approved by the regional ethical review committee (Dnr 204-17).

Organ retrieval was performed in the standard fashion using retrograde aortic perfusion with HTK solution and venous venting through the inferior vena cava. One meter of the distal small intestine (ileum) was resected immediately after the organ perfusion with HTK (3–8 L) and before any other organ was removed. Bowel ends were stapled off and the specimen was placed in an organ bag with cold HTK on ice. After 8 h, 14 h, and 24 h of CS a 10–15 cm ileal segment was removed with a stapler and samples were either placed in 4% formalin or snap frozen.

4.3. Histology

4.3.1. Light Microscopy

Formalin-fixed tissue was paraffinized, embedded, and cut into five-micron sections. Sections were stained with hematoxylin and eosin, and intestinal preservation injury was scored blinded by two experienced observers using the Chiu/Park score [37] on seven fields from three different sections.

Mucus-filled goblet cells (GCs) in the intestinal villi were stained using Alcian Blue staining and counted in ten random fields at high magnification (×400) by a single observer blinded to the study design.

Apoptosis was studied on paraffin sections using immunostaining for active (cleaved) caspase-3 using a Warp Red Chromogen kit (Bio-Care Medical, Concord, CA) according to the manufacturer's instructions. Briefly, after deparaffinization, rehydration, and antigen retrieval using citrate buffer (10 mM, pH 6.0), sections were blocked and then incubated with primary rabbit antibody against cleaved caspase-3 (1:100, #D175; Cell Signaling Technology, Danvers, MA) for 1 h at room temperature followed by incubation with an anti-rabbit probe, a rabbit alkaline phosphatase polymer and warp red chromogen. Nuclei were stained using Myers hematoxylin. Positively labeled enterocytes were counted on ten random fields at high magnification (×400) by a single observer. Polymorphonuclear neutrophils (PMN) were stained using the Naphtol AS-D chloroacetate esterase kit (Sigma Chemicals, St Louis, Mo) and counted in the villi on ten random fields at high magnification (×400).

4.3.2. Immunofluorescence

Paraffin sections were deparaffinized and rehydrated, then antigen retrieval was performed (citrate buffer). After species-specific blocking, slides were incubated overnight at 4 °C with antibodies against zonula occludens (ZO-1; 1:100, Invitrogen AB, Lidingö, Sweden) and claudin-3 (1:100; Abcam, UK). Thereafter, slides were incubated with secondary antibody conjugated with Alexa 488 and Alexa 594 (1:200; Invitrogen). The sections were counterstained with 4'6'-diamidino-2-phenylindole, mounted with aqueous mounting medium (Vector Laboratories, Burlingame, CA, USA), and examined by fluorescence microscopy (Leica). Nuclei on the villi were also counted. Image acquisition and processing were performed using the Leica LAS software.

4.3.3. Western Blot Analyses of Intestinal Mucosa

Western blot protein analysis was performed using whole tissue frozen specimens as described earlier [15). In brief, after electrophoresis and protein transfer on poly-vinyl-difluoride membranes, the membranes were blocked, then incubated overnight at 4 °C with primary antibody against claudin-3 (34-1700, Invitrogen AB, Lidingö, Sweden), claudin-4 (32-9400, Invitrogen AB), tricellulin (48-8400, Invitrogen AB), cytokeratin-8 (ab53708, Abcam, Cambridge, UK), ZO-1 (33-9100, Invitrogen AB), occludin (71-1500, Invitrogen AB), and the loading control glyceraldehyde-3-phosphate dehydrogenase (GAPDH, IMG-5143A, Imgenex, San Diego, CA). After repeated washings, a secondary antibody was applied for 1 h at room temperature and visualization was carried out using the chemoluminescent enzyme substrate CDP-Star (Tropix, Bedford, MA). The signal intensities of specific bands were detected and analyzed using a Chemidox XRS cooled charge-couple device camera and Quantity One

software (BioRad Laboratories, Hercules, CA). GAPDH was used as loading control. For each sample, the optical density of primary antibody was normalized to GAPDH. Before re-probing with a new primary antibody, the membranes were incubated with stripping buffer (Re-Blot Plus Mild Solution 10×, Millipore, Temecula, CA, USA).

4.4. Statistical Analysis

Nonparametric methods were used for statistical comparisons. Statistical differences between independent groups were calculated using the Kruskal–Wallis test corrected for multiple comparisons using the Tukey test, followed by the Mann–Whitney U test (GraphPad Prism6; GraphPad Software, La Jolla, CA). Data are presented as median (range) unless otherwise stated. Results were considered as statistically significant at $p < 0.05$.

Supplementary Materials: Supplementary materials can be found at http://www.mdpi.com/1422-0067/20/13/3135/s1.

Author Contributions: Conceptualization: J.M.S., A.C., and M.O.; Methodology: J.M.S., A.C., M.H., A.P., A.-R.B., J.L., L.P.J., B.H., M.I., A.M.P., and M.O.; Formal Analysis: J.M.S., A.C., A.P., and M.O.; Writing—Original Draft Preparation: J.M.S., A.C., M.H., and M.O.; Writing—Review and Editing: A.P., A.-R.B., J.L., L.P.J., B.H., M.I., and A.M.P.; Funding Acquisition—M.O. and B.H.

Funding: Funding for this study was provided by grants from the Swedish state under the agreement between the Swedish government and the country councils (grants ALFGBG-695931 and ALFGBG-812881) as well as grant PNIIRU-TE-2012-3-0430 from the Executive Agency for Higher Education, Research, Development, and Innovation Funding (Romania) (both to M.O.).

Conflicts of Interest: The authors declare no conflict of interest.

References

1. Abu-Elmagd, K.M.; Costa, G.; Bond, G.J.; Soltys, K.; Sindhi, R.; Wu, T.; Koritsky, D.A.; Schuster, B.; Martin, L.; Cruz, R.J.; et al. Five hundred intestinal and multivisceral transplantations at a single center: Major advances with new challenges. *Ann. Surg.* **2009**, *250*, 567–581. [CrossRef] [PubMed]
2. Clouse, J.W.; Kubal, C.A.; Fridell, J.A.; Mangus, R.S. Posttransplant complications in adult recipients of intestine grafts without bowel decontamination. *J. Surg. Res.* **2018**, *225*, 125–130. [CrossRef] [PubMed]
3. Huard, G.; Schiano, T.D.; Moon, J.; Iyer, K. Severe acute cellular rejection after intestinal transplantation is associated with poor patient and graft survival. *Clin. Transplant.* **2017**, *31*. [CrossRef] [PubMed]
4. Varkey, J.; Simrén, M.; Jalanko, H.; Oltean, M.; Saalman, R.; Gudjonsdottir, A.; Gäbel, M.; Borg, H.; Edenholm, M.; Bentdal, O.; et al. Fifteen years' experience of intestinal and multivisceral transplantation in the Nordic countries. *Scand J. Gastroenterol.* **2015**, *50*, 278–290. [CrossRef] [PubMed]
5. Tesi, R.J.; Jaffe, B.M.; McBride, V.; Haque, S. Histopathologic changes in human small intestine during storage in Viaspan organ preservation solution. *Arch. Pathol. Lab. Med.* **1997**, *121*, 714. [PubMed]
6. deRoover, A.; de Leval, L.; Gilmaire, J.; Detry, O.; Boniver, J.; Honoré, P.; Meurisse, M. A new model for human intestinal preservation: Comparison of University of Wisconsin and Celsior preservation solutions. *Transplant. Proc.* **2004**, *36*, 270–272. [CrossRef] [PubMed]
7. Oltean, M.; Churchill, T.A. Organ-specific solutions and strategies for the intestinal preservation. *Int. Rev. Immunol.* **2014**, *33*, 234–244. [CrossRef] [PubMed]
8. Grant, D.; Hurlbut, D.; Zhong, R.; Wang, P.Z.; Chen, H.F.; Garcia, B.; Behme, R.; Stiller, C.; Duff, J. Intestinal permeability and bacterial translocation following small bowel transplantation in the rat. *Transplantation* **1991**, *52*, 221–224. [CrossRef] [PubMed]
9. Oltean, M.; Zhu, C.; Mera, S.; Pullerits, R.; Mattsby-Baltzer, I.; Mölne, J.; Hallberg, E.; Blomgren, K.; Olausson, M. Reduced liver injury and cytokine release after transplantation of preconditioned intestines. *J. Surg. Res.* **2009**, *154*, 30–37. [CrossRef] [PubMed]
10. Grant, D.; Duff, J.; Zhong, R.; Garcia, B.; Lipohar, C.; Keown, P.; Stiller, C. Successful intestinal transplantation in pigs treated with cyclosporine. *Transplantation* **1988**, *45*, 279–284. [CrossRef]

11. Pirenne, J.; Benedetti, E.; Gruessner, A.; Moon, C.; Hakim, N.; Fryer, J.P.; Troppmann, C.; Nakhleh, R.E.; Gruessner, R.W. Combined transplantation of small and large bowel. FK506 versus cyclosporine A in a porcine model. *Transplantation* **1996**, *61*, 1685–1694. [CrossRef] [PubMed]
12. Pakarinen, M.P.; Kuusanmäki, P.; Lauronen, J.; Paavonen, T.; Halttunen, J. Effects of ileum transplantation and chronic rejection on absorption and synthesis of cholesterol in pigs. *Pediatr. Surg. Int.* **2003**, *19*, 656–661. [CrossRef] [PubMed]
13. Weih, S.; Kessler, M.; Fonouni, H.; Golriz, M.; Nickkholgh, A.; Schmidt, J.; Holland-Cunz, S.; Mehrabi, A. Review of various techniques of small bowel transplantation in pigs. *J. Surg. Res.* **2011**, *171*, 709–718. [CrossRef] [PubMed]
14. Schaefer, N.; Tahara, K.; Schuchtrup, S.; Websky, M.V.; Overhaus, M.; Schmidt, J.; Wirz, S.; Abu-Elmagd, K.M.; Kalff, J.C.; Hirner, A.; et al. Perioperative glycine treatment attenuates ischemia/reperfusion injury and ameliorates smooth muscle dysfunction in intestinal transplantation. *Transplantation* **2008**, *85*, 1300–1310. [CrossRef] [PubMed]
15. Oltean, M.; Joshi, M.; Björkman, E.; Oltean, S.; Casselbrant, A.; Herlenius, G.; Olausson, M. Intraluminal polyethylene glycol stabilizes tight junctions and improves intestinal preservation in the rat. *Am. J. Transplant* **2012**, *12*, 2044–2051. [CrossRef]
16. Oltean, M.; Jiga, L.; Hellström, M.; Söfteland, J.; Papurica, M.; Hoinoiu, T.; Ionac, M.; Casselbrant, A. A sequential assessment of the preservation injury in porcine intestines. *J. Surg. Res.* **2017**, *216*, 149–157. [CrossRef] [PubMed]
17. Blikslager, A.T.; Roberts, M.C.; Rhoads, J.M.; Argenzio, R.A. Is reperfusion injury an important cause of mucosal damage after porcine intestinal ischemia? *Surgery* **1997**, *121*, 526–534. [CrossRef]
18. Ikeda, H.; Yang, C.L.; Tong, J.; Nishimaki, H.; Masuda, K.; Takeo, T.; Kasai, K.; Itoh, G. Rat small intestinal goblet cell kinetics in the process of restitution of surface epithelium subjected to ischemia-reperfusion injury. *Dig. Dis. Sci.* **2002**, *47*, 590–601. [CrossRef] [PubMed]
19. Grootjans, J.; Hundscheid, I.H.; Lenaerts, K.; Boonen, B.; Renes, I.B.; Verheyen, F.K.; Dejong, C.H.; von Meyenfeldt, M.F.; Beets, G.L.; Buurman, W.A. Ischaemia-induced mucus barrier loss and bacterial penetration are rapidly counteracted by increased goblet cell secretory activity in human and rat colon. *Gut* **2013**, *62*, 250–258. [CrossRef]
20. Lopez-Pedrosa, J.M.; Torres, M.I.; Fernández, M.I.; Ríos, A.; Gil, A. Severe malnutrition alters lipid composition and fatty acid profile of small intestine in newborn piglets. *J Nutr.* **1998**, *128*, 224–233. [CrossRef]
21. Kubes, P.; Hunter, J.; Granger, D.N. Ischemia/reperfusion-induced feline intestinal dysfunction: Importance of granulocyte recruitment. *Gastroenterology* **1992**, *103*, 807–812. [CrossRef]
22. Dabrowska, D.; Jablonska, E.; Iwaniuk, A.; Garley, M. Many ways–one destination: Different types of neutrophils death. *Int. Rev. Immunol.* **2019**, *38*, 18–32. [CrossRef] [PubMed]
23. Kohli, V.; Selzner, M.; Madden, J.F.; Bentley, R.C.; Clavien, P.A. Endothelial cell and hepatocyte deaths occur by apoptosis after ischemia-reperfusion injury in the rat liver. *Transplantation* **1999**, *67*, 1099–1105. [CrossRef] [PubMed]
24. Jani, A.; Ljubanovic, D.; Faubel, S.; Kim, J.; Mischak, R.; Edelstein, C.L. Caspase inhibition prevents the increase in caspase-3, -2, -8 and -9 activity and apoptosis in the cold ischemic mouse kidney. *Am. J. Transplant* **2004**, *4*, 1246–1254. [CrossRef] [PubMed]
25. Oltean, M.; Hellström, M.; Ciuce, C.; Zhu, C.; Casselbrant, A. Luminal solutions protect mucosal barrier during extended preservation. *J. Surg. Res.* **2015**, *194*, 289–296. [CrossRef] [PubMed]
26. Casselbrant, A.; Söfteland, J.M.; Hellström, M.; Malinauskas, M.; Oltean, M. Luminal polyethylene glycol alleviates intestinal preservation injury irrespective of molecular size. *J. Pharmacol. Exp. Ther.* **2018**, *366*, 29–36. [CrossRef] [PubMed]
27. Grootjans, J.; Hodin, C.M.; de Haan, J.J.; Derikx, J.P.; Rouschop, K.M.; Verheyen, F.K.; van Dam, R.M.; Dejong, C.H.; Buurman, W.A.; Lenaerts, K. Level of activation of the unfolded protein response correlates with Paneth cell apoptosis in human small intestine exposed to ischemia/reperfusion. *Gastroenterology* **2011**, *140*, 529–539. [CrossRef]
28. Kwon, O.; Phillips, C.L.; Molitoris, B.A. Ischemia induces alterations in actin filaments in renal vascular smooth muscle cells. *Am. J. Physiol. Renal. Physiol.* **2002**, *282*, F1012-9. [CrossRef]

29. Shi, T.; Moulton, V.R.; Lapchak, P.H.; Deng, G.M.; Dalle Lucca, J.J.; Tsokos, G.C. Ischemia-mediated aggregation of the actin cytoskeleton is one of the major initial events resulting in ischemia-reperfusion injury. *Am. J. Physiol. Gastrointest. Liver Physiol.* **2009**, *296*, G339–G347. [CrossRef]
30. Turner, J.R. Molecular basis of epithelial barrier regulation: From basic mechanisms to clinical application. *Am. J. Pathol.* **2006**, *169*, 1901–1909. [CrossRef]
31. Takizawa, Y.; Kishimoto, H.; Kitazato, T.; Tomita, M.; Hayashi, M. Changes in protein and mRNA expression levels of claudin family after mucosal lesion by intestinal ischemia/reperfusion. *Int. J. Pharm.* **2012**, *426*, 82–89. [CrossRef] [PubMed]
32. Fujita, H.; Chiba, H.; Yokozaki, H.; Sakai, N.; Sugimoto, K.; Wada, T.; Kojima, T.; Yamashita, T.; Sawada, N. Differential expression and subcellular localization of claudin-7, -8, -12, -13, and -15 along the mouse intestine. *J. Histochem. Cytochem.* **2006**, *54*, 933–944. [CrossRef] [PubMed]
33. Koudstaal, L.G.; 't Hart, N.A.; Ottens, P.J.; van den Berg, A.; Ploeg, R.J.; van Goor, H.; Leuvenink, H.G. Brain death induces inflammation in the donor intestine. *Transplantation* **2008**, *86*, 148–154. [CrossRef] [PubMed]
34. Pullerits, R.; Oltean, S.; Flodén, A.; Oltean, M. Circulating resistin levels are early and significantly increased in deceased brain dead organ donors, correlate with inflammatory cytokine response and remain unaffected by steroid treatment. *J. Transl. Med.* **2015**, *13*, 201. [CrossRef] [PubMed]
35. Matsumoto, C.S.; Kaufman, S.S.; Girlanda, R.; Little, C.M.; Rekhtman, Y.; Raofi, V.; Laurin, J.M.; Shetty, K.; Fennelly, E.M.; Johnson, L.B.; et al. Utilization of donors who have suffered cardiopulmonary arrest and resuscitation in intestinal transplantation. *Transplantation* **2008**, *86*, 941–946. [CrossRef] [PubMed]
36. Fischer-Fröhlich Königsrainer, A.; Schaffer, R.; Schaub, F.; Pratschke, J.; Pascher, A.; Steurer, W.; Nadalin, S. Organ donation: When should we consider intestinal donation. *Transpl. Int.* **2012**, *25*, 1229–1240. [CrossRef] [PubMed]
37. Park, P.O.; Haglund, U.; Bulkley, G.B.; Falt, K. The sequence of development of intestinal tissue injury after strangulation ischemia and reperfusion. *Surgery* **1990**, *107*, 574. [PubMed]

International Journal of
Molecular Sciences

MDPI

Article

Detailed Clinical Features of Deafness Caused by a Claudin-14 Variant

Tomohiro Kitano [1], Shin-ichiro Kitajiri [1,*], Shin-ya Nishio [1,2] and Shin-ichi Usami [1,2]

[1] Department of Otorhinolaryngology, Shinshu University School of Medicine, 3-1-1 Asahi, Matsumoto, Nagano 390-8621, Japan; tomokitano@shinshu-u.ac.jp (T.K.); nishio@shinshu-u.ac.jp (S.N.); usami@shinshu-u.ac.jp (S.U.)

[2] Department of Hearing Implant Sciences, Shinshu University School of Medicine, 3-1-1 Asahi, Matsumoto, Nagano 390-8621, Japan

* Correspondence: kitajiri@shinshu-u.ac.jp; Tel.: +81-263-37-2666

Received: 23 July 2019; Accepted: 14 September 2019; Published: 16 September 2019

Abstract: Tight junctions are cellular junctions that play a major role in the epithelial barrier function. In the inner ear, claudins, occludin, tricellulin, and angulins form the bicellular or tricellular binding of membrane proteins. In these, one type of claudin gene, *CLDN14*, was reported to be responsible for human hereditary hearing loss, DFNB29. Until now, nine pathogenic variants have been reported, and most phenotypic features remain unclear. In the present study, genetic screening for 68 previously reported deafness causative genes was carried out to identify *CLDN14* variants in a large series of Japanese hearing loss patients, and to clarify the prevalence and clinical characteristics of DFNB29 in the Japanese population. One patient had a homozygous novel variant (c.241C>T: p.Arg81Cys) (0.04%: 1/2549). The patient showed progressive bilateral hearing loss, with post-lingual onset. Pure-tone audiograms indicated a high-frequency hearing loss type, and the deterioration gradually spread to other frequencies. The patient showed normal vestibular function. Cochlear implantation improved the patient's sound field threshold levels, but not speech discrimination scores. This report indicated that claudin-14 is essential for maintaining the inner ear environment and suggested the possible phenotypic expansion of DFNB29. This is the first report of a patient with a tight junction variant receiving a cochlear implantation.

Keywords: tight junction; Claudin-14; *CLDN14*; hearing loss; vestibular function; cochlear implantation

1. Introduction

1.1. Hearing Loss

Hearing loss (HL) is the most common sensory impairment and is diagnosed in approximately two in every 1000 children [1]. At least 60% of all childhood nonsyndromic sensorineural hearing loss is caused by genetic factors [2]. The inheritance patterns of this form of HL include autosomal recessive, autosomal dominant, X-linked, and mitochondrial. Autosomal recessive nonsyndromic hereditary HL (ARNSHL) is typically prelingual, and accounts for approximately 70% of nonsyndromic hereditary HL patients [3]. Thus far, 75 causative genes for ARNSHL have been identified [4]. One form of ARNSHL is DFNB29 (OMIM #: 614035), which is caused by variants in the *CLDN14* gene.

1.2. Tight Junctions in the Inner Ear

For our sound receiving process, it is necessary to convert sound vibration to nerve action potential (mechano-transduction) [5]. The center for this mechano-transduction is the cochlea, located in the inner ear. The cochlea is filled with two types of lymph fluid, the endolymph and perilymph. These fluids are completely different in their chemical composition: the perilymph resembles extracellular

fluids in general [6,7] but the endolymph has the characteristics of an intracellular fluid in that it has high K^+ and low Na^+ concentrations [8]. Furthermore, the electrical potential of the endolymph, i.e., endocochlear potential (EP) is positive by approximately 80 to 90 mV relative to the perilymph [9,10]. It is now widely accepted that these characteristics of the endolymph (high K^+ concentration and EP) are indispensable for cochlear hair cells to transduce acoustic stimuli into electrical signals [11]. The barrier function of the epithelial cell sheet prevents paracellular permeability, and the separation of these two fluids is essential for the maintenance of their differences in composition [12]. Tight junctions (TJs) are cellular junctions that play a major role in epithelial barrier function. In the inner ear, claudins, occludin, tricellulin, and the angulin family proteins (angulin-1/*LSR*, angulin-2/*ILDR1*, and angulin-3/*ILDR2*) form the bicellular or tricellular binding of membrane proteins. Among these, claudin-14, tricellulin, and angulin-2 are reported to be responsible for human deafness DFNB29, DFNB49, and DFNB42, respectively [13–15].

The claudins are a family of proteins that play a major role in epithelial barrier function, especially in bicellular junctions. There are 24 claudins that have been identified in humans thus far [13,16–18], with at least 10 of these reported to be expressed in the inner ear [19]. Their expression can be categorized into three types: (1) claudin-1, claudin-2, claudin-3, claudin-9, claudin-10, claudin-12, claudin-14, and claudin-18 that are expressed in multiple sites such as the organ of Corti, Reissner's membrane, the spiral limbus, and the marginal cells of the stria vascularis; (2) claudin-8 that is expressed in all the aforementioned sites except for the organ of Corti; and (3) claudin-11 that is expressed only in the basal cells of the stria vascularis [19]. The barrier functions are speculated to be dependent on the combinations of these claudins, and previous reports have shown claudin-9, claudin-11, and claudin-14 to be critical for hearing functions [20–25], with mutations in these proteins causing deafness in humans and mice. Murine studies have indicated that claudin-11 (cldn-11) knockout mice demonstrate hearing loss due to reduced EP [20,21]. Other studies have indicated that, as a result of the rapid degeneration of cochlear hair cells shortly after birth, *Cldn9* mutant mice and *Cldn14* mutant mice demonstrate hearing loss. However, these two animal models do not display reduced EP [22,23]. The variations within these phenotypes are thought to be correlated with the multiple functions of the TJs in the inner ear. Thus, the TJs in the epithelial barriers are significantly involved in inner ear function.

1.3. CLDN14 Variants in Deafness

To date, nine different variants in *CLDN14* [13,26–29] have been reported to cause HL in the Pakistani, Greek, and Canadian populations. Seven of the nine variants were reported from Pakistani consanguineous families. The *CLDN14* variants are a relatively common cause of recessive hearing loss, which is responsible for 2.25% of HL patients in a Pakistani study cohort [28], whereas no pathogenic variants were reported from east Asian populations [30,31]. Although previously reported papers have shown some clinical characteristics of patients with *CLDN14* variants, the audiovestibular findings, such as progression and details of vestibular function, remain unclear. In addition, there are no reports on patients with cochlear implantation (CI), thus the outcome of CI is also unknown. In the present study, we used massively parallel DNA sequencing (MPS) to detect pathogenic variants in *CLDN14* among a large series of Japanese HL patients.

Here, we present a patient with a novel variant in the *CLDN14* gene identified from a group of non-consanguineous HL patients and discuss additional clinical features including CI outcomes. This is the first report of a diagnosis of hearing caused by *CLDN14* in an east Asian population and in such a patient receiving a cochlear implant as intervention.

2. Results

2.1. Detected Variant

One possible disease-causing variant, *CLDN14*: NM_144492: c.241C>T, leading to p.Arg81Cys, was homozygously detected in one of 1577 probands with autosomal recessive HL (Table 1, Figure 1),

whereas no pathogenic variants were found in the other 972 probands with autosomal dominant or inheritance pattern of unknown HL. At the same amino acid residue, which is within the first extracellular loop, a different missense change c.242G>A, leading to p.Arg81His, has been reported (Figure 2) [27]. No candidate variants in the other 67 deafness genes were identified in the proband. In detail, the variants in two other genes, *PTPRQ* and *EYA4*, were also detected from the proband but were not segregated. As shown in Figure 1, family segregation was confirmed by using Sanger sequencing. The variant was not identified in ExAC, gnomAD, 3.5KJPN or the 1208 Japanese exome variants, in addition to the 333 in-house Japanese normal hearing control databases.

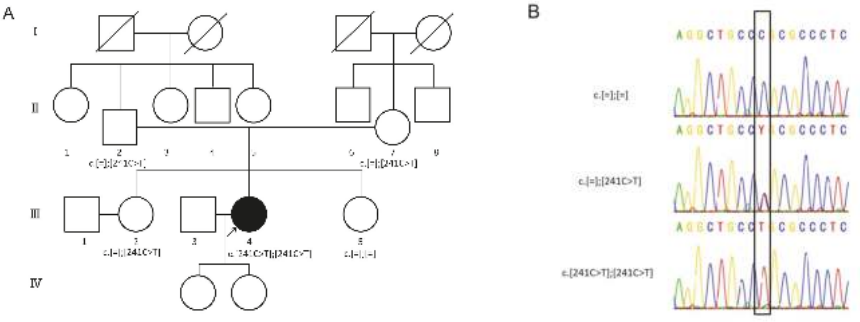

Figure 1. Pedigree and *CLDN14* variants of the family. (**A**) Pedigree shows autosomal recessive inherited hearing loss (HL), (**B**) the electropherograms of this family. Target genome enrichment for 68 previously reported deafness causative genes and massively parallel DNA sequencing are carried out for this proband (III-4). Sanger sequencing is used for family segregation analysis. Genetic analysis results are shown under the proband and family members.

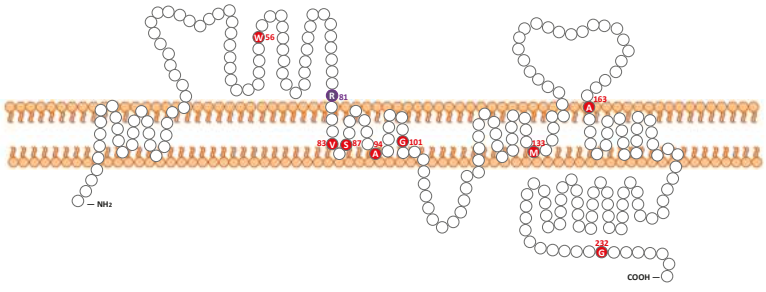

Figure 2. Location of pathogenic variants in Claudin-14. Red colored amino acid residues indicate previously reported claudin-14 variants. The blue colored residue indicates the positions of *CLDN14* p.Arg81His and p.Arg81Cys.

We employed in silico software (SIFT, polyphen-2, LRT, Mutation Taster, etc.), and almost all scores indicated "damaging" (Table 1). The corresponding amino acid was well conserved across species (170/170 (100%) in vertebrates). Taken together, according to the American College of Medical Genetics (ACMG) guideline, the variant was classified as "likely pathogenic" (PS4, PM2, and PM5).

2.2. Clinical Findings

The proband was a 37-year-old female. The newborn hearing screening program had not yet started at birth and there were no particular complications in the perinatal period. The female proband also passed an elementary school health checkup at six years of age, but was suspected of hearing loss at age nine and was referred to an otolaryngology clinic at a local general hospital.

Pure-tone audiograms showed steep high-frequency sensorineural HL (SNHL) with an average of 77 dBHL in both ears (Figure 3A). It appeared to progress slowly, and the proband began to wear hearing aids bilaterally at 11 years of age. Over a period of 20 years, their residual hearing in the lower frequencies gradually deteriorated and hearing aids became ineffective. At the age of 34, the proband consulted our hospital for further examination. Otoscopic examination revealed a normal tympanic membrane. Computed tomography (CT) and magnetic resonance imaging (MRI) of the temporal bones showed no malformations, hearing level was approximately 100 dBHL in both ears, but the left ear showed moderate residual hearing in the lower frequencies. We performed vestibular assessment (caloric test and cervical-ocular vestibular evoked myogenic potentials, i.e., c/oVEMPs) as preoperative examinations prior to CI. The caloric test, cVEMPs, and oVEMPs represent the function of the semicircular canal, the saccule and inferior vestibular nerve, and the utricle and superior vestibular nerve, respectively. As shown in Figure 3B, all vestibular testing showed normal vestibular functions.

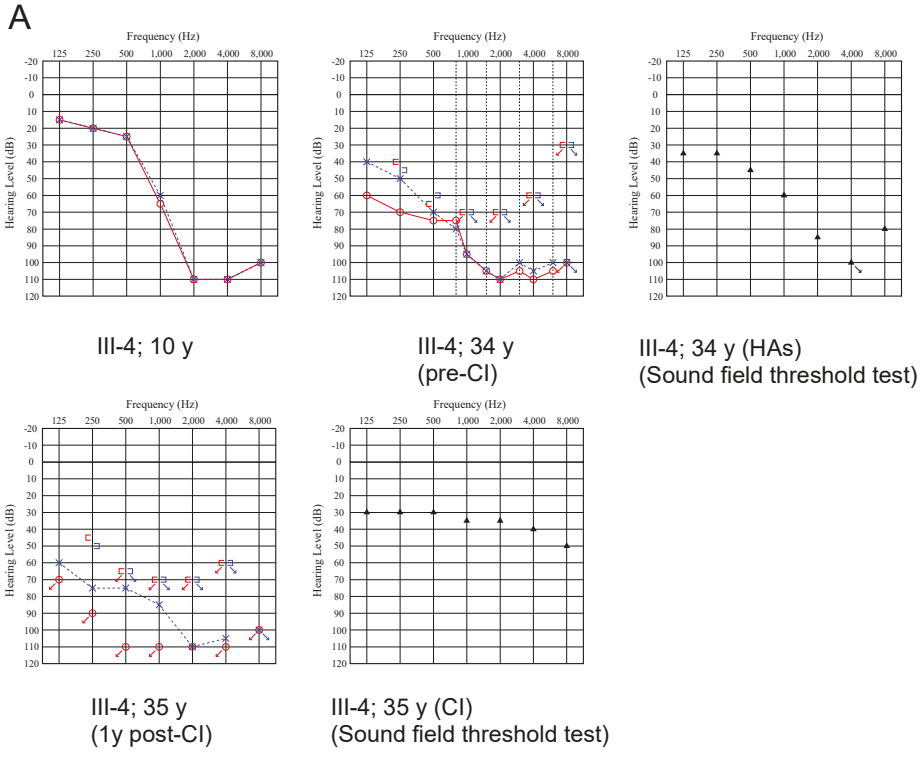

Figure 3. *Cont.*

B

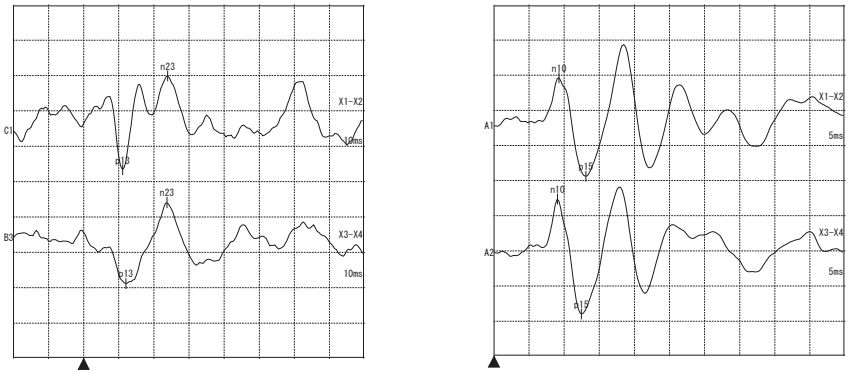

Figure 3. (**A**) Pure-tone audiometry (PTA) shows bilateral progressive sensorineural hearing loss in the proband. After a cochlear implantation (CI) in the right ear, sound field hearing threshold tests with a CI show 40 dBSPL. Red: right ear, Blue: left ear, Circle and Cross: Right and left ear air conduction hearing level respectively, Square bracket: Bone conduction hearing level, Triangle: both ears with intervention, Arrow: over measurement limit (**B**) There are no obvious differences between each ear in the cervical vestibular evoked myogenic potentials (right), and ocular vestibular evoked myogenic potentials (left).

The proband underwent a CI (MED-EL FLEX28) in the right ear at the age 35. Sound field threshold levels were improved from 77.5 dBSPL (with hearing aids) to 37.5 dBSPL (with the cochlear implant) (Figure 3A). To evaluate speech perception outcomes, the proband underwent speech discrimination testing (using the 67S Japanese monosyllable test, presenting in 65 dBSPL). Contrary to the good improvement in sound field threshold levels, the proband's speech perception outcomes improved from 12% to only 32% two years after receiving a CI.

3. Discussion

3.1. Frequency of CLDN14-Associated HL in the Japanese Population

We discovered a novel causative variant in the *CLDN14* gene as a cause of progressive SNHL in a Japanese patient. To date, a total of nine pathogenic variants in *CLDN14* have been reported (Table 2, Figure 2). Among them, seven were reported from Pakistan, and one each from Greece and Canada. Otherwise, according to the previous reports, no pathogenic variants of *CLDN14* have been detected in the Korean and Chinese populations [30,31]. Hence, this is the first report of a causative *CLDN14* variant in an east Asian population.

The incidence of *CLDN14* variants was 0.04% (1/2549) among the Japanese HL patients, and 0.06% (1/1577) among the families with autosomal recessive HL in the Japanese population. In clear contrast to this, variants of *CLDN14* account for 2.25% of autosomal recessive HL in the Pakistani population. In this study, the patient was identified from a non-consanguineous family and the parents of the proband were from a geographically remote area, whereas almost all of the previous reports were from consanguineous families [13,27–29]. As no pathogenic *CLDN14* variants were found in our cohort, but one HL patient with a homozygous *CLDN14* variant was identified, it is necessary to consider such rare HL cases.

Table 1. Possible causative variant identified in this study.

		Prediction Score								Allele Frequency in Controls		
Nucleotide Change	Amino Acid Change	SIFT *	PolyPhen2_HVAR *	LRT *	Mut_Taster *	Mut_Assessor *	REVEL *	CADD	Evolutional Conservation **	ExAC	gnomAD	3.5kJPN
c.241C > T	p.R81C	0.78	0.88	0.84	0.81	0.98	0.89	27.6	Yes (100%)	0.000042	0.000037	0

* The prediction scores of each algorithm included on the ANNOVAR software were converted from the original scoring system. Scores closer to 1.0 indicated the mutation was more damaging, and those closer to 0 indicated they were more tolerant. ** Conserved in 170 vertebrates from the HGMD professional.

Table 2. Summary of clinical features associated with *CLDN14* variants.

			HL		Pure-Tone Audiometry						
Nucleotide Change	**Genotype**	**Amino Acid Change**	**Onset**	**Progression**	**Severity of HL**	**Audiometric Configuration**	**Consanguineous Marriage**	**Vestibuler Function**	**Hearing Intervention**	**Family Origin**	**Reference**
c.167G > A	homozygote	p.Trp56 *	NA	No	severe to profound	gently sloping	Yes	NA	NA	Pakistan	Lee et al. 2011 [27]
c.241C > T	homozygote	p.Arg81Cys	9 y.o.	Yes	Severe	steeply sloping	No	Normal	CI	Japan	This study
c.242G > A	homozygote	p.Arg81His	NA	No	severe to profound	gently sloping	Yes	NA	NA	Pakistan	Lee et al. 2011 [27]
c.254T > A	homozygote	p.Val85Asp	prelingual	No	moderate to profound	HF	Yes	NA	NA	Pakistan	Wilcox et al. 2001 [13], Bashir et al. 2013 [28]
c.259_260TC > AT	homozygote	p.Ser87Ile	prelingual	No	severe to profound	flat	Yes	NA	NA	Pakistan	Bashir et al. 2013 [28]
c.281C > T	homozygote	p.Ala94Val	NA	No	moderate to profound	flat, DE	Yes	NA	NA	Pakistan	Bashir et al. 2013 [28]
c.301G > A	homozygote	p.Gly101Arg	NA	NA	NA	NA	NA	NA	NA	Greece	Wattenhofer et al. 2005 [26]
c.398delT	homozygote	p.Met133Argfs *24	congenital	NA	moderate to profound	gently sloping	Yes	NA	NA	Pakistan	Wilcox et al. 2001 [13], Bashir et al. 2013 [28]
c.488C > T	homozygote	p.Ala163Val	5–7 y.o.	Yes	mild to severe	steeply sloping	Yes	Normal	HA	Canada	Pater et al. 2016 [29]
c.694G > A	homozygote	p.Gly232Arg	NA	No	severe to profound	gently sloping	Yes	NA	NA	Pakistan	Lee et al. 2011 [27]

Abbreviations: HF, high-frequency hearing loss; DE, deaf; CI, cochlear implant; HA, hearing aid; N/A, not available.

3.2. Clinical Characteristics

3.2.1. Progression and Onset of DFNB29

Until Pater et al. reported the progression of HL [29], the phenotype of DFNB29 was associated with non-progressive, congenital or prelingual HL with a variable degree of severity [13,26–28]. In this report, serial audiograms showed hearing deterioration especially at low frequencies (125 to 500 Hz). The average threshold progression rate of HL in the low frequencies was about 1.6 dB/year. Moreover, in this case, HL in the high frequencies was already impaired from the first decade, but there may have been no problem at birth as there was no problem in articulation. According to Pater's report, the phenotype of DFNB29 showed no hearing impairment until three years of age, and its onset occurred after age four especially in the higher frequencies. After that it progressed to almost deaf at above 2 kHz by nine years of age, therefore, it might be that our patient had a similar course. Indeed, in our case, no hearing impairment was detected at the elementary school health checkup at six years of age and it was only suspected at nine years of age. Lee et al. reported HL patients with another amino acid change, p.Arg81His [27], at the same amino acid residue. In that report, the phenotype was described as non-progressive prelingual HL. The audiogram indicated bilateral severe to profound HL with a gentle slope at 20 years of age. From our study and the previous reports, the hearing deterioration in patients with *CLDN14* remains unclear, and further study including serial audiograms is required to clarify this.

3.2.2. Vestibular Examination

We could not identify any dysfunction on the vestibular examinations. According to past reports, claudin-14 is also expressed in the vestibule of mice (such as in the sensory epithelia) [19]. Vestibular function in *Cldn14* knockout model mice has not been reported and the details remain unknown. This is the first report to mention in detail the vestibular function, including caloric testing, cVEMPs, and oVEMPs. Endolymph in cochlear is characterized by extremely high resting potential called EP, in addition to high K^+ concentration. In contrast, in the vestibular endolymph, the K^+ concentration is high, but no EP can be detected. Claudin-14 may be necessary for maintaining a barrier to resist EP, but not K^+.

3.2.3. Outcome of Cochlear Implantation

This is the first report showing the outcome for a CI for a *CLDN14*-associated HL patient. A CI represents the most successful neural prosthesis in clinical cases [32]. For patients with severe to profound SNHL, CI has been established as the standard therapy [33]. The implant is surgically implanted and works by transducing acoustic energy into an electrical signal, with an electrode array in the cochlea used to stimulate the surviving spiral ganglion cells of the auditory nerve [34].

As mentioned above, the patient showed relatively poor improvement in speech discrimination scores, whereas good improvement in sound field threshold levels was observed. Since the cochlear implant directly stimulates the cochlear nerve, the influence of the inner ear should be excluded. Thus, it is likely that the unsatisfactory speech discrimination was due to deficiencies in the spiral ganglion or central auditory pathway. In our previous study, *CLDN14* was expressed at the same level in the organ of Corti and spiral ganglions [35]. Including this report, there have been no cases with intellectual disability indicating central involvement; therefore, it is possible that the spiral ganglion may be involved in claudin-14 associated HL.

4. Materials and Methods

4.1. Subjects

All procedures were approved by the Shinshu University Ethical Committee (No. 387—4 September 2012 and No. 576—2 May 2017) as well as the respective Ethical Committees of the

other participating institutions described elsewhere [36] and were carried out after obtaining written informed consent from all subjects (or from their next of kin, caretaker, or guardian in the case of minors or children). A total of 2549 probands from unrelated Japanese HL families were enrolled from the 67 otolaryngology departments across Japan participating in the present study from May 2012 to September 2016. The age of the probands ranged from 0 to 79 years (mean ± SD: 22.1 ± 19.7). The hereditary patterns of the HL in the families of the probands were autosomal dominant in 602, autosomal recessive in 1577, and unknown inheritance mode in 370.

4.2. Variant Analysis

For the genetic analysis for this proband, we performed target genome enrichment for 68 previously reported genetic causes for deafness and MPS analysis described elsewhere [37]. In brief, amplicon libraries were prepared using an Ion AmpliSeq™ Custom Panel (Applied Biosystems, Life Technologies, Carlsbad, CA, USA), in accordance with the manufacturer's instructions, for 68 genes reported to cause nonsyndromic hereditary HL [37]. Emulsion PCR and sequencing was performed according to the manufacturer's instructions. The detailed protocol has been described elsewhere [38,39]. MPS was performed with an Ion Proton™ system using the Ion PI™ Hi-Q™ Sequencing 200 Kit and Ion PI™ Chip (ThermoFisher Scientific, Waltham, MA, USA) according to the manufacturers' instructions. The sequence data were mapped against the human genome sequence (build GRCh37/hg19) with a Torrent Mapping Alignment Program. The mean depth of coverage of 68 target genes was 363.0. The percentage of each region with more than 20 times coverage (indicating the percentage of each region sequenced 20 times or more by MPS) was 95.31%. After sequence mapping, the DNA variant regions were piled up with Torrent Variant Caller plug-in software. After variant detection, their effects were analyzed using ANNOVAR software [40,41].

The missense, nonsense, insertion/deletion, and splicing variants were selected from among the identified variants. Variants were further selected as less than 1% of (1) the ExAC [42,43], (2) gnomAD [44], (3) 3.5KJPN [45], (4) the Human Genetic Variation Database (dataset for 1208 Japanese exome variants) [46], and (5) the 333 in-house Japanese normal hearing controls. Direct sequencing was utilized to confirm the selected variants. The pathogenicity of a variant was evaluated by ACMG (American College of Medical Genetics, Bethesda, MD, USA) standards and guidelines [47]. For missense variants, in particular, functional prediction software, including Sorting Intolerant from Tolerant (SIFT) [48], Polymorphism Phenotyping (PolyPhen2) [49], Likelihood Ratio Test (LRT) [50], Mutation Taster [51], Mutation Assessor [52], Rare Exome Variant Ensemble Learner (REVEL) [53], and Combined Annotation Dependent Depletion (CADD) [54] were used on the ANNOVAR software. Conservation of the variant site was also evaluated in 170 vertebrates from the HGMD professional [55]. Segregation analysis was performed for the proband and family members.

4.3. Clinical Evaluations

The age of onset of HL, the incidence of progressive HL, and episodes of vertigo and dizziness were analyzed based on the medical charts of the probands with the *CLDN14* variant.

Pure-tone audiometry was performed to evaluate HL. The pure-tone average (PTA) was calculated from the audiometric thresholds at four frequencies (0.5, 1, 2, and 4 kHz). If an individual did not respond to the maximum hearing level at a frequency, 5 dB was added to the maximum hearing level. The severity of HL was classified into mild (PTA: 20–40 dBHL), moderate (41–70 dBHL), severe (71–95 dBHL), and profound (>95 dBHL). The audiometric configurations were categorized as low-frequency, mid-frequency, high-frequency (gently or steeply sloping), flat, and deaf [56].

The vestibular examination findings, including caloric testing and the measurement of cervical and ocular vestibular evoked myogenic potentials (c/oVEMPs), were analyzed. Caloric testing involved the measurement of the maximum slow phase velocity (SPV) by cold water irrigation (20 °C, 5 mL, 20 s). We defined a maximum SPV value below 10 deg/s as representing areflexia and a value between 10 and 20 deg/s as representing hyporeflexia. For cVEMPs testing, electromyography (EMG) was

performed using a pair of surface electrodes mounted on the upper half and sternal head of the sternocleidomastoid muscle, respectively. The electrographic signal was recorded using a Neuropack evoked potential recorder (Nihon Kohden Co Ltd., Tokyo, Japan). Clicks lasting for 0.1 ms at 105 dBnHL were presented through a headphone. The stimulation rate was 5 Hz, the bandpass filter intensity was 20 to 2000 Hz, and the analysis time was 50 ms. The responses to 100 stimuli were averaged twice. The oVEMPs testing was measured by bone-conductive vibration (BCV). The BCV was delivered in 4 ms tone bursts of 500 Hz vibration (rise and fall time = 1 ms and plateau time = 2 ms) by using a hand-held 4810 mini-shaker (Bruel and Kjaer, Naerum, Denmark), which was placed on the midline (Fz) of the forehead. The active electrode was located over the inferior orbital margin and a reference electrode was placed 2 cm below the active electrode. The ground electrode was placed on the chin. The patients laid in a supine position on a bed and looked up at an angle of approximately 30 degrees above straight ahead during the recording. The signals were amplified and bandpass filtered between 20 and 2000 Hz. The stimulus intensity was 115 dB force level, 500 Hz with an analysis time of 40 ms, and 50 responses were averaged for each run. The VEMPs asymmetry was calculated as follows: asymmetry ratio (AR) = (larger amplitude – smaller amplitude) × 100/(larger amplitude + smaller amplitude). In this study, an asymmetry ratio of >30% was defined as a decreased reaction and no reaction in amplitude VEMPs as absent.

Intervention for HL, including the use of hearing aids or cochlear implants, was investigated. To evaluate speech perception outcomes, speech discrimination scores (using the 67S Japanese monosyllable test) were used. The subjects sat 1 m away from the sound source facing zero-degree azimuth, and recorded monosyllable words in quiet were presented in the sound field at 65 dBSPL.

5. Conclusions

We present a patient with a novel variant in the *CLDN14* gene identified from a non-consanguineous family. This is the first report of *CLDN14*-associated HL in an east Asian population. Serial audiograms indicated high-frequency hearing loss type, and the deterioration gradually spread to other frequencies, finally resulting in deafness. The patient showed normal vestibular function for caloric testing, cVEMPs, and oVEMPs. This is also the first report of an HL patient with a tight junction variant receiving a CI. The CI improved the proband's sound field threshold levels, but not their speech discrimination scores. This information contributes to our understanding, diagnosis, and treatment of HL caused by TJ disorders.

Author Contributions: Conceptualization, S.U.; methodology, S.N.; software, S.N.; validation, T.K., S.K., S.N. and S.U.; formal analysis, S.N.; investigation, T.K.; resources, T.K. and S.N.; data curation, S.N.; writing—original draft preparation, T.K.; writing—review and editing, S.K. and S.U.; visualization, T.K.; supervision, S.U.; project administration, S.U.; funding acquisition, S.U.

Funding: This research was funded by a Health and Labor Sciences Research Grant for Research on Rare and Intractable diseases and Comprehensive Research on Disability Health and Welfare from the Ministry of Health, Labor and Welfare of Japan (S.U. H29-Nanchitou(Nan)-Ippan-031), a Grant-in-Aid from Japan Agency for Medical Research and Development (AMED) (S.U. 16kk0205010h001, 18ek0109363h0001), and a Grant-in-Aid for Scientific Research (A) from the Ministry of Education, Science and Culture of Japan (S.U. 15H02565).

Acknowledgments: The authors thank the proband and their family members who participated in this study. We would also like to thank Sachiko Matsuda and Fumiko Tomioka for their technical assistance, and Ayano Koide for her assistance with visualization.

Conflicts of Interest: The authors declare no conflicts of interest. The funders had no role in the design of the study; in the collection, analyses, or interpretation of data; in the writing of the manuscript, or in the decision to publish the results.

Data Availability: The sequencing data are available in the DDBJ databank of Japan (Accession number: JGAS00000000191).

Abbreviations

HL	Hearing loss
ARNSHL	Autosomal recessive nonsyndromic hereditary hearing loss
EP	Endocochlear potential
TJ	Tight junction
CI	Cochlear implantation
MPS	Massively parallel DNA sequencing
PTA	Pure-tone average
cVEMPs	Cervical vestibular evoked myogenic potentials
oVEMPs	Ocular vestibular evoked myogenic potentials
SNHL	Sensorineural hearing loss
dBSPL	Decibel sound pressure level
dBHL	Decibel hearing level

References

1. Morton, C.C.; Nance, W.E. Newborn Hearing Screening—A Silent Revolution. *N. Engl. J. Med.* **2006**, *354*, 2151–2164. [CrossRef] [PubMed]
2. Smith, R.J.H.; Bale, J.F.; White, K.R. Sensorineural hearing loss in children. *Lancet* **2005**, *365*, 879–890. [CrossRef]
3. Hilgert, N.; Smith, R.J.H.; Van Camp, G. Forty-six genes causing nonsyndromic hearing impairment: Which ones should be analyzed in DNA diagnostics? *Mutat. Res.* **2009**, *681*, 189–196. [CrossRef] [PubMed]
4. Hereditary Hearing Loss Homepage. Available online: https://hereditaryhearingloss.org/ (accessed on 13 May 2019).
5. Richardson, G.P.; de Monvel, J.B.; Petit, C. How the Genetics of Deafness Illuminates Auditory Physiology. *Annu. Rev. Physiol.* **2011**, *73*, 311–334. [CrossRef] [PubMed]
6. Wangemann, P.; Schacht, J. Homeostatic Mechanisms in the Cochlea. In *The Cochlea*; Dallos, P., Popper, A.N., Fay, R.R., Eds.; Springer: New York, NY, USA, 1996; Volume 8, pp. 130–185.
7. Ferrary, E.; Sterkers, O. Mechanisms of endolymph secretion. *Kidney Int.* **1998**, *65*, S98–S103.
8. Sterkers, O.; Ferrary, E.; Amiel, C. Production of inner ear fluids. *Phys. Rev.* **1988**, *68*, 1083–1128. [CrossRef] [PubMed]
9. Tasaki, I.; Spyroupoulos, C.S. Stria vascularis as source of endocochlear potential. *J. Neurophysiol.* **1959**, *22*, 149–155. [CrossRef]
10. Konishi, T.; Hamrick, P.E.; Walsh, P.J. Ion transport in guinea pig cochlea. I. Potassium and sodium transport. *Acta Otolaryngol.* **1978**, *86*, 22–34. [CrossRef]
11. Hudspeth, A.J. How the ear's works work. *Nature* **1989**, *341*, 397–404. [CrossRef]
12. Nunes, F.D.; Lopez, L.N.; Lin, H.W.; Davies, C.; Azevedo, R.B.; Gow, A.; Kachar, B. Distinctsubdomain organization and molecular composition of a tight junction with adherens junction features. *J. Cell Sci.* **2006**, *119*, 4819–4827. [CrossRef]
13. Wilcox, E.R.; Burton, Q.L.; Naz, S.; Riazuddin, S.; Smith, T.N.; Ploplis, B.; Belyantseva, I.; Ben-Yosef, T.; Liburd, N.A.; Morell, R.J.; et al. Mutations in the gene encoding tight junction claudin-14 cause autosomal recessive deafness DFNB29. *Cell* **2001**, *104*, 165–172. [CrossRef]
14. Riazuddin, S.; Ahmed, Z.M.; Fanning, A.S.; Lagziel, A.; Kitajiri, S.; Ramzan, K.; Khan, S.N.; Chattaraj, P.; Friedman, P.L.; Anderson, J.M.; et al. Tricellulin Is a Tight-Junction Protein Necessary for Hearing. *Am. J. Hum. Genet.* **2006**, *79*, 1040–1051. [CrossRef]
15. Borck, G.; Rehman, A.U.; Lee, K.; Pogoda, H.; Kakar, N.; von Ameln, S.; Grillet, N.; Hildebrand, M.S.; Ansar, M.; Basit, S.; et al. Loss-of-Function Mutations of ILDR1 Cause Autosomal-Recessive Hearing Impairment DFNB42. *Am. J. Hum. Genet.* **2011**, *88*, 127–137. [CrossRef]
16. Furuse, M.; Fujita, K.; Hiiragi, T.; Fujimoto, K.; Tsukita, S. Claudin-1 and -2: Novel integral membrane proteins localizing at tight junctions with no sequence similarity to occludin. *J. Cell Biol.* **1998**, *141*, 1539–1550. [CrossRef] [PubMed]
17. Elkouby-Naor, L.; Ben-Yosef, T. Functions of claudin tight junction proteins and their complex interactions in various physiologicalsystems. *Int. Rev. Cell Mol. Biol.* **2010**, *279*, 1–32. [PubMed]

18. Gunzel, D.; Fromm, M. Claudins and other tight junction proteins. *Compr. Physiol.* **2012**, *2*, 1819–1852. [PubMed]
19. Kitajiri, S.-I.; Furuse, M.; Morita, K. Expression patterns of claudins, tight junction adhesion molecules, in the inner ear. *Hear. Res.* **2004**, *187*, 25–34. [CrossRef]
20. Gow, A.; Davies, C.; Southwood, C.M.; Frolenkov, G.; Chrustowski, M.; Ng, L.; Yamauchi, D.; Marcus, D.C.; Kachar, B. Deafness in Claudin 11-null mice reveals the critical contribution of basal cell tight junctions to stria vascularis function. *J. Neurosci.* **2004**, *24*, 7051–7062. [CrossRef] [PubMed]
21. Kitajiri, S.; Miyamoto, T.; Mineharuetal, A. Compartmentalization established by claudin-11-based tight junctions in stria vascularis is required for hearing through generation of endocochlear potential. *J. Cell Sci.* **2004**, *117*, 5087–5096. [CrossRef]
22. Ben-Yosef, T.; Belyantseva, I.A.; Saunders, T.L.; Hughes, E.D.; Kawamoto, K.; Van Itallie, C.M.; Beyer, L.A.; Halsey, K.; Gardner, D.J.; Wilcox, E.R.; et al. Claudin 14 knockout mice, a model for autosomal recessive deafness DFNB29, are deaf due to cochlear hair cell degeneration. *Hum. Mol. Genet.* **2003**, *12*, 2049–2061. [CrossRef] [PubMed]
23. Nakano, Y.; Kim, S.H.; Kim, H.M.; Sanneman, J.D.; Zhang, Y.; Smith, R.J.; Marcus, D.C.; Wangemann, P.; Nessler, R.A.; Banfi, B. A claudin-9—Based ion permeability barrier is essential for hearing. *PLoS Genet.* **2009**, *5*, e1000610. [CrossRef] [PubMed]
24. Matter, K.; Balda, M.S. Signalling to and from tight junctions. *Nat. Rev. Mol. Cell Biol.* **2003**, *4*, 225–237. [CrossRef]
25. Schneeberger, E.E.; Lynch, R.D. The tight junction: A multifunctional complex. *Am. J. Physiol. Cell Physiol.* **2004**, *286*, C1213–C1228. [CrossRef] [PubMed]
26. Wattenhofer, M.; Reymond, A.; Falciola, V.; Charollais, A.; Caille, D.; Borel, C.; Lyle, R.; Estivill, X.; Petersen, M.B.; Meda, P.; et al. Different mechanisms preclude mutant CLDN14 proteins from forming tight junctions in vitro. *Hum. Mutat.* **2005**, *25*, 543–549. [CrossRef] [PubMed]
27. Lee, K.; Ansar, M.; Andrade, P.B.; Khan, B.; Santos-Cortez, R.L.P.; Ahmad, W.; Leal, S.M. Novel CLDN14 mutations in Pakistani families with autosomal recessive non-syndromic hearing loss. *Am. J. Med. Genet. A* **2012**, *158*, 315–321. [CrossRef] [PubMed]
28. Bashir, Z.-E.-H.; Latief, N.; Belyantseva, I.A.; Iqbal, F.; Amer Riazuddin, S.; Khan, S.N.; Friedman, T.B.; Riazuddin, S.; Riazuddin, S. Phenotypic variability of CLDN14 mutations causing DFNB29 hearing loss in the Pakistani population HHS Public Access. *J. Hum. Genet.* **2013**, *58143*, 102–108. [CrossRef] [PubMed]
29. Pater, J.A.; Benteau, T.; Griffin, A.; Penney, C.; Stanton, S.G.; Predham, S.; Kielley, B.; Squires, J.; Zhou, J.; Li, Q.; et al. A common variant in CLDN14 causes precipitous, prelingual sensorineural hearing loss in multiple families due to founder effect. *Hum. Genet.* **2017**, *136*, 107–118. [CrossRef] [PubMed]
30. Kim, M.-A.; Kim, Y.-R.; Sagong, B.; Cho, H.-J.; Bae, J.W.; Kim, J.; Lee, J.; Park, H.-J.; Choi, J.Y.; Lee, K.-Y.; et al. Genetic Analysis of Genes Related to Tight Junction Function in the Korean Population with Non-Syndromic Hearing Loss. *PLoS ONE* **2014**, *9*, e95646. [CrossRef] [PubMed]
31. Lu, Y.; Yao, J.; Wei, Q.; Xu, J.; Xing, G.; Cao, X. Genetic analysis of CLDN14 in the Chinese population affected with non-syndromic hearing loss. *Int. J. Pediatr. Otorhinolaryngol.* **2018**, *105*, 6–11. [CrossRef] [PubMed]
32. Roche, J.P.; City, I.; Hansen, M.R. On the Horizon: Cochlear Implant Technology. *Otolaryngol. Clin. North Am.* **2016**, *48*, 1097–1116. [CrossRef] [PubMed]
33. Wilson, B.S. Getting a decent (but sparse) signal to the brain for users of cochlear implants. *Hear. Res.* **2014**, *322*, 24–38. [CrossRef] [PubMed]
34. Deep, N.L.; Dowling, E.M.; Jethanamest, D.; Carlson, M.L. Cochlear Implantation: An Overview. *J. Neurol. Surg. Part B* **2019**, *80*, 169–177. [CrossRef]
35. Nishio, S.; Takumi, Y.; Usami, S. Laser-capture micro dissection combined with next-generation sequencing analysis of cell type-specific deafness gene expression in the mouse cochlea. *Hear. Res.* **2017**, *348*, 87–97. [CrossRef]
36. Nishio, S.Y.; Usami, S.I. Deafness Gene Variations in a 1120 Nonsyndromic Hearing Loss Cohort: Molecular Epidemiology and Deafness Mutation Spectrum of Patients in Japan. *Ann. Otol. Rhinol. Laryngol.* **2015**, *124*, 49S–60S. [CrossRef] [PubMed]
37. Kitano, T.; Miyagawa, M.; Nishio, S.-Y.; Moteki, H.; Oda, K.; Ohyama, K.; Miyazaki, H.; Hidaka, H.; Nakamura, K.-I.; Murata, T.; et al. POU4F3 mutation screening in Japanese hearing loss patients: Massively parallel DNA sequencing-based analysis identified novel variants associated with autosomal dominant hearing loss. *PLoS ONE* **2017**, *12*, 1–15. [CrossRef] [PubMed]

38. Miyagawa, M.; Nishio, S.Y.; Ikeda, T.; Fukushima, K.; Usami, S.I. Massively Parallel DNA Sequencing Successfully Identifies New Causative Mutations in Deafness Genes in Patients with Cochlear Implantation and EAS. *PLoS ONE* **2013**, *8*, e75793. [CrossRef] [PubMed]
39. Nishio, S.Y.; Moteki, H.; Usami, S.I. Simple and efficient germline copy number variant visualization method for the Ion AmpliSeq™ custom panel. *Mol. Genet. Genomic Med.* **2018**, *6*, 678–686. [CrossRef] [PubMed]
40. Chang, X.; Wang, K. wANNOVAR: Annotating genetic variants for personal genomes via the web. *J. Med. Genet.* **2012**, *49*, 433–436. [CrossRef]
41. Wang, K.; Li, M.; Hakonarson, H. ANNOVAR: Functional annotation of genetic variants from high-throughput sequencing data. *Nucleic Acids Res.* **2010**, *38*, e164. [CrossRef]
42. Abboud, H.E.; Abecasis, G.; Aguilar-Salinas, C.A.; Arellano-Campos, O.; Atzmon, G.; Aukrust, I.; Barr, C.L.; Bell, G.I.; Bergen, S.; Bjørkhaug, L.; et al. Analysis of protein-coding genetic variation in 60,706 humans. *Nature* **2016**, *536*, 285–291.
43. The Exome Aggregation Consortium Database (ExAC). Available online: http://exac.broadinstitute.org/ (accessed on 13 May 2019).
44. The Genome Aggregation Database (gnomAD). Available online: https://gnomad.broadinstitute.org/ (accessed on 13 May 2019).
45. Integrative Japanese Genome Variation Database (3.5KJPN). Available online: https://ijgvd.megabank.tohoku.ac.jp/statistics/statistics-3.5kjpn-all (accessed on 13 May 2019).
46. Narahara, M.; Higasa, K.; Nakamura, S.; Tabara, Y.; Kawaguchi, T.; Ishii, M.; Matsubara, K.; Matsuda, F.; Yamada, R. Large-scale East-Asian eQTL mapping reveals novel candidate genes for LD mapping and the genomic landscape of transcriptional effects of sequence variants. *PLoS ONE* **2014**, *9*, e100924. [CrossRef] [PubMed]
47. Richards, S.; Aziz, N.; Bale, S.; Bick, D.; Das, S.; Gastier-Foster, J.; Grody, W.W.; Hegde, M.; Lyon, E.; Spector, E.; et al. Standards and guidelines for the interpretation of sequence variants: A joint consensus recommendation of the American College of Medical Genetics and Genomics and the Association for Molecular Pathology. *Genet. Med.* **2015**, *17*, 405–424. [CrossRef] [PubMed]
48. Kumar, P.; Henikoff, S.; Ng, P.C. Predicting the effects of coding non-synonymous variants on protein function using the SIFT algorithm. *Nat. Protoc.* **2009**, *4*, 1073–1081. [CrossRef] [PubMed]
49. Adzhubei, I.A.; Schmidt, S.; Peshkin, L.; Ramensky, V.E.; Gerasimova, A.; Bork, P.; Kondrashov, A.S.; Sunyaev, S.R. A method and server for predicting damaging missense mutations. *Nat. Methods* **2010**, *7*, 248–249. [CrossRef] [PubMed]
50. Chun, S.; Fay, J.C. Identification of deleterious mutations within three human genomes. *Genome Res.* **2009**, *19*, 1553–1561. [CrossRef]
51. Schwarz, J.M.; Rödelsperger, C.; Schuelke, M.; Seelow, D. MutationTaster evaluates disease-causing potential of sequence alterations. *Nat. Methods* **2010**, *7*, 575–576. [CrossRef]
52. Reva, B.; Antipin, Y.; Sander, C. Predicting the functional impact of protein mutations: Application to cancer genomics. *Nucleic Acids Res.* **2011**, *39*, 37–43. [CrossRef]
53. Ioannidis, N.M.; Rothstein, J.H.; Pejaver, V.; Middha, S.; McDonnell, S.K.; Baheti, S.; Musolf, A.; Li, Q.; Holzinger, E.; Karyadi, D.; et al. REVEL: An Ensemble Method for Predicting the Pathogenicity of Rare Missense Variants. *Am. J. Hum. Genet.* **2016**, *99*, 877–885. [CrossRef]
54. Kircher, M.; Witten, D.M.; Jain, P.; O'Roak, B.J.; Cooper, G.M.; Shendure, J. A general framework for estimating the relative pathogenicity of human genetic variants. *Nat. Genet.* **2014**, *46*, 310–315. [CrossRef]
55. The Human Gene Mutation Database Professional (HGMD). Available online: http://www.hgmd.cf.ac.uk/ (accessed on 13 May 2019).
56. Mazzoli, M.; Van Camp, G.; Newton, V.; Giarbini, N.; Declau, F.; Parving, A. Recommendations for the Description of Genetic and Audiological Data for Families with Nonsyndromic Hereditary Hearing Impairment. *Audiol. Med.* **2003**, *1*, 148–150.

International Journal of
Molecular Sciences

MDPI

Review

Tight Junctions of the Outer Blood Retina Barrier

Aisling Naylor, Alan Hopkins, Natalie Hudson and Matthew Campbell *

Smurfit Institute of Genetics, Trinity College Dublin, Dublin 2, Ireland; aisling.naylor@ucdconnect.ie (A.N.); ahopkin@tcd.ie (A.H.); natalie.hudson@tcd.ie (N.H.)
* Correspondence: campbem2@tcd.ie; Tel.: +353-1-8961-482; Fax: +353-1-8963-848

Received: 21 November 2019; Accepted: 19 December 2019; Published: 27 December 2019

Abstract: The outer blood retina barrier (oBRB) formed by the retinal pigment epithelium (RPE) is critical for maintaining retinal homeostasis. Critical to this modified neuro-epithelial barrier is the presence of the tight junction structure that is formed at the apical periphery of contacting cells. This tight junction complex mediates size-selective passive diffusion of solutes to and from the outer segments of the retina. Unlike other epithelial cells, the apical surface of the RPE is in direct contact with neural tissue and it is centrally involved in the daily phagocytosis of the effete tips of photoreceptor cells. While much is known about the intracellular trafficking of material within the RPE, less is known about the role of the tight junction complexes in health and diseased states. Here, we provide a succinct overview of the molecular composition of the RPE tight junction complex in addition to highlighting some of the most common retinopathies that involve a dysregulation of RPE integrity

Keywords: retinal pigment epithelium; retinopathy; tight junction

1. Introduction

The blood retina barrier (BRB) is fundamental in establishing and maintaining a suitable environment for optimum retinal function [1]. While the inner blood retina barrier (iBRB) is composed of tight junctions (TJs) between retinal capillary endothelial cells, the so-called outer blood retina barrier (oBRB) is formed by the TJs between retinal pigment epithelial (RPE) cells. This oBRB acts to regulate and filter molecular movement of solutes and nutrients from the choroid to the sub-retinal space. Impairment of either of these barriers can lead to the accumulation of blood-borne proteins and other potentially toxic solutes within the retina [1] (differences between the oBRB and iBRB are summarised further in Table 1).

The RPE is composed of a single layer of epithelial cells separating the neural retinal from the underlying Bruch's membrane and fenestrated choriocapillaris. TJs connecting neighbouring RPE cells block the movement of plasma components and toxic molecules into the retina as well as allowing for a controlled flow of fluid and solutes across an osmotic gradient from the choroidal vasculature to the outer retina [2]. The retina has the highest oxygen consumption per weight of any tissue in the body and the BRB (both outer and inner) is essential in providing a distinct and regulated source of nutrients to facilitate for this high metabolic rate [3]. TJs at both the iBRB and oBRB are complex, dynamic structures [4] and in the context of these barriers, the integrity of these TJs is crucial to sight.

Specifically, the oBRB allows for the survival of the photoreceptors (PRs) by supporting essential functions including filtering and transport of nutrients and photoreceptor outer segment (POS) phagocytosis. Other important functions of the RPE include absorption of out of focus and scattered light, retinal adhesion, and vitamin A transport and processing, and re-isomerisation of all-trans-retinal to 11-cis retinal, which is crucial for the visual cycle [2,5]. The RPE is essential for visual function, a failure of any one of these functions can lead to degeneration of the retina, loss of visual function, and blindness [2]. The RPE is highly polarized and can be divided into apical and basolateral sides. The

apical surface is in direct contact with the POS and the basolateral side acts as a barrier in its interaction with the highly permeable and highly perfused choriocapillaris of the choroid [6].

TJs allow for high degrees of selectivity in paracellular barrier function in both the iBRB and the oBRB. TJs are unique assemblies of transmembrane proteins and peripheral cytoplasmic proteins. Transmembrane proteins include the claudins, the MARVEL (Mal and related proteins for vesicle trafficking and membrane link) family and junctional adhesion molecules (JAMs), which span the plasma membrane. Peripheral cytoplasmic proteins such as zonula occludens-1, (ZO-1), -2 (ZO-2) and -3 (ZO-3) anchor these transmembrane proteins to the cytoskeleton and are vital in the initial formation and distinct organization of TJs [7,8].

In principle, the inner and outer BRBs are performing inherently similar roles of paracellular diffusion regulation; however, the molecular composition varies considerably in these junctions. In this review, we will discuss the structure and functions of the oBRB, and how its disruption contributes to the pathogenesis of a variety of ocular conditions including diabetic retinopathy (DR), age related macular degeneration (AMD), central serous chorioretinopathy (CSCR), Sorsby's fundus dystrophy, Retinitis Pigmentosa (RP), and conditions associated with mutations in CLDN-19, the gene encoding for the TJ protein claudin-19.

Table 1. A summary of the key differences between the outer blood retina barrier (oBRB) and inner blood retinal barrier (iBRB).

Outer Blood Retinal Barrier	Inner Blood Retinal Barrier
Formed by tight junctions (TJ) between neighbouring retinal pigment epithelium (RPE) cells [1]. Rests on underlying Bruch's membrane [1]	Formed by TJ between neighbouring retinal endothelial cells [1]. Rests on a basal lamina that is covered by the processes of astrocytes and Müller cells [1]
Regulates the paracellular movement of fluids and molecules between the choriocapillaris and the retina [1]	Regulates the paracellular movement of fluids and molecules across retinal capillaries [1]
Claudin-19 is the predominant claudin [9], claudin-3 and -10 are also expressed [10]	Claudin-5 is the most predominant claudin, claudin-1 and -2 are also expressed [11]
Plays a fundamental role in the microenvironment of the outer retina [1] including regulating access of nutrients from blood to photoreceptors (PRs), eliminating waste products, and maintaining retinal adhesion [1]	Plays a fundamental role in the microenvironment of the neural retina [1]
The relationship between the RPE apical villi and PR is considered to be crucial in maintaining visual function [1]	Regulatory signals of the retinal neuronal circuitry are transmitted by astrocytes, muller cells and pericytes thereby influencing the activity of the iBRB [1]

2. The Retinal Pigment Epithelium (RPE)

The RPE is composed of a single layer of cells joined laterally towards their apices by TJs between adjacent plasma membranes (Figure 1a demonstrates the topographic relationship of the RPE within the retina and Figure 1b demonstrates the structure and function of the RPE as described in this section). The apical membrane faces the photoreceptor outer segments (POS) and the basolateral membrane faces Bruch's membrane, thereby separating the RPE from the choroid [2]. In a planar view, RPE cells exhibit a hexagonal shape. Microvilli extend from the apical surface of the RPE and envelop both rod and cone POS. The apical microvilli cloak a greater length of rods than cones [12]. They increase the RPE surface area 30-fold and promote a unique metabolic and functional relationship between the RPE cells and PRs, which is considered to be critical for the maintenance of visual function [1,13].

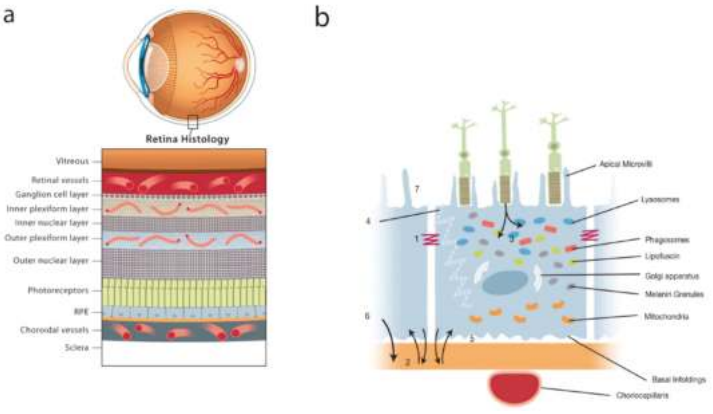

Figure 1. (**a**) Topographic relationship of the retinal pigment epithelium (RPE) within the retina. RPE anatomy and function. (**b**) The functions of the RPE are labelled as follows: (1) Tight junction (TJ) of the outer blood retina barrier (oBRB); (2) Transport of fluid, nutrients, and metabolites (paracellular and transcellular); (3) Phagocytosis of photoreceptor outer segments (POS); (4) Absorption of scattered light; (5) Retinal adhesion; (6) Paracrine secretion (including vascular endothelial growth factor (VEGF)); (7) Maintaining balance across the sub-retinal space.

Laterally, the RPE membrane is the site of cell communication and adhesion. Apically, the composite of gap junctions, adherens junctions (AJs), and TJs form a physical barrier and are involved in the maintenance of cell polarity and the prevention of intramembranous diffusion between the basolateral and apical membrane domains [4,14]. Unlike most epithelia however, the RPE is unusual as its apical surface abuts solid tissue rather than a lumen. This variance allows the neural retina to influence epithelial polarity and the structure and function of TJs [4].

The infoldings of the RPE basal plasma membrane is typical of cells adept in transport. Intracellularly, the organelles tend to display domain specific distribution, with melanosomes primarily in the apical cytoplasm and the mitochondria, Golgi, and nucleus located basally [13].

The RPE has many functions that are vital to the maintenance of normal ocular function and homeostasis. These include phagocytosis of shed POS, retinoid conversion and storage, absorption of scattered light, RPE to PR apposition, and ion and fluid transport [13]. With such a broad spectrum of essential activities involved in vision, it is clear that primary dysregulation of these cells can lead to serious clinical effects, and indeed, given its interaction in many pathways, they must also be vulnerable to secondary damage.

The role of RPE junctional complexes in preventing paracellular movement of molecules and ions make RPE cells the protectors and key effectors of the oBRB [4]. However, they do not form an absolute and persistent wall. In fact, the RPE is moderately leaky in order to support the unique needs of the PRs. This is demonstrated by assessing transepithelial electrical resistance (TEER), which is a measure of paracellular ion movement. By inhibiting the passage of certain ions, TJs allow the RPE to regulate transport and establish concentration gradients between the neural retina and Bruch's membrane [4].

In the context of the oBRB, TJs establish a barrier between the sub-retinal space and the choriocapillaris. RPE cells are responsible for the movement of nutrients and metabolic end products and serve to maintain the ion balance in the sub-retinal space [13]. Channels and pumps mediate the movement of ions and molecules via the transcellular pathway. In one direction, the RPE transports electrolytes and water from the sub-retinal space to the choroid, and in the other direction, the RPE transports glucose and other nutrients from the blood to the PRs [2]. Paracellular resistance is significantly higher than transcellular resistance, subsequently, water transport occurs mainly through transcellular pathways mediated by aquaporin-1 and -4 [2]. The Na^+/K^+-ATPase, which is located

apically in RPE cells, provides the energy for the transport of electrolytes and water from the sub retinal space to the choroid [13]. A substantial amount of water is produced due to the large metabolic turnover of the retina. This constant elimination of water from the inner retina to the choroid produces an elimination force between the retina and RPE. This force is lost by the inhibition of the Na^+/K^+-ATPase. Proper anatomical apposition between RPE and PR cells is essential to the optics of the eye and health of PR cells [13].

Due to exposure to an intense level of light, toxic substances accumulate in PR cells daily [15]. In order for PRs to carry out their role of light transduction efficiently, the POS undergo a constant renewal process [15]. Each rod regenerates its outer segment in 7–12 days [13]. New POS are built at the cilium from the base of the outer segments. The highest concentration of radicals, photo damaged proteins, and lipids are located in the tips, which are shed from the PRs. Shed POS are phagocytosed by the RPE and the process of disk shedding and phagocytosis is tightly coordinated between the RPE and PR [15]. Through this coordinated POS tip shedding and the formation of new POS, a constant length of POS is maintained [15]. Lipofuscin compounds accumulate in the RPE as a consequence of the cells' role in phagocytosing the POS membrane [13]. The RPE facilitates the recycling of the digested shed POS, allowing for essential molecules to be recycled to PRs [2,15]. This process of POS shedding is under circadian control, with the major burst of phagocytosis taking place with the onset of light [16].

The RPE also produces a number of growth factors and other soluble proteins that are essential for the maintenance and structure of the retina and the choriocapillaris [6]. Vascular endothelial growth factor (VEGF) is secreted in low concentrations at the basolateral surface of the RPE in the healthy eye where it prevents endothelial cell apoptosis and is essential for maintaining an intact endothelium associated with the choriocapillaris. It is thought to act as a permeability factor stabilizing the fenestrations of the endothelium [2,13].

3. Tight Junctions (TJs)

TJs are composed of transmembrane proteins and peripheral membrane proteins that interact with each other to form a complex network. Transmembrane proteins extend into the paracellular space, creating a seal characteristic of TJs [3]. These proteins include the MARVEL and claudin family members and JAMs. Scaffolding proteins including ZO-1, ZO-2, and ZO-3 bind to transmembrane proteins, linking these to the cytoskeleton [14]. The TJs create a barrier to paracellular diffusion of solutes as well as the maintenance of cell polarity between the basolateral and apical plasma membrane domains, which are often referred to as the "barrier" and "fence" function, respectively [17].

Since their identification via electron microscopy in 1963, we have learnt a great deal more about the location and composition of TJs [18]. In ultra-thin sections of brain tissues, TJs appear like a sequence of fusions (or kisses), which are formed between two adjacent cells by the outer leaflets of the plasma membrane. At higher magnification, it becomes clear that the membranes are not fused, but rather, are in tight contact with each other [14].

Secretions of the neural retina regulate the assembly, maturation, and tissue-specific properties of these TJs [4]. Initially, adhesive membrane proteins of AJs and TJs form adhesion complexes at sites of cell-to-cell contact. Subsequently, they organise into zipper like structures by lateral adhesion along the cell border [7]. The intracellular partners of transmembrane adhesive proteins also vary during junction maturation and stabilization. Adhesions are in dynamic equilibrium, even after stable contacts have been formed and recycle continuously between the plasma membrane and cytoplasm [8]. In epithelial cells, TJs and AJs follow a well-defined spatial distribution along the cellular cleft with TJs located at the most apical regions and AJs below them [8]. TJs make the most significant contribution to the paracellular component of TEER [4].

The TAMP (TJ-associated MARVEL protein) family members include occludin (MarvelD1), tricellulin (MarvelD2), and MarvelD3 [19,20]. They contain a conserved four-transmembrane MARVEL (Mal and related proteins for vesicle trafficking and membrane link) domain [21]. Occludin, tricellulin,

and marvelD3 have both redundant and unique contributions to epithelial function [19,20]. Occludin was the first transmembrane protein identified in the TJ. It has a molecular mass of 65 kDa, with two extracellular loops, aforementioned four transmembrane loops and its amino and carboxy termini localised intracytoplasmically [22]. Occludin binds directly with the three ZO proteins [8,23] and these interactions are required for the TJ localisation of occludin [20]. Occludin's two extracellular loops are involved in cell–cell adhesion and regulating paracellular permeability, respectively [3]. The C-terminal interacts with ZO-1 and ZO-2 and the last 150 amino acids interact with F-actin [3,22,23]. Expression of C-terminally truncated occludin in MDCKII cells resulted in increased paracellular permeability [24,25]. Over-expression of chicken occludin in MDCK cells leads to an increase in TEER, and therefore a decrease in paracellular permeability [3,26]. In combination, this suggests that occludin plays a potentially pivotal role in established paracellular permeability.

Occludin plays an essential regulatory role in the function of TJs, however, it is unnecessary for TJ formation [27–30]. Occludin associates with ZO-1 at the TJ upon recruitment by JAM-A [7]. This interaction is essential in modulating the function of occludin at the TJ [3]. Occludin has a half-life of approximately 1.5 h and rapidly dissociates from the TJ, indicating that it may facilitate TJs in adapting rapidly to physiologic changes [30,31]. Phosphorylation of occludin has been shown to act as an important regulatory mechanism. Post-translational phosphorylation status of occludin has been found to influence its location within the TJ and its regulation of paracellular permeability [26,32,33]. Threonine and serine phosphorylation of occludin appears to occur in conjunction with the preservation of TJ integrity [3]. Conversely, tyrosine phosphorylation of occludin appears to disrupt the association of ZO-1 and occludin, and demonstrates increased paracellular permeability [3]. In phosphorylated occludin, the binding of Z0-1, Z0-2, and Z0-3 to the C-terminal tail were decreased in comparison to non-phosphorylated occludin [3,34].

The Claudins are a family of transmembrane proteins of which there are more than 24 established members [14]. Like occludin, claudins have four membrane spanning regions, two extracellular loops, and two cytoplasmic termini/intracellular domains [14]. C-terminal amino acids encode PDZ-binding motifs, which are highly conserved throughout the claudin family. Through the C-terminal domain, claudins directly interact with peripheral PDZ-domain containing proteins including- ZO-1, ZO-2, and ZO-3 [14]. The first extracellular domain determines TEER and paracellular charge selectivity [35].

Claudin proteins mediate robust cell–cell adhesion and directly regulate permeability and selectivity [14,36]. They are almost certainly the main proteins important for TJ strand formation [14,30]. Claudins form pores facilitating the passive diffusion of molecules through the paracellular space [37]. Each claudin is thought to have a unique effect on selectivity and permeability [28,37] with the specific paracellular properties of different epithelia resulting from their individual pattern of claudin expression [36]. In the RPE, the claudins that are expressed vary among species [30]. In humans, claudin-3, claudin-10, and claudin-19 were detected in TJs [10] whereas in chicks, claudin-19 is not expressed and claudin-20 is the major claudin [9]. Some claudins have a limited distribution expressed in a tissue-specific manner, for example, claudin-5 appears to be confined to endothelial cells [8,38]. Claudin-1 to claudin-8 bind directly with ZO-1, ZO-2, and ZO-3 [8,39] via the cytoplasmic domain of claudins and the first PDZ domain of ZO proteins [39].

Claudin-19 is expressed and enriched in the RPE, where it is by far the predominant claudin [9]. High levels of claudin-19 are also found in the kidneys [9]. Claudin-19 determines permeability and semi-selectivity of the TJs in the RPE. By knocking-down claudin-19, the expressed claudin-3 was inadequate to form effective TJs. In contrast, the knockdown of claudin-3 demonstrated no effects [9]. Mutated claudin-19 affects multiple stages of RPE and retinal differentiation through its effects on multiple functions of the RPE [40,41]. Of note, claudin-10 was only expressed in a subset of cells [10].

The JAMs are a family of transmembrane proteins, of which four members have been identified: JAM-A, JAM-B, JAM-C, and JAM4/JAML [14]. JAMs are known to interact with many other proteins and may modulate TJ function by targeting other proteins to the TJ [8,14]. JAM-A can co-localize with occludin, ZO-1, and cingulin [7]. JAMs are members of the immunoglobulin superfamily and

are expressed in epithelial cells along with endothelial cells, platelets, and leukocytes [14]. They are composed of a single transmembrane domain, and an extracellular domain containing two Ig-like motifs [14]. A PDZ-binding motif at the C terminus appears to be involved with the mediation of interaction with TJ scaffolding proteins, which appears to be important for the proper function of the TJ [42].

Peripheral membrane proteins anchor transmembrane proteins to the actin cytoskeleton and allow them to organize in the membrane and initiate cell signalling [3,14]. These include ZO-1, ZO-2, ZO-3, and cingulin [7].

The ZO proteins belong to the family of membrane associated guanylate kinases (MAGUK) that possesses a distinct molecular organisation. The core structure is composed of one or more PDZ domains, a Src homology 3 (SH3) domain, and a guanylate kinase (GUK) domain [14,43]. ZO-1 was the first TJ protein discovered in both epithelial and endothelial cells [44,45]. ZO-2 and ZO-3 were later discovered to localise to TJs with a similar sequence homology to ZO-1 [45]. ZO-1 has been shown to play a central role in the assembly and function of TJs [14]. PDZ domains facilitate the formation of specific multi-protein complexes including those necessary for TJ formation by recruiting downstream proteins in a signalling pathway [3]. At the TJ, the PDZ domain binds to the actin cytoskeleton through the C-terminal end and forms a bridge between the C-terminal sequences of occludin and β-actin [3]. It interacts with ZO-2 and ZO-3, its binding partners, through its second PDZ domain [11,43]. ZO proteins form a complex with AJ proteins in non-polarised cells where TJs have not formed, but upon polarisation, ZO proteins can separate from the AJ and concentrate in the TJ where they interact with TJ proteins such as claudins and occludin [46]. ZO-1 has also been found to participate in the regulation of gene expression via its binding in the nucleus to a transcription factor called Zonula-Occludens Associated Nucleic Acid-Binding protein (ZONAB). This interaction may allow TJs to regulate epithelial cell proliferation and cell density [47,48].

ZO-1 has been shown to be present in many ocular tissues including several retinal layers in the mammalian retina. This displays the role of ZO-1 in a wide portfolio of cellular functions in addition to mediating barrier function [3].

4. Role in Pathology

As we have established, the RPE has a wide ranging and diverse number of functions and the oBRB plays a crucial role in establishing the optimal conditions for the functioning of PRs and as such, also for visual function. In this section, we will discuss how the disruption of the oBRB contributes to the pathogenesis of a range of ocular pathologies namely DR, and diabetic macular oedema (DMO), AMD, CSCR, Sorsby's fundal dystrophy, and RP, and also examine conditions associated with mutations in CLDN-19. It should be noted that this is not a complete list of all ocular conditions caused by the disruption of the oBRB, however, for the purpose of the review, we will focus solely on these conditions.

5. Diabetic Retinopathy

Diabetic retinopathy (DR) is the leading cause of blindness among working aged individuals in developed countries. In type 1 diabetes, proliferative diabetic retinopathy (PDR) is the most common sight threatening lesion and is characterised by neovascularisation secondary to a hypoxic insult [2]. In type 2 diabetes, DMO is the primary cause of visual loss, resulting from vascular leakage due to the breakdown of the iBRB [2]. It has been well described previously that iBRB alteration from endothelial cell dysfunction leads to DMO and subsequently retinopathy progression [1]. However, less is known about the role of the oBRB in DR.

There is growing evidence for diabetes induced oBRB dysfunction as observed in both human and animal studies [49,50]. The oBRB specific leakage has been visualised in diabetic and ischemic rodents demonstrating diabetic and ischemia-induced breakdown of TJs in the RPE, with one study reporting that the oBRB contributed a third of the total vascular leakage in diabetic retinas [51]. Significant depletion of occludin in the RPE of ischemic and diabetic rodents was also observed, suggesting that

this leakage is a consequence of the breakdown of TJs in the oBRB [51]. In rodents with early stages of diabetes (those without discernible vascular leakage or TJ breakdown), reduced RPE absorptive capacity occurred before the breakdown of TJ strands [52]. In examining ZO-1 staining in hyperglycaemic rats, the TJ appeared wider and demonstrated small holes [52]. It was found that as a consequence of these conditions, the retina becomes highly hypoxic, which causes the upregulation of hypoxia inducible factor-1 (HIF) alpha and VEGF [39]. Upregulation of the VEGF signalling pathway ultimately leads to the loss of barrier function and TJ-integrity in the oBRB [51,52]. The oBRB breakdown then results in the leakage of blood contents and influx of osmolytes, which precedes subretinal oedema and exudative retinal detachment [51]. Furthermore, hyperglycaemia induces a loss of Na^+/K^+-ATPase function, which could impair the transport of water from the sub retinal space to choriocapillaris and consequently might contribute to DMO development [2].

6. Age-Related Macular Degeneration (AMD)

Age-related macular degeneration (AMD) is the leading cause of central retinal vision loss in developed countries, with an estimated one in 10 people over the age of 55 showing signs of the condition [53]. It is a complex, multifactorial disease characterised by RPE dysfunction and macular PR loss [13]. Advanced AMD presents in two forms that are generally referred to as "dry" or "wet". Choroidal neovascularisation (CNV) is associated with wet AMD and occurs when new blood vessels sprout from the underlying choroidal vasculature and disrupt the integrity of the retina, leading to acute visual loss [54,55]. Geographic atrophy (GA) secondary to dry AMD occurs when the RPE begins to degenerate in the region of the macula leading to cone PR cell death and eventual central vision loss [55,56].

As discussed, the basal surface of the RPE rests on Bruch's membrane. In the aging eye, extracellular material is deposited in Bruch's membrane [13] and as a result, the thickness of Bruch's membrane increases and permeability decreases [56,57]. Aging involves an accumulation of oxidative insults and a concomitant decrease in protective mechanisms [58]. The accumulation of lipofuscin in the RPE has been suggested to act as a starting point [15]. The initial triggers for age-related degenerative diseases are thought to be oxidative damage [15,58]. In patients with AMD, the RPE's adaptive response to stress becomes dysregulated and an increasing imbalance of protective and toxic factors contributes to macular damage and the development of retinal lesions [15]. Reduced capacity of the RPE to absorb light energy is also an important factor in the cascade of events leading to AMD [15].

VEGF is secreted from the basolateral side of healthy RPE cells and is involved in the regulation of choroidal vasculature. Overexpression of VEGF is an important factor in the pathogenesis of CNV in wet AMD [6]. An imbalance between pro-angiogenic and anti-angiogenic factor in favour of the formation of new vessels [59] is likely to occur as a result of local hypoxia, inflammation, and dysregulated wound healing secondary to RPE cell loss [15]. It is the integrity of the oBRB that keeps the choroidal vascular response from invading the retina and changing dry into wet AMD [1] and the loss of this RPE–RPE attachment can induce VEGF overexpression [60]. RPE degeneration, tears, drusen formation, or apoptosis associated with aging can cause a loss of the RPE–RPE attachment [60]. Intravitreal agents that block VEGF have revolutionised the care of patients with wet AMD, decreasing growth, and leakage from CNV lesions, and preventing moderate and severe visual loss [59].

7. Central Serous Chorioretinopathy (CSCR)

Central serous chorioretinopathy (CSCR) is a disease of the retina characterised by serous detachment of the neurosensory retina secondary to focal lesions of the RPE. The mechanism whereby sub retinal fluid is produced is poorly understood [61]. It is thought that the choroidal vascular hyperpermeability occurs in CSCR, possibly as a result of stasis, ischaemia, or inflammation. Once the hydrostatic pressure is sufficiently high, the RPE is pushed forward, leading to discontinuing of the barrier and promoting pigment epithelial detachments. This overwhelms the barrier function of the RPE and leads to fluid accumulation within the RPE [62].

8. Sorsby's Fundus Dystrophy

Sorsby's fundus dystrophy is an autosomal dominant condition of the central retina. Similar to AMD, there is an accumulation of drusen deposits in Bruch's membrane [13]. It is caused by variants in the gene for tissue inhibitor of metalloproteinases-3 (TIMP-3), which has been found in the drusen-like deposits that occur in patients with the condition [63]. TIMP-3 functions to regulate the thickness of Bruch's membrane by inhibiting matrix metalloproteinases and also inhibits VEGF signalling and therefore angiogenesis [63]. Sorsby's fundus dystrophy leads to eventual CNV and PR cell loss [63].

9. Retinitis Pigmentosa

Retinitis Pigmentosa (RP) is the term given to a set of hereditary retinal diseases that feature degeneration of rod and cone PRs and characteristic retinal deposits [64]. In most cases, it is due to the primary degeneration of rods with secondary cone degeneration [65]. In the first instance, RP patients typically lose night vision, followed by peripheral vision, and eventually central vision later in life [64,66]. Rhodopsin was the first gene identified and encodes rod visual pigment. The gene products localised in rods being involved in several visual pathways including a protein of rod visual transduction, cytoskeleton proteins, trafficking proteins, and PR differentiation [65]. There are at least 200 different mutations in more than 60 genes that are linked to RP [67]. Many of the pathways vary dramatically ranging from visual pigments to visual cycle to metabolism and RNA splicing [65]. In RHO(-/-) knockout mice (mice that carry a targeted disruption of the rhodopsin gene and present with rapid PR degeneration) upregulation of ZO-1 has been demonstrated when compared to wild type [66]. This finding may represent a physiological response to PR cell degeneration and appears to be associated with the retinal vasculature of the RHO (−/−) mice. In RHO (−/−) mice, blood vessels appear more clustered and thicker in appearance compared to the wild-type [66]. In contrast, a study looking at retinal degeneration 9 (Rd9) mice (mice that represent a rare model of X-linked RP) demonstrate a decrease in the intensity of ZO-1 staining [67].

In addition, RP may be complicated by cystoid macular oedema (CMO), which represents an important and treatable cause of central visual loss in RP [68]. The underlying pathogenesis remains unclear, however, breakdown of the BRB is a proposed mechanism for the development of CMO in RP [68]. The release of toxic products from the degenerating retina or RPE may cause CMO by disrupting the BRB. The iBRB is the primary site of vascular leakage in RP complicated by CMO in both patients with early and severe RP. Interestingly, patients with more extensive RP demonstrated greater leakage through the RPE compared to those with less extensive RP [69]. In eyes with RP alone, albumin leakage was greatest from the iBRB, however, in RP-associated with other complications such as aphakia and glaucoma leakage varied between iBRB and oBRB [70].

Mutations in CLDN-19

As discussed earlier, claudin-19 is the predominant claudin in the human RPE [9]. Mutations in CLDN-19 cause the renal disease familial hypomagnesemia with hypercalciuria and nephrocalcinosis (FHHNC); ocular involvement (FHHNCOI) results in a varied array of ocular defects demonstrating incomplete penetrance [40,41]. In severe cases, symptoms appear in infants as young as 4–9 months old including bilateral macular coloboma, chorioretinal degeneration, nystagmus, strabismus, and visual loss [41]. Another study has reported that patients affected this mutation present with disrupted optic disc development resulting in near blindness and horizontal nystagmus [40]. The pathogenesis of such defects in FHHNCOI is yet to be determined.

10. Conclusions

In conclusion, the RPE is a single layer of cells that separates the neural retina from the underlying Bruch's membrane and choroid. The TJs between the RPE form the oBRB, which is essential for the maintenance of visual function. In this review, we discussed the RPE and the oBRB in detail and

examined the effect of its dysfunction, which can lead to an array of pathological ocular conditions. Understanding the complex molecular function of the oBRB will inform our understanding of a range of retinal diseases and could ultimately lead to the development of therapies aimed at restoring oBRB function and integrity.

Author Contributions: Conceptualisation, A.N.; A.H.; N.H.; and M.C.; Writing—original draft preparation, A.N.; and A.H; Writing—review and editing, A.N.; N.H.; and M.C.; supervision, N.H.; and M.C. All authors have read and agreed to the published version of the manuscript.

Funding: Work in the Campbell lab at Trinity College Dublin is supported by grants from Science Foundation Ireland (SFI), (12/YI/B2614 and 11/PI/1080), The Health Research Board of Ireland (HRB), the BrightFocus Foundation, and Enterprise Ireland (EI). The Campbell lab at TCD is also supported by an SFI Centres grant supported in part by a research grant from SFI under grant number 16/RC/3948 and co-funded under the European Regional Development fund by FutureNeuro industry partners.

Conflicts of Interest: The authors declare no conflicts of interest.

References

1. Cunha-Vaz, J.; Bernardes, R.; Lobo, C. Blood-retinal barrier. *Eur. J. Ophthalmol.* **2011**, *21*, 3–9. [CrossRef]
2. Simó, R.; Villarroel, M.; Corraliza, L.; Hernández, C.; Garcia-Ramírez, M. The Retinal pigment epithelium: Something more than a constituent of the blood-retinal barrier—Implications for the pathogenesis of diabetic retinopathy. *J. Biomed. Biotechnol.* **2010**, *2010*, 190724. [CrossRef] [PubMed]
3. Campbell, M.; Humphries, P. The blood-retina barrier. In *Biology and Regulation of Blood-Tissue Barriers*; Cheng, C.Y., Ed.; Advances in Experimental Medicine and Biology; Springer: New York, NY, USA, 2013; pp. 70–84, ISBN 978-1-4614-4711-5.
4. Rizzolo, L.J. Development and role of tight junctions in the retinal pigment epithelium. *Int. Rev. Cytol.* **2007**, *258*, 195–234. [CrossRef] [PubMed]
5. Marmorstein, A.D.; Finnemann, S.C.; Bonhila, V.L.; Rodriguez-Boulan, E. Morphogenesis of the retinal pigment epithelium: Toward understanding retinal degenerative diseases. *Ann. N.Y. Acad. Sci.* **1998**, *857*, 1–12. [CrossRef] [PubMed]
6. Marneros, A.G.; Fan, J.; Yokoyama, Y.; Gerber, H.P.; Ferrara, N.; Crouch, R.K.; Olsen, B.R. Vascular endothelial growth factor expression in the retinal pigment epithelium Is essential for choriocapillaris development and visual function. *Am. J. Pathol.* **2005**, *167*, 1451–1459. [CrossRef]
7. Bazzoni, G.; Martínez-Estrada, O.M.; Orsenigo, F.; Cordenonsi, M.; Citi, S.; Dejana, E. Interaction of Junctional Adhesion Molecule with the Tight Junction Components ZO-1, Cingulin, and Occludin. *J. Biol. Chem.* **2000**, *275*, 20520–20526. [CrossRef]
8. Bazzoni, G.; Dejana, E. Endothelial cell-to-cell junctions: Molecular organization and role in vascular homeostasis. *Physiol. Rev.* **2004**, *84*, 869–901. [CrossRef]
9. Peng, S.; Rao, V.S.; Adelman, R.A.; Rizzolo, L.J. Claudin-19 and the barrier properties of the human retinal pigment epithelium. *Investig. Ophthalmol. Vis. Sci.* **2011**, *52*, 1392–1403. [CrossRef]
10. Peng, S.; Adelman, R.A.; Rizzolo, L.J. Minimal effects of VEGF and anti-VEGF drugs on the permeability or selectivity of RPE tight junctions. *Investig. Ophthalmol. Vis. Sci.* **2010**, *51*, 3216–3225. [CrossRef]
11. Luo, Y.; Xiao, W.; Zhu, X.; Mao, Y.; Liu, X.; Chen, X.; Huang, J.; Tang, S.; Rizzollo, L.W. Differential expression of claudins in retinas during normal development and the angiogenesis of oxygen induced retinopathy. *Investig. Ophthalmol. Vis. Sci.* **2011**, *52*, 7556–7564. [CrossRef]
12. Anderson, D.H.; Fisher, S.K. The relationship of primate foveal cones to the pigment epithelium. *J. Ultrastruct. Res.* **1979**, *67*, 23–32. [CrossRef]
13. Sparrow, J.R.; Hicks, D.; Hamel, C.P. The retinal pigment epithelium in health and disease. *Curr. Mol. Med.* **2010**, *10*, 802–823. [CrossRef] [PubMed]
14. Shin, K.; Fogg, V.C.; Margolis, B. Tight junctions and cell polarity. *Annu. Rev. Cell Dev. Biol.* **2006**, *22*, 207–235. [CrossRef] [PubMed]
15. Strauss, O. The retinal pigment epithelium in visual function. *Physiol. Rev.* **2005**, *85*, 845–881. [CrossRef]
16. Besharse, J.C.; Hollyfield, J.G.; Raybron, M.E. Photoreceptor outer segments: Accelerated membrane renewal in rods after exposure to light. *Science* **1997**, *196*, 536–538. [CrossRef]

17. Sakakibara, A.; Furuse, M.; Saitou, M.; Ando-Akatsuka, Y.; Tsukita, S. Possible involvement of phosphorylation of occludin in tight junction formation. *J. Cell Biol.* **1997**, *137*, 1393–1401. [CrossRef]
18. Farquhar, M.G.; Palade, G.E. Junctional complexes in various epithelia. *J. Cell Biol.* **1963**, *17*, 375–412. [CrossRef]
19. Diaz-Coranguez, M.; Liu, X.; Antonetti, D.A. Tight junctions in cell proliferation. *Int. J. Mol. Sci.* **2019**, *20*, 5972. [CrossRef]
20. Raleigh, D.R.; Marchiando, A.M.; Zhang, Y.; Shen, L.; Sasaki, H.; Wang, Y.; Long, M.; Turner, L.R. Tight junction-associated MARVEL proteins marvelD3, tricellulin and occludin have distinct but overlapping functions. *Mol. Biol. Cell* **2010**, *21*, 1200–1213. [CrossRef]
21. Mariano, C.; Sasaki, H.; Brites, D.; Brito, M.A. A look at tricellulin and its role in tight junction formation and maintenance. *Eur. J. Cell Biol.* **2011**, *90*, 787–796. [CrossRef]
22. Furuse, M.; Hirase, T.; Itoh, M.; Nagafuchi, A.; Yonemura, S.; Tsukita, S.; Tsukita, S. Occludin: A novel integral membrane protein localizing at tight junctions. *J. Cell Biol.* **1993**, *123*, 1777–1788. [CrossRef]
23. Furuse, M.; Itoh, T.; Hirase, A.; Nagafuchi, S.; Yonemura, S.; Tsukita, S.; Tsukita, S. Direct association of occludin with ZO-1 and its possible involvement in the localization of occludin at tight junctions. *J. Cell Biol.* **1994**, *127*, 1617–1626. [CrossRef]
24. Balda, M.S.; Whitney, J.A.; Flores, C.; Gonzalez, S.; Cereijido, M.; Matter, K. Functional dissociation of paracellular permeability and transepithelial electrical resistance and disruption of the apical-basolateral intramembrane diffusion barrier by expression of a mutant tight junction membrane protein. *J. Cell Biol.* **1996**, *134*, 1031–1049. [CrossRef] [PubMed]
25. Chen, Y.; Merzdorf, C.; Paul, D.L.; Goodenough, D.A. COOH terminus of occludin is required for tight junction barrier function in early Xenopus embryos. *J. Cell Biol.* **1997**, *138*, 891–899. [CrossRef] [PubMed]
26. Feldman, G.J.; Mullin, J.M.; Ryan, M.P. Occludin: Structure, function and regulation. *Adv. Drug Deliv. Rev.* **2005**, *57*, 883–917. [CrossRef] [PubMed]
27. Saitou, M.; Fujimoto, K.; Doi, Y.; Fujimoto, T.; Furuse, M.; Takano, H.; Noda, T.; Tsukita, S. Occludin-deficient embryonic stem cells can differentiate into polarized epithelial cells bearing tight junctions. *J. Cell Biol.* **1998**, *141*, 397–408. [CrossRef] [PubMed]
28. Saitou, M.; Furuse, M.; Sasaki, H.; Schulzke, J.D.; Fromm, M.; Takano, H.; Noda, T.; Tsukita, S. Complex phenotype of mice lacking occludin, a component of tight junction strands. *Mol. Biol. Cell* **2000**, *11*, 4131–4142. [CrossRef]
29. Wong, V.; Gumbiner, B.M. A synthetic peptide corresponding to the extracellular domain of occludin perturbs the tight junction permeability barrier. *J. Cell Biol.* **1997**, *136*, 399–409. [CrossRef]
30. Rizzolo, L.; Peng, S.; Luo, Y.; Xiao, W. Integration of tight junctions and claudins with the barrier functions of the retinal pigment epithelium. *Prog. Retin. Eye Res.* **2011**, *30*, 296–323. [CrossRef]
31. Traweger, A.; Fang, D.; Liu, Y.C.; Stelzhammer, W.; Krizbai, I.A.; Bauer, H.C.; Bauer, H. The Tight-Junction Specific Protein Occludin is a Functional Target of the E3 Ubiquitin-Protein Ligase Itch. *J. Biol. Chem.* **2002**, *277*, 10201–10208. [CrossRef]
32. Wong, V. Phosphorylation of occludin correlates with occludin localization and function at the tight junction. *Am. J. Physiol.* **1997**, *273*, 1859–1867. [CrossRef] [PubMed]
33. Staddon, J.M.; Smales, C.; Schulze, C.; Esch, F.S.; Rubin, L.L. p120, a p120-related protein (p100), and the cadherin/catenin complex. *J. Cell Biol.* **1995**, *130*, 369–381. [CrossRef] [PubMed]
34. Kale, G.; Naren, A.P.; Sheth, P.; Rao, R.K. Tyrosine phosphorylation of occludin attenuates its interactions with ZO-1, ZO-2, and ZO-3. *Biochem. Biophys. Res. Commun.* **2003**, *302*, 324–329. [CrossRef]
35. Colegio, O.R.; Van Itallie, C.; Rahner, C.; Anderson, J.M. Claudin extracellular domains determine paracellular charge selectivity and resistance but not tight junction fibril architecture. *Am. J. Physiol. Cell Physiol.* **2003**, *284*, 1346–1354. [CrossRef]
36. Colegio, O.R.; Van Itallie, C.; McCrea, H.J. Claudins create charge-selective channels in the paracellular pathway between epithelial cells. *Am. J. Physiol. Cell Physiol.* **2002**, *282*, 142–147. [CrossRef]
37. Van Italie, C.M.; Anderson, J.M. Claudins and paracellular transport. *Annu. Rev. Physiol.* **2006**, *68*, 403–429. [CrossRef]
38. Morita, K.; Sasaki, H.; Furuse, M.; Tsukita, S. Endothelial claudin: Claudin-5/TMVCF constitutes tight junction strands in endothelial cells. *J. Cell Biol.* **1999**, *147*, 185–194. [CrossRef]

39. Itoh, M.; Furuse, M.; Morita, K.; Kubota, K.; Saitou, M.; Tsukita, S. Direct binding of three tight junction-associated MAGUKs, ZO-1, ZO-2, and ZO-3, with the COOH termini of claudins. *J. Cell Biol.* **1999**, *147*, 1351–1363. [CrossRef]
40. Konrad, M.; Schaller, A.; Seelow, D.; Pandey, A.V.; Waldegger, S.; Lesslauer, A.; Vitzthum, H.; Suzuki, Y.; Luk, J.M.; Becker, C.; et al. Mutations in the tight-junction gene claudin 19 (CLDN19) are associated with renal magnesium wasting, renal failure, and severe ocular involvement. *Am. J. Hum. Genet.* **2006**, *79*, 949–957. [CrossRef]
41. Wang, S.B.; Xu, T.; Peng, S.; Singh, D.; Ghiassi-Nejed, M.; Adelman, R.A.; Rizzolo, L.J. Disease-associated mutations of claudin-19 disrupt retinal neurogenesis and visual function. *Commun. Biol.* **2019**, *2*, 113. [CrossRef]
42. Mandell, K.J.; Parkos, C.A. The JAM family of proteins. *Adv. Drug Deliv. Rev.* **2005**, *57*, 857–867. [CrossRef] [PubMed]
43. Gonzalez-Mariscal, L.; Betanzos, A.; Avila-Flores, A. MAGUK proteins: Structure and role in the tight junction. *Semin. Cell. Dev. Biol.* **2000**, *11*, 315–324. [CrossRef] [PubMed]
44. Stevenson, B.R.; Siliciano, J.D.; Mooseker, M.S.; Goodenough, D.A. Identification of ZO-1: A high molecular weight polypeptide associated with the tight junction (zonula occludens) in a variety of epithelia. *J. Cell Biol.* **1986**, *103*, 755–766. [CrossRef] [PubMed]
45. Tsukita, S.; Furuse, M.; Itoh, M. Multifunctional strands in tight junctions. *Nat. Rev. Mol. Cell Biol.* **2001**, *2*, 285–293. [CrossRef]
46. Muller, S.L.; Portwich, M.; Schmidt, A.; Utepbergenov, D.I.; Huber, O.; Blasig, I.E.; Krause, G. The tight junction protein occludin and the adherens junction protein α-catenin share a common interaction mechanism with ZO-1. *J. Biol. Chem.* **2005**, *280*, 3747–3756. [CrossRef]
47. Balda, M.S.; Matter, K. The tight junction protein ZO-1 and an interacting transcription factor regulate ErbB-2 expression. *EMBO. J.* **2000**, *19*, 2024–2033. [CrossRef]
48. Balda, M.S.; Garrett, M.D.; Matter, K. The ZO-1-associated Y-box factor ZONAB regulates epithelial cell proliferation and cell density. *J. Cell Biol.* **2003**, *160*, 423–432. [CrossRef]
49. Vinores, S.A.; Gadegbeku, C.; Campochiaro, P.A.; Green, W.R. Immunohistochemical localization of blood-retinal barrier breakdown in human diabetics. *Am. J. Pathol.* **1989**, *134*, 231–235. [CrossRef]
50. Xia, T.; Rizzolo, L.J. Effects of diabetic retinopathy on the barrier functions of the retinal pigment epothelium. *Vis. Res.* **2017**, *129*, 72–81. [CrossRef]
51. Xu, H.Z.; Le, Y.Z. Significant of outer blood-retina breakdown in diabetes and ischaemia. *Investig. Ophthalmol. Vis. Sci.* **2011**, *53*, 2160–2164. [CrossRef]
52. Desjardins, D.M.; Yates, P.W.; Dahrouj, M.; Yiu, Y.; Crosson, C.E.; Ablonczy, Z. Progressive early breakdown of retinal pigment epithelium function in hyperglycaemic rats. *Investig. Ophthalmol. Vis. Sci.* **2016**, *57*, 2706–2713. [CrossRef] [PubMed]
53. Wong, W.L.; Su, X.; Li, X.; Cheung, C.M.; Klein, R.; Cheng, C.Y.; Wong, T.Y. Global prevalence of age-related macular degeneration and disease burden projection for 2020 and 2040: A systematic review and meta-analysis. *Lancet Glob. Health* **2014**, *2*, 106–116. [CrossRef]
54. Chakravarthy, U.; Evans, J.; Rosenfeld, P.J. Age related macular degeneration. *BMJ* **2010**, *340*, 981. [CrossRef] [PubMed]
55. Cook, H.L.; Pater, P.J.; Tufail, A. Age-related macular degeneration: Diagnosis and management. *Br. Med. Bull.* **2008**, *85*, 127–149. [CrossRef]
56. Fleckenstein, M.; Mitchell, P.; Freund, K.B.; Sadda, S.; Holz, F.G.; Brittain, C.; Henry, E.C.; Ferrara, D. The progression of geographic atrophy secondary to age-related macular degeneration. *Ophthalmology* **2018**, *125*, 369–390. [CrossRef]
57. Ramrattan, R.S.; van der Schaft, T.L.; Mooy, C.M.; de Bruijn, W.C.; Mulder, P.G.; de Jong, P.T. Morphometric analysis of Bruch's membrane, the choriocapillaris, and the choroid in aging. *Investig. Ophthalmol. Vis. Sci.* **1994**, *35*, 2857–2864.
58. Chen, M.; Xu, H. Parainflammation, chronic inflammation, and age related macular degeneration. *J. Leukoc. Biol.* **2015**, *98*, 713–723. [CrossRef]
59. Brassler, S.B. Introduction: Understanding the role of angiogenesis and antiangiogenic agents in age-related macular degeneration. *Ophthalmology* **2009**, *116*, S1–S7. [CrossRef]

60. Farjood, F.; Vargis, E. Physical disruption of cell-cell contact induced VEGF expression in RPE cells. *Mol. Vis.* **2017**, *23*, 431–446, pmc:5524271.
61. Wang, M.; Munch, I.C.; Hasler, P.W.; Prunte, C.; Larsen, M. Central serous retinopathy. *Acta. Ophthalmol. Scand.* **2008**, *86*, 126–145. [CrossRef]
62. Nicholson, B.; Noble, J.; Forooghian, F.; Meyerle, C. Central serous chorioretinopathy: Update on pathophysiology and treatment. *Surv. Ophthalmol.* **2014**, *58*, 103–126. [CrossRef] [PubMed]
63. Christensen, D.R.G.; Brown, F.E.; Cree, A.J.; Ratnayaka, J.A.; Lotery, A.J. Sorsby fundus dystrophy—A review of pathology and disease mechanisms. *Exp. Eye Res.* **2017**, *165*, 35–46. [CrossRef] [PubMed]
64. Hartong, D.T.; Berson, E.L.; Dryja, T.P. Retinitis Pigmentosa. *Lancet* **2006**, *368*, 1795–1809. [CrossRef]
65. Hamel, C. Retinitis Pigmentosa. *Orphanet J. Rare Dis.* **2006**, *1*, 40. [CrossRef]
66. Campbell, M.; Humphries, M.; Kennan, A.; Kenna, P.; Humphries, P.; Brankin, B. Aberrant retinal tight junction and adherens junction protein expression in an animal model of autosomal recessive Retinitis pigmentosa: The Rho (−/−) mouse. *Exp. Eye Res.* **2006**, *83*, 484–492. [CrossRef]
67. Falasconi, F.; Biagioni, M.; Novelli, E.; Piabo, I.; Gargini, C.; Strettoi, E. Retinal phenotype in the rd9 mutant mouse, a model of X-linked RP. *Front. Neurosci.* **2019**, *13*, 991. [CrossRef]
68. Wang, W.; Kini, A.; Wang, Y.; Liu, T.; Chen, Y.; Vukmanic, E.; Emery, D.; Liu, Y.; Jin, L.; Lee, S.J.; et al. Metabolic deregulation of the blood-outer retinal barrier in retinitis pigmentosa. *Cell Rep.* **2019**, *28*, 1323–1334. [CrossRef]
69. Vinores, S.A.; Kuchle, M.; Derevjanik, N.L.; Henderer, J.D.; Mahlow, J.; Green, W.R.; Campochiaro, P.A. Blood-retinal barrier breakdown in retinitis pigmentosa: Light and electron microscopic immunolocalization. *Histol. Histopathol.* **1995**, *10*, 913–923.
70. Strong, S.; Liew, G.; Michaelides, M. Retinitis pigmentosa-associated cystoid macular oedema: Pathogenesis and avenues of intervention. *Br. J. Ophthalmol.* **2017**, *101*, 31–37. [CrossRef]

International Journal of
Molecular Sciences

MDPI

Review

Cerebral Cavernous Malformation Proteins in Barrier Maintenance and Regulation

Shu Wei [1,2,†], Ye Li [2,†], Sean P. Polster [3], Christopher R. Weber [2], Issam A. Awad [3] and Le Shen [2,3,*]

1 Graduate Program in Public Health and Preventive Medicine, Wuhan University of Science and Technology, Wuhan 430081, China; shuwza@gmail.com
2 Department of Pathology, The University of Chicago, Chicago, IL 60615, USA; yli170@bsd.uchicago.edu (Y.L.); cweber@bsd.uchicago.edu (C.R.W.)
3 Section of Neurosurgery, Department of Surgery, The University of Chicago, Chicago, IL 60615, USA; spolster@uchicago.edu (S.P.P.); iawad@uchicago.edu (I.A.A.)
* Correspondence: leshen@uchicago.edu
† These authors contributed equally.

Received: 10 December 2019; Accepted: 15 January 2020; Published: 20 January 2020

Abstract: Cerebral cavernous malformation (CCM) is a disease characterized by mulberry shaped clusters of dilated microvessels, primarily in the central nervous system. Such lesions can cause seizures, headaches, and stroke from brain bleeding. Loss-of-function germline and somatic mutations of a group of genes, called *CCM* genes, have been attributed to disease pathogenesis. In this review, we discuss the impact of *CCM* gene encoded proteins on cellular signaling, barrier function of endothelium and epithelium, and their contribution to CCM and potentially other diseases.

Keywords: cerebral cavernous malformation; endothelial barrier; epithelial barrier; Rho; ROCK; MEKK3

1. Introduction

One of the key functions of endothelial and epithelial cells is to create a barrier that separates different tissue compartments, and in the case of skin, epithelial cells separate body and outer environment. Compromised barrier function leads to abnormal mixing of different tissue components, which can contribute to pathogenesis of many diseases. In this review, we focus on a group of proteins that participates in the development of a neurovascular disease, cerebral cavernous malformation (CCM), and examine their impact on cellular signaling and barrier function.

2. Clinical Features of CCM

CCM (also known as cavernous angioma) disease is characterized by the development of abnormally dilated capillaries, primarily in the central nervous system (Figure 1) [1]. Grossly, these lesions appear to be blood filled, mulberry shaped clusters of thin-walled small vessels. Histologically, the nested microvessels have little supporting tissue and intervening parenchyma, and the dilated vessels are lined by a single layer of dysmorphic endothelial cells. Thrombi frequently form in these vessels, and hemosiderin deposits can be seen adjacent to these capillaries, indicating chronic bleeding (Figure 2). CCM patients are mostly diagnosed by magnetic resonance imaging initiated due to neurological changes, including headache, seizures, and other neurological deficits, such as nausea or vomiting, weakness or numbness, slurred speech, and altered vision. About 25% to 50% of CCM patients do not have clinical symptoms, and only a small fraction of these patients is identified incidentally [2,3]. The prevalence of CCM is about 0.5% in the general population [4,5], and about 70% to 80% of CCM patients have one lesion, and the other 20% to 30% of CCM patients have more than one lesion [6,7]. Most of the patients with one lesion have the sporadic form of the disease without a

family history, while the majority of the patients who have more than one lesion have a family history with autosomal dominant Mendelian inheritance.

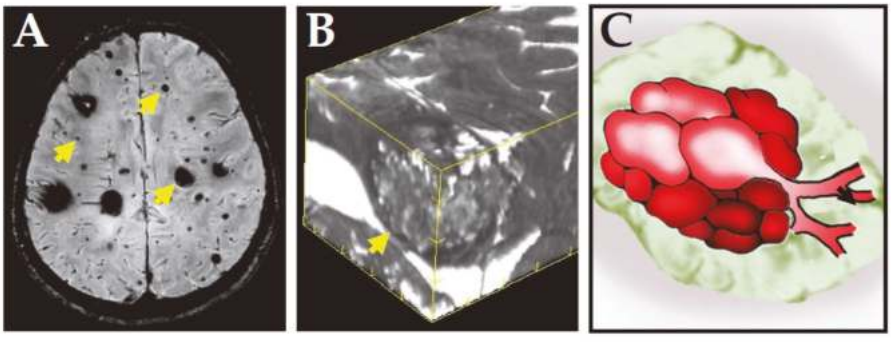

Figure 1. Radiological presentation of CCM. (**A**) MRI image of the brain of a familial CCM patient. Susceptibility weighted imaging showed multiple dark CCM lesions with various sizes. Arrows indicate representative lesions. (**B**) 3D reconstruction of T2 weighted imaging of a CCM lesion. It shows the lesion is not uniform, but with popcorn appearance. The arrow indicates the location of the lesion. (**C**) Schematic presentation of a CCM lesion showing it is composed of nested dilated microvessels.

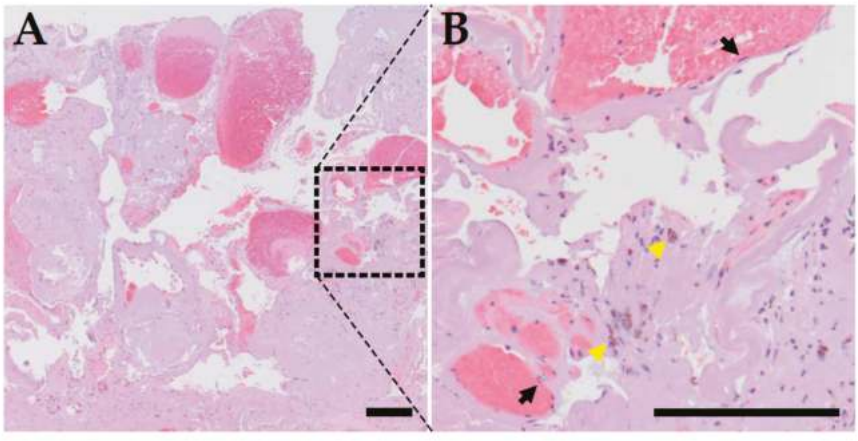

Figure 2. Histopathological presentation of CCM. (**A**) H&E staining of a surgically resected CCM lesion. It is composed of clusters of thin walled dilated microvessels with no supporting smooth muscle cells beneath the endothelial cell layer and no intervening brain parenchyma. Thrombi are present within the lumen of capillaries within the CCM lesion. (**B**) High power image of the boxed region of panel A. Black arrows point to individual endothelial cells lining the inner surface of dilated capillaries, and yellow arrowheads point to hemosiderin deposition adjacent to the capillaries, a sign of chronic bleeding. Bar = 200 μm.

3. Genetics of CCM

Based on linkage analyses, three gene loci (*CCM1* [7q21-22], *CCM2* [7p15-p13], and *CCM3* [3q25.2-q27]) have been identified in the germ-line of familial cases [8–10]. Subsequently, the genes within these loci are identified to be *CCM1/KRIT1*, *CCM2/MGC4607*, and *CCM3/PDCD10* [11–16]. Of all familial CCM patients, ~60% have *CCM1* mutations, ~20% have *CCM2* mutations, ~10% have *CCM3* mutations, and a minority of familial CCM patients do not have mutations in these

three genes [17]. Although mutations of *KRIT1*, *CCM2*, and *PDCD10* genes are all associated with histologically identical CCM lesions, patients with *PDCD10* mutations have the most severe phenotype, with earlier symptomatic onset [18,19]. A large fraction of mutations identified in patients are located in the coding region of *CCM* genes and are loss-of-function mutations [20]. DNA sequencing of lesional tissue and endothelial cells from familial CCM patients showed that in addition to germ-line mutations, these harbor somatic mutations of *CCM* genes, suggesting a two-hit mechanism for CCM pathogenesis [21,22]. Somatic mutations in the same *CCM* genes have been identified in sporadic lesions, indicating that loss of CCM function also contributes to sporadic disease development [23]. This also suggests that biomarkers and therapeutic targets aimed at the familial disease will also apply in sporadic CCM cases.

CCM proteins are conserved molecules. Orthologs of all three *CCM* genes have been identified in *Caenorhabditis elegans*. The *KRIT1* ortholog *kri-1* germline affects animal longevity and germ cell survival [24,25], and *ccm-2* participates in such processes [26]. The *PDCD10* ortholog *ccm-3* is required for excretory canal organization and germline tube development through affecting a large array of cellular events, including actomyosin organization, cell polarity and endocytic recycling [26–28]. In zebrafish, *krit1* and *ccm2* loss leads to dilation of major vessels, with spreading of endothelial cells [29], and a C-terminally truncated PDCD10 causes a similar phenotype [30]. Although *Ccm* heterozygous knockout mice have little or no potential to develop CCM–like lesions in the brain, when they are on a genetically instable background ($Msh2^{-/-}$ or $Trp53^{-/-}$), these mice have a significantly higher lesion burden [19,31,32]. These findings demonstrate that loss of heterozygosity is likely an important driving force for CCM pathogenesis. Mouse studies further show that KRIT1, CCM2, and PDCD10 participate in CCM pathogenesis. Deletion of *Krit1*, *Ccm2*, and *Pdcd10* genes all cause embryonic lethality due to cardiovascular defects [33–35]. Conventional homozygous *Krit1* and *Ccm2* deletion both cause defects in branchial arch artery formation [33,34], while *Pdcd10* deletion causes vasculogenesis and hematopoiesis defects [35]. When embryonic lethality is circumvented by tamoxifen-induced postnatal deletion of floxed *Ccm* genes, CCM-like lesion formation ensues, primarily in the cerebellum, suggesting they are CCM disease causing genes [36–39]. Consistent with human studies, mice with *Pdcd10* deletion also showed a more severe phenotype than mice with *Krit1* or *Ccm2* mutations, indicating PDCD10 may affect KRIT1 and CCM2-independent events [19]. Recent evidence reveals that clonally expanded mutated endothelial cells only comprise a fraction of cells lining CCM lesions, suggesting endothelial cells with *CCM* deletions may co-opt endothelial cells without *CCM* mutations to participate in CCM disease [40].

4. CCM Proteins and Their Interactions

KRIT1 (Krev interaction trapped protein-1, CCM1) is the largest of the three CCM proteins, with 529 amino acid residues [41]. It was first identified through its binding to the small GTPase Rap1 (also called Krev-1), and it is comprised of an N-terminal Nudix domain, three NPxY/F motifs, an ankyrin-repeat region, and a C-terminal FERM (band 4.1, ezrin, radixin, moesin) domain (Figure 3). Through its N-terminal Nudix domain and NPxY/F motif containing region, KRIT1 interacts with the β1-integrin binding protein ICAP1 to limit β1-integrin activation [42,43]. The KRIT1 FERM domain binds to a transmembrane protein Heg1 and the small GTPase Rap1 and is important for KRIT1 to localize to the plasma membrane [41,44–46]. Consistent with its role in cytoskeletal regulation, KRIT1 also directly associates with microtubules [47].

CCM2 is a 444 amino acid residue protein, with a phosphotyrosine-binding domain (PTB) at its N-terminus and a C-terminal harmonin-homology domain (HHD) [13,48]. It was first characterized as an osmosensing scaffolding protein that binds to small GTPase Rac1 and protein kinases MEKK3 and MKK3 [49]. CCM2 is central to the CCM protein complex organization, as it can bind to both KRIT1 and PDCD10 (programmed cell death 10, CCM3) (Figure 3) [50–52]. The CCM2 PTB domain binds directly with the KRIT1 NPxY/F motif, and LD-like motif of CCM2 (within the linker region between the PTB and HHD domains) binds to the focal adhesion targeting (FAT) homology domain of PDCD10 [51–54].

Binding between KRIT1 and CCM2 is important for CCM2 localization [51,54], while the interaction between CCM2 and PDCD10 controls CCM2 and PDCD10 protein stability, as CCM2 depletion decreases cellular PDCD10 protein content, and PDCD10 depletion reduces CCM2 protein abundance [53]. CCM2 also associates with F-actin, bringing the actin regulating small GTPase Rac1 to the proximity of the actin cytoskeleton [55]. A paralog of CCM2, CCM2L, also exists [56]. Although CCM2L can bind to KRIT1 and compete with CCM2 for KRIT1 binding, it does not bind to PDCD10 [56]. Similar to CCM2, CCM2L also interacts with MEKK3 [57], but the significance of CCM2L for CCM disease pathogenesis and its effect on CCM protein complex organization and function remains poorly defined [58].

PDCD10 (CCM3) protein has 212 amino acid residues and consists of an N-terminal dimerization domain and a C-terminus FAT homology domain (Figure 3) [59]. It was first discovered as a gene upregulated during myeloid cell apoptosis [60]. In addition to binding to CCM2 [50], PDCD10 can bind to components of another protein complex, the striatin interacting phosphatase and kinase (STRIPAK) complex, through its dimerization domain. These proteins include striatin itself and germinal center kinase (GCK) III group of serine/threonine protein kinases MST4/MASK, MST3/STK24, and STK25/YSK1/SOK1 and other STRIPAK complex components, including STRIP1/FAM40A and STRIP2/FAM40B [61–67]. Although PDCD10 can bind to CCM2, PDCD10 primarily resides within the STRIPAK complex, rather than the CCM protein complex, in cells [63,64]. Furthermore, PDCD10 can bind to an array of other proteins, including paxillin, PTPN13, UNC13D [50,67–70]. Similar to KRIT1 and CCM2, PDCD10 also interacts with cytoskeletal regulating small GTPases. Cdc42 can co-immunoprecipitate with PDCD10, and Cdc42 deletion causes a CCM-like phenotype, suggesting Cdc42 and PDCD10 resides in the same CCM pathogenic pathway [71]. In addition, PDCD10 can directly bind to RIPOR1/FAM65A, a RhoA associated protein, providing a link between PDCD10 and RhoA signaling [72].

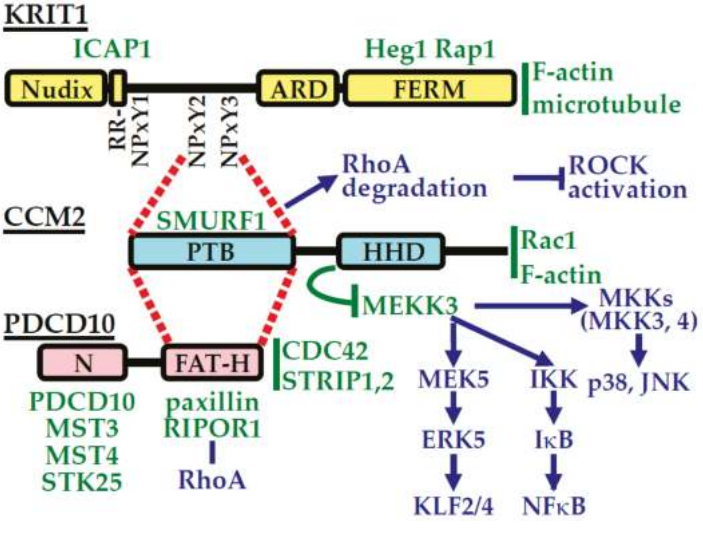

Figure 3. CCM protein domain organization and protein interactions. CCM protein domain organizations are presented schematically. Direct interaction partners are shown in green letters. Locations of the letters indicate rough interaction sites for these binding proteins. If a binding site is unknown, the binding partner is listed to the right of each CCM protein. Key pathways affected by CCM protein and their interaction partners are shown in blue letters. Dashed red lines indicate interaction sites between individual CCM proteins.

5. CCM Proteins and Cellular Signaling

Because each of the CCM proteins has a multitude of interaction partners, it is not surprising that these proteins can impact multiple signaling pathways and cellular processes, including endothelial to mesenchymal transition, autophagy, exocytosis, and Golgi complex organization [63,69,72–75]. One of the best understood CCM controlled signaling pathways is the RhoA-Rho-associated coiled-coil kinase (ROCK) signaling. Decreased expression of any of the CCM proteins leads to increased RhoA and ROCK activity [19,30,34,54,76,77], which in turn increases myosin regulatory light chain (MLC) phosphorylation, causing actomyosin contraction that affects cell migration and intercellular junction integrity. Through its PTB domain, CCM2 can bind to the E3 ubiquitin ligase Smad ubiquitin regulatory factor 1 (Smurf1) [76,78], which ubiquitinates RhoA to promote its degradation [78]. In the absence of CCM2, Smurf1-mediated RhoA degradation is reduced, leading to RhoA accumulation and increased ROCK activity [78]. Depletion of PDCD10 and its binding partners STK25, STRIP1/FAM40A, STRIP2/FAM40B, and RIPTOR/FAM65A all increase MLC phosphorylation, indicating PDCD10 may affect RhoA-ROCK activity through these proteins [19,30,65]. The enhanced RhoA-ROCK signaling is a critical component of CCM pathogenesis, which is further detailed below.

Another relatively well understood CCM-regulated pathway is the MEKK3 signaling. As discussed above, CCM2 directly interacts with MEKK3 [49]. Both *Krit1* and *Ccm2* deletion leads to activation of the MEKK3-MEK5-ERK5-KLF2/4 signaling cascade, causing increased Adamts4/5 expression [57,79,80]. These changes disrupt both embryonic cardiac development and promote CCM-like lesion formation in neonatal mice [79,80]. Consistent with the findings that CCM2 negatively regulates MEKK3, and MEKK3 is required for immune related receptor signaling [81–84], MEKK3 activating ligands lipopolysaccharide (LPS), IL-1β, and pI:pC can all promote CCM-like lesion formation [85]. There is some evidence that aberrantly activated MEKK3 signaling can lead to increased RhoA-ROCK signaling, but the exact mechanism for this potential crosstalk and its contribution to CCM disease need to be further elucidated [79,80,85,86].

CCM proteins have also been implicated in cell death regulation. The *C. elegans KRIT1* ortholog *kri-1* is required to promote irradiation-induced germ cell death through a cell-nonautonomous fashion [25], while in neuroblastoma cells, CCM2 is critical for the TrkA receptor tyrosine kinase to induce tumor cell death [87,88]. As its name suggests, PDCD10 has also been associated with apoptosis regulation. In endothelial cells, overexpression of PDCD10 promotes endothelial apoptosis, and in cardiomyocytes, PDCD10 expression is required for ischemic reperfusion injury-induced cell death [89,90]. However, the exact effect of PDCD10 on apoptosis is still under debate. For example, PDCD10 is up-regulated during oxidative stress, but one report suggested such upregulation promotes tumor cell survival, while another report suggested such upregulation enhances apoptosis [91,92]. Thus, how CCM proteins affect cell death and proliferation to impact human health and disease remains to be further explored.

6. CCM Proteins Participate in Endothelial Barrier Maintenance and Regulation

Early morphological studies showed that CCM lesions are lined by altered endothelial cells with disrupted cell–cell connections, including tight junctions [93,94]. Using MRI based in vivo permeability measurements, it is now clear that CCM lesions have increased vascular permeability [95,96]. In white matter regions away from CCM lesions, patients with familial CCM disease (harboring a germline mutation) have higher baseline permeability than patients with sporadic disease, indicating *CCM* mutations globally affect blood–brain barrier function [95,96]. Furthermore, baseline brain white matter vascular permeability can be used to distinguish familial CCM patients with non-aggressive and aggressive disease, and between stable and non-stable CCM disease [95,96]. These data suggest blood–brain barrier defect regulates CCM clinical disease presentation.

Consistent with patient-based studies, cell culture and mouse studies demonstrated how CCM proteins may affect endothelial barrier function. All three CCM proteins can limit RhoA-ROCK signaling in endothelial cells, although PDCD10 may use a mechanism distinctive of KRIT1 and CCM2 [19,54,65]. The small GTPase RhoA and the other two CCM protein binding small GTPases Rac1

and Cdc42 are cytoskeletal regulators that control barrier function [97–99]. In the case of RhoA, its effector ROCK can either directly or indirectly induce MLC phosphorylation, leading to perijunctional actomyosin contraction, which in turn causes intercellular junction remodeling to increase paracellular permeability [100]. Indeed, decreased KRIT1, CCM2 and PDCD10 expression all promote MLC phosphorylation, stress fiber formation, junctional protein redistribution, and barrier dysfunction in endothelial cells [19,34,54,101].

In addition to maintaining baseline endothelial barrier, KRIT1 also participates in endothelial barrier regulation. While tumor necrosis factor (TNF) increased arteriole and venule permeability in wild type mice, it failed to induce barrier loss in *Krit1* heterozygous knockout mice [101,102]. In contrast, histamine-induced vascular permeability increase occurred normally in *Krit1* heterozygous knockout mice [101,102]. However, another report suggests KRIT1 is required for preservation of endothelial barrier following stimuli [103]. KRIT1 depletion in cultured endothelial cells attenuated prostacyclin-induced perijunctional F-actin accumulation and tightening of endothelial barrier and enhanced cyclic stretch-induced Rho activation and endothelial barrier disruption [103]. In vivo studies further showed that *Krit1* heterozygous knockout exacerbated barrier loss induced by combined treatment of high tidal volume mechanical ventilation and TRAP6, a thrombin receptor activating peptide. This treatment also increased protein and cell content of bronchoalveolar lavage fluid, indicating partial KRIT1 loss participates in lung damage [103]. These data suggest KRIT1 may participate in endothelial barrier regulation in a stimulus-dependent manner and contribute to endothelial dysfunction-related diseases.

Because of the robust ROCK activation in CCM depleted endothelial cells, ROCK became a leading target for novel CCM therapy. ROCK inhibition not only reverses CCM depletion-induced stress fiber formation and barrier loss in vitro but also limits *Ccm* deletion-induced loss of endothelial barrier function in vivo [19,34,54,101]. Pharmacological studies further show that ROCK inhibition by fasudil, atorvastatin, and a newly identified ROCK2 specific inhibitor limits CCM-like lesion formation in multiple mouse models of CCM [104–106], highlighting ROCK inhibition may be a valid therapy for CCM disease. This proof of concept is currently being tested in a clinical trial (NCT02603328) [107].

Besides RhoA-ROCK signaling, additional cellular processes have been implicated for CCM proteins to regulate endothelial barrier. Vascular endothelial growth factor (VEGF) not only promotes endothelial growth, but also increases endothelial permeability [108]. It has been demonstrated that loss of KRIT1 and PDCD10, but not CCM2, increases VEGF production in endothelial cells, and VEGF in turn acts on VEGFR2 to increase endothelial permeability [109]. However, existing evidence also suggests that PDCD10 is required for proper VEGFR2 signaling [35], indicating the relationship between CCM proteins and VEGF and its signaling may be complex. In KRIT1 depleted cells or heterozygous knockout mice, endothelial reactive oxygen species (ROS) production is elevated, at least partially, through upregulated NAPDH oxidase expression [102,110]. When an endothelial targeting ROS scavenger was used, the increased vascular permeability was reduced in KRIT1 deficient mice, demonstrating ROS production also plays a role for KRIT1 to regulate endothelial barrier [102]. However, the molecular mechanisms for ROS to affect barrier function in endothelium, in the presence or absence of KRIT1, remain to be elucidated.

7. Tight Junctions and CCM Disease

One of the major determinants of the endothelial barrier is the tight junction. In contrast to well demarcated tight junction, adherens junction, and gap junction domains within the apical junctional complex of epithelial cells, these domains are frequently mixed at cell–cell contact sites between endothelial cells [111]. Such junctions can vary significantly in endothelial cells of different origins. Microvascular endothelial cell bodies can have a thickness of 0.3 μm, with cell–cell junction depth of ~0.5–0.9 μm, while endothelial cells from arteries and high endothelial venules the cell–cell contact sites may reach 3–10 μm in height [111]. In the brain, the endothelial cells, pericytes at the abluminal side of endothelial cells, and astrocyte end feet together form the neurovascular unit to create the

highly impermeable blood–brain barrier [112]. At the endothelial junctional complex, the adherens junction component VE-cadherin provides adhesive force at the cell–cell junctions, and the tight junction proteins are critical for limiting permeability between individual endothelial cells.

The tight junction seals the paracellular space between individual cavity lining cells and is created and maintained by a large number of transmembrane proteins. The four-transmembrane-domain-containing claudin family consists of more than 25 members in mammals. Some of the claudins (including claudin-1, -3, -5) are barrier forming, while some claudin family members are forming size and charge selective pores that allow charged ions and small molecules to pass (including claudin-2, -10, -15) [113]. In the brain microvascular endothelium, the most dominantly expressed claudin is the barrier forming claudin-5 [114,115]. Although claudin-5 is not required for brain microvascular endothelial tight junction organization, its knockout increased brain microvascular permeability, leading to neonatal death [116]. The four-transmembrane domain-containing tight-junction-associated MARVEL protein (TAMP) family contains occludin, tricellulin, and marveld3 [117], and these proteins generally impact macromolecular permeability [118,119]. Occludin knockout itself does not disrupt normal epithelial tight junction organization, but causes brain calcification, particularly around small vessels [120]. Patients with homozygous recessive occludin mutations have a more severe brain phenotype, with band-like calcification with simplified gyration and polymicrogyria [121]. This suggests occludin plays a critical role in brain development, likely through affecting brain endothelial function. Additional tight junction proteins belong to the immunoglobulin superfamily of proteins with a single transmembrane domain (e.g., junctional adhesion molecule A, JAM-A and Coxsackie and adenovirus receptor, CAR) and popeye family of proteins with three transmembrane domains (Popdc1/Bves). In the intestine, JAM-A maintains proper epithelial macromolecular barrier function and limits intestinal inflammation [122,123], and endothelial JAM-A promotes leukocyte transmigration [73,124]. Similarly, CAR participates in epithelial barrier maintenance [125], and CAR affects shear stress induced endothelial immune response [126].

Multiple plaque proteins concentrate at the cytoplasmic side of the tight junction. These proteins typically bind to multiple transmembrane tight junction proteins, other tight junction plaque proteins, and the cytoskeleton, thus stabilize tight junction organization. Zonula occludens (ZO) family proteins (ZO-1, -2, -3) is a well-studied family of tight junction plaque proteins [127]. They can bind to almost all transmembrane tight junction proteins, heterodimerize among different ZO proteins, and associate with the actin cytoskeleton [127]. ZO-1 knockout mice are embryonic lethal, with defects in vascular endothelial cells [128], a finding supported by in vitro endothelial cell studies [129]. Cingulin family is another group of tight junction plaque proteins (cingulin, paracingulin/cingulin-like/JACOP) that can interact with occludin, JAM-A, ZO proteins, myosin and actin filaments, which are also required for proper endothelial function, including brain endothelial barrier function [130,131].

Many CCM affected signaling events can regulate the tight junction. As discussed above, Rho-ROCK signaling increases MLC phosphorylation to impact actomyosin contraction, which in turn regulates tight junction protein expression and localization [132–135]. In addition, ROCK can directly phosphorylate occludin and claudin-5, and such phosphorylation events are associated with blood brain barrier dysfunction [136]. Interaction between endothelial cells and basement membrane induces β1-integrin engagement, increases MLC phosphorylation in an MLC kinase and ROCK -dependent fashion to promote claudin-5, occludin, and ZO-1 reorganization at the cell–cell junction [137]. This pathway is likely affected by CCM proteins through KRIT1 binding to the β1-integrin signaling inhibitor ICAP-1, a protein that can also bind to ROCK [138–140]. The KRIT1 binding small GTPase Rap1 enhances tight junction protein localization at endothelial cell–cell contact sites and promotes endothelial barrier function [141]. Consistent with this, the Rap1 activating guanine-nucleotide-exchange factor EPAC also maintains endothelial barrier, prevents VEGF and TNF-induced endothelial permeability increase, and limits claudin-5, occludin, and ZO-1 disorganization at the cell–cell junctions [142]. Another small GTPase, Rasip1, is an effector of Rap1, which down-regulates RhoA activity through ArhGAP29 [143–145]. Rasip1 can also interact with the KRIT1 interacting transmembrane protein Heg1 [146], thus KRIT1 can bring Rasip1 and Rap1

close to one another through KRIT1-Heg1 interaction. Furthermore, engagement between individual JAM-A molecules at intercellular junctions can activate Rap1 to preserve epithelial and endothelial barrier functions through JAM-A interaction with the tight junction protein ZO-2, the adherens junction protein AF-6, and PDZ-GEF1/2 [147,148]. These data provide a complex signaling network for the tight junction proteins (JAM-A and ZO-2) and other cell surface adhesion molecules (β1-integrin and Heg1) to affect CCM-dependent cellular signaling pathways to impact tight junction barrier.

Consistent with such findings, resected CCM lesions have reduced occludin, claudin-5, and ZO-1 staining, and decreased tight junction protein expression has between associated with the tendency for local bleeding and edema [149,150]. In *Krit1* deleted brain microvascular endothelial cells, loss of claudin-5 and ZO-1 protein can be readily observed by immunofluorescent staining and western blot [151], and PDCD10 depletion in brain microvascular endothelial cells decreases claudin-5, occludin, and ZO-1 protein abundance, likely through an ERK1/2 and cortactin-dependent process [152]. A recent study suggests PDCD10 depletion in brain endothelial cells upregulates gap junction protein connexin 43 expression and increases gap junction communication, a phenomenon only minimally seen in KRIT1 or CCM2 depleted cells [153]. Such changes are associated with redistribution of tight junction proteins to gap junctions, and the connexin 43 gap junction inhibitor GAP27 can reverse tight junction disorganization and decrease endothelial barrier permeability in PDCD10 depleted cells [153]. These indicate increased gap junction function participates in tight junction disruption in *CCM3* disease. With such findings, it is likely that tight junction protein disorganization downstream of RhoA-ROCK signaling and gap junction is a key effector driving CCM pathogenesis, and it is possible that normalizing tight junction protein expression and localization at the cell–cell junctions can limit CCM development or lesional bleeding. However, the specific roles of tight junction proteins in CCM initiation and progression remain to be formally tested, likely by using transgenic or knockout mice.

8. CCM Proteins Impact Intestinal Homeostasis

In contrast to a plethora of studies on the function of CCM proteins in endothelial cells, we just start to appreciate their roles in epithelial cells. By investigating the effects of KRIT1 in β-catenin signaling, Glading and Ginsberg revealed KRIT1 depletion increases β-catenin transcriptional activity in both endothelial and epithelial cells [154]. This is functionally significant, as *Apc* mutation induced more intestinal polyp formation in *Krit1* heterozygous knockout mice with increased intestinal epithelial nuclear β-catenin accumulation [154]. A recent *C. elegans* study suggested KRIT1 can also form a complex with CCM2 to promote zinc transporter expression to cause Zn^{2+} storage in the intestinal granules, indicating KRIT1 may also impact intestinal epithelial transport [26].

Despite these findings, it was not known if CCM proteins can regulate barrier function in epithelium. Our group addressed this question by studying KRIT1 function in intestinal epithelial Caco-2 cells, a well characterized model to study intestinal epithelial barrier maintenance and regulation [155]. In this model, KRIT1 depletion caused a reduction of epithelial barrier function, characterized by selectively increased relative permeability of small cations, including Na^+, to the anion Cl^- [155]. Such a change is consistent with decreased expression of claudin-1, a tight junction protein that limits small ion permeability, in KRIT1-depleted Caco-2 cells [155,156]. In contrast to the effect of KRIT1 on endothelial cells, intestinal epithelial KRIT1 depletion does not induce MLC phosphorylation, and ROCK inhibition does not reverse KRIT1 depletion-induced barrier loss [155]. This indicates that KRIT1 regulates epithelial and endothelial barrier function through distinct mechanisms. In Caco-2 monolayers, decreasing actomyosin contractility by inhibiting either ROCK or myosin ATPase activity both reduced epithelial barrier function, along with elevated permeability to both small and large cations. These changes are inhibited in KRIT1-depleted Caco-2 monolayers, indicating KRIT1 also participates in actomyosin contraction-induced barrier regulation [155]. Furthermore, KRIT1-depleted epithelial monolayers are resistant to osmotic stress and enteric pathogen *Salmonella typhimurium*-induced epithelial barrier regulation (Figure 4), suggesting KRIT1 may impact gastrointestinal pathophysiology. With the above data, it is surprising to find

that KRIT1 depletion exacerbates TNF-induced epithelial barrier loss. Mechanistic studies suggest this loss is due to aberrantly activated apoptosis in KRIT1-depleted monolayers, but we currently do not know how this occurs [155]. Nevertheless, these data suggest KRIT1 regulates epithelial barrier function through at least two distinct pathways: one is actomyosin and tight junction-dependent barrier maintenance and regulation, and the other is tight junction-independent epithelial apoptosis. Such findings not only point to a role for KRIT1 to mediate the crosstalk between distinctive epithelial barrier regulation pathways, but also suggest KRIT1 may coordinate tight junction barrier maintenance, regulation, and epithelial apoptosis to impact intestinal disease development.

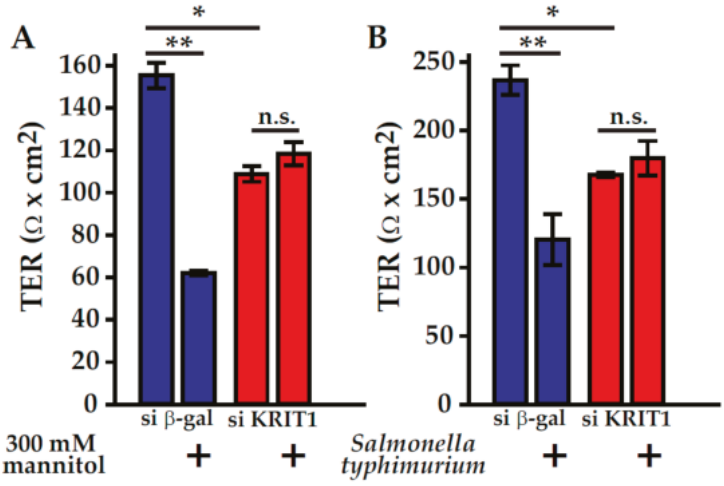

Figure 4. KRIT1 depletion limits pathophysiological stimuli-induced epithelial barrier dysfunction. KRIT1 depletion by stable transfection of a siRNA expressing plasmid decreased epithelial barrier function (A-B, assessed by transepithelial resistant (TER) measurements) in differentiated Caco-2 intestinal epithelial monolayers grown on semi-permeable Transwell inserts [155]. (**A**) Hyperosmotic stress induced by including 300 mM mannitol in Hank's balanced salt solution caused barrier loss in control (siRNA against β-galactosidase transfected, blue bars) Caco-2 monolayers. In contrast, no barrier loss was induced in KRIT1 depleted (siRNA against KRIT1 transfected, red bars) Caco-2 monolayers. (**B**) *Salmonella typhimurium* (strain ATCC 14028) infection by including bacteria in apical culture media caused barrier loss in control, but not KRIT1 depleted Caco-2 monolayers. Mean with standard error (triplicate samples) are shown. One-way ANOVA analysis with Bonferroni correction was used (* $p < 0.05$, ** $p < 0.01$).

An understanding of the potential contribution of the gastrointestinal tract to CCM disease development was stemmed from the surprising finding that neonatal mice with the same induced endothelial specific *Ccm* deletion can have drastically different CCM-like lesion burdens when they were raised in different animal facilities [85]. Fecal microbiome analysis showed that mice susceptible to *Ccm* deletion-induced lesion formation have a Gram-negative bacteria rich microbiome relative to resistant mice. Such a fecal microbiome provides the cell wall product LPS as the ligand to activate the endothelial TLR4-MEKK3-KLR2/4 signaling pathway to promote CCM development [85]. This view is further supported by the finding that germ-free mice and mice treated with antibiotics have lower lesion burden [85]. Because familial CCM patients have genetic mutations of *CCM* genes in all organs and cell types, this study also raised the possibility that CCM could function in the gastrointestinal tract to influence CCM disease development. Indeed, when *Pdcd10* was deleted in the intestinal epithelium, it promoted endothelial *Pdcd10* deletion-induced lesion formation [157]. In contrast, intestinal epithelial specific deletion of *Krit1* does not impact endothelial *Krit1* deletion-induced lesion

formation [157]. This finding may at least partially explain why patients with *PDCD10* mutations have a more aggressive CCM disease than patients with *KRIT1* mutations. In addition to impacting CCM-like disease development, constitutive intestinal epithelial specific *Pdcd10* deletion alone shortened mouse life span, reduced intestinal mucus layer thickness, enlarged goblet cells, and caused intestinal inflammation [157]. These findings indicate PDCD10 is required for intestinal homeostasis and may impact intestinal disease development, which needs to be further investigated.

9. Conclusions and Future Directions

Through their many binding partners, CCM proteins impact many cellular events. The most prominent effect of CCM proteins on cellular signaling is their ability to limit RhoA-ROCK activity and MEKK3-MEK5-ERK5-KLF signaling, events that are important for endothelial function and CCM lesion formation. Despite such detailed understanding, we are just starting to grasp the full spectrum of CCM protein functions. Understanding how CCM proteins affect endothelial function through a variety of pathways to impact CCM disease and identifying therapies to preserve and promote normal CCM function in the brain remain top priorities for CCM research. With the finding that CCM proteins also function in intestinal epithelial cells, it becomes pressing to understand CCM protein functions in the gut, in the context of both CCM disease and other intestinal disorders. It also points to a need to understand CCM protein signaling in other cell types and organs. Such studies will not only advance our understanding of CCM protein biology, but also provide targets to modulate cellular functions to benefit human health.

Author Contributions: Initial draft, S.W., Y.L., and L.S.; contribution of figures, Y.L., S.P.P., C.R.W., and L.S.; draft revision, S.W., Y.L., S.P.P., C.R.W., I.A.A., and L.S. All authors have read and agreed to the published version of the manuscript.

Funding: The original research performed by the author group was partially supported by United States Department of Defense Congress Directed Medical Research Program Discovery Award W81XWH-18-1-0501 (to L.S), National Institutes of Health grants K01 DK092381 (to L.S.), P30 DK042086 (to L.S.), P01 NS092521 (to I.A.A.), and UL1 TR001863 (to I.A.A.). The University of Chicago Safadi Clinical and Translational Neuroscience Awards (to L.S. and S.P.), American Association of Neurological Surgeons/Congress of Neurological Surgeons Joint Cerebrovascular Section Robert J. Dempsey MD Cerebrovascular Research Grant (to S.P.).

Acknowledgments: We thank Wenli Dai, Li Dong, and Jimian Yu for comments and proofreading of the manuscript.

Conflicts of Interest: The authors declare no conflict of interest.

Abbreviations

CCM	cerebral cavernous malformation
EPAC	Rap1 guanine-nucleotide-exchange factor
FAT	focal adhesion targeting
FERM	band 4.1, ezrin, radixin, moesin
GCK	germinal center kinase
HHD	harmonin-homology domain
JAM	junctional adhesion molecule
KRIT1	Krev interaction trapped protein-1
LPS	lipopolysaccharide
MLC	myosin regulatory light chain
PDCD10	programmed cell death 10
PTB	phosphotyrosine-binding domain
ROCK	Rho-associated coiled-coil kinase
ROS	reactive oxygen species
Smurf1	Smad ubiquitin regulatory factor 1
STRIPAK	striatin interacting phosphatase and kinase
TER	transepithelial resistance
TNF	tumor necrosis factor
VEGF	vascular endothelial growth factor
ZO	zonula occludens

References

1. Awad, I.A.; Polster, S.P. Cavernous angiomas: Deconstructing a neurosurgical disease. *J. Neurosurg.* **2019**, *131*, 1–13. [CrossRef]
2. Morris, Z.; Whiteley, W.N.; Longstreth, W.T., Jr.; Weber, F.; Lee, Y.C.; Tsushima, Y.; Alphs, H.; Ladd, S.C.; Warlow, C.; Wardlaw, J.M.; et al. Incidental findings on brain magnetic resonance imaging: Systematic review and meta-analysis. *Br. Med. J.* **2009**, *339*, b3016. [CrossRef]
3. Moore, S.A.; Brown, R.D., Jr.; Christianson, T.J.; Flemming, K.D. Long-term natural history of incidentally discovered cavernous malformations in a single-center cohort. *J. Neurosurg.* **2014**, *120*, 1188–1192. [CrossRef]
4. Flemming, K.D.; Graff-Radford, J.; Aakre, J.; Kantarci, K.; Lanzino, G.; Brown, R.D., Jr.; Mielke, M.M.; Roberts, R.O.; Kremers, W.; Knopman, D.S.; et al. Population-Based Prevalence of Cerebral Cavernous Malformations in Older Adults: Mayo Clinic Study of Aging. *JAMA Neurol.* **2017**, *74*, 801–805. [CrossRef] [PubMed]
5. Otten, P.; Pizzolato, G.P.; Rilliet, B.; Berney, J. [131 cases of cavernous angioma (cavernomas) of the CNS, discovered by retrospective analysis of 24,535 autopsies]. *Neurochirurgie* **1989**, *35*, 82–83, 128–131.
6. Flemming, K.D.; Link, M.J.; Christianson, T.J.; Brown, R.D., Jr. Prospective hemorrhage risk of intracerebral cavernous malformations. *Neurology* **2012**, *78*, 632–636. [CrossRef] [PubMed]
7. Al-Shahi Salman, R.; Berg, M.J.; Morrison, L.; Awad, I.A. Hemorrhage from cavernous malformations of the brain: Definition and reporting standards. Angioma Alliance Scientific Advisory Board. *Stroke* **2008**, *39*, 3222–3230. [CrossRef] [PubMed]
8. Gunel, M.; Awad, I.A.; Anson, J.; Lifton, R.P. Mapping a gene causing cerebral cavernous malformation to 7q11.2-q21. *Proc. Natl. Acad. Sci. USA* **1995**, *92*, 6620–6624. [CrossRef] [PubMed]
9. Marchuk, D.A.; Gallione, C.J.; Morrison, L.A.; Clericuzio, C.L.; Hart, B.L.; Kosofsky, B.E.; Louis, D.N.; Gusella, J.F.; Davis, L.E.; Prenger, V.L. A locus for cerebral cavernous malformations maps to chromosome 7q in two families. *Genomics* **1995**, *28*, 311–314. [CrossRef] [PubMed]
10. Craig, H.D.; Gunel, M.; Cepeda, O.; Johnson, E.W.; Ptacek, L.; Steinberg, G.K.; Ogilvy, C.S.; Berg, M.J.; Crawford, S.C.; Scott, R.M.; et al. Multilocus linkage identifies two new loci for a mendelian form of stroke, cerebral cavernous malformation, at 7p15-13 and 3q25.2-27. *Hum. Mol. Genet.* **1998**, *7*, 1851–1858. [CrossRef]
11. Laberge-le Couteulx, S.; Jung, H.H.; Labauge, P.; Houtteville, J.P.; Lescoat, C.; Cecillon, M.; Marechal, E.; Joutel, A.; Bach, J.F.; Tournier-Lasserve, E. Truncating mutations in *CCM1*, encoding *KRIT1*, cause hereditary cavernous angiomas. *Nat. Genet.* **1999**, *23*, 189–193. [CrossRef] [PubMed]
12. Sahoo, T.; Johnson, E.W.; Thomas, J.W.; Kuehl, P.M.; Jones, T.L.; Dokken, C.G.; Touchman, J.W.; Gallione, C.J.; Lee-Lin, S.Q.; Kosofsky, B.; et al. Mutations in the gene encoding *KRIT1*, a Krev-1/rap1a binding protein, cause cerebral cavernous malformations (*CCM1*). *Hum. Mol. Genet.* **1999**, *8*, 2325–2333. [CrossRef] [PubMed]
13. Liquori, C.L.; Berg, M.J.; Siegel, A.M.; Huang, E.; Zawistowski, J.S.; Stoffer, T.; Verlaan, D.; Balogun, F.; Hughes, L.; Leedom, T.P.; et al. Mutations in a gene encoding a novel protein containing a phosphotyrosine-binding domain cause type 2 cerebral cavernous malformations. *Am. J. Hum. Genet.* **2003**, *73*, 1459–1464. [CrossRef] [PubMed]
14. Denier, C.; Goutagny, S.; Labauge, P.; Krivosic, V.; Arnoult, M.; Cousin, A.; Benabid, A.L.; Comoy, J.; Frerebeau, P.; Gilbert, B.; et al. Mutations within the MGC4607 gene cause cerebral cavernous malformations. *Am. J. Hum. Genet.* **2004**, *74*, 326–337. [CrossRef] [PubMed]
15. Guclu, B.; Ozturk, A.K.; Pricola, K.L.; Bilguvar, K.; Shin, D.; O'Roak, B.J.; Gunel, M. Mutations in apoptosis-related gene, *PDCD10*, cause cerebral cavernous malformation 3. *Neurosurgery* **2005**, *57*, 1008–1013. [CrossRef] [PubMed]
16. Bergametti, F.; Denier, C.; Labauge, P.; Arnoult, M.; Boetto, S.; Clanet, M.; Coubes, P.; Echenne, B.; Ibrahim, R.; Irthum, B.; et al. Mutations within the programmed cell death 10 gene cause cerebral cavernous malformations. *Am. J. Hum. Genet.* **2005**, *76*, 42–51. [CrossRef]
17. Zafar, A.; Quadri, S.A.; Farooqui, M.; Ikram, A.; Robinson, M.; Hart, B.L.; Mabray, M.C.; Vigil, C.; Tang, A.T.; Kahn, M.L.; et al. Familial Cerebral Cavernous Malformations. *Stroke* **2019**, *50*, 1294–1301. [CrossRef]
18. Denier, C.; Labauge, P.; Bergametti, F.; Marchelli, F.; Riant, F.; Arnoult, M.; Maciazek, J.; Vicaut, E.; Brunereau, L.; Tournier-Lasserve, E.; et al. Genotype-phenotype correlations in cerebral cavernous malformations patients. *Ann. Neurol.* **2006**, *60*, 550–556. [CrossRef]

19. Shenkar, R.; Shi, C.; Rebeiz, T.; Stockton, R.A.; McDonald, D.A.; Mikati, A.G.; Zhang, L.; Austin, C.; Akers, A.L.; Gallione, C.J.; et al. Exceptional aggressiveness of cerebral cavernous malformation disease associated with *PDCD10* mutations. *Genet. Med. Off. J. Am. Coll. Med Genet.* **2015**, *17*, 188–196. [CrossRef]
20. Spiegler, S.; Rath, M.; Paperlein, C.; Felbor, U. Cerebral Cavernous Malformations: An Update on Prevalence, Molecular Genetic Analyses, and Genetic Counselling. *Mol. Syndromol.* **2018**, *9*, 60–69. [CrossRef]
21. Gault, J.; Shenkar, R.; Recksiek, P.; Awad, I.A. Biallelic somatic and germ line *CCM1* truncating mutations in a cerebral cavernous malformation lesion. *Stroke* **2005**, *36*, 872–874. [CrossRef] [PubMed]
22. Akers, A.L.; Johnson, E.; Steinberg, G.K.; Zabramski, J.M.; Marchuk, D.A. Biallelic somatic and germline mutations in cerebral cavernous malformations (CCMs): Evidence for a two-hit mechanism of CCM pathogenesis. *Hum. Mol. Genet.* **2009**, *18*, 919–930. [CrossRef] [PubMed]
23. McDonald, D.A.; Shi, C.; Shenkar, R.; Gallione, C.J.; Akers, A.L.; Li, S.; De Castro, N.; Berg, M.J.; Corcoran, D.L.; Awad, I.A.; et al. Lesions from patients with sporadic cerebral cavernous malformations harbor somatic mutations in the *CCM* genes: Evidence for a common biochemical pathway for CCM pathogenesis. *Hum. Mol. Genet.* **2014**, *23*, 4357–4370. [CrossRef]
24. Berman, J.R.; Kenyon, C. Germ-cell loss extends C-elegans life span through regulation of DAF-16 by kri-1 and lipophilic-hormone signaling. *Cell* **2006**, *124*, 1055–1068. [CrossRef] [PubMed]
25. Ito, S.; Greiss, S.; Gartner, A.; Derry, W.B. Cell-Nonautonomous Regulation of *C. elegans* Germ Cell Death by kri-1. *Curr. Biol.* **2010**, *20*, 333–338. [CrossRef] [PubMed]
26. Chapman, E.M.; Lant, B.; Ohashi, Y.; Yu, B.; Schertzberg, M.; Go, C.; Dogra, D.; Koskimaki, J.; Girard, R.; Li, Y.; et al. A conserved CCM complex promotes apoptosis non-autonomously by regulating zinc homeostasis. *Nat. Commun.* **2019**, *10*, 1791. [CrossRef]
27. Pal, S.; Lant, B.; Yu, B.; Tian, R.L.; Tong, J.F.; Krieger, J.R.; Moran, M.F.; Gingras, A.C.; Derry, W.B. CCM-3 Promotes *C. elegans* Germline Development by Regulating Vesicle Trafficking Cytokinesis and Polarity. *Curr. Biol.* **2017**, *27*, 868–876. [CrossRef]
28. Lant, B.; Yu, B.; Goudreault, M.; Holmyard, D.; Knight, J.D.R.; Xu, P.; Zhao, L.; Chin, K.; Wallace, E.; Zhen, M.; et al. CCM-3/STRIPAK promotes seamless tube extension through endocytic recycling. *Nat. Commun.* **2015**, *6*, 6449. [CrossRef]
29. Hogan, B.M.; Bussmann, J.; Wolburg, H.; Schulte-Merker, S. *Ccm1* cell autonomously regulates endothelial cellular morphogenesis and vascular tubulogenesis in zebrafish. *Hum. Mol. Genet.* **2008**, *17*, 2424–2432. [CrossRef]
30. Zheng, X.J.; Xu, C.; Di Lorenzo, A.; Kleaveland, B.; Zou, Z.Y.; Seiler, C.; Chen, M.; Cheng, L.; Xiao, J.P.; He, J.; et al. CCM3 signaling through sterile 20-like kinases plays an essential role during zebrafish cardiovascular development and cerebral cavernous malformations. *J. Clin. Investig.* **2010**, *120*, 2795–2804. [CrossRef]
31. Plummer, N.W.; Gallione, C.J.; Srinivasan, S.; Zawistowski, J.S.; Louis, D.N.; Marchuk, D.A. Loss of p53 sensitizes mice with a mutation in *Ccm1* (*KRIT1*) to development of cerebral vascular malformations. *Am. J. Pathol.* **2004**, *165*, 1509–1518. [CrossRef]
32. McDonald, D.A.; Shenkar, R.; Shi, C.; Stockton, R.A.; Akers, A.L.; Kucherlapati, M.H.; Kucherlapati, R.; Brainer, J.; Ginsberg, M.H.; Awad, I.A.; et al. A novel mouse model of cerebral cavernous malformations based on the two-hit mutation hypothesis recapitulates the human disease. *Hum. Mol. Genet.* **2011**, *20*, 211–222. [CrossRef] [PubMed]
33. Whitehead, K.J.; Plummer, N.W.; Adams, J.A.; Marchuk, D.A.; Li, D.Y. *Ccm1* is required for arterial morphogenesis: Implications for the etiology of human cavernous malformations. *Development* **2004**, *131*, 1437–1448. [CrossRef]
34. Whitehead, K.J.; Chan, A.C.; Navankasattusas, S.; Koh, W.; London, N.R.; Ling, J.; Mayo, A.H.; Drakos, S.G.; Jones, C.A.; Zhu, W.; et al. The cerebral cavernous malformation signaling pathway promotes vascular integrity via Rho GTPases. *Nat. Med.* **2009**, *15*, 177–184. [CrossRef]
35. He, Y.; Zhang, H.; Yu, L.; Gunel, M.; Boggon, T.J.; Chen, H.; Min, W. Stabilization of VEGFR2 signaling by cerebral cavernous malformation 3 is critical for vascular development. *Sci. Signal.* **2010**, *3*, ra26. [CrossRef] [PubMed]
36. Boulday, G.; Rudini, N.; Maddaluno, L.; Blecon, A.; Arnould, M.; Gaudric, A.; Chapon, F.; Adams, R.H.; Dejana, E.; Tournier-Lasserve, E. Developmental timing of CCM2 loss influences cerebral cavernous malformations in mice. *J. Exp. Med.* **2011**, *208*, 1835–1847. [CrossRef]

37. Mleynek, T.M.; Chan, A.C.; Redd, M.; Gibson, C.C.; Davis, C.T.; Shi, D.S.; Chen, T.; Carter, K.L.; Ling, J.; Blanco, R.; et al. Lack of CCM1 induces hypersprouting and impairs response to flow. *Hum. Mol. Genet.* **2014**, *23*, 6223–6234. [CrossRef]
38. Chan, A.C.; Drakos, S.G.; Ruiz, O.E.; Smith, A.C.; Gibson, C.C.; Ling, J.; Passi, S.F.; Stratman, A.N.; Sacharidou, A.; Revelo, M.P.; et al. Mutations in 2 distinct genetic pathways result in cerebral cavernous malformations in mice. *J. Clin. Investig.* **2011**, *121*, 1871–1881. [CrossRef]
39. Cunningham, K.; Uchida, Y.; O'Donnell, E.; Claudio, E.; Li, W.; Soneji, K.; Wang, H.; Mukouyama, Y.S.; Siebenlist, U. Conditional deletion of *Ccm2* causes hemorrhage in the adult brain: A mouse model of human cerebral cavernous malformations. *Hum. Mol. Genet.* **2011**, *20*, 3198–3206. [CrossRef]
40. Detter, M.R.; Snellings, D.A.; Marchuk, D.A. Cerebral Cavernous Malformations Develop Through Clonal Expansion of Mutant Endothelial Cells. *Circ. Res.* **2018**, *123*, 1143–1151. [CrossRef]
41. Serebriiskii, I.; Estojak, J.; Sonoda, G.; Testa, J.R.; Golemis, E.A. Association of Krev-1/rap1a with Krit1, a novel ankyrin repeat-containing protein encoded by a gene mapping to 7q21-22. *Oncogene* **1997**, *15*, 1043–1049. [CrossRef] [PubMed]
42. Liu, W.; Draheim, K.M.; Zhang, R.; Calderwood, D.A.; Boggon, T.J. Mechanism for KRIT1 release of ICAP1-mediated suppression of integrin activation. *Mol. Cell* **2013**, *49*, 719–729. [CrossRef] [PubMed]
43. Zawistowski, J.S.; Serebriiskii, I.G.; Lee, M.F.; Golemis, E.A.; Marchuk, D.A. KRIT1 association with the integrin-binding protein ICAP-1: A new direction in the elucidation of cerebral cavernous malformations (CCM1) pathogenesis. *Hum. Mol. Genet.* **2002**, *11*, 389–396. [CrossRef]
44. Kleaveland, B.; Zheng, X.; Liu, J.J.; Blum, Y.; Tung, J.J.; Zou, Z.; Sweeney, S.M.; Chen, M.; Guo, L.; Lu, M.M.; et al. Regulation of cardiovascular development and integrity by the heart of glass-cerebral cavernous malformation protein pathway. *Nat. Med.* **2009**, *15*, 169–176. [CrossRef] [PubMed]
45. Gingras, A.R.; Liu, J.J.; Ginsberg, M.H. Structural basis of the junctional anchorage of the cerebral cavernous malformations complex. *J. Cell Biol.* **2012**, *199*, 39–48. [CrossRef]
46. Gingras, A.R.; Puzon-McLaughlin, W.; Ginsberg, M.H. The structure of the ternary complex of Krev interaction trapped 1 (KRIT1) bound to both the Rap1 GTPase and the heart of glass (HEG1) cytoplasmic tail. *J. Biol. Chem.* **2013**, *288*, 23639–23649. [CrossRef] [PubMed]
47. Gunel, M.; Laurans, M.S.; Shin, D.; DiLuna, M.L.; Voorhees, J.; Choate, K.; Nelson-Williams, C.; Lifton, R.P. *KRIT1*, a gene mutated in cerebral cavernous malformation, encodes a microtubule-associated protein. *Proc. Natl. Acad. Sci. USA* **2002**, *99*, 10677–10682. [CrossRef]
48. Fisher, O.S.; Zhang, R.; Li, X.; Murphy, J.W.; Demeler, B.; Boggon, T.J. Structural studies of cerebral cavernous malformations 2 (CCM2) reveal a folded helical domain at its C-terminus. *FEBS Lett.* **2013**, *587*, 272–277. [CrossRef]
49. Uhlik, M.T.; Abell, A.N.; Johnson, N.L.; Sun, W.; Cuevas, B.D.; Lobel-Rice, K.E.; Horne, E.A.; Dell'Acqua, M.L.; Johnson, G.L. Rac-MEKK3-MKK3 scaffolding for p38 MAPK activation during hyperosmotic shock. *Nat. Cell Biol.* **2003**, *5*, 1104–1110. [CrossRef]
50. Hilder, T.L.; Malone, M.H.; Bencharit, S.; Colicelli, J.; Haystead, T.A.; Johnson, G.L.; Wu, C.C. Proteomic identification of the cerebral cavernous malformation signaling complex. *J. Proteome Res.* **2007**, *6*, 4343–4355. [CrossRef]
51. Zhang, J.; Rigamonti, D.; Dietz, H.C.; Clatterbuck, R.E. Interaction between krit1 and malcavernin: Implications for the pathogenesis of cerebral cavernous malformations. *Neurosurgery* **2007**, *60*, 353–359. [CrossRef] [PubMed]
52. Zawistowski, J.S.; Stalheim, L.; Uhlik, M.T.; Abell, A.N.; Ancrile, B.B.; Johnson, G.L.; Marchuk, D.A. CCM1 and CCM2 protein interactions in cell signaling: Implications for cerebral cavernous malformations pathogenesis. *Hum. Mol. Genet.* **2005**, *14*, 2521–2531. [CrossRef] [PubMed]
53. Draheim, K.M.; Li, X.; Zhang, R.; Fisher, O.S.; Villari, G.; Boggon, T.J.; Calderwood, D.A. CCM2-CCM3 interaction stabilizes their protein expression and permits endothelial network formation. *J. Cell Biol.* **2015**, *208*, 987–1001. [CrossRef] [PubMed]
54. Stockton, R.A.; Shenkar, R.; Awad, I.A.; Ginsberg, M.H. Cerebral cavernous malformations proteins inhibit Rho kinase to stabilize vascular integrity. *J. Exp. Med.* **2010**, *207*, 881–896. [CrossRef]
55. Hilder, T.L.; Malone, M.H.; Johnson, G.L. Hyperosmotic induction of mitogen-activated protein kinase scaffolding. *Methods Enzym.* **2007**, *428*, 297–312. [CrossRef]

56. Zheng, X.; Xu, C.; Smith, A.O.; Stratman, A.N.; Zou, Z.; Kleaveland, B.; Yuan, L.; Didiku, C.; Sen, A.; Liu, X.; et al. Dynamic regulation of the cerebral cavernous malformation pathway controls vascular stability and growth. *Dev. Cell* **2012**, *23*, 342–355. [CrossRef]
57. Cullere, X.; Plovie, E.; Bennett, P.M.; MacRae, C.A.; Mayadas, T.N. The cerebral cavernous malformation proteins CCM2L and CCM2 prevent the activation of the MAP kinase MEKK3. *Proc. Natl. Acad. Sci. USA* **2015**, *112*, 14284–14289. [CrossRef]
58. Rosen, J.N.; Sogah, V.M.; Ye, L.Y.; Mably, J.D. Ccm2-like is required for cardiovascular development as a novel component of the Heg-CCM pathway. *Dev. Biol.* **2013**, *376*, 74–85. [CrossRef]
59. Li, X.; Zhang, R.; Zhang, H.; He, Y.; Ji, W.; Min, W.; Boggon, T.J. Crystal structure of CCM3, a cerebral cavernous malformation protein critical for vascular integrity. *J. Biol. Chem.* **2010**, *285*, 24099–24107. [CrossRef]
60. Wang, Y.; Liu, H.; Zhang, Y.; Ma, D. cDNA cloning and expression of an apoptosis-related gene, humanTFAR15 gene. *Sci. China C Life Sci.* **1999**, *42*, 323–329. [CrossRef]
61. Ma, X.; Zhao, H.; Shan, J.; Long, F.; Chen, Y.; Zhang, Y.; Han, X.; Ma, D. PDCD10 interacts with Ste20-related kinase MST4 to promote cell growth and transformation via modulation of the ERK pathway. *Mol. Biol. Cell* **2007**, *18*, 1965–1978. [CrossRef] [PubMed]
62. Ceccarelli, D.F.; Laister, R.C.; Mulligan, V.K.; Kean, M.J.; Goudreault, M.; Scott, I.C.; Derry, W.B.; Chakrabartty, A.; Gingras, A.C.; Sicheri, F. CCM3/PDCD10 heterodimerizes with germinal center kinase III (GCKIII) proteins using a mechanism analogous to CCM3 homodimerization. *J. Biol. Chem.* **2011**, *286*, 25056–25064. [CrossRef] [PubMed]
63. Fidalgo, M.; Fraile, M.; Pires, A.; Force, T.; Pombo, C.; Zalvide, J. CCM3/PDCD10 stabilizes GCKIII proteins to promote Golgi assembly and cell orientation. *J. Cell Sci.* **2010**, *123*, 1274–1284. [CrossRef]
64. Goudreault, M.; D'Ambrosio, L.M.; Kean, M.J.; Mullin, M.J.; Larsen, B.G.; Sanchez, A.; Chaudhry, S.; Chen, G.I.; Sicheri, F.; Nesvizhskii, A.I.; et al. A PP2A phosphatase high density interaction network identifies a novel striatin-interacting phosphatase and kinase complex linked to the cerebral cavernous malformation 3 (CCM3) protein. *Mol. Cell Proteom.* **2009**, *8*, 157–171. [CrossRef] [PubMed]
65. Suryavanshi, N.; Furmston, J.; Ridley, A.J. The STRIPAK complex components FAM40A and FAM40B regulate endothelial cell contractility via ROCKs. *BMC Cell Biol.* **2018**, *19*, 26. [CrossRef] [PubMed]
66. Gordon, J.; Hwang, J.; Carrier, K.J.; Jones, C.A.; Kern, Q.L.; Moreno, C.S.; Karas, R.H.; Pallas, D.C. Protein phosphatase 2a (PP2A) binds within the oligomerization domain of striatin and regulates the phosphorylation and activation of the mammalian Ste20-Like kinase Mst3. *BMC Biochem.* **2011**, *12*, 54. [CrossRef] [PubMed]
67. Voss, K.; Stahl, S.; Schleider, E.; Ullrich, S.; Nickel, J.; Mueller, T.D.; Felbor, U. CCM3 interacts with CCM2 indicating common pathogenesis for cerebral cavernous malformations. *Neurogenetics* **2007**, *8*, 249–256. [CrossRef]
68. Li, X.; Ji, W.; Zhang, R.; Folta-Stogniew, E.; Min, W.; Boggon, T.J. Molecular recognition of leucine-aspartate repeat (LD) motifs by the focal adhesion targeting homology domain of cerebral cavernous malformation 3 (CCM3). *J. Biol. Chem.* **2011**, *286*, 26138–26147. [CrossRef]
69. Zhang, Y.; Tang, W.; Zhang, H.; Niu, X.; Xu, Y.; Zhang, J.; Gao, K.; Pan, W.; Boggon, T.J.; Toomre, D.; et al. A network of interactions enables CCM3 and STK24 to coordinate UNC13D-driven vesicle exocytosis in neutrophils. *Dev. Cell* **2013**, *27*, 215–226. [CrossRef]
70. Dibble, C.F.; Horst, J.A.; Malone, M.H.; Park, K.; Temple, B.; Cheeseman, H.; Barbaro, J.R.; Johnson, G.L.; Bencharit, S. Defining the Functional Domain of Programmed Cell Death 10 through Its Interactions with Phosphatidylinositol-3,4,5-Trisphosphate. *PLoS ONE* **2010**, *5*, e11740. [CrossRef]
71. Castro, M.; Lavina, B.; Ando, K.; Alvarez-Aznar, A.; Abu Taha, A.; Brakebusch, C.; Dejana, E.; Betsholtz, C.; Gaengel, K. CDC42 Deletion Elicits Cerebral Vascular Malformations via Increased MEKK3-Dependent KLF4 Expression. *Circ. Res.* **2019**, *124*, 1240–1252. [CrossRef] [PubMed]
72. Mardakheh, F.K.; Self, A.; Marshall, C.J. RHO binding to FAM65A regulates Golgi reorientation during cell migration. *J. Cell Sci.* **2016**, *129*, 4466–4479. [CrossRef] [PubMed]
73. Maddaluno, L.; Rudini, N.; Cuttano, R.; Bravi, L.; Giampietro, C.; Corada, M.; Ferrarini, L.; Orsenigo, F.; Papa, E.; Boulday, G.; et al. EndMT contributes to the onset and progression of cerebral cavernous malformations. *Nature* **2013**, *498*, 492–496. [CrossRef] [PubMed]

74. Marchi, S.; Corricelli, M.; Trapani, E.; Bravi, L.; Pittaro, A.; Delle Monache, S.; Ferroni, L.; Patergnani, S.; Missiroli, S.; Goitre, L.; et al. Defective autophagy is a key feature of cerebral cavernous malformations. *EMBO Mol. Med.* **2015**, *7*, 1403–1417. [CrossRef]
75. Zhou, H.J.; Qin, L.; Zhang, H.; Tang, W.; Ji, W.; He, Y.; Liang, X.; Wang, Z.; Yuan, Q.; Vortmeyer, A.; et al. Endothelial exocytosis of angiopoietin-2 resulting from CCM3 deficiency contributes to cerebral cavernous malformation. *Nat. Med.* **2016**, *22*, 1033–1042. [CrossRef]
76. Crose, L.E.; Hilder, T.L.; Sciaky, N.; Johnson, G.L. Cerebral cavernous malformation 2 protein promotes smad ubiquitin regulatory factor 1-mediated RhoA degradation in endothelial cells. *J. Biol. Chem.* **2009**, *284*, 13301–13305. [CrossRef]
77. Glading, A.; Han, J.; Stockton, R.A.; Ginsberg, M.H. KRIT-1/CCM1 is a Rap1 effector that regulates endothelial cell cell junctions. *J. Cell Biol.* **2007**, *179*, 247–254. [CrossRef]
78. Wang, H.R.; Zhang, Y.; Ozdamar, B.; Ogunjimi, A.A.; Alexandrova, E.; Thomsen, G.H.; Wrana, J.L. Regulation of cell polarity and protrusion formation by targeting RhoA for degradation. *Science* **2003**, *302*, 1775–1779. [CrossRef]
79. Zhou, Z.; Rawnsley, D.R.; Goddard, L.M.; Pan, W.; Cao, X.J.; Jakus, Z.; Zheng, H.; Yang, J.; Arthur, J.S.; Whitehead, K.J.; et al. The cerebral cavernous malformation pathway controls cardiac development via regulation of endocardial MEKK3 signaling and KLF expression. *Dev. Cell* **2015**, *32*, 168–180. [CrossRef]
80. Zhou, Z.; Tang, A.T.; Wong, W.Y.; Bamezai, S.; Goddard, L.M.; Shenkar, R.; Zhou, S.; Yang, J.; Wright, A.C.; Foley, M.; et al. Cerebral cavernous malformations arise from endothelial gain of MEKK3-KLF2/4 signalling. *Nature* **2016**, *532*, 122–126. [CrossRef]
81. Huang, Q.; Yang, J.; Lin, Y.; Walker, C.; Cheng, J.; Liu, Z.G.; Su, B. Differential regulation of interleukin 1 receptor and Toll-like receptor signaling by MEKK3. *Nat. Immunol.* **2004**, *5*, 98–103. [CrossRef] [PubMed]
82. Li, K.; Wang, M.; Hu, Y.; Xu, N.; Yu, Q.; Wang, Q. TAK1 knockdown enhances lipopolysaccharide-induced secretion of proinflammatory cytokines in myeloid cells via unleashing MEKK3 activity. *Cell. Immunol.* **2016**, *310*, 193–198. [CrossRef] [PubMed]
83. Samanta, A.K.; Huang, H.J.; Bast, R.C., Jr.; Liao, W.S. Overexpression of MEKK3 confers resistance to apoptosis through activation of NFkappaB. *J. Biol. Chem.* **2004**, *279*, 7576–7583. [CrossRef] [PubMed]
84. Yang, J.; Lin, Y.; Guo, Z.; Cheng, J.; Huang, J.; Deng, L.; Liao, W.; Chen, Z.; Liu, Z.; Su, B. The essential role of MEKK3 in TNF-induced NF-kappaB activation. *Nat. Immunol.* **2001**, *2*, 620–624. [CrossRef] [PubMed]
85. Tang, A.T.; Choi, J.P.; Kotzin, J.J.; Yang, Y.; Hong, C.C.; Hobson, N.; Girard, R.; Zeineddine, H.A.; Lightle, R.; Moore, T.; et al. Endothelial TLR4 and the microbiome drive cerebral cavernous malformations. *Nature* **2017**, *545*, 305–310. [CrossRef]
86. Fisher, O.S.; Deng, H.; Liu, D.; Zhang, Y.; Wei, R.; Deng, Y.; Zhang, F.; Louvi, A.; Turk, B.E.; Boggon, T.J.; et al. Structure and vascular function of MEKK3-cerebral cavernous malformations 2 complex. *Nat. Commun.* **2015**, *6*, 7937. [CrossRef]
87. Harel, L.; Costa, B.; Tcherpakov, M.; Zapatka, M.; Oberthuer, A.; Hansford, L.M.; Vojvodic, M.; Levy, Z.; Chen, Z.Y.; Lee, F.S.; et al. CCM2 mediates death signaling by the TrkA receptor tyrosine kinase. *Neuron* **2009**, *63*, 585–591. [CrossRef]
88. Costa, B.; Kean, M.J.; Ast, V.; Knight, J.D.; Mett, A.; Levy, Z.; Ceccarelli, D.F.; Badillo, B.G.; Eils, R.; Konig, R.; et al. STK25 protein mediates TrkA and CCM2 protein-dependent death in pediatric tumor cells of neural origin. *J. Biol. Chem.* **2012**, *287*, 29285–29289. [CrossRef]
89. Wu, Z.; Qi, Y.; Guo, Z.; Li, P.; Zhou, D. miR-613 suppresses ischemia-reperfusion-induced cardiomyocyte apoptosis by targeting the programmed cell death 10 gene. *Biosci. Trends* **2016**, *10*, 251–257. [CrossRef]
90. Chen, L.; Tanriover, G.; Yano, H.; Friedlander, R.; Louvi, A.; Gunel, M. Apoptotic functions of PDCD10/CCM3, the gene mutated in cerebral cavernous malformation 3. *Stroke* **2009**, *40*, 1474–1481. [CrossRef]
91. Zhang, H.; Ma, X.; Deng, X.; Chen, Y.; Mo, X.; Zhang, Y.; Zhao, H.; Ma, D. PDCD10 interacts with STK25 to accelerate cell apoptosis under oxidative stress. *Front. Biosci.* **2012**, *17*, 2295–2305. [CrossRef] [PubMed]
92. Fidalgo, M.; Guerrero, A.; Fraile, M.; Iglesias, C.; Pombo, C.M.; Zalvide, J. Adaptor protein cerebral cavernous malformation 3 (CCM3) mediates phosphorylation of the cytoskeletal proteins ezrin/radixin/moesin by mammalian Ste20-4 to protect cells from oxidative stress. *J. Biol. Chem.* **2012**, *287*, 11556–11565. [CrossRef] [PubMed]
93. Wong, J.H.; Awad, I.A.; Kim, J.H. Ultrastructural pathological features of cerebrovascular malformations: A preliminary report. *Neurosurgery* **2000**, *46*, 1454–1459. [CrossRef] [PubMed]

94. Tu, J.; Stoodley, M.A.; Morgan, M.K.; Storer, K.P. Ultrastructural characteristics of hemorrhagic, nonhemorrhagic, and recurrent cavernous malformations. *J. Neurosurg.* **2005**, *103*, 903–909. [CrossRef]
95. Girard, R.; Fam, M.D.; Zeineddine, H.A.; Tan, H.; Mikati, A.G.; Shi, C.; Jesselson, M.; Shenkar, R.; Wu, M.; Cao, Y.; et al. Vascular permeability and iron deposition biomarkers in longitudinal follow-up of cerebral cavernous malformations. *J. Neurosurg.* **2017**, *127*, 102–110. [CrossRef]
96. Mikati, A.G.; Khanna, O.; Zhang, L.; Girard, R.; Shenkar, R.; Guo, X.; Shah, A.; Larsson, H.B.; Tan, H.; Li, L.; et al. Vascular permeability in cerebral cavernous malformations. *J. Cereb. Blood Flow Metab.* **2015**, *35*, 1632–1639. [CrossRef]
97. Murali, A.; Rajalingam, K. Small Rho GTPases in the control of cell shape and mobility. *Cell. Mol. Life Sci.* **2014**, *71*, 1703–1721. [CrossRef]
98. Citalan-Madrid, A.F.; Garcia-Ponce, A.; Vargas-Robles, H.; Betanzos, A.; Schnoor, M. Small GTPases of the Ras superfamily regulate intestinal epithelial homeostasis and barrier function via common and unique mechanisms. *Tissue Barriers* **2013**, *1*, e26938. [CrossRef]
99. van Buul, J.D.; Geerts, D.; Huveneers, S. Rho GAPs and GEFs: Controling switches in endothelial cell adhesion. *Cell Adhes. Migr.* **2014**, *8*, 108–124. [CrossRef]
100. Shen, Q.; Wu, M.H.; Yuan, S.Y. Endothelial contractile cytoskeleton and microvascular permeability. *Cell Health Cytoskelet.* **2009**, *2009*, 43–50. [CrossRef]
101. Corr, M.; Lerman, I.; Keubel, J.M.; Ronacher, L.; Misra, R.; Lund, F.; Sarelius, I.H.; Glading, A.J. Decreased Krev interaction-trapped 1 expression leads to increased vascular permeability and modifies inflammatory responses *in vivo*. *Arter. Thromb. Vasc. Biol.* **2012**, *32*, 2702–2710. [CrossRef] [PubMed]
102. Goitre, L.; DiStefano, P.V.; Moglia, A.; Nobiletti, N.; Baldini, E.; Trabalzini, L.; Keubel, J.; Trapani, E.; Shuvaev, V.V.; Muzykantov, V.R.; et al. Up-regulation of NADPH oxidase-mediated redox signaling contributes to the loss of barrier function in KRIT1 deficient endothelium. *Sci. Rep.* **2017**, *7*, 8296. [CrossRef] [PubMed]
103. Meliton, A.; Meng, F.; Tian, Y.; Shah, A.A.; Birukova, A.A.; Birukov, K.G. Role of Krev Interaction Trapped-1 in Prostacyclin-Induced Protection against Lung Vascular Permeability Induced by Excessive Mechanical Forces and Thrombin Receptor Activating Peptide 6. *Am. J. Respir. Cell Mol. Biol.* **2015**, *53*, 834–843. [CrossRef] [PubMed]
104. McDonald, D.A.; Shi, C.; Shenkar, R.; Stockton, R.A.; Liu, F.; Ginsberg, M.H.; Marchuk, D.A.; Awad, I.A. Fasudil decreases lesion burden in a murine model of cerebral cavernous malformation disease. *Stroke* **2012**, *43*, 571–574. [CrossRef] [PubMed]
105. Shenkar, R.; Shi, C.; Austin, C.; Moore, T.; Lightle, R.; Cao, Y.; Zhang, L.; Wu, M.; Zeineddine, H.A.; Girard, R.; et al. RhoA Kinase Inhibition with Fasudil Versus Simvastatin in Murine Models of Cerebral Cavernous Malformations. *Stroke* **2017**, *48*, 187–194. [CrossRef] [PubMed]
106. Shenkar, R.; Peiper, A.; Pardo, H.; Moore, T.; Lightle, R.; Girard, R.; Hobson, N.; Polster, S.P.; Koskimaki, J.; Zhang, D.; et al. Rho Kinase Inhibition Blunts Lesion Development and Hemorrhage in Murine Models of Aggressive *Pdcd10/Ccm3* Disease. *Stroke* **2019**, *50*, 738–744. [CrossRef] [PubMed]
107. Polster, S.P.; Stadnik, A.; Akers, A.L.; Cao, Y.; Christoforidis, G.A.; Fam, M.D.; Flemming, K.D.; Girard, R.; Hobson, N.; Koenig, J.I.; et al. Atorvastatin Treatment of Cavernous Angiomas with Symptomatic Hemorrhage Exploratory Proof of Concept (AT CASH EPOC) Trial. *Neurosurgery* **2019**, *85*, 843–853. [CrossRef]
108. Lange, C.; Storkebaum, E.; de Almodovar, C.R.; Dewerchin, M.; Carmeliet, P. Vascular endothelial growth factor: A neurovascular target in neurological diseases. *Nat. Rev. Neurol.* **2016**, *12*, 439–454. [CrossRef]
109. DiStefano, P.V.; Kuebel, J.M.; Sarelius, I.H.; Glading, A.J. KRIT1 protein depletion modifies endothelial cell behavior via increased vascular endothelial growth factor (VEGF) signaling. *J. Biol. Chem.* **2014**, *289*, 33054–33065. [CrossRef]
110. Goitre, L.; Balzac, F.; Degani, S.; Degan, P.; Marchi, S.; Pinton, P.; Retta, S.F. KRIT1 regulates the homeostasis of intracellular reactive oxygen species. *PLoS ONE* **2010**, *5*, e11786. [CrossRef]
111. Wallez, Y.; Huber, P. Endothelial adherens and tight junctions in vascular homeostasis, inflammation and angiogenesis. *Biochim. Biophys. Acta* **2008**, *1778*, 794–809. [CrossRef] [PubMed]
112. Daneman, R.; Prat, A. The blood-brain barrier. *Cold Spring Harb. Perspect. Biol.* **2015**, *7*, a020412. [CrossRef] [PubMed]
113. Gunzel, D.; Yu, A.S. Claudins and the modulation of tight junction permeability. *Physiol. Rev.* **2013**, *93*, 525–569. [CrossRef] [PubMed]

114. Castro Dias, M.; Coisne, C.; Lazarevic, I.; Baden, P.; Hata, M.; Iwamoto, N.; Francisco, D.M.F.; Vanlandewijck, M.; He, L.; Baier, F.A.; et al. Claudin-3-deficient C57BL/6J mice display intact brain barriers. *Sci. Rep.* **2019**, *9*, 203. [CrossRef] [PubMed]
115. Ohtsuki, S.; Yamaguchi, H.; Katsukura, Y.; Asashima, T.; Terasaki, T. mRNA expression levels of tight junction protein genes in mouse brain capillary endothelial cells highly purified by magnetic cell sorting. *J. Neurochem.* **2008**, *104*, 147–154. [CrossRef]
116. Nitta, T.; Hata, M.; Gotoh, S.; Seo, Y.; Sasaki, H.; Hashimoto, N.; Furuse, M.; Tsukita, S. Size-selective loosening of the blood-brain barrier in claudin-5-deficient mice. *J. Cell Biol.* **2003**, *161*, 653–660. [CrossRef]
117. Raleigh, D.R.; Marchiando, A.M.; Zhang, Y.; Shen, L.; Sasaki, H.; Wang, Y.; Long, M.; Turner, J.R. Tight junction-associated MARVEL proteins marveld3, tricellulin, and occludin have distinct but overlapping functions. *Mol. Biol. Cell* **2010**, *21*, 1200–1213. [CrossRef]
118. Buschmann, M.M.; Shen, L.; Rajapakse, H.; Raleigh, D.R.; Wang, Y.; Lingaraju, A.; Zha, J.; Abbott, E.; McAuley, E.M.; Breskin, L.A.; et al. Occludin OCEL-domain interactions are required for maintenance and regulation of the tight junction barrier to macromolecular flux. *Mol. Biol. Cell* **2013**, *24*, 3056–3068. [CrossRef]
119. Krug, S.M.; Amasheh, S.; Richter, J.F.; Milatz, S.; Gunzel, D.; Westphal, J.K.; Huber, O.; Schulzke, J.D.; Fromm, M. Tricellulin Forms a Barrier to Macromolecules in Tricellular Tight Junctions without Affecting Ion Permeability. *Mol. Biol. Cell* **2009**, *20*, 3713–3724. [CrossRef]
120. Saitou, M.; Furuse, M.; Sasaki, H.; Schulzke, J.D.; Fromm, M.; Takano, H.; Noda, T.; Tsukita, S. Complex phenotype of mice lacking occludin, a component of tight junction strands. *Mol. Biol. Cell* **2000**, *11*, 4131–4142. [CrossRef]
121. O'Driscoll, M.C.; Daly, S.B.; Urquhart, J.E.; Black, G.C.; Pilz, D.T.; Brockmann, K.; McEntagart, M.; Abdel-Salam, G.; Zaki, M.; Wolf, N.I.; et al. Recessive mutations in the gene encoding the tight junction protein occludin cause band-like calcification with simplified gyration and polymicrogyria. *Am. J. Hum. Genet.* **2010**, *87*, 354–364. [CrossRef]
122. Laukoetter, M.G.; Nava, P.; Lee, W.Y.; Severson, E.A.; Capaldo, C.T.; Babbin, B.A.; Williams, I.R.; Koval, M.; Peatman, E.; Campbell, J.A.; et al. JAM-A regulates permeability and inflammation in the intestine *in vivo*. *J. Exp. Med.* **2007**, *204*, 3067–3076. [CrossRef] [PubMed]
123. Otani, T.; Nguyen, T.P.; Tokuda, S.; Sugihara, K.; Sugawara, T.; Furuse, K.; Miura, T.; Ebnet, K.; Furuse, M. Claudins and JAM-A coordinately regulate tight junction formation and epithelial polarity. *J. Cell Biol.* **2019**, *218*, 3372–3396. [CrossRef] [PubMed]
124. Schmitt, M.M.N.; Megens, R.T.A.; Zernecke, A.; Bidzhekov, K.; van den Akker, N.M.; Rademakers, T.; van Zandvoort, M.A.; Hackeng, T.M.; Koenen, R.R.; Weber, C. Endothelial Junctional Adhesion Molecule-A Guides Monocytes into Flow-Dependent Predilection Sites of Atherosclerosis. *Circulation* **2014**, *129*, 66–76. [CrossRef] [PubMed]
125. Cohen, C.J.; Shieh, J.T.; Pickles, R.J.; Okegawa, T.; Hsieh, J.T.; Bergelson, J.M. The coxsackievirus and adenovirus receptor is a transmembrane component of the tight junction. *Proc. Natl. Acad. Sci. USA* **2001**, *98*, 15191–15196. [CrossRef] [PubMed]
126. Chung, J.; Kim, K.H.; An, S.H.; Lee, S.; Lim, B.K.; Kang, S.W.; Kwon, K. Coxsackievirus and adenovirus receptor mediates the responses of endothelial cells to fluid shear stress. *Exp. Mol. Med.* **2019**, *51*, 1–15. [CrossRef]
127. Fanning, A.S.; Anderson, J.M. Zonula Occludens-1 and-2 Are Cytosolic Scaffolds That Regulate the Assembly of Cellular Junctions. *Ann. N. Y. Acad. Sci.* **2009**, *1165*, 113–120. [CrossRef]
128. Katsuno, T.; Umeda, K.; Matsui, T.; Hata, M.; Tamura, A.; Itoh, M.; Takeuchi, K.; Fujimori, T.; Nabeshima, Y.; Noda, T.; et al. Deficiency of zonula occludens-1 causes embryonic lethal phenotype associated with defected yolk sac angiogenesis and apoptosis of embryonic cells. *Mol. Biol. Cell* **2008**, *19*, 2465–2475. [CrossRef]
129. Tornavaca, O.; Chia, M.; Dufton, N.; Almagro, L.O.; Conway, D.E.; Randi, A.M.; Schwartz, M.A.; Matter, K.; Balda, M.S. ZO-1 controls endothelial adherens junctions, cell-cell tension, angiogenesis, and barrier formation. *J. Cell Biol.* **2015**, *208*, 821–838. [CrossRef] [PubMed]
130. Schossleitner, K.; Rauscher, S.; Groger, M.; Friedl, H.P.; Finsterwalder, R.; Habertheuer, A.; Sibilia, M.; Brostjan, C.; Fodinger, D.; Citi, S.; et al. Evidence That Cingulin Regulates Endothelial Barrier Function In Vitro and *In Vivo*. *Arter. Throm. Vas.* **2016**, *36*, 647–654. [CrossRef] [PubMed]

131. Chrifi, I.; Hermkens, D.; Brandt, M.M.; van Dijk, C.G.M.; Burgisser, P.E.; Haasdijk, R.; Pei, J.Y.; van de Kamp, E.H.M.; Zhu, C.B.; Blonden, L.; et al. Cgnl1, an endothelial junction complex protein, regulates GTPase mediated angiogenesis. *Cardiovasc. Res.* **2017**, *113*, 1776–1788. [CrossRef] [PubMed]
132. McKenzie, J.A.; Ridley, A.J. Roles of Rho/ROCK and MLCK in TNF-alpha-induced changes in endothelial morphology and permeability. *J. Cell. Physiol.* **2007**, *213*, 221–228. [CrossRef]
133. Persidsky, Y.; Heilman, D.; Haorah, J.; Zelivyanskaya, M.; Persidsky, R.; Weber, G.A.; Shimokawa, H.; Kaibuchi, K.; Ikezu, T. Rho-mediated regulation of tight junctions during monocyte migration across the blood-brain barrier in HIV-1 encephalitis (HIVE). *Blood* **2006**, *107*, 4770–4780. [CrossRef] [PubMed]
134. Wojciak-Stothard, B.; Potempa, S.; Eichholtz, T.; Ridley, A.J. Rho and Rac but not Cdc42 regulate endothelial cell permeability. *J. Cell Sci.* **2001**, *114*, 1343–1355. [PubMed]
135. Terry, S.; Nie, M.; Matter, K.; Balda, M.S. Rho signaling and tight junction functions. *Physiology* **2010**, *25*, 16–26. [CrossRef]
136. Yamamoto, M.; Ramirez, S.H.; Sato, S.; Kiyota, T.; Cerny, R.L.; Kaibuchi, K.; Persidsky, Y.; Ikezu, T. Phosphorylation of claudin-5 and occludin by rho kinase in brain endothelial cells. *Am. J. Pathol.* **2008**, *172*, 521–533. [CrossRef]
137. Izawa, Y.; Gu, Y.H.; Osada, T.; Kanazawa, M.; Hawkins, B.T.; Koziol, J.A.; Papayannopoulou, T.; Spatz, M.; Del Zoppo, G.J. beta1-integrin-matrix interactions modulate cerebral microvessel endothelial cell tight junction expression and permeability. *J. Cereb. Blood Flow Metab.* **2018**, *38*, 641–658. [CrossRef]
138. Faurobert, E.; Rome, C.; Lisowska, J.; Manet-Dupe, S.; Boulday, G.; Malbouyres, M.; Balland, M.; Bouin, A.P.; Keramidas, M.; Bouvard, D.; et al. CCM1-ICAP-1 complex controls beta 1 integrin-dependent endothelial contractility and fibronectin remodeling. *J. Cell Biol.* **2013**, *202*, 545–561. [CrossRef]
139. Millon-Fremillon, A.; Brunner, M.; Abed, N.; Collomb, E.; Ribba, A.S.; Block, M.R.; Albiges-Rizo, C.; Bouvard, D. Calcium and calmodulin-dependent serine/threonine protein kinase type II (CaMKII)-mediated intramolecular opening of integrin cytoplasmic domain-associated protein-1 (ICAP-1alpha) negatively regulates beta1 integrins. *J. Biol. Chem.* **2013**, *288*, 20248–20260. [CrossRef]
140. Stroeken, P.J.M.; Alvarez, B.; Van Rheenen, J.; Wijnands, Y.M.; Geerts, D.; Jalink, K.; Roos, E. Integrin cytoplasmic domain-associated protein-1 (ICAP-1) interacts with the ROCK-I kinase at the plasma membrane. *J. Cell. Physiol.* **2006**, *208*, 620–628. [CrossRef]
141. Wittchen, E.S.; Worthylake, R.A.; Kelly, P.; Casey, P.J.; Quilliam, L.A.; Burridge, K. Rap1 GTPase inhibits leukocyte transmigration by promoting endothelial barrier function. *J. Biol. Chem.* **2005**, *280*, 11675–11682. [CrossRef] [PubMed]
142. Ramos, C.J.; Lin, C.; Liu, X.; Antonetti, D.A. The EPAC-Rap1 pathway prevents and reverses cytokine-induced retinal vascular permeability. *J. Biol. Chem.* **2018**, *293*, 717–730. [CrossRef] [PubMed]
143. Wilson, C.W.; Parker, L.H.; Hall, C.J.; Smyczek, T.; Mak, J.; Crow, A.; Posthuma, G.; De Maziere, A.; Sagolla, M.; Chalouni, C.; et al. Rasip1 regulates vertebrate vascular endothelial junction stability through Epac1-Rap1 signaling. *Blood* **2013**, *122*, 3678–3690. [CrossRef] [PubMed]
144. Post, A.; Pannekoek, W.J.; Ross, S.H.; Verlaan, I.; Brouwer, P.M.; Bos, J.L. Rasip1 mediates Rap1 regulation of Rho in endothelial barrier function through ArhGAP29. *Proc. Natl. Acad. Sci. USA* **2013**, *110*, 11427–11432. [CrossRef] [PubMed]
145. Xu, K.; Sacharidou, A.; Fu, S.; Chong, D.C.; Skaug, B.; Chen, Z.J.; Davis, G.E.; Cleaver, O. Blood vessel tubulogenesis requires Rasip1 regulation of GTPase signaling. *Dev. Cell* **2011**, *20*, 526–539. [CrossRef]
146. de Kreuk, B.J.; Gingras, A.R.; Knight, J.D.R.; Liu, J.J.; Gingras, A.C.; Ginsberg, M.H. Heart of glass anchors Rasip1 at endothelial cell-cell junctions to support vascular integrity. *eLife* **2016**, *5*, e11394. [CrossRef]
147. Severson, E.A.; Parkos, C.A. Structural determinants of Junctional Adhesion Molecule A (JAM-A) function and mechanisms of intracellular signaling. *Curr. Opin. Cell Biol.* **2009**, *21*, 701–707. [CrossRef]
148. Giannotta, M.; Benedetti, S.; Tedesco, F.S.; Corada, M.; Trani, M.; D'Antuono, R.; Millet, Q.; Orsenigo, F.; Galvez, B.G.; Cossu, G.; et al. Targeting endothelial junctional adhesion molecule-A/EPAC/Rap-1 axis as a novel strategy to increase stem cell engraftment in dystrophic muscles. *EMBO Mol. Med.* **2014**, *6*, 239–258. [CrossRef]
149. Schneider, H.; Errede, M.; Ulrich, N.H.; Virgintino, D.; Frei, K.; Bertalanffy, H. Impairment of tight junctions and glucose transport in endothelial cells of human cerebral cavernous malformations. *J. Neuropathol. Exp. Neurol.* **2011**, *70*, 417–429. [CrossRef]

150. Jakimovski, D.; Schneider, H.; Frei, K.; Kennes, L.N.; Bertalanffy, H. Bleeding propensity of cavernous malformations: Impact of tight junction alterations on the occurrence of overt hematoma. *J. Neurosurg.* **2014**, *121*, 613–620. [CrossRef]
151. Lopez-Ramirez, M.A.; Fonseca, G.; Zeineddine, H.A.; Girard, R.; Moore, T.; Pham, A.; Cao, Y.; Shenkar, R.; de Kreuk, B.J.; Lagarrigue, F.; et al. Thrombospondin1 (TSP1) replacement prevents cerebral cavernous malformations. *J. Exp. Med.* **2017**, *214*, 3331–3346. [CrossRef] [PubMed]
152. Stamatovic, S.M.; Sladojevic, N.; Keep, R.F.; Andjelkovic, A.V. PDCD10 (CCM3) regulates brain endothelial barrier integrity in cerebral cavernous malformation type 3: Role of CCM3-ERK1/2-cortactin cross-talk. *Acta Neuropathol.* **2015**, *130*, 731–750. [CrossRef] [PubMed]
153. Johnson, A.M.; Roach, J.P.; Hu, A.; Stamatovic, S.M.; Zochowski, M.R.; Keep, R.F.; Andjelkovic, A.V. Connexin 43 gap junctions contribute to brain endothelial barrier hyperpermeability in familial cerebral cavernous malformations type III by modulating tight junction structure. *FASEB J.* **2018**, *32*, 2615–2629. [CrossRef] [PubMed]
154. Glading, A.J.; Ginsberg, M.H. Rap1 and its effector KRIT1/CCM1 regulate beta-catenin signaling. *Dis. Models Mech.* **2010**, *3*, 73–83. [CrossRef]
155. Wang, Y.; Li, Y.; Zou, J.; Polster, S.P.; Lightle, R.; Moore, T.; Dimaano, M.; He, T.C.; Weber, C.R.; Awad, I.A.; et al. The cerebral cavernous malformation disease causing gene KRIT1 participates in intestinal epithelial barrier maintenance and regulation. *FASEB J.* **2019**, *33*, 2132–2143. [CrossRef]
156. McCarthy, K.M.; Francis, S.A.; McCormack, J.M.; Lai, J.; Rogers, R.A.; Skare, I.B.; Lynch, R.D.; Schneeberger, E.E. Inducible expression of claudin-1-myc but not occludin-VSV-G results in aberrant tight junction strand formation in MDCK cells. *J. Cell Sci.* **2000**, *113*, 3387–3398.
157. Tang, A.T.; Sullivan, K.R.; Hong, C.C.; Goddard, L.M.; Mahadevan, A.; Ren, A.; Pardo, H.; Peiper, A.; Griffin, E.; Tanes, C.; et al. Distinct cellular roles for PDCD10 define a gut-brain axis in cerebral cavernous malformation. *Sci. Transl. Med.* **2019**, *11*. [CrossRef]

International Journal of
Molecular Sciences

MDPI

Review

Structure and Junctional Complexes of Endothelial, Epithelial and Glial Brain Barriers

Mariana Castro Dias *, Josephine A. Mapunda, Mykhailo Vladymyrov and Britta Engelhardt *

Theodor Kocher Institute, University of Bern, 3012 Bern, Switzerland; josephine.mapunda@tki.unibe.ch (J.A.M.); mykhailo.vladymyrov@tki.unibe.ch (M.V.)

* Correspondence: mariana.dias@tki.unibe.ch (M.C.D.); bengel@tki.unibe.ch (B.E.)

Received: 14 October 2019; Accepted: 26 October 2019; Published: 29 October 2019

Abstract: The homeostasis of the central nervous system (CNS) is ensured by the endothelial, epithelial, mesothelial and glial brain barriers, which strictly control the passage of molecules, solutes and immune cells. While the endothelial blood-brain barrier (BBB) and the epithelial blood-cerebrospinal fluid barrier (BCSFB) have been extensively investigated, less is known about the epithelial and mesothelial arachnoid barrier and the glia limitans. Here, we summarize current knowledge of the cellular composition of the brain barriers with a specific focus on describing the molecular constituents of their junctional complexes. We propose that the brain barriers maintain CNS immune privilege by dividing the CNS into compartments that differ with regard to their role in immune surveillance of the CNS. We close by providing a brief overview on experimental tools allowing for reliable in vivo visualization of the brain barriers and their junctional complexes and thus the respective CNS compartments.

Keywords: brain barriers; blood-brain barrier; neurovascular unit; blood-cerebrospinal fluid barrier; arachnoid barrier; glia limitans; tight junctions; adherens junctions

1. Introduction

The brain barriers established by the endothelial blood-brain barrier (BBB), the epithelial blood-cerebrospinal fluid barrier (BCSFB), the meningeal brain barriers and the blood spinal cord barrier are essential for maintaining central nervous system (CNS) homeostasis [1]. While the structural and junctional components of the BBB and of the BCSFB of the choroid plexus (ChP) have been vastly explored and described, much less is known about the cells and junctional complexes establishing the meningeal barriers and the glia limitans.

Development of the CNS vasculature begins with the process of vasculogenesis, where angioblasts, which originate from the mesoderm, move to the head region and form the primary perineural vascular plexus around the developing brain. The proliferating neuroectodermal tissue is invaded by vascular sprouts from the primary perineural plexus establishing the brain vasculature by a process called angiogenesis. The unique barrier properties of the brain endothelial cells are not intrinsic and are rather induced by a process referred to as barriergenesis by the continuous crosstalk with the developing neuroectodermal tissue [2–5].

The ChP develops from different locations along the dorsal axis of the neural tube, with the hindbrain ChP of the fourth ventricle being the first to be formed, once the neural tube is closed [6]. While the ChP stroma develops from mesenchymal cells, the ChP epithelium derives from neuroepithelial cells. Despite the different origin along the rostral-caudal axis of the developing nervous system, the mature ChP epithelia are morphologically similar (reviewed in Reference [6]).

The meningeal barriers comprise three layers: the dura mater, the arachnoid mater and the pia mater, and cover the brain and the spinal cord from its earliest stages of development, establishing

a protective covering of the CNS in the adult. Our current understanding of the development of the meninges has not much advanced beyond identifying the origins of pial, arachnoid and dural fibroblasts in the frontal brain from neural crest, and in the midbrain, hindbrain and spinal cord from mesoderm [7]. Despite their differences in developmental origin, the cells of the pia, arachnoid and dura mater have been described to establish functionally similar barriers. However, the respective barrier function may be established by different molecular components of their junctional complexes [8–11].

Taken together, junctional complexes established between cells of the brain barriers might not only differ between the different barriers but also within one respective barrier along the rostral-caudal axis. Here, we summarize the current knowledge of the brain barriers, with a particular focus on the molecular components of their junctional complexes. Additionally, we suggest that visualization of brain barriers junctional complexes provides useful landmarks for in vivo imaging of immune surveillance of the CNS.

2. Blood-Brain Barrier and Its Central Players: Cellular and Acellular Components of the Neurovascular Unit (NVU)

The brain vasculature is a big and complex network composed of arteries and arterioles, capillaries, venules and veins, which allows for the vital distribution of nutrients and oxygen to the CNS at the level of the microvasculature, namely arterioles, capillaries and post-capillary venules [12]. Brain microvascular endothelial cells, referred to as the blood-brain barrier (BBB), possess unique features restricting the free passage of ions, molecules and cells from the blood into the CNS parenchyma, while facilitating the transport of toxic compounds out of the CNS [13,14]. Development and maintenance of BBB characteristics in CNS microvascular endothelium relies on the continuous crosstalk between cellular and acellular elements of the CNS. In the adult, the entity of BBB endothelium, pericytes, astrocytes, and the basal membranes are thus collectively referred to as the neurovascular unit (NVU) (represented in Figure 1) [15]. Maintenance of a functional NVU is a prerequisite for BBB function and requires understanding of the specific contributions of these cells to barrier function.

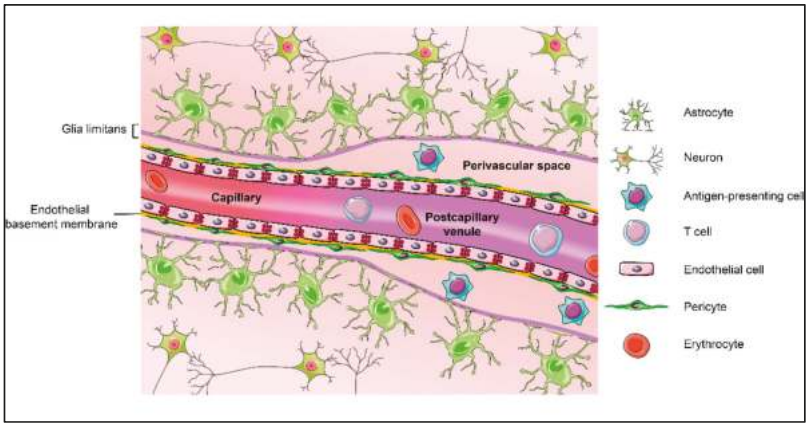

Figure 1. Schematic representation of the components of the neurovascular unit at the level of brain capillaries and post-capillary venules. Drawings of the individual cell types were adapted from Servier Medical Art (http://smart.servier.com/), licensed under a Creative Common Attribution 3.0 Generic License.

2.1. Endothelial Cells

Most studies of the BBB focus on the capillary endothelial cells, due to their unique properties [16,17]. Besides lacking fenestrae, these endothelial cells are brought together by the presence of continuous and complex tight junctions that prohibit free diffusion of molecules across

the BBB via the paracellular route [18–20]. Additionally, they have very low pinocytosis rates when compared to the peripheral endothelium [21,22]. Of notice, the major facilitator superfamily domain-containing protein 2 (Mfsd2a), a membrane transport protein, is specifically expressed in the CNS endothelium and acts as a key regulator suppressing vesicular activity at the BBB [23,24]. To ensure the passage of nutrients from the blood into the CNS and to remove potential toxic agents from the brain, the BBB endothelial cells express specific transporters and efflux pumps [25–27]. In particular, the efflux pump MDR1/P-glycoprotein (Pgp) translocates potentially harmful lipophilic or endogenous molecules from the CNS to the blood [28]. The glucose transporter GLUT-1 (*SLC2A1)* is also highly enriched in the BBB endothelium, allowing for glucose delivery to the CNS [29]. The barrier characteristics referred to above are also present at the level of the endothelial cells forming the BBB in the post-capillary venules. While the capillaries represent a barrier for solutes and ions, leukocyte trafficking is regulated at the level of the post-capillary venules where the endothelial cells express specific adhesion molecules [1,30].

Additionally, the luminal side of the brain endothelium is covered by the glycocalyx, a carbohydrate-rich mesh of anionic polymers, which acts as a first physical barrier between the blood and the vessel wall [31]. In peripheral microvessels, the glycocalyx regulates vascular permeability to water and to albumin, and glycocalyx breakdown results in plasma leakage and enhanced leukocyte recruitment, in vivo [32,33]. Recent advances in in vivo imaging have allowed to confirm barrier forming role of the glycocalyx in peripheral vessels [34] and at the level of the BBB [35].

However, there are areas of the brain, the circumventricular organs, where the capillaries lack BBB properties and rather have fenestrae allowing blood components to freely pass towards specialized neurons serving neuroendocrine and neurosensory functions [36]. In addition, the ChP vasculature is characterized by fenestrae allowing free access of blood components into the ChP stroma [37].

2.2. Mural Cells: Smooth Muscle Cells and Pericytes

Mural cells comprise smooth muscle cells and pericytes. While pericytes, embedded in the endothelial basement membrane, incompletely cover the capillaries, smooth muscle cells seem to completely surround arterioles and to a lower degree venules and, together with the endothelial basement membrane, compose the tunica media [38]. Additionally, smooth muscle cells express contractile proteins such as alpha-smooth muscle actin, which allows for the control of vessel diameter and blood flow [38–41]. Recent studies have assigned additional roles of pericytes in regulating blood flow at the level of capillaries [42], which has initiated a debate on the role of arteriolar smooth muscle cell or capillary pericyte contractility in regulating regional cerebral blood flow. At the same time, pericytes are morphologically and functionally distinct from smooth muscle cells [43], which is further supported by the recent discoveries on their different gene expression profile in CNS blood vessels [44]. Pericytes interact with the endothelial cells via specific adhesion points that can either form peg-and-socket junctions, due to the presence of N-cadherin [45], or can occur as adhesion plaques, gap junctions and even tight junctions [46–48]. In the brain, endothelial coverage by pericytes is extremely high, with an endothelial cell/pericyte ratio between 1:1 to 3:1 [49]. Additionally, pericytes are involved in wound healing, angiogenesis, deposition of extracellular matrix and, during embryogenesis, have a strong role in BBB formation by suppressing vesicular activity in brain endothelial cells [43,50,51]. In the adult stage, loss of pericytes impairs BBB properties of endothelial cells by affecting their gene expression profile leading to increased vesicular trafficking and loss of polarization of astrocytic endfeet [51]. Moreover, pericytes regulate expression of cellular adhesion molecules in the BBB endothelium [50–52].

2.3. Basement Membrane

Pericytes and endothelial cells secrete and are surrounded by the extracellular matrix proteins that comprise the endothelial basement membrane. It is a crosslinked network composed of type IV collagen, α4 and α5 laminins, nidogen, heparan sulphate proteoglycans and some glycoproteins [53]. A unique

feature of CNS microvessels is the presence of a second basement membrane, referred to as parenchymal basement membrane, which is secreted by astrocytes [53,54]. With a composition of α1 and α2 laminins at the brain surface and with α2 laminins at the perivascular spaces, the parenchymal basement membranes are molecularly distinct from the endothelial basement membrane [55]. At the capillary level it merges with the endothelial basement membrane, while at the level of post-capillary venules there is a small perivascular space between those two basement membranes. The three-dimensional configuration and the components of these basement membranes host specific signaling cues for cellular growth and survival during the development and further maintenance of the BBB, while giving physical support to the vasculature [56] (reviewed in Reference [57]).

2.4. Astrocytes

Astrocytes also assume a tight relationship with the endothelium and the mural cells. These glial cells are widely present throughout the CNS and perform a supportive role that regulates the neuronal microenvironment by controlling neurotransmitters and electrolytes balance, synapse formation and clearance of axonal debris [16,58,59]. Furthermore, they have extensive cellular protrusions that cover blood vessels and neuronal synapses, promoting a direct link between neuronal circuits and the vasculature [16]. The astrocytic endfeet are in direct contact with the microvasculature of the CNS, covering a large part of the abluminal aspect of CNS microvessels [39]. Astrocytic processes express a range of proteins, including α-dystroglycan and dystrophin, which link the astrocyte endfoot to the parenchymal basement membrane, and the water channel aquaporin 4, which plays a crucial role regulating water homeostasis in the CNS [60,61]. Astrocytes have been described as an important intermediate in promoting endothelial cell barrier properties, as well as secreting the components of the parenchymal basement membrane, as mentioned above [16,53,62]. Additionally, the astrocytic endfeet and the parenchymal basement membrane form a second barrier of the CNS called glia limitans [1]. Several in vitro studies showed that with a co-culture of astrocytes and endothelial cells, the junctional complexes between adjacent endothelial cells upregulate its main proteins, contributing to an increase in barrier integrity [63,64]. Moreover, secretion of sonic hedgehog, retinoic acid and angiopoietin-1 by astrocytes supports the barrier properties of brain endothelial cells [65,66]. On the other hand, the interaction of astrocytes with endothelial cells is also very important, with endothelial-secreted factors such as LIF1 promoting astrocytic differentiation [67].

3. Molecular Constituents of the BBB

The BBB acts as a physical and metabolic barrier due to the unique biochemical make-up of the BBB endothelial cells. Here we will only focus on describing the molecules establishing the paracellular diffusion barrier of the BBB, which are proteins composing tight junctions, adherens junctions, transmembrane proteins localized at cell-to-cell contacts outside the organized tight junctions and adherens junctions, and intracellular junctional scaffolding proteins.

3.1. BBB Tight Junctions (TJs)

TJs localized between adjacent endothelial cells are core elements actively involved in the establishment of a paracellular barrier, which limits free diffusion of ions and molecules at cell-cell junctions, adopting a "gate" function. TJs were discovered by transmission electron microscopy studies and described as focal points were the membranes of adjacent cells come together, obliterating the intercellular cleft [68]. Freeze-fracture electron microscopy showed that the TJ strands of the BBB endothelium resemble rather those of epithelial cells by producing predominantly protoplasmic (P-face) associated continuous and complex particle strands [69–74]. Although the exact mechanism underlying P-face and exoplasmic (E-face) association of TJ particles remain to be shown, occludin and claudins are localized to the TJ particle strands and thus it is hypothesized that a high fraction of P-face associated TJs correlates with increased avidity of the transmembrane TJ proteins to the actin cytoskeleton elements [73].

Besides blocking paracellular diffusion, TJs are proposed to act as a "fence" by creating an intramembrane diffusion barrier. This not only stops free passage of proteins and lipids across the lipid bilayer [75], but also prohibits an intermixing of the components of the plasma membrane, creating distinct apical and basolateral membrane sites [76]. Additionally, they distribute selected membrane components to the cell surface and allow for accumulation of internal scaffolding proteins, essential to establish a link to the cytoskeleton [77]. Altogether, the "gate and fence" function that TJs assume is essential to assure the regulation of a physiological barrier. Most of the gathered knowledge about TJs is derived from epithelial cells and readily assumed to hold true for endothelial cells, despite lacking formal proof [78]. In terms of molecular composition, TJs are composed of transmembrane proteins, cytoplasmic plaque proteins, signaling proteins and adapters that bind these complexes to the actin cytoskeleton. Transmembrane proteins are suggested to be the elements playing the barrier and fence role, since they are constituted by transmembrane, cytoplasmic and extracellular domains. Three groups of transmembrane proteins are found to be localized in TJs: the claudins, the immunoglobulin superfamily junctional adhesion molecules (JAMs) and the tight junction-associated MARVEL proteins (TAMP) [78,79].

Claudins are the major components of TJs and to date, 27 members of this family have been identified in mammals [80]. Their general structure consists of an intracellular NH_2 domain, four transmembrane domains, two different extracellular loops (ECL1 and ECL2) and one intracellular COOH terminus [79]. In their C-terminus, most of the claudins possess a PDZ-binding motif used to interact with the TJ-associated scaffolding proteins [81]. ECL1 is involved in regulating the paracellular tightness and ion permeability, while ECL2 mediates cis/trans claudin-claudin interactions [82,83]. In vitro data showed that in contrast to other TJ transmembrane proteins, claudins are sufficient to form TJs strands in fibroblasts and that paracellular permeability is increased upon disruption of claudins, which suggests that this family of proteins is essential for barrier formation [84–87]. It has been suggested that specific barrier functions demand expression of different combinations of claudins, which is believed to influence the charge and size-selective properties of the barrier [88]. Claudins such as claudins-1, -3, -5, -11, -14 and -19 act as TJ sealing membrane proteins, while claudins-2, -10, -15 and -17 are involved in ion pore formation between two adjacent cells [89]. Claudin-deficient mice have been extremely helpful to understand the specific function of individual claudins in specific tissue barriers. For example, claudin-1 deficiency leads to epidermal permeability barrier defects in the skin, while lack of claudin-11 causes defects in CNS myelin sheaths [90,91]. Regarding the BBB endothelium, claudin-1, claudin-3, claudin-5, claudin-11 and claudin-12 were described to be expressed in the BBB endothelial cells [92–95]. Claudin-5 is specifically expressed in endothelial cells with very high expression in brain endothelium [50]. Lack of claudin-5 leads to perinatal death in mice, due to exacerbated BBB permeability to tracers smaller than 800 Da [92,96]. Supporting the important role of claudin-5 in BBB TJs, inducible knock-down of claudin-5 in adult mice was found to lead to seizures and behavioral changes, due to loss of BBB properties [97]. Despite this dramatic failure of BBB TJ functions, mice lacking claudin-5 still present morphologically intact and P-face associated TJs in the BBB, which suggests that claudins other than claudin-5 maintain BBB TJs in these mice [92]. Claudin-3 has been described as an additional component of BBB TJs, mediating TJ maturation during development by acting as a downstream target of Wnt/β-catenin signaling [50,98,99]. Additional evidence for a role of claudin-3 in regulating BBB integrity was derived from studies in an animal model for multiple sclerosis or in human glioblastoma multiforme, were claudin-3 immunostaining was found to be specifically lost in inflamed CNS microvessels [98]. These observations supported a role for claudin-3 in maintaining junctional BBB integrity. Making use of a novel claudin-3 deficient mouse and advanced transcriptomic profiling of brain endothelial cells we and others recently made the unexpected observation that claudin-3 mRNA cannot be detected in brain endothelial cells and thus claudin-3 is not expressed in brain endothelial cells and does not contribute to BBB TJs [100–102]. Disturbingly, we found most of the claudin-3 detecting antibodies to produce comparable junctional immunostainings of brain endothelial cells in wild-type and claudin-3-deficient mice suggesting that available claudin-3

antibodies cross-react with another junctional molecule and do not allow to the reliable detection of expression and junctional localization of claudin-3 protein [102]. In addition, positive immunostaining for claudin-1 and claudin-11 has been reported in mouse brain endothelium [103] [93,95]. However, we and others showed that claudin-1 mRNA is not detectable in brain endothelial cells [44,104,105]. In fact, endothelial specific inducible ectopic expression of claudin-1 in BBB endothelium reduces BBB leakiness in an animal model of multiple sclerosis and ameliorates clinical signs of the disease further supporting absence of claudin-1 at the BBB [104]. Similarly, claudin-11 mRNA was not detected in brain endothelial cells in single-cell RNA sequencing datasets from mouse brain microvessels, but its expression was readily detected in oligodendrocytes [44,105].

Finally, claudin-12 is an atypical member of the claudin family because it does not have a PDZ-binding motif [69]. Prominent junctional immunostaining for claudin-12 [92] suggested its localization to BBB TJs. However, by establishing a claudin-12 deficient mouse we could recently show that expression of claudin-12 in microvascular brain endothelial cells is low to absent and is not required for barrier function of the BBB [106]. Analysis of the localization of claudin-12 protein in brain endothelial cells was again hampered by the lack of antibodies specifically detecting claudin-12 in wild-type but not in claudin-12 deficient mice.

Taken together, reports describing junctional localization of claudin-1, claudin-3, and claudin-12 proteins in brain endothelial cells may be inaccurate due to not well-defined cross-reactivities and thus false-positive staining of claudin antibodies. Cross-reactivity of the anti-claudin antibodies may be due to the high degree of conservation and a common amino acid sequence within some members of the claudin family, which could potentiate a cross-reactivity of anti-claudin antibodies [83]. Furthermore, recent studies described detection of claudin-11 at the protein level in BBB endothelial cells in mice especially in the spinal cord and man [93,94]. As single-cell RNAseq analysis of brain endothelial cells failed to detect claudin-11 in these cells [44,105] and so, it is mandatory to explore if claudin 11 mRNA levels are too low for detection in the single-cell RNAseq screens or if detection of claudin-11 protein in these studies is again due to the cross-reaction of claudin-11 antibodies with other junctional entities.

Thus, at present, claudin-5 is the only claudin confirmed to be expressed at the mRNA and protein level in brain endothelial cells, to be localized to BBB TJs and to play a major role in BBB TJs integrity. Advanced transcriptome profiling studies have identified additional claudins, e.g., claudin-25/CLDND1 to be expressed in brain microvascular endothelial cells, with their exact function to be determined [44,105].

The TAMP family comprises the proteins occludin, tricellulin and MARVELD3 [107–109], which have four transmembrane domains and a MARVEL (MAL-related proteins for vesicle trafficking and membrane link) domain. To date, occludin and tricellulin were found to be expressed at the TJs of the BBB [110,111]. Occludin, the first transmembrane protein discovered to be localized exclusively in TJs, is highly expressed in endothelial cells of the CNS and was suggested to play a role in barrier integrity [107,110–113]. However, occludin-deficient epithelial cells develop morphologically intact TJs and consequently maintain barrier function [114]. On the other hand, phosphorylation of occludin was shown to regulate endothelial permeability and to be necessary for cortical actin organization in various endothelial cell models [115–117]. Additionally, occludin-deficient mice do not show impaired TJs, but are characterized by chronic inflammation, poor TJ integrity and by calcifications in the brain [118]. These results suggest that occludin may be involved in calcium movement across the BBB and in the regulation of TJ stability and barrier function, rather than TJ assembly. Another member of the TAMP family is tricellulin, which, as the name indicates, is specifically localized to tricellular junctions, a point in which three adjacent cells meet (reviewed in Reference [119]). Albeit being widely described in epithelial monolayers, recently expression of tricellulin was described in endothelial cells forming the BBB and the blood–retinal barrier [111,120], underscoring the epithelial nature of these endothelial barriers. The precise function of tricellulin in endothelial cells forming the BBB and blood–retinal barrier remains however to be described.

The third group of proteins found in BBB TJs are the members of the JAM family, JAM-A, JAM-B and JAM-C. These proteins are immunoglobulin (Ig)-like molecules composed of a single transmembrane domain, two extracellular Ig domains and a PDZ-binding motif in their C-terminus that allows for an interaction with cytoplasmic proteins linking the JAMs to the actin cytoskeleton [121,122]. JAMs are highly enriched in the TJs of epithelial and endothelial cells [123–127] and are the tight junction-associated transmembrane proteins that regulate cell polarity by interacting with Par3 [128,129]. JAM-A immunostaining was found at the BBB and as JAM-A upon transfection into CHO cells establishes a barrier, JAM-A has been suggested to contribute to BBB integrity [126]. It was additionally described to regulate the migration of monocytes across BBB cell-to-cell contacts [130]. Recently, we have described JAM-B to be localized to BBB TJs but discovered that JAM-B-deficient mice have an intact BBB, which suggests that JAM-B is not required for proper BBB function [131]. JAM-B has been found to bind α4β1-integrin and interestingly mediates α4β1-integrin mediated migration of $CD8^+$ T cells into the CNS but is not involved in the α4β1-integrin-mediated migration of $CD4^+$ T cells across the BBB [131–134]. The third member of the family, JAM-C was also found to be expressed in brain endothelial cells. Albeit C57BL/6 mice deficient for JAM-C develop a hydrocephalus, this is not due to impairment of BBB function, suggesting that JAM-C is not required for BBB junctional integrity [125,135].

The claudins, occludin and the JAMs expressed in TJs connect to the cytoskeleton via the interaction with intracellular scaffolding proteins, which form the TJ plaque. The membrane-associated guanylate kinase (MAGUK) proteins represent the major subgroup of scaffolding proteins at the TJs [136,137]. These proteins are structurally similar, since they share one or more PDZ domains, an SH3 domain and a catalytically inactive guanylate kinase (GUK) domain and are overall involved in the establishment of cell-cell adhesion, cell polarity and cell survival [138]. Zona occludens (ZO) proteins were the first proteins of the MAGUK family to be identified, with ZO-1 and ZO-2 localizing to endothelial TJs, which is essential for the formation of TJ strands [139,140]. Lack of ZO-1 and ZO-2 in mice is embryonically lethal [140,141]. ZO-1 can be found in the BBB TJs, interacting with claudins, occludin, JAMs and ZO-2, and promoting a link between these proteins and the actin cytoskeleton, by binding to F-actin [142]. It is also a main regulator of tension at vascular endothelial (VE)-cadherin-based adherens junction complexes, mainly binding to α-catenin and recruiting important mediators for junctional assembly and stability [69,143]. Additionally, cingulin, afadin (AF-6) and 7H6 antigen are also involved in the coupling of the junctional complexes to the cytoskeleton, supporting TJ structure and stability [144,145]. Cingulin connects ZO-2, AF-6 and JAMs to F-actin, while 7H6 acts towards maturation and maintenance of TJs [146–148].

3.2. Adherens Junctions (AJs) of the BBB

Adherens junctions (Ajs) have a role distinct from TJs. Prior to TJ formation, cell-cell contacts are established by AJs, which is a prerequisite for TJ maturation and maintenance. Thus, AJs are generally required for TJ formation, and a continuous crosstalk between AJs and TJs is necessary for the organization and preservation of the junctional complexes (reviewed in Reference [149]). VE-cadherin is the main protein of the endothelial AJs and is involved in blood vessel assembly and endothelial stabilization and survival [150,151]. Its intracellular domains engage p120 catenin and β-catenin [152,153]. By binding to β-catenin, α-catenin acts as a bridge between the cadherins and the actin cytoskeleton, since it binds to vinculin, α-actinin, ZO-1 or formin-1 [154,155]. Interestingly, VE-cadherin promotes expression of claudin-5 in endothelial cells derived from murine embryonic stem cells [156], supporting the notion that mature AJs are prerequisite for the establishment of TJs. Nectin is an additional component of the AJs of the BBB and connects to the actin cytoskeleton via AF-6. The nectin-AF-6 complex contributes to the formation of AJs and stabilization of TJs [157,158].

Additional molecules are found to be localized at the endothelial cell-cell junctions, outside of the organized AJs and TJs. Platelet endothelial cell adhesion molecule-1 (PECAM-1) is a transmembrane protein that belongs to the Ig superfamily. It is highly concentrated and restricted to the endothelial

junctions but is found outside the organized TJs and AJs complexes [159,160]. However, it plays a very important role in angiogenesis with a mechanosensory function and is involved in the regulation of vascular integrity as PECAM-1-deficient mice show impaired BBB junctional integrity [161–163]. CD99 is an additional protein localized in the endothelial cell junctional complexes, outside of TJs or AJs [164,165]. This protein is a highly O-glycosylated type I transmembrane protein not belonging to any protein family. CD99 mediates leukocyte trafficking across the BBB, with any additional role in BBB junctional integrity remaining to be shown [166]. A schematic representation of the molecular composition of the junctional complexes of the BBB endothelium as known today is illustrated in Figure 2.

Although a large number of molecules localized at the cell-to-cell contacts of the BBB within TJ, AJs and beyond has thus been described, their dynamic interplay and regulation during CNS homeostasis and how their expression and localization changes during neurological disorders when BBB function is impaired remains to be investigated in more detail. In addition, species differences in the expression of molecular constituents of the BBB junctional complexes have been described [94,167,168], an aspect that is important when aiming to translate observations from animal models to the human BBB.

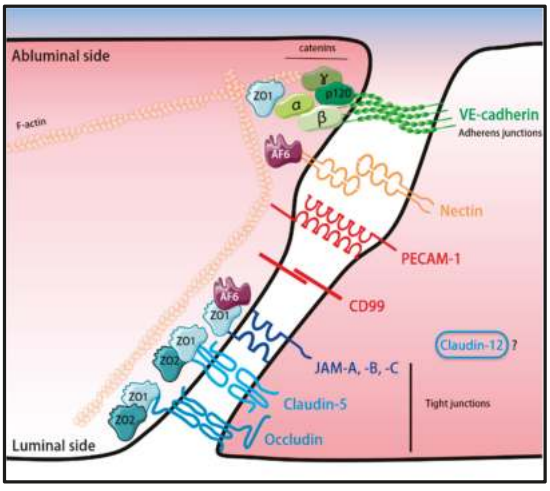

Figure 2. Schematic representation of the junctional complexes of the BBB. The proteins that compose the tight and adherens junctions are connected to the cytoskeleton via intracellular scaffolding proteins, ZO-1, ZO-2 and AF-6. Despite being expressed at low levels by the BBB endothelial cells [106], the subcellular location and function of claudin-12 remains to be defined. The forms of the individual proteins were adapted from Servier Medical Art (http://smart.servier.com/), licensed under a Creative Common Attribution 3.0 Generic License.

4. The Epithelial Blood-Cerebrospinal Fluid Barrier of the Choroid Plexus

The development and maintenance of the CNS is assured by the cerebrospinal fluid (CSF), found in the spinal and brain subarachnoid space, cisterns, sulci and in the cerebral ventricles [169,170]. Importantly, the CSF is produced by the ChP, a highly vascularized secretory tissue that extends into all four cerebral ventricles. The ChP folds out from the ventricular walls and is composed of a highly vascularized stroma that is surrounded by a monolayer of epithelial cells [171]. Because the dense network of capillaries that irrigate the ChP is fenestrated and thus permissive to the passage of blood derived molecules, the epithelial cells surrounding the ChP stroma build a BCSFB [18,172]. Accordingly, the molecules that diffuse from the blood across the ChP vascular wall reach the ChP stroma but are hindered by the epithelial BCSFB to reach the CSF [37].

In accordance to the endothelial BBB, TJs and AJs are present in the BCSFB epithelium, ensuring not only the barrier function but also the apicobasal polarity of the BCSFB [173]. Claudin-1, claudin-2, claudin-3 and claudin-11, together with occludin and ZO-1, were identified to be expressed in the TJs of the BCSFB [100,174–176]. JAM-A, but not JAM-B, is found in the epithelium of the BCSFB, while JAM-C is only present in the BCSFB of the ChP of the fourth ventricle [125,131,149]. In the epithelial monolayer, TJs are apically localized and distinguishable from the AJs, which are in the basolateral compartment [149]. Claudin-1-deficient mice die post-natal due to failure of epidermal barrier function [90], suggesting that lack of claudin-1 at the BCSFB is not essential for BCSFB maturation during embryogenesis. However, the precise role of claudin-1 at the BCSFB needs further investigations. Claudin-2 deficient mice show reduced reabsorption of Na^+ in the proximal tubule of the kidney suggesting a role for claudin-2 in paracellular transport of small cations across the BCSFB [177]. Interestingly, claudin-11 is suggested to induce parallel running TJs strands observed at the BCSFB, but also in myelin sheaths of oligodendrocytes and Sertoli cells, which all express claudin-11 [37,91]. According to the claudin-11 expression pattern, claudin-11 deficient mice display defects in spermatogenesis [91] and show behavioral defects [178]. If any of the CNS related defects is due to lack of claudin-11 at the BCSFB has not been addressed to date [90,91,177,179]. In addition, claudin-3 may be involved in maintenance of BCSFB TJ integrity, since its absence was found to impair BCSFB integrity in a mouse model for multiple sclerosis [180] which was however not confirmed in a second study [102]. Thus, similar to the TJs complexes of the BBB, the precise understanding of the interplay between TJ sealing claudins as claudin-1, claudin-3 and those allowing for transport of water and cations, as claudin-2 in BCSFB TJs, remain to be explored.

Like any other epithelial barrier, the BCSFB epithelial cells establish AJs, where the transmembrane E-cadherin binds to the catenin complex, which anchors the AJs to the epithelial actin cytoskeleton allowing to control adhesive interactions between the BCSFB epithelial cells [149,181].

A schematic representation of the junctional complexes at the ChP BCSFB can be found in Figure 3. In order to set up concentration gradients and assure proper brain function, cellular transporters are also present in the BCSFB. While efflux transporters from the ABC family oversee the return of lipophilic solutes to the blood, solute carrier (SLC) transporters are responsible for the delivery of ions and amino acids to the CSF. Additionally, water flow from the blood to the CSF is in addition to claudin-2 mediated by aquaporin 1 (AQP1) [182].

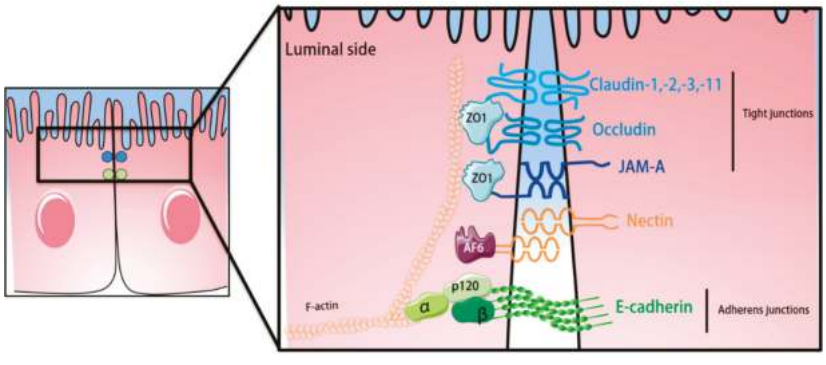

Figure 3. Schematic representation of the junctional complexes of the BCSFB at the choroid plexus. In similarity to the BBB, the proteins that compose the tight and adherens junctions of the choroid plexus BCSFB are connected to the cytoskeleton via intracellular scaffolding proteins and are localized in the apical part of the choroid plexus epithelial cells. The shapes of the proteins were adapted from Servier Medical Art (http://smart.servier.com/), licensed under a Creative Common Attribution 3.0 Generic License.

5. The Meningeal Brain Barriers

The meninges constitute three layers, the dura mater, the arachnoid mater and pia mater, which sheath the brain and spinal cord (represented in Figure 4) [183,184]. For decades, the meninges were known for their role in protecting the brain and spinal cord. In recent years, studies have shown that the meninges also play a vital role in the development of the skull and the brain [9,185,186]. Additionally, studies in rats have shown the presence of stomata on the leptomeningeal coverings of the blood vessels in the sub arachnoid space suggesting that the meningeal layers might be a potential route for the transportation of humoral immune factors from the CSF to perivascular or vascular mural spaces [187].

In humans the dura mater is characterized by three different layers, specifically the periosteal, the meningeal and the border cell layer, with the latter forming the border to the arachnoid barrier cells. The dural border cell layer is composed of flattened fibroblasts with scattered intercellular junctions and pronounced extracellular spaces lacking extracellular collagen [10,183,184,188]. It has been shown that the dura and dural border cell layer are immunoreactive to AQP1 [8]. Although junctions have been described between dura mater fibroblasts, their molecular composition is unknown. The dura mater lacks a BBB [189], thus the arachnoid barrier establishes a BCSFB between the dura mater and the subarachnoid space.

The arachnoid mater is divided into two layers—the arachnoid barrier cell layer and the arachnoid trabeculae, extending into the subarachnoid space. The arachnoid barrier cell layer is characterized by closely joined cells connected by an extensive and continuous system of TJs [190] [191,192]. On the other hand, the arachnoid trabecular cells are characterized by the presence of sporadic fibroblasts [1,10,184]. The molecular composition of arachnoid barrier TJs is not yet well explored and may depend on the origin of these cells from the neural crest or mesoderm, which may lead to the development of epithelial or mesothelial junctional complexes, respectively. Recent studies have shown positive immunostaining for claudin-11 in arachnoid barrier cells in the brains of both humans and rodents [8,189], suggesting that the arachnoid BCSFB establishes TJs similar to those at the ChP BCSFB. Arachnoid barrier cells also express AQP1, the water channels expressed by ChP BCSFB epithelial cells. In addition, existence of AJs between arachnoid barrier fibroblasts has been supported by detection of junctional localization of E-cadherin between the arachnoid cells of the brain in mice [55,193,194]. Presence of junctional proteins in the arachnoidal cells has been further supported as culture of human arachnoid granulations, which are described as projections of the arachnoid membrane into the dural sinuses, have demonstrated the presence of cytoskeletal and junctional proteins [194]. In addition, gap junctions and desmosomes ensure arachnoid barrier function. The presence of connexin 43 composed gap junctions provides electrical and metabolic coupling of arachnoid barrier cells relevant for the regulation of CSF passage across this barrier [194,195]. Desmosomes between arachnoid barrier epithelial or mesothelial cells establish mechanical stability of this barrier by anchoring these junctional structures to the intermediate filament network of the cells [194,196–198]. A potential functional impact on the different developmental origin of arachnoid barrier cells from the neural crest or mesoderm and thus the possible maturation of epithelial versus mesothelial junctional complexes has not yet been investigated. Thus, a detailed analysis of region-specific differences in the molecular composition of arachnoid barrier junctional complexes and their role in regulating barrier formation remains to be performed.

Below the arachnoid barrier there is a subarachnoid space filled with cerebrospinal fluid. Towards the brain and spinal cord tissue the subarachnoid space is lined by the cells forming the pia mater. The pia mater is composed of evenly flattened cells that line all the surface of the brain and spinal cord. The cells of the pia mater lack TJs and do not form a barrier for solutes. At the same time, they are joined by desmosomes and gap junctions [199]. In accordance to the arachnoid barrier, the precise junctional compositions and the regional differences in their composition due to the different developmental origin of the pia mater cells remains to be investigated.

The pia mater is separated from the brain and spinal cord parenchyma by glia limitans formed by the parenchymal basement membrane and astrocyte endfeet [1,184]. In the healthy CNS there is no TJs between astrocyte endfeet, which are rather linked by gap junctions and not well-defined intercellular junctions [190]. Bradbury and colleagues speculated already in 1975 that this suggests that the astrocytic glia limitans establishes a border between the CSF and the brain parenchyma [190]. This notion is further supported by the observation that during neuroinflammation, when BBB integrity is impaired, reactive astrocytes can form TJs possibly prohibiting the parenchymal entry of humoral and cellular factors from the blood stream [200,201]. TJs in reactive astrocytes are composed of JAM-A, claudin-1 and claudin-4. While both claudins have been shown to play a vital role in glial scar formation, JAM-A rather seems to regulate the migration of immune cells across the glia limitans [201,202].

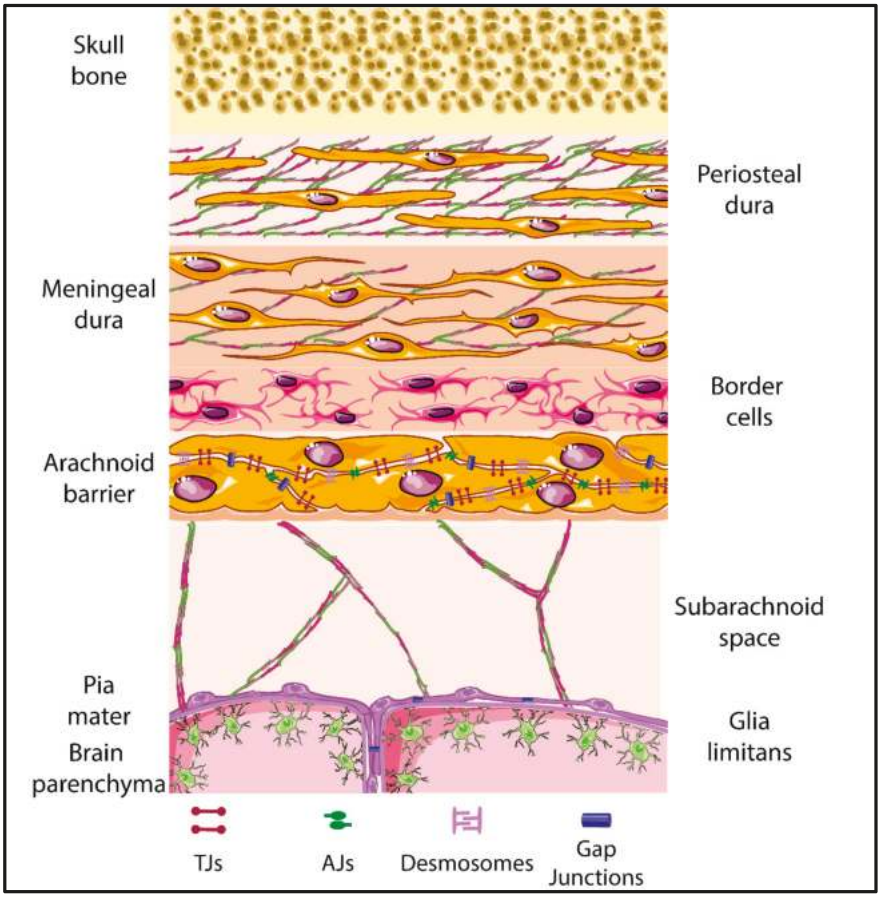

Figure 4. Schematic representation of the meningeal layers. The different layers and cellular composition of the meningeal layers are displayed. Tight junctions are highlighted between the arachnoid barrier cells as parallel lines, with adherens junctions, desmosomes and gap junctions also being represented. The shapes of the cell types were adapted from Servier Medical Art (http://smart.servier.com/), licensed under a Creative Common Attribution 3.0 Generic License.

6. Visualization of the Junctional Complexes of the Brain Barriers

Recent advances in high end in vivo imaging techniques including two-photon intravital microscopy (2P-IVM) have allowed for unprecedented observations of immune cell entry into the CNS during immune surveillance and neuroinflammation. We have proposed that the brain barriers play a vital role in separating compartments in the CNS that provide different access to the immune cells. Advanced imaging has also allowed for precise localization of cellular junctional molecules [203,204] in vitro and in vivo. Exploring the visualization of molecularly distinct junctional complexes in epithelial, endothelial, mesothelial and glial barriers thus provides a novel option for visualization of these barriers by fluorescent imaging using immunofluorescence staining or transgenic reporter mouse models. Furthermore, visualization of junctional complexes in these barriers allows for the study of cellular pathways of immune cell trafficking across these barriers using in vivo live cell imaging [205]. Here, we provide a brief overview of the main tools allowing for reliable visualization of CNS barrier components and thus CNS compartments by confocal and 2P-IVM imaging in healthy and neuroinflammatory conditions. In that context, several published studies have employed endothelial and epithelial junctional reporter mice models to study immune cell trafficking into the CNS.

There are few major approaches allowing for visualization of junctional complexes in brain barriers. First, transgenic mouse models, where a fluorescent reporter is expressed under the promoter of the junctional protein expressed in the respective cell, can be employed. In this case, the soluble fluorescent protein will be visible in the whole volume of the cells expressing the corresponding junctional protein. For example, claudin-5, which has been identified as a major constituent of the TJs of CNS endothelial cells, was used to create the Tg (Cldn5-GFP) Cbet/U reporter mouse line [44], where green fluorescence protein (GFP) is expressed under the control of the claudin-5 promoter. The strong GFP signal in the CNS endothelial cells makes this mouse model very useful for direct visualization of CNS blood vessels by 2P-IVM (Figure 5).

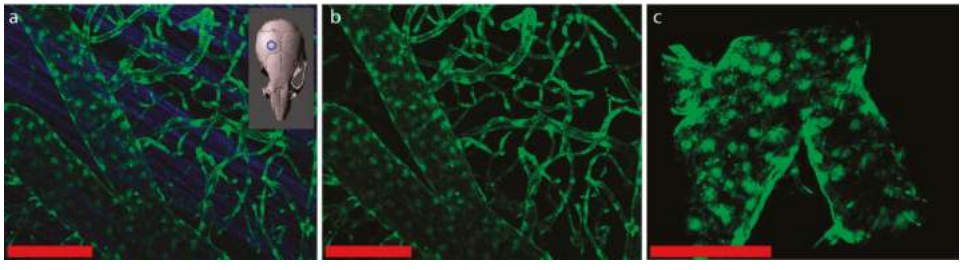

Figure 5. Representative images of the cranial and spinal cord window 2P-IVM imaging of the claudin-5-GFP reporter mouse. (**a**) The cranial window was placed over the right hemisphere of the mouse brain as depicted on the insert. Second harmonic generation in blue derives from collagen fibers in the dura mater. The strong GFP signal visible throughout the brain endothelial cells allows for imaging of the vessels along the entire vascular tree. (**b**) Cranial window region from (a) after removal of the dura mater. (**c**) Cervical spinal cord window. High magnification image showing the dorsal vein and branching veins. Scale bars = 100μm.

Alternatively, knock-in mouse models can be employed where the fluorescent protein is fused to the respective junctional molecule. This approach enables visualization of the subcellular localization of the respective junctional molecule in the cells via the fluorescent tag. For example, the VE-cadherin-GFP knock-in mouse [206], expressing a C-terminal GFP fusion protein of VE-cadherin in the endogenous VE-cadherin locus, enables live imaging of vascular AJs. This model provides a GFP signal, the strength of which is dependent on endogenous VE-cadherin expression. It is suitable for 2P-IVM of vascular AJs in blood vessels of the brain and spinal cord of healthy mice, but also in mice suffering from experimental autoimmune encephalomyelitis (aEAE), an animal model for multiple sclerosis

(Figure 6). In the dura mater, in addition to the blood vessels lined by VE-cadherin expressing vascular endothelial cells, the lymphatic vessels composed of lymphatic endothelial cells, expressing lower levels of VE-cadherin, can be visualized using the VE-cadherin-GFP knock-in reporter mouse model. VE-cadherin-GFP+ blood vessels can be distinguished from VE-cadherin GFP+ lymphatic vessels by the absence of signal of a fluorescent tracer such as orange TRITC Dextran (500 kDa) injected into the blood stream prior to imaging (Figure 6, red arrows). The VE-cadherin-GFP knock-in mouse is thus highly suitable for visualization of the endothelial AJs in the brain and spinal cord along the entire vascular tree. Additionally, it allows for imaging and distinguishing the dural blood and lymphatic vessels on the surface of the brain.

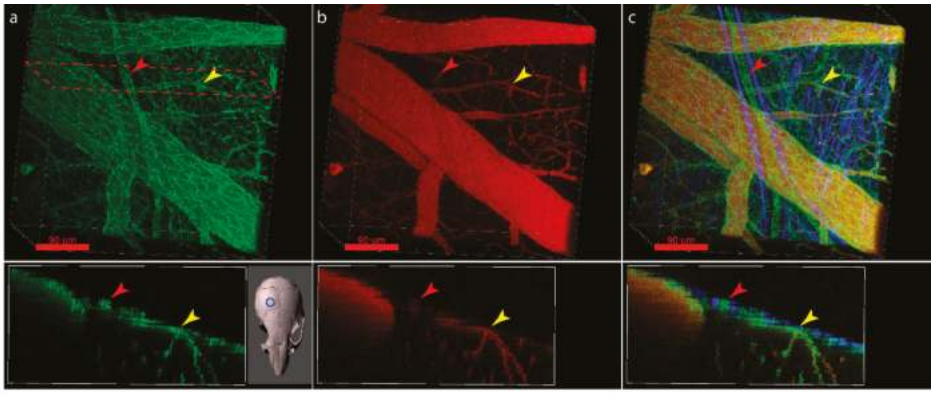

Figure 6. Visualization of CNS and meningeal endothelial AJs using the VE-Cadherin-GFP reporter mouse. (**a**) Cranial window allowing to visualize meningeal, subarachnoid, subpial and cortical vascular VE-cadherin-GFP+ AJs. (**b**) Cranial window preparation from (a) highlighting blood vessels after i.v. injection of TRITC Dextran. (**c**) Overlay of a and b and the second harmonic generation of the collagen fibers in the dura allow to distinguish VE-cadherin-GFP+ TRITC+ blood vessels and VE-cadherin-GFP+ TRITC^{neg} lymphatic vessels in the dura mater. Examples of blood and lymphatic vessels of similar caliber size are highlighted with a yellow and red arrowhead, respectively. The cranial window was placed over the right hemisphere of the mouse brain as depicted in the insert below (a). Top row—3D stack, bottom—XZ maximum intensity projection of 20 µm along Y at the cross section highlighted at the top. Scale bars = 90µm.

Similarly, the E-Cadherin-CFP knock-in mouse expressing the fluorescent protein monomer Cyan (mCFP) fused to the C-terminus of E-cadherin enables visualization of the AJs of epithelial cells [207]. This mouse model may be potentially suitable to visualize AJs between neural crest derived arachnoid barrier cells in the frontal brain, as a recent report demonstrated specific expression of E-cadherin in AJs between arachnoid barrier cells [55]. Once in vivo imaging techniques for the ChP are established it may also be used for visualization of AJs complexes of the ChP BCSFB in vivo.

In vivo imaging of BBB TJ complexes in the mouse has already been successfully reported [205]. To this end a reporter mouse expressing claudin-5 fused to eGFP under the control of the Tie-2 promoter was established [205]. This mouse model has allowed for visualization of claudin-5 in BBB TJs in vivo and direct observation of the cellular pathway of T-cell migration across the BBB owing to the strong expression of eGFP-CLN-5. Potential shortcomings of these models are that claudin-5-GFP is expressed under the control of the Tie-2 promoter, activity of which is regulated by inflammatory mediators. In addition, Tie-2 driven expression is not restricted to endothelium but allows for expression of the transgene in myeloid cells. This may impact on the molecular composition of the BBB TJ and thus its integrity and may be significantly different from physiological conditions.

Another shortcoming of the fusion protein models is the potential impact of the relatively big fluorescent proteins on the appropriate localization of junctional molecules and their interaction with intracellular scaffolding proteins. This issue can be addressed by employing self-complementing split fluorescent proteins [208,209], where only a small part of the florescent protein is used to tag the complex of interest, for example the GFP_{11} fragment of only 16 amino acids formed of a single β-strand in case of the $GFP_{1–10D7/11M3\ OPT}$ split protein [210]. The GFP1-10 fragment overexpressed in the corresponding cell remains non-fluorescent until complementation with the GFP_{11} fused to the target protein.

Additional fluorescent reporter mouse models can be obtained with the versatile aid of the Cre/loxP system. For example, by crossing the Ai14 line [211], where the fluorescent protein is expressed upon deletion of the loxP-flanked stop cassette in the Rosa26 locus, with lines expressing Cre under a brain barrier specific promoter [212], will allow to produce reporter mouse models with the respective fluorescent reporter.

Visualization of the BCSFB can be achieved by employing the FOXJ1-GFP reporter mouse or FOXJ1 Cre models [213], specific for the ciliated epithelial cells, or the transthyretin reporter [214], specific for the ChP epithelial cells.

To distinguish capillary and post-capillary segments of the CNS vascular tree, differential visualization of smooth muscle cells and pericytes can be used. For example, the expression of Cre and eGFP under the promoter of smooth muscle myosin heavy chain was developed to visualize the vascular and non-vascular smooth muscle cells [215]. Visualization of pericytes can be achieved with the Pdgfrb-Cre mouse models [216] or the NG2 reporter mouse lines [212]. In the latter cases, one has however to take into account that expression of the reporters may not be entirely exclusive to the brain barrier cells. NG2 is additionally expressed in oligodendrocyte precursor and smooth muscle cells, and Pdgfrb is also found to be expressed in oligodendrocytes, fibroblasts and smooth muscle cells.

Finally, in peripheral vascular beds visualization of junctional components has been achieved by intravenous injection of fluorescently tagged non-function blocking antibodies targeting, e.g., PECAM-1 to label endothelial cell junctions in vivo [217]. This approach may fail to detect junctional components in the complex and tight BBB TJs in the absence of neuroinflammation, as the antibodies may fail to reach their target. However, during neuroinflammation, when BBB TJ integrity is impaired this may provide a rapid approach for in vivo imaging of BBB junctions.

At the surface of the brain or spinal cord assignment of a vascular structure to a specific layer within the meninges or a compartment in the CNS can be facilitated by making use of the second harmonic generation (SHG) signal [218] obtained from collagen type I secreted in large amounts mainly by the fibroblasts in the dura mater. In 2P-IVM, using a short-pulse laser with an excitation wavelength in the range of 800–1300 nm, the excitation light can be separated from the emitted SHG signal, the wavelength of which is half of the excitation wavelength. SHG allows for localization of CNS compartments rich in collagens, especially the dura mater and, to a certain degree, the arachnoid barrier and pial layers (Figure 6). Furthermore, in some cases these compartments can be distinguished by the collagen fibers morphology [219] and can serve as a reliable landmark in the context of visualization of brain barriers by 2P-IVM.

Various small molecule tracers, such as TRITC and FITC Dextran, nanoparticles can be employed to visualize the luminal compartment of blood or lymphatic vessels. In neuroinflammation, imaging junctional complexes combined with the injection of vascular fluorescent tracers may allow to image BBB junctional leakiness. By injecting tracers into the ventricles or into the cisterna magna, distribution of the fluorescent tracers has been successfully applied to visualize paravascular CSF drainage pathways along subarachnoid vessels [220] allowing to determine CSF flow and the distribution of humoral factors in the CNS. Combining these methodologies with reporter mice for the brain barriers will allow advances in our understanding of CNS immune surveillance.

7. Conclusions

Despite decades of research, there are still a lot of unresolved questions concerning the precise molecular composition and interaction of TJs and AJs of the brain barriers, which have hampered the development of therapeutic strategies targeting the brain barriers in neuroinflammatory disorders. Regarding the BBB, it has been recently confirmed by several reports that claudin-1 and claudin-3 are absent from BBB endothelial cells and thus, claudin-5 is the only critical TJ claudin proven to date to contribute for the mouse BBB function [102]. However, when BBB endothelial cells lack caudin-5, TJs remain morphologically intact [92], which indicates that another claudin must maintain TJ morphology as visualized by transmission electron microscopy. Since we have recently reported that also claudin-12 is not required for proper BBB TJ function [106], the protein that maintains morphologically intact BBB TJs in the absence of claudin-5 remains to be identified. This approach is currently hampered by the lack of suitable antibodies detecting claudins with high and reliably specificity.

Structural and cellular junctions of meningeal barriers are less studied as compared to the BBB and the BCSFB. Meningeal barriers from the front and posterior region of the nervous system have been described to develop from different origins and therefore will have a different molecular make-up of their respective junctional complexes which may lead to regional differences in meningeal barrier functions.

A first set of available tools for in vivo visualization of the junctional components of the different brain barriers allows to study the dynamic interactions of immune cells with the brain barriers during health and neuroinflammation. Identifying the junctional components of the endothelial, epithelial, meningeal and glial brain barriers will set the stage for developing further mouse models, which will allow for in vivo imaging of the brain barriers. With these tools, one can thus explore their function in maintaining CNS immune surveillance and the impact of brain barrier disruption in neuroinflammation in vivo.

Author Contributions: M.C.D.: writing and editing; J.A.M.: writing and editing; M.V.: writing and editing; B.E.: concept, writing, editing, supervision, funding acquisition.

Funding: This research was funded by European Union FP7 ITN project nEUROinflammation (607962), EU FP7 small integrated project JUSTBRAIN (241861), and the Fidelity Bermuda Foundation. J.A.M. is funded by a Swiss Government Excellence Scholarship.

Acknowledgments: We thank Urban Deutsch for the valuable scientific input.

Conflicts of Interest: The authors declare no conflicts of interest.

Abbreviations

aEAE	Active EAE
AF-6	Afadin
AJs	Adherens junctions
AQP1	Aquaporin 1
BBB	Blood-brain barrier
BCSFB	Blood-cerebrospinal-fluid barrier
CLDN	Claudin
CLDND1	Claudin domain containing 1
CNS	Central nervous system
ChP	Choroid plexus
CSF	Cerebrospinal fluid
ECL	Extracellular loop
E-cadherin	Epithelial cadherin
E-face	Exoplasmic face
FITC	Fluorescein
GFP	Green fluorescent protein

JAMs	Junctional adhesion molecules
MAGUK	Membrane-associated guanylate kinase
Mfsd2a	Major facilitator superfamily domain-containing protein 2
mCFP	monomer cyan fluorescent protein
N-cadherin	Neural cadherin
NG2	Neuronal-glial antigen 2
NVU	Neurovascular unit
Pdgfrb	Platelet derived growth factor receptor beta
PECAM-1	Platelet endothelial cell adhesion molecule 1
P-face	Protoplasmic face
Pgp	P-glycoprotein
SHG	Second harmonic generation
SLC	Solute carrier
TAMP	Tight junction-associated MARVEL proteins
Tg	Transgenic
TJs	Tight junctions
TRITC	Tetramethylrhodamine
VCAM-1	Vascular cell adhesion molecule 1
VE-cadherin	Vascular endothelial cadherin
ZO	Zona occludens
2P-IVM	Two-photon intravital microscopy

References

1. Engelhardt, B.; Vajkoczy, P.; Weller, R.O. The movers and shapers in immune privilege of the cns. *Nat. Immunol.* **2017**, *18*, 123–131. [CrossRef]
2. Engelhardt, B. Development of the blood-brain barrier. *Cell Tissue Res.* **2003**, *314*, 119–129. [CrossRef] [PubMed]
3. Engelhardt, B.; Sorokin, L. The blood-brain and the blood-cerebrospinal fluid barriers: Function and dysfunction. *Semin. Immunopathol.* **2009**, *31*, 497–511. [CrossRef] [PubMed]
4. Greenberg, D.A.; Jin, K. From angiogenesis to neuropathology. *Nature* **2005**, *438*, 954–959. [CrossRef] [PubMed]
5. Lee, H.S.; Han, J.; Bai, H.J.; Kim, K.W. Brain angiogenesis in developmental and pathological processes: Regulation, molecular and cellular communication at the neurovascular interface. *FEBS J.* **2009**, *276*, 4622–4635. [CrossRef]
6. Lun, M.P.; Monuki, E.S.; Lehtinen, M.K. Development and functions of the choroid plexus-cerebrospinal fluid system. *Nat. Rev. Neurosci.* **2015**, *16*, 445–457. [CrossRef]
7. DeSisto, J.; O'Rourke, R.; Bonney, S.; Jones, H.E.; Guimiot, F.; Jones, K.L.; Siegenthaler, J. A Cellular Atlas of the Developing Meninges Reveals Meningeal Fibroblast Diversity and Function. *Dev. Cell* **2019**, 53. Available online: https://papers.ssrn.com/sol3/papers.cfm?abstract_id=3396490 (accessed on 30 May 2019). [CrossRef]
8. Weller, R.O.; Sharp, M.M.; Christodoulides, M.; Carare, R.O.; Mollgard, K. The meninges as barriers and facilitators for the movement of fluid, cells and pathogens related to the rodent and human cns. *Acta Neuropathol.* **2018**, *135*, 363–385. [CrossRef]
9. Richtsmeier, J.T.; Flaherty, K. Hand in glove: Brain and skull in development and dysmorphogenesis. *Acta Neuropathol.* **2013**, *125*, 469–489. [CrossRef]
10. Mack, J.; Squier, W.; Eastman, J.T. Anatomy and development of the meninges: Implications for subdural collections and csf circulation. *Pediatr. Radiol.* **2009**, *39*, 200–210. [CrossRef]
11. Angelov, D.N.; Vasilev, V.A. Morphogenesis of rat cranial meninges. A light—And electron-microscopic study. *Cell Tissue Res.* **1989**, *257*, 207–216. [CrossRef] [PubMed]
12. Daneman, R.; Prat, A. The blood-brain barrier. *Cold Spring Harb. Perspect. Biol.* **2015**, *7*, a020412. [CrossRef] [PubMed]
13. Zlokovic, B.V. The blood-brain barrier in health and chronic neurodegenerative disorders. *Neuron* **2008**, *57*, 178–201. [CrossRef] [PubMed]

14. Liebner, S.; Dijkhuizen, R.M.; Reiss, Y.; Plate, K.H.; Agalliu, D.; Constantin, G. Functional morphology of the blood-brain barrier in health and disease. *Acta Neuropathol.* **2018**, *135*, 311–336. [CrossRef] [PubMed]
15. Muoio, V.; Persson, P.B.; Sendeski, M.M. The neurovascular Unit-Concept review. *Acta Physiol.* **2014**, *210*, 790–798. [CrossRef] [PubMed]
16. Abbott, N.J.; Ronnback, L.; Hansson, E. Astrocyte-Endothelial interactions at the Blood-Brain barrier. *Nat. Rev. Neurosci.* **2006**, *7*, 41–53. [CrossRef] [PubMed]
17. Ge, S.; Song, L.; Pachter, J.S. Where is the blood-brain barrier... Really? *J. Neurosci. Res.* **2005**, *79*, 421–427. [CrossRef]
18. Brightman, M.W.; Reese, T.S. Junctions between intimately apposed cell membranes in the vertebrate brain. *J. Cell Biol.* **1969**, *40*, 648–677. [CrossRef]
19. Wolburg, H.; Lippoldt, A. Tight junctions of the blood-brain barrier: Development, composition and regulation. *Vasc. Pharmacol.* **2002**, *38*, 323–337. [CrossRef]
20. Huber, J.D.; Egleton, R.D.; Davis, T.P. Molecular physiology and pathophysiology of tight junctions in the blood-brain barrier. *Trends Neurosci.* **2001**, *24*, 719–725. [CrossRef]
21. Reese, T.S.; Karnovsky, M.J. Fine structural localization of a blood-brain barrier to exogenous peroxidase. *J. Cell Biol.* **1967**, *34*, 207–217. [CrossRef] [PubMed]
22. Coomber, B.L.; Stewart, P.A. Morphometric analysis of cns microvascular endothelium. *Microvasc. Res.* **1985**, *30*, 99–115. [CrossRef]
23. Ben-Zvi, A.; Lacoste, B.; Kur, E.; Andreone, B.J.; Mayshar, Y.; Yan, H.; Gu, C. Mfsd2a is critical for the formation and function of the blood-brain barrier. *Nature* **2014**, *509*, 507–511. [CrossRef] [PubMed]
24. Andreone, B.J.; Chow, B.W.; Tata, A.; Lacoste, B.; Ben-Zvi, A.; Bullock, K.; Deik, A.A.; Ginty, D.D.; Clish, C.B.; Gu, C. Blood-brain barrier permeability is regulated by lipid transport-dependent suppression of caveolae-mediated transcytosis. *Neuron* **2017**, *94*, 581–594. [CrossRef]
25. Betz, A.L.; Goldstein, G.W. Polarity of the blood-brain barrier: Neutral amino acid transport into isolated brain capillaries. *Science* **1978**, *202*, 225–227. [CrossRef]
26. Betz, A.L.; Firth, J.A.; Goldstein, G.W. Polarity of the blood-brain barrier: Distribution of enzymes between the luminal and antiluminal membranes of brain capillary endothelial cells. *Brain Res.* **1980**, *192*, 17–28. [CrossRef]
27. Daneman, R. The blood-brain barrier in health and disease. *Ann. Neurol.* **2012**, *72*, 648–672. [CrossRef]
28. Ha, S.N.; Hochman, J.; Sheridan, R.P. Mini review on molecular modeling of p-glycoprotein (pgp). *Curr. Top. Med. Chem.* **2007**, *7*, 1525–1529. [CrossRef]
29. Cornford, E.M.; Hyman, S.; Swartz, B.E. The human brain glut1 glucose transporter: Ultrastructural localization to the blood-brain barrier endothelia. *J. Cereb. Blood Flow Metab. Off. J. Int. Soc. Cereb. Blood Flow Metab.* **1994**, *14*, 106–112. [CrossRef]
30. Aird, W.C. Phenotypic heterogeneity of the endothelium: I. Structure, function, and mechanisms. *Circ. Res.* **2007**, *100*, 158–173. [CrossRef]
31. Nieuwdorp, M.; Meuwese, M.C.; Vink, H.; Hoekstra, J.B.; Kastelein, J.J.; Stroes, E.S. The endothelial glycocalyx: A potential barrier between health and vascular disease. *Curr. Opin. Lipidol.* **2005**, *16*, 507–511. [CrossRef] [PubMed]
32. Salmon, A.H.; Ferguson, J.K.; Burford, J.L.; Gevorgyan, H.; Nakano, D.; Harper, S.J.; Bates, D.O.; Peti-Peterdi, J. Loss of the endothelial glycocalyx links albuminuria and vascular dysfunction. *J. Am. Soc. Nephrol. JASN* **2012**, *23*, 1339–1350. [CrossRef] [PubMed]
33. Lukasz, A.; Hillgruber, C.; Oberleithner, H.; Kusche-Vihrog, K.; Pavenstadt, H.; Rovas, A.; Hesse, B.; Goerge, T.; Kumpers, P. Endothelial glycocalyx breakdown is mediated by angiopoietin-2. *Cardiovasc. Res.* **2017**, *113*, 671–680. [CrossRef] [PubMed]
34. Betteridge, K.B.; Arkill, K.P.; Neal, C.R.; Harper, S.J.; Foster, R.R.; Satchell, S.C.; Bates, D.O.; Salmon, A.H.J. Sialic acids regulate microvessel permeability, revealed by novel in vivo studies of endothelial glycocalyx structure and function. *J. Physiol.* **2017**, *595*, 5015–5035. [CrossRef]
35. Kutuzov, N.; Flyvbjerg, H.; Lauritzen, M. Contributions of the glycocalyx, endothelium, and extravascular compartment to the blood-brain barrier. *Proc. Natl. Acad. Sci. USA* **2018**, *115*, E9429–E9438. [CrossRef]
36. Duvernoy, H.M.; Risold, P.Y. The circumventricular organs: An atlas of comparative anatomy and vascularization. *Brain Res. Rev.* **2007**, *56*, 119–147. [CrossRef]

37. Wolburg, H.; Paulus, W. Choroid plexus: Biology and pathology. *Acta Neuropathol.* **2010**, *119*, 75–88. [CrossRef]
38. Hartmann, D.A.; Underly, R.G.; Grant, R.I.; Watson, A.N.; Lindner, V.; Shih, A.Y. Pericyte structure and distribution in the cerebral cortex revealed by high-resolution imaging of transgenic mice. *Neurophotonics* **2015**, *2*, 041402. [CrossRef]
39. Mathiisen, T.M.; Lehre, K.P.; Danbolt, N.C.; Ottersen, O.P. The perivascular astroglial sheath provides a complete covering of the brain microvessels: An electron microscopic 3d reconstruction. *Glia* **2010**, *58*, 1094–1103. [CrossRef]
40. Khennouf, L.; Gesslein, B.; Brazhe, A.; Octeau, J.C.; Kutuzov, N.; Khakh, B.S.; Lauritzen, M. Active role of capillary pericytes during stimulation-induced activity and spreading depolarization. *Brain J. Neurol.* **2018**, *141*, 2032–2046. [CrossRef]
41. Hill, R.A.; Tong, L.; Yuan, P.; Murikinati, S.; Gupta, S.; Grutzendler, J. Regional blood flow in the normal and ischemic brain is controlled by arteriolar smooth muscle cell contractility and not by capillary pericytes. *Neuron* **2015**, *87*, 95–110. [CrossRef] [PubMed]
42. Hall, C.N.; Reynell, C.; Gesslein, B.; Hamilton, N.B.; Mishra, A.; Sutherland, B.A.; O'Farrell, F.M.; Buchan, A.M.; Lauritzen, M.; Attwell, D. Capillary pericytes regulate cerebral blood flow in health and disease. *Nature* **2014**, *508*, 55–60. [CrossRef] [PubMed]
43. Armulik, A.; Genove, G.; Betsholtz, C. Pericytes: Developmental, physiological, and pathological perspectives, problems, and promises. *Dev. Cell* **2011**, *21*, 193–215. [CrossRef] [PubMed]
44. Vanlandewijck, M.; He, L.; Mae, M.A.; Andrae, J.; Ando, K.; Del Gaudio, F.; Nahar, K.; Lebouvier, T.; Lavina, B.; Gouveia, L.; et al. A molecular atlas of cell types and zonation in the brain vasculature. *Nature* **2018**, *554*, 475–480. [CrossRef]
45. Gerhardt, H.; Wolburg, H.; Redies, C. N-Cadherin mediates pericytic-endothelial interaction during brain angiogenesis in the chicken. *Dev. Dyn. Off. Publ. Am. Assoc. Anat.* **2000**, *218*, 472–479. [CrossRef]
46. Courtoy, P.J.; Boyles, J. Fibronectin in the microvasculature: Localization in the pericyte-endothelial interstitium. *J. Ultrastruct. Res.* **1983**, *83*, 258–273. [CrossRef]
47. Cuevas, P.; Gutierrez-Diaz, J.A.; Reimers, D.; Dujovny, M.; Diaz, F.G.; Ausman, J.I. Pericyte endothelial gap junctions in human cerebral capillaries. *Anat. Embryol.* **1984**, *170*, 155–159. [CrossRef]
48. Larson, D.M.; Carson, M.P.; Haudenschild, C.C. Junctional transfer of small molecules in cultured bovine brain microvascular endothelial cells and pericytes. *Microvasc. Res.* **1987**, *34*, 184–199. [CrossRef]
49. Shepro, D.; Morel, N.M. Pericyte physiology. *FASEB J. Off. Publ. Fed. Am. Soc. Exp. Biol.* **1993**, *7*, 1031–1038. [CrossRef]
50. Daneman, R.; Zhou, L.; Agalliu, D.; Cahoy, J.D.; Kaushal, A.; Barres, B.A. The mouse blood-brain barrier transcriptome: A new resource for understanding the development and function of brain endothelial cells. *PLoS ONE* **2010**, *5*, e13741. [CrossRef]
51. Armulik, A.; Genove, G.; Mae, M.; Nisancioglu, M.H.; Wallgard, E.; Niaudet, C.; He, L.; Norlin, J.; Lindblom, P.; Strittmatter, K.; et al. Pericytes regulate the blood-brain barrier. *Nature* **2010**, *468*, 557–561. [CrossRef] [PubMed]
52. Villasenor, R.; Ozmen, L.; Messaddeq, N.; Gruninger, F.; Loetscher, H.; Keller, A.; Betsholtz, C.; Freskgard, P.O.; Collin, L. Trafficking of endogenous immunoglobulins by endothelial cells at the blood-brain barrier. *Sci. Rep.* **2016**, *6*, 25658. [CrossRef] [PubMed]
53. Sorokin, L. The impact of the extracellular matrix on inflammation. *Nat. Rev. Immunol.* **2010**, *10*, 712–723. [CrossRef]
54. Hallmann, R.; Horn, N.; Selg, M.; Wendler, O.; Pausch, F.; Sorokin, L.M. Expression and function of laminins in the embryonic and mature vasculature. *Physiol. Rev.* **2005**, *85*, 979–1000. [CrossRef] [PubMed]
55. Hannocks, M.J.; Pizzo, M.E.; Huppert, J.; Deshpande, T.; Abbott, N.J.; Thorne, R.G.; Sorokin, L. Molecular characterization of perivascular drainage pathways in the murine brain. *J. Cereb. Blood Flow Metab. Off. J. Int. Soc. Cereb. Blood Flow Metab.* **2018**, *38*, 669–686. [CrossRef] [PubMed]
56. Yurchenco, P.D.; Patton, B.L. Developmental and pathogenic mechanisms of basement membrane assembly. *Curr. Pharm. Des.* **2009**, *15*, 1277–1294. [CrossRef] [PubMed]
57. Thomsen, M.S.; Routhe, L.J.; Moos, T. The vascular basement membrane in the healthy and pathological brain. *J. Cereb. Blood Flow Metab. Off. J. Int. Soc. Cereb. Blood Flow Metab.* **2017**, *37*, 3300–3317. [CrossRef]

58. Zhang, Y.; Barres, B.A. Astrocyte heterogeneity: An underappreciated topic in neurobiology. *Curr. Opin. Neurobiol.* **2010**, *20*, 588–594. [CrossRef]
59. Allaman, I.; Belanger, M.; Magistretti, P.J. Astrocyte-neuron metabolic relationships: For better and for worse. *Trends Neurosci.* **2011**, *34*, 76–87. [CrossRef]
60. Noell, S.; Wolburg-Buchholz, K.; Mack, A.F.; Beedle, A.M.; Satz, J.S.; Campbell, K.P.; Wolburg, H.; Fallier-Becker, P. Evidence for a role of dystroglycan regulating the membrane architecture of astroglial endfeet. *Eur. J. Neurosci.* **2011**, *33*, 2179–2186. [CrossRef]
61. Wolburg, H.; Wolburg-Buchholz, K.; Fallier-Becker, P.; Noell, S.; Mack, A.F. Structure and functions of aquaporin-4-based orthogonal arrays of particles. *Int. Rev. Cell Mol. Biol.* **2011**, *287*, 1–41. [PubMed]
62. Janzer, R.C.; Raff, M.C. Astrocytes induce blood-brain barrier properties in endothelial cells. *Nature* **1987**, *325*, 253–257. [CrossRef] [PubMed]
63. Siddharthan, V.; Kim, Y.V.; Liu, S.; Kim, K.S. Human astrocytes/astrocyte-conditioned medium and shear stress enhance the barrier properties of human brain microvascular endothelial cells. *Brain Res.* **2007**, *1147*, 39–50. [CrossRef] [PubMed]
64. Colgan, O.C.; Collins, N.T.; Ferguson, G.; Murphy, R.P.; Birney, Y.A.; Cahill, P.A.; Cummins, P.M. Influence of basolateral condition on the regulation of brain microvascular endothelial tight junction properties and barrier function. *Brain Res.* **2008**, *1193*, 84–92. [CrossRef] [PubMed]
65. Alvarez, J.I.; Dodelet-Devillers, A.; Kebir, H.; Ifergan, I.; Fabre, P.J.; Terouz, S.; Sabbagh, M.; Wosik, K.; Bourbonniere, L.; Bernard, M.; et al. The hedgehog pathway promotes blood-brain barrier integrity and cns immune quiescence. *Science* **2011**, *334*, 1727–1731. [CrossRef]
66. Gurnik, S.; Devraj, K.; Macas, J.; Yamaji, M.; Starke, J.; Scholz, A.; Sommer, K.; Di Tacchio, M.; Vutukuri, R.; Beck, H.; et al. Angiopoietin-2-induced blood-brain barrier compromise and increased stroke size are rescued by ve-ptp-dependent restoration of tie2 signaling. *Acta Neuropathol.* **2016**, *131*, 753–773. [CrossRef]
67. Engelhardt, B.; Liebner, S. Novel insights into the development and maintenance of the blood-brain barrier. *Cell Tissue Res.* **2014**, *355*, 687–699. [CrossRef]
68. Farquhar, M.G.; Palade, G.E. Junctional complexes in various epithelia. *J. Cell Biol.* **1963**, *17*, 375–412. [CrossRef]
69. Itoh, M.; Furuse, M.; Morita, K.; Kubota, K.; Saitou, M.; Tsukita, S. Direct binding of three tight junction-associated maguks, zo-1, zo-2, and zo-3, with the cooh termini of claudins. *J. Cell Biol.* **1999**, *147*, 1351–1363. [CrossRef]
70. Simionescu, M.; Simionescu, N.; Palade, G.E. Segmental differentiations of cell junctions in the vascular endothelium. Arteries and veins. *J. Cell Biol.* **1976**, *68*, 705–723. [CrossRef]
71. Muhleisen, H.; Wolburg, H.; Betz, E. Freeze-fracture analysis of endothelial cell membranes in rabbit carotid arteries subjected to short-term atherogenic stimuli. *Virchows Arch. B Cell Pathol. Incl. Mol. Pathol.* **1989**, *56*, 413–417. [CrossRef] [PubMed]
72. Nagy, Z.; Peters, H.; Huttner, I. Fracture faces of cell junctions in cerebral endothelium during normal and hyperosmotic conditions. *Lab. Investig. J. Tech. Methods Pathol.* **1984**, *50*, 313–322.
73. Liebner, S.; Kniesel, U.; Kalbacher, H.; Wolburg, H. Correlation of tight junction morphology with the expression of tight junction proteins in blood-brain barrier endothelial cells. *Eur. J. Cell Biol.* **2000**, *79*, 707–717. [CrossRef] [PubMed]
74. Lippoldt, A.; Kniesel, U.; Liebner, S.; Kalbacher, H.; Kirsch, T.; Wolburg, H.; Haller, H. Structural alterations of tight junctions are associated with loss of polarity in stroke-prone spontaneously hypertensive rat blood-brain barrier endothelial cells. *Brain Res.* **2000**, *885*, 251–261. [CrossRef]
75. Diamond, J.M. Twenty-first bowditch lecture. The epithelial junction: Bridge, gate, and fence. *Physiologist* **1977**, *20*, 10–18.
76. van Meer, G.; Gumbiner, B.; Simons, K. The tight junction does not allow lipid molecules to diffuse from one epithelial cell to the next. *Nature* **1986**, *322*, 639–641. [CrossRef]
77. Fanning, A.S.; Anderson, J.M. Protein modules as organizers of membrane structure. *Curr. Opin. Cell Biol.* **1999**, *11*, 432–439. [CrossRef]
78. Bauer, H.C.; Krizbai, I.A.; Bauer, H.; Traweger, A. "You shall not pass"—Tight junctions of the blood brain barrier. *Front. Neurosci.* **2014**, *8*, 392. [CrossRef]
79. Gunzel, D.; Yu, A.S. Claudins and the modulation of tight junction permeability. *Physiol. Rev.* **2013**, *93*, 525–569. [CrossRef]

80. Mineta, K.; Yamamoto, Y.; Yamazaki, Y.; Tanaka, H.; Tada, Y.; Saito, K.; Tamura, A.; Igarashi, M.; Endo, T.; Takeuchi, K.; et al. Predicted expansion of the claudin multigene family. *FEBS Lett.* **2011**, *585*, 606–612. [CrossRef]
81. Stiffler, M.A.; Chen, J.R.; Grantcharova, V.P.; Lei, Y.; Fuchs, D.; Allen, J.E.; Zaslavskaia, L.A.; MacBeath, G. Pdz domain binding selectivity is optimized across the mouse proteome. *Science* **2007**, *317*, 364–369. [CrossRef] [PubMed]
82. Colegio, O.R.; Van Itallie, C.; Rahner, C.; Anderson, J.M. Claudin extracellular domains determine paracellular charge selectivity and resistance but not tight junction fibril architecture. *Am. J. Physiol. Cell Physiol.* **2003**, *284*, C1346–C1354. [CrossRef] [PubMed]
83. Krause, G.; Winkler, L.; Piehl, C.; Blasig, I.; Piontek, J.; Muller, S.L. Structure and function of extracellular claudin domains. *Ann. N. Y. Acad. Sci.* **2009**, *1165*, 34–43. [CrossRef]
84. Furuse, M.; Fujita, K.; Hiiragi, T.; Fujimoto, K.; Tsukita, S. Claudin-1 and -2: Novel integral membrane proteins localizing at tight junctions with no sequence similarity to occludin. *J. Cell Biol.* **1998**, *141*, 1539–1550. [CrossRef] [PubMed]
85. Furuse, M.; Furuse, K.; Sasaki, H.; Tsukita, S. Conversion of zonulae occludentes from tight to leaky strand type by introducing claudin-2 into madin-darby canine kidney i cells. *J. Cell Biol.* **2001**, *153*, 263–272. [CrossRef]
86. Van Itallie, C.; Rahner, C.; Anderson, J.M. Regulated expression of claudin-4 decreases paracellular conductance through a selective decrease in sodium permeability. *J. Clin. Investig.* **2001**, *107*, 1319–1327. [CrossRef]
87. Amasheh, S.; Schmidt, T.; Mahn, M.; Florian, P.; Mankertz, J.; Tavalali, S.; Gitter, A.H.; Schulzke, J.D.; Fromm, M. Contribution of claudin-5 to barrier properties in tight junctions of epithelial cells. *Cell Tissue Res.* **2005**, *321*, 89–96. [CrossRef]
88. Anderson, J.M.; Van Itallie, C.M. Physiology and function of the tight junction. *Cold Spring Harb. Perspect. Biol.* **2009**, *1*, a002584. [CrossRef]
89. Amasheh, S.; Meiri, N.; Gitter, A.H.; Schoneberg, T.; Mankertz, J.; Schulzke, J.D.; Fromm, M. Claudin-2 expression induces cation-selective channels in tight junctions of epithelial cells. *J. Cell Sci.* **2002**, *115*, 4969–4976. [CrossRef]
90. Furuse, M.; Hata, M.; Furuse, K.; Yoshida, Y.; Haratake, A.; Sugitani, Y.; Noda, T.; Kubo, A.; Tsukita, S. Claudin-based tight junctions are crucial for the mammalian epidermal barrier: A lesson from claudin-1-deficient mice. *J. Cell Biol.* **2002**, *156*, 1099–1111. [CrossRef]
91. Gow, A.; Southwood, C.M.; Li, J.S.; Pariali, M.; Riordan, G.P.; Brodie, S.E.; Danias, J.; Bronstein, J.M.; Kachar, B.; Lazzarini, R.A. Cns myelin and sertoli cell tight junction strands are absent in osp/claudin-11 null mice. *Cell* **1999**, *99*, 649–659. [CrossRef]
92. Nitta, T.; Hata, M.; Gotoh, S.; Seo, Y.; Sasaki, H.; Hashimoto, N.; Furuse, M.; Tsukita, S. Size-selective loosening of the blood-brain barrier in claudin-5-deficient mice. *J. Cell Biol.* **2003**, *161*, 653–660. [CrossRef] [PubMed]
93. Uchida, Y.; Sumiya, T.; Tachikawa, M.; Yamakawa, T.; Murata, S.; Yagi, Y.; Sato, K.; Stephan, A.; Ito, K.; Ohtsuki, S.; et al. Involvement of claudin-11 in disruption of blood-brain, -spinal cord, and -arachnoid barriers in multiple sclerosis. *Mol. Neurobiol.* **2019**, *56*, 2039–2056. [CrossRef] [PubMed]
94. Berndt, P.; Winkler, L.; Cording, J.; Breitkreuz-Korff, O.; Rex, A.; Dithmer, S.; Rausch, V.; Blasig, R.; Richter, M.; Sporbert, A.; et al. Tight junction proteins at the blood-brain barrier: Far more than claudin-5. *Cell. Mol. Life Sci. CMLS* **2019**, *76*, 1987–2002. [CrossRef]
95. Sladojevic, N.; Stamatovic, S.M.; Johnson, A.M.; Choi, J.; Hu, A.; Dithmer, S.; Blasig, I.E.; Keep, R.F.; Andjelkovic, A.V. Claudin-1-dependent destabilization of the blood-brain barrier in chronic stroke. *J. Neurosci. Off. J. Soc. Neurosci.* **2019**, *39*, 743–757. [CrossRef]
96. Morita, K.; Sasaki, H.; Furuse, M.; Tsukita, S. Endothelial claudin: Claudin-5/tmvcf constitutes tight junction strands in endothelial cells. *J. Cell Biol.* **1999**, *147*, 185–194. [CrossRef]
97. Greene, C.; Kealy, J.; Humphries, M.M.; Gong, Y.; Hou, J.; Hudson, N.; Cassidy, L.M.; Martiniano, R.; Shashi, V.; Hooper, S.R.; et al. Dose-dependent expression of claudin-5 is a modifying factor in schizophrenia. *Mol. Psychiatry* **2018**, *23*, 2156–2166. [CrossRef]

98. Wolburg, H.; Wolburg-Buchholz, K.; Kraus, J.; Rascher-Eggstein, G.; Liebner, S.; Hamm, S.; Duffner, F.; Grote, E.H.; Risau, W.; Engelhardt, B. Localization of claudin-3 in tight junctions of the blood-brain barrier is selectively lost during experimental autoimmune encephalomyelitis and human glioblastoma multiforme. *Acta Neuropathol.* **2003**, *105*, 586–592.
99. Liebner, S.; Corada, M.; Bangsow, T.; Babbage, J.; Taddei, A.; Czupalla, C.J.; Reis, M.; Felici, A.; Wolburg, H.; Fruttiger, M.; et al. Wnt/beta-catenin signaling controls development of the blood-brain barrier. *J. Cell Biol.* **2008**, *183*, 409–417. [CrossRef]
100. Steinemann, A.; Galm, I.; Chip, S.; Nitsch, C.; Maly, I.P. Claudin-1, -2 and -3 are selectively expressed in the epithelia of the choroid plexus of the mouse from early development and into adulthood while claudin-5 is restricted to endothelial cells. *Front. Neuroanat.* **2016**, *10*, 16. [CrossRef]
101. Kominsky, S.L.; Tyler, B.; Sosnowski, J.; Brady, K.; Doucet, M.; Nell, D.; Smedley, J.G.; McClane, B.; Brem, H.; Sukumar, S. Clostridium perfringens enterotoxin as a novel-targeted therapeutic for brain metastasis. *Cancer Res.* **2007**, *67*, 7977–7982. [CrossRef] [PubMed]
102. Castro Dias, M.; Coisne, C.; Lazarevic, I.; Baden, P.; Hata, M.; Iwamoto, N.; Francisco, D.M.F.; Vanlandewijck, M.; He, L.; Baier, F.A.; et al. Claudin-3-deficient c57bl/6j mice display intact brain barriers. *Sci. Rep.* **2019**, *9*, 203. [CrossRef] [PubMed]
103. Liebner, S.; Fischmann, A.; Rascher, G.; Duffner, F.; Grote, E.H.; Kalbacher, H.; Wolburg, H. Claudin-1 and claudin-5 expression and tight junction morphology are altered in blood vessels of human glioblastoma multiforme. *Acta Neuropathol.* **2000**, *100*, 323–331. [CrossRef] [PubMed]
104. Pfeiffer, F.; Schafer, J.; Lyck, R.; Makrides, V.; Brunner, S.; Schaeren-Wiemers, N.; Deutsch, U.; Engelhardt, B. Claudin-1 induced sealing of blood-brain barrier tight junctions ameliorates chronic experimental autoimmune encephalomyelitis. *Acta Neuropathol.* **2011**, *122*, 601–614. [CrossRef] [PubMed]
105. Zhang, Y.; Chen, K.; Sloan, S.A.; Bennett, M.L.; Scholze, A.R.; O'Keeffe, S.; Phatnani, H.P.; Guarnieri, P.; Caneda, C.; Ruderisch, N.; et al. An rna-sequencing transcriptome and splicing database of glia, neurons, and vascular cells of the cerebral cortex. *J. Neurosci. Off. J. Soc. Neurosci.* **2014**, *34*, 11929–11947. [CrossRef] [PubMed]
106. Castro Dias, M.; Coisne, C.; Baden, P.; Enzmann, G.; Garrett, L.; Becker, L.; Holter, S.M.; Hrabe de Angelis, M.; Deutsch, U.; Engelhardt, B. Claudin-12 is not required for blood-brain barrier tight junction function. *Fluids Barriers CNS* **2019**, *16*, 30. [CrossRef]
107. Furuse, M.; Hirase, T.; Itoh, M.; Nagafuchi, A.; Yonemura, S.; Tsukita, S.; Tsukita, S. Occludin: A novel integral membrane protein localizing at tight junctions. *J. Cell Biol.* **1993**, *123*, 1777–1788. [CrossRef]
108. Ikenouchi, J.; Furuse, M.; Furuse, K.; Sasaki, H.; Tsukita, S.; Tsukita, S. Tricellulin constitutes a novel barrier at tricellular contacts of epithelial cells. *J. Cell Biol.* **2005**, *171*, 939–945. [CrossRef]
109. Steed, E.; Rodrigues, N.T.; Balda, M.S.; Matter, K. Identification of marveld3 as a tight junction-associated transmembrane protein of the occludin family. *BMC Cell Biol.* **2009**, *10*, 95. [CrossRef]
110. Hirase, T.; Staddon, J.M.; Saitou, M.; Ando-Akatsuka, Y.; Itoh, M.; Furuse, M.; Fujimoto, K.; Tsukita, S.; Rubin, L.L. Occludin as a possible determinant of tight junction permeability in endothelial cells. *J. Cell Sci.* **1997**, *110*, 1603–1613.
111. Iwamoto, N.; Higashi, T.; Furuse, M. Localization of angulin-1/lsr and tricellulin at tricellular contacts of brain and retinal endothelial cells in vivo. *Cell Struct. Funct.* **2014**, *39*, 13015. [CrossRef] [PubMed]
112. Balda, M.S.; Whitney, J.A.; Flores, C.; Gonzalez, S.; Cereijido, M.; Matter, K. Functional dissociation of paracellular permeability and transepithelial electrical resistance and disruption of the apical-basolateral intramembrane diffusion barrier by expression of a mutant tight junction membrane protein. *J. Cell Biol.* **1996**, *134*, 1031–1049. [CrossRef] [PubMed]
113. McCarthy, K.M.; Skare, I.B.; Stankewich, M.C.; Furuse, M.; Tsukita, S.; Rogers, R.A.; Lynch, R.D.; Schneeberger, E.E. Occludin is a functional component of the tight junction. *J. Cell Sci.* **1996**, *109*, 2287–2298. [PubMed]
114. Saitou, M.; Fujimoto, K.; Doi, Y.; Itoh, M.; Fujimoto, T.; Furuse, M.; Takano, H.; Noda, T.; Tsukita, S. Occludin-deficient embryonic stem cells can differentiate into polarized epithelial cells bearing tight junctions. *J. Cell Biol.* **1998**, *141*, 397–408. [CrossRef]
115. Kuwabara, H.; Kokai, Y.; Kojima, T.; Takakuwa, R.; Mori, M.; Sawada, N. Occludin regulates actin cytoskeleton in endothelial cells. *Cell Struct. Funct.* **2001**, *26*, 109–116. [CrossRef] [PubMed]

116. Murakami, T.; Felinski, E.A.; Antonetti, D.A. Occludin phosphorylation and ubiquitination regulate tight junction trafficking and vascular endothelial growth factor-induced permeability. *J. Biol. Chem.* **2009**, *284*, 21036–21046. [CrossRef]
117. Wachtel, M.; Frei, K.; Ehler, E.; Fontana, A.; Winterhalter, K.; Gloor, S.M. Occludin proteolysis and increased permeability in endothelial cells through tyrosine phosphatase inhibition. *J. Cell Sci.* **1999**, *112*, 4347–4356.
118. Saitou, M.; Furuse, M.; Sasaki, H.; Schulzke, J.D.; Fromm, M.; Takano, H.; Noda, T.; Tsukita, S. Complex phenotype of mice lacking occludin, a component of tight junction strands. *Mol. Biol. Cell* **2000**, *11*, 4131–4142. [CrossRef]
119. Higashi, T.; Miller, A.L. Tricellular junctions: How to build junctions at the trickiest points of epithelial cells. *Mol. Biol. Cell* **2017**, *28*, 2023–2034. [CrossRef]
120. Mariano, C.; Palmela, I.; Pereira, P.; Fernandes, A.; Falcao, A.S.; Cardoso, F.L.; Vaz, A.R.; Campos, A.R.; Goncalves-Ferreira, A.; Kim, K.S.; et al. Tricellulin expression in brain endothelial and neural cells. *Cell Tissue Res.* **2013**, *351*, 397–407. [CrossRef]
121. Martin-Padura, I.; Lostaglio, S.; Schneemann, M.; Williams, L.; Romano, M.; Fruscella, P.; Panzeri, C.; Stoppacciaro, A.; Ruco, L.; Villa, A.; et al. Junctional adhesion molecule, a novel member of the immunoglobulin superfamily that distributes at intercellular junctions and modulates monocyte transmigration. *J. Cell Biol.* **1998**, *142*, 117–127. [CrossRef] [PubMed]
122. Garrido-Urbani, S.; Bradfield, P.F.; Imhof, B.A. Tight junction dynamics: The role of junctional adhesion molecules (jams). *Cell Tissue Res.* **2014**, *355*, 701–715. [CrossRef] [PubMed]
123. Aurrand-Lions, M.; Duncan, L.; Ballestrem, C.; Imhof, B.A. Jam-2, a novel immunoglobulin superfamily molecule, expressed by endothelial and lymphatic cells. *J. Biol. Chem.* **2001**, *276*, 2733–2741. [CrossRef] [PubMed]
124. Liu, Y.; Nusrat, A.; Schnell, F.J.; Reaves, T.A.; Walsh, S.; Pochet, M.; Parkos, C.A. Human junction adhesion molecule regulates tight junction resealing in epithelia. *J. Cell Sci.* **2000**, *113*, 2363–2374. [PubMed]
125. Wyss, L.; Schafer, J.; Liebner, S.; Mittelbronn, M.; Deutsch, U.; Enzmann, G.; Adams, R.H.; Aurrand-Lions, M.; Plate, K.H.; Imhof, B.A.; et al. Junctional adhesion molecule (jam)-c deficient c57bl/6 mice develop a severe hydrocephalus. *PLoS ONE* **2012**, *7*, e45619. [CrossRef] [PubMed]
126. Padden, M.; Leech, S.; Craig, B.; Kirk, J.; Brankin, B.; McQuaid, S. Differences in expression of junctional adhesion molecule-a and beta-catenin in multiple sclerosis brain tissue: Increasing evidence for the role of tight junction pathology. *Acta Neuropathol.* **2007**, *113*, 177–186. [CrossRef]
127. Arrate, M.P.; Rodriguez, J.M.; Tran, T.M.; Brock, T.A.; Cunningham, S.A. Cloning of human junctional adhesion molecule 3 (jam3) and its identification as the jam2 counter-receptor. *J. Biol. Chem.* **2001**, *276*, 45826–45832. [CrossRef]
128. Ebnet, K.; Aurrand-Lions, M.; Kuhn, A.; Kiefer, F.; Butz, S.; Zander, K.; Meyer zu Brickwedde, M.K.; Suzuki, A.; Imhof, B.A.; Vestweber, D. The junctional adhesion molecule (jam) family members jam-2 and jam-3 associate with the cell polarity protein par-3: A possible role for jams in endothelial cell polarity. *J. Cell Sci.* **2003**, *116*, 3879–3891. [CrossRef]
129. Ebnet, K.; Suzuki, A.; Horikoshi, Y.; Hirose, T.; Meyer Zu Brickwedde, M.K.; Ohno, S.; Vestweber, D. The cell polarity protein asip/par-3 directly associates with junctional adhesion molecule (jam). *EMBO J.* **2001**, *20*, 3738–3748. [CrossRef]
130. Williams, D.W.; Calderon, T.M.; Lopez, L.; Carvallo-Torres, L.; Gaskill, P.J.; Eugenin, E.A.; Morgello, S.; Berman, J.W. Mechanisms of hiv entry into the cns: Increased sensitivity of hiv infected cd14+cd16+ monocytes to ccl2 and key roles of ccr2, jam-a, and alcam in diapedesis. *PLoS ONE* **2013**, *8*, e69270. [CrossRef]
131. Tietz, S.; Perinat, T.; Greene, G.; Enzmann, G.; Deutsch, U.; Adams, R.; Imhof, B.; Aurrand-Lions, M.; Engelhardt, B. Lack of junctional adhesion molecule (jam)-b ameliorates experimental autoimmune encephalomyelitis. *Brain Behav. Immun.* **2018**, *73*, 3–20. [CrossRef] [PubMed]
132. Cunningham, S.A.; Rodriguez, J.M.; Arrate, M.P.; Tran, T.M.; Brock, T.A. Jam2 interacts with $alpha_4beta_1$. Facilitation by jam3. *J. Biol. Chem.* **2002**, *277*, 27589–27592. [CrossRef] [PubMed]
133. Ludwig, R.J.; Hardt, K.; Hatting, M.; Bistrian, R.; Diehl, S.; Radeke, H.H.; Podda, M.; Schon, M.P.; Kaufmann, R.; Henschler, R.; et al. Junctional adhesion molecule (jam)-b supports lymphocyte rolling and adhesion through interaction with alpha4beta1 integrin. *Immunology* **2009**, *128*, 196–205. [CrossRef] [PubMed]

134. Martin-Blondel, G.; Pignolet, B.; Tietz, S.; Yshii, L.; Gebauer, C.; Perinat, T.; Van Weddingen, I.; Blatti, C.; Engelhardt, B.; Liblau, R. Migration of encephalitogenic cd8 t cells into the central nervous system is dependent on the alpha4beta1-integrin. *Eur. J. Immunol.* **2015**, *45*, 3302–3312. [CrossRef] [PubMed]
135. Mochida, G.H.; Ganesh, V.S.; Felie, J.M.; Gleason, D.; Hill, R.S.; Clapham, K.R.; Rakiec, D.; Tan, W.H.; Akawi, N.; Al-Saffar, M.; et al. A homozygous mutation in the tight-junction protein jam3 causes hemorrhagic destruction of the brain, subependymal calcification, and congenital cataracts. *Am. J. Hum. Genet.* **2010**, *87*, 882–889. [CrossRef] [PubMed]
136. Funke, L.; Dakoji, S.; Bredt, D.S. Membrane-associated guanylate kinases regulate adhesion and plasticity at cell junctions. *Annu. Rev. Biochem.* **2005**, *74*, 219–245. [CrossRef]
137. Dimitratos, S.D.; Woods, D.F.; Stathakis, D.G.; Bryant, P.J. Signaling pathways are focused at specialized regions of the plasma membrane by scaffolding proteins of the maguk family. *Bioessays News Rev. Mol. Cell. Dev. Biol.* **1999**, *21*, 912–921. [CrossRef]
138. Gonzalez-Mariscal, L.; Betanzos, A.; Avila-Flores, A. Maguk proteins: Structure and role in the tight junction. *Semin. Cell Dev. Biol.* **2000**, *11*, 315–324. [CrossRef]
139. Umeda, K.; Ikenouchi, J.; Katahira-Tayama, S.; Furuse, K.; Sasaki, H.; Nakayama, M.; Matsui, T.; Tsukita, S.; Furuse, M.; Tsukita, S. Zo-1 and zo-2 independently determine where claudins are polymerized in tight-junction strand formation. *Cell* **2006**, *126*, 741–754. [CrossRef]
140. Katsuno, T.; Umeda, K.; Matsui, T.; Hata, M.; Tamura, A.; Itoh, M.; Takeuchi, K.; Fujimori, T.; Nabeshima, Y.; Noda, T.; et al. Deficiency of zonula occludens-1 causes embryonic lethal phenotype associated with defected yolk sac angiogenesis and apoptosis of embryonic cells. *Mol. Biol. Cell* **2008**, *19*, 2465–2475. [CrossRef]
141. Xu, J.; Kausalya, P.J.; Phua, D.C.; Ali, S.M.; Hossain, Z.; Hunziker, W. Early embryonic lethality of mice lacking zo-2, but not zo-3, reveals critical and nonredundant roles for individual zonula occludens proteins in mammalian development. *Mol. Cell. Biol.* **2008**, *28*, 1669–1678. [CrossRef] [PubMed]
142. Van Itallie, C.M.; Anderson, J.M. Architecture of tight junctions and principles of molecular composition. *Semin. Cell Dev. Biol.* **2014**, *36*, 157–165. [CrossRef] [PubMed]
143. Tornavaca, O.; Chia, M.; Dufton, N.; Almagro, L.O.; Conway, D.E.; Randi, A.M.; Schwartz, M.A.; Matter, K.; Balda, M.S. Zo-1 controls endothelial adherens junctions, cell-cell tension, angiogenesis, and barrier formation. *J. Cell Biol.* **2015**, *208*, 821–838. [CrossRef] [PubMed]
144. Hawkins, B.T.; Davis, T.P. The blood-brain barrier/neurovascular unit in health and disease. *Pharmacol. Rev.* **2005**, *57*, 173–185. [CrossRef]
145. Davies, D.C. Blood-brain barrier breakdown in septic encephalopathy and brain tumours. *J. Anat.* **2002**, *200*, 639–646. [CrossRef]
146. Cordenonsi, M.; D'Atri, F.; Hammar, E.; Parry, D.A.; Kendrick-Jones, J.; Shore, D.; Citi, S. Cingulin contains globular and coiled-coil domains and interacts with zo-1, zo-2, zo-3, and myosin. *J. Cell Biol.* **1999**, *147*, 1569–1582. [CrossRef]
147. Balda, M.S.; Matter, K. The tight junction protein zo-1 and an interacting transcription factor regulate erbb-2 expression. *EMBO J.* **2000**, *19*, 2024–2033. [CrossRef]
148. Satoh, H.; Zhong, Y.; Isomura, H.; Saitoh, M.; Enomoto, K.; Sawada, N.; Mori, M. Localization of 7h6 tight junction-associated antigen along the cell border of vascular endothelial cells correlates with paracellular barrier function against ions, large molecules, and cancer cells. *Exp. Cell Res.* **1996**, *222*, 269–274. [CrossRef]
149. Tietz, S.; Engelhardt, B. Brain barriers: Crosstalk between complex tight junctions and adherens junctions. *J. Cell Biol.* **2015**, *209*, 493–506. [CrossRef]
150. Carmeliet, P.; Lampugnani, M.G.; Moons, L.; Breviario, F.; Compernolle, V.; Bono, F.; Balconi, G.; Spagnuolo, R.; Oosthuyse, B.; Dewerchin, M.; et al. Targeted deficiency or cytosolic truncation of the ve-cadherin gene in mice impairs vegf-mediated endothelial survival and angiogenesis. *Cell* **1999**, *98*, 147–157. [CrossRef]
151. Crosby, C.V.; Fleming, P.A.; Argraves, W.S.; Corada, M.; Zanetta, L.; Dejana, E.; Drake, C.J. Ve-cadherin is not required for the formation of nascent blood vessels but acts to prevent their disassembly. *Blood* **2005**, *105*, 2771–2776. [CrossRef] [PubMed]
152. Yap, A.S.; Niessen, C.M.; Gumbiner, B.M. The juxtamembrane region of the cadherin cytoplasmic tail supports lateral clustering, adhesive strengthening, and interaction with $p120^{ctn}$. *J. Cell Biol.* **1998**, *141*, 779–789. [CrossRef] [PubMed]

153. Shibamoto, S.; Hayakawa, M.; Takeuchi, K.; Hori, T.; Miyazawa, K.; Kitamura, N.; Johnson, K.R.; Wheelock, M.J.; Matsuyoshi, N.; Takeichi, M.; et al. Association of p120, a tyrosine kinase substrate, with e-cadherin/catenin complexes. *J. Cell Biol.* **1995**, *128*, 949–957. [CrossRef] [PubMed]
154. Rimm, D.L.; Koslov, E.R.; Kebriaei, P.; Cianci, C.D.; Morrow, J.S. Alpha 1(e)-catenin is an actin-binding and -bundling protein mediating the attachment of f-actin to the membrane adhesion complex. *Proc. Natl. Acad. Sci. USA* **1995**, *92*, 8813–8817. [CrossRef] [PubMed]
155. Kobielak, A.; Fuchs, E. Alpha-catenin: At the junction of intercellular adhesion and actin dynamics. *Nat. Rev. Mol. Cell Biol.* **2004**, *5*, 614–625. [CrossRef]
156. Taddei, A.; Giampietro, C.; Conti, A.; Orsenigo, F.; Breviario, F.; Pirazzoli, V.; Potente, M.; Daly, C.; Dimmeler, S.; Dejana, E. Endothelial adherens junctions control tight junctions by ve-cadherin-mediated upregulation of claudin-5. *Nat. Cell Biol.* **2008**, *10*, 923–934. [CrossRef]
157. Indra, I.; Hong, S.; Troyanovsky, R.; Kormos, B.; Troyanovsky, S. The adherens junction: A mosaic of cadherin and nectin clusters bundled by actin filaments. *J. Investig. Dermatol.* **2013**, *133*, 2546–2554. [CrossRef]
158. Takai, Y.; Irie, K.; Shimizu, K.; Sakisaka, T.; Ikeda, W. Nectins and nectin-like molecules: Roles in cell adhesion, migration, and polarization. *Cancer Sci.* **2003**, *94*, 655–667. [CrossRef]
159. Newman, P.J. The biology of pecam-1. *J. Clin. Investig.* **1997**, *99*, 3–8. [CrossRef]
160. Lyck, R.; Ruderisch, N.; Moll, A.G.; Steiner, O.; Cohen, C.D.; Engelhardt, B.; Makrides, V.; Verrey, F. Culture-induced changes in blood-brain barrier transcriptome: Implications for amino-acid transporters in vivo. *J. Cereb. Blood Flow Metab. Off. J. Int. Soc. Cereb. Blood Flow Metab.* **2009**, *29*, 1491–1502. [CrossRef]
161. Graesser, D.; Solowiej, A.; Bruckner, M.; Osterweil, E.; Juedes, A.; Davis, S.; Ruddle, N.H.; Engelhardt, B.; Madri, J.A. Altered vascular permeability and early onset of experimental autoimmune encephalomyelitis in pecam-1-deficient mice. *J. Clin. Investig.* **2002**, *109*, 383–392. [CrossRef]
162. Wimmer, I.; Tietz, S.; Nishihara, H.; Deutsch, U.; Sallusto, F.; Gosselet, F.; Lyck, R.; Muller, W.A.; Lassmann, H.; Engelhardt, B. Pecam-1 stabilizes blood-brain barrier integrity and favors paracellular t-cell diapedesis across the blood-brain barrier during neuroinflammation. *Front. Immunol.* **2019**, *10*, 711. [CrossRef] [PubMed]
163. Privratsky, J.R.; Newman, P.J. Pecam-1: Regulator of endothelial junctional integrity. *Cell Tissue Res.* **2014**, *355*, 607–619. [CrossRef] [PubMed]
164. Schenkel, A.R.; Mamdouh, Z.; Chen, X.; Liebman, R.M.; Muller, W.A. Cd99 plays a major role in the migration of monocytes through endothelial junctions. *Nat. Immunol.* **2002**, *3*, 143–150. [CrossRef] [PubMed]
165. Bixel, G.; Kloep, S.; Butz, S.; Petri, B.; Engelhardt, B.; Vestweber, D. Mouse cd99 participates in t-cell recruitment into inflamed skin. *Blood* **2004**, *104*, 3205–3213. [CrossRef]
166. Winger, R.C.; Harp, C.T.; Chiang, M.Y.; Sullivan, D.P.; Watson, R.L.; Weber, E.W.; Podojil, J.R.; Miller, S.D.; Muller, W.A. Cutting edge: CD99 is a novel therapeutic target for control of t cell-mediated central nervous system autoimmune disease. *J. Immunol.* **2016**, *196*, 1443–1448. [CrossRef]
167. Hoshi, Y.; Uchida, Y.; Tachikawa, M.; Inoue, T.; Ohtsuki, S.; Terasaki, T. Quantitative atlas of blood-brain barrier transporters, receptors, and tight junction proteins in rats and common marmoset. *J. Pharm. Sci.* **2013**, *102*, 3343–3355. [CrossRef]
168. O'Brown, N.M.; Pfau, S.J.; Gu, C. Bridging barriers: A comparative look at the blood-brain barrier across organisms. *Genes Dev.* **2018**, *32*, 466–478. [CrossRef]
169. Lehtinen, M.K.; Bjornsson, C.S.; Dymecki, S.M.; Gilbertson, R.J.; Holtzman, D.M.; Monuki, E.S. The choroid plexus and cerebrospinal fluid: Emerging roles in development, disease, and therapy. *J. Neurosci. Off. J. Soc. Neurosci.* **2013**, *33*, 17553–17559. [CrossRef]
170. Redzic, Z.B.; Preston, J.E.; Duncan, J.A.; Chodobski, A.; Szmydynger-Chodobska, J. The choroid plexus-cerebrospinal fluid system: From development to aging. *Curr. Top. Dev. Biol.* **2005**, *71*, 1–52.
171. Kaur, C.; Rathnasamy, G.; Ling, E.A. The choroid plexus in healthy and diseased brain. *J. Neuropathol. Exp. Neurol.* **2016**, *75*, 198–213. [CrossRef] [PubMed]
172. Hurley, J.V.; Anderson, R.M.; Sexton, P.T. The fate of plasma protein which escapes from blood vessels of the choroid plexus of the rat—An electron microscope study. *J. Pathol.* **1981**, *134*, 57–70. [CrossRef] [PubMed]
173. Liddelow, S.A.; Temple, S.; Mollgard, K.; Gehwolf, R.; Wagner, A.; Bauer, H.; Bauer, H.C.; Phoenix, T.N.; Dziegielewska, K.M.; Saunders, N.R. Molecular characterisation of transport mechanisms at the developing mouse blood-csf interface: A transcriptome approach. *PLoS ONE* **2012**, *7*, e33554. [CrossRef]

174. Wolburg, H.; Wolburg-Buchholz, K.; Liebner, S.; Engelhardt, B. Claudin-1, claudin-2 and claudin-11 are present in tight junctions of choroid plexus epithelium of the mouse. *Neurosci. Lett.* **2001**, *307*, 77–80. [CrossRef]
175. Aijaz, S.; Balda, M.S.; Matter, K. Tight junctions: Molecular architecture and function. *Int. Rev. Cytol.* **2006**, *248*, 261–298. [PubMed]
176. Kratzer, I.; Vasiljevic, A.; Rey, C.; Fevre-Montange, M.; Saunders, N.; Strazielle, N.; Ghersi-Egea, J.F. Complexity and developmental changes in the expression pattern of claudins at the blood-csf barrier. *Histochem. Cell Biol.* **2012**, *138*, 861–879. [CrossRef]
177. Muto, S.; Hata, M.; Taniguchi, J.; Tsuruoka, S.; Moriwaki, K.; Saitou, M.; Furuse, K.; Sasaki, H.; Fujimura, A.; Imai, M.; et al. Claudin-2-deficient mice are defective in the leaky and cation-selective paracellular permeability properties of renal proximal tubules. *Proc. Natl. Acad. Sci. USA* **2010**, *107*, 8011–8016. [CrossRef]
178. Maheras, K.J.; Peppi, M.; Ghoddoussi, F.; Galloway, M.P.; Perrine, S.A.; Gow, A. Absence of claudin 11 in cns myelin perturbs behavior and neurotransmitter levels in mice. *Sci. Rep.* **2018**, *8*, 3798. [CrossRef]
179. Gow, A.; Davies, C.; Southwood, C.M.; Frolenkov, G.; Chrustowski, M.; Ng, L.; Yamauchi, D.; Marcus, D.C.; Kachar, B. Deafness in claudin 11-null mice reveals the critical contribution of basal cell tight junctions to stria vascularis function. *J. Neurosci. Off. J. Soc. Neurosci.* **2004**, *24*, 7051–7062. [CrossRef]
180. Kooij, G.; Kopplin, K.; Blasig, R.; Stuiver, M.; Koning, N.; Goverse, G.; van der Pol, S.M.; van Het Hof, B.; Gollasch, M.; Drexhage, J.A.; et al. Disturbed function of the blood-cerebrospinal fluid barrier aggravates neuro-inflammation. *Acta Neuropathol.* **2014**, *128*, 267–277. [CrossRef]
181. Vestweber, D. Cadherins in tissue architecture and disease. *J. Mol. Med.* **2015**, *93*, 5–11. [CrossRef] [PubMed]
182. Liddelow, S.A. Development of the choroid plexus and blood-csf barrier. *Front. Neurosci.* **2015**, *9*, 32. [CrossRef] [PubMed]
183. Decimo, I.; Fumagalli, G.; Berton, V.; Krampera, M.; Bifari, F. Meninges: From protective membrane to stem cell niche. *Am. J. Stem. Cells* **2012**, *1*, 92–105. [PubMed]
184. Haines, D.E.; Mihailoff, G.A. Fundamental neuroscience for basic and clinical application. In *Science Direct*; Elsevier Publishing Company: Amsterdam, The Netherlands, 2018; pp. 107–121.
185. Bifari, F.; Berton, V.; Pino, A.; Kusalo, M.; Malpeli, G.; Di Chio, M.; Bersan, E.; Amato, E.; Scarpa, A.; Krampera, M.; et al. Meninges harbor cells expressing neural precursor markers during development and adulthood. *Front. Cell. Neurosci.* **2015**, *9*, 383. [CrossRef]
186. Bjornsson, C.S.; Apostolopoulou, M.; Tian, Y.; Temple, S. It takes a village: Constructing the neurogenic niche. *Dev. Cell* **2015**, *32*, 435–446. [CrossRef]
187. Pizzo, M.E.; Wolak, D.J.; Kumar, N.N.; Brunette, E.; Brunnquell, C.L.; Hannocks, M.J.; Abbott, N.J.; Meyerand, M.E.; Sorokin, L.; Stanimirovic, D.B.; et al. Intrathecal antibody distribution in the rat brain: Surface diffusion, perivascular transport and osmotic enhancement of delivery. *J. Physiol.* **2018**, *596*, 445–475. [CrossRef]
188. Gagan, J.R.; Tholpady, S.S.; Ogle, R.C. Cellular dynamics and tissue interactions of the dura mater during head development. *Birth Defects Res. Part C Embryo Today Rev.* **2007**, *81*, 297–304. [CrossRef]
189. Saunders, N.R.; Habgood, M.D.; Mollgard, K.; Dziegielewska, K.M. The biological significance of brain barrier mechanisms: Help or hindrance in drug delivery to the central nervous system? *F1000Research* **2016**, *10*, 5. [CrossRef]
190. Nabeshima, S.; Reese, T.S.; Landis, D.M.; Brightman, M.W. Junctions in the meninges and marginal glia. *J. Comp. Neurol.* **1975**, *164*, 127–169. [CrossRef]
191. Coles, J.A.; Myburgh, E.; Brewer, J.M.; McMenamin, P.G. Where are we? The anatomy of the murine cortical meninges revisited for intravital imaging, immunology, and clearance of waste from the brain. *Prog. Neurobiol.* **2017**, *156*, 107–148. [CrossRef]
192. Yasuda, K.; Cline, C.; Vogel, P.; Onciu, M.; Fatima, S.; Sorrentino, B.P.; Thirumaran, R.K.; Ekins, S.; Urade, Y.; Fujimori, K.; et al. Drug transporters on arachnoid barrier cells contribute to the blood-cerebrospinal fluid barrier. *Drug Metab. Dispos. Biol. Fate Chem.* **2013**, *41*, 923–931. [CrossRef] [PubMed]
193. Figarella-Branger, D.; Pellissier, J.F.; Bouillot, P.; Bianco, N.; Mayan, M.; Grisoli, F.; Rougon, G. Expression of neural cell-adhesion molecule isoforms and epithelial cadherin adhesion molecules in 47 human meningiomas: Correlation with clinical and morphological data. *Mod. Pathol. Off. J. U. S. Can. Acad. Pathol.* **1994**, *7*, 752–761.

194. Holman, D.W.; Grzybowski, D.M.; Mehta, B.C.; Katz, S.E.; Lubow, M. Characterization of cytoskeletal and junctional proteins expressed by cells cultured from human arachnoid granulation tissue. *Cereb. Fluid Res.* **2005**, *2*, 9. [CrossRef] [PubMed]
195. Grafstein, B.; Liu, S.; Cotrina, M.L.; Goldman, S.A.; Nedergaard, M. Meningeal cells can communicate with astrocytes by calcium signaling. *Ann. Neurol.* **2000**, *47*, 18–25. [CrossRef]
196. Kartenbeck, J.; Schwechheimer, K.; Moll, R.; Franke, W.W. Attachment of vimentin filaments to desmosomal plaques in human meningiomal cells and arachnoidal tissue. *J. Cell Biol.* **1984**, *98*, 1072–1081. [CrossRef]
197. Murphy, M.; Chen, J.N.; George, D.L. Establishment and characterization of a human leptomeningeal cell line. *J. Neurosci. Res.* **1991**, *30*, 475–483. [CrossRef]
198. Hasegawa, M.; Yamashima, T.; Kida, S.; Yamashita, J. Membranous ultrastructure of human arachnoid cells. *J. Neuropathol. Exp. Neurol.* **1997**, *56*, 1217–1227. [CrossRef]
199. Rudolf Nieuwenhuys, J.V.; van Huijzen, C. *The Human Central Nervous System: A Synopsis and Atlas*; Springer Berlin Heidelberg: Berlin, Germany, 2007; Chapter 4.
200. Kebir, H.; Kreymborg, K.; Ifergan, I.; Dodelet-Devillers, A.; Cayrol, R.; Bernard, M.; Giuliani, F.; Arbour, N.; Becher, B.; Prat, A. Human T_H17 lymphocytes promote blood-brain barrier disruption and central nervous system inflammation. *Nat. Med.* **2007**, *13*, 1173–1175. [CrossRef]
201. Horng, S.; Therattil, A.; Moyon, S.; Gordon, A.; Kim, K.; Argaw, A.T.; Hara, Y.; Mariani, J.N.; Sawai, S.; Flodby, P.; et al. Astrocytic tight junctions control inflammatory cns lesion pathogenesis. *J. Clin. Investig.* **2017**, *127*, 3136–3151. [CrossRef]
202. Stamatovic, S.M.; Sladojevic, N.; Keep, R.F.; Andjelkovic, A.V. Relocalization of junctional adhesion molecule a during inflammatory stimulation of brain endothelial cells. *Mol. Cell. Biol.* **2012**, *32*, 3414–3427. [CrossRef]
203. Schlingmann, B.; Overgaard, C.E.; Molina, S.A.; Lynn, K.S.; Mitchell, L.A.; Dorsainvil White, S.; Mattheyses, A.L.; Guidot, D.M.; Capaldo, C.T.; Koval, M. Regulation of claudin/zonula occludens-1 complexes by hetero-claudin interactions. *Nat. Commun.* **2016**, *7*, 12276. [CrossRef] [PubMed]
204. Kaufmann, R.; Piontek, J.; Grull, F.; Kirchgessner, M.; Rossa, J.; Wolburg, H.; Blasig, I.E.; Cremer, C. Visualization and quantitative analysis of reconstituted tight junctions using localization microscopy. *PLoS ONE* **2012**, *7*, e31128. [CrossRef] [PubMed]
205. Paul, D.; Baena, V.; Ge, S.; Jiang, X.; Jellison, E.R.; Kiprono, T.; Agalliu, D.; Pachter, J.S. Appearance of claudin-5^+ leukocytes in the central nervous system during neuroinflammation: A novel role for endothelial-derived extracellular vesicles. *J. Neuroinflamm.* **2016**, *13*, 292. [CrossRef] [PubMed]
206. Winderlich, M.; Keller, L.; Cagna, G.; Broermann, A.; Kamenyeva, O.; Kiefer, F.; Deutsch, U.; Nottebaum, A.F.; Vestweber, D. Ve-ptp controls blood vessel development by balancing tie-2 activity. *J. Cell Biol.* **2009**, *185*, 657–671. [CrossRef] [PubMed]
207. Snippert, H.J.; van der Flier, L.G.; Sato, T.; van Es, J.H.; van den Born, M.; Kroon-Veenboer, C.; Barker, N.; Klein, A.M.; van Rheenen, J.; Simons, B.D.; et al. Intestinal crypt homeostasis results from neutral competition between symmetrically dividing lgr5 stem cells. *Cell* **2010**, *143*, 134–144. [CrossRef]
208. Feng, S.; Sekine, S.; Pessino, V.; Li, H.; Leonetti, M.D.; Huang, B. Improved split fluorescent proteins for endogenous protein labeling. *Nat. Commun.* **2017**, *8*, 370. [CrossRef]
209. Kamiyama, D.; Sekine, S.; Barsi-Rhyne, B.; Hu, J.; Chen, B.; Gilbert, L.A.; Ishikawa, H.; Leonetti, M.D.; Marshall, W.F.; Weissman, J.S.; et al. Versatile protein tagging in cells with split fluorescent protein. *Nat. Commun.* **2016**, *7*, 11046. [CrossRef]
210. Cabantous, S.; Terwilliger, T.C.; Waldo, G.S. Protein tagging and detection with engineered self-assembling fragments of green fluorescent protein. *Nat. Biotechnol.* **2005**, *23*, 102–107. [CrossRef]
211. Madisen, L.; Zwingman, T.A.; Sunkin, S.M.; Oh, S.W.; Zariwala, H.A.; Gu, H.; Ng, L.L.; Palmiter, R.D.; Hawrylycz, M.J.; Jones, A.R.; et al. A robust and high-throughput cre reporting and characterization system for the whole mouse brain. *Nat. Neurosci.* **2010**, *13*, 133–140. [CrossRef]
212. Hartmann, D.A.; Underly, R.G.; Watson, A.N.; Shih, A.Y. A murine toolbox for imaging the neurovascular unit. *Microcirculation* **2015**, *22*, 168–182. [CrossRef]
213. Ostrowski, L.E.; Hutchins, J.R.; Zakel, K.; O'Neal, W.K. Targeting expression of a transgene to the airway surface epithelium using a ciliated cell-specific promoter. *Mol. Ther. J. Am. Soc. Gene Ther.* **2003**, *8*, 637–645. [CrossRef]

214. Johnson, B.A.; Coutts, M.; Vo, H.M.; Hao, X.; Fatima, N.; Rivera, M.J.; Sims, R.J.; Neel, M.J.; Kang, Y.J.; Monuki, E.S. Accurate, strong, and stable reporting of choroid plexus epithelial cells in transgenic mice using a human transthyretin bac. *Fluids Barriers CNS* **2018**, *15*, 22. [CrossRef] [PubMed]
215. Xin, H.B.; Deng, K.Y.; Rishniw, M.; Ji, G.; Kotlikoff, M.I. Smooth muscle expression of cre recombinase and egfp in transgenic mice. *Physiol. Genom.* **2002**, *10*, 211–215. [CrossRef]
216. Cuttler, A.S.; LeClair, R.J.; Stohn, J.P.; Wang, Q.; Sorenson, C.M.; Liaw, L.; Lindner, V. Characterization of pdgfrb-cre transgenic mice reveals reduction of rosa26 reporter activity in remodeling arteries. *Genesis* **2011**, *49*, 673–680. [CrossRef] [PubMed]
217. Girbl, T.; Lenn, T.; Perez, L.; Rolas, L.; Barkaway, A.; Thiriot, A.; Del Fresno, C.; Lynam, E.; Hub, E.; Thelen, M.; et al. Distinct compartmentalization of the chemokines cxcl1 and cxcl2 and the atypical receptor ackr1 determine discrete stages of neutrophil diapedesis. *Immunity* **2018**, *49*, 1062–1076. [CrossRef] [PubMed]
218. Zipfel, W.R.; Williams, R.M.; Christie, R.; Nikitin, A.Y.; Hyman, B.T.; Webb, W.W. Live tissue intrinsic emission microscopy using multiphoton-excited native fluorescence and second harmonic generation. *Proc. Natl. Acad. Sci. USA* **2003**, *100*, 7075–7080. [CrossRef] [PubMed]
219. Nam, M.H.; Baek, M.; Lim, J.; Lee, S.; Yoon, J.; Kim, J.; Lee, M.S.; Soh, K.S. Discovery of a novel fibrous tissue in the spinal pia mater by polarized light microscopy. *Connect. Tissue Res.* **2014**, *55*, 147–155. [CrossRef]
220. Iliff, J.J.; Wang, M.; Liao, Y.; Plogg, B.A.; Peng, W.; Gundersen, G.A.; Benveniste, H.; Vates, G.E.; Deane, R.; Goldman, S.A.; et al. A paravascular pathway facilitates csf flow through the brain parenchyma and the clearance of interstitial solutes, including amyloid beta. *Sci. Transl. Med.* **2012**, *4*, 147ra111. [CrossRef]

International Journal of
Molecular Sciences

MDPI

Article

Regional Differences in Tight Junction Protein Expression in the Blood–DRG Barrier and Their Alterations after Nerve Traumatic Injury in Rats

Thomas J. Lux [1], Xiawei Hu [1], Adel Ben-Kraiem [1], Robert Blum [2], Jeremy Tsung-Chieh Chen [1,*,†] and Heike L. Rittner [1,*,†]

[1] Department of Anaesthesiology, University Hospital of Wuerzburg, 97074 Wuerzburg, Germany; thomas.lux@stud-mail.uni-wuerzburg.de (T.J.L.); xiawei_hu@163.com (X.H.); Ben_A@ukw.de (A.B.-K.)
[2] Institute of Clinical Neurobiology, University Hospital of Wuerzburg, 94074 Wuerzburg, Germany; Blum_R@ukw.de
* Correspondence: chen_j1@ukw.de (J.T.-C.C.); rittner_h@ukw.de (H.L.R.); Tel.: +49-931-170-7870047 (H.L.R.)
† These authors contributed equally to this work.

Received: 9 December 2019; Accepted: 28 December 2019; Published: 31 December 2019

Abstract: The nervous system is shielded by special barriers. Nerve injury results in blood–nerve barrier breakdown with downregulation of certain tight junction proteins accompanying the painful neuropathic phenotype. The dorsal root ganglion (DRG) consists of a neuron-rich region (NRR, somata of somatosensory and nociceptive neurons) and a fibre-rich region (FRR), and their putative epi-/perineurium (EPN). Here, we analysed blood–DRG barrier (BDB) properties in these physiologically distinct regions in Wistar rats after chronic constriction injury (CCI). *Cldn5*, *Cldn12*, and *Tjp1* (rats) mRNA were downregulated 1 week after traumatic nerve injury. Claudin-1 immunoreactivity (IR) found in the EPN, claudin-19-IR in the FRR, and ZO-1-IR in FRR-EPN were unaltered after CCI. However, laser-assisted, vessel specific qPCR, and IR studies confirmed a significant loss of claudin-5 in the NRR. The NRR was three-times more permeable compared to the FRR for high and low molecular weight markers. NRR permeability was not further increased 1-week after CCI, but significantly more $CD68^+$ macrophages had migrated into the NRR. In summary, NRR and FRR are different in naïve rats. Short-term traumatic nerve injury leaves the already highly permeable BDB in the NRR unaltered for small and large molecules. Claudin-5 is downregulated in the NRR. This could facilitate macrophage invasion, and thereby neuronal sensitisation and hyperalgesia. Targeting the stabilisation of claudin-5 in microvessels and the BDB barrier could be a future approach for neuropathic pain therapy.

Keywords: tight junction; claudin-5; neuropathic pain; nerve injury; dorsal root ganglion

1. Introduction

Neuropathic pain is defined as a "pain caused by a lesion or disease of the somatosensory nervous system". The etiologies range from metabolic conditions like diabetes mellitus, autoimmune disorders, infectious diseases and chemotherapy-induced neuropathies to traumatic nerve injury and postoperative conditions. Overall, 7–10% of the general population are affected, and their quality of life is significantly lowered [1]. The heterogeneity of etiologies leading to neuropathic pain indicates that a multitude of not yet understood factors participate in the pathogenesis of neuropathic pain [2]. A causative therapy is currently often impossible [3]. While conventional analgesics, e.g., cyclooxygenase inhibitors such as ibuprofen, have little effect on neuropathic pain, symptomatic treatments include antidepressants, antiepileptics, and opioids, but the efficacy of these drugs is moderate [2]. Attempts to develop pathophysiology-oriented drugs have not delivered the desired

results at this point. A better understanding of the mechanisms behind neuropathic phenotypes, therefore, is necessary to find new diagnostic and therapeutic approaches.

Several distinct animal models are used for research in neuropathy. Models are separated into peripheral nerve injury, central pain, drug-induced neuropathy, and disease-induced approaches [4]. Since the introduction of the chronic constriction injury (CCI) model for traumatic neuropathy in 1988 [1], it has been commonly used to understand the pathophysiology of mononeuropathies. Animals are subjected to four ligations of the sciatic nerve, which cause focal ischemia, intraneural edema, and Wallerian degeneration, and subsequently, regeneration. This results in a behavioral phenotype with signs of spontaneous pain and thermal and mechanical hypersensitivity [2]. Hypersensitivity reaches its maximum after 7 d [5], but nociceptive thresholds return to normal within the next 3–6 weeks depending on the noxious stimulus [6]. The local (inflammatory) reaction caused by cell damage at the ligature site does not explain the phenotype after CCI sufficiently. Changes in the dorsal root ganglion (DRG), such as infiltration of macrophages (ED1 for CD68 in rats) and CD8+ lymphocytes have been reported [7]. Furthermore, sprouting of sympathetic axons into the DRG after CCI has been observed [8]. These findings are thought to participate in the pathogenesis of traumatic mononeuropathies. Only about 30% of the neurons of the L4/5 DRGs are afferences from the sciatic nerve. Since other areas of the L4/5 dermatome show few to no changes after CCI, a combination of neuronal and environmental changes must be elementary. Electrophysiological and histopathological studies identified reduced nerve conduction velocity and axonal damage, as correlates of A-fiber damage and sensitization of C-fibers, as probable causes for this phenotype.

Even slight environmental changes disrupt physiological function of neural tissues. Therefore, the entry points to the nervous system are protected. Highly specialized barriers guard myelinated fibers (myelin barrier, MB), the peripheral nerve (blood–nerve barrier), the DRG (blood–DRG barrier, BDB), the spinal cord (blood–spinal-cord barrier), and the brain (blood–brain barrier). The names originate from the protected region, and each of them can be subdivided into the different tissue interfaces, e.g., the endothelial vessels or the perineurium, each fulfilling different physiological demands. Key features for this sealing function are tight junction proteins. The specific tight junction protein composition determines the barriers characteristics. While many of these characteristics are similar in the blood–nerve barrier and blood–brain barrier, distinct features, such as absence of several neurotransmitter transporters and lack of astrocytes in the periphery, qualify the blood–nerve barrier as a specialized, unique structure [9].

After axonal injury or acute demyelination, extravasation of blood-borne molecules such as albumin and intraneural edema as correlates of blood–nerve barrier leakage can be observed [10]. Studies of the blood–nerve barrier in nerve injury models have revealed downregulation of *Cldn1*, *Cldn5*, *Ocln*, *Tjp1* (ZO-1) and *Jam3* (JAMC) mRNA in the sciatic nerve [10–14] as well as *Tjp1* (ZO-1), *Cldn5* and *Ocln* in the spinal cord of rats [15,16]. Similar studies observed reductions of *Cldn1* and *Tjp1* (ZO-1) mRNA and immunoreactivity (IR) in the sciatic nerves of mice [13]. Endothelial cells of the blood–nerve barrier are disrupted with increased permeability as soon as 6 h after CCI surgery, while the neuropathic phenotype develops over days [9]. So, barrier disruption occurs early after nerve injury even before hypersensitivity.

Surprisingly, the BDB has barely been studied before. Regions in the DRG can be divided: Somata of primary sensory neurons reside in DRGs (neuron rich region (NRR)) in contrast to fiber rich regions (FRR). It is known that the BDB is considerably more permeable and contains a higher density of capillaries [17–19]. Claudin-5 IR was detected in the NRR, while claudin-1 and occludin were found in the FRR [19]. However, no quantitative data of either protein or mRNA in all areas, including epi-/perineurium (EPN), are currently available in naïve animals or after neuropathy. Furthermore, whole tissue analysis can be insensitive to small changes of specific barriers and novel techniques, making selective analysis necessary.

In this study, we wanted to fully characterize the BDB and its alteration in neuropathy. To this end, we defined four regions in the DRG: the neuron-rich and the fiber-rich regions (NRR,

FRR), and their putative epi-/perineurial regions (NRR-EPN, FRR-EPN). We used these regions and region-selective techniques to analyze typical tight junction proteins known from the blood nerve and myelin barrier in control rats and in neuropathy and evaluated functional properties of the BDB. Tight junction proteins, including claudin-1, were detected in the nerve perineurium, claudin-5 was found in endoneurial vessels, ZO-1 was ubiquitously detected in the nerve, and claudin-12 and 19 were present in Schwann cells.

2. Results

2.1. Claudin-1, Claudin-19, and ZO-1 Immunoreactivity Is Tissue Specific in Rat DRGs

To characterize the BDB and its molecular structure, we quantified the immunoreactivity (IR) in the DRG, considering its different regions. After separating the DRGs distinct areas, claudin-1, claudin-5, claudin-12, claudin-19, and ZO-1, IR was semi-quantified and compared between the NRR, FRR, and the putative EPN of DRGs after CCI.

While claudin-1 IR was up to five times higher in the EPN as in the inner regions of the DRG (Figure 1b,f), claudin-19 IR was highest in the FRR (Figure 1d,f) and ZO-1 IR was highest in the FRR-EPN (Figure 1e,f). Claudin-5 and claudin-12 expressions were not region specific. The mean intensity of claudin-5 IR was low, but areas with strong signals, mostly associated with claudin-1 signals, were observed (Figure 3). In brightfield images, these areas resembled vessels. This was also seen for ZO-1-IR, which was expressed in the structures resembling capillaries and in the EPN. Claudin-12 was not only found in putative Schwann cell structures, but neurons as well. In contrast, claudin-19-IR was detected in typical paranodal structures of Schwann cells.

2.2. Nocifensive Responsiveness after Nerve Injury

We next wanted to test whether neuropathy results in alterations of the BDB. To demonstrate the validity of the neuropathy CCI model, mechanical nociceptive thresholds were recorded for both rear limbs before and one week after CCI via the von-Frey test.

While there was no change in the sensitivity in the contralateral paw, the limb with nerve injury exhibited a decrease of the mechanical withdrawal threshold to 34% of the previous baseline value (Figure 2), indicating mechanical hypersensitivity in neuropathy.

2.3. Downregulation of Tight Junction Protein mRNA Expression after CCI in Rodents

For evaluation of tight junction protein expression patterns during CCI, we analyzed the mRNA levels of *Cldn1*, *Cldn5*, *Cldn12*, *Cldn19,* and *Tjp1* (ZO-1) in rats' whole DRGs. The expression levels of *Cldn5*, *Cldn12*, and *Tjp1* (ZO-1) mRNA were reduced by 28%, 45% and 26%, respectively after CCI compared to sham (Figure 3).

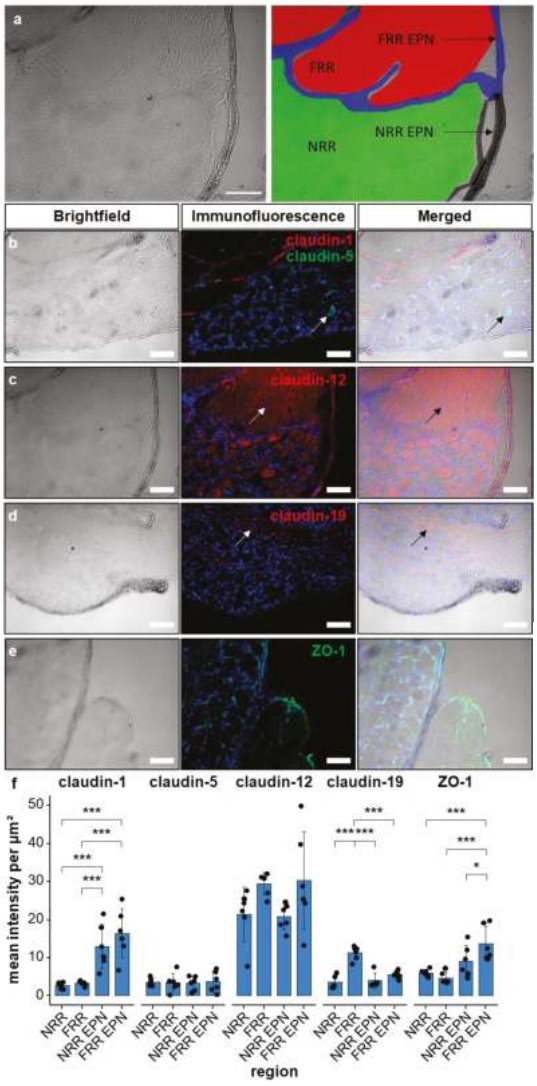

Figure 1. Claudin-1 immunoreactivity (IR) and ZO-1 IR are preferentially found in epi-/perineurium in rats' dorsal root ganglia (DRGs), while claudin-19 IR is most abundant in the fiber-rich region. Classification into neuron rich region (NRR, green), NRR epi-/perineurium (EPN, black), fiber rich region (FRR, red), and FRR-EPN (blue) is shown in (**a**). Control DRG sections (CL) from Wistar rats were immunostained. IRs of claudin-1, claudin-5, and ZO-1 were quantified and compared between NRR and FRR, together with their putative EPN. Representative stainings for claudin-1 (red), claudin-5 (green) (**b**), claudin-12 (**c**), claudin-19 (**d**), and ZO-1 (**e**) are shown. Arrows point to structures identified as vessels (**b**), Schwann cells (**c**), and paranodes of Schwann cells (**d**). Quantification of the signal intensity in the specified areas (**f**). (Scale bars = 100 µm; $n = 5$ or 6; claudin-1: NRR versus NRR-EPN, NRR versus FRR-EPN, FRR versus NRR-EPN, and FRR versus FRR-EPN: $p < 0.0001$; ZO-1: FRR-EPN versus NRR: $p = 0.0003$; FRR-EPN versus NRR-EPN: $p = 0.0138$; FRR-EPN versus NRR: $p = 0.00018$. No normal distribution: ZO-1 FRR. No variance homogeneity: claudin-1. Two-way ANOVA, Tukey HSD. * $p < 0.05$, *** $p < 0.001$).

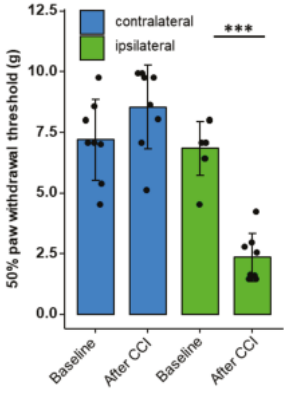

Figure 2. Mechanical hypersensitivity in rats after chronic constriction injury (CCI). Male Wistar rats underwent chronic constriction injury (CCI). Mechanical nociceptive thresholds were evaluated before and one week after CCI (n = 8, Von-Frey test; repeated measures ANOVA, *** $p < 0.001$).

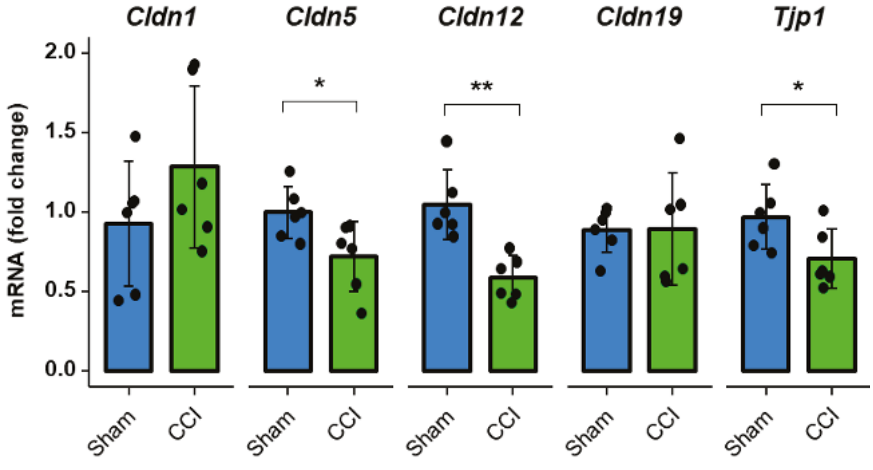

Figure 3. Tight junction protein mRNA expression in rat DRGs is downregulated one week after CCI. Wistar rats were treated with CCI. Relative mRNA expressions of *Cldn1*, *Cldn5*, *Cldn12*, *Cldn19*, and *Tjp1* (ZO-1) in comparison to sham operated animals were analyzed with qPCR after one week. (n = 6; *Cldn5*: $p = 0.0338$; *Cldn12* $p = 0.0021$, *Tjp1* (ZO-1) $p = 0.0419$. No variance homogeneity: *Cldn19* rats. Welch two-sample t-test, Wilcoxon rank sum test: * $p < 0.05$, ** $p < 0.01$).

2.4. Claudin-5 Expression in Vessels Is Reduced Only in the NRR after CCI

Comparison of the tight junction protein IR between naive and CCI rats in the distinct regions did not reveal significant differences (Figures 4 and 5). Only a tendency was observed for claudin-12 in the FRR and claudin-19 for the FRR-EPN ($p = 0.057$).

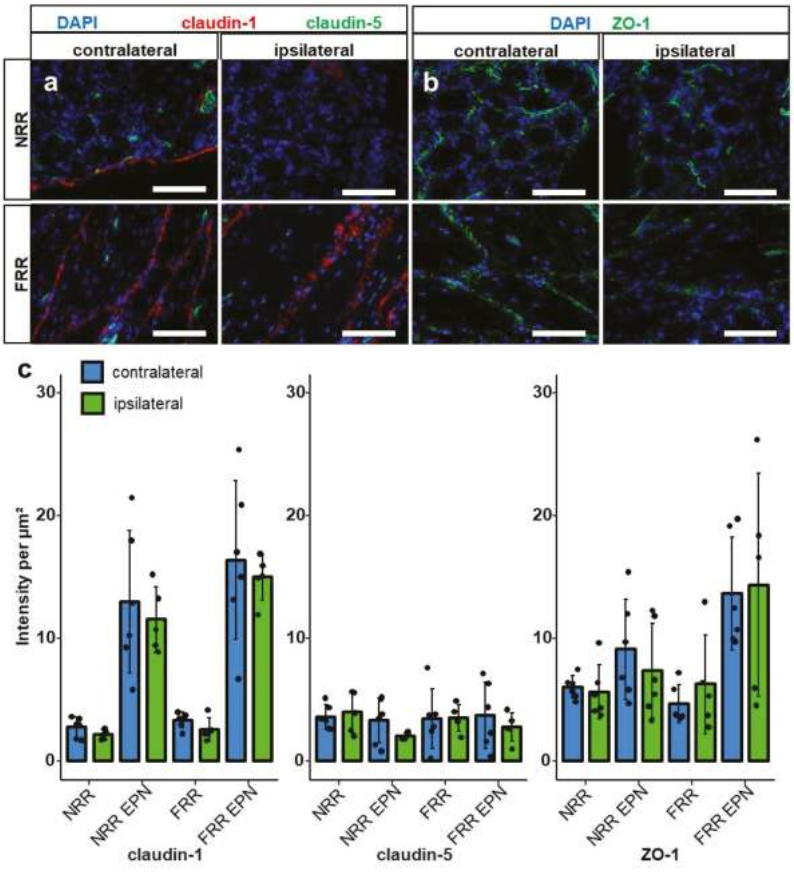

Figure 4. Claudin-1 and ZO-1 IR are unchanged after CCI. DRG sections from Wistar rats with 7 d CCI and naïve controls were immunostained. IRs of claudin-1, claudin-5, and ZO-1 were quantified and compared between IL and CL DRGs after CCI in the neuron rich region (NRR) and fiber rich region (FRR), and their putative EPN are presented as light intensity per μm^2. Representative sections of claudin-1 (red) and claudin-5 (green) (**a**), and ZO-1 (green) (**b**) are shown. Quantification of the signal intensity in the specified areas: significant differences between regions were not indicated, as they are already analyzed in Figure 1 (**c**). (Scale bars = 100 µm. $n = 5$ or 6; claudin-1: NRR versus NRR-EPN, NRR versus FRR-EPN, FRR versus NRR-EPN, and FRR versus FRR-EPN: $p < 0.0001$; ZO-1: FRR-EPN versus NRR: $p = 0.0003$; FRR-EPN versus NRR-EPN: $p = 0.0138$; FRR-EPN versus NRR: $p = 0.00018$. No normal distribution: ZO-1 CL FRR. No variance homogeneity: claudin-1 CL. Two-way ANOVA, Tukey HSD).

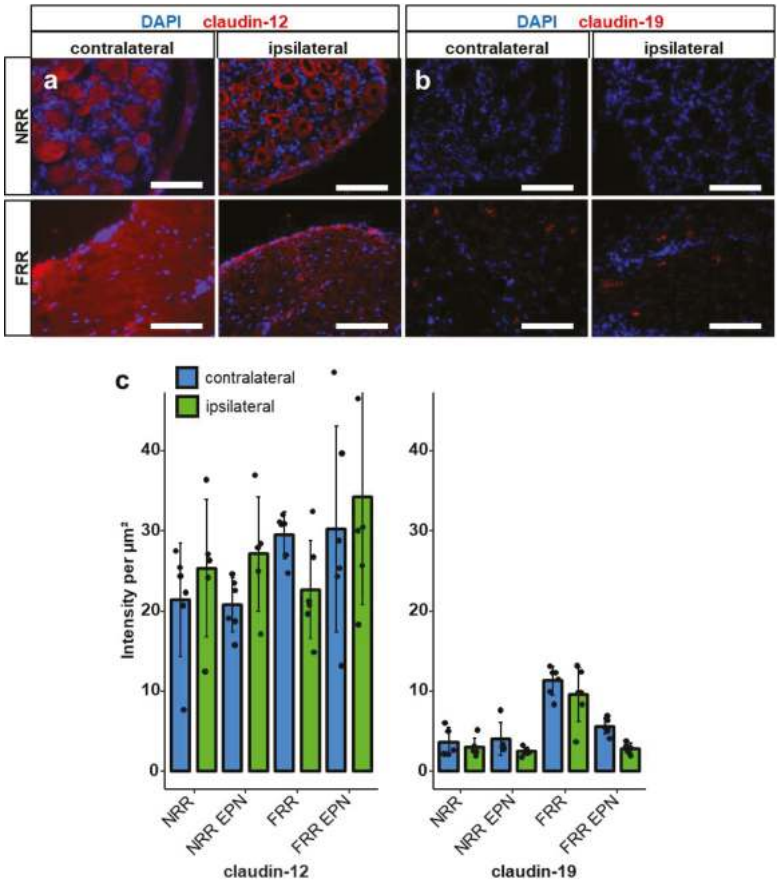

Figure 5. Claudin-19 and claudin-12-IR are unaltered after CCI. After CCI, DRG sections of Wistar rats were immunostained. IRs of claudin-12 and claudin-19 were quantified as light intensity per μm^2. and compared between IL and CL DRGs after CCI in the NRR and FRR, and their putative EPNs. Representative sections of claudin-12 (red) (**a**) and claudin-19 (red) (**b**) are shown. Quantification of the signal intensity in the specified areas: significant differences between regions are not indicated, as they were already analyzed in Figure 1 (**c**). (Scale bars = 100 µm. $n = 5$ or 6; claudin-19: FRR versus NRR, FRR versus NRR-EPN, and FRR versus FRR-EPN: $p < 0.0001$. No normal distribution: claudin-19 CL NRR-EPN. Two-way ANOVA, Tukey HSD).

Since the method is optimized for homogenously expressed proteins and lacks sensitivity for proteins with clustered expression, e.g., in vessels, we analyzed claudin-5 using a different approach. We co-stained the tissue with von Willebrand Factor (vWF) to analyze capillaries in the NRR and FRR (Figure 6). Selective analysis of vessels revealed higher vWF IR in vessels of the FRR compared with the NRR, but no change after CCI. Analysis of claudin-5 within vessels could also show higher IR in the FRR than in the NRR area. Most importantly, we observed a reduction of claudin-5 signal in the vessels of the NRR after CCI.

To verify these results on a mRNA level, we dissected capillaries from the FRR and the NRR by laser dissection in sham and CCI rats 1 d to reflect the mRNA alterations preceding protein expression. No changes were observed for *Vwf* and *Cldn5* mRNA in the FRR, but *Cldn5* was significantly downregulated in the NRR.

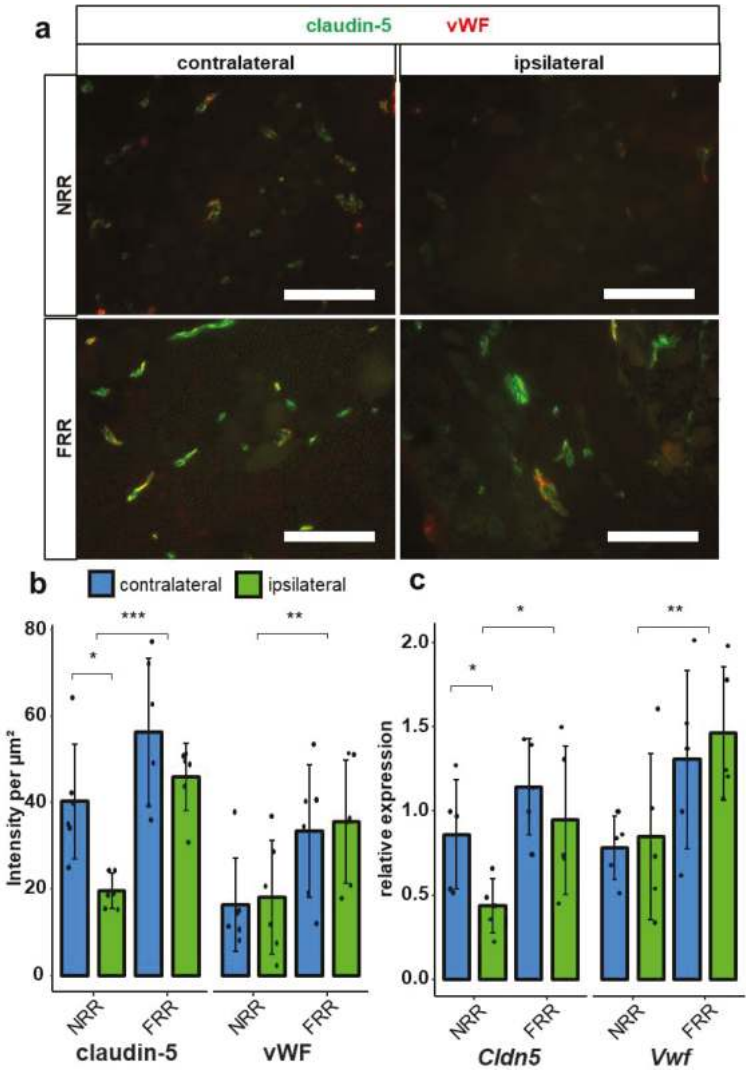

Figure 6. Claudin-5 IR within vessels and *Cldn5* mRNA in the NRR are reduced in rat DRGs. DRG sections from Wistar rats after CCI were immunostained. Quantification of claudin-5 and van Willebrand factor (vWF) IRs and comparison between IL and CL DRGs after CCI in the NRR and FRR as light intensity per μm^2. Tissue samples from the NRR and vessels of the FRR were obtained using laser microdissection (LMD). Claudin-5 and vWF mRNA were quantified as relative expression (to GAPDH) via RT-qPCR. Representative sections of co-stainings with claudin-5 (green) and vWF (red) (**a**). Quantification of the claudin-5 and vWF IR (**b**) $n = 6$; claudin-5: FRR versus NRR, $p = 0.000261$; NRR: CL versus CCI, $p = 0.02985$; vWF: NRR versus FRR, $p = 0.00515$. No normal distribution: claudin-5 FRR CCI, vWF NRR CL. No variance homogeneity: claudin-5 FRR. Two-way ANOVA, Tukey HSD.) And quantification of mRNA expression (**c**) $n = 5$; *Cldn5*: NRR versus FRR, $p = 0.0136$; CL versus IL: $p = 0.0448$; *Vwf*: NRR versus FRR, $p = 0.00838$; two-way ANOVA, Tukey HSD) in the specified areas. (Scale bars = 100 µm. * $p < 0.05$, ** $p < 0.01$, *** $p < 0.001$.) All results are summarized in Table 1.

Table 1. Regional expression of tight junction proteins within rat DRGs. Neuron-rich region (NRR), fiber-rich region (FRR), epi-/perineurium (EPN).

Protein	Expression Pattern
Claudin-1	NRR-EPN and FRR-EPN > NRR and FRR
Claudin-5 (in vessels)	FRR > NRR
ZO-1	FRR-EPN > NRR, FRR, NRR-EPN
Claudin-19	FRR > NRR, NRR-EPN, FRR-EPN

2.5. Permeability of the DRG and Migration of Macrophages

To finally evaluate functional properties of the BDB, we established an assay for vessel permeability with FITC-dextran (70 kDa). After intravenous application, the dye accumulated in the perineurium and within vessels, diffusing a few micrometers into the tissue. Hence, the NRR was 2.35 times more permeable than the FRR; however, no difference after CCI was observed (Figure 7). In the next step, we analyzed the permeability for small molecules using Hoechst reagent (562 Da) after systemic administration in vivo. Hoechst reagent ubiquitously diffused into the tissue and then stained nuclei. We detected significantly higher (3.51 times) permeability in the NRR region compared to the FRR but no change after CCI.

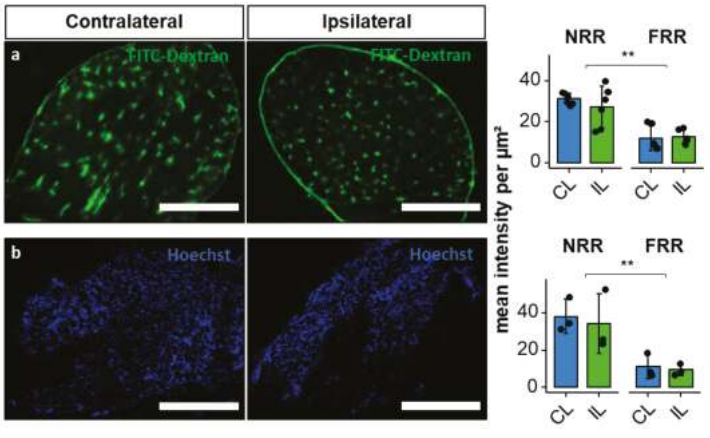

Figure 7. Blood–DRG barrier (BDB) permeability for large molecules in the NRR is higher compared to FRR of DRGs, but has no change after CCI. Wistar rats after 7 d CCI were perfused with FITC-dextran ((**a**), 70 kDa) and Hoechst reagent ((**b**), 562 Da). NRR and FRR of ipsilateral (IL) and contralateral (CL) DRG sections were analyzed. Representative images of the IL show comparable IR. Quantification of FITC-dextran ($n = 6$, NRR versus FRR: $p < 0.001$; two-way ANOVA, Tukey HSD) and Hoechst ($n = 3$, NRR versus FRR $p = 0.002$; two-way ANOVA, Tukey HSD) Immunofluorescence as intensity per µm^2. (Scale bars = 100 µm; ** $p < 0.01$.)

CD68$^+$ cells and CD68 immunoreactivity was quantified in the NRR in naive animals DRGs, and contralateral and ipsilateral DRGs after CCI to assess macrophage migration (Figure 8). CD68$^+$ cells per µm^2 were significantly increased in the IL DRGs after CCI compared to CL, while there was only a tendency ($p = 0.065$) compared to naive DRGs. The anti-CD68 immunoreactivity per µm^2 was significantly higher in IL DRGs after CCI, compared to naive DRGs.

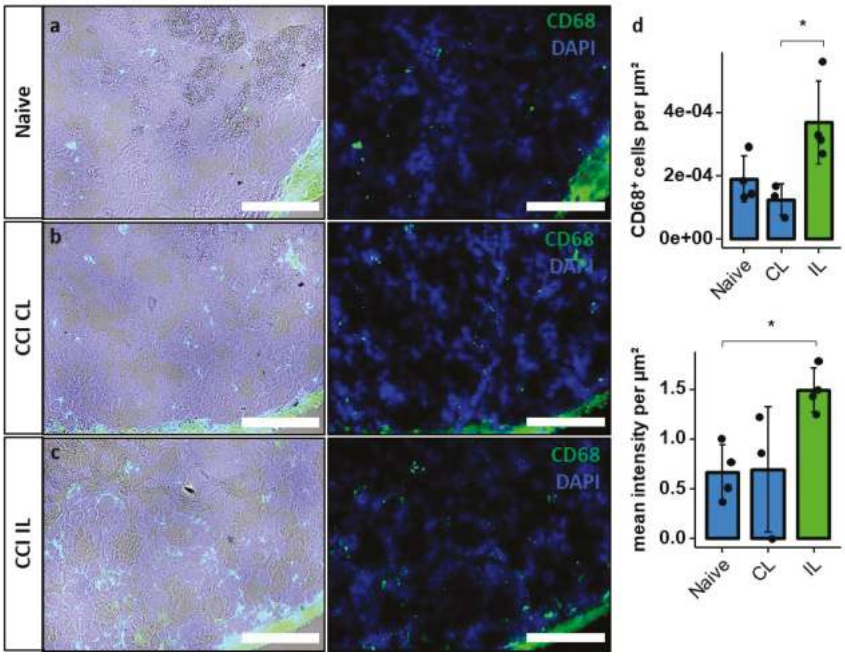

Figure 8. Increased macrophage invasion in the NRR after CCI. DRGs of naive (**a**) and contralateral (CL) (**b**) and ipsilateral (IL) (**c**) DRGs of Wistar rats 7d after CCI were harvested and stained using DAPI and anti-CD68 antibodies (left: immunofluorescence with brightfield; right: only immunofluorescence). In the NRR, CD68+ cells were counted manually, and signal intensity was measured. Both were quantified per μm^2 (**d**). (n = 3 or 4; CD68+ cells per μm^2: CL versus IL, $p = 0.024$; mean intensity per μm^2: Naive versus IL, $p = 0.038$. Two-way ANOVA, Tukey HSD; scale bars = 100 µm; * $p < 0.05$).

3. Discussion

In our study we further characterized the BDB and examined whether traumatic neuropathy not only results in blood–nerve barrier and blood spinal cord barrier breakdown but also affects the BDB. We revealed higher ZO-1 expression in the FRR EPN compared to the NRR and observed regional expression differences for claudin-1 (highest expression in NRR ENP and FRR EPN), claudin-5 (higher expression in the FRR compared to the NRR), and claudin-19 (highest expression in the FRR), as indicated in Table 1. After CCI, claudin-5 IR and *Cldn5* mRNAs were selectively reduced in the vessels of the NRR. The NRR containing somatosensory neurons was 2–3 times more permeable to low and high molecular weight dyes compared to the nerve fiber area with no further increase in permeability after CCI. However more CD68+ macrophages migrated into the NRR.

While the blood–nerve barrier is focus of current literature, the BDB is, so far, almost neglected. As an imperative link between the peripheral nerve and the spinal cord, open questions should be discussed more thoroughly, as they could reveal important knowledge for understanding the peripheral sensory system. The BDB is very similar to the blood–nerve barrier regarding morphology and tight junction protein composition, but its NRR barrier is leaky in its physiological state compared to the blood–nerve barrier. In accordance with our data, intravenously injected Hoechst dye or FITC-dextran diffusion out of capillaries can already be observed in DRGs of naive rats, while dyes only accumulate in peripheral nerves after blood–nerve barrier breakdown [18,20]. A clinically relevant consequence of these characteristics is the accumulation of drugs in the DRG, which can be favorable in case of opioids or undesirable in case of chemotherapeutic drugs causing neuropathies. This hints towards a concept of the DRG being more than a simple relay-station, but being an important signal modulator sensitive

to endogenous and exogenous stimuli [21]. In addition to molecules, cells can migrate into the DRG. Macrophages reside in the DRG and further migrate into the DRG to shape an immune response in neuropathy [22,23]. So, opening of the BDB could facilitate these pathophysiological processes.

We identified that claudin-1, a major sealing tight junction protein, is predominantly expressed in the EPN of both the NRR and the FRR, as they show the highest claudin-1 IRs. *Cldn1* KO is lethal due to dehydration, as claudin-1 is key component of the epidermal barrier in the stratum granulosum in mice [24]. Besides this and other vital functions, claudin-1 is physiologically expressed in the peripheral and central nervous system as part of the blood–nerve barrier and blood–brain barrier. Studies of peripheral nerves observed high expression of *Cldn1* in the perineurium [13,25,26], but also in Schmidt-Lantermann incisures, paranodal loops of myelinating Schwann cells, and the mesaxon [8,27]. Previous studies performed on rats [12,28] and mice [13] also described a reduction of *Cldn1* mRNA and protein levels in the sciatic nerve after nerve injury. Downregulation of *Cldn1* mRNA starts around 3 h after CCI, and is lowest after 7 d [12]. In the DRG, we determined no significant differences of *Clnd1* mRNA in the whole DRG and claudin-1-IR in the subregions between naïve and CCI groups. Therefore, the EPN around rat DRGs seems not to be affected by CCI, although it is possible that intraspecies differences exist for mice, and more importantly, humans, in this and other barrier proteins.

Expression of claudin-12 by glial cells has been observed in the blood–brain barrier [29,30] and blood–nerve barrier [31]. We confirmed *Cldn12* mRNA expression in the DRG. High levels of claudn-12 IR were detected within the somata, and in or around the fibers of neurons. The role of claudin-12 during nerve injury has not been examined yet. In our study, *Cldn12* mRNA was downregulated after CCI in the DRG. Even though we could not observe lower claudin-12 IR, the signal morphology seems disturbed from a more homogenous to a clustered distribution after CCI. While the biological relevance of the signal in the soma is unclear, the distribution and the change of claudin-12 after CCI should certainly be investigated further.

Claudin-19 is expressed in myelinating glia cells in the PNS, but not the CNS [32]. Tight junction formation in myelinating cells is disrupted without claudin-19 [33]. *Cldn19* KO mice are fertile and vital, but show the phenotype of a peripheral neuropathy, causing mainly motor defects, but in 50%, nerve conduction deficits as well [32]. In our study, claudin-19 IR was clustered and highest in the FRR, and in the space between the neurons' somata in the NRR. These clusters could very well resemble the paranodal regions, like those already described in the sciatic nerve [31]. In agreement previous findings of claudin-19 expression in vessels and the perineurium, there were low signals in the EPNs of both regions [32], although we have previously seen this in the nerve [34]. Neither *Cldn19* mRNA levels nor claudin-19 IR were altered in the DRG proximal to the CCI injury.

ZO-1, an intracellular tight junction associated protein, forms complexes with claudin-1 and is required for correct arrangement of tight junctions [33]. *Tjp1*-KO is lethal, and disruption has been linked to neurological disorders [35]. ZO-1 is mostly expressed in the perineurium [31], vessels, and myelinated Schwann cells in the sciatic nerves of humans [31] and mice [36]. In our study, ZO-1 IR signal was detected predominantly in the EPN, like claudin-1's IR, and in clustered regions in all areas. The ZO-1 clusters colocalized with claudin-5, and are, therefore, most likely vessels. *Tjp1* was downregulated in whole DRGs. In our IF study, we detected the highest levels of ZO-1 IR expression in the FRR-EPN but no alterations after CCI. These findings match with the existing data from studies in the mouse sciatic nerve [36].

Considered the most important tight junction protein of the brain barrier, *Cldn5* mRNA expression is >100-fold higher than other tight junction protein expression in endothelial cells [37]. While *Cldn5* KO mice are macroscopically vital, increased brain barrier permeation by molecules of <800 Da and death 10 d after birth were observed [38]. In the blood–nerve barrier, *Cldn5* is expressed in the endoneurial vessels, and the myelinating Schwann cells of humans [31] and rats [39]. In costainings, claudin-5 IR colocalized with vWF, indicating vessel-specific location. The density of claudin-5 IR within vessels was higher in the FRR than in the NRR. This was accompanied by lower permeability for FITC-dextran and Hoechst dye in the FRR. Therefore, we assume lower claudin-5 expression in vessels as a key-factor

for leakiness of the NRR's BDB under physiological conditions. A downregulation of *Cldn5* mRNA in the blood–nerve barrier has consistently been reported after nerve injury in rats [12,28]. In whole DRGs, we observed a *Cldn5* mRNA downregulation. Regional quantification of mean IR within vessels and regional *qPCR* also revealed claudin-5 downregulation after CCI, but only in the NRR. A lower *Cldn5* expression could significantly impact the function of the BDB, making it even more permeable for potentially harmful substances and immune cell invasion. Indeed, we confirmed increased invasion of macrophages in our model in the ipsilateral DRG after CCI, as shown previously in rats [22] and mice [23]. To evaluate possible BDB breakdown regarding permeability for small and large molecules, we performed a perfusion assay with FITC-dextran and Hoechst reagent as representative molecules with high and low molecular weights. We could detect higher permeation for both reagents in the NRR compared to the FRR but no change 1-week after CCI. Even though claudin-5 downregulation in brain vessels results in barrier breakdown accompanied by permeation of small molecules, there are several explanations as why we could not detect this in the DRG: Firstly, the permeability of the NRR in CL DRGs is high, so additional claudin-5 might have little additional impact. Secondly, our permeability assays were established in experimental setups where the baseline showed little to no signal, and therefore, were optimized to detect differences in "low-signal" scenarios. Therefore, high saturations probably caused lower sensitivity. Thirdly, possible compensatory mechanisms might prevent a further increase of BDB permeability, such that there simply is no change. Further studies investigating the BDB after, e.g., long-term CCI or impact of claudin-5 on immune cell migration could clarify these questions.

The structural peculiarities of the DRG are not very well understood: DRG neurons have no afferent synapses and the precise function of the pseudo-unipolar feature is still not known. The somata reside at the end of the T-stem; nevertheless, afferent spikes are connected to the cell bodies and many DRG neurons exhibit specialized membrane characteristics, necessary for the initiation of action potentials. The role of these membranes in signal transmission or generation is not known. Why is the DRG or at least the NRR not as well protected as the nerve? What are the implications? Indeed, not only capillaries but also satellite cells surrounding neurons are permeable. Marker molecules in the extracellular space can access the soma membrane of DRG neurons by diffusion independent of neuropathy [40]. It is, therefore, possible that DRGs carry out some as-yet unidentified chemosensory functions associated with the body's internal milieu. Interference with this delicate homeostasis might lead to increased sensitivity in neuropathy [41]. Interestingly, selectively silencing ectopic activity in the DRG with low dose local anesthetics in neuropathy reduces hypersensitivity [42]. Hypersensitivity could have been triggered by proalgesic molecules bypassing the BDB in neuropathy.

Both methods used, qPCR and IHC, provide specific insights into biological systems within their limitations: The great sensitivity of qPCR can prove even slight changes, but provides spatial resolution only if laser dissection is performed in addition. Furthermore, qPCR data need to be correlated with protein data to generate viable evidence. Antibody-based protein labelling on the other hand, provides an insight into expression and distribution in situ, if a sensitive and specific antibody is used. In our study mRNA data did not fully match our IHC results. While mRNA levels do not necessarily correlate with protein expression, methodological aspects also must be considered, especially for *Cldn5* expression. Whole DRG and LSM qPCR showed a significant difference between *Cldn5* mRNA levels after CCI. Our first method of semi quantification lacks sensitivity regarding proteins, which are not homogenously distributed within one specified region. Therefore, we opted to analyze claudin-5 IR in the vessel area in addition. In summary, tight junctions in the DRG can only be studied sufficiently if different tissues are analyzed separately.

What are the clinical implications? One obvious problem in pain research is the lack of suitable biomarkers and objective measures of pain—especially possible malfunctions of the pain pathway in the primary afferent neuron in the pain pathway [43]. Thus, imaging of the DRG could fill this gap in certain painful conditions. Indeed, alterations of DRG volume have been noted in chemotherapy-induced neuropathy, and two genetic diseases, Fabry disease and neurofibromatosis [44–48]. Alterations in the

permeability at the blood tissue interface have been observed in long-standing Fabry disease in the NRR, indicating a concomitant dysfunctional DRG perfusion [47,48]. In the case of Fabry disease, this observation could to be the consequence of glycolipid accumulation. Unfortunately, pain intensity was not examined in the study. Also, it is not known so far, whether other types of neuropathic pain, including nerve injury or metabolic diseases, also have alterations in the BDB, and specifically, an increased leakage, as observed in the nerve [49]. Nevertheless, magnetic resonance imaging and BDB permeability could be very early in vivo markers for involvement of the peripheral nervous system. Secondly, if BDB breakdown is clinically relevant and contributes to pain generation then stabilization of the BDB (e.g., the wnt [34] and hedgehog pathway [12], as shown for the blood–nerve barrier) could also improve pain relief. Claudin-5 is regulated by steroids [50]. So, one might speculate that the epidural steroids used in the clinic could also improve BDB barrier sealing. Thirdly, the leaky BDB—already under baseline conditions—could facilitate targeting of the ectopic firing from the DRG for pain treatment, e.g., via dilute local anesthetics [42,51].

4. Materials and Methods

4.1. Animals

Twenty 8–12 weeks old male rats Wistar rats (Janvier) were kept in cages of six in a 12 h light cycle with water and food ad libitum. All animal protocols were approved by the local authorities (Regierung Unterfranken, RUF55.2.2-2532-2-612-16, 18 April 2018) and were in accordance with the ARRIVE guidelines.

4.2. Chronic Constriction Injury

Rats were randomized to the surgery and sham control groups. Surgery of the animals was performed under deep isoflurane anesthesia (1.8 vol%, fiO_2). Adequate anesthesia was assumed when paw withdrawal was absent. After skin incision and exposition of the sciatic nerve by blunt preparation, four loose silk ligatures (Perma Silk 6.0, Ethicon Inc., Somerville, NJ, USA) were used in rats with approximately 1 mm spacing in between [10,52]. After loosely tightening the ligatures, the skin was stitched (Prolene 5.0, Ethicon Inc., Somerville, NJ, USA). For sham operations, the same procedure was performed without applying the silk ligatures. All procedures were performed unilaterally, and the following experiments used the IL DRGs. As controls we used sham surgery (qPCR) or CL DRGs.

4.3. Behavioural Tests

Mechanical nociceptive thresholds were tested with the von-Frey test [53]. Rats were positioned on a wire mesh. Filaments were applied in ascending order. The initially used hair value was 1 g. In general, the filaments were applied to the plantar surface of the ipsilateral and contralateral hind paw and were held for 1–3 s until the filaments were bent to an angle of 45°. Each limb was tested three times. We determined the withdrawal threshold of the hind-limbs to a mechanical stimulus by using 50% paw withdrawal threshold (PWT) method.

4.4. Reverse Transcription qPCR (RT-qPCR)

Quantification of mRNA of whole DRGs was performed using qPCR. RNA was first extracted from the samples using TRIzol™ Reagent (Invitrogen, Carlsbad, CA, USA); then, reverse transcribed to cDNA using the High capacity cDNA Reverse Transcriptase Kit (Applied Biosystems, Foster City, CA, USA) according to the manufacturer's instructions. For RT-qPCR, the PowerUpTM SYBR Green Master Mix was used following the manufacturer's protocol with primers for *Cldn1*, *Cldn5*, *Cldn12*, *Cldn19*, and *Tjp1* (ZO-1) (Table 2).

Table 2. List of primers used in qRT-PCR analysis.

Gene	Species	Forward Primers	Reverse Primers
Gapdh	rat	5′-AGTCTACTGGCGTCTTCAC-3′	5′-TCATATTTCTCGTGGTTCAC-3′
Cldn1	rat	5′-GGGACAACATCGTGACTGCT-3′	5′-CCACTAATGTCGCCAGACCTG-3′
Cldn5	rat	5′-AAATTCTGGGTCTGGTGCTG-3′	5′-GCCGGTCAAGGTAACAAAGA-3′
Cldn12	rat	5′-AACTGGCCAAGTGTCTGGTC-3′	5′-AGACCCCCTGAGCTAGCAAT-3′
Cldn19	rat	5′-TGCTGAAGGACCCATCTG-3′	5′-TGTGCTTGCTGTGAGAACTG-3′
ZO-1 (Tjp1)	rat	5′-CACGATGCTCAGAGACGAAGG-3′	5′-TTCTACATATGGAAGTTGGGGATC-3′

Total RNA from capillaries and neuron rich areas from rats DRGs was extracted using the RNeasy® Micro Kit (Qiagen, Venlo, The Netherlands). Total RNA (1 µg) was transcribed to cDNA using the high-capacity cDNA kit (Applied Biosystems, Foster City, CA, USA) following the manufacturer's instructions. *Gapdh* and *18S* were used as reference genes for quantification. Analysis via qPCR was performed with the following primers with the Taqman method: *Cldn5* (Rn01753146_s1, Thermo Scientific, Waltham, MA, USA) and *Vwf* (Rn01492158_m1, Thermo Scientific, Waltham, MA, USA). qPCR analysis was carried out using the StepOnePlus Real-Time PCR System (Applied Biosystems, Foster City, CA, USA) with the following program: 95 °C for 20 s followed by 45 cycles at 95 °C for 1 s and 60 °C for 20 s. Samples were analyzed as triplicates. Relative quantification of mRNA was calculated using the $2^{-\Delta\Delta CT}$ method, in which CT represents the threshold cycle value.

4.5. Immunofluorescence and Microscopy

After euthanizing the rats, the DRGs were harvested, embedded in Tissue Tek O.C.T. Compound (Sakura Finetek Europe B.V., AV Alphen aan den Rijn, The Netherlands), and snap frozen in liquid nitrogen. The samples were stored at −20 °C until further processing. Cryosections of 10 µm thickness were cut at −20 °C in a cryostat (Leica Biosystems CM3050 S Research Cryostat, Leica Biosystems Nussloch GmbH, Nussloch, Germany) and the slides were stored at −20 °C.

For fixation, the slides were immersed in 4% paraformaldehyde (Sigma Aldrich, St. Louis, MO, USA) in PBS (Sigma Aldrich, St. Louis, MO, USA). The fixed samples were blocked with 10% donkey serum in 0.3% Triton X-100 (Sigma-Aldrich, St. Louis, MO, USA) in PBS for 1 h at room temperature. After blocking, slides were incubated with the putative primary antibody in 10% donkey serum in PBS for 16 h at 4 °C: rabbit claudin-1 antibody (1:100, Invitrogen, Waltham, MA, USA, number 51-9000), mouse claudin-5-Alexa488 conjugate antibody (1:200, Invitrogen, number 352588), claudin-12 (1:100, IBL, number 18801), rabbit claudin-19 (1:100, gift from Hou, St. Louis, USA [54]), mouse ZO-1-Alexa488 conjugate antibody (1:200, Invitrogen, number 339188), rabbit vWF antibody (1:100, Dako, Santa Clara, CA, USA, A0082), and mouse anti rat CD68 antibody (1:100; Bio-rad, Hercules, CA, USA, MCA341R). Claudin-1 and claudin-5 or vWF and claudin-5 antibodies were applied together as a co-stain. Primary antibody incubation was followed by thorough washing in PBS and incubation with secondary antibodies: for claudin-1, claudin-12, and claudin-19, Alexa fluor 555 donkey anti-rabbit antibodies (1:1000, Life Technologies, Invitrogen, MolecularProbes Inc., Eugene OR, USA, A31572) were used. The anti-claudin-5 and -ZO-1 antibodies were already conjugated with Alexa fluor 488. Before mounting, the samples were washed, and Hoechst 33342 solution was applied for five minutes at room temperature for counterstaining the nuclei (1 µg/mL in PBS, Thermo Scientific, Waltham, MA, USA). The sections were mounted with Vectashield Antifade Mounting Medium (Vector Laboratories, Burlingame, CA, USA).

Imaging of the fluorophore labeled sections was performed within one session with the same settings for each antibody (Biorevo BZ-9000-E, Keyence, Osaka, Japan). All images were saved as RGB 8-bit Tagged Image File Format (TIFF) files for further analysis.

4.6. Laser Microdissection

DRGs from Wistar rats were embedded in Tissue-Tek O.C.T compound (Sakura Finetek Europe B.V., AV Alphen aan den Rijn, The Netherlands) and stored at −80 °C. Cryosections of 20 µm were

collected on Arcturus® polyethylene naphtalate membrane slides (Applied Biosystems, Foster City, CA, United States) using a cryostat (Leica Biosystems CM3050 S Research Cryostat, Leica Biosystems Nussloch GmbH, Nussloch, Germany). The slides were treated with Rnase AWAY® spray (Sigma Aldrich, St. Louis, MO, USA) before section collection. Before laser microdissection (LMD), sections were stained with toluidine blue. The slides were examined under a microscope coupled with a 355 nm laser (Leica®). Using the Leica LMD V7.6 software. capillaries were delimited and cut in the fiber rich area. Then, the entire neuron rich area was selected and sectioned as demonstrated in Figure 9. Samples were collected by gravity in 0.2 mL PCR SoftTubes (Biozym Scientific GmbH, Hessisch Oldendorf, Niedersachsen, Germany) and stored at −80 °C until reverse transcription qPCR.

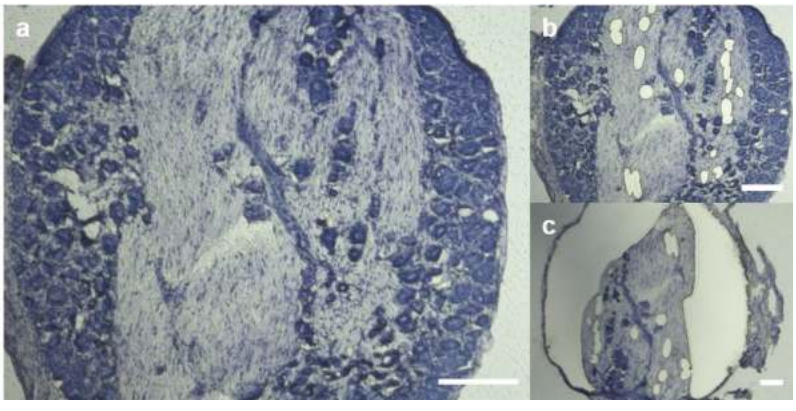

Figure 9. Stepwise sample acquisition of specific rat DRG regions via laser microdissection. Area specific samples of sham operated and rats 1 d after CCI were prepared after toluidine staining. Images of representative sections before dissection (**a**), and after acquisition of vessels in the FRR (**b**) and removal of the NRR (**c**) are shown. Scale bars measure 200 μm.

4.7. Permeability of DRG Capillaries

Anaesthetized rats were laid down in a supine position on a pad. The 5th intercostal space was opened and enlarged by a retractor to open the thorax. The pericardium was stripped, exposing the heart anterior wall, and 12 mL of FITC dextran (70 kDa; 10 mg/mL; Sigma-Aldrich, St. Loui, MO, USA, FD70) or Hoechst 33342 (562 Da; 10 mg/mL; Sigma-Aldrich, St. Louis, MO, USA, 14533) solution was injected into the left ventricle using a syringe. The dye-perfused rats were sacrificed by decapitation after 1 min. DRGs were dissected and embedded in Tissue-Tek. Frozen samples were cut into 10 μm-thick sections on a cryostat at −20 °C. Without any fixation, microscope glass slides containing tissue sections were mounted and were imaged by fluorescence microscopy. The permeability of the DRG was determined by the measuring the fluorescence of FITC dextran in the NRR and FRR.

4.8. Image Analysis

All acquired images were analyzed with Fiji/ImageJ (version 1.52e, Open Source). Brightfield images of rat DRGs were used to distinguish the fiber rich region (FRR) and the neuron rich region (NRR), and their putative epi-/perineuria (FRR-EPN, NRR-EPN), as demonstrated in Figure 1a; and they were saved as regions of interest (ROIs). For vessel specific analysis, ROIs were created using vWF counterstaining and brightfield images.

4.9. Statistical Analysis

RStudio (version 1.1447, Open Source) was used for statistical analysis and plot generation. Datasets were tested for normal distribution and variance homogeneity using the Shapiro–Wilk normality test and Levene's test of equality of variances. Datapoints were distributed normally with homogenous variances if not stated otherwise. Statistical significance of paw withdrawal threshold (Figure 2) was tested via repeated measures ANOVA. mRNA data was tested using Welch's two sample *t*-test or Wilcoxon rank sum test if criteria for the *t*-test were not met. Two-factor ANOVA followed by Tukey's test was used for analysis of immunoreactivity studies. All plots show means ± standard deviations. Significance was assumed as $p < 0.05$ (* $p < 0.05$; ** $p < 0.01$; *** $p < 0.001$) [55].

5. Conclusions

Neurons and non-neuronal cells in the DRG regulate the perceptual quality of pain. We found reduced claudin-5 protein and mRNA expression in the NRR of the DRG following peripheral nerve injury by CCI. Measuring dye diffusion, we observed that the permeability in the NRR is higher compared to FRR in the DRG in naïve rats. Despite of reduced claudin-5, permeability to small and large molecules remained unchanged. Nerve injury-induced macrophage accumulation in the NRR was increased, indicating a possible role of tight junction proteins in cell migration.

Further studies of the BDB will decipher its function and role in pain. Whether BDB permeability, e.g., in MR imaging, will be a suitable biomarker for painful affection of the PNS, has to be studied in the future in preclinical models and patient cohorts.

Author Contributions: Conceptualization, T.J.L., J.T.-C.C. and H.L.R.; Data curation, T.J.L. and J.T.-C.C.; Formal analysis, T.J.L. and J.T.-C.C.; Funding acquisition, R.B. and H.L.R.; Investigation, T.J.L., X.H., A.B.-K. and R.B.; Methodology, T.J.L., A.B.-K., R.B. and J.T.-C.C.; Project administration, H.L.R.; Resources, R.B. and H.L.R.; Software, T.J.L.; Supervision, R.B. and H.L.R.; Validation, T.J.L., X.H., J.T.-C.C. and H.L.R.; Visualization, T.J.L.; Writing—original draft, T.J.L.; Writing—review & editing, T.J.L., R.B., J.T.-C.C. and H.L.R. All authors have read and agreed to the published version of the manuscript.

Funding: This research was funded by the German Research Foundation (DFG, Ri-817/13-1 and 817/15-1), the Graduate School of Life Sciences (GSLS, University of Wuerzburg), the German Academic Scholarship Foundation, and the Interdisciplinary Center for Clinical Studies Wuerzburg (IZKF, ND-368).

Acknowledgments: We thank Nicola Drosczinsky for acquiring rat DRG PCR data and Isabel U.C. Otto for technical assistance with the immunohistochemistry. We are also acknowledging Solange Sauer for helping with the LSM experiments.

Conflicts of Interest: The authors declare no conflict of interest. The funders had no role in the design of the study; in the collection, analyses, or interpretation of data; in the writing of the manuscript, or in the decision to publish the results.

Abbreviations

BDB	blood–DRG barrier
CCI	chronic constriction injury
cldn1	claudin-1
cldn5	claudin-5
cldn12	claudin-12
cldn19	claudin-19
DRG	dorsal root ganglion
EPN	epi-/perineurium
FRR	fiber-rich region
IR	immunoreactivity
LMD	laser microdissection
MB	myelin barrier
NRR	neuron-rich region
vWF	von Willebrandt factor

References

1. Bennett, G.J.; Xie, Y.K. A peripheral mononeuropathy in rat that produces disorders of pain sensation like those seen in man. *Pain* **1988**, *33*, 87–107. [CrossRef]
2. Colloca, L.; Ludman, T.; Bouhassira, D.; Baron, R.; Dickenson, A.H.; Yarnitsky, D.; Freeman, R.; Truini, A.; Attal, N.; Finnerup, N.B.; et al. Neuropathic pain. *Nat. Rev. Dis. Primers* **2017**, *3*, 17002. [CrossRef] [PubMed]
3. Finnerup, N.B.; Attal, N.; Haroutounian, S.; McNicol, E.; Baron, R.; Dworkin, R.H.; Gilron, I.; Haanpää, M.; Hansson, P.; Jensen, T.S.; et al. Pharmacotherapy for neuropathic pain in adults: A systematic review and meta-analysis. *Lancet Neurol.* **2015**, *14*, 162–173. [CrossRef]
4. Joshi, S.K.; Honore, P. Animal models of pain for drug discovery. *Expert Opin. Drug Discov.* **2006**, *1*, 323–334. [CrossRef] [PubMed]
5. De Vry, J.; Kuhl, E.; Franken-Kunkel, P.; Eckel, G. Pharmacological characterization of the chronic constriction injury model of neuropathic pain. *Eur. J. Pharmacol.* **2004**, *491*, 137–148. [CrossRef] [PubMed]
6. Dowdall, T.; Robinson, I.; Meert, T. Comparison of five different rat models of peripheral nerve injury. *Pharmacol. Biochem. Behav.* **2005**, *80*, 93–108. [CrossRef] [PubMed]
7. Hu, P.; Bembrick, A.L.; Keay, K.A.; McLachlan, E.M. Immune cell involvement in dorsal root ganglia and spinal cord after chronic constriction or transection of the rat sciatic nerve. *Brain Behav. Immun.* **2007**, *21*, 599–616. [CrossRef]
8. Ramer, M.S.; Bisby, M.A. Rapid sprouting of sympathetic axons in dorsal root ganglia of rats with a chronic constriction injury. *Pain* **1997**, *70*, 237–244. [CrossRef]
9. Reinhold, A.; Rittner, H. Barrier function in the peripheral and central nervous system—A review. *Pflügers Arch. Eur. J. Physiol.* **2017**, *469*, 123–134. [CrossRef]
10. Reinhold, A.-K.; Yang, S.; Chen, J.T.-C.; Hu, L.; Sauer, R.-S.; Krug, S.M.; Mambretti, E.M.; Fromm, M.; Brack, A.; Rittner, H.L. Tissue plasminogen activator and neuropathy open the blood-nerve barrier with upregulation of microRNA-155-5p in male rats. *Biochim. Et Biophys. Acta (BBA) Mol. Basis Dis.* **2019**, *1865*, 1160–1169. [CrossRef]
11. Moreau, N.; Dieb, W.; Mauborgne, A.; Bourgoin, S.; Villanueva, L.; Pohl, M.; Boucher, Y. Hedgehog Pathway-Mediated Vascular Alterations Following Trigeminal Nerve Injury. *J. Dent. Res.* **2017**, *96*, 450–457. [CrossRef] [PubMed]
12. Moreau, N.; Mauborgne, A.; Bourgoin, S.; Couraud, P.O.; Romero, I.A.; Weksler, B.B.; Villanueva, L.; Pohl, M.; Boucher, Y. Early alterations of Hedgehog signaling pathway in vascular endothelial cells after peripheral nerve injury elicit blood-nerve barrier disruption, nerve inflammation, and neuropathic pain development. *Pain* **2016**, *157*, 827–839. [CrossRef] [PubMed]
13. Reinhold, A.K.; Schwabe, J.; Lux, T.J.; Salvador, E.; Rittner, H.L. Quantitative and Microstructural Changes of the Blood-Nerve Barrier in Peripheral Neuropathy. *Front. Neurosci.* **2018**, *12*, 12. [CrossRef] [PubMed]
14. Lim, T.K.; Shi, X.Q.; Martin, H.C.; Huang, H.; Luheshi, G.; Rivest, S.; Zhang, J. Blood-nerve barrier dysfunction contributes to the generation of neuropathic pain and allows targeting of injured nerves for pain relief. *Pain* **2014**, *155*, 954–967. [CrossRef]
15. Sauer, R.S.; Kirchner, J.; Yang, S.; Hu, L.; Leinders, M.; Sommer, C.; Brack, A.; Rittner, H.L. Blood-spinal cord barrier breakdown and pericyte deficiency in peripheral neuropathy. *Ann. N. Y. Acad. Sci.* **2017**, *1405*, 71–88. [CrossRef]
16. Echeverry, S.; Shi, X.Q.; Rivest, S.; Zhang, J. Peripheral nerve injury alters blood-spinal cord barrier functional and molecular integrity through a selective inflammatory pathway. *J. Neurosci.* **2011**, *31*, 10819–10828. [CrossRef]
17. Jimenez-Andrade, J.M.; Herrera, M.B.; Ghilardi, J.R.; Vardanyan, M.; Melemedjian, O.K.; Mantyh, P.W. Vascularization of the Dorsal Root Ganglia and Peripheral Nerve of the Mouse: Implications for Chemical-Induced Peripheral Sensory Neuropathies. *Mol. Pain* **2008**, *4*, 10. [CrossRef]
18. Abram, S.E.; Yi, J.; Fuchs, A.; Hogan, Q.H. Permeability of injured and intact peripheral nerves and dorsal root ganglia. *Anesthesiology* **2006**, *105*, 146–153. [CrossRef]
19. Hirakawa, H.; Okajima, S.; Nagaoka, T.; Kubo, T.; Takamatsu, T.; Oyamada, M. Regional differences in blood-nerve barrier function and tight-junction protein expression within the rat dorsal root ganglion. *Neuroreport* **2004**, *15*, 405–408. [CrossRef]

20. Liu, Q.; Wang, X.; Yi, S. Pathophysiological Changes of Physical Barriers of Peripheral Nerves After Injury. *Front. Neurosci.* **2018**, *12*. [CrossRef]
21. Bendszus, M.; Stoll, G. Technology Insight: Visualizing peripheral nerve injury using MRI. *Nat. Clin. Pract. Neurol.* **2005**, *1*, 45–53. [CrossRef] [PubMed]
22. Dubovy, P.; Tuckova, L.; Jancalek, R.; Svizenska, I.; Klusakova, I. Increased invasion of ED-1 positive macrophages in both ipsi- and contralateral dorsal root ganglia following unilateral nerve injuries. *Neurosci. Lett.* **2007**, *427*, 88–93. [CrossRef] [PubMed]
23. Simeoli, R.; Montague, K.; Jones, H.R.; Castaldi, L.; Chambers, D.; Kelleher, J.H.; Vacca, V.; Pitcher, T.; Grist, J.; Al-Ahdal, H.; et al. Exosomal cargo including microRNA regulates sensory neuron to macrophage communication after nerve trauma. *Nat. Commun.* **2017**, *8*, 1778. [CrossRef] [PubMed]
24. Furuse, M.; Hata, M.; Furuse, K.; Yoshida, Y.; Haratake, A.; Sugitani, Y.; Noda, T.; Kubo, A.; Tsukita, S. Claudin-based tight junctions are crucial for the mammalian epidermal barrier: A lesson from claudin-1-deficient mice. *J. Cell Biol.* **2002**, *156*, 1099–1111. [CrossRef] [PubMed]
25. Pummi, K.P.; Heape, A.M.; Grenman, R.A.; Peltonen, J.T.; Peltonen, S.A. Tight junction proteins ZO-1, occludin, and claudins in developing and adult human perineurium. *J. Histochem. Cytochem.* **2004**, *52*, 1037–1046. [CrossRef] [PubMed]
26. Hackel, D.; Krug, S.M.; Sauer, R.S.; Mousa, S.A.; Bocker, A.; Pflucke, D.; Wrede, E.J.; Kistner, K.; Hoffmann, T.; Niedermirtl, B.; et al. Transient opening of the perineurial barrier for analgesic drug delivery. *Proc. Natl. Acad. Sci. USA* **2012**, *109*, E2018–E2027. [CrossRef]
27. Parmantier, E.; Lynn, B.; Lawson, D.; Turmaine, M.; Namini, S.S.; Chakrabarti, L.; McMahon, A.P.; Jessen, K.R.; Mirsky, R. Schwann cell-derived Desert hedgehog controls the development of peripheral nerve sheaths. *Neuron* **1999**, *23*, 713–724. [CrossRef]
28. Hirakawa, H.; Okajima, S.; Nagaoka, T.; Takamatsu, T.; Oyamada, M. Loss and recovery of the blood-nerve barrier in the rat sciatic nerve after crush injury are associated with expression of intercellular junctional proteins. *Exp. Cell Res.* **2003**, *284*, 196–210. [CrossRef]
29. Haseloff, R.F.; Dithmer, S.; Winkler, L.; Wolburg, H.; Blasig, I.E. Transmembrane proteins of the tight junctions at the blood-brain barrier: Structural and functional aspects. *Semin Cell Dev. Biol.* **2015**, *38*, 16–25. [CrossRef]
30. Obermeier, B.; Daneman, R.; Ransohoff, R.M. Development, maintenance and disruption of the blood-brain barrier. *Nat. Med.* **2013**, *19*, 1584–1596. [CrossRef]
31. Alanne, M.H.; Pummi, K.; Heape, A.M.; Grenman, R.; Peltonen, J.; Peltonen, S. Tight junction proteins in human Schwann cell autotypic junctions. *J. Histochem. Cytochem.* **2009**, *57*, 523–529. [CrossRef] [PubMed]
32. Miyamoto, T.; Morita, K.; Takemoto, D.; Takeuchi, K.; Kitano, Y.; Miyakawa, T.; Nakayama, K.; Okamura, Y.; Sasaki, H.; Miyachi, Y.; et al. Tight junctions in Schwann cells of peripheral myelinated axons: A lesson from claudin-19-deficient mice. *J. Cell Biol.* **2005**, *169*, 527–538. [CrossRef] [PubMed]
33. Günzel, D.; Yu, A.S.L. Claudins and the Modulation of Tight Junction Permeability. *Physiol. Rev.* **2013**, *93*, 525. [CrossRef] [PubMed]
34. Sauer, R.S.; Krug, S.M.; Hackel, D.; Staat, C.; Konasin, N.; Yang, S.; Niedermirtl, B.; Bosten, J.; Gunther, R.; Dabrowski, S.; et al. Safety, efficacy, and molecular mechanism of claudin-1-specific peptides to enhance blood-nerve-barrier permeability. *J. Control Release* **2014**, *185*, 88–98. [CrossRef] [PubMed]
35. Katsuno, T.; Umeda, K.; Matsui, T.; Hata, M.; Tamura, A.; Itoh, M.; Takeuchi, K.; Fujimori, T.; Nabeshima, Y.; Noda, T.; et al. Deficiency of zonula occludens-1 causes embryonic lethal phenotype associated with defected yolk sac angiogenesis and apoptosis of embryonic cells. *Mol. Biol. Cell* **2008**, *19*, 2465–2475. [CrossRef] [PubMed]
36. Morita, K.; Sasaki, H.; Furuse, M.; Tsukita, S. Endothelial claudin: Claudin-5/TMVCF constitutes tight junction strands in endothelial cells. *J. Cell Biol.* **1999**, *147*, 185–194. [CrossRef]
37. Ohtsuki, S.; Sato, S.; Yamaguchi, H.; Kamoi, M.; Asashima, T.; Terasaki, T. Exogenous expression of claudin-5 induces barrier properties in cultured rat brain capillary endothelial cells. *J. Cell. Physiol.* **2007**, *210*, 81–86. [CrossRef]
38. Nitta, T.; Hata, M.; Gotoh, S.; Seo, Y.; Sasaki, H.; Hashimoto, N.; Furuse, M.; Tsukita, S. Size-selective loosening of the blood-brain barrier in claudin-5-deficient mice. *J. Cell Biol.* **2003**, *161*, 653–660. [CrossRef]
39. Poliak, S.; Matlis, S.; Ullmer, C.; Scherer, S.S.; Peles, E. Distinct claudins and associated PDZ proteins form different autotypic tight junctions in myelinating Schwann cells. *J. Cell Biol.* **2002**, *159*, 361–372. [CrossRef]

40. Shinder, V.; Devor, M. Structural basis of neuron-to-neuron cross-excitation in dorsal root ganglia. *J. Neurocytol.* **1994**, *23*, 515–531. [CrossRef]
41. Devor, M. Unexplained peculiarities of the dorsal root ganglion. *Pain* **1999**, *82* (Suppl. 6), S27–S35. [CrossRef]
42. Yatziv, S.L.; Devor, M. Suppression of neuropathic pain by selective silencing of DRG ectopia using non-blocking concentrations of lidocaine. *Pain* **2019**. [CrossRef] [PubMed]
43. Tracey, I.; Woolf, C.J.; Andrews, N.A. Composite Pain Biomarker Signatures for Objective Assessment and Effective Treatment. *Neuron* **2019**, *101*, 783–800. [CrossRef] [PubMed]
44. Godel, T.; Pham, M.; Heiland, S.; Bendszus, M.; Baumer, P. Human dorsal-root-ganglion perfusion measured in-vivo by MRI. *Neuroimage* **2016**, *141*, 81–87. [CrossRef] [PubMed]
45. Apostolidis, L.; Schwarz, D.; Xia, A.; Weiler, M.; Heckel, A.; Godel, T.; Heiland, S.; Schlemmer, H.P.; Jager, D.; Bendszus, M.; et al. Dorsal root ganglia hypertrophy as in vivo correlate of oxaliplatin-induced polyneuropathy. *PLoS ONE* **2017**, *12*, e0183845. [CrossRef]
46. Godel, T.; Mautner, V.F.; Farschtschi, S.; Pham, M.; Schwarz, D.; Kronlage, M.; Gugel, I.; Heiland, S.; Bendszus, M.; Baumer, P. Dorsal root ganglia volume differentiates schwannomatosis and neurofibromatosis 2. *Ann. Neurol.* **2018**, *83*, 854–857. [CrossRef]
47. Godel, T.; Baumer, P.; Pham, M.; Kohn, A.; Muschol, N.; Kronlage, M.; Kollmer, J.; Heiland, S.; Bendszus, M.; Mautner, V.F. Human dorsal root ganglion in vivo morphometry and perfusion in Fabry painful neuropathy. *Neurology* **2017**, *89*, 1274–1282. [CrossRef]
48. Godel, T.; Kohn, A.; Muschol, N.; Kronlage, M.; Schwarz, D.; Kollmer, J.; Heiland, S.; Bendszus, M.; Mautner, V.F.; Baumer, P. Dorsal root ganglia in vivo morphometry and perfusion in female patients with Fabry disease. *J. Neurol.* **2018**, *265*, 2723–2729. [CrossRef]
49. Baumer, P.; Reimann, M.; Decker, C.; Radbruch, A.; Bendszus, M.; Heiland, S.; Pham, M. Peripheral nerve perfusion by dynamic contrast-enhanced magnetic resonance imaging: Demonstration of feasibility. *Investig. Radiol.* **2014**, *49*, 518–523. [CrossRef]
50. Salvador, E.; Shityakov, S.; Förster, C. Glucocorticoids and endothelial cell barrier function. *Cell Tissue Res.* **2014**, *355*, 597–605. [CrossRef]
51. Deer, T.R.; Pope, J.E.; Lamer, T.J.; Grider, J.S.; Provenzano, D.; Lubenow, T.R.; FitzGerald, J.J.; Hunter, C.; Falowski, S.; Sayed, D.; et al. The Neuromodulation Appropriateness Consensus Committee on Best Practices for Dorsal Root Ganglion Stimulation. *Neuromodulation* **2019**, *22*, 1–35. [CrossRef] [PubMed]
52. Sauer, R.-S.; Rittner, H.L.; Roewer, N.; Sohajda, T.; Shityakov, S.; Brack, A.; Broscheit, J.-A. A Novel Approach for the Control of Inflammatory Pain: Prostaglandin E2 Complexation by Randomly Methylated β-Cyclodextrins. *Anesth. Analg.* **2017**, *124*, 675–685. [CrossRef] [PubMed]
53. Chaplan, S.R.; Bach, F.W.; Pogrel, J.W.; Chung, J.M.; Yaksh, T.L. Quantitative assessment of tactile allodynia in the rat paw. *J. Neurosci. Methods* **1994**, *53*, 55–63. [CrossRef]
54. Hou, J.; Renigunta, A.; Gomes, A.S.; Hou, M.; Paul, D.L.; Waldegger, S.; Goodenough, D.A. Claudin-16 and claudin-19 interaction is required for their assembly into tight junctions and for renal reabsorption of magnesium. *Proc. Natl. Acad. Sci. USA* **2009**, *106*, 15350–15355. [CrossRef]
55. Damoiseaux, J.G.; Döpp, E.A.; Calame, W.; Chao, D.; MacPherson, G.G.; Dijkstra, C.D. Rat macrophage lysosomal membrane antigen recognized by monoclonal antibody ED1. *Immunology* **1994**, *83*, 140–147. [PubMed]

International Journal of
Molecular Sciences

MDPI

Review

Tight Junction Proteins and the Biology of Hepatobiliary Disease

Natascha Roehlen [1,2], Armando Andres Roca Suarez [1,2], Houssein El Saghire [1,2], Antonio Saviano [1,2,3], Catherine Schuster [1,2], Joachim Lupberger [1,2] and Thomas F. Baumert [1,2,3,*]

1 Institut de Recherche sur les Maladies Virales et Hépatiques, Inserm UMR1110, F-67000 Strasbourg, France; natascha.roehlen@etu.unistra.fr (N.R.); andres.roca-suarez@etu.unistra.fr (A.A.R.S.); elsaghire@unistra.fr (H.E.S.); saviano@unistra.fr (A.S.); catherine.schuster@unistra.fr (C.S.); joachim.lupberger@unistra.fr (J.L.)
2 Université de Strasbourg, F-67000 Strasbourg, France
3 Pôle Hepato-digestif, Institut Hopitalo-universitaire, Hôpitaux Universitaires de Strasbourg, F-67000 Strasbourg, France
* Correspondence: thomas.baumert@unistra.fr; Tel.: +33-3688-53703

Received: 4 November 2019; Accepted: 21 January 2020; Published: 28 January 2020

Abstract: Tight junctions (TJ) are intercellular adhesion complexes on epithelial cells and composed of integral membrane proteins as well as cytosolic adaptor proteins. Tight junction proteins have been recognized to play a key role in health and disease. In the liver, TJ proteins have several functions: they contribute as gatekeepers for paracellular diffusion between adherent hepatocytes or cholangiocytes to shape the blood-biliary barrier (BBIB) and maintain tissue homeostasis. At non-junctional localizations, TJ proteins are involved in key regulatory cell functions such as differentiation, proliferation, and migration by recruiting signaling proteins in response to extracellular stimuli. Moreover, TJ proteins are hepatocyte entry factors for the hepatitis C virus (HCV)—a major cause of liver disease and cancer worldwide. Perturbation of TJ protein expression has been reported in chronic HCV infection, cholestatic liver diseases as well as hepatobiliary carcinoma. Here we review the physiological function of TJ proteins in the liver and their implications in hepatobiliary diseases.

Keywords: Claudin; occludin; blood-biliary barrier; chronic liver disease; hepatocellular carcinoma; cholangiocellular carcinoma; NISCH syndrome

1. Introduction

Tight junctions (TJ) are protein complexes on epithelial cells in all organs of the body and establish paracellular diffusion barriers between different compartments. The distinct cell polarity and selective paracellular diffusion hereby provides the molecular basis of tissue homeostasis [1]. Structurally, TJs consist of transmembrane proteins that function as the diffusion barriers and cytosolic proteins that interface the junctional complexes with the cytoskeleton [1]. While initially TJs were believed to serve as simple paracellular gates, in the past years, accumulating data have identified additional functions of TJs proteins. By maintaining cellular differentiation, intercellular communication as well as assembly of signaling proteins, TJ proteins have been shown to orchestrate inside-out and outside-in signaling, hereby affecting cell proliferation, migration, apoptosis, and inflammation [2–4]. On the other hand, several growth factors, cytokines, and signaling cascades induce and regulate localization and expression of TJ proteins, hereby affecting epithelial differentiation and barrier integrity [5,6].

In the healthy liver, TJ proteins are expressed on hepatocytes, cholangiocytes, and nonparenchymal cells such as endothelial cells [5,7,8]. While TJ proteins on hepatocytes build the blood-biliary barrier (BBIB) and are hijacked during hepatitis C virus (HCV) infection, TJ proteins on cholangiocytes line the intrahepatic bile ducts [7,9,10]. Besides their localization at the apical membrane, TJ proteins have

also been described to be localized at the basolateral membrane and in the cytoplasm of hepatocytes. In these non-junctional localizations, TJ proteins regulate cell-matrix interactions, intracellular signaling and proliferation, migration, and invasion [11]. Perturbation of TJ structure, protein expression, and localization have frequently been described in chronic liver and biliary diseases, indicating their fundamental role in liver biology [12]. This review provides an overview of TJ proteins being expressed in the liver, their function in maintaining TJ structure and cell signaling outside of TJs, as well as their implication in hepatobiliary diseases.

2. Biology of Tight Junction Proteins

2.1. Structure and Composition of Tight Junctions

Tight junctions are shaped by intercellular protein-protein complexes connecting plasma membranes of neighboring cells. Thus, TJs often appear as "kissing points" by electron microscopy. Two models of TJ structure exist: the protein model and the protein-lipid hybrid model. The protein model postulates construction of the junctional diffusion barrier by transmembrane proteins on both sides, interacting in a homotypic or heterotypic way (shown in Figure 1a), whereas the hybrid model proposes membrane hemifusions built by inverted lipid micelles and stabilized by transmembrane proteins [1]. Yet no consensus on the ultrastructural appearance has been reached. However, in both cases, TJs build a regulatory semipermeable gate that enables selective paracellular diffusion depending on the size and charge of the corresponding molecule [1]. Moreover, TJs form an intramembrane barrier (also referred to as "fence function"), that restricts exchange between the cells' apical and basolateral surfaces [13]. However, whether the fence function of TJs is critical or not for the establishment of a polarized phenotype has been a matter of debate, taking into account that it has been observed how epithelial cells are able to polarize in the absence of cell-cell junctions [14,15].

The transmembrane domains of TJs on epithelial cells are mainly built by tetraspanin-associated proteins of the claudin (CLDN) family and the junctional proteins occludin (OCLN) and MarvelD3, which contain a MAL and related proteins for vesicle trafficking and membrane link (MARVEL) domain. Moreover, junctional adhesion molecules (JAMs) have been reported as integral membrane proteins in TJs [16,17]. Tricellular TJ proteins characterize cell adhesion between three neighboring cells and include tricellulin [18], lipolysis-stimulated lipoprotein receptor (LSR) [19], as well as immunoglobulin-like domain containing receptor (ILDR1 and ILDR2) [20]. Representatives of the cytosolic junctional plaque on the other hand are adapter proteins as Zonula occludens 1-3 (ZO1-3), membrane-associated guanylate kinase inverted (MAGI) proteins, and cingulin [1] (Figure 1a).

OCLN was the first identified transmembrane protein in TJs and belongs to the large protein family of Marvel-domain-containing proteins [21]. In contrast to the multiple and differentially expressed members of CLDN family, only one OCLN transcript has been described, which however occurs in differently spliced variants. With a size of 65 kDa, OCLN contains four transmembrane domains, one small intracellular loop, two extracellular loops, and intracellular localized C and N terminals (Figure 1a) [22].

The family of CLDN proteins comprises 27 members in mammals [23]. According to their physiological role in paracellular permeability, CLDNs can further be subgrouped into sealing CLDNs (CLDN1, 3, 5, 11, 14, and 19), cation-selective (CLDN2, 10b and 15) and anion-selective paracellular channel forming CLDNs (CLDN10a and 17), as well as water-permeable CLDNs (CLDN2 and 15). For the remaining CLDNs, their roles on epithelial barriers are not yet fully understood [24]. These 20–27 kDa proteins consist of four transmembrane domains, two extracellular loops, and a cytoplasmatic carboxyl tail (Figure 1a). As integral proteins of TJs, CLDNs are reported to regulate ion and water permeability of the paracellular barrier [1,25,26].

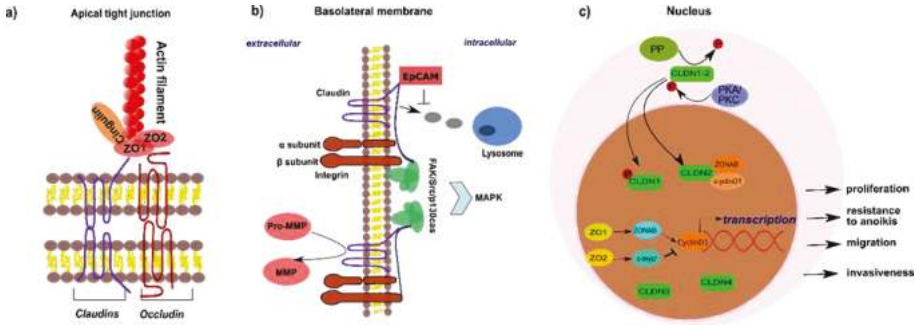

Figure 1. Functions of tight junction proteins at different subcellular localizations. Tight junction proteins are expressed at three different locations within epithelial cells with different functions including the apical membrane (**a**), the basolateral membrane (**b**), and in the nucleus (**c**). (**a**) At the apical membrane, tight junctions (TJs) are typically built by integral membrane proteins of the CLDN or Marvel-domain containing protein family (e.g., occludin—OCLN) that connect via C-terminus bound adapter proteins to intracellular actin filaments. (**b**) In the normal intestinal mucosa and in various cancer cell types, basolateral localized CLDNs have been found to regulate activation of pro-MMPs into MMPs and to interact with integrins at focal adhesion complexes, hereby affecting main intracellular signaling cascades such as the MAPK pathway. Investigations on colon cancer cell lines indicate EpCAM to specifically stabilize expression of CLDN1 and 7 at the basolateral membrane and to prevent their lysosomal degradation. (**c**) Nuclear localization has been reported for ZO1 and ZO2 as well as CLDN1-4 in various cancer cell types and is regulated by posttranslational modification. Within the nucleus, CLDN2 retains cyclinD1 and ZONAB hereby enhancing cell proliferation. Specific interaction of ZO1 with the transcription factor ZONAB regulates G1/S-phase progression by increasing cyclin D1, while ZO2 inhibits transcription of cyclin D1 by binding to c-myc. CLDN (Claudin); c-myc (MYC proto-oncogene); EpCAM (epithelial cell adhesion molecule); FAK (focal adhesion kinase); MAPK (Mitogen-activated protein kinase); MMP (Matrix-metalloproteinase); PKA (protein kinase A); PKC (protein kinase C); PP (protein phosphatase); Src (steroid receptor coactivator); ZO1 (Zonula occludens 1); ZO2 (Zonula occludens 2); ZONAB (ZO1-associated nucleic acid binding protein).

With four transmembrane domains, cytoplasmatic C- and N-terminals, and two extracellular loops, tricellulin shows strong structural similarity to CLDNs and OCLN [18,27]. While OCLN and CLDN represent the main transmembrane proteins of apical cell adhesions between two cells (bicellular tight junction, bTJ), tricellulin is mainly enriched at tricellular contact regions (tricellular tight junction, tTJ), although also been identified in bTJs [18]. LSR, ILDR1 and 2, which are commonly described as the angulin family, have been reported to recruit tricellulin to tTJ [20].

JAMs belong to the immunoglobulin superfamily (IgSF). Originally discovered on leucocytes as key players of leucocyte-endothelial cell interaction and trans-endothelial migration, JAM-A-C as well as the related IgSF members CAR, endothelial cell-selective adhesion molecule (ESAM), and JAM-4 were later described to be enriched in epithelial and endothelial TJs. Consisting of two IgSF domains, two Ig-like domains, one single transmembrane domain, and a PDZ-domain binding cytoplasmatic tail, these proteins contribute to barrier formation and TJ associated signaling [16,17].

Besides transmembrane proteins, TJs consist of junctional plaque components that connect the junctional membrane with the cytoskeleton. ZO proteins are the most important adapter proteins, that connect CLDN, OCLN, and tricellulin with the cytoskeleton, hereby enabling clustering of protein complexes to the intracellular domains of TJs (Figure 1a). Apart from TJs, ZO proteins have also been described in cadherin-based adherens junctions and gap junctions [28]. Three ZO proteins (ZO1-3) with high structural similarity have been discovered. ZO1, the best described member of the family of ZO proteins represents a 220 kDa scaffolding protein, that includes three types of functional domains, a Src homology 3 domain (SH3), three PDZ domains, a proline rich and a guanylate kinase domain [29,30].

ZO proteins directly interact with the intracellular actin filaments and the first PDZ domain has been shown to associate with the C-terminus of CLDN and OCLN proteins, hereby regulating TJ assembly (Figure 1a) [31,32]. Other representatives of the junctional plaque are cingulin and 7H6 [33,34]. For a detailed review regarding the general structure and composition of TJs see [35,36].

The TJ complex is known to be highly dynamic with continuous remodeling by clathrin-mediated endocytic recycling [37–40]. Recycled or newly produced TJ proteins are sorted in the Golgi-network and transported by specific trafficking proteins to the desired localizations [41,42]. On the other hand, several growth factors, cytokines, and signaling cascades induce and regulate localization and expression of TJ proteins, hereby affecting epithelial differentiation and barrier integrity [5,6].

Knockout (KO) studies in cultured epithelial cells indicate an increase of paracellular permeability by loss of single CLDN proteins [43,44]. In contrast, KO of OCLN does not alter baseline barrier function, but attenuates cytokine-induced increase in trans-epithelial resistance [45]. Knockdown of tricellulin using siRNA decreases trans-epithelial electrical resistance and increases the paracellular permeability in cultured epithelial cells [18]. JAM-A in vitro and in vivo KO studies revealed increased epithelial permeability potentially due to perturbed regulation of CLDN expression and induction of apoptosis [46,47]. Loss of ZO1 retards but not completely hampers TJ formation, probably due to compensatory upregulation of ZO2. Thus, assembly of CLDN and OCLN proteins to TJs takes longer in the absence of ZO1 but does not block eventual establishment of the polarized epithelial structure with functional TJs within hours in cell culture [15]. However, KO of ZO1 and knockdown of ZO2 by RNA interference results in diffuse distribution of integral TJ proteins in epithelial cells with severe perturbation of the paracellular barrier [48]. While to our knowledge KO of 7H6 in epithelial cells has not yet been analyzed, its localization would suggest a paracellular barrier function [49,50]. In mice invivo KO or knockdown of TJ proteins results in a wide variety of phenotypes, ranging from a normal phenotype without any disease to lethality [51–55]. Furthermore, there are differences in the phenotype of TJ protein loss of function in mice and humans: e.g., while CLDN1 KO in a mouse model has shown to be lethal [52], congenital CLDN1 KO loss-of function mutations in human patients can manifest in a highly variable phenotype ranging normal health without disease to neonatal sclerosing cholangitis and ichthyosis of variable severity (NISCH syndrome), potentially due to compensatory upregulation of other CLDN members [56]. This indicates differential functions of the TJ orthologs in mice and humans and suggests that a complete loss of TJ proteins can be functionally compensated as shown for CLDN1 in humans.

2.2. Non-Junctional Localization of Tight Junction Proteins

Several TJ proteins have been described to be also localized outside of TJs at the basolateral membrane, in the cytoplasm, and in the nucleus. Non-junctional TJ proteins exert key regulatory functions on cell proliferation, cell adhesion, as well as migration and invasion [11]. As an example, CLDN1, 2, and 7 regulate cell-matrix interaction by forming complexes with integrin proteins at focal adhesions on the basolateral membrane of human lung, melanoma, colon, as well as breast cancer cells (Figure 1b) [57–61]. These interactions have not only been shown to affect epithelial adhesion to the matrix and cell proliferation [59], but also to be associated with cancer progression and metastasis [61]. The epithelial cell adhesion molecule (EpCAM) specifically stabilizes this non-junctional CLDN expression and regulates its lysosomal degradation (Figure 1b) [62]. In line with the potential pro-oncogenic function of CLDN proteins at the basolateral membrane, interaction of EpCAM with CLDN7 was reported to promote tumor progression and cell dissemination [63].

Several studies link basolateral CLDN expression with expression and activity of matrix metalloproteinases (MMPs) [64–66]. At the basolateral membrane of epithelial cells, secreted MMPs are able to degrade extracellular matrix proteins [67]. Interestingly, CLDN proteins have been shown to recruit and activate pro-MMP, hereby promoting migration and invasion of the corresponding cancer cells (Figure 1b) [68].

Nuclear localization has been reported for ZO1/ZO2 [69,70] and CLDN1-4 [71–74] in several types of cancer cells. The conditions or inducers under which these TJ proteins localize in the nucleus are poorly understood. However, in the case of CLDN1, phosphorylation by protein kinase A and C (PKA and PKC) has been shown to promote nuclear import [75]. Nuclear import of CLDN2 on the other hand is induced by dephosphorylation [72]. Functional investigations in colon cancer cells indicate nuclear localization of CLDN proteins to be associated with resistance to anoikis as well as migration and invasiveness [71], while nuclear localization of ZO1/ZO2 affects cell cycle progression and cell proliferation by transcriptional regulation of cyclin D1 in tumorous and non-tumorous epithelial cells [76,77] (Figure 1c).

3. Tight Junction Proteins and Their Role in Signaling

In colon and liver cancer cells, TJ proteins functionally crosstalk with key cellular signaling pathways, including PI3K/AKT, Wnt/β-catenin, and EGFR/ERK signaling [78–80]. Proteomic analysis of OCLN and CLDNs revealed numerous binding partners, that are known to be involved in cell signaling and trafficking, such as kinases, phosphatases, signaling adaptors, and receptor proteins [81,82]. A strong body of evidence indicates functional crosstalk of CLDN proteins with the EGFR signaling pathway. Dhawan et al. reported CLDN2 overexpression to promote cell proliferation in an EGFR-dependent manner in colon tumor cells [79]. De Souza et al. found EGF to increase CLDN3 expression via ERK and PI3K signaling, hereby accelerating colorectal tumor cell migration in vitro [83]. Finally, EGFR signaling has been shown to mediate the formation of a CD81-CLDN1 complex, hereby enabling entry of HCV into hepatocytes [82,84] (Figure 2).

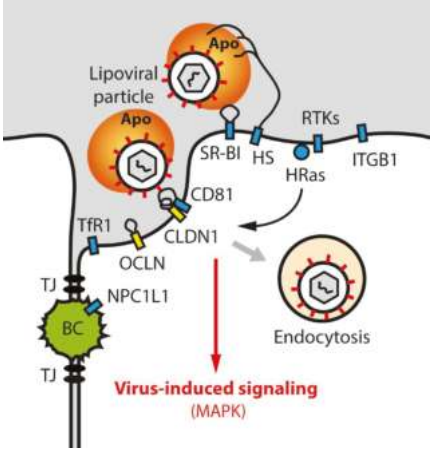

Figure 2. Hepatitis C virus (HCV) entry process and signaling. HCV lipoviral particle entry into hepatocytes requires a complex orchestration of entry factors that involves non-junctional TJ proteins CLDN1 and OCLN and virus-induced host signaling. Apo (Apolipoproteins), BC (Bile canaliculi), CD81 (Cluster of Differentiation 81), CLDN1 (Claudin-1), HRas (HRas Proto-Oncogene, GTPase), HS (Heparan sulfate), ITGB1 (Integrin Subunit Beta 1), MAPK (Mitogen-activated protein kinase), NPC1L1 (Niemann-Pick C1-like protein 1), OCLN (Occludin), RTK (Receptor tyrosine kinases), SR-BI (Scavenger Receptor Class B Member 1), TfR1 (Transferrin Receptor 1), TJ (Tight junction).

Several studies further associate CLDN proteins with proapoptotic signaling. Singh et al. indicated CLDN1 as a driver of resistance to anoikis in colon cancer cells, a form of self-programmed death in epithelial cells following detachment from the surrounding extracellular matrix. Mechanistically, CLDN1 was found to directly interact with steroid receptor coactivator (Src), a non-receptor tyrosine kinase that binds to extracellular matrix proteins and plays a pivotal role in cellular signal transduction,

promoting survival, proliferation, and angiogenesis in its activated form. The authors postulated the presence of a multiprotein complex consisting of CLDN1, ZO1, and Src2 that regulates activation of Src downstream oncogenic signaling [85]. Another cellular self-defense mechanism, Fas-mediated apoptosis, has been shown to alter OCLN and ZO1 expression in lung epithelia [86].

Furthermore, several studies indicate TJ proteins to function as intracellular signaling platforms, involved in regulation of cell differentiation and growth. Indeed, Spadaro et al. reported conformational changes of ZO1 to induce recruitment of the transcription factor DbpA to TJs in epithelial (Eph4) cells, hereby affecting cell proliferation [87]. In lung cells, interaction between CLDN18 and the signaling molecule Yes-associated protein (YAP) has been shown to affect colony formation and progenitor cell proliferation [88].

Posttranslational modification of TJ transmembrane proteins by growth factor signaling pathways fine-tune the TJ barrier function. Mitogen-activated protein kinase (MAPK) [89] and PKA [90] have been shown to phosphorylate CLDN1 at TJs of cerebral and lung endothelial cells, hereby affecting TJ permeability. Phosphorylation of CLDN5, induced by cyclic-AMP potentiates the blood–brain barrier [90], while PKA mediated phosphorylation of CLDN16 affects Mg2+ transport in kidney cells [91]. Vascular endothelial growth factor (VEGF) signaling perturbs hepatocellular TJ integrity by targeting OCLN via the PKC pathway [92]. Moreover, several studies indicate that cytokines, which are upregulated during inflammation, affect TJ protein expression. For example, Ni and coworkers demonstrated that TNF-α-induced phosphorylation of OCLN in human cerebral endothelial cells via MAPK, modulates TJ permeability [93]. Moreover, OCLN phosphorylation regulates its interaction with ZO1 in kidney cancer cells [94]. Exposure of intestinal epithelial cells with TNF-α hampers TJ permeability via NF-κB-dependent downregulation of ZO1 expression and altered junctional localization [95]. Loss of epithelial cell-to-cell junctions including TJs, represents a typical and early event in the evolution of epithelial-mesenchymal transition (EMT). EMT describes a process by which epithelial cells lose epithelial characteristics and acquire mesenchymal properties including the ability of migration and invasion [96,97].

4. Tight Junction Proteins in the Liver and the Blood-Biliary Barrier

Epithelial cells in the liver, namely hepatocytes and cholangiocytes, form the parenchymal structure of the organ and are characterized by a distinct cell polarity. TJs between neighboring hepatocytes separate the hepatocyte cell membrane into basal (sinusoidal), basolateral, and apical (bile canalicular) domains. By sealing the paracellular space, TJs and other adhesion complexes build the physiological BBIB, that segregates blood-containing basal hepatic sinusoids from apical bile canaliculi [9]. The BBIB hereby enables simultaneous execution of two major functions of the liver: the production and secretion of bile and the continuous metabolic exchange with the portal and systemic circulation allowing detoxification and excretion of proteins and coagulation factors. In particular, the apical bile canalicular domain of hepatocytes is characterized by numerous bile transporters and microvilli, that are required for bile secretion and absorption, while the basolateral sinusoidal domain is specialized in metabolic exchange with the blood [98]. CLDNs 1-3 and OCLN are expressed in TJs of hepatocytes and cholangiocytes [53,99,100]. While transmembrane TJ proteins on hepatocytes build the BBIB and shape bile canaliculi, TJs on cholangiocytes line the intrahepatic bile ducts [7]. The gallbladder on the other hand, shows physiologically strong expression of CLDNs 2, 3, 7, and OCLN. The hepatic sinusoidal endothelium strongly expresses CLDN5 [8].

In the normal liver and in contrast to other TJ proteins, tricellulin expression in hepatocytes and biliary epithelial cells strongly variates between individuals but is accentuated at tricellular contacts in colocalization with CLDN1 and CLDN4 [101]. In contrast to their weak expression on hepatocytes, the junctional adaptor proteins 7H6 and ZO1 are enriched in bile canaliculi [33,102].

KO studies in mice suggest a crucial role of CLDN2 and 3 for the BBIB. Thus, KO of the channel-forming CLDN2 lead to cholesterol gallstone disease due to a decrease in paracellular water transport [53]. CLDN3 KO in mice on the other hand, increases the paracellular phosphate ion transport

of hepatic tight junctions, resulting in calcium phosphate core formation. Cholesterol overdose causes the cholesterol gallstone disease in these mice [99].

5. Tight Junction Proteins in Chronic Hepatobiliary Diseases

Chronic liver diseases constitute a global health problem, associated with high mortality due to its complications of liver cirrhosis and cancer [103]. Major causes comprise chronic hepatitis B virus (HBV) and HCV infection, alcoholic and metabolic liver disease such as non-alcoholic steatohepatitis. Decompensated liver cirrhosis is the fourth most common cause of death in adults in central Europe [104,105]. Downregulated expression or impaired function of TJ proteins have frequently been associated with chronic liver diseases [12]. Loss of the BBIB, which is maintained by junctional adhesion complexes including TJs represents a common feature in mice models of chronic liver injury [106,107]. Takaki et al. observed loss of TJ protein expression, including CLDN3 and ZO1 following hepatectomy and reappearance several days after surgery. This suggests a functional role of TJ proteins in liver regeneration [108]. Moreover, alterations related to the expression of TJ proteins have been implicated in chronic HCV infection, biliary diseases, and liver cancer.

5.1. Tight Junction Proteins and HCV Infection

Chronic HCV infection represents a serious global health problem affecting more than 71 million people worldwide and potentially leads to liver fibrosis, cirrhosis, and hepatocellular carcinoma (HCC) [109–111]. Cell entry is a critical step in the HCV life cycle and involves a complex multi-step process consisting of viral attachment to the hepatocyte cell membrane and internalization [10,112]. HCV requires a complex orchestration of host dependency factors including among others CLDN1, OCLN, CD81, and SR-B1. Mechanistically, EGFR signaling promotes CLDN1-CD81 coreceptor association, which is a prerequisite for the internalization of the virus (Figure 2).

OCLN on the other hand, is believed to act downstream of the other cell entry factors CD81, CLDN1, and SRB1 during the HCV entry process [113,114]. OCLN interacts with HCV surface glycoprotein E2 via its extracellular loop 2 (ECL2) [115]. Of note, transgenic expression of human OCLN enables HCV infection of non-permissive species like mice [116–118]. However, the exact mechanism and localization of OCLN-HCV interaction is not fully understood. Considering its role for HCV cell entry, alterations in CLDN1 and OCLN expression levels and their functional consequences have been a focus of interest in the HCV field within the last years. Hepatic expression of CLDN1 and OCLN was found to be increased in liver biopsies of patients with chronic HCV infection [119]. In accordance, HCV liver graft infection is associated with OCLN and CLDN1 upregulation [120].

Anti-CLDN1 antibodies prevent and eliminate chronic HCV infection in cell-based and animal models without any detectable adverse effects and especially without disrupting TJ integrity or function [121–124]. The safety profile was further confirmed in human liver-chimeric mice and is most likely related to the molecular mechanism of action of CLDN1 monoclonal antibodies (mAbs) targeting the non-junctional expressed CLDN1 on hepatocytes without binding to CLDN1 localized in TJs [123–125]. Xiao et al. reported synergistic effects of anti-CLDN1 mAb with direct-acting antivirals as antiviral approaches for difficult-to-treat patients [126,127]. Confirming the functional role of OCLN in HCV entry, previous mechanistic monoclonal antibodies targeting ECL2 of OCLN were efficient in the prevention of infection both in cell culture and human liver chimeric mice without detectable side effects [114,128,129].

5.2. Tight Junction Proteins in Hepatocellular Carcinoma

Primary liver cancer is the sixth most frequent and second most deadly type of cancer in the world, with HCC being the most common histological subtype (75%–85%) [130]. Several members of the CLDN family have been reported to be perturbed during hepatocarcinogenesis. CLDN1, 4, 5, 7, and 10 are overexpressed in HCC [80,131–135]. Low levels of CLDN5 and high levels of CLDN7 were found to be independent prognostic factors [131]. Similarly, CLDN10 overexpression in

HCC correlated with poor patients' outcome and tumor recurrence [133,136]. In contrast, CLDN14 downregulation in HCCs correlates with advanced tumor stage and poor overall survival [137] and CLDN3 expression is decreased in HCC [138]. Bouchagier and coworkers reported an overexpression of OCLN in HCC tumors compared to non-neoplastic liver tissues, which positively correlated with a favorable prognosis [131]. Orban et al. on the other hand, found decreased OCLN mRNA and protein levels in HCC [102]. These opposing findings may be due to different histological grading of the analyzed HCC samples and a potential dedifferentiation characterized by decreased OCLN levels. Decreased cell migration and proliferation following treatment of HCC cells with different compounds was accompanied by upregulation of OCLN expression, indicating mesenchymal-epithelial transition (MET) [139–141] and thus supporting the findings from Bouchagier et al. Expression of tricellulin is very heterogeneous in HCC tissues, but seems to be positively correlated with poor prognosis [101]. Downregulation of ZO1 on the other hand, associates with poor prognosis in HCC patients undergoing hepatectomy [142]. Collectively, these studies suggest a pathogenic role of TJ proteins in hepatocarcinogenesis.

Studies on TJ protein expression in chronic liver diseases together with clinical correlations are summarized in Table 1.

Table 1. Perturbation of TJ proteins in chronic liver diseases.

Liver Disease	Tight Junction Protein	Perturbation	Potential Clinical Impact	References
HCV infection	CLDN1	• Overexpression in chronically HCV-infected liver tissue • Upregulation upon HCV liver graft infection	• SNPs in *CLDN1* promoter confer susceptibility to HCV infection • Crucial HCV entry factor, antiviral target	[143,144] [119,121,124], [120,122,123]
	OCLN	• Overexpression in chronically HCV-infected liver tissue • Upregulation upon HCV liver graft infection	• Crucial HCV entry factor, antiviral target	[114,119,120,128,129,145]
HCC	CLDN1	• Upregulated in the large majority of HCCs	• Correlation of expression with patients' survival • Therapeutic target	[80,131,132,134,135]
	CLDN3, CLDN14	• Downregulated/low expression in HCC	• Unknown	[137,138]
	CLDN4, 5, 7 and 10	• Upregulated in HCC	• Unknown	[131] [133,136]
	OCLN	• Both downregulated and upregulated described in HCC	• Positive correlation of expression with good prognosis	[102,131]
	Tricellulin	• Heterogeneous	• Positive correlation with poor prognosis	[101]
	ZO1	-	• Low expression correlates with HCC recurrence after hepatic resection	[142]

6. Tight Junction Proteins in Biliary Diseases

Considering that TJ proteins on bile canaliculi are major contributors to the BBIB, TJ integrity has frequently been investigated in biliary diseases. Indeed, disruption of bile duct epithelial barrier plays a crucial role in the pathogenesis of chronic biliary diseases [7]. Studies in animal models of cholestatic disease hereby revealed secondary expressional and morphologic alterations of the tight junctional network upon cholestatic liver injury [146]. Perturbation of TJ proteins could further be found in human biliary liver diseases as primary sclerosing cholangitis (PSC) [147] and cholangiocellular carcinoma (CCA) [148]. Moreover, primary perturbation of TJ proteins caused by homozygous mutations have been identified to account for cholestatic syndromes, including progressive familial intrahepatic cholestasis (PFIC) type 4 [149,150] and the neonatal ichthyosis-sclerosing cholangitis (NISCH) syndrome [151].

6.1. Tight Junction Proteins in Primary Biliary Cirrhosis and Secondary Sclerosing Cholangitis

Primary biliary cirrhosis (PBC) and PSC represent etiologies of chronic liver disease that are characterized by cholestasis and an increased risk of developing liver cirrhosis and cancer. Mediated by immunological mechanisms of bile duct destruction, patients typically present with elevated serum levels of bile acids [152,153]. Ultrastructural studies of damaged bile ducts in PBC show electron-dense deposits in enlarged intercellular spaces, infiltrated by immune cells indicating perturbated barrier integrity [154]. TJ proteins are responsible for the main barrier formations maintaining the BBIB and preventing bile regurgitation from the biliary tract. In this context, downregulation of the TJ proteins 7H6 and ZO1 in bile ducts in PBC and in hepatocytes in PSC has been suggested to account for the increased paracellular permeability observed in chronic cholestatic liver diseases. Consequently, toxic bile acids can enter the periductal area and promote the infiltration of immune cells, eventually leading to inflammatory driven progression of bile injury. Interestingly, the expression of these TJ proteins is preserved in PBC patients treated with ursodeoxycholic acid [147].

6.2. Primary Perturbation of Tight Junction Proteins in Biliary Diseases: NISCH Syndrome and PFIC Type 4

NISCH syndrome represents an extremely rare autosomal-recessive ichthyosis syndrome caused by mutations in the *CLDN1* gene leading to its abolished expression in liver and skin (KO phenotype). First being described in 2002, only 12 cases have been reported [151,155–161]. The clinical manifestation is variable ranging from absent or regressive cholestasis to progressive liver disease with liver failure. The hepatic feature of this syndrome is characterized by neonatal sclerosing cholangitis with elevated serum bile acids and hepatomegaly. Additional non-hepatic manifestations can include dental anomalies, mild psychomotor delay, ichthyosis, and scalp hypotrichosis as well as scarring alopecia [56,151]. The human phenotype hereby strongly deviates from the one observed in CLDN1-KO mice that present severely wrinkled appearance of the skin and death within 24 h after birth [52], indicating differential function of CLDNs in mice and humans. Thus, increased paracellular permeability and secondary bile injury due to CLDN1 absence in patients with NISCH syndrome [44] may be compensated by overexpression of other TJ protein members in the liver, explaining the variable phenotype [56]. Alternatively, mutations in other genes may be responsible for part of the observed phenotype. In conclusion, these findings demonstrate that CLDN1 is not essential for life in humans and its absence has a variable clinical phenotype.

Loss of ZO2 on the other hand, is observed in PFIC type 4 [149,150]. Mechanistically, a mutation in the *ZO2* gene has been described to hamper proper localization of CLDN1 in TJs of cholangiocytes in the liver despite normal protein levels, hereby increasing paracellular permeability to bile acids [149]. Clinical signs of cholestasis appear within the first year of life in patients homozygous for this mutation and are typically contrasted by normal levels of γ-glutamyl transferase activity (GGT). Progressing into secondary biliary cirrhosis, affected patients present with severe liver disease at a young age, often requiring liver transplantation [149]. A missense mutation in the first PDZ domain of ZO2, that binds

to CLDN1 in TJs has further been described in patients with familial hypercholanemia, characterized by pruritus and fat malabsorption but without progressive liver disease [162].

6.3. Tight Junction Proteins in Cholangiocellular Carcinoma

Cholangiocellular carcinoma (CCA) represents the second most common primary liver cancer type. With an overall incidence rate of 2/100000 it belongs to the rather rare cancer subtypes, though within the last few years, a dramatic increase in prevalence and mortality have been documented [163–165]. In contrast to the strong linkage of liver fibrosis/cirrhosis with HCC, most CCAs occur sporadically. However, known risk factors are PSC and HBV/HCV associated liver cirrhosis [166–169].

Several studies have reported evidence for potential functional implication of TJ proteins in CCA. CLDN3, 7, 8, and 10 expression were found to be decreased in intrahepatic CCAs compared to normal tissues. Significantly lower expression of CLDN1, 8, and 10 was also found in extrahepatic CCA, while CLDN1, 2, 3, 7, 8, and 10 are decreased in CCA of the gallbladder [148]. The most significant alteration of CLDN expression between CCA and adjacent liver tissue was found for CLDN10, as it was markedly decreased in all forms of bile duct cancers [148]. Moreover, in contrast to its restricted membrane localization in normal bile epithelia, intrahepatic CCA showed cytoplasmatic localization of CLDN10. Based on the negative staining in HCC and normal mature hepatocytes, CLDN4 and CLDN7 have been suggested as immunohistochemical markers of cholangiocellular differentiation in primary liver cancer [170,171]. In view of its preserved or even elevated expression in intra- and extrahepatic CCA, especially CLDN4 represents an attractive histological marker of CCA [148]. Interestingly, downregulation of CLDN4 by siRNA led to decreased migration and invasion of CCA cell lines [172]. CLDN18, that has been intensively studied in relation to gastric cancer is expressed in 40% of intrahepatic CCAs and is associated with lymph node metastasis and poor prognosis [173].

In intrahepatic CCA, tricellulin is decreased compared to adjacent tumor tissue, while patients with preserved tricellulin expression had significantly better clinical outcome and lower histological grading [101]. Downregulation of ZO1 and OCLN are associated with progression in biliary tract cancers [174].

All reported perturbations of TJ protein expressions in chronic hepatobiliary diseases are summarized in Table 2.

Table 2. Perturbation of TJ proteins in chronic biliary diseases.

Biliary Disease	TJ Protein	Perturbation	Potential Clinical Implication	References
Primary biliary cirrhosis (PBC)	ZO1	• Downregulation in bile ducts of patients with PBC	• Increased paracellular permeability • Preservation of ZO-1 expression in patients treated with ursodeoxycholic acid	[147]
Primary sclerosing cholangitis (PSC)	ZO1	• Downregulation on hepatocytes of patients with PSC	• Increased paracellular permeability	[147]
Progressive familial intrahepatic cholestasis (PFIC) type 4	ZO2	• Loss of expression	• Failed localization of CLDN1 to TJs on cholangiocytes despite normal CLDN1 protein levels • Increased paracellular permeability • Progressive chronic liver disease	[149,150]
Familial hypercholanemia	ZO2	• Missense mutation in the first PDZ domain of ZO2	• Perturbed localization of CLDN1 in TJs • Pruritus, fat malabsorption, elevated serum bile acid concentrations	[162]
NISCH syndrome	CLDN1	• Loss of CLDN1 expression due to homozygous *CLDN1* mutation (functional KO)	• Variable clinical outcome from mild to absent disease to neonatal sclerosing cholangitis and ichthyosis (with functional impact of additional mutations unknown) • Increased paracellular permeability	[56,151]
CCA	CLDN1–3, 7, 8, and 10	• Perturbed expression in intrahepatic, extrahepatic CCA, and/or CCA of the gallbladder	• CLDN7: suggested as histological marker to distinguish CCA from HCC	[148,170]
	CLDN4	• Perturbed expression in CCA	• Suggested as histological marker to distinguish HCC and CCA	[148,170–172]
	CLDN18	• Expressed in 40% of intrahepatic CCAs	• Expression is associated with lymph node metastasis and poor prognosis	[173]
	Tricellulin	• Downregulated in CCA	• Positive correlation of expression with clinical outcome and low staging	[101]
	OCLN	• Downregulated in CCA	• Correlation of downregulated expression with tumor progression	[148]
	ZO1	• Downregulated in CCA	• Correlation of downregulated expression with tumor progression	[148]

7. Summary

Tight junction proteins on hepatocytes and cholangiocytes play an important functional role as paracellular gatekeepers and represent the molecular basis of the BBIB, enabling exertion of two major function of the liver: production and secretion of bile as well as metabolic exchange and detoxification. Moreover, non-junctional TJ proteins at the basolateral membrane and in the nucleus exert key functions in cellular signaling, apoptosis, and migration. The TJ proteins CLDN1 and OCLN on the basolateral membrane of hepatocytes serve as entry factors for HCV—a major cause of liver disease and cancer worldwide. Highlighting its function as regulators of paracellular permeability enabling maintenance of the BBIB, secondary perturbation of TJ proteins has been described in biliary diseases, including PSC and PBC. In humans, the complete loss of distinct TJ proteins is not lethal, and the associated clinical phenotypes are highly variable as described for NISCH-syndrome or PFIC type 3. Finally, up- or downregulation of TJ protein expression in hepatobiliary cancer suggests a functional implication of TJ proteins in key cell regulatory signaling cascades potentially associated with carcinogenesis.

Author Contributions: N.R. and T.F.B. conceptualized the N.R. performed the literature review and wrote the manuscript. J.L., C.S. and T.F.B. revised the manuscript, J.L., A.S., H.E.S. and A.A.R.S. prepared original figures. All authors have read and agreed to the published version of the manuscript.

Funding: The authors acknowledge support by ARC, Paris and Institut Hospital-Universitaire, Strasbourg (TheraHCC, TheraHCC2.0 IHUARC IHU201301187 and IHUARC2019 IHU201901299 to T.F.B.), the European Union (ERC-AdG-2014-671231-HEPCIR, EU H2020-667273-HEPCAR and ERC-PoC-2016-PRELICAN, ERC-PoC-2018-HEPCAN to T.F.B), Agence nationale de recherche sur le sida et les hépatites virales (ANRS, ECTZ35076) and the Foundation of the University of Strasbourg. This work was done under the framework of the LABEX ANR-10-LABX-0028_HEPSYS and Inserm Plan Cancer (Plan Cancer 2014-2019, Action 13.1, appel à projets 2018) and benefits from funding from the state managed by the French National Research Agency as part of the Investments for the future. N. R. is supported by a fellowship of the German Research Foundation (DFG) (RO 5983/1-1 to NR).

Conflicts of Interest: Inserm, the University of Strasbourg, the Strasbourg University Hospitals and the IHU have filed patent applications and patents on Claudin-1 specific monoclonal antibodies for prevention and treatment of HCV infection and hepatocellular carcinoma which have been licensed to Alentis Therapeutics, Basel, Switzerland.

Abbreviations

Akt	AKT serine/threonine kinase
Apo	Apolipoprotein
BBIB	Blood-biliary barrier
bTJ	Bicellular tight junction
CCA	Cholangiocellular carcinoma
CD81	Cluster of differentiation 81
CLDN	Claudin
c-myc	MYC proto-oncogene
ECL2	Extracellular loop 2
EGFR	Epidermal growth factor receptor
EMT	Epithelial-mesenchymal transition
EpCAM	Epithelial cell adhesion molecule
ESAM	Endothelial cell-selective adhesion molecule
FAK	Focal adhesion kinase
GGT	γ-glutamyl transferase
HBV	Hepatitis B virus
HCC	Hepatocellular carcinoma
HCV	Hepatitis C virus
HRas	HRas proto-oncogene, GTPase
HS	Heparan sulfate
IgSF	Immunoglobulin superfamily
ILDR	Immunoglobulin-like domain containing receptor

ITGB1	Integrin subunit beta 1
JAM	Junctional adhesion molecules
KO	Knockout
LSR	Lipolysis-stimulated lipoprotein receptor
mAbs	Monoclonal antibodies
MAGI	Membrane-associated guanylate kinase inverted
MAPK	Mitogen-activated protein kinase
MARVEL	MAL and related proteins for vesicle trafficking and membrane link
MET	Mesenchymal-epithelial transition
MMP	Matrix metalloproteinase
NISCH	Neonatal ichthyosis-sclerosing cholangitis
NPC1L1	Niemann-Pick C1-like protein 1
OCLN	Occludin
PBC	Primary biliary cirrhosis
PFIC	Progressive familial intrahepatic cholestasis
PKA	Protein kinase A
PKC	Protein kinase C
PP	Protein phosphatase
PSC	Primary sclerosing cholangitis
RTK	Receptor tyrosine kinase
SH3	Src homology 3 domain
SNPs	Single nucleotide polymorphisms
SR-BI	Scavenger receptor class B member 1
Src	Steroid receptor coactivator
TfR1	Transferrin receptor 1
TJ	Tight junction
tTJ	Tricellular tight junction
TNF-α	Tumor necrosis factor alpha
VEGF	Vascular endothelial growth factor
YAP	Yes-associated protein
ZO	Zonula occludens
ZONAB	ZO1-associated nucleic acid binding protein

References

1. Zihni, C.; Mills, C.; Matter, K.; Balda, M.S. Tight junctions: From simple barriers to multifunctional molecular gates. *Nat. Rev. Mol. Cell Biol.* **2016**, *17*, 564–580. [CrossRef] [PubMed]
2. Severson, E.A.; Parkos, C.A. Mechanisms of outside-in signaling at the tight junction by junctional adhesion molecule A. *Ann. N. Y. Acad. Sci.* **2009**, *1165*, 10–18. [CrossRef] [PubMed]
3. Singh, A.B.; Uppada, S.B.; Dhawan, P. Claudin proteins, outside-in signaling, and carcinogenesis. *Pflug. Arch.* **2017**, *469*, 69–75. [CrossRef] [PubMed]
4. Farkas, A.E.; Capaldo, C.T.; Nusrat, A. Regulation of epithelial proliferation by tight junction proteins. *Ann. N. Y. Acad. Sci.* **2012**, *1258*, 115–124. [CrossRef]
5. Kojima, T.; Sawada, N. Expression and function of claudins in hepatocytes. *Methods Mol. Biol.* **2011**, *762*, 233–244. [CrossRef]
6. Gonzalez-Mariscal, L.; Tapia, R.; Chamorro, D. Crosstalk of tight junction components with signaling pathways. *Biochim. Biophys. Acta* **2008**, *1778*, 729–756. [CrossRef]
7. Rao, R.K.; Samak, G. Bile duct epithelial tight junctions and barrier function. *Tissue Barriers* **2013**, *1*, e25718. [CrossRef]
8. Sakaguchi, T.; Suzuki, S.; Higashi, H.; Inaba, K.; Nakamura, S.; Baba, S.; Kato, T.; Konno, H. Expression of tight junction protein claudin-5 in tumor vessels and sinusoidal endothelium in patients with hepatocellular carcinoma. *J. Surg. Res.* **2008**, *147*, 123–131. [CrossRef]

9. Kojima, T.; Yamamoto, T.; Murata, M.; Chiba, H.; Kokai, Y.; Sawada, N. Regulation of the blood-biliary barrier: Interaction between gap and tight junctions in hepatocytes. *Med. Electron. Microsc.* **2003**, *36*, 157–164. [CrossRef]
10. Miao, Z.; Xie, Z.; Miao, J.; Ran, J.; Feng, Y.; Xia, X. Regulated Entry of Hepatitis C Virus into Hepatocytes. *Viruses* **2017**, *9*, 100. [CrossRef]
11. Hagen, S.J. Non-canonical functions of claudin proteins: Beyond the regulation of cell-cell adhesions. *Tissue Barriers* **2017**, *5*, e1327839. [CrossRef]
12. Zeisel, M.B.; Dhawan, P.; Baumert, T.F. Tight junction proteins in gastrointestinal and liver disease. *Gut* **2018**. [CrossRef]
13. Markov, A.G.; Aschenbach, J.R.; Amasheh, S. The epithelial barrier and beyond: Claudins as amplifiers of physiological organ functions. *IUBMB Life* **2017**, *69*, 290–296. [CrossRef]
14. Baas, A.F.; Kuipers, J.; van der Wel, N.N.; Batlle, E.; Koerten, H.K.; Peters, P.J.; Clevers, H.C. Complete polarization of single intestinal epithelial cells upon activation of LKB1 by STRAD. *Cell* **2004**, *116*, 457–466. [CrossRef]
15. Umeda, K.; Matsui, T.; Nakayama, M.; Furuse, K.; Sasaki, H.; Furuse, M.; Tsukita, S. Establishment and characterization of cultured epithelial cells lacking expression of ZO-1. *J. Biol. Chem.* **2004**, *279*, 44785–44794. [CrossRef]
16. Ebnet, K.; Suzuki, A.; Ohno, S.; Vestweber, D. Junctional adhesion molecules (JAMs): More molecules with dual functions? *J. Cell Sci.* **2004**, *117*, 19–29. [CrossRef]
17. Ebnet, K. Junctional Adhesion Molecules (JAMs): Cell Adhesion Receptors with Pleiotropic Functions in Cell Physiology and Development. *Physiol. Rev.* **2017**, *97*, 1529–1554. [CrossRef]
18. Ikenouchi, J.; Furuse, M.; Furuse, K.; Sasaki, H.; Tsukita, S.; Tsukita, S. Tricellulin constitutes a novel barrier at tricellular contacts of epithelial cells. *J. Cell Biol.* **2005**, *171*, 939–945. [CrossRef]
19. Masuda, S.; Oda, Y.; Sasaki, H.; Ikenouchi, J.; Higashi, T.; Akashi, M.; Nishi, E.; Furuse, M. LSR defines cell corners for tricellular tight junction formation in epithelial cells. *J. Cell Sci.* **2011**, *124*, 548–555. [CrossRef]
20. Higashi, T.; Tokuda, S.; Kitajiri, S.; Masuda, S.; Nakamura, H.; Oda, Y.; Furuse, M. Analysis of the 'angulin' proteins LSR, ILDR1 and ILDR2–tricellulin recruitment, epithelial barrier function and implication in deafness pathogenesis. *J. Cell Sci.* **2013**, *126*, 966–977. [CrossRef]
21. Furuse, M.; Hirase, T.; Itoh, M.; Nagafuchi, A.; Yonemura, S.; Tsukita, S.; Tsukita, S. Occludin: A novel integral membrane protein localizing at tight junctions. *J. Cell Biol.* **1993**, *123*, 1777–1788. [CrossRef] [PubMed]
22. Cummins, P.M. Occludin: One protein, many forms. *Mol. Cell. Biol.* **2012**, *32*, 242–250. [CrossRef] [PubMed]
23. Mineta, K.; Yamamoto, Y.; Yamazaki, Y.; Tanaka, H.; Tada, Y.; Saito, K.; Tamura, A.; Igarashi, M.; Endo, T.; Takeuchi, K.; et al. Predicted expansion of the claudin multigene family. *FEBS Lett.* **2011**, *585*, 606–612. [CrossRef] [PubMed]
24. Gunzel, D.; Fromm, M. Claudins and other tight junction proteins. *Compr. Physiol.* **2012**, *2*, 1819–1852. [CrossRef]
25. Tamura, A.; Tsukita, S. Paracellular barrier and channel functions of TJ claudins in organizing biological systems: Advances in the field of barriology revealed in knockout mice. *Semin. Cell Dev. Biol.* **2014**, *36*, 177–185. [CrossRef]
26. Tanaka, H.; Tamura, A.; Suzuki, K.; Tsukita, S. Site-specific distribution of claudin-based paracellular channels with roles in biological fluid flow and metabolism. *Ann. N. Y. Acad. Sci.* **2017**, *1405*, 44–52. [CrossRef]
27. Chiba, H.; Osanai, M.; Murata, M.; Kojima, T.; Sawada, N. Transmembrane proteins of tight junctions. *Biochim. Biophys. Acta* **2008**, *1778*, 588–600. [CrossRef]
28. Bauer, H.; Zweimueller-Mayer, J.; Steinbacher, P.; Lametschwandtner, A.; Bauer, H.C. The dual role of zonula occludens (ZO) proteins. *J. Biomed. Biotechnol.* **2010**, *2010*, 402593. [CrossRef]
29. Tsukita, S.; Furuse, M.; Itoh, M. Molecular architecture of tight junctions: Occludin and ZO-1. *Soc. Gen. Physiol. Ser.* **1997**, *52*, 69–76.
30. Willott, E.; Balda, M.S.; Fanning, A.S.; Jameson, B.; Van Itallie, C.; Anderson, J.M. The tight junction protein ZO-1 is homologous to the Drosophila discs-large tumor suppressor protein of septate junctions. *Proc. Natl. Acad. Sci. USA* **1993**, *90*, 7834–7838. [CrossRef]
31. Guillemot, L.; Paschoud, S.; Pulimeno, P.; Foglia, A.; Citi, S. The cytoplasmic plaque of tight junctions: A scaffolding and signalling center. *Biochim. Biophys. Acta* **2008**, *1778*, 601–613. [CrossRef] [PubMed]

32. Li, Y.; Fanning, A.S.; Anderson, J.M.; Lavie, A. Structure of the conserved cytoplasmic C-terminal domain of occludin: Identification of the ZO-1 binding surface. *J. Mol. Biol.* **2005**, *352*, 151–164. [CrossRef] [PubMed]
33. Zhong, Y.; Saitoh, T.; Minase, T.; Sawada, N.; Enomoto, K.; Mori, M. Monoclonal antibody 7H6 reacts with a novel tight junction-associated protein distinct from ZO-1, cingulin and ZO-2. *J. Cell Biol.* **1993**, *120*, 477–483. [CrossRef] [PubMed]
34. Citi, S.; Sabanay, H.; Jakes, R.; Geiger, B.; Kendrick-Jones, J. Cingulin, a new peripheral component of tight junctions. *Nature* **1988**, *333*, 272–276. [CrossRef] [PubMed]
35. Tsukita, S.; Furuse, M.; Itoh, M. Multifunctional strands in tight junctions. *Nat. Rev. Mol. Cell Biol.* **2001**, *2*, 285–293. [CrossRef]
36. Tsukita, S.; Tanaka, H.; Tamura, A. The Claudins: From Tight Junctions to Biological Systems. *Trends Biochem. Sci.* **2019**, *44*, 141–152. [CrossRef] [PubMed]
37. Shen, L.; Weber, C.R.; Turner, J.R. The tight junction protein complex undergoes rapid and continuous molecular remodeling at steady state. *J. Cell Biol.* **2008**, *181*, 683–695. [CrossRef]
38. Chalmers, A.D.; Whitley, P. Continuous endocytic recycling of tight junction proteins: How and why? *Essays Biochem.* **2012**, *53*, 41–54. [CrossRef]
39. Ivanov, A.I.; Nusrat, A.; Parkos, C.A. Endocytosis of the apical junctional complex: Mechanisms and possible roles in regulation of epithelial barriers. *Bioessays* **2005**, *27*, 356–365. [CrossRef]
40. Ivanov, A.I.; Nusrat, A.; Parkos, C.A. Endocytosis of epithelial apical junctional proteins by a clathrin-mediated pathway into a unique storage compartment. *Mol. Biol. Cell* **2004**, *15*, 176–188. [CrossRef]
41. Lu, R.; Stewart, L.; Wilson, J.M. Scaffolding protein GOPC regulates tight junction structure. *Cell Tissue Res.* **2015**, *360*, 321–332. [CrossRef] [PubMed]
42. Lu, R.; Johnson, D.L.; Stewart, L.; Waite, K.; Elliott, D.; Wilson, J.M. Rab14 regulation of claudin-2 trafficking modulates epithelial permeability and lumen morphogenesis. *Mol. Biol. Cell* **2014**, *25*, 1744–1754. [CrossRef]
43. Gunzel, D.; Yu, A.S. Claudins and the modulation of tight junction permeability. *Physiol. Rev.* **2013**, *93*, 525–569. [CrossRef]
44. Grosse, B.; Cassio, D.; Yousef, N.; Bernardo, C.; Jacquemin, E.; Gonzales, E. Claudin-1 involved in neonatal ichthyosis sclerosing cholangitis syndrome regulates hepatic paracellular permeability. *Hepatology* **2012**, *55*, 1249–1259. [CrossRef] [PubMed]
45. Van Itallie, C.M.; Fanning, A.S.; Holmes, J.; Anderson, J.M. Occludin is required for cytokine-induced regulation of tight junction barriers. *J. Cell Sci.* **2010**, *123*, 2844–2852. [CrossRef] [PubMed]
46. Laukoetter, M.G.; Nava, P.; Lee, W.Y.; Severson, E.A.; Capaldo, C.T.; Babbin, B.A.; Williams, I.R.; Koval, M.; Peatman, E.; Campbell, J.A.; et al. JAM-A regulates permeability and inflammation in the intestine in vivo. *J. Exp. Med.* **2007**, *204*, 3067–3076. [CrossRef]
47. Vetrano, S.; Rescigno, M.; Cera, M.R.; Correale, C.; Rumio, C.; Doni, A.; Fantini, M.; Sturm, A.; Borroni, E.; Repici, A.; et al. Unique role of junctional adhesion molecule-a in maintaining mucosal homeostasis in inflammatory bowel disease. *Gastroenterology* **2008**, *135*, 173–184. [CrossRef] [PubMed]
48. Umeda, K.; Ikenouchi, J.; Katahira-Tayama, S.; Furuse, K.; Sasaki, H.; Nakayama, M.; Matsui, T.; Tsukita, S.; Furuse, M.; Tsukita, S. ZO-1 and ZO-2 independently determine where claudins are polymerized in tight-junction strand formation. *Cell* **2006**, *126*, 741–754. [CrossRef] [PubMed]
49. Satoh, H.; Zhong, Y.; Isomura, H.; Saitoh, M.; Enomoto, K.; Sawada, N.; Mori, M. Localization of 7H6 tight junction-associated antigen along the cell border of vascular endothelial cells correlates with paracellular barrier function against ions, large molecules, and cancer cells. *Exp. Cell Res.* **1996**, *222*, 269–274. [CrossRef]
50. Zhong, Y.; Enomoto, K.; Isomura, H.; Sawada, N.; Minase, T.; Oyamada, M.; Konishi, Y.; Mori, M. Localization of the 7H6 antigen at tight junctions correlates with the paracellular barrier function of MDCK cells. *Exp. Cell Res.* **1994**, *214*, 614–620. [CrossRef]
51. Kage, H.; Flodby, P.; Gao, D.; Kim, Y.H.; Marconett, C.N.; DeMaio, L.; Kim, K.J.; Crandall, E.D.; Borok, Z. Claudin 4 knockout mice: Normal physiological phenotype with increased susceptibility to lung injury. *Am. J. Physiol. Lung Cell. Mol. Physiol.* **2014**, *307*, L524–L536. [CrossRef] [PubMed]
52. Furuse, M.; Hata, M.; Furuse, K.; Yoshida, Y.; Haratake, A.; Sugitani, Y.; Noda, T.; Kubo, A.; Tsukita, S. Claudin-based tight junctions are crucial for the mammalian epidermal barrier: A lesson from claudin-1-deficient mice. *J. Cell Biol.* **2002**, *156*, 1099–1111. [CrossRef] [PubMed]

53. Matsumoto, K.; Imasato, M.; Yamazaki, Y.; Tanaka, H.; Watanabe, M.; Eguchi, H.; Nagano, H.; Hikita, H.; Tatsumi, T.; Takehara, T.; et al. Claudin 2 deficiency reduces bile flow and increases susceptibility to cholesterol gallstone disease in mice. *Gastroenterology* **2014**, *147*, 1134–1145. [CrossRef] [PubMed]
54. Katsuno, T.; Umeda, K.; Matsui, T.; Hata, M.; Tamura, A.; Itoh, M.; Takeuchi, K.; Fujimori, T.; Nabeshima, Y.; Noda, T.; et al. Deficiency of zonula occludens-1 causes embryonic lethal phenotype associated with defected yolk sac angiogenesis and apoptosis of embryonic cells. *Mol. Biol. Cell* **2008**, *19*, 2465–2475. [CrossRef]
55. Saitou, M.; Furuse, M.; Sasaki, H.; Schulzke, J.D.; Fromm, M.; Takano, H.; Noda, T.; Tsukita, S. Complex phenotype of mice lacking occludin, a component of tight junction strands. *Mol. Biol. Cell* **2000**, *11*, 4131–4142. [CrossRef]
56. Hadj-Rabia, S.; Baala, L.; Vabres, P.; Hamel-Teillac, D.; Jacquemin, E.; Fabre, M.; Lyonnet, S.; De Prost, Y.; Munnich, A.; Hadchouel, M.; et al. Claudin-1 gene mutations in neonatal sclerosing cholangitis associated with ichthyosis: A tight junction disease. *Gastroenterology* **2004**, *127*, 1386–1390. [CrossRef]
57. Izraely, S.; Sagi-Assif, O.; Klein, A.; Meshel, T.; Ben-Menachem, S.; Zaritsky, A.; Ehrlich, M.; Prieto, V.G.; Bar-Eli, M.; Pirker, C.; et al. The metastatic microenvironment: Claudin-1 suppresses the malignant phenotype of melanoma brain metastasis. *Int. J. Cancer* **2015**, *136*, 1296–1307. [CrossRef]
58. Ding, L.; Lu, Z.; Foreman, O.; Tatum, R.; Lu, Q.; Renegar, R.; Cao, J.; Chen, Y.H. Inflammation and disruption of the mucosal architecture in claudin-7-deficient mice. *Gastroenterology* **2012**, *142*, 305–315. [CrossRef]
59. Lu, Z.; Kim, D.H.; Fan, J.; Lu, Q.; Verbanac, K.; Ding, L.; Renegar, R.; Chen, Y.H. A non-tight junction function of claudin-7-Interaction with integrin signaling in suppressing lung cancer cell proliferation and detachment. *Mol. Cancer* **2015**, *14*, 120. [CrossRef]
60. Ding, L.; Wang, L.; Sui, L.; Zhao, H.; Xu, X.; Li, T.; Wang, X.; Li, W.; Zhou, P.; Kong, L. Claudin-7 indirectly regulates the integrin/FAK signaling pathway in human colon cancer tissue. *J. Hum. Genet.* **2016**, *61*, 711–720. [CrossRef]
61. Tabaries, S.; Dong, Z.; Annis, M.G.; Omeroglu, A.; Pepin, F.; Ouellet, V.; Russo, C.; Hassanain, M.; Metrakos, P.; Diaz, Z.; et al. Claudin-2 is selectively enriched in and promotes the formation of breast cancer liver metastases through engagement of integrin complexes. *Oncogene* **2011**, *30*, 1318–1328. [CrossRef] [PubMed]
62. Wu, C.J.; Mannan, P.; Lu, M.; Udey, M.C. Epithelial cell adhesion molecule (EpCAM) regulates claudin dynamics and tight junctions. *J. Biol. Chem.* **2013**, *288*, 12253–12268. [CrossRef] [PubMed]
63. Nubel, T.; Preobraschenski, J.; Tuncay, H.; Weiss, T.; Kuhn, S.; Ladwein, M.; Langbein, L.; Zoller, M. Claudin-7 regulates EpCAM-mediated functions in tumor progression. *Mol. Cancer Res* **2009**, *7*, 285–299. [CrossRef] [PubMed]
64. Agarwal, R.; D'Souza, T.; Morin, P.J. Claudin-3 and claudin-4 expression in ovarian epithelial cells enhances invasion and is associated with increased matrix metalloproteinase-2 activity. *Cancer Res.* **2005**, *65*, 7378–7385. [CrossRef]
65. Leotlela, P.D.; Wade, M.S.; Duray, P.H.; Rhode, M.J.; Brown, H.F.; Rosenthal, D.T.; Dissanayake, S.K.; Earley, R.; Indig, F.E.; Nickoloff, B.J.; et al. Claudin-1 overexpression in melanoma is regulated by PKC and contributes to melanoma cell motility. *Oncogene* **2007**, *26*, 3846–3856. [CrossRef]
66. Yoon, C.H.; Kim, M.J.; Park, M.J.; Park, I.C.; Hwang, S.G.; An, S.; Choi, Y.H.; Yoon, G.; Lee, S.J. Claudin-1 acts through c-Abl-protein kinase Cdelta (PKCdelta) signaling and has a causal role in the acquisition of invasive capacity in human liver cells. *J. Biol. Chem.* **2010**, *285*, 226–233. [CrossRef]
67. Conlon, G.A.; Murray, G.I. Recent advances in understanding the roles of matrix metalloproteinases in tumour invasion and metastasis. *J. Pathol.* **2019**, *247*, 629–640. [CrossRef]
68. Torres-Martinez, A.C.; Gallardo-Vera, J.F.; Lara-Holguin, A.N.; Montano, L.F.; Rendon-Huerta, E.P. Claudin-6 enhances cell invasiveness through claudin-1 in AGS human adenocarcinoma gastric cancer cells. *Exp. Cell Res.* **2017**, *350*, 226–235. [CrossRef]
69. Gottardi, C.J.; Arpin, M.; Fanning, A.S.; Louvard, D. The junction-associated protein, zonula occludens-1, localizes to the nucleus before the maturation and during the remodeling of cell-cell contacts. *Proc. Natl. Acad. Sci. USA* **1996**, *93*, 10779–10784. [CrossRef]
70. Islas, S.; Vega, J.; Ponce, L.; Gonzalez-Mariscal, L. Nuclear localization of the tight junction protein ZO-2 in epithelial cells. *Exp. Cell Res.* **2002**, *274*, 138–148. [CrossRef]
71. Dhawan, P.; Singh, A.B.; Deane, N.G.; No, Y.; Shiou, S.R.; Schmidt, C.; Neff, J.; Washington, M.K.; Beauchamp, R.D. Claudin-1 regulates cellular transformation and metastatic behavior in colon cancer. *J. Clin. Investig.* **2005**, *115*, 1765–1776. [CrossRef] [PubMed]

72. Ikari, A.; Watanabe, R.; Sato, T.; Taga, S.; Shimobaba, S.; Yamaguchi, M.; Yamazaki, Y.; Endo, S.; Matsunaga, T.; Sugatani, J. Nuclear distribution of claudin-2 increases cell proliferation in human lung adenocarcinoma cells. *Biochim. Biophys. Acta* **2014**, *1843*, 2079–2088. [CrossRef] [PubMed]
73. Todd, M.C.; Petty, H.M.; King, J.M.; Piana Marshall, B.N.; Sheller, R.A.; Cuevas, M.E. Overexpression and delocalization of claudin-3 protein in MCF-7 and MDA-MB-415 breast cancer cell lines. *Oncol. Lett.* **2015**, *10*, 156–162. [CrossRef] [PubMed]
74. Cuevas, M.E.; Gaska, J.M.; Gist, A.C.; King, J.M.; Sheller, R.A.; Todd, M.C. Estrogen-dependent expression and subcellular localization of the tight junction protein claudin-4 in HEC-1A endometrial cancer cells. *Int. J. Oncol.* **2015**, *47*, 650–656. [CrossRef] [PubMed]
75. French, A.D.; Fiori, J.L.; Camilli, T.C.; Leotlela, P.D.; O'Connell, M.P.; Frank, B.P.; Subaran, S.; Indig, F.E.; Taub, D.D.; Weeraratna, A.T. PKC and PKA phosphorylation affect the subcellular localization of claudin-1 in melanoma cells. *Int. J. Med. Sci.* **2009**, *6*, 93–101. [CrossRef] [PubMed]
76. Sourisseau, T.; Georgiadis, A.; Tsapara, A.; Ali, R.R.; Pestell, R.; Matter, K.; Balda, M.S. Regulation of PCNA and cyclin D1 expression and epithelial morphogenesis by the ZO-1-regulated transcription factor ZONAB/DbpA. *Mol. Cell. Biol.* **2006**, *26*, 2387–2398. [CrossRef]
77. Huerta, M.; Munoz, R.; Tapia, R.; Soto-Reyes, E.; Ramirez, L.; Recillas-Targa, F.; Gonzalez-Mariscal, L.; Lopez-Bayghen, E. Cyclin D1 is transcriptionally down-regulated by ZO-2 via an E box and the transcription factor c-Myc. *Mol. Biol. Cell* **2007**, *18*, 4826–4836. [CrossRef]
78. Singh, A.B.; Sharma, A.; Smith, J.J.; Krishnan, M.; Chen, X.; Eschrich, S.; Washington, M.K.; Yeatman, T.J.; Beauchamp, R.D.; Dhawan, P. Claudin-1 up-regulates the repressor ZEB-1 to inhibit E-cadherin expression in colon cancer cells. *Gastroenterology* **2011**, *141*, 2140–2153. [CrossRef]
79. Dhawan, P.; Ahmad, R.; Chaturvedi, R.; Smith, J.J.; Midha, R.; Mittal, M.K.; Krishnan, M.; Chen, X.; Eschrich, S.; Yeatman, T.J.; et al. Claudin-2 expression increases tumorigenicity of colon cancer cells: Role of epidermal growth factor receptor activation. *Oncogene* **2011**, *30*, 3234–3247. [CrossRef]
80. Suh, Y.; Yoon, C.H.; Kim, R.K.; Lim, E.J.; Oh, Y.S.; Hwang, S.G.; An, S.; Yoon, G.; Gye, M.C.; Yi, J.M.; et al. Claudin-1 induces epithelial-mesenchymal transition through activation of the c-Abl-ERK signaling pathway in human liver cells. *Oncogene* **2013**, *32*, 4873–4882. [CrossRef]
81. Fredriksson, K.; Van Itallie, C.M.; Aponte, A.; Gucek, M.; Tietgens, A.J.; Anderson, J.M. Proteomic analysis of proteins surrounding occludin and claudin-4 reveals their proximity to signaling and trafficking networks. *PLoS ONE* **2015**, *10*, e0117074. [CrossRef] [PubMed]
82. Zona, L.; Lupberger, J.; Sidahmed-Adrar, N.; Thumann, C.; Harris, H.J.; Barnes, A.; Florentin, J.; Tawar, R.G.; Xiao, F.; Turek, M.; et al. HRas signal transduction promotes hepatitis C virus cell entry by triggering assembly of the host tetraspanin receptor complex. *Cell Host Microbe* **2013**, *13*, 302–313. [CrossRef] [PubMed]
83. De Souza, W.F.; Fortunato-Miranda, N.; Robbs, B.K.; de Araujo, W.M.; de-Freitas-Junior, J.C.; Bastos, L.G.; Viola, J.P.; Morgado-Diaz, J.A. Claudin-3 overexpression increases the malignant potential of colorectal cancer cells: Roles of ERK1/2 and PI3K-Akt as modulators of EGFR signaling. *PLoS ONE* **2013**, *8*, e74994. [CrossRef]
84. Lupberger, J.; Zeisel, M.B.; Xiao, F.; Thumann, C.; Fofana, I.; Zona, L.; Davis, C.; Mee, C.J.; Turek, M.; Gorke, S.; et al. EGFR and EphA2 are host factors for hepatitis C virus entry and possible targets for antiviral therapy. *Nat. Med.* **2011**, *17*, 589–595. [CrossRef] [PubMed]
85. Singh, A.B.; Sharma, A.; Dhawan, P. Claudin-1 expression confers resistance to anoikis in colon cancer cells in a Src-dependent manner. *Carcinogenesis* **2012**, *33*, 2538–2547. [CrossRef] [PubMed]
86. Herrero, R.; Prados, L.; Ferruelo, A.; Puig, F.; Pandolfi, R.; Guillamat-Prats, R.; Moreno, L.; Matute-Bello, G.; Artigas, A.; Esteban, A.; et al. Fas activation alters tight junction proteins in acute lung injury. *Thorax* **2019**, *74*, 69–82. [CrossRef] [PubMed]
87. Spadaro, D.; Le, S.; Laroche, T.; Mean, I.; Jond, L.; Yan, J.; Citi, S. Tension-Dependent Stretching Activates ZO-1 to Control the Junctional Localization of Its Interactors. *Curr. Biol.* **2017**, *27*, 3783–3795. [CrossRef]
88. Zhou, B.; Flodby, P.; Luo, J.; Castillo, D.R.; Liu, Y.; Yu, F.X.; McConnell, A.; Varghese, B.; Li, G.; Chimge, N.O.; et al. Claudin-18-mediated YAP activity regulates lung stem and progenitor cell homeostasis and tumorigenesis. *J. Clin. Investig.* **2018**, *128*, 970–984. [CrossRef]
89. Fujibe, M.; Chiba, H.; Kojima, T.; Soma, T.; Wada, T.; Yamashita, T.; Sawada, N. Thr203 of claudin-1, a putative phosphorylation site for MAP kinase, is required to promote the barrier function of tight junctions. *Exp. Cell Res.* **2004**, *295*, 36–47. [CrossRef]

90. Ishizaki, T.; Chiba, H.; Kojima, T.; Fujibe, M.; Soma, T.; Miyajima, H.; Nagasawa, K.; Wada, I.; Sawada, N. Cyclic AMP induces phosphorylation of claudin-5 immunoprecipitates and expression of claudin-5 gene in blood-brain-barrier endothelial cells via protein kinase A-dependent and -independent pathways. *Exp. Cell Res.* **2003**, *290*, 275–288. [CrossRef]
91. Ikari, A.; Ito, M.; Okude, C.; Sawada, H.; Harada, H.; Degawa, M.; Sakai, H.; Takahashi, T.; Sugatani, J.; Miwa, M. Claudin-16 is directly phosphorylated by protein kinase A independently of a vasodilator-stimulated phosphoprotein-mediated pathway. *J. Cell. Physiol.* **2008**, *214*, 221–229. [CrossRef]
92. Schmitt, M.; Horbach, A.; Kubitz, R.; Frilling, A.; Haussinger, D. Disruption of hepatocellular tight junctions by vascular endothelial growth factor (VEGF): A novel mechanism for tumor invasion. *J. Hepatol.* **2004**, *41*, 274–283. [CrossRef] [PubMed]
93. Ni, Y.; Teng, T.; Li, R.; Simonyi, A.; Sun, G.Y.; Lee, J.C. TNFalpha alters occludin and cerebral endothelial permeability: Role of p38MAPK. *PLoS ONE* **2017**, *12*, e0170346. [CrossRef] [PubMed]
94. Elias, B.C.; Suzuki, T.; Seth, A.; Giorgianni, F.; Kale, G.; Shen, L.; Turner, J.R.; Naren, A.; Desiderio, D.M.; Rao, R. Phosphorylation of Tyr-398 and Tyr-402 in occludin prevents its interaction with ZO-1 and destabilizes its assembly at the tight junctions. *J. Biol. Chem.* **2009**, *284*, 1559–1569. [CrossRef] [PubMed]
95. Ma, T.Y.; Iwamoto, G.K.; Hoa, N.T.; Akotia, V.; Pedram, A.; Boivin, M.A.; Said, H.M. TNF-alpha-induced increase in intestinal epithelial tight junction permeability requires NF-kappa B activation. *Am. J. Physiol. Gastrointest. Liver Physiol.* **2004**, *286*, G367–G376. [CrossRef]
96. Kalluri, R. EMT: When epithelial cells decide to become mesenchymal-like cells. *J. Clin. Investig.* **2009**, *119*, 1417–1419. [CrossRef]
97. Lamouille, S.; Xu, J.; Derynck, R. Molecular mechanisms of epithelial-mesenchymal transition. *Nat. Rev. Mol. Cell Biol.* **2014**, *15*, 178–196. [CrossRef]
98. Gissen, P.; Arias, I.M. Structural and functional hepatocyte polarity and liver disease. *J. Hepatol.* **2015**, *63*, 1023–1037. [CrossRef]
99. Tanaka, H.; Imasato, M.; Yamazaki, Y.; Matsumoto, K.; Kunimoto, K.; Delpierre, J.; Meyer, K.; Zerial, M.; Kitamura, N.; Watanabe, M.; et al. Claudin-3 regulates bile canalicular paracellular barrier and cholesterol gallstone core formation in mice. *J. Hepatol.* **2018**, *69*, 1308–1316. [CrossRef]
100. Rahner, C.; Mitic, L.L.; Anderson, J.M. Heterogeneity in expression and subcellular localization of claudins 2, 3, 4, and 5 in the rat liver, pancreas, and gut. *Gastroenterology* **2001**, *120*, 411–422. [CrossRef]
101. Somoracz, A.; Korompay, A.; Torzsok, P.; Patonai, A.; Erdelyi-Belle, B.; Lotz, G.; Schaff, Z.; Kiss, A. Tricellulin expression and its prognostic significance in primary liver carcinomas. *Pathol. Oncol. Res.* **2014**, *20*, 755–764. [CrossRef] [PubMed]
102. Orban, E.; Szabo, E.; Lotz, G.; Kupcsulik, P.; Paska, C.; Schaff, Z.; Kiss, A. Different expression of occludin and ZO-1 in primary and metastatic liver tumors. *Pathol. Oncol. Res.* **2008**, *14*, 299–306. [CrossRef] [PubMed]
103. Byass, P. The global burden of liver disease: A challenge for methods and for public health. *BMC Med.* **2014**, *12*, 159. [CrossRef] [PubMed]
104. D'Amico, G.; Morabito, A.; D'Amico, M.; Pasta, L.; Malizia, G.; Rebora, P.; Valsecchi, M.G. Clinical states of cirrhosis and competing risks. *J. Hepatol.* **2018**, *68*, 563–576. [CrossRef]
105. Marcellin, P.; Kutala, B.K. Liver diseases: A major, neglected global public health problem requiring urgent actions and large-scale screening. *Liver Int.* **2018**, *38*, 2–6. [CrossRef]
106. Pradhan-Sundd, T.; Zhou, L.; Vats, R.; Jiang, A.; Molina, L.; Singh, S.; Poddar, M.; Russell, J.; Stolz, D.B.; Oertel, M.; et al. Dual catenin loss in murine liver causes tight junctional deregulation and progressive intrahepatic cholestasis. *Hepatology* **2018**, *67*, 2320–2337. [CrossRef]
107. Pradhan-Sundd, T.; Vats, R.; Russell, J.O.; Singh, S.; Michael, A.A.; Molina, L.; Kakar, S.; Cornuet, P.; Poddar, M.; Watkins, S.C.; et al. Dysregulated Bile Transporters and Impaired Tight Junctions During Chronic Liver Injury in Mice. *Gastroenterology* **2018**, *155*, 1218–1232-e24. [CrossRef]
108. Takaki, Y.; Hirai, S.; Manabe, N.; Izumi, Y.; Hirose, T.; Nakaya, M.; Suzuki, A.; Mizuno, K.; Akimoto, K.; Tsukita, S.; et al. Dynamic changes in protein components of the tight junction during liver regeneration. *Cell Tissue Res.* **2001**, *305*, 399–409. [CrossRef]
109. Liang, T.J.; Rehermann, B.; Seeff, L.B.; Hoofnagle, J.H. Pathogenesis, natural history, treatment, and prevention of hepatitis C. *Ann. Intern. Med.* **2000**, *132*, 296–305. [CrossRef]
110. Thrift, A.P.; El-Serag, H.B.; Kanwal, F. Global epidemiology and burden of HCV infection and HCV-related disease. *Nat. Rev. Gastroenterol. Hepatol.* **2017**, *14*, 122–132. [CrossRef]

111. WHO. *Global Hepatitis Report*; WHO: Geneva, Switzerland, 2017.
112. Douam, F.; Lavillette, D.; Cosset, F.L. The mechanism of HCV entry into host cells. *Prog. Mol. Biol. Transl Sci.* **2015**, *129*, 63–107. [CrossRef] [PubMed]
113. Sourisseau, M.; Michta, M.L.; Zony, C.; Israelow, B.; Hopcraft, S.E.; Narbus, C.M.; Parra Martin, A.; Evans, M.J. Temporal analysis of hepatitis C virus cell entry with occludin directed blocking antibodies. *PLoS Pathog.* **2013**, *9*, e1003244. [CrossRef] [PubMed]
114. Shimizu, Y.; Shirasago, Y.; Kondoh, M.; Suzuki, T.; Wakita, T.; Hanada, K.; Yagi, K.; Fukasawa, M. Monoclonal Antibodies against Occludin Completely Prevented Hepatitis C Virus Infection in a Mouse Model. *J. Virol.* **2018**, *92*, e02258-17. [CrossRef] [PubMed]
115. Liu, S.; Kuo, W.; Yang, W.; Liu, W.; Gibson, G.A.; Dorko, K.; Watkins, S.C.; Strom, S.C.; Wang, T. The second extracellular loop dictates Occludin-mediated HCV entry. *Virology* **2010**, *407*, 160–170. [CrossRef] [PubMed]
116. Dorner, M.; Horwitz, J.A.; Robbins, J.B.; Barry, W.T.; Feng, Q.; Mu, K.; Jones, C.T.; Schoggins, J.W.; Catanese, M.T.; Burton, D.R.; et al. A genetically humanized mouse model for hepatitis C virus infection. *Nature* **2011**, *474*, 208–211. [CrossRef] [PubMed]
117. Dorner, M.; Horwitz, J.A.; Donovan, B.M.; Labitt, R.N.; Budell, W.C.; Friling, T.; Vogt, A.; Catanese, M.T.; Satoh, T.; Kawai, T.; et al. Completion of the entire hepatitis C virus life cycle in genetically humanized mice. *Nature* **2013**, *501*, 237–241. [CrossRef] [PubMed]
118. Ding, Q.; von Schaewen, M.; Hrebikova, G.; Heller, B.; Sandmann, L.; Plaas, M.; Ploss, A. Mice Expressing Minimally Humanized CD81 and Occludin Genes Support Hepatitis C Virus Uptake In Vivo. *J. Virol.* **2017**, *91*, e01799-16. [CrossRef]
119. Nakamuta, M.; Fujino, T.; Yada, R.; Aoyagi, Y.; Yasutake, K.; Kohjima, M.; Fukuizumi, K.; Yoshimoto, T.; Harada, N.; Yada, M.; et al. Expression profiles of genes associated with viral entry in HCV-infected human liver. *J. Med. Virol.* **2011**, *83*, 921–927. [CrossRef]
120. Mensa, L.; Crespo, G.; Gastinger, M.J.; Kabat, J.; Perez-del-Pulgar, S.; Miquel, R.; Emerson, S.U.; Purcell, R.H.; Forns, X. Hepatitis C virus receptors claudin-1 and occludin after liver transplantation and influence on early viral kinetics. *Hepatology* **2011**, *53*, 1436–1445. [CrossRef]
121. Krieger, S.E.; Zeisel, M.B.; Davis, C.; Thumann, C.; Harris, H.J.; Schnober, E.K.; Mee, C.; Soulier, E.; Royer, C.; Lambotin, M.; et al. Inhibition of hepatitis C virus infection by anti-claudin-1 antibodies is mediated by neutralization of E2-CD81-claudin-1 associations. *Hepatology* **2010**, *51*, 1144–1157. [CrossRef]
122. Fofana, I.; Krieger, S.E.; Grunert, F.; Glauben, S.; Xiao, F.; Fafi-Kremer, S.; Soulier, E.; Royer, C.; Thumann, C.; Mee, C.J.; et al. Monoclonal anti-claudin 1 antibodies prevent hepatitis C virus infection of primary human hepatocytes. *Gastroenterology* **2010**, *139*, 953–964. [CrossRef] [PubMed]
123. Colpitts, C.C.; Tawar, R.G.; Mailly, L.; Thumann, C.; Heydmann, L.; Durand, S.C.; Xiao, F.; Robinet, E.; Pessaux, P.; Zeisel, M.B.; et al. Humanisation of a claudin-1-specific monoclonal antibody for clinical prevention and cure of HCV infection without escape. *Gut* **2018**, *67*, 736–745. [CrossRef] [PubMed]
124. Mailly, L.; Xiao, F.; Lupberger, J.; Wilson, G.K.; Aubert, P.; Duong, F.H.T.; Calabrese, D.; Leboeuf, C.; Fofana, I.; Thumann, C.; et al. Clearance of persistent hepatitis C virus infection in humanized mice using a claudin-1-targeting monoclonal antibody. *Nat. Biotechnol.* **2015**, *33*, 549–554. [CrossRef] [PubMed]
125. Fofana, I.; Fafi-Kremer, S.; Carolla, P.; Fauvelle, C.; Zahid, M.N.; Turek, M.; Heydmann, L.; Cury, K.; Hayer, J.; Combet, C.; et al. Mutations that alter use of hepatitis C virus cell entry factors mediate escape from neutralizing antibodies. *Gastroenterology* **2012**, *143*, 223–233. [CrossRef]
126. Xiao, F.; Fofana, I.; Thumann, C.; Mailly, L.; Alles, R.; Robinet, E.; Meyer, N.; Schaeffer, M.; Habersetzer, F.; Doffoel, M.; et al. Synergy of entry inhibitors with direct-acting antivirals uncovers novel combinations for prevention and treatment of hepatitis C. *Gut* **2014**. [CrossRef]
127. Xiao, F.; Fofana, I.; Heydmann, L.; Barth, H.; Soulier, E.; Habersetzer, F.; Doffoel, M.; Bukh, J.; Patel, A.H.; Zeisel, M.B.; et al. Hepatitis C virus cell-cell transmission and resistance to direct-acting antiviral agents. *PLoS Pathog.* **2014**, *10*, e1004128. [CrossRef]
128. Okai, K.; Ichikawa-Tomikawa, N.; Saito, A.C.; Watabe, T.; Sugimoto, K.; Fujita, D.; Ono, C.; Fukuhara, T.; Matsuura, Y.; Ohira, H.; et al. A novel occludin-targeting monoclonal antibody prevents hepatitis C virus infection in vitro. *Oncotarget* **2018**, *9*, 16588–16598. [CrossRef]
129. Michta, M.L.; Hopcraft, S.E.; Narbus, C.M.; Kratovac, Z.; Israelow, B.; Sourisseau, M.; Evans, M.J. Species-specific regions of occludin required by hepatitis C virus for cell entry. *J. Virol.* **2010**, *84*, 11696–11708. [CrossRef]

130. Bray, F.; Ferlay, J.; Soerjomataram, I.; Siegel, R.L.; Torre, L.A.; Jemal, A. Global cancer statistics 2018, GLOBOCAN estimates of incidence and mortality worldwide for 36 cancers in 185 countries. *CA Cancer J. Clin.* **2018**, *68*, 394–424. [CrossRef]
131. Bouchagier, K.A.; Assimakopoulos, S.F.; Karavias, D.D.; Maroulis, I.; Tzelepi, V.; Kalofonos, H.; Kardamakis, D.; Scopa, C.D.; Tsamandas, A.C. Expression of claudins-1, -4, -5, -7 and occludin in hepatocellular carcinoma and their relation with classic clinicopathological features and patients' survival. *In Vivo* **2014**, *28*, 315–326.
132. Holczbauer, A.; Gyongyosi, B.; Lotz, G.; Torzsok, P.; Kaposi-Novak, P.; Szijarto, A.; Tatrai, P.; Kupcsulik, P.; Schaff, Z.; Kiss, A. Increased expression of claudin-1 and claudin-7 in liver cirrhosis and hepatocellular carcinoma. *Pathol. Oncol. Res.* **2014**, *20*, 493–502. [CrossRef]
133. Huang, G.W.; Ding, X.; Chen, S.L.; Zeng, L. Expression of claudin 10 protein in hepatocellular carcinoma: Impact on survival. *J. Cancer Res. Clin. Oncol.* **2011**, *137*, 1213–1218. [CrossRef] [PubMed]
134. Zhou, S.; Parham, D.M.; Yung, E.; Pattengale, P.; Wang, L. Quantification of glypican 3, beta-catenin and claudin-1 protein expression in hepatoblastoma and paediatric hepatocellular carcinoma by colour deconvolution. *Histopathology* **2015**, *67*, 905–913. [CrossRef] [PubMed]
135. Kim, J.H.; Kim, E.L.; Lee, Y.K.; Park, C.B.; Kim, B.W.; Wang, H.J.; Yoon, C.H.; Lee, S.J.; Yoon, G. Decreased lactate dehydrogenase B expression enhances claudin 1-mediated hepatoma cell invasiveness via mitochondrial defects. *Exp. Cell Res.* **2011**, *317*, 1108–1118. [CrossRef] [PubMed]
136. Cheung, S.T.; Leung, K.L.; Ip, Y.C.; Chen, X.; Fong, D.Y.; Ng, I.O.; Fan, S.T.; So, S. Claudin-10 expression level is associated with recurrence of primary hepatocellular carcinoma. *Clin. Cancer Res.* **2005**, *11*, 551–556. [PubMed]
137. Li, C.P.; Cai, M.Y.; Jiang, L.J.; Mai, S.J.; Chen, J.W.; Wang, F.W.; Liao, Y.J.; Chen, W.H.; Jin, X.H.; Pei, X.Q.; et al. CLDN14 is epigenetically silenced by EZH2-mediated H3K27ME3 and is a novel prognostic biomarker in hepatocellular carcinoma. *Carcinogenesis* **2016**, *37*, 557–566. [CrossRef]
138. Jiang, L.; Yang, Y.D.; Fu, L.; Xu, W.; Liu, D.; Liang, Q.; Zhang, X.; Xu, L.; Guan, X.Y.; Wu, B.; et al. CLDN3 inhibits cancer aggressiveness via Wnt-EMT signaling and is a potential prognostic biomarker for hepatocellular carcinoma. *Oncotarget* **2014**, *5*, 7663–7676. [CrossRef]
139. Gerardo-Ramirez, M.; Lazzarini-Lechuga, R.; Hernandez-Rizo, S.; Jimenez-Salazar, J.E.; Simoni-Nieves, A.; Garcia-Ruiz, C.; Fernandez-Checa, J.C.; Marquardt, J.U.; Coulouarn, C.; Gutierrez-Ruiz, M.C.; et al. GDF11 exhibits tumor suppressive properties in hepatocellular carcinoma cells by restricting clonal expansion and invasion. *Biochim. Biophys. Acta Mol. Basis Dis.* **2019**, *1865*, 1540–1554. [CrossRef]
140. Hou, X.; Yang, L.; Jiang, X.; Liu, Z.; Li, X.; Xie, S.; Li, G.; Liu, J. Role of microRNA-141-3p in the progression and metastasis of hepatocellular carcinoma cell. *Int. J. Biol. Macromol.* **2019**, *128*, 331–339. [CrossRef]
141. Wang, S.C.; Lin, X.L.; Li, J.; Zhang, T.T.; Wang, H.Y.; Shi, J.W.; Yang, S.; Zhao, W.T.; Xie, R.Y.; Wei, F.; et al. MicroRNA-122 triggers mesenchymal-epithelial transition and suppresses hepatocellular carcinoma cell motility and invasion by targeting RhoA. *PLoS ONE* **2014**, *9*, e101330. [CrossRef]
142. Nagai, T.; Arao, T.; Nishio, K.; Matsumoto, K.; Hagiwara, S.; Sakurai, T.; Minami, Y.; Ida, H.; Ueshima, K.; Nishida, N.; et al. Impact of Tight Junction Protein ZO-1 and TWIST Expression on Postoperative Survival of Patients with Hepatocellular Carcinoma. *Dig. Dis.* **2016**, *34*, 702–707. [CrossRef]
143. Bekker, V.; Chanock, S.J.; Yeager, M.; Hutchinson, A.A.; von Hahn, T.; Chen, S.; Xiao, N.; Dotrang, M.; Brown, M.; Busch, M.P.; et al. Genetic variation in CLDN1 and susceptibility to hepatitis C virus infection. *J. Viral. Hepat.* **2010**, *17*, 192–200. [CrossRef]
144. Zadori, G.; Gelley, F.; Torzsok, P.; Sarvary, E.; Doros, A.; Deak, A.P.; Nagy, P.; Schaff, Z.; Kiss, A.; Nemes, B. Examination of claudin-1 expression in patients undergoing liver transplantation owing to hepatitis C virus cirrhosis. *Transplant. Proc.* **2011**, *43*, 1267–1271. [CrossRef] [PubMed]
145. Liu, S.; Yang, W.; Shen, L.; Turner, J.R.; Coyne, C.B.; Wang, T. Tight junction proteins claudin-1 and occludin control hepatitis C virus entry and are downregulated during infection to prevent superinfection. *J. Virol.* **2009**, *83*, 2011–2014. [CrossRef]
146. De Vos, R.; Desmet, V.J. Morphologic changes of the junctional complex of the hepatocytes in rat liver after bile duct ligation. *Br. J. Exp. Pathol.* **1978**, *59*, 220–227.
147. Sakisaka, S.; Kawaguchi, T.; Taniguchi, E.; Hanada, S.; Sasatomi, K.; Koga, H.; Harada, M.; Kimura, R.; Sata, M.; Sawada, N.; et al. Alterations in tight junctions differ between primary biliary cirrhosis and primary sclerosing cholangitis. *Hepatology* **2001**, *33*, 1460–1468. [CrossRef]

148. Nemeth, Z.; Szasz, A.M.; Tatrai, P.; Nemeth, J.; Gyorffy, H.; Somoracz, A.; Szijarto, A.; Kupcsulik, P.; Kiss, A.; Schaff, Z. Claudin-1, -2, -3, -4, -7, -8, and -10 protein expression in biliary tract cancers. *J. Histochem. Cytochem.* **2009**, *57*, 113–121. [CrossRef]
149. Sambrotta, M.; Strautnieks, S.; Papouli, E.; Rushton, P.; Clark, B.E.; Parry, D.A.; Logan, C.V.; Newbury, L.J.; Kamath, B.M.; Ling, S.; et al. Mutations in TJP2 cause progressive cholestatic liver disease. *Nat. Genet.* **2014**, *46*, 326–328. [CrossRef]
150. Vitale, G.; Gitto, S.; Vukotic, R.; Raimondi, F.; Andreone, P. Familial intrahepatic cholestasis: New and wide perspectives. *Dig. Liver Dis.* **2019**, *51*, 922–933. [CrossRef]
151. Baala, L.; Hadj-Rabia, S.; Hamel-Teillac, D.; Hadchouel, M.; Prost, C.; Leal, S.M.; Jacquemin, E.; Sefiani, A.; De Prost, Y.; Courtois, G.; et al. Homozygosity mapping of a locus for a novel syndromic ichthyosis to chromosome 3q27–q28. *J. Investig. Dermatol.* **2002**, *119*, 70–76. [CrossRef]
152. Lindor, K.D.; Gershwin, M.E.; Poupon, R.; Kaplan, M.; Bergasa, N.V.; Heathcote, E.J. American Association for Study of Liver, D. Primary biliary cirrhosis. *Hepatology* **2009**, *50*, 291–308. [CrossRef] [PubMed]
153. Karlsen, T.H.; Folseraas, T.; Thorburn, D.; Vesterhus, M. Primary sclerosing cholangitis—A comprehensive review. *J. Hepatol.* **2017**, *67*, 1298–1323. [CrossRef] [PubMed]
154. Nakanuma, Y.; Tsuneyama, K.; Gershwin, M.E.; Yasoshima, M. Pathology and immunopathology of primary biliary cirrhosis with emphasis on bile duct lesions: Recent progress. *Semin. Liver Dis.* **1995**, *15*, 313–328. [CrossRef] [PubMed]
155. Feldmeyer, L.; Huber, M.; Fellmann, F.; Beckmann, J.S.; Frenk, E.; Hohl, D. Confirmation of the origin of NISCH syndrome. *Hum. Mutat.* **2006**, *27*, 408–410. [CrossRef] [PubMed]
156. Nagtzaam, I.F.; van Geel, M.; Driessen, A.; Steijlen, P.M.; van Steensel, M.A. Bile duct paucity is part of the neonatal ichthyosis-sclerosing cholangitis phenotype. *Br. J. Dermatol.* **2010**, *163*, 205–207. [CrossRef] [PubMed]
157. Shah, I.; Bhatnagar, S. NISCH syndrome with hypothyroxinemia. *Ann. Hepatol.* **2010**, *9*, 299–301. [CrossRef]
158. Kirchmeier, P.; Sayar, E.; Hotz, A.; Hausser, I.; Islek, A.; Yilmaz, A.; Artan, R.; Fischer, J. Novel mutation in the CLDN1 gene in a Turkish family with neonatal ichthyosis sclerosing cholangitis (NISCH) syndrome. *Br. J. Dermatol.* **2014**, *170*, 976–978. [CrossRef]
159. Youssefian, L.; Vahidnezhad, H.; Saeidian, A.H.; Sotoudeh, S.; Zeinali, S.; Uitto, J. Gene-Targeted Next-Generation Sequencing Identifies a Novel CLDN1 Mutation in a Consanguineous Family With NISCH Syndrome. *Am. J. Gastroenterol.* **2017**, *112*, 396–398. [CrossRef]
160. Nagtzaam, I.F.; Peeters, V.P.M.; Vreeburg, M.; Wagner, A.; Steijlen, P.M.; van Geel, M.; van Steensel, M.A.M. Novel CLDN1 mutation in ichthyosis-hypotrichosis-sclerosing cholangitis syndrome without signs of liver disease. *Br. J. Dermatol.* **2018**, *178*, e202–e203. [CrossRef]
161. Szepetowski, S.; Lacoste, C.; Mallet, S.; Roquelaure, B.; Badens, C.; Fabre, A. NISCH syndrome, a rare cause of neonatal cholestasis: A case report. *Arch. Pediatr.* **2017**, *24*, 1228–1234. [CrossRef]
162. Carlton, V.E.; Harris, B.Z.; Puffenberger, E.G.; Batta, A.K.; Knisely, A.S.; Robinson, D.L.; Strauss, K.A.; Shneider, B.L.; Lim, W.A.; Salen, G.; et al. Complex inheritance of familial hypercholanemia with associated mutations in TJP2 and BAAT. *Nat. Genet.* **2003**, *34*, 91–96. [CrossRef] [PubMed]
163. Patel, T. Increasing incidence and mortality of primary intrahepatic cholangiocarcinoma in the United States. *Hepatology* **2001**, *33*, 1353–1357. [CrossRef] [PubMed]
164. Saha, S.K.; Zhu, A.X.; Fuchs, C.S.; Brooks, G.A. Forty-Year Trends in Cholangiocarcinoma Incidence in the U.S: Intrahepatic Disease on the Rise. *Oncologist* **2016**, *21*, 594–599. [CrossRef] [PubMed]
165. Von Hahn, T.; Ciesek, S.; Wegener, G.; Plentz, R.R.; Weismuller, T.J.; Wedemeyer, H.; Manns, M.P.; Greten, T.F.; Malek, N.P. Epidemiological trends in incidence and mortality of hepatobiliary cancers in Germany. *Scand. J. Gastroenterol.* **2011**, *46*, 1092–1098. [CrossRef]
166. Ehlken, H.; Schramm, C. Primary sclerosing cholangitis and cholangiocarcinoma: Pathogenesis and modes of diagnostics. *Dig. Dis.* **2013**, *31*, 118–125. [CrossRef]
167. Shaib, Y.H.; El-Serag, H.B.; Davila, J.A.; Morgan, R.; McGlynn, K.A. Risk factors of intrahepatic cholangiocarcinoma in the United States: A case-control study. *Gastroenterology* **2005**, *128*, 620–626. [CrossRef]
168. Ralphs, S.; Khan, S.A. The role of the hepatitis viruses in cholangiocarcinoma. *J. Viral. Hepat.* **2013**, *20*, 297–305. [CrossRef]
169. Tyson, G.L.; El-Serag, H.B. Risk factors for cholangiocarcinoma. *Hepatology* **2011**, *54*, 173–184. [CrossRef]

170. Jakab, C.; Kiss, A.; Schaff, Z.; Szabo, Z.; Rusvai, M.; Galfi, P.; Szabara, A.; Sterczer, A.; Kulka, J. Claudin-7 protein differentiates canine cholangiocarcinoma from hepatocellular carcinoma. *Histol. Histopathol.* **2010**, *25*, 857–864. [CrossRef]
171. Lodi, C.; Szabo, E.; Holczbauer, A.; Batmunkh, E.; Szijarto, A.; Kupcsulik, P.; Kovalszky, I.; Paku, S.; Illyes, G.; Kiss, A.; et al. Claudin-4 differentiates biliary tract cancers from hepatocellular carcinomas. *Mod. Pathol.* **2006**, *19*, 460–469. [CrossRef]
172. Bunthot, S.; Obchoei, S.; Kraiklang, R.; Pirojkul, C.; Wongkham, S.; Wongkham, C. Overexpression of claudin-4 in cholangiocarcinoma tissues and its possible role in tumor metastasis. *Asian Pac. J. Cancer Prev.* **2012**, *13*, 71–76. [PubMed]
173. Shinozaki, A.; Shibahara, J.; Noda, N.; Tanaka, M.; Aoki, T.; Kokudo, N.; Fukayama, M. Claudin-18 in biliary neoplasms. Its significance in the classification of intrahepatic cholangiocarcinoma. *Virchows Arch.* **2011**, *459*, 73–80. [CrossRef] [PubMed]
174. Nemeth, Z.; Szasz, A.M.; Somoracz, A.; Tatrai, P.; Nemeth, J.; Gyorffy, H.; Szijarto, A.; Kupcsulik, P.; Kiss, A.; Schaff, Z. Zonula occludens-1, occludin, and E-cadherin protein expression in biliary tract cancers. *Pathol. Oncol. Res.* **2009**, *15*, 533–539. [CrossRef] [PubMed]

International Journal of
Molecular Sciences

MDPI

Review

The Integral Role of Tight Junction Proteins in the Repair of Injured Intestinal Epithelium

Zachary M. Slifer and Anthony T. Blikslager *

Department of Clinical Sciences, College of Veterinary Medicine, North Carolina State University, Raleigh, NC 27607, USA; zmslifer@ncsu.edu
* Correspondence: Anthony_Blikslager@ncsu.edu

Received: 30 August 2019; Accepted: 14 October 2019; Published: 1 February 2020

Abstract: The intestinal epithelial monolayer forms a transcellular and paracellular barrier that separates luminal contents from the interstitium. The paracellular barrier consists of a highly organized complex of intercellular junctions that is primarily regulated by apical tight junction proteins and tight junction-associated proteins. This homeostatic barrier can be lost through a multitude of injurious events that cause the disruption of the tight junction complex. Acute repair after injury leading to the reestablishment of the tight junction barrier is crucial for the return of both barrier function as well as other cellular functions, including water regulation and nutrient absorption. This review provides an overview of the tight junction complex components and how they link to other plasmalemmal proteins, such as ion channels and transporters, to induce tight junction closure during repair of acute injury. Understanding the components of interepithelial tight junctions and the mechanisms of tight junction regulation after injury is crucial for developing future therapeutic targets for patients experiencing dysregulated intestinal permeability.

Keywords: barrier function; tight junction; repair; occludin; claudin; NHE2; ClC-2

1. Intestinal Epithelium as a Selective Barrier

The intestine is lined with a monolayer of columnar epithelium that maintains two critical functions: (1) selectively filtering luminal contents, including nutrients, water and electrolytes, to allow for their translocation into the circulation and (2) forming a barrier to prevent the translocation of luminal toxins, commensal or pathogenic microorganisms, and foreign antigens into the circulation [1]. Under homeostatic conditions, these functions are regulated by both transcellular and paracellular pathways, the latter of which are primarily maintained by apical tight junction proteins through paracellular pore and leak permeability pathways [2,3]. The paracellular pathway is associated with the charge and size selective transport of materials through the space between intestinal epithelial cells.

Intestinal barrier homeostasis is disrupted through tight junction protein dysregulation, which occurs via a variety of injurious events, including microbial degradation and bacterial toxin exposure, exposure to cytotoxic agents, exposure to pro-inflammatory cytokines such as IFNγ and TNFα, intestinal autoimmune disease such as Celiac disease, and intestinal ischemia [4–9]. The loss of tight junction integrity results in the formation of a third pathway, known as the high-capacity and nonselective unrestricted permeability pathway, which can allow for the unrestricted movement of microorganisms and large proteins across the paracellular space [10]. An inability to rapidly repair the tight junctions in order to restore epithelial barrier function is detrimental to the patient, as it can result in various pathologies, including sepsis and multiple organ dysfunction [11,12]. Therefore, understanding factors that can regulate the tight junction complex during repair of injured intestinal epithelium is crucial for developing future therapeutic targets.

2. Tight Junction Protein Structure

Tight junctions are made up of a number of protein elements, including transmembrane claudins (total of 27 mammalian claudins), as well as myelin and lymphocyte (MAL) and related proteins for vesicle trafficking and membrane link (MARVEL) [13–18]. MARVEL domain-containing proteins are a component of a larger group of tight junction-associated MARVEL proteins (TAMPS) that include transmembrane proteins such as occludin and tricellulin [18–20]. Other tight junction-associated transmembrane molecules include junctional adhesion molecules (JAM-1, -2, and -3) that can regulate the formation of tight junctions and migration of neutrophils [21–26]. Additionally, intracellular scaffold proteins such as zonula occludens (ZO) -1, -2, and -3 play an integral role in tight junction protein assembly and link tight junction transmembrane proteins with the actin cytoskeleton [27–30].

Intestinal claudins exist in two different classes: sealing claudins and pore-forming claudins [31]. Increased membrane expression of sealing proteins results in a 'tighter' epithelial barrier, further restricting the movement of luminal contents through the paracellular space. Sealing tight junction proteins include claudins-1, -3, -4, -5, -8, -11, -14, 18, and -19 [17]. Alternatively, increased membrane expression of pore-forming proteins (including claudins-2, -10a/-10b, -15, -16, and -17) reduces the selectivity for luminal contents that can pass between epithelial cells, thereby increasing paracellular permeability [17]. Each pore-forming claudin has an ionic charge specificity for cations or anions as well as ionic size selectivity, thereby increasing the permeability for ions based on claudin-specific permeability characteristics. An interesting interaction between the two classes of claudins has been observed with the displacement of pore-forming claudins by sealing claudins. For example, in a claudin-8 transfected Madin–Darby canine kidney II (MDCK II) cell line in which claudin-8 expression occurred in the absence of doxycycline, claudin-8 displacement of claudin-2 was visualized upon immunofluorescent imaging [32,33]. Specifically, claudin-8 served to replace claudin-2 in tight junction strands in this model, which reduced the number of functional paracellular cation pores [32].

Tight junction protein expression in the intestinal tract is tissue- and age-specific. For example, claudin-2 is normally expressed in the human small intestine but is reported to be expressed only in the colonic crypt of fetal humans and absent in the adult colon under homeostatic conditions [34]. Overall, claudin-2 generally exhibits higher expression in leaky epithelial tissues, such as colonic tissues from a subset of patients with inflammatory bowel disease [35]. Additionally, its protein expression was detected throughout the crypt–villus axis of human small intestines but was only detected in undifferentiated crypt cells of human colonic tissue [36]. Other claudins follow suit regarding crypt–luminal axis expression with some pore-forming claudins (-2, -10, -13, -15) being restricted to the intestinal crypt base in murine tissue while other sealing claudins (-3, -4, -7, -8) are expressed in luminal epithelial cells [37–40].

Special Functions of Select Tight Junction Proteins

As discussed throughout the remainder of this review, regulation of tight junction proteins is a vital component of epithelial barrier repair after injury. However, specific tight junction proteins can have additional special functions that are species and age dependent. In the case of claudin-4, there is an age-dependent disparity between cellular localization of tight junction proteins [41]. Intestinal porcine claudin-4 is localized to the apical surface of porcine jejunal enterocytes within the first two days of age and only localizes to the lateral surface between adjacent epithelial cells beyond two days of age [41]. This age-specificity of claudin-4 localization in piglet jejunum may be due to immunological naivety that newborn piglets experience. Piglets must be able to acquire and absorb immunoglobulins and other immune-related molecules, including cytokines and antimicrobial peptides, from colostrum within the first day of life to prevent death via bacterial sepsis [42]. It is reported that this age-specific, apical surface localization of claudin-4 occurs in jejunal enterocytes at the same period of time in which the vital immune macromolecules are absorbed into the bloodstream [41]. Therefore, this special function of claudin-4 localization is necessary to allow for the proper uptake of immune molecules by the piglet, and subsequent relocalization to the lateral surface may aid in sealing of the paracellular space between adjacent epithelial cells once the immune constituents are absorbed.

Another tight junction protein, tricellulin, serves a special function in the tight junction barrier where more than two epithelial cells meet. Tight junction strands between two adjacent epithelial cells typically associated laterally to pair with another tight junction strand, forming bicellular tight junctions between the two cells [43]. However, these bicellular tight junctions are not continuous at tricellular epithelial cell contacts and have therefore been described as tricellular tight junction proteins. While traditional tight junction proteins, such as occludin and claudins, are found in both bicellular and tricellular tight junctions, tricellulin is concentrated to the tricellular tight junction and its knockdown in the EpH4 cell line of immortalized mouse mammary gland epithelium resulted in altered organization of bicellular tight junction proteins [20]. Additionally, tricellulin has been shown to not affect the permeability for ions while forming a barrier to macromolecules in tricellulin-transfected MDCK II cells overexpressing tricellulin in the tricellular tight junctions [44]. Overall, it is crucial to consider all components and special functions of tight junction proteins when studying tight junction structure. Furthermore, the understanding of these tight junction special functions may be crucial to restoring barrier function following injury.

3. Acute Mechanisms of Repair in Injured Intestinal Epithelium

When the monolayer of intestinal epithelium is injured, such as that which occurs during ischemia/reperfusion injury or exposure to pathogenic microbes such as rotavirus [45,46], detachment of the epithelium from the basement membrane and separation of adjacent epithelial cells from one another due to dysregulation and loss of tight junctional proteins occurs. Furthermore, the loss of polarity-establishing tight junctional proteins results in the loss of cell polarity, which abolishes apical and basolateral positioning of localized molecules such as ion channels/transporters, resulting in their mislocalization [47]. When homeostatic positioning of ion channels and transporters is lost, this can subsequently lead to the dysregulation of a multitude of cellular functions including water absorption/secretion, intracellular and organelle pH, and nutrient absorption.

Once the cause of intestinal injury is resolved, such as restoration of blood flow in ischemic injury, rapid mechanisms of intestinal mucosal repair take place in a well-orchestrated series of reparative events. Initially, small intestinal villi contract via the contraction of myofibroblasts adjacent to the epithelial basement membrane and centrally along the central lacteal. Villus contraction is characterized histologically by a quantitatively diminished villus height [48] and occurs in response to mediators such as PGE_2 [49]. Villus contraction results in reduction of the denuded surface area that remains to be covered by epithelial cells. Simultaneously, restitution of epithelial cells shouldering the site of injury occurs to cover the denuded area [50]. These cells depolarize to disassemble microvilli, allowing for subsequent lamellipodia-driven movement via actin–myosin treadmilling, while maintaining transient attachment to the basement membrane through integrins [11]. Although the underlying intestinal layers may not appear exposed to luminal contents since the mucosa is no longer denuded, the unrestricted permeability pathway via poorly formed tight junctions allows for microorganisms and macromolecules to cross the epithelial barrier. In order for the tight junction barrier and cell polarity to be restored, tight junction proteins internalized during injury, such as the endocytosis of occludin that accompanies anoxic injury in Caco-2 cells, must be reinserted back into the membrane via recycling endosomes [51–53]. Ultimately, following these acute repair mechanisms, crypt cells can proliferate and differentiate to restore the proper number of epithelial cells to the monolayer in order to regain full homeostatic function.

4. Regulation of Tight Junctions via Ion Channels/Transporters

Closure of the tight junction after acute intestinal injury is paramount in restoring barrier function and returning to homeostatic functioning. Tight junction proteins can be regulated by many factors, including cytokines, growth factors, and nutrients. For example, transport of glucose by SGLT1 has been shown to result in the physiological opening of tight junctions in an NHE3-dependent mechanism [54]. Alternatively, ion channel/transporters, including proteins from the Na^+/H^+ exchanger (NHE) family as well as chloride channel protein 2 (ClC-2) have also been shown to regulate tight junction proteins,

specifically after intestinal ischemic injury [55–57]. This review will examine the reparative role of these transport proteins specifically related to restoration of junctions.

4.1. NHE2 and Intestinal Repair

The gastrointestinal epithelium is home to many ion transporters that are collectively responsible for regulating homeostatic cell functions, including the regulation of nutrient absorption, cytosolic and organelle pH, water absorption and secretion, and cell volume [58]. One major family of ion transporters in the human GI tract is the *SLC9* gene family, also known as the NHE family. NHE isoforms belonging to the *SLC9A* gene subgroup (*SLC9A1-9*) can be either plasmalemmal or intracellular, depending on the isoform and tissue location within the gut [59]. Additionally, the Na^+/H^+ exchanger 5 (NHE5) is the only isoform for which expression has not been shown in the gastrointestinal tract [60]. These proteins are responsible for the electroneutral antiport of Na^+ into intestinal epithelium in exchange for H^+ secreted from the cell to maintain cellular pH and volume.

An additional function of NHEs that continues to be explored is the link between NHEs and the tight junction. One mechanism that links NHEs to the tight junction is through binding to the actin cytoskeleton. Specifically, Na^+/H^+ exchanger 3 (NHE3) has been shown to bind directly to the actin cytoskeleton and indirectly through various binding partners, including ezrin [61,62]. The ezrin protein is known to link the plasma membrane to the cytoskeleton in its active, phosphorylated conformation through binding to actin with its C-terminal region [63–65]. This interaction with the cytoskeleton has been shown to regulate plasma membrane tension, which is involved in motility and endocytosis [66]. Ezrin links the cytoskeleton to the plasma membrane through binding of its N-terminal region to either membrane lipids or cytoplasmic regions of transmembrane proteins, including NHE3 [66,67]. Thus, by linking transmembrane proteins such as NHE3 to the cytoskeleton, there is an indirect link between transmembrane proteins and tight junction proteins.

Of the NHE isoforms that have been described in the gut, Na^+/H^+ exchanger 2 (NHE2) is one of the least described NHEs in regards to its homeostatic and pathophysiologic functionality. However, NHE2 has been linked to paracellular barrier function and tight junction regulation during the recovery of injured intestinal epithelium [55,56]. In both porcine and murine models of intestinal ischemic injury, NHE2, rather than NHE1 or NHE3, appears to be the primary NHE responsible for regulating tight junction proteins during the recovery of ischemia-injured intestines [55,56]. During ex vivo recovery of porcine intestinal ischemia, selective pharmacologic inhibition of NHE2 enhanced epithelial recovery, as evidenced by significant elevations in transepithelial electrical resistance (TER) while inhibition of NHE1 or NHE3 did not elicit a recovery response [56]. In the same study, this NHE2-specific inhibitory effect on recovery was independent of epithelial restitution, and NHE2 was shown to co-immunoprecipitate with ezrin/radixin/moesin (ERM)-binding phosphoprotein 50 (EBP50), also known as NHE regulatory factor 1 (NHERF1), in ischemia-injured porcine ileum. These data suggest that NHE2 regulates restoration of the tight junction barrier during recovery of intestinal ischemia and is potentially linked to the actin cytoskeleton through binding partners (Figure 1). Although NHE2 is also implicated in the in vivo recovery of murine intestinal ischemia, the genetic knockout of NHE2 in the murine model has the inverse effect when compared to pharmacologic inhibition of NHE2 in the porcine model of intestinal ischemia [55]. Specifically, NHE2 null mice exhibit increased blood-to-lumen ^{3}H-mannitol flux at 1.5 and 3 hours after ischemic injury as well as a change in localization of occludin and claudin-1 from the membrane to the cytosol when compared to wild-type mice [55]. Additionally, epithelial restitution after intestinal ischemia was unaffected by the absence of NHE2 in this model. It is important to note that pharmacologic inhibition or genetic knockout of NHE2 may affect intracellular pH (pH_i) since NHEs are known to contribute to pH_i changes, and these potential pH_i changes can affect charge selectivity of the paracellular pathway [68,69]. However, further studies will be required to determine if NHE-mediated changes in pH_i are linked to alterations in the tight junction. Together, this information suggests that NHE2 regulates acute recovery after intestinal ischemic injury in a tight junction-dependent manner, whereas its absence delays restoration of tight junction barrier function.

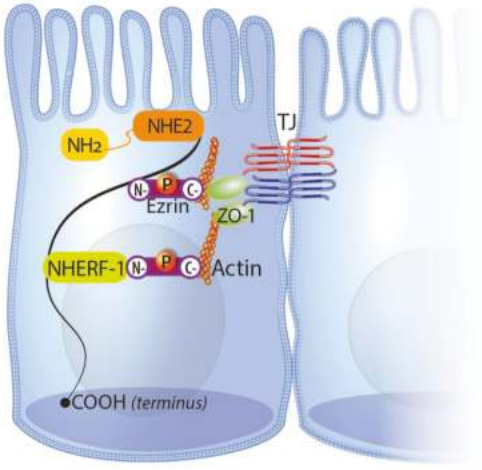

Figure 1. Schematic representation of the potential link of NHE2 to the actin cytoskeleton and subsequently the tight junction through binding partners. The primary candidate protein linking NHE2 to the actin cytoskeleton is phosphorylated ezrin. Based on information known about NHE3 and data from NHE2 in vivo studies, NHE2 may bind directly to ezrin or indirectly through additional binding partners, including NHERF1/EBP50.

4.2. ClC-2 and Intestinal Repair

Chloride secretion from intestinal epithelium into the lumen is crucial for homeostatic water absorption/secretion via maintaining an osmotic balance with luminal accumulation of both chloride and sodium ions. This subsequently allows for proper mucosal hydration of the epithelial layer, which protects the lumen as food passes through the intestine [70]. The primary protein responsible for chloride transport into the intestinal lumen is the apically located cystic fibrosis transmembrane receptor (CFTR) [71]. However, another contributor to transepithelial chloride transport within intestinal epithelium is the voltage-gated ClC-2 protein, one of nine mammalian proteins belonging to the chloride channel (ClC) protein family [72]. ClC-2 has been shown to localize in the plasma membrane at tight junction complexes within mouse intestinal epithelium [73] or has plasmalemmal basolateral localization within guinea pig colons [74], suggesting species- or tissue-specific localization of ClC-2.

In addition to its role in transepithelial chloride transport, ClC-2 has been shown to regulate intestinal tight junction barrier function in various injury models. After porcine intestinal ischemic injury, stimulation of ClC-2 with the ClC-2 agonist lubiprostone during ex vivo recovery on Ussing chambers resulted in marked increases in TER and reduced mucosal-to-serosal mannitol flux [57]. Contrasting the effect of ClC-2 stimulation with lubiprostone, the genetic absence of ClC-2 in a murine model of intestinal ischemia resulted in significant increases in blood-to-lumen mannitol clearance while also reducing expression of membrane-bound occludin and claudin-1 after up to 3 hours of in vivo recovery [75]. In this murine model, occludin co-localized with ClC-2 after co-immunoprecipitation studies, and its localization to the tight junction region was diffuse in ClC-2 null mice after up to 3 hours of recovery [75]. Additionally, in a murine model of dextran sulfate sodium (DSS)-induced colitis, the absence of ClC-2 increased disease severity, as measured through significant losses in body weight and significant increases in disease activity index [76]. ClC-2 null mice treated with DSS also demonstrated significantly increased expression of claudin-2 and reduced occludin expression in the same study. Interestingly, a recent in vitro study established Caco-2 cells overexpressing ClC-2 (Caco-2^{ClCN2}), and this ClC-2 overexpression resulted in a decrease of the pore-forming claudin-2 protein while maintaining claudin-1 and claudin-4 protein levels to that of control cells [77]. As an aside, although cell volume and pH_i is partially regulated by ClC-2 and thus the genetic knockout

of ClC-2 can affect these intracellular factors, studies will be needed to determine if ClC-2-mediated changes in these intracellular factors have an effect on the tight junction [78,79]. Based on these studies, there appears to be a mechanistic link between ClC-2 and the regulation of membrane claudin expression, but further studies will need to be carried out to determine how ClC-2 plays a role in claudin expression patterns. Nonetheless, current data suggest the critical role of ClC-2 in barrier function during recovery from epithelial injury while also reinforcing the link between ClC-2 and the tight junction barrier.

The link between ClC-2 and the tight junction was initially shown to exist through intracellular caveolar trafficking of occludin via interaction with both caveolin-1 and the small GTPase Rab5 in a cell line derived from human intestinal Caco-2 cells (Figure 2) [80]. This connection between ClC-2, occludin, and caveolin-1 was further supported in vivo with a model of DSS-induced colitis. ClC-2 null mice treated with DSS had significantly displaced occludin/caveolin-1 densitometry readings toward high-density, detergent-soluble fractions of sucrose density gradient-based fractions when compared to wild-type mice treated with DSS [76]. These data suggest that after DSS-induced colitis, occludin and caveolin-1 are strongly associated in the cytosol of mice lacking ClC-2 but not in mice normally expressing ClC-2. In tandem, overexpression of ClC-2 in Caco-2^{ClCN2} cells was reported to not only exhibit enhanced tight junction barrier function through significant increases in TER and reductions in apical-to-basal inulin flux, but this ClC-2 overexpression further connected ClC-2 to caveolin-1 and caveolar trafficking of occludin [77]. Specifically, ClC-2 overexpression in Caco-2^{ClCN2} cells exhibited both significantly increased occludin protein and reduced endocytosis of occludin when compared to control cells while simultaneously diminishing both caveolin-1 protein and caveolae assembly [77]. Furthermore, this study reported that selective inhibition of ClC-2 lead to both reduced occludin protein and increased caveolin-1 protein. Taken together, there is strong evidence from both in vitro and in vivo models that links ClC-2 to the tight junction protein occludin and its regulation by caveolar trafficking. Based on the presented evidence, it is believed that ClC-2 facilitates the shuttling of endocytosed tight junction proteins back to the apical–lateral membrane to repair injured tight junctions. However, further mechanistic studies are required out to determine the precise mechanisms of these events.

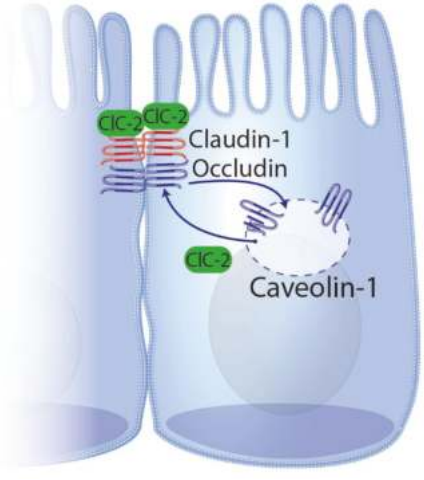

Figure 2. Schematic representation of the link between ClC-2 and caveolar trafficking of occludin. This schematic is a slight modification from a previously published figure [81] to more closely associate ClC-2 to both the tight junction complex and to caveolin-1-associated endocytosis and recycling of tight junction proteins such as occludin. Note that the representation of ClC-2 at the tight junction complex is not exclusively apical in localization, which leaves room for ClC-2 to be more closely associated with occludin in the membrane.

5. Conclusions

Injury of intestinal epithelium affects both the epithelial cells and the junctional structures that link them. A great deal of attention has been focused on mechanisms of epithelial restitution, but a lesser level of attention has been paid to the reassembly of tight junctions within repairing epithelium. This intriguing process appears to be intimately associated with ion channels, which in the case of NHE2 and ClC-2, is facilitated by a close association with tight junction regulatory proteins. With ClC-2 in particular, the mechanism of ion channel-facilitated tight junction reassembly has been linked to endosomal recycling of tight junction proteins, with evidence of restoration of the positioning of tight junction integral membrane proteins during the reparative process, and increased membrane expression of sealing claudins with cellular over-expression of ClC-2. However, how precisely ion channels interact with structures such as endosomes, and how this facilitates insertion of sealing tight junction proteins at the repairing tight junction will require further study. Nonetheless, it does appear that ion channels such as NHE2 and ClC-2 have a greater cellular function than ion transport alone. It is conceivable that the transport of select ions accompanies a structural change that sets off a series of signaling events associated with tight junction reassembly, but this will require additional mechanistic work. Ultimately, further studies to uncover the relationship between ion channels and reassembly of tight junctions has the potential to lead to novel therapeutic targets for patients with increased intestinal paracellular permeability.

Funding: The APC was funded by USDA-NIFA, 2017-67015-26804 (to ATB).

Conflicts of Interest: The authors declare no conflict of interest.

References

1. Groschwitz, K.R.; Hogan, S.P. Intestinal barrier function: Molecular regulation and disease pathogenesis. *J. Allergy Clin. Immunol.* **2009**, *124*, 3–22. [CrossRef] [PubMed]
2. Turner, J.R. Intestinal mucosal barrier function in health and disease. *Nat. Rev. Immunol.* **2009**, *9*, 799–809. [CrossRef] [PubMed]
3. Liang, G.H.; Weber, C.R. Molecular aspects of tight junction barrier function. *Curr. Opin. Pharmacol.* **2014**, *19*, 84–89. [CrossRef] [PubMed]
4. König, J.; Wells, J.; Cani, P.D.; García-Ródenas, C.L.; Macdonald, T.; Mercenier, A.; Whyte, J.; Troost, F.; Brummer, R.J. Human Intestinal Barrier Function in Health and Disease. *Clin. Transl. Gastroenterol.* **2016**, *7*, e196. [CrossRef] [PubMed]
5. El Asmar, R.; Panigrahi, P.; Bamford, P.; Berti, I.; Not, T.; Coppa, G.V.; Catassi, C.; Fasano, A. Host-dependent zonulin secretion causes the impairment of the small intestine barrier function after bacterial exposure. *Gastroenterology* **2002**, *123*, 1607–1615. [CrossRef]
6. Al-Sadi, R. Mechanism of cytokine modulation of epithelial tight junction barrier. *Front. Biosci.* **2009**, *14*, 2765–2778. [CrossRef]
7. Broekaert, N.; Devreese, M.; Demeyere, K.; Berthiller, F.; Michlmayr, H.; Varga, E.; Adam, G.; Meyer, E.; Croubels, S. Comparative in vitro cytotoxicity of modified deoxynivalenol on porcine intestinal epithelial cells. *Food Chem. Toxicol.* **2016**, *95*, 103–109. [CrossRef]
8. Schumann, M.; Siegmund, B.; Schulzke, J.D.; Fromm, M. Celiac Disease: Role of the Epithelial Barrier. *Cell. Mol. Gastroenterol. Hepatol.* **2017**, *3*, 150–162. [CrossRef]
9. Li, Q.; Zhang, Q.; Wang, C.; Liu, X.; Qu, L.; Gu, L.; Li, N.; Li, J. Altered distribution of tight junction proteins after intestinal ischaemia/reperfusion injury in rats. *J. Cell. Mol. Med.* **2009**, *13*, 4061–4076. [CrossRef]
10. Odenwald, M.A.; Turner, J.R. The intestinal epithelial barrier: A therapeutic target? *Nat. Rev. Gastroenterol. Hepatol.* **2017**, *14*, 9–21. [CrossRef]
11. Blikslager, A.T.; Moeser, A.J.; Gookin, J.L.; Jones, S.L.; Odle, J. Restoration of Barrier Function in Injured Intestinal Mucosa. *Physiol. Rev.* **2007**, *87*, 545–564. [CrossRef] [PubMed]
12. Gonzalez, L.M.; Moeser, A.J.; Blikslager, A.T. Animal models of ischemia-reperfusion-induced intestinal injury: Progress and promise for translational research. *Am. J. Physiol. Gastrointest Liver Physiol.* **2015**, *308*, G63–G75. [CrossRef] [PubMed]

13. Furuse, M. Claudin-1 and -2: Novel Integral Membrane Proteins Localizing at Tight Junctions with No Sequence Similarity to Occludin. *J. Cell Biol.* **1998**, *141*, 1539–1550. [CrossRef] [PubMed]
14. Tsukita, S.; Tanaka, H.; Tamura, A. The Claudins: From Tight Junctions to Biological Systems. *Trends Biochem. Sci.* **2019**, *44*, 141–152. [CrossRef]
15. Chiba, H.; Osanai, M.; Murata, M.; Kojima, T.; Sawada, N. Transmembrane proteins of tight junctions. *Biochim. Biophys. Acta BBA Biomembr.* **2008**, *1778*, 588–600. [CrossRef]
16. Günzel, D.; Fromm, M. Claudins and Other Tight Junction Proteins. *Compr. Physiol.* **2012**, *2*, 1819–1852.
17. Günzel, D.; Yu, A.S.L. Claudins and the Modulation of Tight Junction Permeability. *Physiol. Rev.* **2013**, *93*, 525–569. [CrossRef]
18. Van Itallie, C.M.; Anderson, J.M. Phosphorylation of tight junction transmembrane proteins: Many sites, much to do. *Tissue Barriers* **2018**, *6*, e1382671. [CrossRef]
19. Furuse, M. Occludin: A novel integral membrane protein localizing at tight junctions. *J. Cell Biol.* **1993**, *123*, 1777–1788. [CrossRef]
20. Ikenouchi, J.; Furuse, M.; Furuse, K.; Sasaki, H.; Tsukita, S.; Tsukita, S. Tricellulin constitutes a novel barrier at tricellular contacts of epithelial cells. *J. Cell Biol.* **2005**, *171*, 939–945. [CrossRef]
21. Martin-Padura, I.; Lostaglio, S.; Schneemann, M.; Williams, L.; Romano, M.; Fruscella, P.; Panzeri, C.; Stoppacciaro, A.; Ruco, L.; Villa, A.; et al. Junctional Adhesion Molecule, a Novel Member of the Immunoglobulin Superfamily That Distributes at Intercellular Junctions and Modulates Monocyte Transmigration. *J. Cell Biol.* **1998**, *142*, 117–127. [CrossRef] [PubMed]
22. Palmeri, D. Vascular Endothelial Junction-associated Molecule, a Novel Member of the Immunoglobulin Superfamily, Is Localized to Intercellular Boundaries of Endothelial Cells. *J. Biol. Chem.* **2000**, *275*, 19139–19145. [CrossRef] [PubMed]
23. Liang, T.W.; Chiu, H.H.; Gurney, A.; Sidle, A.; Tumas, D.B.; Schow, P.; Foster, J.; Klassen, T.; Dennis, K.; Demarco, R.A.; et al. Vascular endothelial-junctional adhesion molecule (VE-JAM)/JAM 2 interacts with T, NK, and dendritic cells through JAM 3. *J. Immunol.* **2002**, *168*, 1618–1626. [CrossRef] [PubMed]
24. Ebnet, K.; Aurrand-Lions, M.; Kiefer, F.; Butz, S.; Zander, K.; Zu Brickwedde, M.K.M.; Kuhn, A.; Suzuki, A.; Imhof, B.A.; Vestweber, D. The junctional adhesion molecule (JAM) family members JAM-2 and JAM-3 associate with the cell polarity protein PAR-3: A possible role for JAMs in endothelial cell polarity. *J. Cell Sci.* **2003**, *116*, 3879–3891. [CrossRef] [PubMed]
25. Garrido-Urbani, S.; Bradfield, P.F.; Imhof, B.A. Tight junction dynamics: The role of junctional adhesion molecules (JAMs). *Cell Tissue Res.* **2014**, *355*, 701–715. [CrossRef] [PubMed]
26. Zemans, R.L.; Colgan, S.P.; Downey, G.P. Transepithelial migration of neutrophils: Mechanisms and implications for acute lung injury. *Am. J. Respir. Cell Mol. Biol.* **2009**, *40*, 519–535. [CrossRef] [PubMed]
27. Stevenson, B.R.; Siliciano, J.D.; Mooseker, M.S.; Goodenough, D.A. Identification of ZO-1: A high molecular weight polypeptide associated with the tight junction (zonula occludens) in a variety of epithelia. *J. Cell Biol.* **1986**, *103*, 755–766. [CrossRef]
28. Gumbiner, B.; Lowenkopf, T.; Apatira, D. Identification of a 160-kDa polypeptide that binds to the tight junction protein ZO-1. *Proc. Natl. Acad. Sci. USA* **1991**, *88*, 3460–3464. [CrossRef]
29. Jesaitis, L.A. Molecular characterization and tissue distribution of ZO-2, a tight junction protein homologous to ZO-1 and the Drosophila discs-large tumor suppressor protein. *J. Cell Biol.* **1994**, *124*, 949–961. [CrossRef]
30. Balda, M.S. Assembly of the tight junction: The role of diacylglycerol. *J. Cell Biol.* **1993**, *123*, 293–302. [CrossRef]
31. Shen, L.; Weber, C.R.; Raleigh, D.R.; Yu, D.; Turner, J.R. Tight junction pore and leak pathways: A dynamic duo. *Annu. Rev. Physiol.* **2011**, *73*, 283–309. [CrossRef] [PubMed]
32. Yu, A.S.L.; Yin, H.; Havrilla, C.M.; Gao, L.; Morrow, J.D.; Porter, N.A.; Enck, A.H.; Lencer, W.I.; Schneeberger, E.E. Claudin-8 Expression in Madin-Darby Canine Kidney Cells Augments the Paracellular Barrier to Cation Permeation. *J. Biol. Chem.* **2003**, *278*, 17350–17359. [CrossRef]
33. France, M.M.; Turner, J.R. The mucosal barrier at a glance. *J. Cell Sci.* **2017**, *130*, 307–314. [CrossRef]
34. Luettig, J.; Rosenthal, R.; Barmeyer, C.; Schulzke, J. Claudin-2 as a mediator of leaky gut barrier during intestinal inflammation. *Tissue Barriers* **2015**, *3*, e977176. [CrossRef] [PubMed]
35. Zeissig, S.; Burgel, N.; Gunzel, D.; Richter, J.; Mankertz, J.; Wahnschaffe, U.; Kroesen, A.J.; Zeitz, M.; Fromm, M.; Schulzke, J.D. Changes in expression and distribution of claudin 2, 5 and 8 lead to discontinuous tight junctions and barrier dysfunction in active Crohn's disease. *Gut* **2007**, *56*, 61–72. [CrossRef] [PubMed]

36. Escaffit, F.; Boudreau, F.; Beaulieu, J.F. Differential expression of claudin-2 along the human intestine: Implication of GATA-4 in the maintenance of claudin-2 in differentiating cells. *J. Cell. Physiol.* **2005**, *203*, 15–26. [CrossRef] [PubMed]
37. Garcia-Hernandez, V.; Quiros, M.; Nusrat, A. Intestinal epithelial claudins: Expression and regulation in homeostasis and inflammation. *Ann. N. Y. Acad. Sci.* **2017**, *1397*, 66–79. [CrossRef] [PubMed]
38. Rahner, C.; Mitic, L.L.; Anderson, J.M. Heterogeneity in expression and subcellular localization of claudins 2, 3, 4, and 5 in the rat liver, pancreas, and gut. *Gastroenterology* **2001**, *120*, 411–422. [CrossRef]
39. Fujita, H.; Chiba, H.; Yokozaki, H.; Sakai, N.; Sugimoto, K.; Wada, T.; Kojima, T.; Yamashita, T.; Sawada, N. Differential Expression and Subcellular Localization of Claudin-7, -8, -12, -13, and -15 Along the Mouse Intestine. *J. Histochem. Cytochem.* **2006**, *54*, 933–944. [CrossRef]
40. Holmes, J.L.; Van Itallie, C.M.; Rasmussen, J.E.; Anderson, J.M. Claudin profiling in the mouse during postnatal intestinal development and along the gastrointestinal tract reveals complex expression patterns. *Gene Expr. Patterns* **2006**, *6*, 581–588. [CrossRef]
41. Pasternak, J.A.; Kent-Dennis, C.; Van Kessel, A.G.; Wilson, H.L. Claudin-4 Undergoes Age-Dependent Change in Cellular Localization on Pig Jejunal Villous Epithelial Cells, Independent of Bacterial Colonization. *Mediat. Inflamm.* **2015**, *2015*, 1–14. [CrossRef] [PubMed]
42. Butler, J.E.; Lager, K.M.; Splichal, I.; Francis, D.; Kacskovics, I.; Sinkora, M.; Wertz, N.; Sun, J.; Zhao, Y.; Brown, W.R.; et al. The piglet as a model for B cell and immune system development. *Vet. Immunol. Immunopathol.* **2009**, *128*, 147–170. [CrossRef] [PubMed]
43. Tsukita, S.; Furuse, M.; Itoh, M. Multifunctional strands in tight junctions. *Nat. Rev. Mol. Cell Biol.* **2001**, *2*, 285–293. [CrossRef] [PubMed]
44. Krug, S.M.; Amasheh, S.; Richter, J.F.; Milatz, S.; Günzel, D.; Westphal, J.K.; Huber, O.; Schulzke, J.D.; Fromm, M. Tricellulin Forms a Barrier to Macromolecules in Tricellular Tight Junctions without Affecting Ion Permeability. *Mol. Biol. Cell* **2009**, *20*, 3713–3724. [CrossRef]
45. Ciarlet, M.; Conner, M.E.; Finegold, M.J.; Estes, M.K. Group A Rotavirus Infection and Age-Dependent Diarrheal Disease in Rats: A New Animal Model To Study the Pathophysiology of Rotavirus Infection. *J. Virol.* **2002**, *76*, 41–57. [CrossRef]
46. Estes, M.K.; Kang, G.; Zeng, C.Q.; Crawford, S.E.; Ciarlet, M. Pathogenesis of Rotavirus Gastroenteritis. *Novartis Found. Symp.* **2001**, *238*, 82–96; discussion 96–100.
47. Klunder, L.J.; Faber, K.N.; Dijkstra, G.; Van Ijzendoorn, S.C. Mechanisms of Cell Polarity–Controlled Epithelial Homeostasis and Immunity in the Intestine. *Cold Spring Harb. Perspect. Biol.* **2017**, *9*, a027888. [CrossRef]
48. Moore, R.; Carlson, S.; Madara, J.L. Villus contraction aids repair of intestinal epithelium after injury. *Am. J. Physiol. Liver Physiol.* **1989**, *257*, G274–G283. [CrossRef]
49. Gookin, J.L.; Galanko, J.A.; Blikslager, A.T.; Argenzio, R.A. PG-mediated closure of paracellular pathway and not restitution is the primary determinant of barrier recovery in acutely injured porcine ileum. *Am. J. Physiol. Liver Physiol.* **2003**, *285*, G967–G979. [CrossRef]
50. Dignass, A.U. Mechanisms and Modulation of Intestinal Epithelial Repair. *Inflamm. Bowel Dis.* **2001**, *7*, 68–77. [CrossRef]
51. Utech, M.; Mennigen, R.; Bruewer, M. Endocytosis and recycling of tight junction proteins in inflammation. *J. Biomed. Biotechnol.* **2010**, *2010*, 484987. [CrossRef] [PubMed]
52. Stamatovic, S.M.; Johnson, A.M.; Sladojevic, N.; Keep, R.F.; Andjelkovic, A.V. Endocytosis of tight junction proteins and the regulation of degradation and recycling. *Ann. N. Y. Acad. Sci.* **2017**, *1397*, 54–65. [CrossRef] [PubMed]
53. Jin, Y.; Blikslager, A.T. Myosin light chain kinase mediates intestinal barrier dysfunction via occludin endocytosis during anoxia/reoxygenation injury. *Am. J. Physiol. Physiol.* **2016**, *311*, C996–C1004. [CrossRef] [PubMed]
54. Turner, J.R.; Black, E.D.; Ward, J.; Tse, C.M.; Uchwat, F.A.; Alli, H.A.; Donowitz, M.; Madara, J.L.; Angle, J.M. Transepithelial resistance can be regulated by the intestinal brush-border Na(+)/H(+) exchanger NHE3. *Am. J. Physiol. Cell Physiol.* **2000**, *279*, C1918–C1924. [CrossRef]
55. Moeser, A.J.; Nighot, P.K.; Ryan, K.A.; Simpson, J.E.; Clarke, L.L.; Blikslager, A.T. Mice lacking the Na+/H+ exchanger 2 have impaired recovery of intestinal barrier function. *Am. J. Physiol. Gastrointest Liver Physiol.* **2008**, *295*, G791–G797. [CrossRef]

56. Moeser, A.J.; Nighot, P.K.; Ryan, K.A.; Wooten, J.G.; Blikslager, A.T. Prostaglandin-mediated inhibition of Na+/H+ exchanger isoform 2 stimulates recovery of barrier function in ischemia-injured intestine. *Am. J. Physiol. Gastrointest Liver Physiol.* **2006**, *291*, G885–G894. [CrossRef]
57. Moeser, A.J.; Nighot, P.K.; Engelke, K.J.; Ueno, R.; Blikslager, A.T. Recovery of mucosal barrier function in ischemic porcine ileum and colon is stimulated by a novel agonist of the ClC-2 chloride channel, lubiprostone. *Am. J. Physiol. Liver Physiol.* **2007**, *292*, G647–G656. [CrossRef]
58. Feranchak, A.P. Ion channels in digestive health and disease. *J. Pediatr. Gastroenterol. Nutr.* **2003**, *37*, 230–241. [CrossRef]
59. Donowitz, M.; Ming Tse, C.; Fuster, D. SLC9/NHE gene family, a plasma membrane and organellar family of Na(+)/H(+) exchangers. *Mol. Asp. Med.* **2013**, *34*, 236–251. [CrossRef]
60. Gurney, M.A.; Laubitz, D.; Ghishan, F.K.; Kiela, P.R. Pathophysiology of Intestinal Na(+)/H(+) exchange. *Cell Mol. Gastroenterol. Hepatol.* **2017**, *3*, 27–40. [CrossRef]
61. Kurashima, K.; D'Souza, S.; Szaszi, K.; Ramjeesingh, R.; Orlowski, J.; Grinstein, S. The apical Na(+)/H(+) exchanger isoform NHE3 is regulated by the actin cytoskeleton. *J. Biol. Chem.* **1999**, *274*, 29843–29849. [CrossRef] [PubMed]
62. Donowitz, M.; Li, X. Regulatory Binding Partners and Complexes of NHE3. *Physiol. Rev.* **2007**, *87*, 825–872. [CrossRef] [PubMed]
63. Yao, X.; Cheng, L.; Forte, J.G. Biochemical Characterization of Ezrin-Actin Interaction. *J. Biol. Chem.* **1996**, *271*, 7224–7229. [CrossRef] [PubMed]
64. Vaheri, A.; Carpén, O.; Heiska, L.; Helander, T.S.; Jääskeläinen, J.; Majander-Nordenswan, P.; Sainio, M.; Timonen, T.; Turunen, O. The ezrin protein family: Membrane-cytoskeleton interactions and disease associations. *Curr. Opin. Cell Biol.* **1997**, *9*, 659–666. [CrossRef]
65. Bosk, S.; Braunger, J.A.; Gerke, V.; Steinem, C. Activation of F-Actin Binding Capacity of Ezrin: Synergism of PIP2 Interaction and Phosphorylation. *Biophys. J.* **2011**, *100*, 1708–1717. [CrossRef] [PubMed]
66. Brückner, B.R.; Pietuch, A.; Nehls, S.; Rother, J.; Janshoff, A. Ezrin is a Major Regulator of Membrane Tension in Epithelial Cells. *Sci. Rep.* **2015**, *5*, 14700. [CrossRef]
67. Hayashi, H.; Tamura, A.; Krishnan, D.; Tsukita, S.; Suzuki, Y.; Kocinsky, H.S.; Aronson, P.S.; Orlowski, J.; Grinstein, S.; Alexander, R.T. Ezrin is Required for the Functional Regulation of the Epithelial Sodium Proton Exchanger, NHE3. *PLoS ONE* **2012**, *8*, e55623.
68. Praetorius, J.; Andreasen, D.; Jensen, B.L.; Ainsworth, M.A.; Friis, U.G.; Johansen, T. NHE1, NHE2, and NHE3 contribute to regulation of intracellular pH in murine duodenal epithelial cells. *Am. J. Physiol. Liver Physiol.* **2000**, *278*, G197–G206. [CrossRef]
69. Schneeberger, E.E.; Lynch, R.D. Tight junctions. Their structure, composition, and function. *Circ. Res.* **1984**, *55*, 723–733. [CrossRef]
70. Barrett, K.E.; Keely, S.J. Chloride Secretion by the Intestinal Epithelium: Molecular Basis and Regulatory Aspects. *Annu. Rev. Physiol.* **2000**, *62*, 535–572. [CrossRef] [PubMed]
71. Frizzell, R.A.; Hanrahan, J.W. Physiology of Epithelial Chloride and Fluid Secretion. *Cold Spring Harb. Perspect. Med.* **2012**, *2*, a009563. [CrossRef] [PubMed]
72. Poroca, D.R.; Pelis, R.M.; Chappe, V.M. ClC Channels and Transporters: Structure, Physiological Functions, and Implications in Human Chloride Channelopathies. *Front. Pharmacol.* **2017**, *8*, 151. [CrossRef] [PubMed]
73. Gyomorey, K.; Yeger, H.; Ackerley, C.; Garami, E.; Bear, C.E. Expression of the chloride channel ClC-2 in the murine small intestine epithelium. *Am. J. Physiol. Physiol.* **2000**, *279*, C1787–C1794. [CrossRef] [PubMed]
74. Catalan, M.; Niemeyer, M.I.; Cid, L.; Sepúlveda, F.V. Basolateral ClC-2 chloride channels in surface colon epithelium: Regulation by a direct effect of intracellular chloride. *Gastroenterology* **2004**, *126*, 1104–1114. [CrossRef] [PubMed]
75. Nighot, P.K.; Blikslager, A.T. ClC-2 regulates mucosal barrier function associated with structural changes to the villus and epithelial tight junction. *Am. J. Physiol. Liver Physiol.* **2010**, *299*, G449–G456. [CrossRef] [PubMed]
76. Nighot, P.; Young, K.; Nighot, M.; Rawat, M.; Sung, E.J.; Maharshak, N.; Plevy, S.E.; Ma, T.; Blikslager, A. Chloride channel ClC-2 is a key factor in the development of DSS-induced murine colitis. *Inflamm. Bowel Dis.* **2013**, *19*, 2867–2877. [CrossRef] [PubMed]

77. Nighot, P.K.; Leung, L.; Ma, T.Y. Chloride channel ClC- 2 enhances intestinal epithelial tight junction barrier function via regulation of caveolin-1 and caveolar trafficking of occludin. *Exp. Cell Res.* **2017**, *352*, 113–122. [CrossRef]
78. Roman, R.M.; Smith, R.L.; Feranchak, A.P.; Clayton, G.H.; Doctor, R.B.; Fitz, J.G. ClC-2 chloride channels contribute to HTC cell volume homeostasis. *Am. J. Physiol. Liver Physiol.* **2001**, *280*, G344–G353. [CrossRef]
79. Nighot, M.P.; Nighot, P.K.; Ma, T.Y.; Malinowska, D.H.; Shull, G.E.; Cuppoletti, J.; Blikslager, A.T. Genetic Ablation of the ClC-2 Cl- Channel Disrupts Mouse Gastric Parietal Cell Acid Secretion. *PLoS ONE* **2015**, *10*, e0138174. [CrossRef]
80. Nighot, P.K.; Blikslager, A.T. Chloride channel ClC-2 modulates tight junction barrier function via intracellular trafficking of occludin. *Am. J. Physiol. Physiol.* **2012**, *302*, C178–C187. [CrossRef]
81. Jin, Y.; Blikslager, A.T. ClC-2 regulation of intestinal barrier function: Translation of basic science to therapeutic target. *Tissue Barriers* **2015**, *3*, e1105906. [CrossRef] [PubMed]

International Journal of
Molecular Sciences

MDPI

Review

Claudins in the Renal Collecting Duct

Janna Leiz [1,2] and Kai M. Schmidt-Ott [1,2,3,*]

[1] Department of Nephrology and Intensive Care Medicine, Charité-Universitätsmedizin Berlin, 12203 Berlin, Germany; janna.leiz@charite.de
[2] Molecular and Translational Kidney Research, Max-Delbrück-Center for Molecular Medicine in the Helmholtz Association (MDC), 13125 Berlin, Germany
[3] Berlin Institute of Health (BIH), 10178 Berlin, Germany
* Correspondence: kai.schmidt-ott@charite.de; Tel.: +49-(0)30-450614671

Received: 22 October 2019; Accepted: 20 December 2019; Published: 28 December 2019

Abstract: The renal collecting duct fine-tunes urinary composition, and thereby, coordinates key physiological processes, such as volume/blood pressure regulation, electrolyte-free water reabsorption, and acid-base homeostasis. The collecting duct epithelium is comprised of a tight epithelial barrier resulting in a strict separation of intraluminal urine and the interstitium. Tight junctions are key players in enforcing this barrier and in regulating paracellular transport of solutes across the epithelium. The features of tight junctions across different epithelia are strongly determined by their molecular composition. Claudins are particularly important structural components of tight junctions because they confer barrier and transport properties. In the collecting duct, a specific set of claudins (Cldn-3, Cldn-4, Cldn-7, Cldn-8) is expressed, and each of these claudins has been implicated in mediating aspects of the specific properties of its tight junction. The functional disruption of individual claudins or of the overall barrier function results in defects of blood pressure and water homeostasis. In this concise review, we provide an overview of the current knowledge on the role of the collecting duct epithelial barrier and of claudins in collecting duct function and pathophysiology.

Keywords: epithelial barrier; barrier formation; collecting duct; tight junction; claudin

1. Introduction

Selective barriers formed by epithelial monolayers are vital for many critical physiological processes [1]. These barriers are composed of intercellular multiprotein complexes along the apical-basal axis of epithelial cells creating direct cell-cell interactions and forming apical junctional complexes [2]. These complexes include tight junctions (TJs), adherens junctions, and desmosomes.

TJs are the most apical and diverse of these junctional complexes. They are formed by transmembrane as well as cytoplasmic proteins and are linked to the cytoskeleton. The protein composition of TJs varies greatly among different epithelia and determines the barrier properties and permeability [3].

Overall, TJs serve a dual function in epithelial layers acting as (a) a fence, separating membrane proteins between the apical and basolateral membrane and (b) as a gate by regulating size- and charge-selective movements of ions, solutes, and small molecules via the paracellular route [4–7]. Consequently, TJs are not only critical to establish and maintain cell adhesion and epithelial polarity but are also necessary to create selective paracellular permeability between compartments.

Several studies show that the main protein family mediating TJ characteristics and functions are the membrane-spanning claudins. So far, more than 25 different claudins have been identified, and at least 10 of them are expressed in spatiotemporal patterns along the renal nephron (for a detailed review see [8]).

Structurally, the transmembrane proteins connect in both *cis* and *trans* to neighboring claudins of the same, as well as the opposing, cell membranes forming TJ strands [9]. Claudins are sufficient to arrange those strands when expressed in cells lacking endogenous TJ formation [10].

Here, we review the role of claudins in epithelial barrier formation with emphasis on the renal collecting duct as well as their implications in collecting duct physiology and function.

2. The Renal Collecting Duct

The renal collecting duct is the most distal part of the renal tubules. It connects renal nephrons with the renal pelvis and—together with the distal convoluted tubule and the connecting tubule—it contributes to the aldosterone-sensitive distal nephron. In general, the renal collecting duct plays important roles in fine-tuning urinary composition, extracellular fluid volume, electrolyte balance, blood pressure regulation, water homeostasis, and acid-base regulation [11,12].

Although most of the water and solute reabsorption in the kidney occurs in the more upstream segments of the nephron, transport variability in the renal collecting duct is significantly higher, and ion and water transport are under strict hormonal control [11]. This permits to adjust reabsorption and secretion to prevalent physiological conditions and to control the body's water and electrolyte balance closely.

The main solutes reabsorbed in the collecting duct are sodium (Na+) and chloride (Cl−), while potassium (K+) is secreted into the urine [13] (Figure 1). Transport of these ions occurs via the transcellular route—mediated by channels and membrane transporters—and via the paracellular route—mediated by TJs.

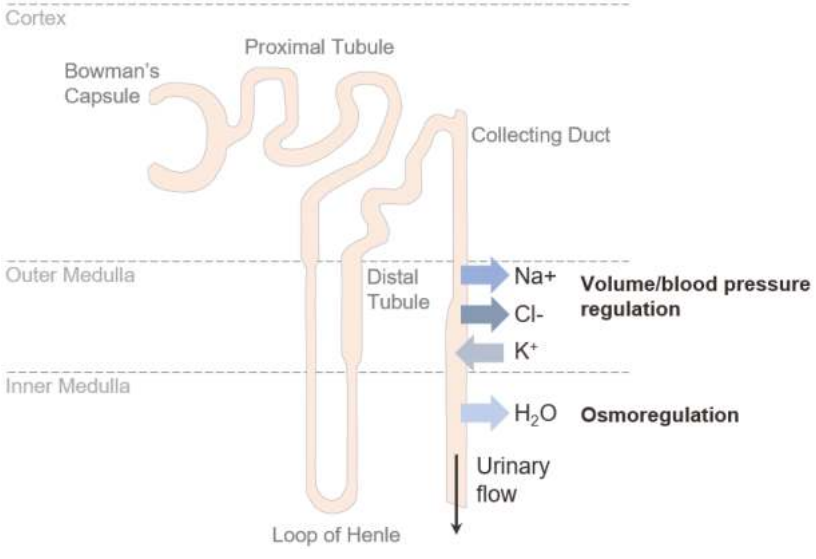

Figure 1. Transport in the renal collecting duct. In the renal collecting duct Na+ and Cl− are reabsorbed, while K+ is secreted into the urine. A steep osmolality gradient between the interstitium and lumen across the epithelial barrier is the driving force for water reabsorption.

3. Claudins and Their Roles in Collecting Duct Epithelial Barrier Formation and Paracellular Ion Transport

In general, claudins can be pore- or barrier-forming [14]. As in other segments of the renal nephron, it is believed that the expressed claudins are the main mediators of TJ permeability characteristics, and thus, control the paracellular pathway in the collecting duct [9,15]. Among the predominately

expressed claudins in the renal collecting duct are claudin-3 (Cldn-3), -4 (Cldn-4), -7 (Cldn-7) and -8 (Cldn-8) [16,17]. Furthermore, a recently published study proposes a role for claudin-19 (Cldn-19) in the renal collecting duct [18]. Overall, the present knowledge strongly supports the theory that these claudins either enforce the epithelial barrier in general or build a paracellular Cl− channel, while other aspects of their functions are less clear (Table 1).

Table 1. Claudins expressed in the renal collecting duct and their proposed function in barrier formation and collecting duct tight junctions.

Claudin	Proposed Function in the Collecting Duct Tight Junction	Knockout Phenotype In Vivo
Cldn-3	General barrier function [19,20]	Increase in urinary pH, no electrolyte abnormalities [21]
Cldn-4	Cl− channel, cation barrier [22]	Hypotension, hypochloremia, metabolic alkalosis, renal wasting of Na+ and Cl− [23]
Cldn-7	Cl− and Na+ channel [24–27]	Severe renal salt wasting, dehydration [27]
Cldn-8	Cl− channel, cation barrier [28,29]	Hypotension, hypochloremia, metabolic alkalosis, renal wasting of Na+ and Cl− [29]
Cldn-19	Adaption of barrier selectivity to osmolality [18]	-

In the following sections, we will briefly review the published literature on the functions of these claudins in the collecting duct. As a general note, it should be acknowledged that gain-of-function studies utilizing overexpression of claudins in cell lines have a general limitation due to the influence of the endogenous components of the TJ in each cell line. The expressed claudins in the respective chosen model make it difficult to determine the exact impact of single claudins on permeability characteristics. In contrast, loss-of-function studies, if carried out in the appropriate system (i.e., the collecting duct in vivo or cell lines that accurately represent collecting duct epithelia), are more appropriate to outline the molecular functions of each claudin.

3.1. Cldn-3

Several studies have found that Cldn-3 enforces the paracellular barrier [19,20]. Its overexpression in otherwise leaky Madin-Darby Canine Kidney (MDCK) II cells leads to an altered TJ structure with increased transepithelial resistance (TER) and decreased permeability for ions as well as molecules of 332 Da and 4 kDa, indicating a general role for Cldn-3 in barrier formation and enforcement [19]. Furthermore, Cldn-3 has been described to promote tubule formation in vitro and might thus play a role during tubule morphogenesis in the developing kidney [30]. The conditional knockout of Cldn-3 resulted in increased urinary pH without any effect on urine or plasma electrolytes [21]. However, the collecting duct-specific role of Cldn-3 has not been studied so far.

3.2. Cldn-7

Cldn-7-deficient mice die shortly after birth due to severe renal salt wasting and dehydration [27]. Interestingly, collecting duct cells isolated from Cldn-7-deficient mice demonstrate an increase in TER and show decreased paracellular permeability for both Na+ and Cl− [31]. This suggests that Cldn-7 may form a non-selective paracellular channel facilitating Cl− and Na+ reabsorption in collecting ducts.

Different and partially conflicting roles of Cldn-7 have been suggested in other experimental systems, complicating the interpretation of Cldn-7 biology. Overexpression of Cldn-7 in LLC-PK1 cells induces an increase in TER accompanied by a reduced Cl− and elevated Na+ conductance [24]. In contrast, the knockdown of Cldn-7 in those cells leads to loss of anion selectivity and decreased Cl− permeation, whereas in cation-selective MDCK cells, knockdown of Cldn-7 leads to increased Na+ permeability [25]. Mutation experiments in vitro demonstrated the importance of specific negatively charged amino acids in the extracellular loop of Cldn-7 for paracellular permeability and charge

selectivity [32]. These contrasting results could indicate different roles for Cldn-7, depending on the cellular background, and endogenously expressed TJ components.

3.3. Cldn-4 and Cldn-8

Both, Cldn-4 and Cldn-8, are thought to serve as a cation barrier [33–35] and an anion channel [22]. This hypothesis is supported by data from in vivo experiments. Collecting duct-specific knockout of either Cldn-4 or Cldn-8, causes hypotension, hypochloremia, metabolic alkalosis and renal wasting of Na+ and Cl− [23,29]. These phenotypes would be consistent with Cldn-4 and Cldn-8 acting as paracellular Cl− channels, which are necessary for a paracellular "chloride shunt" required for effective transcellular Na+ reabsorption (via the epithelial sodium channel).

Different effects of Cldn-4 overexpression on charge selectivity, depending on the used cell model, have been described. Overexpression of Cldn-4 leads to an increase in TER in cation-selective MDCK II and anion-selective LLC-PK1 cells, but a decrease in Na+ permeability is only observed in MDCK II cells [34].

Cldn-8 has been shown to be necessary to recruit Cldn-4 to the TJ and to implement the protein into the junctional complex. In the absence of Cldn-8, Cldn-4 is mainly found in the endoplasmic reticulum and the Golgi complex, but not in the apical cell membrane where TJs are located [22]. Thus, Cldn-8 knockout causes a functional double knockout on the TJ level due to its requirement for correct Cldn-4 localization [22].

3.4. Cldn-19

In addition to the longer known claudins of the renal collecting duct described above, a recently published study indicates a role for Cldn-19, which had previously been linked to thick ascending limb functions [36–38]. Cldn-19 is associated with tightness and cation selectivity of the epithelial barrier. Interestingly, the TJ localization of Cldn-19 is promoted by a low osmolality, whereas high osmolality favors an intracellular localization, suggesting that it may contribute to tonicity-induced changes in paracellular ion selectivity [18]. This role of a claudin in epithelial adaption to the changing osmolality along the corticomedullary axis provides an interesting aspect of TJ physiology but collecting duct-specific knockout models of Cldn-19 have not yet been generated.

4. The Collecting Duct Epithelial Barrier in Electrolyte-Free Water Reabsorption

Although water transport in the renal collecting duct is not directly facilitated by water channel-forming claudins (contrasting with observations of Cldn-2 in the proximal tubule [39]), TJs in the collecting duct contribute to water reabsorption indirectly.

The driving force for water reabsorption in the renal collecting duct is a steep osmolality gradient formed by high concentrations of osmolytes in the interstitium, which increases towards the renal medulla [40]. The tight collecting duct epithelial barrier is crucial to maintain the osmolality gradient between the tubular lumen and the interstitium.

Water transport in the renal collecting duct is mainly controlled by arginine vasopressin (AVP), also called antidiuretic hormone. If the water content in the body is low, AVP binds to its type 2 receptor (V2R) localized in the basal cell membrane of collecting duct principal cells and stimulates the expression of aquaporin-2 (AQP2) water channels. Furthermore, AVP triggers a signaling cascade leading to the accumulation of AQP2 in the apical membrane (for a detailed review see [11,41]). This mechanism enables reabsorption of electrolyte-free water from the intraluminal urine and forms the basis of urinary concentrating ability. Inactivation of either V2R or AQP2 leads to polyuria with massive excretion of electrolyte-free water, a condition called nephrogenic diabetes insipidus [42].

A recent study has demonstrated the importance of an intact epithelial barrier in the renal collecting duct for efficient water reabsorption [43]. Deletion of the transcriptional regulator Grainyhead-like 2 (Grhl2), an epithelial transcription factor that induces the expression of barrier-enforcing molecular TJ components including Cldn-4 [44], results in a leaky collecting duct epithelium and a decreased

TER across the collecting duct epithelium. Leakage of interstitial osmolytes across the Grhl2-deficient collecting duct epithelium is associated with defective retention of osmolytes in the interstitium of the inner medulla. Grhl2-deficient mice show signs of diabetes insipidus and fail to concentrate their urine adequately, although AQP-mediated water transport across the apical and basolateral membranes of Grhl2-deficient collecting ducts is intact [43]. This indicates that a tight collecting duct epithelial barrier is crucial for the maintenance of osmolality gradients and for effective collecting duct water reabsorption. Interestingly, Grhl2 deficiency (unlike deficiencies of individual claudins) was not associated with abnormalities of Cl− and Na+ reabsorption. It needs to be acknowledged that Grhl2 functions are not restricted to the effects on the TJ, which may explain the difference in phenotypes. In addition, it is possible that the barrier defect of Grhl2-deficient collecting duct cells is more profound, leading to non-ion-selective leakage of interstitial osmolytes into hypotonic urine.

5. Aldosterone and Its Role in Transcellular and Paracellular Transport Regulation

In the renal collecting duct, Na+ transport is separated from Cl− transport [45]. Na+ reabsorption from the intraluminal urine occurs transcellularly via the epithelial sodium channel (ENaC) that locates to the apical membrane of collecting duct principal cells. This generates a lumen-negative potential, providing a driving force for K+ secretion via the renal outer medullary potassium channel (ROMK). In contrast, Cl− reabsorption in the collecting duct occurs predominantly via the paracellular route. This "chloride shunt" is important to limit the built-up of a lumen-negative potential and, thereby, facilitates continued Na+ reabsorption and prevents excessive K+ secretion.

The key regulator of ENaC is aldosterone, a hormone secreted from the adrenal gland in response to hyperkalemia and hypovolemia [11,46]. Overall, aldosterone plays a central role in blood pressure regulation by controlling plasma Na+ and K+ levels and thus indirectly influences water retention or loss. However, growing evidence supports the hypothesis that aldosterone controls Na+ reabsorption and K+ secretion not only by regulating the abundance of ENaC and increasing transcellular transport but also by adjusting paracellular Cl− permeability in multiple ways:

For instance, aldosterone triggers the expression of Cldn-8 when ENaC is active, presumably to seal the paracellular route for Na+ back flux. Thereby net flux of Na+ can be increased [28].

Additionally, aldosterone regulates channel-activating protease 1 (Cap1) [47]. Cap1, in turn, stimulates ENaC and inhibits the Cl− conductivity by directly regulating Cldn-4 *trans*-interactions [23,48]. Thereby K+ secretion is favored over Cl− reabsorption (Figure 2a).

Aldosterone also induces the phosphorylation and activation of the with no lysine kinases 4 (WNK4) [49]. Expression of WNK4 in MDCK II cells has been shown to reduce the TER and increase Cl− permeability, without affecting TJ structure [50]. Activated WNK4 phosphorylates Cldn-4 on threonine residues decreasing the cells' TER and increasing apical to basal anion passage [51].

In the absence of aldosterone, WNK4 inhibits ENaC and ROMK activity and thus directly opposes Cap1 [52,53]. WNK4 phosphorylation suspends this inhibition (Figure 2b). Taken together, this indicates the possibility that aldosterone might regulate claudins through Cap1 and WNK4, coordinating Cl− reabsorption or K+ secretion, respectively.

Kahle and colleagues proposed WNK4 as the functional switch regulating Na+ and Cl− reabsorption independently from K+ secretion depending on the physiological conditions [53]. However, the factors facilitating different functional states of WNK4 haven't been provided, and to our knowledge, it is still unknown how the reverse actions of Cap1 and WNK4, that are both mediated by aldosterone, are regulated to decide in favor of K+ secretion or Cl− reabsorption, respectively.

In diabetes, the role of aberrant aldosterone signaling in the progression of renal disease has long been established [54,55]. Mediated by the divergent aldosterone levels, Cldn-4 and Cldn-8 are overexpressed in the distal nephron from type 1 diabetic rats, and the expression of WNK4 and its co-localization with Cldn-4 and Cldn-8 is also increased [56,57]. This might result in increased activation of Cldn-4 and Cldn-8 by WNK4 under diabetic conditions and could implicate disturbed paracellular

transport in renal disease progression. However, additional experimental evidence verifying this hypothesis is needed.

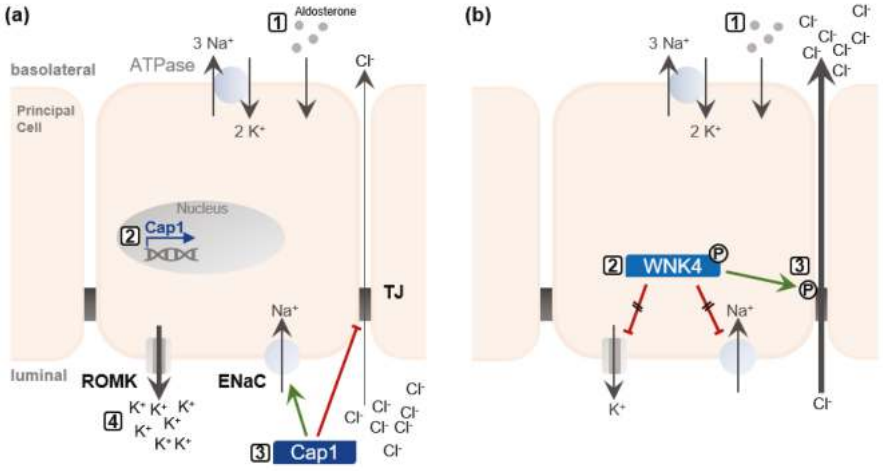

Figure 2. (**a**) Aldosterone-mediated induction of channel-activating protease 1 (Cap1) activates Na+ reabsorption, but simultaneously inhibits the paracellular "chloride shunt", resulting in excessive K+ excretion. When aldosterone is secreted (1), it triggers the expression of Cap1 in principal cells of the renal collecting duct (2). Cap1 inhibits Cl− reabsorption directly by disrupting *trans*-interactions of Cldn-4. Simultaneously, Cap1 activates apical Na+ channels (ENaC), and thus, increases the transcellular reabsorption of Na+ (3). Consequently, the growing luminal negative potential drives K+ secretion into the urine via renal outer medullary potassium (ROMK) channels (4). (**b**) Aldosterone activates ENaC, ROMK, and the paracellular "chloride shunt" via with no lysine kinases 4 (WNK4) phosphorylation. When aldosterone is secreted (1), it leads to the phosphorylation of WNK4. This suspends the tonic inhibition of ROMK and ENaC by WNK4 (2). Furthermore, WNK4 phosphorylates claudins located to the tight junctions (TJs) of the renal collecting duct and thereby increases Cl− reabsorption (3). Green arrows indicate positive regulation, red lines indicate inhibition.

6. Chloride Reabsorption in Renal Collecting Ducts and Potential Involvement in Disease

The aldosterone-sensitive distal nephron is the main side of Cl− reabsorption. It occurs via multiple ways, including paracellular transport via TJs as well as transcellular pathways in intercalated cells [12,23,29] and is driven by the lumen-negative transepithelial potential generated by the unilateral Na+ reabsorption to maintain electroneutrality (Figure 3). As in aldosterone signaling, it becomes increasingly evident that crosstalk between paracellular and transcellular transport occurs.

The importance of efficient Cl− reabsorption becomes obvious in claudin-deficient mouse models. For example, Cldn-7 deficiency in mice is lethal within 12 days after birth due to severe salt-wasting and subsequent chronic dehydration (see above) [27]. Cldn-$7^{-/-}$ mice show reduced ROMK and increased ENaC, Aqp2, and Na+ Cl− cotransporter mRNA. These changes in channel expressions are probably due to a compensatory mechanism to inhibit further urinary loss of salt and water [27].

It has long been established that accumulation of luminal Cl− depolarizes the membrane, and thereby, inhibits the apical Na+ channel ENaC [58]. Several studies also have demonstrated that pathological increases in Cl− reabsorption are associated with diseases, such as pseudo-hypoaldosteronism type II (PHA-II) or Gordon's syndrome.

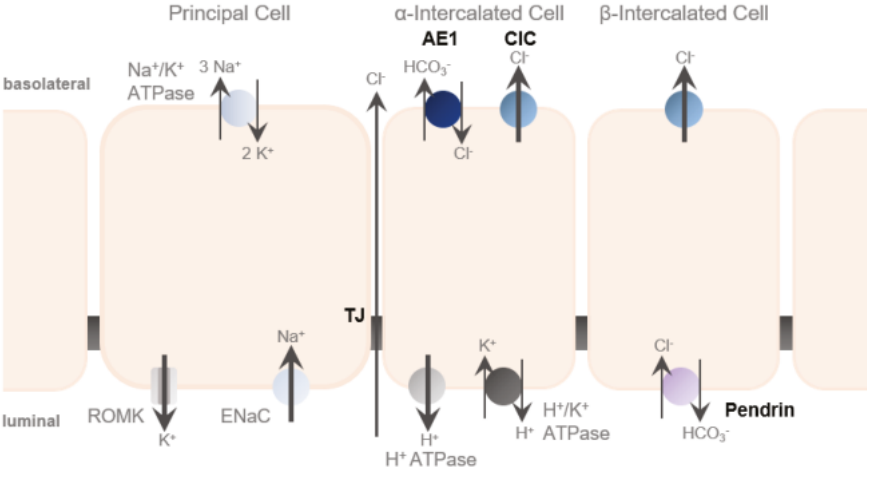

Figure 3. Chloride transport in the renal collecting duct. Chloride is transported via the paracellular route mediated by tight junctions (TJs), as well as, via the transcellular route using transporters and channels in α- and β-intercalated cells (depicted in bold).

PHA-II is a rare Mendelian syndrome leading to hypertension, hyperkalemia, and metabolic acidosis [59]. These symptoms are the exact opposite of the Cldn-4 and Cldn-8 knockout phenotypes in mice [23,29].

Interestingly, a long-known causative gene for PHA-II is WNK4 [60], and WNK4 can regulate Cl− conductance presumably by phosphorylation of Cldn-4 and Cldn-8 [50]. The PHA-II-causing mutation of WNK4 increases paracellular Cl− permeability in vitro [49,50]. Consistent with the proposed Cl− pore activity of Cldn-4 and Cldn-8, this is an additional indicator of an activating effect of claudin phosphorylation by WNK4. Furthermore, a recent study demonstrates that WNK4 is overexpressed in Cldn-7-deficient cultured, collecting duct cells [31]. Conversely, the PHA-II mutant of WNK4 is associated with increased Cldn-7 phosphorylation and enhanced paracellular Cl− conductivity [26]. This adds a new aspect and raises the possibility that claudins might act both up- and down-stream of WNK4 to regulate paracellular transport.

Another gene associated with PHA-II is KLHL3, encoding Kelch-like protein 3 [61,62]. Interestingly, KLHL3 normally induces ubiquitination and degradation of Cldn-8, while disease-associated mutations of KLHL3 abolish the interaction of KLHL3 with Cldn-8 [29]. In addition, KLHL3 leads to the ubiquitination of WNK4. In line with PHA-II symptoms, loss of KLHL3 increases Cl- permeability in vivo [29], which may contribute to the disease phenotype.

7. Conclusions

Collecting duct epithelia express claudins enforcing a high TER such as Cldn-3, -4, -7, -8, and -19, consistent with a demand for strong epithelial barrier function in the presence of steep transepithelial gradients. Based on our current knowledge, these claudins are thought to either support a tight barrier in general or to act as a cation barrier and/or an anion channel.

Consequently, the renal collecting duct is comprised of an especially tight epithelial barrier compared to other, more upstream segments of the nephron. As a result, the collecting duct lumen and interstitium are strictly separated. Nevertheless, the TJs of the collecting duct exhibit a regulated paracellular permeability for ions such as Cl-. Hence, the collecting duct TJ participates in a range of physiological functions:

It allows for controlled paracellular transport of Cl- to the interstitium, which is important in the setting of Na+ reabsorption via ENaC and secretion of K+ via ROMK.

It prevents paracellular diffusion and back flux of osmolytes into the urine and thus promotes the formation of steep gradients across the epithelium, which are necessary to drive electrolyte-free water reabsorption.

Future research will be needed to elucidate further the precise mechanisms that regulate TJ properties and that mediate crosstalk between paracellular and transcellular transport processes and how these processes relate to renal pathophysiology.

Author Contributions: Writing—original draft preparation: J.L., K.M.S.-O.; Writing—review and editing: J.L., K.M.S.-O. All authors have read and agreed to the published version of the manuscript.

Funding: This work was supported by the German Research Foundation (DFG) Research Training Group GRK 2318, by Collaborative Research Grant 1365, and by Research Unit FOR 2841. We acknowledge support from the German Research Foundation (DFG) and the Open Access Publication Fund of Charité-Universitätsmedizin Berlin.

Conflicts of Interest: The authors declare no conflict of interest.

Abbreviations

AQP	Aquaporin
AVP	Arginine vasopressin
Cap1	Channel-activating protease 1
Cldn	Claudin
Cl-	Chloride
ENaC	Epithelial sodium channel
Grhl2	Grainyhead-like 2
K+	Potassium
KLHL3	Kelch-like protein 3
MDCK	Madin-Darby Canine Kidney
mIMCD3	Mouse inner medullary collecting duct
Na+	Sodium
NCC	Na+ Cl− cotransporter
PHA-II	Pseudohypoaldosteronism type II (also known as Gordon's syndrome)
ROMK	Renal outer medullary potassium channel
TER	Transepithelial resistance
TJ	Tight junction
V2R	Vasopressin type 2 receptor
WNK4	With no lysine kinases 4

References

1. Powell, D.W. Barrier function of epithelia. *Am. J. Phys.* **1981**, *241*, G275–G288. [CrossRef] [PubMed]
2. Farquhar, M.G.; Palade, G.E. Junctional complexes in various epithelia. *J. Cell Biol.* **1963**, *17*, 375–412. [CrossRef] [PubMed]
3. Denker, B.M.; Sabath, E. The biology of epithelial cell tight junctions in the kidney. *J. Am. Soc. Nephrol.* **2011**, *22*, 622–625. [CrossRef] [PubMed]
4. Furuse, M.; Fujita, K.; Hiiragi, T.; Fujimoto, K.; Tsukita, S. Claudin-1 and -2: Novel integral membrane proteins localizing at tight junctions with no sequence similarity to occludin. *J. Cell Biol.* **1998**, *141*, 1539–1550. [CrossRef]
5. Colegio, O.R.; Van Itallie, C.M.; McCrea, H.J.; Rahner, C.; Anderson, J.M. Claudins create charge-selective channels in the paracellular pathway between epithelial cells. *Am. J. Physiol. Cell Physiol.* **2002**, *283*, C142–C147. [CrossRef]
6. Schneeberger, E.E.; Robert, D.L. The tight junction: A multifunctional complex. *Am. J. Physiol. Cell Physiol.* **2004**, *286*, C1213–C1228. [CrossRef]
7. Diamond, J.M. The epithelial junction: Bridge, gate, and fence. *Physiologist* **1977**, *20*, 10–18.
8. Yu, A.S. Claudins and the kidney. *J. Am. Soc. Nephrol.* **2015**, *26*, 11–19. [CrossRef]
9. Furuse, M.; Sasaki, H.; Tsukita, S. Manner of Interaction of Heterogeneous Claudin Species within and Between Tight Junction Strands. *J. Cell Biol.* **1999**, *147*, 891–903. [CrossRef]

10. Furuse, M.; Sasaki, H.; Fujimoto, K.; Tsukita, S. A Single Gene Product, Claudin-1 or -2, Reconstitutes Tight Junction Strands and Recruits Occludin in Fibroblasts. *J. Cell Biol.* **1998**, *143*, 391–401. [CrossRef]
11. Pearce, D.; Soundararajan, R.; Trimpert, C.; Kashlan, O.B.; Deen, P.M.T.; Kohan, D.E. Collecting duct principal cell transport processes and their regulation. *Clin. J. Am. Soc. Nephrol.* **2015**, *10*, 135–146. [CrossRef]
12. Rao, R.; Bhalla, V.; Pastor-Soler, N.M. Intercalated Cells of the Kidney Collecting Duct in Kidney Physiology. *Semin. Nephrol.* **2019**, *39*, 353–367. [CrossRef] [PubMed]
13. Wang, W.H.; Giebisch, G. Regulation of potassium (K) handling in the renal collecting duct. *Pflug. Arch.* **2009**, *458*, 157–168. [CrossRef] [PubMed]
14. Krause, G.; Winkler, L.; Mueller, S.L.; Haseloff, R.F.; Piontek, J.; Blasig, I.E. Structure and function of claudins. *Biochim. Biophys. Acta* **2008**, *1778*, 631–645. [CrossRef] [PubMed]
15. Simon, D.B.; Lu, Y.; Choate, K.A.; Velazquez, H.; Al-Sabban, E.; Praga, M.; Casari, G.; Bettinelli, A.; Colussi, G.; Rodriguez-Soriano, J.; et al. Paracellin-1, a Renal Tight Junction Protein Required for Paracellular Mg2+Resorption. *Science* **1999**, *285*, 103–106. [CrossRef] [PubMed]
16. Kiuchi-Saishin, Y.; Gotoh, S.; Furuse, M.; Takasuga, A.; Tano, Y.; Tsukita, S. Differential Expression Patterns of Claudins, Tight Junction Membrane Proteins, in Mouse Nephron Segments. *J. Am. Soc. Nephrol.* **2002**, *13*, 875–886. [PubMed]
17. Li, W.Y.; Huey, C.L.; Yu, A.S.L. Expression of claudin-7 and -8 along the mouse nephron. *Am. J. Physiol. Ren. Physiol.* **2004**, *286*, F1063–F1071. [CrossRef]
18. Ziemens, A.; Sonntag, S.R.; Wulfmeyer, V.C.; Edemir, B.; Bleich, M.; Himmerkus, N. Claudin 19 Is Regulated by Extracellular Osmolality in Rat Kidney Inner Medullary Collecting Duct Cells. *Int. J. Mol. Sci.* **2019**, *20*, 4401. [CrossRef]
19. Milatz, S.; Krug, S.M.; Rosenthal, R.; Gunzel, D.; Muller, D.; Schulzke, J.D.; Amasheh, S.; Fromm, M. Claudin-3 acts as a sealing component of the tight junction for ions of either charge and uncharged solutes. *Biochim. Biophys. Acta* **2010**, *1798*, 2048–2057. [CrossRef]
20. Coyne, C.B.; Gambling, T.M.; Boucher, R.C.; Carson, J.L.; Johnson, L.G. Role of claudin interactions in airway tight junctional permeability. *Am. J. Physiol. Lung Cell Mol. Physiol.* **2003**, *285*, L1166–L1178. [CrossRef]
21. Schröder, K. Generierung und Charakterisierung ei-nes Claudin-3-defizienten Mausmodells. *Humboldt-Universität zu Berlin, Mathematisch-Naturwissenschaftliche Fakultät I*. 2013. Available online: https://edoc.hu-berlin.de/handle/18452/17423 (accessed on 23 December 2019).
22. Hou, J.; Renigunta, A.; Yang, J.; Waldegger, S. Claudin-4 forms paracellular chloride channel in the kidney and requires claudin-8 for tight junction localization. *Proc. Natl. Acad. Sci. USA* **2010**, *107*, 18010–18015. [CrossRef] [PubMed]
23. Gong, Y.; Yu, M.; Yang, J.; Gonzales, E.; Perez, R.; Hou, M.; Tripathi, P.; Hering-Smith, K.S.; Hamm, L.L.; Hou, J. The Cap1-claudin-4 regulatory pathway is important for renal chloride reabsorption and blood pressure regulation. *Proc. Natl. Acad. Sci. USA* **2014**, *111*, E3766–E3774. [CrossRef] [PubMed]
24. Alexandre, M.D.; Lu, Q.; Chen, Y.H. Overexpression of claudin-7 decreases the paracellular Cl- conductance and increases the paracellular Na+ conductance in LLC-PK1 cells. *J. Cell Sci.* **2005**, *118*, 2683–2693. [CrossRef] [PubMed]
25. Hou, J.; Gomes, A.S.; Paul, D.L.; Goodenough, D.A. Study of claudin function by RNA interference. *J. Biol. Chem.* **2006**, *281*, 36117–36123. [CrossRef]
26. Tatum, R.; Zhang, Y.; Lu, Q.; Kim, K.; Jeansonne, B.G.; Chen, Y.H. WNK4 phosphorylates ser(206) of claudin-7 and promotes paracellular Cl(-) permeability. *FEBS Lett.* **2007**, *581*, 3887–3891. [CrossRef]
27. Tatum, R.; Zhang, Y.; Salleng, K.; Lu, Z.; Lin, J.J.; Lu, Q.; Jeansonne, B.G.; Ding, L.; Chen, Y.H. Renal salt wasting and chronic dehydration in claudin-7-deficient mice. *Am. J. Physiol. Ren. Physiol.* **2010**, *298*, F24–F34. [CrossRef]
28. Amasheh, S.; Milatz, S.; Krug, S.M.; Bergs, M.; Amasheh, M.; Schulzke, J.D.; Fromm, M. Na+ absorption defends from paracellular back-leakage by claudin-8 upregulation. *Biochem. Biophys. Res. Commun.* **2009**, *378*, 45–50. [CrossRef]
29. Gong, Y.; Wang, J.; Yang, J.; Gonzales, E.; Perez, R.; Hou, J. KLHL3 regulates paracellular chloride transport in the kidney by ubiquitination of claudin-8. *Proc. Natl. Acad. Sci. USA* **2015**, *112*, 4340–4345. [CrossRef]
30. Haddad, N.; El Andalousi, J.; Khairallah, H.; Yu, M.; Ryan, A.K.; Gupta, I.R. The tight junction protein claudin-3 shows conserved expression in the nephric duct and ureteric bud and promotes tubulogenesis in vitro. *Am. J. Physiol. Ren. Physiol.* **2011**, *301*, F1057–F1065. [CrossRef]

31. Fan, J.; Tatum, R.; Hoggard, J.; Chen, Y.H. Claudin-7 Modulates Cl(-) and Na(+) Homeostasis and WNK4 Expression in Renal Collecting Duct Cells. *Int. J. Mol. Sci.* **2019**, *20*, 3798. [CrossRef]
32. Alexandre, M.D.; Jeansonne, B.G.; Renegar, R.H.; Tatum, R.; Chen, Y.H. The first extracellular domain of claudin-7 affects paracellular Cl- permeability. *Biochem. Biophys. Res. Commun.* **2007**, *357*, 87–91. [CrossRef] [PubMed]
33. Van Itallie, C.; Rahner, C.; Anderson, J.M. Regulated expression of claudin-4 decreases paracellular conductance through a selective decrease in sodium permeability. *J. Clin. Investig.* **2001**, *107*, 1319–1327. [CrossRef] [PubMed]
34. Van Itallie, C.M.; Fanning, A.S.; Anderson, J.M. Reversal of charge selectivity in cation or anion-selective epithelial lines by expression of different claudins. *Am. J. Physiol. Ren. Physiol.* **2003**, *285*, F1078–F1084. [CrossRef] [PubMed]
35. Yu, A.S.; Enck, A.H.; Lencer, W.I.; Schneeberger, E.E. Claudin-8 expression in Madin-Darby canine kidney cells augments the paracellular barrier to cation permeation. *J. Biol. Chem.* **2003**, *278*, 17350–17359. [CrossRef]
36. Konrad, M.; Schaller, A.; Seelow, D.; Pandey, A.V.; Waldegger, S.; Lesslauer, A.; Vitzthum, H.; Suzuki, Y.; Luk, J.M.; Becker, C.; et al. Mutations in the Tight-Junction Gene Claudin 19 (CLDN19) Are Associated with Renal Magnesium Wasting, Renal Failure, and Severe Ocular Involvement. *Am. J. Hum. Genet.* **2006**, *79*, 949–957. [CrossRef]
37. Angelow, S.; El-Husseini, R.; Kanzawa, S.A.; Yu, A.S. Renal localization and function of the tight junction protein, claudin-19. *Am. J. Physiol. Ren. Physiol.* **2007**, *293*, F166–F177. [CrossRef]
38. Hou, J.; Renigunta, A.; Konrad, M.; Gomes, A.S.; Schneeberger, E.E.; Paul, D.L.; Waldegger, S.; Goodenough, D.A. Claudin-16 and claudin-19 interact and form a cation-selective tight junction complex. *J. Clin. Investig.* **2008**, *118*, 619–628. [CrossRef]
39. Rosenthal, R.; Milatz, S.; Krug, S.M.; Oelrich, B.; Schulzke, J.D.; Amasheh, S.; Gunzel, D.; Fromm, M. Claudin-2, a component of the tight junction, forms a paracellular water channel. *J. Cell Sci.* **2010**, *123*, 1913–1921. [CrossRef]
40. Knepper, M.A.; Kwon, T.H.; Nielsen, S. Molecular physiology of water balance. *N. Engl. J. Med.* **2015**, *372*, 1349–1358. [CrossRef]
41. Ranieri, M.; Di Mise, A.; Tamma, G.; Valenti, G. Vasopressin-aquaporin-2 pathway: Recent advances in understanding water balance disorders. *F1000Res* **2019**, *8*, F1000. [CrossRef]
42. Loonen, A.J.M.; Knoers, N.V.A.M.; van Os, C.H.; Deen, P.M.T. Aquaporin 2 Mutations in Nephrogenic Diabetes Insipidus. *Semin. Nephrol.* **2008**, *28*, 252–265. [CrossRef] [PubMed]
43. Hinze, C.; Ruffert, J.; Walentin, K.; Himmerkus, N.; Nikpey, E.; Tenstad, O.; Wiig, H.; Mutig, K.; Yurtdas, Z.Y.; Klein, J.D.; et al. GRHL2 Is Required for Collecting Duct Epithelial Barrier Function and Renal Osmoregulation. *J. Am. Soc. Nephrol.* **2018**, *29*, 857–868. [CrossRef] [PubMed]
44. Aue, A.; Hinze, C.; Walentin, K.; Ruffert, J.; Yurtdas, Y.; Werth, M.; Chen, W.; Rabien, A.; Kilic, E.; Schulzke, J.D.; et al. A Grainyhead-Like 2/Ovo-Like 2 Pathway Regulates Renal Epithelial Barrier Function and Lumen Expansion. *J. Am. Soc. Nephrol.* **2015**, *26*, 2704–2715. [CrossRef] [PubMed]
45. Sansom, S.C.; Weinman, E.J.; O'Neil, R.G. Microelectrode assessment of chloride-conductive properties of cortical collecting duct. *Am. J. Physiol. Cell Physiol.* **1984**, *274*, F291–F302. [CrossRef] [PubMed]
46. Fine, D.; Meiselas, L.E.; Auerbach, T. The effect of acute hypovolemia on the release of "aldosterone" and on the renal excretion of sodium. *J. Clin. Investig.* **1958**, *37*, 232–243. [CrossRef] [PubMed]
47. Narikiyo, T.; Kitamura, K.; Adachi, M.; Miyoshi, T.; Iwashita, K.; Shiraishi, N.; Nonoguchi, H.; Chen, L.-M.; Chai, K.X.; Chao, J.; et al. Regulation of prostasin by aldosterone in the kidney. *J. Clin. Investig.* **2002**, *109*, 401–408. [CrossRef]
48. Vallet, V.; Chraibi, A.; Gaeggeler, H.-P.; Horisberger, J.-D.; Rossier, B.C. An epithelial serine protease activates the amiloride-sensitive sodium channel. *Nature* **1997**, *389*, 607–610. [CrossRef]
49. Yamauchi, K.; Rai, T.K.K.; Sohara, E.; Suzuki, T.; Itoh, T.; Suda, S.; Hayama, A.; Sasaki, S.; Uchida, S. Disease-causing mutant WNK4 increases paracellular chloride permeability and phosphorylates claudins. *Proc. Natl. Acad. Sci. USA* **2004**, *101*, 4690–4694. [CrossRef]
50. Kahle, K.T.; MacGregor, G.G.; Wilson, F.H.; Van Hoek, A.N.; Brown, D.; Ardito, T.; Kashgarian, M.; Giebisch, G.; Hebert, S.C.; Boulpaep, E.L.; et al. Paracellular Cl- permeability is regulated by WNK4 kinase: Insight into normal physiology and hypertension. *Proc. Natl. Acad. Sci. USA* **2004**, *101*, 14877–14882. [CrossRef]

51. Le Moellic, C.; Boulkroun, S.; Gonzalez-Nunez, D.; Dublineau, I.; Cluzeaud, F.; Fay, M.; Blot-Chabaud, M.; Farman, N. Aldosterone and tight junctions: Modulation of claudin-4 phosphorylation in renal collecting duct cells. *Am. J. Physiol. Cell Physiol.* **2005**, *289*, C1513–C1521. [CrossRef]
52. Ring, A.M.; Cheng, S.X.; Leng, Q.; Kahle, K.T.; Rinehart, J.; Lalioti, M.D.; Volkman, H.M.; Wilson, F.H.; Hebert, S.C.; Lifton, R.P. WNK4 regulates activity of the epithelial Na+ channel in vitro and in vivo. *Proc. Natl. Acad. Sci. USA* **2007**, *104*, 4020–4024. [CrossRef]
53. Kahle, K.T.; Wilson, F.H.; Leng, Q.; Lalioti, M.D.; O'Connell, A.D.; Dong, K.; Rapson, A.K.; MacGregor, G.G.; Giebisch, G.; Hebert, S.C.; et al. WNK4 regulates the balance between renal NaCl reabsorption and K+ secretion. *Nat. Genet.* **2003**, *35*, 372–376. [CrossRef]
54. Siragy, H.M.; Awad, A.; Abadir, P.; Webb, R. The angiotensin II type 1 receptor mediates renal interstitial content of tumor necrosis factor-alpha in diabetic rats. *Endocrinology* **2003**, *144*, 2229–2233. [CrossRef]
55. Hollenberg, N.K.; Stevanovic, R.; Agarwal, A.; Lansang, M.C.; Price, D.A.; Laffel, L.M.; Williams, G.H.; Fisher, N.D. Plasma aldosterone concentration in the patient with diabetes mellitus. *Kidney Int.* **2004**, *65*, 1435–1439. [CrossRef]
56. Molina-Jijon, E.; Rodriguez-Munoz, R.; Namorado Mdel, C.; Pedraza-Chaverri, J.; Reyes, J.L. Oxidative stress induces claudin-2 nitration in experimental type 1 diabetic nephropathy. *Free Radic. Biol. Med.* **2014**, *72*, 162–175. [CrossRef]
57. Molina-Jijon, E.; Rodriguez-Munoz, R.; Gonzalez-Ramirez, R.; Namorado-Tonix, C.; Pedraza-Chaverri, J.; Reyes, J.L. Aldosterone signaling regulates the over-expression of claudin-4 and -8 at the distal nephron from type 1 diabetic rats. *PLoS ONE* **2017**, *12*, e0177362. [CrossRef]
58. Canessa, C.M.; Schild, L.; Buell, G.; Thorens, B.; Gautschi, I.; Horisberger, J.-D.; Rossier, B.C. Amiloride-sensitive epithelial Na+ channel is made of three homologous subunits. *Nature* **1994**, *367*, 463–467. [CrossRef]
59. Gordon, R.D. Syndrome of hypertension and hyperkalemia with normal glomerular filtration rate. *Hypertension* **1986**, *8*, 93–102. [CrossRef]
60. Wilson, F.H.; Disse-Nicodeme, S.; Choate, K.A.; Ishikawa, K.; Nelson-Williams, C.; Desitter, I.; Gunel, M.; Milford, D.V.; Lipkin, G.W.; Achard, J.-M.; et al. Human hypertension caused by mutations in WNK kinase. *Science* **2001**, *293*, 1107–1112. [CrossRef]
61. Boyden, L.M.; Choi, M.; Choate, K.A.; Nelson-Williams, C.J.; Farhi, A.; Toka, H.R.; Tikhonova, I.R.; Bjornson, R.; Mane, S.M.; Colussi, G.; et al. Mutations in kelch-like 3 and cullin 3 cause hypertension and electrolyte abnormalities. *Nature* **2012**, *482*, 98–102. [CrossRef]
62. Louis-Dit-Picard, H.; Barc, J.; Trujillano, D.; Miserey-Lenkei, S.; Bouatia-Naji, N.; Pylypenko, O.; Beaurain, G.; Bonnefond, A.; Sand, O.; Simian, C.; et al. KLHL3 mutations cause familial hyperkalemic hypertension by impairing ion transport in the distal nephron. *Nat. Genet.* **2012**, *44* (Suppl. S1–S3), 456–460. [CrossRef]

International Journal of
Molecular Sciences

MDPI

Article

Claudin-7 Modulates Cl^- and Na^+ Homeostasis and WNK4 Expression in Renal Collecting Duct Cells

Junming Fan [1,2], Rodney Tatum [1], John Hoggard [1] and Yan-Hua Chen [1,3,*]

[1] Department of Anatomy and Cell Biology, Brody School of Medicine, East Carolina University, Greenville, NC 27834, USA
[2] Institute of Hypoxia Medicine, School of Basic Medical Sciences, Wenzhou Medical University, Wenzhou 325035, China
[3] East Carolina Diabetes and Obesity Institute, East Carolina University, Greenville, NC 27834, USA
* Correspondence: cheny@ecu.edu; Tel.: +1-252-744-1341; Fax: +1-252-744-2850

Received: 11 July 2019; Accepted: 30 July 2019; Published: 3 August 2019

Abstract: Claudin-7 knockout ($CLDN7^{-/-}$) mice display renal salt wasting and dehydration phenotypes. To address the role of CLDN7 in kidneys, we established collecting duct (CD) cell lines from $CLDN7^{+/+}$ and $CLDN7^{-/-}$ mouse kidneys. We found that deletion of CLDN7 increased the transepithelial resistance (TER) and decreased the paracellular permeability for Cl^- and Na^+ in $CLDN7^{-/-}$ CD cells. Inhibition of transcellular Cl^- and Na^+ channels has no significant effect on TER or dilution potentials. Current-voltage curves were linear in both $CLDN7^{+/+}$ and $CLDN7^{-/-}$ CD cells, indicating that the ion flux was through the paracellular pathway. The impairment of Cl^- and Na^+ permeability phenotype can be rescued by CLDN7 re-expression. We also found that WNK4 (its mutations lead to hypertension) expression, but not WNK1, was significantly increased in $CLDN7^{-/-}$ CD cell lines as well as in primary $CLDN7^{-/-}$ CD cells, suggesting that the expression of WNK4 was modulated by CLDN7. In addition, deletion of CLDN7 upregulated the expression level of the apical epithelial sodium channel (ENaC), indicating a potential cross-talk between paracellular and transcellular transport systems. This study demonstrates that CLDN7 plays an important role in salt balance in renal CD cells and modulating WNK4 and ENaC expression levels that are vital in controlling salt-sensitive hypertension.

Keywords: Claudin-7; tight junctions; permeability; WNK4; epithelial sodium channel (ENaC), collecting duct cells

1. Introduction

Maintaining electrolytes and body fluids across epithelial layers in kidneys within the physiological range is of vital importance for blood pressure regulation. Chloride (Cl^-) and sodium (Na^+), two predominant extracellular ionic components in kidneys, determine the extracellular electrolyte balance and regulate the blood pressure in the segment of the collecting duct (CD) [1]. It is well known that sodium reabsorption in the CD is an active process through the apical epithelial sodium channel (ENaC) and is driven by the basolateral Na^+-K^+-ATPase. On the other hand, chloride reabsorption is driven by the lumen-negative transepithelial potential and mainly occurs through tight junctions (TJs), the gatekeeper of the paracellular pathway in CD [1–3].

TJ is a multi-molecular complex and plays an essential role in regulating ions and small molecules passing through the apical to basal compartment of the epithelial cells [4,5]. Claudins (CLDN), a family of transmembrane proteins with at least 24 members in mouse and human, are the most important structural and functional components of the TJs and the principal regulators in defining the properties of paracellular ion permeability of the epithelial cells [6,7]. There are more than ten CLDN members expressed in kidneys, and they are closely associated with their corresponding

segment-specific ion reabsorption characters [6,8]. Deficiency or aberrant expression of distinct CLDNs has been reported to be associated with disturbance of electrolytes, which can lead to high blood pressure or hypertension-related diseases. For example, mutations in CLDN16 and CLDN19 in humans resulted in kidney disorders exhibiting renal magnesium wasting and hypercalciuria [9,10]. Mice with CLDN16 knockdown exhibit defects in paracellular cation selectivity and develop severe renal wasting of magnesium and calcium [11]. A study by Muto et al. [12] demonstrated that CLDN2-deficient mice show a significant decrease in net transepithelial reabsorption of Na^+ and Cl^- in proximal tubules, causing a loss of Na^+ selectivity and therefore relative Cl^- selectivity in the proximal tubule paracellular pathway. Results from Krug et al. [13] reported that Madin-Darby Canine Kidney (MDCK) C7 cells with CLDN17 overexpression show an increase in paracellular anion permeability and switch from cation-selective to anion-selective. Knockdown of CLDN17 in LLC-PK1 cells support CLDN17 as an anion channel. In addition, mice with CLDN10 deletion in the thick ascending limb show the impairment in paracellular Na^+ permeability and hypermagnesemia [14], and can rescue CLDN16-deficient mice from hypomagnesemia and hypercalciuria [15].

Pseudohypoaldosteronism type II (PHAII) is an autosomal-dominant hereditary hypertensive disease that is characterized by hyperkalemia and metabolic acidosis [16,17]. In 2001, Wilson et al. [18] found that the mutations in WNK4, a serine/threonine kinase with No K (lysine), were linked to the pathogenesis of PHAII. Since then, many studies have shown that several membrane channels and transporters are the molecular targets of WNK4 [16,19–24]. Since WNK4 is localized at the TJs of distal nephrons, TJ proteins could also serve as additional targets for WNK4. Indeed, two groups have reported that WNK4 regulates the paracellular Cl^- permeability in MDCK II cells [25,26], and the latest study documented by Chen et al. showed that mice with knockin Cl^--insensitive mutant WNK4 displayed hypertension, hyperkalemia, hyperactive NCC, and the authors concluded that WNK4 is a physiological intracellular Cl^- sensor [24]. Our previous study also showed that claudin-7 is the substrate of WNK4 and can be phosphorylated by WNK4 at serine^{206} in its COOH-terminus [27].

Although it is well characterized how transcellular channels and transports work in regulating Cl^- and Na^+ transport in the CD of the kidney [12,14], the molecular targets of the paracellular pathway responsible for Cl^- and Na^+ transport have not been fully elucidated. It has been reported that CLDN4 served as a Cl^- channel in mouse kidney CD cells that require the presence of CLDN8 [28]. We have previously reported that the first extracellular domain of CLDN7 affects paracellular Cl^- permeability [29]. In addition, overexpression of CLDN7 in LLC-PK1 cells decreased the paracellular Cl^- conductance and increased Na^+ conductance [30].

To study the role of CLDN7 in vivo, we generated a CLDN7 knockout (CLDN7$^{-/-}$) mouse model and discovered that CLDN7-deficient mice exhibited renal salt wasting, chronic dehydration, and severe intestinal defects, and that 90% of the pups died within 10 days after birth [31]. The kidney phenotypes suggest that CLDN7 plays an indispensable role in keeping salt homeostasis in distal nephrons. However, the functional role of CLDN7 in the distal nephron remains unclear. In this study, we isolated and purified CD cells from CLDN7$^{+/+}$ and CLDN7$^{-/-}$ mouse kidneys using Dolichos biflorus lectin-coated Dynabeads, and immortalized these cells into cell lines by Lenti-SV40 virus infection. These CD cells express AQP2, CLDN3, and CLDN4, but not CLDN2, a proximal tubule marker. We found that transepithelial resistance (TER) was significantly increased and paracellular Cl^- and Na^+ permeability was decreased in CLDN7$^{-/-}$ CD cells. These phenotypes can be rescued by the transfection of CLDN7 into CLDN7$^{-/-}$ CD cells. In addition, we found in this study that WNK4 expression, but not WNK1, was significantly increased, and so was the ENaC level in CLDN7$^{-/-}$ CD cells. These results suggest the potential influence of the paracellular pathway on transcellular pathway. Defects in the paracellular ion transport may affect transcellular transport systems, leading to the ionic imbalance in kidneys.

2. Results

2.1. Generation of CD Cell Lines Isolated from CLDN7$^{+/+}$ and CLDN7$^{-/-}$ Mouse Kidneys

To study the role of claudin-7 in CDs, we generated CD cell lines isolated and purified from CLDN7$^{+/+}$ and CLDN7$^{-/-}$ mouse kidneys using Dolichos biflorus lectin-coated Dynabeads, and then immortalized these cells into multiple cell lines by Lenti-SV40 virus infection. The immortalized CLDN7$^{+/+}$ and CLDN7$^{-/-}$ CD cells have an epithelial morphology as shown in Figure 1A. CLDN7$^{+/+}$ CD cells have a strong CLDN7 immunostaining signal localized at cell–cell contact area, while CLDN7 signal was absent in CLDN7$^{-/-}$ CD cells as expected (Figure 1B, top panel). CLDN3, CLDN4, and AQP2 were known to be expressed in CD cells, and their presences were confirmed by both immunofluorescence microscopy and western blot analysis (Figure 1B,C). It was observed that AQP2 signal was quite weak at the cell membrane in CLDN7$^{-/-}$ CD cells (Figure 1B); however, the protein expression level was similar between CLDN7$^{+/+}$ and CLDN7$^{-/-}$ CD cells (Figure 1C). CLDN8 signal was undetectable in both CLDN7$^{+/+}$ and CLDN7$^{-/-}$ CD cells (data unpublished).

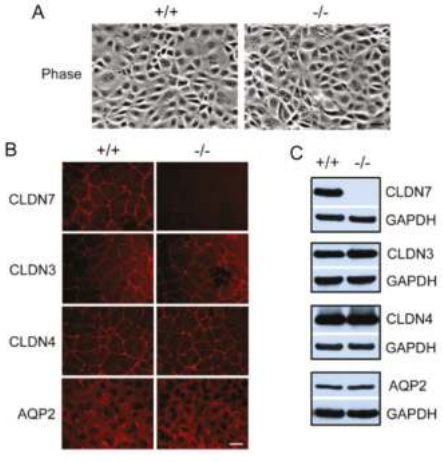

Figure 1. Characterization of immortalized mouse collecting duct (CD) cell lines. (**A**) Phase images of CLDN7$^{+/+}$ (+/+) and CLDN7$^{-/-}$ (–/–) CD cells. CD cells from 4-day old mouse CLDN7$^{+/+}$ and CLDN7$^{-/-}$ kidneys were isolated and purified by Dolichos biflorus lectin-coated Dynabeads. These purified CD cells were immortalized into cell lines using SV40 virus. The stable CD cells were grown on coverslips for 5–7 days before fixation for fluorescent light microcopy. Bar: 30 μm. (**B**) CLDN7$^{+/+}$ and CLDN7$^{-/-}$ CD cells were immunostained with antibodies against CLDN7, CLDN3, CLDN4, and AQP2 and detected by Cy3-conjugated anti-rabbit secondary antibody. CLDN7$^{+/+}$ CD cells showed a strong anti-CLDN7 immunostaining and this signal was completely absent in CLDN7$^{-/-}$ CD cells. Both CLDN3 and CLDN4 have similar staining patterns in CLDN7$^{+/+}$ and CLDN7$^{-/-}$ CD cells. AQP2 is a marker protein for CD principle cells and its membrane staining was much weaker in CLDN7$^{-/-}$ than in CLDN7$^{+/+}$ CD cells. Bar: 20 μm. (**C**) Western blot analysis confirmed the absence of CLDN7 protein in CLDN7$^{-/-}$ CD cells. CLDN3, CLDN4, and AQP2 expression levels were similar between CLDN7$^{+/+}$ and CLDN7$^{-/-}$ CD cells. GAPDH signal was used as a loading control.

2.2. Decreased Paracellular Cl^- and Na^+ Permeability in CLDN7$^{-/-}$ CD Cells

To examine CLDN7-based CD cell electrophysiology, we first measured the TER of CLDN7$^{+/+}$ and CLDN7$^{-/-}$ CD cells. The TER of CLDN7$^{+/+}$ CD cells has an average value of 510 ± 43 Ω.cm^2. Deletion of CLDN7 dramatically increased TER to 1115 ± 96 Ω.cm^2 (Figure 2A), suggesting an increase in barrier function induced by CLDN7 absence in CD cells.

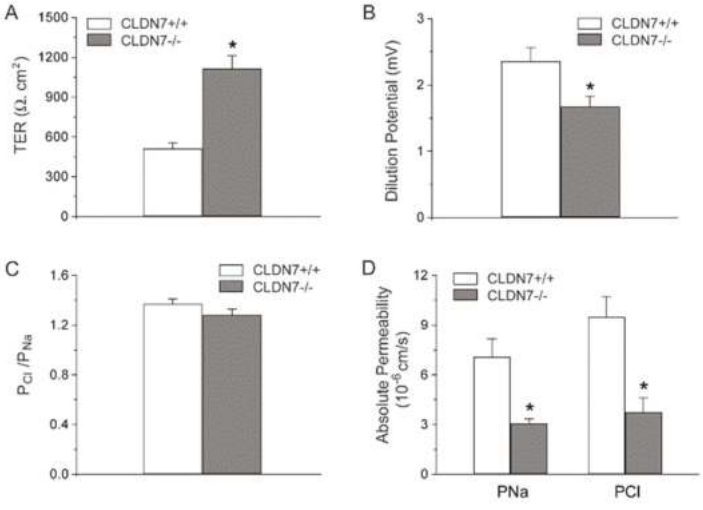

Figure 2. Deletion of CLDN7 increased transepithelial resistance (TER) and decreased paracellular Cl^- and Na^+ permeability on CD cell monolayers. (**A**) TER was measured on monolayers cultured for 7 days. (**B**) CD cells were grown on collagen-coated Snapwell filters for 7 days to reach the full confluence. The filter rings containing cell monolayers were mounted into EasyMount chambers. Both apical and basal chambers were filled with buffer containing 140 mM NaCl. Subsequently, buffer in the basal chamber was replaced by 70 mM NaCl, and dilution potentials were measured. (**C**) The ratio of the absolute permeability of Cl^- to Na^+ (P_{Cl}/P_{Na}) was calculated using the Goldman–Hodgkin–Katz equation. The ratio of P_{Cl}/P_{Na} was >1 in $CLDN7^{+/+}$, indicating that these CD cells were more permeable to Cl^- than Na^+. (**D**) The absolute permeability for P_{Cl} and P_{Na} was calculated according to the method of simplified Kimizuka and Koketsu equations. * $p < 0.05$. $n = 3$.

To further examine the ion permeability in our established CD cell lines, we performed dilution potential experiments. Our data showed that dilution potentials measured from $CLDN7^{-/-}$ CD cells were significantly reduced compared to those of $CLDN7^{+/+}$ CD cells (Figure 2B). However, the ratio of absolute permeability of Cl^- (P_{Cl}) to Na^+ (P_{Na}) was slightly decreased for $CLDN7^{-/-}$ CD cells, but without statistical significance (Figure 2C). Deletion of CLDN7 in CD cells depressed the permeation of Cl^- and Na^+ as indicated by their reduced absolute permeability values of Cl^- (P_{Cl}) and Na^+ (P_{Na}) (Figure 2D). Inhibition of epithelial Na^+ and Cl^- channels had no significant effect on TER or dilution potentials either in $CLDN7^{+/+}$ or $CLDN7^{-/-}$ CD cells, indicating that the impairment of Cl^- and Na^+ permeability in $CLDN7^{-/-}$ CD cells is through the paracellular pathway (data unpublished). Moreover, current–voltage curves were linear in both $CLDN7^{+/+}$ and $CLDN7^{-/-}$ CD cells, consistent with the conductance being attributable to the paracellular pathway for ion flux (data unpublished). Our results indicate that CLDN7 plays a vital role in NaCl reabsorption in mouse CD cells. Deletion of CLDN7 decreases paracellular permeability to Cl^- and Na^+, suggesting CLDN7 may serve as a non-selective paracellular channel in CD cells.

2.3. Increased Expression Levels of WNK4 and ENaC in $CLDN7^{-/-}$ CD Cells

We reported previously that CLDN7 was colocalized with WNK4 in kidneys and that they formed a protein complex when co-expressed in kidney epithelial cells [27]. To investigate whether CLDN7 deletion affects the expression of WNK4 and other kinases and ion channels, we performed real-time RT-PCR experiments. We found that deletion of CLDN7 significantly increased WNK4, SGK-1, and ENaC-α mRNA levels, while there were no significant changes in ROMK and AQP2 mRNA levels (Figure 3A).

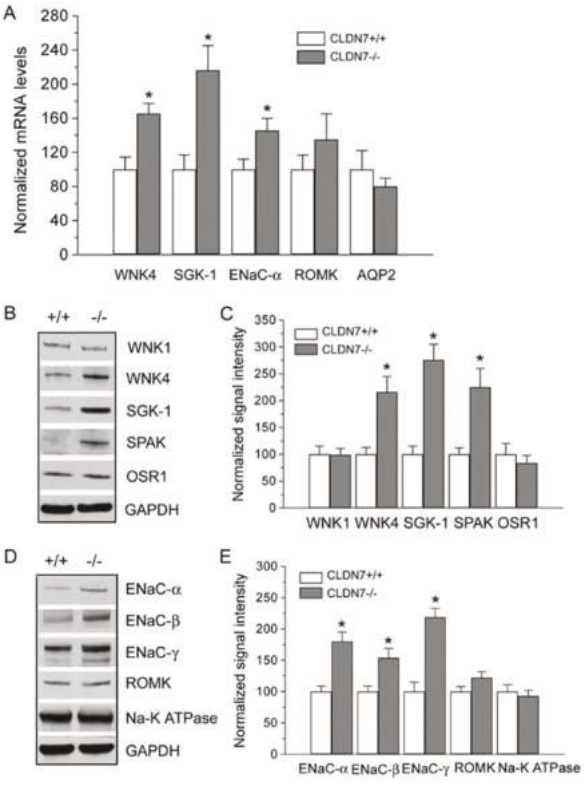

Figure 3. Deletion of CLDN7 had a significant effect on gene and protein expression levels of WNK4, SGK-1, and ENaC. (**A**) Real-time RT-PCR analysis of WNK4, SGK-1, ENaC-α, ROMK, and AQP2 mRNA levels in CLDN7$^{+/+}$ and CLDN7$^{-/-}$ CD cells. Each measurement was normalized to its β-actin level. * $p < 0.05$. $n = 3$. (**B**) Western blotting analysis of several protein kinase levels in CD cells. CLDN7$^{+/+}$ and CLDN7$^{-/-}$ CD cells were lysed in RIPA (radio-immunoprecipitation assay) buffer and a total of 30 μg protein for each lane was loaded onto the SDS NuPAGE gel. Membranes were blotted against WNK1, WNK4, SGK-1, SPARK, and OSR1. GAPDH (glyceraldehyde 3-phosphate dehydrogenase) staining was used as a loading control. (**C**) Densitometry analysis of protein expression levels shown on (**B**). Each band intensity for CLDN7$^{+/+}$ CD cells was normalized and set as a reference. * $p < 0.05$. $n = 3$. (**D**) Western blotting analysis of several ion channel levels in CD cells. Equal amounts of CLDN7$^{+/+}$ and CLDN7$^{-/-}$ CD cell lysates were loaded onto the SDS NuPAGE gel and the membranes were probed against ENaC-α, -β, -γ, ROMK, and Na^+-K^+-ATPase. (**E**) Densitometry analysis of protein expression levels shown on (**D**). Each band intensity for CLDN7$^{+/+}$ CD cells was normalized and set as a reference. * $p < 0.05$. $n = 3$.

Immunoblotting analysis also showed that the protein expression levels of WNK4, SGK-1, and SPAK were all clearly increased, but WNK1 and OSR1 levels were unchanged in CLDN7$^{-/-}$ CD cells compared to those in CLDN7$^{+/+}$ CD cells (Figure 3B,C). Interestingly, we found that the expression levels of ENaC-α, -β and –γ were all elevated with no changes in ROMK and Na-K-ATPase in CLDN7$^{-/-}$ CD cells (Figure 3D,E). We have confirmed these results in the primary CLDN7$^{+/+}$ and CLDN7$^{-/-}$ CD cells as shown in Figure 4. The phase images of primary CD cells isolated from CLDN7$^{+/+}$ and CLDN7$^{-/-}$ kidneys were shown in Figure 4A (top panel). Anti-CLDN4 and anti-AQP2 antibodies were used to stain CD cells (Figure 4A). After CD cells were removed, the remaining cells were immunostained with CLDN4 and found to be CLDN4-negative (Figure 4A, bottom panel).

Consistent with the immortalized CLDN7$^{-/-}$ CD cells, CLDN7 deletion clearly increased WNK4, SGK-1, and ENaC subunit's expression levels with no significant effects on WNK1, ROMK, or AQP2 expression levels in primary CLDN7$^{-/-}$ CD cells (Figure 4B,C).

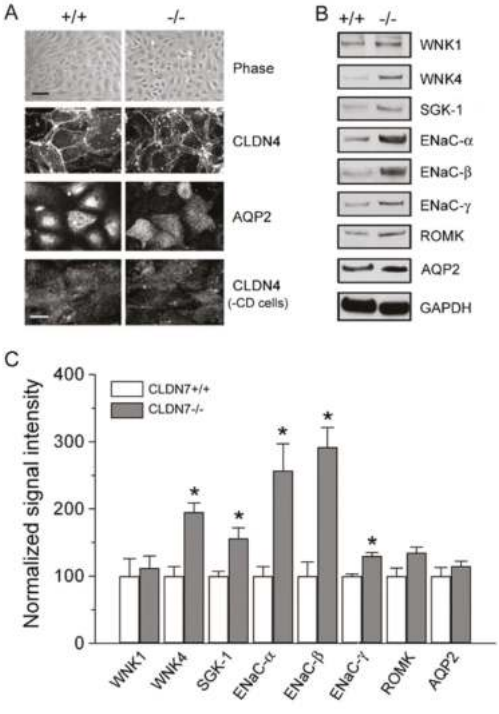

Figure 4. Deletion of CLDN7 had a significant effect on protein expression levels of representative kinases and ion channel on primary CD cells. (**A**) The establishment of primary cultures of CD cells isolated from kidneys of CLDN7$^{+/+}$ and CLDN7$^{-/-}$ pups. The top panel shows the phase images of primary CD cells isolated from kidneys of 5-day old CLDN7$^{+/+}$ and CLDN7$^{-/-}$ pups after cultured in 12-well plates for a week to form a complete monolayer. Bar: 40 μm. The cultured primary CLDN7$^{+/+}$ and CLDN7$^{-/-}$ CD cells were immunostained with anti-CLDN4 and anti-AQP2 antibodies. The last panel shows the remaining cells immunostained with anti-CLDN4 antibody after removal of CD cells. Bar: 15 μm. (**B**) The primary CD cells were lysed in RIPA buffer and a total of 30 μg protein for each lane was loaded onto the SDS NuPAGE gel. Membranes were blotted against WNK1, WNK4, SGK-1, ENaC-α, -β, and -γ, ROMK, and AQP2. GAPDH was used as a loading control. (**C**) Densitometry analysis of protein expression levels shown on (**B**). Each band intensity for CLDN7$^{+/+}$ CD cells was normalized and set as a reference. * $p < 0.05$. $n = 4$.

2.4. Rescued Function of Ion Permeability in Immortalized CLDN7$^{+/+}$ CD Cells with CLDN7 Knockdown

As we observed an increase in barrier function and a decrease in Cl^- and Na^+ permeability in CLDN7$^{-/-}$ CD cells, we tried to stably transfect CLDN7 back ('rescue') into CLDN7$^{-/-}$ CD cells to study whether CLDN7 could revert the phenotype. However, we were unable to obtain the stable cell lines after many attempts. Therefore, herein we designed specific shRNAs to knock down the expression of CLDN7 in CLDN7$^{+/+}$ CD (KD) cells and then transfected CLDN7 back into these KD cells. Immunofluorescent staining and western blot analysis confirmed the knockdown of the expression of CLDN7 in CLDN7$^{+/+}$ CD cells by CLDN7 shRNA (Figure 5A–C). Similarly as in CLDN7$^{-/-}$ CD cells, CLDN7 KD induced an increase in WNK4 and SGK-1 expression while AQP2, CLDN3, and CLDN4

expressions were unchanged (Figure 5B,C). In addition, we found that CLDN7 KD also significantly increased the TER value by 61.2% compared with the scrambled controls (Figure 5D). Moreover, CLDN7 KD decreased dilution potential (DP) (Figure 5E) and Cl^- and Na^+ permeability (Figure 5G) as we found in CLDN7$^{-/-}$ CD cells without a significant change in PCl/PNa (Figure 5F).

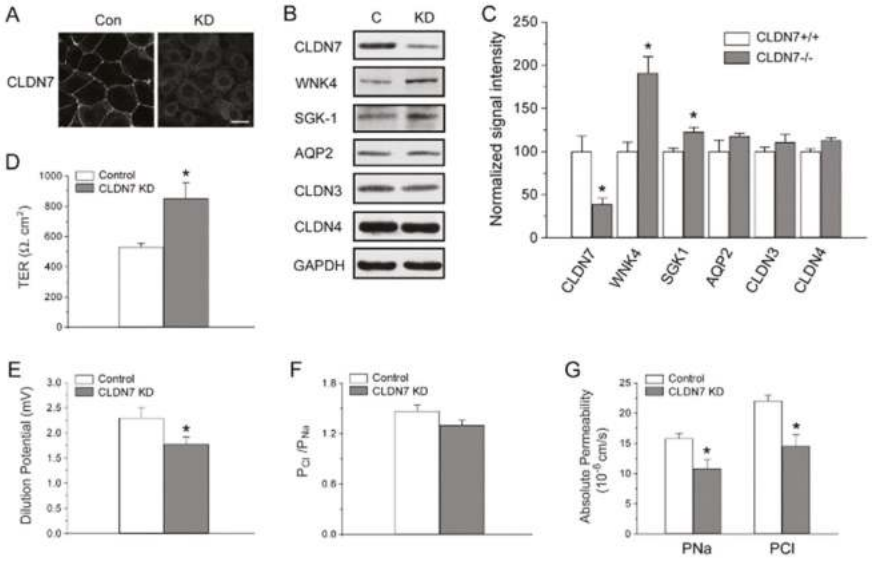

Figure 5. Knockdown of CLDN7 in CLDN7$^{+/+}$ CD cells decreased paracellular Cl^- and Na^+ permeability. (**A**) CLDN7$^{+/+}$ CD cells were transfected with either control (Con) or CLDN7 shRNA (KD) vector. The indirect immunofluorecent method shows the reduced immunostaining signal of CLDN7 in KD cells compared to that of control cells. (**B**) The control and knockdown (KD) cell lysates were subject to western blot analysis. Membranes were probed against CLDN7, WNK4, SGK-1, AQP2, CLDN3, and CLDN4. GAPDH was used as a loading control. (**C**) Densitometry analysis of protein expression levels shown on (**B**). Each band intensity for CLDN7$^{+/+}$ CD cells was normalized and set as a reference. * $p < 0.05$. $n = 3$. (**D**) The control and KD CD cells were cultured in Transwell plates coated with collagen. TER was measured on monolayers cultured for 7 days. (**E**) The control and KD CD cells were grown on collagen-coated Snapwell filters for 7 days. The dilution potentials were measured as described in Figure 2B. (**F**) The ratio of the absolute permeability of Cl^- to Na^+ (P_{Cl}/P_{Na}) was calculated using the Goldman–Hodgkin–Katz equation. (**G**) The calculated absolute permeability for P_{Cl} and P_{Na} was significantly reduced in KD cells compared to that of control cells. * $p < 0.05$. $n = 3$.

Transfection of CLDN7 back to the CLDN7$^{+/+}$ KD cells (KD+CLDN7) increased the protein expression of CLDN7 to 88.2% of the control cell value (Figure 6A). The TER and DP were also back to the values similar to those in control cells (Figure 6B,C). Although there was no significant difference in PCl/PNa among the control, KD, and KD+CLDN7 CD cells (Figure 6D), Cl^- and Na^+ permeability was recovered to 91.1% and 90.4% in CLDN7 rescued cells, respectively (Figure 6E).

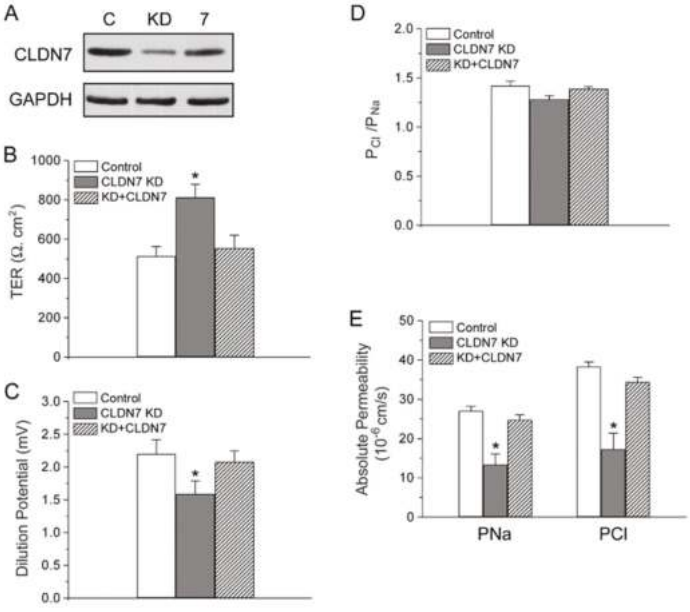

Figure 6. Re-expression ('rescue') of CLDN7 in CLDN7$^{+/+}$ CD cells with CLDN7 knockdown restored paracellular Cl^- and Na^+ permeability. (**A**) CD cells from control (C), CLDN7 knockdown (KD), KD with CLDN7 cDNA transfection (7) were lysed in RIPA buffer and subjected to western blotting. The membrane was blotted with anti-CLDN7 antibody. (**B**) TER values were measured on cell monolayers cultured for 7 days on collagen-coated Transwell plates. (**C**) Dilution potentials were measured as described in Figure 2B. (**D**) The ratio of the absolute permeability of Cl^- to Na^+ (P_{Cl}/P_{Na}), and (**E**) the absolute permeability for P_{Cl} and P_{Na} were calculated as described in Figure 2C,D, respectively. * $p < 0.05$ compared to control and KD+CLDN7. $n = 3$.

3. Discussion

In this study, we have shown that mouse renal CD cells with CLDN7 deletion exhibited significant decrease in paracellular Cl^- and Na^+ permeability. At the same time, the TER in CLDN7$^{-/-}$ CD cells was greatly increased while the dilution potential was decreased. The paracellular ion permeability in CLDN7$^{+/+}$ CD cells with CLDN7 knockdown resembled that of CLDN7$^{-/-}$ CD cells. Re-expression ('rescue') CLDN7 in CLDN7$^{+/+}$ KD cells restored the role of CLDN7 in paracellular Cl^- and Na^+ permeability. In addition, our study demonstrates that deletion of CLDN7 upregulates WNK4 expression at both mRNA and protein levels in our immortalized CD cells as well as in the primary CD cells, indicating that CLDN7 may play an important role in regulating WNK4 expression in kidneys. Interestingly, ENaC expression was also upregulated in immortalized and primary CLDN7$^{-/-}$ CD cells compared to that of CLDN7$^{+/+}$ CD cells, suggesting a potential influence of paracellular pathway on transcellular pathway.

It is known that CLDN7 is highly expressed in the distal nephron of the kidney [32]. We reported previously that CLDN7-deficient mice exhibited renal salt wasting and chronic dehydration [31]. To investigate the function of CLDN7 in distal nephron, we used the novel approach to isolate, purify, and immortalize the CD cells from CLDN7$^{+/+}$ and CLDN7$^{-/-}$ mouse kidneys. This approach allows us to study the role of CLDN7 in renal epithelial cells in a controlled environment without the stimulation of hormones and other circulating factors. We found that the TER value was around 500 $\Omega.cm^2$ for CLDN7$^{+/+}$ CD cells, which was consistent with the literature on isolated rabbit CDs [33]. However, deletion of CLDN7 increased TER value to more than 1000 $\Omega.cm^2$. The increase in TER is due to the

decrease in paracellular Cl^- and Na^+ permeability. We reported previously that overexpression of CLDN7 in LLC-PK1 cells decreases the paracellular Cl^- conductance and increases paracellular Na^+ conductance [30]. It is possible that the effect of overexpression or knockdown of the same gene in different cell lines may have different functional consquences as we have observed in human lung cancer cells [34] and our unpublished data. It is known that the paracellular pathway in the CD system is mainly Cl^- selective [1,35]. However, Cl^- reabsorption must match that of Na^+ in order to maintain the homeostasis of luminal fluids and electrolytes. Our current study suggests that CLDN7 may form a non-selective paracellular channel in renal CD cells and play a critical role in Cl^- and Na^+ homeostasis in distal nephrons.

WNK4 is localized at TJs of distal nephrons and has been shown to selectively increase paracellular Cl^- permeability and phosphorylate claudins in MDCK cells [18,25,26], and many studies have revealed that mutations of WNK4 are involved in the pathogenesis of PHAII [18,24,36,37]. We previously found that CLDN7 was a substrate of WNK4, and that phosphorylation of CLDN7 by WNK4 promoted the paracellular Cl^- permeability in kidney epithelial cells [27]. Interestingly, we found in this study that deletion of CLDN7 significantly increased WNK4 expression in CD cell lines as well as in primary CD cells (Figures 3B and 4B), suggesting a previously unrecognized involvement of CLDN7 in the regulation of WNK4. In addition, ENaC expression was also increased in both $CLDN7^{-/-}$ immortalized and primary CD cells, which could be mediated through the up-regulation of SGK-1 since it has been reported that SGK-1 stimulates the membrane expression and the activity of ENaC [38–40]. It will be interesting to see in future studies whether ENaC channel activity is altered in $CLDN7^{-/-}$ CD cells.

It has been reported that CLDN4 forms a paracellular Cl^- channel in the kidney and requires CLDN8 for TJ localization [28]. However, in our CLDN7 CD cell lines, CLDN4 was well localized to the cell junction area in both $CLDN7^{+/+}$ and $CLDN7^{-/-}$ CD cells, though the CLDN8 signal was undetectable. It is possible that different renal epithelial cells may behave differently depending on the TJ components and claudin compositions.

4. Materials and methods

4.1. Antibodies and Reagents

Rabbit polyclonal anti-CLDN3 and CLDN4 antibodies were purchased from Invitrogen (Thermo Fisher Scientific, Waltham, MA, USA). Rabbit polyclonal anti-CLDN7 antibody was obtained from Immuno-Biological Laboratories (Gunma, Japan). AQP2 polyclonal antibody was purchased from CALBIOCHEM (Sigma-Aldrich, St. Louis, MO, USA). Rabbit anti-WNK4 antibody was described previously [41]. The WNK1 antibody was obtained from Novus Biologicals (Centennial, CO, USA). Anti-SGK-1 and Anti-SPAK antibodies were from Cell Signaling Technology (Danvers, MA, USA). OSR1 antibody was purchased from Abcam (Cambridge, MA, USA). All chemicals and reagents were purchased from Sigma and/or Fisher Scientific unless noted otherwise. Transwell and Snapwell plates were from Corning Costar (Corning, NY, USA).

4.2. Isolation and Immortalization of CD Cells from $CLDN7^{+/+}$ and $CLDN7^{-/-}$ Mouse Kidneys

The kidneys were removed quickly from 4–5-day-old $CLDN7^{+/+}$ and $CLDN7^{-/-}$ mice generated in this laboratory [31], minced into 1 mm^3 pieces, and digested in Hanks' Balanced Salt Solution (HBSS, Invitrogen, ThermoFisher Scientific, Waltham, MA USA) containing 0.2% collagenase A and 0.2% hyaluronidase (Sigma, St. Louis, MO, USA). After 30 min incubation at 37 °C, DNase I (100 U/mL) was added to the cell suspension to prevent cell clumping. Then the cell suspension went through a cell strainer and the collected cells were incubated with Dolichos biflorus lectin-coated Dynabeads (Invitrogen, ThermoFisher Scientific) in a tube at 8 °C for 20 min. The tube was placed in a magnet for 2 min and the supernatant was discarded. The beads-bound cells were washed with PBS, separated from the supernatant by the magnet, and re-suspended in an established renal CD medium [42]. To release the cells from the beads, DNase was added to the tube containing beads-bound cells.

The released cells and beads were separated by the magnet, and the supernatant with released cells were cultured in DMEM/Ham's F12 medium containing 5% fetal bovine serum, 2.5 μg/mL transferrin, 1 μM thyronine T_3, 30 μM sodium selenate, 2 mM L-glutamine, 15 mM HEPES, 100 U/mL penicillin, and 100 μg/mL streptomycinneomycin in a humidified 5% CO_2-air atmosphere at 37 °C. The purified CD cells were immortalized into cell lines using Lenti-SV40 virus infection according to the manufacturer's instructions (Applied Biological Materials Inc. Richmond, Canada). At least three CD cell lines were established by the above methods and used in the current study. All animal experiments were approved by the East Carolina University Animal Care and Use Committee (AUP#A172b, date of approval 16 December 2011).

4.3. Electrophysiological Measurements

Transepithelial resistant (TER) measurements: CLDN7$^{+/+}$ and CLDN7$^{-/-}$ CD cells were plated onto collagen-coated Transwell inserts at the density of 1.5×10^5 cells/cm^2 and cultured for 7–10 days. After the monolayer reached confluence, the resistance across each filter was measured by a Millicell-ERS Volt-Ohm meter (Millipore, Bedford, MA, USA). All TER values were calculated by subtracting the resistance measured in the blank insert from the resistance measured in the insert with the monolayer and then multiplied by the surface area of the membrane.

Dilution potential measurements: CLDN7$^{+/+}$ and CLDN7$^{-/-}$ CD cells were grown on Snapwell membranes coated with collagens. The apical and basal chambers were filled with P1 buffer containing (in mM): 140 NaCl, 2 $CaCl_2$, 1 $MgCl_2$, 10 HEPES, and 10 glucose (pH 7.3). To measure the dilution potential (DP), the basal chamber was switched from P1 to P2 buffer containing (in mM): 70 NaCl, 140 mannitol, 2 $CaCl_2$, 1 $MgCl_2$, 10 HEPES, and 10 glucose (pH 7.3). During the experiments, the buffer was maintained at 37 °C and bubbled constantly with 95% air and 5% CO_2. Dilution potential measurements and calculations were conducted as described in Alexandre et al. [30] and Yu et al. [43]. Briefly, the ion permeability ratio of the monolayer to Cl^- over the permeability to Na^+ ($\beta = P_{Cl}/P_{Na}$) was calculated from the dilution potential using the Goldman–Hodgkin–Katz equation. The absolute permeability values of Na^+ (P_{Na}) and Cl^- (P_{Cl}) were calculated according to the following equations, $P_{Na} = G \cdot (RT/F^2)/(\alpha(1 + \beta)$ and $P_{Cl} = P_{Na} \cdot \beta$. Here, the conductance per unit surface area (G) of the membrane can be measured by Ohm's law, α is the NaCl activity, and β is the ratio of the permeability of Cl^- to that of Na^+ as determined by the Goldman–Hodgkin–Katz equation [43]. Amiloride (100 μM, Sigma, St Louis, MO, USA), niflumic acid (NFA, 100 μM), and 4,4′-diisothiocyanatostilbene-2,2′-disulfonic acid (DIDS, 100 μM) were added to the solution to block epithelial sodium and chloride channels in CD cells.

4.4. RNA Extraction and Quantitative Real-Time PCR

The total RNA of CLDN7$^{+/+}$ and CLDN7$^{-/-}$ CD cells were isolated using a Qiagen RNeasy kit (Qiagen, Valencia, CA, USA), and the first-strand cDNA was synthesized with a Qiagen First Strand Kit according to the manufacturer's instructions. Quantitative real-time RT-PCR (qRT-PCR) was performed as previously described [44]. For each target gene, the relative gene expression was performed in triplicates and the cycle threshold (Ct) values were normalized to the internal control β-actin gene expression level and analyzed by $2^{-\Delta\Delta Ct}$ method [45].

4.5. Statistical Analysis

Statistical analysis was performed using Origin50 and VassarStats programs. The differences between two groups were analyzed using the unpaired two-tailed Student's t-test. One-way ANOVA was performed if comparisons involved more than two groups. Data are expressed as mean ± S.E.M. and *n* indicates the number of independent experiments. A *p*-value of <0.05 was considered significant.

5. Conclusion

In conclusion, our present study highlights a critical role of CLDN7 in Cl^- and Na^+ homeostasis in CD cells of kidneys and the involvement of CLDN7 in WNK4 regulation. In addition, the increased expression of ENaC in stable and primary CLDN7$^{-/-}$ CD cells suggests the influence of an altered paracellular pathway on the transcellular pathway. Future studies should involve the functional analysis of ENaC channel activity in the presence and absence of CLDN7. Therefore, our mouse CD cell lines provide a unique model for investigating the crosstalk between paracellular and transcellular pathways and how this interaction affects the ionic balance of the kidney and blood pressure in the body.

Author Contributions: Conceptualization, Y.-H.C.; Methodology, J.F., R.T., and J.H.; Validation and Data Curation, J.F., R.T., and J.H.; Funding Acquisition, Y.-H.C.; Supervision, Y.-H.C.; Writing-Original Draft Preparation, J.F.; Writing-Review and Editing, Y.-H.C.

Funding: This research was supported by National Institutes of Health grants HL085752 and DK103166 to Y.H.C.

Acknowledgments: We sincerely thank Lawrence Palmer (Weill Medical College of Cornell University) for providing ENaC antibodies and Alan Yu (University of Kansas Medical Center) for helpful discussion. We thank Beverly Jeansonne and Joani Zary Oswald for their technical assistance.

Conflicts of Interest: The authors disclose no conflicts of interest.

References

1. Sansom, S.C.; Weinman, E.J.; O'Neil, R.G. Microelectrode assessment of chloride-conductive properties of cortical collecting duct. *Am. J. Physiol.* **1984**, *247*, F291–F302. [CrossRef] [PubMed]
2. Schuster, V.L.; Stokes, J.B. Chloride transport by the cortical and outer medullary collecting duct. *Am. J. Physiol.* **1987**, *253*, F203–F212. [CrossRef] [PubMed]
3. Hou, J. Paracellular transport in the collecting duct. *Curr. Opin. Nephrol. Hypertens.* **2016**, *25*, 424–428. [CrossRef] [PubMed]
4. Denker, B.M.; Sabath, E. The biology of epithelial cell tight junctions in the kidney. *J. Am. Soc. Nephrol.* **2011**, *22*, 622–625. [CrossRef] [PubMed]
5. Van Itallie, C.M.; Anderson, J.M. Claudins and epithelial paracellular transport. *Annu. Rev. Physiol.* **2006**, *68*, 403–429. [CrossRef] [PubMed]
6. Balkovetz, D.F. Claudins at the gate: Determinants of renal epithelial tight junction paracellular permeability. *Am. J. Physiol. Renal Physiol.* **2006**, *290*, F572–F579. [CrossRef] [PubMed]
7. Mineta, K.; Yamamoto, Y.; Yamazaki, Y.; Tanaka, H.; Tada, Y.; Saito, K.; Tamura, A.; Igarashi, M.; Endo, T.; Takeuchi, K.; et al. Predicted expansion of the claudin multigene family. *FEBS Lett.* **2011**, *585*, 606–612. [CrossRef] [PubMed]
8. Kiuchi-Saishin, Y.; Gotoh, S.; Furuse, M.; Takasuga, A.; Tano, Y.; Tsukita, S. Differential expression patterns of claudins, tight junction membrane proteins, in mouse nephron segments. *J. Am. Soc. Nephrol.* **2002**, *13*, 875–886.
9. Konrad, M.; Schaller, A.; Seelow, D.; Pandey, A.V.; Waldegger, S.; Lesslauer, A.; Vitzthum, H.; Suzuki, Y.; Luk, J.M.; Becker, C.; et al. Mutations in the tight-junction gene claudin 19 (CLDN19) are associated with renal magnesium wasting, renal failure, and severe ocular involvement. *Am. J. Hum. Genet.* **2006**, *79*, 949–957. [CrossRef]
10. Simon, D.B.; Lu, Y.; Choate, K.A.; Velazquez, H.; Al-Sabban, E.; Praga, M.; Casari, G.; Bettinelli, A.; Colussi, G.; Rodriguez-Soriano, J.; et al. Paracellin-1, a renal tight junction protein required for paracellular Mg2+ resorption. *Science* **1999**, *285*, 103–106. [CrossRef]
11. Hou, J.; Shan, Q.; Wang, T.; Gomes, A.S.; Yan, Q.; Paul, D.L.; Bleich, M.; Goodenough, D.A. Transgenic RNAi depletion of claudin-16 and the renal handling of magnesium. *J. Biol. Chem.* **2007**, *282*, 17114–17122. [CrossRef] [PubMed]
12. Muto, S.; Hata, M.; Taniguchi, J.; Tsuruoka, S.; Moriwaki, K.; Saitou, M.; Furuse, K.; Sasaki, H.; Fujimura, A.; Imai, M.; et al. Claudin-2-deficient mice are defective in the leaky and cation-selective paracellular permeability properties of renal proximal tubules. *Proc. Natl. Acad. Sci. USA* **2010**, *107*, 8011–8016. [CrossRef] [PubMed]

13. Krug, S.M.; Gunzel, D.; Conrad, M.P.; Rosenthal, R.; Fromm, A.; Amasheh, S.; Schulzke, J.D.; Fromm, M. Claudin-17 forms tight junction channels with distinct anion selectivity. *Cell Mol. Life Sci.* **2012**, *69*, 2765–2778. [CrossRef] [PubMed]
14. Breiderhoff, T.; Himmerkus, N.; Stuiver, M.; Mutig, K.; Will, C.; Meij, I.C.; Bachmann, S.; Bleich, M.; Willnow, T.E.; Muller, D. Deletion of claudin-10 (Cldn10) in the thick ascending limb impairs paracellular sodium permeability and leads to hypermagnesemia and nephrocalcinosis. *Proc. Natl. Acad. Sci. USA* **2012**, *109*, 14241–14246. [CrossRef]
15. Breiderhoff, T.; Himmerkus, N.; Drewell, H.; Plain, A.; Gunzel, D.; Mutig, K.; Willnow, T.E.; Muller, D.; Bleich, M. Deletion of claudin-10 rescues claudin-16-deficient mice from hypomagnesemia and hypercalciuria. *Kidney Int.* **2018**, *93*, 580–588. [CrossRef]
16. Furgeson, S.B.; Linas, S. Mechanisms of type I and type II pseudohypoaldosteronism. *J. Am. Soc. Nephrol.* **2010**, *21*, 1842–1845. [CrossRef]
17. Healy, J.K. Pseudohypoaldosteronism type II: History, arguments, answers, and still some questions. *Hypertension* **2014**, *63*, 648–654. [CrossRef]
18. Wilson, F.H.; Disse-Nicodeme, S.; Choate, K.A.; Ishikawa, K.; Nelson-Williams, C.; Desitter, I.; Gunel, M.; Milford, D.V.; Lipkin, G.W.; Achard, J.M.; et al. Human hypertension caused by mutations in WNK kinases. *Science* **2001**, *293*, 1107–1112. [CrossRef]
19. Arroyo, J.P.; Gamba, G. Advances in WNK signaling of salt and potassium metabolism: Clinical implications. *Am. J. Nephrol.* **2012**, *35*, 379–386. [CrossRef]
20. Welling, P.A.; Chang, Y.P.; Delpire, E.; Wade, J.B. Multigene kinase network, kidney transport, and salt in essential hypertension. *Kidney Int.* **2010**, *77*, 1063–1069. [CrossRef]
21. Kahle, K.T.; Ring, A.M.; Lifton, R.P. Molecular physiology of the WNK kinases. *Annu. Rev. Physiol.* **2008**, *70*, 329–355. [CrossRef]
22. Wang, W.H.; Giebisch, G. Regulation of potassium (K) handling in the renal collecting duct. *Pflugers Arch.* **2009**, *458*, 157–168. [CrossRef]
23. Kahle, K.T.; Wilson, F.H.; Leng, Q.; Lalioti, M.D.; O'Connell, A.D.; Dong, K.; Rapson, A.K.; MacGregor, G.G.; Giebisch, G.; Hebert, S.C.; et al. WNK4 regulates the balance between renal NaCl reabsorption and K+ secretion. *Nat. Genet.* **2003**, *35*, 372–376. [CrossRef]
24. Chen, J.C.; Lo, Y.F.; Lin, Y.W.; Lin, S.H.; Huang, C.L.; Cheng, C.J. WNK4 kinase is a physiological intracellular chloride sensor. *Proc. Natl. Acad. Sci. USA* **2019**, *116*, 4502–4507. [CrossRef]
25. Kahle, K.T.; Macgregor, G.G.; Wilson, F.H.; Van Hoek, A.N.; Brown, D.; Ardito, T.; Kashgarian, M.; Giebisch, G.; Hebert, S.C.; Boulpaep, E.L.; et al. Paracellular Cl- permeability is regulated by WNK4 kinase: Insight into normal physiology and hypertension. *Proc. Natl. Acad. Sci. USA* **2004**, *101*, 14877–14882. [CrossRef]
26. Yamauchi, K.; Rai, T.; Kobayashi, K.; Sohara, E.; Suzuki, T.; Itoh, T.; Suda, S.; Hayama, A.; Sasaki, S.; Uchida, S. Disease-causing mutant WNK4 increases paracellular chloride permeability and phosphorylates claudins. *Proc. Natl. Acad. Sci. USA* **2004**, *101*, 4690–4694. [CrossRef]
27. Tatum, R.; Zhang, Y.; Lu, Q.; Kim, K.; Jeansonne, B.G.; Chen, Y.H. WNK4 phosphorylates ser(206) of claudin-7 and promotes paracellular Cl(-) permeability. *FEBS Lett.* **2007**, *581*, 3887–3891. [CrossRef]
28. Hou, J.; Renigunta, A.; Yang, J.; Waldegger, S. Claudin-4 forms paracellular chloride channel in the kidney and requires claudin-8 for tight junction localization. *Proc. Natl. Acad. Sci. USA* **2010**, *107*, 18010–18015. [CrossRef]
29. Alexandre, M.D.; Jeansonne, B.G.; Renegar, R.H.; Tatum, R.; Chen, Y.H. The first extracellular domain of claudin-7 affects paracellular Cl- permeability. *Biochem. Biophys. Res. Commun.* **2007**, *357*, 87–91. [CrossRef]
30. Alexandre, M.D.; Lu, Q.; Chen, Y.H. Overexpression of claudin-7 decreases the paracellular Cl- conductance and increases the paracellular Na+ conductance in LLC-PK1 cells. *J. Cell. Sci.* **2005**, *118*, 2683–2693. [CrossRef]
31. Tatum, R.; Zhang, Y.; Salleng, K.; Lu, Z.; Lin, J.J.; Lu, Q.; Jeansonne, B.G.; Ding, L.; Chen, Y.H. Renal salt wasting and chronic dehydration in claudin-7-deficient mice. *Am. J. Physiol. Renal Physiol.* **2010**, *298*, F24–34. [CrossRef]
32. Li, W.Y.; Huey, C.L.; Yu, A.S. Expression of claudin-7 and -8 along the mouse nephron. *Am. J. Physiol. Renal Physiol.* **2004**, *286*, F1063–F1071. [CrossRef]
33. Muto, S.; Yasoshima, K.; Yoshitomi, K.; Imai, M.; Asano, Y. Electrophysiological identification of alpha- and beta-intercalated cells and their distribution along the rabbit distal nephron segments. *J. Clin. Invest.* **1990**, *86*, 1829–1839. [CrossRef]

34. Lu, Z.; Ding, L.; Hong, H.; Hoggard, J.; Lu, Q.; Chen, Y.H. Claudin-7 inhibits human lung cancer cell migration and invasion through ERK/MAPK signaling pathway. *Exp. Cell Res.* **2011**, *317*, 1935–1946. [CrossRef]
35. Light, D.B.; Schwiebert, E.M.; Fejes-Toth, G.; Naray-Fejes-Toth, A.; Karlson, K.H.; McCann, F.V.; Stanton, B.A. Chloride channels in the apical membrane of cortical collecting duct cells. *Am. J. Physiol.* **1990**, *258*, F273–F280. [CrossRef]
36. Lopez-Cayuqueo, K.I.; Chavez-Canales, M.; Pillot, A.; Houillier, P.; Jayat, M.; Baraka-Vidot, J.; Trepiccione, F.; Baudrie, V.; Busst, C.; Soukaseum, C.; et al. A mouse model of pseudohypoaldosteronism type II reveals a novel mechanism of renal tubular acidosis. *Kidney Int.* **2018**, *94*, 514–523. [CrossRef]
37. Susa, K.; Sohara, E.; Rai, T.; Zeniya, M.; Mori, Y.; Mori, T.; Chiga, M.; Nomura, N.; Nishida, H.; Takahashi, D.; et al. Impaired degradation of WNK1 and WNK4 kinases causes PHAII in mutant KLHL3 knock-in mice. *Hum. Mol. Genet.* **2014**, *23*, 5052–5060. [CrossRef]
38. Alvarez de la Rosa, D.; Zhang, P.; Naray-Fejes-Toth, A.; Fejes-Toth, G.; Canessa, C.M. The serum and glucocorticoid kinase sgk increases the abundance of epithelial sodium channels in the plasma membrane of Xenopus oocytes. *J. Biol. Chem.* **1999**, *274*, 37834–37839. [CrossRef]
39. Faletti, C.J.; Perrotti, N.; Taylor, S.I.; Blazer-Yost, B.L. sgk: An essential convergence point for peptide and steroid hormone regulation of ENaC-mediated Na+ transport. *Am. J. Physiol. Cell Physiol.* **2002**, *282*, C494–500. [CrossRef]
40. Loffing, J.; Zecevic, M.; Feraille, E.; Kaissling, B.; Asher, C.; Rossier, B.C.; Firestone, G.L.; Pearce, D.; Verrey, F. Aldosterone induces rapid apical translocation of ENaC in early portion of renal collecting system: Possible role of SGK. *Am. J. Physiol. Renal. Physiol.* **2001**, *280*, F675–682. [CrossRef]
41. Jeansonne, B.; Lu, Q.; Goodenough, D.A.; Chen, Y.H. Claudin-8 interacts with multi-PDZ domain protein 1 (MUPP1) and reduces paracellular conductance in epithelial cells. *Cell Mol. Biol. (Noisy-le-grand)* **2003**, *49*, 13–21.
42. Bens, M.; Duong Van Huyen, J.P.; Cluzeaud, F.; Teulon, J.; Vandewalle, A. CFTR disruption impairs cAMP-dependent Cl(-) secretion in primary cultures of mouse cortical collecting ducts. *Am. J. Physiol. Renal Physiol.* **2001**, *281*, F434–442. [CrossRef]
43. Yu, A.S. Electrophysiological characterization of claudin ion permeability using stably transfected epithelial cell lines. *Methods Mol. Biol.* **2011**, *762*, 27–41.
44. Ding, L.; Lu, Z.; Foreman, O.; Tatum, R.; Lu, Q.; Renegar, R.; Cao, J.; Chen, Y.H. Inflammation and disruption of the mucosal architecture in claudin-7-deficient mice. *Gastroenterology* **2012**, *142*, 305–315. [CrossRef]
45. Dussault, A.A.; Pouliot, M. Rapid and simple comparison of messenger RNA levels using real-time PCR. *Biol. Proced. Online* **2006**, *8*, 1–10. [CrossRef]

International Journal of
Molecular Sciences

MDPI

Article

Claudin-19 Is Regulated by Extracellular Osmolality in Rat Kidney Inner Medullary Collecting Duct Cells

Annalisa Ziemens [1], Svenja R. Sonntag [1,2], Vera C. Wulfmeyer [1,3], Bayram Edemir [4], Markus Bleich [1] and Nina Himmerkus [1,*]

1 Institute of Physiology, Christian-Albrecht-University Kiel, Hermann-Rodewald-Str. 5, 24118 Kiel, Germany
2 Department of Ophthalmology, University of Lübeck, Ratzeburger Allee 160, 23538 Lübeck, Germany
3 Department of Nephrology and Hypertension, Hannover Medical School, Carl-Neuberg-Str. 1, 30625 Hannover, Germany
4 Department of Internal Medicine IV, Hematology and Oncology, University Hospital Halle, Ernst-Grube-Str. 40, 06120 Halle (Saale), Germany
* Correspondence: n.himmerkus@physiologie.uni-kiel.de; Tel.: +49-431-880-2038

Received: 26 July 2019; Accepted: 4 September 2019; Published: 7 September 2019

Abstract: The inner medullary collecting duct (IMCD) is subject to severe changes in ambient osmolality and must either allow water transport or be able to seal the lumen against a very high osmotic pressure. We postulate that the tight junction protein claudin-19 is expressed in IMCD and that it takes part in epithelial adaptation to changing osmolality at different functional states. Presence of claudin-19 in rat IMCD was investigated by Western blotting and immunofluorescence. Primary cell culture of rat IMCD cells on permeable filter supports was performed under different osmotic culture conditions and after stimulation by antidiuretic hormone (AVP). Electrogenic transepithelial transport properties were measured in Ussing chambers. IMCD cells cultivated at 300 mosm/kg showed high transepithelial resistance, a cation selective paracellular pathway and claudin-19 was mainly located in the tight junction. Treatment by AVP increased cation selectivity but did not alter transepithelial resistance or claudin-19 subcellular localization. In contrast, IMCD cells cultivated at 900 mosm/kg had low transepithelial resistance, anion selectivity, and claudin-19 was relocated from the tight junctions to intracellular vesicles. The data shows osmolality-dependent transformation of IMCD epithelium from tight and sodium-transporting to leaky, with claudin-19 expression in the tight junction associated to tightness and cation selectivity under low osmolality.

Keywords: barrier function; paracellular permeability; antidiuretic hormone

1. Introduction

The inner medullary collecting duct (IMCD) is the last segment of the nephron. It is embedded in the unique structure of the inner medulla together with descending and ascending thin limbs of Henle's loop and the accompanying vasa recta, which are specialized capillaries [1,2]. Maintenance of body water homeostasis under extreme variations in water intake is achieved under hormonal regulation, especially AVP signaling. Thereby, urine osmolality can vary between 50 mosm/kg and 1500 mosm/kg in humans. Of high importance is the interstitial osmolality provided by the main osmolytes, NaCl and urea, and the cortico-medullary concentration gradient established by the loop of Henle [3,4] countercurrent concentration system. During antidiuresis, interstitial and intraluminal osmolality is high and the transepithelial gradient is levelled by the water flux from the lumen to the interstitium through water channel insertion into the cell membrane. Under water diuresis, interstitial osmolality is lower; however, high NaCl concentration is conserved and mainly urea concentration is changing with diuretic state [5,6]. Therefore, the now transcellularly water tight collecting duct faces a high transepithelial osmotic gradient. The interstitial accumulation of urea during antidiuresis is

tightly controlled by antidiuretic hormone (AVP) but also by other factors (e.g., endothelin, PGE2) [4]. Hypertonicity and urea are thereby cell stressors and cellular osmo-homeostasis has to be controlled and adapted under these changing conditions [7,8]. Osmo-protective responses include accumulation of compatible organic osmolytes, abundance of heat shock proteins, and control of transmembrane water flux by water channels. Ionic and osmotic gradients under both antidiuresis or water diuresis between the luminal and the interstitial side of the epithelium do not only challenge the transcellular barrier, but also the paracellular route. The paracellular cleft between epithelial cells is specifically sealed by the tight junction (TJ). This complex is composed of a variety of different proteins fulfilling a broad spectrum of tasks in addition to barrier formation and provision of permeability, including anchoring the TJ proteins to the cytoskeleton and cell signaling. The proteins responsible for tightness and permeability are claudins, a family comprising more than 25 different members to date (for review, see [9–11]). From a functional perspective, IMCD paracellular properties can vary with respect to water permeability and ion selectivity. Under diuretic conditions, in the absence of AVP, the collecting duct is sealed against water permeation [12]. In antidiuresis, water channels provide a high transcellular water permeability. Early studies in the 1990s by Flamion et al. suggested a potential additional paracellular route for water in IMCD under strong antidiuresis [13]. So far, different claudins have been described for collecting ducts (claudin-3, -4, -7, -8, -10, -19) [14]. Especially, claudin-4 and -8 have been implicated in paracellular selectivity and ion transport [15]. Claudin-19 was described first in 2004 [16] and in the kidney, it is mainly expressed in the thick ascending limb of Henle's Loop (TAL) [17–19]. Mutations in humans lead to familial hypomagnesemia with hypercalciuria and nephrocalcinosis (FHHNC, OMIM 610036, [17]) which also can be caused by mutations in claudin-16 [20,21]. Both TAL claudins are required for functional TAL Ca^{2+} and Mg^{2+} transport [19,22]. In 2006, Lee et al. described a different expression pattern identified by antibody staining, showing claudin-19 in the distal tubule (i.e., mainly TAL) and the collecting duct in humans and rats [23]. In RNA-seq analysis of microdissected rat kidney tubule segments, claudin-19 mRNA has been found in more upstream collecting duct segments but hardly any in IMCD [24]. By immunofluorescence staining, our group repetitively encountered claudin-19 expression in segments more distal to the TAL and decided to investigate its expression and function in the inner medulla.

We hypothesize that claudin-19 is part of the IMCD TJ, that IMCD cells adapt to osmolality or AVP stimulation, and that claudin-19 takes part in this adaptation. We used the well-established model of primary cultivated inner medullary collecting duct cells grown on permeable supports (IMCDs) [25,26]. Cells were cultivated under hormone stimulation and different osmotic challenges. Under cell culture conditions with proliferating cells not yet confluent and therefore not yet forming a complete epithelial layer, naturally occurring highly variable osmotic conditions are not easy to copy. We focused on long term (days) basolateral changes, omitting transepithelial gradients. Plasma-isotonicity represented cortical conditions and two increasing medullary osmolalities represented either the medullary axis or different diuretic states. Under low osmolality, claudin-19 localized to the TJ of IMCD, most likely fulfilling the sealing function and being responsible for high transepithelial resistance.

2. Results

2.1. Claudin19 Is Expressed in Inner Medullary Collecting Duct

We investigated claudin-19 expression using WB analysis in both mouse and rat tissue. Along the nephron of the mouse (Figure 1A), claudin-19 protein was absent in glomeruli and proximal tubule (PT). In TAL and all segments further downstream, claudin-19 was expressed and protein abundance was highest in TAL, medullary CD (mCD), and in papilla tissue. Qualitatively similar results were obtained along the rat nephron and here we could specifically detect claudin-19 also in dissected and isolated IMCD (Figure 1B). We performed claudin-19 immunofluorescence staining in mouse and rat inner medulla (Figure 1C,D). Claudin-19 was expressed in both, IMCD and thin limbs. In IMCD, claudin-19 was located mostly in the TJ, i.e., line- or dot-shaped fluorescence along the apical cell cleft

but also extending to the lateral cell borders (Figure 1D). In addition, some intracellular vesicular staining was visible at the basal cell pole of the IMCD cells. Costaining with the intercalated cell anion exchanger AE1 confirmed IMCD localization. Thin limb TJs showed the typical meandering pattern (Figure 1C [27]). Next, we investigated claudin-19 protein in rat kidney tissue in a more quantitative approach and tried to extract membrane proteins first using the mild nonionic detergent triton-x-100 (Triton), followed by a harsher extraction of the remaining membrane proteins by incubation with the anionic surfactant sodium dodecyl sulfate (SDS). As shown in Figure 1E, inner medullary claudin-19 is mainly already solubilized by Triton extraction, whereas outer medullary claudin-19 (i.e., mainly TAL) only solubilized in the presence of SDS, indicating a different TJ structure and organization.

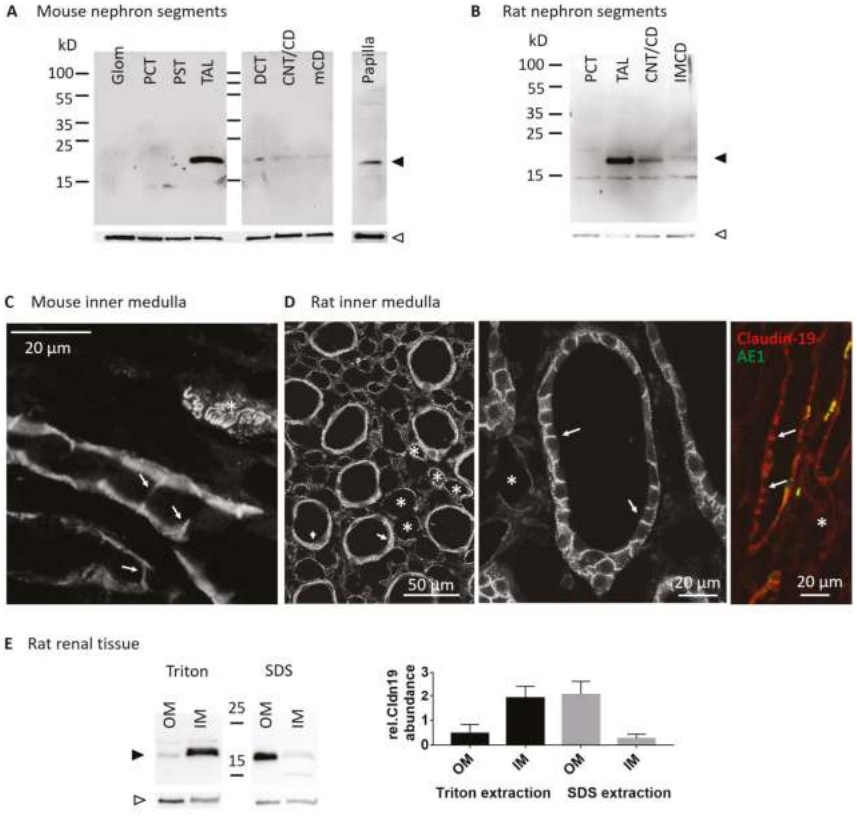

Figure 1. Claudin-19 in rodent kidney tissue. (**A**) Western blot of mouse kidney segments: glomeruli (Glom), proximal convoluted tubule (PCT), proximal straight tubule (PST), thick ascending limb (TAL), distal convoluted tubule (DCT), connecting tubule/cortical CD (CNT/CD), medullary CD (mCD), and papilla. Upper part: claudin-19 (black arrowhead), lower part: β-actin (white arrowhead). (**B**) Western blot of rat kidney segments: proximal convoluted tubule (PCT), thick ascending limb (TAL), connecting tubule and cortical CD (CNT/CD) and inner medullary collecting duct (IMCD). Claudin-19 and β-actin indicated as in A. Immunofluorescence of claudin-19 in mouse (**C**) and rat (**D**) inner medulla, arrows indicate claudin-19 TJ expression in IMCD, asterisks indicate thin limbs. AE1 (green) costaining in claudin-19 (red) positive IMCD in rat inner medulla. (**E**) Western blot of rat kidney tissue: Triton and SDS solubilized protein extracts of Cortex, outer medulla (OM) and inner medulla (IM), claudin-19 and β-actin indicated as in A. Summary of $n = 2$ independent extraction experiments showing Triton solubilization mainly in IM and SDS solubilization mainly in OM.

2.2. AVP Signaling Is Preserved in IMCD Cells at Different Osmotic Culture Conditions

In a first set of experiments, we tested the IMCD culture cells for basic physiological function. Therefore, IMCD cells were cultured under 300 mosm/kg (300-IMCD) and 600 mosm/kg (600-IMCD) conditions for five days and finally treated for 24 h with AVP. As shown in Figure 2 for 300-IMCD, subcellular localization of AQP2 was assessed by immunostaining. Although some AQP2 still remained in intracellular vesicles, AQP2 membrane staining markedly increased, revealing intact AVP signaling also after several days of cell culture. The same results were obtained for 600-IMCD (data not shown).

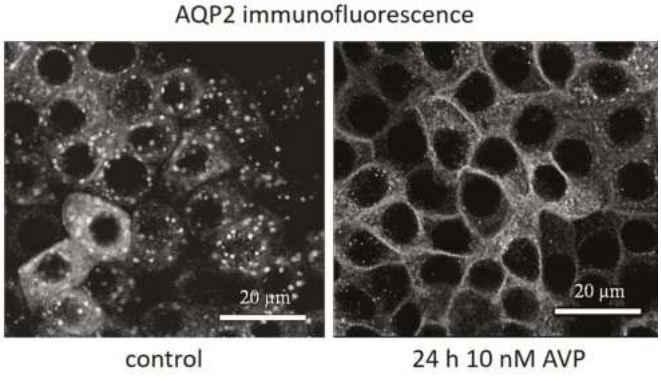

Figure 2. Effect of antidiuretic hormone (AVP) on subcellular AQP2 localization in 300-IMCD. AVP stimulation induced AQP2 insertion into the plasma membrane.

2.3. AVP Treatment Changes IMCD Cell Electrophysiological Properties but not Claudin-19 Localization

In two independent experimental series, 300-IMCD (Figure 3) or 600-IMCD (Figure 4) were cultivated for 24 h in the absence (control) or presence of 10 nmol/L AVP prior to the electrophysiological measurements. Under 300 mosm/kg conditions, mimicking strong water-diuresis or cortical osmolality, IMCD cells showed low, but consistently negative transepithelial voltage (V_{te}) and a transepithelial resistance (R_{te}) in the range of 310 Ωcm^2. These properties were not changed by AVP treatment. Accordingly, equivalent short-circuit current I'_{sc} also remained unaltered by AVP treatment (Figure 3A). Paracellular permeability properties were tested in the continuous presence of 50 µmol/L amiloride (V_{te} in the presence of amiloride was virtually abolished as shown in insert in Figure 3A) by applying an iso-osmotic NaCl concentration gradient with low NaCl (30 mmol/L) at the luminal side. In Figure 3B, two representative original chart recordings are shown to illustrate the development of a lumen-positive diffusion potential (DP) after application of the iso-osmotic NaCl gradient, indicating preferred diffusion of Na^+ ions towards the lumen. After AVP treatment, DP increased, resulting in higher cation selectivity as summarized in Figure 3C. To test whether claudin-19 subcellular localization was altered by AVP stimulation, we compared filters of both groups for the relative distribution of claudin-19 within the cells. Under control as well as under AVP treatment, almost all claudin-19 staining was localized in thin lines representing membrane, i.e., TJ staining (Figure 3D,E). There was no difference in the tight junction scores (2.70 ± 0.06 and 2.77 ± 0.05), respectively.

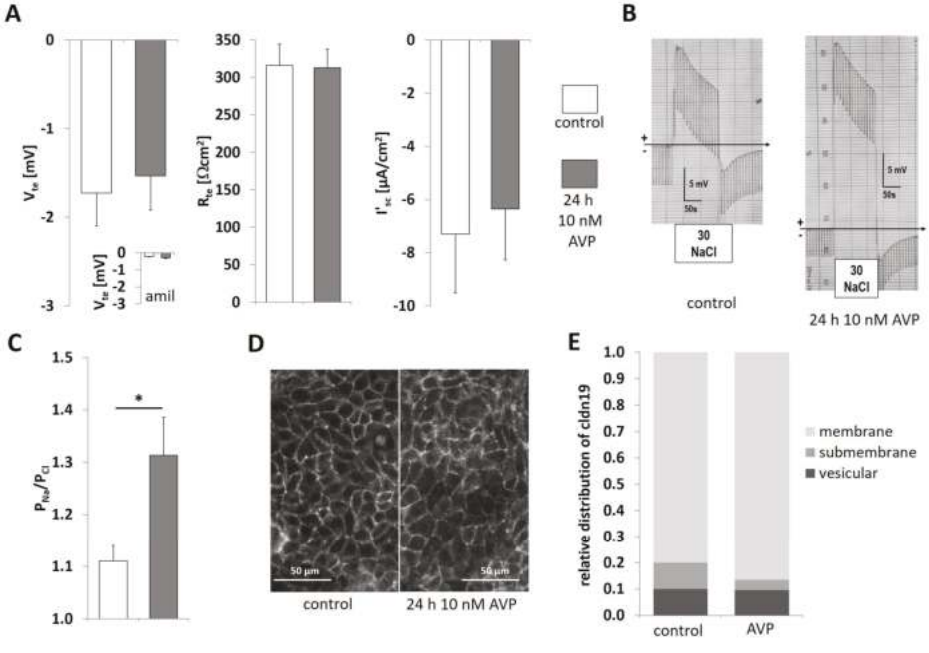

Figure 3. 300-IMCD under AVP stimulation (10 nmol/L). (**A**) Electrophysiological properties with transepithelial voltage V_{te}, transepithelial resistance R_{te}, and equivalent short-circuit current I'_{sc}, with or without 24 h prestimulation with AVP. Insert in V_{te} panel: V_{te} in the presence of 50 µM amiloride. (**B**) Original experiments showing 30 mmol/L NaCl diffusion potentials, (**C**) summarized permeability ratio PNa/PCl. Data are means ± SEM, n = 13,13; * $p < 0.05$. (**D**) Immunofluorescence of claudin-19 in 300-IMCD with or without 24 h prestimulation with AVP, (**E**) summarized subcellular localization of claudin-19 in the categories of membrane TJ staining, submembrane and intracellular vesicular staining, n = 13, 13.

The same parameters were also measured under 600 mosm/kg (Figure 4) culture conditions, which is a more physiological osmolar condition for inner medulla. Osmolality was adjusted by adding urea as well as NaCl. In comparison to 300-IMCD (Figure 3), V_{te} and R_{te} of 600-IMCDs was lower. In addition, V_{te} and I'_{sc} became less negative under AVP treatment, whereas R_{te} increased (Figure 4A). DP was measured after luminal exchange to iso-osmotic 50 mmol/L NaCl to generate a NaCl concentration gradient comparable to the previous experiments in 300-IMCD. In absolute contrast to 300-IMCD (Figure 3B,C), we now observed lumen negative diffusion voltage (Figure 4B), indicating pronounced anion selectivity (Figure 4C). There was no significant effect of AVP on paracellular selectivity as shown in original recordings (Figure 4B) and summary (Figure 4C). Claudin-19 subcellular distribution was not different between control situation und AVP treatment (Figure 4D,E; tight junction score 1.76 ± 0.07 and 1.93 ± 0.03, respectively). However, claudin-19 subcellular distribution was again markedly changed by osmolality, with a shift to submembrane and even more intracellular vesicular representation at 600-IMCD.

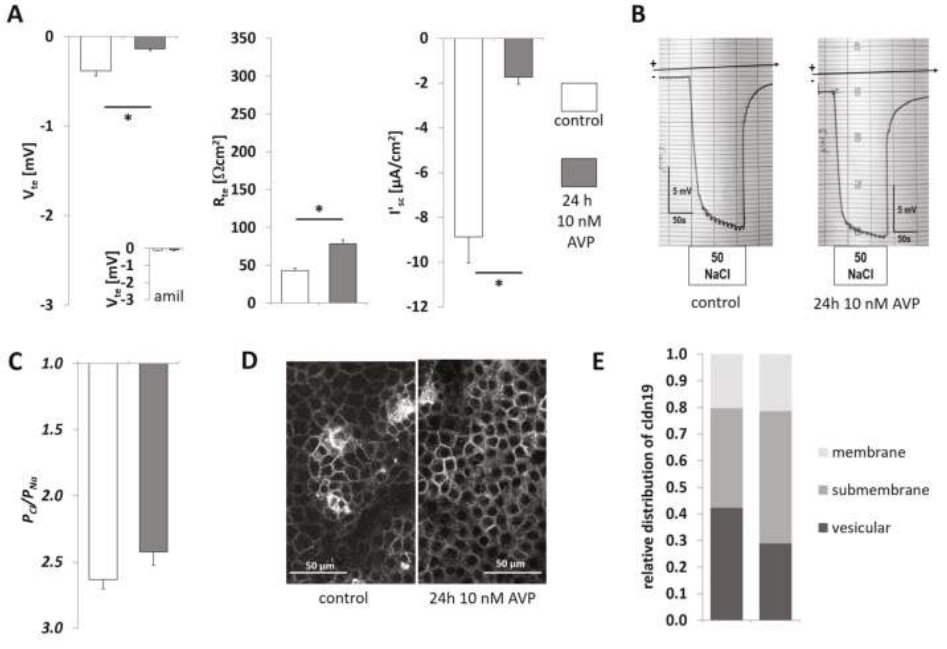

Figure 4. 600-IMCD under AVP stimulation (10 nmol/L). (**A**) Electrophysiological properties with transepithelial voltage V_{te}, transepithelial resistance R_{te}, and equivalent short-circuit current I'_{sc}, with or without 24 h prestimulation with AVP. Insert in V_{te} panel: V_{te} in the presence of 50 µM amiloride. (**B**) Original experiments showing 50 mmol/L NaCl diffusion potentials, (**C**) summarized permeability ratio P_{Cl}/P_{Na}. Data are means ± SEM, n = 12,12; * $p < 0.05$. (**D**) Immunofluorescence of claudin-19 in 600-IMCD, (**E**) summarized subcellular localization of claudin-19 in the categories of membrane TJ staining, submembrane and intracellular vesicular staining, n = 8, 7.

2.4. Differences in Extracellular Osmolality Determine IMCD-Cell Trans- and Paracellular Properties

The observation that osmolality strongly changed the transepithelial properties of IMCD-cells prompted us to further examine this strikingly strong effect of ambient osmolality on claudin-19 function. Therefore, we performed a new independent set of experiments cultivating IMCD cells in parallel under 300 mosm/kg, 600 mosm/kg, and 900 mosm/kg (900-IMCD) to mimic stronger antidiuresis. Transepithelial resistance measured daily under culture condition (TER) was monitored and cells reached peak resistance values at day 6 under all three osmolality regimens (Figure 5). Interestingly, the average resistance varied considerably between the three groups. Whereas cells grown under plasma isotonic conditions (300-IMCD) reached TER values of around 550 Ωcm^2, TER of 600-IMCDs was five times and TER of 900-IMCDs even 10 times lower.

Subsequently, filters were measured in Ussing Chamber experiments at day 5. Figure 6 shows electrophysiological properties in more detail. Only 300-IMCDs showed noteworthy lumen negative V_{te}, which disappeared under high osmolality. The resistance measurements during cell culture (TER, Figure 5) were corroborated. 300-IMCD displayed ca. 400 Ωcm^2, 600-IMCDs ca. 70 Ωcm^2, and 900-IMCD only ca. 27 Ωcm^2 (Figure 6A). Consistently, only 300-IMCD showed a lumen negative transcellular transport current I'_{sc} in this set of experiments. Paracellular selectivity was then assessed using comparable transepithelial NaCl concentration gradients adjusted to medium NaCl concentrations, respectively (Table 1, Figure 6B). Whereas 300-IMCD consistently showed a lumen positive DP, indicating cation selectivity (left original recording in Figure 6B), and all 900-IMCD a lumen negative DP, indicating anion selectivity (right original recording in Figure 6B), 600-IMCD

displayed either lumen positive or lumen negative DP. Ion permeability ratios for Na^+ and Cl^- are summarized in Figure 6C. 300-IMCDs were cation selective and 900-IMCDs anion selective, 600-IMCD showing a moderate anion selectivity close to unity. Absolute permeability was calculated from these ratios and R_{te}. As the effect of osmolality on R_{te} of IMCD was much more pronounced than the changes in ion selectivity, the effect of higher osmolality was an increase for P_{Na} and even more for P_{Cl}. Figure 6D depicts the calculated permeabilities for Na^+ and Cl^- with an up to 25-fold increase in P_{Cl} comparing 300-IMCD and 900-IMCD.

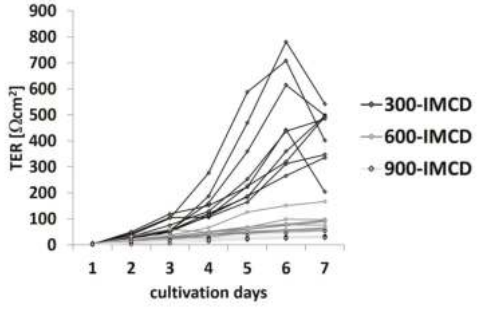

Figure 5. Time course of transepithelial resistance (TER) under culture conditions after seeding for nine different preparations with the filters of 300-IMCD, 600-IMC, and 900-IMCD, respectively.

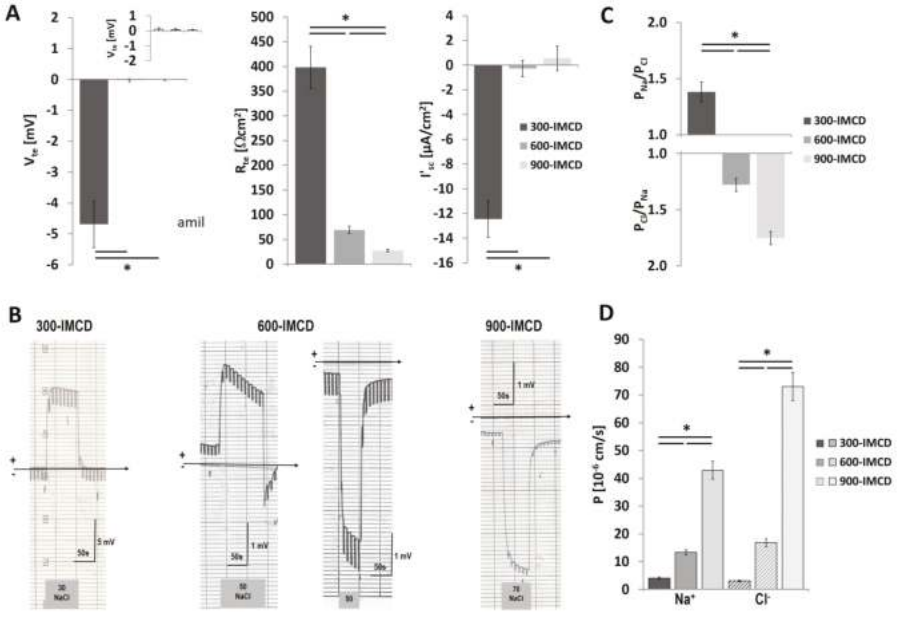

Figure 6. Comparison between 300-IMCD, 600-IMCD, and 900-IMCD after five days of cultivation. (**A**) Electrophysiological properties with transepithelial voltage V_{te}, transepithelial resistance R_{te} and equivalent short-circuit current I'_{sc}. Insert in Vte panel: Vte in the presence of 50 μM amiloride. (**B**) Original experiments showing 30 mmol/L NaCl (300-IMCD), 50 mmol/L (600-IMCD), and 70 mmol/L (900-IMCD) diffusion potentials. (**C**) Summarized permeability ratio PNa/PCl and PCl/PNa, respectively. (**D**) Calculated Na^+ and Cl^- permeabilities. Data are means ± SEM, n = 24, 39, 46; * $p < 0.05$.

Table 1. Composition of experimental solutions used in Ussing chamber experiments. Concentrations are given in mmol/L. pH was adjusted to pH 7.4.

	Control Solution			Low NaCl Solution		
	'300'	'600'	'900'	'300'	'600'	'900'
NaCl	145	245	345	30	50	70
KH_2PO_4	0.4	0.4	0.4	0.4	0.4	0.4
K_2HPO_4	1.6	1.6	1.6	1.6	1.6	1.6
$MgCl_2$	1	1	1	1	1	1
Ca-gluconate	1.3	1.3	1.3	1.3	1.3	1.3
glucose	5	5	5	5	5	5
urea	-	100	200	-	100	200
mannitol	-	-	-	230	390	550

2.5. Effect of the Different Osmolality on IMCD Transport Properties

300-IMCD showed a lumen negative I'_{sc} which was almost completely abolished by luminal amiloride application, indicating functionally expressed ENaC (Figure 7A). 600-IMCD showed basically no amiloride-dependent I'_{sc} but, astonishingly, 900-IMCD became slightly lumen positive after amiloride application. Sodium transport was verified by the measurement of changes in sodium concentration under cell culture conditions within 24 h. Luminal and basolateral cell culture medium was collected and compared directly before the Ussing chamber experiments. Only 300-IMCD showed sodium reabsorption decreasing the luminal sodium concentration (Figure 7B). 600-IMCD and 900-IMCD did not achieve a significant difference in luminal versus basolateral sodium concentration. To investigate whether osmolality affected the overall tightness of the epithelium for larger molecules, we applied 40 kDa FITC–dextran to one compartment of the cell culture and measured the fluorescence in the trans-compartment. In comparison to the empty cell culture filters, confluent cell layers showed hardly any FITC–dextran permeability confirming intact cell layers. Only 900-IMCD showed a slightly higher 40 kD FITC–dextran permeability (Figure 7C), still minute in comparison to empty filters.

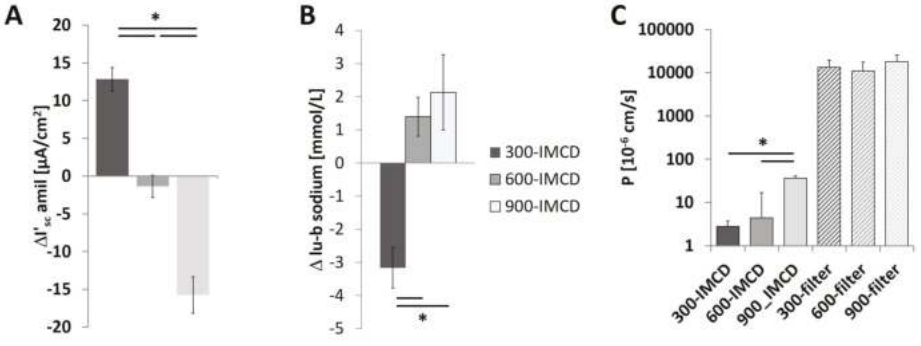

Figure 7. Transepithelial transport parameters of 300-IMCD, 600-IMCD, and 900-IMCD after five days' cultivation. (**A**) Amiloride-sensitive equivalent short-circuit current $\Delta I'_{sc}$. (**B**) Na^+ concentration difference between luminal and basolateral cultivation medium, (**C**) summarized 40 kD FITC–dextran permeability. Data are means ± SEM, IMCD filters: n = 10,11,11; empty filters: n = 3, 3, 3; * $p < 0.05$.

2.6. Differences in Extracellular Osmolality Change Claudin-19 Subcellular Localization

Finally, we compared the subcellular localization of claudin-19 in the different IMCD cultures and corroborated the findings already implicated by the AVP experiments. Whereas in 300-IMCD most claudin-19 was localized to the tight junction and appeared as a sharp line (Figure 8A), the percentage of submembrane and intracellular vesicular staining increased at higher cell culture medium osmolality (Figure 8B,C). Representative immunofluorescence stainings for claudin-19 are shown in (Figure 8A–C)

and the observations are summarized as relative distribution between membrane, submembrane, and vesicular compartments (Figure 8D). 300-IMCD showed nearly 70% TJ staining (TJ score 2.69 ± 0.10), 600-IMCD expression pattern was intermediate (TJ score 1.80 ± 0.11), and in 900-IMCD, more than 90% of claudin-19 was distributed to small intracellular vesicular-like structures (TJ score 1.13 ± 0.08).

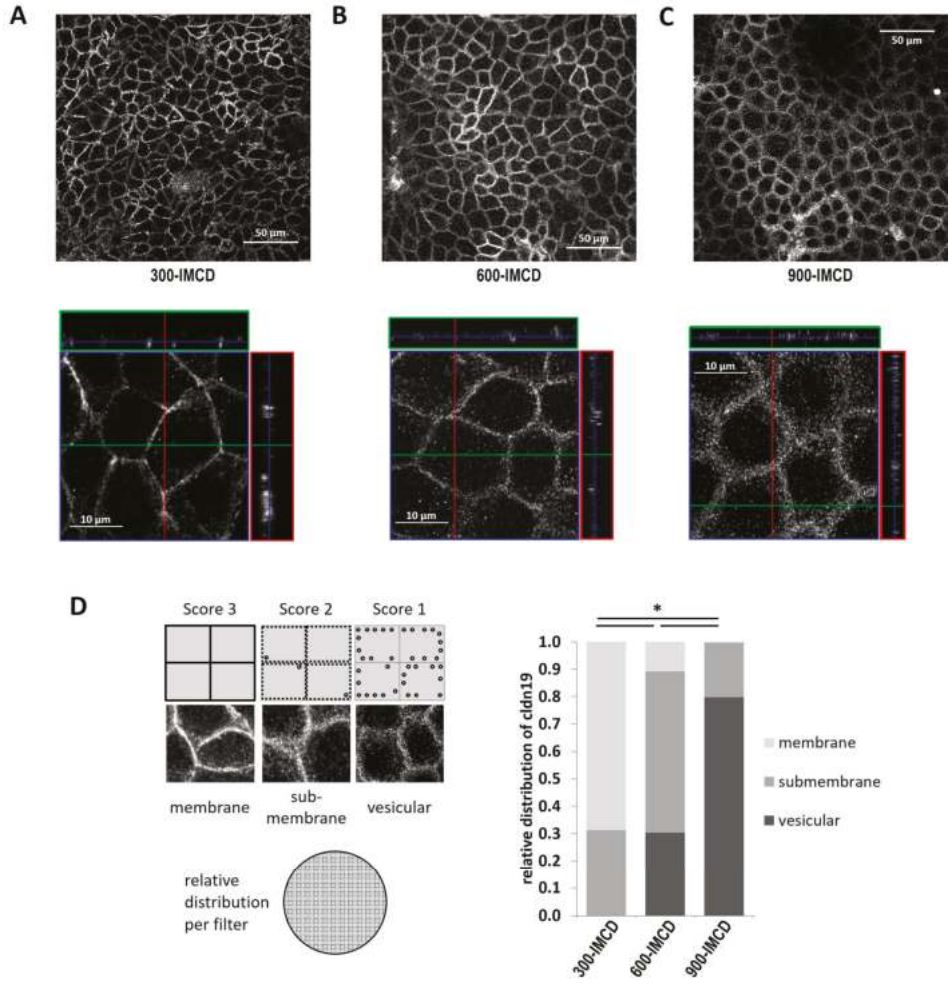

Figure 8. Immunofluorescence of claudin-19 (**A**) in 300-IMCD, (**B**) in 600-IMCD, and (**C**) in 900-IMCD, shown in an xy-overview (upper panel) and a representative z-stack (lower panel). (**D**) Summarized subcellular localization of claudin-19 in the categories of membrane TJ staining, submembrane and intracellular vesicular staining (schematic drawing), n = 12, 14, 12.

2.7. Further Observations

This study mainly focused on the expression and localization of claudin-19 under different osmotic cell culture conditions. However, in comparison to the changing subcellular localization of claudin-19, which we investigated in detail, we could not find a similar pattern in the expression of claudin-8 (Figure 9A). In addition, the TJ associated scaffolding protein ZO-1 localized nicely to the tight junction belt of IMCD under all conditions (Figure 9B), independent of osmolality.

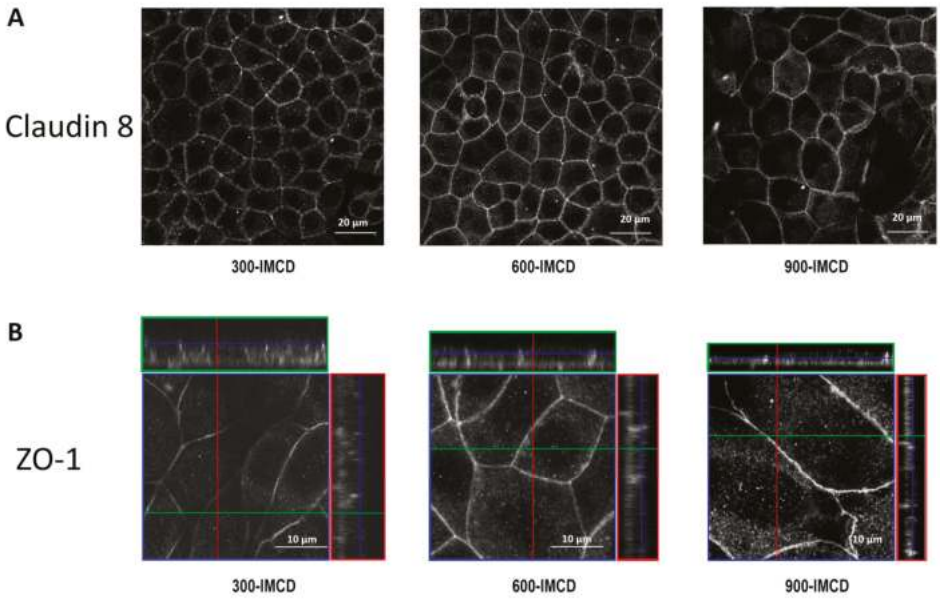

Figure 9. Immunofluorescence of claudin-8 in xy-overview in 300-IMCD, 600-IMCD, and 900-IMCD (**A**). Z-stacks of immunofluorescence of ZO-1 in 300-IMCD, 600-IMCD, and 900-IMCD (**B**).

Furthermore, the z-stacks in Figure 8; Figure 9 show that osmotic cell culture conditions also influenced cell height and size. Especially 900-IMCD, although covering the total area of the filter, were rather flat and more expanded, suggesting a reduced number of available cells.

3. Discussion

We and others have investigated the expression and function of a variety of claudins along the nephron [28,29]; however, there are still several claudins in this large protein family which are not fully characterized with respect to their expression and functional role. Refinement of Western Blot analysis and immunofluorescence of claudin-19 protein in isolated renal tubules showed substantial expression in medullary and inner medullary collecting ducts. As these tubules are exposed to varying interstitial osmolality depending on the diuretic state and at the same time have to serve different needs with respect to permeability and barrier function, we hypothesized that claudin-19 is involved in medullary and inner medullary collecting duct function and might be under the control of antidiuretic hormone and osmolality.

We used primary IMCD cells cultivated under hormonal and osmotic challenges to investigate their electrophysiological transport properties as well as subcellular localization of claudin-19 under these conditions. AVP partially influenced electrophysiological properties and did this in an osmolality depended manner: 300 mosm/kg—increase in cation selectivity (Figure 3), 600 mosm/kg—decrease in transcellular transport and increase in R_{te} (Figure 4). Claudin-19 subcellular localization, however, remained unaffected by the hormone. More strikingly, low osmolality increased R_{te} substantially and translocated claudin-19 to the tight junction, whereas high osmolality resulted in rather low R_{te} and removal of claudin-19 from the TJ to intracellular vesicles (Figures 6–8). In addition, paracellular selectivity changed from cation to anion selectivity with increasing extracellular osmolality.

Although the data are shown in comparison to isotonic conditions, we consider 600 mosm/kg as "physiological" osmolality for our experiments, a tonicity more attributed to the outer medulla [3] and the more outer parts of inner medulla. This is in line with former publications [25,30] and takes the cone-like structure of the inner medulla into account. However, towards the tip of the papilla, even

higher osmolalities are to be expected in rodents as rats, which excrete urine with osmolality values between 1500 and 2500 mosm/kg [27,31]. The electrophysiological findings of our primary cell culture under hyperosmotic conditions (600-IMCD and 900-IMCD) reproduced the findings from native, isolated perfused papillary collecting ducts rather well, with a slightly lumen positive V_{te} (< 1 mV) and R_{te} of about 148 Ωcm^2 [32]. We could corroborate the presence of claudin-19 protein in IMCD in native tissue (Figure 1) as well as in primary cell culture (Figures 3, 4 and 8). This is in accordance with the finding of Lee et al. [23] but did not find its way into the recently published expression profiles along the nephron where claudin-19 so far is not included in the collecting duct [28,29]. Our data is also in line with the transcriptome, which is negative for the tubule segments upstream the TAL but positive for the TAL and downstream, including IMCD. The lower metabolism of cells in the medulla might explain why protein abundance is high in comparison to the low mRNA levels found for claudin-19 in the IMCD transcriptome [24].

Acute effects of changes in osmolality on paracellular properties have been investigated mainly in established renal epithelia cell lines. In MDCK cells, mimicking proximal tubules, small steps of osmolality increase (10–20 mosm/kg by addition of glucose or mannitol) were tested to imitate diabetic nephropathy with conflicting results. After 24–72 h hyperosmotic challenge using glucose, R_{te} decreased, while cation selectivity increased (increase in claudin-2 expression and reduction in claudin-1 and -3; [33]). In contrast, mannitol increased R_{te} by decreasing claudin-2 expression and increasing claudin-1 within the same time-frame [34]. Collecting ducts face more pronounced changes in osmolality due to the unique urinary concentration mechanisms [4]. A lot of studies have been performed in IMCD3 cells, collecting duct cells originally derived from mouse inner medulla, challenging them acutely by increasing tonicity and looking for cellular adaptations within hours or the first days. Fast changes to higher osmolality triggered apoptotic events [35]; a combination of NaCl and urea was better tolerated [36]. Altogether, IMCD3 adapted well to higher osmolality if changes were induced stepwise [37]. In primary IMCD cells, changes in tonicity also lead to adaptation, partially to apoptosis and to vast changes in gene expression [8,26]. In our experiments, we observed tonicity-dependent changes in cell shape, with expanded and flat cells under high osmolality. This might be attributed to the higher susceptibility of the cells to undergo apoptosis. Still the epithelial monolayer was intact. In this study, we did not further investigate apoptosis, but we confined our experiments on physiological transport properties and tight junction protein expression. Adaptation described for IMCD3 also included changes in the TJ proteins [38,39]. Claudin-4 was thereby under the control of the scaffolding multi-PDZ domain protein 1 (MUPP-1) and showed higher expression in IMCD3 cells adapted to high osmolalities. In native murine papilla, claudin-4 expression was upregulated after water deprivation of mice [39]. In addition, we could show that ascending thin limbs reacted to water load by increasing the cation preference of their paracellular pathway [27]. Otherwise, not much is known about inner medullary adaptation of the paracellular pathway to changing environments. For this study, we focused our investigation mainly on claudin-19 in long-term adaptation experiments and on functional states.

Plasma isotonic conditions are most probably an environment rarely faced by IMCD cells in native inner medulla. One explanation for the changes seen here, especially functional ENaC expression (Figure 7A) and directed Na^+ transport (Figure 7B), could be that the cells undergo a transition to cortical collecting duct properties; a kind of 'corticalization'. All three ENaC subunits are expressed in all parts of the connecting tubule and the collecting duct [40]. However, without aldosterone stimulation, functional ENaC in the luminal membrane plays a crucial role mainly in the connecting tubule [41] and even in the cortical collecting duct of mice, lumen negative V_{te} as an indicator of the presence of ENaC is not measured [42] in the absence of aldosterone. As already mentioned, IMCDs did not show negative V_{te} [32]. Accordingly, water homeostasis has been implicated in the regulation of ENaC. Crambert et al. could show that water deprivation in mice increased ENaC expression in cortical, but not outer medullary CDs, and in a collecting cell line, hyperosmolality sufficed to reduce ENaC expression [43]. On the other side, low osmolality at the luminal side, but not necessarily at the

basolateral side, would be indicative for water diuresis, which would require a sealing against water flux and the assimilation of luminal and basolateral osmolalities [12].

How could known claudin-19 properties support collecting duct function? Under isotonic conditions, claudin-19 appears to be localized in the TJ (Figures 3 and 8). In TAL, claudin-19 confers Ca^{2+} and Mg^{2+} permeability to the tight junction, together with claudin-16 [22,44]. If claudin-19 alone is expressed in MDCK cells, it seems to act as cation barrier [18], whereas expression in a per-se anion selective background (porcine kidney cells, LLC-PK1), claudin-19 reduces anion selectivity [45]. Altogether, translocation of claudin-19 to the tight junction might be responsible for the increase in R_{te} and the accompanying cation selectivity. So far, no other direct interaction partners of claudin-19, in analogy to claudin-16/19 interaction, have been described. Obviously, the TJ structure and accessibility to detergents was remarkably different between the outer and the inner medulla (Figure 1). The TAL presents the main tubular component of the inner stripe of outer medulla (we excluded the outer stripe for a more secure exclusion of cortex), whereas in the inner medulla, the collecting duct is probably the main component by cell mass. Hence, outer medulla claudin-19 originates mainly from TAL and inner medulla claudin-19 mainly from IMCD, both showing completely different dissolving profiles. It has been proposed that the tight junction complex can be part of or be associated with cholesterol-enriched "lipid rafts" of plasma membranes. These lipid rafts consist of cholesterol and sphingomyelin to form a tightly packed membrane lipid region [46]. The extractability of, e.g., claudin-4, is strongly dependent on the detergent used for solubilization [47]. Triton solubility increases with lipid raft disruption. Sugibayashi et al. showed in MDCK cells that this disruption increased solubility to Triton for claudin-4, -5, and occludin, but not for claudin-1, -2, and -3, indicating that in this cell system, claudin-4 and claudin-5 were organized in lipid rafts, whereas claudin-1, -2, and -3 were not [48]. In analogy, we would propose that claudin-19 could be part of a lipid raft (TAL) or not (CD) depending on the structure and composition of the respective TJ.

Increasing osmolalities in the cultivation medium dramatically decreased R_{te} and increased ion permeability, especially for Cl^-. High osmolalities on both sides of the IMCD epithelium mimic conditions of strong antidiuresis, also independent of the original stimulus by AVP [49]. The gradual removal of claudin-19 into intracellular compartments and vesicular structures (Figure 8) could partially explain the reduction in R_{te}. However, literature and our own first findings emphasize the complexity of the regulation and composition of the paracellular pathway. A parallel increase in claudin-4 as described by Lanaspa et al. [39] could contribute in addition, especially with regard to the increase in anion selectivity. Claudin-8, a direct interaction partner of claudin-4, however, does not show regulation, at least on the level of subcellular localization (Figure 9). Under high osmotic conditions on both sides of the epithelium, osmotic pressure across the epithelium is low and, potentially, tricellular sealing, an additional route for water, ions, and macromolecules, could be less stringent [50]. One indicator for this could be the slightly increasing permeability for the high-molecular 40 kD FITC dextran marker in 600-IMCD and especially 900-IMCD. Other claudins (e.g., claudin-7) and expressional or post-translational regulations of TJ properties have to be considered in future studies to finally complete the picture.

Although AVP is the main controlling hormone of renal water handling [4,49], we could corroborate that local osmolality changes were able to regulate IMCD transport properties and claudin expression independently, similar to the findings of Lanaspa and coworkers [38,39]. Whereas in these studies TJ proteins have been described as targets for regulation, intriguingly, it has also been proposed that the TJ itself could serve as sensor for osmolality and tonicity changes, thereby becoming the origin of regulation (reviewed in [51]). In MDCK cells, acute changes in transepithelial osmotic gradients dramatically changed paracellular selectivity and claudin localization as well as cytoskeleton remodeling [52]. Besides these changes by cell culture osmolality, AVP itself showed effects on paracellular properties as it increased cation selectivity in 300-IMCD. However, these changes were independent of claudin-19, or at least not dependent on subcellular localization of the claudin. We speculate from findings in medullary TAL that mechanisms like claudin-19 phosphorylation could be part of the effect of AVP.

In TAL, we could show that AVP directly increased cation selectivity within minutes, without changing claudin-10b localization, indicating that phosphorylation rather than recruitment to the membrane may be involved [53].

In conclusion, we propose that claudin-19 is part of the collecting duct TJ complex. Its presence in the TJ is under the control of ambient interstitial tonicity. Under iso-osmotic conditions, it is responsible for a high electrical transepithelial resistance and contributes to the tonicity-induced changes in paracellular ion selectivity.

4. Materials and Methods

4.1. Animals

All experiments were performed in accordance with the German law on animal protection and approved by the local authorities (animal ethics protocol number V312-72241.121-2). C57 Bl6/J mice, Wistar or Sprague-Dawley rats were housed under a 12 h light cycle with free access to water and chow.

4.2. Cell Culture

Cell culture medium of 300 mosm/kg was used as basic medium. It consisted of high glucose DMEM (PAA Laboratories, Coelbe, Germany) enriched with 1% Ultroser G (CytoGen, Wetzlar, Germany), 1% nonessential amino acids (PAA Laboratories), 1% L-Glutamine (PAA Laboratories; 200 mmol/L), and 1% penicillin/streptomycin (PAA Laboratories). For 600 mosm/kg medium, 100 mmol/L NaCl and 100 mmol/L urea were added; for 900 mosm/kg medium, 200 mmol/L NaCl and 200 mmol/L urea were added, respectively.

IMCD cells for primary cell cultures were isolated as described previously [25,26]. Briefly, 200–300 g Wistar or Sprague-Dawley rats ($n = 20$) of both sexes were sacrificed. Under sterile conditions, the inner medulla of both kidneys was dissected, transferred to enzyme solution (0.2% hyaluronidase type I (Sigma Aldrich, St. Louis, MO, USA) and 0.2% collagenase type II (Biochrom AG, Berlin, Germany) in PBS and digested for 90 min in a thermoshaker (37 °C, 850 rpm). The suspension of cells and tubular fragments was washed in PBS twice by centrifugation und resuspension in 600 mosm/kg medium. Cells were seeded on collagen IV-coated (mouse collagen IV, BD Biosciences, Heidleberg, Germany; 0.2 µg/cm) Costar Transwell Permeable supports (Sigma Aldrich, St. Louis, USA); 0.33 cm^2) at densities of 350,000 cells/cm^2 or 600,000 cells/cm^2. Cells were cultivated at 37 °C and 8% CO_2. After a 24 h settlement period in 600 mosm/kg medium, cells were transferred to 300, 600, or 900 mosm/kg medium, respectively, and cultivation lasted 5–7 days in total. Medium was changed and transepithelial resistance was monitored daily (EVOM2µ, World Precision Instruments). All filters were checked for confluency after the experimental procedure by visual control for complete epithelial coverage of the filter. Filters with gaps in confluency were excluded from analysis.

4.3. Immunohistochemistry

After Ussing chamber measurements, the filters were fixed in 0.4% PFA in PBS at 4 °C overnight. In addition, cryosections (3 µm) of perfusion fixed kidneys of Sprague-Dawley rats and of C57Bl/6 J mice [54] were heated in 0.3% triton-x-100 in PBS (PBST-T) for antigen retrieval. Filters as well as kidney slices were washed extensively in PBS-T and blocked with 1% bovine serum albumin in PBS-T. Filters and cryosections were incubated with primary antibody in 1% BSA overnight at 4°C. The claudin-19 antibody, a kind gift of J. Hou (Department of Internal Medicine, Washington University Renal Division, USA), has been successfully used in a Claudin-19 KD animal model [21]) and was used in a dilution of 1:300, Antibodies used in addition: rabbit anti-aquaporin-, 1:100 (Alomone labs, Jerusalem, Israel), rabbit anti-claudin-8 and rabbit anti-ZO-1 (both Thermo Fisher, Waltham, USA), guinea pig anti-AE1 (kind gift of C. Wagner, University of Zürich, Institute of Physiology, Zürich, Switzerland). After three additional washing steps (PBS-T), filters were incubated with the respective secondary antibody (1:400; AlexaFluo 488, donkey anti-rabbit, AlexaFluo 633, goat anti-rabbit; AlexaFluo 488 goat anti-guinea

pig, Thermo Fisher) for 60 min at room temperature. After final extensive washing (PBS-T), filters and cryosections were embedded in Moviol-Dabco. Pictures were taken either confocally (LSM 510, Axiovert 200 M; Zeiss, Jena, Germany) or with Apotome2 (AX 10, Zeiss). Filters were analyzed for the subcellular staining pattern of claudin-19 in three categories as ordinal scale reflecting the functional expression of claudin-10 (see scheme in Figure 8: score 3 for membrane associated tight junction staining (clear lines), score 2 for submembrane staining (diffuse scattering lines), and score 1 for vesicular staining (dotted intracellular staining). For each filter the percentage of the different categories was given with 5–10% precision and each filter was attributed then an overall TJ score between 1 (all claudin-19 in intracellular vesicles) and 3 (all claudin-19 in TJ).

4.4. Western Blotting

Enzymatic and enzymatically assisted dissection was used to generate sorted tubular samples [27,55]. After flank incision under deep anesthesia the left kidney of Sprague-Dawley rats was perfused with enzyme solution: 2 mg/mL collagenase Type II in incubation solution (in mmol/L: 140 NaCl, 0.4 KH_2PO_4, 1.6 K_2HPO_4, 1 $MgSO_4$, 10 sodium acetate, 1 α-ketoglutarate, 1.3 calcium gluconate, 5 glycine, containing 48 mg/L trypsin inhibitor and 25 mg/L DNase I, pH 7.4, at 37 °C). Mice kidneys were similarly perfused via the abdominal vein [45]. Tubular segments from 6–8 week C57 Bl/6J or Sprague-Dawley rats were sorted after digestion as described in [45,55] or dissected manually from thin transversal kidney slices at 4 °C in sorting solution (incubation solution supplemented with 0.5 mg/L albumin). For Western blotting, approximately 20–50 tubules per segment were sorted and stored in 20–25 µL 1× Laemmli solution at −80 °C prior to use. For membrane protein solubilization, rat kidneys (6–8 week) were cut in transversal slices at 4 °C and under visual control the papilla (inner medulla, IM) and outer medulla (OM) were prepared, the later with a safety margin to cortex. Therefore, OM mainly comprises the inner stripe. Tissues were snap frozen in liquid nitrogen and stored at −80 °C. After thawing tissues were homogenized with a glass teflon homogenizer in Triton buffer (in mmol/L: 20 Tris–HCl, 50 NaCl, 2 EDTA, 1% Triton-x-100, pH 7.6, protease inhibitor cocktail (Roche, Basel, Switzerland) and incubated for 2 h on ice. After 30 min centrifugation at 21,000× *g* and 4 °C, the supernatant was transferred to a new reaction tube, a sample was kept for determination of protein content (NanoDrop, Thermo Scientific, Waltham, MA, USA) and the tube stored at −20 °C after addition of Laemmli concentrate. The remaining pellet was resuspended in SDS buffer (in mmol/L: 20 Tris–HCl, 50 NaCl, 2 EDTA, 1% SDS, pH 7.6, protease inhibitor cocktail (Roche)), incubated for one additional hour at 4 °C, and then processed as described for the Triton samples. After thawing and denaturation, samples were separated in 15% polyacrylamide minigels and electrophoretically transferred to nitrocellulose membranes. Membranes were blocked for 60 min with 5% BSA in PBS–Tween (0.1% Tween in PBS) and incubated with primary antibody (anti-claudin-19, 1:2000) at 4 °C overnight. Membranes were further incubated for 2 h at RT with the secondary antibodies (Dianova, goat anti-rabbit-HRP) and imaged using a ChemiDoc Imaging system (Biorad, Herkules, USA). Procedure was repeated with anti-β-actin for loading control.

4.5. Electrophysiology

IMCD cells grown on filter supports were measured in a modified Ussing Chamber (EP Devices, Leuven, Belgium). Measurements were performed under the osmolality corresponding to the respective cultivation conditions and experimental solutions are enlisted in Table 1. After a short equilibration period, luminal amiloride (50 µmol/L) was applied to inhibit ENaC driven transepithelial Na^+ transport. In the presence of luminal amiloride, the transepithelial voltage was close to zero in all cases. Next, diffusion potentials were obtained by consecutively replacing the luminal solution by low-NaCl solution and application of a 1:5 luminal to basolateral NaCl concentration gradient (iso-osmotic; 30, 50, and 70 mmol/L NaCl, respectively, see Table 1). All obtained potentials were corrected for their respective calculated liquid junction potentials [56]. Permeability ratio P_{Na}/P_{Cl} was calculated using the Goldman–Hodgkin–Katz flux equation. Absolute permeability of Na^+ was obtained using the

simplified Kimizuka–Koketsu equation [54,57]. Absolute permeability for Cl^- was calculated from the respective permeability ratio and P_{Na}.

4.6. FITC Dextran Permeability Measurement

The 40 kDa FITC–dextran conjugate ((Sigma Aldrich, St. Louis, USA) stock solution was dialyzed (8000–10,000 MWCO) to remove free FITC. Under cell culture conditions, 26 μM FITC dextran was added to the luminal compartment of nine filters per osmolality condition. Fluorescence in the basolateral compartment was measured at time points 0 and 30 min in a plate reader (Tecan, Männedorf, Switzerland). Calibration curves were conducted to calculate FITC–dextran concentration. FITC–dextran flow rate was given as change in concentration over time in the chamber volume. Permeability coefficient (P) was calculated relating the flow rate to the respective filter area and the initial concentration difference as driving force. Permeability of empty filters under the different osmolality conditions was determined accordingly.

4.7. Electrolyte Measurement

Luminal and basolateral cell culture supernatants of the last 24 h of cultivation were collected, Na^+ and K^+ concentrations measured by flame photometry (EFOX 5053, Eppendorf, Hamburg, Germany), and basolateral to luminal differences in electrolyte concentrations were calculated.

4.8. Statistics

Electrophysiological data are presented as means ± SEM. Two groups were tested by unpaired *t*-test or Mann–Whitney test. Three groups were tested with one-way ANOVA followed by Tukey post-hoc testing or Kruskal–Wallis test and Dunn's post-hoc test. All statistical analyses were performed using GraphPad Prism including the test for normal distribution (D'Agostino & Pearson normality test). Immunofluorescence subcellular staining data are presented as a stacked-column graph, giving the respective category as a percentage. Filter-scores were tested with nonparametric Mann–Whitney *U*-Test or Kruskal–Wallis test and Dunn's post-hoc test.

Author Contributions: Conceptualization, A.Z., S.R.S., N.H. and B.E.; Methodology, A.Z., S.R.S., M.B.; Software, N.H. and S.R.S; Validation, N.H. and M.B.; Formal Analysis, A.Z., S.R.S. and N.H.; Investigation, A.Z., S.R.S., V.C.W. and N.H.; Resources, M.B.; Data Curation, N.H., A.Z., S.R.S. and V.C.W.; Writing—Original Draft Preparation, A.Z., S.R.S. and N.H.; Writing—Review & Editing, V.C.W., B.E. and M.B.; Visualization, A.Z., S.R.S. and N.H.; Supervision, M.B. and N.H.; Project Administration, N.H., M.B.; Funding Acquisition, M.B.

Funding: This research received no external funding

Acknowledgments: We greatly appreciate the expert technical assistance from T. Stegman and R. Lingg as well as the support by the animal facility of the Christian-Albrechts-University Kiel. We thank Jianghui Hou, Division of Nephrology, Washington University School of Medicine, St. Louis, USA, for providing the claudin-19 antibody. Funding was provided by the Christian-Albrechts-University Kiel.

Conflicts of Interest: The authors declare no conflicts of interest.

Abbreviations

IMCD	Inner medullary collecting duct
AVP	Arginine vasopressin
PG2	Prostaglandin E2
TJ	Tight junction
TAL	Thick ascending limb
PT	Proximal tubule
PCT	Proximal convoluted tubule

PST	Proximal straight
DCT	Distal convoluted tubule
CNT/CD	Connecting tubule and cortical collecting duct
mCD	Medullary collecting duct (outer stripe of outer medulla)
SDS	sodium dodecyl sulfate
AQP2	Aquaporin 2
V_{te}	Transepithelial voltage
R_{te}	Transepithelial resistance
I'_{sc}	Equivalent short circuit current
TER	Transepithelial resistance (cell culture)
DP	Diffusion potential

References

1. Dantzler, W.H.; Pannabecker, T.L.; Layton, A.T.; Layton, H.E. Urine concentrating mechanism in the inner medulla of the mammalian kidney: Role of three-dimensional architecture. *Acta Physiol.* **2011**, *202*, 361–378. [CrossRef] [PubMed]
2. Pannabecker, T.L. Comparative physiology and architecture associated with the mammalian urine concentrating mechanism: Role of inner medullary water and urea transport pathways in the rodent medulla. *Am. J. Physiol. Regul. Integr. Comp. Physiol.* **2013**, *304*, R488–R503. [CrossRef] [PubMed]
3. Sands, J.M.; Layton, H.E. The physiology of urinary concentration: An update. *Semin. Nephrol.* **2009**, *29*, 178–195. [CrossRef] [PubMed]
4. Fenton, R.A.; Knepper, M.A. Mouse models and the urinary concentrating mechanism in the new millennium. *Physiol. Rev.* **2007**, *87*, 1083–1112. [CrossRef] [PubMed]
5. Sheen, M.R.; Kim, J.-A.; Lim, S.W.; Jung, J.-Y.; Han, K.-H.; Jeon, U.S.; Park, S.-H.; Kim, J.; Kwon, H.M. Interstitial tonicity controls TonEBP expression in the renal medulla. *Kidney Int.* **2009**, *75*, 518–525. [CrossRef] [PubMed]
6. Maril, N.; Margalit, R.; Mispelter, J.; Degani, H. Sodium magnetic resonance imaging of diuresis: Spatial and kinetic response. *Magn. Reson. Med.* **2005**, *53*, 545–552. [CrossRef] [PubMed]
7. Berl, T. How Do Kidney Cells Adapt to Survive in Hypertonic Inner Medulla? *Trans. Am. Clin. Climatol. Assoc.* **2009**, *120*, 389. [PubMed]
8. Schulze Blasum, B.; Schröter, R.; Neugebauer, U.; Hofschröer, V.; Pavenstädt, H.; Ciarimboli, G.; Schlatter, E.; Edemir, B. The kidney-specific expression of genes can be modulated by the extracellular osmolality. *FASEB J.* **2016**, *30*, 3588–3597. [CrossRef] [PubMed]
9. Günzel, D.; Yu, A.S.L. Claudins and the modulation of tight junction permeability. *Physiol. Rev.* **2013**, *93*, 525–569. [CrossRef]
10. Günzel, D.; Fromm, M. Claudins and other tight junction proteins. *Compr. Physiol.* **2012**, *2*, 1819–1852.
11. González-Mariscal, L.; Tapia, R.; Chamorro, D. Crosstalk of tight junction components with signaling pathways. *Biochim. Biophys. Acta* **2008**, *1778*, 729–756. [CrossRef] [PubMed]
12. Gong, Y.; Himmerkus, N.; Sunq, A.; Milatz, S.; Merkel, C.; Bleich, M.; Hou, J. ILDR1 is important for paracellular water transport and urine concentration mechanism. *Proc. Natl. Acad. Sci. USA* **2017**, *114*, 5271–5276. [CrossRef] [PubMed]
13. Flamion, B.; Spring, K.R.; Abramow, M. Adaptation of inner medullary collecting duct to dehydration involves a paracellular pathway. *Am. J. Physiol.* **1995**, *268*, F53–F63. [CrossRef] [PubMed]
14. Muto, S. Physiological roles of claudins in kidney tubule paracellular transport. *Am. J. Physiol. Ren. Physiol.* **2017**, *312*, F9–F24. [CrossRef] [PubMed]
15. Hou, J.; Renigunta, A.; Yang, J.; Waldegger, S. Claudin-4 forms paracellular chloride channel in the kidney and requires claudin-8 for tight junction localization. *Proc. Natl. Acad. Sci. USA* **2010**, *107*, 18010–18015. [CrossRef] [PubMed]
16. Luk, J.M.; Tong, M.-K.; Mok, B.W.; Tam, P.-C.; Yeung, W.S.B.; Lee, K.-F. Sp1 site is crucial for the mouse claudin-19 gene expression in the kidney cells. *FEBS Lett.* **2004**, *578*, 251–256. [CrossRef] [PubMed]

17. Konrad, M.; Schaller, A.; Seelow, D.; Pandey, A.V.; Waldegger, S.; Lesslauer, A.; Vitzthum, H.; Suzuki, Y.; Luk, J.M.; Becker, C.; et al. Mutations in the tight-junction gene claudin 19 (CLDN19) are associated with renal magnesium wasting, renal failure, and severe ocular involvement. *Am. J. Hum. Genet.* **2006**, *79*, 949–957. [CrossRef] [PubMed]
18. Angelow, S.; El-Husseini, R.; Kanzawa, S.A.; Yu, A.S.L. Renal localization and function of the tight junction protein, claudin-19. *Am. J. Physiol. Ren. Physiol.* **2007**, *293*, F166–F177. [CrossRef] [PubMed]
19. Hou, J.; Renigunta, A.; Konrad, M.; Gomes, A.S.; Schneeberger, E.E.; Paul, D.L.; Waldegger, S.; Goodenough, D.A. Claudin-16 and claudin-19 interact and form a cation-selective tight junction complex. *J. Clin. Investig.* **2008**, *118*, 619–628. [CrossRef]
20. Weber, S.; Hoffmann, K.; Jeck, N.; Saar, K.; Boeswald, M.; Kuwertz-Broeking, E.; Meij, I.I.C.; Knoers, N.V.A.M.; Cochat, P.; Suláková, T.; et al. Familial hypomagnesaemia with hypercalciuria and nephrocalcinosis maps to chromosome 3q27 and is associated with mutations in the PCLN-1 gene. *Eur. J. Hum. Genet.* **2000**, *8*, 414–422. [CrossRef]
21. Hou, J.; Renigunta, A.; Gomes, A.S.; Hou, M.; Paul, D.L.; Waldegger, S.; Goodenough, D.A. Claudin-16 and claudin-19 interaction is required for their assembly into tight junctions and for renal reabsorption of magnesium. *Proc. Natl. Acad. Sci. USA* **2009**, *106*, 15350–15355. [CrossRef] [PubMed]
22. Günzel, D.; Haisch, L.; Pfaffenbach, S.; Krug, S.M.; Milatz, S.; Amasheh, S.; Hunziker, W.; Müller, D. Claudin function in the thick ascending limb of Henle's loop. *Ann. N. Y. Acad. Sci.* **2009**, *1165*, 152–162. [CrossRef] [PubMed]
23. Lee, N.P.Y.; Tong, M.K.; Leung, P.P.; Chan, V.W.; Leung, S.; Tam, P.-C.; Chan, K.-W.; Lee, K.-F.; Yeung, W.S.B.; Luk, J.M. Kidney claudin-19: Localization in distal tubules and collecting ducts and dysregulation in polycystic renal disease. *FEBS Lett.* **2006**, *580*, 923–931. [CrossRef] [PubMed]
24. Lee, J.W.; Chou, C.-L.; Knepper, M.A. Deep Sequencing in Microdissected Renal Tubules Identifies Nephron Segment-Specific Transcriptomes. *J. Am. Soc. Nephrol.* **2015**, *26*, 2669–2677. [CrossRef] [PubMed]
25. Maric, K.; Oksche, A.; Rosenthal, W. Aquaporin-2 expression in primary cultured rat inner medullary collecting duct cells. *Am. J. Physiol.* **1998**, *275*, F796–F801. [CrossRef] [PubMed]
26. Schenk, L.K.; Rinschen, M.M.; Klokkers, J.; Kurian, S.M.; Neugebauer, U.; Salomon, D.R.; Pavenstaedt, H.; Schlatter, E.; Edemir, B. Cyclosporin-A Induced Toxicity in Rat Renal Collecting Duct Cells: Interference with Enhanced Hypertonicity Induced Apoptosis. *Cell. Physiol. Biochem.* **2010**, *26*, 887–900. [CrossRef]
27. Sonntag, S.R.; Ziemens, A.; Wulfmeyer, V.C.; Milatz, S.; Bleich, M.; Himmerkus, N. Diuretic state affects ascending thin limb tight junctions. *Am. J. Physiol. Renal Physiol.* **2018**, *314*, F190–F195. [CrossRef]
28. Gong, Y.; Hou, J. Claudins in barrier and transport function-the kidney. *Pflug. Arch.* **2017**, *469*, 105–113. [CrossRef]
29. Yu, A.S.L. Claudins and the kidney. *J. Am. Soc. Nephrol.* **2015**, *26*, 11–19. [CrossRef]
30. Ruhfus, B.; Bauernschmitt, H.G.; Kinne, R.K. Properties of a polarized primary culture from rat renal inner medullary collecting duct (IMCD) cells. *Cell. Dev. Biol. Anim.* **1998**, *34*, 227–231. [CrossRef]
31. Cil, O.; Ertunc, M.; Onur, R. The diuretic effect of urea analog dimethylthiourea in female Wistar rats. *Hum. Exp. Toxicol.* **2012**, *31*, 1050–1055. [CrossRef]
32. Husted, R.F.; Hayashi, M.; Stokes, J.B. Characteristics of papillary collecting duct cells in primary culture. *Am. J. Physiol.* **1988**, *255*, F1160–F1169. [CrossRef] [PubMed]
33. Mongelli-Sabino, B.M.; Canuto, L.P.; Collares-Buzato, C.B. Acute and chronic exposure to high levels of glucose modulates tight junction-associated epithelial barrier function in a renal tubular cell line. *Life Sci.* **2017**, *188*, 149–157. [CrossRef] [PubMed]
34. Canuto, L.P.; Collares-Buzato, C.B. Increased osmolality enhances the tight junction-mediated barrier function in a cultured renal epithelial cell line. *Cell Biol. Int.* **2019**, *43*, 73–82. [CrossRef] [PubMed]
35. Michea, L.; Ferguson, D.R.; Peters, E.M.; Andrews, P.M.; Kirby, M.R.; Burg, M.B. Cell cycle delay and apoptosis are induced by high salt and urea in renal medullary cells. *Am. J. Physiol. Ren. Physiol.* **2000**, *278*, F209–F218. [CrossRef] [PubMed]
36. Santos, B.C.; Chevaile, A.; Hébert, M.J.; Zagajeski, J.; Gullans, S.R. A combination of NaCl and urea enhances survival of IMCD cells to hyperosmolality. *Am. J. Physiol.* **1998**, *274*, F1167–F1173. [CrossRef] [PubMed]
37. Capasso, J.M.; Rivard, C.J.; Berl, T. Long-term adaptation of renal cells to hypertonicity: Role of MAP kinases and Na-K-ATPase. *Am. J. Physiol. Ren. Physiol.* **2001**, *280*, F768–F776. [CrossRef] [PubMed]

38. Lanaspa, M.A.; Almeida, N.E.; Andres-Hernando, A.; Rivard, C.J.; Capasso, J.M.; Berl, T. The tight junction protein, MUPP1, is up-regulated by hypertonicity and is important in the osmotic stress response in kidney cells. *Proc. Natl. Acad. Sci. USA* **2007**, *104*, 13672–13677. [CrossRef] [PubMed]
39. Lanaspa, M.A.; Andres-Hernando, A.; Rivard, C.J.; Dai, Y.; Berl, T. Hypertonic stress increases claudin-4 expression and tight junction integrity in association with MUPP1 in IMCD3 cells. *Proc. Natl. Acad. Sci. USA* **2008**, *105*, 15797–15802. [CrossRef]
40. Hager, H.; Kwon, T.H.; Vinnikova, A.K.; Masilamani, S.; Brooks, H.L.; Frøkiaer, J.; Knepper, M.A.; Nielsen, S. Immunocytochemical and immunoelectron microscopic localization of alpha-, beta-, and gamma-ENaC in rat kidney. *Am. J. Physiol. Ren. Physiol.* **2001**, *280*, F1093–F1106. [CrossRef]
41. Ronzaud, C.; Loffing, J.; Bleich, M.; Gretz, N.; Gröne, H.-J.; Schütz, G.; Berger, S. Impairment of sodium balance in mice deficient in renal principal cell mineralocorticoid receptor. *J. Am. Soc. Nephrol.* **2007**, *18*, 1679–1687. [CrossRef] [PubMed]
42. Leviel, F.; Hübner, C.A.; Houillier, P.; Morla, L.; El Moghrabi, S.; Brideau, G.; Hatim, H.; Parker, M.D.; Kurth, I.; Kougioumtzes, A.; et al. The Na^+-dependent chloride-bicarbonate exchanger SLC4A8 mediates an electroneutral Na^+ reabsorption process in the renal cortical collecting ducts of mice. *J. Clin. Investig.* **2010**, *120*, 1627–1635. [CrossRef] [PubMed]
43. Crambert, G.; Ernandez, T.; Lamouroux, C.; Roth, I.; Dizin, E.; Martin, P.-Y.; Féraille, E.; Hasler, U. Epithelial sodium channel abundance is decreased by an unfolded protein response induced by hyperosmolality. *Physiol. Rep.* **2014**, *2*, e12169. [CrossRef] [PubMed]
44. Milatz, S.; Himmerkus, N.; Wulfmeyer, V.C.; Drewell, H.; Mutig, K.; Hou, J.; Breiderhoff, T.; Müller, D.; Fromm, M.; Bleich, M.; et al. Mosaic expression of claudins in thick ascending limbs of Henle results in spatial separation of paracellular Na^+ and Mg^{2+} transport. *Proc. Natl. Acad. Sci. USA* **2017**, *114*, E219–E227. [CrossRef] [PubMed]
45. Gong, Y.; Renigunta, V.; Himmerkus, N.; Zhang, J.; Renigunta, A.; Bleich, M.; Hou, J. Claudin-14 regulates renal Ca(+)(+) transport in response to CaSR signalling via a novel microRNA pathway. *EMBO J.* **2012**, *31*, 1999–2012. [CrossRef] [PubMed]
46. Nusrat, A.; Parkos, C.A.; Verkade, P.; Foley, C.S.; Liang, T.W.; Innis-Whitehouse, W.; Eastburn, K.K.; Madara, J.L. Tight junctions are membrane microdomains. *J. Cell Sci.* **2000**, *113*, 1771–1781. [PubMed]
47. Mitic, L.L. Expression, solubilization, and biochemical characterization of the tight junction transmembrane protein claudin-4. *Protein Sci.* **2003**, *12*, 218–227. [CrossRef] [PubMed]
48. Sugibayashi, K.; Onuki, Y.; Takayama, K. Displacement of tight junction proteins from detergent-resistant membrane domains by treatment with sodium caprate. *Eur. J. Pharm. Sci.* **2009**, *36*, 246–253. [CrossRef]
49. Wilson, J.L.L.; Miranda, C.A.; Knepper, M.A. Vasopressin and the regulation of aquaporin-2. *Clin. Exp. Nephrol.* **2013**, *17*, 751–764. [CrossRef]
50. Krug, S.M.; Amasheh, S.; Richter, J.F.; Milatz, S.; Günzel, D.; Westphal, J.K.; Huber, O.; Schulzke, J.D.; Fromm, M. Tricellulin forms a barrier to macromolecules in tricellular tight junctions without affecting ion permeability. *Mol. Biol. Cell* **2009**, *20*, 3713–3724. [CrossRef]
51. Tokuda, S.; Yu, A.S.L. Regulation of Epithelial Cell Functions by the Osmolality and Hydrostatic Pressure Gradients: A Possible Role of the Tight Junction as a Sensor. *Int. J. Mol. Sci.* **2019**, *20*, 3513. [CrossRef] [PubMed]
52. Tokuda, S.; Hirai, T.; Furuse, M. Effects of osmolality on paracellular transport in MDCK II cells. *PLoS ONE* **2016**, *11*, 1–21. [CrossRef] [PubMed]
53. Himmerkus, N.; Plain, A.; Marques, R.D.; Sonntag, S.R.; Paliege, A.; Leipziger, J.; Bleich, M. AVP dynamically increases paracellular Na^+ permeability and transcellular NaCl transport in the medullary thick ascending limb of Henle's loop. *Pflug. Arch.* **2017**, *469*, 149–158. [CrossRef] [PubMed]
54. Plain, A.; Wulfmeyer, V.C.; Milatz, S.; Klietz, A.; Hou, J.; Bleich, M.; Himmerkus, N. Corticomedullary difference in the effects of dietary Ca^{2+} on tight junction properties in thick ascending limbs of Henle's loop. *Pflug. Arch.* **2016**, *468*, 293–303. [CrossRef] [PubMed]
55. Pohl, M.; Kaminski, H.; Castrop, H.; Bader, M.; Himmerkus, N.; Bleich, M.; Bachmann, S.; Theilig, F. Intrarenal renin angiotensin system revisited: Role of megalin-dependent endocytosis along the proximal nephron. *J. Biol. Chem.* **2010**, *285*, 41935–41946. [CrossRef] [PubMed]

56. Barry, P.H.; Lynch, J.W. Liquid junction potentials and small cell effects in patch-clamp analysis. *J. Membr. Biol.* **1991**, *121*, 101–117. [CrossRef]
57. Kimizuka, H.; Koketsu, K. Ion transport through cell membrane. *J. Theor. Biol.* **1964**, *6*, 290–305. [CrossRef]

International Journal of
Molecular Sciences

MDPI

Article

Claudin-12 Knockout Mice Demonstrate Reduced Proximal Tubule Calcium Permeability

Allein Plain [1], Wanling Pan [1], Deborah O'Neill [1], Megan Ure [1], Megan R. Beggs [1,2], Maikel Farhan [2,3], Henrik Dimke [4,5], Emmanuelle Cordat [1] and R. Todd Alexander [1,2,3,*]

1 Department of Physiology, The University of Alberta, Edmonton, AB T6J 2R7, Canada; aplain@gmail.com (A.P.); pan2@ualberta.ca (W.P.); oneilld@ualberta.ca (D.O.); ure@ualberta.ca (M.U.); mbeggs@ualberta.ca (M.R.B.); cordat@ualberta.ca (E.C.)
2 The Women's & Children's Health Research Institute, 11405-87 Avenue, Edmonton, AB T6G 1C9 Canada; maikel@ualberta.ca
3 Department of Pediatrics, The University of Alberta, Edmonton, AB T6J 2R7, Canada
4 Department of Cardiovascular and Renal Research, Institute of Molecular Medicine, University of Southern Denmark, 5230 Odense, Denmark; hdimke@health.sdu.dk
5 Department of Nephrology, Odense University Hospital, 5000 Odense, Denmark
* Correspondence: todd2@ualberta.ca; Tel.: +1-(780)-248-5560

Received: 17 January 2020; Accepted: 15 March 2020; Published: 18 March 2020

Abstract: The renal proximal tubule (PT) is responsible for the reabsorption of approximately 65% of filtered calcium, primarily via a paracellular pathway. However, which protein(s) contribute this paracellular calcium pore is not known. The claudin family of tight junction proteins confers permeability properties to an epithelium. Claudin-12 is expressed in the kidney and when overexpressed in cell culture contributes paracellular calcium permeability (P_{Ca}). We therefore examined claudin-12 renal localization and its contribution to tubular paracellular calcium permeability. Claudin-12 null mice (KO) were generated by replacing the single coding exon with β-galactosidase from *Escherichia coli*. X-gal staining revealed that claudin-12 promoter activity colocalized with aquaporin-1, consistent with the expression in the PT. PTs were microperfused ex vivo and P_{Ca} was measured. P_{Ca} in PTs from KO mice was significantly reduced compared with WT mice. However, urinary calcium excretion was not different between genotypes, including those on different calcium containing diets. To assess downstream compensation, we examined renal mRNA expression. Claudin-14 expression, a blocker of P_{Ca} in the thick ascending limb (TAL), was reduced in the kidney of KO animals. Thus, claudin-12 is expressed in the PT, where it confers paracellular calcium permeability. In the absence of claudin-12, reduced claudin-14 expression in the TAL may compensate for reduced PT calcium reabsorption.

Keywords: proximal tubule; calcium permeability; claudin-12

1. Introduction

Calcium is essential for a myriad of physiological functions including intracellular signal transduction, blood clotting, and as a structural component of bone. It is therefore tightly maintained within a narrow physiologic range in serum. This is achieved through hormonal regulation by parathyroid hormone (PTH), vitamin D, and fibroblast growth factor 23 (FGF23). These hormones, in turn, mediate coordinated interactions between intestinal calcium absorption/secretion, bone resorption/deposition and filtration at the renal glomerulus, and consequent reabsorption along the nephron. The majority, approximately two-thirds of filtered calcium, is reabsorbed by the proximal tubule [1]. This occurs via a paracellular route, primarily driven by the reabsorption of water from the proximal tubule [2–6]. A failure to reabsorb calcium from the proximal tubule has been implicated in

the pathogenesis of kidney stone formation [7]. Thus, understanding the molecular mediators of this process is a prerequisite to finding improved therapies for this disease.

Paracellular fluxes not only rely on a driving force, but are also dependent on the permeability of the epithelium to the ion being transported. The proximal tubule has significant permeability to Ca^{2+}, enabling paracellular Ca^{2+} flux [1,3–5]. Claudins are a family of four pass membrane proteins expressed in the tight junction that confer paracellular permeability to the tight junction [8]. Claudin-2 is expressed in the proximal tubule and claudin-2 knockout (KO) mice display increased urinary calcium excretion relative to their wild type littermates, consistent with claudin-2 conferring calcium permeability to the proximal tubule [8,9]. Claudin-2 and claudin-12 are expressed in the intestine, and are implicated in mediating calcium permeability [10,11]. Claudin-12 mRNA has been detected in the kidney [2,12]. We have previously reported claudin-12 expression in a renal proximal tubular cell culture model, opossum kidney (OK) cells [13], and mRNA expression has been identified in proximal tubules, where it could also contribute paracellular Ca^{2+} permeability [14].

To study claudin-12 renal expression and if it contributes Ca^{2+} permeability to the renal tubule, claudin-12 KO mice were generated by replacing the single coding exon with β-galactosidase from *E. coli*. The knockout mice grew and behaved similarly to their wild type (WT) littermates. We did not detect differences in plasma electrolytes nor in calciotropic hormone levels between KO and WT mice. We observed predominant X-gal staining in the renal cortex that colocalized with aquaporin-1, indicating expression of claudin-12 in the renal proximal tubule. We therefore perfused proximal tubules from claudin-12 KO mice and found reduced paracellular Ca^{2+} permeability. The KO mice did not however have increased urinary Ca^{2+} excretion. We thus examined the expression of genes that participate in tubular Ca^{2+} transport and found decreased expression of the paracellular Ca^{2+} blocker, claudin-14 [15], and propose that increased thick ascending limb (TAL) Ca^{2+} reabsorption compensates for reduced proximal tubular Ca^{2+} reabsorption in claudin-12 knockout mice.

2. Results

2.1. Generation of a Global Claudin-12 Knockout Model

In order to examine the renal localization and potential tubular transport role of claudin-12, we generated a global claudin-12 knockout mouse. The claudin-12 gene (*Cldn12*) was replaced by homologous recombination of exon 4, the only coding exon of the *Cld12* gene, with the β-galactosidase coding sequence from *E. coli* (Figure 1A). Specific PCR reactions failed to amplify the wild type sequence from KO animals. Similarly, PCR with primers specific for β-galactosidase did not amplify a product from wild type DNA. However, appropriate size PCR fragments could be amplified from both the wild type *Cld12* gene and β-galactosidase from heterozygous mice (Figure 1C). Moreover, quantitative real-time PCR performed on cDNA generated from RNA isolated from whole kidney of wild type mice detected *Cld12* that was not detectable in knockout mice (Figure 1B), consistent with known renal *Cld12* expression [2]. Unfortunately, we have been unable to identify a commercially available antibody or generate an antibody that was specific for claudin-12, as was previously reported by Professor Tsukita's group [16], and more recently by a group studying claudin-12 in nervous tissue [17]. We therefore performed a sequencing reaction on DNA from wild type and claudin-12 KO mice using a primer specific for a sequence approximately 50 bp 5′ to the start cogon in exon 4 of claudin-12. This confirmed that the claudin-12 coding sequence had been replaced with β-galactosidase (Figure 1D).

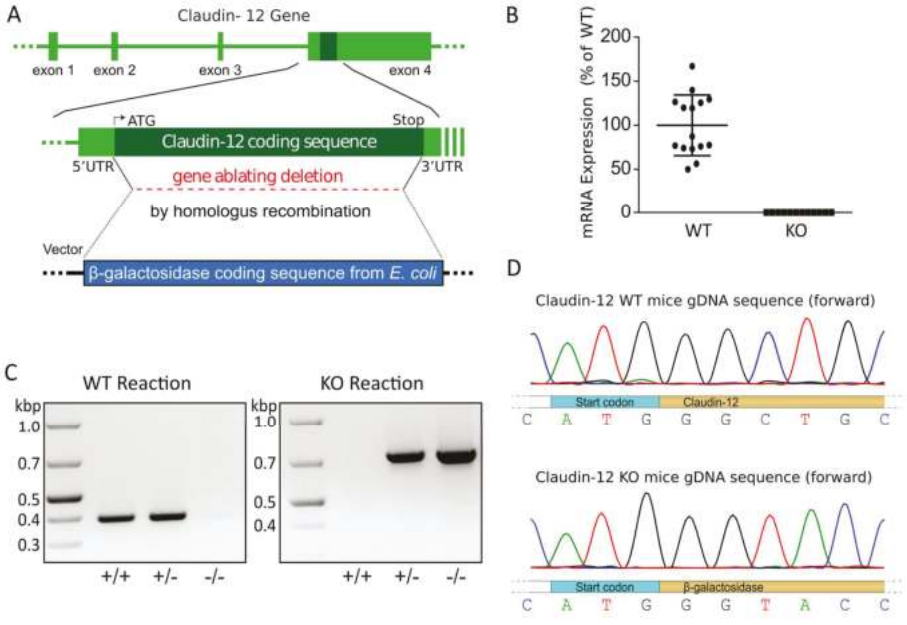

Figure 1. Claudin-12 knockout mouse model. (**A**) Claudin-12 gene deletion targeting strategy. (**B**) Relative claudin-12 mRNA expression normalized to GAPDH, from kidneys of wild type (WT) or claudin-12 knockout mice (KO). (**C**) Genotyping reactions of wild type (+/+), heterozygous (+/−), or claudin-12 knockout (−/−) mice using specific primers for the coding exon of claudin-12 (WT reaction) or the β-galactosidase coding sequence from *E. coli* (KO reaction). (**D**) Sequencing results of the gDNA sequence of claudin-12 WT or KO mice.

2.2. Claudin-12 is Expressed in the Renal Proximal Tubule

In order to localize claudin-12 expression in the kidney, we performed X-gal staining of kidney sections on wild type mice and heterozygous littermates (Figure 2). No staining was evident on the wild type kidney section (Figure 2A). However, we observed prominent staining in the knockout renal cortex, consistent with claudin-12 promoter activity (Figure 2B). Interestingly, the greatest amount of color production was in the juxtamedullary region, with virtually no color produced in the medulla. Higher power images of the cortical region clearly demonstrate β-galactosidase expression concentrated in some, but not all, of the tubules present in the juxtamedullary cortex (Figure 2C). The tubules with greatest β-galactosidase expression were the largest, had an obvious brush border, and were the most abundant in the cortex, consistent with claudin-12 promoter activity in the proximal tubule.

In order to more precisely define claudin-12 renal cortical expression, we performed immunofluorescence localization with tubule segment-specific markers on renal sections from heterozygous mice, after X-gal staining. Aquaporin I (AQP1), a marker of the proximal tubule in the renal cortex [18], colocalized with X-gal production (Figure 3A), confirming predominant localization to the proximal tubule. AQP1 is also present in the thin descending limb in loop of Henle [18], but we limited our assessment to the cortex. For the identification of the thick ascending limb, distal convoluted tubule, and collecting duct, we performed immunostaining with the sodium–potassium–chloride cotransporter II (NKCC2, Figure 3B), the sodium–chloride cotransporter (NCC, Figure 3C), and carbonic anhydrase II (CAII, Figure 3D), respectively. Although CAII is present in the proximal tubule, expression is very low and the greatest expression by far is in the collecting duct (intercalated cells); thus, CAII can be used as a marker of this segment [19]. We observed AQP1 co-staining with X-gal stained tubules. However, none of the other markers demonstrated significant

X-gal co-staining, which is consistent with predominant, if not exclusive, expression of claudin-12 in the renal proximal tubule. Importantly, this method of colocalization cannot exclude low levels of claudin-12 mRNA expression.

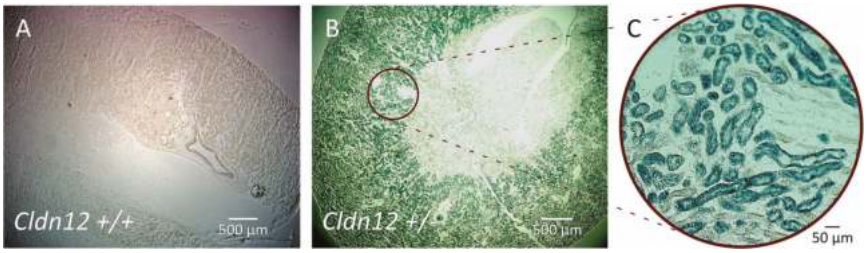

Figure 2. X-gal staining of kidney sections from wild type (**A**) and heterozygous (**B**) mice. β-galactosidase is expressed in the renal cortex in knockout kidney slices and not in wild type ones. Higher power image (**C**).

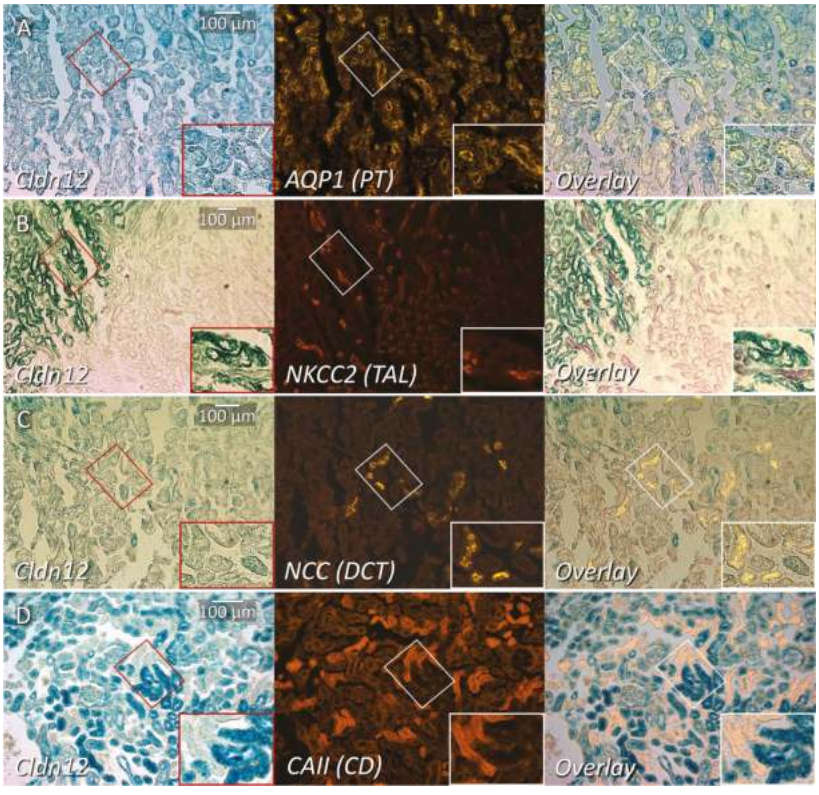

Figure 3. Co-staining of cortical renal tubule markers with X-gal on kidney slices from claudin-12 heterozygous mice. X-gal staining representing claudin-12 promoter expression (Cld12) co-stained with: (**A**) aquaporin-1 (AQP1), (**B**) sodium–potassium–chloride cotransporter 2 (NKCC2), (**C**) sodium–chloride cotransporter (NCC), or (**D**) carbonic anhydrase II (CAII); markers of the proximal tubule (PT), thick ascending limb (TAL), distal collecting tubule (DCT) and collecting duct respectively. The box in the right lower corner is a digitally magnified image from the smaller area depicted with the same shape.

2.3. Claudin-12 Deletion Decreases Sodium and Calcium Permeability of the Proximal Tubule

We next turned our attention to the putative role of claudin-12 in the proximal tubule. To this end, we microperfused freshly isolated straight proximal tubules (Figure 4A) from either wild type (WT) or knockout (KO) mice, as this is the segment which demonstrated the most intense X-gal staining. We recorded transepithelial voltage across the tubule (Figure 4B,C) and used a current pulse (13 nA) to calculate the transepithelial resistance. The transepithelial resistance, transepithelial voltage, and short-circuit current determined before and after the addition of ouabain were indistinguishable between WT and KO animals (Figure 4D–F). Ouabain inhibits the Na^+/K^+ATPase, eliminating transepithelial Na^+ transport (as it is the driving force for vectorial Na^+ flux). Importantly, as we were applying a dilution potential across the tubule to measure permeability, not flux, this did not alter our measurement. Ouabain dramatically reduced the transepithelial voltage and consequently the short-circuit current. This is consistent with transcellular transport being substantially reduced, as would be expected. Thus, any subsequent changes in transepithelial voltage generated after the addition of ouabain are primarily due to the paracellular movement of ions induced by the change in the basolateral solution composition. Importantly, the decrease in transcellular transport was not statistically different between WT and KO tubules.

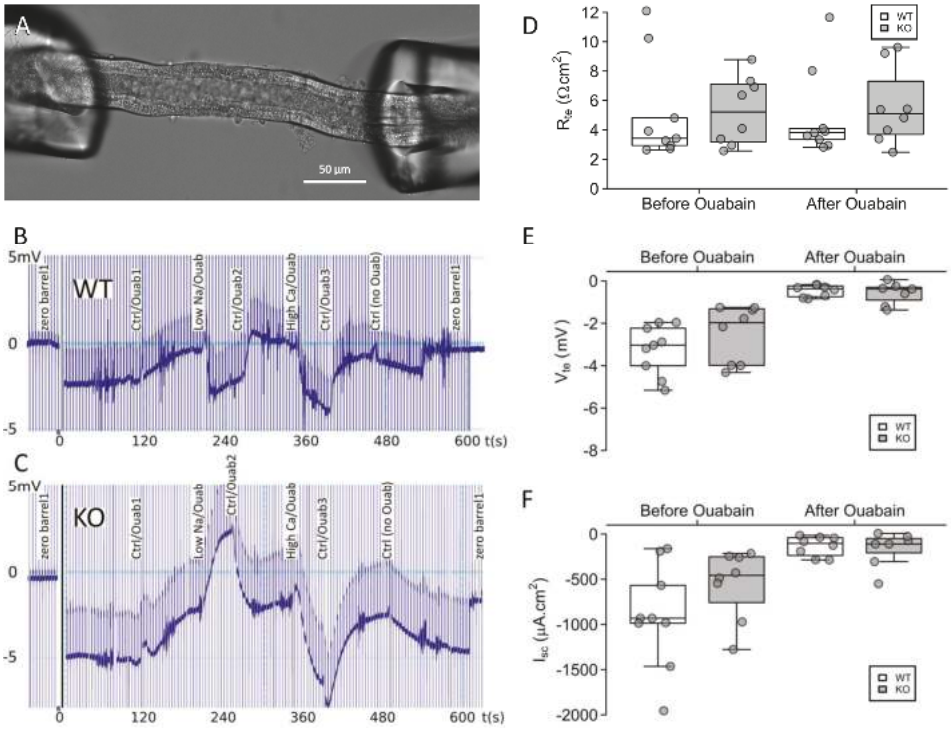

Figure 4. Microperfused proximal tubules from claudin-12 knockout (KO) and wild type (WT) mice. (**A**) Representative image of a proximal tubule perfused ex vivo. (**B**,**C**) Representative recording traces from original experiments in proximal tubules from WT (**B**) and KO (**C**) animals. Basolateral addition of ouabain, and solutions containing a low sodium or high calcium concentration altered the trace by first reducing transcellular transport, and then generating diffusion potentials. (**D**–**F**) Transepithelial resistance (R_{te}), transepithelial voltage (V_{te}), and short-circuit current (I_{sc}) before and after the addition of ouabain.

Next, we imposed a sodium chloride concentration gradient, by adding a solution containing low sodium to the basolateral side, and measured the diffusion potential generated across the tubule. With this result and the resistance, we calculated the permeability ratio of sodium to chloride (Figure 5A, P_{Na}/P_{Cl}). Interestingly we observed an increase in the potential difference (PD) across the tubule in the KO mice, as opposed to a decrease in PD in the WT animals, consistent with altered relative sodium to chloride permeability. We then imposed a calcium to sodium diffusion gradient across the tubule, recorded the diffusion potential generated and used this to calculate the permeability ratio of calcium to sodium (Figure 5A, P_{Ca}/P_{Na}). From these ratios and the resistance, we were able to calculate the absolute permeabilities of the tubule to sodium, chloride, and calcium (Figure 5B). Straight proximal tubules from claudin-12 KO mice displayed a reduced sodium relative to chloride permeability ratio (1.27 ± 0,05 in the WT compared with 0.89 ± 0.17 in the KO), which was the result of decreased sodium permeability ($3.8 \pm 1.3 \times 10^{-4}$ cm/s in WT vs. $2.5 \pm 0.4 \times 10^{-4}$ cm/s in KO), and not increased chloride permeability (Figure 5). Hence, the deletion of claudin-12 changes the selectivity of the straight proximal tubule to relatively more anion permeable, i.e., claudin-12 confers cation selectivity to the straight portion of the renal proximal tubule.

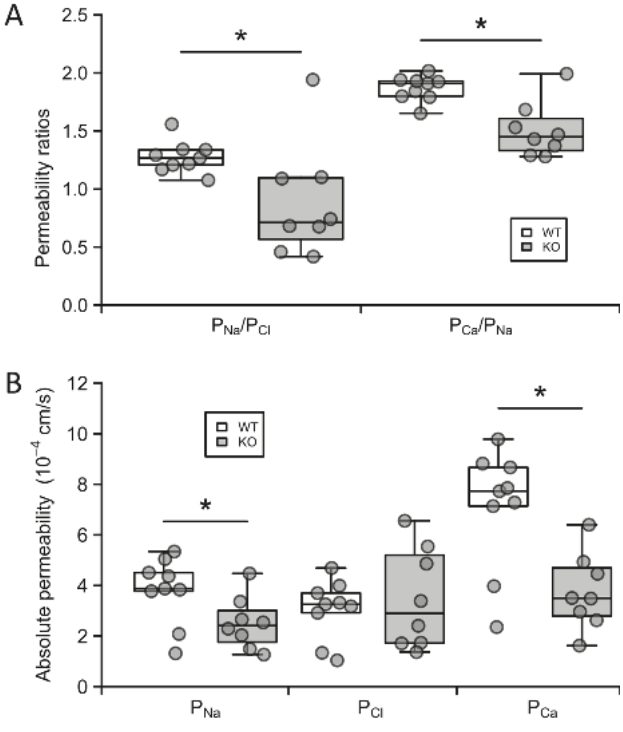

Figure 5. Ion permeabilities in proximal tubules from claudin-12 knockout (KO) and wild type (WT) mice. (**A**) Sodium–chloride and calcium–sodium permeability ratios. (**B**) Absolute permeabilities to sodium, chloride, and calcium. *—$p < 0.05$.

We next examined the calcium permeability characteristics of the proximal tubule. Interestingly, straight proximal tubules from wild type mice displayed a calcium to sodium permeability ratio of about 2 (P_{Ca}/P_{Na} = 1.87 ± 0.04, Figure 5A), inferring that this part of the nephron is approximately twice as permeable to calcium as to sodium. Further, the deletion of claudin-12 resulted in a greater reduction in permeability to calcium than to sodium (P_{Ca}/P_{Na} = 1.51 ± 0.08, Figure 5A), which was also reflected in decreased absolute calcium permeability ($7.1 \pm 0.8 \times 10^{-4}$ cm/s in the WT compared

with $3.8 \pm 0.5 \times 10^{-4}$ cm/s in the KO) (Figure 5B, P_{Ca}). These results indicate that the straight portion of the proximal tubule has selective calcium permeability and that claudin-12 confers some, but not all, of the selective and total permeability to calcium.

2.4. Claudin-12 Null Mice Do not Have Hypercalciuria

We hypothesized that reduced calcium permeability in the proximal tubule of claudin-12 knockout mice would result in increased urinary calcium excretion and/or hormonal compensation. We therefore housed mice in metabolic cages with water and chow provided ad libitum. The claudin-12 knockout mice weighed the same as their wild type littermates and no differences were observed in water or chow ingested, urine volume, or fecal weight (Table 1). Further, analysis of serum at the end of the metabolic cage experiments failed to identify significant differences in plasma electrolytes, including Ca^{2+}, creatinine, glucose, and blood urea nitrogen (BUN) (Table 2). Importantly, we did not find differences in the circulating levels of parathyroid hormone (PTH), FGF23, nor the active form of vitamin D, 1,25 dihydroxy vitamin D_3/calcitriol (Table 2). Finally, we examined urinary and fecal excretion. We did not detect a significant difference in the urinary excretion of all electrolytes examined, including Ca^{2+} and Na^+ (Table 3). We also did not observe an alteration in urinary excretion of creatinine, consistent with the same glomerular filtration rate in both genotypes (Table 3). In summary, claudin-12 knockout mice, despite reduced proximal tubular Na^+ and Ca^{2+} permeability, do not display altered urinary excretion of these ions, or hormonal compensation.

Table 1. Metabolic cage data.

	WT (n = 12–13)	KO (n = 17–19)	p-Value
Female Weight, g	26.8 ± 1.3 (n = 10)	26.6 ± 0.7 (n = 9)	0.918
Male Weight, g	29.4 ± 0.9 (n = 3)	30.9 ± 0.8 (n = 10)	0.337
H_2O drunk, mL/24 h	6.0 ± 0.4	6.3 ± 0.3	0.426
Chow eaten, g	4.8 ± 0.2	5.3 ± 0.2	0.068
$Ca^{2+}{}_{ingested}$ [1], µmol/24 h	1138 ± 46	1266 ± 46	0.068
Urine volume, mL/24 h	1.6 ± 0.2	1.7 ± 0.2	0.603
Fecal excretion [2], g/24 h	5.8 ± 0.3	6.4 ± 0.3	0.162
Fecal calcium excretion			
$Ca^{2+}{}_{feces}$, µmol/24 h	1065 ± 53	1116 ± 57	0.536
$Ca^{2+}{}_{feces}/Ca^{2+}{}_{ingested}$	0.94 ± 0.04	0.88 ± 0.03	0.177

[1] Calculated from chow eaten per animal. [2] Dry feces weight.

Table 2. Serum values.

	WT (n = 12–13)	KO (n = 17–19)	p-Value
Na^+, mmol/L	150.7 ± 1.2	150.9 ± 0.6	0.820
K^+, mmol/L	4.7 ± 0.2	4.6 ± 0.2	0.784
Cl^-, mmol/L [1]	119 ± 1	117 ± 0.7	0.180
Ca^{2+}, mmol/L	2.4 ± 0.2	2.5 ± 0.1	0.369
Cr, µmol/L	0.030 ± 0.004	0.036 ± 0.004	0.315
Glucose, mmol/L	8.8 ± 0.5	9.3 ± 0.4	0.389
BUN, mmol/L [1]	29.2 ± 1.5	29.3 ± 1.5	0.954
PTH, pg/mL	421 ± 85	332 ± 52	0.370
FGF23, pg/mL	273 ± 16	306 ± 14	0.173
Vitamin D3, pg/mL	81 ± 15	80 ± 11	0.971

[1] WT n = 6, age (WT&KO) between 3 and 6 months.

Wild type and knockout mice were then fed a normal (0.6% wt/wt), low (0.01% wt/wt) or high (2.0% wt/wt) calcium diet, to evaluate if altering calcium intake would alter urinary calcium excretion (Table 4). The diets increased or reduced urinary calcium excretion as expected, but no clear differences

between genotypes were observed for either FE_{Ca} or plasma Ca^{2+} levels between genotypes on the different diets.

Table 3. Urinary ion excretion.

	WT (n = 12)	KO (n = 13)	p-Value
Na^+/Creatinine	31 ± 8	39 ± 9	0.495
Cl^-/Creatinine	140 ± 45	136 ± 33	0.951
K^+/Creatinine	99 ± 25	93 ± 21	0.855
Ca^{2+}/Creatinine	0.24 ± 0.05	0.22 ± 0.04	0.819
PO_4^{3-}/Creatinine	5.4 ± 0.8	5.0 ± 0.7	0.688
Creatinine, µmol/24 h	12 ± 2	16 ± 3	0.377

Table 4. Urine ion excretion normalized to the creatinine of WT and KO mice on different calcium-containing diets.

	Normal			High Ca			Low Ca		
	WT (n = 12)	KO (n = 8)	p-Value	WT (n = 14)	KO (n = 15)	p-Value	WT (n = 15)	KO (n = 11)	p-Value
Urine Ca^{2+}/Cr	0.88 ± 0.08	0.79 ± 0.07	0.456	2.65 ± 0.48	3.10 ± 0.52	0.555	0.62 ± 0.03	0.60 ± 0.01	0.614
FE Ca	0.63 ± 0.15	0.37 ± 0.21	0.323	1.88 ± 0.46	1.67 ± 0.31	0.703	0.55 ± 0.14	0.31 ± 0.07	0.178

2.5. Renal Compensation in Claudin-12 KO Mice

Having failed to identify urinary wasting of Ca^{2+} or Na^+ or apparent hormonal compensation, we turned our attention to possible intrarenal compensatory mechanisms. Firstly, we examined the cortical protein expression of Claudin-10 and -2, which are also known to be expressed in the proximal tubule (Figure 6A–D). We found that both were significantly reduced in expression, in the KO mice.

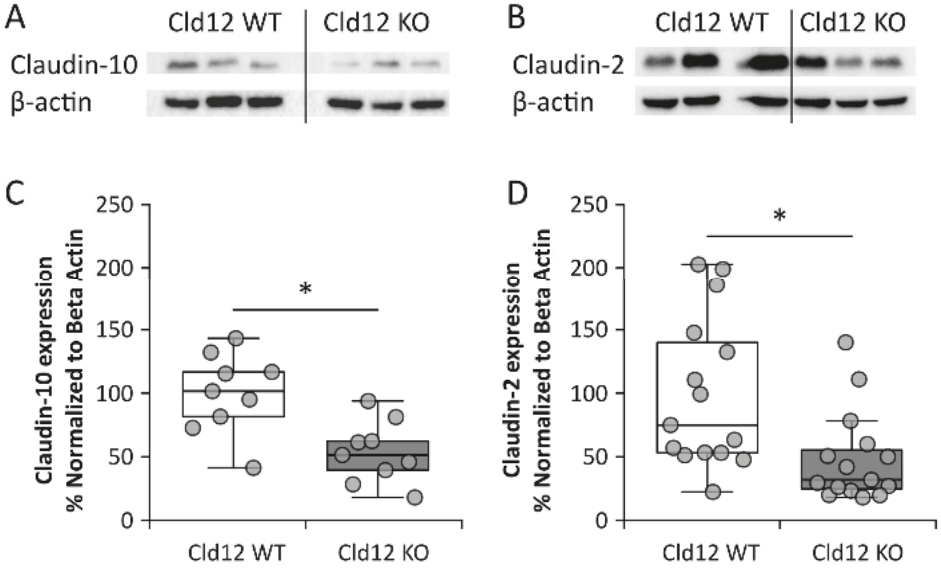

Figure 6. Claudin-12 wild type (WT) and knockout (KO) mouse renal cortical protein expression. (**A**,**C**) Claudin-10 and (**B**,**D**) Claudin-2. * $p < 0.05$.

We also isolated RNA from the whole kidney of wild type and claudin-12 KO mice and performed a quantitative real-time PCR. We did not find a significant difference in the expression of genes mediating

transcellular Ca^{2+} reabsorption from the distal convoluted tubule except for PMCA1b, which was slightly reduced (Figure 7A). We also failed to identify significant differences in the expression of apical sodium transport proteins along the nephron (Figure 7B). Further, consistent with the absence of a significant difference in circulating calcitriol levels, we did not find differences in the expression of renal enzymes regulating the amount of this hormone in plasma, the vitamin D receptor, the calcium sensing receptor (CaSR), nor in klotho (Figure 7C). Finally, we assessed the expression of renal claudins (Figure 7D) and found that claudin-1, -8, and -14 had a significantly reduced expression in the knockout animals. Claudin-14 reduction is particularly interesting as it is only expressed in the cortical TAL [20], the nephron segment responsible for the reabsorption of around 25% of filtered calcium [1]. When present, claudin-14 attenuates calcium reabsorption from the TAL via the paracellular pathway [15]. Reduced expression in the knockout mice may therefore reflect increased TAL calcium reabsorption, in compensation for decreased proximal tubule calcium reabsorption.

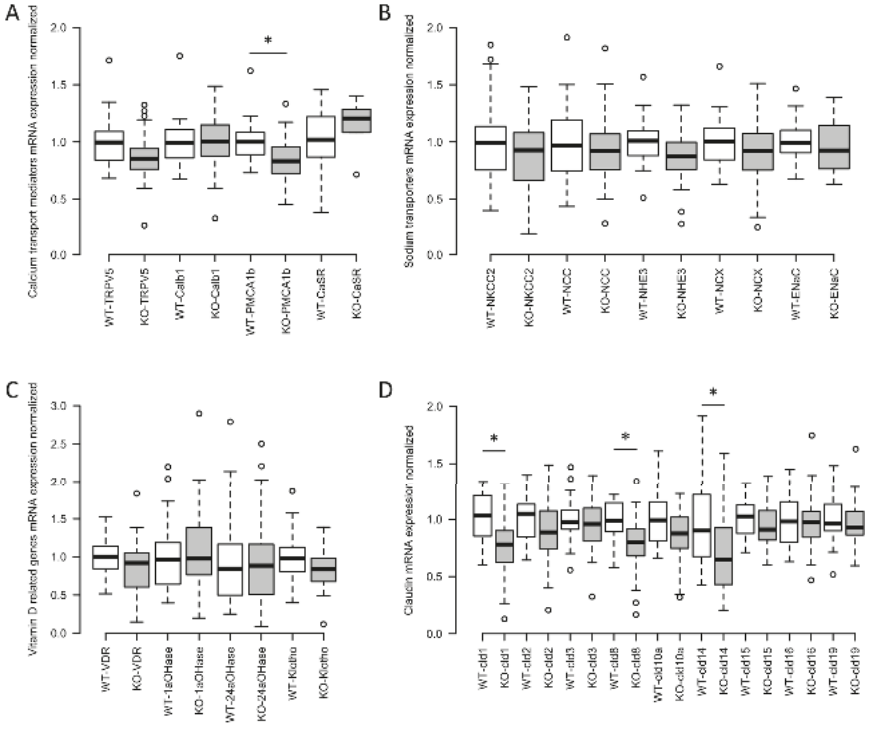

Figure 7. Claudin-12 wild type (WT) and knockout (KO) mouse renal mRNA expression of key genes involved in Ca^{2+} transport. (**A**) Calcium transport mediators: transient receptor potential cation channel subfamily V member 5 (TRPV5), calbindin 1 (Calb1), plasma membrane calcium ATPase 1b (PMCA1b), and calcium sensing receptor (CaSR). (**B**) Sodium transporters: sodium–potassium–chloride cotransporter 2 (NKCC2), sodium–chloride cotransporter (NCC), sodium-hydrogen exchanger 3 (NHE3), sodium–calcium exchanger (NCX), and epithelial sodium channel (ENaC). (**C**) Vitamin D related genes: vitamin D receptor (VDR), 25-hydroxyvitamin D 1 alpha hydroxylase (1aOHase), 24-hydroxylase (24aOHase), and klotho. (**D**) Renal claudins involved in cation transport normalized to 18S as house-keeping gene: claudins 1, 2, 3, 8, 10a, 14, 15, 16, and 19. n = 26 and 35, respectively. *—significant with Benjamini–Hochberg critical value for false discovery rate of 0.05. ° represents values that are above or below 1.5 times the interquartile range.

3. Discussion

Evidence supports a role for claudin-12 in contributing paracellular Ca^{2+} permeability in the intestine [11]. Claudin-12 mRNA is expressed in the kidney, and a proximal tubule cell culture model [10,13,21]. The proximal tubule is the location of the greatest amount of Ca^{2+} reabsorption along the nephron and this occurs via the paracellular pathway [1,3–5]. To date the tight junction proteins contributing calcium permeability to this segment have been incompletely defined. We therefore hypothesized that claudin-12 contributes paracellular permeability to the proximal tubule and generated a claudin-12 KO mouse, by replacing the only coding exon of the claudin-12 gene with β-galactosidase to assess this possibility. This model enabled us to localize *Cldn12* to the renal proximal tubule, and by perfusing tubules ex vivo from wild type mice and claudin-12 KO animals, we confirmed that *Cldn12* does indeed contribute Ca^{2+} and Na^{+} permeability to this segment. However, the deletion of *Cldn12* does not induce hypercalciuria or an increase in calciotropic hormone levels.

Direct measurement of Ca^{2+} permeability of the straight portion of the proximal tubule of wild type and claudin-12 KO mice revealed relative selectivity for Ca^{2+} over Na^{+}, which was attenuated in the absence of claudin-12. This strongly supports *Cldn12* contributing to the Ca^{2+} permeability of the proximal tubule. It is surprising then that claudin-12 null mice did not display hypercalciuria in response to a failure to reabsorb Ca^{2+} from the proximal straight tubule. Further, there appeared to be no systemic compensation for reduced paracellular Ca^{2+} permeability in the proximal nephron, as calciotropic hormone levels were also unchanged. What then may explain our observations? Potentially altered permeability of the proximal tubule is compensated by an increased driving force for Ca^{2+} across this segment. This could occur via generating a more lumen positive potential difference across the segment, or increasing water reabsorption from the proximal tubule, which would in turn either enhance the Ca^{2+} concentration gradient or convective driving force for paracellular Ca^{2+} [22]. We did not observe a significant difference in baseline transepithelial voltage (Vte) across tubules perfused ex vivo between wild type and knockout mice (Vte WT = −3.2 ± 0.4 mV, $n = 9$ and KO = −2.5 ± 0.5 mV, $n = 8$, $p = 0.253$), making the former explanation unlikely. Further, we did not observe altered expression of the major Na^{+} transporter in the proximal tubule, sodium hydrogen exchanger isoform 3(NHE3), suggesting that this is not the explanation, although altered NHE3 activity can occur in the absence of altered expression [23–25]. Instead, we observed decreased *Cldn14* expression, consistent with increased Ca^{2+} reabsorption from the TAL in compensation. Claudin-14 interacts in the cortical TAL (cTAL) tight junction with the claudin-16/19 complex, reducing permeability to calcium, and thus calcium absorption from this segment [15,26]. This suggests that increased Ca^{2+} reabsorption from the TAL is compensating for reduced proximal tubule Ca^{2+} reabsorption.

How might *Cldn14* expression be altered in the absence of changes in circulating Ca^{2+} or PTH levels? The expression of Cldn14 is increased by the activation of the calcium sensing receptor (CaSR) in the basolateral membrane of the TAL [15]. Plasma Ca^{2+} levels were not different between wild type and claudin-12 KO mice, however, we were unable to assess the local concentration of Ca^{2+} in the peritubular space of the cortical TAL (where *Cldn14* is expressed [20]). Interestingly, the cTAL runs linearly into the juxtamedullary cortex, and Figure 3 reveals that the cTAL directly abuts tubules with significant *Cldn12* promoter activity. Consistent with this observation, microdissection of straight segments of proximal tubules frequently demonstrated the close adherence of a cTAL (Figure 8). Perhaps, then, reduced reabsorption of Ca^{2+} from the straight portion of the proximal tubule, leads to a lower concentration of Ca^{2+} in the juxtamedullary interstitium, and thus reduced CaSR activation? This would result in increased cTAL Ca^{2+} permeability and increased reabsorption from this segment, in compensation. The proposed proximal tubule–cTAL crosstalk would explain our lack of alteration in urinary Ca^{2+} excretion and the lack of hormonal compensation. However, this hypothesis requires further experimental testing to support it.

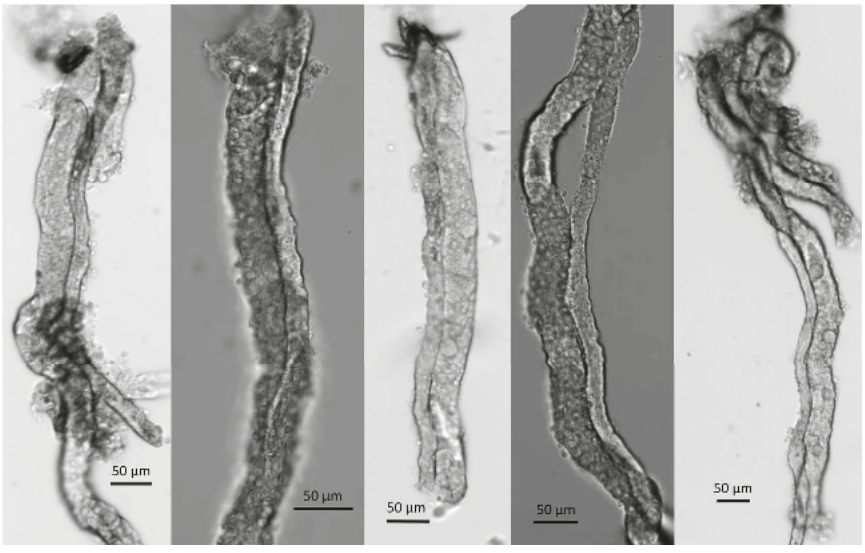

Figure 8. Examples of cTAL (thinner tubule) attached to the straight portion of the pars recta of the proximal tubule (thicker tubule).

Claudin-2 has also been implicated in paracellular intestinal Ca^{2+} absorption. In addition, this protein has been clearly localized to the proximal tubule, where it contributes paracellular Na^{+} permeability [9,11,27]. Proximal tubule paracellular Na^{+} permeability contributes a significant amount of net Na^{+} reabsorption from this segment. Using the paracellular pathway and the concentration gradient/convection forces induced by the considerable water flux across this segment increases the efficiency of this process, thereby reducing the energy required [28]. Interestingly, claudin-2 KO mice display hypercalciuria [9]. It is therefore tempting to speculate that claudin-2 also contributes proximal tubule Ca^{2+} permeability as we observe for claudin-12. Further specific studies will be required to support this. Why claudin-2 KO mice demonstrate hypercalciuria and claudin-12 null mice do not is unclear, but is perhaps due to a greater abundance of claudin-2 in the proximal tubule.

PTH is released from the parathyroid gland in response to low plasma calcium levels. It acts directly on the proximal tubule to inhibit transcellular sodium reabsorption and likely paracellular $Ca2^{+}$ reabsorption [22]. It also acts on the distal convoluted tubule/connecting tubule to increase Ca^{2+} reabsorption [29]. FGF23 is another phosphocalciotropic hormone that acts on the proximal tubule to inhibit sodium phosphate cotransport, and on the distal convoluted tubule/connecting tubule to augment Ca^{2+} absorption [30,31]. Although we did not detect a significant difference in the circulating amounts of these hormones between wild type and claudin-12 KO mice, there were large variations in plasma levels. It is thus possible that alterations in these hormones could be compensating for the reduced paracellular Ca^{2+} permeability in the proximal tubule.

The lack of a specific claudin-12 antibody has limited our ability to confirm protein localization. This is despite trying several commercially available antibodies and generating two of our own. It should be emphasized that we are not the only group to experience this difficulty [12,17]. Regardless, we have shown clearly the absence of claudin-12 DNA in the knockout mice and the inability to detect messenger RNA in the kidney of knockout mice. Moreover, the claudin-12 KO mice that we generated do not have alterations in the endogenous promoter, and we replaced the coding sequence with a reporter β-galactosidase, which clearly demonstrates an expression in the renal cortex, as seen in Figure 2. We are therefore confident that *Cldn12* is expressed in the renal proximal tubule where it

confers Ca^{2+} permeability. We should emphasize that we cannot exclude lower levels of expression in other nephron segments.

In conclusion, using a mutant mouse engineered to have β-galactosidase replace the coding exon of *Cldn12*, we were able to localize claudin-12 expression to the renal proximal tubule. Microperfusion studies on this model revealed reduced Na^+ and Ca^{2+} permeability consistent with claudin-12 conferring paracellular Ca^{2+} permeability to the proximal tubule. Surprisingly the knockout mice did not have increased urinary Ca^{2+} excretion, or alterations in calciotropic hormone levels. We propose that this is due to a proximal tubule–TAL crosstalk leading to reduced *Cldn14* expression and consequently increased Ca^{2+} reabsorption from the TAL, in compensation for decreased proximal tubule Ca^{2+} reabsorption.

4. Materials and Methods

4.1. Generation of Cld12 KO Mice

A claudin-12 null strain was generated through the UC Davies Knock Out Mouse Project (KOMP). The gene encoding claudin-12 is located on chromosome 5, and contains four exons with the coding sequence encoded by exon four (NCBI Gene: 64945). A targeting vector (Velocigene cassette ZEN-Ub1, KOMP Repository category number 13208L1) was used to replace exon four with the neomycin resistance gene and the lacZ reporter gene by homologous recombination in VGB6 embryonic stem (ES) cells derived from the mouse strain C57BL/6NTac. The mouse strain used for this research project, KOMP ES cell line $Cldn12^{tm1(KOMP)Vlcg}$, RRID:MMRRC_053773-UCD, was obtained from the Mutant Mouse Resource and Research Center (MMRRC) at the University of California at Davis, an NIH-funded strain repository, and was donated to the MMRRC by The KOMP Repository, UC Davis Mouse Biology Program. This created a 760-bp deletion between positions 5507663–5508422 of Chromosome 5 resulting in heterozygotes (HET) ES cells (Figure 1A). Subsequently, the recombinant ES cells were used to generate HET mice. Littermates were used as controls. Intercrossing of heterozygotes yielded claudin-12 deficient mice (KO). Genotypes were confirmed by RT-PCR, and gene sequencing (Figure 1B–D).

4.2. Metabolic Cage Studies

Metabolic Cage studies were performed as previously reported [2,15]. Three month-old wild type (WT), or claudin-12 deficient (KO) mice were placed in metabolic cages for three days with free access to normal rodent diet chow (LabDiet® 5001, Fort Worth, TX, USA) and water. Weight, chow eaten, and water consumed were measured daily. Urine and feces were collected every 24 h for analysis. Only samples from day three were used for analysis. Then, animals were anesthetized using pentobarbital sodium, and blood was collected for analysis of serum creatinine via high-performance liquid chromatography. We also performed a blood gas at that time. Kidneys were harvested and snap frozen in liquid nitrogen and stored at −80 °C. Metabolic cage studies on wild type and claudin-12 KO mice fed different calcium containing diets (low = 0.01% TD. 95027, normal = 0.6% TD.97191, or high = 2% TD.00374, all from Harlan Laboratories, Madison, WI, USA) were performed as previously described [15]. All experimental procedures were approved on 3 October 2013 by the Animal Care and Use Committee for Health Sciences at the University of Alberta (protocol number 00000213).

4.3. Measurement of Urinary, Fecal, and Plasma Electrolytes

Serum electrolytes, blood urea nitrogen, and glucose were measured with a handheld blood gas analyzer (Vet Scan i-STAT1 Analyzer, Abaxis, Union City, CA, USA) as previously described [15]. Feces from the last 24-h collection were dried for 48 h in an incubator (Labline, Imperial III Incubator, Mumbai, India) at 55 °C, and then homogenized with a mortar and pestle. A sample of 0.7 g per mouse was then taken and solubilized in nitric acid for elemental analysis. Nitric acid (70%) was added to the samples in two sequential steps: the first 0.3 mL were added when the sample was at 65 °C, then 0.7

mL were added once fumes subsided after about 30 min. The mix was then heated to 85 °C and boiled until the fumes stopped (approximately 1 h later). Subsequently, 1 mL of 30% H_2O_2 was added, again in two steps: first, 0.2 mL were added while the sample was still at 85 °C. Once boiling stopped, the sample was allowed to cool for 10 min before adding the remaining 0.8 mL. After another 10 min at room temperature, the samples were heated again to 85 °C until the reaction stopped (approximately 1 h later). The samples were adjusted to 5 mL with ddH_2O and used for analysis. The calcium content was measured using the QuantiChrom Ca^{2+} Assay Kit (Catalog number: DICA-500) from BioAssay Systems (Hayward, CA, USA).

Urine electrolyte content was measured by ion chromatography. All experiments were performed with a Dionex Aquion Ion Chromatography (IC) System (category number 22176-60004, Thermo Fisher Scientific Inc., Mississauga, ON, Canada) equipped with an autosampler. The cation and anion eluents were prepared as per the manufacturer's instructions. The anion eluent consisted of a 4.5 mM Na_2CO_3/1.5 mM $NaHCO_3$ in ddH_2O, and the cation eluent consisted of 20 mM Methanesulfonic acid in ddH2O. All reagents and samples were filtered with a 0.2 µm syringe filter (category number 03-391-1B, Thermo Fisher Scientific Inc., Mississauga, ON, Canada), and stored in high density polyethylene containers that had been thoroughly cleaned with deionized water to avoid any traces of ions. Calibration standard curves were produced using Dionex five anion standard (category number 037157, Thermo Fisher Scientific Inc., Mississauga, ON, Canada) and Dionex six cation-I standard (category number 040187, Thermo Fisher Scientific Inc., Mississauga, ON, Canada). Thermo Scientific Chromeleon 7 Chromatography Data System (CDS) software was used for automation and data handling. High-performance liquid chromatography (HPLC) was used to detect creatinine concentration in urine and blood samples. All experiments were performed with a Dionex UltiMate 3000 HPLC System (Thermo Scientific, ISO-3100SD PUMP category number 5040.0011; TCC-3000SD Column Thermostat, category number 5730.0010, and VWD-3100 DETECTOR, category number 5074.0005, Thermo Fisher Scientific Inc., Mississauga, ON, Canada). UV detection of samples occurred at 216 nm and the pump flow rate was set at 0.2 mL/min accordingly. The HPLC eluent was prepared as per the manufacturer's instructions. The eluent consisted of acetonitrile (category number A-0626-17, Thermo Scientific)/Trifluoroacetic acid category number T-3258-PB05, Thermo Scientific, Mississauga, ON, Canada) in ddH_2O. All reagents and samples were filtered using 0.2 µM syringe filters (Thermo Scientific, category number 03-391-1B, Mississauga, ON, Canada) and stored in glass containers that had been thoroughly cleaned with deionized water to avoid sample adsorption. Calibration standard curves were produced using creatinine from Acros Organics, NJ, USA, category number AC228940250. Thermo Scientific Chromeleon 7 Chromatography Data System (CDS) software was used for automation and data handling.

4.4. Measurement of Hormone Levels

PTH was measured by ELISA according the manufacturer's instructions (mouse PTH 1-84 ELISA Kit, Immutopics Inc., category number 60-2305, San Diego, CA, USA) and Vitamin D levels were determined by a radioimmunoassay (1,25-Dihydroxy Vitamin D RIA kit, Immunodiagnostic systems, category number AA-54F1, Immunodiagnostic Systems Inc, Gaithersburg, MD, USA), according to the manufacturer's instructions as previously reported [2,15]. FGF23 was quantified by ELISA according to the manufacturer's instructions (FGF-23 ELISA Kit, Kainos, category number CY-4000, Tokyo, Japan).

4.5. X-Gal Staining and Immunofluorescence Microscopy on Renal Sections

We performed X-gal staining on 8-µm renal cryosections fixed with periodate–lysine–paraformaldehyde and prepared as previously reported [2]. Sections were first washed three times with fresh phosphate buffered saline, then rinsed briefly with distilled water. Next sections were incubated for approximately 3 h in X-gal solution, which consisted of a 1:40 dilution of pure X-gal (Sigma-Aldrich, Oakville ON, Canada) dissolved in 4% DMSO with a dilution buffer consisting of potassium ferricyanide crystalline 5 mM, potassium ferricyanide trihydrate 5 mM, $MgCl_2$ 2 mM, and PBS 100 mM, to allow the development of a

blue color. Wild type littermate sections were taken as a negative control. Then, sections were rinsed with PBS twice for 5 min before mounting with DAKO (Carpinteria, CA, USA) or undergoing immunostaining, essentially as previously reported [19,32]. In brief, antigen retrieval was performed with sodium citrate, and then washed three times with TN buffer (0.1 M Tris/HCl and 0.15 M NaCl, pH 7.6). Then the section was incubated with 0.3% H_2O_2 in TN buffer for 30 min. Sections were then washed three times with TN buffer before blocking for 1 h with TN buffer containing 0.5% Blocking Reagent (Perkin Elmer, MA, USA) and 0.05% Tween 20. Next, primary antibodies were applied in TN buffer (1:1500 anti-NKCC2, Developmental Studies Hybridoma Bank University of Iowa, USA, 1:500 anti- CAII (Santa Cruz Biotechnology Inc, Dallas, TX, USA, 1:500 anti-AQP1, Santa Cruz Biotechnology Inc., Dallas, TX USA or 1:500 Anti-NCC, Stress Marq Biosciences Inc. Victoria, BC, Canada), overnight all diluted in TN buffer. The slides were then washed three times with TN buffer and then a Cy3 conjugated secondary antibody of either donkey anti-mouse (NKCC2, CAII), anti-rabbit (NCC), or anti-goat (AQP1) was applied in the TN buffer containing 0.05% Tween-20 (TNT) for an hour. Finally, the slides were washed three times with TNT buffer before being mounted and visualized with an Olympus BX51 microscope equipped with a X-cite Series 120Q light source (Lumen Dynamics Inc. Mississauga, ON, Canada) and an Infinity 3, 1.4 Megapixel Cooled, color Camera (Lumenera, Ottawa, ON, Canada).

4.6. Proximal Tubular Perfusion and Electrophysiology

Proximal tubules were isolated and microperfused essentially as previously described [33]. To this end, kidneys were collected from three month-old claudin-12 WT and KO mice, swiftly decapsulated and sliced transversely. Cortical and juxtamedullary straight proximal tubules where mechanically dissected from the slices at 4 °C on a Leica M165C dissecting microscope and transferred to an Axi Observer Zeiss microscope for microperfusion. A Vestavia Scientific, LLC (Atlanta, GA, USA) microperfusion system of concentric micropipettes was used to hold and microperfuse the tubules as described previously [34]. The glass pipettes where built on a Luigs & Neumann GmbH microforge (Ratingen, Germany). We used for the external holding pipettes sodalime glass capillaries (Hilgenberg, Germany, category number 1409679), and elongated double-barreled glass capillary (Theta-Bo-glasscapillaries, Hilgenberg, Germany, category number 1402401) for the double-barreled perfusion pipettes. A silver wire of 0.2-mm diameter was inserted in one of the barrels of the perfusion pipette to be later connected to a pulse generator. We injected currents of 13 nA for one second every other second via a 150-MΩ resistor into the perfused tubules. The generated voltage deflections where used to later calculate the transepithelial resistance using the cable equation. The perfusion system was connected to a pressure pump that was designed at the Institute of Physiology of the University of Kiel, Germany, to keep a constant luminal flow through the perfused tubules. The bath and tubule lumen (via one of the barrels of the perfusion pipette) where connected via agar bridges (3M KCl, 3% agar) to silver–chloride electrodes, Ag/AgCl (RC-3, World Precision Instruments, Sarasota, FL, USA), which were themselves connected to ground, an amplifier, and to an impedance converter. The signal was digitalized with a PowerLab 8/SP and recorded with LabChart data acquisition and analysis software (LabChart 4.2, ADInstruments–North America, Colorado Springs, CO, USA). This enabled the recording of the transepithelial voltage and the transepithelial voltage deflections throughout the course the experiments. The length and diameter of the tubules were measured on the digital images taken using Zen 2.6 Blue Edition Carl Zeiss Microscopy modular image-processing and analysis software (Carl Zeiss Canada, Toronto, ON, Canada). Images were captured with a Hamamatsu ORCA-Flash4.0 V3 digital camera, model C13440-20CU (Hamamatsu Corporation - Americas, Bridgewater, NJ, USA).

In order to measure calcium permeability, tubules were first perfused with modified Ringer's control solution (132 mM NaCl, 0.4 mM KH_2PO_4, 1.4 mM K_2HPO_4, 1.2 mM $MgCl_2 \cdot 6H_2O$, 5 mM Na-Acetate $\cdot 3H_2O$, 2.5 mM $NaHCO_3$, 1.3 mM $CaCl_2$, 5 mM L-alanine, and 5 mM glucose) in a running bath of the same control solution. Subsequently, the bath solution was exchanged to the same control solution containing ouabain (10 μM). Once voltage recordings stabilized, we changed the basolateral solution to first induce a NaCl dilution potential, and then a Na^+-Ca^{2+} bi-ionic diffusion potential (all

the solutions contained 10 μM ouabain) (Figure 4B,C). The 70 mM low sodium solution (65 mM NaCl, 0.4 mM KH_2PO_4, 1.4 mM $K_2HPO_4 \cdot 3H_2O$, 1.2 mM $MgCl_2 \cdot 6H_2O$, 5 mM Na-Acetate $\cdot 3H_2O$, 2.5 mM $NaHCO_3$, 1.3 mM $CaCl_2$, 5 mM L-alanine, 5 mM Glucose, and 112 mannitol) and the 72.5 mM high calcium containing solution (3.6 mM KCl, 72.5 mM $CaCl_2 \cdot 2H_2O$, 5 mM glucose, and 3mM HEPES) were designed using the control solution as the base. The sodium–chloride permeability ratios and the calcium–sodium permeability ratios were then calculated using the Goldmann–Hodgin–Katz flux equation. The absolute permeability to sodium was calculated using the simplified Kimizuka–Koketsu equation, and the absolute permeabilities to chloride and calcium obtained from this value and the permeability ratios [35,36].

4.7. Quantitative Real-Time PCR and Immunoblotting

Quantitative real-time PCR and immunoblotting were performed essentially as previously described [2,15,16,21]. Total mRNA was extracted from $\frac{1}{2}$ of a snap frozen kidney from three month-old mice using the TRIzol Reagent (Invitrogen, Carlsbad, CA, USA) according to the manufacturer's instructions. After treatment with DNAse (ThermoScientific, Vilnius, LT, USA, category number EN052), cDNA was reverse transcribed from the isolated total mRNA. Primers and probes were obtained from Applied Biosystems Inc. (Foster City, CA, USA). A quantity of 5 μL (125 ng of cDNA) was used as a template to determine the gene expression by qPCR. TaqMan universal qPCR master mix (Applied Biosystems Inc, Foster City, CA, USA), primer, probe, and RNAse-free water were mixed together, then added to cDNA that had been placed in a 384-well plate (Applied Biosystems Inc, Foster City, CA, USA). Internal control mRNA levels of 18S ribosomal RNA were measured. Expression levels were quantified with an ABI Prism 7900 HT Sequence Detection System (Applied Biosystems Inc, Foster City, CA, USA), and 18S was used for normalization of RNA as none of the experimental perturbations resulted in a significant change in its expression. Immunoblotting was carried out using an anti-claudin-10 (Invitrogen Inc., category number 38-8400, a subsidy of Thermo Fischer Inc., Mississauga, ON, Canada) or anti-claudin-2 (Thermo Fischer Inc., category number 32-5600, Mississauga, ON, Canada) and appropriate secondary antibodies, and then quantified as previously described [2].

4.8. Statistical Analysis

The differences between group mean were assessed by Student's t test with a Bonferroni correction for multiple comparisons applied when needed. The Shapiro–Wilk test was used to evaluate the data for normal distribution when pertinent. The results are presented as mean ± SEM (n = number of animals throughout) and considered significant at $p < 0.05$. Renal mRNA expression was analyzed using the Benjamini–Hochberg procedure, with a critical value for false discovery rate of 0.05 [37].

Author Contributions: Conceptualization and design, A.P., W.P., D.O., M.U., M.R.B., M.F., H.D., E.C. and R.T.A.; experimental data acquisition, A.P., W.P., D.O., M.U. and M.F.; data analysis and interpretation, A.P., W.P., D.O., M.U., M.R.B., M.F., E.C. and R.T.A.; figure preparation, A.P., W.P. and M.U.; manuscript drafting, A.P. and R.T.A.; editing and revision of the manuscript, A.P., W.P., D.O., M.U., M.R.B., M.F., H.D., E.C. and R.T.A.; funding acquisition, R.T.A. All authors have read and agreed to the published version of the manuscript.

Funding: This work was funded by grants from the Women and Children's Health Research Institute, which is supported by the Stollery Children's Hospital Foundation, and the Canadian Institutes of Health Research (CIHR, MOP 136891) and the Kidney Foundation of Canada to R.T.A., who is the Canada Research Chair in Renal Epithelial Transport Physiology.

Conflicts of Interest: The authors declare no conflicts of interest. The funders had no role in the design of the study, in the collection, analyses, or interpretation of data, in the writing of the manuscript, or in the decision to publish the results.

Abbreviations

PT	Renal proximal tubule
KO	Null (knock-out) mice
WT	Wild-type mice
P_X	Paracellular permeability to ion *X*
(c)TAL	(cortical) Thick ascending limb of the Henle's loop
PTH	Parathyroid hormone
FGF23	Fibroblast growth factor 23
ES	Embryonic stem cells
HET	Heterozygotes
AQP1	Aquaporin I
NKCC2	Sodium–potassium–chloride cotransporter II
NCC	Sodium–chloride cotransporter
CAII	Carbonic anhydrase II
BUN	Blood urea nitrogen
PMCA1b	Plasma membrane Ca^{2+} ATPase, isoform 1b
NHE3	Sodium–hydrogen exchanger type 3
CaSR	Calcium sensing receptor

References

1. Suki, W.N. Calcium transport in the nephron. *Am. J. Physiol.* **1979**, *237*, F1–F6. [CrossRef] [PubMed]
2. Pan, W.; Borovac, J.; Spicer, Z.; Hoenderop, J.G.; Bindels, R.J.; Shull, G.E.; Doschak, M.R.; Cordat, E.; Alexander, R.T. The epithelial sodium/proton exchanger, NHE3, is necessary for renal and intestinal calcium (re)absorption. *Am. J. Physiol.* **2012**, *302*, F943–F956. [CrossRef] [PubMed]
3. Brunette, M.; Aras, M. A microinjection study of nephron permeability to calcium and magnesium. *Am. J. Physiol.* **1971**, *221*, 1442–1448. [CrossRef] [PubMed]
4. Frick, A.; Rumrich, G.; Ullrich, K.J.; Lassiter, W.E. Microperfusion study of calcium transport in the proximal tubule of the rat kidney. *Pflug. Arch. Gesamte Physiol. Menschen Tiere* **1965**, *286*, 109–117. [CrossRef] [PubMed]
5. Murayama, Y.; Morel, F.; Le Grimellec, C. Phosphate, calcium and magnesium transfers in proximal tubules and loops of Henle, as measured by single nephron microperfusion experiments in the rat. *Pflug. Arch.* **1972**, *333*, 1–16. [CrossRef]
6. Edwards, A.; Bonny, O. A model of calcium transport and regulation in the proximal tubule. *Am. J. Physiol.* **2018**, *315*, F942–F953. [CrossRef]
7. Worcester, E.M.; Coe, F.L.; Evan, A.P.; Bergsland, K.J.; Parks, J.H.; Willis, L.R.; Clark, D.L.; Gillen, D.L. Evidence for increased postprandial distal nephron calcium delivery in hypercalciuric stone-forming patients. *Am. J. Physiol.* **2008**, *295*, F1286–F1294. [CrossRef]
8. Yu, A.S. Claudins and the kidney. *J. Am. Soc. Nephrol.* **2015**, *26*, 11–19. [CrossRef]
9. Muto, S.; Hata, M.; Taniguchi, J.; Tsuruoka, S.; Moriwaki, K.; Saitou, M.; Furuse, K.; Sasaki, H.; Fujimura, A.; Imai, M.; et al. Claudin-2-deficient mice are defective in the leaky and cation-selective paracellular permeability properties of renal proximal tubules. *Proc. Natl. Acad. Sci. USA* **2010**, *107*, 8011–8016. [CrossRef] [PubMed]
10. Beggs, M.R.; Appel, I.; Svenningsen, P.; Skjodt, K.; Alexander, R.T.; Dimke, H. Expression of transcellular and paracellular calcium and magnesium transport proteins in renal and intestinal epithelia during lactation. *Am. J. Physiol.* **2017**, *313*, F629–F640. [CrossRef]
11. Fujita, H.; Sugimoto, K.; Inatomi, S.; Maeda, T.; Osanai, M.; Uchiyama, Y.; Yamamoto, Y.; Wada, T.; Kojima, T.; Yokozaki, H.; et al. Tight junction proteins claudin-2 and -12 are critical for vitamin D-dependent Ca^{2+} absorption between enterocytes. *Mol. Biol. Cell* **2008**, *19*, 1912–1921. [CrossRef]
12. Kiuchi-Saishin, Y.; Gotoh, S.; Furuse, M.; Takasuga, A.; Tano, Y.; Tsukita, S. Differential expression patterns of claudins, tight junction membrane proteins, in mouse nephron segments. *J. Am. Soc. Nephrol.* **2002**, *13*, 875–886. [PubMed]

13. Borovac, J.; Barker, R.S.; Rievaj, J.; Rasmussen, A.; Pan, W.; Wevrick, R.; Alexander, R.T. Claudin-4 forms a paracellular barrier, revealing the interdependence of claudin expression in the loose epithelial cell culture model opossum kidney cells. *Am. J. Physiol. Cell Physiol.* **2012**, *303*, C1278–C1291. [CrossRef] [PubMed]
14. Abuazza, G.; Becker, A.; Williams, S.S.; Chakravarty, S.; Truong, H.T.; Lin, F.; Baum, M. Claudins 6, 9 and 13 are developmentally expressed renal tight junction proteins. *Am. J. Physiol. Renal Physiol.* **2006**, *291*, F1132–F1141. [CrossRef] [PubMed]
15. Dimke, H.; Desai, P.; Borovac, J.; Lau, A.; Pan, W.; Alexander, R.T. Activation of the Ca^{2+}-sensing receptor increases renal claudin-14 expression and urinary Ca^{2+} excretion. *Am. J. Physiol. Renal Physiol.* **2013**, *304*, F761–F769. [CrossRef]
16. Krishnan, D.; Pan, W.; Beggs, M.R.; Trepiccione, F.; Chambrey, R.; Eladari, D.; Cordat, E.; Dimke, H.; Alexander, R.T. Deficiency of Carbonic Anhydrase II Results in a Urinary Concentrating Defect. *Front. Physiol.* **2017**, *8*, 1108. [CrossRef]
17. Castro Dias, M.; Coisne, C.; Baden, P.; Enzmann, G.; Garrett, L.; Becker, L.; Holter, S.M.; German Mouse Clinic, C.; Hrabe de Angelis, M.; Deutsch, U.; et al. Claudin-12 is not required for blood-brain barrier tight junction function. *Fluids Barriers CNS* **2019**, *16*, 30. [CrossRef]
18. Sabolic, I.; Valenti, G.; Verbavatz, J.M.; Van Hoek, A.N.; Verkman, A.S.; Ausiello, D.A.; Brown, D. Localization of the CHIP28 water channel in rat kidney. *Am. J. Physiol.* **1992**, *263*, C1225–C1233. [CrossRef]
19. Vilas, G.; Krishnan, D.; Loganathan, S.K.; Malhotra, D.; Liu, L.; Beggs, M.R.; Gena, P.; Calamita, G.; Jung, M.; Zimmermann, R.; et al. Increased water flux induced by an aquaporin-1/carbonic anhydrase II interaction. *Mol. Biol. Cell* **2015**, *26*, 1106–1118. [CrossRef]
20. Gong, Y.; Renigunta, V.; Himmerkus, N.; Zhang, J.; Renigunta, A.; Bleich, M.; Hou, J. Claudin-14 regulates renal Ca^{++} transport in response to CaSR signalling via a novel microRNA pathway. *EMBO J.* **2012**, *31*, 1999–2012. [CrossRef] [PubMed]
21. Rievaj, J.; Pan, W.; Cordat, E.; Alexander, R.T. The Na^+/H^+ exchanger isoform 3 is required for active paracellular and transcellular Ca^{2+} transport across murine cecum. *Am. J. Physiol. Gastrointest. Liver Physiol.* **2013**, *305*, G303–G313. [CrossRef] [PubMed]
22. Alexander, R.T.; Dimke, H.; Cordat, E. Proximal tubular NHEs: Sodium, protons and calcium? *Am. J. Physiol. Renal Physiol.* **2013**, *305*, F229–F236. [CrossRef] [PubMed]
23. Schultheis, P.J.; Clarke, L.L.; Meneton, P.; Miller, M.L.; Soleimani, M.; Gawenis, L.R.; Riddle, T.M.; Duffy, J.J.; Doetschman, T.; Wang, T.; et al. Renal and intestinal absorptive defects in mice lacking the NHE3 Na^+/H^+ exchanger. *Nat. Genet.* **1998**, *19*, 282–285. [CrossRef] [PubMed]
24. Leong, P.K.; Devillez, A.; Sandberg, M.B.; Yang, L.E.; Yip, D.K.; Klein, J.B.; McDonough, A.A. Effects of ACE inhibition on proximal tubule sodium transport. *Am. J. Physiol. Renal Physiol.* **2006**, *290*, F854–F863. [CrossRef]
25. Riquier-Brison, A.D.; Leong, P.K.; Pihakaski-Maunsbach, K.; McDonough, A.A. Angiotensin II stimulates trafficking of NHE3, NaPi2, and associated proteins into the proximal tubule microvilli. *Am. J. Physiol. Renal Physiol.* **2010**, *298*, F177–F186. [CrossRef]
26. Plain, A.; Wulfmeyer, V.C.; Milatz, S.; Klietz, A.; Hou, J.; Bleich, M.; Himmerkus, N. Corticomedullary difference in the effects of dietary Ca^{2+} on tight junction properties in thick ascending limbs of Henle's loop. *Pflug. Arch.* **2016**, *468*, 293–303. [CrossRef]
27. Enck, A.H.; Berger, U.V.; Yu, A.S. Claudin-2 is selectively expressed in proximal nephron in mouse kidney. *Am. J. Physiol. Renal Physiol.* **2001**, *281*, F966–F974. [CrossRef]
28. Pei, L.; Solis, G.; Nguyen, M.T.; Kamat, N.; Magenheimer, L.; Zhuo, M.; Li, J.; Curry, J.; McDonough, A.A.; Fields, T.A.; et al. Paracellular epithelial sodium transport maximizes energy efficiency in the kidney. *J. Clin. Investig.* **2016**, *126*, 2509–2518. [CrossRef]
29. Greger, R.; Lang, F.; Oberleithner, H. Distal site of calcium reabsorption in the rat nephron. *Pflug. Arch.* **1978**, *374*, 153–157. [CrossRef]
30. Gattineni, J.; Bates, C.; Twombley, K.; Dwarakanath, V.; Robinson, M.L.; Goetz, R.; Mohammadi, M.; Baum, M. FGF23 decreases renal NaPi-2a and NaPi-2c expression and induces hypophosphatemia in vivo predominantly via FGF receptor 1. *Am. J. Physiol. Renal Physiol.* **2009**, *297*, F282–F291. [CrossRef]
31. Olauson, H.; Lindberg, K.; Amin, R.; Jia, T.; Wernerson, A.; Andersson, G.; Larsson, T.E. Targeted deletion of Klotho in kidney distal tubule disrupts mineral metabolism. *J. Am. Soc. Nephrol.* **2012**, *23*, 1641–1651. [CrossRef]

32. Ure, M.E.; Heydari, E.; Pan, W.; Ramesh, A.; Rehman, S.; Morgan, C.; Pinsk, M.; Erickson, R.; Herrmann, J.M.; Dimke, H.; et al. A variant in a cis-regulatory element enhances claudin-14 expression and is associated with pediatric-onset hypercalciuria and kidney stones. *Hum. Mutat.* **2017**, *38*, 649–657. [CrossRef] [PubMed]
33. Wiebe, S.A.; Plain, A.; Pan, W.; O'Neill, D.; Braam, B.; Alexander, R.T. NHE8 attenuates Ca^{2+} influx into NRK cells and the proximal tubule epithelium. *Am. J. Physiol. Renal Physiol.* **2019**, *317*, F240–F253. [CrossRef] [PubMed]
34. Greger, R. Cation selectivity of the isolated perfused cortical thick ascending limb of Henle's loop of rabbit kidney. *Pflug. Arch.* **1981**, *390*, 30–37. [CrossRef] [PubMed]
35. Gunzel, D.; Stuiver, M.; Kausalya, P.J.; Haisch, L.; Krug, S.M.; Rosenthal, R.; Meij, I.C.; Hunziker, W.; Fromm, M.; Muller, D. Claudin-10 exists in six alternatively spliced isoforms that exhibit distinct localization and function. *J. Cell Sci.* **2009**, *122*, 1507–1517. [CrossRef] [PubMed]
36. Kimizuka, H.; Koketsu, K. Ion transport through cell membrane. *J. Theor. Biol.* **1964**, *6*, 290–305. [CrossRef]
37. Thissen, D.; Steinberg, L.; Kuang, D. Quick and easy implementation of the Benjamini-Hochberg procedure for controlling the false positive rate in multiple comparisons. *J. Educ. Behav. Stat.* **2002**, *27*, 77–83. [CrossRef]

International Journal of
Molecular Sciences

MDPI

Review

A Novel Claudinopathy Based on Claudin-10 Mutations

Susanne Milatz *

Institute of Physiology, Kiel University, Christian-Albrechts-Platz 4, 24118 Kiel, Germany

Received: 15 October 2019; Accepted: 27 October 2019; Published: 30 October 2019

Abstract: Claudins are key components of the tight junction, sealing the paracellular cleft or composing size-, charge- and water-selective paracellular channels. Claudin-10 occurs in two major isoforms, claudin-10a and claudin-10b, which constitute paracellular anion or cation channels, respectively. For several years after the discovery of claudin-10, its functional relevance in men has remained elusive. Within the past two years, several studies appeared, describing patients with different pathogenic variants of the *CLDN10* gene. Patients presented with dysfunction of kidney, exocrine glands and skin. This review summarizes and compares the recently published studies reporting on a novel autosomal-recessive disorder based on claudin-10 mutations.

Keywords: tight junction; paracellular permeability; paracellular sodium transport; thick ascending limb; nephropathy; HELIX syndrome; hypokalemia; hypermagnesemia; anhidrosis; gland dysfunction

1. Introduction

1.1. Claudin-10

The protein family of claudins is a key component of the tight junction (TJ). Claudins comprise four transmembrane segments (TM1-4), two extracellular segments (ECS1 and 2) and intracellular N- and C-termini. Embedded in the plasma membranes of adjacent cells, they interact with each other within the same plasma membrane but also across the paracellular cleft, with claudins of the neighboring cell (cis- or trans-interaction, respectively). By this means, they form a complex strand meshwork and determine tightness and selectivity of the bicellular TJ. Whereas most claudins exhibit a mainly sealing function, some claudins form size-, charge- and water-selective channels through the TJ [1–18].

The claudin family encompasses at least 24 members in mammals. The human gene encoding claudin-10 (*CLDN10*) contains six exons and gives rise to two major isoforms: claudin-10a and -10b. According to their usage of either exon 1a or 1b, they differ in their TM1 and ECS1 (Figure 1). As ECS1 acts as main determinant of charge selectivity, claudin-10a and -10b strands exhibit contrarian permeability properties.

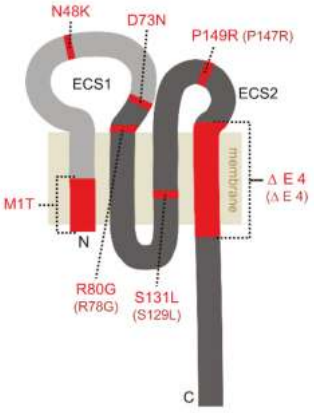

Figure 1. Predicted topology of claudin-10. The two major isoforms claudin-10a and claudin-10b differ in their first transmembrane segment and most of the first extracellular segment (ECS1), both shown in light grey. The remaining protein sequence is identical (shown in dark grey). The mutations discovered to date (red) comprise single amino acid substitutions or large deletions (M1T, ΔE4) and affect either both claudin-10a and claudin-10b or only claudin-10b. The existing claudin-10a variants with respective residue numbering are depicted in parentheses.

Due to claudin-10a's equipment with seven positive and only one negative amino acid in ECS1, it is predestined to form a paracellular anion channel [10,12]. Expression of human claudin-10a in the poorly ion permeable cell line MDCK C7 resulted in a decrease in transepithelial resistance (TER) without alteration in preference for Na^+ or Cl^- [12]. Moreover, claudin-10a expression increased the relative NO_{3-} permeability but decreased the permeability to the anion pyruvate, suggesting that claudin-10a modifies the anion preference of the paracellular pathway [12].

ECS1 of claudin-10b comprises four positive and five negative amino acids. In most cell culture models, heterologous expression of human or murine claudin-10b led to a marked decrease in TER that was based on an increase in Na^+ permeability over Cl^- permeability ($P_{Na}{}^+/P_{Cl}{}^-$). Further studies revealed a relative strong permeability to all monovalent cations with preference for Na^+, a lesser permeability to divalent cations and impermeability to larger molecules (4 kDa dextran) or water of the claudin-10b-based paracellular channel [10,12,13,19].

Claudin-10a and -10b do not only differ significantly in their function but also with respect to their expression in the body. Whereas claudin-10a appears to be restricted to the kidney, claudin-10b has been detected in many tissues, including kidney, skin, salivary glands, sweat glands, brain, lung and pancreas [10,12,20]. Along the kidney tubule, claudin-10a is expressed in the proximal tubule to the S3 segment whereas the main expression site of claudin-10b is the thick ascending limb of Henle's loop (TAL). Claudin-10b is found along the whole medullary–cortical axis of TAL from inner stripe of outer medulla (ISOM) to outer stripe of outer medulla (OSOM) to the renal cortex. In ISOM TAL, to current knowledge, solely claudin-10b constitutes the bicellular TJ, where it facilitates Na^+ reabsorption [21,22]. Towards OSOM and cortex, a TAL mosaic claudin expression is found. Claudin-10b equips part of the TJs, whereas the remaining TJs contain a complex of claudin-3, -16, -19 and to a smaller extent claudin-14 [21–23]. This complex is involved in the reabsorption of divalent cations such as Ca^{2+} and Mg^{2+} in the TAL. The thin limb of Henle also incorporates claudin-10, as yet the identity of the present isoform is unknown [24].

An important insight into the physiological role of claudin-10b was provided by the mouse model generated by Breiderhoff et al., lacking claudin-10 in the entire loop of Henle. These mice featured a strongly reduced paracellular Na^+ selectivity in the TAL that led to a urinary concentration defect and was accompanied by hypermagnesemia, polyuria, polydipsia, elevated plasma urea levels and

compensatorily increased K^+ and H^+ secretion [25,26]. This misbalanced TAL electrolyte handling was accompanied by a severe medullary nephrocalcinosis in these animals.

1.2. Claudinopathies

So far, a number of human hereditary diseases based on defects in claudin-1, -14, -16 and -19 have been reported [27–32]. However, for 18 years after the discovery of claudin-10, its functional relevance in men has remained unclear. On the one hand, defects in the *CLDN10* gene are rare and clinical manifestations occur mainly in patients with biallelic defects (autosomal recessive disorder). On the other hand, some patients presented with symptoms many years ago but were originally misdiagnosed with Bartter syndrome or Gitelman syndrome. Both diseases are characterized by a salt-losing nephropathy with an imbalance in Ca^{2+} and Mg^{2+} homeostasis. In Bartter syndrome, the transcellular NaCl reabsorption in the TAL is disrupted, due to mutations in the Na-K-Cl cotransporter 2 (NKCC2), the renal outer medullary potassium channel (ROMK1) or the Cl^- channel Kb (ClC-Kb) [33–36]. Gitelman syndrome is caused by mutations affecting the Na^+-Cl^- cotransporter (NCC) in the distal convoluted tubule [37]. Nowadays, whole-exome sequencing is available at lower cost and increasingly used to identify the cause of rare mendelian disorders. In 2017, three studies reported on patients with different pathogenic variants of *CLDN10* [38–40]. Hadj-Rabia et al. coined a novel disease syndrome, summarizing the clinical manifestations of their patients (HELIX for hypohidrosis, electrolyte imbalance, lacrimal gland dysfunction, ichthyosis, xerostomia) [39]. This review aims to summarize and compare the data of Bongers et al., Hadj-Rabia et al., Klar et al. and a case report by Meyers et al., all describing a novel claudinopathy based on *CLDN10* mutations [38–41].

2. Clinical Manifestations

To date, a total of 22 patients carrying homozygous or compound heterozygous *CLDN10* mutations have been reported, their ages ranging from 4 to 53 years. Patients were mostly born in consanguineous families and first symptoms often occurred in early childhood, sometimes directly after birth. Patients presented with first symptoms as anhidrosis, xerostomia, alacrima, muscle cramps, falls, or chest pain. Table 1 provides a summary of all patient groups and their clinical manifestations.

Table 1. Summary of all patient groups, their *CLDN10* variants and clinical manifestations.

Publication	Bongers et al. [38]	Bongers et al. [38]	Klar et al. [40]	Hadj-Rabia et al. [39]	Hadj-Rabia et al. [39]	Meyers et al. [41]
Number of patients	1 (patient 1)	1 (patient 2)	13	4 (family A)	2 (family B)	1
Claudin-10a variant	P147R, ΔE4	wildtype, P147R	wildtype	S129L	wildtype	R78G
Claudin-10b variant	P149R, ΔE4	D73N, P149R	N48K	S131L	M1T	R80G
Loss of claudin-10b function	partial/complete	partial	partial	complete	complete *	not analyzed
Extrarenal manifestations						
Xerostomia	yes	yes	yes	yes	yes	yes
Alacrima	n.r.	yes	yes	yes	yes	yes
Hypohidrosis	yes	yes	yes	yes	yes	yes
Dermatological manifestations in addition to hypohidrosis	yes	yes	no	yes	yes	no

Table 1. *Cont.*

Publication	Bongers et al. [38]	Bongers et al. [38]	Klar et al. [40]	Hadj-Rabia et al. [39]	Hadj-Rabia et al. [39]	Meyers et al. [41]
Renal function						
Hypermagnesemia	yes	no	yes	yes	yes **	yes
Urinary magnesium	rather high ***	normal ***	low	low or normal	rather high	n.r.
Plasma/serum calcium	upper normal range	upper normal range	normal	1 increased, 3 normal	normal	n.r.
Hypocalciuria	yes	yes	yes	yes	yes	yes
Hypokalemia	yes	yes	no	yes **	yes **	yes
Metabolic alkalosis	yes	yes	n.r.	n.r.	n.r.	n.r.
Plasma aldosterone	n.r.	n.r.	n.r.	normal or high	normal or high	high
Polyuria	yes	no	no	inconsistent	inconsistent	yes
Polydipsia	n.r.	n.r.	n.r.	yes	yes	yes
Estimated Estimated glomerular filtration rate	decreased	normal	lower normal range	normal or decreased	normal	decreased
Kidney form/size	small right kidney	normal	normal	n.r.	normal	normal
Nephrocalcinosis	no	no	n.r.	no	no	no
Blood pressure	lower normal range	low to normal	n.r.	low	low	normal

* with the exception of normal deposition in eccrine sweat glands. ** considering the patient's age. *** compared to heterozygous family members. n.r. not reported

2.1. Hypohidrosis, Xerostomia and Alacrima

Hypohidrosis with intolerance to heat was frequently reported as one of the first symptoms observed in early childhood. Apparently, all known patients suffer from hypohidrosis, including the two patients described by Bongers et al., who did not complain about reduced sweating at the outset but confirmed hypohidrosis subsequently [38], (personal communication with Tom Nijenhuis, Radboud University Medical Center, Nijmegen). Klar et al. evaluated heat intolerance in two patients by exposure to heat for 20 min, which resulted in a rapidly increased body temperature from 37 °C to 39.6 °C and an increase in heart rate [40]. Generalized hypohidrosis was verified using starch-iod test applied on different body parts, corroborating a severe dysfunction of eccrine sweat glands.

Likewise, xerostomia due to reduced saliva production is apparently a typical symptom of *CLDN10* defects as it has been documented in all known patients including the patients examined by Bongers et al. [39–41]; (personal communication with Tom Nijenhuis). Hadj-Rabia et al. analyzed xerostomia by saliva secretion rate measurements in three adult patients [39]. As a result, the flow of fluid was reduced by 98% in patients compared to healthy controls. Moreover, the fluid/mucus ratio of saliva was dramatically decreased in patients with *CLDN10* variants. Hadj-Rabia also documented a poor dental condition with severe enamel wear and generalized gingival inflammation of their patients [39]. This is attributed to aptyalism but might also be a consequence of disturbed enamel mineralization (amelogenesis imperfecta) as claudin-10 expression was found in ameloblasts of mice [42].

Alacrima (the inability to produce tears) was described in the majority of patients and was confirmed using Schirmer's test by Hadj-Rabia et al. [39–41].

2.2. Dermatological Manifestations in Addition to Hypohidrosis

The occurrence of ichthyosis and other dermatological manifestations among patients was rather inconsistent. Hadj-Rabia described mild forms of ichthyosis with a thickened stratum corneum, palmar hyperlinearity and plantar keratoderma in two unrelated families with different *CLDN10* variants. Histological analysis of skin biopsies revealed slight epidermal hyperplasia and an abnormally high number of dilated eccrine sweat glands. The patients examined by Bongers et al. reported dry skin in retrospect, and dermatological consultation showed palmar hyperlinearity and plantar hyperkeratosis (personal communication with Tom Nijenhuis). In contrast, patients examined by Klar et al. and Meyers et al. showed no dermatological manifestations apart from hypohidrosis [40,41]. Morphology and number of eccrine sweat glands appeared normal in patients examined by Klar et al. [40].

2.3. Kidney Dysfunction

A number of features revealing a renal dysfunction in patients has been reported. All patients showed a disturbance in electrolyte balance, becoming manifest in hypermagnesemia, hypokalemia and hypocalciuria. Hypermagnesemia was present in the majority of patients, most pronounced in childhood and decreasing with age (Figure 2A). In contrast, hypokalemia was most severe in adults with the exception of the patient group examined by Klar et al. [40],(Figure 2B). These patients had serum K^+ levels in the upper normal range or higher in adulthood. The reason for that discrepancy remains unclear. Admittedly, more longitudinal intraindividual data over a longer time period are required for confirmation of the apparent age dependencies depicted in Figure 2. Bongers et al. reported that hypokalemia was accompanied by metabolic alkalosis in their patients [38].

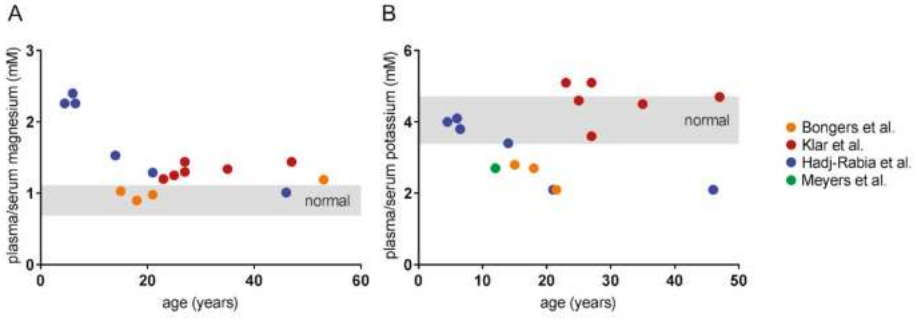

Figure 2. Available plasma/serum values of patients plotted against their age. (**A**) Hypermagnesemia is most pronounced in children and decreases with age. (**B**) Plasma/serum potassium levels decline with age, revealing a marked hypokalemia in adolescence. The only exception is the patient group examined by Klar et al [40]. Values were partly obtained by conversion into mmol/L. The publication by Bongers et al. provided data points of the same patients at different ages [38].

Of note, hypocalciuria appears to be a common manifestation as it was distinct in all tested patients and at all ages with plasma/serum Ca^{2+} in the normal or upper normal range. Despite the strong incidence of hypermagnesemia and hypocalciuria, most patients showed no decrease in urinary Mg^{2+} or an elevation of plasma/serum Ca^{2+}. The reason for this is not clear. However, it appears that renal Ca^{2+} and Mg^{2+} reabsorption and handling are tightly but differentially regulated.

In some patients, plasma aldosterone levels were determined and revealed hyperaldosteronism [39, 41]. The underlying cause of the electrolyte disorder and hyperaldosteronism is a NaCl wasting in the TAL, the main expression site of claudin-10b. Plasma/serum Na^+ appeared mostly normal if tested, presumably due to compensation in the more distal parts of the nephron. However, slight hypochloremia was present in few patients [39–41].

Bongers et al. tested the urine concentrating ability of one patient [38]. As a result, the patient showed a reduced response to thirsting and the application of the synthetic vasopressin analogue ddAVP. Verification of an adequate aquaporin-2 response in the collecting duct pointed to a dysfunction of NaCl reabsorption in the TAL as cause for an insufficient build-up of interstitial tonicity. In line with the reduced urine concentrating ability, this patient suffered from polyuria. Overall, the occurrence of polyuria and polydipsia among patients was rather inconsistent and might also be partially attributed to xerostomia.

The estimated glomerular filtration rate (eGFR) as indicator for kidney function was determined in most patients. It ranged from low to normal and decreased with time in some patients, indicating a progressive renal insufficiency. With one exception, kidneys analyzed by computer tomography scans were normal in form and size and, in contrast to the mouse model, nephrocalcinosis was not detected in any patient [38–41]. However, several patients of Klar et al. suffered from recurrent kidney pain due to nephrolithiasis [40]. If determined, the patient's blood pressure ranged from low to normal. Some patients complained of atypical chest pain, heart palpitations, collapse, falls, or muscle cramps. Klar et al. additionally analyzed lung and pancreas function without abnormal findings [40].

3. Protein Variants and Their Functional Analyses

Figure 1 displays all naturally occurring claudin-10 variants reported so far. Four mutations apply to both claudin-10a and claudin-10b proteins, whereas three defects affect only claudin-10b. Markedly, there are no obvious differences between the six patients with both defective isoforms and the 16 patients with defective claudin-10b and unaffected or only heterozygously affected claudin-10a, at least none that could be easily attributed to that special factor (Table 1). Of note, to date no patients with exclusive claudin-10a variants (without affection of claudin-10b) were described, also pointing to a minor role of claudin-10a defects in men.

Because of the predominant importance of claudin-10b defects in patients, most in vitro studies were carried out using the mutants of this isoform. Several analyses addressed localization, strand formation and channel function of mutated claudin-10b vs. wildtype protein. In the following, the denomination of claudin-10 variants refers to the alteration in claudin-10b protein, i.e., the amino acid exchange or deletion.

3.1. Membrane Localization

Correct trafficking to the membrane of a claudin variant is a fundamental prerequisite for a physiological function within the TJ. Similar to the wild type protein, the claudin-10b N48K mutant analyzed by Klar et al. resided in the cell membrane when heterologously expressed in the epithelial cell line MDCK C7. However, the subcellular distribution of N48K suggested an increased intracellular accumulation [40]. A very similar distribution in MDCK C7 cells was observed for the variants D73N and P149R investigated by Bongers et al. [38]. In sharp contrast, their third variant ΔE4 was very weakly expressed and did not localize to the cell membrane. This variant lacks TM4 which inevitably leads to exclusion from the plasma membrane. Likewise, the variant S131L with a missense mutation in TM3 analyzed by Hadj-Rabia et al. showed no detectable presence at the plasma membrane when expressed in a mouse TAL cell culture [39]. Contradictorily, the claudin-10 variant M1T probably lacking part of TM1 revealed normal deposition in eccrine sweat glands of a skin biopsy but was not localized in the TAL of a kidney biopsy [39]. Klar et al. also performed immunostainings of sweat glands and observed a normal localization of N48K in membranes facing the lumen but also an abnormally strong intracellular distribution without accumulation in canaliculi, pointing to a reduced delivery to the TJs [40].

Overall, the analyzed claudin-10b mutations resulted either in complete absence from the plasma membrane (especially those affecting one of the transmembrane segments) or, on the other hand, can basically insert into the plasma membrane, although an increased distribution outside the TJ suggests a reduced function.

3.2. TJ Strand Formation

Strand formation is the consequence of cis- and trans-interaction between claudins. In case of claudin-10b and its mutants, interaction with itself (homophilic interaction) is of particular importance as claudin-10b is not capable of interaction with any other claudin in the TAL [22]. Trans-interaction (with claudins in the opposing plasma membrane) can be detected by heterologous expression of the appropriate claudin in TJ-free HEK 293 cells and subsequent microscopic analysis of so-called contact enrichment. If the claudin is capable of autonomous strand formation, it enriches at cell–cell-contacts of two transfected cells compared to the remaining cell membrane. Bongers et al. reported a basal capability of trans-interaction and TJ formation for variants D73N and P149R but not for the truncated variant ΔE4 [38]. Klar et al. did not detect a significant contact enrichment of their mutant N48K, tantamount to a perturbed homophilic trans-interaction [40]. Moreover, homophilic cis-interaction was analyzed by Förster resonance energy transfer (FRET) and revealed an exaggerated oligomerization of N48K proteins. Ultrastructural analysis using freeze fracture electron microscopy showed that N48K formed few particle-typed TJ strands with less compact meshworks, compared to wildtype claudin-10b [40].

Overall, the few claudin-10b variants analyzed with respect to interaction properties mostly showed a fundamental capability of homophilic interaction and strand formation. Nonetheless, quality and/or quantity of interaction and strand assembly were impaired. As anticipated, the lack of a transmembrane segment resulted in a complete loss of function.

3.3. Channel Function

Analyses of claudin-10b mutant channel properties by means of electrophysiological measurements are available only for the N48K variant, as yet. Klar et al. stably transfected MDCK C7 cells and compared claudin-10b N48K-with wildtype-expressing cells [40]. The cation selectivity (P_{Na}/P_{Cl}) of N48K-expressing cells was first similar to that of claudin-10b wildtype-transfected cells but progressively decreased with passaging, more and more resembling that for clones with a weak expression of claudin-10b wildtype. Moreover, N48K-expressing cells showed a higher TER and altered relative permeabilities to other monovalent cations, compared to claudin-10 wildtype-expressing cells. Together, the results suggest that the channels formed by N48K have a subnormal Na^+ permeability and that the overall number of channels is markedly reduced [40].

In an attempt to mimic sweat secretion, Klar et al. used a 3D cell culture model by growing MDCK C7 cells in Matrigel. Epithelial cells formed three-dimensional cysts with the apical side towards the lumen. Cysts formed by wildtype-claudin-10b-expressing cells increased their lumen by transcellular Cl^- secretion, followed by claudin-10b-mediated Na^+ permeation and subsequent water transport. N48K-expressing cysts, in contrast, showed considerably less lumen expansion, indicating a reduced overall Na^+ conductance. In line with electrophysiological studies, this is probably caused by a combination of a reduction in single channel Na^+ conductance and a reduction in the overall number of channels [40].

3.4. Protein Structure

In order to determine the cause of the impairments brought about by single amino acid substitutions in claudin-10b, Klar et al. and Hadj-Rabia et al. provided 3D homology models of N48K or S131L, respectively, based on the crystal structure of murine claudin-15 [39,40,43]. The N48K mutation, localized in ECS1, appears to disrupt an intramolecular bridging between different backbones in ECS1 and membrane–ECS1-transition. Moreover, a potential electrostatic interaction could be disturbed by the replacement of an uncharged residue by a positively charged one. These alterations are presumed to perturb protein interaction and function indirectly [40]. The S131L mutation analyzed by Hadj-Rabia et al. affects TM3 and is suggested to clash sterically with several of the surrounding residues, especially of TM1 and -2 and by this perturbing the compactness of the helical bundle [39].

Furthermore, an intrahelical stabilizing hydrogen bond is lost by the amino acid substitution. As a consequence of the helical bundle destabilization, the S131L variant fails to insert into the cell membrane and is retained in the cytosol.

The impact of the amino acid substitutions D73N, R80G and P149R on protein folding or pore formation remain temporarily unsolved, also because functional data on the particular variants are scarce or absent. In general, substitution of a charged residue by an uncharged one in ECS1 (D73N, R80G) is considered critical for ion pore formation. On the other hand, neither D73 nor R80 have been shown to be important for charge selectivity of pore-forming claudins (for review see [44]). However, R80 is localized at the predicted transition between ECS1 and TM2 and might be crucial for the formation of the helical bundle. P149 in ECS2 is conserved in the majority of claudins. It is suggested to stabilize ECS2 conformation and to play a role in correct TJ strand arrangement [45].

3.5. Short Summary of Functional Analyses

Taken together, claudin-10b variants with truncations in one of the transmembrane segments necessarily show a complete loss of function as they are not inserted into the plasma membrane whereas variants with point mutations in one of the loops often keep a certain residual function. Nevertheless, localization, interaction and channel function can be impaired to a certain extent. Point mutations in transmembrane segments still have a high probability to severely affect membrane localization, probably depending on the substituting residue. The comparatively poor viability of cells expressing claudin-10b mutant proteins compared to wildtype-expressing cells and the increased degradation of mutant proteins due to suboptimal folding and localization as observed for several variants appear to be a common incidence and presumably contribute pivotally to the harmfulness of mutations [38–40].

Of course, the question arises to which extent site and type of claudin-10b mutation determine the clinical outcome. The most prominent differences between patient groups with particular *CLDN10* variants concern plasma/serum potassium values and the dermatological phenotype. However, with the actual number of patients and the information available it is difficult to assess a possible correlation and future studies will probably help to clarify that issue.

4. Mechanisms of Disease

The naturally occurring claudin-10 mutations discovered during the last years result in a complete or partial loss of function of the claudin-10b isoform and subsequently in a reduced or absent paracellular Na^+ permeation in the TAL as well as in sweat, salivary and lacrimal glands. Figures 3 and 4 illustrate the mechanistic principles, particularly the role of claudn-10b in epithelial transport, underlying a correct organ function.

4.1. Kidney

As mentioned above, the exact role of claudin-10a in the proximal tubule is not understood, as yet. Based on cell culture experiments, a function as paracellular anion channel is assumed (Figure 3A). However, the data presented in the reviewed studies indicate a rather minor role in the pathogenesis of claudin-10 defects. It appears likely that possible impairments affecting the proximal tubule can be distally compensated to a certain degree as it was shown for the loss of claudin-2 in a mouse model [46]. After all, future studies will have to clarify the physiological relevance of claudin-10a.

In the TAL, half of the Na^+ is reabsorbed paracellularly via the claudin-10b paracellular channel as a consequence of transcellular net uptake of Cl^- involving NKCC2 (Figure 3B). In TAL of the ISOM, claudin-10b dominates the TJ, although claudin-3, -16 and -19 are expressed intracellularly. Towards OSOM and cortex, an additional epithelial cell type occurs, expressing claudin-3, -16 and -19 but no claudin-10b. These cells form TJ complexes that are spatially separated from claudin-10b TJs and are involved in the reabsorption of Mg^{2+} and Ca^{2+}. The residual TJs assembled exclusively by claudin-10b enable a backflux of Na^+ into the lumen, due to its concentration gradient, thus adding to the lumen-positive potential and supporting the paracellular reabsorption of Mg^{2+} and Ca^{2+} [21,22,47].

An impaired claudin-10b function would reduce the Na^+ reabsorption in the TAL by the paracellular portion and lead to a compensatorily increased electrogenic Na^+ reabsorption via the epithelial sodium channel (ENaC) in the more distal nephron segments. This, in turn, would promote K^+ and H^+ loss. Whereas hyperaldosteronism, hypokalemia and metabolic alkalosis in patients with pathogenic claudin-10b variants are the consequence of compensatory mechanisms in the distal nephron, hypermagnesemia and hypocalciuria can be attributed to an exaggerated paracellular reabsorption of Mg^{2+} and Ca^{2+} in the TAL. In the mouse model described by Breiderhoff et al., the lack of claudin-10b in the TAL results in an increased distribution of the TJ complex containing claudin-16 and -19 over all TJs, including those in the ISOM, where normally only claudin-10b is constituting the TJ [22,25,26,48]. If a similar process takes place in men with *CLDN10* variants that lead to a reduced claudin-10b insertion into TAL TJs, it would explain the hypermagnesemia, in line with the mouse model. Apparently, in patients, the reabsorption of Mg^{2+} and Ca^{2+} is shifted from cortex/OSOM TAL to ISOM TAL and the lack of claudin-10b-based Na^+ backflux as additional driving force in cortex/OSOM TAL is thereby overcompensated.

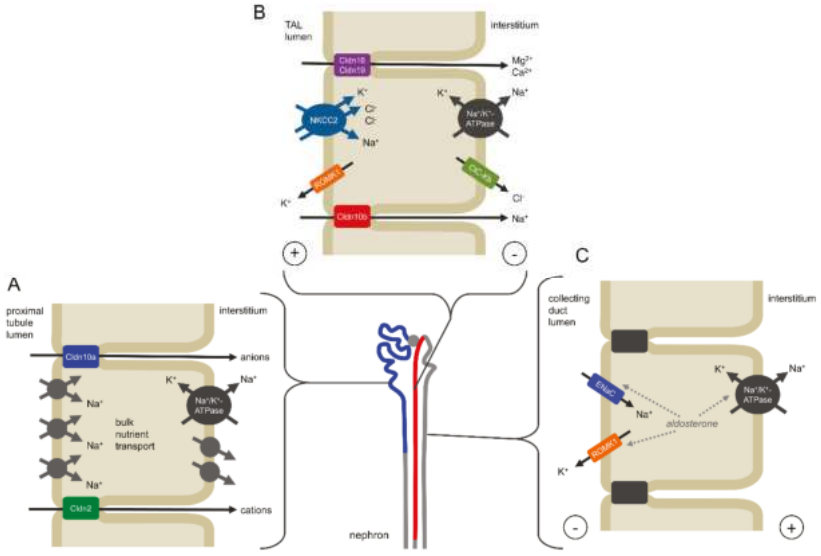

Figure 3. Mechanisms of claudin-10 function in the kidney. (**A**) Claudin-10a is expressed in the renal proximal tubule to the S3 segment (shown in blue) where it forms a paracellular anion pathway. Patients with pathogenic variants of both claudin-10a and claudin-10b appear to have no clinical manifestations different from patients with only claudin-10b variants, suggesting a minor role of an impaired claudin-10a function and/or compensation in more distal nephron segments. (**B**) Claudin-10b is mainly localized in the thick ascending limb of Henle's loop (TAL, shown in red) where it facilitates the paracellular reabsorption of Na^+. Na^+, 2 Cl^- and K^+ enter the epithelial cell by the secondary active NKCC2 transporter. Whereas Na^+ and Cl^- leave the cell basolaterally, K^+ is recirculated via the ROMK1 channel. This results in a net reabsorption of Cl^- and causes a lumen-positive transepithelial potential, which in turn drives paracellular Na^+ reabsorption via claudin-10b. Towards the distal TAL segment the expression of claudin-16 and -19 is involved in the paracellular reabsorption of Mg^{2+} and Ca^{2+}. Here, Na^+ can backflux into the lumen along its concentration gradient, thus adding to the lumen-positive potential as a driving force for Mg^{2+}- and Ca^{2+} reabsorption. An impairment of claudin-10b function would result in a NaCl wasting in the TAL and an expansion of claudin-16 and -19 over all TJs, causing hypermagnesemia and hypocalciuria. (**C**) Na^+ wasting in the TAL is compensated in the more distal nephron involving electrogenic transport via ENaC, promoting secretion of K^+ and causing hypokalemia.

However, the reasons for the magnitude of hypokalemia and hypermagnesemia depending on the patients' age remain unsolved.

4.2. Glands

In glands, a concerted secretion of ions and water across the glandular epithelium is required in order to produce sweat, saliva or lacrimal fluid, respectively (Figure 4). Molecular mechanisms in the secretory coil of sweat glands as well as in salivary and lacrimal acinar cells are partially understood and share certain mechanistic similarities [49–56]. Stimulation of G-protein-coupled muscarinergic receptors by acetylcholine results in an increased intracellular concentration of free Ca^{2+}, which activates apical Cl^- channels and basolateral K^+ channels. Subsequent activation of NKCC1 in the basolateral membrane leads to an influx of Na^+, K^+ and Cl^- into secretory cells. Na^+ and K^+ circulate across the basolateral membrane via NKCC1, the Na^+/K^+-ATPase and/or K^+ channels, respectively. The transcellular net flux of Cl^- via apical channels and basolateral NKCC1 generates a lumen-negative transepithelial potential and drives the paracellular secretion of Na^+ via claudin-10b channels. This is followed by transcellular water secretion involving aquaporin-5 water channels. Although an additional paracellular water secretion is frequently suggested, the strict water impermeability of claudin-10b-based TJs [13] and the implausibility of claudin-10b to form heterogeneous TJs with other claudins [22] rather argue against it.

An impairment of claudin-10b distribution or function as reported by Klar et al. would result in a complete abrogation of Na^+ and subsequent water secretion in sweat, salivary and lacrimal glands and become manifest in hypohidrosis, aptyalism and alacrima as observed in patients [40].

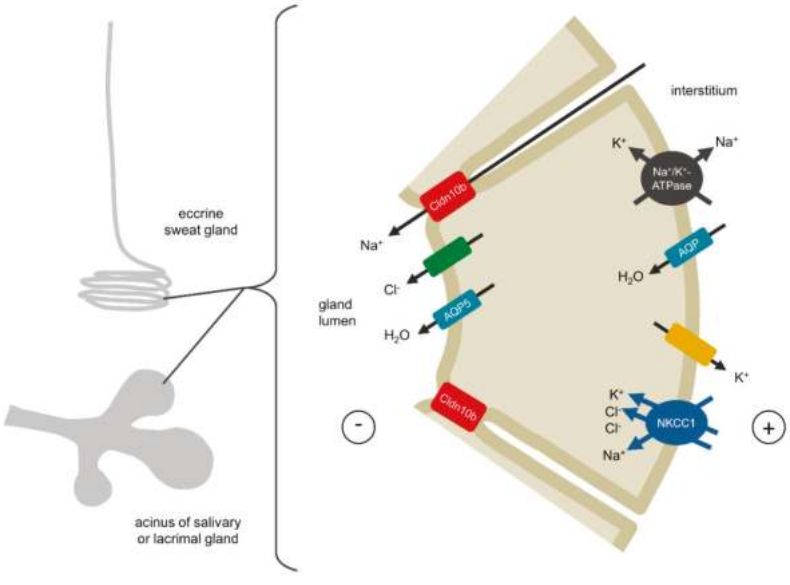

Figure 4. Mechanisms of claudin-10b function in the secretory portion of sweat glands and the acinar cells of salivary and lacrimal glands. During secretion, apical Cl^- channels and basolateral K^+ channels are activated. Na^+, 2 Cl^- and K^+ enter the cell via the basolaterally expressed NKCC1 transporter. Cl^- is secreted into the lumen whereas Na^+ and K^+ leave the cell basolaterally. The secretion of Cl^- drives Na^+ transport via the paracellular claudin-10b channel and transcellular water transport via aquaporins. An abrogation of the claudin-10b-mediated Na^+ transport would result in a complete dysfunction of sweat, saliva and tear secretion.

4.3. Skin

At present it remains unsolved whether dermatological manifestations such as ichthyosis and dry skin are a mere consequence of sweat gland dysfunction or may also be augmented by defective claudin-10 proteins in the epidermis. The mechanical barrier function of the skin is maintained on the one hand by the stratum corneum containing dead, cornified cells (corneocytes) and by the TJs on the other hand (for review see [57]). Functional TJs are localized in the stratum granulosum where they form a liquid–liquid interface barrier. The role of claudins in epidermal barrier function is illustrated by the phenotype of patients with pathogenic variants of the *CLDN1* gene. Patients lacking functional claudin-1 suffer from NISCH syndrome (neonatal ichthyosis–sclerosing cholangitis). The thick, scaly skin of ichthyosis is assumed to result from the skin compensating for barrier dysfunction [58]. On the other hand, claudins are expressed not only in the stratum granulosum but in all living layers of the epidermis and are probably involved in the differentiation of stratum granulosum cells to corneocytes.

Claudin-10 mRNA was detected in human skin biopsies and was found to be downregulated in patients with psoriasis vulgaris [59–61]. Immunohistochemical staining of rodent skin revealed an intracellular localization in the stratum basale [20] or in the stratum corneum [62]. The finding that claudin-10 is expressed beyond the stratum granulosum points to a possible function aside from its role as an ion pathway in the epidermis. However, its particular function in the skin has yet to be unraveled.

5. Summary

The four studies of Bongers et al., Klar et al., Hadj-Rabia et al. and Meyers et al. describe a novel claudinopathy that is based on mutations in the *CLDN10* gene and is characterized by an impaired function of mainly claudin-10b. Patients show a salt-losing nephropathy without hypercalciuria (as in Bartter syndrome) or hypomagnesemia (as in Gitelman syndrome). Main symptoms probably occurring in the majority of present and future patients are:

- age-dependent hypermagnesemia, age-dependent hypokalemia, hypocalciuria;
- hypohidrosis, xerostomia, alacrima;
- possibly dermatological abnormalities.

The severity of clinical manifestations may depend on site and type of mutation. Patients expressing a claudin-10b variant with a defect in one of the transmembrane regions, especially a truncation, are at high risk to develop the full severity of the phenotype. In this respect, genotyping of future patients may further help to correlate mutation type and course of disease. Further functional analysis of found *CLDN10* variants may provide a more detailed insight into the protein function. The reviewed studies demonstrate the significance of proper claudin-10b function for kidney, skin and gland physiology.

Funding: This work received no external funding.

Acknowledgments: I thank Nina Himmerkus (Institute of Physiology, Kiel University, Kiel, Germany) and Tom Nijenhuis (Radboud University Medical Center, Nijmegen, The Netherlands) for reading the manuscript draft and for helpful discussions and suggestions.

Conflicts of Interest: The author declares no conflict of interest.

References

1. Van Itallie, C.; Rahner, C.; Anderson, J.M. Regulated expression of claudin-4 decreases paracellular conductance through a selective decrease in sodium permeability. *J. Clin. Invest.* **2001**, *107*, 1319–1327. [CrossRef] [PubMed]
2. Furuse, M.; Furuse, K.; Sasaki, H.; Tsukita, S. Conversion of zonulae occludentes from tight to leaky strand type by introducing claudin-2 into Madin-Darby canine kidney I cells. *J. Cell Biol.* **2001**, *153*, 263–272. [CrossRef] [PubMed]

3. Furuse, M.; Hata, M.; Furuse, K.; Yoshida, Y.; Haratake, A.; Sugitani, Y.; Noda, T.; Kubo, A.; Tsukita, S. Claudin-based tight junctions are crucial for the mammalian epidermal barrier: a lesson from claudin-1-deficient mice. *J. Cell Biol.* **2002**, *156*, 1099–1111. [CrossRef] [PubMed]
4. Amasheh, S.; Meiri, N.; Gitter, A.H.; Schöneberg, T.; Mankertz, J.; Schulzke, J.D.; Fromm, M. Claudin-2 expression induces cation-selective channels in tight junctions of epithelial cells. *J. Cell. Sci.* **2002**, *115*, 4969–4976. [CrossRef] [PubMed]
5. Colegio, O.R.; Van Itallie, C.M.; McCrea, H.J.; Rahner, C.; Anderson, J.M. Claudins create charge-selective channels in the paracellular pathway between epithelial cells. *Am. J. Physiol., Cell Physiol.* **2002**, *283*, C142–147. [CrossRef]
6. Nitta, T.; Hata, M.; Gotoh, S.; Seo, Y.; Sasaki, H.; Hashimoto, N.; Furuse, M.; Tsukita, S. Size-selective loosening of the blood-brain barrier in claudin-5-deficient mice. *J. Cell Biol.* **2003**, *161*, 653–660. [CrossRef]
7. Van Itallie, C.M.; Fanning, A.S.; Anderson, J.M. Reversal of charge selectivity in cation or anion-selective epithelial lines by expression of different claudins. *Am. J. Physiol. Ren. Physiol.* **2003**, *285*, F1078–1084. [CrossRef]
8. Yu, A.S.L.; Enck, A.H.; Lencer, W.I.; Schneeberger, E.E. Claudin-8 expression in Madin-Darby canine kidney cells augments the paracellular barrier to cation permeation. *J. Biol. Chem.* **2003**, *278*, 17350–17359. [CrossRef]
9. Amasheh, S.; Schmidt, T.; Mahn, M.; Florian, P.; Mankertz, J.; Tavalali, S.; Gitter, A.H.; Schulzke, J.-D.; Fromm, M. Contribution of claudin-5 to barrier properties in tight junctions of epithelial cells. *Cell Tissue Res.* **2005**, *321*, 89–96. [CrossRef]
10. Van Itallie, C.M.; Rogan, S.; Yu, A.; Vidal, L.S.; Holmes, J.; Anderson, J.M. Two splice variants of claudin-10 in the kidney create paracellular pores with different ion selectivities. *Am. J. Physiol. Ren. Physiol.* **2006**, *291*, F1288–F1299. [CrossRef]
11. Angelow, S.; Schneeberger, E.E.; Yu, A.S.L. Claudin-8 expression in renal epithelial cells augments the paracellular barrier by replacing endogenous claudin-2. *J. Membr. Biol.* **2007**, *215*, 147–159. [CrossRef] [PubMed]
12. Günzel, D.; Stuiver, M.; Kausalya, P.J.; Haisch, L.; Krug, S.M.; Rosenthal, R.; Meij, I.C.; Hunziker, W.; Fromm, M.; Muller, D. Claudin-10 exists in six alternatively spliced isoforms that exhibit distinct localization and function. *J. Cell. Sci.* **2009**, *122*, 1507–1517. [CrossRef] [PubMed]
13. Rosenthal, R.; Milatz, S.; Krug, S.M.; Oelrich, B.; Schulzke, J.-D.; Amasheh, S.; Günzel, D.; Fromm, M. Claudin-2, a component of the tight junction, forms a paracellular water channel. *J. Cell. Sci.* **2010**, *123*, 1913–1921. [CrossRef] [PubMed]
14. Milatz, S.; Krug, S.M.; Rosenthal, R.; Günzel, D.; Müller, D.; Schulzke, J.-D.; Amasheh, S.; Fromm, M. Claudin-3 acts as a sealing component of the tight junction for ions of either charge and uncharged solutes. *Biochim. Biophys. Acta* **2010**, *1798*, 2048–2057. [CrossRef] [PubMed]
15. Tamura, A.; Hayashi, H.; Imasato, M.; Yamazaki, Y.; Hagiwara, A.; Wada, M.; Noda, T.; Watanabe, M.; Suzuki, Y.; Tsukita, S. Loss of claudin-15, but not claudin-2, causes Na+ deficiency and glucose malabsorption in mouse small intestine. *Gastroenterology* **2011**, *140*, 913–923. [CrossRef] [PubMed]
16. Krug, S.M.; Günzel, D.; Conrad, M.P.; Rosenthal, R.; Fromm, A.; Amasheh, S.; Schulzke, J.D.; Fromm, M. Claudin-17 forms tight junction channels with distinct anion selectivity. *Cell. Mol. Life Sci.* **2012**, *69*, 2765–2778. [CrossRef]
17. Tanaka, H.; Yamamoto, Y.; Kashihara, H.; Yamazaki, Y.; Tani, K.; Fujiyoshi, Y.; Mineta, K.; Takeuchi, K.; Tamura, A.; Tsukita, S. Claudin-21 Has a Paracellular Channel Role at Tight Junctions. *Mol. Cell. Biol.* **2016**, *36*, 954–964. [CrossRef]
18. Rosenthal, R.; Günzel, D.; Piontek, J.; Krug, S.M.; Ayala-Torres, C.; Hempel, C.; Theune, D.; Fromm, M. Claudin-15 forms a water channel through the tight junction with distinct function compared to claudin-2. *Acta Physiol (Oxf)* **2019**, e13334. [CrossRef]
19. Inai, T.; Kamimura, T.; Hirose, E.; Iida, H.; Shibata, Y. The protoplasmic or exoplasmic face association of tight junction particles cannot predict paracellular permeability or heterotypic claudin compatibility. *Eur. J. Cell Biol.* **2010**, *89*, 547–556. [CrossRef]
20. Inai, T.; Sengoku, A.; Guan, X.; Hirose, E.; Iida, H.; Shibata, Y. Heterogeneity in expression and subcellular localization of tight junction proteins, claudin-10 and -15, examined by RT-PCR and immunofluorescence microscopy. *Arch. Histol. Cytol.* **2005**, *68*, 349–360. [CrossRef]

21. Plain, A.; Wulfmeyer, V.C.; Milatz, S.; Klietz, A.; Hou, J.; Bleich, M.; Himmerkus, N. Corticomedullary difference in the effects of dietary Ca^{2+} on tight junction properties in thick ascending limbs of Henle's loop. *Pflugers Arch.* **2016**, *468*, 293–303. [CrossRef] [PubMed]
22. Milatz, S.; Himmerkus, N.; Wulfmeyer, V.C.; Drewell, H.; Mutig, K.; Hou, J.; Breiderhoff, T.; Müller, D.; Fromm, M.; Bleich, M.; et al. Mosaic expression of claudins in thick ascending limbs of Henle results in spatial separation of paracellular Na^+ and Mg^{2+} transport. *Proc. Natl. Acad. Sci. USA* **2017**, *114*, E219–E227. [CrossRef] [PubMed]
23. Gong, Y.; Renigunta, V.; Himmerkus, N.; Zhang, J.; Renigunta, A.; Bleich, M.; Hou, J. Claudin-14 regulates renal Ca^{++} transport in response to CaSR signalling via a novel microRNA pathway. *EMBO J.* **2012**, *31*, 1999–2012. [CrossRef]
24. Lee, J.W.; Chou, C.-L.; Knepper, M.A. Deep Sequencing in Microdissected Renal Tubules Identifies Nephron Segment-Specific Transcriptomes. *J. Am. Soc. Nephrol.* **2015**, *26*, 2669–2677. [CrossRef] [PubMed]
25. Breiderhoff, T.; Himmerkus, N.; Stuiver, M.; Mutig, K.; Will, C.; Meij, I.C.; Bachmann, S.; Bleich, M.; Willnow, T.E.; Müller, D. Deletion of claudin-10 (Cldn10) in the thick ascending limb impairs paracellular sodium permeability and leads to hypermagnesemia and nephrocalcinosis. *Proc. Natl. Acad. Sci. U.S.A.* **2012**, *109*, 14241–14246. [CrossRef]
26. Seker, M.; Fernandez-Rodriguez, C.; Martinez-Cruz, L.A.; Müller, D. Mouse models of human claudin-associated disorders: benefits and limitations. *Int. J. Mol. Sci.* **2019**. submitted for publication.
27. Weber, S.; Hoffmann, K.; Jeck, N.; Saar, K.; Boeswald, M.; Kuwertz-Broeking, E.; Meij, I.I.; Knoers, N.V.; Cochat, P.; Suláková, T.; et al. Familial hypomagnesaemia with hypercalciuria and nephrocalcinosis maps to chromosome 3q27 and is associated with mutations in the PCLN-1 gene. *Eur. J. Hum. Genet.* **2000**, *8*, 414–422. [CrossRef]
28. Wilcox, E.R.; Burton, Q.L.; Naz, S.; Riazuddin, S.; Smith, T.N.; Ploplis, B.; Belyantseva, I.; Ben-Yosef, T.; Liburd, N.A.; Morell, R.J.; et al. Mutations in the gene encoding tight junction claudin-14 cause autosomal recessive deafness DFNB29. *Cell* **2001**, *104*, 165–172. [CrossRef]
29. Hadj-Rabia, S.; Baala, L.; Vabres, P.; Hamel-Teillac, D.; Jacquemin, E.; Fabre, M.; Lyonnet, S.; De Prost, Y.; Munnich, A.; Hadchouel, M.; et al. Claudin-1 gene mutations in neonatal sclerosing cholangitis associated with ichthyosis: a tight junction disease. *Gastroenterology* **2004**, *127*, 1386–1390. [CrossRef]
30. Thorleifsson, G.; Holm, H.; Edvardsson, V.; Walters, G.B.; Styrkarsdottir, U.; Gudbjartsson, D.F.; Sulem, P.; Halldorsson, B.V.; de Vegt, F.; d'Ancona, F.C.H.; et al. Sequence variants in the CLDN14 gene associate with kidney stones and bone mineral density. *Nat. Genet.* **2009**, *41*, 926–930. [CrossRef]
31. Konrad, M.; Schaller, A.; Seelow, D.; Pandey, A.V.; Waldegger, S.; Lesslauer, A.; Vitzthum, H.; Suzuki, Y.; Luk, J.M.; Becker, C.; et al. Mutations in the tight-junction gene claudin 19 (CLDN19) are associated with renal magnesium wasting, renal failure, and severe ocular involvement. *Am. J. Hum. Genet.* **2006**, *79*, 949–957. [CrossRef] [PubMed]
32. Kausalya, P.J.; Amasheh, S.; Günzel, D.; Wurps, H.; Müller, D.; Fromm, M.; Hunziker, W. Disease-associated mutations affect intracellular traffic and paracellular Mg2+ transport function of Claudin-16. *J. Clin. Invest.* **2006**, *116*, 878–891. [CrossRef] [PubMed]
33. Simon, D.B.; Karet, F.E.; Hamdan, J.M.; DiPietro, A.; Sanjad, S.A.; Lifton, R.P. Bartter's syndrome, hypokalaemic alkalosis with hypercalciuria, is caused by mutations in the Na-K-2Cl cotransporter NKCC2. *Nat. Genet.* **1996**, *13*, 183–188. [CrossRef] [PubMed]
34. Simon, D.B.; Karet, F.E.; Rodriguez-Soriano, J.; Hamdan, J.H.; DiPietro, A.; Trachtman, H.; Sanjad, S.A.; Lifton, R.P. Genetic heterogeneity of Bartter's syndrome revealed by mutations in the K+ channel, ROMK. *Nat. Genet.* **1996**, *14*, 152–156. [CrossRef] [PubMed]
35. Watanabe, S.; Fukumoto, S.; Chang, H.; Takeuchi, Y.; Hasegawa, Y.; Okazaki, R.; Chikatsu, N.; Fujita, T. Association between activating mutations of calcium-sensing receptor and Bartter's syndrome. *Lancet* **2002**, *360*, 692–694. [CrossRef]
36. Vargas-Poussou, R.; Huang, C.; Hulin, P.; Houillier, P.; Jeunemaître, X.; Paillard, M.; Planelles, G.; Déchaux, M.; Miller, R.T.; Antignac, C. Functional characterization of a calcium-sensing receptor mutation in severe autosomal dominant hypocalcemia with a Bartter-like syndrome. *J. Am. Soc. Nephrol.* **2002**, *13*, 2259–2266. [CrossRef]

37. Simon, D.B.; Nelson-Williams, C.; Bia, M.J.; Ellison, D.; Karet, F.E.; Molina, A.M.; Vaara, I.; Iwata, F.; Cushner, H.M.; Koolen, M.; et al. Gitelman's variant of Bartter's syndrome, inherited hypokalaemic alkalosis, is caused by mutations in the thiazide-sensitive Na-Cl cotransporter. *Nat. Genet.* **1996**, *12*, 24–30. [CrossRef]
38. Bongers, E.M.H.F.; Shelton, L.M.; Milatz, S.; Verkaart, S.; Bech, A.P.; Schoots, J.; Cornelissen, E.A.M.; Bleich, M.; Hoenderop, J.G.J.; Wetzels, J.F.M.; et al. A Novel Hypokalemic-Alkalotic Salt-Losing Tubulopathy in Patients with *CLDN10* Mutations. *JASN* **2017**, *28*, 3118–3128. [CrossRef]
39. Hadj-Rabia, S.; Brideau, G.; Al-Sarraj, Y.; Maroun, R.C.; Figueres, M.-L.; Leclerc-Mercier, S.; Olinger, E.; Baron, S.; Chaussain, C.; Nochy, D.; et al. Multiplex epithelium dysfunction due to CLDN10 mutation: the HELIX syndrome. *Genet Med* **2018**, *20*, 190–201. [CrossRef]
40. Klar, J.; Piontek, J.; Milatz, S.; Tariq, M.; Jameel, M.; Breiderhoff, T.; Schuster, J.; Fatima, A.; Asif, M.; Sher, M.; et al. Altered paracellular cation permeability due to a rare CLDN10B variant causes anhidrosis and kidney damage. *PLoS Genet* **2017**, *13*, e1006897. [CrossRef]
41. Meyers, N.; Nelson-Williams, C.; Malaga-Dieguez, L.; Kaufmann, H.; Loring, E.; Knight, J.; Lifton, R.P.; Trachtman, H. Hypokalemia Associated With a Claudin 10 Mutation: A Case Report. *Am. J. Kidney Dis.* **2019**, *73*, 425–428. [CrossRef] [PubMed]
42. Hata, M.; Kawamoto, T.; Kawai, M.; Yamamoto, T. Differential expression patterns of the tight junction-associated proteins occludin and claudins in secretory and mature ameloblasts in mouse incisor. *Med. Mol. Morphol.* **2010**, *43*, 102–106. [CrossRef] [PubMed]
43. Suzuki, H.; Nishizawa, T.; Tani, K.; Yamazaki, Y.; Tamura, A.; Ishitani, R.; Dohmae, N.; Tsukita, S.; Nureki, O.; Fujiyoshi, Y. Crystal structure of a claudin provides insight into the architecture of tight junctions. *Science* **2014**, *344*, 304–307. [CrossRef] [PubMed]
44. Milatz, S.; Breiderhoff, T. One gene, two paracellular ion channels-claudin-10 in the kidney. *Pflugers Arch.* **2017**, *469*, 115–121. [CrossRef] [PubMed]
45. Piontek, J.; Winkler, L.; Wolburg, H.; Müller, S.L.; Zuleger, N.; Piehl, C.; Wiesner, B.; Krause, G.; Blasig, I.E. Formation of tight junction: determinants of homophilic interaction between classic claudins. *FASEB J.* **2008**, *22*, 146–158. [CrossRef]
46. Pei, L.; Solis, G.; Nguyen, M.T.X.; Kamat, N.; Magenheimer, L.; Zhuo, M.; Li, J.; Curry, J.; McDonough, A.A.; Fields, T.A.; et al. Paracellular epithelial sodium transport maximizes energy efficiency in the kidney. *J. Clin. Invest.* **2016**, *126*, 2509–2518. [CrossRef]
47. Shan, Q.; Himmerkus, N.; Hou, J.; Goodenough, D.A.; Bleich, M. Insights into driving forces and paracellular permeability from claudin-16 knockdown mouse. *Ann. N. Y. Acad. Sci.* **2009**, *1165*, 148–151. [CrossRef]
48. Breiderhoff, T.; Himmerkus, N.; Drewell, H.; Plain, A.; Günzel, D.; Mutig, K.; Willnow, T.E.; Müller, D.; Bleich, M. Deletion of claudin-10 rescues claudin-16-deficient mice from hypomagnesemia and hypercalciuria. *Kidney Int.* **2018**, *93*, 580–588. [CrossRef]
49. Murota, H.; Matsui, S.; Ono, E.; Kijima, A.; Kikuta, J.; Ishii, M.; Katayama, I. Sweat, the driving force behind normal skin: an emerging perspective on functional biology and regulatory mechanisms. *J. Dermatol. Sci.* **2015**, *77*, 3–10. [CrossRef]
50. Cui, C.-Y.; Schlessinger, D. Eccrine sweat gland development and sweat secretion. *Exp. Dermatol.* **2015**, *24*, 644–650. [CrossRef]
51. Roussa, E. Channels and transporters in salivary glands. *Cell Tissue Res.* **2011**, *343*, 263–287. [CrossRef] [PubMed]
52. Baker, O.J. Current trends in salivary gland tight junctions. *Tissue Barriers* **2016**, *4*, e1162348. [CrossRef] [PubMed]
53. Proctor, G.B. The physiology of salivary secretion. *Periodontol. 2000* **2016**, *70*, 11–25. [CrossRef] [PubMed]
54. Tsubota, K.; Hirai, S.; King, L.S.; Agre, P.; Ishida, N. Defective cellular trafficking of lacrimal gland aquaporin-5 in Sjögren's syndrome. *Lancet* **2001**, *357*, 688–689. [CrossRef]
55. Walcott, B.; Birzgalis, A.; Moore, L.C.; Brink, P.R. Fluid secretion and the Na+-K+-2Cl- cotransporter in mouse exorbital lacrimal gland. *Am. J. Physiol. Cell Physiol.* **2005**, *289*, C860–C867. [CrossRef]
56. Rocha, E.M.; Alves, M.; Rios, J.D.; Dartt, D.A. The aging lacrimal gland: changes in structure and function. *Ocul Surf* **2008**, *6*, 162–174. [CrossRef]
57. Yokouchi, M.; Kubo, A. Maintenance of tight junction barrier integrity in cell turnover and skin diseases. *Exp. Dermatol.* **2018**, *27*, 876–883. [CrossRef]

58. Segre, J.A. Epidermal barrier formation and recovery in skin disorders. *J. Clin. Invest.* **2006**, *116*, 1150–1158. [CrossRef]
59. Brandner, J.M.; Kief, S.; Grund, C.; Rendl, M.; Houdek, P.; Kuhn, C.; Tschachler, E.; Franke, W.W.; Moll, I. Organization and formation of the tight junction system in human epidermis and cultured keratinocytes. *Eur. J. Cell Biol.* **2002**, *81*, 253–263. [CrossRef]
60. Suárez-Fariñas, M.; Fuentes-Duculan, J.; Lowes, M.A.; Krueger, J.G. Resolved psoriasis lesions retain expression of a subset of disease-related genes. *J. Invest. Dermatol.* **2011**, *131*, 391–400. [CrossRef]
61. Kast, J.I.; Wanke, K.; Soyka, M.B.; Wawrzyniak, P.; Akdis, D.; Kingo, K.; Rebane, A.; Akdis, C.A. The broad spectrum of interepithelial junctions in skin and lung. *J. Allergy Clin. Immunol.* **2012**, *130*, 544–547.e4. [CrossRef] [PubMed]
62. Troy, T.-C.; Rahbar, R.; Arabzadeh, A.; Cheung, R.M.-K.; Turksen, K. Delayed epidermal permeability barrier formation and hair follicle aberrations in Inv-Cldn6 mice. *Mech. Dev.* **2005**, *122*, 805–819. [CrossRef] [PubMed]

International Journal of
Molecular Sciences

MDPI

Review

Claudin-2: Roles beyond Permeability Functions

Shruthi Venugopal, Shaista Anwer and Katalin Szászi *

Keenan Research Centre for Biomedical Science of the St. Michael's Hospital and Department of Surgery, University of Toronto, Toronto, ON M5B 1W8, Canada; shruti.venugopal@gmail.com (S.V.); shaista.anwer@mail.utoronto.ca (S.A.)

* Correspondence: katalin.szaszi@unityhealth.to; Tel.: +1-416-8471752

Received: 13 October 2019; Accepted: 9 November 2019; Published: 12 November 2019

Abstract: Claudin-2 is expressed in the tight junctions of leaky epithelia, where it forms cation-selective and water permeable paracellular channels. Its abundance is under fine control by a complex signaling network that affects both its synthesis and turnover in response to various environmental inputs. Claudin-2 expression is dysregulated in many pathologies including cancer, inflammation, and fibrosis. Claudin-2 has a key role in energy-efficient ion and water transport in the proximal tubules of the kidneys and in the gut. Importantly, strong evidence now also supports a role for this protein as a modulator of vital cellular events relevant to diseases. Signaling pathways that are overactivated in diseases can alter claudin-2 expression, and a good correlation exists between disease stage and claudin-2 abundance. Further, loss- and gain-of-function studies showed that primary changes in claudin-2 expression impact vital cellular processes such as proliferation, migration, and cell fate determination. These effects appear to be mediated by alterations in key signaling pathways. The specific mechanisms linking claudin-2 to these changes remain poorly understood, but adapters binding to the intracellular portion of claudin-2 may play a key role. Thus, dysregulation of claudin-2 may contribute to the generation, maintenance, and/or progression of diseases through both permeability-dependent and -independent mechanisms. The aim of this review is to provide an overview of the properties, regulation, and functions of claudin-2, with a special emphasis on its signal-modulating effects and possible role in diseases.

Keywords: claudin-2; tight junctions; epithelium; cancer; inflammation; fibrosis; paracellular permeability; proliferation; migration

1. Introduction

Claudin-2 and the Claudin Family of Tight Junction Proteins

Epithelial cells maintain tissue homeostasis by forming a protective layer to separate the internal milieu from the outside. The epithelium mediates highly regulated directional transport and thus controls the exchange of water and solutes. Tight junctions (TJ) are found at the apical side of the junctional complexes that connect epithelial cells. Their primary role is to generate cell polarity (referred to as fence function), control paracellular transport (gate function), and provide signaling input for a wide variety of cellular events (reviewed in [1–3]). The TJs are comprised of a multitude of transmembrane and intracellular proteins. The claudin family of TJ membrane proteins consists of 26 (human) or 27 (rodents) small (20-25 kDa) tetraspan proteins expressed in a tissue-specific manner in epithelial and endothelial cells [4–6]. The number of claudins varies between species, and in some species e.g., fish there are a much higher number of claudins, probably due to a larger need for osmoregulation. In this review, we only focus on the mammalian claudin-2. Tsukita and colleagues found that the mouse and human orthologs mostly clustered together, except for claudin-13, which is absent in humans [6–8].

Claudins form the backbone of the TJ strand and determine junctional permeability. Based on permeability properties, members of the claudin family can be classified into channel forming and sealing proteins [2,4,9,10]. The composition of the TJ strand, i.e., the types and ratio of claudins expressed, determines the permeability of the TJs, which can be altered by selectively replacing specific claudins [11].

Claudin-2 was one of the first claudins identified by Tsukita and co-workers as a member of a new class of TJ transmembrane proteins that share tetraspan topology with occludin but have no homology with it [12,13]. Subsequent studies revealed that claudin-2 has a high degree of homology with claudins 1–10, 14, 15, 17 and 19, a group referred to as classic claudins [10]. The mouse and human orthologs of claudin-2 share 70% sequence homology, while their promoters possess a homology of 84% [14,15]. Claudin-2 is a cation-selective channel forming TJ protein expressed in leaky epithelia [16–19]. In this review, we will refer to paracellular channel formation by claudin-2 as its *permeability function*. Importantly, expression of claudin-2 is dynamically modulated by a variety of conditions, and compelling evidence now indicates that altered claudin-2 expression affects vital biological processes, such as proliferation, migration and cell fate decision. These effects cannot be explained by the permeability function of claudin-2, and they appear to be mediated by specific signaling pathways and transcription factors. This newly emerging, incompletely understood role of claudin-2 will be referred to as its signal-modulating function and will be the focus of this review. In fact, such a novel role is in line with the emerging non-classical functions described for several other claudins [20–22].

We will first provide an overview of the properties of claudin-2, and the key inputs regulating its expression. This will be followed by a discussion of its functions including the mounting evidence of its signal-modulating function, and its link to various diseases.

2. Properties of Claudin-2

2.1. Expression

Under physiological conditions, claudin-2 mRNA is enriched in the kidneys, where it is exclusively expressed in the proximal tubules, and in the gastrointestinal tract, where the highest expression was reported in the small intestine, liver, gall bladder, and pancreas [23–25]. It is also detectable at lower levels in the stomach and colon [24]. Interestingly, claudin-2 expression was also reported outside of epithelia, e.g., in endothelial cells [26,27] and macrophages (e.g., [28]), but it is not clear whether this represents a physiological localization. As discussed later (see Section 5), pathological conditions affect claudin-2 levels, and may also alter its expression pattern, therefore these observations might indicate pathological expression. Indeed, interleukins and Transforming Growth Factor β1 (TGFβ1) were shown to induce claudin-2 expression in macrophages [28]. Whether claudin-2 has a role in non-epithelial cells remains undetermined.

2.2. Structure and Interactions

Claudin-2 is a 230 amino acid transmembrane protein, with a calculated molecular mass of 24.5 kDa. Alternatively spliced transcript variants with different 5′ untranslated regions have been found for the claudin-2 gene, although their relevance remains unknown. Like other members of the family, claudin-2 is a tetraspan membrane protein consisting of two extracellular domains (ECL1 and ECL2), a small intracellular loop connecting the second and third transmembrane sections and short intracellular N and C terminal portions (Figure 1) ([12,13] and see [5,10] for review on claudin structure). ECL1 (amino acids 29–81), is responsible for paracellular charge selectivity and permeability [29]. The narrow fluid-filled pores of the claudin-2 channel are lined by polar side chains of ECL1 [16,29–32]. Mutagenesis studies revealed that the cation specificity of the channel is due to electrostatic interactions between the transported cations and the negatively charged carboxyl sidechain of D65 and the aromatic residue of Y67 [16,31]. These residues allow cations to permeate in a fully or partially dehydrated state.

Intramolecular cis interactions between C54 and C64, two highly conserved cysteines in ECL1 stabilize the TJ pore [33].

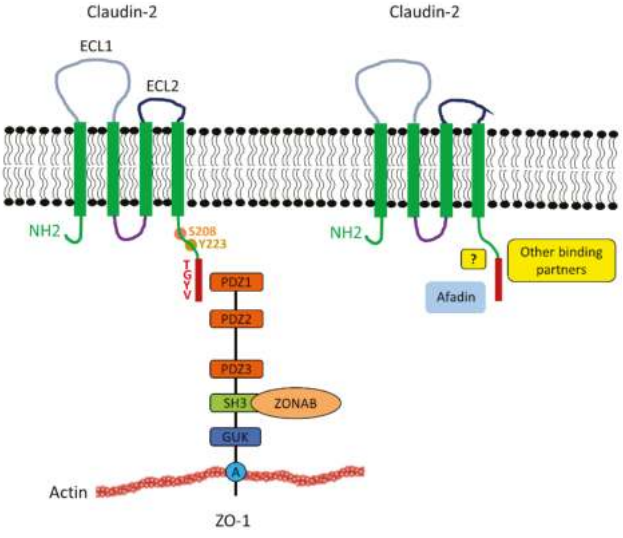

Figure 1. Claudin-2 structure and interactions with cytosolic multidomain adapters. Claudin-2 consists of two extracellular loops, the longer ECL1 (grey) and shorter ECL2 (black). Claudin-2 also contains 4 transmembrane domains (green box), a cytoplasmic loop (purple), a short N-terminal region and a longer C-terminal region (green). Claudin-2 interacts with the ZO family of TJ plaque proteins (for clarity only ZO1 is depicted) through its PDZ-binding motif - TGYV located at the end of the C-terminus (indicated by the red box). The domains of ZO1 depicted include PDZ1, PDZ2, and SH3, mediating binding of a variety of proteins to create large multiprotein complexes; GUK and A, for actin binding segment. The SH3 domain of ZO-1 was shown to bind to the transcription factor ZONAB, which may play a role in the proliferative effects of claudin-2 (Section 4.2). Afadin is a recently identified claudin-2 partner. The mode of coupling (direct biding or indirect association through adapters) remains to be established. Other newly identified candidate binding partners for claudin-2 include Scrib, Arhgap21, PDLIM2/7, and Rims-2 [34]. The claudin-2 tail contains many potential phosphorylation sites. Among these, Y223 affects the affinity of the PDZ binding domain [35], and S208 appears to be a switch for membrane retention and lysosomal or nuclear localization (see Sections 3.4 and 4.2).

Claudin-2 forms both homo- and heterotypic adhesions, via cis (i.e., molecules in the same cell) and trans (between molecules in neighboring cells) interactions. Cis homodimerization of claudin-2 requires the transmembrane domains and may have a role in organizing the TJ strands [36]. On the other hand, trans homophilic interactions are thought to promote cell-cell adhesion (e.g., [37]). Atomic force microscopy studies probing properties of the interactions between the extracellular loops of claudin-2 revealed that ECL1 was sufficient for homophilic trans interaction, and ECL2 did not mediate these [38]. This is different from what was shown for some other claudins (e.g., claudin-5) [39], where ECL2 had a role in trans interactions, and the reason for such difference remains unknown. Thus, the exact role of the claudin-2 ECL2 is not yet established, since it was not found to be involved in determining permeability or homotypic interactions. Of note, however, a peptide (DFYSP) mimicking a highly conserved region in claudin-2, induced endocytosis, and degradation of the protein [40]. This finding suggests that ECL2 might be key for maintaining claudin-2 at the membrane through a yet to be revealed mechanism.

Some heterotypic trans interactions of claudin-2 have also been described. Claudin-2 can bind to claudin-3 but not to claudin-1 on neighboring cells [41]. However, to date, there is limited information on these interactions, and the exact structural basis for the trans interactions of claudin-2 remains to be mapped. Interestingly, an antagonistic relationship was demonstrated between claudin-2 and two other claudins, and this was implicated in cytokine-induced junction reorganization. Fluorescence recovery after photobleaching (FRAP) analysis of GFP-tagged claudin-4 revealed that claudin-2 and -4 compete with one another for residency at the TJs [42]. Further, claudin-8 was shown to displace claudin-2 from the junctions, resulting in elevated transepithelial resistance (TER) [43].

The intracellular interactions of claudin-2 are pivotal for its signal-modulating functions. However, we only have a limited understanding of the protein network associated with claudin-2. The last four C-terminal amino acids of claudins correspond to a PDZ domain-binding motif, and in classic claudins, the two C-terminal amino acids (YV) are 100% conserved. Specificity for different PDZ domains is determined by variation in the neighboring amino acids close to the PDZ domain-binding motifs [44]. In claudin-2, the last 4 amino acids are T-G-Y-V (N- to C-term). This PDZ-binding motif was shown to associate with a variety of TJ plaque scaffold proteins including the membrane-associated guanylate kinase (MAGUK) family adapters ZO-1-3 [45] (Figure 1). Recently, Tabaries et al. identified several new candidate claudin-2 binding partners [34]. These will be described in more detail in Section 4.4.

The intracellular portions of claudin-2 also undergoes post-translational modifications including phosphorylation [46–48], sumoylation [49], and nitration [50] (see Section 3.4). The effects of posttranslational modifications are not fully understood.

3. Regulation of Claudin-2

3.1. Context-Dependent Regulation of Claudin-2

The TJs are continuously remodeled in response to environmental cues. In line with this, claudin-2 expression is dynamically modulated by a multitude of inputs in a context-dependent manner that affect both synthesis and turnover (Figure 2). Protein half-life and trafficking are fine-tuned by a variety of post-translational modifications and interactions with a large array of proteins. Many of the pathways that control claudin-2 are dysregulated in various diseases, resulting in disease-associated changes in claudin-2 expression (see Section 5). In general, studies to decipher the mechanisms controlling claudin-2 were performed in cell lines, and it is important to emphasize that significant context-dependent discrepancies are abundant in the literature. Specifically, some treatments were found to be stimulatory in one cell type, but inhibitory in another. Some of these differences may reflect the complex and likely organ-specific regulation of the protein. In support of this notion, the claudin-2 promoter was affected in the opposite direction by EGF in Caco2 colon cancer and in MDCK tubular epithelial cells [51]. However, some caution is warranted when evaluating data in the literature on claudin-2 regulation in cell lines, as the experiments are impacted not only by difference in origin, culture conditions and passage number of the cells, but also a multitude of other parameters. For example, our studies call attention to the importance of cell confluence and junction maturity as a factor in claudin-2 expression regulation. We found that in LLC-PK1 tubular cells, claudin-2 expression was low in subconfluent cultures and increased as confluence was established [52]. Treatment time is another important parameter that is not always taken into consideration when comparing studies. In tubular and intestinal cell lines the effect of TNFα proved to be opposite depending on the length of treatment [53]. Despite these discrepancies in findings, several mechanisms of claudin-2 regulation are now well established.

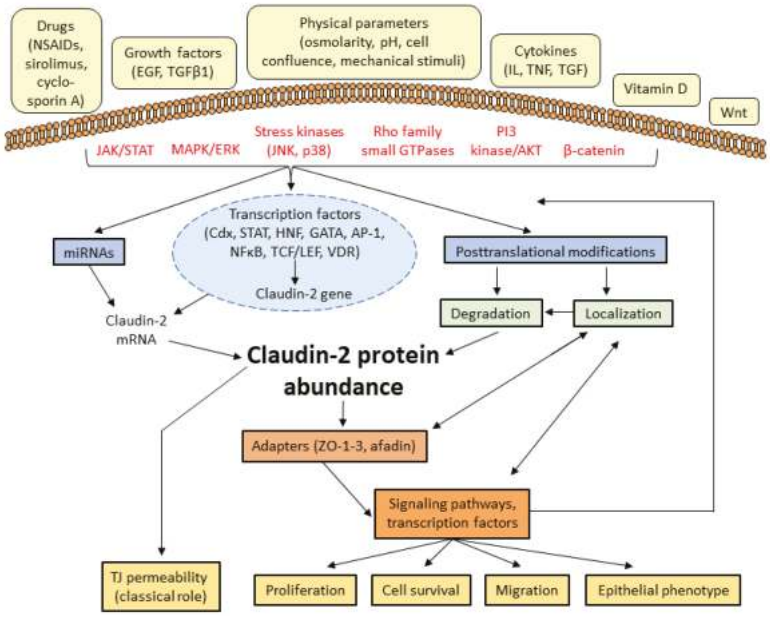

Figure 2. Schematic overview of claudin-2 regulation and its downstream effects. Various extracellular stimuli activate signaling pathways that impact claudin-2 expression by altering its synthesis, and via post-transcriptional and post-translational modifications. In addition to its permeability effects, altered claudin-2 expression also modulates various cellular processes likely acting via a number of downstream signaling pathways and transcription factors (see Table 1 for details on the signaling and effects downstream from claudin-2).

3.2. Signal Transduction Pathways Regulating Claudin-2 Expression

A multitude of signaling pathways, many of which are pro-proliferative and cancer-related, were shown to affect claudin-2 abundance. These pathways affect all aspects of claudin-2 regulation, including the control of synthesis via a set of transcription factors, as well as turn-over and localization of the protein. These latter are affected by post-translational modifications and interactions with various proteins (Figure 2). Many pathways affect multiple aspects of claudin-2 control, and the transcriptional effects are often intertwined with the control of turnover. In this section we will summarize the most studied stimuli and pathways that affect claudin-2 expression, highlighting the mode of their action. The transcription factors affecting claudin-2 will be discussed in more detail in Section 3.3.

One of the best-explored regulators of claudin-2 is the epidermal growth factor receptor (EGFR) and its effectors. Both the Ras/Raf/MEK/ERK and the phosphoinositide 3-kinase (PI3K)/Akt/nuclear factor-κB (NF-κB) pathways were found to target claudin-2 [54–56]. EGFR and ERK signaling were shown to affect claudin-2 in many tissues and could mediate effects of a variety of inputs. As mentioned above, both negative and positive effects were reported, highlighting the importance of context (e.g., [51,53,57–62]. EGFR can also mediate effects of other stimuli. For example, histone deacetylases including HDAC4 appear to affect claudin-2 via EGFR and ERK signaling [63,64]. Thus, HDAC inhibitors, that are in use or under consideration for therapy may have a major impact on claudin-2.

The effects of various cytokines on claudin-2 were extensively explored. For example, several interleukins, including IL-1β, 6, 9, 13, and 22 control claudin-2, and some were shown to act via the Jak/Stat pathway [65–67]. The effect of TNFα might be organ-specific, as it was verified to have different effects on claudin-2 in intestinal and tubular cells (e.g., [53,56]).

Kinases, downstream from various receptors may alter claudin-2 synthesis, but direct phosphorylation of the protein could also affect turnover (see Section 3.4). For most of the kinases, these details have yet to be established. Src kinases reduced claudin-2 expression [68,69], while protein kinase C (PKC) family members and the stress kinase JNK augmented it (e.g., [70–73]). Regulation of claudin-2 by Wnt/β-catenin signaling and Rho family small GTPases could also be significant both physiologically and in diseases [52,53,74]. RhoA/Rho kinase and Rac/Pak control both resting claudin-2 levels [52,53,75] and its localization [76].

Finally, several miRNAs, including miR-488, miR-16, and the miR-199a-5p/214-3p gene cluster were also implicated in claudin-2 control [54,77,78]. For example, the miR-199a-5p/214-3p gene cluster was found to be downstream from serum response factor (SRF), a pro-fibrotic transcription factor, and was implicated in high glucose-induced claudin-2 downregulation in peritoneal mesothelial cells undergoing epithelial-mesenchymal transition (EMT) [78].

3.3. Transcription Factors controlling claudin-2 expression

The TATA-less claudin-2 promoter has binding sites for several transcription factors [14]. Regulation by Caudal-related homeobox (Cdx) homeodomain proteins, hepatocyte nuclear factor (HNF)-1, GATA 2 and -4, AP1, Vitamin D Receptor, TCF/LEF1 and STATs was verified experimentally [14,23,55,72,74,79]. Many of these have significant roles in pathology (see Section 5). HNF-1α and GATA-4 are responsible for claudin-2 expression in specific locations of the gastrointestinal tract, but not in the kidney, highlighting a key organ-specific difference [23,80]. In contrast, GATA-2 was suggested to control claudin-2 in lung and kidney cells [70]. Cdx proteins are intestine-specific transcription factors with significant functions in gut differentiation and carcinogenesis (reviewed in [81]). The claudin-2 promoter is activated by both Cdx1 and 2, which might mediate the effects of the ERK pathway in cancer cells [14,55,82–84]. Interestingly, Cdx factors can collaborate with β-catenin-T cell factor (TCF)/lymphoid enhancer factor (LEF) [74] and HNF-1α [14]. The Cdx1 binding site also contains a functional vitamin D response element, which can directly interact with the Vitamin D Receptor transcription factor [79]. This could be significant for intestinal Ca2+ absorption. Finally, the AP1 complex can mediate the effects of JNK and ERK on the claudin-2 promoter [55,60,72,85], while STATs are effectors of interleukins [65,72].

Many stimuli were shown to decrease claudin-2 levels. This downregulation could be due to inhibition of the above signaling pathways and transcription factors. For example, hyperosmolarity was found to reduce claudin-2 promoter activity by inhibiting PKCβ-dependent GATA-2 transcriptional activity [70]. In addition, transcriptional repressors might also act directly on the claudin-2 promoter. Several EMT-inducing transcription factors are known repressors of tight junction protein genes [86,87]. Accordingly, the transcription factor Snail can induce a drop in claudin-2 [88]. Significantly, the exact mechanisms responsible for claudin-2 downregulation remain mostly unclear. For example, we do not yet have a mechanistic understanding of claudin-2 downregulation in tubular cells (Section 5.3), and the reported negative effects of Src kinases remain unexplained [68,69]. Considering the emerging consequences of reduced claudin-2 expression, a better understanding of these mechanisms will be critical.

3.4. Claudin-2 Turnover, Trafficking, and Posttranslational Modifications

Claudin-2 is a high turnover protein that dynamically cycles between the membrane and intracellular pools [89]. Claudins are connected to both the microtubules and the actomyosin belt through adapter proteins, and these play key roles in assembly and remodeling of the TJs [90–92]. Junctional localization of claudin-2 is not only a prerequisite for permeability functions, but also increases the protein's half-life (e.g., [52,93]). TJ insertion can be promoted or hindered via interactions with membrane and adapter proteins. As mentioned in Section 2.2. claudin-4 and 8 were shown to exclude claudin-2 from the membrane [42,43]. In contrast, ZO family adapters augment the localization of claudin-2 to the TJs. Silencing of ZO-1 and 2 reduced claudin-2 levels, likely in part by enhancing its

degradation [52,67,94,95]. Interestingly, however, loss of ZO-1 also inhibited the claudin-2 promoter, suggesting the existence of feedback regulation between claudin-2 turnover and synthesis [52].

Claudin-2 is retrieved from the TJs by endocytosis. This process was found to be clathrin-dependent in lung and kidney cells [40,48,58]. Other studies have demonstrated a direct binding between claudin-2 and the endocytic scaffold protein caveolin-1 [96,97]. Cytokine-induced gut permeability increase was found to be dependent on caveolin-1 and myosin light chain-dependent endocytosis of TJ proteins [98]. In general, the actomyosin belt plays an essential role in promoting TJ protein retrieval induced by cytokines [91,99], although its specific role in claudin-2 retrieval remains less well established.

The fate of endocytosed claudin-2 is poorly understood. One study found recycling of the endocytosed protein back to the TJs [89]. Several other studies showed that it is targeted for lysosomal degradation (e.g., [40,47,71]). The small GTPases Rab14 and the atypical PKCι, an essential regulator of apico-basal polarity were implicated in the control of claudin-2 trafficking [71]. The autophagy pathway can also target claudin-2 [100,101]. TNFα-induced inhibition of autophagic degradation was suggested to elevate claudin-2 expression in intestinal cells [102]. TNFα also caused an acute ERK-dependent decrease in claudin-2 degradation in tubular cells [53]. Interestingly, similar to some other claudins, claudin-2 was also shown to translocate to the nucleus [103] (see Section 4.2).

Post-translational modifications appear to be key determinants of claudin-2 localization, and turnover, and likely control protein-protein interactions. The claudin-2 intracellular segment contains several potential phosphorylation sites. Phosphorylation of Y224 in human claudin-2 (referred to in some papers as Tyr-6) was shown to affect the affinity of the ZO-1 PDZ binding domain [35], which may impact trafficking. In many publications, the numbering of the position of the C-terminal claudin residues follows the convention that the C-terminal amino acid is referred to as the P0 residue. Subsequent residues toward the N terminus are termed P−1, P−2, etc. Thus, the tyrosine in question is often referred to as position P-6. The possible importance of this site is supported by the fact that many claudins have a tyrosine at this position [35]. S208 is another site that was shown to be phosphorylated. It was implicated in the control of membrane retention, lysosomal localization, and degradation, as well as nuclear localization [46,48,103]. Accordingly, a non-phosphorylatable mutant (S208A) was found to be more cytosolic and lysosomal, while the phospho-mimetic mutant (S208E) localized more to the plasma membrane. Interestingly, mutants, that prevent claudin-2 from insertion to the TJs were found to be poorly phosphorylated, suggesting that TJ insertion is a necessary step for the protein to become phosphorylated. Since the S208 site was implicated both in membrane retention and nuclear localization [46,48,103], it is conceivable that a coupling between claudin-2 TJ insertion and nuclear localization may exist. Accordingly, S208 phosphorylation (e.g., by PKC) could induce plasma membrane localization of claudin-2, while dephosphorylation of this site might promote nuclear translocation [46,48,103].

Claudin-2 also undergoes other post-translational modifications. Sumoylation was found to control membrane localization, ubiquitination, and degradation of claudin-2 [49], and nitration of tyrosine residues was associated with reduced expression [50]. Despite these emerging data, however, we still poorly understand how claudin-2 trafficking and fate are determined.

Importantly, many details of the complex, multilevel regulation of claudin-2 are closely linked to its pathogenic roles, and therefore an improved understanding of the molecular details will be pivotal for further insight into its dysregulation.

4. Functions of Claudin-2

4.1. Permeability Functions

Claudin-2 forms paracellular cation and water permeable channels. An elegant study by Weber et al. used a novel trans-TJ patch-clamp technique to show that the claudin-2 channel exhibits symmetrical and reversible conductance of ~90 pS [32]. They found that the channel is gated with one open and two distinct closed states. Claudin-2, on the other hand, is relatively impermeable to

uncharged solutes [17,18], but permeable to cations and water [104]. Interestingly, water transport is mediated by the same pore that allows cation transport ([105] and reviewed in [106]).

These permeability properties are well verified in cell lines and knockout mouse models. Claudin-2 overexpression and silencing in various cell lines decreases and increases TER, respectively [17,18,53,104,107]. Claudin-2 silencing also eliminates preference of the paracellular pathway towards Na^+ over Cl^- [19].

Knockout mouse models also revealed that the selective, site-specific localization and cation channel properties of claudin-2 are essential for highly specialized functions in the kidneys and the bile duct (reviewed in [108]). In the kidney, claudin-2 is pivotal for efficient Na^+ and water reabsorption in the proximal tubules. Accordingly, the S2 segment of the proximal tubules in claudin-2 KO mice showed significantly reduced net transepithelial reabsorption of Na^+, Cl^-, and water [109]. Although the mice had normal Na^+ homeostasis when fed a regular diet, administration of salt revealed Na^+ handling deficiencies in the kidneys. This suggests that under resting conditions the kidneys could compensate for the loss of the passive claudin-2-mediated Na^+ transport, but under stress, this capacity was insufficient. This conclusion was also supported by findings from Pei et al. [110]. They showed that in claudin-2 knockout mice, upregulation of active transcellular pathways took over the role of passive paracellular Na^+ transport. However, claudin-2 appears to be vital for energy efficiency of the proximal tubular Na^+ reabsorption process, and the higher energy-demand for transcellular transport resulted in medullary hypoxia and increased susceptibility to renal ischemia-reperfusion injury in the claudin-2 KO mice (see also Section 5.3).

In addition to a significant role in ion transport, studies using KO mice also revealed that claudin-2-mediated water transport contributes 23-30% of total water absorption in the proximal tubules [106]. Taken together, the permeability function of claudin-2 in the kidneys is fundamental for Na^+ and water homeostasis and blood pressure regulation [106,109,111].

In the liver and bile system, claudin-2 is highly expressed in hepatocytes and cholangiocytes and plays a central role in water transport associated with bile generation. Accordingly, in claudin-2 KO mice, the rate of bile flow was found to be reduced by half, resulting in a significant increase in bile concentration, and gallstones [112].

In the small intestine, claudin-2 plays a role in luminal Na^+ homeostasis. Surprisingly, however, it was found to be dispensable for Na^+-driven nutrient transport [113]. This contrasted with the role of claudin-15, which proved to be indispensable for both luminal Na^+ transport and Na^+-driven absorption of vital nutrients. The absence of these two claudins in double knockout mice resulted in severe malnutrition [114].

Taken together, claudin-2 plays a key role as a paracellular permeability molecule. However, as discussed in the next sections, emerging evidence suggests that its functions go beyond permeability.

4.2. Role in Proliferation

Evidence is mounting that claudin-2 is not only a paracellular channel protein, but also acts as a signal modulator and integrator (Table 1). This conclusion is derived in part from the correlation between claudin-2 expression and altered outcomes, and in part from overexpression and silencing studies that reveal the effects of altered claudin-2 expression on various outcomes. Importantly, dysregulation of claudin-2 expression appears to be an important event in several diseases (see Section 5).

As discussed in Section 3.2, many proliferative pathways affect claudin-2 expression, and these are often dysregulated in diseases, including in cancer. In fact, a strong correlation has been established by many studies between proliferation/cell viability and altered claudin-2 expression. For example, the silencing of the TJ adapter protein cingulin in kidney tubular cells simultaneously elevated claudin-2 levels and caused a RhoA-dependent increase in G1/S phase transition [75]. In A549 lung adenocarcinoma cells, ephrinA1 reduced both claudin-2 expression and proliferation, and both were mediated by Cdx-2 [115]. Recently, miR-488 was shown to suppress both claudin-2 expression and cell viability in colorectal carcinoma cells [77].

These correlations, however, do not prove a causative connection. More definitive proof is provided by gain- and loss-of-function experiments in a variety of cell lines, showing that primary claudin-2 expression changes can alter proliferation (e.g., [67,103,116]). The experimental evidence connecting claudin-2 with downstream effects is summarized in Table 1. Experimental interventions that reduce claudin-2 expression in lung cancer cells reduce proliferation (see Section 5.1) [64,117]. Thus, claudin-2 might be a permissive factor for proliferation and may act as a mediator of pro-proliferative signaling. Accordingly, silencing claudin-2 in the colon cancer cell line Caco-2 and in tubular cells prevented EGF- and TNFα-induced increase in cell proliferation [51,67].

Claudin-2 impacts cell cycle progression and expression of cell cycle regulators both in cultured cells and in a transgenic mouse model [67,103,116]. In a Villin-claudin-2 transgenic mouse model that overexpresses claudin-2 in the colon, the proliferation of colon cells was augmented by claudin-2 overexpression via the PI-3Kinase/Bcl-2 pathway [116]. In lung cancer cells claudin-2 controls the G1/S transition through cyclin D1 and E1 [103]. This effect was mediated by the Y-box transcription factor Zonula occludens 1-associated nucleic acid-binding protein (ZONAB). ZONAB is known to shuttle between the TJs and the nucleus. Interestingly, claudin-2 was also found in the nucleus where it formed a complex with ZO-1 and ZONAB [103]. Moreover, its nuclear levels increased during the G1/S transition. Interaction between claudin-2 and ZONAB was also demonstrated in colon cancer cells, where symplekin, a transcriptional regulator that cooperates with nuclear ZONAB, was shown to control claudin-2 levels [118]. The molecular underpinning of the nuclear translocation of claudin-2 remains insufficiently understood. No classic nuclear localization sequence is recognizable in claudin-2, but mutagenesis studies revealed that the C-terminal cytosolic segment (but not the PDZ domain) was essential for nuclear transport. As discussed in Section 3.4 S208 phosphorylation is a key regulator of nuclear localization, and a phospho-incompetent mutant (S208A) was found to be more nuclear.

Another cell cycle regulator affected by claudin-2 is $p27^{kip1}$ (cyclin-dependent kinase inhibitor 1B, CDKN1B). The expression of this molecule is high in quiescent cells, where it blocks cell cycle entry. We found that claudin-2 silencing elevated $p27^{kip1}$ levels, and this effect was mediated by the GEF-H1/RhoA pathway [67]. Since $p27^{kip1}$ has tumor suppressor effects, its regulation by claudin-2 might be relevant for carcinogenesis.

Altered claudin-2 expression affects several other transcription factors too. Sp1, a zinc finger transcription factor belonging to the Sp/KLF family and c-jun, part of the AP1 early response complex were found to be affected by claudin-2. Specifically, claudin-2 knockdown decreased the levels of phosho-c-Jun and reduced nuclear Sp1 [119,120]. Importantly, these transcription factors also regulate cell proliferation (e.g., [121]) suggesting another possible link.

Recently, claudin-2 was shown to affect miRNAs. This effect was implicated in the control of self-renewal in colon cancer stem cells [122]. Although the mechanisms that connect claudin-2 to miRNA regulation remain undefined, such effects might link claudin-2 to many downstream events.

Finally, yet another intriguing observation is that claudin-2 can localize along the primary cilium [123]. Claudin-2 is dispensable for ciliogenesis, and its exact role in the cilium remains unclear. However, since the primary cilium is present only in quiescent cells and its disassembly is necessary for cell proliferation [124], this intriguing observation clearly warrants further exploration.

4.3. Migration

The effects of claudin-2 on cell migration may be relevant in both cancer biology and tissue regeneration. Although many studies found that claudin-2 affects migration, significant contradictions are notable among these (Table 1). Specifically, both claudin-2 overexpression and silencing were shown to enhance migration, pointing to context-dependent factors.

In support of a role for claudin-2 in augmenting motility, in various cancer cells claudin-2 overexpression correlates with enhanced migration. In gastric cancer cells, the Helicobacter pylori virulence factor cytotoxin-associated gene (CagA) augmented both claudin-2 expression and invasiveness [82] (see Section 5.1). In line with a stimulatory role, in several cells, a decrease in

claudin-2 abundance reduced migration. Non-steroidal anti-inflammatory drugs (NSAIDs), that may provide protection against cancer, reduced both migration and claudin-2 expression in colon, stomach, and lung cancer cell lines [125]. In these studies, the authors provided further evidence for a causal link, by showing that overexpression of claudin-2 stimulated migration and that claudin-2 re-expression restored migration following drug treatment.

Underlying mechanisms for a positive effect of claudin-2 on migration are yet to be unraveled, but a few possible players have emerged. Matrix metalloproteases (MMP) might be important mediators of the effect. This family of zinc-dependent proteases contains over 25 members. Several of them were shown to aid migration through the digestion of extracellular substrates [126] and are considered as potential therapeutic targets. Claudin-2 was shown to affect MMP9 activity, although surprisingly claudin-2 decrease and increase exerted a similar augmenting effect [120,127]. Inhibition of A549 cancer cell migration in a wound-healing assay by claudin-2 knockdown was attributed to reduced MMP-9 expression and activity due to Sp1 inhibition [120]. However, this might not be a universal effect, as claudin-2 overexpression-induced augmented migration of Caco-2 cells proved independent of MMPs [128].

As opposed to the above-described effects, some studies have found that claudin-2 exerts an inhibitory effect on migration. In MDCK tubular cells inducible knockdown of claudin-2 increased MMP-9 mRNA and activity, and this enhanced migration in a wound-healing assay [120]. Similarly, hyperosmotic stress-induced decrease in claudin-2 expression in the same cell line led to augmented migration, and the phenotype was rescued by re-expression of claudin-2 [70]. Of note, MDCK cells are not derived from cancer, but from normal renal tubular epithelial cells, which might explain the different effects on migration. Claudin-2 loss was also shown to augment migration downstream from the transcription factor Spi-B. This factor is normally restricted to the lymphocyte lineage, but it is frequently expressed in lung cancer. Further, it was shown to repress the transcription of claudin-2, which led to enhanced invasiveness [129]. Another study suggested that in osteosarcoma cells claudin-2 loss augmented migration via the afadin/ERK pathway [130]. Along the same lines miR-488 was shown to regulate invasion and lymph node metastasis in colon cancer cells through claudin-2-dependent control of the MAPK pathway [77].

Another mechanism whereby claudin-2 might affect migration is through effects on EMT [131,132]. This process involves a coordinated genetic reprogramming, during which cells lose their epithelial characteristics and gain mesenchymal properties, including enhanced motility. This process is key during embryonic development and wound healing, but also plays a role in cancer metastasis formation. Tight junction downregulation is a hallmark of full-blown EMT [86], but interestingly, multiple studies now suggest a reciprocal correlation too, namely active EMT-regulating roles for claudins. For example, claudin-1 overexpression was shown to promote EMT, while claudin-3 suppressed it [133,134]. While the exact role of claudin-2 in this process remains to be fully established, we recently found that claudin-2 silencing enhanced RhoA-mediated activation of Myocardin-Related Transcription Factor (MRTF), and upregulated Slug, two pro-EMT transcription factors [67]. The potential role of these in altered migration following claudin-2 loss remains unknown.

Taken together, claudin-2 was shown to have both a positive and a negative effect on migration, suggesting a need for optimal claudin-2 levels for efficient migration regulation. Clearly, further mechanistic inquiries will be required to establish the context-dependent mechanisms and importance of these effects.

Table 1. Summary of the experimental evidence for a causal link between claudin-2 expression and functional outcomes.

Cell Line or Transgenic Mouse	Change in Claudin-2 Expression	Downstream Functional Effect	Signaling Components Downstream from Claudin-2	Ref.
Villin-claudin-2 transgenic mice	Claudin-2 overexpression	Increased colonocyte proliferation	PI-3K/Bcl-2 pathway	[116]
Caco2 human colon cancer cell	Claudin-2 silencing	Reduced EGF-induced proliferation		[51]
SW480 and HCT116 colon cancer cell lines	Claudin-2 overexpression	Increased proliferation and anchorage-independent growth		
LLC-PK1 porcine kidney tubular cells	Claudin-2 silencing	Reduced proliferation	GEF-H1-mediated RhoA activation, increase in $p27^{kip1}$	[67]
		Pro-fibrotic epithelial shift	RhoA-mediated MRTF activation	
A549 human lung adenocarcinoma cells	Claudin-2 downregulation/ knockdown	Reduced G1/S transition	Cyclin D1 and E1, ZONAB	[103]
		Increased sensitivity to anti-cancer agents; increased intracellular drug accumulation and reduced efflux	Decrease in phosho-c-Jun and nuclear Sp1; reduced expression of multidrug resistance-associated protein/ABCC2	[119]
		Reduced migration	Decreased Sp1, reduced MMP-9 expression, activity	[120]
A549 human lung adenocarcinoma cells	Flavonoid- or epigenetic inhibitor-induced claudin-2 downregulation;	Reduced proliferation; partial rescue of phenotype by claudin-2 reexpression		[64,117]
HT-29 colorectal cancer cell line	Symplekin silencing-induced claudin-2 downregulation;	Reduced anchorage-dependent growth and Zonab nuclear localization; rescue of phenotype by claudin-2 reexpression		[118]
A549 human lung adenocarcinoma cells	Endocytosis and lysosomal degradation of claudin-2 induced by a peptide mimic (DFYSP) of a conserved ECL2 region	Claudin-2 accumulation in the lysosomes, cellular injury and necrotic cell death	Cathepsin B release from lysosomes	[40]
MDCK canine tubular cells	Inducible knockdown of claudin-2	Enhanced migration in a wound-healing assay	Increased MMP-9 mRNA and activity	[120]
Human colon cancer stem-like cells (patient-derived CCP1 cells)	Claudin-2 overexpression	Self-renewal of cancer stem cells; enhanced tumor initiation, progression, and metastasis	YAP and miRNAs (especially miR-222-3p)	[122]
Caco2 human colon cancer cell	Claudin-2 overexpression	Enhanced migration	Effect independent from MMP-2 and 9	[128]
AGS stomach carcinoma cells	Claudin-2 overexpression	Enhanced migration	Likely via increased MMP-1, -2 and 9 expression	[125]

Table 1. *Cont.*

Cell Line or Transgenic Mouse	Change in Claudin-2 Expression	Downstream Functional Effect	Signaling Components Downstream from Claudin-2	Ref.
T-84 colonic adenocarcinoma, AGS and KATO-III stomach carcinoma cells; A549 lung adenocarcinoma cell lines	Claudin-2 silencing Claudin-2 overexpression Non-steroidal anti-inflammatory drugs (NSAIDs)-induced claudin-2 downregulation	Reduced migration Augmented migration Reduced migration; claudin-2 reexpression counteracted the effect		[125]
U2OS osteosarcoma cell line	Claudin-2 overexpression	Reduced migration and invasion	Afadin-mediated ERK inhibition	[130]
Fetal osteoblast cell line hFOB.1.19	Claudin-2 silencing	Augmented migration and invasion	ERK activation, afadin reduction	
Claudin-2 KO mice	Claudin-2 KO	Augmented TNFα-induced colorectal inflammation	NFκB, myosin light chain kinase	[135]
Claudin-2 KO mice	Claudin-2 KO	Augmented energy demand of transport processes; increased ischemia-reperfusion kidney injury		[110]

4.4. Signal-Modulating Effects of Claudin-2: Emerging Mechanisms Underlying Roles in Biological Processes

As discussed in Sections 4.2 and 4.3, evidence is mounting that claudin-2 affects cell behavior (Table 1). However, a coherent picture of the underlying mechanisms has yet to emerge. Many studies suggest that claudin-2 may be a signal modulator and integrator protein. Nevertheless, an in-depth understanding of how claudin-2 is linked with altered signaling pathways remains elusive.

The TJ cytoplasmic plaque contains a large array of signaling and regulatory proteins. These are connected to the TJ membrane proteins by various adapters. For many of these proteins, recruitment to the junctions results in inactivation, or a spatial restriction of activity (for review see [90,136,137]). The specific role of individual claudins in the organizing of the cytoplasmic plaque is not yet resolved. As mentioned in Section 2.2, the cytoplasmic tail of claudin-2 interacts with multiple proteins, but the claudin-2 interactome has not yet been fully mapped, and context-dependent regulation of the interactions remains unknown. As mentioned earlier, a recent study from the Siegel group identified some candidate binding partners of the claudin-2 PDZ domain [34]. Using metastatic breast cancer cells with elevated claudin-2 expression, they demonstrated that the last three C-terminal amino acids of claudin-2 (comprising the PDZ-binding motif) are necessary for anchorage-independent growth. They identified several potential partners of this motif, including afadin, which is an actin filament- and Rap1 small GTPase-binding protein encoded by the MLLT4/AF-6 gene. Loss of afadin impaired colony formation of breast cancer cells in soft agar and reduced lung and liver metastasis, verifying the significance of the claudin-2/afadin complex. Importantly, some of their findings suggested the existence of afadin-independent mechanisms too. The identified potential other partners, including the polarity protein Scrib, the small GTPase regulator Arhgap21, PDZ-LIM domain-containing proteins (PDLIM) 2 and 7, and the exocytosis-controlling Rims-2 (regulating synaptic membrane exocytosis protein 2) may mediate such downstream effects. However, whether these are direct binding partners or interact via adapters, and their potential functional significance remains to be established.

The crosstalk between claudin-2 and the cytoskeleton may play a central role in mediating downstream effects. Claudin-2, as all TJ membrane proteins, is anchored to the junctional actomyosin belt and microtubules through adaptor proteins. Among these, ZO family proteins directly bind claudins, and connect to F-actin either directly, or indirectly through actin-binding proteins [138,139]. Thus, it is conceivable that altered claudin-2 expression might affect the organization of the prejunctional cytoskeleton. In support of this, we recently found that in tubular cells, claudin-2 silencing altered acto-myosin organization through RhoA [67].

The microtubules also play a role in junction regulation and might be affected by the TJ organization. Cingulin and its paralog paracingulin interact with TJ proteins, likely through ZO adapters, and thus connect to actin. Cingulin also binds the microtubules and has a role in organizing the microtubular planar apical network in mammary epithelial cells [140,141]. Further, association of cingulin with actin filaments and the microtubules was found to be regulated by phosphorylation and plays a crucial role in the control of the epithelial barrier [141]. The specific roles of individual claudins as organizers of the cytoplasmic plaque complexes and their impact on the cytoskeleton are yet to be uncovered. Nevertheless, it is conceivable that some of the signal modulating effects of claudin-2 is mediated by an impact on the acto-myosin or the MTs.

Interestingly, claudin-2 appears to have a bidirectional relationship with the cytoskeleton and some signaling pathways. Specifically, some of the pathways modulated by claudin-2 can also regulate its expression. This suggests the existence of various regulatory feedback cycles (Figure 2). Such regulatory loops also pose a challenge for defining clear "upstream" and "downstream" events. The ERK and Rho signaling pathways are prominent examples of this complexity. The role of MEK/ERK signaling in basal and stimulus-induced claudin-2 expression is well documented [53,55,60,61,85,142,143]. Besides, a recent study reported the converse effect: claudin-2 silencing was found to augment MEK/ERK1/2 signaling [130], an effect that may help to restore claudin-2 levels. A complex relationship also exists between Rho family small GTPases and claudin-2. We found that RhoA/Rho-kinase are negative regulators of claudin-2 expression in cultured tubular cells [53]. On the other hand, as mentioned above,

in the same cells claudin-2 silencing enhanced RhoA activity through the exchange factor GEF-H1, suggesting that in resting cells, claudin-2 might suppress RhoA activation [67]. Thus, claudin-2 loss can augment Rho activity, which in turn may further reduce claudin-2 expression, in a possible self-augmenting cycle.

5. Claudin-2 in Diseases

A growing number of studies document altered claudin-2 expression, phosphorylation and/or localization in various pathological conditions. Initially, the described claudin expression alterations were considered an epiphenomenon, i.e., they were assumed to arise due to the underlying disease process but were thought not to be causally contributing to pathogenesis. Nevertheless, interest in pathological alterations in claudin-2 expression was boosted by the hope that it can be used as a diagnostic and/or prediction marker. As described in Section 4, in the past years, strong evidence accumulated in support of a causal link between claudin-2 dysregulation and functional alterations, the key points of which are the following. First, signaling pathways that are known to be overactivated in diseases can alter claudin-2 expression, and a good correlation exists between disease stage and claudin-2 expression. Second, loss-of-function and gain-of-function studies recapitulate some aspects of the functional changes. Thus, primary changes in claudin-2 expression can alter cell behavior. The mounting experimental evidence prompted a paradigm shift, favoring a pathogenic role for claudin-2. Although dysregulation of claudin-2 is likely not a primary cause, pathological changes in claudin-2 abundance and/or localization might play significant roles in the generation, maintenance and/or progression of diseases.

In the following sections, we will provide an overview of the evidence linking claudin-2 to cancer, and various non-malignant pathologies, such as inflammatory gastrointestinal and kidney diseases.

5.1. Claudin-2 in Cancer and Metastasis Formation

An expanding body of literature documents dysregulated claudin-2 expression in gastric, colorectal, lung, breast, and renal carcinomas and in osteosarcoma (e.g., [51,144–148]. As described in Sections 4.2 and 4.3, claudin-2 levels affect processes underlying carcinogenesis and metastasis formation, including proliferation, migration and epithelial-mesenchymal transition. The following overview however also highlights that the role of claudin-2 is likely complex, and differences in its impact might exist not only based on tissue origin but also cancer stage.

Cancers of the gastrointestinal tract—Claudin-2 is highly expressed in gastric and colorectal cancers and its expression level shows a good correlation with the development of these tumors. For example, a gradual increase was observed in claudin-2-positivity in various stages of gastric carcinogenesis from no expression in gastritis to elevated expression in dysplasia and gastric intestinal-type adenocarcinoma [149]. In fact, in this study, 73% of adenocarcinoma samples were found to be claudin-2 positive.

As described in Sections 3.2 and 3.3, claudin-2 is the target of key signaling pathways and transcription factors central to gastrointestinal cancers. One prominent example is the significant correlation between Cdx2 and claudin-2 expression in gastric dysplasia and cancer [150]. Further, a potentially important link between claudin-2 and H. pylori was also uncovered. H. pylori infection shows a strong correlation with gastric cancer [151], and the virulence factor CagA is considered a gastric oncogene. During infection, this protein is translocated into and reprograms the gastric cells. Interestingly, CagA augmented claudin-2 expression in gastric cells, and promoted invasiveness through effects on Cdx2 [82].

Hyperactivation of Wnt signaling and the consequent increase in gene transcription by TCF/ LEF is a hallmark of colon cancer (reviewed in [152]). Wnt-1 was shown to increase claudin-2 promoter activity through β-catenin/LEF-1 [74]. Increased claudin-2 and β-catenin expression were detected in active inflammatory bowel disease (IBD), adenomas, and IBD-associated dysplasia, but not in acute,

self-limited colitis [153]. These data suggest that β-catenin might mediate an increase in claudin-2 during carcinogenesis.

EGFR signaling is yet another key pathway linking colon cancer and claudin-2. EGFR activation upregulated claudin-2 in colon cancer cells, and claudin-2 expression was decreased in the colon of waved-2 mice that have EGFR activation deficiency [51] (see also Section 3.2 on the effects of EGFR on claudin-2).

Taken together, these studies suggest that the initial upregulation of claudin-2 could be due to the overactivation of the above-discussed pathways, and this may promote carcinogenesis. To prove a causal link between elevated claudin-2 and the properties of cancer, exogenous claudin-2 was overexpressed in colorectal cancer cell lines. An increase in claudin-2 expression promoted colonocyte proliferation and anchorage-independent colony formation and stimulated tumor formation in colorectal cancer xenografts (e.g., [51,116]). Further, claudin-2 expression was a negative predictor for post-chemotherapy disease-free survival of colon cancer patients [51].

Another key role of claudin-2 could be its effect on colorectal cancer stem-like cells [122]. Claudin-2 promoted self-renewal of these cells via miRNAs and the hippo effector yes-associated protein (YAP). Interestingly, claudin-2 was also detected in human colorectal cancer-associated fibroblasts (CAFs). This finding is especially intriguing since claudin-2 is regarded as an epithelial molecule. Its expression in CAFs was linked to KRAS mutation status and correlated with reduced progression-free survival [154]. Of note, claudin-2 was also shown to be enriched in macrophages associated with mammary tumors [28]. Thus, an attractive hypothesis is that claudin-2 may increase proliferation/survival and migration of fibroblasts and macrophages in the tumor environment.

Lung cancer—Primary lung cancer is among the deadliest types of tumors worldwide, and adenocarcinomas are the most frequent forms of non-small cell lung cancer. Claudin-2 expression in normal bronchial epithelium is low [85]. In contrast, according to one study, two-thirds of examined lung adenocarcinoma samples overexpressed claudin-2 [145]. Surprisingly, in these cells, claudin-2 was found mostly in cytoplasmic granules. Adenocarcinoma is often associated with upregulated EGFR activity and KRAS/MEK/ERK signaling. Indeed, EGFR signaling is key in upregulating claudin-2 in the human lung adenocarcinoma cell line A549 [60]. These cells were used in a series of studies to demonstrate that claudin-2 may be a therapeutic target in lung cancer. The studies showed that rapid proliferation of A549 cells required claudin-2. Accordingly, claudin-2 knockdown impaired cell growth and migration [103,120] and elevated sensitivity for anti-cancer agents [119]. Importantly, a variety of interventions, including epigenetic inhibitors and various flavonoids reduced claudin-2 expression and decreased proliferation. These effects were counteracted by retransfection of claudin-2 [64,117]. Claudin-2 abundance can also be reduced by a peptide that mimics a sequence in ECL2. This peptide-induced endocytosis and lysosomal accumulation of claudin-2, resulting in lysosomal damage and necrotic cell death [40]. Taken together, these studies provided strong evidence that targeting claudin-2 can mitigate proliferation and raised hope that this approach will prove useful in cancer therapy (see further elaboration in Section 5.4).

Osteosarcoma and breast cancer—Interestingly, in some tumors, claudin-2 expression is decreased. Osteosarcoma cells have lower claudin-2 expression than normal osteoblasts [130], and this is associated with enhanced migration. In breast cancer, increased or decreased claudin-2 expression might be associated with different cancer types and stages [155,156]. As discussed below, in this type of tumor, claudin-2 expression appears to correlate with metastasis formation.

Metastasis—The importance of claudin-2 in metastasis is also emerging. Claudin-2 might affect migration via a variety of effects. Its possible role in migration was discussed in Section 4.3. Beyond general effects on migration, claudin-2 also appears to affect metastasis through mediating specific adhesion of the metastatic cells, thereby promoting invasion into distant organs. Interestingly, the exact role of claudin-2 in metastasis appears to vary based on the site of invasion. In some breast cancer reduction in claudin-2 was associated with lymph node metastasis and higher clinical stage [156]. In contrast, claudin-2 overexpression was shown to augment breast carcinoma metastasis to the liver. Claudin-2 expression is elevated in liver metastases compared to primary breast cancer cells [157].

Indeed, claudin-2 promoted attachment and survival of metastatic cells specifically in the liver and enhanced their interactions with hepatocytes [37]. Due to these effects, claudin-2 was found to be a negative prognostic factor that predicts liver metastasis in breast cancer [158]. Metastatic breast cancer cells showed a general increase in adhesion to the extracellular matrix, as claudin-2 promoted surface expression of α2β1- and α5β1-integrins [157]. However, while these effects might contribute to invasiveness in general, enhanced interaction between hepatocytes and breast cancer cells proved to be independent of integrins. Instead, the effect required the first claudin-2 extracellular loop (ECL1) and was likely attributable to homotypic trans interactions between claudin-2 molecules. Thus, claudin-2 in the metastatic breast cancer cells can bind to claudin-2 on hepatocytes, thereby promoting their adhesion to the liver [157]. Further, the PDZ-binding motif (YV) in claudin-2 was found to be necessary for anchorage-dependent growth and metastases [34]. These exciting findings raise hope that blocking peptides or neutralizing antibodies against the identified domain might be effective in reducing liver metastasis (see Section 5.4).

5.2. Claudin-2 in Gut Inflammation

Claudin-2 emerged as an important factor in IBD, a term describing conditions such as ulcerative colitis and Crohn's disease. These chronic diseases are hallmarked by compromised epithelial barrier and are thought to be caused by a dysregulated immune response in the gut (e.g., reviewed in [159,160]). Increased paracellular permeability is likely a critical pathogenic factor. Specifically, the disease appears to be maintained by a vicious cycle: increased epithelial permeability due to dysregulation of TJ proteins elicits an aberrant immune response, and the ensuing inflammation further disrupts TJs and aggravates the condition. The effects of inflammation on epithelial permeability have been long known. Elevated claudin-2 expression in IBD is attributed to the presence of cytokines (e.g., [56,161,162] and reviewed in [159,163]). The permeability function of claudin-2 appears to be central in IBD, although a causal link is hard to decipher. Studies in transgenic mice explored and verified the role of the permeability function of claudin-2. In contrast, little is known about the possible significance of claudin-2 as a signal modulator in IBD. Somewhat surprisingly, recent studies point to a possible protective role of claudin-2 against injury. A transgenic mouse with targeted overexpression of claudin-2 in the colon was protected against colitis-associated injury [116]. This study also highlighted the complex roles of claudin-2 in intestinal homeostasis and IBD. Claudin-2 overexpression in the colon augmented mucosal permeability but did not by itself cause inflammation. Instead, the mice had longer colons and elongated crypts, a result of accelerated colonocyte proliferation. Most notably, despite the leaky colon, the mice were significantly protected against experimental colitis, and inflammation-associated gene expression was sharply downregulated. Some of the effects could be the result of reduced apoptosis and augmented regeneration due to faster proliferation. Thus, in this respect, claudin-2 elevation may at least initially confer some protection in IBD. This notion is also supported by another study that used claudin-2 null mice to explore the effects of intraperitoneally injected TNFα and experimental colitis [135]. The data revealed augmented colorectal inflammation in the KO mice compared to WT animals. These effects were mediated by NF-κB signaling. The mice also had increased expression of IL-6 and IL-1β and higher intestinal myosin light chain kinase levels. Overall, these studies suggest that increased claudin-2 expression might suppress inflammatory signals. Importantly, although the proliferative effect observed could be beneficial for regeneration, this is a double-edged sword. IBD elevates the risk for developing colorectal cancer and augmented claudin-2 expression could contribute to this. As mentioned in Section 5.1, claudin-2 levels rise with the development of dysplasia and cancer. This raises the intriguing possibility that elevated claudin-2 expression might be a crucial connection between inflammation and cancer. Thus, while elevated claudin-2 might protect against injury and enhance regeneration, it could raise the risk of cancer.

The role of claudin-2 in intestinal diseases might go beyond IBD, as it was also implicated in diseases caused by enteropathogenic bacteria. Salmonella invasion elevated claudin-2 protein and mRNA levels both in cultured cells and in the intestine of mice. Upregulation of claudin-2, in turn, elevated permeability and promoted internalization of the bacteria [73]. Finally, recent studies raise the

possibility that claudin-2 might contribute to chronic pancreatitis, a progressive inflammatory disease that is frequently associated with alcohol consumption. A genome-wide association search found that polymorphisms of the claudin-2 locus confer an increased risk of alcohol-induced pancreatitis [164]. Since claudin-2 is essential for bile formation, it will be interesting to see if claudin-2 polymorphism might also predispose for gall bladder disease and gallstones.

5.3. Claudin-2 in Kidney Disease

Claudin-2 mRNA levels are highest in the kidney, where it is a key mediator of cation and water transport in the proximal tubules (reviewed in [165–167]). Although a direct role of claudin-2 in kidney disease has not been definitively established, several observations suggest a possible link.

Claudin-2 is affected by inflammatory cytokines in tubular cells. Specifically, short-term TNFα treatment caused an increase in claudin-2 abundance [53]. In contrast, prolonged (>8h) TNF-α or IL-1β treatment downregulated claudin-2 expression [53,67]. Interestingly, a large variety of potentially harmful stimuli can downregulate claudin-2 expression in tubular cells. In addition to these cytokines, metabolic acidosis [168], changes in osmolarity [48,127], oxidants [169], EGF [58,170], sheer stress [171], the flavonoid quercetin [172], and drugs, such as the immunosuppressants sirolimus and cyclosporine A [173], reduce claudin-2 levels. Reduced claudin-2 expression was also recorded in various kidney disease animal models, including cisplatin-induced nephrotoxicity [174], diabetic nephropathy [50] and obstructive nephropathy-induced fibrosis [67]. These findings are of significance because claudin-2 was found to exert a protective effect against kidney injury by reducing the energy demand of transport processes [110]. Further, as mentioned above loss of claudin-2 in tubular cells induced RhoA activation, and claudin-2 knockout mice had elevated RhoA activity [67]. This led to reduced proliferation and activation of MRTF, a transcription factor that mediates profibrotic epithelial transition [67,175]. Thus, reduced claudin-2 expression in stress conditions might increase susceptibility for injury and may promote fibrosis.

Finally, the proximal tubular paracellular pathway also plays a central role in Ca2+ reabsorption. Accordingly, claudin-2 null mice were hypercalciuric, a condition that enhances kidney stone formation [109]. Thus, conditions that reduce the abundance of claudin-2 in the kidney might also lead to kidney stone disease, a condition affecting a significant portion of the population.

5.4. Development of Therapies Targeting Claudin-2

Several studies raise hope that targeting claudin-2 could have beneficial effects. Indeed, in a proof of principle study, a monoclonal antibody that recognizes the first extracellular loop (ECL1) of claudin-2 was shown to prevent TNFα-induced TJ disruption [176]. The same group recently generated a human-rat chimeric monoclonal antibody against claudin-2 and showed that it accumulated in claudin-2 positive sarcoma xenografts. The antibody also suppressed tumor growth [177]. Importantly, no major adverse effects were found.

Taken together, accumulating evidence supports that claudin-2 can be considered a diagnostic and prognostic marker in various diseases and is an exciting potential therapeutic target.

6. Open Questions

Claudin-2 is now established as a pathogenic factor in several diseases due to its permeability-dependent and -independent functions. The recognition that claudins have major signal modulator, permeability-independent functions reenergized claudin research, leading to an explosion in the number of studies published. Although the fact that altered claudin-2 expression affects signaling and cell behavior is firmly established, many questions remain unanswered. It is worthwhile to articulate some of these as they set the direction for future research. Importantly, our understanding of mechanisms mediating pathological dysregulation of claudin-2 is still incomplete, which precludes the design of interventions. There are also fundamental unanswered questions regarding the mechanisms that link claudin-2 to various downstream events. We do not know the role of claudin-2 localization in its signal-modulating effects. Are these effects mediated by TJ localized claudin-2? Given that claudin-2

was shown to reside in other compartments (cytosolic vesicles, nucleus), some of the non-classical effects may well be mediated by these claudin-2 sub-pools. Further, many studies revealed the importance of altered claudin-2 expression in the downstream effects, but we do not know whether these are exclusively related to the number of molecules or if further regulation (e.g., by distinct posttranslational modifications) are also involved. Extra- and intracellular binding partners of claudin-2 are likely crucial mediators of signal-modulating effects. Indeed, TJ-localized claudin-2 can interact with other membrane proteins and may act as a sensor of neighboring cells. However, it is not clear whether claudin-2 needs to be engaged for its signal-modulating effects. Further, the claudin-2 interactome is only now starting to emerge and uncovering the context-dependent regulation of interactions will be key for a better understanding. Adapters in the TJ plaque generate signaling complexes, that may change depending on the availability of claudin-2, leading to recruitment or release of signaling intermediates and alterations in the cytoskeleton organization. However, the specific role of claudin-2 in such events remains unknown. Ongoing research from many groups will likely help fill these knowledge gaps leading to a better mechanistic understanding of the signal-modulating effects of claudin-2. The emerging knowledge has already informed the design of interventions targeting claudin-2. Such future therapies have the potential to benefit many patients with a broad spectrum of diseases.

Author Contributions: Writing–Original Draft Preparation, S.V., S.A., K.S.; Review & Editing, S.V., S.A., K.S.; Visualization, S.A.; Supervision, K.S.; Funding Acquisition, K.S.

Funding: This research was funded by the KIDNEY FOUNDATION OF CANADA, the CANADIAN INSTITUTES OF HEALTH RESEARCH (CIHR), grant number: PJT-149058 and MOP-142409; and NATURAL SCIENCES AND ENGINEERING RESEARCH COUNCIL OF CANADA (NSERC) grant number: RGPIN-2017-06517. Shaista Anwer received scholarships from the Research Training Center of the St Michael's Hospital and University of Toronto through an open fellowship.

Acknowledgments: The authors would like to express their gratitude to Andras Kapus and Mirjana Jerkic for critical reading of the manuscript.

Conflicts of Interest: The authors declare no conflict of interest.

Abbreviations

CagA	CagA: cytotoxin-associated gene
Cdx	Caudal-related homeobox
EGF	epidermal growth factor
EGFR	epidermal growth factor receptor
EMT	epithelial-mesenchymal transition
HNF	hepatocyte nuclear factor
IBD	inflammatory bowel disease
IL	Interleukin
MMP	matrix metalloprotease
TGFβ1	transforming growth factor β1
TNF	tumor necrosis factor
PDZ	postsynaptic density, disc-large, ZO-1
TCF/LEF	T cell factor/lymphoid enhancer factor
ZONAB	Zonula occludens 1-associated nucleic acid-binding protein
TJ	tight junctions
ZO	zonula occludens

References

1. Zihni, C.; Mills, C.; Matter, K.; Balda, M.S. Tight junctions: From simple barriers to multifunctional molecular gates. *Nat. Rev. Mol. Cell Biol.* **2016**, *17*, 564–580. [CrossRef] [PubMed]
2. Van Itallie, C.M.; Anderson, J.M. Architecture of tight junctions and principles of molecular composition. *Semin. Cell Dev. Biol.* **2014**, *36*, 157–165. [CrossRef] [PubMed]

3. Shen, L.; Weber, C.R.; Raleigh, D.R.; Yu, D.; Turner, J.R. Tight junction pore and leak pathways: A dynamic duo. *Annu. Rev. Physiol.* **2011**, *73*, 283–309. [CrossRef] [PubMed]
4. Gunzel, D.; Fromm, M. Claudins and other tight junction proteins. *Compr. Physiol.* **2012**, *2*, 1819–1852. [PubMed]
5. Tsukita, S.; Tanaka, H.; Tamura, A. The Claudins: From Tight Junctions to Biological Systems. *Trends Biochem. Sci.* **2019**, *44*, 141–152. [CrossRef] [PubMed]
6. Mineta, K.; Yamamoto, Y.; Yamazaki, Y.; Tanaka, H.; Tada, Y.; Saito, K.; Tamura, A.; Igarashi, M.; Endo, T.; Takeuchi, K.; et al. Predicted expansion of the claudin multigene family. *FEBS Lett.* **2011**, *585*, 606–612. [CrossRef] [PubMed]
7. Lal-Nag, M.; Morin, P.J. The claudins. *Genome Biol.* **2009**, *10*, 235. [CrossRef] [PubMed]
8. Wu, J.; Helftenbein, G.; Koslowski, M.; Sahin, U.; Tureci, O. Identification of new claudin family members by a novel PSI-BLAST based approach with enhanced specificity. *Proteins* **2006**, *65*, 808–815. [CrossRef] [PubMed]
9. Furuse, M. Molecular basis of the core structure of tight junctions. *Cold Spring Harb. Perspect. Biol.* **2010**, *2*, a002907. [CrossRef] [PubMed]
10. Krause, G.; Winkler, L.; Mueller, S.L.; Haseloff, R.F.; Piontek, J.; Blasig, I.E. Structure and function of claudins. *Biochim. Biophys. Acta* **2008**, *1778*, 631–645. [CrossRef] [PubMed]
11. Capaldo, C.T.; Nusrat, A. Claudin switching: Physiological plasticity of the Tight Junction. *Semin. Cell Dev. Biol.* **2015**, *42*, 22–29. [CrossRef] [PubMed]
12. Furuse, M.; Fujita, K.; Hiiragi, T.; Fujimoto, K.; Tsukita, S. Claudin-1 and -2: Novel integral membrane proteins localizing at tight junctions with no sequence similarity to occludin. *J. Cell Biol.* **1998**, *141*, 1539–1550. [CrossRef] [PubMed]
13. Furuse, M.; Sasaki, H.; Fujimoto, K.; Tsukita, S. A single gene product, claudin-1 or -2, reconstitutes tight junction strands and recruits occludin in fibroblasts. *J. Cell Biol.* **1998**, *143*, 391–401. [CrossRef] [PubMed]
14. Sakaguchi, T.; Gu, X.; Golden, H.M.; Suh, E.; Rhoads, D.B.; Reinecker, H.C. Cloning of the human claudin-2 5'-flanking region revealed a TATA-less promoter with conserved binding sites in mouse and human for caudal-related homeodomain proteins and hepatocyte nuclear factor-1alpha. *J. Biol. Chem* **2002**, *277*, 21361–21370. [CrossRef] [PubMed]
15. Gunzel, D.; Yu, A.S. Claudins and the modulation of tight junction permeability. *Physiol. Rev.* **2013**, *93*, 525–569. [CrossRef] [PubMed]
16. Yu, A.S.; Cheng, M.H.; Angelow, S.; Gunzel, D.; Kanzawa, S.A.; Schneeberger, E.E.; Fromm, M.; Coalson, R.D. Molecular basis for cation selectivity in claudin-2-based paracellular pores: Identification of an electrostatic interaction site. *J. Gen. Physiol.* **2009**, *133*, 111–127. [CrossRef] [PubMed]
17. Furuse, M.; Furuse, K.; Sasaki, H.; Tsukita, S. Conversion of zonulae occludentes from tight to leaky strand type by introducing claudin-2 into Madin-Darby canine kidney I cells. *J. Cell Biol.* **2001**, *153*, 263–272. [CrossRef] [PubMed]
18. Amasheh, S.; Meiri, N.; Gitter, A.H.; Schoneberg, T.; Mankertz, J.; Schulzke, J.D.; Fromm, M. Claudin-2 expression induces cation-selective channels in tight junctions of epithelial cells. *J. Cell Sci.* **2002**, *115*, 4969–4976. [CrossRef] [PubMed]
19. Hou, J.; Gomes, A.S.; Paul, D.L.; Goodenough, D.A. Study of claudin function by RNA interference. *J. Biol. Chem.* **2006**, *281*, 36117–36123. [CrossRef] [PubMed]
20. Gupta, I.R.; Ryan, A.K. Claudins: Unlocking the code to tight junction function during embryogenesis and in disease. *Clin. Genet.* **2010**, *77*, 314–325. [CrossRef] [PubMed]
21. Kwon, M.J. Emerging roles of claudins in human cancer. *Int. J. Mol. Sci.* **2013**, *14*, 18148–18180. [CrossRef] [PubMed]
22. Hagen, S.J. Non-canonical functions of claudin proteins: Beyond the regulation of cell-cell adhesions. *Tissue Barriers* **2017**, *5*, e1327839. [CrossRef] [PubMed]
23. Escaffit, F.; Boudreau, F.; Beaulieu, J.F. Differential expression of claudin-2 along the human intestine: Implication of GATA-4 in the maintenance of claudin-2 in differentiating cells. *J. Cell Physiol.* **2005**, *203*, 15–26. [CrossRef] [PubMed]
24. Aung, P.P.; Mitani, Y.; Sanada, Y.; Nakayama, H.; Matsusaki, K.; Yasui, W. Differential expression of claudin-2 in normal human tissues and gastrointestinal carcinomas. *Virchows Arch.* **2006**, *448*, 428–434. [CrossRef] [PubMed]

25. Markov, A.G.; Veshnyakova, A.; Fromm, M.; Amasheh, M.; Amasheh, S. Segmental expression of claudin proteins correlates with tight junction barrier properties in rat intestine. *J. Comp. Physiol. B* **2010**, *180*, 591–598. [CrossRef] [PubMed]
26. Lippoldt, A.; Liebner, S.; Andbjer, B.; Kalbacher, H.; Wolburg, H.; Haller, H.; Fuxe, K. Organization of choroid plexus epithelial and endothelial cell tight junctions and regulation of claudin-1, -2 and -5 expression by protein kinase C. *Neuroreport* **2000**, *11*, 1427–1431. [CrossRef] [PubMed]
27. Tan, X.; Li, D.; Wang, X.; Zeng, Y.; Yan, Y.; Yang, L. Claudin-2 downregulation by KSHV infection is involved in the regulation of endothelial barrier function. *J. Cutan Pathol.* **2014**, *41*, 630–639. [CrossRef] [PubMed]
28. Van den Bossche, J.; Laoui, D.; Morias, Y.; Movahedi, K.; Raes, G.; De Baetselier, P.; Van Ginderachter, J.A. Claudin-1, claudin-2 and claudin-11 genes differentially associate with distinct types of anti-inflammatory macrophages in vitro and with parasite- and tumour-elicited macrophages in vivo. *Scand J. Immunol.* **2012**, *75*, 588–598. [CrossRef] [PubMed]
29. Colegio, O.R.; Van Itallie, C.; Rahner, C.; Anderson, J.M. Claudin extracellular domains determine paracellular charge selectivity and resistance but not tight junction fibril architecture. *Am. J. Physiol. Cell Physiol.* **2003**, *284*, C1346–C1354. [CrossRef] [PubMed]
30. Colegio, O.R.; Van Itallie, C.M.; McCrea, H.J.; Rahner, C.; Anderson, J.M. Claudins create charge-selective channels in the paracellular pathway between epithelial cells. *Am. J. Physiol. Cell Physiol.* **2002**, *283*, C142–C147. [CrossRef] [PubMed]
31. Li, J.; Zhuo, M.; Pei, L.; Rajagopal, M.; Yu, A.S. Comprehensive cysteine-scanning mutagenesis reveals Claudin-2 pore-lining residues with different intrapore locations. *J. Biol. Chem* **2014**, *289*, 6475–6484. [CrossRef] [PubMed]
32. Weber, C.R.; Liang, G.H.; Wang, Y.; Das, S.; Shen, L.; Yu, A.S.; Nelson, D.J.; Turner, J.R. Claudin-2-dependent paracellular channels are dynamically gated. *Elife* **2015**, *4*, e09906. [CrossRef] [PubMed]
33. Li, J.; Angelow, S.; Linge, A.; Zhuo, M.; Yu, A.S. Claudin-2 pore function requires an intramolecular disulfide bond between two conserved extracellular cysteines. *Am. J. Physiol. Cell Physiol.* **2013**, *305*, C190–C196. [CrossRef] [PubMed]
34. Tabaries, S.; McNulty, A.; Ouellet, V.; Annis, M.G.; Dessureault, M.; Vinette, M.; Hachem, Y.; Lavoie, B.; Omeroglu, A.; Simon, H.G.; et al. Afadin cooperates with Claudin-2 to promote breast cancer metastasis. *Genes Dev.* **2019**, *33*, 180–193. [CrossRef] [PubMed]
35. Nomme, J.; Antanasijevic, A.; Caffrey, M.; Van Itallie, C.M.; Anderson, J.M.; Fanning, A.S.; Lavie, A. Structural Basis of a Key Factor Regulating the Affinity between the Zonula Occludens First PDZ Domain and Claudins. *J. Biol. Chem.* **2015**, *290*, 16595–16606. [CrossRef] [PubMed]
36. Van Itallie, C.M.; Mitic, L.L.; Anderson, J.M. Claudin-2 forms homodimers and is a component of a high molecular weight protein complex. *J. Biol. Chem.* **2011**, *286*, 3442–3450. [CrossRef] [PubMed]
37. Tabaries, S.; Dupuy, F.; Dong, Z.; Monast, A.; Annis, M.G.; Spicer, J.; Ferri, L.E.; Omeroglu, A.; Basik, M.; Amir, E.; et al. Claudin-2 promotes breast cancer liver metastasis by facilitating tumor cell interactions with hepatocytes. *Mol. Cell Biol.* **2012**, *32*, 2979–2991. [CrossRef] [PubMed]
38. Lim, T.S.; Vedula, S.R.; Hunziker, W.; Lim, C.T. Kinetics of adhesion mediated by extracellular loops of claudin-2 as revealed by single-molecule force spectroscopy. *J. Mol. Biol.* **2008**, *381*, 681–691. [CrossRef] [PubMed]
39. Piontek, J.; Winkler, L.; Wolburg, H.; Muller, S.L.; Zuleger, N.; Piehl, C.; Wiesner, B.; Krause, G.; Blasig, I.E. Formation of tight junction: Determinants of homophilic interaction between classic claudins. *FASEB J.* **2008**, *22*, 146–158. [CrossRef] [PubMed]
40. Ikari, A.; Taga, S.; Watanabe, R.; Sato, T.; Shimobaba, S.; Sonoki, H.; Endo, S.; Matsunaga, T.; Sakai, H.; Yamaguchi, M.; et al. Clathrin-dependent endocytosis of claudin-2 by DFYSP peptide causes lysosomal damage in lung adenocarcinoma A549 cells. *Biochim. Biophys. Acta* **2015**, *1848*, 2326–2336. [CrossRef] [PubMed]
41. Furuse, M.; Sasaki, H.; Tsukita, S. Manner of interaction of heterogeneous claudin species within and between tight junction strands. *J. Cell Biol.* **1999**, *147*, 891–903. [CrossRef] [PubMed]
42. Capaldo, C.T.; Farkas, A.E.; Hilgarth, R.S.; Krug, S.M.; Wolf, M.F.; Benedik, J.K.; Fromm, M.; Koval, M.; Parkos, C.; Nusrat, A. Proinflammatory cytokine-induced tight junction remodeling through dynamic self-assembly of claudins. *Mol. Biol. Cell* **2014**, *25*, 2710–2719. [CrossRef] [PubMed]

43. Angelow, S.; Schneeberger, E.E.; Yu, A.S. Claudin-8 expression in renal epithelial cells augments the paracellular barrier by replacing endogenous claudin-2. *J. Membr Biol.* **2007**, *215*, 147–159. [CrossRef] [PubMed]
44. Zhang, Y.; Yeh, S.; Appleton, B.A.; Held, H.A.; Kausalya, P.J.; Phua, D.C.; Wong, W.L.; Lasky, L.A.; Wiesmann, C.; Hunziker, W.; et al. Convergent and divergent ligand specificity among PDZ domains of the LAP and zonula occludens (ZO) families. *J. Biol. Chem.* **2006**, *281*, 22299–22311. [CrossRef] [PubMed]
45. Itoh, M.; Furuse, M.; Morita, K.; Kubota, K.; Saitou, M.; Tsukita, S. Direct binding of three tight junction-associated MAGUKs, ZO-1, ZO-2, and ZO-3, with the COOH termini of claudins. *J. Cell Biol.* **1999**, *147*, 1351–1363. [CrossRef] [PubMed]
46. Van Itallie, C.M.; Tietgens, A.J.; LoGrande, K.; Aponte, A.; Gucek, M.; Anderson, J.M. Phosphorylation of claudin-2 on serine 208 promotes membrane retention and reduces trafficking to lysosomes. *J. Cell Sci.* **2012**, *125*, 4902–4912. [CrossRef] [PubMed]
47. Yamauchi, K.; Rai, T.; Kobayashi, K.; Sohara, E.; Suzuki, T.; Itoh, T.; Suda, S.; Hayama, A.; Sasaki, S.; Uchida, S. Disease-causing mutant WNK4 increases paracellular chloride permeability and phosphorylates claudins. *Proc. Natl. Acad. Sci. USA* **2004**, *101*, 4690–4694. [CrossRef] [PubMed]
48. Fujii, N.; Matsuo, Y.; Matsunaga, T.; Endo, S.; Sakai, H.; Yamaguchi, M.; Yamazaki, Y.; Sugatani, J.; Ikari, A. Hypotonic Stress-Induced Down-Regulation of Claudin-1 and -2 Mediated by Dephosphorylation and Clathrin-Dependent Endocytosis in Renal Tubular Epithelial Cells. *J. Biol. Chem.* **2016**, *291*, 24787–24799. [CrossRef] [PubMed]
49. Van Itallie, C.M.; Mitic, L.L.; Anderson, J.M. SUMOylation of claudin-2. *Ann. N. Y. Acad. Sci.* **2012**, *1258*, 60–64. [CrossRef] [PubMed]
50. Molina-Jijon, E.; Rodriguez-Munoz, R.; Namorado Mdel, C.; Pedraza-Chaverri, J.; Reyes, J.L. Oxidative stress induces claudin-2 nitration in experimental type 1 diabetic nephropathy. *Free Radic. Biol. Med.* **2014**, *72*, 162–175. [CrossRef] [PubMed]
51. Dhawan, P.; Ahmad, R.; Chaturvedi, R.; Smith, J.J.; Midha, R.; Mittal, M.K.; Krishnan, M.; Chen, X.; Eschrich, S.; Yeatman, T.J.; et al. Claudin-2 expression increases tumorigenicity of colon cancer cells: Role of epidermal growth factor receptor activation. *Oncogene* **2011**, *30*, 3234–3247. [CrossRef] [PubMed]
52. Amoozadeh, Y.; Anwer, S.; Dan, Q.; Venugopal, S.; Shi, Y.; Branchard, E.; Liedtke, E.; Ailenberg, M.; Rotstein, O.D.; Kapus, A.; et al. Cell confluence regulates claudin-2 expression: Possible role for ZO-1 and Rac. *Am. J. Physiol. Cell Physiol.* **2018**, *314*, C366–C378. [CrossRef] [PubMed]
53. Amoozadeh, Y.; Dan, Q.; Xiao, J.; Waheed, F.; Szaszi, K. Tumor necrosis factor-alpha induces a biphasic change in claudin-2 expression in tubular epithelial cells: Role in barrier functions. *Am. J. Physiol. Cell Physiol.* **2015**, *309*, C38–C50. [CrossRef] [PubMed]
54. Sonoki, H.; Sato, T.; Endo, S.; Matsunaga, T.; Yamaguchi, M.; Yamazaki, Y.; Sugatani, J.; Ikari, A. Quercetin Decreases Claudin-2 Expression Mediated by Up-Regulation of microRNA miR-16 in Lung Adenocarcinoma A549 Cells. *Nutrients* **2015**, *7*, 4578–4592. [CrossRef] [PubMed]
55. Suzuki, T.; Yoshinaga, N.; Tanabe, S. Interleukin-6 (IL-6) regulates claudin-2 expression and tight junction permeability in intestinal epithelium. *J. Biol. Chem.* **2011**, *286*, 31263–31271. [CrossRef] [PubMed]
56. Mankertz, J.; Amasheh, M.; Krug, S.M.; Fromm, A.; Amasheh, S.; Hillenbrand, B.; Tavalali, S.; Fromm, M.; Schulzke, J.D. TNFalpha up-regulates claudin-2 expression in epithelial HT-29/B6 cells via phosphatidylinositol-3-kinase signaling. *Cell Tissue Res.* **2009**, *336*, 67–77. [CrossRef] [PubMed]
57. Singh, A.B.; Harris, R.C. Epidermal growth factor receptor activation differentially regulates claudin expression and enhances transepithelial resistance in Madin-Darby canine kidney cells. *J. Biol. Chem.* **2004**, *279*, 3543–3552. [CrossRef] [PubMed]
58. Ikari, A.; Takiguchi, A.; Atomi, K.; Sugatani, J. Epidermal growth factor increases clathrin-dependent endocytosis and degradation of claudin-2 protein in MDCK II cells. *J. Cell Physiol.* **2011**, *226*, 2448–2456. [CrossRef] [PubMed]
59. Kim, T.I.; Poulin, E.J.; Blask, E.; Bukhalid, R.; Whitehead, R.H.; Franklin, J.L.; Coffey, R.J. Myofibroblast keratinocyte growth factor reduces tight junctional integrity and increases claudin-2 levels in polarized Caco-2 cells. *Growth Factors* **2012**, *30*, 320–332. [CrossRef] [PubMed]
60. Ikari, A.; Sato, T.; Watanabe, R.; Yamazaki, Y.; Sugatani, J. Increase in claudin-2 expression by an EGFR/MEK/ERK/c-Fos pathway in lung adenocarcinoma A549 cells. *Biochim. Biophys. Acta* **2012**, *1823*, 1110–1118. [CrossRef] [PubMed]

61. Lipschutz, J.H.; Li, S.; Arisco, A.; Balkovetz, D.F. Extracellular signal-regulated kinases 1/2 control claudin-2 expression in Madin-Darby canine kidney strain I and II cells. *J. Biol. Chem.* **2005**, *280*, 3780–3788. [CrossRef] [PubMed]
62. Martin-Martin, N.; Ryan, G.; McMorrow, T.; Ryan, M.P. Sirolimus and cyclosporine A alter barrier function in renal proximal tubular cells through stimulation of ERK1/2 signaling and claudin-1 expression. *Am. J. Physiol. Renal Physiol.* **2010**, *298*, F672–F682. [CrossRef] [PubMed]
63. Ahmad, R.; Kumar, B.; Pan, K.; Dhawan, P.; Singh, A.B. HDAC-4 regulates claudin-2 expression in EGFR-ERK1/2 dependent manner to regulate colonic epithelial cell differentiation. *Oncotarget* **2017**, *8*, 87718–87736. [CrossRef] [PubMed]
64. Hichino, A.; Okamoto, M.; Taga, S.; Akizuki, R.; Endo, S.; Matsunaga, T.; Ikari, A. Down-regulation of Claudin-2 Expression and Proliferation by Epigenetic Inhibitors in Human Lung Adenocarcinoma A549 Cells. *J. Biol. Chem.* **2017**, *292*, 2411–2421. [CrossRef] [PubMed]
65. Wang, Y.; Mumm, J.B.; Herbst, R.; Kolbeck, R.; Wang, Y. IL-22 Increases Permeability of Intestinal Epithelial Tight Junctions by Enhancing Claudin-2 Expression. *J. Immunol.* **2017**, *199*, 3316–3325. [CrossRef] [PubMed]
66. Tian, L.; Li, Y.; Zhang, J.; Chang, R.; Li, J.; Huo, L. IL-9 promotes the pathogenesis of ulcerative colitis through STAT3/SOCS3 signaling. *Biosci. Rep.* **2018**, *38*, 9476–9487. [CrossRef] [PubMed]
67. Dan, Q.; Shi, Y.; Rabani, R.; Venugopal, S.; Xiao, J.; Anwer, S.; Ding, M.; Speight, P.; Pan, W.; Alexander, R.T.; et al. Claudin-2 suppresses GEF-H1, RHOA, and MRTF thereby impacting proliferation and profibrotic phenotype of tubular cells. *J. Biol. Chem.* **2019**, *294*, 15446–15465. [CrossRef] [PubMed]
68. Tabaries, S.; Annis, M.G.; Hsu, B.E.; Tam, C.E.; Savage, P.; Park, M.; Siegel, P.M. Lyn modulates Claudin-2 expression and is a therapeutic target for breast cancer liver metastasis. *Oncotarget* **2015**, *6*, 9476–9487. [CrossRef] [PubMed]
69. Garcia-Hernandez, V.; Flores-Maldonado, C.; Rincon-Heredia, R.; Verdejo-Torres, O.; Bonilla-Delgado, J.; Meneses-Morales, I.; Gariglio, P.; Contreras, R.G. EGF regulates claudin-2 and -4 expression through Src and STAT3 in MDCK cells. *J. Cell Physiol.* **2015**, *230*, 105–115. [CrossRef] [PubMed]
70. Ikari, A.; Fujii, N.; Hahakabe, S.; Hayashi, H.; Yamaguchi, M.; Yamazaki, Y.; Endo, S.; Matsunaga, T.; Sugatani, J. Hyperosmolarity-Induced Down-Regulation of Claudin-2 Mediated by Decrease in PKCbeta-Dependent GATA-2 in MDCK Cells. *J. Cell Physiol.* **2015**, *230*, 2776–2787. [CrossRef] [PubMed]
71. Lu, R.; Dalgalan, D.; Mandell, E.K.; Parker, S.S.; Ghosh, S.; Wilson, J.M. PKCiota interacts with Rab14 and modulates epithelial barrier function through regulation of claudin-2 levels. *Mol. Biol. Cell* **2015**, *26*, 1523–1531. [CrossRef] [PubMed]
72. Al-Sadi, R.; Ye, D.; Boivin, M.; Guo, S.; Hashimi, M.; Ereifej, L.; Ma, T.Y. Interleukin-6 modulation of intestinal epithelial tight junction permeability is mediated by JNK pathway activation of claudin-2 gene. *PLoS ONE* **2014**, *9*, e85345. [CrossRef] [PubMed]
73. Zhang, Y.G.; Wu, S.; Xia, Y.; Sun, J. Salmonella infection upregulates the leaky protein claudin-2 in intestinal epithelial cells. *PLoS ONE* **2013**, *8*, e58606. [CrossRef] [PubMed]
74. Mankertz, J.; Hillenbrand, B.; Tavalali, S.; Huber, O.; Fromm, M.; Schulzke, J.D. Functional crosstalk between Wnt signaling and Cdx-related transcriptional activation in the regulation of the claudin-2 promoter activity. *Biochem. Biophys. Res. Commun.* **2004**, *314*, 1001–1007. [CrossRef] [PubMed]
75. Guillemot, L.; Citi, S. Cingulin regulates claudin-2 expression and cell proliferation through the small GTPase RhoA. *Mol. Biol. Cell* **2006**, *17*, 3569–3577. [CrossRef] [PubMed]
76. Bruewer, M.; Hopkins, A.M.; Hobert, M.E.; Nusrat, A.; Madara, J.L. RhoA, Rac1, and Cdc42 exert distinct effects on epithelial barrier via selective structural and biochemical modulation of junctional proteins and F-actin. *Am. J. Physiol. Cell Physiol.* **2004**, *287*, C327–C335. [CrossRef] [PubMed]
77. Wang, Y.B.; Shi, Q.; Li, G.; Zheng, J.H.; Lin, J.; Qiu, W. MicroRNA-488 inhibits progression of colorectal cancer via inhibition of the mitogen-activated protein kinase pathway by targeting claudin-2. *Am. J. Physiol. Cell Physiol.* **2019**, *316*, C33–C47. [CrossRef] [PubMed]
78. Che, M.; Shi, T.; Feng, S.; Li, H.; Zhang, X.; Feng, N.; Lou, W.; Dou, J.; Tang, G.; Huang, C.; et al. The MicroRNA-199a/214 Cluster Targets E-Cadherin and Claudin-2 and Promotes High Glucose-Induced Peritoneal Fibrosis. *J. Am. Soc. Nephrol.* **2017**, *28*, 2459–2471. [CrossRef] [PubMed]
79. Zhang, Y.G.; Wu, S.; Lu, R.; Zhou, D.; Zhou, J.; Carmeliet, G.; Petrof, E.; Claud, E.C.; Sun, J. Tight junction CLDN2 gene is a direct target of the vitamin D receptor. *Sci. Rep.* **2015**, *5*, 10642. [CrossRef] [PubMed]

80. Lepage, D.; Belanger, E.; Jones, C.; Tremblay, S.; Allaire, J.M.; Bruneau, J.; Asselin, C.; Perreault, N.; Menendez, A.; Gendron, F.P.; et al. Gata4 is critical to maintain gut barrier function and mucosal integrity following epithelial injury. *Sci. Rep.* **2016**, *6*, 36776. [CrossRef] [PubMed]
81. Guo, R.J.; Suh, E.R.; Lynch, J.P. The role of Cdx proteins in intestinal development and cancer. *Cancer Biol. Ther.* **2004**, *3*, 593–601. [CrossRef] [PubMed]
82. Song, X.; Chen, H.X.; Wang, X.Y.; Deng, X.Y.; Xi, Y.X.; He, Q.; Peng, T.L.; Chen, J.; Chen, W.; Wong, B.C.; et al. pylori-encoded CagA disrupts tight junctions and induces invasiveness of AGS gastric carcinoma cells via Cdx2-dependent targeting of Claudin-2. *Cell Immunol.* **2013**, *286*, 22–30. [CrossRef] [PubMed]
83. Sakamoto, H.; Mutoh, H.; Sugano, K. Expression of Claudin-2 in intestinal metaplastic mucosa of Cdx2-transgenic mouse stomach. *Scand J. Gastroenterol.* **2010**, *45*, 1273–1280. [CrossRef] [PubMed]
84. Wang, W.; Chen, S.W.; Zhu, J.; Zuo, S.; Ma, Y.Y.; Chen, Z.Y.; Zhang, J.L.; Chen, G.W.; Liu, Y.C.; Wang, P.Y. Intestinal alkaline phosphatase inhibits the translocation of bacteria of gut-origin in mice with peritonitis: Mechanism of action. *PLoS ONE* **2015**, *10*, e0124835. [CrossRef] [PubMed]
85. Peter, Y.; Comellas, A.; Levantini, E.; Ingenito, E.P.; Shapiro, S.D. Epidermal growth factor receptor and claudin-2 participate in A549 permeability and remodeling: Implications for non-small cell lung cancer tumor colonization. *Mol. Carcinog.* **2009**, *48*, 488–497. [CrossRef] [PubMed]
86. Wang, Y.; Shi, J.; Chai, K.; Ying, X.; Zhou, B.P. The Role of Snail in EMT and Tumorigenesis. *Curr. Cancer Drug Targets* **2013**, *13*, 963–972. [CrossRef] [PubMed]
87. Burns, W.C.; Thomas, M.C. The molecular mediators of type 2 epithelial to mesenchymal transition (EMT) and their role in renal pathophysiology. *Expert Rev. Mol. Med.* **2010**, *12*, e17. [CrossRef] [PubMed]
88. Carrozzino, F.; Soulie, P.; Huber, D.; Mensi, N.; Orci, L.; Cano, A.; Feraille, E.; Montesano, R. Inducible expression of Snail selectively increases paracellular ion permeability and differentially modulates tight junction proteins. *Am. J. Physiol. Cell Physiol.* **2005**, *289*, C1002–C1014. [CrossRef] [PubMed]
89. Dukes, J.D.; Whitley, P.; Chalmers, A.D. The PIKfyve inhibitor YM201636 blocks the continuous recycling of the tight junction proteins claudin-1 and claudin-2 in MDCK cells. *PLoS ONE* **2012**, *7*, e28659. [CrossRef] [PubMed]
90. Vasileva, E.; Citi, S. The role of microtubules in the regulation of epithelial junctions. *Tissue Barriers* **2018**, *6*, 1539596. [CrossRef] [PubMed]
91. Shen, L. Tight junctions on the move: Molecular mechanisms for epithelial barrier regulation. *Ann. N. Y. Acad. Sci.* **2012**, *1258*, 9–18. [CrossRef] [PubMed]
92. Nusrat, A.; Turner, J.R.; Madara, J.L. Molecular physiology and pathophysiology of tight junctions. IV. Regulation of tight junctions by extracellular stimuli: Nutrients, cytokines, and immune cells. *Am. J. Physiol. Gastrointest Liver Physiol.* **2000**, *279*, G851–G857. [CrossRef] [PubMed]
93. Van Itallie, C.M.; Colegio, O.R.; Anderson, J.M. The cytoplasmic tails of claudins can influence tight junction barrier properties through effects on protein stability. *J. Membr. Biol.* **2004**, *199*, 29–38. [CrossRef] [PubMed]
94. Van Itallie, C.M.; Fanning, A.S.; Bridges, A.; Anderson, J.M. ZO-1 stabilizes the tight junction solute barrier through coupling to the perijunctional cytoskeleton. *Mol. Biol. Cell* **2009**, *20*, 3930–3940. [CrossRef] [PubMed]
95. Raya-Sandino, A.; Castillo-Kauil, A.; Dominguez-Calderon, A.; Alarcon, L.; Flores-Benitez, D.; Cuellar-Perez, F.; Lopez-Bayghen, B.; Chavez-Munguia, B.; Vazquez-Prado, J.; Gonzalez-Mariscal, L. Zonula occludens-2 regulates Rho proteins activity and the development of epithelial cytoarchitecture and barrier function. *Biochim. Biophys. Acta* **2017**, *1864*, 1714–1733. [CrossRef] [PubMed]
96. Ares, G.; Buonpane, C.; Sincavage, J.; Yuan, C.; Wood, D.R.; Hunter, C.J. Caveolin 1 is Associated with Upregulated Claudin 2 in Necrotizing Enterocolitis. *Sci. Rep.* **2019**, *9*, 4982. [CrossRef] [PubMed]
97. Itallie, C.M.; Anderson, J.M. Caveolin binds independently to claudin-2 and occludin. *Ann. N. Y. Acad. Sci.* **2012**, *1257*, 103–107. [CrossRef] [PubMed]
98. Marchiando, A.M.; Shen, L.; Graham, W.V.; Weber, C.R.; Schwarz, B.T.; Austin, J.R., 2nd; Raleigh, D.R.; Guan, Y.; Watson, A.J.; Montrose, M.H.; et al. Caveolin-1-dependent occludin endocytosis is required for TNF-induced tight junction regulation in vivo. *J. Cell Biol.* **2010**, *189*, 111–126. [CrossRef] [PubMed]
99. Cunningham, K.E.; Turner, J.R. Myosin light chain kinase: Pulling the strings of epithelial tight junction function. *Ann. N. Y. Acad. Sci.* **2012**, *1258*, 34–42. [CrossRef] [PubMed]
100. Nighot, P.K.; Hu, C.A.; Ma, T.Y. Autophagy enhancement of intestinal epithelial tight junction barrier function by targeting claudin-2 degradation. *J. Biol. Chem.* **2015**, *290*, 7234–7246. [CrossRef] [PubMed]

101. Zhang, C.; Yan, J.; Xiao, Y.; Shen, Y.; Wang, J.; Ge, W.; Chen, Y. Inhibition of Autophagic Degradation Process Contributes to Claudin-2 Expression Increase and Epithelial Tight Junction Dysfunction in TNF-alpha Treated Cell Monolayers. *Int. J. Mol. Sci.* **2017**, *18*, 910–919.
102. Huang, L.; Jiang, Y.; Sun, Z.; Gao, Z.; Wang, J.; Zhang, D. Autophagy Strengthens Intestinal Mucosal Barrier by Attenuating Oxidative Stress in Severe Acute Pancreatitis. *Dig. Dis. Sci.* **2018**, *63*, 910–919. [CrossRef] [PubMed]
103. Ikari, A.; Watanabe, R.; Sato, T.; Taga, S.; Shimobaba, S.; Yamaguchi, M.; Yamazaki, Y.; Endo, S.; Matsunaga, T.; Sugatani, J. Nuclear distribution of claudin-2 increases cell proliferation in human lung adenocarcinoma cells. *Biochim. Biophys. Acta* **2014**, *1843*, 2079–2088. [CrossRef] [PubMed]
104. Rosenthal, R.; Milatz, S.; Krug, S.M.; Oelrich, B.; Schulzke, J.D.; Amasheh, S.; Gunzel, D.; Fromm, M. Claudin-2, a component of the tight junction, forms a paracellular water channel. *J. Cell Sci.* **2010**, *123*, 1913–1921. [CrossRef] [PubMed]
105. Rosenthal, R.; Gunzel, D.; Krug, S.M.; Schulzke, J.D.; Fromm, M.; Yu, A.S. Claudin-2-mediated cation and water transport share a common pore. *Acta Physiol. (Oxf)* **2017**, *219*, 521–536. [CrossRef] [PubMed]
106. Rosenthal, R.; Gunzel, D.; Theune, D.; Czichos, C.; Schulzke, J.D.; Fromm, M. Water channels and barriers formed by claudins. *Ann. N. Y. Acad. Sci.* **2017**, *1397*, 100–109. [CrossRef] [PubMed]
107. Borovac, J.; Barker, R.S.; Rievaj, J.; Rasmussen, A.; Pan, W.; Wevrick, R.; Alexander, R.T. Claudin-4 forms a paracellular barrier, revealing the interdependence of claudin expression in the loose epithelial cell culture model opossum kidney cells. *Am. J. Physiol. Cell Physiol.* **2012**, *303*, C1278–C1291. [CrossRef] [PubMed]
108. Tanaka, H.; Tamura, A.; Suzuki, K.; Tsukita, S. Site-specific distribution of claudin-based paracellular channels with roles in biological fluid flow and metabolism. *Ann. N. Y. Acad. Sci.* **2017**, *1405*, 44–52. [CrossRef] [PubMed]
109. Muto, S.; Hata, M.; Taniguchi, J.; Tsuruoka, S.; Moriwaki, K.; Saitou, M.; Furuse, K.; Sasaki, H.; Fujimura, A.; Imai, M.; et al. Claudin-2-deficient mice are defective in the leaky and cation-selective paracellular permeability properties of renal proximal tubules. *Proc. Natl. Acad. Sci. USA* **2010**, *107*, 8011–8016. [CrossRef] [PubMed]
110. Pei, L.; Solis, G.; Nguyen, M.T.; Kamat, N.; Magenheimer, L.; Zhuo, M.; Li, J.; Curry, J.; McDonough, A.A.; Fields, T.A.; et al. Paracellular epithelial sodium transport maximizes energy efficiency in the kidney. *J. Clin. Investig.* **2016**, *126*, 2509–2518. [CrossRef] [PubMed]
111. Schnermann, J.; Huang, Y.; Mizel, D. Fluid reabsorption in proximal convoluted tubules of mice with gene deletions of claudin-2 and/or aquaporin1. *Am. J. Physiol. Renal Physiol.* **2013**, *305*, F1352–F1364. [CrossRef] [PubMed]
112. Matsumoto, K.; Imasato, M.; Yamazaki, Y.; Tanaka, H.; Watanabe, M.; Eguchi, H.; Nagano, H.; Hikita, H.; Tatsumi, T.; Takehara, T.; et al. Claudin 2 deficiency reduces bile flow and increases susceptibility to cholesterol gallstone disease in mice. *Gastroenterology* **2014**, *147*, 1134–1145. [CrossRef] [PubMed]
113. Tamura, A.; Hayashi, H.; Imasato, M.; Yamazaki, Y.; Hagiwara, A.; Wada, M.; Noda, T.; Watanabe, M.; Suzuki, Y.; Tsukita, S. Loss of claudin-15, but not claudin-2, causes Na+ deficiency and glucose malabsorption in mouse small intestine. *Gastroenterology* **2011**, *140*, 913–923. [CrossRef] [PubMed]
114. Wada, M.; Tamura, A.; Takahashi, N.; Tsukita, S. Loss of claudins 2 and 15 from mice causes defects in paracellular Na+ flow and nutrient transport in gut and leads to death from malnutrition. *Gastroenterology* **2013**, *144*, 369–380. [CrossRef] [PubMed]
115. Sukka-Ganesh, B.; Mohammed, K.A.; Kaye, F.; Goldberg, E.P.; Nasreen, N. Ephrin-A1 inhibits NSCLC tumor growth via induction of Cdx-2 a tumor suppressor gene. *BMC Cancer* **2012**, *12*, 309. [CrossRef] [PubMed]
116. Ahmad, R.; Chaturvedi, R.; Olivares-Villagomez, D.; Habib, T.; Asim, M.; Shivesh, P.; Polk, D.B.; Wilson, K.T.; Washington, M.K.; Van Kaer, L.; et al. Targeted colonic claudin-2 expression renders resistance to epithelial injury, induces immune suppression, and protects from colitis. *Mucosal Immunol.* **2014**, *7*, 1340–1353. [CrossRef] [PubMed]
117. Sonoki, H.; Tanimae, A.; Endo, S.; Matsunaga, T.; Furuta, T.; Ichihara, K.; Ikari, A. Kaempherol and Luteolin Decrease Claudin-2 Expression Mediated by Inhibition of STAT3 in Lung Adenocarcinoma A549 Cells. *Nutrients* **2017**, *9*, 597. [CrossRef] [PubMed]
118. Buchert, M.; Papin, M.; Bonnans, C.; Darido, C.; Raye, W.S.; Garambois, V.; Pelegrin, A.; Bourgaux, J.F.; Pannequin, J.; Joubert, D.; et al. Symplekin promotes tumorigenicity by up-regulating claudin-2 expression. *Proc. Natl. Acad. Sci. USA* **2010**, *107*, 2628–2633. [CrossRef] [PubMed]

119. Maruhashi, R.; Akizuki, R.; Sato, T.; Matsunaga, T.; Endo, S.; Yamaguchi, M.; Yamazaki, Y.; Sakai, H.; Ikari, A. Elevation of sensitivity to anticancer agents of human lung adenocarcinoma A549 cells by knockdown of claudin-2 expression in monolayer and spheroid culture models. *Biochim. Biophys. Acta Mol. Cell Res.* **2018**, *1865*, 470–479. [CrossRef] [PubMed]
120. Ikari, A.; Sato, T.; Takiguchi, A.; Atomi, K.; Yamazaki, Y.; Sugatani, J. Claudin-2 knockdown decreases matrix metalloproteinase-9 activity and cell migration via suppression of nuclear Sp1 in A549 cells. *Life Sci.* **2011**, *88*, 628–633. [CrossRef] [PubMed]
121. Behrens, A.; Sibilia, M.; Wagner, E.F. Amino-terminal phosphorylation of c-Jun regulates stress-induced apoptosis and cellular proliferation. *Nat. Genet.* **1999**, *21*, 326–329. [CrossRef] [PubMed]
122. Paquet-Fifield, S.; Koh, S.L.; Cheng, L.; Beyit, L.M.; Shembrey, C.; Molck, C.; Behrenbruch, C.; Papin, M.; Gironella, M.; Guelfi, S.; et al. Tight Junction Protein Claudin-2 Promotes Self-Renewal of Human Colorectal Cancer Stem-like Cells. *Cancer Res.* **2018**, *78*, 2925–2938. [CrossRef] [PubMed]
123. Larre, I.; Castillo, A.; Flores-Maldonado, C.; Contreras, R.G.; Galvan, I.; Munoz-Estrada, J.; Cereijido, M. Ouabain modulates ciliogenesis in epithelial cells. *Proc. Natl. Acad. Sci. USA* **2011**, *108*, 20591–20596. [CrossRef] [PubMed]
124. Sanchez, I.; Dynlacht, B.D. Cilium assembly and disassembly. *Nat. Cell Biol.* **2016**, *18*, 711–717. [CrossRef] [PubMed]
125. Mima, S.; Takehara, M.; Takada, H.; Nishimura, T.; Hoshino, T.; Mizushima, T. NSAIDs suppress the expression of claudin-2 to promote invasion activity of cancer cells. *Carcinogenesis* **2008**, *29*, 1994–2000. [CrossRef] [PubMed]
126. Dreymueller, D.; Theodorou, K.; Donners, M.; Ludwig, A. Fine Tuning Cell Migration by a Disintegrin and Metalloproteinases. *Mediators Inflamm.* **2017**, *2017*, 9621724. [CrossRef] [PubMed]
127. Ikari, A.; Takiguchi, A.; Atomi, K.; Sato, T.; Sugatani, J. Decrease in claudin-2 expression enhances cell migration in renal epithelial Madin-Darby canine kidney cells. *J. Cell Physiol.* **2011**, *226*, 1471–1478. [CrossRef] [PubMed]
128. Takehara, M.; Nishimura, T.; Mima, S.; Hoshino, T.; Mizushima, T. Effect of claudin expression on paracellular permeability, migration and invasion of colonic cancer cells. *Biol. Pharm Bull.* **2009**, *32*, 825–831. [CrossRef] [PubMed]
129. Du, W.; Xu, X.; Niu, Q.; Zhang, X.; Wei, Y.; Wang, Z.; Zhang, W.; Yan, J.; Ru, Y.; Fu, Z.; et al. Spi-B-Mediated Silencing of Claudin-2 Promotes Early Dissemination of Lung Cancer Cells from Primary Tumors. *Cancer Res.* **2017**, *77*, 4809–4822. [CrossRef] [PubMed]
130. Zhang, X.; Wang, H.; Li, Q.; Li, T. CLDN2 inhibits the metastasis of osteosarcoma cells via down-regulating the afadin/ERK signaling pathway. *Cancer Cell Int.* **2018**, *18*, 160. [CrossRef] [PubMed]
131. Campbell, K.; Casanova, J. A common framework for EMT and collective cell migration. *Development* **2016**, *143*, 4291–4300. [CrossRef] [PubMed]
132. Chaffer, C.L.; San Juan, B.P.; Lim, E.; Weinberg, R.A. EMT, cell plasticity and metastasis. *Cancer Metastasis Rev.* **2016**, *35*, 645–654. [CrossRef] [PubMed]
133. Che, J.; Yue, D.; Zhang, B.; Zhang, H.; Huo, Y.; Gao, L.; Zhen, H.; Yang, Y.; Cao, B. Claudin-3 Inhibits Lung Squamous Cell Carcinoma Cell Epithelial-mesenchymal Transition and Invasion via Suppression of the Wnt/beta-catenin Signaling Pathway. *Int. J. Med. Sci.* **2018**, *15*, 339–351. [CrossRef] [PubMed]
134. Suh, Y.; Yoon, C.H.; Kim, R.K.; Lim, E.J.; Oh, Y.S.; Hwang, S.G.; An, S.; Yoon, G.; Gye, M.C.; Yi, J.M.; et al. Claudin-1 induces epithelial-mesenchymal transition through activation of the c-Abl-ERK signaling pathway in human liver cells. *Oncogene* **2013**, *32*, 4873–4882. [CrossRef] [PubMed]
135. Nishida, M.; Yoshida, M.; Nishiumi, S.; Furuse, M.; Azuma, T. Claudin-2 Regulates Colorectal Inflammation via Myosin Light Chain Kinase-Dependent Signaling. *Dig. Dis. Sci.* **2013**, *58*, 1546–1559. [CrossRef] [PubMed]
136. Guillemot, L.; Paschoud, S.; Pulimeno, P.; Foglia, A.; Citi, S. The cytoplasmic plaque of tight junctions: A scaffolding and signalling center. *Biochim. Biophys. Acta* **2008**, *1778*, 601–613. [CrossRef] [PubMed]
137. Balda, M.S.; Matter, K. Tight junctions as regulators of tissue remodelling. *Curr. Opin. Cell Biol.* **2016**, *42*, 94–101. [CrossRef] [PubMed]
138. Hartsock, A.; Nelson, W.J. Adherens and tight junctions: Structure, function and connections to the actin cytoskeleton. *Biochim. Biophys. Acta* **2008**, *1778*, 660–669. [CrossRef] [PubMed]

139. Herve, J.C.; Derangeon, M.; Sarrouilhe, D.; Bourmeyster, N. Influence of the scaffolding protein Zonula Occludens (ZOs) on membrane channels. *Biochim. Biophys. Acta* **2014**, *1838*, 595–604. [CrossRef] [PubMed]
140. Yano, T.; Matsui, T.; Tamura, A.; Uji, M.; Tsukita, S. The association of microtubules with tight junctions is promoted by cingulin phosphorylation by AMPK. *J. Cell Biol.* **2013**, *203*, 605–614. [CrossRef] [PubMed]
141. Yano, T.; Torisawa, T.; Oiwa, K.; Tsukita, S. AMPK-dependent phosphorylation of cingulin reversibly regulates its binding to actin filaments and microtubules. *Sci. Rep.* **2018**, *8*, 15550. [CrossRef] [PubMed]
142. Pollack, V.; Sarkozi, R.; Banki, Z.; Feifel, E.; Wehn, S.; Gstraunthaler, G.; Stoiber, H.; Mayer, G.; Montesano, R.; Strutz, F.; et al. Oncostatin M-induced effects on EMT in human proximal tubular cells: Differential role of ERK signaling. *Am. J. Physiol. Renal Physiol.* **2007**, *293*, F1714–F1726. [CrossRef] [PubMed]
143. Kinugasa, T.; Sakaguchi, T.; Gu, X.; Reinecker, H.C. Claudins regulate the intestinal barrier in response to immune mediators. *Gastroenterology* **2000**, *118*, 1001–1011. [CrossRef]
144. Kinugasa, T.; Huo, Q.; Higashi, D.; Shibaguchi, H.; Kuroki, M.; Tanaka, T.; Futami, K.; Yamashita, Y.; Hachimine, K.; Maekawa, S.; et al. Selective up-regulation of claudin-1 and claudin-2 in colorectal cancer. *Anticancer Res.* **2007**, *27*, 3729–3734. [CrossRef]
145. Moldvay, J.; Jackel, M.; Paska, C.; Soltesz, I.; Schaff, Z.; Kiss, A. Distinct claudin expression profile in histologic subtypes of lung cancer. *Lung Cancer* **2007**, *57*, 159–167. [CrossRef] [PubMed]
146. Xin, S.; Huixin, C.; Benchang, S.; Aiping, B.; Jinhui, W.; Xiaoyan, L.; Yu, W.B.; Minhu, C. Expression of Cdx2 and claudin-2 in the multistage tissue of gastric carcinogenesis. *Oncology* **2007**, *73*, 357–365. [CrossRef] [PubMed]
147. Lin, Z.; Zhang, X.; Liu, Z.; Liu, Q.; Wang, L.; Lu, Y.; Liu, Y.; Wang, M.; Yang, M.; Jin, X.; et al. The distinct expression patterns of claudin-2, -6, and -11 between human gastric neoplasms and adjacent non-neoplastic tissues. *Diagn. Pathol.* **2013**, *8*, 133. [CrossRef] [PubMed]
148. Virman, J.; Soini, Y.; Kujala, P.; Luukkaala, T.; Salminen, T.; Sunela, K.; Kellokumpu-Lehtinen, P.L. Claudins as prognostic factors for renal cell cancer. *Anticancer Res.* **2014**, *34*, 4181–4187. [PubMed]
149. Song, X.; Li, X.; Tang, Y.; Chen, H.; Wong, B.; Wang, J.; Chen, M. Expression of claudin-2 in the multistage process of gastric carcinogenesis. *Histol. Histopathol.* **2008**, *23*, 673–682. [PubMed]
150. Jung, H.; Jun, K.H.; Jung, J.H.; Chin, H.M.; Park, W.B. The expression of claudin-1, claudin-2, claudin-3, and claudin-4 in gastric cancer tissue. *J. Surg. Res.* **2011**, *167*, e185–e191. [CrossRef] [PubMed]
151. Chen, S.Y.; Zhang, R.G.; Duan, G.C. Pathogenic mechanisms of the oncoprotein CagA in H. pylori-induced gastric cancer (Review). *Oncol. Rep.* **2016**, *36*, 3087–3094. [CrossRef] [PubMed]
152. Basu, S.; Haase, G.; Ben-Ze'ev, A. Wnt signaling in cancer stem cells and colon cancer metastasis. *F1000Research* **2016**, *5*. [CrossRef] [PubMed]
153. Weber, C.R.; Nalle, S.C.; Tretiakova, M.; Rubin, D.T.; Turner, J.R. Claudin-1 and claudin-2 expression is elevated in inflammatory bowel disease and may contribute to early neoplastic transformation. *Lab. Investig.* **2008**, *88*, 1110–1120. [CrossRef] [PubMed]
154. Mezheyeuski, A.; Strell, C.; Hrynchyk, I.; Guren, T.K.; Dragomir, A.; Doroshenko, T.; Pashkova, O.; Gorgun, J.; Ruksha, K.; Pfeiffer, P.; et al. Treatment-related survival associations of claudin-2 expression in fibroblasts of colorectal cancer. *Virchows Arch.* **2018**, *472*, 395–405. [CrossRef] [PubMed]
155. Soini, Y. Claudins 2, 3, 4, and 5 in Paget's disease and breast carcinoma. *Hum. Pathol.* **2004**, *35*, 1531–1536. [CrossRef] [PubMed]
156. Kim, T.H.; Huh, J.H.; Lee, S.; Kang, H.; Kim, G.I.; An, H.J. Down-regulation of claudin-2 in breast carcinomas is associated with advanced disease. *Histopathology* **2008**, *53*, 48–55. [CrossRef] [PubMed]
157. Tabaries, S.; Dong, Z.; Annis, M.G.; Omeroglu, A.; Pepin, F.; Ouellet, V.; Russo, C.; Hassanain, M.; Metrakos, P.; Diaz, Z.; et al. Claudin-2 is selectively enriched in and promotes the formation of breast cancer liver metastases through engagement of integrin complexes. *Oncogene* **2011**, *30*, 1318–1328. [CrossRef] [PubMed]
158. Kimbung, S.; Kovacs, A.; Bendahl, P.O.; Malmstrom, P.; Ferno, M.; Hatschek, T.; Hedenfalk, I. Claudin-2 is an independent negative prognostic factor in breast cancer and specifically predicts early liver recurrences. *Mol. Oncol.* **2014**, *8*, 119–128. [CrossRef] [PubMed]
159. Barmeyer, C.; Fromm, M.; Schulzke, J.D. Active and passive involvement of claudins in the pathophysiology of intestinal inflammatory diseases. *Pflugers Arch.* **2017**, *469*, 15–26. [CrossRef] [PubMed]
160. Landy, J.; Ronde, E.; English, N.; Clark, S.K.; Hart, A.L.; Knight, S.C.; Ciclitira, P.J.; Al-Hassi, H.O. Tight junctions in inflammatory bowel diseases and inflammatory bowel disease associated colorectal cancer. *World J. Gastroenterol.* **2016**, *22*, 3117–3126. [CrossRef] [PubMed]

161. Amasheh, M.; Fromm, A.; Krug, S.M.; Amasheh, S.; Andres, S.; Zeitz, M.; Fromm, M.; Schulzke, J.D. TNFalpha-induced and berberine-antagonized tight junction barrier impairment via tyrosine kinase, Akt and NFkappaB signaling. *J. Cell Sci.* **2010**, *123*, 4145–4155. [CrossRef] [PubMed]
162. Zeissig, S.; Burgel, N.; Gunzel, D.; Richter, J.; Mankertz, J.; Wahnschaffe, U.; Kroesen, A.J.; Zeitz, M.; Fromm, M.; Schulzke, J.D. Changes in expression and distribution of claudin 2, 5 and 8 lead to discontinuous tight junctions and barrier dysfunction in active Crohn's disease. *Gut* **2007**, *56*, 61–72. [CrossRef] [PubMed]
163. Luettig, J.; Rosenthal, R.; Barmeyer, C.; Schulzke, J.D. Claudin-2 as a mediator of leaky gut barrier during intestinal inflammation. *Tissue Barriers* **2015**, *3*, e977176. [CrossRef] [PubMed]
164. Aghdassi, A.A.; Weiss, F.U.; Mayerle, J.; Lerch, M.M.; Simon, P. Genetic susceptibility factors for alcohol-induced chronic pancreatitis. *Pancreatology* **2015**, *15*, S23–S31. [CrossRef] [PubMed]
165. Gong, Y.; Hou, J. Claudins in barrier and transport function-the kidney. *Pflugers Arch.* **2017**, *469*, 105–113. [CrossRef] [PubMed]
166. Fromm, M.; Piontek, J.; Rosenthal, R.; Gunzel, D.; Krug, S.M. Tight junctions of the proximal tubule and their channel proteins. *Pflugers Arch.* **2017**, *469*, 877–887. [CrossRef] [PubMed]
167. Szaszi, K.; Amoozadeh, Y. New insights into functions, regulation, and pathological roles of tight junctions in kidney tubular epithelium. *Int. Rev. Cell Mol. Biol.* **2014**, *308*, 205–271. [PubMed]
168. Balkovetz, D.F.; Chumley, P.; Amlal, H. Downregulation of claudin-2 expression in renal epithelial cells by metabolic acidosis. *Am. J. Physiol. Renal Physiol.* **2009**, *297*, F604–F611. [CrossRef] [PubMed]
169. Gonzalez, J.E.; DiGeronimo, R.J.; Arthur, D.E.; King, J.M. Remodeling of the tight junction during recovery from exposure to hydrogen peroxide in kidney epithelial cells. *Free Radic Biol. Med.* **2009**, *47*, 1561–1569. [CrossRef] [PubMed]
170. Singh, A.B.; Sugimoto, K.; Dhawan, P.; Harris, R.C. Juxtacrine activation of EGFR regulates claudin expression and increases transepithelial resistance. *Am. J. Physiol. Cell Physiol.* **2007**, *293*, C1660–C1668. [CrossRef] [PubMed]
171. Maggiorani, D.; Dissard, R.; Belloy, M.; Saulnier-Blache, J.S.; Casemayou, A.; Ducasse, L.; Gres, S.; Belliere, J.; Caubet, C.; Bascands, J.L.; et al. Shear Stress-Induced Alteration of Epithelial Organization in Human Renal Tubular Cells. *PLoS ONE* **2015**, *10*, e0131416. [CrossRef] [PubMed]
172. Gamero-Estevez, E.; Andonian, S.; Jean-Claude, B.; Gupta, I.; Ryan, A.K. Temporal Effects of Quercetin on Tight Junction Barrier Properties and Claudin Expression and Localization in MDCK II Cells. *Int. J. Mol. Sci.* **2019**, *20*, 4889. [CrossRef] [PubMed]
173. Martin-Martin, N.; Dan, Q.; Amoozadeh, Y.; Waheed, F.; McMorrow, T.; Ryan, M.P.; Szaszi, K. RhoA and Rho kinase mediate cyclosporine A and sirolimus-induced barrier tightening in renal proximal tubular cells. *Int. J. Biochem. Cell Biol.* **2012**, *44*, 178–188. [CrossRef] [PubMed]
174. Trujillo, J.; Molina-Jijon, E.; Medina-Campos, O.N.; Rodriguez-Munoz, R.; Reyes, J.L.; Loredo, M.L.; Tapia, E.; Sanchez-Lozada, L.G.; Barrera-Oviedo, D.; Pedraza-Chaverri, J. Renal tight junction proteins are decreased in cisplatin-induced nephrotoxicity in rats. *Toxicol. Mech. Methods* **2014**, *24*, 520–528. [CrossRef] [PubMed]
175. Bialik, J.F.; Ding, M.; Speight, P.; Dan, Q.; Miranda, M.Z.; Di Ciano-Oliveira, C.; Kofler, M.M.; Rotstein, O.D.; Pedersen, S.F.; Szaszi, K.; et al. Profibrotic epithelial phenotype: A central role for MRTF and TAZ. *Sci. Rep.* **2019**, *9*, 4323. [CrossRef] [PubMed]
176. Takigawa, M.; Iida, M.; Nagase, S.; Suzuki, H.; Watari, A.; Tada, M.; Okada, Y.; Doi, T.; Fukasawa, M.; Yagi, K.; et al. Creation of a Claudin-2 Binder and Its Tight Junction-Modulating Activity in a Human Intestinal Model. *J. Pharmacol. Exp. Ther.* **2017**, *363*, 444–451. [CrossRef] [PubMed]
177. Hashimoto, Y.; Hata, T.; Tada, M.; Iida, M.; Watari, A.; Okada, Y.; Doi, T.; Kuniyasu, H.; Yagi, K.; Kondoh, M. Safety evaluation of a human chimeric monoclonal antibody that recognizes the extracellular loop domain of claudin-2. *Eur. J. Pharm. Sci.* **2018**, *117*, 161–167. [CrossRef] [PubMed]

International Journal of
Molecular Sciences

MDPI

Article

Brazilian Green Propolis Rescues Oxidative Stress-Induced Mislocalization of Claudin-1 in Human Keratinocyte-Derived HaCaT Cells

Kana Marunaka [1], Mao Kobayashi [1], Shokoku Shu [1], Toshiyuki Matsunaga [2] and Akira Ikari [1,*]

[1] Laboratory of Biochemistry, Department of Biopharmaceutical Sciences, Gifu Pharmaceutical University, Gifu 501-1196, Japan
[2] Education Center of Green Pharmaceutical Sciences, Gifu Pharmaceutical University, Gifu 502-8585, Japan
* Correspondence: ikari@gifu-pu.ac.jp; Tel.: +81-58-230-8124; Fax: +81-58-230-8124

Received: 9 July 2019; Accepted: 7 August 2019; Published: 8 August 2019

Abstract: Claudin-1 (CLDN1) is expressed in the tight junction (TJ) of the skin granular layer and acts as a physiological barrier for the paracellular transport of ions and nonionic molecules. Ultraviolet (UV) and oxidative stress may disrupt the TJ barrier, but the mechanism of and protective agents against this effect have not been clarified. We found that UVB and hydrogen peroxide (H_2O_2) caused the internalization of CLDN1 and increased the paracellular permeability of lucifer yellow, a fluorescent marker, in human keratinocyte-derived HaCaT cells. Therefore, the mechanism of mislocalization of CLDN1 and the protective effect of an ethanol extract of Brazilian green propolis (EBGP) were investigated. The UVB- and H_2O_2-induced decreases in CLDN1 localization were rescued by EBGP. H_2O_2 decreased the phosphorylation level of CLDN1, which was also rescued by EBGP. Wild-type CLDN1 was distributed in the cytosol after treatment with H_2O_2, whereas T191E, its H_2O_2-insensitive phosphorylation-mimicking mutant, was localized at the TJ. Both protein kinase C activator and protein phosphatase 2A inhibitor rescued the H_2O_2-induced decrease in CLDN1 localization. The tight junctional localization of CLDN1 and paracellular permeability showed a negative correlation. Our results indicate that UVB and H_2O_2 could induce the elevation of paracellular permeability mediated by the dephosphorylation and mislocalization of CLDN1 in HaCaT cells, which was rescued by EBGP. EBGP and its components may be useful in preventing the destruction of the TJ barrier through UV and oxidative stress.

Keywords: claudin-1; hydrogen peroxide; phosphorylation

1. Introduction

The skin forms a barrier between the body and its external environment in order to prevent the intrusion of pathogens and the uncontrolled loss of internal water and solutes. The epidermis is the outermost layer of skin and provides the first line of defense against ultraviolet (UV) radiation and other environmental factors. UV is divided into three ranges based on wavelength: UVA (320–400 nm), UVB (280–320 nm), and UVC (100–290 nm). Among these, UVC is unlikely to be present in terrestrial sunlight because it is blocked by the ozone layer, whereas UVA and UVB can come into contact with the skin. The skin can be separated by the basement membrane into two layers, the dermis and epidermis. The mammalian epidermis is composed of four layers, including the basal, spinous, granular, and cornified layers [1]. UVA can penetrate the dermal layer of the skin and reach the capillaries, whereas UVB is blocked in the upper dermis. According to wavelength-dependent studies, UVB radiation has more cytotoxic and mutagenic effects than UVA does [2,3]. Long-term exposure to UVB induces damage to both the dermal and epidermal skin [4]. UVB-induced cell death is caused through directly induced DNA damage and indirect action mediated by the generation of

reactive oxygen species (ROS) and nitric oxide [5]. The main causes of UV-induced DNA damage are 2,3-cyclobutane pyrimidine dimer and a pyrimidine (6-4) pyrimidone photoproduct [6]. In contrast, it is not fully understood what mechanisms are involved in damage to the skin barrier under low toxic conditions. An investigation of the effect of each toxic factor on the tight junction (TJ) barrier may be needed in order to clarify the molecular mechanism.

Human skin keratinocytes form a TJ at the most apical pole of the lateral membrane between neighboring cells. The TJ prevents the abnormal paracellular movement of water, solutes, and pathogens. Claudins (CLDNs) and occludin are integral membrane proteins in TJ, and they comprise a large family of 27 subtypes in mammals [7,8]. Among them, CLDN1 and CLDN4 are highly expressed in human keratinocytes [9]. Most CLDNs contain carboxyl-terminal PSD95/Dlg/ZO-1 (PDZ)-binding motifs that mediate interactions between CLDNs and scaffolding proteins such as ZO-1 and ZO-2. These scaffolding proteins indirectly link CLDNs to actin filaments. CLDN1-deficient mice develop aberrant stratum corneum barrier functions in the skin [10]. A premature stop codon of CLDN1, resulting in a lack of CLDN1 protein, has been identified in neonatal ichthyosis and sclerosing cholangitis syndrome, a disorder characterized by scalp hypotrichosis, ichthyosis, scarring alopecia, and sclerosing cholangitis [11]. Therefore, CLDN1 may have an important role in maintaining the barrier function in the skin.

An antioxidant effect is one of the key factors in reducing skin injury, aging, and cancer risk, and antioxidant activities have been reported in components extracted from plants, fruits, vegetables, and bee propolis [12,13]. Propolis contains many classes of compounds, including flavonoids, phenolic acids, and others. The components of propolis are different in each area [14]. The ethanol extract of Brazilian green propolis (EBGP) exerts strong antioxidant activity in mouse skin [15] and protects human keratinocytes against UV-induced apoptosis [16]. In addition, hydroalcoholic extracts of Brazilian propolis improve dermal burn healing [17]. EBGP may be useful in protecting skin damage from various external stimuli, but the effect of EBGP on the TJ barrier has not been examined.

Human keratinocyte-derived HaCaT cells can easily be plated as a monolayer and form the TJ [18]. Therefore, they may be useful in examining the function of TJ in the skin. In the present study, we investigated the effects of ROS and EBGP on the cellular localization and function of CLDN1 in HaCaT cells. In addition, the molecular mechanism of tight junctional localization of CLDN1 was assessed by immunoprecipitation, immunoblotting, and immunofluorescence measurements.

2. Results

2.1. Effect of UVB Radiation on the Production of ROS

The production of ROS and H_2O_2 in HaCaT cells was measured using 2′,7′-dichlorodihydrofluorescein diacetate (H_2DCFDA) and Hydrop, respectively. UVB radiation dose-dependently induced the fluorescence intensities of H_2DCFDA and Hydrop (Figure 1A,B). UVB radiation between 10 and 50 mJ/cm^2 may have increased the production of ROS and H_2O_2. Cell viability was dose-dependently decreased by exposure to UVB (Figure 1C). The effects were significant over 10 mJ/cm^2, but the percentage of cell toxicity was less than 40%. UVB radiation up to 50 mJ/cm^2 may have produced relatively low toxic conditions. To clarify the effects of ROS on viability, the cells were transiently exposed to H_2O_2 for 3 h. H_2O_2 dose-dependently decreased cell viability (Figure 1D). We decided to treat the cells with 50 mJ/ cm^2 UVB or 200 μM H_2O_2 in subsequent experiments.

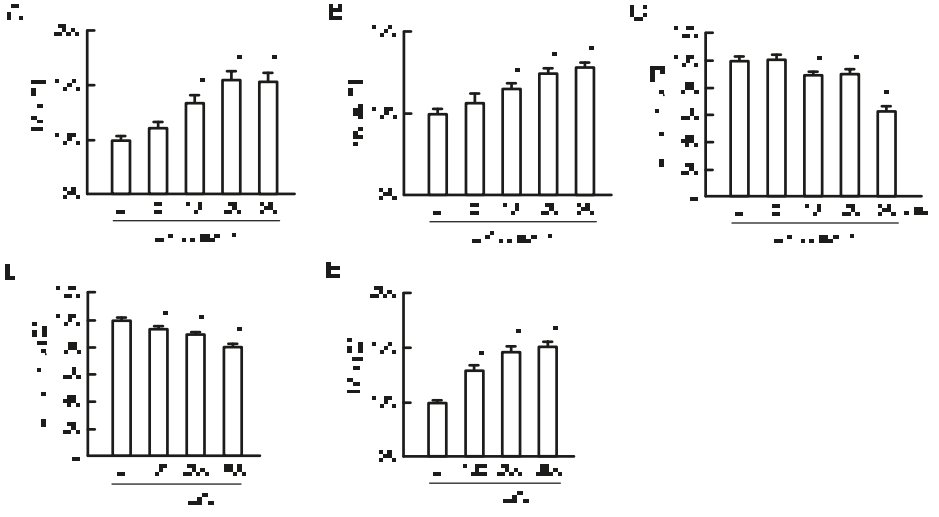

Figure 1. Effects of UVB and H_2O_2 on reactive oxygen species (ROS) production and cell toxicity in HaCaT cells. (**A**,**B**) Cells exposed to UVB were cultured for 3 h and then incubated with 2′,7′-dichlorodihydrofluorescein diacetate (H_2DCFDA) (ROS) and Hydrop (H_2O_2) for 30 min. The florescence intensities of each dye were measured using an Infinite F200 Pro microplate reader and are shown relative to the values (0 mJ/cm^2). (**C**,**D**) Cells were exposed to UVB or transiently exposed to H_2O_2 for 3 h, and then they were cultured for 24 h. Cell viability was measured using a WST-1 assay. (**E**) Cells were exposed to H_2O_2 for 3 h, and then they were incubated with H_2DCFDA. The florescence intensities of H_2DCF are shown as relative to the values in 0 μM H_2O_2. n = 4–6; *** $p < 0.001$ and ** $p < 0.01$ significantly different from 0 mJ/cm^2 UVB or 0 μM H_2O_2.

2.2. *Effect of H_2O_2 on the Cell Localization of TJ Protein*

Immunofluorescence measurements showed that CLDN1, CLDN4, and ZO-1 were localized at the TJ under control conditions (Figure 2A,B). The fluorescence signal of CLDN1 at the TJ was not changed by treatment with 200 μM H_2O_2 for 3 h, but it became weaker at 6 h. In contrast, those of CLDN4 and ZO-1 were unchanged. CLDN1 was relocalized at the TJ after 48 h. The amount of CLDN1 protein was unchanged by H_2O_2 treatment, but that of CLDN4 transiently increased at 6 h (Figure 2C).

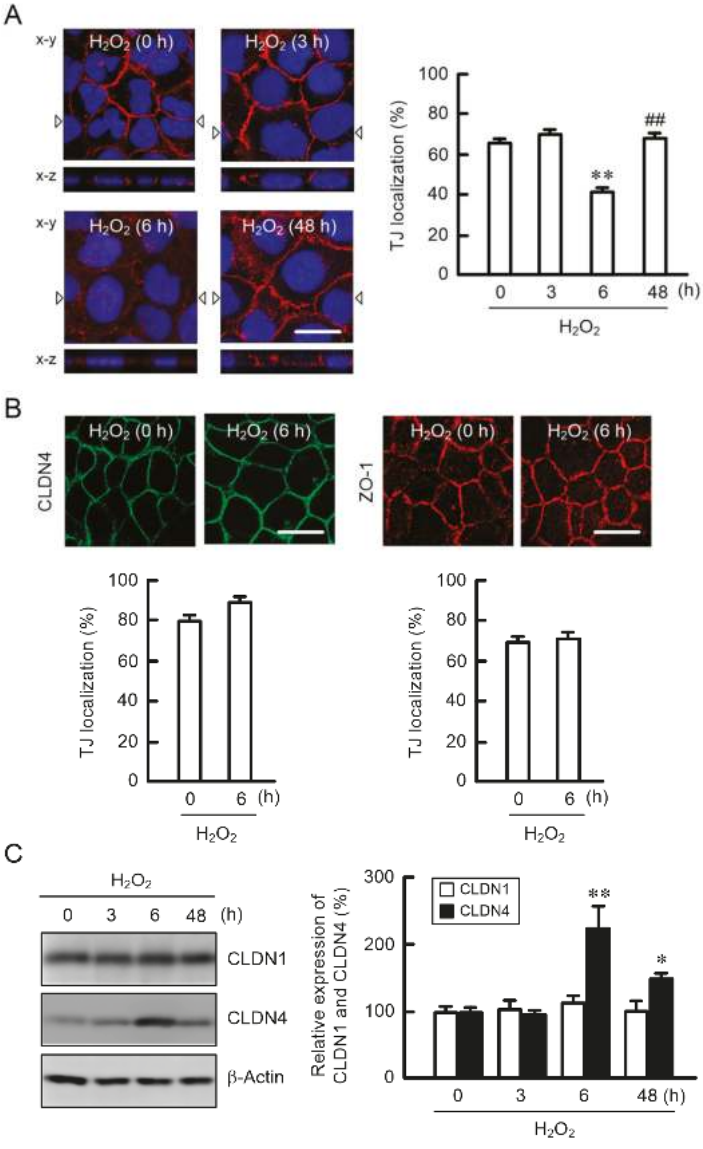

Figure 2. Effects of H_2O_2 on the localization and expression of claudins (CLDNs). Cells exposed to 200 μM H_2O_2 were cultured for 0, 3, 6, and 48 h. (**A**) The cells were immunostained with anti-CLDN1 (red) antibodies and DAPI (nuclear marker). The low panels (x-z) show the vertical sections indicated by the triangles of x-y images. Scale bars indicate 10 μm. The fluorescence values of CLDN1 at the tight junction (TJ) are shown as a percentage of the total fluorescence values. (**B**) The cells were immunostained with anti-CLDN4 (green) or anti-ZO-1 (red) antibodies. The fluorescence values of CLDN4 and ZO-1 at the TJ are shown as a percentage of the total fluorescence values. (**C**) Cell lysates were applied to 12.5% SDS-PAGE and blotted with anti-CLDN1, anti-CLDN4, and β-actin antibodies. The expression levels of CLDN1 and CLDN4 are represented relative to the values at 0 h. n = 3–8; ** $p < 0.01$ and * $p < 0.05$ significantly different from 0 h; ## $p < 0.01$ significantly different from 6 h.

2.3. Effects of EBGP on the UVB- and H_2O_2-Induced Destruction of the TJ Barrier

The function of the TJ barrier was evaluated using transepithelial electrical resistance (TER) and lucifer yellow (LY) flux with HaCaT cells cultured on Transwell inserts. TER decreased after 6 h of treatment with UVB or H_2O_2, then returned to the control level after 48 h (Figure 3A). EBGP-induced cell toxicity was examined using a 2-(4-Iodophenyl)-3-(4-nitrophenyl)-5-(2,4-disulfophenyl)-2*H*-tetrazolium (WST-1) assay. Cell viability was not significantly changed by EBGP at concentrations less than 20 μg/mL, but decreased at 50 μg/mL (Figure 3B). The H_2O_2-induced mislocalization of CLDN1 was significantly rescued by 10 μg/mL EBGP (Figure 3C), but not by 50 μg/mL EBGP. Similarly, the TJ localization of CLDN1 was decreased by UVB, which was rescued by 10 μg/mL EBGP. Both H_2O_2 and UVB caused a decrease in TER and an increase in LY flux, indicating that H_2O_2 and UVB induced the destruction of the TJ barrier. These effects were rescued by EBGP (Figure 3D). These results indicated that UVB and H_2O_2 may have induced the destruction of the TJ barrier mediated by the loss of CLDN1 in the TJ, which was rescued by EBGP.

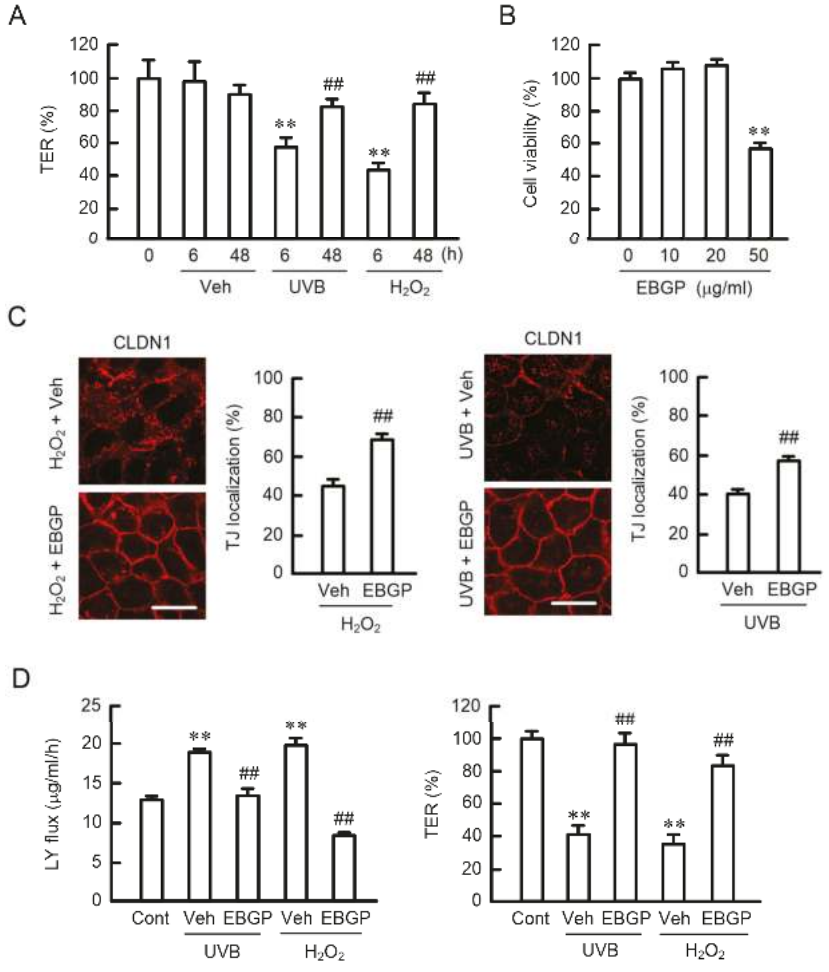

Figure 3. Effects of UVB, H_2O_2, and Brazilian green propolis (EBGP) on TJ permeability. (**A**) Cells plated on Transwell inserts were incubated with 50 mJ/cm^2 UVB or 200 μM H_2O_2 for the periods indicated. Transepithelial electrical resistance (TER) was measured using a volt-ohmmeter and is represented as a

percentage of the values at 0 h. (**B**) Cells were incubated in the presence or absence of EBGP for 24 h. Cell viability was measured using a WST-1 assay. (**C**) The cells were pre-incubated in the absence (Veh) or presence of 10 μg/mL EBGP for 30 min, followed by exposure to UVB or H_2O_2 for 6 h. The cells were immunostained with anti-CLDN1 antibodies. Scale bars indicate 10 μm. The TJ localization of CLDN1 is represented as the percentage of total amount. (**D**) The cells were pre-incubated in the absence (Veh) or presence of 10 μg/mL EBGP for 30 min, followed by exposure to UVB or H_2O_2 for 6 h. Control cells (Cont) were not treated with UVB or H_2O_2. TER was measured using a volt-ohmmeter and is represented as a percentage of the values in control cells. Paracellular lucifer yellow (LY) flux was analyzed using fluorescence spectrometry. $n = 4$; ** $p < 0.01$ significantly different from 0 h, 0 μg/mL, or Cont; $^{\#\#}$ $p < 0.01$ significantly different from 6 h of UVB and H_2O_2 or Veh of UVB and H_2O_2.

2.4. Effect of CLDN1 Expression on the TJ Barrier

To confirm the involvement of CLDN1, we examined the effect of knockdown of CLDN1 expression. The mRNA expression of CLDN1 was decreased by the introduction of CLDN1 small interfering RNAs (siRNAs) (Figure 4A). The knockdown of CLDN1 induced a decrease in TER and an increase in LY flux (Figure 4B), indicating that CLDN1 had an important role in the regulation of the TJ barrier. H_2O_2 significantly changed neither TER nor LY flux in CLDN1 knockdown cells (Figure 4C). In addition, EBGP showed no recovery effects on the TJ barrier. These results indicated that CLDN1 was necessary for the EBGP-induced rescue effect of the TJ barrier.

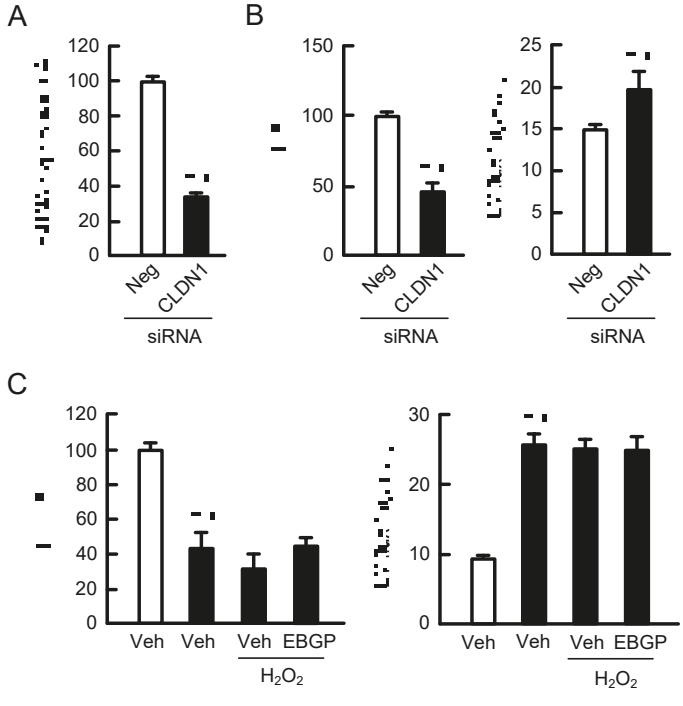

Figure 4. Destruction of the TJ barrier by a decrease in CLDN1 expression. The cells were transfected with negative (Neg and open bars) or CLDN1 (closed bars) small interfering RNAs (siRNAs). (**A**) The expression level of CLDN1 mRNA was measured using real-time PCR. (**B**) TER and paracellular LY flux were analyzed using a volt-ohmmeter and fluorescence spectrometry, respectively. (**C**) The cells were incubated in the absence (Veh) or presence of 200 μM H_2O_2 and 10 μg/mL EBGP for 6 h. TER and paracellular LY flux were analyzed. $n = 4$; ** $p < 0.01$ significantly different from Veh.

2.5. Effects of Endocytosis Inhibitors on the Localization of CLDN1

The localization of plasma membrane protein is regulated by endocytotic processes, including clathrin- and caveolae-dependent pathways. The H_2O_2-induced mislocalization of CLDN1 was inhibited by monodansylcadaverine (MDC), a clathrin-dependent endocytosis inhibitor, but not by methyl-β-cyclodextrin (MβCD), a caveolae-dependent endocytosis inhibitor (Figure 5A), indicating that H_2O_2 may increase the internalization of CLDN1 mediated by the clathrin-dependent endocytosis pathway. An increase in the paracellular permeability caused by H_2O_2 was rescued by MDC, but not by MβCD (Figure 5B). These results coincided with the effect of MDC on the H_2O_2-induced mislocalization of CLDN1 in the immunofluorescence measurements. The recovery effect of MDC was blocked by the knockdown of CLDN1 expression. These results support that the disappearance of CLDN1 in TJ may induce disruption of the TJ barrier. The localization of some CLDNs has been reported to change according to their phosphorylation status [19–21]. Therefore, we decided to investigate the effect of H_2O_2 on the phosphorylation of CLDN1.

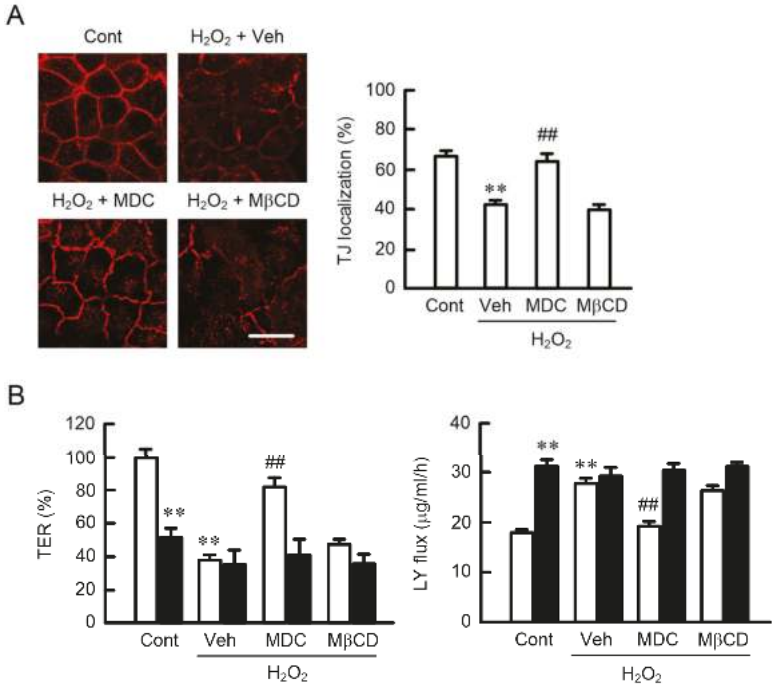

Figure 5. Rescue of the H_2O_2-induced mislocalization of CLDN1 by monodansylcadaverine (MDC). (**A**) Cells were pre-incubated in the absence (Veh) or presence of 5 μM MDC and 10 μM methyl-β-cyclodextrin (MβCD) for 30 min, followed by exposure to 200 μM H_2O_2. Control cells (Cont) were not treated with H_2O_2 and endocytosis inhibitors. The cells were immunostained with anti-CLDN1 antibodies. Scale bars indicate 10 μm. The TJ localization of CLDN1 is represented as the percentage of the total amount. (**B**) Negative (open bars) or CLDN1 siRNA-transfected cells (closed bars) were incubated with H_2O_2, MDC, and MβCD. TER and paracellular LY flux were analyzed using a volt-ohmmeter and fluorescence spectrometry, respectively. n = 4–6; ** $p < 0.01$ significantly different from Cont or Cont of negative siRNA; ## $p < 0.01$ significantly different from Veh of H_2O_2.

2.6. Effects of Phosphorylation Mimic Mutants of CLDN1 on the TJ Barrier

H_2O_2 transiently decreased the phosphothreonine (p-Thr) levels of CLDN1 after 3–6 h (Figure 6A). In contrast, phosphoserine (p-Ser) levels were unchanged by H_2O_2 (data not shown). The H_2O_2-induced

dephosphorylation of CLDN1 was inhibited by EBGP (Figure 6B). It has been reported previously that CLDN1 may be phosphorylated at T191 and T195 [22]. To clarify the dephosphorylation site of CLDN1 associated with H_2O_2 treatment, we investigated the effects of phosphorylation mimic mutants of CLDN1, T191E, and T195E. In the absence of H_2O_2, the wild-type (WT), T191E, and T195E proteins were localized in the TJ area. H_2O_2 increased the intracellular distribution of WT and T195E, but T191E was still mainly localized in the TJ area (Figure 6C). Compared to WT in the absence of H_2O_2, T191E showed a similar TJ barrier function, but T195E did not (Figure 6D). These results indicated that the phosphorylation of T191 may be necessary for the TJ localization of CLDN1.

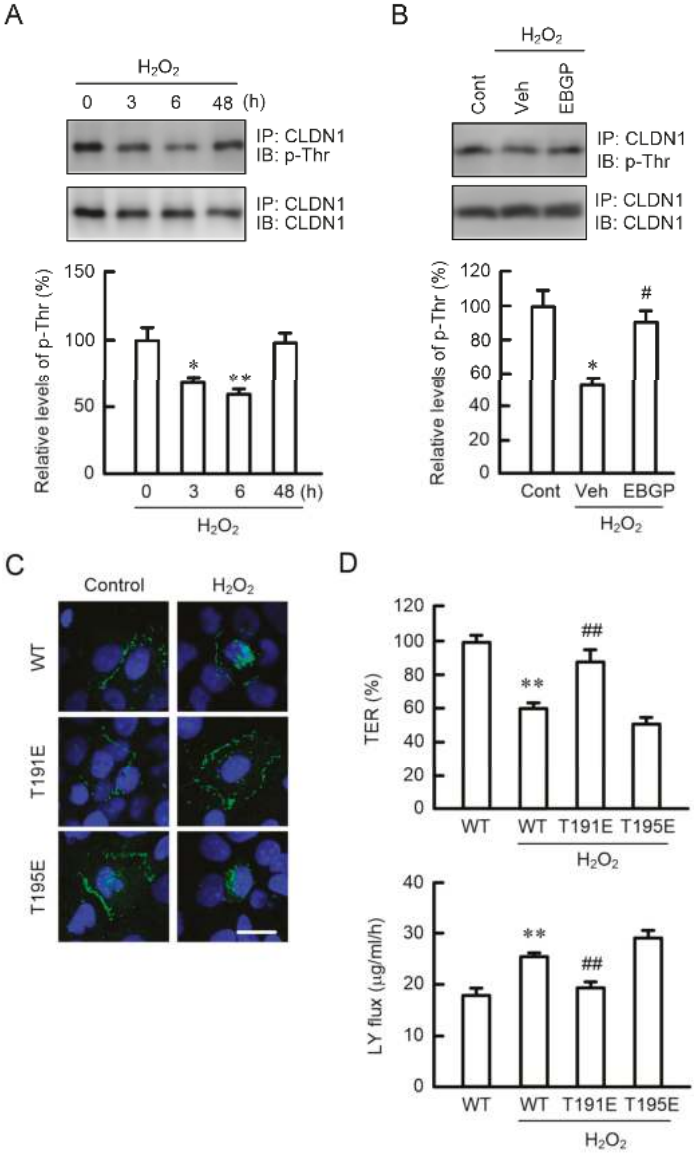

Figure 6. Effects of phosphorylation mimic mutants on H_2O_2-induced barrier destruction. (**A**) Cell lysates were prepared from the cells exposed to 200 μM H_2O_2 for the periods indicated. (**B**) Cell lysates

were prepared from the cells exposed to 200 μM H_2O_2 in the absence (Veh) or presence of 10 μg/mL EBGP for 6 h. After immunoprecipitation with anti-CLDN1 antibodies, the immunoprecipitants were applied to 12.5% SDS-PAGE and blotted with antiphosphothreonine (p-Thr) and anti-CLDN1 antibodies. The levels of p-Thr are represented relative to the values at 0 h or the control (Cont). (**C**,**D**) Cells were transfected with FLAG-tagged wild-type (WT), T191E, and T195E CLDN1. At 48 h after transfection, the cells were exposed to 200 μM H_2O_2 for 6 h. (**C**) The cells were immunostained with anti-FLAG antibodies (green) and DAPI (blue), a nuclear marker. Scale bars indicate 10 μm. (**D**) TER and paracellular LY flux were analyzed using a volt-ohmmeter and fluorescence spectrometry, respectively. n = 3–4; ** $p < 0.01$ and * $p < 0.05$ significantly different from 0 h, Cont, or WT alone; $^{\#\#}$ $p < 0.01$ and $^{\#}$ $p < 0.05$ significantly different from Veh with H_2O_2 or WT with H_2O_2.

2.7. Phosphorylation of CLDN1 by PKC

The phosphorylation level of CLDN1 is regulated by atypical PKC and protein phosphatases (PPs) [23]. Go6976, a selective PKCα and β isoform inhibitor, decreased p-Thr levels and the TJ localization of CLDN1 (Figure 7A,B). H_2O_2 decreased PKC activity and increased PP activities, which were significantly inhibited by EBGP (Figure 7C). To support the involvement of PKC, we examined the effects of phorbol 12-myristate 13-acetate (PMA), a PKC activator, and cantharidin, a PP2A inhibitor, on the TJ barrier. The H_2O_2-induced mislocalization of CLDN1 was inhibited by both PMA and cantharidin (Figure 7D). Similarly, the reduction in the TJ barrier function by H_2O_2 was significantly rescued by both PMA and cantharidin (Figure 7E,F). The recovery effects of PMA and cantharidin were blocked by the knockdown of CLDN1 expression. These results indicated that PKC activator and PP inhibitor could rescue the H_2O_2-induced mislocalization of CLDN1.

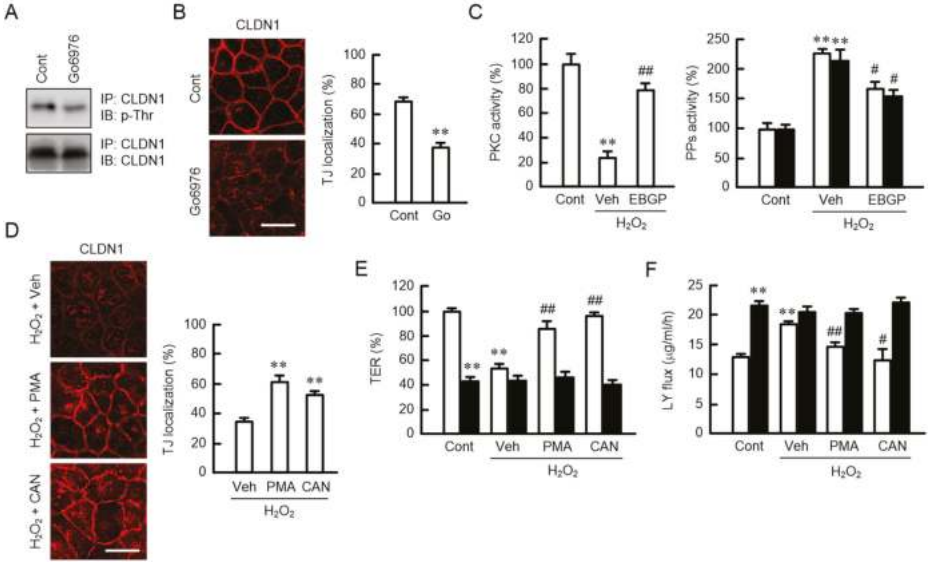

Figure 7. Upregulation of the TJ localization and phosphorylation of CLDN1 by PKC. (**A**,**B**) Cells were incubated in the absence (Cont) or presence of 10 μM Go6976 (Go) for 30 min (**A**) or 6 h (**B**). (**A**) After immunoprecipitation with anti-CLDN1 antibodies, the immunoprecipitants were blotted with anti-p-Thr and anti-CLDN1 antibodies. (**B**) The cells were immunostained with anti-CLDN1 antibodies. Scale bars indicate 10 μm. The TJ localization of CLDN1 is represented as the percentage of the total amount. (**C**) Cell lysates were prepared from the cells exposed to 200 μM H_2O_2 in the presence (EBGP) and absence (Veh) of 10 μg/mL EBGP. Control cells (Cont) were not treated with H_2O_2 and EBGP. PKC activity was measured using a CycLex PKC Super Family Kinase Assay Kit. Protein phosphatase (PP)

activities were measured using pNPP in neutral (open bars) and alkaline (closed bars) conditions. (**D**) The cells were pre-incubated with vehicle (Veh), 100 nM phorbol 12-myristate 13-acetate (PMA), or 1 μM cantharidin (CAN) for 30 min, followed by exposure to 200 μM H_2O_2 for 6 h. The cells were immunostained with anti-CLDN1 antibodies. The TJ localization of CLDN1 is represented as the percentage of the total amount. Scale bars indicate 10 μm. (**E**,**F**) Negative (open bars) or CLDN1 siRNA-transfected cells (closed bars) were incubated with H_2O_2, PMA, and CAN for 6 h. Control cells (Cont) were not treated with H_2O_2 and these drugs. TER and paracellular LY flux were analyzed using a volt-ohmmeter and fluorescence spectrometry, respectively. $n = 3–8$; ** $p < 0.01$ and * $p < 0.05$ significantly different from Cont, Cont of negative, or Veh with H_2O_2; $^{\#\#}$ $p < 0.01$ and $^{\#}$ $p < 0.05$ significantly different from Veh with H_2O_2.

3. Discussion

Disruption of the TJ barrier in the skin is caused by UV exposure and oxidative stress. In previous research, TJ integrity has been examined using high doses of UV, which can induce noticeable cell damage [24]. The production of ROS and H_2O_2 was increased by UVB in a dose-dependent manner (Figure 1A,B). ROS production has been reported to be increased by UVB irradiation in a dose- and time-dependent manner [25]. Park et al. [26] reported that ROS production was increased 1.3-fold by UVB irradiation (10 mJ/cm^2) and incubation for 8 h in HaCaT cells, which is similar to our data. Transient H_2O_2 treatment increased the production of ROS and decreased cell viability in a dose-dependent manner (Figure 1D,E). The percentage of damaged cells was about 10%–20% in the present experimental conditions of transient H_2O_2 treatment. Transient H_2O_2 (200 μM) treatment induced the mislocalization of CLDN1 without affecting the amount of CLDN1 protein (Figure 2). There was no apparent change in CLDN4 localization, but the amount of CLDN4 protein increased transiently after 6 h of H_2O_2 treatment. Recently, El-Chami et al. [27] reported that H_2O_2 (1 mM, a higher concentration than in our study) induced the mislocalization of CLDN1, CLDN4, and occludin in a continuous cell line of rat epidermal keratinocytes. We suggest that oxidative stress selectively induces the mislocalization of CLDN1 in low-level cell toxic conditions.

The protein level of CLDN1 is decreased in atopic dermatitis, whereas that of CLDN4 is increased [28]. The loss of CLDN1 localization in the TJ may induce a compensatory elevation of CLDN4 expression. Nevertheless, the barrier function of TJ was decreased after 6 h of transient H_2O_2 treatment (Figure 3A). The TJ barrier function was reduced by the knockdown of CLDN1 by siRNA (Figure 4A,B). Furthermore, the rescue effects of EBGP on the decrease in TER and increase in LY flux by H_2O_2 were blocked by the knockdown of CLDN1 (Figure 4C). There results indicate that CLDN1 has an important role in the maintenance of the TJ barrier. Previously, Furuse et al. [29] have reported that a continuous TJ was observed in the stratum granulosum of the epidermis in CLDN1-deficient mice and in WT mice using ultrathin section electron microscopy. However, a small molecule tracer (~600 D) passes through the TJ of the epidermis in CLDN1-deficient mice, whereas the diffusion is prevented at the TJ in WT mice. We suggest that CLDN1 cannot be replaced by CLDN4 in the skin.

The H_2O_2-induced mislocalization of CLDN1 was inhibited by a clathrin-dependent endocytosis inhibitor (Figure 5A), suggesting that H_2O_2 enhances the endocytosis of CLDN1 from the TJ to intracellular compartments. Although the protein levels of CLDN1 did not change, we did not detect the subcellular localization of CLDN1 in the organelle (Figure 2). We have to clarify the subcellular localization of CLDN1 using organelle markers in further studies. The p-Thr level of CLDN1 was decreased by H_2O_2 (Figure 6A). The phosphorylation status of proteins is regulated by various protein kinases and PPs. Go6976 induced the dephosphorylation and mislocalization of CLDN1 (Figure 7). On the contrary, the H_2O_2-induced mislocalization of CLDN1 was rescued by the PKC activator PMA. These results suggest that the TJ localization of CLDN1 is upregulated by PKC-dependent phosphorylation. Dephosphorylation of CLDN1 is caused by the activation of PP2A [23]. H_2O_2 increased PP activities, and the mislocalization of CLDN1 was rescued by a PP inhibitor, cantharidin, indicating that PPs may also be involved in the dephosphorylation of CLDN1 by H_2O_2. CLDN1 is phosphorylated in both renal tubular MDCK I and colonic HT29 cells,

but PKC-induced changes in the phosphorylation state were detected only in MDCK I cells [21]. The regulatory mechanism for the phosphorylation of CLDN1 may be different in each tissue.

Threonine phosphorylation sites of CLDN1 by PKC were predicted at T191 and T195 using the NetPhos 2.0 and Disphos 1.3 servers [22]. A phosphorylation mimic T191E mutant was localized to the TJ and maintained the TJ barrier in cells treated with H_2O_2, whereas WT and a T195E mutant lost their localization and barrier function in the TJ (Figure 6C,D). These results indicate that phosphorylation at T191 may be necessary for CLDN1 to localize to the TJ in HaCaT cells. The necessity of phosphorylation at T191 has been reported using human embryonic kidney 293 cells [30] and MDCK cells [31].

H_2O_2 caused a decrease in CLDN1 localization in TJ and an increase in paracellular permeability, which were rescued by EBGP (Figure 3C,D). Similar effects were observed in the UVB-treated cells. Although the effect of EBGP may be due to antioxidant activity, some cinnamic acid derivatives and flavonoids, which are contained in propolis, have beneficial effects on PKC. Artepillin C enhances adipocyte differentiation and glucose uptake mediated by the activation of PKC [32]. Chlorogenic acid prevents α-amino-hydroxy-5-methyl-isoxazole-4-propionate-mediated excitotoxicity in optic nerve oligodendrocytes through a PKC-dependent pathway [33]. Caffeic acid phenethyl ester inhibits the expression and activity of PP2A [34]. Our preliminary data indicate that kaempferide, which is abundant in EBGP [35], had lower antioxidant activity compared to EBGP, but it rescued the H_2O_2-induced mislocalization of CLDN1 and the reduction in the TJ barrier function. The components of propolis, including kaempferide, vary depending on the area [14]. A comparison of the effects of propolis produced in various places may be good for the identification of active components. Further studies are needed on which components of EBGP can rescue the H_2O_2-induced mislocalization of CLDN1 using human keratinocytes and what doses are effective. The identification of active components could lead to expanding the range of raw substances beyond green propolis, which could prove useful for the same functions.

In conclusion, we found that UVB irradiation increased ROS production, including H_2O_2, and both UVB and H_2O_2 caused the mislocalization of CLDN1 in HaCaT cells. The H_2O_2-induced mislocalization of CLDN1 was rescued by EBGP, PMA, and cantharidin. H_2O_2 decreased PKC activity and increased PP activities, which were inhibited by EBGP. Go6976 decreased p-Thr levels and the TJ localization of CLDN1. These results suggest that the TJ localization of CLDN1 is controlled by PKC. H_2O_2 decreased the p-Thr level of CLDN1, but this effect was blocked by EBGP. The T191E CLDN1 mutant was localized to the TJ after treatment with H_2O_2. We suggest that the phosphorylation of CLDN1 at T191 is necessary for its localization in the TJ. EBGP and its components may be useful in preventing the destruction of the TJ barrier by UVB and oxidative stress.

4. Materials and Methods

4.1. Materials

Rabbit anti-CLDN1, mouse anti-CLDN4, and rabbit anti-ZO-1 antibodies were obtained from Thermo Fisher Scientific (San Diego, CA, USA). Goat anti-β-actin and mouse anti-FLAG antibodies were from Santa Cruz Biotechnology (Santa Cruz, CA, USA) and Wako Pure Chemical (Osaka, Japan), respectively. Mouse anti-p-Ser and anti-p-Thr antibodies were from Sigma-Aldrich (Saint Louis, MO, USA). EBGP, LY, H_2DCFDA, and PMA were from Yamada Bee Company, Inc. (Lot: LY-009, Okayama, Japan), Biotium (Fremont, CA, USA), Thermo Fisher Scientific, and LC Laboratories (Woburn, MA, USA), respectively. OxiOrange and Hydrop were from Goryo Chemical (Hokkaido, Japan). All other reagents were of the highest grade of purity available.

4.2. Cell Culture

HaCaT cells, an immortalized nontumorigenic human keratinocyte-derived cell line [36], were grown in Dulbecco's Modified Eagle's Medium (Sigma-Aldrich) supplemented with 5% fetal bovine serum (FBS, Sigma-Aldrich), 0.07 mg/mL penicillin-G potassium, and 0.14 mg/mL streptomycin

sulfate in a 5% CO_2 atmosphere at 37 °C. One day before experiments, cells were transferred to FBS-free medium. Cell viability was examined using a WST-1 assay.

4.3. UVB Irradiation

UVB irradiation was carried out using a UV Crosslinker CL-1000M (Analytik Jena, Upland, CA, USA), which emits most of its energy within the UVB range (peaking at 302 nm). HaCaT cells were irradiated at a dose of 5–50 mJ/cm^2 in Hank's balanced salt solution. After UVB radiation, cells were incubated in fresh medium until analysis.

4.4. Production of Reactive Oxygen Species

H_2DCFDA can detect several ROS, including H_2O_2, ·OH, and peroxy radical, whereas OxiOrange and Hydrop selectively detect ·OH and H_2O_2, respectively. HaCaT cells were incubated with these ROS-sensitive fluorescent probes for 30 min. The fluorescence intensity of each probe was detected using an Infinite F200 Pro microplate reader (Tecan, Mannedorf, Switzerland).

4.5. Confocal Microscopy

Cells were plated on cover glasses. After forming a confluent monolayer, the cells were incubated with cold methanol for 10 min at −30 °C and then permeabilized with 0.2% Triton X-100 for 10 min. Following permeabilization, the cells were blocked with 4% Block Ace (Dainippon Sumitomo Pharma, Osaka, Japan) for 30 min and incubated with anti-CLDN1, anti-CLDN4, anti-FLAG, or anti-ZO-1 antibodies (1:100 dilution) for 16 h at 4 °C, followed by incubation with Alexa Fluor 488- or 555-conjugated secondary antibodies (1:100 dilution). The fluorescence images were observed using an LSM 700 confocal microscope (Carl Zeiss, Jena, Germany).

4.6. SDS-Polyacrylamide Gel Electrophoresis and Immunoblotting

Cells were scraped into cold phosphate-buffered saline and precipitated by centrifugation. They were lysed in a RIPA buffer containing 150 mM NaCl, 0.5 mM EDTA, 1% Triton X-100, 0.1% SDS, 50 mM Tris-HCl (pH 8.0), and a protease inhibitor cocktail (Sigma-Aldrich) and were sonicated for 20 s. After centrifugation at 6000× *g* for 5 min, the supernatants were collected and used as cell lysates, which included membrane and cytoplasmic proteins. Samples were applied to SDS-polyacrylamide gel electrophoresis (SDS-PAGE) and blotted onto a polyvinylidene fluoride membrane. The membrane was then incubated with the respective primary antibody (1:1000 dilution) at 4 °C for 16 h, followed by a peroxidase-conjugated secondary antibody (1:3000 dilution) at room temperature for 1.5 h. Finally, the blots were incubated in EzWestLumi Plus (Atto, Tokyo, Japan) or ImmunoStar Basic (Wako Pure Chemical) and scanned with a C-DiGit Blot Scanner (LI-COR Biotechnology, Lincoln, NE, USA). The blots were stripped and reprobed with an anti-β-actin antibody. Band density was quantified using ImageJ software (National Institute of Health software). The signals were normalized using a β-actin loading control.

4.7. Measurement of Paracellular Permeability

Cells were plated on Transwell plates (0.4 μm pore size, Corning Inc., Corning, NY, USA). After forming a confluent monolayer, TER was measured using a Millicell-ERS epithelial volt-ohmmeter (Millipore, Billerica, MA, USA). TER values (ohms × cm^2) were normalized by the area of the monolayer and were calculated by subtracting the blank values from the filter and the bathing medium. The paracellular permeability to LY, a fluorescent paracellular flux marker, for 1 h from upper to lower compartments was measured with an Infinite F200 Pro microplate reader.

4.8. Isolation of Total RNA and Quantitative Real-Time Polymerase Chain Reaction

Total RNA was extracted using a TRI reagent (Sigma-Aldrich). Reverse transcription and quantitative real-time polymerase chain reaction (PCR) was performed as described previously [37]. The primer pairs used for PCR were human CLDN1 (sense: 5′-ATGAGGATGGCTGTCATTGG-3′; antisense: 5′-ATTGACTGGGGTCATAGGGT-3′) and human β-actin (sense: 5′-CCTGAGGCACTCTTCCAGCCTT-3′; antisense: 5′-TGCGGATGTCCACGTCACACTTC-3′).

4.9. PKC and Serine/Threonine Protein Phosphatase Activity Assays

Cells were harvested in 1× Passive Buffer (Promega, Madison, WI, USA). PKC activity was measured using a CycLex PKC Super Family Kinase Assay Kit (Medical & Biological Laboratories, Nagoya, Japan) in accordance with the manufacturer's protocol. Serine/threonine PP activities were investigated using paranitrophenylphosphate (pNPP) as a substrate at pH 7.5 (neutral condition) and pH 8.4 (alkaline condition). The hydrolysis of pNPP was measured by monitoring the absorbance at 405 nm.

4.10. Vector Construction and Transfection

A vector containing human CLDN1 cDNA was prepared as described previously [31] and was called CLDN1/pCMV, which encoded a FLAG tag at the amino terminus. Mutants of T191E and T195E were generated as described previously [31]: siRNAs against CLDN1 (SASI_Hs01_00211216) and a negative control (SIC-001) were purchased from Sigma-Aldrich. Plasmid vector and siRNAs were transfected into cells using Lipofectamine 2000, as recommended by the manufacturer.

4.11. Statistics

Results are presented as means ± S.E.M. Differences between groups were analyzed using one-way analysis of variance, and corrections for multiple comparison were made using Tukey's multiple comparison test. Comparisons between two groups were made using Student's *t*-test. Statistical analyses were performed using KaleidaGraph version 4.5.1 software (Synergy Software, Reading, PA, USA). Significant differences were assumed at $p < 0.05$.

Author Contributions: K.M., M.K., and S.S. performed the experiments and analyzed the data. T.M. contributed to the experiment plan and to the discussion of the manuscript. A.I. contributed to supervision of the project, interpretation of the data, and writing the paper.

Funding: This work was supported in part by grants from the Yamada Research Grant from Yamada Bee Company, Inc., and the Koyanagi-foundation.

Conflicts of Interest: The authors declare no conflict of interest.

Abbreviations

CLDN	Claudin
Ct	Threshold cycle
FBS	Fetal bovine serum
EBGP	Ethanol extract of Brazilian green propolis
H_2DCFDA	2′,7′-Dichlorodihydrofluorescein diacetate
H_2O_2	Hydrogen peroxide
LY	Lucifer yellow
MβCD	Methyl-β-cyclodextrin
MDC	Monodansylcadaverine
p-Ser	Phosphoserine
p-Thr	Phosphothreonine
PCR	Polymerase chain reaction
PDZ	PSD95/Dlg/ZO-1
PMA	Phorbol 12-myristate 13-acetate

pNPP	Paranitrophenylphosphate
PPs	Protein phosphatases
ROS	Reactive oxygen species
SDS-PAGE	SDS-polyacrylamide gel electrophoresis
siRNA	Small interfering RNA
TER	Transepithelial electrical resistance
TJ	Tight junction
UV	Ultraviolet
WST-1	2-(4-Iodophenyl)-3-(4-nitrophenyl)-5-(2,4-disulfophenyl)-2*H*-tetrazolium
WT	Wild-type

References

1. Coolen, N.A.; Schouten, K.C.; Middelkoop, E.; Ulrich, M.M. Comparison between human fetal and adult skin. *Arch. Dermatol. Res.* **2010**, *302*, 47–55. [CrossRef] [PubMed]
2. Young, A.R.; Chadwick, C.A.; Harrison, G.I.; Nikaido, O.; Ramsden, J.; Potten, C.S. The similarity of action spectra for thymine dimers in human epidermis and erythema suggests that DNA is the chromophore for erythema. *J. Investig. Dermatol.* **1998**, *111*, 982–988. [CrossRef] [PubMed]
3. De Gruijl, F.R. Action spectrum for photocarcinogenesis. *Recent Results Cancer Res.* **1995**, *139*, 21–30. [PubMed]
4. Moon, S.E.; Youn, J.I.; Kim, J.A. The effect of ultraviolet-B exposure scheduling on the photodamage of hairless mouse skin. *Photodermatol. Photoimmunol. Photomed.* **2000**, *16*, 74–77. [CrossRef] [PubMed]
5. Pustisek, N.; Situm, M. UV-radiation, apoptosis and skin. *Coll. Antropol.* **2011**, *35* (Suppl. 2), 339–341.
6. Ichihashi, M.; Ueda, M.; Budiyanto, A.; Bito, T.; Oka, M.; Fukunaga, M.; Tsuru, K.; Horikawa, T. UV-induced skin damage. *Toxicology* **2003**, *189*, 21–39. [CrossRef]
7. Mineta, K.; Yamamoto, Y.; Yamazaki, Y.; Tanaka, H.; Tada, Y.; Saito, K.; Tamura, A.; Igarashi, M.; Endo, T.; Takeuchi, K.; et al. Predicted expansion of the claudin multigene family. *FEBS Lett.* **2011**, *585*, 606–612. [CrossRef]
8. Turksen, K.; Troy, T.C. Barriers built on claudins. *J. Cell Sci.* **2004**, *117*, 2435–2447. [CrossRef]
9. Basler, K.; Bergmann, S.; Heisig, M.; Naegel, A.; Zorn-Kruppa, M.; Brandner, J.M. The role of tight junctions in skin barrier function and dermal absorption. *J. Control. Release* **2016**, *242*, 105–118. [CrossRef]
10. Sugawara, T.; Iwamoto, N.; Akashi, M.; Kojima, T.; Hisatsune, J.; Sugai, M.; Furuse, M. Tight junction dysfunction in the stratum granulosum leads to aberrant stratum corneum barrier function in claudin-1-deficient mice. *J. Dermatol. Sci.* **2013**, *70*, 12–18. [CrossRef]
11. Hadj-Rabia, S.; Baala, L.; Vabres, P.; Hamel-Teillac, D.; Jacquemin, E.; Fabre, M.; Lyonnet, S.; De Prost, Y.; Munnich, A.; Hadchouel, M.; et al. Claudin-1 gene mutations in neonatal sclerosing cholangitis associated with ichthyosis: A tight junction disease. *Gastroenterology* **2004**, *127*, 1386–1390. [CrossRef] [PubMed]
12. Zhou, Y.; Zheng, J.; Li, Y.; Xu, D.P.; Li, S.; Chen, Y.M.; Li, H.B. Natural Polyphenols for Prevention and Treatment of Cancer. *Nutrients* **2016**, *8*, 515. [CrossRef] [PubMed]
13. Sawicka, D.; Car, H.; Borawska, M.H.; Niklinski, J. The anticancer activity of propolis. *Folia Histochem. Cytobiol.* **2012**, *50*, 25–37. [CrossRef] [PubMed]
14. Toreti, V.C.; Sato, H.H.; Pastore, G.M.; Park, Y.K. Recent progress of propolis for its biological and chemical compositions and its botanical origin. *Evid. Based Complement. Alternat. Med.* **2013**, *2013*, 697390. [CrossRef] [PubMed]
15. Fonseca, Y.M.; Marquele-Oliveira, F.; Vicentini, F.T.; Furtado, N.A.; Sousa, J.P.; Lucisano-Valim, Y.M.; Fonseca, M.J. Evaluation of the Potential of Brazilian Propolis against UV-Induced Oxidative Stress. *Evid. Based Complement. Alternat. Med.* **2011**, *2011*, 863917. [CrossRef] [PubMed]
16. Kim, H.B.; Yoo, B.S. Propolis Inhibits UVA-Induced Apoptosis of Human Keratinocyte HaCaT Cells by Scavenging ROS. *Toxicol. Res.* **2016**, *32*, 345–351. [CrossRef]
17. De Almeida, E.B.; Cordeiro Cardoso, J.; Karla de Lima, A.; de Oliveira, N.L.; de Pontes-Filho, N.T.; Oliveira Lima, S.; Leal Souza, I.C.; de Albuquerque-Junior, R.L. The incorporation of Brazilian propolis into collagen-based dressing films improves dermal burn healing. *J. Ethnopharmacol.* **2013**, *147*, 419–425. [CrossRef] [PubMed]

18. Li, J.; Li, Q.; Geng, S. Alltrans retinoic acid alters the expression of the tight junction proteins Claudin1 and 4 and epidermal barrier functionassociated genes in the epidermis. *Int. J. Mol. Med.* **2019**, *43*, 1789–1805. [PubMed]
19. D'Souza, T.; Agarwal, R.; Morin, P.J. Phosphorylation of claudin-3 at threonine 192 by cAMP-dependent protein kinase regulates tight junction barrier function in ovarian cancer cells. *J. Biol. Chem.* **2005**, *280*, 26233–26240. [CrossRef]
20. Ikari, A.; Matsumoto, S.; Harada, H.; Takagi, K.; Hayashi, H.; Suzuki, Y.; Degawa, M.; Miwa, M. Phosphorylation of paracellin-1 at Ser217 by protein kinase A is essential for localization in tight junctions. *J. Cell Sci.* **2006**, *119*, 1781–1789. [CrossRef]
21. Sjo, A.; Magnusson, K.E.; Peterson, K.H. Protein kinase C activation has distinct effects on the localization, phosphorylation and detergent solubility of the claudin protein family in tight and leaky epithelial cells. *J. Membr. Biol.* **2010**, *236*, 181–189. [CrossRef] [PubMed]
22. Ahmad, W.; Shabbiri, K.; Ijaz, B.; Asad, S.; Sarwar, M.T.; Gull, S.; Kausar, H.; Fouzia, K.; Shahid, I.; Hassan, S. Claudin-1 required for HCV virus entry has high potential for phosphorylation and O-glycosylation. *Virol. J.* **2011**, *8*, 229. [CrossRef] [PubMed]
23. Nunbhakdi-Craig, V.; Machleidt, T.; Ogris, E.; Bellotto, D.; White, C.L.; Sontag, E. Protein phosphatase 2A associates with and regulates atypical PKC and the epithelial tight junction complex. *J. Cell Biol.* **2002**, *158*, 967–978. [CrossRef] [PubMed]
24. Alhasaniah, A.; Sherratt, M.J.; O'Neill, C.A. The Impact of Ultraviolet Radiation on Barrier Function in Human Skin: Molecular Mechanisms and Topical Therapeutics. *Curr. Med. Chem.* **2018**, *25*, 5503–5511. [CrossRef] [PubMed]
25. Hu, Y.; Ma, Y.; Wu, S.; Chen, T.; He, Y.; Sun, J.; Jiao, R.; Jiang, X.; Huang, Y.; Deng, L.; et al. Protective Effect of Cyanidin-3-O-Glucoside against Ultraviolet B Radiation-Induced Cell Damage in Human HaCaT Keratinocytes. *Front. Pharmacol.* **2016**, *7*, 301. [CrossRef] [PubMed]
26. Park, E.J.; Kim, Y.M.; Chang, K.C. Hemin Reduces HMGB1 Release by UVB in an AMPK/HO-1-dependent Pathway in Human Keratinocytes HaCaT Cells. *Arch. Med. Res.* **2017**, *48*, 423–431. [CrossRef] [PubMed]
27. El-Chami, C.; Haslam, I.S.; Steward, M.C.; O'Neill, C.A. Organic osmolytes preserve the function of the developing tight junction in ultraviolet B-irradiated rat epidermal keratinocytes. *Sci. Rep.* **2018**, *8*, 5167. [CrossRef]
28. Gruber, R.; Bornchen, C.; Rose, K.; Daubmann, A.; Volksdorf, T.; Wladykowski, E.; Vidal, Y.S.S.; Peters, E.M.; Danso, M.; Bouwstra, J.A.; et al. Diverse regulation of claudin-1 and claudin-4 in atopic dermatitis. *Am. J. Pathol.* **2015**, *185*, 2777–2789. [CrossRef]
29. Furuse, M.; Hata, M.; Furuse, K.; Yoshida, Y.; Haratake, A.; Sugitani, Y.; Noda, T.; Kubo, A.; Tsukita, S. Claudin-based tight junctions are crucial for the mammalian epidermal barrier: A lesson from claudin-1-deficient mice. *J. Cell Biol.* **2002**, *156*, 1099–1111. [CrossRef]
30. Shiomi, R.; Shigetomi, K.; Inai, T.; Sakai, M.; Ikenouchi, J. CaMKII regulates the strength of the epithelial barrier. *Sci. Rep.* **2015**, *5*, 13262. [CrossRef]
31. Fujii, N.; Matsuo, Y.; Matsunaga, T.; Endo, S.; Sakai, H.; Yamaguchi, M.; Yamazaki, Y.; Sugatani, J.; Ikari, A. Hypotonic stress-induced down-regulation of claudin-1 and -2 mediated by dephosphorylation and clathrin-dependent endocytosis in renal tubular epithelial cells. *J. Biol. Chem.* **2016**, *291*, 24787–24799. [CrossRef] [PubMed]
32. Choi, S.S.; Cha, B.Y.; Iida, K.; Lee, Y.S.; Yonezawa, T.; Teruya, T.; Nagai, K.; Woo, J.T. Artepillin C, as a PPARgamma ligand, enhances adipocyte differentiation and glucose uptake in 3T3-L1 cells. *Biochem. Pharmacol.* **2011**, *81*, 925–933. [CrossRef] [PubMed]
33. Rebai, O.; Amri, M. Chlorogenic Acid Prevents AMPA-Mediated Excitotoxicity in Optic Nerve Oligodendrocytes Through a PKC and Caspase-Dependent Pathways. *Neurotox. Res.* **2018**, *34*, 559–573. [CrossRef] [PubMed]
34. Avci, C.B.; Sahin, F.; Gunduz, C.; Selvi, N.; Aydin, H.H.; Oktem, G.; Topcuoglu, N.; Saydam, G. Protein phosphatase 2A (PP2A) has a potential role in CAPE-induced apoptosis of CCRF-CEM cells via effecting human telomerase reverse transcriptase activity. *Hematology* **2007**, *12*, 519–525. [CrossRef] [PubMed]
35. Andrade, J.K.S.; Denadai, M.; de Oliveira, C.S.; Nunes, M.L.; Narain, N. Evaluation of bioactive compounds potential and antioxidant activity of brown, green and red propolis from Brazilian northeast region. *Food Res. Int.* **2017**, *101*, 129–138. [CrossRef] [PubMed]

36. Boukamp, P.; Petrussevska, R.T.; Breitkreutz, D.; Hornung, J.; Markham, A.; Fusenig, N.E. Normal keratinization in a spontaneously immortalized aneuploid human keratinocyte cell line. *J. Cell Biol.* **1988**, *106*, 761–771. [CrossRef] [PubMed]
37. Sonoki, H.; Tanimae, A.; Endo, S.; Matsunaga, T.; Furuta, T.; Ichihara, K.; Ikari, A. Kaempherol and Luteolin Decrease Claudin-2 Expression Mediated by Inhibition of STAT3 in Lung Adenocarcinoma A549 Cells. *Nutrients* **2017**, *9*, 597. [CrossRef]

International Journal of
Molecular Sciences

MDPI

Article

Drinking and Water Handling in the Medaka Intestine: A Possible Role of Claudin-15 in Paracellular Absorption?

Christian K. Tipsmark [1,*], Andreas M. Nielsen [2], Maryline C. Bossus [1,3], Laura V. Ellis [1], Christina Baun [4], Thomas L. Andersen [4], Jes Dreier [5], Jonathan R. Brewer [5] and Steffen S. Madsen [1,2]

1 Department of Biological Sciences, University of Arkansas, SCEN 601, Fayetteville, AR 72701, USA; maryline.bossus@lyon.edu (M.C.B.); lvellis@email.uark.edu (L.V.E.); steffen@biology.sdu.dk (S.S.M.)
2 Department of Biology, University of Southern Denmark, Campusvej 55, 5230 Odense M, Denmark; Amorck@live.dk
3 Department of Math and Sciences, Lyon College, 2300 Highland Rd, Batesville, AR 72501, USA
4 Department of Nuclear Medicine, Odense University Hospital, Sdr. Boulevard 29, 5000 Odense C, Denmark; Christina.Baun@rsyd.dk (C.B.); Thomas.Andersen@rsyd.dk (T.L.A.)
5 Department of Biochemistry and Molecular Biology, University of Southern Denmark, Campusvej 55, 5230 Odense M, Denmark; jes.dreier@cpr.ku.dk (J.D.); brewer@memphys.sdu.dk (J.R.B.)
* Correspondence: tipsmark@uark.edu; Tel.: +1-479-575-8436

Received: 14 February 2020; Accepted: 6 March 2020; Published: 8 March 2020

Abstract: When euryhaline fish move between fresh water (FW) and seawater (SW), the intestine undergoes functional changes to handle imbibed SW. In Japanese medaka, the potential transcellular aquaporin-mediated conduits for water are paradoxically downregulated during SW acclimation, suggesting paracellular transport to be of principal importance in hyperosmotic conditions. In mammals, intestinal claudin-15 (CLDN15) forms paracellular channels for small cations and water, which may participate in water transport. Since two *cldn15* paralogs, *cldn15a* and *cldn15b*, have previously been identified in medaka, we examined the salinity effects on their mRNA expression and immunolocalization in the intestine. In addition, we analyzed the drinking rate and intestinal water handling by adding non-absorbable radiotracers, 51-Cr-EDTA or 99-Tc-DTPA, to the water. The drinking rate was >2-fold higher in SW than FW-acclimated fish, and radiotracer experiments showed anterior accumulation in FW and posterior buildup in SW intestines. Salinity had no effect on expression of *cldn15a*, while *cldn15b* was approximately 100-fold higher in FW than SW. Despite differences in transcript dynamics, Cldn15a and Cldn15b proteins were both similarly localized in the apical tight junctions of enterocytes, co-localizing with occludin and with no apparent difference in localization and abundance between FW and SW. The stability of the Cldn15 protein suggests a physiological role in water transport in the medaka intestine.

Keywords: aquaporin; claudin; drinking rate; epithelial fluid transport; enterocyte; occludin; osmoregulation; paracellular

1. Introduction

In fresh water (FW) fishes, the intestinal epithelium must limit excessive fluid absorption while securing dietary ion uptake [1]; in seawater (SW), imbibed water is absorbed in a solute-linked process [1,2]. Therefore, the functional plasticity of the enterocytic epithelium is a critical factor in euryhaline fish that are capable of going through salinity transitions. Elevated intestinal aquaporin (Aqp/*aqp*) abundance in eel [3–5] and salmonids [6] in response to SW transfer have led to propose a transcellular water path in these species [7];

however, in medaka, a consistent downregulation of several intestinal Aqp/*aqp* isoforms after SW transfer has challenged this model and suggests a major involvement of a paracellular pathway [8].

Transepithelial water transport has been suggested to be mainly transcellular via Aqps, but this matter is still under debate [9,10]. Thus, in leaky epithelia, similar to the intestine, fluid transport may primarily be paracellular as proposed based on a corneal model [9] or include both components as proposed for marine fish [2]. Taking species differences into account, it appears that the medaka intestine may be a choice comparative model to study paracellular fluid transport because a tight junction defined path seems central, as suggested by Madsen et al. [8].

Proteins belonging to the claudin (Cldn) superfamily are the main determinants of tight junction permeability properties and thus important regulators of paracellular transport [11,12]. Cldns are integral membrane proteins with 4 trans-membrane domains and two extracellular loops (ECL). The amino acid residues of the first ECL are critical for the permselectivity of the junction they create in homo- or hetero-dimeric and -tetrameric combinations [13–16]. There are 27 claudins (CLDNs) paralogs described in mammals [12]; in the teleost lineage, an extensive expansion of the *cldn* gene family due to gene duplications has led to a higher number with e.g., 56 in Fugu [17] and 54 in zebrafish [18]. The specific permselectivity has been investigated for several mammalian CLDN paralogs, and there are many examples of barrier-forming as well as specific anion- and cation-pore-forming CLDNs [12]. In addition, there are a few examples of CLDNs contributing to creating water-permeable pores. This has been convincingly demonstrated for CLDN2 [19], which has functional significance in the mammalian kidney, and most recently intestinal CLDN15 has also been assigned such a role [20] in addition to the cation-pore-forming properties of both CLDNs [12]. However, Na^+ and water fluxes through CLDN15 inhibit each other in functional contrast to CLDN2 [20]. Based on amino acid homology, especially in the first ECL, it is often assumed that fish Cldns give rise to the same permeability properties as mammalian orthologues, but only a few have been investigated thoroughly [21,22]. Mutational analysis and MD simulations [15,16] based on the crystal structure [23] have shown that especially amino acid D55 is critical for CLDN15 pore formation. In support for a similar function in medaka to the mammalian orthologue is the conservation of this amino acid in both medaka Cldn15a and Cldn15b.

A given tissue often shows the expression of several CLDN paralogs [12]. In the mammalian nephron, this is coupled to a highly segmental pattern of expression [24]. In the mammalian intestine, CLDN15 appears to be one of the most abundant CLDNs, at least in the small intestine [25–27], and it plays a critical role in the gut ontogeny of both mammals and fish [28,29]. In mice, CLDN15-mediated Na^+ back-flux into the intestinal lumen is essential for active glucose absorption through the Na^+/glucose cotransporter, safeguarding monosaccharide uptake [30]. In fishes, Cldn15a paralogs have been found to be expressed specifically in the gastrointestinal (GI) tract (salmon [31,32], zebrafish [33], medaka [34]). In medaka, we previously identified an additional new paralog, Cldn15b, which is also primarily expressed in the intestine at levels several orders of magnitude higher than any other examined organs [34].

To develop our knowledge about paracellular versus transcellular fluid transport, it will be valuable to expand our understanding of water transport and enterocyte tight junctions in medaka. Furthermore, the functional plasticity of the intestine during salinity change in this euryhaline fish is useful when seeking to understand basic principles. Therefore, the goals of this work were to first study drinking behavior and water handling in response to changes in the osmotic environment, which are unknown in adult medaka. Secondly, we examined the expression and localization of the two Cldn15 paralogs in relation to hypo- to hyperosmotic acclimation based on the assumption that intestinal Cldn15 is implicated in water transport, as seen in other models.

2. Results

2.1. Drinking Rate and Intestinal Handling of Imbibed Water

In preliminary experiments using both FW- and SW-acclimated fish, it was assured that the intestinal accumulation of radioactivity in fish continued linearly in excess of 3 h, and gut-passage time

after drinking thus was well in excess of 3 h (data not shown). Therefore, the drinking rate estimation was based on a 3 h incubation in 51-Cr-EDTA containing water. The drinking rate was relatively high in FW-acclimated medaka (5 μL/g/h) but was doubled in fish acclimated to SW (Figure 1). Drinking rate measurements were based on counting radioactivity in the GI tract after incubation and a 1 h rinsing period in clean water.

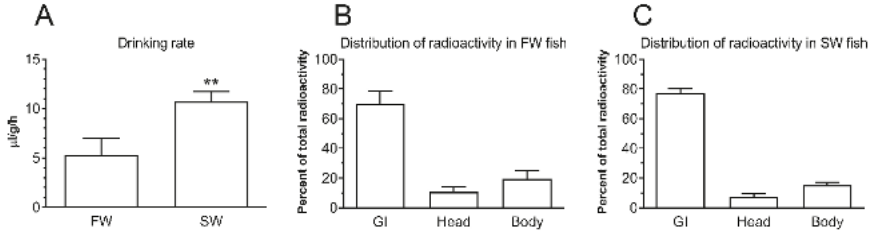

Figure 1. (**A**) Drinking rate (μL/g/h) in fresh water (FW) and seawater (SW)-acclimated medaka estimated by radioactivity in the entire gastrointestinal tract after incubation in 51-Cr-EDTA traced FW or SW for 3 h followed by rinsing in clean water for 1 h. ** $p < 0.01$. In (**B**) (FW) and (**C**) (SW), the radioactivity content of the gastrointestinal tract (GI, imbibed) is compared to radioactivity absorbed to the head and remaining body parts.

The head and body carcass where counted separately after the experiment, and the radioactivity content in these parts amounted to 8–10% and 15–20%, respectively, of the total radioactivity of the fish (Figure 1B,C). It is assumed that this is mainly due to attachment to the external mucus layer in these body parts, as Cr-EDTA has been shown to be a non-absorbable marker, which means that it does not cross the intestinal epithelium [35].

When dissected intestines were carefully fragmented into 0.5 cm segments and analyzed, it was found that radioactivity was evenly distributed but with a trend of showing higher levels at the anterior end of the FW intestine (Figure 2A). In the SW-acclimated fish, the radioactivity clearly accumulated toward the posterior end of the intestine (Figure 2B).

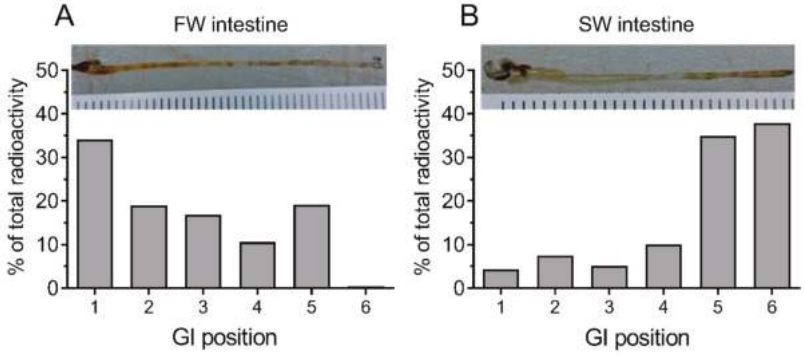

Figure 2. Distribution of radioactivity longitudinally in the gastrointestinal (GI) tract of fish allowed to drink 51-Cr-EDTA traced FW (**A**) or SW (**B**) water for 3 h. After incubation, the entire GI tract was ligatured into 0.5 cm segments and each segment was then transferred to a scintillation vial and scanned for radioactive content. The entire intestine was approximately 3 cm in length, as shown in the inserted photographs.

The progressive movement of imbibed water along the intestine was followed in a more direct way by a series of single photon emission computed tomography–computed tomography (SPECT-CT) scans of intact, euthanized fish after incubation in 99-Tc-DTPA-traced water (Figure 3). The imaging

series showed an initial high intensity of tracer in the esophageal end of the GI tract with a more posterior distribution as the incubation time was increased. The precipitation of mineral salts (Mg- and Ca-carbonates) could be seen in the CT images of SW-acclimated fish ca 2/3 down the intestine (white arrow in Figure 3D).

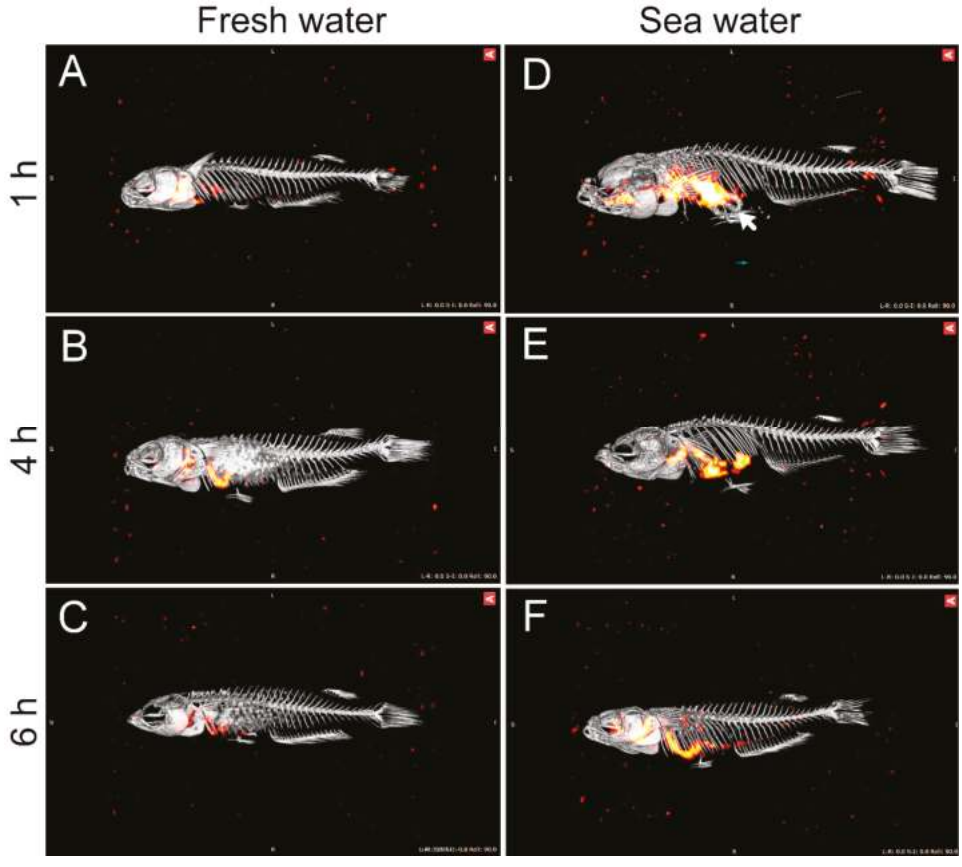

Figure 3. Visualization of the movement of imbibed water along the gastrointestinal tract of medaka acclimated to FW (**A**–**C**) or SW (**D**–**F**). Images are merged from single photon emission computed tomography (SPECT) (red intensity layer) and computed tomography (CT) (gray) scans of fish which had been incubated in 99-Tc-DTPA traced FW or SW for 1 h followed by transfer to non-radioactive FW or SW for 1 h (**A**, **D**), 4 h (**B**, **E**), or 6 h (**C**, **F**). The SPECT layer visualizes the localization (and intensity) of imbibed isotope-labeled water and the CT layer visualizes mineralized structures (skeleton and mineral precipitates in the SW intestines, white arrow in **D**). Note that 99-Tc has a short half-life (6 h), which influences the apparent intensities of the imbibed isotope. The fish was approximately 3 cm in length.

2.2. Transcript Levels and Response to Salinity

The transcript levels of selected targets were analyzed in intestines from medaka long-term acclimated to FW and SW (Figure 4). The absorptive Na^+, K^+,$2Cl^-$ cotransporter (*nkcc2*) level was several-fold higher in SW than FW fish, whereas *cldn15b*, *aqp1a*, and *aqp8ab* levels were significantly reduced in SW compared to FW fish. *cldn15a* was unaffected by long-term salinity acclimation. The salinity-induced changes in transcript levels observed in long-term acclimated fish were reproduced

in a 7-day time course experiment (Figure 5), with *nkcc2*, *cldn15b*, *aqp1a*, and *aqp8ab* all being significantly affected by both salinity and time (two-way ANOVA). Since there was a significant interaction between the two factors on these transcripts, the effect of SW was time-dependent. Thus, the SW effect on *nkcc2* was significant at all time-points, but it was the highest after 168 h. The effect on cldn15b was significant only after 24 h and 168 h days, while both *aqps* decreased already after 6 h and 24 h but not significantly so at the 168 h time point. *cldn15a* was unaffected by salinity during the 7-day time course experiment, as observed in long-term acclimated fish.

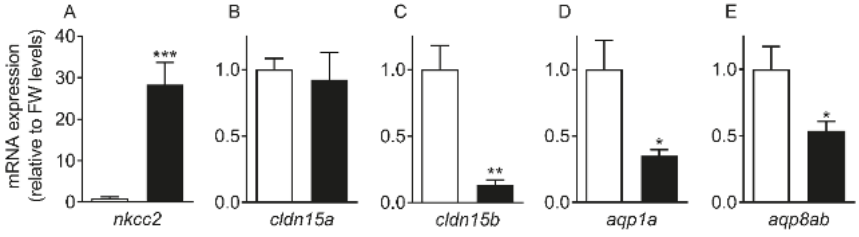

Figure 4. Transcript levels of *nkcc2* (**A**), *cldn15a* (**B**), *cldn15b* (**C**), *aqp1a* (**D**), and *aqp8ab* (**E**) in intestine from medaka acclimated to FW (white bars) or SW (black bars). Fish were acclimated to the respective salinities for over one month prior to sampling ($n = 8$). Expression levels represent the mean value ± SEM relative to FW levels. Asterisks indicate a significant difference from FW expression (* $p < 0.05$, ** $p < 0.01$, *** $p < 0.001$).

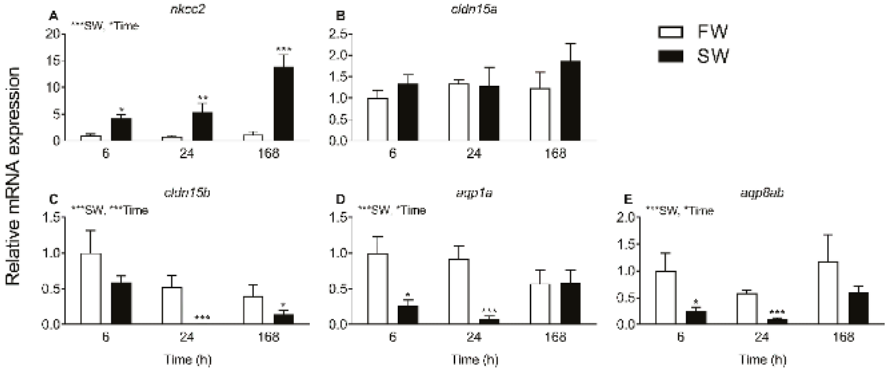

Figure 5. Effect of FW-to-SW transfer on intestinal transcript levels of *nkcc2* (**A**), *cldn15a* (**B**), *cldn15b* (**C**), *aqp1a* (**D**), and *aqp8ab* (**E**). Fish were transferred from FW-to-SW (black bars) or FW-to-FW (white bars) as a control and sampled at 6, 24, and 168 h ($n = 6$). Expression levels represent the mean value ± SEM relative to the 6 h-FW group. Asterisks next to SW and Time refers to the overall effects of a factor with two-way ANOVA. All targets with overall effects also had a significant interaction between factors, so the differences between time-matched groups were analyzed with Bonferroni multiple comparisons test (* $p < 0.05$, ** $p < 0.01$, *** $p < 0.001$) to identify the time-dependence of SW effects.

2.3. Cldn15 Localization in the Intestinal Epithelium

Cldn15a and Cldn15b showed similar localization in the intestinal epithelium. Immunoreactivity was confined to the apical area of enterocytes with distinct "hot spots" in the apical junction area between enterocytes (Figures 6 and 7). At lower magnification, these hot spots were partly masked by the non-specific staining of the brush-border area at variable intensity (Figure 6A,C).

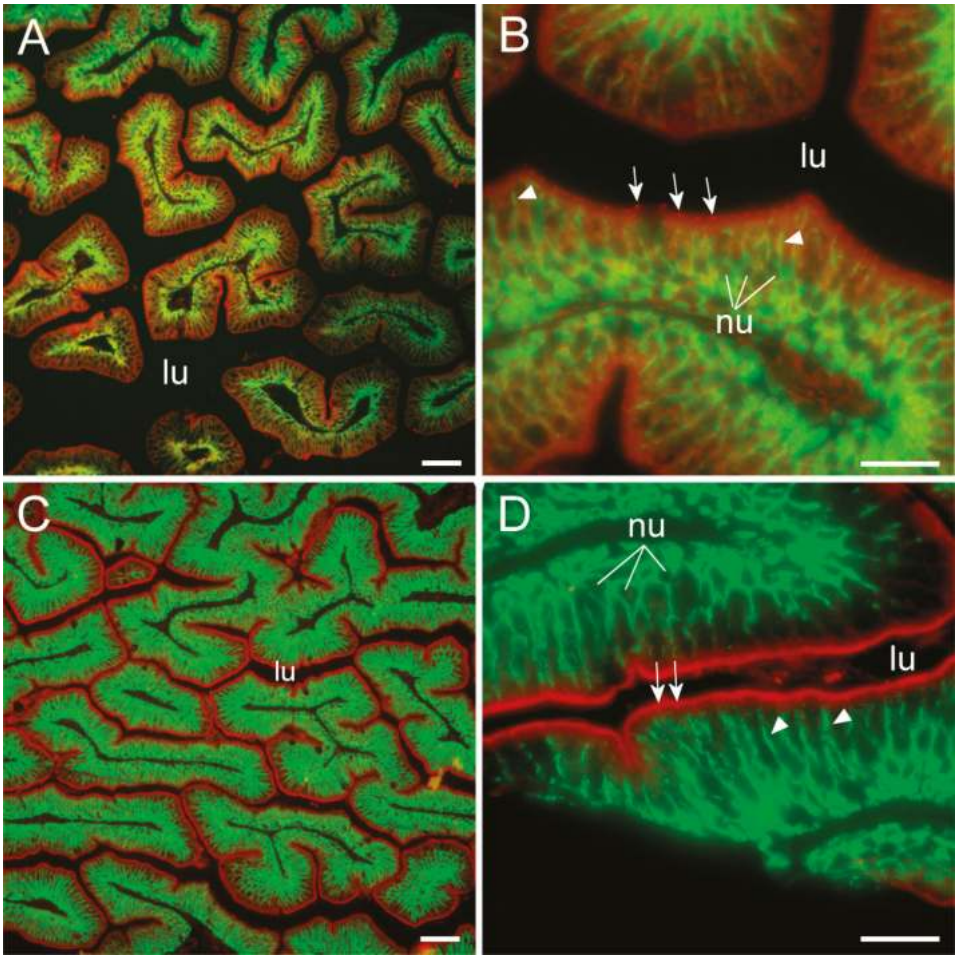

Figure 6. Immunofluorescence micrographs showing apical localization of Cldn15a (red, in **A** and **B**), and Cldn15b (red in **C** and **D**) and basolateral localization of the Na^+,K^+-ATPase alpha subunit (green) in FW-acclimated medaka middle intestine. (**A**) and (**C**) are at 200× magnification, (**B**) and (**D**) are at 1000× magnification. lu = lumen, nu = nuclei; in (**B**) and (**C**) arrows point to Cldn "hot spots" in the tight junction zones; arrowheads point to lateral membranes. Size bars indicate 50 μm (**A**, **C**) or 20 μm (**B**, **D**).

However, these "hot spots" became particularly evident at higher magnification (Figure 6B,D, Figure 7) and when inspecting the tissues with confocal and STED microscopy, which has a much narrower z-plane focus (Figures 8 and 9). Control incubation without primary Cldn15 antibodies showed a very faint general fluorescence without the distinct "hot spots" (insert in Figure 7A). Na^+,K^+-ATPase alpha subunit immunostaining revealed parallel lateral membranes, which were slightly spaced between neighboring cells, thus creating the lateral intercellular space (e.g., see Figure 6D, Figure 8A,B, marked with arrowheads). Near the basal borders, the membrane staining surrounded the nuclei, which appeared as circular dark "holes" in the images (marked "nu" in Figures 6–8). The distinct Cldn staining was apical to the Na^+,K^+-ATPase staining, i.e., at the end of

an axis extrapolated from the lateral membrane area. Thus, there was no co-localization of the two antibodies. This indicates that the two Cldn15 proteins are located in the tight junction zone.

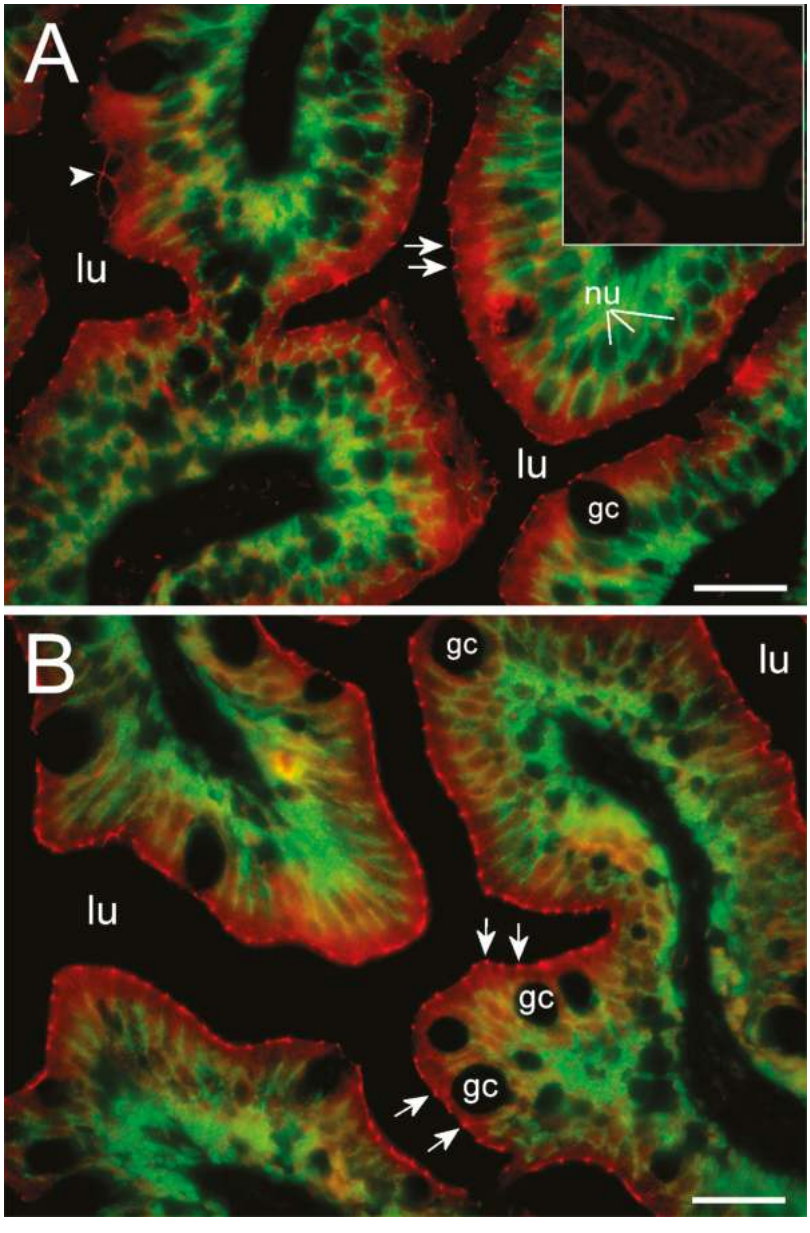

Figure 7. Immunofluorescence micrographs showing apical localization of Cldn15a (red in **A**) and Cldn15b (red in **B**) and basolateral localization of the Na^+,K^+-ATPase alpha subunit (green) in SW-acclimated medaka middle intestine. The insert in the upper left corner shows control without primary antibodies. Images are at 1000× magnification. lu = lumen, gc = goblet cell, nu = nuclei; arrows point to "hot spots" in the tight junction zones; Size bars indicate 20 μm.

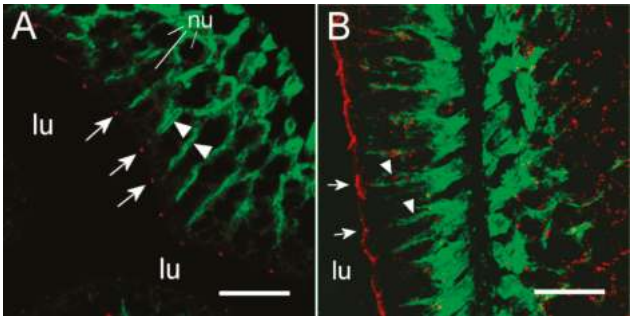

Figure 8. Confocal images showing apical localization of Cldn15a (red in **A**) and Cldn15b (red in **B**) and basolateral localization of Na^+,K^+-ATPase alpha subunit (green) in SW-acclimated medaka middle intestine. lu = lumen; arrows point to Cldn15 "hot spots" in the tight junction zones; arrowheads point to lateral membranes of enterocytes clearly separating the intercellular space. Size bars indicate 10 μm.

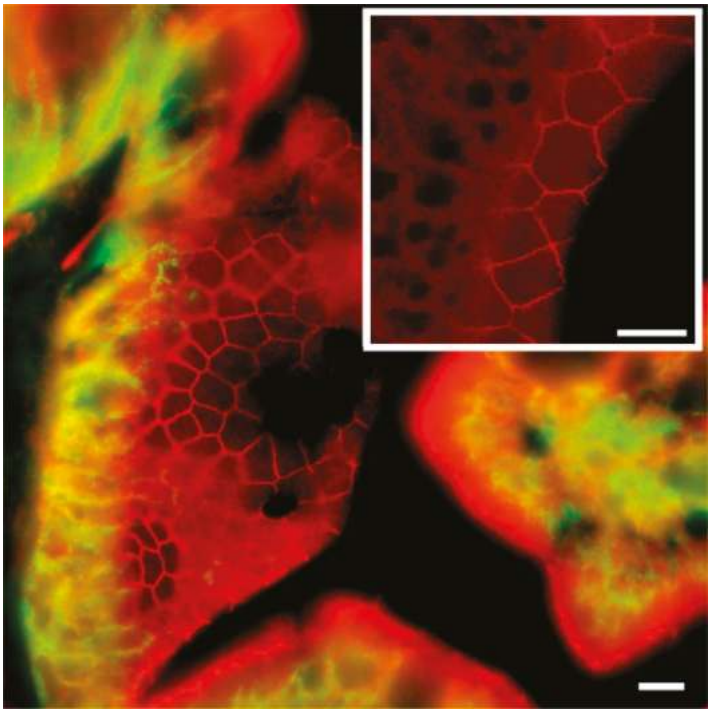

Figure 9. Confocal STED images showing the apical localization of Cldn15b (red) in SW-acclimated medaka middle intestine. Large image shows double staining with the anti-Na^+,K^+-ATPase alpha subunit (green). Na^+,K^+-ATPase is localized in basolateral membranes as shown in Figures 6–8, and it is absent in the apical area, where the tight junctions are located. Thus, the mosaic-like pattern of Cldn15b is without green overlay. The subfigure shows a subsection of the apical area focusing on the tight junction area. Size bars indicate 5 μm.

Occasionally, the section plane was slightly tilted and therefore made it possible to obtain a zoomed view of the apical junction area just below the brush border zone (Figure 9). In these cases, confocal STED microscopy showed a beautiful polygonal staining revealing the three-dimensional

junction zone surrounding the individual enterocytes. These polygons varied from simple tetragons to heptagons in shape, indicating enterocytes surrounded by four to seven neighboring cells.

We also performed a double labeling with Cldn15b and occludin antibodies (Figure 10). This revealed a complete co-localization of the two proteins, thus validating that Cldn15 is indeed localized in the tight junction between enterocytes.

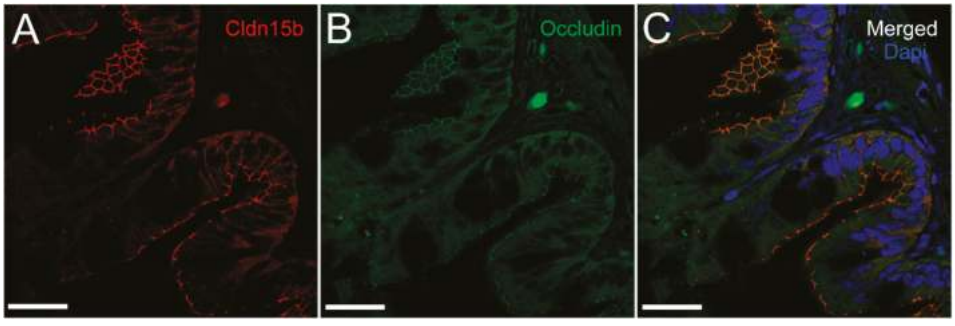

Figure 10. Confocal images showing Cldn15b (**A**, red), occludin (**B**, green) and co-localization (**C**, merged) in SW-acclimated medaka middle intestine. In (**C**), nuclei are stained blue with DAPI. Size bars indicate 20 μm.

3. Discussion

Japanese medaka can move between FW and SW while maintaining osmotic homeostasis. Based on our knowledge from several other teleosts, this requires high functional plasticity in e.g., the intestine, which in FW contributes to maintain ion balance and in SW switches to fluid absorption to compensate for dehydration [36]. Fluid absorption in fishes is driven by solute transport and is generally assumed to occur mainly through a transcellular pathway [2,7]. Accordingly, intestinal *aqp* expression is elevated during hyperosmotic exposure in order to develop the transcellular pathway [37,38]. This paradigm was challenged in previous studies, where we and others showed that in medaka *spp*., unlike in other species studied, intestinal *aqp*/Aqp expression is downregulated at both transcript and protein levels when fish are exposed to hyperosmotic conditions [8,39]. This paradox suggests that the paracellular pathway may be of higher importance, at least in the medaka. The recent report that the mammalian tight junction CLDN15 may create intestinal water channels [20] led us to investigate the role of the medaka orthologues in relation to fluid absorption. With limited knowledge about medaka drinking behavior and intestinal water handling, we set out by examining salinity effects on drinking behavior and water handling and then addressing the specific expression of *cldn15*. If involved in paracellular fluid absorption, our expectation was that *cldn15* expression would increase after SW exposure.

3.1. Drinking Rate and Intestinal Handling of Imbibed Water

After transition to SW, drinking rates and fluid absorption in the intestine increase in most examined fish species [36]. In order to understand intestinal function using the adult medaka model, we had to describe its drinking behavior and water handling, which was until now unknown. We demonstrated that the drinking rate was 5 μL/g/h and 10 μL/g/h in FW and SW medaka, respectively (Figure 1); thus, SW-transfer doubled oral water intake, which was presumably due to the need to compensate for osmotic water loss in the concentrated environment. This is similar to what has been observed in other euryhaline fish [35,40,41] including Japanese medaka larvae [42], and rates are comparable to other studies albeit on the high side [43]. Drinking rate is inversely related to body mass [43] and probably related to surface-to-volume ratio aspects, and most fishes examined up to now were larger fish (5–800 g). The medaka used in these experiments are small (0.4–0.6 g), and the smaller SW fish examined so far have comparable drinking rates (*Pholis gunnelus*, 2–10 g: 12 μL/g/h; *Aphanius*

dispar, 0.4–1 g: 10 μL/g/h; see [43]). It is often assumed that FW fish should keep oral water intake to a minimum in order to not put excessive strain on the kidney in a hypotonic environment [36]. This is certainly the case in some FW teleosts (e.g., 0.4 μL/g/h in 0.1–2.5 g *Platichthys flesus* [44]). However, there are also reports of significant drinking in FW teleosts in the μL/g/h-range [41,45,46], and this also seems to be the case in FW medaka. We do not have any physiological explanation as to why FW drinking rates were so relatively high compared to most other reported studies. Feeding events could possibly be accompanied by the swallowing of small amounts of water, but normally, including the present study, fish are unfed during drinking rate measurements. Stress is another factor that may affect drinking and water turnover, but the fish were left undisturbed during the whole experiment, so we must assume that it is negligible. It has been speculated that drinking in FW may be a source of divalent ions such as Ca^{2+} [45], but the significance of this was rejected by Lin et al. [46] based on quantitative analyses in tilapia.

When analyzing the segmental distribution of 51-Cr-EDTA-traced water in the intestine (Figure 2), our data showed that in FW fish, 51-Cr-EDTA was for the most part located anteriorly in contrast with a more posterior accumulation in SW fish. This is in perfect agreement with Kaneko and Hasegawa's [42] observations in medaka larvae, using a laser scanning technique to visualize intestinal water handling. This suggests that imbibed water in FW fish is taken up by osmosis in the anterior intestine were the tracers accumulate, and the volume regulatory problem associated must then be corrected by the kidney. While it is difficult to get reliable measurements of luminal fluid in small medaka, a study on FW tilapia showed that anterior, middle, and posterior luminal osmolality is close to plasma levels [47]. This corroborates an equilibration of the luminal fluid (FW) with plasma in the anterior intestine. In SW, after initial desalination in the esophagus, the luminal fluid osmolality in tilapia is similar all along the intestine and is higher than plasma osmolality [47]. Therefore, water uptake must rely on solute-driven transport into the lateral intercellular space in the anterior parts of the intestine [6] in combination with $CaCO_3$ precipitation in the posterior end to increase the concentration of free water molecules [2,36]. Therefore, continuous water flow along the intestine means that 51-Cr-EDTA tends to accumulate in the posterior section in SW fish. The accumulation of the non-absorbable tracer, 99-Tc-DTPA, at the posterior end indirectly supports the progressive absorption of water. This was further supported by the SPECT/CT imaging, in which the progress of water movement in the intestine was visualized directly in live fish (Figure 3). In SW fish, CT scans further revealed mineral precipitation in the posterior intestine, suggesting bicarbonate secretion, which induces Mg- and Ca-carbonate precipitation that helps drive osmotic water transport across the intestinal epithelium [2].

3.2. Transcript Levels and Response to Salinity

The progress of SW acclimation was followed by transcript analyses of a few selected targets representing intestinal NaCl uptake (*nkcc2*), which is needed to establish solute-driven water absorption and a possible transcellular water uptake pathway (*aqp1a, aqp8ab*) (Figures 4 and 5). As expected, there was a steep increase in *nkcc2* in SW, suggesting increased NaCl transport across the apical enterocytic brush border membrane. The data also confirmed the paradoxical drop in *aqp1a* and *aqp8ab* expression found in previous studies [*O. latipes*: 8; *O. dancena*: 39]. Thus, based on *aqp* dynamics, transcellular water transport is not supported in SW medaka; and it remains puzzling as to why *aqp* expression is kept higher in the FW condition. The time-course experiment showed that *cldn15b* was not significant affected by SW before 24 h and 168 h while the inhibitory effect on the two *aqps* was apparent at the 6 h and 24 h mark but not significant at the 168 h time point. Thus, while the dynamics of regulation are not straightforward, the overall inhibitory effect of SW on *cldn15b*, *aqp1a*, and *aqp8ab* observed previously was confirmed [8,34].

Based on similarities to the mammalian CLDN15 shown in Figure 11, we hypothesized that the two medaka orthologs, *cldn15a* and *cldn15b*, may share functional properties in terms of forming cation and water pores and therefore may contribute to paracellular water absorption in SW medaka. In fishes (medaka [34]; salmon [31,32]; zebrafish [33]) and mammals [12], CLDN15 orthologs are expressed

especially, but not exclusively, in the GI tract. In Atlantic salmon, SW acclimation was shown to induce elevated intestinal *cldn15a* mRNA expression [32], and a different study in the same species documented higher transepithelial resistance in SW than FW intestine measured *ex vivo* [48]. Taken together, this seems counterintuitive if teleost Cldn15 paralogs such as the mammalian ortholog form cation selective pores, and thereby theoretically should *decrease* epithelial resistance rather than increase it. We did not find any effect of salinity on *cldn15a* mRNA levels in medaka. However, Na^+ and water fluxes through human CLDN15 was recently shown to inhibit each other [20], and it is possible that physiological significance depends on the local chemical conditions, which may be very different in FW and SW intestines. We found a roughly 100-fold decrease of the *cldn15b* paralog when fish are acclimated to SW, which based on an expected possible role in creating a water pore is somewhat surprising. The high FW expression level of this paralog suggests a specific role in the FW intestine, which may be related to Na^+/glucose cotransport or K^+ uptake from the diet. The interpretation of Cldn data is not straightforward, because Cldn15 may interact with other proteins and Cldn paralogs when co-expressed in enterocytes [25], and the properties and physiological significance may change depending on salinity and intestinal location. Therefore, the expression of other intestinal Cldns should be investigated in future studies.

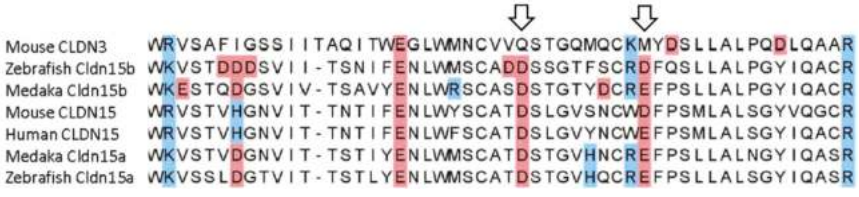

Figure 11. Alignment of the first extracellular loop of CLDN15 from human and mouse, and the orthologues from Japanese medaka and zebrafish shows that the residues critical to pore formation (D55 and D64) are found in both teleost Cldn15 paralogues. There are also differences from mammalian CLDN15; for example, both medaka Cldn15a and Cldn15b have an R63 residue and Cldn15a has an added H60. Amino acids are highlighted in red when acidic and in blue when basic. Arrows marks aspartic acids (D55 and D64), which are found to be important for cation and the water pore function of CLDN15 [11,12,15,16]. Mouse CLDN3 has been classified as a barrier protein and included as a reference. Sequences used: Human CLDN15: Acc. No. NP_001172009; Mouse CLDN15: Acc. No. NP_068365; Mouse CLDN3: NP_034032; Medaka Cldn15a: XP_004079873; Medaka Cldn15b: XP_004076514; Zebrafish Cldn15a: NP_956698; Zebrafish Cldn15b: NP_001035404.

3.3. Cldn15 Localization in the Intestinal Epithelium

To our knowledge, this is the first study showing enterocyte tight junction Cldn localization in a teleost fish. By using high-resolution fluorescence microscopy (Figures 6–9), we were able to demonstrate that Cldn15a and Cldn15b showed similar localization in the intestinal epithelium regardless of salinity. The use of Na^+,K^+-ATPase immunostaining to visualize basolateral membranes showed that parallel lateral membranes were slightly spaced between neighboring cells, thus creating the lateral intercellular space possibly involved in solvent drag [7]. Discrete Cldn15 immunoreaction was seen apically to Na^+,K^+-ATPase immunoreaction, demarcating apical and basolateral membranes with no co-localization of the two antibodies. The antibodies gave some apparent non-specific staining of the brush border zone, which had variable intensity between sections. It is possible that this is created by non-specific adsorption to the mucus layer in this area. Nonetheless, the specific immunoreaction of both Cldn15 antibodies was restricted to a very narrow apical-most zone, which was below the brush border and in direct extension from membranes bordering the lateral intercellular space. In cellular cross-sections at high resolution, this appeared as an apical dot-like staining, and when viewed from above in a frontal section, the pattern appeared as a circumcellular polygonal pattern, which is characteristic of epithelial tight junctions. This became particularly evident at higher magnification

when using high-resolution STED microscopy. The co-localization of Cldn15b with the tight junction marker occludin confirmed a role in control of the paracellular intestinal barrier. The localization is identical to that of CLDN15 throughout the mouse intestine [49] and that of occludin in the goldfish intestine [50]. Despite their classification as tight-junction proteins, several other intestinal CLDNs (e.g., CLDN-1, -3, -4, -5, and -7) are localized further away from the apical zone in lateral and basolateral membranes in mammals (see [25]). Based on the mRNA analyses, we expected to see a significant downregulation of Cldn15b after SW-exposure, but we did not find any significant change in the localization and immunoreactivity of neither Cldn15 paralog. There was a trend that the "hot spots" of Cldn staining appeared more intense in SW specimens, but it was not possible to quantify this (compare Figure 6B,D with Figure 7A,B). Unfortunately, the antibodies did not function for Western blots, and further quantification efforts are not possible at present. Thus, we conclude that the Cldn15-based apical tight junction component is resilient to changes in salinity, suggesting that it may contribute to paracellular fluid transport.

3.4. Conclusion and Perspectives

The drinking rate in FW medaka is quite high though still increasing when fish are challenged with hyperosmotic conditions. This suggests that the need for fluid absorption increases as dehydration threatens osmotic homeostasis. Several Aqp isoforms are expressed in the medaka intestine [8], but paradoxically, the most abundant forms (Aqp1a, Aqp8ab, and Aqp10 [8]) are significantly downregulated in SW, in parallel with the increased demand for fluid uptake. This led us to hypothesize that in medaka, the paracellular pathway may be more important when fish move into a hyperosmotic environment. The present data do not reject this hypothesis but do not provide strong support, either. Cldn15 paralogs make a significant constituent of the apical tight junction complex and may thereby create a paracellular water (and Na^+) leak pathway. However, there are no signs that this is reinforced during SW acclimation.

The present study leaves behind a couple of questions: (1) What is the physiological significance of drinking in FW, and is this water really absorbed in the intestine? (2) What is the significance of uncoupled transcript and protein dynamics with regard to the Cldn15b paralog? We have attempted to analyze unidirectional water fluxes across isolated gut segments ex vivo using tritiated water as a tracer in an Ussing chamber setup, but so far, the data are inconclusive due to the fragility of the tissue. Future research in this area should pursue the functional aspects of water transport in this species by including vivo knock-down technology as well as analyses of luminal fluid chemical composition.

4. Materials and Methods

4.1. Fish and Rearing Conditions

The Japanese medaka (*Oryzias latipes*) used for this study came from two different sources. The fish (CAB strain) used for histological examinations, drinking rate, and drinking-related experiments were purchased from the UMS AMAGEN (Centre national de la recherche scientifique, Gif-sur-Yvette, France) and held in tanks with biofiltered FW or 30 ppt at 24–26 °C and exposed to a 12:12 light:dark photoperiod. These fish were generally fed four times per day with TetraMin® flakes (Tetra GmbH, Melle, Germany), and the food was withheld 2 days before any experimentation. The experimental procedures were approved by the Danish Animal Experiments Inspectorate in accordance with the European convention for the protection of vertebrate animals used for experiments and other scientific purposes (#86/609/EØF). Long-term acclimated fish for transcriptional analysis were obtained from Aquatic Research Organisms, Inc. (Hampton, NH, USA; CAB strain) and held in biofiltered FW or 30 ppt SW and sampled after 1 month of acclimation. They were fed daily with TetraMin tropical flakes (Tetra, United Pet Group, Blacksburg, VA, USA), and food was withheld 2 days prior to any sampling. To investigate the early response to hyperosmotic environments, 10 female and 10 male FW-acclimated medaka were transferred to both sham FW conditions and SW (30 ppt; Instant Ocean,

Spectrum Brands, Blacksburg, VA, USA; n = 40) and sampled after 6, 24, and 168 h (n = 6 per group). All handling and experimental procedures were approved by the Animal Care and Use Committee of the University of Arkansas (IACUC 17091).

4.2. Drinking Rate Measurements

A series of experiments was performed to estimate the rate of drinking in FW and SW-acclimated medaka. The gamma emitter 51-Cr-EDTA (PerkinElmer, NEZ147001MCNSA1, Waltham, MA, USA) was used as a non-absorbable marker for these experiments. The tracer (5 MBq) was added to the water (1 L of FW or 30 ppt SW), and the fish (n = 10–12) were then transferred to the experimental tank [35,40]. They were allowed to drink for 3 h, after which they were transferred to clean water (1 L) for 3 min and transferred to another tank with clean water (1 L) for 30 min. Then, the fish were anaesthetized in 100 mg/L MS-222 (Tricaine methanesulfonate) and killed by cervical dislocation. Before dissection, the fish were blotted by a paper towel and weighed to the nearest mg. The intestine was carefully ligatured at the anterior and posterior ends, removed from the body, and transferred to a 5 mL scintillation vial. The head was separated from the body with remaining organs and transferred to separate scintillation vials. All samples had 0.5 mL of distilled water added, and they were counted on a PerkinElmer 1480 WizardTM 3" Automatic gamma counter. The radioactivity of a 1.0 mL water sample was measured to estimate the specific radioactivity of the drinking water. Background radioactivity was counted on a 1.0 mL non-radioactive water sample. All samples were corrected for background, and the specific drinking rate (μL/g/h) was calculated as DR = sa/(bw*time), DR = drinking rate, sa = background-corrected specific activity (counts/minute); bw = body weight; time = time in radioactive water. Prior to these experiments, the accumulation of 51-Cr radioactivity was investigated and found to be linear in excess of 3 h.

4.3. Water Passage through the GI Tract

Medaka are agastric fish, meaning that the esophagus is directly connected to the anterior part of the tube-like intestine. In order to trace the passage of imbibed water in FW and SW-acclimated fish, two fish were allowed to drink for 3 h in water to which 51-Cr-EDTA had been added as described above. After this the fish were anaesthetized in MS-222 and killed by cervical dislocation, and the complete GI tract was ligatured at both ends and removed from the fish. Then, segments of 5–6 mm were ligatured and carefully dissected into scintillation vials to estimate the longitudinal distribution of radioactivity. The counting and calculations were done according to the above methodology, and the data were graphed in percent of total radioactivity as a function of longitudinal position.

4.4. Single Photon Emission Computed Tomography (SPECT)–Computed Tomography (CT) Scanning

In order to visualize the intestinal passage of imbibed water, a series of experiments was done in which fish were allowed to drink water with added non-absorbable marker 99-Tc-DTPA (Technetium-99mTc-diethylene-triamine-pentaacetic acid). This short-lived gamma emitter ($T_{1/2}$ = 6.0067 h) is a widely used clinical radiophamaceutical for renal diagnosis and functioning. Subsequently, the fish were analyzed by SPECT-CT scanning. SPECT scanning is used for three-dimensional analysis of the radiochemical, while CT scanning creates a three-dimensional X-ray image, and when the two images are merged, a high-resolution image localizing the radiochemical to internal structures is obtained. All SPECT/CT scans were performed on a Siemens INVEON multimodality pre-clinical scanner (Siemens pre-clinical solutions, Knoxville, TN, USA).

Three fish were used for experiments in FW and SW, respectively, with imaging time-points at 1, 4, and 6 h for each group. For each salinity, two fish were transferred to a container with 100 mL water with the addition of 3.5 GBq Tc-99-DTPA, and one fish was transferred to a container with 100 mL of water with the addition of 5 GBq Tc-99-DTPA. Due to the short half-life of the 99-Tc isotope, a relatively high specific activity in the water is needed in order to obtain a good signal-to-noise ratio for visualization; thus, a higher activity was required for the late imaging group. All fish were allowed to

drink in the labeled water for 1 h. Then, they were transferred to separate containers with 1 L of clean water for 5 min, followed by transfer to a second container with 1 L of clean water to rid the external surface for radioactivity. For each salinity, one fish was then euthanized in an overdose of MS-222 after a total of 1, 4, and 6 h after transfer to clean water and analyzed by SPECT-CT scanning in order to analyze the progressive movement of the imbibed isotope through the GI tract. After euthanasia, each fish was wrapped in plastic to avoid dehydration during the following imaging. The fish was placed in a lateral position on a dedicated SPECT/CT pre-clinical bed (25 mm).

CT scans were performed with the following settings; 360° rotation with 360 projections and 2 × 2 bin. The magnification was set at medium, yielding an isotropic pixel size of 40.00 µm and a trans-axial field view of 42 mm. The tube voltage was set to 80 kV, the current was 500 µA, and each projection was exposed for 1000 ms. CT scans were reconstructed using Feldkamp algorithm, with a Sheep–Logan filter and slight noise reduction. SPECT images were acquired using mouse high-resolution single pinhole collimators. A full 360° rotation with 60 projections and a fixed radius of 25 mm yielded a reconstructed 28 mm trans-axial field of view. A 20% energy window centered on the energy peak of 99mTc at 140 keV was used. Acquisition duration was set to 100 sec/projection. CT and SPECT images were co-registered using a transformation matrix and SPECT data was reconstructed using the Siemens MAP3D algorithm (matrix 128 × 128, 0.5 mm pixels, 16 iterations, and 6 subsets).

4.5. RNA Isolation, cDNA Synthesis, and qPCR

RNA isolation was conducted according to the manufacturer's protocol (TRI Reagent®; Sigma Aldrich, St. Lois, MO, USA). All samples were homogenized using a Power Max 200 rotating knife homogenizer (Advanced Homogenizing System; Manufactured by PRO Scientific for Henry Troemner LLC, Thorofare, NJ, USA). First, 500 ng of total RNA was used for cDNA synthesis using the Applied Biosystems High Capacity cDNA Reverse Transcription kit (Thermo Fisher, Waltham, MA, USA). Used primers were previously validated and published in Bossus et al. [34] and Madsen et al. [6]. Elongation Factor 1 alpha (*ef1α*), beta actin (*βact*), and ribosomal protein L7 (*rpl7*) were analyzed as normalization genes in all experiments. Quantitative PCR was run on a Bio-Rad CFX96 platform (BioRad, Hercules, CA, USA) using SYBR® Green JumpStart (Sigma Aldrich). qPCR cycling was conducted using the following protocol: a denaturation/activation step (94 °C) for 3 min, 40 cycles of a 15 s denaturation step (94 °C) followed by an annealing/elongation step for 60 s (60 °C), and finally a melting curve analysis at an interval of 5 s per degree from 55 to 94 °C. The absence of primer–dimer association was verified with no template controls (NTC). As an alternative to DNAse treatment, the absence of significant genomic DNA amplification was confirmed using total RNA samples instead of cDNA in a no reverse transcriptase control (NRT). Primer amplification efficiency was analyzed using a standard curve method with dilutions of the primers from 2 to 16 times. Amplification efficiency was used to calculate the relative copy numbers of the individual targets. Relative copy numbers were calculated by $E_a^{\Delta Ct}$, where Ct is the threshold cycle number and E_a is the amplification efficiency. Data were normalized to the geometric mean of the three normalization genes.

4.6. Immunofluorescence, Confocal, and Stimulated Emission Depletion (STED) Microscopy

The preparation of medaka intestines for immunofluorescence microscopy followed the procedures described previously [51]. Sections (0.5 cm) from the middle part of the intestines from medaka acclimated to FW and 30 ppt SW were sampled and fixed overnight in 4% buffered paraformaldehyde at 4 °C. After rinsing several times in 70% EtOH, the tissues were dehydrated overnight through a graded series of EtOH and xylene followed by embedding in 60 °C paraffin. Five-micron-thick transversal sections were cut on a microtome, and sections were placed on Superfrost plus (Gerhard Menzel GmbH, Braunschweig, Germany) slides before being dried overnight at 55 °C. Then, the tissue sections were hydrated through washes in xylene, 99%, 96%, and 70% EtOH and finally Na citrate (10 mM Na-citrate, pH 6.0). Antigen retrieval was performed by boiling the sections in the citrate solution for 5 min in a microwave oven and leaving them in the warm citrate solution for 30 min before

being washed in 1× PBS (in mmol L^{-1}: 137 NaCl, 2.7 KCl, 1.5 KH_2PO_4, 4.3 Na_2HPO_4, pH 7.3). Then, representative sections were blocked by incubation in 2% goat serum and 2% bovine serum albumin in 1× PBS for 1 h at room temperature. This was followed by dual labeling with a cocktail of an affinity purified polyclonal rabbit antibody against medaka Cldn15a or Cldn15b, respectively, in combination with the monoclonal mouse α5 antibody, which recognizes the alpha-subunit of the Na^+,K^+-ATPase in all vertebrates (The Developmental Studies Hybridoma Bank developed under auspices of the National Institute of Child Health Development and maintained by The University of Iowa, Department of Biological Sciences, Iowa City, IA, USA). In a separate experiment, sections were dual-labeled with Cldn15b and an occludin mouse monoclonal antibody (Invitrogen, product # 33-1500) in order to verify localization in the tight junction zone. Primary antibodies were diluted in 2% goat serum and 2% bovine serum albumin in PBS and incubated overnight at 4 °C. The polyclonal Cldn antibodies were custom-made in rabbits by Genscript (Piscataway, NJ, USA) against the following epitopes near the C-termini: Japanese medaka Cldn15a PAPTRSVVASTYGR, GenBank accession XP_004079873.1; Japanese medaka Cldn15b SHAAPSNYDRNAYV, GenBank accession XP_004076514.1). They were used at the concentrations 0.5 μg/mL (Cldn15a), 0.6 μg/mL (Cldn15b), and 5 μg/mL (occludin). The α5 antibody was used at 0.2 μg/mL.

For immunofluorescence and confocal microscopy, the following secondary antibodies were used for visualization: Alexa Flour® 568 Donkey Anti-Rabbit IgG (H+L) at 1 ug/mL and Oregon Green® 488 Goat Anti-Mouse IgG (H+L) at 2ug/mL (Invitrogen™ Molecular ProbesTM, Carlsbad, CA, USA). The incubation time was 1 h at 37 °C for the secondary antibody. Then, sections were washed repeatedly in PBS, and coverslips were mounted using ProLong Gold antifade reagent (Invitrogen).

For STED microscopy, we used higher Cldn antibody concentrations: 0.7 μg/mL (Cldn15a) and 0.9 μg/mL (Cldn15b). The secondary antibodies used for STED were goat-anti-rabbit Abberior® STAR 488 and goat-anti-mouse Abberior® STAR 440SX (Sigma-Aldrich) at 1:200 and 1:1000 dilution, respectively. Negative control incubations with 2% BSA in PBS instead of primary antibodies were made routinely. The fluorescence was inspected on a Leica HC microscope (Manheim, Germany) and pictures of representative areas were captured using a Leica DC200 camera. Confocal images were taken on a Zeiss LSM510 META confocal microscope (CarlZeiss, Oberkochen, Germany) using a 63× objective with oil immersion. STED images were recorded using a Leica TSC SP8 STED setup. The excitation was done at 500 nm using a white light laser for Abberior® STAR 488 and at 458 using an Argon laser for Abberior® STAR 440SXP. The depletion laser (STED laser) was a 592 nm CW for both channels. The emission was recorded at 510–560 nm using the gated hybrid detector (0.3 ns) in counting mode for the Abberior® STAR 488 and at 500–550 nm using the non-gated hybrid detector in counting mode for the Abberior® STAR 440SXP. The images were cross-talk corrected and deconvoluted using Huygens™ (Hilversum, Netherland). The deconvolution was done to further increase the resolution of the images and decrease the background.

4.7. Statistical Analyses

All data analysis was conducted using GraphPad Prism 8.0 software (San Diego, CA, USA). Data from the salinity transfer experiments were analyzed using Bonferroni adjusted two-tailed Student's t-test in experiments with two groups and two-way ANOVA followed by Bonferroni's multiple comparisons test of time-matched groups in experiments with more groups. Drinking rates were analyzed using two-tailed Student's t-test. When required, data were log or square root transformed to meet the ANOVA assumption of homogeneity of variances as tested with Bartlett's test. Significant differences were accepted when $p < 0.05$.

Author Contributions: S.S.M., A.M.N., M.C.B. and C.K.T. conceived the idea and designed the project; A.M.N., M.C.B., and L.V.E. performed the transcript analyses; A.M.N performed the fluorescence and confocal microscopy; J.D. and J.R.B. performed the STED microscopy and image analyses; C.B. and T.L.A. performed the SPECT/CT scanning experiments and data analyses; A.M.N. and S.S.M. performed the drinking rate experiments; S.S.M. and C.K.T. wrote the manuscript. All authors have read and agreed to the published version of the manuscript.

Funding: This work was supported by a grant from the Danish Research Council for Independent Research (DFF-4181-00020) to SSM, and the National Science Foundation [IOS 1251616] and Arkansas Biosciences Institute to CKT.

Acknowledgments: The authors acknowledge the Danish Molecular Biomedical Imaging Center (DaMBIC, University of Southern Denmark) for the use of the bioimaging facilities.

Conflicts of Interest: The authors declare no conflict of interest. The funders had no role in the design of the study; in the collection, analyses, or interpretation of data; in the writing of the manuscript, or in the decision to publish the results.

Abbreviations

ANOVA	Analysis of variance
AQP	Aquaporin
CLDN	Claudin
CT	Computed tomography
DR	Drinking rate
DTPA	Diethylenetriamine penta-acetic acid
EDTA	2,2′,2′′,2′′′-(Ethane-1,2-diyldinitrilo)-tetraacetic acid
FW	Fresh water
GI	Gastrointestinal tract
NKCC	Sodium-potassium-chloride-cotransporter
SEM	Standard error of the mean
STED	Stimulated Emission Depletion
SPECT	Single photon emission computed tomography
SW	Seawater
PPT	Parts per thousand

References

1. Madsen, S.S.; Engelund, M.B.; Cutler, C.P. Water transport and functional dynamics of aquaporins in osmoregulatory organs of fishes. *Biol. Bull.* **2015**, *229*, 70–92. [CrossRef] [PubMed]
2. Whittamore, J.M. Osmoregulation and epithelial water transport: Lessons from the intestine of marine teleost fish. *J. Comp. Physiol.* **2012**, *182B*, 13–19. [CrossRef] [PubMed]
3. Aoki, M.; Kaneko, T.; Katoh, F.; Hasegawa, S.; Tsutsui, N.; Aida, K. Intestinal water absorption through aquaporin 1 expressed in the apical membrane of mucosal epithelial cells in seawater-adapted Japanese eel. *J. Exp. Biol.* **2003**, *206*, 3495–3505. [CrossRef] [PubMed]
4. Cutler, C.P.; Philips, C.; Hazon, N.; Cramb, G. Aquaporin 8 (AQP8) intestinal mRNA expression increases in response to salinity acclimation in yellow and silver European eels (*Anguilla anguilla*). *Comp. Biochem. Physiol.* **2009**, *153A*, S78. [CrossRef]
5. Martinez, A.S.; Cutler, C.P.; Wilson, G.D.; Phillips, C.; Hazon, N.; Cramb, G. Cloning and expression of three aquaporin homologues from the European eel (*Anguilla anguilla*): Effects of seawater acclimation and cortisol treatment on renal expression. *Biol. Cell* **2005**, *97*, 615–627. [CrossRef]
6. Madsen, S.S.; Olesen, J.H.; Bedal, K.; Engelund, M.B.; Velasco-Santamaria, Y.M.; Tipsmark, C.K. Functional characterization of water transport and cellular localization of three aquaporin paralogs in the salmonid intestine. *Front. Physiol.* **2011**, *2*, 56. [CrossRef]
7. Sundell, K.S.; Sundh, H. Intestinal fluid absorption in anadromous salmonids: Importance of tight junctions and aquaporins. *Front. Physiol.* **2012**, *3*, 388. [CrossRef]
8. Madsen, S.S.; Bujak, J.; Tipsmark, C.K. Aquaporin expression in the Japanese medaka (*Oryzias latipes*) in freshwater and seawater: Challenging the paradigm of intestinal water transport? *J. Exp. Biol.* **2014**, *217*, 3108–3121. [CrossRef]
9. Fischbarg, J. Fluid transport across leaky epithelia: Central role of the tight junction and supporting role of aquaporins. *Physiol. Rev.* **2010**, *90*, 1271–1290. [CrossRef]
10. Laforenza, U. Water channel proteins in the gastrointestinal tract. *Mol. Aspects Med.* **2012**, *33*, 642–650. [CrossRef]

11. Günzel, D.; Fromm, M. Claudins and other tight junction proteins. *Compr. Physiol.* **2012**, *2*, 1819–1852. [CrossRef] [PubMed]
12. Günzel, D.; Yu, A.S.L. Claudins and the modulation of tight junction permeability. *Physiol. Rev.* **2013**, *93*, 525–569. [CrossRef] [PubMed]
13. Angelow, S.; Yu, A.S.L. Structure-function studies of claudin extracellular domains by cysteine-scanning mutagenesis. *J. Biol. Chem.* **2009**, *284*, 29205–29217. [CrossRef] [PubMed]
14. Li, J.; Angelow, S.; Linge, A.; Zhuo, M.; Yu, A.S. Claudin-2 pore function requires an intramolecular disulfide bond between two conserved extracellular cysteines. *Am. J. Physiol.* **2013**, *305*, C190–C196. [CrossRef]
15. Samanta, P.; Wang, Y.; Fuladi, S.; Zou, J.; Li, Y.; Shen, L.; Weber, C.; Khalili-Araghi, F. Molecular determination of claudin-15 organization and channel selectivity. *J. Gen. Physiol.* **2018**, *150*, 949–968. [CrossRef]
16. Alberini, G.; Benfenati, F.; Maragliano, L. Molecular dynamics simulations of ion selectivity in a claudin-15 paracellular channel. *J. Phys. Chem. B* **2018**, *122*, 10783–10792. [CrossRef]
17. Loh, Y.H.; Christoffels, A.; Brenner, S.; Hunziker, W.; Venkatesh, B. Extensive expansion of the claudin gene family in the teleost fish, *Fugu rubripes*. *Genome Res.* **2004**, *14*, 1248–1257. [CrossRef]
18. Baltzegar, D.A.; Reading, B.J.; Brune, E.S.; Borski, R.J. Phylogenetic revision of the claudin gene family. *Mar. Genomics* **2013**, *11*, 17–26. [CrossRef]
19. Rosenthal, R.; Milatz, S.; Krug, S.M.; Oelrich, B.; Schulzke, J.-D.; Amasheh, S.; Günzel, D.; Fromm, M. Claudin-2, a component of the tight junction, forms a paracellular water channel. *J. Cell Sci.* **2010**, *123*, 1913–1921. [CrossRef]
20. Rosenthal, R.; Gunzel, D.; Piontek, J.; Krug, S.M.; Ayala-Torres, C.; Hempel, C.; Theune, D.; Fromm, M. Claudin-15 forms a water channel through the tight junction with distinct function compared to claudin-2. *Acta Physiol.* **2020**, *228*, e13334. [CrossRef]
21. Engelund, M.B.; Yu, A.S.L.; Li, J.; Madsen, S.S.; Færgeman, N.J.; Tipsmark, C.K. Functional characterization and localization of a gill-specific claudin isoform in Atlantic salmon. *Am. J. Physiol.* **2012**, *302*, R300–R322. [CrossRef] [PubMed]
22. Kwong, R.W.M.; Perry, S.F. The tight junction protein claudin-b regulates epithelial permeability and sodium handling in larval zebrafish, *Danio rerio*. *Am. J. Physiol.* **2013**, *304*, R504–R513. [CrossRef] [PubMed]
23. Suzuki, H.; Nishizawa, T.; Tani, K.; Yamazaki, Y.; Tamura, A.; Ishitani, R.; Dohmae, N.; Tsukita, S.; Nureki, O.; Fujiyoshi, Y. Crystal structure of a claudin provides insight into the architecture of tight junctions. *Science* **2014**, *344*, 304–307. [CrossRef] [PubMed]
24. Hou, J.; Rajagopal, M.; Yu, A.S.L. Claudins and the kidney. *Annu. Rev. Physiol.* **2013**, *75*, 479–501. [CrossRef]
25. Garcia-Hernandez, V.; Quiros, M.; Nusrat, A. Intestinal epithelial claudins: Expression and regulation in homeostasis and inflammation. *Ann. N. Y. Acad. Sci.* **2017**, *1397*, 66–79. [CrossRef]
26. Holmes, J.L.; Van Itallie, C.M.; Rasmussen, J.E.; Anderson, J.M. Claudin profiling in the mouse during postnatal intestinal development and along the gastrointestinal tract reveals complex expression patterns. *Gene Expr. Patterns* **2006**, *6*, 581–588. [CrossRef]
27. Lu, Z.; Ding, L.; Lu, Q.; Chen, Y.H. Claudins in intestines: Distribution and functional significance in health and diseases. *Tissue Barriers* **2013**, *1*, e24978. [CrossRef]
28. Tamura, A.; Kitano, Y.; Hatam, M.; Katsuno, T.; Moriwaki, K.; Sasaki, H.; Hayashi, H.; Suzuki, Y.; Noda, T.; Furuse, M.; et al. Megaintestine in claudin-15 deficient mice. *Gastroenterology* **2008**, *134*, 523–534. [CrossRef]
29. Bagnat, M.; Cheung, I.D.; Mostov, K.E.; Stainier, D.Y. Genetic control of single lumen formation in the zebrafish gut. *Nat. Cell Biol.* **2007**, *9*, 954–960. [CrossRef]
30. Tamura, A.; Hayashi, H.; Imasato, M.; Yamazaki, Y.; Hagiwara, A.; Wada, M.; Noda, T.; Watanabe, M.; Suzuki, Y.; Tsukita, S. Loss of claudin-15, but not claudin-2, causes Na^+ deficiency and glucose malabsorption in mouse small intestine. *Gastroenterology* **2011**, *140*, 913–923. [CrossRef]
31. Tipsmark, C.K.; Kiilerich, P.; Nilsen, T.O.; Ebbesson, L.O.E.; Stefansson, S.O.; Madsen, S.S. Branchial expression patterns of claudin isoforms in Atlantic salmon during seawater acclimation and smoltification. *Am. J. Physiol.* **2008**, *294*, R1563–R1574. [CrossRef] [PubMed]
32. Tipsmark, C.K.; Sørensen, K.J.; Hulgard, K.; Madsen, S.S. Claudin-15 and-25b expression in the intestinal tract of Atlantic salmon in response to seawater acclimation, smoltification and hormone treatment. *Comp. Biochem. Physiol.* **2010**, *155A*, 361–370. [CrossRef] [PubMed]

33. Clelland, E.S.; Kelly, S.P. Tight junction proteins in zebrafish ovarian follicles: Stage specific mRNA abundance and response to 17beta-estradiol, human chorionic gonadotropin, and maturation inducing hormone. *Gen. Comp. Endocrinol.* **2010**, *168*, 388–400. [CrossRef] [PubMed]
34. Bossus, M.C.; Madsen, S.S.; Tipsmark, C.K. Functional dynamics of claudin expression in Japanese medaka (*Oryzias latipes*): Response to environmental salinity. *Comp. Biochem. Physiol.* **2015**, *187A*, 74–85. [CrossRef] [PubMed]
35. Usher, M.L.; Talbot, C.; Eddy, F.B. Drinking in Atlantic salmon smolts transferred to seawater and the relationship between drinking and feeding. *Aquaculture* **1988**, *73*, 237–246. [CrossRef]
36. Marshall, W.S.; Grosell, M. Ion transport, osmoregulation, and acid-base regulation. In *The Physiology of Fishes*; Evans, D.H., Clairborne, J.B., Eds.; Taylor and Francis Group: Boca Raton, FL, USA, 2006; pp. 177–210.
37. Cerdá, J.; Finn, R.N. Piscine aquaporins: An overview of recent advances. *J. Exp. Zool.* **2010**, *313A*, 623–650. [CrossRef]
38. Tipsmark, C.K.; Sørensen, K.J.; Madsen, S.S. Aquaporin expression dynamics in osmoregulatory tissues of Atlantic salmon during smoltification and seawater acclimation. *J. Exp. Biol.* **2010**, *213*, 368–379. [CrossRef]
39. Kim, Y.K.; Lee, S.Y.; Kim, B.S.; Kim, D.S.; Nam, Y.K. Isolation and mRNA expression analysis of aquaporin isoforms in marine medaka *Oryzias dancena*, a euryhaline teleost. *Comp. Biochem. Physiol.* **2014**, *171A*, 1–8. [CrossRef]
40. Perrott, M.N.; Grierson, C.E.; Hazon, N.; Balment, R.J. Drinking behaviour in sea water and fresh water teleosts, the role of the renin-angiotensin system. *Fish. Physiol. Biochem.* **1992**, *10*, 161–168. [CrossRef]
41. Fuentes, J.; Bury, N.R.; Carroll, S.; Eddy, F.B. Drinking in Atlantic salmon presmolts (*Salmo salar* L.) and juvenile rainbow trout (*Oncorhynchus mykiss* Walbaum) in response to cortisol and sea water challenge. *Aquaculture* **1996**, *141*, 129–137. [CrossRef]
42. Kaneko, T.; Hasegawa, S. Application of laser scanning microscopy to morphological observations on drinking in freshwater medaka larvae and those exposed to 80% seawater. *Fish. Sci.* **1999**, *65*, 492–493. [CrossRef]
43. Fuentes, J.; Eddy, F.B. Drinking in marine, euryhaline and freshwater teleost fish. In *Ionic Regulation in Animals: A Tribute to Professor W.T.W. Potts*; Hazon, N., Eddy, F.B., Flik, G., Eds.; Springer: Berlin/Heidelberg, Germany, 1997; pp. 136–149.
44. Hutchinson, S.; Hawkins, L.E. The influence of salinity on water balance in 0-group flounders, *Platichthys flesus* (L). *J. Fish. Biol.* **1990**, *36*, 751–764. [CrossRef]
45. Tytler, P.; Tatner, M.; Findlay, C. The ontogeny of drinking in the rainbow trout, *Oncorhychus mykiss*. (Walbaum). *J. Fish. Biol.* **1990**, *36*, 867–875. [CrossRef]
46. Lin, L.Y.; Weng, C.F.; Hwang, P.P. Regulation of drinking rate in euryhaline tilapia larvae (*Oreochromis mossambicus*) during salinity challenges. *Physiol. Biochem. Zool.* **2001**, *74*, 171–177. [CrossRef] [PubMed]
47. Grosell, M. Intestinal transport processes in marine fish osmoregulation. In *Fish. Osmoregulation*; Baldisserotto, B., Mancera, J.M., Kapoor, B.G., Eds.; Science Publishers: Enfield, NH, USA, 2007; pp. 333–357.
48. Sundell, K.; Jutfelt, F.; Agustsson, T.; Olsen, R.E.; Sandblom, E.; Hansen, T.; Bjornsson, B.T. Intestinal transport mechanisms and plasma cortisol levels during normal and out-of-season parr–smolt transformation of Atlantic salmon, *Salmo salar*. *Aquaculture* **2003**, *222*, 265–285. [CrossRef]
49. Fujita, H.; Chiba, H.; Yokozaki, H.; Sakai, N.; Sugimoto, K.; Wada, T.; Kojima, T.; Yamashita, T.; Sawada, N. Differential expression and subcellular localization of claudin-7, -8, -12, -13, and -15 along the mouse intestine. *J. Histochem. Cytochem.* **2006**, *54*, 933–944. [CrossRef] [PubMed]
50. Chasiotis, H.; Kelly, S.P. Occludin immunolocalization and protein expression in goldfish. *J. Exp. Biol.* **2008**, *211*, 1524–1534. [CrossRef]
51. Engelund, M.B.; Madsen, S.S. Tubular localization and expressional dynamics of aquaporins in the kidney of seawater-challenged Atlantic salmon. *J. Comp. Physiol. B* **2015**, *185B*, 207–223. [CrossRef]

International Journal of
Molecular Sciences

MDPI

Review

Regulation of Epithelial Cell Functions by the Osmolality and Hydrostatic Pressure Gradients: A Possible Role of the Tight Junction as a Sensor

Shinsaku Tokuda [1,2,*] and Alan S. L. Yu [2]

[1] Department of Respiratory Medicine, Graduate School of Medicine, Kyoto University, Kyoto 606-8507, Japan
[2] Division of Nephrology and Hypertension, Department of Internal Medicine, University of Kansas Medical Center, Kansas City, KS 66160, USA
* Correspondence: tokku@kuhp.kyoto-u.ac.jp

Received: 24 May 2019; Accepted: 16 July 2019; Published: 17 July 2019

Abstract: Epithelia act as a barrier to the external environment. The extracellular environment constantly changes, and the epithelia are required to regulate their function in accordance with the changes in the environment. It has been reported that a difference of the environment between the apical and basal sides of epithelia such as osmolality and hydrostatic pressure affects various epithelial functions including transepithelial transport, cytoskeleton, and cell proliferation. In this paper, we review the regulation of epithelial functions by the gradients of osmolality and hydrostatic pressure. We also examine the significance of this regulation in pathological conditions especially focusing on the role of the hydrostatic pressure gradient in the pathogenesis of carcinomas. Furthermore, we discuss the mechanism by which epithelia sense the osmotic and hydrostatic pressure gradients and the possible role of the tight junction as a sensor of the extracellular environment to regulate epithelial functions.

Keywords: tight junction; osmolality; hydrostatic pressure; cancer; sensor

1. Introduction

In multicellular organisms, epithelia act as a barrier to the external environment and contribute to maintain the homeostasis in the internal environment. The environmental conditions including osmolality and hydrostatic pressure (HP) constantly changes with the biological activity [1–3]. The epithelia are required to regulate their functions including transepithelial transport in accordance with the changes in the environmental condition to maintain the homeostasis in the internal environment. It has been reported that differences of the osmolality and HP between the apical and basal sides of the epithelia affects various epithelial functions as reviewed in this paper.

In this paper, we review these reports and illustrate the effects of osmotic and HP gradients in the regulation of epithelial functions. Furthermore, we examine the significance of the regulation in pathological conditions and discuss the mechanism by which epithelia sense the gradients of osmolality and HP.

2. Effects of Osmolality on the Epithelia and Endothelia

2.1. Regulation of Osmolality in the Body

When there is a concentration difference of a certain substance between a semipermeable membrane which is permeable to water but not to the substance, the substance exerts a driving force for the water movement and the driving force is called osmotic pressure or osmolality. Epithelia act as a barrier to the external environment and osmolality in the apical side of the epithelia constantly changes with

the biological activity. For example, the osmolality in the apical side of an intestine dramatically and dynamically changes with diet and its digestion. The osmolality in the surface of an airway epithelium changes with secretion and moisture, and urine osmolality fluctuates in accordance with the regulation of osmolality in a body (see below).

In contrast, the osmolality inside the body is strictly regulated within a narrow range (275–295 mOsm/kg) [4,5]. The regulation of osmolality is mainly performed in the kidney except in aquatic animals. The excretion of free water in urine is regulated in the kidney, which is further regulated by hormones such as antidiuretic hormone (ADH) [6]. In the interstitium of the kidney, the osmotic gradient is formed from medulla toward cortex (high osmolality in medulla) [5,7]. The glomerular filtrate flows through renal tubules, and renal tubules go down to medulla and then make a sharp loop (Henle's loop) and return to cortex. The permeability of water in renal tubules after the Henle's loop is very low and the filtrate grows hypotonic as sodium chloride is reabsorbed. Then the renal tubules gather into collecting ducts and again go down to medulla [5,7]. In collecting ducts, water is absorbed in accordance with the amount of aquaporin (AQP) in the cell membranes and ADH regulates the amount of AQP in the apical cell membrane [6]. As such, the amount of free water excretion in urine is regulated and osmolality in the body is kept within a narrow range. The osmolality in urine ranges from 30 to 1200 mOsm/kg in humans [5,7].

Therefore, osmolality in the apical side constantly changes whereas osmolality in the basal side is kept in a narrow range in most epithelia. Then, what kind of effects does the osmotic change have on the epithelia?

2.2. Effect of Osmolality on Cell Volume and Other Cell Functions

The effects of osmolality on cells received attention as early as 1930s. In the 1960s, the regulation of cell volume after the osmotic changes in the extracellular environment was actively investigated by using erythrocytes. When the extracellular osmolality is lowered, water flows into the cells as most cell membranes of animal cells have high water permeability and results in cell swelling. Then, cells start to restore their volume to their original size by excreting potassium chloride (regulatory volume decrease: RVD). In contrast, when the extracellular osmolality is raised, water flows out from the cells and results in cell shrinkage. Then cells start to restore their volume by the uptake of sodium chloride (regulatory volume increase: RVI). The mechanism of osmotic cell volume regulation has been intensively investigated, and transporters and channels involved in RVD and RVI have been identified [8,9]. Furthermore, cell volume alteration by the osmotic changes have been known to have an impact on various cell functions including cell proliferation, cell apoptosis, metabolism, epithelial transport and migration [1,10].

2.3. Effects of the Osmotic Gradient Between Apical and Basal Sides on the Epithelia

As noted above, osmolality in the apical side changes constantly whereas osmolality in the basal side is kept in a narrow range. This explains why there are often differences of the osmolality between apical and basal sides in most epithelia. Interestingly, the difference of the osmolality (the osmotic gradient across the epithelia) is known to affect various epithelial functions in a different manner from osmotic volume changes. In this paper, we focus on the studies which clearly show that the osmotic gradient between apical and basal sides, but not increase or decrease of osmolality in both sides, affects epithelial functions.

2.3.1. Jejunum

The osmolality in the apical side of the intestinal epithelium drastically changes with the diet, and the osmotic gradient affects transepithelial transport of a jejunal epithelium in a guinea pig [11]. Madara has reported that increase of the osmolality in the apical side with mannitol (up to 600 mOsm) elevates transepithelial electrical resistance (TER) whereas increase of the osmolality in the basal side has no effect on TER and increase of the osmolality in both sides slightly reduces TER [11].

Thus, the osmotic gradient from the apical to basal side is thought to elevate TER. TER reflects ion permeability across the epithelia. There are two pathways for ions across the epithelia: a transcellular pathway via apical and basal cell membranes and a paracellular pathway across intercellular space. The permeability of the paracellular pathway is regulated by tight junctions (TJs) [12–14]. To study the effect of the osmotic gradient on TJs, Madara investigated morphological changes in TJs by freeze-fracture electron microscopy. Apical hyperosmolality induces increase in number and depth of TJ strands (Figure 1A, [11]). Thus, the osmotic gradient from apical to basal side increases transepithelial ion permeability with the morphological changes in TJs in the jejunum. These changes may contribute the regulation of ion absorption in the jejunum.

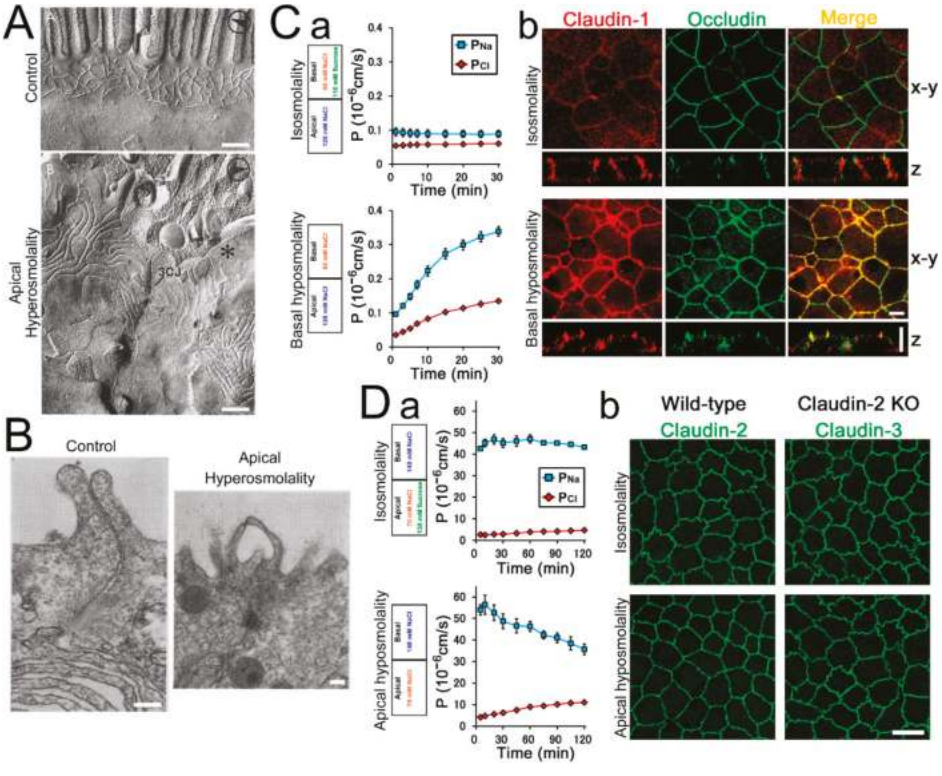

Figure 1. Effects of the osmotic gradient in various epithelia. (**A**) Freeze-fracture electron micrographs in the jejunal epithelium. Apical osmolality was increased to 600 mOsm with mannitol and cells were fixed 20 min after the osmotic changes. Apical hyperosmolality increased tight junction (TJ) strand number and depth. Scale bar = 200 nm. From Madara. *J. Cell Biol.* 1983 [11] with permission. (**B**) Transmission electron micrographs in the bladder epithelium. Apical osmolality was increased with 240 mM urea and cells were fixed 10 min after the osmotic changes. Apical hyperosmolality induced bleb formation between TJ strands. Scale bar = 200 nm. From Wade et al., *Am. J. Physiol.* 1973 [15] with permission. (**C**) Effects of basal hypoosmolality on *Xenopus* A6 cells. (**a**) Basal osmolality was decreased by the reduction of NaCl concentration or counterbalanced by the addition of sucrose, and permeability of sodium and chloride (P_{Na} and P_{Cl}) were calculated from transepithelial resistance and dilution potentials in the presence of Na^+, K^+ and Cl^- channel blockers. Basal hypoosmolality increased P_{Na} and P_{Cl} with the selective increase of P_{Na}. (**b**) Immunofluorescence of claudin-1 and occludin.

Cells were fixed 30 min after the osmotic changes. Basal hypoosmolality altered claudin-1 localization to the apical end and claudin-1 showed colocalization with occludin. Scale bar = 5 μm. Modified from Tokuda et al., *Biochem. Biophys. Res. Commun.* 2008 [16] and Tokuda et al., *Biochem. Biophys. Res. Commun.* 2010 [17] with permission. (**D**) Effects of apical hypoosmolality on Madin–Darby canine kidney (MDCK) II cells. (**a**) Apical osmolality was decreased by the reduction of NaCl concentration or counterbalanced by the addition of sucrose. Apical hypoosmolality induced the reduction of cation selectivity. (**b**) Immunofluorescence of claudin-2 or claudin-3 in wild-type and claudin-2 knockout cells. Cells were fixed 30 min after the osmotic changes. Apical hypoosmolality altered the shape of cell–cell contact from zigzag to more straight shape in wild-type cells but not in claudin-2 knockout cells. Scale bar = 10 μm. Modified from Tokuda et al., *PLoS ONE*. 2016 [18] with permission.

2.3.2. Skin

In the skin, osmolality in the apical side changes with the condition of sweat and drying, and the osmotic gradient affects TER in a frog skin [19,20]. The increase of osmolality in the apical side with mannitol, acetamide, or thiourea reduces TER. In contrast, increase of osmolality in the basal side elevates TER. Increase of osmolality in both sides has almost no effect on TER [19]. The decrease of TER with apical hyperosmolality and the increase of TER with basal hyperosmolality is also reported in another study in a frog skin [20]. Thus, the osmotic gradient from apical to basal side reduces TER whereas that from basal to apical side elevates TER in the skin.

2.3.3. Retina

In the retina, a retinal pigment epithelium (RPE) separates retinal (apical) and choroidal (basal) environment and contributes to a blood–retinal barrier (BRB), which provides proper environment for photoreceptor cells. The osmolality in the choroidal side is higher than retinal side in the physiological condition. When the BRB is disrupted in the pathological conditions such as diabetic retinopathy, the osmolality in the retinal side increases and results in the accumulation of water and macular edema [21].

The osmotic gradient is reported to affect the electrophysiological property of the RPE [22]. To measure the electrophysiological property, a microelectrode was placed inside of and across the RPE and electrophysiological measurement including electroretinogram (ERG) was performed in chick retinas. Apical hyperosmolality with 25 mM mannitol induces depolarization of the basal cell membrane with decrease of membrane resistance and amplifies light-evoked c-wave in ERG. Basal hyperosmolality has opposite effects on these measurements and hyperosmolality in both sides has no effect on c-wave in ERG. Thus, the osmotic gradient affects electrophysiological property of the RPE, which may have a role in the regulation of BRB in the physiological and pathological conditions.

2.3.4. Vascular Endothelium

Endothelia in the brain form the blood–brain barrier (BBB) and restrict the permeation of substances into the brain. Infusion of osmotic agents such as mannitol into the carotid artery is known to induce transient increase of TJ permeability in the endothelia in the BBB [23,24], which is considered as the method to improve the drug delivery into the brain for the treatment of brain tumors and other brain diseases [25–27]. Interestingly, the osmotic gradient causes increase of permeability in the endothelia in bovine major cerebral artery [28]. Apical hyperosmolality with 20% mannitol increases albumin permeability in the endothelia. Basal hyperosmolality also increases albumin permeability. In contrast, hyperosmolality in both sides has no effect on albumin permeability. Thus, the osmotic gradient in both directions increases the albumin permeability in the brain endothelia, and the same mechanism may be involved in the increase of BBB permeability by the infusion of mannitol into the carotid artery.

2.3.5. Bladder

As noted above, the urine osmolality fluctuates in accordance with the amount of free water excretion in the urine, thus the osmolality in the apical side of bladder changes with this fluctuation. The osmotic gradient affects the transepithelial transport of bladder epithelium. In toad bladder, apical hyperosmolality with urea increases the permeability of sucrose and water. Basal hyperosmolality or hyperosmolality in both sides has almost no effect on the permeability of sucrose and reduces water permeability [29]. Interestingly, apical hyperosmolality induces bleb formation between TJ strands (Figure 1B, [15]). The blebs are also formed in basal hypoosmolality but not in basal hyperosmolality, hyperosmolality in both sides, apical hypoosmolality or hypoosmolality in both sides. Thus, the osmotic gradient from apical to basal side increases permeability of sucrose and water with structural changes in TJs, which is thought to contribute the regulation of transepithelial transport in the bladder.

2.3.6. Kidney, Distal Tubule

As noted above, the osmolality of apical and basal sides in renal tubules varies in each segment of nephron, and the osmotic gradient is known to affect transepithelial transport in *Xenupus* A6 cells, a model of distal tubule cells [16,17]. In A6 cells, basal hypoosmolality reduces TER. The permeability of sodium (P_{Na}) is selectively increased than that of chloride (P_{Cl}) (Figure 1C). A counterbalance of the osmotic gradient by adding sucrose eliminates the reduction of TER. Apical hyperosmolality also reduces TER with the selective increase of P_{Na} [16]. The osmotic gradient from apical to basal side also affects the localization of the claudin, a family protein of an integral membrane protein in TJs. Claudins are major constituent of tight junction strands and thought to be a major determinant of TJ permeability [30–32]. In A6 cells, claudin-1 is mainly localized in the entire lateral cell membrane and shows no colocalization with occludin (other TJ protein mainly localized at TJs). The osmotic gradient from apical to basal side alters the localization of claudin-1 to the apical end of the lateral membrane and claudin-1 shows colocalization with occludin (Figure 1C) [17]. In contrast, osmotic gradient from basal to apical side reduces TER with an equal increase in P_{Na} and P_{Cl} [16,17]. The selective increase of P_{Na} by the osmotic gradient from apical to basal side is also observed in Madin–Darby canine kidney (MDCK) I cells, a model of distal tubule cells [18]. Thus, the osmotic gradient from apical to basal side reduce TER with selective increase of P_{Na} in distal tubule cell models, and the regulation of transepithelial transport by the osmotic gradient may have a role in the regulation of ion reabsorption in the distal nephron.

2.3.7. Kidney, Proximal Tubule

Sodium chloride is filtered in the glomerulus and approximately 70% of sodium chloride in the glomerular filtrate is absorbed in proximal tubules. The proximal tubules have high water permeability and the osmotic gradient created by the reabsorption of sodium generates the driving force for water absorption. However, the filtrate in the apical side of the proximal tubules flows before the osmolality in the apical and basal sides become equal and thus the osmolality in the basal side is slightly higher than the apical side in proximal tubules [33–35]. In addition, fluctuation of plasma osmolality in the physiological conditions such as the changes in sodium chloride or blood glucose concentration in the plasma affects the osmolality of the filtrate in the proximal tubules. The osmotic gradient is known to affect the permeability of TJs in MDCK II cells, a model of proximal tubule cells [18]. TJs of MDCK II cells have high ion permeability with cation selectivity. Claudin-2 is expressed in MDCK II cells as well as proximal tubule cells in vivo, and claudin-2 is known to form highly conductive channels with cation selectivity in TJ strands and to be a major determinant of the permeability property of TJs in MDCK II cells [36–38]. Interestingly, apical hypoosmolality induces a reduction of cation selectivity in MDCK II cells (Figure 1D). A counterbalance of the osmotic gradient by adding sucrose or mannitol eliminates the reduction of cation selectivity. Basal hyperosmolality also reduces cation selectivity and basal hypoosmolality, apical hyperosmolality, or hyperosmolality

in both sides does not affect cation selectivity. The expression level of claudin-2 is not changed two hours after the apical hypoosmolality. Thus, the osmotic gradient from basal to apical side is thought to cause the reduction of cation selectivity in MDCK II cells. In addition, the osmotic gradient from basal to apical side induces bleb formation between TJ strands with the changes in actin filaments. Furthermore, the osmotic gradient from basal to apical side alters the shape of cell–cell contact in MDCK II cells from zigzag to more straight shape (Figure 1D). Interestingly, the reduction of cation selectivity, the bleb formation and the alteration in the shape of cell–cell contact are not observed in claudin-2 knockout MDCK II cells, suggesting that claudin-2 mediates these changes. Since claudin-2 is expressed in proximal tubules in vivo, the regulation of charge selectivity in TJs by the osmotic gradient may have a role in the regulation of ion reabsorption in the proximal tubules in the physiological conditions.

2.3.8. Summary

Effects of the osmotic gradient on epithelia and endothelia are summarized in Table 1. The osmotic gradient is involved in the regulation of various cell functions in various epithelia and endothelia. The cell functions regulated by the osmotic gradient include transepithelial transport (paracellula transport in many cases), polarization and resistance of cell membrane, actin filaments and shape of cell–cell contact. Interestingly, the direction of the osmotic gradient which induces cell responses and the regulated cell functions are different among the types of epithelia. Therefore, it is speculated that epithelia distinguish the direction of the osmotic gradient and each epithelium has a different mechanism to regulate cell functions, which is likely to reflect a difference of physiological roles in each epithelium.

Table 1. Effects of the osmotic gradient on epithelia and endothelia.

Organ	Type of the Osmotic Gradient	Cell Response	References
Jejunum	Apical hyper (600 mOsm with mannitol)	TER, TJ strand number↑	[11]
Skin	Apical hyper (210 mM mannitol, acetamide, thiourea)	TER↓	[19,20]
	Basal hyper (210 mM mannitol, acetamide, thiourea)	TER↑	
Retina	Apical hyper (25 mM mannitol)	depolarization, Rt↓ in basal cell membrane	[22]
(RPE)	Basal hyper (25 mM mannitol)	polarization, Rt↑ in basal cell membrane	
Brain	Apical hyper (1100 mM mannitol)	$P_{albumin}$↑	[28]
(Endothelia)	Basal hyper (1100 mM mannitol)	$P_{albumin}$↑	
Bladder	Apical hyper (240 mM Urea)	$P_{sucrose}$↑, P_{H2O}↑	[15,29]
	Apical hyper (240 mM Urea) or Basal hypo	Bleb formation between TJ strands	
Kidney	Basal hypo or Apical hyper (120 mM NaCl)	TER↓, Claudin-1 localization to TJs	[16–18]
(Distal tubule)	Apical hypo or Basal hyper (120 mM NaCl)	TER↓	
Kidney	Apical hypo or Basal hyper (70 mM NaCl)	Cation selectivity↓, Bleb formation between TJ	[18]
(Proximal tubule)		strands, Changes in cell–cell contact shape	
Gallbladder	Apical hyper (100 mM sucrose)	TER↑, $P_{sucrose}$↓, $P_{1,4\text{-butanediol}}$↓	[39]

RPE = retinal pigment epithelium; Hyper = hyperosmolality; Hypo = hypoosmolality; TER = transepithelial electrical resistance; ↑ = increase; ↓ = decrease; TJ = tight junction; P_X = permeability of X; Rt = resistance.

3. Effects of HP on the Epithelia and Endothelia

As shown in Table 1, the osmotic gradient is involved in the regulation of various cell functions in various epithelia and endothelia. If the permeability of the substances used in the studies in Table 1 across the epithelial sheets is lower than water permeability, the concentration difference of the substances is assumed to act as a driving force for the water movement across the epithelia. To put in perspective the magnitude of this, the concentration difference of just 1 mM osmotically active solute (fasting blood glucose level fluctuates from 3.9 to 6.1 mM in the physiological condition) is estimated to be 26 cmH_2O. Surprisingly, HP less than 26 cmH_2O has been reported to have great impact on epithelial functions as we will review here.

3.1. HP in the Body

As in the case of osmolality, HP in the apical side constantly changes in accordance with biological activity. For example, the HP in the apical side of intestine drastically changes with diet. HP in a gallbladder and a bladder changes with the amount of storage (bile and urine, respectively).

In the lung, respiration affects the pressure in the airway and the pressure in the apical side of alveoli periodically becomes negative in inspiration and positive in expiration. In contrast, HP in the basal side (interstitial fluid pressure: IFP) is regulated in a certain range. Most loose tissues have slightly negative IFP (−1 to −3 cmH_2O) and the negative value is relatively high in the lung IFP (−10 cmH_2O). In contrast, IFP in the encased tissues such as kidney shows slightly positive values (0 to 2 cmH_2O) [7,40,41]. Therefore, it is thought that HP is higher in the apical side in most epithelia in the physiological condition and the HP gradient between apical and basal sides fluctuates with the biological activity.

3.2. Effects of HP on Epithelia

3.2.1. Intestine

In the intestine, HP in the apical side dynamically and drastically changes with diet, and water transport in the intestine is affected by the HP gradient. In the isolated dog jejunum and ileum, water is absorbed from the apical to the basal side in normal conditions. The HP from the apical to the basal side up to 20 cmH_2O has no effect on water transport. In contrast, HP from basal to apical side reduces the water absorption dependent on the pressure and the direction of water movement is reversed at 4 cmH_2O [42]. Similar effects of the HP gradient on water transport is observed in a small intestine in a hamster and a colon in a rat [43,44]. Thus, the HP gradient from basal side suppresses water absorption in the intestinal epithelia.

3.2.2. Trachea

Chronic inflammation in the trachea such as asthma is known to increase permeability of airway epithelia. On the other hand, chronic inflammation is also known to increase IFP (see Section 3.4), and the HP gradient from the basal side affects the transepithelial transport in the tracheal epithelia. HP from basal side increases transepithelial conductance (reciprocal of electrical resistance) and permeability of mannitol and albumin in dog tracheal epithelium, transepithelial conductance and permeability of 70 kDa and 2000 kDa dextran in bovine tracheal epithelium, and permeability of 70 kDa dextran in guinea pig tracheal epithelium [45–47]. HP from apical from basal side has no effect on transepithelial transport in dog and bovine tracheal epithelia whereas it induces small increase in the permeability of 70 kDa dextran in guinea pig tracheal epithelium. Thus, the HP gradient from basal side increases the permeability of tracheal epithelium, which may be involved in the pathogenesis of asthma and other airway diseases.

3.2.3. Alveolus

The HP in alveoli periodically alters with respiration. In addition, the pressure is thought to be affected in various clinical conditions such as acute respiratory distress syndrome (ARDS), interstitial pneumonia, and mechanical ventilation. The HP gradient affects transcellular transport in alveolar epithelia. In *Xenopus* alveoli, sodium is absorbed and chloride and potassium are secreted via the epithelial sodium channel (ENaC), chloride, and potassium channels in the apical cell membrane, respectively. The HP from the apical side reduces short-circuit current (Isc) from apical to basal side, the reflection of net ion transport across the epithelia. The HP from the basal side also reduces Isc whereas the increase of the HP in both sides has no effect on Isc, suggesting both directions of the HP gradients reduce Isc. The blocker of ENaC or a chloride channel enhances the reduction of Isc induced by the HP from apical side whereas the potassium channel blocker decreases the reduction of Isc [48,49]. Thus, the HP gradient from apical side increases sodium and chloride secretion and reduces potassium secretion via the transcellular pathway in the alveolar epithelia.

3.2.4. Kidney, Distal Tubule

In the renal tubules, HP is applied from apical side by the flow of filtrate, and the HP gradient is known to affect various cell functions of *Xenopus* A6 cells [50,51]. The HP from basal side increases

transepithelial conductance dependent on the degree of pressure. The HP from basal side also alters the structure of actin filaments and claudin-1 localization at the lateral side, increases cell height and stimulates transcellular chloride secretion (Figure 2A). The HP from apical side or the increase of the HP in both sides does not induce these changes. Thus, the HP gradient from the basal side affects various cell functions including transepithelial conductance, actin structure, claudin-1 localization, cell height, and transcellular transport in A6 cells.

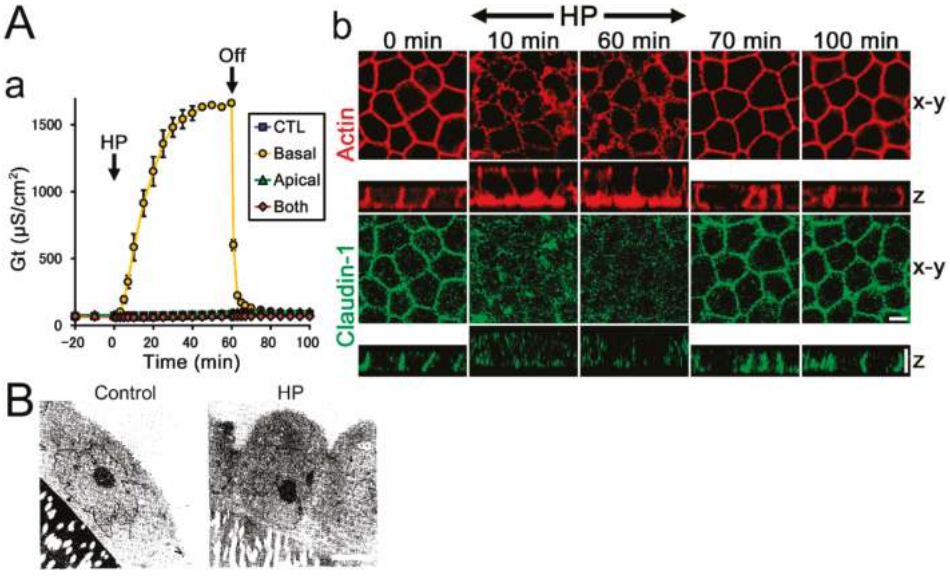

Figure 2. Effects of the hydrostatic pressure (HP) gradient in renal distal tubule cells and podocytes. (**A**) Effects of HP on *Xenopus* A6 cells. (**a**) Time course of transepithelial conductance. 8 cmH_2O HP was applied from apical, basal, or both sides from time 0 to 60 min. The HP from basal side increased transepithelial conductance with reversibility. (**b**) Immunofluorescence of F-actin and claudin-1. 8 cmH_2O HP from basal side was applied from time 0 to 60 min. HP from basal side increased cell height and altered actin structure and claudin-1 localization with reversibility. Modified from Tokuda et al., *Biochem. Biophys. Res. Commun.* 2009 [51] with permission. (**B**) Transmission electron micrographs of podocytes. 1 cmH_2O HP was applied from basal side for three days. Podocyte cells showed more round shape and had wide intercellular space when the HP was applied from basal side. Scale bar = 5 μm. From Coers et al., *Pathobiology.* 1996 [52] with permission.

3.2.5. Glomerulus

In the glomerulus, glomerular epithelial cells (podocytes) play an important role in glomerular filtration. The podocytes have TJs in fetal period, but they develop slit diaphragms, special structure for the glomerular filtration, during the development, and lose TJs [53]. When podocytes are isolated and cultured in vitro, they dedifferentiate and lose various characteristics within 24 h, and they form TJs again. The glomerular filtrate flows from basal to apical side in a podocyte cell sheet in vivo, and the HP gradient from basal side has been reported to affect various characteristics of the podocytes [52]. When podocyte cells from a rat cell line are cultured on a membrane filter and 1 cmH_2O HP is applied from basal side by changing the height of culture medium, the podocyte cell sheet forms a large whirl-like configuration compared with the control (no HP gradient) condition. Furthermore, podocyte cells show more round shape and have wide intercellular space and deep intercellular indentations (Figure 2B). The HP from basal side also induces the reduction of TER and the loss of keratine-18 expression, one of the dedifferentiation markers in the isolated podocytes,

in some cells. Thus, the HP gradient from a the basal side affects various characteristics in podocytes, and it is speculated that these changes may be related to the redifferentiation of podocytes.

3.2.6. Bladder

In the bladder, the HP from an apical side fluctuates with the amount of urine storage. The HP gradient is known to affect transepithelial transport of the bladder epithelium [54–56]. The HP from an apical side increases Isc from apical to basal side whereas HP from a basal side decreases Isc in the bullfrog bladder [54]. The increase of Isc by the HP from apical side is also observed in the rabbit bladder, which is inhibited by ENaC, chloride and potassium channel blockers [55,56]. Thus, the HP gradient from an apical side affects sodium absorption and chloride and potassium secretion in the bladder epithelium, which is thought to contribute to the regulation of ion absorption and excretion in the bladder.

3.2.7. Mammary Gland

In mammary glands, HP in the apical side fluctuates with milk production and breastfeeding and the permeability of TJs in mammary epithelia is known to be affected by the status of milk storage in vivo. The HP gradient has been reported to affect transepithelial transport in cultured mammary epithelial HC11 cells [57,58]. The HP from basal side decreases TER and changes the direction of Isc. The increase of HP in both sides has no effect on TER. Thus, the HP gradient from a basal side affects TER and transcellular transport, which may be involved in the regulation of transepithelial transport in milk production and breastfeeding.

3.2.8. Summary

Effects of the HP gradient on epithelia are summarized in Table 2. There are several reports which show that HP from the apical or basal side affects transepithelial transport in gallbladder, hepatocyte, nasal epithelia, and proximal tubule [59–62]. However, these reports do not have clear data that shows that the gradient is a definitive cause of the changes due to the purpose of the studies and/or the difficulty in an experimental system, and we do not include these studies in the Table 2. Nevertheless, there is a possibility that the HP gradient is also involved in the regulation of cell functions in these epithelia.

As shown in Table 2, the HP gradient is involved in the regulation of various cell functions in various epithelia. The cell functions regulated by the HP gradient include transepithelial transport (transcellular and paracellular transport), cytoskeleton and cell shape. Surprisingly, only several to several tens cmH_2O HP gradients induce various cell responses, which are less than the osmotic pressure induced by the 1 mM concentration difference of the nonionized osmotic substance as a driving force for the water movement (26 cmH_2O). In addition, the HP gradient and the osmotic gradient which are assumed to generate the water movement of a same direction induce different cell responses in some cases (see the cases in the jejunum and the distal tubule in Tables 1 and 2). Therefore, the osmotic gradient and the HP gradient are thought to affect various cell functions through different mechanisms (see Section 4).

Furthermore, the direction of the HP gradient which induces cell responses and the regulated cell functions are different among the types of epithelia. Thus, it is speculated that epithelia distinguish the direction of the HP gradient and each epithelium has a different mechanism to regulate cell functions, which is likely to reflect the difference of physiological roles in each epithelium.

Table 2. Effects of the HP gradient on epithelia.

Organ	Type of HP Gradient	Cell Response	References
Jejunum, ileum	Basal (20 cmH_2O)	Water absorption↓	[42–44]
Trachea	Basal (5–20 cmH_2O)	TER↓, $P_{mannitol}$↑, P_{water}↑, $P_{70kDa\ or\ 2000kDa\ dextran}$↑, $P_{albumin}$↑	[45–47]
	Apical (20 cmH_2O)	$P_{70kDa\ dextran}$↑	
Alveolus	Apical (5 cmH_2O) Basal (5 cmH_2O)	Isc↓, K^+ secretion↓, Na^+ absorption↑, Cl^- secretion↑ Isc↓	[48,49]
Kidney (Distal tubule)	Basal (8 cmH_2O)	TER↓, Cl^- secretion↑, Claudin-1 localization, Actin structure, Cell height	[50,51]
Kidney (Podocyte)	Basal (1 cmH_2O)	Cell shape, TER↓, Expression of keratin-18↓	[52]
Bladder	Apical (1–8 cmH_2O)	Na^+ absorption↑, Cl^- secretion↑, K^+ secretion↑	[54–56]
Mammary gland	Basal (10.2 cmH_2O)	TER↓, Isc↓	[57,58]
Cervical epithelium	Basal (2.1 cmH_2O)	TER↓, $P_{pyranine}$↑	[63]

HP = hydrostatic pressure; TER = transepithelial electrical resistance; ↑ = increase; ↓ = decrease; P_X = permeability of X; Isc = short-circuit current.

3.3. Effects of HP on Endothelia

Relatively high HP is applied to the endothelia from the apical side by the blood flow. The pressure is especially high in the artery (approximately 100 cmH_2O), which fluctuates with heartbeats. There are many reports which show that the HP from apical or the basal side affects various endothelial functions such as transendothelial transport, cell adhesion, cell shape, intracellular Ca^{2+} concentration, expression of cytokines and so on [64–72]. On the other hand, the increase of 50–270 cmH_2O HP to the whole cell by using specialized pressure chamber also affects various endothelial functions including transendothelial electrical resistance, cytoskeletons, cell proliferation, and expression of cytokines and cell adhesion proteins [73–77]. Furthermore, smaller HP (2 to 27 cmH_2O) is also shown to have effects on F-actin and cell proliferation [78–81], although there is a report which shows that 136 cmH_2O HP has no effect on F-actin and cell proliferation in endothelia [82]. Thus, it is important to distinguish the effect of the increase of the HP on whole cell and the effect of the HP gradient on endothelia. However, there is no study which clearly shows that the HP gradient has an effect on endothelial functions. Thus, there is a possibility that HP gradient affects endothelial cell functions, but currently we do not have enough evidence.

3.4. HP in the Pathological Conditions

The HP in the basal side of epithelia (IFP) is known to change in pathological conditions. For example, IFP is markedly decreased in burn to −27 to −42 cmH_2O [83]. Edema induced by raising vascular pressure increases IFP in a dog lung [84]. On the other hand, acute inflammation induces interstitial edema but the IFP is rather decreased transiently by the reduction of tension in the interstitium due to physical denaturation of collagen [85]. In contrast, in chronic inflammation the IFP is known to be increased; experimental inflammation by the ligation of first maxillary molar in rat gingiva and experimental pulpitis in cat dental pulp induce the increase of IFP [86,87]. Meanwhile, the IFP is also increased in cancer tissues. The increase of IFP was reported in xenograft tumor in animals as early as 1950 [88–90]. The IFP is also increased in most human tumors to 14–54.4 cmH_2O [91–96]. The precise mechanism of the increase of IFP in tumors is still incompletely understood, but fibrosis, fluid accumulation and increase of cell density is thought to be involved in the mechanism [97,98]. In addition, the increase of IFP is known to be the factor associated with poor prognosis in uterine cervical cancer [99,100].

It is worth noting that IFP is increased in both chronic inflammation and carcinomas. The causal association between chronic inflammation and carcinomas is reported in almost all organs [101]. The mechanism of the association is generally thought to be due to immune responses induced by the chronic inflammation; reactive oxygen species from immune cells contribute to the occurrence of gene mutation and cytokines secreted by the immune cells promote cell proliferation, inhibition of apoptosis, angiogenesis, metastasis and epithelial mesenchymal transition (EMT) of the carcinomas [101,102].

On the other hand, since IFP is increased in both chronic inflammation and carcinomas, it is thought that the increased IFP may also contribute the promotion of carcinomas in chronic inflammation.

3.4.1. Effects of HP on Tumor Cells

The increase of HP in the extracellular environment by using a specialized pressure chamber is known to affect the characteristics of cancer cells. In osteosarcoma, the increase of 27 to 68 cmH_2O HP induces promotion or suppression of cell proliferation dependent on cell lines. In the cell lines which show the promotion of cell proliferation by the HP, the HP increases sensitivity to cisplatin, elevates the expression of tissue plasminogen activator (TPA) and vascular endothelial growth factor C (VEGF-C), and suppresses the expression of VEGF-A [103–106]. In lung cancer cells (CL1-5 cells and A549 cells), 27 cmH_2O HP increases migration speed and cell volume with the elevation of the expression of various proteins including AQP1, Snail, vinculin and caveolin-1 [107,108]. In urothelial carcinoma cells, 102–1020 cmH_2O HP promotes apoptosis with the elevation of the expression of Fas ligand, toll-like receptor 6 and connective tissue growth factor in the presence of mitomycin C [109,110]. In addition, extremely high HP more than 1 million cmH_2O induces immunogenic cell death in tumor cells and is used for the method in cancer immunotherapy [111,112]. In contrast, small degree of the HP gradient from a basal side has been known to have carcinogenic effects on the epithelia.

3.4.2. Effects of the HP Gradient on Carcinogenic Properties of Epithelia

When epithelia are cultured on permeable filters and the HP gradient is applied from a basal side by changing the height of culture medium, the HP induces epithelial stratification in some epithelial cell lines including MDCK I cells, Caco-2 cells, a model of colon cancer cells, and EpH4 cells, a model of mammary epithelial cells (Figure 3, [113]). The stratification is not observed when the HP is applied from apical side or the HP in both sides are decreased or increased, suggesting the stratification is caused by the HP gradient from basal side. In MDCK II cells, the HP gradient from a basal side does not induce the stratification, indicating the responsiveness of epithelial stratification to the HP gradient is different among the cell types. The stratification continues to develop in the presence of the HP gradient from a basal side, and the elimination of the HP gradient restores the epithelia to an almost single layer in 2 days after the elimination.

Interestingly, cavities with the characteristics of apical cell polarity are formed within the stratified epithelia. Microvilli are observed at the surface of the cavities, and TJs with the functional barrier assessed by the biotin tracer experiment are formed between the cells surrounding the cavities. It is worth noting that a similar abnormality in cell polarity is observed in the epithelia expressing oncogene and in vivo cancer tissue. When K-ras is expressed in MDCK cells and the cells are culture on permeable filters, epithelial stratification is induced and cavities with microvilli and TJs are observed within the stratification [114]. Similar stratification is reported in rat salivary gland cells (Pa-4 cells) when Raf-1 is expressed and cultured on permeable filter [115]. Furthermore, small cavities with microvilli and TJs are observed within pulmonary metastases of the mammary adenocarcinoma induced by the infection of mammary tumor virus in mice, and the permeation of lanthanum nitrate is blocked by these TJs [116]. Therefore, the epithelial stratification and abnormal cell polarity induced by the HP gradient from a basal side are thought to be common characteristics observed in oncogene expressing cells and in vivo carcinomas.

In addition, the HP gradient from a basal side affects cell proliferation and apoptosis. The proportion of S phase cells assessed by the BrdU assay is elevated by the HP gradient from a basal side, indicating the acceleration of a cell cycle. The HP gradient from a basal side also reduces the amount of dead cells in culture supernatant, and the elimination of the HP gradient induces the emergence of numerous TUNEL positive cells from 6 h after the elimination, suggesting the suppression of apoptosis by the HP gradient. In addition, the HP gradient from a basal side decreases TER and increases P_{Na} with the increase of claudin-2 expression level. Furthermore, the epithelial stratification is suppressed by the activation of protein kinase A (PKA) and promoted by the inhibition

of PKA [113]. Thus, the HP gradient from basal side induces abnormal cell polarity, accelerates cell proliferation and suppresses cell apoptosis, resulting in the epithelial stratification via the PKA pathway.

In contrast to the carcinogenic effects of the HP gradient from a basal side, the outcome of the treatment of the bladder carcinoma by the HP suggests the possibility that the HP gradient from an apical side may have an inhibitory effect on carcinomas.

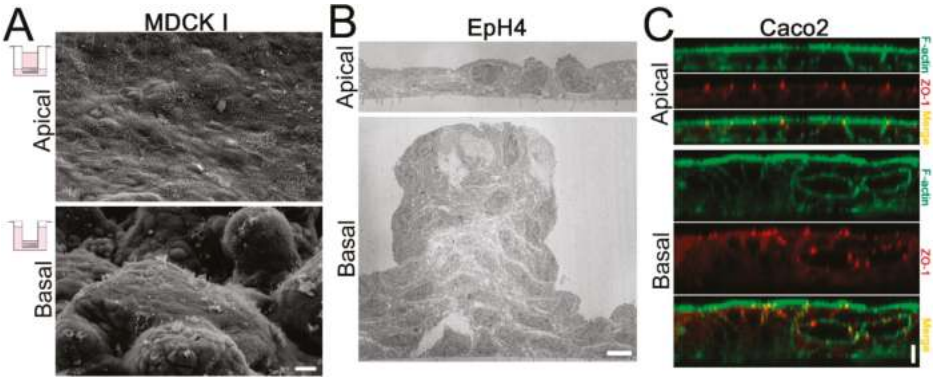

Figure 3. Effects of the HP gradient on carcinogenic properties of epithelia. (**A**) Scanning electron micrographs in MDCK I cells. 0.6 cmH_2O HP was applied from apical or basal side for four days. A bumpy surface with cell masses was observed when the HP was applied from a basal side. Scale bar = 10 μm. (**B**) Transmission electron micrographs in EpH4 cells. 0.6 cmH_2O HP was applied from apical or basal side for four days. HP from a basal side induced stratification. Cavities were observed within the stratification. Scale bar = 5 μm. (**C**) Immunofluorescence of F-actin and ZO-1 in Caco2 cells. 0.6 cmH_2O HP was applied from apical or basal side for eight days. HP from a basal side induced stratification. ZO-1 was localized at the cavities within the stratification. Scale bar = 5 μm. Modified from Tokuda et al., *PLoS ONE*. 2015 [113] with permission.

3.4.3. Treatment of the Bladder Carcinoma by HP from an Apical Side

In 1972, Helmstein developed and introduced a method for the treatment of the bladder carcinoma using HP. In this method, the pressure inside the bladder is kept at the level of diastolic blood pressure for 5–6 h under general anesthesia. Surprisingly, in the studies including the patients with pathological stage T4, the reduction of the tumor has been observed in 70%–100% and complete response has been achieved in 25%–45% [117–121]. The cause of antitumor effect in the HP treatment was speculated to be the ischemia induced by the HP; tumor cells were thought to be more sensitive to the ischemia by the HP than normal cells due to the vulnerability of tumor vessels and changes in metabolism in tumor cells, and the HP from apical side induced cell death only in tumor cells.

The current standard therapy of non-muscle invasive bladder carcinomas is transurethral resection of visible bladder tumor (TURBT) and intravesical instillation of chemotherapy or BCG dependent on the risk factors of recurrence, and the HP treatment for the bladder carcinoma is not performed in current practical clinic. The mechanism of the HP treatment of the bladder carcinoma is still poorly understood, but since the HP gradient from basal side has carcinogenic effects on epithelia and the elimination of the HP gradient induces cell apoptosis [113], it is likely that the HP gradient from apical side in the HP treatment itself may have suppressive effect on tumor cells and contribute to tumor reduction.

3.4.4. Intervention of IFP in Tumors

If the HP gradient from basal side promotes the growth of carcinomas and the elimination of the HP gradient contributes to the treatment of carcinomas, the intervention of the HP gradient in

tumor tissues may be used as the treatment of carcinomas. In the HP treatment of bladder carcinomas, the HP from the apical side is applied under general anesthesia, but it is practically difficult to change the HP in the apical side in other organs. In contrast, various interventions are known to affect the IFP in tumor tissues. In xenograft tumors in mice, hamsters or rats, knockout of Neural/glial antigen 2 (NG2) proteoglycan, hyperthermia (43 °C), and the treatments of the antibody against VEGF receptor-2, ZD6126 (tubulin-binding agent) and inhibitor of platelet-derived growth factor (PDGF) receptor reduce IFP whereas the treatment of angiotensin II elevates IFP [122–127]. However, the mechanism of the increase of IFP in tumor tissues is still not fully understood, and it is difficult to constantly keep the IFP in normal level. Thus, it is currently not feasible to eliminate the HP gradient with the intervention except for the bladder carcinoma. On the other hand, the elucidation of the mechanism in the regulation of epithelial functions by the HP gradient is thought to provide a clue for the alternative method to develop the treatment of carcinomas. Then, how do the epithelia sense the HP gradient?

4. Theoretical Speculation of the Mechanism about How Epithelia Sense Osmotic and HP Gradients

In physiological conditions, there are various differences between the apical and basal environments of the epithelia including osmolality, HP, concentration of various substances, and electrical potential. Steep gradients of osmolality, HP, concentration of various substances, and electrical potential between apical and basal sides are formed at the sites that act as barriers to these differences, and the major barriers are the apical and basal cell membranes and the TJs. It is reasonable to speculate that the sensor(s) of these differences must be located at the site of these steep gradients (Figure 4A). Thus, next we discuss the possibility that either the cell membranes or the TJs act as the sensor of the gradients.

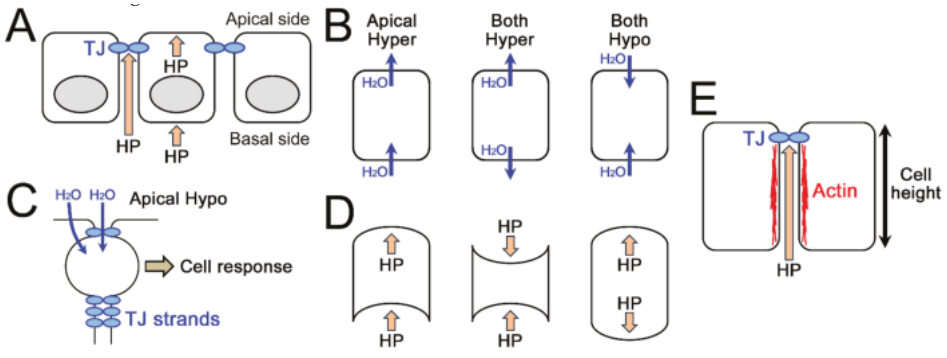

Figure 4. Theoretical speculation of the mechanism about how epithelia sense osmotic and HP gradients. (**A**) A model of epithelium in the HP from basal side. Steep HP gradients are formed at TJs and apical and basal cell membranes. (**B**) The water movement through apical and basal cell membranes in apical hyperosmolality (*left*), hyperosmolality in both sides (*middle*), and hypoosmolality in both sides (*right*). Hyper = hyperosmolality; Hypo = hypoosmolality. (**C**) Possible mechanism of bleb formation between TJ strands in apical hyperosmolality. (**D**) Effects of HP from basal side (*left*), increase of HP in both side (*middle*) and decrease of HP in both sides (*right*) on apical and basal cell membranes. (**E**) Possible effects of HP from basal side on F-actin in the lateral side and cell height.

4.1. Osmolality

The osmotic gradient induces various changes in epithelia (Table 1). It is shown in the studies in Table 1 that either apical or basal hyperosmolality induces cell responses but hyperosmolality in both sides does not induce these responses except for the study in gallbladder. Further, it is also shown that either apical or basal hypoosmolality induces cell response but hypoosmolality in both sides does not induce these responses in the bladder, proximal tubule and distal tubule cells [15–18]. In addition,

the cell responses induced by the osmotic gradient are somewhat different from the responses induced by cell volume changes in hyperosmolality or hypoosmolality [1,10]. Therefore, epithelial cells are thought to sense and respond to the transepithelial osmotic gradient (i.e., the osmotic difference between the two sides) and not merely the overall extracellular osmolality.

First, we will consider the possibility that the apical cell membrane acts as a sensor of apical hyperosmolality. In the apical hyperosmotic condition, water flows out through the apical cell membrane (Figure 4B). In the condition of hyperosmolality in both sides, water also flows out through the apical cell membrane (Figure 4B). If the apical cell membrane is a sensor of the apical hyperosmolality and the water flow through the apical cell membrane induces cell responses, same cell responses should be induced by the hyperosmolality in both sides. However, the cell responses induced by the apical hyperosmolality are not induced by the hyperosmolality in both sides. Thus it is unlikely that the outflow of water through the apical cell membrane by itself is the trigger of cell responses induced by the apical hyperosmolality. Similarly, in the apical hyperosmotic condition, water flows in through the basal cell membrane. In the condition of hypoosmolality in both sides, water also flows in through the basal cell membrane. If the basal cell membrane is a sensor of the apical hyperosmolality and the water flow through the basal cell membrane induces cell responses, same cell responses should be induced by the hypoosmolality in both sides. However, the cell responses induced by the apical hyperosmolality in the bladder and proximal and distal tubule cells are not induced by the hypoosmolality in both sides. Thus it is unlikely that the inflow of water through the basal cell membrane by itself is the trigger of cell responses induced by the apical hyperosmolality (Figure 4B). There remains a possibility that apical and basal membranes act together as a sensor. If this is the case, the possible mechanism is that the water flow from both cell membranes induces the changes in cell membranes, cell shape and/or cytoskeleton and serves as a trigger. However, it may be difficult to distinguish between these changes in the osmotic gradient and those in cell swelling and shrinkage and provide enough sensitivity as a sensor. Therefore, it is not very likely that cell membranes are the sensor of the osmotic gradient.

In contrast, the possibility that TJs act as a sensor of the osmotic gradient is quite plausible. The movement of water and/or osmotic substances through the TJs is assumed to be sensed by TJs. One of the possible mechanisms in this case is that the movement of water and substances through the TJ strands act as shear stress and the shear stress is sensed by the TJ strands. Furthermore, the water movement may cause the accumulation of water between TJ strands because of differences in the water permeability between diffusion across TJ strands and diffusion through the paracellular space between strands, and this water accumulation may serve as a trigger of cell responses (Figure 4C). The bleb formation between TJ strands observed in the presence of the osmotic gradient is thought to support this possibility (Figure 1B, [15,18]). In addition, since TJ permeability is regulated by the osmotic gradient in many cases, TJs may constitute a feedback system in which TJs sense the extracellular environment and regulate the functions of themselves.

4.2. HP

The HP gradient also induces various changes in epithelia (Table 2 and [113]). Some studies in Table 1 show that these changes are not induced by the increase or decrease of HP in both sides [51,52,113]. In addition, the atmospheric pressure fluctuates more than 1 cmH_2O in a day and more than 5 cmH_2O from day to day, and it is unlikely that the fluctuation of atmospheric pressure induces the changes observed in Table 2. Thus, as in the case of osmolality, epithelial cells are thought to distinguish the HP gradient and the changes of HP in both sides.

In the condition of the HP gradient from basal side, it is thought that basal and apical cell membranes are pushed to apical side with the water movement (Figure 4D). In contrast, basal cell membrane is pushed to apical side and apical cell membrane is pushed to basal side with the water movement in the condition that the HP is increased in both sides, and the cell membranes are pushed to opposite direction with the water movement in the condition that HP is decreased in both sides.

Thus, if the cell membranes act as a sensor of the HP gradient, it is unlikely that the push of basal cell membrane to apical side with the water movement by itself or the push of apical cell membrane to apical side by with the water movement itself is the trigger of the responses induced by the HP gradient (Figure 4D). There remains a possibility that the push of apical cell membrane to apical side and basal cell membrane act together as a sensor. If this is the case, the possible mechanism is that as in the case of osmolality, the push of cell membranes induces the changes in cell membranes, cell shape and/or cytoskeleton and serves as a trigger. However, it may be difficult to distinguish between these changes in the HP gradient and those in the increase or decrease of HP in both sides and provide enough sensitivity as a sensor. Therefore, it is not very likely that cell membranes are the sensor of the HP gradient.

In contrast, it is simple to consider the possibility that TJs act as a sensor of the HP gradient. The push of TJ strands to apical or basal side and movement of water through the TJs is sensed by the TJs. One of the possible mechanisms in this case is that the pressure to the TJ strands changes the structure of the intracellular proteins in TJ complexes and the tension applied to the cytoskeleton (Figure 5). The structural changes of F-actin in the lateral side and the increase of cell height by the HP gradient from basal side in *Xenupus* A6 cells may reflect the effect of HP gradient on the tension in F-actin (Figures 2A and 4E, [51]).

In summary, it is likely that TJs act as a sensor of osmotic and HP gradients, although it is difficult to rule out the possibility that apical and basal cell membranes act together as a sensor. Lastly, we further discuss the possible role of TJs as a sensor

4.3. Possible Role of TJs as a Sensor

The TJs are one mode of the junctional complexes located in the most apical part of the complexes [12]. The TJs regulate the permeability of the paracellular pathway [13,14]. Claudins are a family protein of integral membrane proteins (26 members in human) in TJs and a major constituent of TJ strands [30,128,129]. Most epithelia express multiple claudins and expression patterns of claudins are thought to determine the permeability of TJs in each epithelium [31,32]. Most claudins have PDZ binding motif in carboxy-terminal tail and bind to scaffolding proteins in TJs which have PDZ motif such as ZO family proteins, multiple PDZ domain protein (MPDZ) and Pals1-associated tight junction protein (PATJ). These scaffolding proteins further bind to transmembrane proteins including claudins and other proteins, scaffolding proteins, F-actin and many other proteins involved in the regulation of various cell functions including cytoskeleton, transcription, signal transduction, and vesicular trafficking. Thus, TJs is a complex comprised of diverse proteins which are involved in the regulation of various cell functions including cell differentiation, proliferation and apoptosis [130–134].

As discussed above, the sensor of the environmental gradients between apical and basal sides of the epithelia is required to distinguish the direction of the gradient and the difference of the stimulation (such as osmolality and HP) to regulate various cell functions dependent on the physiological requirement in each epithelium. Since claudins are large family proteins and expression patterns of claudins in TJs are different among epithelial and endothelial cell types, TJ strands are thought to be quite diverse among cell types and likely to have the ability to distinguish the direction and the difference of the stimulation dependent on cell types. Furthermore, diverse proteins in TJ complex are thought to be a suitable system to transduce the stimulation sensed by the TJ strands to regulate various cell functions (Figure 5). So far, there is little evidence that shows that TJs act as a sensor of the environmental gradient between apical and basal sides. However, since the changes in the shape of cell–cell contact and F-actin induced by the osmotic gradient from apical to basal side in MDCK II cells are not observed in claudin-2 knockout cells (Figure 1D, [18]), claudin-2 is thought to mediate these changes by the osmotic gradient and likely supports the possibility that TJs act as a sensor. In addition, it is known that the expression pattern of claudins is changed in most carcinomas and changes in the expression level of some claudins affects cell functions such as cell proliferation [135,136]. Since the HP gradient from basal side has carcinogenic effects on epithelia, the altered expression pattern of claudins in

carcinomas may contribute to transduce favorable signals induced by the HP gradient from basal side for cancer growth.

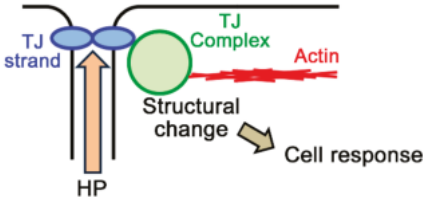

Figure 5. Possible mechanism of TJs as a sensor.

5. Conclusions

Osmotic and HP gradients have great impact on various cell functions in various epithelia. It is required to elucidate the mechanism about how epithelia sense the extracellular environment and regulate cell functions; the mechanism is thought to have physiological and cell biological significance and may contribute to the development of cancer therapy. Theoretical speculation suggests the possibility that TJs are involved in the sensing of osmotic and HP gradients, although obviously more evidence is required. Since TJs are intricate complexes composed of multiple proteins, it is speculated to be challenging to elucidate the mechanism due to the redundancy of many proteins and enormous protein interactions. We expect more examples that indicate the regulation of cell functions by the environmental gradient between apical and basal sides, which may provide a clue for the elucidation of the mechanism.

Funding: This work was supported by JSPS Overseas Research Fellowships to S.T.

Conflicts of Interest: The authors declare no conflict of interest.

Abbreviations

HP	hydrostatic pressure
ADH	antidiuretic hormone
AQP	aquaporin
RVD	regulatory volume decrease
RVI	regulatory volume increase
TER	transepithelial electrical resistance
TJ	tight junction
P_{Na}	permeability of sodium
P_{Cl}	permeability of chloride
MDCK	Madin–Darby canine kidney
RPE	retinal pigment epithelium
BRB	blood–retinal barrier
ERG	electroretinogram
BBB	blood–brain barrier
IFP	interstitial fluid pressure
ARDS	acute respiratory distress syndrome
ENaC	epithelial sodium channel
Isc	short-circuit current
EMT	epithelial mesenchymal transition
TPA	tissue plasminogen activator
VEGF	vascular endothelial growth factor
TURBT	transurethral resection of visible bladder tumor

References

1. Hoffmann, E.K.; Lambert, I.H.; Pedersen, S.F. Physiology of cell volume regulation in vertebrates. *Physiol. Rev.* **2009**, *89*, 193–277. [CrossRef] [PubMed]
2. Swabb, E.A.; Hynes, R.A.; Donowitz, M. Elevated intraluminal pressure alters rabbit small intestinal transport in vivo. *Am. J. Physiol.* **1982**, *242*, 58–64. [CrossRef] [PubMed]
3. Loring, S.H.; Topulos, G.P.; Hubmayr, R.D. Transpulmonary Pressure: The Importance of Precise Definitions and Limiting Assumptions. *Am. J. Respir. Crit. Care Med.* **2016**, *194*, 1452–1457. [CrossRef] [PubMed]
4. Rasouli, M. Basic concepts and practical equations on osmolality: Biochemical approach. *Clin. Biochem.* **2016**, *49*, 936–941. [CrossRef] [PubMed]
5. Sands, J.M.; Layton, H.E. The physiology of urinary concentration: An update. *Semin. Nephrol.* **2009**, *29*, 178–195. [CrossRef] [PubMed]
6. Bankir, L.; Bichet, D.G.; Morgenthaler, N.G. Vasopressin: Physiology, assessment and osmosensation. *J. Intern. Med.* **2017**, *282*, 284–297. [CrossRef] [PubMed]
7. Guyton, A.C.; Hall, J.E. *Textbook of Medical Physiology*, 11th ed.; Elsevier Saunders: Philadelphia, PA, USA, 2006; pp. 187–188, 348–357.
8. Okada, Y.; Maeno, E.; Shimizu, T.; Dezaki, K.; Wang, J.; Morishima, S. Receptor-mediated control of regulatory volume decrease (RVD) and apoptotic volume decrease (AVD). *J. Physiol.* **2001**, *532*, 3–16. [CrossRef] [PubMed]
9. Hoffmann, E.K.; Pedersen, S.F. Cell volume homeostatic mechanisms: Effectors and signalling pathways. *Acta. Physiol.* **2011**, *202*, 465–485. [CrossRef] [PubMed]
10. Lang, F.; Busch, G.L.; Ritter, M.; Völkl, H.; Waldegger, S.; Gulbins, E.; Häussinger, D. Functional significance of cell volume regulatory mechanisms. *Physiol. Rev.* **1998**, *78*, 247–306. [CrossRef]
11. Madara, J.L. Increases in guinea pig small intestinal transepithelial resistance induced by osmotic loads are accompanied by rapid alterations in absorptive-cell tight-junction structure. *J. Cell Biol.* **1983**, *97*, 125–136. [CrossRef] [PubMed]
12. Farquhar, M.G.; Palade, G.E. Junctional complexes in various epithelia. *J. Cell Biol.* **1963**, *17*, 375–412. [CrossRef] [PubMed]
13. Claude, P.; Goodenough, D.A. Fracture faces of zonulae occludentes from "tight" and "leaky" epithelia. *J. Cell. Biol.* **1973**, *58*, 390–400. [CrossRef] [PubMed]
14. Powell, D.W. Barrier function of epithelia. *Am. J. Physiol.* **1981**, *241*, 275–288. [CrossRef] [PubMed]
15. Wade, J.B.; Revel, J.P.; DiScala, V.A. Effect of osmotic gradients on intercellular junctions of the toad bladder. *Am. J. Physiol.* **1973**, *224*, 407–415. [CrossRef] [PubMed]
16. Tokuda, S.; Niisato, N.; Nakajima, K.; Marunaka, Y. Regulation of the paracellular Na+ and Cl- conductances by the NaCl-generated osmotic gradient in a manner dependent on the direction of osmotic gradients. *Biochem. Biophys. Res. Commun.* **2008**, *366*, 464–470. [CrossRef] [PubMed]
17. Tokuda, S.; Miyazaki, H.; Nakajima, K.; Yamada, T.; Marunaka, Y. NaCl flux between apical and basolateral side recruits claudin-1 to tight junction strands and regulates paracellular transport. *Biochem. Biophys. Res. Commun.* **2010**, *393*, 390–396. [CrossRef] [PubMed]
18. Tokuda, S.; Hirai, T.; Furuse, M. Effects of Osmolality on Paracellular Transport in MDCK II Cells. *PLoS ONE* **2016**, *11*, e0166904. [CrossRef] [PubMed]
19. Lindley, B.D.; Hoshiko, T.; Leb, D.E. Effects of D2O and osmotic gradients on potential and resistance of the isolated frog skin. *J. Gen. Physiol.* **1964**, *47*, 773–793. [CrossRef] [PubMed]
20. Ussing, H.H. Relationship between osmotic reactions and active sodium transport in the frog skin epithelium. *Acta. Physiol. Scand.* **1965**, *63*, 141–155. [CrossRef]
21. Willermain, F.; Janssens, S.; Arsenijevic, T.; Piens, I.; Bolaky, N.; Caspers, L.; Perret, J.; Delporte, C. Osmotic stress decreases aquaporin-4 expression in the human retinal pigment epithelial cell line, ARPE-19. *Int. J. Mol. Med.* **2014**, *34*, 533–538. [CrossRef]
22. Shirao, Y.; Steinberg, R.H. Mechanisms of effects of small hyperosmotic gradients on the chick RPE. *Invest. Ophthalmol. Vis. Sci.* **1987**, *28*, 2015–2025. [PubMed]
23. Rapoport, S.I. Effect of concentrated solutions on blood–brain barrier. *Am. J. Physiol.* **1970**, *219*, 270–274. [CrossRef] [PubMed]

24. Nagy, Z.; Pappius, H.M.; Mathieson, G.; Hüttner, I. Opening of tight junctions in cerebral endothelium. I. Effect of hyperosmolar mannitol infused through the internal carotid artery. *J. Comp. Neurol.* **1979**, *185*, 569–578. [CrossRef] [PubMed]
25. Robinson, P.J. Facilitation of drug entry into brain by osmotic opening of the blood–brain barrier. *Clin. Exp. Pharmacol. Physiol.* **1987**, *14*, 887–901. [CrossRef] [PubMed]
26. Rapoport, S.I. Osmotic opening of the blood–brain barrier. *Ann. Neurol.* **1988**, *24*, 677–684. [CrossRef] [PubMed]
27. Kroll, R.A.; Neuwelt, E.A. Outwitting the blood–brain barrier for therapeutic purposes: Osmotic opening and other means. *Neurosurgery* **1998**, *42*, 1083–1100. [CrossRef] [PubMed]
28. Machi, T.; Kassell, N.F.; Scheld, M.W.; Lehmann, G.A. Effect of mannitol on the permeability of cultured endothelial cells. *Fukuoka Igaku Zasshi* **1996**, *87*, 178–183. [PubMed]
29. Urakabe, S.; Handler, J.S.; Orloff, J. Effect of hypertonicity on permeability properties of the toad bladder. *Am. J. Physiol.* **1970**, *218*, 1179–1187. [CrossRef]
30. Furuse, M.; Fujita, K.; Hiiragi, T.; Fujimoto, K.; Tsukita, S. Claudin-1 and -2: Novel integral membrane proteins localizing at tight junctions with no sequence similarity to occludin. *J. Cell Biol.* **1998**, *141*, 1539–1550. [CrossRef]
31. Van Itallie, C.M.; Anderson, J.M. Claudins and epithelial paracellular transport. *Annu. Rev. Physiol.* **2006**, *68*, 403–429. [CrossRef]
32. Günzel, D.; Yu, A.S. Claudins and the modulation of tight junction permeability. *Physiol. Rev.* **2013**, *93*, 525–569. [CrossRef]
33. Green, R.; Giebisch, G. Reflection coefficients and water permeability in rat proximal tubule. *Am. J. Physiol.* **1989**, *257*, 658–668. [CrossRef]
34. Williams, J.C., Jr.; Schafer, J.A. Cortical interstitium as a site for solute polarization during tubular absorption. *Am. J. Physiol.* **1988**, *254*, 813–823. [CrossRef] [PubMed]
35. Schafer, J.A. Transepithelial osmolality differences, hydraulic conductivities, and volume absorption in the proximal tubule. *Annu. Rev. Physiol.* **1990**, *52*, 709–726. [CrossRef] [PubMed]
36. Furuse, M.; Furuse, K.; Sasaki, H.; Tsukita, S. Conversion of zonulae occludentes from tight to leaky strand type by introducing claudin-2 into Madin–Darby canine kidney I cells. *J. Cell Biol.* **2001**, *153*, 263–272. [CrossRef] [PubMed]
37. Amasheh, S.; Meiri, N.; Gitter, A.H.; Schöneberg, T.; Mankertz, J.; Schulzke, J.D.; Fromm, M. Claudin-2 expression induces cation-selective channels in tight junctions of epithelial cells. *J. Cell Sci.* **2002**, *115*, 4969–4976. [CrossRef]
38. Tokuda, S.; Furuse, M. Claudin-2 knockout by TALEN-mediated gene targeting in MDCK cells: Claudin-2 independently determines the leaky property of tight junctions in MDCK cells. *PLoS ONE* **2015**, *10*, e0119869. [CrossRef]
39. Smulders, A.P.; Tormey, J.D.; Wright, E.M. The effect of osmotically induced water flows on the permeability and ultrastructure of the rabbit gallbladder. *J. Membr. Biol.* **1972**, *7*, 164–197. [CrossRef]
40. Scholander, P.F.; Hargens, A.R.; Miller, S.L. Negative pressure in the interstitial fluid of animals. Fluid tensions are spectacular in plants; in animals they are elusively small, but just as vital. *Science* **1968**, *161*, 321–328. [CrossRef]
41. Miserocchi, G.; Passi, A.; Negrini, D.; Del Fabbro, M.; De Luca, G. Pulmonary interstitial pressure and tissue matrix structure in acute hypoxia. *Am. J. Physiol. Lung Cell Mol. Physiol.* **2001**, *280*, 881–887. [CrossRef]
42. Hakim, A.A.; Lifson, N. Effects of pressure on water and solute transport by dog intestinal mucosa in vitro. *Am. J. Physiol.* **1969**, *216*, 276–284. [CrossRef] [PubMed]
43. Wanitschke, R.; Nell, G.; Rummel, W. Influence of hydrostatic pressure gradients on net transfer of sodium and water across isolated rat colonic mucosa. *Naunyn. Schmiedebergs Arch. Pharmacol.* **1977**, *297*, 191–194. [CrossRef] [PubMed]
44. Wilson, T.H. A modified method for study of intestinal absorption in vitro. *J. Appl. Physiol.* **1956**, *9*, 137–140. [CrossRef] [PubMed]
45. Kondo, M.; Finkbeiner, W.E.; Widdicombe, J.H. Changes in permeability of dog tracheal epithelium in response to hydrostatic pressure. *Am. J. Physiol.* **1992**, *262*, 176–182. [CrossRef] [PubMed]
46. Azizi, F.; Matsumoto, P.S.; Wu, D.X.; Widdicombe, J.H. Effects of hydrostatic pressure on permeability of airway epithelium. *Exp. Lung Res.* **1997**, *23*, 257–267. [CrossRef] [PubMed]

47. Gustafsson, B.G.; Persson, C.G. Asymmetrical effects of increases in hydrostatic pressure on macromolecular movement across the airway mucosa. A study in guinea-pig tracheal tube preparations. *Clin. Exp. Allergy* **1991**, *21*, 121–126. [CrossRef] [PubMed]
48. Bogdan, R.; Veith, C.; Clauss, W.; Fronius, M. Impact of mechanical stress on ion transport in native lung epithelium (Xenopus laevis): Short-term activation of Na+, Cl (-) and K+ channels. *Pflugers Arch.* **2008**, *456*, 1109–1120. [CrossRef] [PubMed]
49. Richter, K.; Kiefer, K.P.; Grzesik, B.A.; Clauss, W.G.; Fronius, M. Hydrostatic pressure activates ATP-sensitive K+ channels in lung epithelium by ATP release through pannexin and connexin hemichannels. *FASEB J.* **2014**, *28*, 45–55. [CrossRef]
50. Tokuda, S.; Niisato, N.; Nagai, T.; Taruno, A.; Nakajima, K.; Miyazaki, H.; Yamada, T.; Hosogi, S.; Ohta, M.; Nishio, K.; et al. Regulation of paracellular Na+ and Cl(-) conductances by hydrostatic pressure. *Cell Biol. Int.* **2009**, *33*, 949–956. [CrossRef]
51. Tokuda, S.; Miyazaki, H.; Nakajima, K.; Yamada, T.; Marunaka, Y. Hydrostatic pressure regulates tight junctions, actin cytoskeleton and transcellular ion transport. *Biochem. Biophys. Res. Commun.* **2009**, *390*, 1315–1321. [CrossRef]
52. Coers, W.; Vos, J.T.; Huitema, S.; Dijk, F.; Weening, J.J. Biological alterations of rat podocytes cultured under basolateral hydrostatic pressure. *Pathobiology* **1996**, *64*, 222–232. [CrossRef] [PubMed]
53. Reeves, W.; Caulfield, J.P.; Farquhar, M.G. Differentiation of epithelial foot processes and filtration slits: Sequential appearance of occluding junctions, epithelial polyanion, and slit membranes in developing glomeruli. *Lab. Invest.* **1978**, *39*, 90–100. [PubMed]
54. Stiffler, D.F.; Thornburg, K.L.; Swanson, R.E. Structural and functional responses of the bullfrog urinary bladder to distension caused by hydrostatic pressure gradients. *Arch. Physiol. Biochem.* **2000**, *108*, 405–414. [CrossRef] [PubMed]
55. Ferguson, D.R.; Kennedy, I.; Burton, T.J. ATP is released from rabbit urinary bladder epithelial cells by hydrostatic pressure changes–a possible sensory mechanism? *J. Physiol.* **1997**, *505*, 503–511. [CrossRef] [PubMed]
56. Wang, E.C.; Lee, J.M.; Johnson, J.P.; Kleyman, T.R.; Bridges, R.; Apodaca, G. Hydrostatic pressure-regulated ion transport in bladder uroepithelium. *Am. J. Physiol. Renal Physiol.* **2003**, *285*, 651–663. [CrossRef] [PubMed]
57. Mießler, K.S.; Vitzthum, C.; Markov, A.G.; Amasheh, S. Basolateral pressure challenges mammary epithelial cell monolayer integrity, in vitro. *Cytotechnology* **2018**, *70*, 567–576. [CrossRef]
58. Mießler, K.S.; Markov, A.G.; Amasheh, S. Hydrostatic pressure incubation affects barrier properties of mammary epithelial cell monolayers, in vitro. *Biochem. Biophys. Res. Commun.* **2018**, *495*, 1089–1093. [CrossRef]
59. Eldrup, E.; Frederiksen, O.; Møllgård, K.; Rostgaard, J. Effects of a small serosal hydrostatic pressure on sodium and water transport and morphology in rabbit gall-bladder. *J. Physiol.* **1982**, *331*, 67–85. [CrossRef]
60. Toyota, N.; Miyai, K.; Hardison, W.G. Effect of biliary pressure versus high bile acid flux on the permeability of hepatocellular tight junction. *Lab. Invest.* **1984**, *50*, 536–542.
61. Berg, S.; Wollmer, P.; Andersson, M.; Persson, C.G.; Greiff, L. Effects of experimental changes in nasal airway pressure on mucosal output of plasma. *Clin. Physiol. Funct. Imaging.* **2003**, *23*, 155–158. [CrossRef]
62. Bank, N.; Koch, K.M.; Aynedjian, H.S.; Aras, M. Effect of changes in renal perfusion pressure on the suppression of proximal tubular sodium reabsorption due to saline loading. *J. Clin. Invest.* **1969**, *48*, 271–283. [CrossRef] [PubMed]
63. Gorodeski, G.I. The cultured human cervical epithelium: A new model for studying paracellular transport. *J. Soc. Gynecol. Investig.* **1996**, *3*, 267–280. [CrossRef] [PubMed]
64. DeMaio, L.; Tarbell, J.M.; Scaduto, R.C., Jr.; Gardner, T.W.; Antonetti, D.A. A transmural pressure gradient induces mechanical and biological adaptive responses in endothelial cells. *Am. J. Physiol. Heart Circ. Physiol.* **2004**, *286*, 731–741. [CrossRef] [PubMed]
65. Stamer, W.D.; Roberts, B.C.; Epstein, D.L. Hydraulic pressure stimulates adenosine 3′,5′-cyclic monophosphate accumulation in endothelialcells from Schlemm's canal. *Invest. Ophthalmol. Vis. Sci.* **1999**, *40*, 1983–1988. [PubMed]

66. Lei, Y.; Stamer, W.D.; Wu, J.; Sun, X. Cell senescence reduced the mechanotransduction sensitivity of porcine angular aqueous plexus cells to elevation of pressure. *Invest. Ophthalmol. Vis. Sci.* **2014**, *55*, 2324–2328. [CrossRef] [PubMed]
67. Larsson, B.; Skärby, T.; Edvinsson, L.; Hardebo, J.E.; Owman, C. Vincristine reduces damage of the blood–brain barrier induced by high intravascular pressure. *Neurosci. Lett.* **1980**, *17*, 155–159. [CrossRef]
68. Tsukimoto, K.; Mathieu-Costello, O.; Prediletto, R.; Elliott, A.R.; West, J.B. Ultrastructural appearances of pulmonary capillaries at high transmural pressures. *J. Appl. Physiol.* **1991**, *71*, 573–582. [CrossRef] [PubMed]
69. Patel, M.; Chignalia, A.Z.; Isbatan, A.; Bommakanti, N.; Dull, R.O. Ropivacaine inhibits pressure-induced lung endothelial hyperpermeability in models of acute hypertension. *Life Sci.* **2019**, *222*, 22–28. [CrossRef]
70. Kuebler, W.M.; Ying, X.; Bhattacharya, J. Pressure-induced endothelial Ca(2+) oscillations in lung capillaries. *Am. J. Physiol. Lung Cell Mol. Physiol.* **2002**, *282*, 917–923. [CrossRef]
71. Gan, L.; Doroudi, R.; Hägg, U.; Johansson, A.; Selin-Sjögren, L.; Jern, S. Differential immediate-early gene responses to shear stress and intraluminal pressure in intact human conduit vessels. *FEBS Lett.* **2000**, *477*, 89–94. [CrossRef]
72. Riou, S.; Mees, B.; Esposito, B.; Merval, R.; Vilar, J.; Stengel, D.; Ninio, E.; van Haperen, R.; de Crom, R.; Tedgui, A.; et al. High pressure promotes monocyte adhesion to the vascular wall. *Circ. Res.* **2007**, *100*, 1226–1233. [CrossRef]
73. Prystopiuk, V.; Fels, B.; Simon, C.S.; Liashkovich, I.; Pasrednik, D.; Kronlage, C.; Wedlich-Söldner, R.; Oberleithner, H.; Fels, J. A two-phase response of endothelial cells to hydrostatic pressure. *J. Cell Sci.* **2018**, *131*, jcs206920. [CrossRef]
74. Ohashi, T.; Sugaya, Y.; Sakamoto, N.; Sato, M. Hydrostatic pressure influences morphology and expression of VE-cadherin of vascular endothelial cells. *J. Biomech.* **2007**, *40*, 2399–2405. [CrossRef]
75. Thoumine, O.; Nerem, R.M.; Girard, P.R. Oscillatory shear stress and hydrostatic pressure modulate cell-matrix attachment proteins in cultured endothelial cells. *In Vitro Cell Dev. Biol. Anim.* **1995**, *31*, 45–54. [CrossRef]
76. Hasel, C.; Dürr, S.; Bauer, A.; Heydrich, R.; Brüderlein, S.; Tambi, T.; Bhanot, U.; Möller, P. Pathologically elevated cyclic hydrostatic pressure induces CD95-mediated apoptotic cell death in vascular endothelial cells. *Am. J. Physiol. Cell Physiol.* **2005**, *289*, 312–322. [CrossRef]
77. Shin, H.Y.; Smith, M.L.; Toy, K.J.; Williams, P.M.; Bizios, R.; Gerritsen, M.E. VEGF-C mediates cyclic pressure-induced endothelial cell proliferation. *Physiol. Genomics* **2002**, *11*, 245–251. [CrossRef]
78. Shin, H.Y.; Underwood, R.M.; Fannon, M.W. Fluid pressure is a magnitude-dependent modulator of early endothelial tubulogenic activity: Implications related to a potential tissue-engineering control parameter. *Tissue Eng. Part A* **2012**, *18*, 2590–2600. [CrossRef]
79. Salwen, S.A.; Szarowski, D.H.; Turner, J.N.; Bizios, R. Three-dimensional changes of the cytoskeleton of vascular endothelial cells exposed to sustained hydrostatic pressure. *Med. Biol. Eng. Comput.* **1998**, *36*, 520–527. [CrossRef]
80. Acevedo, A.D.; Bowser, S.S.; Gerritsen, M.E.; Bizios, R. Morphological and proliferative responses of endothelial cells to hydrostatic pressure: Role of fibroblast growth factor. *J. Cell Physiol.* **1993**, *157*, 603–614. [CrossRef]
81. Schwartz, E.A.; Bizios, R.; Medow, M.S.; Gerritsen, M.E. Exposure of human vascular endothelial cells to sustained hydrostatic pressure stimulates proliferation. Involvement of the alphaV integrins. *Circ. Res.* **1999**, *84*, 315–322. [CrossRef]
82. Tworkoski, E.; Glucksberg, M.R.; Johnson, M. The effect of the rate of hydrostatic pressure depressurization on cells in culture. *PLoS ONE* **2018**, *13*, e0189890. [CrossRef]
83. Lund, T.; Wiig, H.; Reed, R.K. Acute postburn edema: Role of strongly negative interstitial fluid pressure. *Am. J. Physiol.* **1988**, *255*, 1069–1074. [CrossRef]
84. Bhattacharya, J.; Gropper, M.A.; Shepard, J.M. Lung expansion and the perialveolar interstitial pressure gradient. *J. Appl. Physiol.* **1989**, *66*, 2600–2605. [CrossRef]
85. Reed, R.K.; Rubin, K. Transcapillary exchange: Role and importance of the interstitial fluid pressure and the extracellular matrix. *Cardiovasc. Res.* **2010**, *87*, 211–217. [CrossRef]
86. Fjaertoft, M.; Johannessen, A.C.; Heyeraas, K.J. Micropuncture measurements of interstitial fluid pressure in normal and inflamed gingiva in rats. *J. Periodontal Res.* **1992**, *27*, 534–538. [CrossRef]
87. Tønder, K.J.; Kvinnsland, I. Micropuncture measurements of interstitial fluid pressure in normal and inflamed dental pulp in cats. *J. Endod.* **1983**, *9*, 105–109. [CrossRef]

88. Young, J.S.; Lumsden, C.E.; Stalker, A.L. The significance of the tissue pressure of normal testicular and of neoplastic (Brown-Pearce carcinoma) tissue in the rabbit. *J. Pathol. Bacteriol.* **1950**, *62*, 313–333. [CrossRef]
89. Boucher, Y.; Baxter, L.T.; Jain, R.K. Interstitial pressure gradients in tissue-isolated and subcutaneous tumors: Implications for therapy. *Cancer Res.* **1990**, *50*, 4478–4484.
90. Boucher, Y.; Jain, R.K. Microvascular pressure is the principal driving force for interstitial hypertension in solid tumors: Implications for vascular collapse. *Cancer Res.* **1992**, *52*, 5110–5114.
91. Roh, H.D.; Boucher, Y.; Kalnicki, S.; Buchsbaum, R.; Bloomer, W.D.; Jain, R.K. Interstitial hypertension in carcinoma of uterine cervix in patients: Possible correlation with tumor oxygenation and radiation response. *Cancer Res.* **1991**, *51*, 6695–6698.
92. Boucher, Y.; Kirkwood, J.M.; Opacic, D.; Desantis, M.; Jain, R.K. Interstitial hypertension in superficial metastatic melanomas in humans. *Cancer Res.* **1991**, *51*, 6691–6694.
93. Less, J.R.; Posner, M.C.; Boucher, Y.; Borochovitz, D.; Wolmark, N.; Jain, R.K. Interstitial hypertension in human breast and colorectal tumors. *Cancer Res.* **1992**, *52*, 6371–6374.
94. Gutmann, R.; Leunig, M.; Feyh, J.; Goetz, A.E.; Messmer, K.; Kastenbauer, E.; Jain, R.K. Interstitial hypertension in head and neck tumors in patients: Correlation with tumor size. *Cancer Res.* **1992**, *52*, 1993–1995.
95. Curti, B.D.; Urba, W.J.; Alvord, W.G.; Janik, J.E.; Smith, J.W., 2nd; Madara, K.; Longo, D.L. Interstitial pressure of subcutaneous nodules in melanoma and lymphoma patients: Changes during treatment. *Cancer Res.* **1993**, *53*, 2204–2207.
96. Nathanson, S.D.; Nelson, L. Interstitial fluid pressure in breast cancer, benign breast conditions, and breast parenchyma. *Ann. Surg. Oncol.* **1994**, *1*, 333–338. [CrossRef]
97. Heldin, C.H.; Rubin, K.; Pietras, K.; Ostman, A. High interstitial fluid pressure—An obstacle in cancer therapy. *Nat. Rev. Cancer* **2004**, *4*, 806–813. [CrossRef]
98. Lunt, S.J.; Fyles, A.; Hill, R.P.; Milosevic, M. Interstitial fluid pressure in tumors: Therapeutic barrier and biomarker of angiogenesis. *Future Oncol.* **2008**, *4*, 793–802. [CrossRef]
99. Milosevic, M.; Fyles, A.; Hedley, D.; Pintilie, M.; Levin, W.; Manchul, L.; Hill, R. Interstitial fluid pressure predicts survival in patients with cervix cancer independent of clinical prognostic factors and tumor oxygen measurements. *Cancer Res.* **2001**, *61*, 6400–6405.
100. Fyles, A.; Milosevic, M.; Pintilie, M.; Syed, A.; Levin, W.; Manchul, L.; Hill, R.P. Long-term performance of interstial fluid pressure and hypoxia as prognostic factors in cervix cancer. *Radiother. Oncol.* **2006**, *80*, 132–137. [CrossRef]
101. Coussens, L.M.; Werb, Z. Inflammation and cancer. *Nature* **2002**, *420*, 860–867. [CrossRef]
102. Hanahan, D.; Weinberg, R.A. Hallmarks of cancer: The next generation. *Cell* **2011**, *144*, 646–674. [CrossRef] [PubMed]
103. Diresta, G.R.; Nathan, S.S.; Manoso, M.W.; Casas-Ganem, J.; Wyatt, C.; Kubo, T.; Boland, P.J.; Athanasian, E.A.; Miodownik, J.; Gorlick, R.; et al. Cell proliferation of cultured human cancer cells are affected by the elevated tumor pressuresthat exist in vivo. *Ann. Biomed. Eng.* **2005**, *33*, 1270–1280. [CrossRef] [PubMed]
104. Nathan, S.S.; DiResta, G.R.; Casas-Ganem, J.E.; Hoang, B.H.; Sowers, R.; Yang, R.; Huvos, A.G.; Gorlick, R.; Healey, J.H. Elevated physiologic tumor pressure promotes proliferation and chemosensitivity in human osteosarcoma. *Clin. Cancer Res.* **2005**, *11*, 2389–2397. [CrossRef]
105. Nathan, S.S.; Huvos, A.G.; Casas-Ganem, J.E.; Yang, R.; Linkov, I.; Sowers, R.; DiResta, G.R.; Gorlick, R.; Healey, J.H. Tumor interstitial fluid pressure may regulate angiogenic factors in osteosarcoma. *J. Orthop. Res.* **2008**, *26*, 1520–1525. [CrossRef] [PubMed]
106. Aung, K.Z.; Pereira, B.P.; Tan, P.H.; Han, H.C.; Nathan, S.S. Interstitial fluid pressure as an alternate regulator of angiogenesis independent of hypoxia driven HIF-1α in solid tumors. *J. Orthop. Res.* **2012**, *30*, 2038–2045. [CrossRef]
107. Kao, Y.C.; Lee, C.H.; Kuo, P.L. Increased hydrostatic pressure enhances motility of lung cancer cells. *Conf. Proc. IEEE Eng. Med. Biol. Soc.* **2014**, *2014*, 2928–2931. [CrossRef]
108. Kao, Y.C.; Jheng, J.R.; Pan, H.J.; Liao, W.Y.; Lee, C.H.; Kuo, P.L. Elevated hydrostatic pressure enhances the motility and enlarges the size of the lung cancercells through aquaporin upregulation mediated by caveolin-1 and ERK1/2 signaling. *Oncogene* **2017**, *36*, 863–874. [CrossRef]
109. Chen, S.K.; Chung, C.A.; Cheng, Y.C.; Huang, C.J.; Ruaan, R.C.; Chen, W.Y.; Li, C.; Tsao, C.W.; Hu, W.W.; Chien, C.C. Hydrostatic pressure enhances mitomycin C induced apoptosis in urothelial carcinoma cells. *Urol. Oncol.* **2014**, *32*, 17–24. [CrossRef]

110. Chen, S.K.; Chung, C.A.; Cheng, Y.C.; Huang, C.J.; Chen, W.Y.; Ruaan, R.C.; Li, C.; Tsao, C.W.; Hu, W.W.; Chien, C.C. Toll-like receptor 6 and connective tissue growth factor are significantly upregulated in mitomycin-C-treated urothelial carcinoma cells under hydrostatic pressure stimulation. *Genet. Test Mol. Biomarkers* **2014**, *18*, 410–416. [CrossRef]
111. Adkins, I.; Hradilova, N.; Palata, O.; Sadilkova, L.; Palova-Jelinkova, L.; Spisek, R. High hydrostatic pressure in cancer immunotherapy and biomedicine. *Biotechnol. Adv.* **2018**, *36*, 577–582. [CrossRef]
112. Shinitzky, M.; Goldman, Y. Immunotherapy of cancer with pressure modified cells. *Isr. Med. Assoc. J.* **2000**, *2*, 615–620. [PubMed]
113. Tokuda, S.; Kim, Y.H.; Matsumoto, H.; Muro, S.; Hirai, T.; Mishima, M.; Furuse, M. Effects of Hydrostatic Pressure on Carcinogenic Properties of Epithelia. *PLoS ONE* **2015**, *10*, e0145522. [CrossRef] [PubMed]
114. Schoenenberger, C.A.; Zuk, A.; Kendall, D.; Matlin, K.S. Multilayering and loss of apical polarity in MDCK cells transformed with viral K-ras. *J. Cell Biol.* **1991**, *112*, 873–889. [CrossRef] [PubMed]
115. Li, D.; Mrsny, R.J. Oncogenic Raf-1 disrupts epithelial tight junctions via downregulation of occludin. *J. Cell Biol.* **2000**, *148*, 791–800. [CrossRef] [PubMed]
116. Pitelka, D.R.; Hamamoto, S.T.; Taggart, B.N. Epithelial cell junctions in primary and metastatic mammary tumors of mice. *Cancer Res.* **1980**, *40*, 1588–1599. [PubMed]
117. Helmstein, K. Treatment of bladder carcinoma by a hydrostatic pressure technique. Report on 43 cases. *Br. J. Urol.* **1972**, *44*, 434–450. [CrossRef] [PubMed]
118. Glashan, R.W. A critical review of the management of bladder neoplasia using a modified form of Helmstein's pressure therapy. *Br. J. Urol.* **1975**, *47*, 57–66. [CrossRef]
119. Hirose, K.; Seto, T.; Takayasu, H. Re-evaluation of hydrostatic pressure treatment for malignant bladder lesions. *J. Urol.* **1977**, *118*, 762–764. [CrossRef]
120. Debré, B.; Steg, A. Hydrostatic distension of the bladder: Technique and indications. 89 cases (author's transl). *Nouv. Presse. Med.* **1981**, *10*, 21–24.
121. Antonsen, H.K.; Lose, G.; Højensgård, J.C. The Helmstein bladder distension treatment for tumours and severe bleeding. *Int. Urol. Nephrol.* **1986**, *18*, 421–427. [CrossRef]
122. Tong, R.T.; Boucher, Y.; Kozin, S.V.; Winkler, F.; Hicklin, D.J.; Jain, R.K. Vascular normalization by vascular endothelial growth factor receptor 2 blockade induces a pressure gradient across the vasculature and improves drug penetration in tumors. *Cancer Res.* **2004**, *64*, 3731–3736. [CrossRef] [PubMed]
123. Skliarenko, J.V.; Lunt, S.J.; Gordon, M.L.; Vitkin, A.; Milosevic, M.; Hill, R.P. Effects of the vascular disrupting agent ZD6126 on interstitial fluid pressure and cell survival in tumors. *Cancer Res.* **2006**, *66*, 2074–2080. [CrossRef] [PubMed]
124. Pietras, K.; Stumm, M.; Hubert, M.; Buchdunger, E.; Rubin, K.; Heldin, C.H.; McSheehy, P.; Wartmann, M.; Ostman, A. STI571 enhances the therapeutic index of epothilone B by a tumor-selective increase of drug uptake. *Clin. Cancer Res.* **2003**, *9*, 3779–3787. [PubMed]
125. Leunig, M.; Goetz, A.E.; Dellian, M.; Zetterer, G.; Gamarra, F.; Jain, R.K.; Messmer, K. Interstitial fluid pressure in solid tumors following hyperthermia: Possible correlation with therapeutic response. *Cancer Res.* **1992**, *52*, 487–490. [PubMed]
126. Ozerdem, U.; Hargens, A.R. A simple method for measuring interstitial fluid pressure in cancer tissues. *Microvasc. Res.* **2005**, *70*, 116–120. [CrossRef] [PubMed]
127. Hori, K.; Suzuki, M.; Saito, S.; Tanda, S.; Zhang, Q.H.; Li, H.C. Changes in vessel pressure and interstitial fluid pressure of normal subcutis and subcutaneous tumor in rats due to angiotensin II. *Microvasc. Res.* **1994**, *48*, 246–256. [CrossRef] [PubMed]
128. Furuse, M.; Sasaki, H.; Fujimoto, K.; Tsukita, S. A single gene product, claudin-1 or -2, reconstitutes tight junction strands and recruits occludin in fibroblasts. *J. Cell Biol.* **1998**, *143*, 391–401. [CrossRef]
129. Mineta, K.; Yamamoto, Y.; Yamazaki, Y.; Tanaka, H.; Tada, Y.; Saito, K.; Tamura, A.; Igarashi, M.; Endo, T.; Takeuchi, K.; et al. Barrier function of epithelia. *FEBS Lett.* **2011**, *585*, 606–612. [CrossRef]
130. Tsukita, S.; Furuse, M.; Itoh, M. Multifunctional strands in tight junctions. *Nat. Rev. Mol. Cell Biol.* **2001**, *2*, 285–293. [CrossRef]
131. Schneeberger, E.E.; Lynch, R.D. The tight junction: A multifunctional complex. *Am. J. Physiol. Cell Physiol.* **2004**, *286*, 1213–1228. [CrossRef]
132. Van Itallie, C.M.; Anderson, J.M. Architecture of tight junctions and principles of molecular composition. *Semin. Cell Dev. Biol.* **2014**, *36*, 157–165. [CrossRef] [PubMed]

133. González-Mariscal, L.; Domínguez-Calderón, A.; Raya-Sandino, A.; Ortega-Olvera, J.M.; Vargas-Sierra, O.; Martínez-Revollar, G. Tight junctions and the regulation of gene expression. *Semin. Cell Dev. Biol.* **2014**, *36*, 213–223. [CrossRef] [PubMed]
134. Zihni, C.; Mills, C.; Matter, K.; Balda, M.S. Tight junctions: From simple barriers to multifunctional molecular gates. *Nat. Rev. Mol. Cell Biol.* **2016**, *17*, 564–580. [CrossRef] [PubMed]
135. Turksen, K.; Troy, T.C. Junctions gone bad: Claudins and loss of the barrier in cancer. *Biochim. Biophys. Acta* **2011**, *1816*, 73–79. [CrossRef] [PubMed]
136. Bhat, A.A.; Uppada, S.; Achkar, I.W.; Hashem, S.; Yadav, S.K.; Shanmugakonar, M.; Al-Naemi, H.A.; Haris, M.; Uddin, S. Tight Junction Proteins and Signaling Pathways in Cancer and Inflammation: A Functional Crosstalk. *Front. Physiol.* **2019**, *9*, 1942. [CrossRef] [PubMed]

International Journal of
Molecular Sciences

MDPI

Review

The Blood–Brain Barrier and Its Intercellular Junctions in Age-Related Brain Disorders

Laura Costea [1], Ádám Mészáros [2,3], Hannelore Bauer [4], Hans-Christian Bauer [5], Andreas Traweger [5], Imola Wilhelm [1,2], Attila E. Farkas [2,6,*,†] and István A. Krizbai [1,2,*,†]

1 Institute of Life Sciences, Vasile Goldiş Western University of Arad, 310414 Arad, Romania; laura.m.costea@gmail.com (L.C.); wilhelm.imola@brc.hu (I.W.)
2 Institute of Biophysics, Biological Research Centre, 6726 Szeged, Hungary; meszaros.adam@brc.hu
3 Doctoral School of Biology, University of Szeged, 6726 Szeged, Hungary
4 Department of Biological Sciences, University of Salzburg, 5020 Salzburg, Austria; hannelore.bauer@sbg.ac.at
5 Institute of Tendon and Bone Regeneration, Paracelsus Medical University—Spinal Cord Injury and Tissue Regeneration Center Salzburg, 5020 Salzburg, Austria; hans.bauer@pmu.ac.at (H.-C.B.); andreas.traweger@pmu.ac.at (A.T.)
6 Department of Physiology, Anatomy and Neuroscience, University of Szeged, 6726 Szeged, Hungary
* Correspondence: farkas.attilae@brc.hu (A.E.F.); krizbai.istvan@brc.hu (I.A.K.); Tel.: +36-62-599601 (A.E.F. & I.A.K.)
† These authors contributed equally to this study.

Received: 12 October 2019; Accepted: 1 November 2019; Published: 3 November 2019

Abstract: With age, our cognitive skills and abilities decline. Maybe starting as an annoyance, this decline can become a major impediment to normal daily life. Recent research shows that the neurodegenerative disorders responsible for age associated cognitive dysfunction are mechanistically linked to the state of the microvasculature in the brain. When the microvasculature does not function properly, ischemia, hypoxia, oxidative stress and related pathologic processes ensue, further damaging vascular and neural function. One of the most important and specialized functions of the brain microvasculature is the blood–brain barrier (BBB), which controls the movement of molecules between blood circulation and the brain parenchyma. In this review, we are focusing on tight junctions (TJs), the multiprotein complexes that play an important role in establishing and maintaining barrier function. After a short introduction of the cell types that modulate barrier function via intercellular communication, we examine how age, age related pathologies and the aging of the immune system affects TJs. Then, we review how the TJs are affected in age associated neurodegenerative disorders: Alzheimer's disease and Parkinson's disease. Lastly, we summarize the TJ aspects of Huntington's disease and schizophrenia. Barrier dysfunction appears to be a common denominator in neurological disorders, warranting detailed research into the molecular mechanisms behind it. Learning the commonalities and differences in the pathomechanism of the BBB injury in different neurological disorders will predictably lead to development of new therapeutics that improve our life as we age.

Keywords: aging; blood–brain barrier; tight junction

1. Introduction

Aging and age-related co-morbidities are rapidly increasing unresolved health and socio-economic problems in developed countries. Decline of cognitive brain functions represents one of the main health challenges of aging and includes vascular and neurodegenerative dementias such as Alzheimer's or Parkinson's disease.

The functional state of the central nervous system (CNS) is greatly dependent on the quality of the vasculature. As the centuries old saying goes: "A man is as old as his arteries". Today, especially for the brain, this concept should be redefined: You are as old as your microvessels and capillaries [1]. There is increasing evidence that the cerebral microvasculature and the neurovascular unit play a critical role in age-related brain dysfunctions. The multitude of brain microvascular changes accompanied by aging includes endothelial dysfunction, blood–brain barrier (BBB) breakdown, decrease in blood flow, microhemorrhages, vessel rarefication and neurovascular uncoupling. In this review, our main focus is the breakdown of the paracellular barrier and tight junctions.

2. Cells of the Neurovascular Unit (NVU)

The vasculature in the brain forms a functional unit with the surrounding neural tissue, thus the term neurovascular unit was coined [2]. A functionally intact neurovascular unit (NVU) is a prerequisite for the proper function of the CNS. The most important cellular components of the NVU are cerebral endothelial cells, pericytes, astrocytic endfeet and neurons; however, other cellular elements like microglia may also play a modulatory role. The main role of the NVU besides neurovascular coupling is the formation of the BBB.

Cerebral endothelial cells (CECs) lining brain capillaries are considered the principal barrier forming endothelial cells. They are interconnected by a continuous line of tight junctions and characterized by a high number of mitochondria and low number of caveolae [3–5]. These characteristics contribute to the formation of a paracellular and transcellular barrier.

Pericytes are localized in the duplication of the basement membrane covering the basal surface of the endothelium. The estimates of pericyte coverage show large variations in the literature [6,7]. Pericytes can secrete a large number of substances that may influence endothelial function including TGFβ, angiopoetin-1 or VEGF. It seems that the differentiation stage of pericytes determines their effect on the endothelium as well [8]. The role of pericytes in the formation of the BBB is supported by the finding that absence of pericytes leads to endothelial hyperplasia, abnormal vasculogenesis and an increased BBB permeability [9,10].

Although the role of astrocytes in the formation of the physical barrier is limited, due to their influence on cerebral endothelial cells they play an important role in the maintenance of the BBB [11]. The astrocytic endfeet ensheath the brain vasculature almost completely [12] and express the water channel protein, aquaporin 4, which is suggested to play a crucial role in creating a bulk flow in the brain parenchyma from arterioles towards venules. This flow was shown to contribute to the clearance of extracellular proteins and metabolic waste products through the newly rediscovered glymphatic system [13,14]. Despite much interest in the glymphatic system, some experimental results do not support or even contradict its function [15]. Thus further refining of the glymphatic hypothesis is likely necessary [16]. Nevertheless, the aquaporin 4 in astrocytic endfeet is indispensable to BBB function as its knockout results in altered brain microvasculature and decreased water exchange through the BBB [17], furthermore its subcellular distribution shows an age dependent depolarization accompanied by decreased protein clearance [18].

The BBB is in the forefront of the defense line of the CNS and restricts the free movement of solutes and cellular elements between the systemic circulation and neuronal tissue. The BBB is involved in the pathogenesis of a large number of CNS disorders [19].

Cell types comprising the NVU are in close communication in order to maintain physiologic function and react to pathologies. Ligand-receptor type intercellular interactions and ion channels were described early as pathways that coordinate the function of the cell types constituting the NVU [20]. An example of bidirectional information exchange is the role of CD146 in coordinating the development of pericyte coverage on brain vasculature during early ontogenesis. At first CD146 is expressed by endothelial cells but as pericyte coverage increases, CD146 expression shifts to pericytes where it acts as a co-receptor of PDGFRβ. Endothelia attached pericytes down-regulate endothelial CD146 via TGFβ1 secretion, promoting BBB maturation [21]. Recently a growing body of evidence suggests that extracellular vesicle—mainly exosome—mediated bidirectional communication coordinates key functions of the NVU at the local and systemic level as well [22–25]. In a mouse model of spinal cord injury, pericyte-derived exosomes improved microcirculation and protected barrier function [26]. In response to traumatic brain injury, the loss of pericytes and consequent impairment of crosstalk among NVU cells causes barrier dysfunction, brain edema and leakage of cerebral vasculature. A recent example of pericyte to endothelial cell communication in the retina is the circular RNA cPWWP2A that is synthesized in pericytes and downregulates angiopoietin 1, occludin and sirtuin-1expression in endothelial cells by sequestering miRNA-579 [27].

3. Brain Capillaries in Aging

With aging, the density of brain vasculature is decreased and cerebrovascular dysfunction appears to precede and accompany cognitive dysfunction and neurodegeneration. Cerebrovascular angiogenesis is decreased and cerebral blood flow is inhibited by anomalous blood vessels such as tortuous arterioles and thick collagen deposits in the walls of veins and venules [28].

In most mammals, the capacity of CECs to divide is limited and endothelial cells are prone to be senescent. Aging is associated with endothelial dysfunction, arterial stiffening and remodeling, impaired angiogenesis, defective vascular repair and with an increasing prevalence of atherosclerosis [29]. In the aging brain cerebral blood flow declines and perfusion pressure either is constant or increases. In Brown-Norway and Fisher 344/Brown-Norway rats that maintain a relatively consistent cortical volume throughout life the densities of arterioles and arteriole-to-arteriole anastomoses on the cortical surface was found to be decreased with age [30]. In a spontaneously hypertensive rat model, long term hypertension was found to gradually destroy BBB, resulting in white matter lesions, one of the most important pathological changes in vascular dementia [31]. At the capillary level, increased capillary diameters and decreased capillary density paired with increased red blood cell velocities were observed [28,32]. Some capillary density measurements in humans contradict these observations, as no changes were observed in the intervascular distance on CD31 stained brain sections [33].

4. Junctional Proteins in Aging and Related Disorders

The paracellular barrier properties of CECs are determined by the tight junction (TJ), which are composed of transmembrane proteins that control the transport across the intercellular space between adjacent cells and cytoplasmic plaque. Claudin 5, member of the 27 strong claudin family, is primarily responsible for controlling the paracellular transport of water and small molecules through capillary vessel walls [34]. Other claudins may contribute to BBB function as well, though the isoforms present in human and murine brain vessels is still under investigation [35,36]. Like claudins, MARVEL (MAL and related proteins for vesicle trafficking and membrane link) proteins especially occludin play a role in restricting paracellular transport and also regulate homeostasis and TJ organization [37–40]. The third group of integral membrane proteins of the TJ belongs to the CTX (cortical thymocyte marker in *Xenopus*) family within the immunoglobulin superfamily such as junctional adhesion molecules (JAM) and coxsackie and adenovirus receptor (CAR). Integral membrane proteins of the TJ are coupled to cytoplasmic plaque proteins that provide a platform for anchoring the junction to the cytoskeleton and for interactions with signaling molecules. The main components of the cytoplasmic plaque are zonula occludens (ZO) proteins [41–43].

Junctional proteins are not restricted to the endothelial cells of the NVU. Recently, pericytic occludin was described in a new role as a NADH oxidase enzyme and an important player in BBB pericyte metabolism including the modulation of pericyte energy sharing with other NVU components via intercellular transport of mitochondria and glucose [44]. Astrocytic occludin was described two decades ago [45], and a recent report proposed a new role for it in RNA metabolism [46]. Astrocytic TJ, composed of claudin 1, 4 and JAM may also form in inflammation to control lymphocyte segregation [47].

4.1. TJ in Aging and Aging Models

Limited data is available on what changes develop in the function of the BBB and the composition and structure of endothelial TJs in the healthy aging human brain. In a meta-analysis of BBB permeability studies, the barrier function was negatively impacted by age. Though there were some discrepancies, paracellular permeability was generally increased in the aged human brain [48]. Multiple accelerated aging animal models are available to complement this data, which we will discuss mainly together with the appropriate aging associated disorders in later paragraphs. Literature data presented in this chapter are summarized in Table 1. In the review we will include large molecule (e.g., albumin or Evans blue albumin) permeability and blood component extravasation as well even though these are not markers of TJ dysfunction but rather indicate transcellular transport or disruption of the vascular wall respectively.

Table 1. Blood–brain barrier (BBB) function and junctional proteins in aging.

Experimental System	Claudin 5	Occludin	ZO-1	Permeability	Other	Authors
BubR1 accelerated aging, cell culture	Discontinuous immunofluorescence for all three.					Baker et al., 2011 [49]
aged mouse and human brain tissue	fragmented, weak immunofluorescence, reduced protein level.		fragmented, weak immunofluorescence	increased 3kDa dextran permeability rescued by sirtuin-1 overexpression.		Stamatovic et al., 2019 [50]
sirtuin-1 overexpression	rescued by sirtuin-1 overexpression					
sirtuin-1 knockdown	reduced claudin 5 mRNA and protein			increased		
senescent female rats				Evans blue extravasation, hippocampus, olfactory bulb		Bake and Sohrabji 2004 [51]
senescent rats	weaker and discontinuous immunofluorescence in hippocampal vessels in senescent compared to young female rats. No change in middle aged vs. young male rats	no change in reproductive senescent vs. young female rats			age and gender dependent IgG extravasation, e.g., increased IgG extravasation in senescent female rat thalamus	Bake et al., 2009 [52]
postmenopausal women	altered distribution					
ovariectomized rats			unaffected	increased	connexin43 redistribution	Wilson et al., 2008 [53]
+estrogen replacement				rescued	rescued	
Pdgfrβ+/−, pericyte deficient mice	All three decreased.					Bell et al., 2010 [54]
24-month-old rats, compared to 12-months-old		protein decreased, mRNA unaffected	mRNA increased, protein unaffected			Mooradian et al., 2003 [55]
24-month-old rats, compared to 3-months-old		protein decreased, mRNA unaffected	protein unaffected			
mouse primary brain microvessel endothelial culture. disrupted endothelial integrin/basal lamina interaction	decreased			increased		Osada et al., 2011 [56]
integrin α5 knockout mice	increased mRNA			improved barrier	resistant to MCAO induced stroke	Roberts et al., 2017 [57]

Experimental results linking BBB dysfunction to declining cognitive function prompted the use of modern in vivo imaging such as dynamic contrast enhanced magnetic resonance imaging to study cerebrovascular permeability. A recent work revealed an age dependent BBB permeability increase in the hippocampus of individuals without any cognitive impairment, which was exacerbated in the case of mild cognitive impairment of Alzheimer's, Huntington's and multiple sclerosis patients [58].

Permeability changes are likely the result of decreased expression and disorganized localization of TJ proteins. As shown in the BubR1 hypomorphic murine model of accelerated aging, claudin 5, occludin and ZO-1 expression of cortical and striatal microvessels were decreased in aged mice, with reactive astrogliosis also apparent at the vessels. BubR1 is a key member of the mitotic checkpoint that ensures accurate chromosome segregation [49]. In an experiment using cells isolated from BubR1 hypomorphic mice, aged CECs (co-cultured with pericytes) showed a discontinuous junctional staining for claudin 5, occludin and ZO-1 and the presence of abnormal cells with smaller cytoplasm that are highly immune-reactive for TJ proteins [59]. The BubR1 hypomorphic CECs also showed increased number of spikes in the claudin 5 staining, reminiscent to those previously described as budding and docking sites for claudin bearing vesicles [60].

Aged mouse and human brains both showed fragmented and weak claudin 5 and ZO-1 staining in microvessels compared to healthy young controls, with an accompanying reduction of claudin 5 protein expression. BBB permeability to 3 kDa dextran was also increased in aged mice. Both claudin 5 levels and BBB function were rescued in transgenic mice overexpressing sirtuin-1, a NAD-dependent deacetylase, while inducible, endothelial-specific knockdown of sirtuin-1 increased barrier permeability and reduced claudin 5 mRNA and protein levels [50]. These results add a novel mode in which sirtuin-1 affects longevity and neurological disorders by maintaining BBB integrity [61,62].

Barrier function of the cerebral vasculature was shown to be under the control of estrogen [63]. Thus, a potential influence of the age-dependent decline of estrogen levels on BBB integrity in postmenopausal women or reproductive senescent female animals appeared plausible. In this context, Bake and Sohrabji [51] showed enhanced extravasation of Evans Blue-albumin in the hippocampus and olfactory bulb of reproductive senescent female rats. Moreover, the localization of the tight junction protein claudin 5 in hippocampal microvessels was affected in senescent female rats compared to young adult ones. In case of human brain microvessels, disrupted distribution and poor junctional localization of claudin 5 was altered in postmenopausal women, in contrast to premenopausal women [52]. Further confirmation to suggest that reproductive hormones regulate BBB permeability came from studies with ovariectomized rats [53]. While expression of ZO-1 was unaffected, redistribution and increased expression of connexin-43 was observed following ovariectomy. Estrogen replacement to young (4 months old) ovariectomized rats restored BBB function, while reproductive senescent animals did not benefit from estrogen treatment or even showed increased BBB permeability in the hippocampus [53].

Further evidence of age-related junctional alterations at the BBB came from a study showing that the cerebral occludin protein content in total cerebral tissue extracts from 24-month-old rats was significantly reduced compared to 12-month-old or 3-month-old male rats without a corresponding change in occludin mRNA. ZO-1 protein levels were found to be unchanged while ZO-1 mRNA was significantly increased in 24-month-old rats compared to 3-month-olds [55].

By using transmission electron microscopy, a decline in the pericytic coverage of aged capillaries has been described over thirty years ago [64]. Beyond the assumption that the age-dependent loss of pericytes decreases the ability of the BBB to compensate for transient leaks, there is evidence that pericytes regulate the expression of TJ/BBB-specific proteins in microvascular endothelial cells. A comparison of claudin 5, ZO-1 and occludin expression in 6–8 month old Pdgfrβ+/− mice has revealed significant reductions of protein expression in pericyte-deficient mice compared to controls [54]. Therefore, it is likely that aging-associated TJ dysregulation may be partly the consequence of pericyte loss.

Integrins are heterodimeric proteins that anchor cells to the extracellular matrix and are involved in ligand dependent bidirectional signaling between the cell and its environment thus playing important roles in all cell functions. Researchers have found connections between integrins and aging [65,66] and neurological disorders [67]. Disruption of cerebral endothelial integrin interaction with the basal lamina lead to decreased claudin 5 levels and BBB integrity [56]. Recently, integrin α5 knockout mice were found resistant to transient middle cerebral artery occlusion (MCAO) induced ischemic stroke with a small initial infarct volume that disappeared within 3 days. The α5 knockout animals showed improved barrier function and higher claudin 5 mRNA levels compared to controls [57].

CTX family proteins have not been directly linked to aging; however, some play important roles in the brain development and function or tumorigenesis and invasiveness. JAM-A in CECs undergoes subcellular relocalization in response to inflammatory stimuli [68] and its levels are reduced in response to brain injury [20]. JAM3 was found to be essential for BBB integrity and for normal lens development in humans. Homozygous mutations of JAM3 in humans led to brain hemorrhage and brain calcification [69], the latter being somewhat similar to calcification in the basal ganglia in occludin knockout mice [70]. Brain endothelial function of CAR is scarcely known. However, it was found to play key roles in neurons in synapse development in the postnatal and adult brain and its loss contributes to cognitive defects [71,72].

4.2. Brain Endothelial TJ in Ischemic Injury

In the healthy brain, practically every neuron has a capillary running next to it. With the rarefaction of capillaries in aging brain, the ability to maintain homogeneous flow during periods of localized ischemia is reduced. Hypoxia and reoxygenation are important components of many disorders that affect the central nervous system, including stroke and dementia [73–75]. The incidence of stroke is increased with age and the prognosis of elderly stroke patients is unfavorable compared to young adults [76,77]. Literature data regarding TJs presented in this chapter are summarized in Table 2.

Table 2. BBB function and junctional proteins in age related disorders, ischemic injury and immune system.

Experimental System	Claudin 5	Occludin	ZO-1	Permeability	Other	Authors
hypoxia, 8% O_2, mouse, brain lysate	unaffected	decreased protein levels disrupted immunofluorescence for both	unchanged protein levels	Na-fluorescein leakage increased	MMP and VEGF dependence	Bauer et al., 2010 [78]
hypoxia in primary bovine brain microvessel endothelial culture		membrane localization perturbed	ZO2 membrane localization perturbed, ZO1 and ZO2 diffuse cytosolic staining	sucrose permeability increased	actin stress fibers, increased actin protein	Mark and Davis 2002 [79]
H_2O_2 ROS +GM6001	unaffected	phosphorylation change, degradation rescues degradation			TEER increase does not rescue	Lischper et al., 2010 [80]
hypoxia/reoxygenation modeled by DMNQ treatment of primary mouse brain microvessel endothelial culture		protein decreased				Krizbai et al., 2005 [81]
hypoxia in bEND.3	altered localization, decreased protein			increased		Koto et al., 2007 [82]
reactive oxygen species	altered localization, decreased protein for both				xanthine oxidase and 100 μM hypoxanthine	Schreibelt et al., 2007. [83]
MCAO, 12 months vs. 2 months old mice	decrease in both age groups, after 3 days less protein in old compared to young		decrease in both age groups, after 1 and 3 days less protein in old	larger Evans blue extravasation in old with stroke		Shen et al., 2019 [84]
young adult rats hypoxia/reoxygenation		phosphorylation	no change in protein	increased		Witt et al., 2003 [85]
young adult rats hypoxia/reoxygenation as above + free radical scavenger tempol		disrupted rescued				Lochhead et al., 2010 [73]
young adult rats hypoxia/reoxygenation	disrupted localization, slightly increase membrane fraction	disrupted localization, slightly increase membrane fraction	disrupted localization	PKC-dependent focal BBB leakage		Willis et al., 2010 [86]
EGFP-Claudin 5 transgenic mouse tMCAO after 24–30 hours after 48–58 hours	eGFP-claudin 5 no change eGFP-claudin 5 non membrane	no change reduced	no change reduced		Claudin 5 transgene protein expression is double of wild type.	Knowland et al., 2014 [87]

Table 2. *Cont.*

Experimental System	Claudin 5	Occludin	ZO-1	Permeability	Other	Authors
600–950 g rats compared to 200–250 g rats		degradation				Kaur et al., 2011 [88]
MCAO, both ages	slightly increased phosphorylation					
tPA after reperfusion, only in old	greatly increased phosphorylation	increased degradation				
rat tMCAO +PP2 Src kinase inhibitor, brain tissue	time dependent decrease of claudin 5 protein and mRNA was rescued by PP2			brain lysate protein decrease was significant from 24, mRNA from 72 hours and persisted 7 days later, fibrinogen leakage from brain coincided claudin 5 decrease and vas rescued by PP2		Bai et al., 2014, [89]
rat microsphere embolism, capillary lysate		decreased amount, increased phosphorylation 6–72 h after microsphere injection	decreased amount	albumin leakage starting from 48 hours		Kago et al., 2006 [90]
rat microsphere embolism, capillary lysate, +PP2		decreased amount and increased phosphorylation rescued by PP2		albumin leakage 6-24h, rescued by PP2		Takenaga et al., 2009 [91]
spontaneously hypertensive rats tMCAO, brain sections	rapid reorganization in localization 3 h after reperfusion + MMP2 activity at vessels. Protein appeared in astrocytes.			Increased gelatinase activity 3 h after reperfusion, rescued by MMP2 inhibition.		Yang et al., 2007, Yang and Rosenberg 2011 [92,93]
brain lysate	decreased mRNA, degraded protein rescued by BB-1101 MMP inhibitor					
spontaneously hypertensive rats tMCAO+GM6001 MMP inhibitor	protein levels were rescued for all three					Yang et al., 2013 [94]
Primary human brain microvascular endothelial cells+PARP inhibition	increased protein levels for both					Rom et al., 2015 [95]

Table 2. *Cont.*

Experimental System	Claudin 5	Occludin	ZO-1	Permeability	Other	Authors
spontaneously hypertensive rats tMCAO + mynocicline	increased protein levels for all three					Yang et al., 2015 [96]
SRF, MRTF-A/-B knockdown hemorrhagic stroke model, whole brain tissue	claudin1, 3, 5 and 12 mRNA and claudin5 protein downregulated		ZO-2 and ZO-3 mRNA downregulated, ZO-1 unaffected			Weinl et al., 2015 [97]
bovine brain microvessel endothelial cells +VEGF		distribution changed from membrane to cytoplasm, protein levels increased		permeability increase, resistance decrease		Wang et al., 2001 [98]
adenoviral expression of IL-1 in VEGFA knockout mouse	VEGFA KO rescued protein expression of brain microvessels in inflammatory lesions for both					Argaw et al., 2012 [99]
EAE in VEGFA KO mouse	VEGFA KO rescued protein expression of brain microvessels in inflammatory lesions					
VEGFR2 blocking antibodies in Cortical VEGF injected wild type mice	rescued protein expression for both					
eNOS inhibition or silencing in human brain microvessel endothelial cells	rescued protein expression					
24 months old mice compared to 3 months old, via fluorescence activated cell sorting	significantly decreased		decreased	IgG leakage	neurovascular inflammation and neuronal stress	Elahy et al., 2015 [100]
SAMP8 mice, 12 vs. 4 months old, permeability				no change in albumin permeability and insulin uptake		Banks et al., 2000 [101]

In vitro studies of hypoxia and hypoxia followed by reoxygenation have revealed much of the cellular mechanisms affected by ischemia in CECs. In oxidative stress, the interactions of occludin with claudins or proteins of the ZO family are affected, directly influencing the formation and function of the TJ. Oxidative stress downregulates occludin, reduces its specific membrane localization and regulatory contribution to barrier tightness via multiple signaling pathways [102].

Significant disruptions were seen in the distribution pattern of occludin after hypoxia [78]. These changes were less apparent in posthypoxic reoxygenation, correlating to the increased protein expression [79]. MCAO caused NADPH oxidase upregulation, ROS (reactive oxygen species) generation, matrix metalloproteinase (MMP)-9 activation, and edema formation [103]. MMP activity in oxidative stress increases paracellular permeability by occludin cleavage. However, applying the same level of MMP activity without oxidative damage, neither is occludin cleaved nor BBB permeability is increased [80]. In an opposite approach, normobaric hyperoxia protected the BBB, and the expression and distribution of occludin against MMP-9–mediated effects in cerebral ischemia [103]. Thus occludin plays a key role in the response of cellular barriers to redox changes and could be a redox sensor at the TJs [104,105]. In a brain endothelial cell culture model of hypoxia/reoxygenation, ERK1/2 was activated and the amount of occludin and barrier function decreased which was exacerbated by glucose deprivation [81]. Hypoxia (1% O_2) altered the location of claudin 5 in the plasma membrane and the level of claudin 5 protein in bEND.3 cells, and these changes were accompanied by an increase in BBB permeability. In vivo, claudin 5 was also significantly reduced under hypoxic conditions [82]. ROS-induced BBB disruption via the redistribution and decrease of claudin 5 and occludin levels was paralleled by cytoskeleton rearrangements. This rearrangement was mediated by RhoA, PI3 kinase and protein kinase B (PKB/Akt), and specific inhibitors prevented ROS-induced monocyte migration across an in vitro model of the BBB [83].

The effect of age on the outcome of ischemic stroke was studied in murine distal MCAO experiments, demonstrating an increased inflammatory reaction in 12 month old mice compared to 2 month olds based on IL-6 and IL-1β levels in the ischemic tissue. At the same time, there was an increased number of CD68 immunoreactive cells, denoting phagocytosis and microglia activation in peri-infarct tissue and the older mice suffered more severe BBB damage as well [84]. Similar BBB permeability increase was observed in young adult rats after one hour of hypoxia (6% O_2) followed by 10 minutes of reoxygenation, which also lead to increased occludin phosphorylation without significant changes in ZO-1 expression [85]. Disrupted occludin staining of brain endothelial cells in rats was reversible by administration of ROS scavengers [73]. Another study under similar conditions showed PKC-dependent focal BBB leakage and disrupted claudin 5, occludin and ZO-1 organization at endothelial cell borders while the protein levels were slightly increased in the membrane fraction for claudin 5 and occludin [86].

Functional changes of the BBB appear shortly after a hypoxic event, but structural TJ changes develop much slower. Using an EGFP-claudin 5 transgenic mouse model, researchers demonstrated a stepwise alteration of the BBB, leading to an increase in transcytosis followed by alterations of TJ proteins, which undergo significant ultrastructural remodeling and localization changes starting at 48–58 h post tMCAO (transient middle cerebral artery occlusion) [87]. Early permeability increase elicited by tissue plasminogen activator (tPA) during reperfusion in elderly rats was accompanied by greatly increased claudin 5 phosphorylation while unphosphorylated claudin 5 decreased compared to the contralateral side. MCAO treatment itself increased claudin 5 phosphorylation slightly. Occludin protein level was decreased in elderly compared to young rats and further degradation was observed in response to MCAO and tPA. These age-dependent differences in claudin 5 phosphorylation and occludin degradation were inferred from redistribution of western blot bands [88].

In a multifocal cerebral ischemia model, Src kinase dependent tyrosine phosphorylation of occludin was found to contribute to barrier disruption. Systemic inhibition of Src resulted in decreased infarct size, decreased VEGF-A, rescuing claudin 5, occludin expression and barrier function [89–91]. Reperfusion experiments following 90-minute hypoxia in spontaneously hypertensive rats revealed

MMP dependence of BBB leakage and the disruption of claudin 5 and occludin at the TJ in vivo. Interestingly the TJ proteins from disrupted endothelial barrier appeared in adjacent astrocytes underlining intercellular communication [92,93]. In vivo use of the MMP inhibitor GM6001 in rats as an early treatment given at the time of MCAO increased the number of vessels and improved ZO-1, occludin and claudin 5 expression in the infarct region 3 weeks after the ischemic injury [94].

In a sterile inflammation model induced by TNF-α in human primary brain microvascular endothelial cells, PARP inhibition promoted BBB barrier function. Furthermore, PARP inhibition in primary endothelial cells improved TEER and increased occludin and claudin 5 protein levels [95]. In spontaneously hypertensive rats that underwent MCAO, minocycline, an inhibitor of PARP-1 and anti-inflammatory, anti-apoptotic and neuroprotective drug, significantly reduced the infarct size and prevented tissue loss, improved perfusion, reduced BBB permeability and increased ZO-1, occludin and claudin 5 protein levels. At the same time, increased MMP-2 and -3 were detected at four weeks, at which time peri-infarct microglia showed M2 activation [96].

In a recent genetic model of intracerebral hemorrhagic stroke and vascular dementia, cerebral small vessel disease symptoms were elicited by inducible knockdown of the transcription factor, serum response factor (SRF) or its cofactors Myocardin Related Transcription Factor (MRTF-A/-B). The microhemorrhagic phenotype observed in this model is attributed to loss of TJ components and is specific for brain tissue. The authors demonstrated mRNA level decrease of claudin 1, 3, 5 and 12, as well as ZO-2 and ZO-3, and significant loss of claudin 5 protein in isolated brain endothelial cells [97].

Exposing mice to normobaric hypoxia led to an increase in brain vascular permeability associated with diminished expression of occludin and inhibition of VEGF attenuated vascular leakage [78]. This confirms the results of studies in primary brain endothelial cells in which VEGF decreased occludin expression [98]. Astrocyte derived VEGF-A acts directly on brain microvasculature to downregulate occludin protein and mRNA in vitro and in mouse models of experimental autoimmune encephalomyelitis (EAE), inducing BBB permeability. In vivo inactivation of astrocytic VEGF-A expression or systemic use of the eNOS inhibitor cavtratin rescued BBB function [99].

4.3. Involvement of Brain Barriers in Aging-Associated Alterations of Immune Functions

Brain barriers are important interfaces for neuroimmune communication and any disturbance may inevitably result in CNS dysfunctions. Aging-associated alterations at the BBB and brain cerebrospinal fluid (BCSF) barrier are thus considered to be one trigger for the development of cognitive impairment(s) in the aged brain (reviewed in [106,107]). Literature data concerning TJs presented in this chapter can be found at the end of Table 2.

While it is well established that migration of immune cells from the blood into the CNS parenchyma is a process occurring in inflammatory and neurodegenerative state, accumulating evidence suggests that immune cells also infiltrate the perivascular space of non-diseased brain, though at very low levels, maintaining and contributing to the surveillance and homeostasis of the CNS (reviewed in [108–110]).

Less information exists concerning age-related immune cell trafficking across the BBB and BCSF, obviously due to the fact that normal aging of the brain is usually accompanied by at least low level inflammatory activity [111]. Leakage of IgG into the cerebral cortex and hippocampus of healthy aged (24 months old) but not young (3 months old) mice were reported [100]. This leakage was accompanied by a decrease in occludin and ZO-1 expression in cerebral endothelial cells but no signs of leukocyte transmigration into the CNS.

A progressive age-related enhancement of TNFα-elicited T cell infiltration in brain parenchyma and choroid plexus of mice was demonstrated by Xu et al. [112]. Further, Stichel and Luebbert [113] reported on the presence of T cells and dendritic-like cells in mouse brain parenchyma at about 12 months of age, with numbers increasing during aging. T cells from aged mice were found to exhibit increased expression of adhesion molecules, such as CD11a and CD49d, facilitating diapedesis [114] and elevated ICAM1 expression was found in brain vasculature of aged human and mouse brains [115].

The role of aging-associated T cell infiltration of the non-diseased brain is still unclear. Results from single-cell RNA-sequencing and immunofluorescence staining of the subventricular zone from young (3 month old) and old (28–29 months) mice suggest that T cells, expressing interferon-γ, were clonally expanded and markedly enriched in the subventricular zone from old mice [116]. In vitro studies have shown that T cells can inhibit the proliferation of neural stem cells in co-cultures in an interferon-γ-dependent mechanism [116]. Thus, it may be assumed that interaction of T cells with neural stem cells in neurogenic niches of old animals may contribute to the proliferative decline of neural stem cells during aging. A distinct role of immune cells was demonstrated in increasing cerebral vascular permeability [117]. Using a mouse model of CD8 T cell-mediated CNS vascular permeability it was shown that CD8 T cells are capable of initiating BBB disruption in a non-apoptotic perforin-dependent manner.

4.4. Alzheimer's Disease (AD)

The blood–brain barrier contributes to the pathology and may play a causative role in the development of the most common neurodegenerative disease afflicting the elderly population: Alzheimer's disease (AD). The involvement of the BBB happens through multiple mechanisms such as barrier disruption, transporter dysfunction and secretion of neurotoxic substances [118,119]. Amyloid-β peptide (Aβ), the main component of senile plaques in the AD influences the expression and localization of TJ proteins [120–122]. The extracellular matrix and TJ proteins are substrates of MMPs, whose activity is also increased in AD and after ischemic injury, which results in lower TJ proteins [123]. Data concerning TJ changes in Alzheimer's, Parkinson's and Huntington's diseases, as well as schizophrenia are summarized in Table 3.

Table 3. BBB function and junctional proteins in age related disorders, neurodegenerative diseases.

Experimental System	Claudin 5	Occludin	ZO-1	Permeability	Other	Authors
Triple-transgenic mice (3 × Tg-AD), 10–11 vs. 4 month old				no change in [3H]-inulin and [14C]-sucrose uptake	Age dependent reduction in cerebrovascular volume, thickened basal membrane	Bourasset et al., 2009, Mehta et al., 2013 [124]
18–20 month old 3 × Tg-AD vs. wild type mice				no change in [3H]-inulin and [14C]-sucrose uptake decreased uptake of passively diffusing markers: [3H] diazepam and [3H] propranolol in AD mice	thickened basal membrane	
rat brain microvessel endothelial cells +Aβ1-42 for 24–72 h, immunofluorescence	disrupted localization after 24 h, increased fluorescence of Claudin 5 and 1.	no change in localization. Decreased fluorescence at 24 hours.	ZO-2 diffuse localization. ZO-2 increased fluorescence at 24 h and decreased at 72 h.			Marco and Skaper 2006 [120]
capillary cerebral amyloid angiopathy (capCAA) patient brain sections	loss of protein in capillaries with amyloid β deposits					Carrano et al., 2011, 2012 [125,126]
hCMEC/D3 cell culture + Aβ1-42 for 24 h	dose dependent, ROS mediated decrease of mRNA for both					
ARPE-19 cell culture + oligomeric Aβ1-42	disrupted membrane staining, significantly decreased mRNA			increased 40 kDa FITC-dextran permeability		Bruban et al., 2009 [127]
subretinal Aβ1-42 injection in C57BL/6 J mice	Similarly disrupted membrane staining of both in young, adult and aged mice.					
bEnd.3+Aβ1-42	decreased protein level		decreased protein levels rescued by inhibition of either RAGE, calcineurin or MMP	increased 40 kDa FITC-dextran permeability rescued by inhibition of calcineurin or MMP		Kook et al., 2012 [128]
8 months old transgenic mice with five familial AD mutations (5XFAD) compared to wild type	TJ cross section length significantly decreased, by transmission electronmicroscopy				RAGE expression was increased in brain capillaries	
bEnd.3	Oligomeric, but not monomeric or fibrillar Aβ1-42 dose dependently decreased protein levels. Protein levels were rescued by silencing RAGE with siRNA or blocking RAGE with a polyclonal antibody.					Wan et al., 2015 [129]

Table 3. *Cont.*

Experimental System	Claudin 5	Occludin	ZO-1	Permeability	Other	Authors
bEnd.3 + oligomeric Aβ1–42	decreased protein levels and increased permeability were rescued by EGb761 in a dose dependent manner				Aβ1–42-Oligo induced expression of MMP-2 and MMP-9 was rescued by blocking RAGE via antibody.	Wan, Cao, et al., 2014 [130]
bEnd.3 cells+ Aβ1-42 and isolated capillaries from 5XFAD mice	exogenous ANXA1 rescued Aβ1-42 induced decrease in protein levels by blocking Rho-ROCK signaling		exogenous ANXA1 rescued Aβ1-42 induced decrease in protein levels by blocking Rho-ROCK signaling			Park et al., 2017 [131]
APOE4 transgene expressing Apoe-/- mice	protein levels were decreased dependent on the pericytic cyclophilin A/NF-κB/MMP9 dependent pathway					Bell et al., 2010 [54]
bEnd.3, CD-1 or PARP-1 KO mouse primary glial culture +Aβ1–42	endothelial protein expression reduced by activated microglia was rescued by PARP inhibition.					Mehrabadi et al., 2017 [132]
MPTP mouse model +caffeine	MPTP treated animals showed decreased protein levels, which was rescued by caffeine.			Caffeine rescued MPTP induced Evans blue leakage in striatum.	Caffeine blocked MPTP-induced increases in MMP9 activity	Chen et al., 2008 [133]
MPTP mouse model +trehalose	immunofluorescent signal was greatly diminished in MPTP animals, which was rescued by trehalose.					Sarkar et al., 2014 [134]
unilateral striatal 6OHDA injection in rats				FITC-albumin or horseradish peroxidase leakage in striatum and substantia nigra in response to 6OHDA		Carvey et al., 2005 [135]
unilateral striatal 6OHDA injection in rats	immunohistochemistry signal decreased	protein levels decreased for both				Huang et al., 2016 [136]
hCMEC/D3 (co-cultured with mouse primary astrocytes) + preformed α-synuclein fibrils	decreased protein levels					Kuan et al., 2016 [137]

Table 3. *Cont.*

Experimental System	Claudin 5	Occludin	ZO-1	Permeability	Other	Authors
Parkinson's Disease patient tissue sections compared to age matched and deep brain stimulated patient tissue	decreased immunofluorescent staining compared to control, rescued by deep brain stimulation.			IgG extravasation		Pienaar et al., 2015 [138]
Parkinson's disease patient tissue sections				blood extravasation		Gray and Woulfe 2015 [139]
Huntington's disease patient putamen samples compared to control		decreased protein levels		extravascular fibrin deposition., increased leakage in caudate and putamen by DCE MRI	abnormal vessel morphology	Drouin-Ouellet et al., 2015 [140]
and R6/2 mouse model, striatal samples		decreased protein levels		increased pinocytic activity and increased albumin extravasation	morphological changes in vessel walls	
iPSC derived brain microvascular endothelial cells from HD patients	miss-localization to the cytoplasm			decreased TEER		Lim et al., 2017 [141]
schizophrenic patient brain tissue	discontinuous localization			anti-psychotic medications dose dependently increased claudin 5 expression		Greene et al., 2018. [142]

Similar to data on permeability in the aging brain, the BBB permeability data of AD patients was heterogeneous. This could partly be ascribed to difficulties in separating different types of dementia and co-morbidities confounding results. In a meta analysis by Farrall and Wardlaw some results show increased BBB permeability in AD compared to controls but the permeability increase is higher and more clear cut for vascular dementia and mixed dementias compared to AD [48]. Murine models of AD allow for more precise control over experiments and make it possible to concentrate on separate aspects of the disease; however, available results are still conflicting. A number of studies showed that the paracellular route is unaffected in murine models of AD. There was a substantially decreased occludin expression in APP/PS1 mice AD model compared to wild-type controls [143]. In some cases, when using an APP/PS1 mouse model there was an unaltered BBB permeability to ^{131}I-albumin [144] and to sodium fluorescein [145]. Even though earlier work showed small localized disruption in Senescence Accelerated Mouse-Prone 8 (SAMP8), no global BBB permeability change was observed when comparing 12 and 4 months old animals [101]. Comparing 11 and 4 months old 3 × Tg-AD mice (triple transgenic mice for familial Alzheimer's disease mutations), Bourasset et al. found no changes in the distribution of vascular space markers ^{3}H-inulin and ^{14}C-sucrose, but found a global reduction in cerebrovascular volume that was most significant in the hippocampus [124]. In a comparison of 18–20 month old 3×Tg-AD and wild type mice researchers also did not find changes in ^{3}H-inulin and ^{14}C-sucrose uptake, while the uptake of passively diffusing markers ^{3}H-diazepam and ^{3}H-propranolol was less in AD mice [146]. These results suggest that in murine AD models global BBB breakdown is not detectable and research probably should focus on local barrier disruption, as data from multiple research groups point to the importance of cerebral amyloid angiopathy in AD and there is ample amount of research revealing the molecular mechanisms behind it.

Regarding TJ proteins in post-mortem human brain, a dramatic loss of claudin 5, occludin and ZO-1 was demonstrated in Aβ-laden capillaries surrounded by NADPH oxidase-2 (NOX-2)-positive activated microglia. Further results show that Aβ is toxic to endothelial cells in the human brain via binding to the receptor for advanced glycation end-products (RAGE) and induction of ROS production, which ultimately leads to disruption of TJs and loss of BBB integrity [125,126]. In a model of age-related macular degeneration, increased formation of ROS was found after administration of the oligomeric form of Aβ1–42 to retinal pigmented epithelial cells [127], which was accompanied by a decrease in the expression of occludin. The Aβ1-42 peptide accumulation around brain microvessels was found to be mediated by transport via RAGE in 5XFAD mice, increasing permeability, disrupting claudin 5, ZO-1 and occludin. This MMP and Ca^{2+}-calcineurin dependent BBB disruption could be prevented in bEnd.3 cells by neutralizing antibodies against RAGE [128], small interfering RNA knockdown of RAGE [129] or *Ginkgo biloba* extract EGb761 [130].

An in vitro study on Aβ1-42-treated bEnd.3 cells showed that AnnexinA1 (ANXA1), an anti-inflammatory messenger, significantly rescued the expression of claudin 5 and ZO-1 and barrier function in Aβ1-42 -treated bEnd.3 cells. Aβ1–42 reduced ANXA1 bEnd.3 cells, and also had reduced expression in capillaries of 5XFAD mice, and the human serum of patients with AD. ANXA1 acted via the inhibition of RhoA-ROCK signaling. In co-culture experiments, pericyte secreted ANXA1 attenuated the Aβ1–42-induced disruption of the tight junction [131].

Pericytes influence the BBB by promoting TJ protein expression in endothelial cells [54] and helping the alignment of TJs [147]. It has also been shown that a loss of pericytes plays a role in AD development and is followed by a decreased expression of TJ proteins [148,149].

The strongest genetic risk factor for late onset AD is Apolipoprotein E4 (ApoE4). ApoE4 and its receptors are expressed throughout the NVU and are linked to many aspects of cerebrovascular dysfunction [150,151]. The molecular mechanisms of ApoE4 mediated neurovascular injury demonstrate how the coordinated effort of multiple cell types maintains a functional NVU. Bell et al. revealed using multiple transgenic mice that the ApoE induced degradation of TJ proteins claudin 5, ZO-1 and occludin and basal membrane protein collagen IV is the result of an intercellular

communication error. ApoE4 secreted by astrocytes is unable to bind LRP1 on pericytes and thus does not block the pericytic cyclophilin A/NF-κB/MMP9 pathway, which results in vascular dysfunction [152].

Soluble Aβ is also known to induce secretion of proinflammatory cytokines (TNF and IL-6) and chemokines, which stimulate the production of MMP-2 and MMP-9 and it also activates the production of ROS [153]. Furthermore, experimental data confirms the involvement of all cells of the NVU in the effect of Aβ. Microglia activated by Aβ treatment shows reduced expression of trophic factors that are responsible for inflammatory resolution and increased pro inflammatory NO and TNFα release. This affects both astrocytes and capillary endothelium leading to reduced BBB integrity and function [132].

AD is also accompanied by tau protein accumulation and hyperphosphorylation, which was shown to promote BBB dysfunction in AD and other tauopathies [154–156].

4.5. Parkinson's Disease (PD)

The BBB is also involved in the progression of the second most common neurodegenerative disorder: Parkinson's disease (PD). The contribution of BBB disruption to PD is not widely studied despite the implication of known BBB damaging mechanisms and agents such as oxidative stress and MMPs in the pathomechanism of the disease [157,158]. Thickened basement membrane in the cingulate cortex and degeneration of the brain microvasculature in PD was reported by Farkas et al. and Guan et al. [159,160]. Gray and Woulfe published the first report of BBB disruption evidenced by blood extravasation in striatal PD tissue in 2015 [139]. Motor function and regional blood flow can be improved in PD patients by deep brain stimulation [161], which is possibly a result of normalizing aberrant microvasculature in PD. In a study regarding the effects of deep brain stimulation of the subthalamic nucleus in PD patients, the decreased immunofluorescence signal of claudin 5, occludin and ZO-1 of PD samples could be rescued by deep brain stimulation treatments [138]. This is in line with multiple studies using experimental parkinsonism models. Significant decrease was detected in the amount of occludin in the striatum, which was associated with increased BBB leakage, in the 1-methyl-4-phenyl-1,2,3,6-tetrahydropyridine (MPTP)-treated mouse model. Increased striatal MMP-9 activity was also detected in the MPTP model with a possible role in TJ opening [133,134]. Increased permeability of the BBB was also observed in the striatum in rats after treatment with unilateral injections with 6-Hydroxydopamine (6OHDA) [135] that leads to downregulation of occludin [136]. Similar to amyloid oligomers in AD the Lewy body component α-synuclein was found to damage BBB. An in vitro study showed that preformed α-synuclein fibrils lead to a decrease in the expression of occludin and ZO-1, but not tricellulin or marveld3, in human brain microvascular endothelial cells [137].

4.6. Huntington's Disease (HD)

Huntington's disease (HD) is a dominantly inherited autosomal neurodegenerative disorder that is not usually considered aging related as it is typically diagnosed at the age of 40, and the onset of the disease can vary from earlier than ten to over eighty years of age. However, recent research indicates that epigenetic age acceleration in specific brain regions is associated with HD [162].

Recently, morphological changes of blood vessels and BBB leakage in the caudate and putamen were observed in HD patients using magnetic resonance imaging. In putamen samples of HD patients and in striatal samples of the HD model R6/2 mice, occludin and claudin 5 protein levels were decreased and evidence of increased BBB permeability was found [140]. More recently, these results were expanded in induced pluripotent stemm cell (iPSC) derived brain microvascular endothelial cells. While in this system no significant changes in TJ protein levels were observed, claudin 5 was found to mislocalize to the cytoplasm of cells derived from HD patients; however, trans endothelial electric resistance (TEER) and MDR1 function was significantly decreased compared to control cell lines. Some of the changes in cell lines derived from HD patients could be attributed to aberrant Wnt signaling [141].

4.7. Schizophrenia

Some aspects of schizophrenia raise the possibility that accelerated aging of the brain can be responsible for some of its symptoms [163]. Individuals with the chromosomal abnormality: 22q11 deletion syndrome (22q11DS) have an increased risk of developing schizophrenia, in fact it occurs in 30% of such individuals. Interestingly, 22q11DS are haploinsufficient for claudin 5. Recent experiments on AAV mediated claudin 5 suppression in mice and inducible claudin 5 knockdown uncovered focal BBB breakdown and behavioral changes. Anti-psychotic medications were found to dose dependently increase claudin 5 expression. Furthermore post mortem analysis of schizophrenic brains revealed aberrant, discontinuous expression of claudin 5 [142].

5. Closing Remarks

Aging comes with the deterioration of all bodily functions of which the loss of cognitive function is possibly the most serious in our heavily information dependent society. With the building evidence that dysfunction of the microvasculature is not just coincident but is part of the underlying mechanisms of aging and associated neurovascular and neurological disorders, new therapeutic possibilities are opened. The significant heterogeneity of BBB disruption data in studies using aging postmortem brain tissue suggests that more data is necessary to clearly understand the role of BBB disruption and to see whether it is a symptom or a cause [48]. It is not surprising that human BBB data before the mid-1990s is mainly regarding permeability; however, even since the discovery of occludin, zonula occludens proteins and claudins, BBB TJ data in the aging brain is scarce and this deficit is just partly made up for by data from aging associated disorders. Furthermore many studies disregard that claudin 5, occludin or ZO1 does not constitute the paracellular barrier by itself and all three should be studied along with permeability to different molecular size tracers at the same time to get a picture of barrier status. Worsening the situation is that the reliability of existing TJ data has been questioned recently [35]. Thus further comprehensive BBB TJ and permeability studies are needed in the field of aging and aging associated disorders. Another focus needs to be the study of both classical and novel intercellular communication pathways between brain capillary endothelium, pericytes, astrocytes, microglia and neurons as the concerted activity of all these cell types is necessary for proper neural function. We are just beginning to understand the depth and mechanisms of intercellular information exchange that makes the NVU a functional unit. The knowledge of how the interdependent functions of the cell types constituting the NVU are affected by the process of aging can lead to the alleviation of age related impairments and a better quality of life.

Author Contributions: All authors participated in researching and discussing literature and writing parts of the manuscripts. L.C., I.A.K. and A.E.F. wrote the paper with input from all authors. All authors approved the final version.

Funding: A.E.F. is supported by the János Bolyai Research Fellowship of the Hungarian Academy of Sciences (BO/00023/17/8) and the New National Excellence Program of the Ministry of Human Capacities (UNKP-19-4-SZTE-43). Work of I.A.K. is supported by the NKFIH (grant numbers: K-116158, GINOP-2.3.2-15-2016-00020 and GINOP-2.3.2-15-2016-0034) and by the UEFISCDI PNCDI III—PCE 2016 Program (project number: PN-III-P4-ID-PCE-2016-0408, 188/2017). Work of I.W. is supported by the NKFIH FK-124114 and the UEFISCDI PN-III-P1–1.1-TE-2016–1352 projects.

Conflicts of Interest: The authors declare no conflict of interest. The funders had no role in the design of the study; in the collection, analyses, or interpretation of data; in the writing of the manuscript, or in the decision to publish the results.

Abbreviations

BBB	blood–brain barrier
TJ	tight-junction
CNS	central nervous system
NVU	neurovascular unit
CEC	Cerebral endothelial cells
ZO-1	zonula occludens 1 protein
MCAO	middle cerebral artery occlusion
Aβ	amyloid-beta protein
Aβ1-42	amyloid-beta peptide containing amino acids 1-42
AD	Alzheimer's disease
MMP	matrix metalloproteinase
PD	Parkinson's disease
HD	Huntington's disease

References

1. Wilhelm, I.; Nyúl-Tóth, Á.; Kozma, M.; Farkas, A.E.; Krizbai, I.A. Role of pattern recognition receptors of the neurovascular unit in inflamm-aging. *Am. J. Physiol. Heart Circ. Physiol.* **2017**, *313*, H1000–H1012. [CrossRef] [PubMed]
2. Iadecola, C. The Neurovascular Unit Coming of Age: A Journey through Neurovascular Coupling in Health and Disease. *Neuron* **2017**, *96*, 17–42. [CrossRef] [PubMed]
3. Brightman, M.W.; Reese, T.S. Junctions between intimately apposed cell membranes in the vertebrate brain. *J. Cell Biol.* **1969**, *40*, 648–677. [CrossRef] [PubMed]
4. Oldendorf, W.H.; Cornford, M.E.; Brown, W.J. The large apparent work capability of the blood-brain barrier: A study of the mitochondrial content of capillary endothelial cells in brain and other tissues of the rat. *Ann. Neurol.* **1977**, *1*, 409–417. [CrossRef]
5. Nag, S. Morphology and molecular properties of cellular components of normal cerebral vessels. *Methods Mol. Med.* **2003**, *89*, 3–36. [CrossRef]
6. Hill, J.; Rom, S.; Ramirez, S.H.; Persidsky, Y. Emerging roles of pericytes in the regulation of the neurovascular unit in health and disease. *J. Neuroimmune Pharm.* **2014**, *9*, 591–605. [CrossRef]
7. Winkler, E.A.; Sengillo, J.D.; Bell, R.D.; Wang, J.; Zlokovic, B.V. Blood-spinal cord barrier pericyte reductions contribute to increased capillary permeability. *Br. J. Cereb. Blood Flow Metab.* **2012**, *32*, 1841–1852. [CrossRef]
8. Thanabalasundaram, G.; Schneidewind, J.; Pieper, C.; Galla, H.J. The impact of pericytes on the blood-brain barrier integrity depends critically on the pericyte differentiation stage. *Int. J. Biochem. Cell Biol.* **2011**, *43*, 1284–1293. [CrossRef]
9. Hellström, M.; Gerhardt, H.; Kalén, M.; Li, X.; Eriksson, U.; Wolburg, H.; Betsholtz, C. Lack of pericytes leads to endothelial hyperplasia and abnormal vascular morphogenesis. *J. Cell Biol.* **2001**, *153*, 543–553. [CrossRef]
10. Armulik, A.; Genové, G.; Mäe, M.; Nisancioglu, M.H.; Wallgard, E.; Niaudet, C.; He, L.; Norlin, J.; Lindblom, P.; Strittmatter, K.; et al. Pericytes regulate the blood-brain barrier. *Nature* **2010**, *468*, 557–561. [CrossRef]
11. Abbott, N.J.; Rönnbäck, L.; Hansson, E. Astrocyte-endothelial interactions at the blood-brain barrier. *Nat. Rev. Neurosci.* **2006**, *7*, 41–53. [CrossRef] [PubMed]
12. Delaney, C.; Campbell, M. The blood brain barrier: Insights from development and ageing. *Tissue Barriers* **2017**, *5*, e1373897. [CrossRef] [PubMed]
13. Verheggen, I.C.M.; Van Boxtel, M.P.J.; Verhey, F.R.J.; Jansen, J.F.A.; Backes, W.H. Interaction between blood-brain barrier and glymphatic system in solute clearance. *Neurosci. Biobehav. Rev.* **2018**, *90*, 26–33. [CrossRef] [PubMed]
14. Iliff, J.J.; Wang, M.; Liao, Y.; Plogg, B.A.; Peng, W.; Gundersen, G.A.; Benveniste, H.; Vates, G.E.; Deane, R.; Goldman, S.A.; et al. A paravascular pathway facilitates CSF flow through the brain parenchyma and the clearance of interstitial solutes, including amyloid beta. *Sci. Transl. Med.* **2012**, *4*, 147ra111. [CrossRef] [PubMed]
15. Smith, A.J.; Verkman, A.S. The "glymphatic" mechanism for solute clearance in Alzheimer's disease: Game changer or unproven speculation? *FASEB J.* **2018**, *32*, 543–551. [CrossRef] [PubMed]

16. Abbott, N.J.; Pizzo, M.E.; Preston, J.E.; Janigro, D.; Thorne, R.G. The role of brain barriers in fluid movement in the CNS: Is there a 'glymphatic' system? *Acta Neuropathol.* **2018**, *135*, 387–407. [CrossRef] [PubMed]
17. Zhang, Y.; Xu, K.; Liu, Y.; Erokwu, B.O.; Zhao, P.; Flask, C.A.; Ramos-Estebanez, C.; Farr, G.W.; LaManna, J.C.; Boron, W.F.; et al. Increased cerebral vascularization and decreased water exchange across the blood-brain barrier in aquaporin-4 knockout mice. *PLoS ONE* **2019**, *14*, e0218415. [CrossRef] [PubMed]
18. Kress, B.T.; Iliff, J.J.; Xia, M.; Wang, M.; Wei, H.S.; Zeppenfeld, D.; Xie, L.; Kang, H.; Xu, Q.; Liew, J.A.; et al. Impairment of paravascular clearance pathways in the aging brain. *Ann. Neurol.* **2014**, *76*, 845–861. [CrossRef]
19. Neuwelt, E.; Abbott, N.J.; Abrey, L.; Banks, W.A.; Blakley, B.; Davis, T.; Engelhardt, B.; Grammas, P.; Nedergaard, M.; Nutt, J.; et al. Strategies to advance translational research into brain barriers. *Lancet Neurol.* **2008**, *7*, 84–96. [CrossRef]
20. Bhowmick, S.; D'Mello, V.; Caruso, D.; Wallerstein, A.; Abdul-Muneer, P.M. Impairment of pericyte-endothelium crosstalk leads to blood-brain barrier dysfunction following traumatic brain injury. *Exp. Neurol.* **2019**, *317*, 260–270. [CrossRef]
21. Chen, J.; Luo, Y.; Hui, H.; Cai, T.; Huang, H.; Yang, F.; Feng, J.; Zhang, J.; Yan, X. CD146 coordinates brain endothelial cell-pericyte communication for blood-brain barrier development. *Proc. Natl. Acad. Sci. USA* **2017**, *114*, E7622–E7631. [CrossRef] [PubMed]
22. Zagrean, A.M.; Hermann, D.M.; Opris, I.; Zagrean, L.; Popa-Wagner, A. Multicellular Crosstalk Between Exosomes and the Neurovascular Unit After Cerebral Ischemia. Therapeutic Implications. *Front. Neurosci.* **2018**, *12*, 811. [CrossRef] [PubMed]
23. Ramirez, S.H.; Andrews, A.M.; Paul, D.; Pachter, J.S. Extracellular vesicles: Mediators and biomarkers of pathology along CNS barriers. *Fluids Barriers CNS* **2018**, *15*, 19. [CrossRef] [PubMed]
24. András, I.E.; Toborek, M. Extracellular vesicles of the blood-brain barrier. *Tissue Barriers* **2016**, *4*, e1131804. [CrossRef]
25. Saeedi, S.; Israel, S.; Nagy, C.; Turecki, G. The emerging role of exosomes in mental disorders. *Transl. Psychiatry* **2019**, *9*, 122. [CrossRef]
26. Yuan, X.; Wu, Q.; Wang, P.; Jing, Y.; Yao, H.; Tang, Y.; Li, Z.; Zhang, H.; Xiu, R. Exosomes Derived from Pericytes Improve Microcirculation and Protect Blood-Spinal Cord Barrier After Spinal Cord Injury in Mice. *Front. Mol. Neurosci.* **2019**, *13*, 319. [CrossRef]
27. Liu, C.; Ge, H.M.; Liu, B.H.; Dong, R.; Shan, K.; Chen, X.; Yao, M.D.; Li, X.M.; Yao, J.; Zhou, R.M.; et al. Targeting pericyte-endothelial cell crosstalk by circular RNA-cPWWP2A inhibition aggravates diabetes-induced microvascular dysfunction. *Proc. Natl. Acad. Sci. USA* **2019**, *116*, 7455–7464. [CrossRef]
28. Brown, W.R.; Thore, C.R. Review: Cerebral microvascular pathology in ageing and neurodegeneration. *Neuropathol. Appl. Neurobiol.* **2011**, *37*, 56–74. [CrossRef]
29. Erusalimsky, J.D. Vascular endothelial senescence: From mechanisms to pathophysiology. *J. Appl. Physiol.* **2009**, *106*, 326–332. [CrossRef]
30. Sonntag, W.E.; Lynch, C.D.; Cooney, P.T.; Hutchins, P.M. Decreases in cerebral microvasculature with age are associated with the decline in growth hormone and insulin-like growth factor 1. *Endocrinology* **1997**, *138*, 3515–3520. [CrossRef]
31. Fan, Y.; Yang, X.; Tao, Y.; Lan, L.; Zheng, L.; Sun, J. Tight junction disruption of blood-brain barrier in white matter lesions in chronic hypertensive rats. *Neuroreport* **2015**, *26*, 1039–1043. [CrossRef] [PubMed]
32. Desjardins, M.; Berti, R.; Lefebvre, J.; Dubeau, S.; Lesage, F. Aging-related differences in cerebral capillary blood flow in anesthetized rats. *Neurobiol. Aging* **2014**, *35*, 1947–1955. [CrossRef] [PubMed]
33. Goodall, E.F.; Wang, C.; Simpson, J.E.; Baker, D.J.; Drew, D.R.; Heath, P.R.; Saffrey, M.J.; Romero, I.A.; Wharton, S.B. Age-associated changes in the blood-brain barrier: Comparative studies in human and mouse. *Neuropathol. Appl. Neurobiol.* **2018**, *44*, 328–340. [CrossRef] [PubMed]
34. Nitta, T.; Hata, M.; Gotoh, S.; Seo, Y.; Sasaki, H.; Hashimoto, N.; Furuse, M.; Tsukita, S. Size-selective loosening of the blood-brain barrier in claudin-5–deficient mice. *J. Cell Biol.* **2003**, *161*, 653–660. [CrossRef] [PubMed]
35. Castro Dias, M.; Coisne, C.; Lazarevic, I.; Baden, P.; Hata, M.; Iwamoto, N.; Francisco, D.M.F.; Vanlandewijck, M.; He, L.; Baier, F.A.; et al. Claudin-3-deficient C57BL/6J mice display intact brain barriers. *Sci. Rep.* **2019**, *9*, 203. [CrossRef]

36. Berndt, P.; Winkler, L.; Cording, J.; Breitkreuz-Korff, O.; Rex, A.; Dithmer, S.; Rausch, V.; Blasig, R.; Richter, M.; Sporbert, A.; et al. Tight junction proteins at the blood-brain barrier: Far more than claudin-5. *Cell Mol. Life Sci.* **2019**, *76*, 1987–2002. [CrossRef]
37. Dörfel, M.J.; Westphal, J.K.; Bellmann, C.; Krug, S.M.; Cording, J.; Mittag, S.; Tauber, R.; Fromm, M.; Blasig, I.E.; Huber, O. CK2-dependent phosphorylation of occludin regulates the interaction with ZO-proteins and tight junction integrity. *Cell Commun. Signal.* **2013**, *11*, 40. [CrossRef]
38. Raleigh, D.R.; Boe, D.M.; Yu, D.; Weber, C.R.; Marchiando, A.M.; Bradford, E.M.; Wang, Y.; Wu, L.; Schneeberger, E.E.; Shen, L.; et al. Occludin S408 phosphorylation regulates tight junction protein interactions and barrier function. *J. Cell Biol.* **2011**, *193*, 565–582. [CrossRef]
39. Runkle, E.A.; Sundstrom, J.M.; Runkle, K.B.; Liu, X.; Antonetti, D.A. Occludin localizes to centrosomes and modifies mitotic entry. *J. Biol. Chem.* **2011**, *286*, 30847–30858. [CrossRef]
40. Furuse, M.; Hirase, T.; Itoh, M.; Nagafuchi, A.; Yonemura, S.; Tsukita, S. Occludin: A novel integral membrane protein localizing at tight junctions. *J. Cell Biol.* **1993**, *12 Pt 2*, 1777–1788. [CrossRef]
41. Furuse, M.; Itoh, M.; Hirase, T.; Nagafuchi, A.; Yonemura, S.; Tsukita, S. Direct association of occludin with ZO-1 and its possible involvement in the localization of occludin at tight junctions. *J. Cell Biol.* **1994**, *127 Pt 1*, 1617–1626. [CrossRef]
42. Haskins, J.; Gu, L.; Wittchen, E.S.; Hibbard, J.; Stevenson, B.R. ZO-3, a novel member of the MAGUK protein family found at the tight junction, interacts with ZO-1 and occludin. *J. Cell Biol.* **1998**, *141*, 199–208. [CrossRef] [PubMed]
43. Itoh, M.; Furuse, M.; Morita, K.; Kubota, K.; Saitou, M.; Tsukita, S. Direct binding of three tight junction-associated MAGUKs, ZO-1, ZO-2, and ZO-3, with the COOH termini of claudins. *J. Cell Biol.* **1999**, *147*, 1351–1363. [CrossRef] [PubMed]
44. Castro, V.; Skowronska, M.; Lombardi, J.; He, J.; Seth, N.; Velichkovska, M.; Toborek, M. Occludin regulates glucose uptake and ATP production in pericytes by influencing AMP-activated protein kinase activity. *J. Cereb. Blood Flow Metab.* **2018**, *38*, 317–332. [CrossRef] [PubMed]
45. Bauer, H.; Stelzhammer, W.; Fuchs, R.; Weiger, T.M.; Danninger, C.; Probst, G.; Krizbai, I.A. Astrocytes and neurons express the tight junction-specific protein occludin in vitro. *Exp. Cell Res.* **1999**, *250*, 434–438. [CrossRef] [PubMed]
46. Morgan, S.V.; Garwood, C.J.; Jennings, L.; Simpson, J.E.; Castelli, L.M.; Heath, P.R.; Mihaylov, S.R.; Vaquéz-Villaseñor, I.; Minshull, T.C.; Ince, P.G.; et al. Proteomic and cellular localisation studies suggest non-tight junction cytoplasmic and nuclear roles for occludin in astrocytes. *Eur. J. Neurosci.* **2018**, *47*, 1444–1456. [CrossRef] [PubMed]
47. Horng, S.; Therattil, A.; Moyon, S.; Gordon, A.; Kim, K.; Argaw, A.T.; Hara, Y.; Mariani, J.N.; Sawai, S.; Flodby, P.; et al. Astrocytic tight junctions control inflammatory CNS lesion pathogenesis. *J. Clin. Investig.* **2017**, *127*, 3136–3151. [CrossRef] [PubMed]
48. Farrall, A.J.; Wardlaw, J.M. Blood-brain barrier: Ageing and microvascular disease-systematic review and meta-analysis. *Neurobiol. Aging* **2009**, *30*, 337–352. [CrossRef]
49. Baker, D.J.; Wijshake, T.; Tchkonia, T.; LeBrasseur, N.K.; Childs, B.G.; van de Sluis, B.; Kirkland, J.L.; van Deursen, J.M. Clearance of p16Ink4a-positive senescent cells delays ageing-associated disorders. *Nature* **2011**, *479*, 232–236. [CrossRef]
50. Stamatovic, S.M.; Martinez-Revollar, G.; Hu, A.; Choi, J.; Keep, R.F.; Andjelkovic, A.V. Decline in Sirtuin-1 expression and activity plays a critical role in blood-brain barrier permeability in aging. *Neurobiol. Dis.* **2019**, *126*, 105–116. [CrossRef]
51. Bake, S.; Sohrabji, F. 17beta-estradiol differentially regulates blood-brain barrier permeability in young and aging female rats. *Endocrinology* **2004**, *145*, 5471–5475. [CrossRef] [PubMed]
52. Bake, S.; Friedman, J.A.; Sohrabji, F. Reproductive age-related changes in the blood brain barrier: Expression of IgG and tight junction proteins. *Microvasc. Res.* **2009**, *78*, 413–424. [CrossRef] [PubMed]
53. Wilson, A.C.; Clemente, L.; Liu, T.; Bowen, R.L.; Meethal, S.V.; Atwood, C.S. Reproductive hormones regulate the selective permeability of the blood-brain barrier. *Biochim. Biophys. Acta (BBA) Mol. Basis Dis.* **2008**, *1782*, 401–407. [CrossRef] [PubMed]
54. Bell, R.D.; Winkler, E.A.; Sagare, A.P.; Singh, I.; LaRue, B.; Deane, R.; Zlokovic, B.V. Pericytes control key neurovascular functions and neuronal phenotype in the adult brain and during brain aging. *Neuron* **2010**, *68*, 409–427. [CrossRef] [PubMed]

55. Mooradian, A.D.; Haas, M.J.; Chehade, J.M. Age-related changes in rat cerebral occludin and zonula occludens-1 (ZO-1). *Mech. Ageing Dev.* **2003**, *124*, 143–146. [CrossRef]
56. Osada, T.; Gu, Y.H.; Kanazawa, M.; Tsubota, Y.; Hawkins, B.T.; Spatz, M.; Milner, R.; del Zoppo, G.J. Interendothelial claudin-5 expression depends on cerebral endothelial cell-matrix adhesion by β (1)-integrins. *J. Cereb. Blood Flow Metab.* **2011**, *31*, 1972–1985. [CrossRef] [PubMed]
57. Roberts, J.; de Hoog, L.; Bix, G.J. Mice deficient in endothelial α5 integrin are profoundly resistant to experimental ischemic stroke. *J. Cereb. Blood Flow Metab.* **2017**, *37*, 85–96. [CrossRef] [PubMed]
58. Montagne, A.; Barnes, S.R.; Sweeney, M.D.; Halliday, M.R.; Sagare, A.P.; Zhao, Z.; Toga, A.W.; Jacobs, R.E.; Liu, C.Y.; Amezcua, L.; et al. Blood-brain barrier breakdown in the aging human hippocampus. *Neuron* **2015**, *85*, 296–302. [CrossRef]
59. Yamazaki, Y.; Baker, D.J.; Tachibana, M.; Liu, C.C.; van Deursen, J.M.; Brott, T.G.; Bu, G.; Kanekiyo, T. Vascular Cell Senescence Contributes to Blood-Brain Barrier Breakdown. *Stroke* **2016**, *47*, 1068–1077. [CrossRef]
60. Schlingmann, B.; Overgaard, C.E.; Molina, S.A.; Lynn, K.S.; Mitchell, L.A.; Dorsainvil White, S.; Mattheyses, A.L.; Guidot, D.M.; Capaldo, C.T.; Koval, M. Regulation of claudin/zonula occludens-1 complexes by hetero-claudin interactions. *Nat. Commun.* **2016**, *7*, 12276. [CrossRef]
61. Lee, S.H.; Lee, J.H.; Lee, H.Y.; Min, K.J. Sirtuin signaling in cellular senescence and aging. *BMB Rep.* **2019**, *52*, 24–34. [CrossRef] [PubMed]
62. Herskovits, A.Z.; Guarente, L. SIRT1 in neurodevelopment and brain senescence. *Neuron* **2014**, *81*, 471–483. [CrossRef] [PubMed]
63. Stirone, C.; Duckles, S.P.; Krause, D.N. Multiple forms of estrogen receptor-alpha in cerebral blood vessels: Regulation by estrogen. *Am. J. Physiol. Endocrinol Metab.* **2003**, *284*, E184–E192. [CrossRef] [PubMed]
64. Stewart, P.A.; Magliocco, M.; Hayakawa, K.; Farrell, C.L.; Del Maestro, R.F.; Girvin, J.; Kaufmann, J.C.; Vinters, H.V.; Gilbert, J. A quantitative analysis of blood-brain barrier ultrastructure in the aging human. *Microvasc. Res.* **1987**, *33*, 270–282. [CrossRef]
65. Borghesan, M.; O'Loghlen, A. Integrins in senescence and aging. *Cell Cycle* **2017**, *16*, 909–910. [CrossRef]
66. Labat-Robert, J. Cell-matrix interactions, alteration with aging and age associated diseases. A review. *Pathol. Biol.* **2001**, *49*, 349–352. [CrossRef]
67. Wu, X.; Reddy, D.S. Integrins as receptor targets for neurological disorders. *Pharmacol. Ther.* **2012**, *134*, 68–81. [CrossRef]
68. Stamatovic, S.M.; Sladojevic, N.; Keep, R.F.; Andjelkovic, A.V. Relocalization of junctional adhesion molecule A during inflammatory stimulation of brain endothelial cells. *Mol. Cells Biol.* **2012**, *32*, 3414–3427. [CrossRef]
69. Mochida, G.H.; Ganesh, V.S.; Felie, J.M.; Gleason, D.; Hill, R.S.; Clapham, K.R.; Rakiec, D.; Tan, W.H.; Akawi, N.; Al-Saffar, M.; et al. A homozygous mutation in the tight-junction protein JAM3 causes hemorrhagic destruction of the brain, subependymal calcification, and congenital cataracts. *Am. J. Hum. Genet.* **2010**, *87*, 882–889. [CrossRef]
70. Saitou, M.; Furuse, M.; Sasaki, H.; Schulzke, J.D.; Fromm, M.; Takano, H.; Noda, T.; Tsukita, S. Complex phenotype of mice lacking occludin, a component of tight junction strands. *Mol. Biol. Cell* **2000**, *11*, 4131–4142. [CrossRef]
71. Gonzalez-Lozano, M.A.; Klemmer, P.; Gebuis, T.; Hassan, C.; van Nierop, P.; van Kesteren, R.E.; Smit, A.B.; Li, K.W. Dynamics of the mouse brain cortical synaptic proteome during postnatal brain development. *Sci. Rep.* **2016**, *6*, 35456. [CrossRef] [PubMed]
72. Zussy, C.; Loustalot, F.; Junyent, F.; Gardoni, F.; Bories, C.; Valero, J.; Desarménien, M.G.; Bernex, F.; Henaff, D.; Bayo-Puxan, N.; et al. Coxsackievirus Adenovirus Receptor Loss Impairs Adult Neurogenesis, Synapse Content, and Hippocampus Plasticity. *J. Neurosci.* **2016**, *36*, 9558–9571. [CrossRef] [PubMed]
73. Lochhead, J.J.; McCaffrey, G.; Quigley, C.E.; Finch, J.; DeMarco, K.M.; Nametz, N.; Davis, T.P. Oxidative stress increases blood-brain barrier permeability and induces alterations in occludin during hypoxia-reoxygenation. *J. Cereb. Blood Flow Metab.* **2010**, *30*, 1625–1636. [CrossRef] [PubMed]
74. Raz, L.; Knoefel, J.; Bhaskar, K. The neuropathology and cerebrovascular mechanisms of dementia. *J. Cereb. Blood Flow Metab.* **2016**, *36*, 172–186. [CrossRef]
75. Sugawara, T.; Fujimura, M.; Noshita, N.; Kim, G.W.; Saito, A.; Hayashi, T.; Narasimhan, P.; Maier, C.M.; Chan, P.H. Neuronal death/survival signaling pathways in cerebral ischemia. *NeuroRx* **2004**, *1*, 17–25. [CrossRef]

76. Roy-O'Reilly, M.; McCullough, L.D. Age and Sex Are Critical Factors in Ischemic Stroke Pathology. *Endocrinology* **2018**, *159*, 3120–3131. [CrossRef]
77. Lutski, M.; Zucker, I.; Shohat, T.; Tanne, D. Characteristics and Outcomes of Young Patients with First-Ever Ischemic Stroke Compared to Older Patients: The National Acute Stroke ISraeli Registry. *Front. Neurol.* **2017**, *8*, 421. [CrossRef]
78. Bauer, A.T.; Bürgers, H.F.; Rabie, T.; Marti, H.H. Matrix metalloproteinase-9 mediates hypoxia-induced vascular leakage in the brain via tight junction rearrangement. *J. Cereb. Blood Flow Metab.* **2010**, *30*, 837–848. [CrossRef]
79. Mark, K.S.; Davis, T.P. Cerebral microvascular changes in permeability and tight junctions induced by hypoxia-reoxygenation. *Am. J. Physiol. Heart Circ. Physiol.* **2002**, *282*, H1485–H1494. [CrossRef]
80. Lischper, M.; Beuck, S.; Thanabalasundaram, G.; Pieper, C.; Galla, H.J. Metalloproteinase mediated occludin cleavage in the cerebral microcapillary endothelium under pathological conditions. *Brain Res.* **2010**, *1326*, 114–127. [CrossRef]
81. Krizbai, I.; Bauer, H.; Bresgen, N.; Eckl, P.; Farkas, A.; Szatmari, E.; Traweger, A.; Wejksza, K.; Bauer, H. Effect of oxidative stress on the junctional proteins of cultured cerebral endothelial cells. *Cell. Mol. Neurobiol.* **2005**, *25*, 129–139. [CrossRef] [PubMed]
82. Koto, T.; Takubo, K.; Ishida, S.; Shinoda, H.; Inoue, M.; Tsubota, K.; Okada, Y.; Ikeda, E. Hypoxia disrupts the barrier function of neural blood vessels through changes in the expression of claudin-5 in endothelial cells. *Am. J. Pathol.* **2007**, *170*, 1389–1397. [CrossRef] [PubMed]
83. Schreibelt, G.; Kooij, G.; Reijerkerk, A.; van Doorn, R.; Gringhuis, S.I.; van der Pol, S.; Weksler, B.B.; Romero, I.A.; Couraud, P.O.; Piontek, J.; et al. Reactive oxygen species alter brain endothelial tight junction dynamics via RhoA, PI3 kinase, and PKB signaling. *Faseb. J.* **2007**, *21*, 3666–3676. [CrossRef] [PubMed]
84. Shen, F.; Jiang, L.; Han, F.; Degos, V.; Chen, S.; Su, H. Increased Inflammatory Response in Old Mice is Associated with More Severe Neuronal Injury at the Acute Stage of Ischemic Stroke. *Aging Dis.* **2019**, *10*, 12–22. [CrossRef] [PubMed]
85. Witt, K.A.; Mark, K.S.; Hom, S.; Davis, T.P. Effects of hypoxia-reoxygenation on rat blood-brain barrier permeability and tight junctional protein expression. *Am. J. Physiol. Heart Circ. Physiol.* **2003**, *285*, H2820–H2831. [CrossRef] [PubMed]
86. Willis, C.L.; Meske, D.S.; Davis, T.P. Protein kinase C activation modulates reversible increase in cortical blood-brain barrier permeability and tight junction protein expression during hypoxia and posthypoxic reoxygenation. *J. Cereb. Blood Flow Metab.* **2010**, *30*, 1847–1859. [CrossRef]
87. Knowland, D.; Arac, A.; Sekiguchi, K.J.; Hsu, M.; Lutz, S.E.; Perrino, J.; Steinberg, G.K.; Barres, B.A.; Nimmerjahn, A.; Agalliu, D. Stepwise recruitment of transcellular and paracellular pathways underlies blood-brain barrier breakdown in stroke. *Neuron* **2014**, *82*, 603–617. [CrossRef]
88. Kaur, J.; Tuor, U.I.; Zhao, Z.; Barber, P.A. Quantitative MRI reveals the elderly ischemic brain is susceptible to increased early blood-brain barrier permeability following tissue plasminogen activator related to claudin 5 and occludin disassembly. *J. Cereb. Blood Flow Metab.* **2011**, *31*, 1874–1885. [CrossRef]
89. Bai, Y.; Xu, G.; Xu, M.; Li, Q.; Qin, X. Inhibition of Src phosphorylation reduces damage to the blood-brain barrier following transient focal cerebral ischemia in rats. *Int. J. Mol. Med.* **2014**, *34*, 1473–1482. [CrossRef]
90. Kago, T.; Takagi, N.; Date, I.; Takenaga, Y.; Takagi, K.; Takeo, S. Cerebral ischemia enhances tyrosine phosphorylation of occludin in brain capillaries. *Biochem. Biophys. Res. Commun.* **2006**, *339*, 1197–1203. [CrossRef]
91. Takenaga, Y.; Takagi, N.; Murotomi, K.; Tanonaka, K.; Takeo, S. Inhibition of Src activity decreases tyrosine phosphorylation of occludin in brain capillaries and attenuates increase in permeability of the blood-brain barrier after transient focal cerebral ischemia. *J. Cereb. Blood Flow Metab.* **2009**, *29*, 1099–1108. [CrossRef] [PubMed]
92. Yang, Y.; Estrada, E.Y.; Thompson, J.F.; Liu, W.; Rosenberg, G.A. Matrix metalloproteinase-mediated disruption of tight junction proteins in cerebral vessels is reversed by synthetic matrix metalloproteinase inhibitor in focal ischemia in rat. *J. Cereb. Blood Flow Metab.* **2007**, *27*, 697–709. [CrossRef] [PubMed]
93. Yang, Y.; Rosenberg, G.A. MMP-mediated disruption of claudin-5 in the blood-brain barrier of rat brain after cerebral ischemia. *Methods Mol. Biol.* **2011**, *762*, 333–345. [CrossRef]

94. Yang, Y.; Thompson, J.F.; Taheri, S.; Salayandia, V.M.; McAvoy, T.A.; Hill, J.W.; Estrada, E.Y.; Rosenberg, G.A. Early inhibition of MMP activity in ischemic rat brain promotes expression of tight junction proteins and angiogenesis during recovery. *J. Cereb. Blood Flow Metab.* **2013**, *33*, 1104–1114. [CrossRef] [PubMed]
95. Rom, S.; Zuluaga-Ramirez, V.; Dykstra, H.; Reichenbach, N.L.; Ramirez, S.H.; Persidsky, Y. Poly(ADP-ribose) polymerase-1 inhibition in brain endothelium protects the blood-brain barrier under physiologic and neuroinflammatory conditions. *J. Cereb. Blood Flow Metab.* **2015**, *35*, 28–36. [CrossRef] [PubMed]
96. Yang, Y.; Salayandia, V.M.; Thompson, J.F.; Yang, L.Y.; Estrada, E.Y. Attenuation of acute stroke injury in rat brain by minocycline promotes blood-brain barrier remodeling and alternative microglia/macrophage activation during recovery. *J. Neuroinflammation* **2015**, *12*, 26. [CrossRef] [PubMed]
97. Weinl, C.; Castaneda Vega, S.; Riehle, H.; Stritt, C.; Calaminus, C.; Wolburg, H.; Mauel, S.; Breithaupt, A.; Gruber, A.D.; Wasylyk, B.; et al. Endothelial depletion of murine SRF/MRTF provokes intracerebral hemorrhagic stroke. *Proc. Natl. Acad. Sci. USA* **2015**, *112*, 9914–9919. [CrossRef]
98. Wang, W.; Dentler, W.L.; Borchardt, R.T. VEGF increases BMEC monolayer permeability by affecting occludin expression and tight junction assembly. *Am. J. Physiol. Heart Circ. Physiol.* **2001**, *280*, H434–H440. [CrossRef]
99. Argaw, A.T.; Asp, L.; Zhang, J.; Navrazhina, K.; Pham, T.; Mariani, J.N.; Mahase, S.; Dutta, D.J.; Seto, J.; Kramer, E.G.; et al. Astrocyte-derived VEGF-A drives blood-brain barrier disruption in CNS inflammatory disease. *J. Clin. Investig.* **2012**, *122*, 2454–2468. [CrossRef]
100. Elahy, M.; Jackaman, C.; Mamo, J.C.; Lam, V.; Dhaliwal, S.S.; Giles, C.; Nelson, D.; Takechi, R. Blood-brain barrier dysfunction developed during normal aging is associated with inflammation and loss of tight junctions but not with leukocyte recruitment. *Immun. Ageing* **2015**, *12*, 2. [CrossRef]
101. Banks, W.A.; Farr, S.A.; Morley, J.E. Permeability of the blood-brain barrier to albumin and insulin in the young and aged SAMP8 mouse. *J. Gerontol. A Biol. Sci. Med. Sci.* **2000**, *55*, B601–B606. [CrossRef] [PubMed]
102. Engelhardt, S.; Patkar, S.; Ogunshola, O.O. Cell-specific blood-brain barrier regulation in health and disease: A focus on hypoxia. *Br. J. Pharm.* **2014**, *171*, 1210–1230. [CrossRef] [PubMed]
103. Liu, W.; Sood, R.; Chen, Q.; Sakoglu, U.; Hendren, J.; Cetin, O.; Miyake, M.; Liu, K.J. Normobaric hyperoxia inhibits NADPH oxidase-mediated matrix metalloproteinase-9 induction in cerebral microvessels in experimental stroke. *J. Neurochem.* **2008**, *107*, 1196–1205. [CrossRef] [PubMed]
104. Blasig, I.E.; Bellmann, C.; Cording, J.; del Vecchio, G.; Zwanziger, D.; Huber, O.; Haseloff, R.F. Occludin Protein Family: Oxidative Stress and Reducing Conditions. *Antioxid. Redox Signal.* **2011**, *15*, 1195–1219. [CrossRef] [PubMed]
105. Bellmann, C.; Schreivogel, S.; Günther, R.; Dabrowski, S.; Schümann, M.; Wolburg, H.; Blasig, I.E. Highly conserved cysteines are involved in the oligomerization of occludin-redox dependency of the second extracellular loop. *Antioxid. Redox Signal.* **2014**, *20*, 855–867. [CrossRef] [PubMed]
106. Erickson, M.A.; Banks, W.A. Neuroimmune Axes of the Blood-Brain Barriers and Blood-Brain Interfaces: Bases for Physiological Regulation, Disease States, and Pharmacological Interventions. *Pharm. Rev.* **2018**, *70*, 278–314. [CrossRef] [PubMed]
107. Erickson, M.A.; Banks, W.A. Age-Associated Changes in the Immune System and Blood-Brain Barrier Functions. *Int. J. Mol. Sci.* **2019**, *20*, 1632. [CrossRef]
108. Ransohoff, R.M.; Engelhardt, B. The anatomical and cellular basis of immune surveillance in the central nervous system. *Nat. Rev. Immunol* **2012**, *12*, 623–635. [CrossRef]
109. Ousman, S.S.; Kubes, P. Immune surveillance in the central nervous system. *Nat. Neurosci.* **2012**, *15*, 1096–1101. [CrossRef]
110. Varatharaj, A.; Galea, I. The blood-brain barrier in systemic inflammation. *Brain Behav. Immun.* **2017**, *60*, 1–12. [CrossRef]
111. Gemechu, J.M.; Bentivoglio, M. T Cell Recruitment in the Brain during Normal Aging. *Front. Cell. Neurosci.* **2012**, *6*, 38. [CrossRef] [PubMed]
112. Xu, Y.Z.; Nygård, M.; Kristensson, K.; Bentivoglio, M. Regulation of cytokine signaling and T-cell recruitment in the aging mouse brain in response to central inflammatory challenge. *Brain Behav. Immun.* **2010**, *24*, 138–152. [CrossRef] [PubMed]
113. Stichel, C.C.; Luebbert, H. Inflammatory processes in the aging mouse brain: Participation of dendritic cells and T-cells. *Neurobiol. Aging* **2007**, *28*, 1507–1521. [CrossRef] [PubMed]

114. Ritzel, R.M.; Crapser, J.; Patel, A.R.; Verma, R.; Grenier, J.M.; Chauhan, A.; Jellison, E.R.; McCullough, L.D. Age-Associated Resident Memory CD8 T Cells in the Central Nervous System Are Primed to Potentiate Inflammation after Ischemic Brain Injury. *J. Immunol* **2016**, *196*, 3318–3330. [CrossRef]
115. Miguel-Hidalgo, J.J.; Nithuairisg, S.; Stockmeier, C.; Rajkowska, G. Distribution of ICAM-1 immunoreactivity during aging in the human orbitofrontal cortex. *Brain Behav. Immun.* **2007**, *21*, 100–111. [CrossRef]
116. Dulken, B.W.; Buckley, M.T.; Navarro Negredo, P.; Saligrama, N.; Cayrol, R.; Leeman, D.S.; George, B.M.; Boutet, S.C.; Hebestreit, K.; Pluvinage, J.V.; et al. Single-cell analysis reveals T cell infiltration in old neurogenic niches. *Nature* **2019**, *571*, 205–210. [CrossRef]
117. Suidan, G.L.; Mcdole, J.R.; Chen, Y.; Pirko, I.; Johnson, A.J. Induction of blood brain barrier tight junction protein alterations by CD8 T cells. *PLoS ONE* **2008**, *3*, e3037. [CrossRef]
118. Erickson, M.A.; Banks, W.A. Blood-brain barrier dysfunction as a cause and consequence of Alzheimer's disease. *J. Cereb. Blood Flow Metab.* **2013**, *33*, 1500–1513. [CrossRef]
119. Yamazaki, Y.; Kanekiyo, T. Blood-Brain Barrier Dysfunction and the Pathogenesis of Alzheimer's Disease. *Int. J. Mol. Sci.* **2017**, *18*, 1965. [CrossRef]
120. Marco, S.; Skaper, S.D. Amyloid beta-peptide1–42 alters tight junction protein distribution and expression in brain microvessel endothelial cells. *Neurosci. Lett.* **2006**, *401*, 219–224. [CrossRef]
121. Janota, C.; Lemere, C.A.; Brito, M.A. Dissecting the Contribution of Vascular Alterations and Aging to Alzheimer's Disease. *Mol. Neurobiol.* **2016**, *53*, 3793–3811. [CrossRef] [PubMed]
122. Wan, W.; Chen, H.; Li, Y. The potential mechanisms of Aβ-receptor for advanced glycation end-products interaction disrupting tight junctions of the blood-brain barrier in Alzheimer's disease. *Int. J. Neurosci.* **2014**, *124*, 75–81. [CrossRef] [PubMed]
123. Rosenberg, G.A. Matrix metalloproteinases and their multiple roles in neurodegenerative diseases. *Lancet Neurol.* **2009**, *8*, 205–216. [CrossRef]
124. Bourasset, F.; Ouellet, M.; Tremblay, C.; Julien, C.; Do, T.M.; Oddo, S.; LaFerla, F.; Calon, F. Reduction of the cerebrovascular volume in a transgenic mouse model of Alzheimer's disease. *Neuropharmacology* **2009**, *56*, 808–813. [CrossRef] [PubMed]
125. Carrano, A.; Hoozemans, J.J.; van der Vies, S.M.; van Horssen, J.; de Vries, H.E.; Rozemuller, A.J. Neuroinflammation and blood-brain barrier changes in capillary amyloid angiopathy. *Neurodegener. Dis.* **2012**, *10*, 329–331. [CrossRef] [PubMed]
126. Carrano, A.; Hoozemans, J.J.; van der Vies, S.M.; Rozemuller, A.J.; van Horssen, J.; de Vries, H.E. Amyloid Beta induces oxidative stress-mediated blood-brain barrier changes in capillary amyloid angiopathy. *Antioxid. Redox Signal.* **2011**, *15*, 1167–1178. [CrossRef]
127. Bruban, J.; Glotin, A.L.; Dinet, V.; Chalour, N.; Sennlaub, F.; Jonet, L.; An, N.; Faussat, A.M.; Mascarelli, F. Amyloid-beta (1–42) alters structure and function of retinal pigmented epithelial cells. *Aging Cell* **2009**, *8*, 162–177. [CrossRef]
128. Kook, S.Y.; Hong, H.S.; Moon, M.; Ha, C.M.; Chang, S.; Mook-Jung, I. $A\beta_{1\text{-}42}$-RAGE interaction disrupts tight junctions of the blood-brain barrier via Ca^{2+}-calcineurin signaling. *J. Neurosci.* **2012**, *32*, 8845–8854. [CrossRef]
129. Wan, W.; Cao, L.; Liu, L.; Zhang, C.; Kalionis, B.; Tai, X.; Li, Y.; Xia, S. Aβ (1–42) oligomer-induced leakage in an in vitro blood-brain barrier model is associated with up-regulation of RAGE and metalloproteinases, and down-regulation of tight junction scaffold proteins. *J. Neurochem.* **2015**, *134*, 382–393. [CrossRef]
130. Wan, W.B.; Cao, L.; Liu, L.M.; Kalionis, B.; Chen, C.; Tai, X.T.; Li, Y.M.; Xia, S.J. EGb761 provides a protective effect against Aβ1-42 oligomer-induced cell damage and blood-brain barrier disruption in an in vitro bEnd.3 endothelial model. *PLoS ONE* **2014**, *9*, e113126. [CrossRef]
131. Park, J.C.; Baik, S.H.; Han, S.H.; Cho, H.J.; Choi, H.; Kim, H.J.; Lee, W.; Kim, D.K.; Mook-Jung, I. Annexin A1 restores Aβ1-42-induced blood-brain barrier disruption through the inhibition of RhoA-ROCK signaling pathway. *Aging Cell* **2017**, *16*, 149–161. [CrossRef] [PubMed]
132. Mehrabadi, A.R.; Korolainen, M.A.; Odero, G.; Miller, D.W.; Kauppinen, T.M. Poly(ADP-ribose) polymerase-1 regulates microglia mediated decrease of endothelial tight junction integrity. *Neurochem. Int.* **2017**, *108*, 266–271. [CrossRef] [PubMed]
133. Chen, X.; Lan, X.; Roche, I.; Liu, R.; Geiger, J.D. Caffeine protects against MPTP-induced blood-brain barrier dysfunction in mouse striatum. *J. Neurochem.* **2008**, *107*, 1147–1157. [CrossRef] [PubMed]

134. Sarkar, S.; Chigurupati, S.; Raymick, J.; Mann, D.; Bowyer, J.F.; Schmitt, T.; Beger, R.D.; Hanig, J.P.; Schmued, L.C.; Paule, M.G. Neuroprotective effect of the chemical chaperone, trehalose in a chronic MPTP-induced Parkinson's disease mouse model. *Neurotoxicology* **2014**, *44*, 250–262. [CrossRef] [PubMed]
135. Carvey, P.M.; Zhao, C.H.; Hendey, B.; Lum, H.; Trachtenberg, J.; Desai, B.S.; Snyder, J.; Zhu, Y.G.; Ling, Z.D. 6-Hydroxydopamine-induced alterations in blood-brain barrier permeability. *Eur. J. Neurosci.* **2005**, *22*, 1158–1168. [CrossRef]
136. Huang, L.; Deng, M.; He, Y.; Lu, S.; Ma, R.; Fang, Y. β-asarone and levodopa co-administration increase striatal dopamine level in 6-hydroxydopamine induced rats by modulating P-glycoprotein and tight junction proteins at the blood-brain barrier and promoting levodopa into the brain. *Clin. Exp. Pharm. Physiol.* **2016**, *43*, 634–643. [CrossRef]
137. Kuan, W.L.; Bennett, N.; He, X.; Skepper, J.N.; Martynyuk, N.; Wijeyekoon, R.; Moghe, P.V.; Williams-Gray, C.H.; Barker, R.A. α-Synuclein pre-formed fibrils impair tight junction protein expression without affecting cerebral endothelial cell function. *Exp. Neurol.* **2016**, *285 Pt A*, 72–81. [CrossRef]
138. Pienaar, I.S.; Lee, C.H.; Elson, J.L.; McGuinness, L.; Gentleman, S.M.; Kalaria, R.N.; Dexter, D.T. Deep-brain stimulation associates with improved microvascular integrity in the subthalamic nucleus in Parkinson's disease. *Neurobiol. Dis.* **2015**, *74*, 392–405. [CrossRef]
139. Gray, M.T.; Woulfe, J.M. Striatal blood-brain barrier permeability in Parkinson's disease. *J. Cereb. Blood Flow Metab.* **2015**, *35*, 747–750. [CrossRef]
140. Drouin-Ouellet, J.; Sawiak, S.J.; Cisbani, G.; Lagacé, M.; Kuan, W.L.; Saint-Pierre, M.; Dury, R.J.; Alata, W.; St-Amour, I.; Mason, S.L.; et al. Cerebrovascular and blood-brain barrier impairments in Huntington's disease: Potential implications for its pathophysiology. *Ann. Neurol.* **2015**, *78*, 160–177. [CrossRef]
141. Lim, R.G.; Quan, C.; Reyes-Ortiz, A.M.; Lutz, S.E.; Kedaigle, A.J.; Gipson, T.A.; Wu, J.; Vatine, G.D.; Stocksdale, J.; Casale, M.S.; et al. Huntington's Disease iPSC-Derived Brain Microvascular Endothelial Cells Reveal WNT-Mediated Angiogenic and Blood-Brain Barrier Deficits. *Cell Rep.* **2017**, *19*, 1365–1377. [CrossRef] [PubMed]
142. Greene, C.; Kealy, J.; Humphries, M.M.; Gong, Y.; Hou, J.; Hudson, N.; Cassidy, L.M.; Martiniano, R.; Shashi, V.; Hooper, S.R.; et al. Dose-dependent expression of claudin-5 is a modifying factor in schizophrenia. *Mol. Psychiatry* **2018**, *23*, 2156–2166. [CrossRef] [PubMed]
143. Takechi, R.; Galloway, S.; Pallebage-Gamarallage, M.M.; Mamo, J.C. Chylomicron amyloid-beta in the aetiology of Alzheimer's disease. *Atheroscler. Suppl.* **2008**, *9*, 19–25. [CrossRef]
144. Poduslo, J.F.; Curran, G.L.; Wengenack, T.M.; Malester, B.; Duff, K. Permeability of proteins at the blood-brain barrier in the normal adult mouse and double transgenic mouse model of Alzheimer's disease. *Neurobiol. Dis.* **2001**, *8*, 555–567. [CrossRef] [PubMed]
145. Cheng, Z.; Zhang, J.; Liu, H.; Li, Y.; Zhao, Y.; Yang, E. Central nervous system penetration for small molecule therapeutic agents does not increase in multiple sclerosis- and Alzheimer's disease-related animal models despite reported blood-brain barrier disruption. *Drug Metab. Dispos.* **2010**, *38*, 1355–1361. [CrossRef] [PubMed]
146. Mehta, D.C.; Short, J.L.; Nicolazzo, J.A. Altered brain uptake of therapeutics in a triple transgenic mouse model of Alzheimer's disease. *Pharm. Res.* **2013**, *30*, 2868–2879. [CrossRef] [PubMed]
147. Daneman, R.; Zhou, L.; Kebede, A.A.; Barres, B.A. Pericytes are required for blood-brain barrier integrity during embryogenesis. *Nature* **2010**, *468*, 562–566. [CrossRef]
148. Sagare, A.P.; Bell, R.D.; Zhao, Z.; Ma, Q.; Winkler, E.A.; Ramanathan, A.; Zlokovic, B.V. Pericyte loss influences Alzheimer-like neurodegeneration in mice. *Nat. Commun.* **2013**, *4*, 2932. [CrossRef]
149. Sengillo, J.D.; Winkler, E.A.; Walker, C.T.; Sullivan, J.S.; Johnson, M.; Zlokovic, B.V. Deficiency in mural vascular cells coincides with blood-brain barrier disruption in Alzheimer's disease. *Brain Pathol.* **2013**, *23*, 303–310. [CrossRef]
150. Tai, L.M.; Thomas, R.; Marottoli, F.M.; Koster, K.P.; Kanekiyo, T.; Morris, A.W.; Bu, G. The role of APOE in cerebrovascular dysfunction. *Acta Neuropathol.* **2016**, *131*, 709–723. [CrossRef]
151. Brandon, J.A.; Farmer, B.C.; Williams, H.C.; Johnson, L.A. Apoe and Alzheimer's Disease: Neuroimaging of Metabolic and Cerebrovascular Dysfunction. *Front. Aging Neurosci.* **2018**, *10*, 180. [CrossRef] [PubMed]
152. Bell, R.D.; Winkler, E.A.; Singh, I.; Sagare, A.P.; Deane, R.; Wu, Z.; Holtzman, D.M.; Betsholtz, C.; Armulik, A.; Sallstrom, J.; et al. Apolipoprotein E controls cerebrovascular integrity via cyclophilin A. *Nature* **2012**, *485*, 512–516. [CrossRef] [PubMed]

153. Daneman, R.; Prat, A. The blood-brain barrier. *Cold Spring Harb. Perspect. Biol.* **2015**, *7*, a020412. [CrossRef] [PubMed]
154. Zenaro, E.; Piacentino, G.; Constantin, G. The blood-brain barrier in Alzheimer's disease. *Neurobiol. Dis.* **2017**, *107*, 41–56. [CrossRef]
155. Sweeney, M.D.; Sagare, A.P.; Zlokovic, B.V. Blood-brain barrier breakdown in Alzheimer disease and other neurodegenerative disorders. *Nat. Rev. Neurol.* **2018**, *14*, 133–150. [CrossRef]
156. Greene, C.; Hanley, N.; Campbell, M. Claudin-5: Gatekeeper of neurological function. *Fluids Barriers CNS* **2019**, *16*, 3. [CrossRef]
157. Lee, H.; Pienaar, I.S. Disruption of the blood-brain barrier in Parkinson's disease: Curse or route to a cure? *Front. Biosci. (Landmark Ed.)* **2014**, *19*, 272–280. [CrossRef]
158. Pan, Y.; Nicolazzo, J.A. Impact of aging, Alzheimer's disease and Parkinson's disease on the blood-brain barrier transport of therapeutics. *Adv. Drug Deliv. Rev.* **2018**, *135*, 62–74. [CrossRef]
159. Farkas, E.; De Jong, G.I.; de Vos, R.A.; Jansen Steur, E.N.; Luiten, P.G. Pathological features of cerebral cortical capillaries are doubled in Alzheimer's disease and Parkinson's disease. *Acta Neuropathol.* **2000**, *100*, 395–402. [CrossRef]
160. Guan, J.; Pavlovic, D.; Dalkie, N.; Waldvogel, H.J.; O'Carroll, S.J.; Green, C.R.; Nicholson, L.F. Vascular degeneration in Parkinson's disease. *Brain Pathol.* **2013**, *23*, 154–164. [CrossRef]
161. Hill, K.K.; Campbell, M.C.; McNeely, M.E.; Karimi, M.; Ushe, M.; Tabbal, S.D.; Hershey, T.; Flores, H.P.; Hartlein, J.M.; Lugar, H.M.; et al. Cerebral blood flow responses to dorsal and ventral STN DBS correlate with gait and balance responses in Parkinson's disease. *Exp. Neurol.* **2013**, *241*, 105–112. [CrossRef] [PubMed]
162. Horvath, S.; Langfelder, P.; Kwak, S.; Aaronson, J.; Rosinski, J.; Vogt, T.F.; Eszes, M.; Faull, R.L.; Curtis, M.A.; Waldvogel, H.J.; et al. Huntington's disease accelerates epigenetic aging of human brain and disrupts DNA methylation levels. *Aging (Albany Ny)* **2016**, *8*, 1485–1512. [CrossRef] [PubMed]
163. Okusaga, O.O. Accelerated aging in schizophrenia patients: The potential role of oxidative stress. *Aging Dis.* **2014**, *5*, 256–262. [CrossRef] [PubMed]

International Journal of
Molecular Sciences

MDPI

Review

Role of Claudin Proteins in Regulating Cancer Stem Cells and Chemoresistance-Potential Implication in Disease Prognosis and Therapy

Saiprasad Gowrikumar [1], Amar B. Singh [1,2,3] and Punita Dhawan [1,2,3,*]

[1] Department of Biochemistry and Molecular Biology, University of Nebraska Medical Center, Omaha, NE 68198-5870, USA; sai.gowrikumar@unmc.edu (S.G.); amar.singh@unmc.edu (A.B.S.)
[2] VA Nebraska-Western Iowa Health Care System, Omaha, NE 68105, USA
[3] Department of Biochemistry and Molcular Biology, Fred and Pamela Buffet Cancer Center, University of Nebraska Medical Center, Omaha, NE 68105, USA
* Correspondence: punita.dhawan@unmc.edu; Tel.: +(402)-559-6587

Received: 27 October 2019; Accepted: 13 December 2019; Published: 20 December 2019

Abstract: Claudins are cell–cell adhesion proteins, which are expressed in tight junctions (TJs), the most common apical cell-cell adhesion. Claudin proteins help to regulate defense and barrier functions, as well as differentiation and polarity in epithelial and endothelial cells. A series of studies have now reported dysregulation of claudin proteins in cancers. However, the precise mechanisms are still not well understood. Nonetheless, studies have clearly demonstrated a causal role of multiple claudins in the regulation of epithelial to mesenchymal transition (EMT), a key feature in the acquisition of a cancer stem cell phenotype in cancer cells. In addition, claudin proteins are known to modulate therapy resistance in cancer cells, a feature associated with cancer stem cells. In this review, we have focused primarily on highlighting the causal link between claudins, cancer stem cells, and therapy resistance. We have also contemplated the significance of claudins as novel targets in improving the efficacy of cancer therapy. Overall, this review provides a much-needed understanding of the emerging role of claudin proteins in cancer malignancy and therapeutic management.

Keywords: claudins; cancer; stem cell; chemoresistance

1. Introduction

1.1. Tight Junctions

Tight junctions (TJs) are the sites where tissues interface directly with the external environment or internal compartments that are contiguous with the external environment and are lined by mucosal surfaces, where epithelial cells act insulation for the internal organ. These structures not only provide a protective layer but also act as a selective barrier between the body and the gut lumen that restricts free exchange across the paracellular space [1,2]. There are three main transport mechanisms across the epithelial layers, which include the trans-cellular pathway (passive diffusion), carrier dependent pathway (carrier or receptors), and the paracellular pathway (passage through spaces between cells). Among these transport mechanisms, the apical junctional complex, a crucial factor for the paracellular pathway, is composed of three junctions from apical to basal are known as the tight junction (zonula occludens), adherens junction (zonula adherens), and desmosome (macula adherens) [3]. The TJs are intercellular junctions, which act as permeability barriers in epithelial cells [1]. The tight junction proteins are diverse and include occludins (the first one to be found), claudins, tricellulin, cingulin, and junctional adhesion molecules (JAM). These proteins interact within themselves and with the cellular cytoskeleton to form a complex architecture [4–8]. Among these TJ proteins, claudins are key proteins, acting as both pores and barriers, aiding the paracellular pathway between epithelial cells [9,10].

1.2. Claudins

The functionalities of claudins are as follows: (1) Fence function, responsible for maintaining polarity by differentiating apical and basolateral cell domains; (2) Signaling molecule, involved in cell growth, survival, proliferation, and differentiation; (3) Barrier function, this gate function separates compartments with fluids to avoid intermixing [11]. Claudins were identified as a major integral membrane protein by Tsukita and his colleagues in 1998, before which the only known tight junction protein was occludin [12,13]. Studies conducted to overexpress claudins in fibroblasts, which do not have tight junctions, were able to reconstitute tight junction-like networks of strands, which shows the importance of claudins in tight junction assembly [14]. Several claudin isoforms have been identified in mammals. These have high sequence homology in the first and fourth transmembrane domains and extracellular loops. Further, the homologous classic claudins include claudins 1–10, 14, 15, 17, and 19, and non-classical claudins comprised of claudins 11–13, 16, 18, and 20–27, which are less homologous [15].

The structure of claudins is comprised of four transmembrane domains, the intracellular N and C termini, and the two extracellular loops (ECLs). The claudin structure encompasses N-termini (7 amino acids), C-termini (25–55 amino acids), and loops containing 25–55 aminoacids. The ECLs are involved in barrier and pore formations. There are two ECLs, ECL1 consists of ~50 amino acids with two conserved cysteines involved in the barrier function. Negative and positive charges in ECL1 contribute to pore formation. The schematic representation of the structure of claudins and its classification is depicted (Figure 1). The ECL2 is responsible for homo and heterotypic interactions and was recently shown to be involved in host cell binding and cytotoxicity for the *Clostridium perfringens* enterotoxin. The ECL2 usually has ~25 amino acids, but fewer in claudin-11 and more in claudin-18 [16]. Claudins interact with other TJ-associated proteins through carboxy-terminal tails, which contain a PDZ-domain binding motif [17].

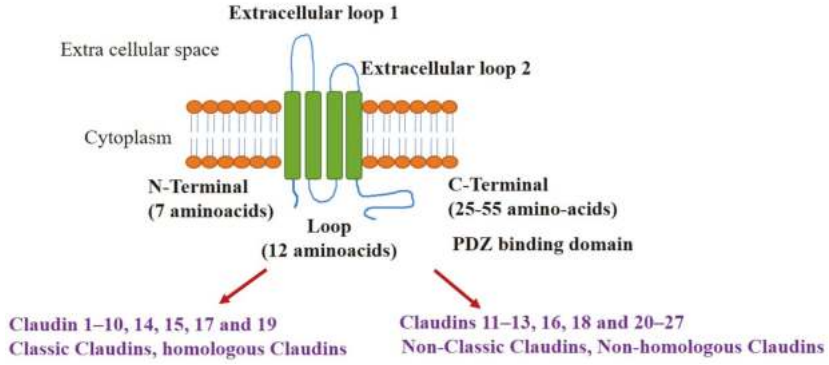

Figure 1. Structural organization of claudin proteins (monomer), and its classification based on homologous sequences between them. Colour code: Green- transmembrane domains; Orange: Bilipid layer, Blue–Extracellular loops/N and C termini.

2. Claudins as Oncogenic Signal Transducer

The expression of claudins varies among different tissue types [18]. As an important structure in regulating paracellular permeability, claudin overexpression influences trans-epithelial resistance (TER) and ion permeability [19–22]. Aberrant expressions of claudins have been reported in various cancers. Some of the claudins known to be frequently dysregulated in cancers are claudin-1, -3, -4, and -7 [23]. A large body of evidence highlights claudins as pro and anti-tumorigenic factors [24–31]. The potential of claudins to act as proto-oncogene or tumor promotor in various cancers are summarized in Table 1. In addition, several recent studies have also demonstrated the importance of claudins as tumor

suppressors [24–31]. A recent study by Chang et al. in 2019 provided evidence for intestinal hyperplasia and adenomas in claudin-7 knockdown mice [32]. Consistent with this, claudin-7 was downregulated in colon cancer patient samples as compared to normal tissue [33]. These effects of claudin-7 were achieved by inhibiting phosphorylation and nuclear localization of Akt. Conversely, claudin-7 association with Epithelial cell adhesion molecule (EPCAM) supports proliferation, upregulation of anti-apoptotic proteins, and drug resistance [33]. Claudin-18 knockout mice spontaneously developed lung adenocarcinomas, and its mRNA expression was decreased in lung adenocarcinomas. Claudin-18 inhibits Akt signaling through modulation of yes-associated protein/Taz (Yap/Taz) and insulin-like growth factor (IGF-1R) signaling in lung cancer [34]. Further, the depletion of claudin-3 induced tumor burden by enhancing β-catenin activity through (IL)-6/STAT3 signaling in colon cancer [35]. Yet another study by Che et al. in 2018 [36] identified claudin-3 as a suppressor of lung squamous cell carcinoma cells, in which overexpression of claudin-3 inhibited invasion, migration, and EMT of lung squamous cell carcinoma. Similarly, claudin-4 accelerates cell migration and invasion in ovarian tumor cell lines, in support of this, peptide-mediated silencing of claudin-4 in ovarian cancer cells exhibited lower tumor burden [37]. Claudin-6 was shown to be a tumor suppressor through genetic manipulation studies in cervical carcinoma cells wherein loss of claudin-6 exacerbated cell proliferation and tumor growth [38,39]. An array of articles from Dhawan et al., have proved a significant role of claudin-1 as a tumor promoter in colon cancer [40,41]. In one of their reports, increased claudin-1 expression was causally associated with metastasis [40]. In contrast to claudin-1, claudin-7 has an inverse role on EMT, wherein it causes mesenchymal to epithelial transformation (MET) in Rab25 dependent manner to combat colon cancer [42]. Similarly, claudin-2 is upregulated in colon cancer and is involved in cancer progression. Claudin-2 suppression in colon cancer cells has led to decreased cell proliferation through the modulation of EGF signaling [43]. Opposite colon cancer, claudin-1 is frequently down-regulated in invasive human breast cancer. Recently, mutations of claudin-1 have been reported in breast cancer, which has led to claudin-1 transcript variants shorter than classical claudin-1 transcript [44]. Taken together, it appears that the deregulated claudin composition in any given epithelial cells sheet may modify the signaling and associated changes in protein partnering to modulate oncogenesis.

Table 1. Claudins as tumour promotor/suppressor.

Claudins Subtype	Cancer Type	Proto-Oncogene	Reference
Claudin-6	Gastric cancer	Tumour promotor	[25]
Claudin-1	Colon cancer	Tumour promotor	[40,45]
Claudin-3	Ovarian cancer	Tumour promotor	[22]
Claudin-4	Ovarian cancer	Tumour promotor	[22]
Claudin-6	Breast cancer, Gastric cancer	Tumour promotor	[26,27]
Claudin-7	Colon cancer	Tumour promotor	[46]
Claudin-2	Lung cancer	Tumour promotor	[28]
Claudin-1	Gastric cancer	Tumour suppressor	[47]
Claudin-1	Lung cancer	Tumour suppressor	[29]
Claudin-3	Ovarian cancer	Tumour suppressor	[31]
Claudin-4	Ovarian cancer	Tumour suppressor	[31]
Claudin-7	Lung cancer	Tumour suppressor	[30]
Claudin-11	Gastric cancer	Tumour suppressor	[48]
Claudin-2	Osteosarcoma	Tumour suppressor	[49]

To glimpse how claudins can achieve its pro or anti-tumorigenic effect, understanding the regulation of claudins in normal and cancer cells is essential. Recently it has been demonstrated that claudins are not a static and rigid seal of the paracellular space; rather, they are dynamically capable of responding to various biochemical and mechanical stimuli through reshaping and remodeling [50,51]. Epigenetic regulation of claudins has recently gained significant importance. The claudin-3 promotor

is known to possess low DNA methylation and high histone H3 acetylation for its expression in ovarian cancer cells [52]. DNA hypomethylation of the claudin-4 promotor is an important factor for its high expressions in gastric cancer [53]. Downregulation of claudin 1 via DNA promoter methylation is reported in estrogen receptor-positive breast cancer [54]. Claudins are also regulated at the transcriptional level by different transcription factors. A study has reported novel post-transcriptional regulation of claudin-1 in colon cancer cells [55], the authors documented the role of histone deacetylase (HDAC)-dependent histone acetylation as a key post-transcriptional regulation over claudin-1 expression, as found through HDAC inhibitor studies. Studies demonstrate the interaction of Slug and Snail (transcriptional factors) with the E-box element in the claudin-1 promoter causes inhibition of claudin-1. Snail is known to act as a transcription factor causing repression of E-cadherin (E-CAD) and has a potential role in promoting tumorigenesis. Slug is also a pivotal transcription factor involved in cell migration during embryogenesis and in tumor cell invasion and migration [56]. Yet another transcriptional factor known to be associated with claudin-1 is Runt-related transcription factor 3 (RUNX3), which is a gastric tumor suppressor [47]. Caudal homeobox proteins (Cdx1 & Cdx2) and GATA binding protein 4, GATA4) are known activators of claudin-1 promoters in colon cancer [57]. Sp1 is a transcriptional factor known to regulate claudin-3 and claudin-4 promoter activity in ovarian cancer [52,58]. Apart from these transcriptional regulations, claudins are also known to be regulated by post-translational modifications involved in their protein localization, interaction with other proteins, and overall turnover [59,60]. The post-translational modification of claudins includes palmitoylation, O-glycosylation, and phosphorylation [61,62]. Phosphorylation is one of the key regulatory modifications for the regulation of intracellular localization and degradation of claudins.

Claudins are phosphorylated by many different enzymes like protein-kinase A/C, protein phosphatase 2A and mitogen-activated protein kinase (MAPK) [63,64]. The localization or dissociation of claudins to TJs is regulated by phosphorylation. For phosphorylated claudin-1, -5, and -16 are localized in the TJs while in contrast, phosphorylated claudin-3 and -4 dissociate from TJs [64–66]. Furthermore, the rho family of small dimeric G proteins mediated phosphorylation of claudin-5 at T207 was recently reported [67]. The phosphorylation of claudin-1 at different serine sites (192, 205, 206, and T191) regulates its assembly at tight junctions [68]. The cAMP-dependent protein kinase (PKA) is known to phosphorylate of claudin-3 at amino acid 192 at the C terminus. Claudin-4 is phosphorylated by atypical PKC (aPKC) at serine195 [65]. Another important posttranslational modification playing a key role in claudin regulation is palmitoylation. Emerging articles have demonstrated the importance of palmitoylation in claudin localization into tight junctions. In claudin-5 self-assembly, palmitoylation restricts specific protein-protein conformations, as reported by Rajagopal et al. [61]. Claudin-7 interacts directly with EpCAM along the basal membrane. Palmitoylation regulates the ability of claudin-7 to interact with integrins, recruiting EpCAM, and concomitantly associate with the actin cytoskeleton [69].

3. Claudins and Stem Cells

Stem cells are crucial for the development and homeostasis of many different tissues. Stem cells are also involved in cell replacement therapies in the case of cell damage or degeneration [70]. Pluripotency of stem cells is defined as self-renewing and differentiating potential into all three germ layers. Human pluripotent stem cells are very promising in regenerative medicine. The stem cell further differentiates into a wide variety of cells under the influence of diverse signaling molecules, growth factors, and transcription factors [71]. Recent research is focused on understanding the signals, which maintain pluripotency or differentiation potential. Various intrinsic and extrinsic factors are involved in stem cell maintenance, self-renewal, and differentiation [71]. On the other hand, stem cells are also an important factor for many tumors. Dysregulated pluripotent stem cells in tumors are more aggressive and have the potential to reform the whole tumor [72]. Thus, it becomes important to selectively remove undifferentiated human pluripotent stem cells (hPSCs) from differentiated cultures. For achieving this, selective pluripotent-specific cell surface markers are needed, which can separate undifferentiating from the differentiated cells. While screening for a highly specific marker protein

specific for the undifferentiated hPSCs, Uri Ben-David et al. [73] found claudin-6 to be highly specific for undifferentiated hPSCs. The expression of claudin-6 was 90-fold higher in undifferentiated hPSCs than in differentiated cells. The proof for the involvement of claudins in epithelial differentiation from embryonic stem cells was first reported by Sugimoto et al. [74], where the potential of claudin-6 to trigger epithelial morphogenesis in mouse stem cells was reported. Also, claudin-6 regulated other tight-junction and microvillus molecules claudin-7, occludin, Zonula occludens (ZO-1α+), and ezrin/radixin/moesin-binding phosphoprotein50, which strongly proved the role of claudins in epithelial differentiation [74]. This was further supported by other studies, which also showed the expression of claudin-6 is an early marker in embryonic stem cells [75,76]. Differentiation of Human Embryonic Stem Cells to Hepatocyte-Like Cells resulted in a decrease in stem cell markers Oct3/4 and Nanog as expected. Along with stem cell markers, claudin-1 declined eventually, whereas claudin-4 increased and was highest at the end stage of differentiation [77].

A growing body of evidence focuses on cancer stem cells in cancer biology. The drawbacks of cancer treatment failures and drug resistance are proved to originate from cancer stem cells, which are a small subpopulation in tumors. Recently the factors regulating cancer stem cells have gained significant importance and opened new avenues for targeted therapies and thus decrease the chance of recurrence of the disease [78]. Cancer stem cells (CSCs) represent a small group of cells in typically heterogeneous tumors, which possess tumor-initiating and self-renewal properties, giving rise to non-tumorigenic progeny. CSCs are enriched after chemotherapy and lead to therapy failure and thus recurrence of cancer. The role of CSCs in tumor relapse, metastasis, and therapeutic refractoriness is well described [79]. The role of claudins in cancer stem cell (CSC) biology is gaining much attention. The WNT pathway is well known to provide the key signals for achieving this particular phenotype. It is also established that the *Wnt* signal transduction pathway is important in normal and malignant stem cells [80]. Recent articles have highlighted the link between claudin and the *Wnt*/β-catenin signaling pathway and the role of CSC in this cross-talk. Claudin-1 and claudin-2 transcription is regulated by WNT*t* signaling, and they are known to regulate the β-Catenin- T-cell factor/lymphoid enhancer-binding factor (TCF/LEF) signaling pathway to regulate CSC [81,82]. In contrast, other claudins negatively regulate WNTsignaling cascades, such as loss of claudin-3 inducing WNT/β-catenin activation, thus aiding in the promotion of colon cancer [35]. Darido et al. provided evidence for Tcf-4 and Sox-9 regulating the expression of claudin-7 [46]. In addition, studies by Prat et al. discovered a new claudin-low molecular subtype of breast cancer [83]. The key characteristics of this subtype are low expression of tight junction and junction adherens proteins (claudin-3, -4 and -7, and E-cadherin), and enriched in stem cell and EMT features. Patients having high-grade invasive ductal breast carcinoma in this subgroup had a poor prognosis, absence of luminal differentiation markers, enhanced EMT markers, expression of immune response genes, and most closely resembled mammary epithelial stem cells. This suggested that low claudin cells might emerge from more immature stem or progenitor cells and comprise cancer stem cells. Thus, identification of the low claudin subtype in breast cancer has shown the potential of claudins in regulating stem cells. In addition, claudin-3 is known to play an oncogenic role in non-small cell lung cancer (NSCLC). One of the major contributing factors for the role of claudin-3 is regulation of cancer stemness and chemoresistance in non-squamous NSCLC. The depletion of claudin-3 was able to combat the formation of spheres and tumor formation as well as increased sensitivity to cisplatin [84]. Further, claudin-3 inhibition by small-molecule inhibitors including withaferin A, estradiol and fulvestrant, suppressed cancer stemness and combated chemoresistance, giving strong evidence for the role of claudin-3 in inducing stemness. Another claudin playing an important role in stem cell regulation is claudin-18 in lung cancer [85], which has been reported to have a role in the aberrant proliferation of alveolar epithelial type II (AT2) cells, resulting in lung enlargement and parenchymal expansion by restrictions on stem/progenitor cell proliferation. Recently, claudin-2 was shown to be restricted in the stem/progenitor cell compartment of intestinal crypts. It enriches aldehyde dehydrogenase $ALDH^{High}$ cancer stem-like cells in heterogeneous colorectal cancer cell populations through the regulation of Yes-associated protein (YAP) activity and miR-222-3p

expression [86]. Overall, these studies give an overview of the potential role of claudins in stem cell biology. The role of claudins in the regulation of stem cells is summarized in Table 2. The claudin mediated enrichment of stem cells provides a new axis-of-evil for a preferential therapeutic target, which has potential clinical consequences.

Table 2. Claudins and stemness.

Claudin Subtype	Stem Cell Related Functions	References
Claudin-6	Early marker in embryonic stem cell.High expression in undifferentiated human pluripotent stem cells (hPSCs). Trigger epithelial morphogenesis in mouse stem cells.	[73,74]
Claudin-1 and 2	Known to regulate the β-Catenin-TCF/LEF signaling pathway to regulate CSC.	[81]
Claudin low subtype in breast cancer	Enriched in stem cells and more EMT.	[83]
Claudin-3	Regulation on cancer stemness and chemoresistance in non-small cell lung cancer (NSCLC).	[84]
Claudin-18	Triggers lung enlargement and parenchymal expansion by restrictions on stem/progenitor cell proliferation.	[85]
Claudin-2	Enrich $ALDH^{High}$ cancer stem-like cells in heterogeneous colorectal cancer cell populations.	[86]

4. Claudins in Chemoresistance

Most cancer patients initially respond to chemotherapy. Eventually, cancer relapses due to chemoresistance resulting in treatment failure causing death. The mechanisms of chemoresistance in cancers are still largely unknown [87]. Since the role of claudins in the regulation of cancer stem cells is well documented, their correlation with drug resistance and distant metastasis is inevitable and obvious [49,88,89]. In brief, claudin-3 and -6 are correlated with lymph node metastasis in squamous cell lung carcinomas [90,91]. Claudin-4 is highly expressed in primary and metastatic prostate cancer [92] and gastric cancer [93,94]. Claudin-1 and -7 have proved to have an inverse role in colon cancer, wherein claudin-1 elevates the metastasis of colon cancer cells. On the other hand, suppression of claudin-7 leads to liver metastasis [40,42]. Epithelial to mesenchymal transition (EMT) is a piece of vital machinery responsible for invasiveness and initiation of metastasis and chemoresistance of cancer cells. Claudins are known inducers of EMT in cancers. Claudin-1 is known to induce EMT in colon, liver, nasopharyngeal carcinoma, and breast cancers [40,95,96]. At the same time, claudin-7 is reported to be involved in establishing MET in colon cancer [36,42]. Claudin-3 suppresses EMT in lung cancer cells [36]. Overall, the potential role of claudins in EMT, Metastasis and CSC enrichment provides the rationale for exploring them as a key factor in establishing drug resistance. Claudins as chemo-resistance modulators is an emerging field of research. In a recent article, the potential of claudin-6 in enhancing chemoresistance to Adriamycin in triple-negative breast cancer (TNBC) was documented [97]. This effect of claudin-6 was mediated through its regulation over the AF-6/extracellular signal–regulated kinases (AF-6/ERK signaling pathway and up-regulation of cancer stem cells. Claudin-3 is also identified as a molecule to combat cisplatin chemoresistance in non-squamous lung carcinoma [84]. Here, claudin-3 overexpressing lung cancer cells were insensitive to cisplatin treatment compared to control cells. Adding to this, knockdown of claudin-3 or claudin-4 in ovarian cancer cells induced resistance to cisplatin by the regulation of Cu transporter CTR1 [98]. Another study by a Japanese group of researchers reported a high expression of claudin-4 in the ovarian cancer tissues of platinum-resistant patients [99]. In lung cancer, claudin-1 is a key deciding factor for metastasis and a responsible factor for drug resistance towards cisplatin through the up-regulation of Unc-51 Like Autophagy Activating Kinase 1 (ULK1) phosphorylation [100,101]. It is also known to enhance drug resistance in liver cancer cells by modulating autophagy to achieve drug resistance. The

role of claudin-7 in drug resistance [102] has also been reported, wherein decreased drug resistance, increased apoptosis and diminished anti-apoptotic PI3K/Akt pathway was achieved by knocking down claudin-7, proving the potentiality in chemo-resistance [103]. It is well known that EpCAM associates with claudin-7 and is known to be involved in cancer metastasis. Florian et al. [69] have provided evidence for the increased migratory potential of pancreatic cancer cells upon EPCAM and claudin-7 association influencing cell-cell adhesion. Interestingly, the EPCAM and claudin-7 association seems to enhance drug resistance against cisplatin through enhancing MAPK and c-Jun N-terminal kinases (JNK) pathways. Altogether, these studies indicate the important role of claudins contributing to drug resistance in cancer cells. The pictorial representation of the role of claudins as a stem cell regulator and its impact in chemoresistance is shown in Figure 2.

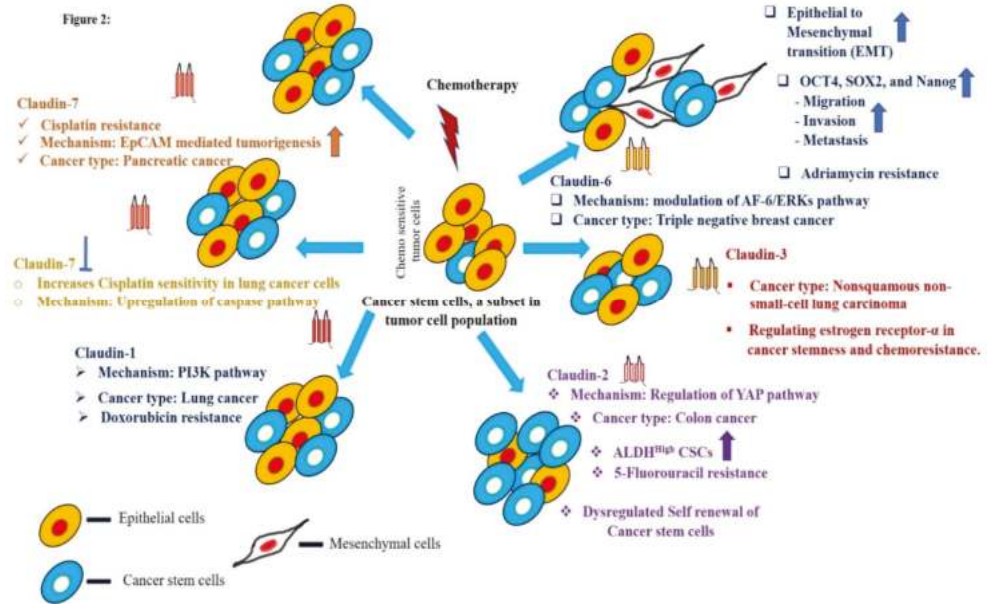

Figure 2. The central role of claudins in the regulation of epithelial to mesenchymal transition (EMT), cancer stem cells, and chemoresistance in various cancers. ⊥- inhibition of claudin-7. The arrows indicate the upregulation and higher enrichment of the mentioned signaling molecules, colour is respective of each claudin.

5. Claudins in Prognosis

Emerging data defining mechanisms through which claudins augment cancer metastasis provides the rationale for exploring claudins as prognostic factors and therapeutic targets in cancer. The importance of claudins is established using cancer cell models, mouse models, and human patient samples. Target molecules for cancer surveillance in high-risk populations are desperately warranted. As a vital emerging modulator in molecular or cellular pathways related to cancers, claudins could be targeted or used as biomarkers for prognosis, diagnosis, and treatments. A number of recent studies have projected a role for claudins as key prognosis factors in cancers. In one of the study Lechpammer et al. [104] demonstrated the potential of claudins as a diagnostic and prognostic factor in renal cell carcinoma. Claudin-1, -3, -4, -7, and -8 were studied in human renal cell carcinomas and oncocytomas. The data from their research showed an inverse correlation between claudin-3 and -4 expression with overall survival in clear cell renal cell carcinomas, and these claudins could be considered for prognosis

in renal cell carcinomas. Claudin-7 and 8 can be implied as useful markers in the identification of renal cell carcinomas from oncocytomas [105].

Claudin-6 was reported as a prognosis factor in NSCLC patients. In this report, the patients with low claudin-6 had a lower survival rate than the patients with high claudin-6. [91] reported low claudin-6 as an independent indicator of prognosis in NSCLC patients. In this study, they documented low claudin-6 in 61 of 123 NSCLC tissue samples, and patients with low claudin-6 expression correlated with lower survival rates than those with high claudin-6 expression. The influence of claudin-3, claudin-7, and claudin-18 in gastric cancer patients were also studied [106]. Claudin-3 and claudin-7 were expressed in 25.4% and 29.9% of the gastric cancer tissues, respectively. However, 51.5% of gastric cancer tissues exhibited reduced expression of claudin-18. Claudin-7 expression correlated with shorter overall survival in gastric cancer patients, while the overall survival was increased in patients with claudin-18 expression. Recently, claudin-3 and -7 are also considered as novel prognostic factors in triple-negative breast cancer (TNBC) through its aberrant immunohistochemical expressions [107]. Claudin-3 cytoplasmic expression is an indicator of poor survival in triple-negative breast cancer. In addition, epigenetic modifications of claudins are reported to be a promising prognosis marker of various cancers. Zhenzhen et al. [106] recently demonstrated that the methylation of claudin-3 is a prognostic factor in gastric adenocarcinoma.

Further, the serum levels of claudin-7 among patients with colorectal cancer (CRC) was significantly reduced and correlated with high tumor stage and high carcinoembryonic antigen levels [108]. Claudin-7 was found to be downregulated in CRC, as reported by Bhat et al. [42], and associated with diminished EMT and tumor progression. These studies give a strong rationale to consider claudin-7 as a biomarker for predicting the development, proliferation, and prognosis of CRC. A claudin-low molecular subtype of breast cancer has been described with a concomitant upregulation of several EMT markers and an enrichment in stem cell features [109]. In an interesting article by Danzinger et al., the importance of claudin-3 in triple-negative breast cancer (TNBC) was documented. It was reported that claudin-3 expression was correlated with a Breast cancer type 1 (BRCA1) mutation [107]. This could help in guiding the decision for BRCA testing for triple-negative breast cancer (TNBC). Also, the expression of claudin-11 has been suggested as a biomarker for advanced-stage cutaneous squamous carcinoma, and reflects the distinct stages of tumor development and differentiation [110]. The clinical significance of claudin-11 was addressed in Laryngeal Squamous Cell Carcinoma (LSCC) by Nissinen et al. [110]. In this study, elevated promoter methylation of claudin-11 in tumor tissues was observed. Patients with lymph node metastasis with an advanced clinical stage showed more methylation in the claudin-11 promoter, which associated with poor overall survival of LSCC patients. In TNBCs, claudin-1, -3, -4, and -7 higher expression rates are more frequent than in other subtypes [111]. Claudin-4 high/claudin-1 low, claudin-4 high/claudin-7 low, and claudin-4 high/claudin-1 low/claudin-7 low types were also significantly correlated with lymph node metastasis, and showed worse survival. Apart from this, a recent article from Upadhaya et al. documented the therapeutic potential of claudin-1 in oral epithelial dysplasia and oral squamous cell carcinoma [112]. Overall the differential expression pattern of claudins may reflect the distinct stages of tumor development and differentiation and have been implied as prognostic factors for early determination of the tumor state.

6. Claudins as Therapeutic Agents

So far, over 100 monoclonal antibody (mAb) products are in clinical trials [113]. In an oncology setting, these monoclonal antibodies can mediate antibody-dependent cellular cytotoxicity (ADCC) and complement-dependent cytotoxicity (CDC) against cancer cells [114]. There is a long-lasting history of antibody-mediated targeting of claudin-1 against hepatitis C virus (HCV) infections, and wherein many researchers have provided proof for the importance of claudins in HCV infections as viral entry point [115,116]. A study by Fofana et al. [117] designed monoclonal antibodies against claudin-1 to combat HCV entry. It was promising to see the antibodies raised against claudin-1 was able to block HCV entry. A recent study by Colpitts et al. has documented the humanization of a claudin-1-specific

monoclonal antibody and was investigated in a large panel of primary human hepatocytes, and was found to be very promising for clinical HCV prevention and cure [118]. These studies hold significance because these antibodies could prevent HCV infection after liver transplantation, and virus spread in chronically infected patients. These antibodies are now being tested in cancer models. Claudins, as a potential target in antibody-based therapies for carcinomas, was investigated by Offner et al. [119]. In this study, the antibodies were raised against the extracellular domains of claudin-1, -3, and -4. Recently Romani et al. engineered a fully human anti-claudin-3 IgG1 antibody (IgGH6) [120], which is specific to claudin-3 and no cross-reactivity with other claudins was observed. Recent work by Cherradi et al. [121] investigated the importance of claudin-1 in different colorectal cancer (CRC) molecular subtypes. There is a differential expression pattern of claudin-1 based on the subtype. A murine monoclonal antibody against the extracellular part of human claudin-1 (6 F6 mAb) was designed and generated, which was specifically able to pick claudin-1 positive CRC cell lines, and no other cross-reactivity was observed. Furthermore, 6 F6 mAb was able to combat colony formation, xenograft growth and metastasis of claudin-1 positive CRC cells suggesting its utility as a therapeutic. Fujiwara et al. recently targeted claudin-4 in CRC using an anti-claudin-4 extracellular domain antibody [122]. The efficacy of the anti-claudin-4 antibody is promising and observed to enhance the anti-tumorigenic potential of 5-fluorouracil (FU) and anti-EGFR antibodies. These works demonstrate the proof of concept for exploiting claudins as targets for monoclonal antibodies in therapies.

Some of the monoclonal antibodies against claudins, including anti-claudin-18.2 (IMAB362-claudin-18.2) and the anti-claudin-6 (IMAB027-claudin-6), have also found their way into clinical trials [123]. Claudin-18.2 is expressed on the outer cell membrane of gastric cancer cells and binds to monoclonal antibodies. The IMAB362 was proven to be clinically safe as the patients were devoid of any side effects. Also, IMAB027 is in an ongoing clinical trial for recurrent advanced ovarian cancer (NCT02054351), and patients have not demonstrated any adverse effects [123]. Clinical trials for claudiximab (claudin-18 targeting) in advanced gastroesophageal cancer patients are also underway [124]. Recently, claudiximab was reported to be a first-in-class chimeric monoclonal antibody for the treatment of gastric cancer targeting claudin-18, which is an important factor in gastric cancer metastasis. This is just the beginning of an exciting journey and more research is warranted to revolutionize claudins targeted monoclonal antibodies in cancer therapy.

Another avenue to exploit Claudins as a therapeutics is their ability to behave as receptors for microbes. *Clostridium perfringens* enterotoxin (CPE) has the potential to bind with claudin receptors. CPE binds to the C-terminal CPE domain at both the first and second extracellular loops (ECL-1 and ECL-2) of claudins [125]. The affinity of CPE to claudins causes a pore leading to calcium influx responsible for host cell death. The claudin–CPE interaction is gaining significance in receptor decoy therapeutics for potential applications in gastrointestinal disease, cancer therapy/diagnoses, and drug delivery [125]. Claudin-3 and claudin-4 have been widely demonstrated to function as CPE receptors [126,127]. The binding ability of CPE to claudins, especially claudin-3 and claudin-4, has raised a great opportunity to target cancers with dysregulated claudin-3 and -4 cancers, especially breast, ovarian, and pancreatic cancers. The binding of CPE to claudin-3 and -4 was documented to induce dose-dependent cytolysis in breast cancer cells expressing claudin-3 and -4 [128]. Recent studies have exploited the CPE mediated targeting of claudin-3 and 4 cancers to target therapy-resistant ovarian cancer, pancreatic, and breast cancer xenografts possessing increased expressions of claudin-3 and -4. In one of the studies, the possibility of CPE binding claudin-3 as a visualization tool for identifying of micrometastatic chemotherapy-resistant ovarian cancer has been demonstrated [129]. The applicability of CPE, claudin-3, and -4 interactions is exploited in gene therapy against colon cancer. Recombinant (recCPE) and optimized CPE expressing vector (optCPE) were demonstrated to have a cytotoxic effect in claudin overexpressing colon cancer cells [130,131]. Further, the recent identification of the crystal structure of claudin-9 revealed that human claudin-9 has high-affinity for the CPE receptor and treatment with CPE caused cell death in human claudin-9 expressing cells [132]. In continuation of these studies, an interesting approach of nanoparticle-based targeting of cancer

cells was documented by researchers, wherein the C-terminus of the CPE was conjugated to gold nanoparticles (AuNPs). This combination binds to claudin expressing tumor cells and kills the cells using gold nanoparticle-mediated laser perforation (GNOME-LP) technique [133,134]. Thus, the clinical relevance and functional importance of claudins in diverse cancers make them potential therapeutic targets.

7. Claudins as a Visualization Tool

The use of monoclonal antibodies against claudins have also been utilized in imaging modalities. Recently, claudin-4 was studied as an imaging tool for x-ray computed tomography (CT) in the prognosis of pancreatic ductal adenocarcinoma (PDAC) [135]. Claudin-4 is a known biomarker in PDAC detection. In this study, researchers reported a novel radiolabeled anti-claudin-4 monoclonal antibody in detecting PDAC using single-photon emission computed tomography (SPECT) imaging. The results showed promising uptake of anti-claudin-4 monoclonal antibody by PDAC tumors and were helpful in early detection and characterization of PDAC malignancy. Also, the researcher later targeted the extracellular domain of claudin-4 (4D3) with monoclonal antibodies (4D3) in combating bladder and lung cancer [136].

Colonoscopic aided screening and polyp and tumor removal have led to the reduced incidence and mortality of colorectal cancer (CRC). However, the lack of specificity is a major pitfall in these approaches and makes them less effective. It is especially difficult to detect the regions of flat dysplasia or serrated polyps, which also possess malignant potential. Thus, a targeted approach for advanced endoscopic techniques is a cornerstone requirement. A promising approach was recently demonstrated for the real-time endoscopic imaging of colonic adenomas [137]. In this study, the researchers exploited claudin-1 as a potential target in endoscopic imaging of colonic adenomas. As claudin-1 is highly expressed in the early development of CRC, endoscopic imaging might be useful for detecting either polypoid or flat precancerous lesions that are difficult to visualize [138]. Peptide (peptide sequence—RTSPSSR), specific to claudin-1, was developed against the extracellular loop of claudin-1. This peptide showed greater intensity for human adenomas, hyperplastic polyps and sessile serrated adenomas thus proposing the possibility of using claudin-1 peptide aided endoscopic imaging for the future clinical translation to detect precancerous lesions. Recently another study by our group demonstrated the significance of claudin-1 as a useful target for near-infrared antibody-based imaging for visualization of colorectal tumors [138]. When animals injected with colon cancer cells subcutaneously were imaged using claudin-1 antibody conjugated LI-COR IR800DyeCW through a LI-COR Pearl Trilogy Fluorescence Imaging System, the system was able to target tumors specifically. These studies pave the way for using claudins as a tool for fluorescence-guided surgery, which will help in more specific targeting of the tumors in a stage-specific manner. A comprehensive representation encompassing the role of claudins and the monoclonal antibodies against claudins as therapeutic and detection tools is given in Figure 3, and the role of claudins as a therapeutic, prognostic, and detection agents is tabulated in Table 3.

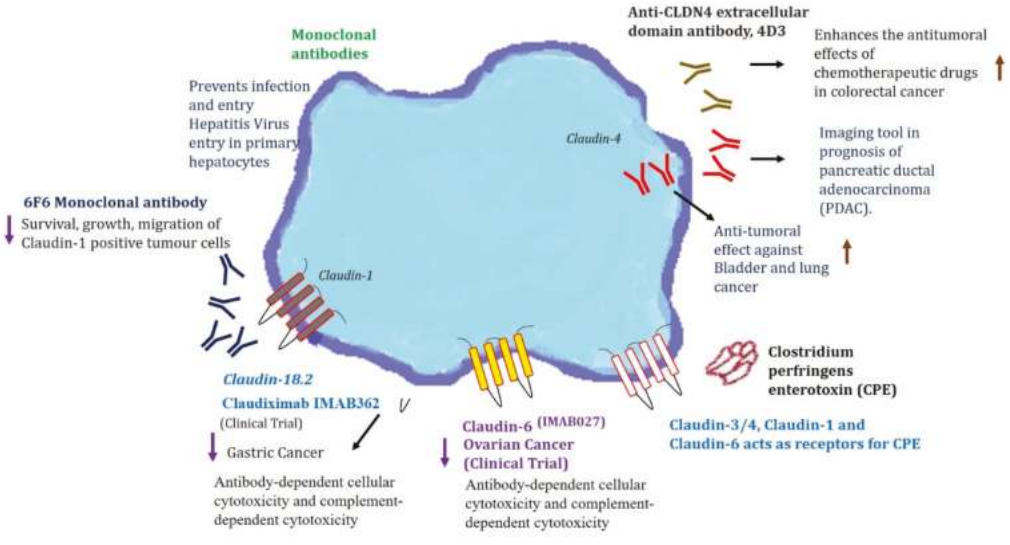

Figure 3. Claudins as an employable platform for prognostic, diagnostic, and therapeutic targets. The upward arrow indicated upregulation and downwards arrow indicated downregulation of the mentioned signaling events.

Table 3. Claudins as prognostic, therapeutic and detection agents.

Claudins Subtype	Disease Type	Therapeutic Agent	Clinical Application	Reference
Claudin-1	Hepatitis C virus infection	Residues within the first extracellular loop. Humanization of a claudin-1-specific monoclonal antibody.	Hepatitis C virus co-receptor. Clinical prevention and cure of Hepatitis C virus(HCV) infection.	[139] [118]
Claudin-6	Ovarian cancer	*Clostridium perfringens* enterotoxin (CPE) cytotoxicity.	CPE-mediated cytotoxicity in Ovarian cancer.	[127]
Claudin-3	Ovarian cancer uterine carcinomas	Human anti-claudin-3 IgG1 antibody.	Candidate for antibody-drug conjugate therapeutic applications.	[120,140]
Claudin-1	Colon cancer	Human claudin-1 (6F6 mAb).	Suppressed survival, growth, and migration of claudin-1 positive cells. Suppressed tumor growth and liver metastasis formation.	[121]
Claudin-4	Colorectal cancer	Anti-claudin-4 extracellular domain antibody.	Enhancer of anti-tumoral effects of chemotherapeutic agents.	[122]
Claudin-4	Pancreatic Cancer (PDAC)	Indium-111 tagged anti-claudin-4 monoclonal antibody.	X-ray computed tomography sided detection of PDAC.	[135]
Claudin-18.2	Gastric and gastroesophageal junction cancer	Chimeric monoclonal antibody that binds to claudin-18.2 (NCT03504397)	Cell death through antibody-dependent cellular cytotoxicity and complement-dependent cytotoxicity.	[123]
Claudin-4	Pancreatic cancer	Claudin-4 binder C-CPE 194	Enhances Tazeffects of anticancer agents via a MAPK pathway.	[141]
Claudin-3 and 4	Prostate cancer	Claudin-3 and claudin-4 targeted *Clostridium perfringens* protoxin	Selectively cytotoxic to PSA-producing prostate cancer cells.	[126]
Claudin-1	Colon cancer	Peptide RTSPSSR, specific to claudin-1 against the extracellular loop of claudin-1.	Specific to human adenomas, hyperplastic polyps, and sessile serrated adenomas.	[137]
Claudin-1	Colon cancer	Claudin-1 antibody conjugated with LI-COR IR800DyeCW	Near-infrared antibody-based imaging for visualization of colorectal tumors.	[138]
Claudin-9	Hepatitis C virus infection	Residues N38 and V45 in the first extracellular loop (EL1) of claudin-9 are responsible for HCV entry. Also found in PBMS (peripheral blood mononuclear cell) contributing to extrahepatic HCV infection.	It can be implicated in the development of drugs to block HCV entry into the liver and peripheral blood mononuclear cell (PBMS).	[142]

Table 3. *Cont.*

Claudins Subtype	Disease Type	Therapeutic Agent	Clinical Application	Reference
Claudin-11	Gastric Cancer	Hyper-methylation of claudin-11 promotor region leads to significant downregulation in gastric cancer.	Identification of the associated signaling cascades might lead to novel approaches in diagnosis and therapy for gastric cancer.	[48]
Claudin-7	Non-small cell lung cancer (NSCLC)	Reduced expression—Poor outcome Claudin-7 low NSCLC—Poor survival. Claudin-7 high NSCLC—High Survival.	Biomarker and a potential therapeutic target in patients with NSCLC.	[143]
Claudin-7	Epithelial Ovarian cancer	Claudin-7 transcripts were significantly enhanced in epithelial ovarian carcinoma patients. Silencing claudin-7 displayed enhanced sensitivity to Cisplatin treatment.	Independent prognostic factor and a key protein in regulating response to platinum-based chemotherapy in the treatment of epithelial ovarian cancer (EOC).	[144]
Claudin-2	Irritable bowel disease (IBD)	Anti-claudin-2 mAb 1A2	Prevent *cis*- and *trans*-interactions of claudin-2, attenuating the formation of leaky tight junction (TJ) seals.	[145]

8. Future Perspectives

The quest for prognostic, diagnostic, and therapeutic markers for many cancers is of high importance. More reliable and earlier detection markers have implications for diagnostic and therapeutic targeting. As the role of claudins in the regulation and enrichment of cancer stem cells and chemo-resistance becomes obvious, targeting claudins for diminishing cancer stem cells, which are cancer-propagating subsets of malignant cells, would be very useful. The potential of the claudin–cancer stem cell axis provides great potential for combating invasive, metastatic, and drug resistance phenotypes of various cancers. Future studies focusing on the role of claudins in cancer stem cells will be warranted to specifically target these populations to curb down residual tumor cells left after standard therapies.

Claudins are gaining their importance as detection and therapeutic agents. Future engineering of more monoclonal antibodies against claudins will have potential applications in targeted therapy, and claudin assisted endoscopy, imaging of various tumors. Also, the antibody-based detections will provide ample opportunity for the early diagnosis of any inflammatory diseases before they reach cancer status. The ongoing clinical trials for monoclonal antibodies against claudins might lead to claudin directed immunotherapies. Recently, small molecules inhibitors have been gaining more attention in cancer biology, as they aid in targeted therapy. No known small molecule inhibitors are currently being researched for claudins. Thus, in the future, screening for more potent inhibitors against claudins is warranted. Overall, to strengthen the therapeutic window of claudins, a more translational view of claudins by researchers is warranted.

Author Contributions: Conceptualization, S.G., P.D., and A.B.S.; methodology, S.G. and P.D.; resources, S.G. and P.D.; writing—original draft preparation, S.G.; writing—review and editing, S.G., A.B.S., and P.D.; supervision, P.D.; project administration, P.D. and A.B.S.; funding acquisition, P.D. and A.B.S. All authors have read and agreed to the published version of the manuscript.

Funding: This study was supported by grant numbers BX002086 (VA merit) and CA216746 (NIH/NCI). Further funding came from a pilot project award from the Fred and Pamela Buffet Cancer Center, which was funded by a National Cancer Institute Cancer Center Support Grant, under award number P30 CA036727 to P.D., BX002761 (VA merit) to A.B.S., and Nebraska research initiative (NRI to P.D and A.B.S).

Conflicts of Interest: The authors declare no conflict of interest.

References

1. Farquhar, M.G.; Palade, G.E. Junctional complexes in various epithelia. *J. Cell Biol.* **1963**, *17*, 375–412. [CrossRef]
2. Schneeberger, E.E.; Lynch, R.D. The tight junction: a multifunctional complex. *Am. J. Physiol.-Cell Physiol.* **2004**, *286*, C1213–C1228. [CrossRef]
3. Niessen, C.M. Tight junctions/adherens junctions: basic structure and function. *J. Investig. Dermatol.* **2007**, *127*, 2525–2532. [CrossRef]
4. Gonzalez-Mariscal, L.; Betanzos, A.; Nava, P.; Jaramillo, B.E. Tight junction proteins. *Prog. Biophys. Mol. Biol.* **2003**, *81*, 1–44. [CrossRef]
5. Stevenson, B.R.; Siliciano, J.D.; Mooseker, M.S.; Goodenough, D.A. Identification of ZO-1: a high molecular weight polypeptide associated with the tight junction (zonula occludens) in a variety of epithelia. *J. Cell Biol.* **1986**, *103*, 755–766. [CrossRef] [PubMed]
6. Citi, S.; Sabanay, H.; Jakes, R.; Geiger, B.; Kendrick-Jones, J. Cingulin, a new peripheral component of tight junctions. *Nature* **1988**, *333*, 272–276. [CrossRef] [PubMed]
7. Furuse, M.; Itoh, M.; Hirase, T.; Nagafuchi, A.; Yonemura, S.; Tsukita, S.; Tsukita, S. Direct association of occludin with ZO-1 and its possible involvement in the localization of occludin at tight junctions. *J. Cell Biol.* **1994**, *127*, 1617–1626. [CrossRef] [PubMed]
8. Nunes, F.D.; Lopez, L.N.; Lin, H.W.; Davies, C.; Azevedo, R.B.; Gow, A.; Kachar, B. Distinct subdomain organization and molecular composition of a tight junction with adherens junction features. *J. Cell Sci.* **2006**, *119*, 4819–4827. [CrossRef] [PubMed]

9. Gunzel, D.; Yu, A.S. Claudins and the modulation of tight junction permeability. *Physiol. Rev.* **2013**, *93*, 525–569. [CrossRef]
10. Angelow, S.; Yu, A.S. Claudins and paracellular transport: an update. *Curr. Opin. Nephrol. Hypertens.* **2007**, *16*, 459–464. [CrossRef]
11. Krause, G.; Protze, J.; Piontek, J. Assembly and function of claudins: Structure-function relationships based on homology models and crystal structures. *Semin. Cell Dev. Biol.* **2015**, *42*, 3–12. [CrossRef] [PubMed]
12. Tsukita, S.; Furuse, M. Occludin and claudins in tight-junction strands: leading or supporting players? *Trends Cell Biol.* **1999**, *9*, 268–273. [CrossRef]
13. Tsukita, S.; Furuse, M. Overcoming barriers in the study of tight junction functions: from occludin to claudin. *Genes Cells* **1998**, *3*, 569–573. [CrossRef] [PubMed]
14. Furuse, M.; Sasaki, H.; Fujimoto, K.; Tsukita, S. A single gene product, claudin-1 or -2, reconstitutes tight junction strands and recruits occludin in fibroblasts. *J. Cell Biol.* **1998**, *143*, 391–401. [CrossRef] [PubMed]
15. Lal-Nag, M.; Morin, P.J. The claudins. *Genome Biol.* **2009**, *10*, 235. [CrossRef]
16. Angelow, S.; Ahlstrom, R.; Yu, A.S. Biology of claudins. *Am. J. Physiol. Renal Physiol.* **2008**, *295*, F867–F876. [CrossRef]
17. Gunzel, D.; Fromm, M. Claudins and other tight junction proteins. *Compr. Physiol.* **2012**, *2*, 1819–1852. [CrossRef]
18. Soini, Y. Expression of claudins 1, 2, 3, 4, 5 and 7 in various types of tumours. *Histopathology* **2005**, *46*, 551–560. [CrossRef]
19. Schlingmann, B.; Molina, S.A.; Koval, M. Claudins: Gatekeepers of lung epithelial function. *Semin. Cell Dev. Biol.* **2015**, *42*, 47–57. [CrossRef]
20. Amasheh, S.; Meiri, N.; Gitter, A.H.; Schoneberg, T.; Mankertz, J.; Schulzke, J.D.; Fromm, M. Claudin-2 expression induces cation-selective channels in tight junctions of epithelial cells. *J. Cell Sci.* **2002**, *115*, 4969–4976. [CrossRef]
21. Wang, Y.; Mumm, J.B.; Herbst, R.; Kolbeck, R.; Wang, Y. IL-22 Increases Permeability of Intestinal Epithelial Tight Junctions by Enhancing Claudin-2 Expression. *J. Immunol.* **2017**, *199*, 3316–3325. [CrossRef] [PubMed]
22. Agarwal, R.; D'Souza, T.; Morin, P.J. Claudin-3 and claudin-4 expression in ovarian epithelial cells enhances invasion and is associated with increased matrix metalloproteinase-2 activity. *Cancer Res.* **2005**, *65*, 7378–7385. [CrossRef] [PubMed]
23. Morin, P.J. Claudin proteins in human cancer: promising new targets for diagnosis and therapy. *Cancer Res.* **2005**, *65*, 9603–9606. [CrossRef] [PubMed]
24. Kage, H.; Flodby, P.; Zhou, B.; Borok, Z. Dichotomous roles of claudins as tumor promoters or suppressors: Lessons from knockout mice. *Cell. Mol. Life Sci.* **2019**, *76*, 4663–4672. [CrossRef] [PubMed]
25. Kohmoto, T.; Masuda, K.; Shoda, K.; Takahashi, R.; Ujiro, S.; Tange, S.; Ichikawa, D.; Otsuji, E.; Imoto, I. Claudin-6 is a single prognostic marker and functions as a tumor-promoting gene in a subgroup of intestinal type gastric cancer. *Gastric Cancer* **2019**, 1–15. [CrossRef]
26. Yafang, L.; Qiong, W.; Yue, R.; Xiaoming, X.; Lina, Y.; Mingzi, Z.; Ting, Z.; Yulin, L.; Chengshi, Q. Role of Estrogen Receptor-alpha in the Regulation of Claudin-6 Expression in Breast Cancer Cells. *J. Breast Cancer* **2011**, *14*, 20–27. [CrossRef]
27. Rendon-Huerta, E.; Teresa, F.; Teresa, G.M.; Xochitl, G.S.; Georgina, A.F.; Veronica, Z.Z.; Montano, L.F. Distribution and expression pattern of claudins 6, 7, and 9 in diffuse- and intestinal-type gastric adenocarcinomas. *J. Gastrointest Cancer* **2010**, *41*, 52–59. [CrossRef]
28. Ikari, A.; Watanabe, R.; Sato, T.; Taga, S.; Shimobaba, S.; Yamaguchi, M.; Yamazaki, Y.; Endo, S.; Matsunaga, T.; Sugatani, J. Nuclear distribution of claudin-2 increases cell proliferation in human lung adenocarcinoma cells. *Biochim. Biophys. Acta* **2014**, *1843*, 2079–2088. [CrossRef]
29. Chao, Y.C.; Pan, S.H.; Yang, S.C.; Yu, S.L.; Che, T.F.; Lin, C.W.; Tsai, M.S.; Chang, G.C.; Wu, C.H.; Wu, Y.Y.; et al. Claudin-1 is a metastasis suppressor and correlates with clinical outcome in lung adenocarcinoma. *Am. J. Respir. Crit. Care Med.* **2009**, *179*, 123–133. [CrossRef]
30. Lu, Z.; Ding, L.; Hong, H.; Hoggard, J.; Lu, Q.; Chen, Y.H. Claudin-7 inhibits human lung cancer cell migration and invasion through ERK/MAPK signaling pathway. *Exp. Cell Res.* **2011**, *317*, 1935–1946. [CrossRef]
31. Shang, X.; Lin, X.; Alvarez, E.; Manorek, G.; Howell, S.B. Tight junction proteins claudin-3 and claudin-4 control tumor growth and metastases. *Neoplasia* **2012**, *14*, 974–985. [CrossRef] [PubMed]

32. Xu, C.; Wang, K.; Ding, Y.H.; Li, W.J.; Ding, L. Claudin-7 gene knockout causes destruction of intestinal structure and animal death in mice. *World J. Gastroenterol.* **2019**, *25*, 584–599. [CrossRef] [PubMed]
33. Nubel, T.; Preobraschenski, J.; Tuncay, H.; Weiss, T.; Kuhn, S.; Ladwein, M.; Langbein, L.; Zoller, M. Claudin-7 regulates EpCAM-mediated functions in tumor progression. *Mol. Cancer Res.* **2009**, *7*, 285–299. [CrossRef] [PubMed]
34. Shimobaba, S.; Taga, S.; Akizuki, R.; Hichino, A.; Endo, S.; Matsunaga, T.; Watanabe, R.; Yamaguchi, M.; Yamazaki, Y.; Sugatani, J.; et al. Claudin-18 inhibits cell proliferation and motility mediated by inhibition of phosphorylation of PDK1 and Akt in human lung adenocarcinoma A549 cells. *Biochim. Biophys. Acta* **2016**, *1863*, 1170–1178. [CrossRef]
35. Ahmad, R.; Kumar, B.; Chen, Z.; Chen, X.; Muller, D.; Lele, S.M.; Washington, M.K.; Batra, S.K.; Dhawan, P.; Singh, A.B. Loss of claudin-3 expression induces IL6/gp130/Stat3 signaling to promote colon cancer malignancy by hyperactivating Wnt/beta-catenin signaling. *Oncogene* **2017**, *36*, 6592–6604. [CrossRef]
36. Che, J.; Yue, D.; Zhang, B.; Zhang, H.; Huo, Y.; Gao, L.; Zhen, H.; Yang, Y.; Cao, B. Claudin-3 Inhibits Lung Squamous Cell Carcinoma Cell Epithelial-mesenchymal Transition and Invasion via Suppression of the Wnt/beta-catenin Signaling Pathway. *Int. J. Med. Sci.* **2018**, *15*, 339–351. [CrossRef]
37. Hicks, D.A.; Galimanis, C.E.; Webb, P.G.; Spillman, M.A.; Behbakht, K.; Neville, M.C.; Baumgartner, H.K. Claudin-4 activity in ovarian tumor cell apoptosis resistance and migration. *BMC Cancer* **2016**, *16*, 788. [CrossRef]
38. Zhang, X.; Ruan, Y.; Li, Y.; Lin, D.; Quan, C. Tight junction protein claudin-6 inhibits growth and induces the apoptosis of cervical carcinoma cells in vitro and in vivo. *Med. Oncol.* **2015**, *32*, 148. [CrossRef]
39. Zhang, X.; Ruan, Y.; Li, Y.; Lin, D.; Liu, Z.; Quan, C. Expression of apoptosis signal-regulating kinase 1 is associated with tight junction protein claudin-6 in cervical carcinoma. *Int. J. Clin. Exp. Pathol.* **2015**, *8*, 5535–5541.
40. Dhawan, P.; Singh, A.B.; Deane, N.G.; No, Y.; Shiou, S.R.; Schmidt, C.; Neff, J.; Washington, M.K.; Beauchamp, R.D. Claudin-1 regulates cellular transformation and metastatic behavior in colon cancer. *J. Clin. Investig.* **2005**, *115*, 1765–1776. [CrossRef]
41. Singh, A.B.; Sharma, A.; Smith, J.J.; Krishnan, M.; Chen, X.; Eschrich, S.; Washington, M.K.; Yeatman, T.J.; Beauchamp, R.D.; Dhawan, P. Claudin-1 up-regulates the repressor ZEB-1 to inhibit E-cadherin expression in colon cancer cells. *Gastroenterology* **2011**, *141*, 2140–2153. [CrossRef] [PubMed]
42. Bhat, A.A.; Pope, J.L.; Smith, J.J.; Ahmad, R.; Chen, X.; Washington, M.K.; Beauchamp, R.D.; Singh, A.B.; Dhawan, P. Claudin-7 expression induces mesenchymal to epithelial transformation (MET) to inhibit colon tumorigenesis. *Oncogene* **2015**, *34*, 4570–4580. [CrossRef] [PubMed]
43. Dhawan, P.; Ahmad, R.; Chaturvedi, R.; Smith, J.J.; Midha, R.; Mittal, M.K.; Krishnan, M.; Chen, X.; Eschrich, S.; Yeatman, T.J.; et al. Claudin-2 expression increases tumorigenicity of colon cancer cells: role of epidermal growth factor receptor activation. *Oncogene* **2011**, *30*, 3234–3247. [CrossRef] [PubMed]
44. Blanchard, A.A.; Zelinski, T.; Xie, J.; Cooper, S.; Penner, C.; Leygue, E.; Myal, Y. Identification of Claudin 1 Transcript Variants in Human Invasive Breast Cancer. *PLoS ONE* **2016**, *11*, e0163387. [CrossRef]
45. Oku, N.; Sasabe, E.; Ueta, E.; Yamamoto, T.; Osaki, T. Tight junction protein claudin-1 enhances the invasive activity of oral squamous cell carcinoma cells by promoting cleavage of laminin-5 gamma2 chain via matrix metalloproteinase (MMP)-2 and membrane-type MMP-1. *Cancer Res.* **2006**, *66*, 5251–5257. [CrossRef]
46. Darido, C.; Buchert, M.; Pannequin, J.; Bastide, P.; Zalzali, H.; Mantamadiotis, T.; Bourgaux, J.F.; Garambois, V.; Jay, P.; Blache, P.; et al. Defective claudin-7 regulation by Tcf-4 and Sox-9 disrupts the polarity and increases the tumorigenicity of colorectal cancer cells. *Cancer Res.* **2008**, *68*, 4258–4268. [CrossRef]
47. Chang, T.L.; Ito, K.; Ko, T.K.; Liu, Q.; Salto-Tellez, M.; Yeoh, K.G.; Fukamachi, H.; Ito, Y. Claudin-1 has tumor suppressive activity and is a direct target of RUNX3 in gastric epithelial cells. *Gastroenterology* **2010**, *138*, 255–265 e251-253. [CrossRef]
48. Agarwal, R.; Mori, Y.; Cheng, Y.; Jin, Z.; Olaru, A.V.; Hamilton, J.P.; David, S.; Selaru, F.M.; Yang, J.; Abraham, J.M.; et al. Silencing of claudin-11 is associated with increased invasiveness of gastric cancer cells. *PLoS One* **2009**, *4*, e8002. [CrossRef]
49. Zhang, X.; Wang, H.; Li, Q.; Li, T. CLDN2 inhibits the metastasis of osteosarcoma cells via down-regulating the afadin/ERK signaling pathway. *Cancer Cell Int.* **2018**, *18*, 160. [CrossRef]
50. Yamazaki, Y.; Tokumasu, R.; Kimura, H.; Tsukita, S. Role of claudin species-specific dynamics in reconstitution and remodeling of the zonula occludens. *Mol. Biol. Cell* **2011**, *22*, 1495–1504. [CrossRef]

51. Matsuda, M.; Kubo, A.; Furuse, M.; Tsukita, S. A peculiar internalization of claudins, tight junction-specific adhesion molecules, during the intercellular movement of epithelial cells. *J. Cell Sci.* **2004**, *117*, 1247–1257. [CrossRef] [PubMed]
52. Honda, H.; Pazin, M.J.; D'Souza, T.; Ji, H.; Morin, P.J. Regulation of the CLDN3 gene in ovarian cancer cells. *Cancer Biol. Ther.* **2007**, *6*, 1733–1742. [CrossRef] [PubMed]
53. Kwon, M.J.; Kim, S.H.; Jeong, H.M.; Jung, H.S.; Kim, S.S.; Lee, J.E.; Gye, M.C.; Erkin, O.C.; Koh, S.S.; Choi, Y.L.; et al. Claudin-4 overexpression is associated with epigenetic derepression in gastric carcinoma. *Lab. Investig.* **2011**, *91*, 1652–1667. [CrossRef] [PubMed]
54. Di Cello, F.; Cope, L.; Li, H.; Jeschke, J.; Wang, W.; Baylin, S.B.; Zahnow, C.A. Methylation of the claudin 1 promoter is associated with loss of expression in estrogen receptor positive breast cancer. *PLoS ONE* **2013**, *8*, e68630. [CrossRef] [PubMed]
55. Krishnan, M.; Singh, A.B.; Smith, J.J.; Sharma, A.; Chen, X.; Eschrich, S.; Yeatman, T.J.; Beauchamp, R.D.; Dhawan, P. HDAC inhibitors regulate claudin-1 expression in colon cancer cells through modulation of mRNA stability. *Oncogene* **2010**, *29*, 305–312. [CrossRef] [PubMed]
56. Martinez-Estrada, O.M.; Culleres, A.; Soriano, F.X.; Peinado, H.; Bolos, V.; Martinez, F.O.; Reina, M.; Cano, A.; Fabre, M.; Vilaro, S. The transcription factors Slug and Snail act as repressors of Claudin-1 expression in epithelial cells. *Biochem. J.* **2006**, *394*, 449–457. [CrossRef]
57. Bhat, A.A.; Sharma, A.; Pope, J.; Krishnan, M.; Washington, M.K.; Singh, A.B.; Dhawan, P. Caudal homeobox protein Cdx-2 cooperates with Wnt pathway to regulate claudin-1 expression in colon cancer cells. *PLoS ONE* **2012**, *7*, e37174. [CrossRef]
58. Honda, H.; Pazin, M.J.; Ji, H.; Wernyj, R.P.; Morin, P.J. Crucial roles of Sp1 and epigenetic modifications in the regulation of the CLDN4 promoter in ovarian cancer cells. *J. Biol. Chem.* **2006**, *281*, 21433–21444. [CrossRef]
59. Shigetomi, K.; Ikenouchi, J. Regulation of the epithelial barrier by post-translational modifications of tight junction membrane proteins. *J. Biochem.* **2018**, *163*, 265–272. [CrossRef]
60. Van Itallie, C.M.; Anderson, J.M. Claudin interactions in and out of the tight junction. *Tissue Barriers* **2013**, *1*, e25247. [CrossRef]
61. Rajagopal, N.; Irudayanathan, F.J.; Nangia, S. Palmitoylation of Claudin-5 Proteins Influences Their Lipid Domain Affinity and Tight Junction Assembly at the Blood-Brain Barrier Interface. *J. Phys. Chem. B* **2019**, *123*, 983–993. [CrossRef] [PubMed]
62. Butt, A.M.; Khan, I.B.; Hussain, M.; Idress, M.; Lu, J.; Tong, Y. Role of post translational modifications and novel crosstalk between phosphorylation and O-beta-GlcNAc modifications in human claudin-1, -3 and -4. *Mol. Biol. Rep.* **2012**, *39*, 1359–1369. [CrossRef] [PubMed]
63. French, A.D.; Fiori, J.L.; Camilli, T.C.; Leotlela, P.D.; O'Connell, M.P.; Frank, B.P.; Subaran, S.; Indig, F.E.; Taub, D.D.; Weeraratna, A.T. PKC and PKA phosphorylation affect the subcellular localization of claudin-1 in melanoma cells. *Int. J. Med. Sci.* **2009**, *6*, 93–101. [CrossRef] [PubMed]
64. D'Souza, T.; Indig, F.E.; Morin, P.J. Phosphorylation of claudin-4 by PKCepsilon regulates tight junction barrier function in ovarian cancer cells. *Exp. Cell Res.* **2007**, *313*, 3364–3375. [CrossRef]
65. D'Souza, T.; Agarwal, R.; Morin, P.J. Phosphorylation of claudin-3 at threonine 192 by cAMP-dependent protein kinase regulates tight junction barrier function in ovarian cancer cells. *J. Biol. Chem.* **2005**, *280*, 26233–26240. [CrossRef]
66. Akizuki, R.; Shimobaba, S.; Matsunaga, T.; Endo, S.; Ikari, A. Claudin-5, -7, and -18 suppress proliferation mediated by inhibition of phosphorylation of Akt in human lung squamous cell carcinoma. *Biochim. Biophys. Acta Mol. Cell Res.* **2017**, *1864*, 293–302. [CrossRef]
67. Yamamoto, M.; Ramirez, S.H.; Sato, S.; Kiyota, T.; Cerny, R.L.; Kaibuchi, K.; Persidsky, Y.; Ikezu, T. Phosphorylation of claudin-5 and occludin by rho kinase in brain endothelial cells. *Am. J. Pathol.* **2008**, *172*, 521–533. [CrossRef]
68. Ahmad, W.; Shabbiri, K.; Ijaz, B.; Asad, S.; Sarwar, M.T.; Gull, S.; Kausar, H.; Fouzia, K.; Shahid, I.; Hassan, S. Claudin-1 required for HCV virus entry has high potential for phosphorylation and O-glycosylation. *Virol. J.* **2011**, *8*, 229. [CrossRef]
69. Heiler, S.; Mu, W.; Zoller, M.; Thuma, F. The importance of claudin-7 palmitoylation on membrane subdomain localization and metastasis-promoting activities. *Cell Commun. Signal.* **2015**, *13*, 29. [CrossRef]
70. Biteau, B.; Hochmuth, C.E.; Jasper, H. Maintaining tissue homeostasis: dynamic control of somatic stem cell activity. *Cell Stem Cell* **2011**, *9*, 402–411. [CrossRef]

71. Romito, A.; Cobellis, G. Pluripotent Stem Cells: Current Understanding and Future Directions. *Stem Cells Int.* **2016**, *2016*, 9451492. [CrossRef] [PubMed]
72. Duinsbergen, D.; Salvatori, D.; Eriksson, M.; Mikkers, H. Tumors originating from induced pluripotent stem cells and methods for their prevention. *Ann. N.Y. Acad. Sci.* **2009**, *1176*, 197–204. [CrossRef] [PubMed]
73. Ben-David, U.; Nudel, N.; Benvenisty, N. Immunologic and chemical targeting of the tight-junction protein Claudin-6 eliminates tumorigenic human pluripotent stem cells. *Nat. Commun.* **2013**, *4*, 1992. [CrossRef] [PubMed]
74. Sugimoto, K.; Ichikawa-Tomikawa, N.; Satohisa, S.; Akashi, Y.; Kanai, R.; Saito, T.; Sawada, N.; Chiba, H. The tight-junction protein claudin-6 induces epithelial differentiation from mouse F9 and embryonic stem cells. *PLoS ONE* **2013**, *8*, e75106. [CrossRef] [PubMed]
75. Wang, L.; Xue, Y.; Shen, Y.; Li, W.; Cheng, Y.; Yan, X.; Shi, W.; Wang, J.; Gong, Z.; Yang, G.; et al. Claudin 6: a novel surface marker for characterizing mouse pluripotent stem cells. *Cell Res.* **2012**, *22*, 1082–1085. [CrossRef] [PubMed]
76. Turksen, K.; Troy, T.C. Claudin-6: a novel tight junction molecule is developmentally regulated in mouse embryonic epithelium. *Dev. Dyn.* **2001**, *222*, 292–300. [CrossRef]
77. Erdelyi-Belle, B.; Torok, G.; Apati, A.; Sarkadi, B.; Schaff, Z.; Kiss, A.; Homolya, L. Expression of Tight Junction Components in Hepatocyte-Like Cells Differentiated from Human Embryonic Stem Cells. *Pathol. Oncol. Res.* **2015**, *21*, 1059–1070. [CrossRef]
78. Abdullah, L.N.; Chow, E.K. Mechanisms of chemoresistance in cancer stem cells. *Clin. Transl. Med.* **2013**, *2*, 3. [CrossRef]
79. Phi, L.T.H.; Sari, I.N.; Yang, Y.G.; Lee, S.H.; Jun, N.; Kim, K.S.; Lee, Y.K.; Kwon, H.Y. Cancer Stem Cells (CSCs) in Drug Resistance and their Therapeutic Implications in Cancer Treatment. *Stem Cells Int.* **2018**, *2018*, 5416923. [CrossRef]
80. Nusse, R. Wnt signaling and stem cell control. *Cell Res.* **2008**, *18*, 523–527. [CrossRef]
81. Miwa, N.; Furuse, M.; Tsukita, S.; Niikawa, N.; Nakamura, Y.; Furukawa, Y. Involvement of claudin-1 in the beta-catenin/Tcf signaling pathway and its frequent upregulation in human colorectal cancers. *Oncol. Res.* **2001**, *12*, 469–476. [CrossRef] [PubMed]
82. Gowrikumar, S.; Ahmad, R.; Uppada, S.B.; Washington, M.K.; Shi, C.; Singh, A.B.; Dhawan, P. Upregulated claudin-1 expression promotes colitis-associated cancer by promoting beta-catenin phosphorylation and activation in Notch/p-AKT-dependent manner. *Oncogene* **2019**, *38*, 5321–5337. [CrossRef] [PubMed]
83. Prat, A.; Parker, J.S.; Karginova, O.; Fan, C.; Livasy, C.; Herschkowitz, J.I.; He, X.; Perou, C.M. Phenotypic and molecular characterization of the claudin-low intrinsic subtype of breast cancer. *Breast Cancer Res.* **2010**, *12*, R68. [CrossRef] [PubMed]
84. Ma, L.; Yin, W.; Ma, H.; Elshoura, I.; Wang, L. Targeting claudin-3 suppresses stem cell-like phenotype in nonsquamous non-small-cell lung carcinoma. *Lung Cancer Manag.* **2019**, *8*, LMT04. [CrossRef] [PubMed]
85. Zhou, B.; Flodby, P.; Luo, J.; Castillo, D.R.; Liu, Y.; Yu, F.X.; McConnell, A.; Varghese, B.; Li, G.; Chimge, N.O.; et al. Claudin-18-mediated YAP activity regulates lung stem and progenitor cell homeostasis and tumorigenesis. *J. Clin. Investig.* **2018**, *128*, 970–984. [CrossRef]
86. Paquet-Fifield, S.; Koh, S.L.; Cheng, L.; Beyit, L.M.; Shembrey, C.; Molck, C.; Behrenbruch, C.; Papin, M.; Gironella, M.; Guelfi, S.; et al. Tight Junction Protein Claudin-2 Promotes Self-Renewal of Human Colorectal Cancer Stem-like Cells. *Cancer Res.* **2018**, *78*, 2925–2938. [CrossRef]
87. Zheng, H.C. The molecular mechanisms of chemoresistance in cancers. *Oncotarget* **2017**, *8*, 59950–59964. [CrossRef]
88. Wang, K.; Li, T.; Xu, C.; Ding, Y.; Li, W.; Ding, L. Claudin-7 downregulation induces metastasis and invasion in colorectal cancer via the promotion of epithelial-mesenchymal transition. *Biochem. Biophys. Res. Commun.* **2019**, *508*, 797–804. [CrossRef]
89. Tabaries, S.; Siegel, P.M. The role of claudins in cancer metastasis. *Oncogene* **2017**, *36*, 1176–1190. [CrossRef]
90. Zhang, L.; Wang, Y.; Zhang, B.; Zhang, H.; Zhou, M.; Wei, M.; Dong, Q.; Xu, Y.; Wang, Z.; Gao, L.; et al. Claudin-3 expression increases the malignant potential of lung adenocarcinoma cells: role of epidermal growth factor receptor activation. *Oncotarget* **2017**, *8*, 23033–23047. [CrossRef]
91. Wang, Q.; Zhang, Y.; Zhang, T.; Han, Z.G.; Shan, L. Low claudin-6 expression correlates with poor prognosis in patients with non-small cell lung cancer. *Onco Targets Ther.* **2015**, *8*, 1971–1977. [CrossRef] [PubMed]

92. Landers, K.A.; Samaratunga, H.; Teng, L.; Buck, M.; Burger, M.J.; Scells, B.; Lavin, M.F.; Gardiner, R.A. Identification of claudin-4 as a marker highly overexpressed in both primary and metastatic prostate cancer. *Br. J. Cancer* **2008**, *99*, 491–501. [CrossRef] [PubMed]
93. Hwang, T.L.; Changchien, T.T.; Wang, C.C.; Wu, C.M. Claudin-4 expression in gastric cancer cells enhances the invasion and is associated with the increased level of matrix metalloproteinase-2 and -9 expression. *Oncol. Lett.* **2014**, *8*, 1367–1371. [CrossRef] [PubMed]
94. Ohtani, S.; Terashima, M.; Satoh, J.; Soeta, N.; Saze, Z.; Kashimura, S.; Ohsuka, F.; Hoshino, Y.; Kogure, M.; Gotoh, M. Expression of tight-junction-associated proteins in human gastric cancer: downregulation of claudin-4 correlates with tumor aggressiveness and survival. *Gastric Cancer* **2009**, *12*, 43–51. [CrossRef]
95. Stebbing, J.; Filipovic, A.; Giamas, G. Claudin-1 as a promoter of EMT in hepatocellular carcinoma. *Oncogene* **2013**, *32*, 4871–4872. [CrossRef]
96. Zhou, B.; Moodie, A.; Blanchard, A.A.; Leygue, E.; Myal, Y. Claudin 1 in Breast Cancer: New Insights. *J. Clin. Med.* **2015**, *4*, 1960–1976. [CrossRef]
97. Yang, M.; Li, Y.; Ruan, Y.; Lu, Y.; Lin, D.; Xie, Y.; Dong, B.; Dang, Q.; Quan, C. CLDN6 enhances chemoresistance to ADM via AF-6/ERKs pathway in TNBC cell line MDAMB231. *Mol. Cell. Biochem.* **2018**, *443*, 169–180. [CrossRef]
98. Shang, X.; Lin, X.; Manorek, G.; Howell, S.B. Claudin-3 and claudin-4 regulate sensitivity to cisplatin by controlling expression of the copper and cisplatin influx transporter CTR1. *Mol. Pharmacol.* **2013**, *83*, 85–94. [CrossRef]
99. Yoshida, H.; Sumi, T.; Zhi, X.; Yasui, T.; Honda, K.; Ishiko, O. Claudin-4: a potential therapeutic target in chemotherapy-resistant ovarian cancer. *Anticancer Res.* **2011**, *31*, 1271–1277.
100. Zhao, Z.; Li, J.; Jiang, Y.; Xu, W.; Li, X.; Jing, W. CLDN1 Increases Drug Resistance of Non-Small Cell Lung Cancer by Activating Autophagy via Up-Regulation of ULK1 Phosphorylation. *Med. Sci. Monit.* **2017**, *23*, 2906–2916. [CrossRef]
101. Akizuki, R.; Maruhashi, R.; Eguchi, H.; Kitabatake, K.; Tsukimoto, M.; Furuta, T.; Matsunaga, T.; Endo, S.; Ikari, A. Decrease in paracellular permeability and chemosensitivity to doxorubicin by claudin-1 in spheroid culture models of human lung adenocarcinoma A549 cells. *Biochim. Biophys. Acta Mol. Cell Res.* **2018**, *1865*, 769–780. [CrossRef] [PubMed]
102. Philip, R.; Heiler, S.; Mu, W.; Buchler, M.W.; Zoller, M.; Thuma, F. Claudin-7 promotes the epithelial-mesenchymal transition in human colorectal cancer. *Oncotarget* **2015**, *6*, 2046–2063. [CrossRef] [PubMed]
103. Hoggard, J.; Fan, J.; Lu, Z.; Lu, Q.; Sutton, L.; Chen, Y.H. Claudin-7 increases chemosensitivity to cisplatin through the upregulation of caspase pathway in human NCI-H522 lung cancer cells. *Cancer Sci.* **2013**, *104*, 611–618. [CrossRef] [PubMed]
104. Lechpammer, M.; Resnick, M.B.; Sabo, E.; Yakirevich, E.; Greaves, W.O.; Sciandra, K.T.; Tavares, R.; Noble, L.C.; DeLellis, R.A.; Wang, L.J. The diagnostic and prognostic utility of claudin expression in renal cell neoplasms. *Mod. Pathol.* **2008**, *21*, 1320–1329. [CrossRef]
105. Osunkoya, A.O.; Cohen, C.; Lawson, D.; Picken, M.M.; Amin, M.B.; Young, A.N. Claudin-7 and claudin-8: immunohistochemical markers for the differential diagnosis of chromophobe renal cell carcinoma and renal oncocytoma. *Hum. Pathol.* **2009**, *40*, 206–210. [CrossRef]
106. Yang, L.; Sun, X.; Meng, X. Differences in the expression profiles of claudin proteins in human gastric carcinoma compared with nonneoplastic mucosa. *Mol. Med. Rep.* **2018**, *18*, 1271–1278. [CrossRef]
107. Danzinger, S.; Tan, Y.Y.; Rudas, M.; Kastner, M.T.; Weingartshofer, S.; Muhr, D.; Singer, C.F.; kConFab, I. Differential Claudin 3 and EGFR Expression Predicts BRCA1 Mutation in Triple-Negative Breast Cancer. *Cancer Investig.* **2018**, *36*, 378–388. [CrossRef]
108. Karabulut, M.; Alis, H.; Bas, K.; Karabulut, S.; Afsar, C.U.; Oguz, H.; Gunaldi, M.; Akarsu, C.; Kones, O.; Aykan, N.F. Clinical significance of serum claudin-1 and claudin-7 levels in patients with colorectal cancer. *Mol. Clin. Oncol.* **2015**, *3*, 1255–1267. [CrossRef]
109. Sabatier, R.; Finetti, P.; Guille, A.; Adelaide, J.; Chaffanet, M.; Viens, P.; Birnbaum, D.; Bertucci, F. Claudin-low breast cancers: clinical, pathological, molecular and prognostic characterization. *Mol. Cancer* **2014**, *13*, 228. [CrossRef]
110. Nissinen, L.; Siljamaki, E.; Riihila, P.; Piipponen, M.; Farshchian, M.; Kivisaari, A.; Kallajoki, M.; Raiko, L.; Peltonen, J.; Peltonen, S.; et al. Expression of claudin-11 by tumor cells in cutaneous squamous cell carcinoma is dependent on the activity of p38delta. *Exp. Dermatol.* **2017**, *26*, 771–777. [CrossRef]

111. Dias, K.; Dvorkin-Gheva, A.; Hallett, R.M.; Wu, Y.; Hassell, J.; Pond, G.R.; Levine, M.; Whelan, T.; Bane, A.L. Claudin-Low Breast Cancer; Clinical & Pathological Characteristics. *PLoS ONE* **2017**, *12*, e0168669. [CrossRef]
112. Upadhaya, P.; Barhoi, D.; Giri, A.; Bhattacharjee, A.; Giri, S. Joint detection of claudin-1 and junctional adhesion molecule-A as a therapeutic target in oral epithelial dysplasia and oral squamous cell carcinoma. *J. Cell. Biochem.* **2019**, *120*, 18117–18127. [CrossRef] [PubMed]
113. Chau, C.H.; Steeg, P.S.; Figg, W.D. Antibody-drug conjugates for cancer. *Lancet* **2019**, *394*, 793–804. [CrossRef]
114. Shuptrine, C.W.; Surana, R.; Weiner, L.M. Monoclonal antibodies for the treatment of cancer. *Semin. Cancer Biol.* **2012**, *22*, 3–13. [CrossRef]
115. Mailly, L.; Xiao, F.; Lupberger, J.; Wilson, G.K.; Aubert, P.; Duong, F.H.T.; Calabrese, D.; Leboeuf, C.; Fofana, I.; Thumann, C.; et al. Clearance of persistent hepatitis C virus infection in humanized mice using a claudin-1-targeting monoclonal antibody. *Nat. Biotechnol.* **2015**, *33*, 549–554. [CrossRef]
116. Fukasawa, M.; Nagase, S.; Shirasago, Y.; Iida, M.; Yamashita, M.; Endo, K.; Yagi, K.; Suzuki, T.; Wakita, T.; Hanada, K.; et al. Monoclonal antibodies against extracellular domains of claudin-1 block hepatitis C virus infection in a mouse model. *J. Virol.* **2015**, *89*, 4866–4879. [CrossRef]
117. Fofana, I.; Krieger, S.E.; Grunert, F.; Glauben, S.; Xiao, F.; Fafi-Kremer, S.; Soulier, E.; Royer, C.; Thumann, C.; Mee, C.J.; et al. Monoclonal anti-claudin 1 antibodies prevent hepatitis C virus infection of primary human hepatocytes. *Gastroenterology* **2010**, *139*, 953–964, 964. e4. [CrossRef]
118. Colpitts, C.C.; Tawar, R.G.; Mailly, L.; Thumann, C.; Heydmann, L.; Durand, S.C.; Xiao, F.; Robinet, E.; Pessaux, P.; Zeisel, M.B.; et al. Humanisation of a claudin-1-specific monoclonal antibody for clinical prevention and cure of HCV infection without escape. *Gut* **2018**, *67*, 736–745. [CrossRef]
119. Offner, S.; Hekele, A.; Teichmann, U.; Weinberger, S.; Gross, S.; Kufer, P.; Itin, C.; Baeuerle, P.A.; Kohleisen, B. Epithelial tight junction proteins as potential antibody targets for pancarcinoma therapy. *Cancer Immunol. Immunother.* **2005**, *54*, 431–445. [CrossRef]
120. Romani, C.; Cocco, E.; Bignotti, E.; Moratto, D.; Bugatti, A.; Todeschini, P.; Bandiera, E.; Tassi, R.; Zanotti, L.; Pecorelli, S.; et al. Evaluation of a novel human IgG1 anti-claudin3 antibody that specifically recognizes its aberrantly localized antigen in ovarian cancer cells and that is suitable for selective drug delivery. *Oncotarget* **2015**, *6*, 34617–34628. [CrossRef]
121. Cherradi, S.; Ayrolles-Torro, A.; Vezzo-Vie, N.; Gueguinou, N.; Denis, V.; Combes, E.; Boissiere, F.; Busson, M.; Canterel-Thouennon, L.; Mollevi, C.; et al. Antibody targeting of claudin-1 as a potential colorectal cancer therapy. *J. Exp. Clin. Cancer Res.* **2017**, *36*, 89. [CrossRef] [PubMed]
122. Fujiwara-Tani, R.; Sasaki, T.; Luo, Y.; Goto, K.; Kawahara, I.; Nishiguchi, Y.; Kishi, S.; Mori, S.; Ohmori, H.; Kondoh, M.; et al. Anti-claudin-4 extracellular domain antibody enhances the antitumoral effects of chemotherapeutic and antibody drugs in colorectal cancer. *Oncotarget* **2018**, *9*, 37367–37378. [CrossRef] [PubMed]
123. Sahin, U.; Schuler, M.; Richly, H.; Bauer, S.; Krilova, A.; Dechow, T.; Jerling, M.; Utsch, M.; Rohde, C.; Dhaene, K.; et al. A phase I dose-escalation study of IMAB362 (Zolbetuximab) in patients with advanced gastric and gastro-oesophageal junction cancer. *Eur. J. Cancer* **2018**, *100*, 17–26. [CrossRef] [PubMed]
124. Singh, P.; Toom, S.; Huang, Y. Anti-claudin 18.2 antibody as new targeted therapy for advanced gastric cancer. *J. Hematol. Oncol.* **2017**, *10*, 105. [CrossRef]
125. Shrestha, A.; Uzal, F.A.; McClane, B.A. The interaction of Clostridium perfringens enterotoxin with receptor claudins. *Anaerobe* **2016**, *41*, 18–26. [CrossRef]
126. Romanov, V.; Whyard, T.C.; Waltzer, W.C.; Gabig, T.G. A claudin 3 and claudin 4-targeted Clostridium perfringens protoxin is selectively cytotoxic to PSA-producing prostate cancer cells. *Cancer Lett.* **2014**, *351*, 260–264. [CrossRef]
127. Lal-Nag, M.; Battis, M.; Santin, A.D.; Morin, P.J. Claudin-6: a novel receptor for CPE-mediated cytotoxicity in ovarian cancer. *Oncogenesis* **2012**, *1*, e33. [CrossRef]
128. Kominsky, S.L.; Vali, M.; Korz, D.; Gabig, T.G.; Weitzman, S.A.; Argani, P.; Sukumar, S. Clostridium perfringens enterotoxin elicits rapid and specific cytolysis of breast carcinoma cells mediated through tight junction proteins claudin 3 and 4. *Am. J. Pathol.* **2004**, *164*, 1627–1633. [CrossRef]
129. Cocco, E.; Shapiro, E.M.; Gasparrini, S.; Lopez, S.; Schwab, C.L.; Bellone, S.; Bortolomai, I.; Sumi, N.J.; Bonazzoli, E.; Nicoletti, R.; et al. Clostridium perfringens enterotoxin C-terminal domain labeled to fluorescent dyes for in vivo visualization of micrometastatic chemotherapy-resistant ovarian cancer. *Int. J. Cancer* **2015**, *137*, 2618–2629. [CrossRef]

130. Pahle, J.; Menzel, L.; Niesler, N.; Kobelt, D.; Aumann, J.; Rivera, M.; Walther, W. Rapid eradication of colon carcinoma by Clostridium perfringens Enterotoxin suicidal gene therapy. *BMC Cancer* **2017**, *17*, 129. [CrossRef]
131. Pahle, J.; Aumann, J.; Kobelt, D.; Walther, W. Oncoleaking: Use of the Pore-Forming Clostridium perfringens Enterotoxin (CPE) for Suicide Gene Therapy. *Methods Mol. Biol.* **2015**, *1317*, 69–85. [CrossRef] [PubMed]
132. Vecchio, A.J.; Stroud, R.M. Claudin-9 structures reveal mechanism for toxin-induced gut barrier breakdown. *Proc. Natl. Acad. Sci. USA* **2019**, *116*, 17817–17824. [CrossRef] [PubMed]
133. Becker, A.; Leskau, M.; Schlingmann-Molina, B.L.; Hohmeier, S.C.; Alnajjar, S.; Murua Escobar, H.; Ngezahayo, A. Functionalization of gold-nanoparticles by the Clostridium perfringens enterotoxin C-terminus for tumor cell ablation using the gold nanoparticle-mediated laser perforation technique. *Sci. Rep.* **2018**, *8*, 14963. [CrossRef] [PubMed]
134. Becker, A.; Lehrich, T.; Kalies, S.; Heisterkamp, A.; Ngezahayo, A. Parameters for Optoperforation-Induced Killing of Cancer Cells Using Gold Nanoparticles Functionalized With the C-terminal Fragment of Clostridium Perfringens Enterotoxin. *Int. J. Mol. Sci.* **2019**, *20*. [CrossRef] [PubMed]
135. Torres, J.B.; Knight, J.C.; Mosley, M.J.; Kersemans, V.; Koustoulidou, S.; Allen, D.; Kinchesh, P.; Smart, S.; Cornelissen, B. Imaging of Claudin-4 in Pancreatic Ductal Adenocarcinoma Using a Radiolabelled Anti-Claudin-4 Monoclonal Antibody. *Mol. Imaging Biol.* **2018**, *20*, 292–299. [CrossRef] [PubMed]
136. Kuwada, M.; Chihara, Y.; Luo, Y.; Li, X.; Nishiguchi, Y.; Fujiwara, R.; Sasaki, T.; Fujii, K.; Ohmori, H.; Fujimoto, K.; et al. Pro-chemotherapeutic effects of antibody against extracellular domain of claudin-4 in bladder cancer. *Cancer Lett.* **2015**, *369*, 212–221. [CrossRef] [PubMed]
137. Rabinsky, E.F.; Joshi, B.P.; Pant, A.; Zhou, J.; Duan, X.; Smith, A.; Kuick, R.; Fan, S.; Nusrat, A.; Owens, S.R.; et al. Overexpressed Claudin-1 Can Be Visualized Endoscopically in Colonic Adenomas In Vivo. *Cell. Mol. Gastroenterol. Hepatol.* **2016**, *2*, 222–237. [CrossRef]
138. Hollandsworth, H.M.; Lwin, T.M.; Amirfakhri, S.; Filemoni, F.; Batra, S.K.; Hoffman, R.M.; Dhawan, P.; Bouvet, M. Anti-Claudin-1 Conjugated to a Near-Infrared Fluorophore Targets Colon Cancer in PDOX Mouse Models. *J. Surg. Res.* **2019**, *242*, 145–150. [CrossRef]
139. Evans, M.J.; von Hahn, T.; Tscherne, D.M.; Syder, A.J.; Panis, M.; Wolk, B.; Hatziioannou, T.; McKeating, J.A.; Bieniasz, P.D.; Rice, C.M. Claudin-1 is a hepatitis C virus co-receptor required for a late step in entry. *Nature* **2007**, *446*, 801–805. [CrossRef]
140. Romani, C.; Comper, F.; Bandiera, E.; Ravaggi, A.; Bignotti, E.; Tassi, R.A.; Pecorelli, S.; Santin, A.D. Development and characterization of a human single-chain antibody fragment against claudin-3: A novel therapeutic target in ovarian and uterine carcinomas. *Am. J. Obstet. Gynecol.* **2009**, *201*, 70 e71–e79. [CrossRef]
141. Kono, T.; Kondoh, M.; Kyuno, D.; Ito, T.; Kimura, Y.; Imamura, M.; Kohno, T.; Konno, T.; Furuhata, T.; Sawada, N.; et al. Claudin-4 binder C-CPE 194 enhances effects of anticancer agents on pancreatic cancer cell lines via a MAPK pathway. *Pharmacol. Res. Perspect.* **2015**, *3*, e00196. [CrossRef] [PubMed]
142. Zheng, A.; Yuan, F.; Li, Y.; Zhu, F.; Hou, P.; Li, J.; Song, X.; Ding, M.; Deng, H. Claudin-6 and claudin-9 function as additional coreceptors for hepatitis C virus. *J. Virol.* **2007**, *81*, 12465–12471. [CrossRef] [PubMed]
143. Yamamoto, T.; Oshima, T.; Yoshihara, K.; Yamanaka, S.; Nishii, T.; Arai, H.; Inui, K.; Kaneko, T.; Nozawa, A.; Woo, T.; et al. Reduced expression of claudin-7 is associated with poor outcome in non-small cell lung cancer. *Oncol. Lett.* **2010**, *1*, 501–505. [CrossRef] [PubMed]
144. Kim, C.J.; Lee, J.W.; Choi, J.J.; Choi, H.Y.; Park, Y.A.; Jeon, H.K.; Sung, C.O.; Song, S.Y.; Lee, Y.Y.; Choi, C.H.; et al. High claudin-7 expression is associated with a poor response to platinum-based chemotherapy in epithelial ovarian carcinoma. *Eur. J. Cancer* **2011**, *47*, 918–925. [CrossRef]
145. Takigawa, M.; Iida, M.; Nagase, S.; Suzuki, H.; Watari, A.; Tada, M.; Okada, Y.; Doi, T.; Fukasawa, M.; Yagi, K.; et al. Creation of a Claudin-2 Binder and Its Tight Junction-Modulating Activity in a Human Intestinal Model. *J. Pharmacol. Exp. Ther.* **2017**, *363*, 444–451. [CrossRef]

International Journal of
Molecular Sciences

MDPI

Review

Claudin-1, A Double-Edged Sword in Cancer

Ajaz A. Bhat [1], Najeeb Syed [1], Lubna Therachiyil [2,3], Sabah Nisar [1], Sheema Hashem [1], Muzafar A. Macha [4,5], Santosh K. Yadav [1], Roopesh Krishnankutty [2], Shanmugakonar Muralitharan [6], Hamda Al-Naemi [6], Puneet Bagga [7], Ravinder Reddy [7], Punita Dhawan [5], Anthony Akobeng [8], Shahab Uddin [2], Michael P. Frenneaux [9], Wael El-Rifai [10] and Mohammad Haris [1,6,*]

1 Division of Translational Medicine, Research Branch, Sidra Medicine, Doha 26999, Qatar; abhat@sidra.org (A.A.B.); nsyed@sidra.org (N.S.); snisar1@sidra.org (S.N.); shashem@sidra.org (S.H.); syadav@sidra.org (S.K.Y.)
2 Translational Research Institute, Academic Health System, Hamad Medical Corporation, Doha 3050, Qatar; LTherachiyil@hamad.qa (L.T.); RKrishnankutty@hamad.qa (R.K.); SKhan34@hamad.qa (S.U.)
3 Department of Pharmaceutical Sciences, College of Pharmacy, QU Health, Qatar University, Doha 2713, Qatar
4 Department of Biotechnology, Central University of Kashmir, Ganderbal, Jammu and Kashmir 191201, India; muzafar.macha1@gmail.com
5 Department of Biochemistry and Molecular Biology, University of Nebraska Medical Center, Omaha, NE 68198, USA; punita.dhawan@unmc.edu
6 Laboratory Animal Research Center, Qatar University, Doha 2713, Qatar; smurli28@qu.edu.qa (S.M.); halnaemi@qu.edu.qa (H.A.-N.)
7 Center for Magnetic Resonance and Optical Imaging, Department of Radiology, Perelman School of Medicine at the University of Pennsylvania, Philadelphia, PA 19104, USA; puneetb@pennmedicine.upenn.edu (P.B.); krr@pennmedicine.upenn.edu (R.R.)
8 Department of Pediatric Gastroenterology, Sidra Medicine, Doha 26999, Qatar; aakobeng@sidra.org
9 Academic Health System, Hamad Medical Corporation, Doha 3050, Qatar; mfrenneaux@hamad.qa
10 Department of Surgery, University of Miami Miller School of Medicine, Miami, FL 33136, USA; welrifai@med.miami.edu
* Correspondence: mharis@sidra.org; Tel.: +974-4003-7407

Received: 25 November 2019; Accepted: 13 January 2020; Published: 15 January 2020

Abstract: Claudins, a group of membrane proteins involved in the formation of tight junctions, are mainly found in endothelial or epithelial cells. These proteins have attracted much attention in recent years and have been implicated and studied in a multitude of diseases. Claudins not only regulate paracellular transepithelial/transendothelial transport but are also critical for cell growth and differentiation. Not only tissue-specific but the differential expression in malignant tumors is also the focus of claudin-related research. In addition to up- or down-regulation, claudin proteins also undergo delocalization, which plays a vital role in tumor invasion and aggressiveness. Claudin (CLDN)-1 is the most-studied claudin in cancers and to date, its role as either a tumor promoter or suppressor (or both) is not established. In some cancers, lower expression of CLDN-1 is shown to be associated with cancer progression and invasion, while in others, loss of CLDN-1 improves the patient survival. Another topic of discussion regarding the significance of CLDN-1 is its localization (nuclear or cytoplasmic vs perijunctional) in diseased states. This article reviews the evidence regarding CLDN-1 in cancers either as a tumor promoter or suppressor from the literature and we also review the literature regarding the pattern of CLDN-1 distribution in different cancers, focusing on whether this localization is associated with tumor aggressiveness. Furthermore, we utilized expression data from The Cancer Genome Atlas (TCGA) to investigate the association between CLDN-1 expression and overall survival (OS) in different cancer types. We also used TCGA data to compare CLDN-1 expression in normal and tumor tissues. Additionally, a pathway interaction analysis was performed to investigate the interaction of CLDN-1 with other proteins and as a future therapeutic target.

Keywords: claudin 1; tight junctions; tumor; metastasis; epithelial to mesenchymal transition

1. Introduction

Claudins and occludin, a group of cell junctional proteins, serve as the backbone of the tight junctions. Claudin family members perform dual roles; some have barrier activities, while others mediate the permeability of small molecules and ions. In addition to the localization pattern, the differential expression of claudins between normal and tumor tissue has drawn attention to these proteins as potential prime candidates for future cancer therapy. Another hot topic of discussion is the tumor-promoter or tumor-suppressor role of claudins. This opens a wide area of research in elucidating how the tissue-specific expression of claudins and their interaction with other molecules in the cell may result in these two opposing effects. Both defective tight junctions and the absence of tight junctions have shown to be associated with the development and progression of certain cancers. In this article, we include a brief introduction of tight junctions, the structure of claudins, and their role in various cancers. We also perform the bioinformatics analysis on TCGA data to supplement the literature review.

1.1. Tight Junctions

Adjacent epithelial cells are sealed into an epithelial barrier by the most apical intercellular junctions called tight junctions. Tight junctions, as a network of continuous strands, separate the plasma membrane into apical and basolateral domains [1,2]. Tight junctions between adjacent cells associate to form paired strands imparting mechanical strength to the cells [3,4] and serve as barriers to control the movement of small molecules and ions across the paracellular space [5–7]. Apart from their mechanical strength, maintaining polarity and paracellular movement, tight junction proteins are able to recruit signaling proteins for various cellular processes [4]. Alterations in the structure and function of tight junctions result in a multitude of diseases, especially adenocarcinoma of various organs [8–10]. The failure of tight junctiontight junctions or tight junction proteins is one of the many key factors that contribute to the progression of cancer, but this is not a universal phenomenon as there can be many other direct or indirect factors that contribute to the development of cancer. The second reason that loss of tight junctions or tight junction proteins is not a universal phenomenon to the development of cancers is that besides the epithelial cancers, there are also non-epithelial tumors such as small subset of laryngeal neoplasms [11], angiomas, lipomas and neuromas [12] which do not display failure of tight junctions but other contributing factors come into play.

1.2. Claudins

Claudins are integral to the structure and function of tight junctions with four membrane-spanning regions, which include two extracellular loops, N- and C-terminal cytoplasmic domains. The extracellular loops are highly conserved, and the C-terminal domain is important for localizing the claudins to tight junctions (Figure 1). Being a part of a multigene family, there are about 27 members of claudins that are unique in their tissue-specific expression and their molecular weight ranges from 20–34 kDa [3]. Claudins play an important role in regulating transepithelial permeability by regulating the epithelium's paracellular permeability to small molecules and ions [5,7,13]. Post-translational modifications such as phosphorylation alter the paracellular functions of claudins, which in turn modulate diverse signal mechanisms [14–17].

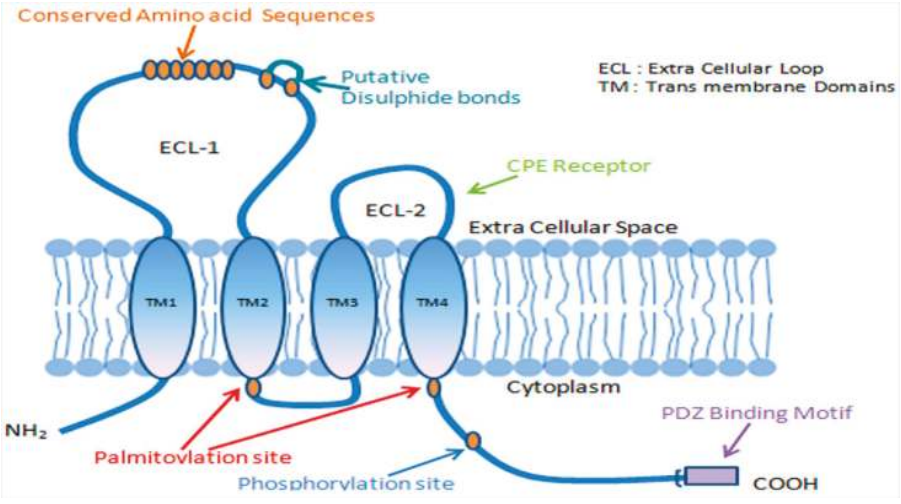

Figure 1. A schematic presentation of tight junction complex involving claudins and other major components. Claudins contain four transmembrane domains (TMD-1, TMD-2, TMD-3, and TMD-4) and two extracellular (ECL) loops. The PDZ-binding domain of the –COOH terminal of claudin undergoes post-transcriptional modification and has been implicated in signal transduction.

1.3. Claudins and Cancer

One of the important factors in cellular transformation and tumorigenesis is the loss of cell-to-cell adhesion [1]. Accordingly, the claudin family of proteins is significantly involved in the progression and growth of several cancers [9,10,18]. Tumor progression is characterized by migration, invasion, and metastasis of cancer cells. Claudins are believed to play a significant role in these processes as their loss contributes to the loss of cell junctions in a tissue-dependent manner [18,19]. Claudins have been also reported to play a vital role in the epithelial–mesenchymal transition (EMT) (Figure 2), a process that favors the spread of carcinomas, generation of cancer stem cells (CSCs) or tumor-initiating cells (TICs), and chemo-resistance [20–23]. The loss of claudins in epithelial cells results in disrupted tight junction function responsible for impaired cell polarity and epithelial integrity [6,7]. Several studies have reported the mislocalization and altered expression of claudins in various cancers [19,24]. The CLDN-1 and CLDN-7 members of the claudin family are primarily found to be downregulated in several invasive cancers including breast, esophageal, and prostate cancers [9,19,25–27]. However, in contrast, overexpression of CLDN-1 has been observed in colon, nasopharyngeal, ovarian and oral squamous cell cancers [9,10], while CLDN-3 and -4 are highly overexpressed in ovarian cancer and upregulated in breast, gastric, pancreatic, prostate and uterine cancers [28–30]. Human carcinomas such as those of the breast, liver, ovary, prostate, colon, liver and stomach are found to exhibit altered expression of claudins [19]. The expression and localization patterns of some of the claudins serve as an important prognostic predictor in many cancers [30,31]. The consensus of whether claudin expression increases or decreases during tumorigenesis is still a debatable topic and open to more research.

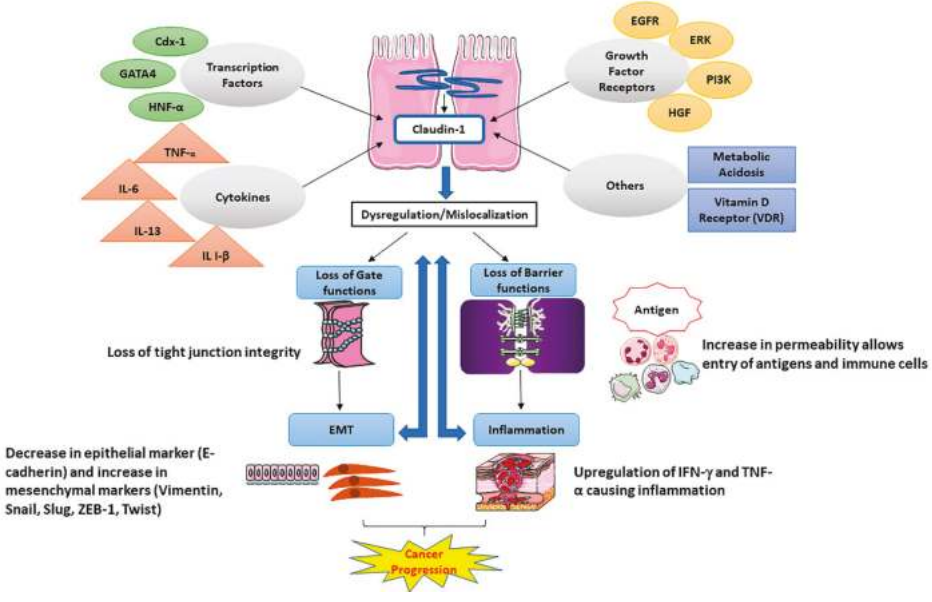

Figure 2. Schematic model of role and regulation of CLDN-1 in a normal or diseased state. In normal physiological conditions, CLDN-1 expression/ integrity is regulated by transcription factors, growth factors and cytokines, which in turn maintain the normal gate function and barrier function of tight junctions. Dysregulation of CLDN-1 expression can result in the compromise of membrane barrier functions and gate functions, which subsequently can lead to the upregulation of the expression of pro-inflammatory markers such as IFN-γ and TNF-α. In cancer, the loss of CLDN-1 facilitates the malignant transformation of cancer cells and epithelial-mesenchymal transition (EMT).

2. Claudin-1 and Cancer; Tumor Promoter or Suppressor

CLDN-1 is a membrane protein that, along with occludin and other claudins form the backbone of the tight junctions and is essential for epithelial barrier functions [32]. It was the first member of the claudin family to be identified with a molecular weight of 22 kDa and is strongly expressed in the intestine, spleen, brain, liver, kidney, and testis [19,33]. Studies have shown the direct involvement of CLDN-1 in the development and progression of several cancers, such as colon cancers [34], oral squamous cell carcinomas [35], breast cancers [36], melanomas [37,38], and in many other cancers as discussed in this review. In some cancers, CLDN-1 has the opposite role where the decreased expression of CLDN-1 is associated with cancer progression, invasion and development of the metastatic phenotype [37,39]. The expression of CLDN-1 in different types of cancer and cancer subtypes is summarized in Table 1. Based on the literature, CLDN-1 is one of the most deregulated claudins in human cancer and can function as a tumor promoter or suppressor depending on the type of cancer (Figure 3) (Table 2). The role of CLDN-1 as a tumor promoter is mostly through its effect on the invasion or motility of cancer cells. Considering the importance of claudins in cancer, targeting claudin expression appears to have promise in the treatment of cancer. The specific role of CLDN-1 in various cancers is discussed in the following sections.

Table 1. Expression of CLDN-1 in different types of cancer.

Type of Cancer	Subtypes	Expression of CLDN-1	References
Breast Cancer	Luminal A	Downregulated	[40]
	Luminal B	Downregulated	[40]
	Triple negative/Basal like	Upregulated	[40]
	HER2 enriched	Downregulated	[41]
	Claudin-low	Downregulated	[41]
Thyroid Cancer	Papillary Thyroid Cancer	Upregulated	[42]
	Follicular Thyroid Cancer	Upregulated	[43]
Colorectal Cancer	Ulcerative Colitis associated Colorectal Cancer	Upregulated	[44]
	Sporadic Colorectal Cancer	Upregulated	[34]
Gastric Adenocarcinoma	-	Upregulated	[45]
Head and Neck Squamous Cell Carcinoma	-	Upregulated	[46]
Hypopharyngeal Squamous Cell Carcinoma	-	Upregulated	[47]
Hepatocellular Carcinoma	-	Downregulated	[48,49]
Lung Adenocarcinoma	-	Downregulated	[50]
Pancreatic Ductal Carcinoma	-	Upregulated	[51]
Epithelial Ovarian Cancer	-	Upregulated	[52,53]
Oral Squamous Cell Carcinoma	-	Upregulated	[35]
Melanoma	-	Upregulated	[38]
Prostate adenocarcinoma	-	Downregulated	[54,55]

"-" no subtypes.

Table 2. Role of CLDN-1 in different cancers.

Cancer Type	Activity	Findings	References
Melanoma	Tumor Promoter	Cytoplasmic expression of CLDN-1 contributes to the migratory capacity of melanoma cells	[56]
Oral Squamous Cell Carcinoma	Tumor Promoter	CLDN-1 enhances the invasive activity of OSC-4 and NOS-2 cell lines by activation of MT1-MMP and MMP-2	[35]
Prostate Cancer	Tumor Suppressor	Loss of CLDN-1 associated with progression of Prostate cancer	[54]
Lung Cancer	Tumor Suppressor	Knockdown of CLDN-1 increased invasive and metastatic activity of lung adenocarcinoma cells	[57]
Breast Cancer	Tumor Promoter in ER-Subtypes	Increases cell migration and also exhibits an anti-apoptotic effect	[40]
	Tumor Suppressor in ER+ Subtypes	Acts as a suppressor of mammary epithelial proliferation Increases apoptosis of breast cancer cells	
Thyroid Cancer	Tumor Promoter	High expression of CLDN-1 found in follicular thyroid carcinoma (FTC-133) and Papillary Thyroid Carcinoma cells	[42,43]
Ovarian Cancer	Tumor Promoter	High expression of CLDN-1 correlated with shorter overall survival in ovarian carcinoma effusions	[58]
Colon Cancer	Tumor Promoter	High CLDN-1 expression in colon carcinoma and metastasis CLDN-1 upregulates the repressor ZEB-1 to reduce expression of E-cadherin in colon cancer cells	[34,59]
Gastric Cancer	Tumor Promoter	High expression of CLDN-1 in gastric cancer associated with poor survival	[60]
Hypopharyngeal Squamous Cell Carcinoma	Tumor Promoter	High expression of CLDN-1 associated with lymph node metastasis and degree of tumor differentiation	[61]
Hepatocellular Carcinoma	Tumor Promoter	CLDN-1 promoted epithelial-mesenchymal transition (EMT) in HCC cells by overexpression of mesenchymal markers (N-cadherin and vimentin)	[48,62,63]
Pancreatic Cancer	Tumor Promoter	TNF-α upregulated CLDN-1 expression, leading to increased proliferation of pancreatic cancer cells	[64]

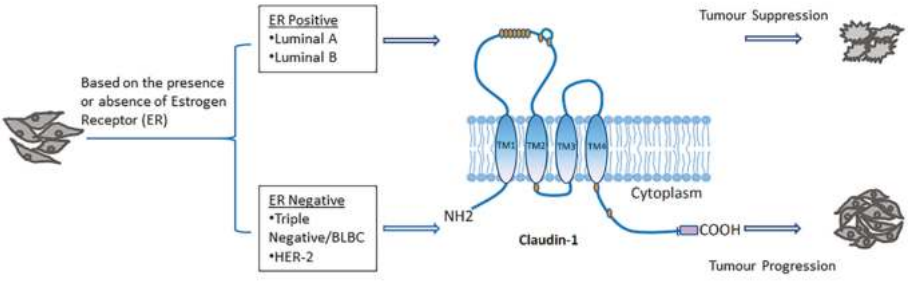

Figure 3. CLDN-1 expression in different subtypes of breast cancer as characterized by the presence or absence of estrogen receptor (ER). Luminal A, and Luminal B subtypes of human invasive breast cancer (ER-positive) exhibit low levels of CLDN-1, which suggests the suppressor role of CLDN-1 in these tumors. However, aggressive forms (ER-negative) exhibit overall high levels of CLDN-1 expression, which signifies CLDN-1 role as a tumor promoter.

2.1. Claudin-1 and Breast Cancer

Breast cancer is the second major cause of death in women, and its heterogeneous molecular nature is a significant obstacle in treatment planning [65]. It has several subtypes, such as human epidermal growth factor receptor 2 (HER2), triple-negative or basal-like, Luminal A and Luminal B type depending on the presence or absence of several hormone receptors like HER2, estrogen, and progesterone [66–68]. Recently, another subtype of breast cancer known as the claudin-low subtype has been reported [67]. Each subtype of breast cancer exhibits unique prognostic features and different molecular markers [69].

The *CLDN-1* gene has been found to be upregulated during the early involution of the mammary gland [70]. The differential expression of CLDN-1 observed in different cancers outlines the complexity of the potential role that it plays in the cancer process. The CLDN-1 expression level in breast cancer differs depending on the cancer subtypes [71]. Studies have shown a correlation between increased malignancy, invasiveness and recurrence of breast cancer with total or partial loss of CLDN-1 expression [36,70]. In most of the invasive human breast cancers such as ER+ luminal A and luminal B, CLDN-1 expression is found to be downregulated, while an increased expression and cytoplasmic delocalization of CLDN-1 has been observed in some of the aggressive ER- basal-like breast cancer (BLBC) subtypes [40,72,73]. CLDN-1 is also found to be downregulated in HER2 enriched and claudin low breast cancer subtypes [41]. CLDN-1 acts as a tumor suppressor in ER+ and as a tumor promoter in ER- cancer subtypes [25]. In hereditary and sporadic breast cancer, CLDN-1 is found to be involved in tumorigenesis by suppressing the proliferation of mammary epithelial cells [74]. Further, CLDN-1 overexpression in MDA-MB 361 breast cancer cells resulted in increased apoptosis [75,76]. While one study reported that the activation of CLDN-1 was repressed by the binding of E-cadherin to CLDN-1 promoter [77], knockdown of CLDN-1 has been found to be associated with decreased cell migration and induction of EMT in breast cancer cells [76]. Another study showed a unique pattern of expression for CLDN-1 in ER-ve and ER+ve tumors. The authors showed that the protein expressions of CLDN-1 were significantly higher in the basal-like subtype of breast cancers (ER-ve, Her-2-ve, EGFR+ve, CK5/6+ve, a subtype largely linked to poor outcome [40]. CLDN-1 expression has also been observed in a small percentage of invasive human breast cancers that exhibit different pathological lesions leading to complexity in CLDN-1 expression [78]. CLDN-1 also possesses tumor-promoting effects by increasing cell migration and by exhibiting anti-apoptotic effects in some breast cancer cell lines like MCF-7 [76,79].

Several proteins interact with CLDN-1 to fuel the progression of breast cancer, including the following: Ephrin B1, ESCRT, CD9 and EpCAM [80–83]. CLDN-1 mediates the tyrosine phosphorylation of Ephrin B1, a transmembrane protein, in a receptor independent manner which provides the evidence

that ephrin-B1 inhibits the formation of the tight cell–cell adhesion in a wide variety of epithelial and cancer cells regardless of the existence of cognate Eph receptors [80]. Endosomal sorting complexes required for transport (ESCRT) machinery are a set of proteins present in the cytosol that are involved in the maintenance of cell polarity and the regulation of membrane-bound proteins [81]. When the function of ESCRT is inhibited, CLDN-1 accumulates in the cytoplasm causing the tight junctions to disassemble and lose cell polarity [25]. The loss of ESCRT function is also linked with increased proliferation and less stable tissue structure in the cancer cells. CLDN-1 is also found to interact with CD9, a transmembrane protein that regulates cell migration, proliferation, differentiation and fusion [82]. CD9 prevents the association between CLDN-1 and tight junctions that could cause the progression of the tumor. The subcellular co-localization of CLDN-1 and CD9 supports their interaction, and this was confirmed in many cell clines including different human breast cancer cell lines [82]. EpCAM (also known as epithelial cell adhesion molecule), another surface transmembrane glycoprotein known to be expressed in some invasive carcinomas is involved in cell proliferation and metastasis and has been shown to protect CLDN-1 from degradation. [83]. This could be a cause for the cytoplasmic accumulation of CLDN-1 in some breast cancer cell lines [76,83]. Several transcript variants for CLDN-1 were found in human invasive breast cancer as a result of splicing and mis splicing events suggesting that through alternative splicing CLDN-1 is downregulated in invasive type of breast cancers [72].

2.2. Claudin-1 and Thyroid Cancer

Thyroid cancer is the most commonly occurring endocrine malignancy [84,85]. A study by Nemeth et al. performed independent microarray expression analyses of two types of thyroid carcinomas, namely papillary thyroid cancer (PTC) and follicular thyroid cancer (FTC) [42]. The study showed that high expression of CLDN-1 is specific for the regional lymph node metastasis associated with PTC [42] and found increased expression of *CLDN-1* gene in PTC [86,87]. Sobel et al. reported high levels of CLDN-1 expression in serous papillary endometrial carcinoma [88]. Another study about the role of CLDN-1 in follicular-cell derived thyroid carcinoma cell lines (FTC-133 and FTC-238) found higher expression of CLDN-1 in the nuclei of FTC-238 cells as compared to the FTC-133 cells [43]. The same study demonstrated the increased pathogenic character of FTC-133 cells by RASV12 transfection was associated with high expression of CLDN-1 and enhanced cell proliferation and migration [43]. Conversely, the downregulation of CLDN-1 by siRNA caused decreased cell invasion and migration accompanied by decreased phospho-PKC expression in the FTC-238 cells, suggesting that the aggressiveness of follicular thyroid carcinoma associated with high CLDN-1 expression can be influenced by PKC activity [43]. Another study described the reduced expression of CLDN-1 in follicular carcinomas vs adenomas, specifically in the poorly-differentiated and undifferentiated types of human thyroid carcinomas [89]. The expression of CLDN-1 was significantly different between malignant and benign thyroid neoplasms, and between follicular and papillary carcinomas [90]. Similarly, papillary carcinomas showed significantly higher positive CLDN-1 expression. While negative CLDN-1 expression was observed in the tissue samples of normal thyroid and solitary-follicular-patterned-nodules [91].

2.3. Claudin-1 and Colorectal Cancer

Colorectal cancer (CRC) is the fourth leading cause of cancer-related deaths and the third most frequently diagnosed malignancy worldwide [92]. Increased expression of CLDN-1 is associated with the progression and metastasis of colon carcinoma [34,93]. In mouse xenograft studies, tumor growth and metastasis is regulated by genetic modulation of CLDN-1 [94]. The nucleus and cytoplasm of colon carcinoma cells and metastatic lesions showed intensified CLDN-1 expression [34]. Many studies suggest that the genes encoding tight junction proteins (TGPs) in CRC are differentially expressed and involved in the process of invasion and cellular transformation [95]. Several studies reported up-regulation of CLDN-1 in CRC [34,44,96,97]. A similar study showed that CLDN-1 overexpression

induced a highly invasive and metastatic potential in CRC cells [34]. Noncancerous cells with normal CLDN-1 expression were found to form a monolayer, whereas cells that overexpressed CLDN-1 grew as aggregates. CLDN-1 regulates cellular morphology and behavior in the colonic epithelium [34,44]. The possible involvement of CLDN-1 in the tumorigenesis of ulcerative colitis (UC)-associated CRC has also been demonstrated [44]. Another study demonstrated that the prognostic factor for CRC is the independent expression of CLDN-1 [98]. Delocalization of CLDN-1 from the membrane to cytoplasm and nuclei of cancer cells supports cancer growth and malignancy [34]. In colon cancer cells, CLDN-1 decreases the expression of E-cadherin by upregulating ZEB-1 repressor resulting in invasion and reduction of anoikis [59].

The level of CLDN-1 mRNA was found to be higher in the distal site of the colon as compared to the proximal site and demonstrated significant effects on xenografted tumors growth in athymic mice by changes in the expression of CLDN-1, showing its role in CRC tumorigenesis [34]. Both mRNA and protein levels of CLDN-1 were found to be upregulated in sporadic human CRC compared to the normal mucosa [34]. Dhawan and colleagues reported that T84 cell transfection with CLDN -1 resulted in aggregation and multilayer formation in transfected T84 cells as compared to the T84 parent cells. The interactions between claudin family members are both homophilic and heterophilic and are considered to play a significant role in the progression of CRC and several other cancers [99]. The progression of colon cancer has been linked with the dysregulation of the CLDN-1 expression causing disorganization of the tight junction fibrils leading to increased paracellular permeability [100]. Increased potential for invasion and metastasis has been demonstrated in xenografts that express CLDN-1 [101]. CLDN-1 positively correlates with CRC cell proliferation and influences the growth and evolution of the tumor. Its expression was also found to be associated with accelerated serrated lesions of CRC and was related to anoikis resistance and cellular dis-cohesion [101]. Moreover, serrated polyps with over-expressed CLDN-1 were found to have a higher potential for the development and progression into higher-grade lesions [101].

Activation of the Wnt signaling pathway is strongly implicated in the development of colorectal cancer [102]. Wnt signaling is activated by the loss of the adenomatous polyposis coli (APC) protein or by the activation of β-catenin mutations [103,104]. CLDN-1, one of the target genes in the Wnt signaling pathway, has two β-catenin binding sites (TCF/LEF) in its promoter region for the activation of the transcription process [105,106]. A study showed that the expression of CLDN-1 was found to be elevated in the intestinal adenomas of the APC in mice as compared to normal tissue [94]. Additionally, high expressions of CLDN-1 are seen in the dysplastic areas of the colon in patients with chronic inflammatory disease [94]. CLDN-1 was overexpressed in metastatic colorectal cancer (mCRC) samples as compared to normal mucosa with differential expression in other CRC subtypes. Consensus molecular subtype CMS2, transit-amplifying and C5 subtypes of the mCRC exhibited higher expression of CLDN-1 [107].

2.4. Claudin-1 and Gastric Cancer

CLDN-1 is highly expressed in gastric cancers [108,109]. High expression of CLDN-1 was reported in intestinal type gastric cancer that correlated with lymph node metastasis, advanced TNM (classification of malignant tumors) stage, recruitment, and activation of MMP-2 and MMP-9, which are all responsible for enhanced cell invasion and metastasis [60,109]. The invasion of gastric adenocarcinoma cells is associated with the levels of CLDN-1 expression as CLDN-1 is found to be upregulated in gastric carcinoma and participates in the metastatic behavior of these cancer cells [45].

One study demonstrated that the localization and correlation of CLDN-1 expression are linked with anoikis resistance in gastric cancer through mediating membrane β-catenin expression and by inducing cell aggregation and inhibiting apoptosis cascade [110]. The authors also observed that the levels of CLDN-1 expression in gastric cancer tissues decreased from well to moderate to poorly differentiated tumors, suggesting that reduced CLDN-1 expression is an adverse prognostic factor predicting a lower

survival rate [110]. However, another study showed that in comparison to CLDN-4, the expression of CLDN-1 was higher in well-to-moderately differentiated gastric adenocarcinomas [111].

2.5. Claudin-1 and Hypopharyngeal Squamous Cell Carcinoma

Head and neck squamous cell carcinoma (HNSCC) is the sixth most frequent tumor worldwide [112]. Tissue microarray and immunohistochemistry assays of surgical samples suggested that CLDN-1 expression is increased in squamous cell cancer [46,113]. It has been shown previously that CLDN-1 induces the generation of tumor lymphatic vessels and increases the lymph node metastasis [47]. Additionally, a study demonstrated that CLDN-1 expression in squamous cancers differs in an organ-specific manner [113]. CLDN-1 was found to be upregulated in hypopharyngeal squamous cell carcinoma (HSCC). This study showed a positive association of CLDN-1 expression with the degree of tumor differentiation and lymph node metastasis [61].

2.6. Claudin-1 and Hepatocellular Carcinoma

Hepatocellular carcinoma (HCC) is the third major cause of death due to cancer and the fifth most common cancer malignancy worldwide [114]. Studies have reported the involvement of CLDN-1in the tumorigenesis and metastasis of HCC [48,63]. HCC cell line experiments demonstrated the role of CLDN-1 in the process of cancer cell invasion [115]. Primary HCC samples were found to be positive for CLDN-1, suggesting its significant role in the formation of metastasis and hepato-carcinogenesis [115]. Another study demonstrated the involvement of CLDN-1 in the epithelial to mesenchymal transition in HCC and hepato-carcinogenesis [62]. One study established that overexpression of CLDN-1 induces MMP-2 in SNU-354, -423 and -449 HCC cells resulting in increased invasion and migration of the cancer cells compared to the normal liver cells and other CLDN-1 expressing HCC cells such as SNU-398 and SNU-475 [63]. However in another study reduced expression of CLDN-1 was reported to be a marker for a poor prognosis in HCC [49], and a further study showed that reduced expression of CLDN-1 reinforced the invasive and cancer stem cell (CSC) like properties of HCC cell lines (Huh7 and Hep3B) in vitro, while the forced expression of CLDN-1 diminished the CSC-like properties of HCC cells [116].

2.7. Claudin-1 and Lung Adenocarcinoma

Lung cancer is one of the leading causes of death worldwide. Several studies have shown that CLDN-1 has a significant role in the pathogenesis of lung cancer [117–119]. In lung cancer, CLDN-1 acts as a cancer invasion/metastasis suppressor [57]. CLDN-1 was found to be associated with increased expressions of cancer metastasis suppressors such as connective tissue growth factor (CTGF), thrombospondin 1 (THBS1), deleted in liver cancer 1 (DLC1), occludin (OCLN), zona occludens 1 (ZO-1) and reduced expressions of cancer metastasis enhancers such as secreted phosphoprotein 1 (SPP1), cut-like homeobox 1 (CUTL1), transforming growth factor-alpha (TGF-α), solute carrier family 2 (facilitated glucose transporter) member 3 (SLC2A3) and placental growth factor (PGF) in lung adenocarcinoma [57]. For patients with lung adenocarcinoma, CLDN-1 is a potential drug treatment target and a useful predictor of prognosis. Studies showed that the invasive ability of HOP62 lung adenocarcinoma cells is increased by knockdown of endogenous expression of CLDN-1 [57]. Immunohistochemistry and RT-PCR analysis showed that CLDN-1 is either reduced or undetected in adenocarcinomas [57]. The authors demonstrated that CLDN-1 overexpression inhibited adenocarcinoma cell dissociation in wound-healing time-lapse images [57].

Inflammatory mediators, such as TNFα, plays a significant role in the process of tumorigenesis [120]. Studies have shown that CLDN-1 is involved in the mediation of inflammatory responses initiated by TNFα in different cancers [64,121,122]. An experiment in human lung cancer cell lines, observed that TNFα induced the expression of CLDN-1, and knockdown of CLDN-1 blocked 75% of TNFα-induced gene expression. In CL1-5 lung cancer cells, cell migration activity was inhibited by over-expression of CLDN-1 and restored by CLDN-1 knockdown in addition to cell invasion ability. The above findings signify a signal mediator role of CLDN-1 in TNFα induced gene expression and cell migration [57]. One

study demonstrated that CLDN-1 expression correlated with Ras and epidermal-growth-factor-receptor (EGFR) expression suggesting the involvement of the latter two signaling pathways in the regulation of CLDN-1 in lung adenocarcinoma [119]. The results of this study demonstrated an association between CLDN-1 and Ras/EFGR in the development of lung cancer and the combination of both has strong clinical significance [119]. Surprisingly, as compared to the previous studies that showed that overexpression of CLDN-1 suppressed metastatic abilities of lung adenocarcinoma cells [50,57], this study showed that patients with positive expressions of both CLDN-1 and Ras/EGFR were found to have poor prognosis as compared to CLDN-1(+) Ras/EGFR(−), CLDN-1(−) Ras/EGFR(+), and CLDN-1(−) and Ras/EGFR(−) patients [119]. Another study found that enhanced cell migration by tumor necrosis factor and a similar morphology like fibroblast was found to be reduced by small CLDN-1 interfering RNA in the cells of lung cancer [121].

2.8. Claudin-1 and Pancreatic Cancer

Pancreatic cancer is the fourth major cause of deaths caused by cancer worldwide, with a strong capacity for metastasis and recurrence [123]. In pancreatic cancer (PC), increased expression of CLDN-1 was found to be associated with epithelial-mesenchymal transition. CLDN-1 is expressed by ductal pancreatic adenocarcinomas as well as intra-ductal papillary mucinous pancreatic tumors. One study demonstrated that 58% positive CLDN-1 immunostaining in ductal pancreatic adenocarcinomas and intraductal papillary pancreatic tumors [51]. Another study showed that through activation of mitogen-activated protein kinase 2 (MEK2), CLDN-1 was involved in cell dissociation of PC cells [124]. A further study observed the role of CLDN-1 in the progression of human PC using the PANC-1 cell line [64]. Increased expression of PARP [poly-(ADP-ribose) polymerase], an apoptosis marker, and decreased PANC-1 proliferation was observed after treatment with TNF-α [64]. Increased proliferation in PANC-1 cells was observed after treatment with TNF-α and CLDN-1 siRNA against CLDN-1, suggesting the cells were resistant to TNF-α-induced apoptosis when transfected with CLDN-1 siRNA. These findings clearly demonstrated that the CLDN-1 expression plays a role in the proliferation of PC cells [64].

2.9. Claudin-1 and Ovarian Cancer

Ovarian cancer affected a significant number of women worldwide and is the seventh most frequent cause of deaths due to cancer in women [125]. The upregulation of the *CLDN-1* gene is found to be associated with ovarian cancer [52]. Studies have shown that overexpression of CLDN-1 caused reduced cell differentiation and a high invasive growth rate [126]. The role of CLDN-1 has been widely studied in two different types of ovarian cancers, namely, ovarian serous and ovarian endometroid carcinoma [127]. The expression of CLDN-1 was shown to be negatively regulated by microRNA-155 (miR-155) which results in reduced proliferation and invasion of human ovarian cancer-initiating cells [52]. Reports have shown that elevated level of CLDN-11, 4, and 7 promotes the growth of both benign and malignant epithelial ovarian cancers [52]. Extensive studies conducted and analyzed for the association of CLDN-1 with survival and anatomical site showed 85% elevation of CLDN-1 expression [58]. Recently, the level of CLDN-1 expression was also investigated in borderline tumors of the ovary (BOT) [53]. A significantly higher level of CLDN-1 expression was associated with the peritoneal implants and micropapillary patterns that are specifically seen only in serous BOT [53].

2.10. Claudin-1 and Oral Squamous Cell Carcinoma

Almost 90% of all oral carcinomas are oral squamous cell carcinomas (OSCC) [128]. It has been shown previously that the invasive activity of OSCC cells is enhanced by CLDN-1 through activation of MMP-1 and 2, resulting in increased cleavage of Laminin-5 γ2 chains. The authors of the study further revealed elevated expression of CLDN-1 in OSC-4 and NOS-2 cell lines which are highly invasive [129]. One study demonstrated the association of high CLDN-1 expression with aggressive histopathologic features such as perineural and vascular invasion and suggested that CLDN-1 might

be directly or indirectly involved in the progression of OSCC [130]. Another study found that the absence of CLDN-1 was associated with poorly differentiated tumors [131]. Immunohistochemical analysis revealed that the presence of CLDN-1 in the invasive front of tumor islands was associated with neck mode metastasis. The results obtained from this study further suggested that the expression of CLDN-1 is linked with the recurrence of OSCC [132].

2.11. Claudin-1 and Melanoma

Melanoma, which arises from melanocytes, causes 75% of deaths related to skin cancers [133]. CLDN-1 was found to be upregulated in melanoma tissues [134]. In melanoma, CLDN-1 is abnormally/aberrantly expressed in the cytoplasm of malignant cells and not in the cell membrane. This may be related to its influence on protein kinase C (PKC) activity [38]. PKC activation caused an increase in transcription and protein expression of CLDN-1 and thus, cell motility [38]. When melanoma cells transfected with CLDN-1, it increased the secretions of matrix metalloproteinase- 2 (MMP-2) reflecting its contribution to the cell invasion process. The data from French, et al. supported the hypothesis that the invasive capacity of melanoma cells is increased by cytoplasmic expression of CLDN-1 and not by the elevated nuclear expression of CLDN-1 [56]. In melanoma patients with brain metastases, the expression of CLDN-1 was downregulated, and the introduction of CLDN-1 retrovirus reduced the tumor aggressiveness and tumor migration ability and diminished micro-metastasis in the brain. This shows that reduction in CLDN-1 supports tumor progression and metastasis and that CLDN-1 can be used as a prognostic predictor for melanoma patients with increased risk of brain metastasis [135].

2.12. Claudin-1 and Prostate Cancer

Prostate cancer is the second most diagnosed malignancy and fifth-most leading cause of cancer deaths in men [136]. The Gleason grading score system is the most commonly used method to evaluate the aggressiveness of prostate cancers, whereas, the changes in the glandular architecture indicate the tumor grades [54]. The typical glandular architecture is supported by cellular polarity and cell-to-cell contact, and thus the alterations and dysregulations of proteins mediating normal cellular connection may impact the histology and Gleason grade [54]. It is suggested that the loss of tight junction protein, CLDN-1, is associated with cancer invasion, progression and the transformation into metastatic phenotype in prostate cancers. A study reported that the lower expression of CLDN-1 correlated with higher prostate-specific antigen in prostate cancer [54]. Further studies are needed to thoroughly investigate the association between prognostic factors and claudins expression in prostate cancer.

3. Claudin-1 and Tight Junction Barrier Function

CLDN-1 is an integral membrane protein that in conjunction with other claudins forms the tight junctions and together plays an essential role in epithelial barrier functions. CLDN-1 has a significant role in epithelial differentiation and loss of CLDN-1 can impair the functioning of tight junctions [137]. Numerous studies have reported the involvement of CLDN-1 in transepithelial electrical resistance (TER) [138,139] and paracellular permeability [140] showing its importance in tight junction barrier functions. The study showed that CLDN-1 increased the TER and reduced paracellular flux in Madin-Darby Canine Kidney (MCDK) cells [138]. While another study reported that induced CLDN-1-myc in MDCK cells resulted in the formation of aberrant tight junction strands independently without the participation of ZO-1 and occludin [139]. CLDN-1 controls the flux of solutes by localizing at tight junctions and modulating the paracellular permeability. Any defect in the expression of CLDN-1 can result in tight junction dysfunction causing increased paracellular permeability leading to various pathologies such as in Neonatal ichthyosis-sclerosing cholangitis (NISCH) syndrome [140]. This study showed that the silencing of CLDN-1 leads to increased hepatic paracellular permeability [140]. Mostly, an increase in the tight junction proteins should lead to an increase in the tight junction integrity but this is not a universal phenomenon as one study reported

that high expression of CLDN-1 resulted in decreased TER and increased permeability causing loss of barrier function in intestinal epithelial cells (IEC-18) treated with TNF-α [141]. The authors explained the reason for this contradictory finding is that the loss of barrier function was due to the reduced expression of occludin protein and not CLDN-1 [141]. Besides, the other study reported that high expression of CLDN-1 resulted in blood–brain-barrier (BBB) leakiness during post-stroke recovery and targeting of CLDN-1 by a CLDN-1 peptide improved the permeability of brain endothelial barrier [142]. So, these studies suggest that the upregulation of CLDN-1 cannot necessarily be universal to the increased barrier function and there might be other contributing factors that regulate these functions, and also we should not rule out the tissue specific expression of claudins as other possibility to their dichotomous roles.

4. Gene Expression, Survival and Pathway Interaction Analysis of claudin-1 across different Cancers

Survival Analysis was performed using online survival analysis tools to assess the influence of CLDN-1 expression on survival in different types of cancer using the Cancer Genome Atlas (TCGA) datasets. This analysis was to investigate whether an alteration in gene expression correlates with poor survival or with tumor recurrence. The data showed that the gene expression of CLDN-1 did not affect survival significantly in cancers like breast invasive carcinoma (BRCA), cervical squamous cell carcinoma and endocervical adenocarcinoma (CESC) and pancreatic adenocarcinoma (PAAD) ($p > 0.05$), but did significantly associate with survival for cancers like thyroid carcinoma (THCA), adrenocortical carcinoma (ACC), rectum adenocarcinoma (READ) (* $p < 0.05$) (Figure 4). All survival analysis was performed using online survival analysis tools.

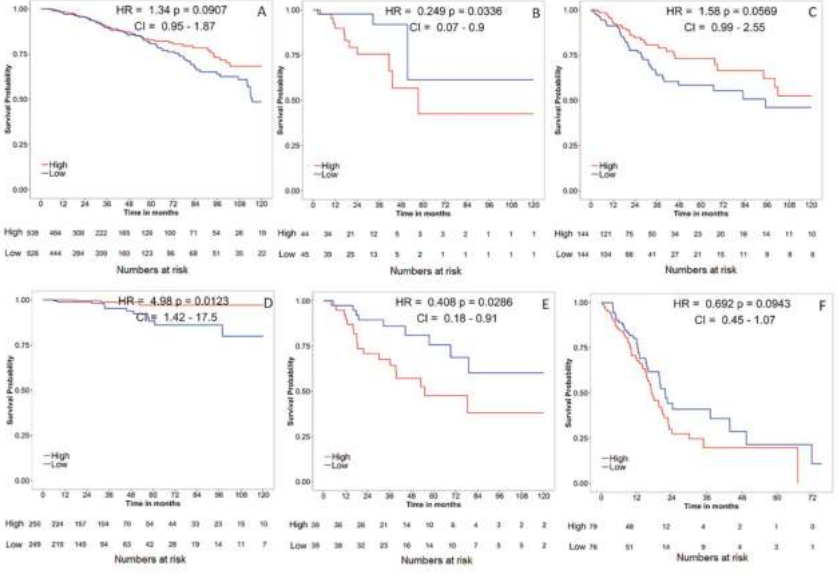

Figure 4. Survival analysis of CLDN-1 in various cancers. The red line denotes higher expression, and the blue line indicates lower expression. (**A**) Breast invasive carcinoma (BRCA); (**B**) rectum adenocarcinoma (READ); (**C**) cervical squamous cell carcinoma and endocervical adenocarcinoma (CESC); (**D**) thyroid carcinoma (THCA); (**E**) adrenocortical carcinoma (ACC); (**F**) pancreatic adenocarcinoma (PAAD).

We further compared the expression of CLDN-1 between tumor and normal tissues for ACC, CESC, PAAD, READ, THCA and BRCA from TCGA datasets. We found that most of the cancers showed significant expression differences of CLDN-1 between tumor and normal type. We observed

that for most of the cancers, tumor tissues have higher expression than normal tissues but for cancer like ACC, CLDN-1 expression in normal tissue was found to be greater than tumor tissues (Figure 5). We did not find any significant difference in CLDN-1 expression between tumor and normal tissue of BRCA.

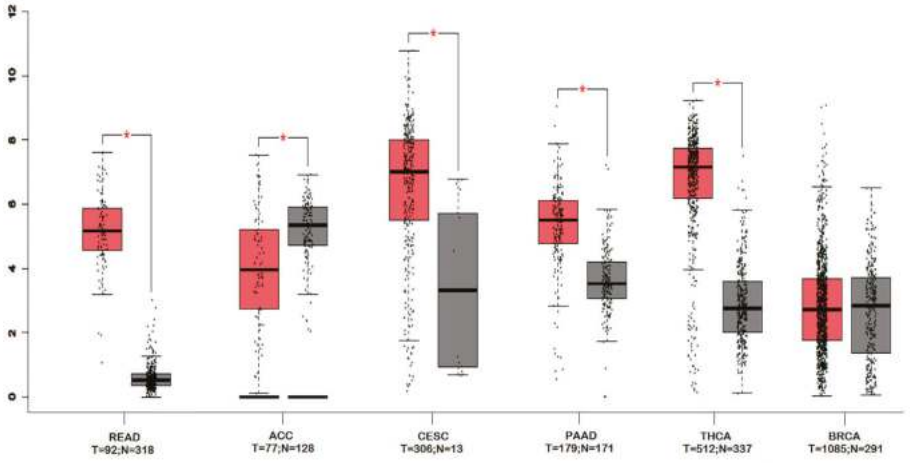

Figure 5. Boxplot showing the distribution of CLDN-1 expression in tumors and normal tissues for different types of cancers. Significant differences are shown with an asterisk (*). Boxplots were generated using GEPIA1 webserver and p-value < 0.01 was considered as significant.

To determine the interaction of CLDN-1 with other genes, we performed gene interaction analysis using the Gene MANIA prediction server. We found that CLDN-1 significantly interacted with several key genes that play an important role in normal cell physiology. Any disturbance in CLDN-1 expression or its partners may result in the manifestation of various diseases including cancers. The interaction of CLDN-1 with other key molecules can be individually analyzed in different cancers. This may highlight the key pathways which can be therapeutically targeted to suppress cancer growth or metastasis (Figure 6).

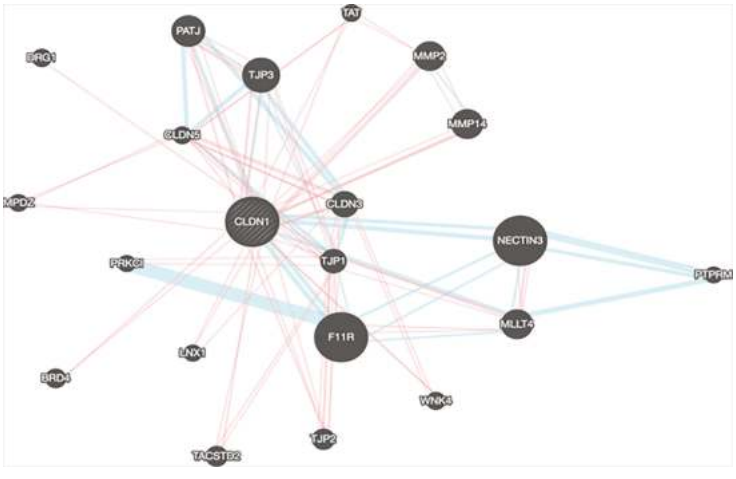

Figure 6. CLDN-1 interaction network using the Gene MANIA prediction server.

5. Claudin-1 as a Drug Target

The involvement of CLDN-1 in various pathological conditions has provided new perceptions into drug development targeting CLDN-1. The approach of targeting CLDN-1 either by monoclonal antibodies or chimeric antibodies has great potential but needs more research to reach the level of clinical trials. The initial studies have laid an important foundation towards the new strategies that could be employed and further modified towards the potential usefulness of CLDN-1 as a therapeutic target. The localization of CLDN-1 as a transmembrane protein makes it a perfect target for the enhanced drug absorption for preventing infection and treating cancer. One of the studies observed that the human hepatocytes treated with mouse anti-CLDN-1 monoclonal antibodies (mAbs), showed improved drug absorption and prevented hepatitis C virus (HCV) infection [143]. A human-mouse chimeric CLDN-1 mAb (clone 3A2) demonstrated cellular cytotoxicity against CLDN-1 expressing cancer cells [144]. The other aspect of claudins that is being exploited for therapeutic targeting is their role in regulating paracellular permeability in different tissues. *Clostridium perfringens* enterotoxin (cCPE) binds with claudin through its claudin binding domain and inhibits the claudin function. It was observed that blocking CLDN-1 with cCPE variants in the Huh7.5 hepatoma cell line inhibited infection of Huh7.5 cells with HCV in a dose-dependent manner and this also opened the epidermal barrier in the reconstructed human epidermis [145]. To eliminate the possible limitation facing CLDN-1 targeted therapies due to genotype-dependent escape via CLDN-6 and CLDN-9 and to improve anti-HCV activity, humanized anti- CLDN-1 monoclonal antibody (mAb) could be an alternative. One study developed functional mAB against extracellular domains of CLDN-1 and found that these antibodies have a very high affinity for intact CLDN-1, efficiently inhibited HCV infections both in vitro and in vivo, further demonstrating that anti-CLDN1 mAbs could be useful in inhibiting HCV infections [146]. In a very recent study, CLDN-1 was successfully targeted with anti-CLDN1 near-infrared fluorophore to track the colorectal cancer cells, and it may provide a novel way for fluorescence-guided surgery of tumor [147].

The main concern with claudin-targeted therapies is the presence of claudins in both normal epithelial cells and cancer cells that makes the targeting difficult. However, it has been observed that claudins are localized at the tight junctions in normal tissues, while in malignant tissues, there is a dysregulation of claudins localization from the tight junctions to the cell surface [24,148]. Claudins with aberrant localization in malignant tumors can be recognized by utilizing the C-terminal claudin-binding domain of cCPE fused with protein synthesis inhibitory factor (C-CPE-PSIF), causing less cytotoxicity to normal cells and a study has shown how CLDN-4 can be used as a target for tumor therapy by fusion of cCPE with PSIF. The results of the study showed that C-CPE-PSIF was cytotoxic to cells with undeveloped tight junctions (preconfluent cultures of Caco-2) and was not cytotoxic to cells with developed tight junctions (postconfluent cultures of Caco-2) [149]. Several other studies have used CLDN-4 as a target for tumor therapy and showed the accumulation of anti-CLDN-4 mAbs specifically in the tumors and reduced the growth of human colorectal and gastric tumors in mice [150]. One study detected CLDN-4 upregulation non-invasively in mice pancreatic ductal adenocarcinoma xenografts by using MRI and ^{18}FDG-PET [151] (for detailed reviews see [152]). In the future, a similar approach can be applied to CLDN-1 by preparation of CLDN-1 targeting molecule and can be tested for cytotoxicity to normal cells.

6. Claudins and Autosomal Recessive Disorders

As explained in the previous sections, the claudin family of proteins is an integral part of tight junctions that determine paracellular selectivity and permeability to small ions by acting as pores or barriers in polarized epithelia. We also discussed how overexpression or reduction of claudins could both promote and limit cancer progression, revealing complex dichotomous roles for claudins depending on cellular context. Besides the fact that the abnormal or deregulated expression of claudins has been associated with different human diseases like cancer, there are also other human disorders such as autosomal recessive disorders that have been reported due to clearly defined mutations in the

corresponding claudin genes. Such disorders are mostly observed in skin, liver, kidney, the inner ear, and the eye. The first evidence that showed a mutation in the claudin family of tight junction proteins causes human disorders were from the group of Lifton [153]. In their study, they reported that the mutations in the human gene, paracellin-1 (PCLN-1)/CLDN-16 causes an autosomal recessive disorder called Familial hypomagnesemia with hypercalcinuria and nephrocalcinosis (FHHNC) characterized with renal Mg^{2+} and Ca^{+} wasting. Later the same group revealed additional evidence that loss of function mutations in paracellin-1 PCLN-1/CLDN-16, are causative of FHHNC [154]. PCLN-1 is related to the claudin family of tight junction proteins and is in tight junctions of the thick ascending limb of Henle (TAL). CLDN-16 is a cattle ortholog of PCLN-1 with ~ 90% sequence homology, and PCLN-1/CLDN16 mutations have been shown to be strongly associated with bovine chronic interstitial nephritis with diffuse zonal fibrosis (CINF) [155]. Although both renal disorders FHHN and CINF are caused by PCLN-1/CLDN16 mutations, but the clinical features of both diseases are quite different which may be due to specific mutations/deletions in the same gene or through species specificity. Since the first report [153], several other tight junction disorders have been shown to cause human diseases including mutations in claudin proteins such as CLDN-1 [156], CLDN-9 [157], CLDN-10 [158], CLDN-14 [159], CLDN-16 [160], CLDN-19 [161] (for detailed reviews see [162]).

7. Conclusions

It is clear from the literature that among all the tight junction proteins, the claudin family of proteins is particularly important in regulating normal cell physiology. Among the claudin family, CLDN-1 is the most extensively studied protein and has been shown to be involved directly or indirectly in the development and progression of cancer, and also has a suppressive role in some cancers. CLDN-1 acts alone or in combination with other molecules to exert its tumor promoting or suppressing effect. Likewise, the shuttling of CLDN-1 between the cell membrane, cytoplasm and nucleus is a deciding factor in the development and progression of cancers. Another important aspect is the involvement of CLDN-1 in many signaling pathways, especially in Wnt and Notch signaling. The association of CLDN-1 with patient survival or recurrence in many cancers suggests its importance as a prognostic marker and as a potential therapeutic target. Also, pathway interaction analysis revealed CLDN-1 interacting partners, which can be further explored as potential drug targets. Based on the complexity of the topic, there is no one statement we can make for CLDN-1 role in cancer or barrier function since it is more intricate (Claudins are upregulated or downregulated in cancer and may or may not play a role in barrier function). In other words, universal statements concerning CLDN-1 and cancer or CLDN-1 and barrier function are dangerous oversimplifications.

Author Contributions: Writing—original draft preparation, A.A.B., L.T., S.N., S.U., M.H.; writing—review and editing, S.H., M.A.M., P.D., W.E.-R., M.P.F., N.S., R.K.; visualization, S.M., H.A.-N., A.A.; supervision, A.A.B., M.H., W.E.-R., S.U., P.B., R.R.; project administration, A.A.B., N.S., S.K.Y., M.H., S.U.; funding acquisition, A.A.B., M.H. All authors have read and agreed to the published version of the manuscript.

Funding: This research was funded by Sidra Medicine to Mohammad Haris (50610110002) and Ajaz A. Bhat (5011041002). Muzafar A. Macha is a recipient of Ramanujan Fellowship from Science and Engineering Research Board (SERB), Department of Science and Technology, Govt. of India, New Delhi.

Acknowledgments: The authors would like to express their gratitude to Vineeta Tanwar (Research Scientist, Ohio State University, Ohio, Columbus, USA) for help in English editing and valuable suggestions to improve the quality of the manuscript. The publication of this article was funded by the Qatar National Library.

Conflicts of Interest: The authors declare no conflict of interest.

Abbreviations

CLDN-1	Claudin-1 protein
CLDN-1	Claudin-1 gene
EMT	Epithelial-mesenchymal transition
CSCs	Cancer stem cells
HER2	Human epidermal growth factor receptor 2
BLBC	Basal-like breast cancer
ER	Estrogen receptor
ESCRT	Endosomal sorting complexes required for transport
EpCAM	Epithelial cell adhesion molecule
PTC	Papillary thyroid cancer
FTC	Follicular thyroid cancer
CRC	Colorectal cancer
mCRC	Metastatic colorectal cancer
UC	Ulcerative colitis
APC	Adenomatous polyposis coli
HNSCC	Head and neck squamous cell carcinoma
HSCC	Hypopharyngeal squamous cell carcinoma
HCC	Hepatocellular carcinoma
CTGF	Connective tissue growth factor
THBS1	Thrombospondin 1
DLC1	Deleted in liver cancer 1
OCLN	Occludin
ZO-1	Zona occludins 1
SPP1	Secreted phosphoprotein 1
CUTL1	Cut-like homeobox 1
TGF-α	Transforming growth factor-alpha
SLC2A3	Solute carrier family 2 (facilitated glucose transporter) member 3
PGF	Placental growth factor
EGFR	Epidermal growth factor
PC	Pancreatic cancer
MEK2	Mitogen activated protein kinase 2
miR-155	microRNA-155
BOT	Borderline tumors of the ovary
OSCC	Oral squamous cell carcinoma
MMP	Matrix metalloproteinase
BRCA	Breast invasive carcinoma
READ	Rectum adenocarcinoma
CESC	Cervical squamous cell carcinoma
THCA	Thyroid carcinoma
ACC	Adrenocortical carcinoma
PAAD	Pancreatic adenocarcinoma
mAbs	Monoclonal antibodies
cCPE	*Clostridium perfringens enterotoxin*
HCV	Hepatitis C virus
TCGA	The cancer genome atlas

References

1. Tsukita, S.; Yamazaki, Y.; Katsuno, T.; Tamura, A.; Tsukita, S. Tight junction-based epithelial microenvironment and cell proliferation. *Oncogene* **2008**, *27*, 6930–6938. [CrossRef]
2. Itoh, M.; Bissell, M.J. The organization of tight junctions in epithelia: Implications for mammary gland biology and breast tumorigenesis. *J. Mammary Gland Biol. Neoplasia* **2003**, *8*, 449–462. [CrossRef] [PubMed]

3. Tsukita, S.; Furuse, M.; Itoh, M. Multifunctional strands in tight junctions. *Nat. Rev. Mol. Cell Biol.* **2001**, *2*, 285–293. [CrossRef] [PubMed]
4. Krause, G.; Winkler, L.; Mueller, S.L.; Haseloff, R.F.; Piontek, J.; Blasig, I.E. Structure and function of claudins. *Biochim. Biophys. Acta* **2008**, *1778*, 631–645. [CrossRef] [PubMed]
5. Tsukita, S.; Furuse, M. Claudin-based barrier in simple and stratified cellular sheets. *Curr. Opin. Cell Biol.* **2002**, *14*, 531–536. [CrossRef]
6. Anderson, J.M.; Van Itallie, C.M. Physiology and function of the tight junction. *Cold Spring Harb. Perspect. Biol.* **2009**, *1*, a002584. [CrossRef]
7. Kirschner, N.; Rosenthal, R.; Furuse, M.; Moll, I.; Fromm, M.; Brandner, J.M. Contribution of tight junction proteins to ion, macromolecule, and water barrier in keratinocytes. *J. Investig. Derm.* **2013**, *133*, 1161–1169. [CrossRef]
8. Soler, A.P.; Miller, R.D.; Laughlin, K.V.; Carp, N.Z.; Klurfeld, D.M.; Mullin, J.M. Increased tight junctional permeability is associated with the development of colon cancer. *Carcinogenesis* **1999**, *20*, 1425–1431. [CrossRef]
9. Singh, A.B.; Sharma, A.; Dhawan, P. Claudin family of proteins and cancer: An overview. *J. Oncol.* **2010**, *2010*, 541957. [CrossRef]
10. Kwon, M.J. Emerging roles of claudins in human cancer. *Int. J. Mol. Sci.* **2013**, *14*, 18148–18180. [CrossRef]
11. Saraydaroglu, O.; Narter, S.; Ozsen, M.; Coskun, H. Non-epithelial tumors of the larynx: Case series of 12 years. *Eur. Arch. Oto-Rhino-Laryngol.* **2019**, *276*, 2843–2847. [CrossRef] [PubMed]
12. Reinert, S. Principles of Management of Neoplastic Salivary Gland Disease. *Maxillofacial Surgery*, 3rd ed. 2017, pp. 657–667. Available online: https://www.sciencedirect.com/book/9780702060564/maxillofacial-surgery (accessed on 13 January 2020).
13. Amasheh, S.; Milatz, S.; Krug, S.M.; Markov, A.G.; Gunzel, D.; Amasheh, M.; Fromm, M. Tight junction proteins as channel formers and barrier builders. *Ann. N. Y. Acad. Sci.* **2009**, *1165*, 211–219. [CrossRef] [PubMed]
14. Ikari, A.; Ito, M.; Okude, C.; Sawada, H.; Harada, H.; Degawa, M.; Sakai, H.; Takahashi, T.; Sugatani, J.; Miwa, M. Claudin-16 is directly phosphorylated by protein kinase a independently of a vasodilator-stimulated phosphoprotein-mediated pathway. *J. Cell Physiol.* **2008**, *214*, 221–229. [CrossRef] [PubMed]
15. Fujibe, M.; Chiba, H.; Kojima, T.; Soma, T.; Wada, T.; Yamashita, T.; Sawada, N. Thr203 of claudin-1, a putative phosphorylation site for map kinase, is required to promote the barrier function of tight junctions. *Exp. Cell Res.* **2004**, *295*, 36–47. [CrossRef] [PubMed]
16. Akizuki, R.; Shimobaba, S.; Matsunaga, T.; Endo, S.; Ikari, A. Claudin-5, -7, and -18 suppress proliferation mediated by inhibition of phosphorylation of akt in human lung squamous cell carcinoma. *Biochim. Biophys Acta* **2017**, *1864*, 293–302. [CrossRef] [PubMed]
17. Findley, M.K.; Koval, M. Regulation and roles for claudin-family tight junction proteins. *Iubmb. Life* **2009**, *61*, 431–437. [CrossRef]
18. Lal-Nag, M.; Morin, P.J. The claudins. *Genome Biol.* **2009**, *10*, 235. [CrossRef]
19. Hewitt, K.J.; Agarwal, R.; Morin, P.J. The claudin gene family: Expression in normal and neoplastic tissues. *BMC Cancer* **2006**, *6*, 186. [CrossRef]
20. Pope, J.L.; Bhat, A.A.; Sharma, A.; Ahmad, R.; Krishnan, M.; Washington, M.K.; Beauchamp, R.D.; Singh, A.B.; Dhawan, P. Claudin-1 regulates intestinal epithelial homeostasis through the modulation of notch-signalling. *Gut* **2014**, *63*, 622–634. [CrossRef]
21. Singh, A.B.; Uppada, S.B.; Dhawan, P. Claudin proteins, outside-in signaling, and carcinogenesis. *Pflug. Arch.* **2017**, *469*, 69–75. [CrossRef]
22. Turksen, K. Claudins and cancer stem cells. *Stem Cell Rev.* **2011**, *7*, 797–798. [CrossRef] [PubMed]
23. Zhou, B.; Flodby, P.; Luo, J.; Castillo, D.R.; Liu, Y.; Yu, F.X.; McConnell, A.; Varghese, B.; Li, G.; Chimge, N.O.; et al. Claudin-18-mediated yap activity regulates lung stem and progenitor cell homeostasis and tumorigenesis. *J. Clin. Investig.* **2018**, *128*, 970–984. [CrossRef] [PubMed]
24. Morin, P.J. Claudin proteins in human cancer: Promising new targets for diagnosis and therapy. *Cancer Res.* **2005**, *65*, 9603–9606. [CrossRef] [PubMed]
25. Zhou, B.; Moodie, A.; Blanchard, A.A.; Leygue, E.; Myal, Y. Claudin 1 in breast cancer: New insights. *J. Clin. Med.* **2015**, *4*, 1960–1976. [CrossRef]

26. Usami, Y.; Chiba, H.; Nakayama, F.; Ueda, J.; Matsuda, Y.; Sawada, N.; Komori, T.; Ito, A.; Yokozaki, H. Reduced expression of claudin-7 correlates with invasion and metastasis in squamous cell carcinoma of the esophagus. *Hum. Pathol.* **2006**, *37*, 569–577. [CrossRef]
27. Miyamoto, K.; Kusumi, T.; Sato, F.; Kawasaki, H.; Shibata, S.; Ohashi, M.; Hakamada, K.; Sasaki, M.; Kijima, H. Decreased expression of claudin-1 is correlated with recurrence status in esophageal squamous cell carcinoma. *Biomed. Res.* **2008**, *29*, 71–76. [CrossRef]
28. Honda, H.; Pazin, M.J.; Ji, H.; Wernyj, R.P.; Morin, P.J. Crucial roles of sp1 and epigenetic modifications in the regulation of the cldn4 promoter in ovarian cancer cells. *J. Biol. Chem.* **2006**, *281*, 21433–21444. [CrossRef]
29. Honda, H.; Pazin, M.J.; D'Souza, T.; Ji, H.; Morin, P.J. Regulation of the cldn3 gene in ovarian cancer cells. *Cancer Biol.* **2007**, *6*, 1733–1742. [CrossRef]
30. Sheehan, G.M.; Kallakury, B.V.; Sheehan, C.E.; Fisher, H.A.; Kaufman, R.P., Jr.; Ross, J.S. Loss of claudins-1 and -7 and expression of claudins-3 and -4 correlate with prognostic variables in prostatic adenocarcinomas. *Hum. Pathol.* **2007**, *38*, 564–569. [CrossRef]
31. Resnick, M.B.; Konkin, T.; Routhier, J.; Sabo, E.; Pricolo, V.E. Claudin-1 is a strong prognostic indicator in stage ii colonic cancer: A tissue microarray study. *Mod. Pathol.* **2005**, *18*, 511–518. [CrossRef]
32. Furuse, M.; Hata, M.; Furuse, K.; Yoshida, Y.; Haratake, A.; Sugitani, Y.; Noda, T.; Kubo, A.; Tsukita, S. Claudin-based tight junctions are crucial for the mammalian epidermal barrier: A lesson from claudin-1-deficient mice. *J. Cell Biol.* **2002**, *156*, 1099–1111. [CrossRef] [PubMed]
33. Morita, K.; Furuse, M.; Fujimoto, K.; Tsukita, S. Claudin multigene family encoding four-transmembrane domain protein components of tight junction strands. *Proc. Natl Acad Sci USA* **1999**, *96*, 511–516. [CrossRef] [PubMed]
34. Dhawan, P.; Singh, A.B.; Deane, N.G.; No, Y.; Shiou, S.R.; Schmidt, C.; Neff, J.; Washington, M.K.; Beauchamp, R.D. Claudin-1 regulates cellular transformation and metastatic behavior in colon cancer. *J. Clin. Investig.* **2005**, *115*, 1765–1776. [CrossRef]
35. Oku, N.; Sasabe, E.; Ueta, E.; Yamamoto, T.; Osaki, T. Tight junction protein claudin-1 enhances the invasive activity of oral squamous cell carcinoma cells by promoting cleavage of laminin-5 gamma2 chain via matrix metalloproteinase (mmp)-2 and membrane-type mmp-1. *Cancer Res.* **2006**, *66*, 5251–5257. [CrossRef]
36. Tokes, A.M.; Kulka, J.; Paku, S.; Szik, A.; Paska, C.; Novak, P.K.; Szilak, L.; Kiss, A.; Bogi, K.; Schaff, Z. Claudin-1, -3 and -4 proteins and mrna expression in benign and malignant breast lesions: A research study. *Breast Cancer Res.* **2005**, *7*, R296–R305. [CrossRef] [PubMed]
37. Cohn, M.L.; Goncharuk, V.N.; Diwan, A.H.; Zhang, P.S.; Shen, S.S.; Prieto, V.G. Loss of claudin-1 expression in tumor-associated vessels correlates with acquisition of metastatic phenotype in melanocytic neoplasms. *J. Cutan. Pathol.* **2005**, *32*, 533–536. [CrossRef]
38. Leotlela, P.D.; Wade, M.S.; Duray, P.H.; Rhode, M.J.; Brown, H.F.; Rosenthal, D.T.; Dissanayake, S.K.; Earley, R.; Indig, F.E.; Nickoloff, B.J.; et al. Claudin-1 overexpression in melanoma is regulated by pkc and contributes to melanoma cell motility. *Oncogene* **2007**, *26*, 3846–3856. [CrossRef]
39. Morohashi, S.; Kusumi, T.; Sato, F.; Odagiri, H.; Chiba, H.; Yoshihara, S.; Hakamada, K.; Sasaki, M.; Kijima, H. Decreased expression of claudin-1 correlates with recurrence status in breast cancer. *Int. J. Mol. Med.* **2007**, *20*, 139–143. [CrossRef]
40. Blanchard, A.A.; Skliris, G.P.; Watson, P.H.; Murphy, L.C.; Penner, C.; Tomes, L.; Young, T.L.; Leygue, E.; Myal, Y. Claudins 1, 3, and 4 protein expression in er negative breast cancer correlates with markers of the basal phenotype. *Virchows Arch.* **2009**, *454*, 647–656. [CrossRef]
41. Lu, S.; Singh, K.; Mangray, S.; Tavares, R.; Noble, L.; Resnick, M.B.; Yakirevich, E. Claudin expression in high-grade invasive ductal carcinoma of the breast: Correlation with the molecular subtype. *Mod. Pathol.* **2013**, *26*, 485–495. [CrossRef]
42. Nemeth, J.; Nemeth, Z.; Tatrai, P.; Peter, I.; Somoracz, A.; Szasz, A.M.; Kiss, A.; Schaff, Z. High expression of claudin-1 protein in papillary thyroid tumor and its regional lymph node metastasis. *Pathol. Oncol. Res.* **2010**, *16*, 19–27. [CrossRef] [PubMed]
43. Zwanziger, D.; Badziong, J.; Ting, S.; Moeller, L.; Schmid, K.; Siebolts, U.; Wickenhauser, C.; Dralle, H.; Fuhrer, D. The impact of claudin-1 on follicular thyroid carcinoma aggressiveness. *Endocr. Relat. Cancer* **2015**, *22*, 819–830. [CrossRef] [PubMed]

44. Kinugasa, T.; Akagi, Y.; Yoshida, T.; Ryu, Y.; Shiratuchi, I.; Ishibashi, N.; Shirouzu, K. Increased claudin-1 protein expression contributes to tumorigenesis in ulcerative colitis-associated colorectal cancer. *Anticancer Res.* **2010**, *30*, 3181–3186. [PubMed]
45. Wu, Y.-L.; Zhang, S.; Wang, G.-R.; Chen, Y.-P. Expression transformation of claudin-1 in the process of gastric adenocarcinoma invasion. *World J. Gastroenterol.* **2008**, *14*, 4943–4948. [CrossRef]
46. Nelhubel, G.A.; Karoly, B.; Szabo, B.; Lotz, G.; Kiss, A.; Tovari, J.; Kenessey, I. The prognostic role of claudins in head and neck squamous cell carcinomas. *Pathol. Oncol. Res.* **2014**, *20*, 99–106. [CrossRef]
47. Li, W.J.; Zhang, Z.L.; Yu, X.M.; Cai, X.L.; Pan, X.L.; Yang, X.Y. Expression of claudin-1 and its relationship with lymphatic microvessel generation in hypopharyngeal squamous cell carcinoma. *Genet. Mol. Res.* **2015**, *14*, 11814–11826. [CrossRef]
48. Holczbauer, A.; Gyongyosi, B.; Lotz, G.; Szijarto, A.; Kupcsulik, P.; Schaff, Z.; Kiss, A. Distinct claudin expression profiles of hepatocellular carcinoma and metastatic colorectal and pancreatic carcinomas. *J. Histochem. Cytochem.* **2013**, *61*, 294–305. [CrossRef]
49. Higashi, Y.; Suzuki, S.; Sakaguchi, T.; Nakamura, T.; Baba, S.; Reinecker, H.C.; Nakamura, S.; Konno, H. Loss of claudin-1 expression correlates with malignancy of hepatocellular carcinoma. *J. Surg. Res.* **2007**, *139*, 68–76. [CrossRef]
50. Paschoud, S.; Bongiovanni, M.; Pache, J.-C.; Citi, S. Claudin-1 and claudin-5 expression patterns differentiate lung squamous cell carcinomas from adenocarcinomas. *Mod. Pathol.* **2007**, *20*, 947–954. [CrossRef]
51. Tsukahara, M.; Nagai, H.; Kamiakito, T.; Kawata, H.; Takayashiki, N.; Saito, K.; Tanaka, A. Distinct expression patterns of claudin-1 and claudin-4 in intraductal papillary–mucinous tumors of the pancreas. *Pathol. Int.* **2005**, *55*, 63–69. [CrossRef]
52. English, D.P.; Santin, A.D. Claudins overexpression in ovarian cancer: Potential targets for clostridium perfringens enterotoxin (cpe) based diagnosis and therapy. *Int. J. Mol. Sci.* **2013**, *14*, 10412–10437. [CrossRef] [PubMed]
53. El-Balat, A.; Schmeil, I.; Gasimli, K.; Sänger, N.; Karn, T.; Ahr, A.; Becker, S.; Arsenic, R.; Holtrich, U.; Engels, K. Claudin-1 is linked to presence of implants and micropapillary pattern in serous borderline epithelial tumours of the ovary. *J. Clin. Pathol.* **2018**, *71*, 1060. [CrossRef]
54. Seo, K.W.; Kwon, Y.K.; Kim, B.H.; Kim, C.I.; Chang, H.S.; Choe, M.S.; Park, C.H. Correlation between claudins expression and prognostic factors in prostate cancer. *Korean J. Urol.* **2010**, *51*, 239–244. [CrossRef] [PubMed]
55. Väre, P.; Loikkanen, I.; Hirvikoski, P.; Vaarala, M.; Soini, Y. Low claudin expression is associated with high gleason grade in prostate adenocarcinoma. *Oncol. Rep.* **2008**, *19*, 25–31. [CrossRef] [PubMed]
56. French, A.D.; Fiori, J.L.; Camilli, T.C.; Leotlela, P.D.; O'Connell, M.P.; Frank, B.P.; Subaran, S.; Indig, F.E.; Taub, D.D.; Weeraratna, A.T. Pkc and pka phosphorylation affect the subcellular localization of claudin-1 in melanoma cells. *Int. J. Med. Sci.* **2009**, *6*, 93–101. [CrossRef] [PubMed]
57. Chao, Y.-C.; Pan, S.-H.; Yang, S.-C.; Yu, S.-L.; Che, T.-F.; Lin, C.-W.; Tsai, M.-S.; Chang, G.-C.; Wu, C.-H.; Wu, Y.-Y.; et al. Claudin-1 is a metastasis suppressor and correlates with clinical outcome in lung adenocarcinoma. *Am. J. Respir. Crit. Care Med.* **2009**, *179*, 123–133. [CrossRef] [PubMed]
58. Kleinberg, L.; Holth, A.; Trope, C.G.; Reich, R.; Davidson, B. Claudin upregulation in ovarian carcinoma effusions is associated with poor survival. *Hum. Pathol.* **2008**, *39*, 747–757. [CrossRef] [PubMed]
59. Singh, A.B.; Sharma, A.; Smith, J.J.; Krishnan, M.; Chen, X.; Eschrich, S.; Washington, M.K.; Yeatman, T.J.; Beauchamp, R.D.; Dhawan, P. Claudin-1 up-regulates the repressor zeb-1 to inhibit e-cadherin expression in colon cancer cells. *Gastroenterology* **2011**, *141*, 2140–2153. [CrossRef]
60. Eftang, L.L.; Esbensen, Y.; Tannaes, T.M.; Blom, G.P.; Bukholm, I.R.; Bukholm, G. Up-regulation of cldn1 in gastric cancer is correlated with reduced survival. *BMC Cancer* **2013**, *13*, 586. [CrossRef]
61. Li, W.; Dong, Q.; Li, L.; Zhang, Z.; Cai, X.; Pan, X. Prognostic significance of claudin-1 and cyclin b1 protein expression in patients with hypopharyngeal squamous cell carcinoma. *Oncol. Lett.* **2016**, *11*, 2995–3002. [CrossRef]
62. Suh, Y.; Yoon, C.H.; Kim, R.K.; Lim, E.J.; Oh, Y.S.; Hwang, S.G.; An, S.; Yoon, G.; Gye, M.C.; Yi, J.M.; et al. Claudin-1 induces epithelial–mesenchymal transition through activation of the c-abl-erk signaling pathway in human liver cells. *Oncogene* **2013**, *32*, 4873–4882. [CrossRef] [PubMed]
63. Stebbing, J.; Filipovic, A.; Giamas, G. Claudin-1 as a promoter of emt in hepatocellular carcinoma. *Oncogene* **2013**, *32*, 4871–4872. [CrossRef] [PubMed]

64. Kondo, J.; Sato, F.; Kusumi, T.; Liu, Y.; Motonari, O.; Sato, T.; Kijima, H. Claudin-1 expression is induced by tumor necrosis factor-alpha in human pancreatic cancer cells. *Int. J. Mol. Med.* **2008**, *22*, 645–649. [PubMed]
65. Cronin, K.A.; Lake, A.J.; Scott, S.; Sherman, R.L.; Noone, A.M.; Howlader, N.; Henley, S.J.; Anderson, R.N.; Firth, A.U.; Ma, J.; et al. Annual report to the nation on the status of cancer, part i: National cancer statistics. *Cancer* **2018**, *124*, 2785–2800. [CrossRef] [PubMed]
66. Sinn, H.P.; Kreipe, H. A brief overview of the who classification of breast tumors, 4th edition, focusing on issues and updates from the 3rd edition. *Breast Care (Basel)* **2013**, *8*, 149–154. [CrossRef]
67. Dai, X.; Li, T.; Bai, Z.; Yang, Y.; Liu, X.; Zhan, J.; Shi, B. Breast cancer intrinsic subtype classification, clinical use and future trends. *Am. J. Cancer Res.* **2015**, *5*, 2929–2943.
68. Yeo, S.K.; Guan, J.L. Breast cancer: Multiple subtypes within a tumor? *Trends Cancer* **2017**, *3*, 753–760. [CrossRef]
69. Dai, X.; Xiang, L.; Li, T.; Bai, Z. Cancer hallmarks, biomarkers and breast cancer molecular subtypes. *J. Cancer* **2016**, *7*, 1281–1294. [CrossRef]
70. Blanchard, A.; Shiu, R.; Booth, S.; Sorensen, G.; DeCorby, N.; Nistor, A.; Wong, P.; Leygue, E.; Myal, Y. Gene expression profiling of early involuting mammary gland reveals novel genes potentially relevant to human breast cancer. *Front. Biosci.* **2007**, *12*, 2221–2232. [CrossRef]
71. Ricardo, S.; Gerhard, R.; Cameselle-Teijeiro, J.F.; Schmitt, F.; Paredes, J. Claudin expression in breast cancer: High or low, what to expect? *Histol. Histopathol.* **2012**, *27*, 1283–1295.
72. Blanchard, A.A.; Zelinski, T.; Xie, J.; Cooper, S.; Penner, C.; Leygue, E.; Myal, Y. Identification of claudin 1 transcript variants in human invasive breast cancer. *PLoS ONE* **2016**, *11*, e0163387. [CrossRef] [PubMed]
73. Swisshelm, K.; Machl, A.; Planitzer, S.; Robertson, R.; Kubbies, M.; Hosier, S. Semp1, a senescence-associated cdna isolated from human mammary epithelial cells, is a member of an epithelial membrane protein superfamily. *Gene* **1999**, *226*, 285–295. [CrossRef]
74. Kramer, F.; White, K.; Kubbies, M.; Swisshelm, K.; Weber, B.H. Genomic organization of claudin-1 and its assessment in hereditary and sporadic breast cancer. *Hum. Genet.* **2000**, *107*, 249–256. [CrossRef] [PubMed]
75. Hoevel, T.; Macek, R.; Swisshelm, K.; Kubbies, M. Reexpression of the tj protein cldn1 induces apoptosis in breast tumor spheroids. *Int. J. Cancer* **2004**, *108*, 374–383. [CrossRef]
76. Zhou, B.; Blanchard, A.; Wang, N.; Ma, X.; Han, J.; Schroedter, I.; Leygue, E.; Myal, Y. Claudin 1 promotes migration and increases sensitivity to tamoxifen and anticancer drugs in luminal-like human breast cancer cells mcf7. *Cancer Investig.* **2015**, 429–439. [CrossRef]
77. Martinez-Estrada, O.M.; Culleres, A.; Soriano, F.X.; Peinado, H.; Bolos, V.; Martinez, F.O.; Reina, M.; Cano, A.; Fabre, M.; Vilaro, S. The transcription factors slug and snail act as repressors of claudin-1 expression in epithelial cells. *Biochem. J.* **2006**, *394*, 449–457. [CrossRef]
78. Myal, Y.; Leygue, E.; Blanchard, A.A. Claudin 1 in breast tumorigenesis: Revelation of a possible novel "claudin high" subset of breast cancers. *J. Biomed. Biotechnol.* **2010**, *2010*, 956897. [CrossRef]
79. Akasaka, H.; Sato, F.; Morohashi, S.; Wu, Y.; Liu, Y.; Kondo, J.; Odagiri, H.; Hakamada, K.; Kijima, H. Anti-apoptotic effect of claudin-1 in tamoxifen-treated human breast cancer mcf-7 cells. *BMC Cancer* **2010**, *10*, 548. [CrossRef]
80. Tanaka, M.; Kamata, R.; Sakai, R. Phosphorylation of ephrin-b1 via the interaction with claudin following cell-cell contact formation. *Embo J.* **2005**, *24*, 3700–3711. [CrossRef]
81. Schmidt, O.; Teis, D. The escrt machinery. *Curr. Biol.* **2012**, *22*, R116–R120. [CrossRef]
82. Kovalenko, O.V.; Yang, X.H.; Hemler, M.E. A novel cysteine cross-linking method reveals a direct association between claudin-1 and tetraspanin cd9. *Mol. Cell Proteom.* **2007**, *6*, 1855–1867. [CrossRef] [PubMed]
83. Wu, C.J.; Mannan, P.; Lu, M.; Udey, M.C. Epithelial cell adhesion molecule (epcam) regulates claudin dynamics and tight junctions. *J. Biol. Chem.* **2013**, *288*, 12253–12268. [CrossRef] [PubMed]
84. Kondo, T.; Ezzat, S.; Asa, S.L. Pathogenetic mechanisms in thyroid follicular-cell neoplasia. *Nat. Rev. Cancer* **2006**, *6*, 292–306. [CrossRef] [PubMed]
85. Kitahara, C.M.; Sosa, J.A. The changing incidence of thyroid cancer. *Nat. Rev. Endocrinol.* **2016**, *12*, 646–653. [CrossRef]
86. Hucz, J.; Kowalska, M.; Jarzab, M.; Wiench, M. Gene expression of metalloproteinase 11, claudin 1 and selected adhesion related genes in papillary thyroid cancer. *Endokrynol. Pol.* **2006**, *57*, 18–25.
87. Fluge, O.; Bruland, O.; Akslen, L.A.; Lillehaug, J.R.; Varhaug, J.E. Gene expression in poorly differentiated papillary thyroid carcinomas. *Thyroid* **2006**, *16*, 161–175. [CrossRef]

88. Sobel, G.; Nemeth, J.; Kiss, A.; Lotz, G.; Szabo, I.; Udvarhelyi, N.; Schaff, Z.; Paska, C. Claudin 1 differentiates endometrioid and serous papillary endometrial adenocarcinoma. *Gynecol. Oncol.* **2006**, *103*, 591–598. [CrossRef]
89. Tzelepi, V.N.; Tsamandas, A.C.; Vlotinou, H.D.; Vagianos, C.E.; Scopa, C.D. Tight junctions in thyroid carcinogenesis: Diverse expression of claudin-1, claudin-4, claudin-7 and occludin in thyroid neoplasms. *Mod. Pathol.* **2008**, *21*, 22–30. [CrossRef]
90. Süren, D.; Yildirim, M.; Sayiner, A.; Alikanoğlu, A.S.; Atalay, I.; Gündüz, U.R.; Kaya, V.; Gündüz, Ş.; Oruç, M.T.; Sezer, C. Expression of claudin 1, 4 and 7 in thyroid neoplasms. *Oncol. Lett.* **2017**, *13*, 3722–3726. [CrossRef]
91. Abd El Atti, R.M.; Shash, L.S. Potential diagnostic utility of cd56 and claudin-1 in papillary thyroid carcinoma and solitary follicular thyroid nodules. *J. Egypt. Natl. Cancer Inst.* **2012**, *24*, 175–184. [CrossRef]
92. Arnold, M.; Sierra, M.S.; Laversanne, M.; Soerjomataram, I.; Jemal, A.; Bray, F. Global patterns and trends in colorectal cancer incidence and mortality. *Gut* **2017**, *66*, 683. [CrossRef] [PubMed]
93. Ouban, A. Claudin-1 role in colon cancer: An update and a review. *Histol. Histopathol.* **2018**, 11980.
94. Pope, J.L.; Ahmad, R.; Bhat, A.A.; Washington, M.K.; Singh, A.B.; Dhawan, P. Claudin-1 overexpression in intestinal epithelial cells enhances susceptibility to adenamatous polyposis coli-mediated colon tumorigenesis. *Mol. Cancer* **2014**, *13*, 167. [CrossRef] [PubMed]
95. Grone, J.; Weber, B.; Staub, E.; Heinze, M.; Klaman, I.; Pilarsky, C.; Hermann, K.; Castanos-Velez, E.; Ropcke, S.; Mann, B.; et al. Differential expression of genes encoding tight junction proteins in colorectal cancer: Frequent dysregulation of claudin-1, -8 and -12. *Int. J. Colorectal Dis.* **2007**, *22*, 651–659. [CrossRef] [PubMed]
96. Kinugasa, T.; Huo, Q.; Higashi, D.; Shibaguchi, H.; Kuroki, M.; Tanaka, T.; Futami, K.; Yamashita, Y.; Hachimine, K.; Maekawa, S.; et al. Selective up-regulation of claudin-1 and claudin-2 in colorectal cancer. *Anticancer Res.* **2007**, *27*, 3729–3734. [CrossRef]
97. de Oliveira, S.S.; de Oliveira, I.M.; De Souza, W.; Morgado-Diaz, J.A. Claudins upregulation in human colorectal cancer. *FEBS Lett.* **2005**, *579*, 6179–6185. [CrossRef]
98. Nakagawa, S.; Miyoshi, N.; Ishii, H.; Mimori, K.; Tanaka, F.; Sekimoto, M.; Doki, Y.; Mori, M. Expression of cldn1 in colorectal cancer: A novel marker for prognosis. *Int. J. Oncol.* **2011**, *39*, 791–796.
99. Huo, Q.; Kinugasa, T.; Wang, L.; Huang, J.; Zhao, J.; Shibaguchi, H.; Kuroki, M.; Tanaka, T.; Yamashita, Y.; Nabeshima, K.; et al. Claudin-1 protein is a major factor involved in the tumorigenesis of colorectal cancer. *Anticancer Res.* **2009**, *29*, 851–857.
100. Wang, K.; Xu, C.; Li, W.; Ding, L. Emerging clinical significance of claudin-7 in colorectal cancer: A review. *Cancer Manag. Res.* **2018**, *10*, 3741–3752. [CrossRef]
101. Caruso, M.; Fung, K.Y.; Moore, J.; Brierley, G.V.; Cosgrove, L.J.; Thomas, M.; Cheetham, G.; Brook, E.; Fraser, L.M.; Tin, T.; et al. Claudin-1 expression is elevated in colorectal cancer precursor lesions harboring the braf v600e mutation. *Transl. Oncol.* **2014**, *7*, 456–463. [CrossRef]
102. Schatoff, E.M.; Leach, B.I.; Dow, L.E. Wnt signaling and colorectal cancer. *Curr. Colorectal Cancer Rep.* **2017**, *13*, 101–110. [CrossRef] [PubMed]
103. Katoh, M. Multilayered prevention and treatment of chronic inflammation, organ fibrosis and cancer associated with canonical wnt/betacatenin signaling activation (review). *Int. J. Mol. Med.* **2018**, 713–725. [CrossRef]
104. Krishnamurthy, N.; Kurzrock, R. Targeting the wnt/beta-catenin pathway in cancer: Update on effectors and inhibitors. *Cancer Treat. Rev.* **2018**, *62*, 50–60. [CrossRef] [PubMed]
105. Miwa, N.; Furuse, M.; Tsukita, S.; Niikawa, N.; Nakamura, Y.; Furukawa, Y. Involvement of claudin-1 in the beta-catenin/tcf signaling pathway and its frequent upregulation in human colorectal cancers. *Oncol. Res.* **2001**, *12*, 469–476. [CrossRef]
106. Bhat, A.A.; Sharma, A.; Pope, J.; Krishnan, M.; Washington, M.K.; Singh, A.B.; Dhawan, P. Caudal homeobox protein cdx-2 cooperates with wnt pathway to regulate claudin-1 expression in colon cancer cells. *PLoS ONE* **2012**, *7*, e37174. [CrossRef]
107. Cherradi, S.; Ayrolles-Torro, A.; Vezzo-Vié, N.; Gueguinou, N.; Denis, V.; Combes, E.; Boissière, F.; Busson, M.; Canterel-Thouennon, L.; Mollevi, C.; et al. Antibody targeting of claudin-1 as a potential colorectal cancer therapy. *J. Exp. Clin. Cancer Res.* **2017**, *36*, 89. [CrossRef]
108. Jung, H.; Jun, K.H.; Jung, J.H.; Chin, H.M.; Park, W.B. The expression of claudin-1, claudin-2, claudin-3, and claudin-4 in gastric cancer tissue. *J. Surg. Res.* **2011**, *167*, e185–e191. [CrossRef]

109. Huang, J.; Li, J.; Qu, Y.; Zhang, J.; Zhang, L.; Chen, X.; Liu, B.; Zhu, Z. The expression of claudin 1 correlates with beta-catenin and is a prognostic factor of poor outcome in gastric cancer. *Int. J. Oncol.* **2014**, *44*, 1293–1301. [CrossRef]
110. Huang, J.; Zhang, L.; He, C.; Qu, Y.; Li, J.; Zhang, J.; Du, T.; Chen, X.; Yu, Y.; Liu, B.; et al. Claudin-1 enhances tumor proliferation and metastasis by regulating cell anoikis in gastric cancer. *Oncotarget* **2015**, *6*, 1652–1665. [CrossRef]
111. Tokuhara, Y.; Morinishi, T.; Matsunaga, T.; Ohsaki, H.; Kushida, Y.; Haba, R.; Hirakawa, E. Claudin-1, but not claudin-4, exhibits differential expression patterns between well- to moderately-differentiated and poorly-differentiated gastric adenocarcinoma. *Oncol. Lett.* **2015**, *10*, 93–98. [CrossRef]
112. Parkin, D.M.; Bray, F.; Ferlay, J.; Pisani, P. Global cancer statistics, 2002. *CA Cancer J. Clin.* **2005**, *55*, 74–108. [CrossRef] [PubMed]
113. Ouban, A.; Hamdan, H.; Hakam, A.; Ahmed, A.A. Claudin-1 expression in squamous cell carcinomas of different organs: Comparative study of cancerous tissues and normal controls. *Int. J. Surg. Pathol.* **2012**, *20*, 132–138. [CrossRef] [PubMed]
114. Ghouri, Y.A.; Mian, I.; Rowe, J.H. Review of hepatocellular carcinoma: Epidemiology, etiology, and carcinogenesis. *J. Carcinog.* **2017**, *16*, 1–18. [PubMed]
115. Yoon, C.-H.; Kim, M.-J.; Park, M.-J.; Park, I.-C.; Hwang, S.-G.; An, S.; Choi, Y.-H.; Yoon, G.; Lee, S.-J. Claudin-1 acts through c-abl-protein kinase cdelta (pkcdelta) signaling and has a causal role in the acquisition of invasive capacity in human liver cells. *J. Biol. Chem.* **2010**, *285*, 226–233. [CrossRef] [PubMed]
116. Chen, Y.-J.; You, M.-L.; Chong, Q.-Y.; Pandey, V.; Zhuang, Q.-S.; Liu, D.-X.; Ma, L.; Zhu, T.; Lobie, P.E. Autocrine human growth hormone promotes invasive and cancer stem cell-like behavior of hepatocellular carcinoma cells by stat3 dependent inhibition of claudin-1 expression. *Int. J. Mol. Sci.* **2017**, *18*, 1274. [CrossRef] [PubMed]
117. Jung, J.H.; Jung, C.K.; Choi, H.J.; Jun, K.H.; Yoo, J.; Kang, S.J.; Lee, K.Y. Diagnostic utility of expression of claudins in non-small cell lung cancer: Different expression profiles in squamous cell carcinomas and adenocarcinomas. *Pathol. Res. Pract.* **2009**, *205*, 409–416. [CrossRef]
118. Soini, Y. Claudins in lung diseases. *Respir. Res.* **2011**, *12*, 70. [CrossRef]
119. Sun, B.-S.; Yao, Y.-Q.; Pei, B.-X.; Zhang, Z.-F.; Wang, C.-L. Claudin-1 correlates with poor prognosis in lung adenocarcinoma. *Thorac. Cancer* **2016**, *7*, 556–563. [CrossRef]
120. Landskron, G.; De la Fuente, M.; Thuwajit, P.; Thuwajit, C.; Hermoso, M.A. Chronic inflammation and cytokines in the tumor microenvironment. *J. Immunol. Res.* **2014**, *2014*, 149185. [CrossRef]
121. Shiozaki, A.; Bai, X.H.; Shen-Tu, G.; Moodley, S.; Takeshita, H.; Fung, S.Y.; Wang, Y.; Keshavjee, S.; Liu, M. Claudin 1 mediates tnfalpha-induced gene expression and cell migration in human lung carcinoma cells. *PLoS ONE* **2012**, *7*, e38049. [CrossRef]
122. Bhat, A.A.; Ahmad, R.; Uppada, S.B.; Singh, A.B.; Dhawan, P. Claudin-1 promotes tnf-α-induced epithelial-mesenchymal transition and migration in colorectal adenocarcinoma cells. *Exp. Cell Res.* **2016**, *349*, 119–127. [CrossRef] [PubMed]
123. Jemal, A.; Siegel, R.; Xu, J.; Ward, E. Cancer statistics, 2010. *CA Cancer J. Clin.* **2010**, *60*, 277–300. [CrossRef] [PubMed]
124. Tan, C.; Cruet-Hennequart, S.; Troussard, A.; Fazli, L.; Costello, P.; Sutton, K.; Wheeler, J.; Gleave, M.; Sanghera, J.; Dedhar, S. Regulation of tumor angiogenesis by integrin-linked kinase (ilk). *Cancer Cell* **2004**, *5*, 79–90. [CrossRef]
125. Reid, B.M.; Permuth, J.B.; Sellers, T.A. Epidemiology of ovarian cancer: A review. *Cancer Biol. Med.* **2017**, *14*, 9–32. [PubMed]
126. Liu, T.; Cheng, W.; Lai, D.; Huang, Y.; Guo, L. Characterization of primary ovarian cancer cells in different culture systems. *Oncol. Rep.* **2010**, *23*, 1277–1284. [PubMed]
127. Zhu, Y.; Sundfeldt, K. Tight junction formation in epithelial ovarian adenocarcinoma. *Acta Obs. Gynecol. Scand.* **2007**, *86*, 1011–1019. [CrossRef]
128. Tandon, P.; Dadhich, A.; Saluja, H.; Bawane, S.; Sachdeva, S. The prevalence of squamous cell carcinoma in different sites of oral cavity at our rural health care centre in loni, maharashtra—A retrospective 10-year study. *Contemp. Oncol.* **2017**, *21*, 178–183. [CrossRef]

129. Habelhah, H.; Okada, F.; Kobayashi, M.; Nakai, K.; Choi, S.; Hamada, J.; Moriuchi, T.; Kaya, M.; Yoshida, K.; Fujinaga, K.; et al. Increased e1af expression in mouse fibrosarcoma promotes metastasis through induction of mt1-mmp expression. *Oncogene* **1999**, *18*, 1771–1776. [CrossRef]
130. Sappayatosok, K.; Phattarataratip, E. Overexpression of claudin-1 is associated with advanced clinical stage and invasive pathologic characteristics of oral squamous cell carcinoma. *Head Neck Pathol.* **2015**, *9*, 173–180. [CrossRef]
131. Lourenco, S.V.; Coutinho-Camillo, C.M.; Buim, M.E.; Pereira, C.M.; Carvalho, A.L.; Kowalski, L.P.; Soares, F.A. Oral squamous cell carcinoma: Status of tight junction claudins in the different histopathological patterns and relationship with clinical parameters. A tissue-microarray-based study of 136 cases. *J. Clin. Pathol.* **2010**, *63*, 609–614. [CrossRef]
132. De Vicente, J.C.; Fernández-Valle, Á.; Vivanco-Allende, B.; Santamarta, T.R.; Lequerica-Fernández, P.; Hernández-Vallejo, G.; Allonca-Campa, E. The prognostic role of claudins -1 and -4 in oral squamous cell carcinoma. *Anticancer Res.* **2015**, *35*, 2949–2959. [PubMed]
133. Jerant, A.F.; Johnson, J.T.; Sheridan, C.D.; Caffrey, T.J. Early detection and treatment of skin cancer. *Am. Fam. Physician* **2000**, *62*, 357–368, 375–376, 381–382.
134. Weeraratna, A.T.; Becker, D.; Carr, K.M.; Duray, P.H.; Rosenblatt, K.P.; Yang, S.; Chen, Y.; Bittner, M.; Strausberg, R.L.; Riggins, G.J.; et al. Generation and analysis of melanoma sage libraries: Sage advice on the melanoma transcriptome. *Oncogene* **2004**, *23*, 2264–2274. [CrossRef] [PubMed]
135. Izraely, S.; Sagi-Assif, O.; Klein, A.; Meshel, T.; Ben-Menachem, S.; Zaritsky, A.; Ehrlich, M.; Prieto, V.G.; Bar-Eli, M.; Pirker, C.; et al. The metastatic microenvironment: Claudin-1 suppresses the malignant phenotype of melanoma brain metastasis. *Int. J. Cancer* **2015**, *136*, 1296–1307. [CrossRef]
136. Wong, M.C.S.; Goggins, W.B.; Wang, H.H.X.; Fung, F.D.H.; Leung, C.; Wong, S.Y.S.; Ng, C.F.; Sung, J.J.Y. Global incidence and mortality for prostate cancer: Analysis of temporal patterns and trends in 36 countries. *Eur. Urol.* **2016**, *70*, 862–874. [CrossRef]
137. Sugawara, T.; Iwamoto, N.; Akashi, M.; Kojima, T.; Hisatsune, J.; Sugai, M.; Furuse, M. Tight junction dysfunction in the stratum granulosum leads to aberrant stratum corneum barrier function in claudin-1-deficient mice. *J. Dermatol. Sci.* **2013**, *70*, 12–18. [CrossRef]
138. Inai, T.; Kobayashi, J.; Shibata, Y. Claudin-1 contributes to the epithelial barrier function in mdck cells. *Eur. J. Cell Biol.* **1999**, *78*, 849–855. [CrossRef]
139. McCarthy, K.M.; Francis, S.A.; McCormack, J.M.; Lai, J.; Rogers, R.A.; Skare, I.B.; Lynch, R.D.; Schneeberger, E.E. Inducible expression of claudin-1-myc but not occludin-vsv-g results in aberrant tight junction strand formation in mdck cells. *J. Cell Sci.* **2000**, *113*, 3387.
140. Grosse, B.; Cassio, D.; Yousef, N.; Bernardo, C.; Jacquemin, E.; Gonzales, E. Claudin-1 involved in neonatal ichthyosis sclerosing cholangitis syndrome regulates hepatic paracellular permeability. *Hepatology* **2012**, *55*, 1249–1259. [CrossRef]
141. Poritz, L.S.; Harris, L.R., 3rd; Kelly, A.A.; Koltun, W.A. Increase in the tight junction protein claudin-1 in intestinal inflammation. *Dig. Dis. Sci.* **2011**, *56*, 2802–2809. [CrossRef]
142. Sladojevic, N.; Stamatovic, S.M.; Johnson, A.M.; Choi, J.; Hu, A.; Dithmer, S.; Blasig, I.E.; Keep, R.F.; Andjelkovic, A.V. Claudin-1-dependent destabilization of the blood–brain barrier in chronic stroke. *J. Neurosci.* **2019**, *39*, 743. [CrossRef] [PubMed]
143. Hashimoto, Y.; Fukasawa, M.; Kuniyasu, H.; Yagi, K.; Kondoh, M. Claudin-targeted drug development using anti-claudin monoclonal antibodies to treat hepatitis and cancer. *Ann. N. Y. Acad. Sci.* **2017**, *1397*, 5–16. [CrossRef] [PubMed]
144. Hashimoto, Y.; Tada, M.; Iida, M.; Nagase, S.; Hata, T.; Watari, A.; Okada, Y.; Doi, T.; Fukasawa, M.; Yagi, K.; et al. Generation and characterization of a human–mouse chimeric antibody against the extracellular domain of claudin-1 for cancer therapy using a mouse model. *Biochem. Biophys. Res. Commun.* **2016**, *477*, 91–95. [CrossRef] [PubMed]
145. Nordin, B.E.; Robertson, A.; Seamark, R.F.; Bridges, A.; Philcox, J.C.; Need, A.G.; Horowitz, M.; Morris, H.A.; Deam, S. The relation between calcium absorption, serum dehydroepiandrosterone, and vertebral mineral density in postmenopausal women. *J. Clin. Endocrinol. Metab.* **1985**, *60*, 651–657. [CrossRef]
146. Fukasawa, M.; Nagase, S.; Shirasago, Y.; Iida, M.; Yamashita, M.; Endo, K.; Yagi, K.; Suzuki, T.; Wakita, T.; Hanada, K.; et al. Monoclonal antibodies against extracellular domains of claudin-1 block hepatitis c virus infection in a mouse model. *J. Virol.* **2015**, *89*, 4866–4879. [CrossRef] [PubMed]

147. Hollandsworth, H.M.; Lwin, T.M.; Amirfakhri, S.; Filemoni, F.; Batra, S.K.; Hoffman, R.M.; Dhawan, P.; Bouvet, M. Anti-claudin-1 conjugated to a near-infrared fluorophore targets colon cancer in pdox mouse models. *J. Surg. Res.* **2019**, *242*, 145–150. [CrossRef]
148. Kominsky, S.L. Claudins: Emerging targets for cancer therapy. *Expert Rev. Mol. Med.* **2006**, *8*, 1–11. [CrossRef]
149. Saeki, R.; Kondoh, M.; Kakutani, H.; Tsunoda, S.-i.; Mochizuki, Y.; Hamakubo, T.; Tsutsumi, Y.; Horiguchi, Y.; Yagi, K. A novel tumor-targeted therapy using a claudin-4-targeting molecule. *Mol. Pharmacol.* **2009**, *76*, 918. [CrossRef]
150. Hashimoto, Y.; Kawahigashi, Y.; Hata, T.; Li, X.; Watari, A.; Tada, M.; Ishii-Watabe, A.; Okada, Y.; Doi, T.; Fukasawa, M.; et al. Efficacy and safety evaluation of claudin-4-targeted antitumor therapy using a human and mouse cross-reactive monoclonal antibody. *Pharmacol. Res. Perspect.* **2016**, *4*, e00266. [CrossRef]
151. Torres, J.B.; Knight, J.C.; Mosley, M.J.; Kersemans, V.; Koustoulidou, S.; Allen, D.; Kinchesh, P.; Smart, S.; Cornelissen, B. Imaging of claudin-4 in pancreatic ductal adenocarcinoma using a radiolabelled anti-claudin-4 monoclonal antibody. *Mol. Imaging Biol.* **2018**, *20*, 292–299. [CrossRef]
152. Hashimoto, Y.; Tachibana, K.; Krug, S.M.; Kunisawa, J.; Fromm, M.; Kondoh, M. Potential for tight junction protein-directed drug development using claudin binders and angubindin-1. *Int. J. Mol. Sci.* **2019**, *20*, 4016. [CrossRef] [PubMed]
153. Simon, D.B.; Lu, Y.; Choate, K.A.; Velazquez, H.; Al-Sabban, E.; Praga, M.; Casari, G.; Bettinelli, A.; Colussi, G.; Rodriguez-Soriano, J.; et al. Paracellin-1, a renal tight junction protein required for paracellular Mg2+ resorption. *Science* **1999**, *285*, 103–106. [CrossRef] [PubMed]
154. Sanjad, S.A.; Hariri, A.; Habbal, Z.M.; Lifton, R.P. A novel pcln-1 gene mutation in familial hypomagnesemia with hypercalciuria and atypical phenotype. *Pediatr. Nephrol.* **2007**, *22*, 503–508. [CrossRef] [PubMed]
155. Hirano, T.; Kobayashi, N.; Itoh, T.; Takasuga, A.; Nakamaru, T.; Hirotsune, S.; Sugimoto, Y. Null mutation of pcln-1/claudin-16 results in bovine chronic interstitial nephritis. *Genome Res.* **2000**, *10*, 659–663. [CrossRef]
156. Hadj-Rabia, S.; Baala, L.; Vabres, P.; Hamel-Teillac, D.; Jacquemin, E.; Fabre, M.; Lyonnet, S.; de Prost, Y.; Munnich, A.; Hadchouel, M.; et al. Claudin-1 gene mutations in neonatal sclerosing cholangitis associated with ichthyosis: A tight junction disease. *Gastroenterology* **2004**, *127*, 1386–1390. [CrossRef]
157. Sineni, C.J.; Yildirim-Baylan, M.; Guo, S.; Camarena, V.; Wang, G.; Tokgoz-Yilmaz, S.; Duman, D.; Bademci, G.; Tekin, M. A truncating cldn9 variant is associated with autosomal recessive nonsyndromic hearing loss. *Hum. Genet.* **2019**, *138*, 1071–1075. [CrossRef]
158. Hadj-Rabia, S.; Brideau, G.; Al-Sarraj, Y.; Maroun, R.C.; Figueres, M.-L.; Leclerc-Mercier, S.; Olinger, E.; Baron, S.; Chaussain, C.; Nochy, D.; et al. Multiplex epithelium dysfunction due to cldn10 mutation: The helix syndrome. *Genet. Med.* **2018**, *20*, 190–201. [CrossRef]
159. Wilcox, E.R.; Burton, Q.L.; Naz, S.; Riazuddin, S.; Smith, T.N.; Ploplis, B.; Belyantseva, I.; Ben-Yosef, T.; Liburd, N.A.; Morell, R.J.; et al. Mutations in the gene encoding tight junction claudin-14 cause autosomal recessive deafness dfnb29. *Cell* **2001**, *104*, 165–172. [CrossRef]
160. Hampson, G.; Konrad, M.A.; Scoble, J. Familial hypomagnesaemia with hypercalciuria and nephrocalcinosis (fhhnc): Compound heterozygous mutation in the claudin 16 (cldn16) gene. *BMC Nephrol.* **2008**, *9*, 12. [CrossRef]
161. Konrad, M.; Schaller, A.; Seelow, D.; Pandey, A.V.; Waldegger, S.; Lesslauer, A.; Vitzthum, H.; Suzuki, Y.; Luk, J.M.; Becker, C.; et al. Mutations in the tight-junction gene claudin 19 (cldn19) are associated with renal magnesium wasting, renal failure, and severe ocular involvement. *Am. J. Hum. Genet.* **2006**, *79*, 949–957. [CrossRef]
162. Seker, M.; Fernandez-Rodriguez, C.; Martinez-Cruz, L.A.; Müller, D. Mouse models of human claudin-associated disorders: Benefits and limitations. *Int. J. Mol. Sci.* **2019**, *20*, 5504. [CrossRef] [PubMed]

MDPI
St. Alban-Anlage 66
4052 Basel
Switzerland
Tel. +41 61 683 77 34
Fax +41 61 302 89 18
www.mdpi.com

International Journal of Molecular Sciences Editorial Office
E-mail: ijms@mdpi.com
www.mdpi.com/journal/ijms

MDPI
St. Alban-Anlage 66
4052 Basel
Switzerland

Tel: +41 61 683 77 34
Fax: +41 61 302 89 18

www.mdpi.com

ISBN 978-3-03936-494-7